Records processed under FOIA Request #2014-8015; Released by CDRH on 12-8-2015

U.S. Department of Health & Human Services

Food and Drug Administration

SAVE REQUEST

USER:	(smw)
FOLDER:	K131337 - 1620 pages
COMPANY:	ORTHO DEVELOPMENT CORP. (ORTHDEVEB)
PRODUCT:	PROSTHESIS, KNEE, PATELLOFEMOROTIBIAL, SEMI-CONSTRAINED, CEMENTED, POLYMER/METAL/POLYMER (JWH)
SUMMARY:	Product: BALANCED KNEE SYSTEM HIGH FLEX VITAMIN E PS TIBIAL INSERT AND PATELLA
DATE REQUESTED:	Oct 19, 2015
DATE PRINTED:	Oct 19, 2015

Note: Printed

Questions? Contact FDA/CDRH/OCE/DID at CDRH-FOISTATUS@fda.hhs.gov or 301-796-8118

Records processed under FOIA Request #2014-8015; Released by CDRH on 12-8-2015

510(k) Summary

NAME OF SPONSOR: Ortho Development Corporation
12187 South Business Park Drive
Draper, Utah 84020

OCT 1 1 2013

510(k) CONTACT: Tom Haueter
Regulatory Affairs Manager
Telephone: (801) 553-9991
Facsimile: (801) 553-9993
Email: thaueter@orthodevelopment.com

DATE PREPARED: April 24, 2013

PROPRIETARY NAME: Balanced Knee® System High Flex Vitamin E PS Tibial Insert and Patella

COMMON NAME: Total Knee Replacement Prosthesis

CLASSIFICATION: 21 CFR 888.3560, Knee joint, patellofemorotibial, polymer/metal/polymer semi-constrained cemented prosthesis, Class II device

DEVICE PRODUCT CODE: OIY, JWH

PREDICATE DEVICES: Balanced Knee® System (K994370), *Ortho Development Corp.*

Balanced Knee® System High Flex PS (K123457), *Ortho Development Corp.*

Highly Cross-Linked Vitamin E UHMWPE Tibial Insert (K091956), *DJO Surgical/Encore Medical*

Questions? Contact FDA/CDRH/OCE/DID at CDRH-FOISTATUS@fda.hhs.gov or 301-796-8118

Records processed under FOIA Request #2014-8015; Released by CDRH on 12-8-2015

Device Description

The Balanced Knee® System High Flex Vitamin E (High Flex Vit E) PS tibial insert and patella are machined from extensively crosslinked, compression molded, Vitamin E UHMWPE. Both components are single use only. The High Flex Vit E PS tibial insert must be used in conjunction with the High Flex PS femoral component (K123457). Used together, these components are designed to accommodate increased range of motion up to 150° of flexion. The High Flex Vit E patella may be used in conjunction with the Balanced Knee® System (BKS) femoral components (K994370), the BKS modular femoral components (K060569), or the High Flex PS femoral components (K123457). Both the High Flex Vit E PS tibial insert and patella may be used in conjunction with the BKS standard and modular tibial trays, tibial augments, and stems to complete the semi-constrained modular knee prosthesis. The tibial trays, tibial augments, and stems were approved under K994370 and K031201.

Intended Use

The Balanced Knee® System High Flex Vitamin E PS tibial insert and patella are intended for use in cemented total knee arthroplasty procedures with the following indications:

1. Loss of knee joint configuration and joint function.
2. Osteoarthritis of the knee joint.
3. Rheumatoid arthritis of the knee joint.
4. Post-traumatic arthritis of the knee joint.
5. Valgus, varus, or flexion deformities of the knee joint.
6. Revision procedures where other treatments or devices have failed.

Technological Characteristics

Feature	Equivalent Device
Indications for Use and Design	Ortho Development: Balanced Knee® System (K994370) Ortho Development: Balanced Knee® System High Flex PS (K123457)
Material: Extensively Crosslinked Vitamin E Polyethylene UHMWPE (α-tocopherol)	DJO Surgical/Encore Medical: Vit E UHMWPE Tibial Insert (K091956)

There is only one difference between the High Flex Vit E PS insert when compared to the BKS High Flex PS insert: the implementation of a different material, crosslinked Vitamin E UHMWPE. Likewise, the High Flex Vit E patella is identical to the BKS patella except for the crosslinked Vitamin E UHMWPE material. The indications for use for the High Flex Vit E PS tibial insert and patella are identical to the indications for use for the BKS High Flex. The crosslinked Vitamin E UHMWPE for the High Flex Vit E PS insert and patella undergoes substantially equivalent fabrication and final processing as its predicate, DJO/Encore's Vitamin E UHMWPE tibial insert.

Questions? Contact FDA/CDRH/OCE/DID at CDRH-FOISTATUS@fda.hhs.gov or 301-796-8118

Records processed under FOIA Request #2014-8015; Released by CDRH on 12-8-2015

Performance Data

The following non-clinical testing was performed to determined substantial equivalence to the predicate devices:

Property	Result
Range of Motion	Up to 150° flexion; Substantially Equivalent to predicate device, BKS High Flex
Femorotibial Constraint	Substantially Equivalent to predicate device, BKS High Flex
Femorotibial Contact Area	Substantially Equivalent to predicate device, BKS High Flex
Patellofemoral Constraint	Substantially Equivalent to predicate device, BKS High Flex
Patellofemoral Contact Area	Substantially Equivalent to predicate device, BKS High Flex
PS Spine Fatigue	Substantially Equivalent
Insert Assembly/ Disassembly	Substantially Equivalent
Crosslinking Characterization of High Flex Vit E	Substantially equivalent or better than BKS
Vitamin E Characterization of High Flex Vit E	Substantially equivalent or better than BKS
High Flex Knee Wear	Decrease in wear over BKS

Basis for Substantial Equivalence

Ortho Development believes that the High Flex Vit E PS tibial insert and patella are substantially equivalent to the previously cleared predicate devices based on similarities in intended use, design, materials, manufacturing methods, packaging, and mechanical performance.

Questions? Contact FDA/CDRH/OCE/DID at CDRH-FOISTATUS@fda.hhs.gov or 301-796-8118

Records processed under FOIA Request #2014-8015; Released by CDRH on 12-8-2015

DEPARTMENT OF HEALTH & HUMAN SERVICES

Public Health Service

Food and Drug Administration
10903 New Hampshire Avenue
Document Control Center - WO66-G609
Silver Spring, MD 20993-0002

October 11, 2013

Ortho Development Corporation
Mr. Tom Haueter
Regulatory Affairs Manager
12187 South Business Park Drive
Draper, Utah 84020

Re: K131337
Trade/Device Name: Balanced Knee® System High Flex Vitamin E PS Tibial Insert and Patella
Regulation Number: 21 CFR 888.3560
Regulation Name: Knee joint patellofemorotibial polymer/metal/polymer semi-constrained cemented prosthesis
Regulatory Class: Class II
Product Code: JWH, OIY
Dated: September 6, 2013
Received: September 9, 2013

Dear Mr. Haueter:

We have reviewed your Section 510(k) premarket notification of intent to market the device referenced above and have determined the device is substantially equivalent (for the indications for use stated in the enclosure) to legally marketed predicate devices marketed in interstate commerce prior to May 28, 1976, the enactment date of the Medical Device Amendments, or to devices that have been reclassified in accordance with the provisions of the Federal Food, Drug, and Cosmetic Act (Act) that do not require approval of a premarket approval application (PMA). You may, therefore, market the device, subject to the general controls provisions of the Act. The general controls provisions of the Act include requirements for annual registration, listing of devices, good manufacturing practice, labeling, and prohibitions against misbranding and adulteration. Please note: CDRH does not evaluate information related to contract liability warranties. We remind you; however, that device labeling must be truthful and not misleading.

If your device is classified (see above) into either class II (Special Controls) or class III (PMA), it may be subject to additional controls. Existing major regulations affecting your device can be found in the Code of Federal Regulations, Title 21, Parts 800 to 898. In addition, FDA may publish further announcements concerning your device in the Federal Register.

Please be advised that FDA's issuance of a substantial equivalence determination does not mean that FDA has made a determination that your device complies with other requirements of the Act or any Federal statutes and regulations administered by other Federal agencies. You must comply with all the Act's requirements, including, but not limited to: registration and listing (21

Questions? Contact FDA/CDRH/OCE/DID at CDRH-FOISTATUS@fda.hhs.gov or 301-796-8118

Records processed under FOIA Request #2014-8015; Released by CDRH on 12-8-2015

CFR Part 807); labeling (21 CFR Part 801); medical device reporting (reporting of medical device-related adverse events) (21 CFR 803); good manufacturing practice requirements as set forth in the quality systems (QS) regulation (21 CFR Part 820); and if applicable, the electronic product radiation control provisions (Sections 531-542 of the Act); 21 CFR 1000-1050.

If you desire specific advice for your device on our labeling regulation (21 CFR Part 801), please contact the Division of Small Manufacturers, International and Consumer Assistance at its toll-free number (800) 638-2041 or (301) 796-7100 or at its Internet address http://www.fda.gov/MedicalDevices/ResourcesforYou/Industry/default.htm. Also, please note the regulation entitled, "Misbranding by reference to premarket notification" (21CFR Part 807.97). For questions regarding the reporting of adverse events under the MDR regulation (21 CFR Part 803), please go to http://www.fda.gov/MedicalDevices/Safety/ReportaProblem/default.htm for the CDRH's Office of Surveillance and Biometrics/Division of Postmarket Surveillance.

You may obtain other general information on your responsibilities under the Act from the Division of Small Manufacturers, International and Consumer Assistance at its toll-free number (800) 638-2041 or (301) 796-7100 or at its Internet address http://www.fda.gov/MedicalDevices/ResourcesforYou/Industry/default.htm.

Sincerely yours,

Erin I. Keith

for

Mark N. Melkerson
Director
Division of Orthopedic Devices
Office of Device Evaluation
Center for Devices and
Radiological Health

Enclosure

Questions? Contact FDA/CDRH/OCE/DID at CDRH-FOISTATUS@fda.hhs.gov or 301-796-8118

Records processed under FOIA Request #2014-8015; Released by CDRH on 12-8-2015

Indication for Use Form
Ortho Development
Balanced Knee® System High Flex Vitamin E PS Tibial Insert and Patella 510(k)

510(k) Number (if known): _K131337_____

Device Name: Balanced Knee® System High Flex Vitamin E PS Tibial Insert and Patella

Indications for Use:

The Balanced Knee® System High Flex Vitamin E PS tibial insert and patella are intended for use in cemented total knee arthroplasty procedures with the following indications:

1. Loss of knee joint configuration and joint function.
2. Osteoarthritis of the knee joint.
3. Rheumatoid arthritis of the knee joint.
4. Post-traumatic arthritis of the knee joint.
5. Valgus, varus, or flexion deformities of the knee joint.
6. Revision procedures where other treatments or devices have failed.

Prescription Use ____X____ (Part 21 CFR 801 Subpart D) AND/OR Over-The-Counter Use _____ (21 CFR 801 Subpart C)

(PLEASE DO NOT WRITE BELOW THIS LINE-CONTINUE ON ANOTHER PAGE IF NEEDED)

Concurrence of CDRH, Office of Device Evaluation (ODE)

Casey L. Hanley, Ph.D.
Division of Orthopedic Devices

Questions? Contact FDA/CDRH/OCE/DID at CDRH-FOISTATUS@fda.hhs.gov or 301-796-8118

Records processed under FOIA Request #2014-8015; Released by CDRH on 12-8-2015

DEPARTMENT OF HEALTH & HUMAN SERVICES

Public Health Service

Food and Drug Administration
10903 New Hampshire Avenue
Document Control Center - WO66-G609
Silver Spring, MD 20993-0002

October 11, 2013

Ortho Development Corporation
Mr. Tom Haueter
Regulatory Affairs Manager
12187 South Business Park Drive
Draper, Utah 84020

Re: K131337
Trade/Device Name: Balanced Knee® System High Flex Vitamin E PS Tibial Insert and Patella
Regulation Number: 21 CFR 888.3560
Regulation Name: Knee joint patellofemorotibial polymer/metal/polymer semi-constrained cemented prosthesis
Regulatory Class: Class II
Product Code: JWH, OIY
Dated: September 6, 2013
Received: September 9, 2013

Dear Mr. Haueter:

We have reviewed your Section 510(k) premarket notification of intent to market the device referenced above and have determined the device is substantially equivalent (for the indications for use stated in the enclosure) to legally marketed predicate devices marketed in interstate commerce prior to May 28, 1976, the enactment date of the Medical Device Amendments, or to devices that have been reclassified in accordance with the provisions of the Federal Food, Drug, and Cosmetic Act (Act) that do not require approval of a premarket approval application (PMA). You may, therefore, market the device, subject to the general controls provisions of the Act. The general controls provisions of the Act include requirements for annual registration, listing of devices, good manufacturing practice, labeling, and prohibitions against misbranding and adulteration. Please note: CDRH does not evaluate information related to contract liability warranties. We remind you; however, that device labeling must be truthful and not misleading.

If your device is classified (see above) into either class II (Special Controls) or class III (PMA), it may be subject to additional controls. Existing major regulations affecting your device can be found in the Code of Federal Regulations, Title 21, Parts 800 to 898. In addition, FDA may publish further announcements concerning your device in the Federal Register.

Please be advised that FDA's issuance of a substantial equivalence determination does not mean that FDA has made a determination that your device complies with other requirements of the Act or any Federal statutes and regulations administered by other Federal agencies. You must comply with all the Act's requirements, including, but not limited to: registration and listing (21

Questions? Contact FDA/CDRH/OCE/DID at CDRH-FOISTATUS@fda.hhs.gov or 301-796-8118

Records processed under FOIA Request #2014-8015; Released by CDRH on 12-8-2015

CFR Part 807); labeling (21 CFR Part 801); medical device reporting (reporting of medical device-related adverse events) (21 CFR 803); good manufacturing practice requirements as set forth in the quality systems (QS) regulation (21 CFR Part 820); and if applicable, the electronic product radiation control provisions (Sections 531-542 of the Act); 21 CFR 1000-1050.

If you desire specific advice for your device on our labeling regulation (21 CFR Part 801), please contact the Division of Small Manufacturers, International and Consumer Assistance at its toll-free number (800) 638-2041 or (301) 796-7100 or at its Internet address http://www.fda.gov/MedicalDevices/ResourcesforYou/Industry/default.htm. Also, please note the regulation entitled, "Misbranding by reference to premarket notification" (21CFR Part 807.97). For questions regarding the reporting of adverse events under the MDR regulation (21 CFR Part 803), please go to http://www.fda.gov/MedicalDevices/Safety/ReportaProblem/default.htm for the CDRH's Office of Surveillance and Biometrics/Division of Postmarket Surveillance.

You may obtain other general information on your responsibilities under the Act from the Division of Small Manufacturers, International and Consumer Assistance at its toll-free number (800) 638-2041 or (301) 796-7100 or at its Internet address http://www.fda.gov/MedicalDevices/ResourcesforYou/Industry/default.htm.

Sincerely yours,

Erin I. Keith

for

Mark N. Melkerson
Director
Division of Orthopedic Devices
Office of Device Evaluation
Center for Devices and
Radiological Health

Enclosure

Questions? Contact FDA/CDRH/OCE/DID at CDRH-FOISTATUS@fda.hhs.gov or 301-796-8118

Records processed under FOIA Request #2014-8015; Released by CDRH on 12-8-2015

Concurrence & Template History Page

Full Submission Number: K131337/S002

For Office of Compliance Contact Information:

http://insideportlets.fda.gov:9010/portal/page?_pageid=197,415881&_dad=portal&_schema=PORTAL&org=318

For Office of Surveillance and Biometrics Contact Information:

http://insideportlets.fda.gov:9010/portal/page?_pageid=197,415881&_dad=portal&_schema=PORTAL&org=423

Digital Signature Concurrence Table	
Reviewer Sign-Off	Michael Owens
Branch Chief Sign-Off	Casey Hanley (10/11/2013)
Division Sign-Off	Erin I. Keith 2013.10.11 14:12:07 -04'00'

f/t:MCO:JNJ:10/11/13:eaf:10/11/13
Template Name: K1(A) – SE after 1996

Template History:

Date of Update	By	Description of Update
7/27/09	Brandi Stuart	Added Updates to Boiler Table
8/7/09	Brandi Stuart	Updated HFZ Table
1/11/10	Diane Garcia	Liability/Warranty sentence added at bottom of 1st page
10/4/11	M. McCabe Janicki	Removed IFU sheet and placed in Forms
9/25/12	Edwena Jones	Added digital signature format
12/12/12	M. McCabe Janicki	Added an extra line between letter signature block and the word "Enclosure". Also, added a missing digit in 4-digit extension on letterhead zip code: "002" should be "0002".
4/2/2013	M. McCabe Janicki	Edited sentence that starts "If you desire specific advice for your device on our labeling regulation (21 CFR Part 801)..." Replaced broken Compliance link with general link to DSMICA.
4/12/2013	Margaret McCabe Janicki	Fixed a typo: Paragraph 1, final sentence, "We remind you, however; that device labeling must be truthful..." Replaced incorrect semicolon with a comma.

Questions? Contact FDA/CDRH/OCE/DID at CDRH-FOISTATUS@fda.hhs.gov or 301-796-8118

Records processed under FOIA Request #2014-8015; Released by CDRH on 12-8-2015

Indication for Use Form
Ortho Development
Balanced Knee® System High Flex Vitamin E PS Tibial Insert and Patella 510(k)

510(k) Number (if known): _K131337_____

Device Name: Balanced Knee® System High Flex Vitamin E PS Tibial Insert and Patella

Indications for Use:

The Balanced Knee® System High Flex Vitamin E PS tibial insert and patella are intended for use in cemented total knee arthroplasty procedures with the following indications:

1. Loss of knee joint configuration and joint function.
2. Osteoarthritis of the knee joint.
3. Rheumatoid arthritis of the knee joint.
4. Post-traumatic arthritis of the knee joint.
5. Valgus, varus, or flexion deformities of the knee joint.
6. Revision procedures where other treatments or devices have failed.

Prescription Use ____X____ (Part 21 CFR 801 Subpart D) AND/OR Over-The-Counter Use _____ (21 CFR 801 Subpart C)

(PLEASE DO NOT WRITE BELOW THIS LINE-CONTINUE ON ANOTHER PAGE IF NEEDED)

Concurrence of CDRH, Office of Device Evaluation (ODE)

Casey L. Hanley, Ph.D.
Division of Orthopedic Devices

Questions? Contact FDA/CDRH/OCE/DID at CDRH-FOISTATUS@fda.hhs.gov or 301-796-8118

Records processed under FOIA Request #2014-8015; Released by CDRH on 12-8-2015

K131337

12187 So. Business Park Drive
Draper, Utah 84020
801-553-9991/fax 553-9993

orthodevelopment.com

ORTHO DEVELOPMENT

FDA CDRH DMC
MAY 14 2013
Received

13 May 2013

This Replacement eCopy is an exact duplicate of the paper copy of the Balanced Knee® System High Flex Vitamin E PS Tibial Insert and Patella Premarket Notification, K131337, except pages 723 and 724 have been updated to clearer images. Those pages were askew in previous paper and electronic submissions. A paper copy of those pages has also been included for replacement.

To rectify the embedded attachments indicated from your email dated May 10th and on page 17 of the FDA's "eCopy Program for Medical Device Submissions" PDF, Sections 23 and 25 were scanned and then included on the eCopy. Ortho Development strives to submit PDFs in their clearest form, but at times will use scans to satisfy the FDA's loading process. Section 25 was also saved as a reduced-size scanned PDF to satisfy the 50 MB-per-section limit. This change lessens the resolution of Section 25 in the eCopy compared to the paper copy.

Thank you for your time in reviewing this submission and please do not hesitate to contact me if you need any further information.

Kind Regards,

Ed Goodman
Director of Quality Assurance/Regulatory Affairs
Ortho Development Corporation
12187 South Business Park Drive
Draper, UT 84020
egoodman@orthodevelopment.com

Questions? Contact FDA/CDRH/OCE/DID at CDRH-FOISTATUS@fda.hhs.gov or 301-796-8118

Records processed under FOIA Request #2014-8015; Released by CDRH on 12-8-2015

K131337

12187 So. Business Park Drive
Draper, Utah 84020
801-553-9991/fax 553-9993

orthodevelopment.com

ORTHO DEVELOPMENT

FDA CDRH DMC
MAY 10 2013
Received

9 May 2013

This Replacement eCopy is an exact duplicate of the paper copy of the Balanced Knee® System High Flex Vitamin E PS Tibial Insert and Patella Premarket Notification, K131337.

Thank you for your time in reviewing this submission and please do not hesitate to contact me if you need any further information.

Kind Regards,

Ed Goodman
Director of Quality Assurance/Regulatory Affairs
Ortho Development Corporation
12187 South Business Park Drive
Draper, UT 84020
egoodman@orthodevelopment.com

2

Questions? Contact FDA/CDRH/OCE/DID at CDRH-FOISTATUS@fda.hhs.gov or 301-796-8118

Records processed under FOIA Request #2014-8015; Released by CDRH on 12-8-2015

K56

FDA CDRH DMC
MAY 09 2013
Received

K131337

ORTHO DEVELOPMENT®

April 26, 2013

Food and Drug Administration
Center for Device and Radiological Health
Document Mail Center – WO66-G609
10903 New Hampshire Avenue
Silver Spring, Maryland 20993-0002

Re: 510(k) Submission
Balanced Knee® System High Flex Vitamin E PS Tibial Insert and Patella

To whom it may concern,

Please find attached the traditional 510(k) submitted by Ortho Development Corporation for the following total knee replacement prosthesis, which is a new device. There are no prior submissions for this device.

Name of Sponsor: Ortho Development Corporation
12187 South Business Park Drive
Draper, Utah 84020

Proprietary Name: Balanced Knee® System High Flex Vitamin E PS Tibial Insert and Patella

Common Name: Total Knee Replacement Prosthesis

Classification: 21 CFR 888.3560, Knee joint, patellofemorotibial, polymer/metal/polymer semi-constrained cemented prosthesis, Class II device

Device Product Code: JWH

The primary use of the device is summarized in the table below:

Question	Yes	No
Is the device intended for prescription use (21 CFR 801 Subpart D)?	X	
Is the device intended for over-the-counter use (21 CFR 807 Subpart C)?		X
Does the device contain components derived from a tissue or other biologic source?		X
Is the device provided sterile?	X	
Is the device intended for single use?	X	
Is the device a reprocessed single use device?		X
Does the device contain a drug?		X
Does the device contain a biologic?		X
Does the device use software?		X
Does the submission include clinical information?		X
Is the device implanted?	X	

Questions? Contact FDA/CDRH/OCE/DID at CDRH-FOISTATUS@fda.hhs.gov or 301-796-8118

Records processed under FOIA Request #2014-8015; Released by CDRH on 12-8-2015

Ortho Development Corporation considers its intent to market this device to be company confidential information per 21 CFR 807.95. Knowledge of this project and product line has been restricted to Ortho Development's employees, suppliers, and agents only.

Please find included one paper copy of the submission and one disc containing an electronic copy per instructions provided on the FDA website.

The Regulatory Affairs Manager of Ortho Development is the official contact and correspondent for this submission. Please direct any correspondence to my attention at:

Tom Haueter
Regulatory Affairs Manager
Telephone: (801) 553-9991
Facsimile: (801) 553-9993
Email: thaueter@orthodevelopment.com

Should you have any immediate questions regarding this submission, please feel free to contact me at your convenience.

Sincerely,

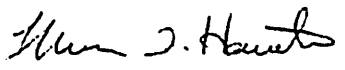

Tom Haueter
Regulatory Affairs Manager
Ortho Development

Questions? Contact FDA/CDRH/OCE/DID at CDRH-FOISTATUS@fda.hhs.gov or 301-796-8118

Records processed under FOIA Request #2014-8015; Released by CDRH on 12-8-2015

12187 So. Business Park Drive
Draper, Utah 84020
801-553-9991/fax 553-9993

orthodevelopment.com

K131337

ORTHO DEVELOPMENT

FDA CDRH DMC
MAY 9 2013
Received

3 May 2013

This eCopy is an exact duplicate of the paper copy of the Balanced Knee® System High Flex Vitamin E PS Tibial Insert and Patella Premarket Notification.

Thank you for your time in reviewing this submission and please do not hesitate to contact me if you need any further information.

Kind Regards,

Ed Goodman
Director of Quality Assurance/Regulatory Affairs
Ortho Development Corporation
12187 South Business Park Drive
Draper, UT 84020
egoodman@orthodevelopment.com

Questions? Contact FDA/CDRH/OCE/DID at CDRH-FOISTATUS@fda.hhs.gov or 301-796-8118

Records processed under FOIA Request #2014-8015; Released by CDRH on 12-8-2015

12187 So. Business Park Drive
Draper, Utah 84020
801-553-9991/fax 553-9993

orthodevelopment.com

ORTHO DEVELOPMENT

3 May 2013

This eCopy is an exact duplicate of the paper copy of the Balanced Knee® System High Flex Vitamin E PS Tibial Insert and Patella Premarket Notification.

Thank you for your time in reviewing this submission and please do not hesitate to contact me if you need any further information.

Kind Regards,

Ed Goodman
Director of Quality Assurance/Regulatory Affairs
Ortho Development Corporation
12187 South Business Park Drive
Draper, UT 84020
egoodman@orthodevelopment.com

Questions? Contact FDA/CDRH/OCE/DID at CDRH-FOISTATUS@fda.hhs.gov or 301-796-8118

Records processed under FOIA Request #2014-8015; Released by CDRH on 12-8-2015

Acceptance Checklist for Traditional 510(k)s

Device Name: Balanced Knee® System High Flex Vitamin E PS Tibial Insert and Patella

Date Prepared: April 24, 2013

Preliminary Questions		
Question	*Response*	*510(k) Section*
1	Yes	Section 3
2	Yes	Section 3
3	N/A	--
4	Yes	Section 3
5	No	--
6	No	--

Organizational Elements		
Question	*Response*	*510(k) Section*
a	Yes	Table of Contents
b	Yes	All
c	Yes	All
d	Yes	Section 2

A. Administrative		
Question	*Response*	*510(k) Section*
1	Yes	All
2	Yes	Section 2
2a	Yes	Section 2
2b	Yes	Section 2
2c	Yes	Section 2
3	Yes	Section 4
4	Yes	Section 5
4a	Yes	Section 5
4b	N/A	N/A
5	Yes	Section 6
6	N/A	N/A
7	N/A	N/A
7a	N/A	N/A
7b	N/A	N/A
8	Yes	Section 9
9	Yes	Section 3
9a	N/A	N/A

B. Device Description		
Question	*Response*	*510(k) Section*
10a	N/A	N/A
10b	Yes	Section 18
11a	Yes	Sections 11 & 13
11b	Yes	Sections 11 & 13
11c	Yes	Sections 11 & 13
12	Yes	Section 11
13a	Yes	Section 11
13b	Yes	Section 11
13c	Yes	Section 11

C. Substantial Equivalence Discussion		
Question	*Response*	*510(k) Section*
14	Yes	Section 12
14a	Yes	Section 12
14b	Yes	Sections 5 & 12
15a	Yes	Section 12
15b	Yes	Section 12
16	Yes	Section 12

D. Proposed Labeling		
Question	*Response*	*510(k) Section*
17	Yes	Section 13
17a	Yes	Sections 4, 5 & 13
17b	Yes	Section 13
18	Yes	Section 13
19a	Yes	Section 13
19b	N/A	N/A
20a	N/A	N/A
20b	Yes	Section 13
20c	N/A	N/A
21	N/A	N/A

E. Sterilization		
Question	*Response*	*510(k) Section*
E	"sterile"	Section 14
22a	Yes	Section 14
22b	Yes	Section 14
22c	Yes	Section 14
23a	Yes	Section 14
23b	Yes	Section 14
23c	Yes	Section 14
23d	Yes	Section 14
23e	Yes	Section 14
24a	Yes	Section 14
24b	Yes	Section 14
24c	Yes	Section 14
24d	Yes	Section 14
25a	N/A	N/A
25b	Yes	Section 14
25c	N/A	N/A

F. Shelf Life		
Question	*Response*	*510(k) Section*
26	Yes	Section 14
27	Yes	Section 14
28	Yes	Section 14

G. Biocompatibility		
Question	*Response*	*510(k) Section*
G	"are"	Section 15
29	Yes	Section 11
30	Yes	Section 15
31	Yes	Section 15

H. Software		
Question	*Response*	*510(k) Section*
H	"does not"	Section 10

I. EMC and Electrical Safety		
Question	*Response*	*510(k) Section*
I	"does not"	Section 10

J. Performance Data - General		
Question	*Response*	*510(k) Section*
36	Yes	Section 18
37a	N/A	N/A
37b	Yes	Section 18
37c	N/A	N/A
38a	Yes	Section 18
38b	Yes	Section 18
39	N/A	N/A

K. Performance Characteristics		
Question	*Response*	*510(k) Section*
K	"is not"	Section 10

Records processed under FOIA Request #2014-8015; Released by CDRH on 12-8-2015

Balanced Knee® System High Flex Vitamin E PS Tibial Insert and Patella 510(k) Submission Table of Contents

Section 1	Medical Device User Fee Cover Sheet
Section 2	CDRH Premarket Revision Submission Cover Sheet
Section 3	510(k) Cover Letter
Section 4	Indications for Use Statement
Section 5	510(k) Summary
Section 6	Truthful and Accurate Statement
Section 7	Class Ill Summary and Certification
Section 8	Financial Certification or Disclosure Statement
Section 9	Declarations of Conformity and Summary Reports
Section 10	Executive Summary
Section 11	Device Description
Section 12	Substantial Equivalence Discussion
Section 13	Proposed Labeling
Section 14	Sterilization and Shelf Life
Section 15	Biocompatibility
Section 16	Software
Section 17	Electromagnetic Compatibility and Electrical Safety
Section 18	Performance Testing - Bench
Section 19	Performance Testing - Animal
Section 20	Performance Testing - Clinical

Questions? Contact FDA/CDRH/OCE/DID at CDRH-FOISTATUS@fda.hhs.gov or 301-796-8118

Records processed under FOIA Request #2014-8015; Released by CDRH on 12-8-2015

Section 1
Medical Device User Fee Cover Sheet

Questions? Contact FDA/CDRH/OCE/DID at CDRH-FOISTATUS@fda.hhs.gov or 301-796-8118

Form Approved: OMB No. 0910-511 Expiration Date: February 28, 2013. See Instructions for OMB Statement.

DEPARTMENT OF HEALTH AND HUMAN SERVICES
FOOD AND DRUG ADMINISTRATION
MEDICAL DEVICE USER FEE COVER SHEET

PAYMENT IDENTIFICATION NUMBER: (b) (4) [redacted]
Write the Payment Identification number on your check.

A completed cover sheet must accompany each original application or supplement subject to fees. If payment is sent by U.S. mail or courier, please include a copy of this completed form with payment. Payment and mailing instructions can be found at: http://www.fda.gov/oc/mdufma/coversheet.html

1. COMPANY NAME AND ADDRESS (include name, street address, city state, country, and post office code)

ORTHO DEVELOPMENT CORPORATION
12187 Business Park Dr

Draper
UT 840208663
US

1.1 EMPLOYER IDENTIFICATION NUMBER (EIN)
(b)(4) [redacted]

2. CONTACT NAME
Thomas Haueter

2.1 E-MAIL ADDRESS
thaueter@orthodevelopment.com

2.2 TELEPHONE NUMBER (include Area code)
801-5539991

2.3 FACSIMILE (FAX) NUMBER (Include Area code)
801-5539993

3. TYPE OF PREMARKET APPLICATION (Select one of the following in each column; if you are unsure, please refer to the application descriptions at the following web site: http://www.fda.gov/oc/mdufma

Select an application type:
[X] Premarket notification(510(k)); except for third party
[ ] 513(g) Request for Information
[ ] Biologics License Application (BLA)
[ ] Premarket Approval Application (PMA)
[ ] Modular PMA
[ ] Product Development Protocol (PDP)
[ ] Premarket Report (PMR)
[ ] Annual Fee for Periodic Reporting (APR)
[ ] 30-Day Notice

3.1 Select a center
[X] CDRH
[ ] CBER

3.2 Select one of the types below
[X] Original Application

Supplement Types:
[ ] Efficacy (BLA)
[ ] Panel Track (PMA, PMR, PDP)
[ ] Real-Time (PMA, PMR, PDP)
[ ] 180-day (PMA, PMR, PDP)

4. ARE YOU A SMALL BUSINESS? (See the instructions for more information on determining this status)
[ ] YES, I meet the small business criteria and have submitted the required qualifying documents to FDA
[X] NO, I am not a small business

4.1 If Yes, please enter your Small Business Decision Number:

5. FDA WILL NOT ACCEPT YOUR SUBMISSION IF YOUR COMPANY HAS NOT PAID AN ESTABLISHMENT REGISTRATION FEE THAT IS DUE TO FDA. HAS YOUR COMPANY PAID ALL ESTABLISHMENT REGISTRATION FEES THAT ARE DUE TO FDA?
[X] YES (All of our establishments have registered and paid the fee, or this is our first device, and we will register and pay the fee within 30 days of FDA's approval/clearance of this device.)
[ ] NO (If "NO," FDA will not accept your submission until you have paid all fees due to FDA. This submission will not be processed; see http://www.fda.gov/cdrh/mdufma for additional information)

6. IS THIS PREMARKET APPLICATION COVERED BY ANY OF THE FOLLOWING USER FEE EXCEPTIONS? IF SO, CHECK THE APPLICABLE EXCEPTION.
[ ] This application is the first PMA submitted by a qualified small business, including any affiliates
[ ] The sole purpose of the application is to support conditions of use for a pediatric population
[ ] This biologics application is submitted under section 351 of the Public Health Service Act for a product licensed for further manufacturing use only
[ ] The application is submitted by a state or federal government entity for a device that is not to be distributed commercially

7. IS THIS A SUPPLEMENT TO A PREMARKET APPLICATION FOR WHICH FEES WERE WAIVED DUE TO SOLE USE IN A PEDIATRIC POPULATION THAT NOW PROPOSES CONDITION OF USE FOR ANY ADULT POPULATION? (If so, the application is subject to the fee that applies for an original premarket approval application (PMA).
[ ] YES [X] NO

PAPERWORK REDUCTION ACT STATEMENT
Public reporting burden for this collection of information is estimated to average 18 minutes per response, including the time for reviewing instructions, searching existing data sources, gathering and maintaining the data needed, and completing and reviewing the collection of information. Send comments regarding this burden estimate or any other aspect of this collection of information, including suggestions for reducing this burden, to the address below.

Department of Health and Human Services, Food and Drug Administration, Office of Chief Information Officer, 1350 Piccard Drive, 4th Floor Rockville, MD 20850
[Please do NOT return this form to the above address, except as it pertains to comments on the burden estimate.]

8. USER FEE PAYMENT AMOUNT SUBMITTED FOR THIS PREMARKET APPLICATION
(b)(4) [redacted] 19-Apr-2013

Form FDA 3601 (01/2007)

"Close Window" Print Cover sheet

Questions? Contact FDA/CDRH/OCE/DID at CDRH-FOISTATUS@fda.hhs.gov or 301-796-8118

Records processed under FOIA Request #2014-8015; Released by CDRH on 12-8-2015

Section 2
CDRH Premarket Review Submission Cover Sheet

Questions? Contact FDA/CDRH/OCE/DID at CDRH-FOISTATUS@fda.hhs.gov or 301-796-8118

Records processed under FOIA Request #2014-8015; Released by CDRH on 12-8-2015

DEPARTMENT OF HEALTH AND HUMAN SERVICES
FOOD AND DRUG ADMINISTRATION

CDRH PREMARKET REVIEW SUBMISSION COVER SHEET

Form Approval
OMB No. 0910-0120
Expiration Date: December 31, 2013
See OMB Statement on page 5.

Date of Submission	User Fee Payment ID Number	FDA Submission Document Number *(if known)*
04/23/2013	(b)(4) [redacted]	

SECTION A — TYPE OF SUBMISSION

PMA	PMA & HDE Supplement	PDP	510(k)	Meeting
☐ Original Submission	☐ Regular (180 day)	☐ Original PDP	☒ Original Submission:	☐ Pre-510(K) Meeting
☐ Premarket Report	☐ Special	☐ Notice of Completion	☒ Traditional	☐ Pre-IDE Meeting
☐ Modular Submission	☐ Panel Track (PMA Only)	☐ Amendment to PDP	☐ Special	☐ Pre-PMA Meeting
☐ Amendment	☐ 30-day Supplement		☐ Abbreviated (Complete section I, Page 5)	☐ Pre-PDP Meeting
☐ Report	☐ 30-day Notice		☐ Additional Information	☐ Day 100 Meeting
☐ Report Amendment	☐ 135-day Supplement		☐ Third Party	☐ Agreement Meeting
☐ Licensing Agreement	☐ Real-time Review			☐ Determination Meeting
	☐ Amendment to PMA & HDE Supplement			☐ Other *(specify)*:
	☐ Other			

IDE	Humanitarian Device Exemption (HDE)	Class II Exemption Petition	Evaluation of Automatic Class III Designation (De Novo)	Other Submission
☐ Original Submission	☐ Original Submission	☐ Original Submission	☐ Original Submission	☐ 513(g)
☐ Amendment	☐ Amendment	☐ Additional Information	☐ Additional Information	☐ Other *(describe submission)*:
☐ Supplement	☐ Supplement			
	☐ Report			
	☐ Report Amendment			

Have you used or cited Standards in your submission? ☒ Yes ☐ No *(If Yes, please complete Section I, Page 5)*

SECTION B — SUBMITTER, APPLICANT OR SPONSOR

Company / Institution Name: Ortho Development Corporation	Establishment Registration Number *(if known)*: 1722511
Division Name *(if applicable)*:	Phone Number *(including area code)*: 801-553-9991
Street Address: 12187 South Business Park Drive	FAX Number *(including area code)*: 801-553-9993
City: Draper	State / Province: UT; ZIP/Postal Code: 84020; Country: USA
Contact Name: Tom Haueter	
Contact Title: Regulatory Affairs Manager	Contact E-mail Address: thaueter@orthodevelopment.com

SECTION C — APPLICATION CORRESPONDENT (e.g., consultant, if different from above)

Company / Institution Name:	
Division Name *(if applicable)*:	Phone Number *(including area code)*:
Street Address:	FAX Number *(including area code)*:
City:	State / Province: ; ZIP Code: ; Country:
Contact Name:	
Contact Title:	Contact E-mail Address:

Questions? Contact FDA/CDRH/OCE/DID at CDRH-FOISTATUS@fda.hhs.gov or 301-796-8118 PSC Form Services (301) 443-6740 EF

Records processed under FOIA Request #2014-8015; Released by CDRH on 12-8-2015

SECTION D1 — REASON FOR APPLICATION - PMA, PDP, OR HDE

- [ ] New Device
- [ ] Withdrawal
- [ ] Additional or Expanded Indications
- [ ] Request for Extension
- [ ] Post-approval Study Protocol
- [ ] Request for Applicant Hold
- [ ] Request for Removal of Applicant Hold
- [ ] Request to Remove or Add Manufacturing Site

- [ ] Change in design, component, or specification:
  - [ ] Software / Hardware
  - [ ] Color Additive
  - [ ] Material
  - [ ] Specifications
  - [ ] Other *(specify below)*

- [ ] Location change:
  - [ ] Manufacturer
  - [ ] Sterilizer
  - [ ] Packager

- [ ] Report Submission:
  - [ ] Annual or Periodic
  - [ ] Post-approval Study
  - [ ] Adverse Reaction
  - [ ] Device Defect
  - [ ] Amendment

- [ ] Process change:
  - [ ] Manufacturing
  - [ ] Packaging
  - [ ] Sterilization
  - [ ] Other *(specify below)*

- [ ] Labeling change:
  - [ ] Indications
  - [ ] Instructions
  - [ ] Performance Characteristics
  - [ ] Shelf Life
  - [ ] Trade Name
  - [ ] Other *(specify below)*

- [ ] Change in Ownership
- [ ] Change in Correspondent
- [ ] Change of Applicant Address

- [ ] Response to FDA correspondence:

- [ ] Other Reason *(specify)*:

SECTION D2 — REASON FOR APPLICATION - IDE

- [ ] New Device
- [ ] New Indication
- [ ] Addition of Institution
- [ ] Expansion / Extension of Study
- [ ] IRB Certification
- [ ] Termination of Study
- [ ] Withdrawal of Application
- [ ] Unanticipated Adverse Effect
- [ ] Notification of Emergency Use
- [ ] Compassionate Use Request
- [ ] Treatment IDE
- [ ] Continued Access

- [ ] Change in:
  - [ ] Correspondent / Applicant
  - [ ] Design / Device
  - [ ] Informed Consent
  - [ ] Manufacturer
  - [ ] Manufacturing Process
  - [ ] Protocol - Feasibility
  - [ ] Protocol - Other
  - [ ] Sponsor

- [ ] Report submission:
  - [ ] Current Investigator
  - [ ] Annual Progress Report
  - [ ] Site Waiver Report
  - [ ] Final

- [ ] Response to FDA Letter Concerning:
  - [ ] Conditional Approval
  - [ ] Deemed Approved
  - [ ] Deficient Final Report
  - [ ] Deficient Progress Report
  - [ ] Deficient Investigator Report
  - [ ] Disapproval
  - [ ] Request Extension of Time to Respond to FDA
  - [ ] Request Meeting
  - [ ] Request Hearing

- [ ] Other Reason *(specify)*:

SECTION D3 — REASON FOR SUBMISSION - 510(k)

- [x] New Device
- [ ] Additional or Expanded Indications
- [ ] Change in Technology

- [ ] Other Reason *(specify)*:

Questions? Contact FDA/CDRH/OCE/DID at CDRH-FOISTATUS@fda.hhs.gov or 301-796-8118

Records processed under FOIA Request #2014-8015; Released by CDRH on 12-8-2015

SECTION E — ADDITIONAL INFORMATION ON 510(K) SUBMISSIONS

Product codes of devices to which substantial equivalence is claimed

1	JWH	2		3		4	
5		6		7		8	

Summary of, or statement concerning, safety and effectiveness information

- [x] 510 (k) summary attached
- [ ] 510 (k) statement

Information on devices to which substantial equivalence is claimed *(if known)*

	510(k) Number		*Trade or Proprietary or Model Name*		*Manufacturer*
1	K994370	1	Balanced Knee System	1	Ortho Development
2	K123457	2	Balanced Knee System High Flex PS	2	Ortho Development
3	K091956	3	Highly Cross-Linked Vitamin E UHMWPE Tibial Insert	3	DJO/Encore Medical
4		4		4	
5		5		5	
6		6		6	

SECTION F — PRODUCT INFORMATION - APPLICATION TO ALL APPLICATIONS

Common or usual name or classification name

Knee joint, patellofemorotibial, polymer/metal/polymer semi-constrained cemented prosthesis

	Trade or Proprietary or Model Name for This Device		Model Number
1	Balanced Knee System High Flex Vitamin E PS Tibial Insert and Patella	1	
2		2	
3		3	
4		4	
5		5	

FDA document numbers of all prior related submissions *(regardless of outcome)*

1 None	2	3	4	5	6
7	8	9	10	11	12

Data Included in Submission

- [x] Laboratory Testing
- [ ] Animal Trials
- [ ] Human Trials

SECTION G — PRODUCT CLASSIFICATION - APPLICATION TO ALL APPLICATIONS

Product Code	C.F.R. Section *(if applicable)*	Device Class
JWH	888.3560	[ ] Class I [x] Class II
Classification Panel: Orthopedic		[ ] Class III [ ] Unclassified

Indications *(from labeling)*

The Balanced Knee System High Flex Vitamin E PS tibial insert and patella are intended for use in cemented total knee arthroplasty procedures with the following indications:

1. Loss of knee joint configuration and joint function.
2. Osteoarthritis of the knee joint.
3. Rheumatoid arthritis of the knee joint.
4. Post-traumatic arthritis of the knee joint.
5. Valgus, varus, or flexion deformities of the knee joint.
6. Revision procedures where other treatments or devices have failed.

Questions? Contact FDA/CDRH/OCE/DID at CDRH-FOISTATUS@fda.hhs.gov or 301-796-8118

Note: Submission of the information entered in Section H does not affect the need to submit device establishment registration.	FDA Document Number *(if known)*

SECTION H — MANUFACTURING / PACKAGING / STERILIZATION SITES RELATING TO A SUBMISSION

☒ Original ☐ Add ☐ Delete	Facility Establishment Identifier (FEI) Number: 1722511	☒ Manufacturer ☐ Contract Sterilizer ☐ Contract Manufacturer ☐ Repackager / Relabeler
Company / Institution Name: Ortho Development Corporation		Establishment Registration Number: 1722511
Division Name *(if applicable)*		Phone Number *(including area code)*: (801) 553-9991
Street Address: 12187 South Business Park Drive		FAX Number *(including area code)*: (801) 553-9993
City: Draper	State / Province: UT	ZIP Code: 84020 / Country: USA
Contact Name: Tom Haueter	Contact Title: Regulatory Affairs Manager	Contact E-mail Address: thaueter@orthodevelopment.com

☐ Original ☐ Add ☐ Delete	Facility Establishment Identifier (FEI) Number	☐ Manufacturer ☒ Contract Sterilizer ☐ Contract Manufacturer ☐ Repackager / Relabeler

(b)(4)

[redacted]

☐ Original ☐ Add ☐ Delete	Facility Establishment Identifier (FEI) Number	☐ Manufacturer ☐ Contract Sterilizer ☒ Contract Manufacturer ☐ Repackager / Relabeler

(b)(4)

[redacted]

Questions? Contact FDA/CDRH/OCE/DID at CDRH-FOISTATUS@fda.hhs.gov or 301-796-8118

Records processed under FOIA Request #2014-8015; Released by CDRH on 12-8-2015

Note: Submission of this information does not affect the need to submit a 2891 or 2891a Device Establishment Registration form.	FDA Document Number *(if known)*

SECTION H *(Continued)*

☐ Original ☐ Add ☐ Delete	Facility Establishment Identifier (FEI) Number	☐ Manufacturer ☐ Contract Sterilizer ☐ Contract Manufacturer ☐ Repackager / Relabeler
Company / Institution Name		Establishment Registration Number
Division Name *(if applicable)*		Phone Number *(including area code)*
Street Address		FAX Number *(including area code)*
City	State / Province	ZIP Code / Country
Contact Name	Contact Title	Contact E-mail Address

☐ Original ☐ Add ☐ Delete	Facility Establishment Identifier (FEI) Number	☐ Manufacturer ☐ Contract Sterilizer ☐ Contract Manufacturer ☐ Repackager / Relabeler
Company / Institution Name		Establishment Registration Number
Division Name *(if applicable)*		Phone Number *(including area code)*
Street Address		FAX Number *(including area code)*
City	State / Province	ZIP Code / Country
Contact Name	Contact Title	Contact E-mail Address

☐ Original ☐ Add ☐ Delete	Facility Establishment Identifier (FEI) Number	☐ Manufacturer ☐ Contract Sterilizer ☐ Contract Manufacturer ☐ Repackager / Relabeler
Company / Institution Name		Establishment Registration Number
Division Name *(if applicable)*		Phone Number *(including area code)*
Street Address		FAX Number *(including area code)*
City	State / Province	ZIP Code / Country
Contact Name	Contact Title	Contact E-mail Address

Questions? Contact FDA/CDRH/OCE/DID at CDRH-FOISTATUS@fda.hhs.gov or 301-796-8118

Records processed under FOIA Request #2014-8015; Released by CDRH on 12-8-2015

SECTION I UTILIZATION OF STANDARDS

Note: Complete this section if your application or submission cites standards or includes a *"Declaration of Conformity to a Recognized Standard"* statement.

	Standards No.	Standards Organization	Standards Title	Version	Date
1	D638	ASTM	Standard Test Method For Tensile Testing Of Plastics	10	01/01/2010
2	D695	ASTM	Standard Test Method For Compressive Properties Of Rigid Plastics	10	01/01/2010
3	D1505	ASTM	Standard Test method for Density of Plastics by the Density-Gradient Technique	10	01/01/2010
4	D4169	ASTM	Standard Practice for Performance Testing of Shipping Containers and Systems	09	01/01/2009
5	D6068	ASTM	Standard Test Method For Determining J-R Curves Of Plastic Materials	96	01/01/1996
6	E647	ASTM	Standard Test Method For Measurement Of Fatigue Crack Growth Rates	08e1	01/01/2008
7	F648	ASTM	Standard Specification for Ultra-High-Molecular-Weight Polyethylene Powder and Fabricated Form for Surgical Implants	10a	01/01/2010

Please include any additional standards to be cited on a separate page.

Public reporting burden for this collection of information is estimated to average 0.5 hour per response, including the time for reviewing instructions, searching existing data sources, gathering and maintaining the data needed, and completing reviewing the collection of information. Send comments regarding this burden estimate or any other aspect of this collection of information, including suggestions for reducing this burden to:

Department of Health and Human Services
Food and Drug Administration
Office of Chief Information Officer
1350 Piccard Drive, Room 400
Rockville, MD 20850

An agency may not conduct or sponsor, and a person is not required to respond to, a collection of information unless it displays a currently valid OMB control number.

Questions? Contact FDA/CDRH/OCE/DID at CDRH-FOISTATUS@fda.hhs.gov or 301-796-8118

Standards for which Declarations of Conformity are provided

(Continued from CDRH Premarket Review Submission Cover Sheet)

Standard Number	Standard Organization	Standard Title	Version	Date
F1223	ASTM	Standard Test Method for Determination of Total Knee Replacement Constraint	08	2008
F1672	ASTM	Standard Specification for Resurfacing Patellar Prosthesis	95	2011
F1886	ASTM	Standard Test Method for Determining Integrity of Seals for Flexible Packaging by Visual Inspection	09	2009
F1980	ASTM	Standard Guide for Accelerated Aging of Sterile Barrier Systems for Medical Devices	07	2011
F2003	ASTM	Standard Practice for Accelerated Aging of Ultra-High Molecular Weight Polyethylene after Gamma Irradiation in Air	02	2008
F2083	ASTM	Standard Specification for Total Knee Prosthesis	11	2011
F2096	ASTM	Standard Test Method for Detecting Gross Leaks in Medical Packaging by Internal Pressurization (Bubble Test)	11	2011
F2102	ASTM	Standard Guide for Evaluating the Extent of Oxidation In Ultra-High-Molecular-Weight Polyethylene Fabricated Forms for Surgical Implants	06e1	2006
F2183	ASTM	Standard Test Method for Small Punch Testing of Ultra-High Molecular Weight Polyethylene	02	2008
F2214	ASTM	Standard Test Method for In Situ Determination of Network Parameters of Crosslinked Ultra High Molecular Weight Polyethylene	02	2008
F2381	ASTM	Standard Test Method for Evaluating Trans-Vinylene Yield in Irradiated Ultra-High-Molecular-Weight Polyethylene	10	2010
F2565	ASTM	Standard Guide for Extensively Irradiation-Crosslinked Ultra-High Molecular Weight Polyethylene Fabricated Forms for Surgical Implant Applications	06	2006
F2625	ASTM	Standard Test Method for Measurement of Enthalpy of Fusion, Percent Crystallinity, and Melting Point of Ultra-High-Molecular-Weight Polyethylene by Means of Differential Scanning Calorimetry	10	2010
TIR30	AAMI	A compendium of processes, materials, test methods and acceptance criteria for cleaning reusable medical devices		2011
ST79	ANSI/AAMI	Comprehensive guide to steam sterilization and sterility assurance in health care facilities		2006
10993-5	ISO	Biological evaluation of medical devices - Part 5: Tests for in vitro cytotoxicity		2009
10993-6	ISO	Biological Evaluation of medical devices - Part 6: Tests for local effects after implantation		2007
10993-7	ISO	Biological evaluation of medical devices - Part 7: Ethylene oxide sterilization residuals		2008
10993-10	ISO	Biological evaluation of medical devices - Part 10: Tests for irritation and skin sensitization		2010
11135-1	ISO	Sterilization of health care products - Ethylene oxide - Part 1: Requirements for development, validation and routine control of a sterilization process for medical devices		2007
11607-1	ISO	Packaging for Terminally Sterilized Medical Devices - Part 1: Requirements for materials, sterile barrier systems and packaging systems		2006
14243-1	ISO	Implants for surgery - Wear of total knee-joint prostheses - Part 1: Loading and displacement parameters for wear-testing machines with load control and corresponding environmental conditions for test		2009
14243-2	ISO	Implants for surgery - Wear of total knee-joint prostheses - Part 2: Methods of measurement		2009
17664	ISO	Sterilization of Medical Devices- Information to be provided by the manufacturer for the processing of resterilizable medical devices		2004
17665	ISO	Sterilization of health care products - Moist heat - Part 1: Requirements for the development, validation, and routine control of a sterilization process for medical devices		2006

Records processed under FOIA Request #2014-8015; Released by CDRH on 12-8-2015

Section 3
510(k) Cover Letter

Questions? Contact FDA/CDRH/OCE/DID at CDRH-FOISTATUS@fda.hhs.gov or 301-796-8118

Records processed under FOIA Request #2014-8015; Released by CDRH on 12-8-2015

ORTHO DEVELOPMENT®

April 26, 2013

Food and Drug Administration
Center for Device and Radiological Health
Document Mail Center – WO66-G609
10903 New Hampshire Avenue
Silver Spring, Maryland 20993-0002

Re: 510(k) Submission
Balanced Knee® System High Flex Vitamin E PS Tibial Insert and Patella

To whom it may concern,

Please find attached the **traditional 510(k)** submitted by Ortho Development Corporation for the following total knee replacement prosthesis, which is a **new device**. There are no prior submissions for this device.

Name of Sponsor: Ortho Development Corporation
12187 South Business Park Drive
Draper, Utah 84020

Proprietary Name: Balanced Knee® System High Flex Vitamin E PS Tibial Insert and Patella

Common Name: Total Knee Replacement Prosthesis

Classification: 21 CFR 888.3560, Knee joint, patellofemorotibial, polymer/metal/polymer semi-constrained cemented prosthesis, Class II device

Device Product Code: JWH

The primary use of the device is summarized in the table below:

Question	Yes	No
Is the device intended for prescription use (21 CFR 801 Subpart D)?	X	
Is the device intended for over-the-counter use (21 CFR 807 Subpart C)?		X
Does the device contain components derived from a tissue or other biologic source?		X
Is the device provided sterile?	X	
Is the device intended for single use?	X	
Is the device a reprocessed single use device?		X
Does the device contain a drug?		X
Does the device contain a biologic?		X
Does the device use software?		X
Does the submission include clinical information?		X
Is the device implanted?	X	

Questions? Contact FDA/CDRH/OCE/DID at CDRH-FOISTATUS@fda.hhs.gov or 301-796-8118

Records processed under FOIA Request #2014-8015; Released by CDRH on 12-8-2015

Ortho Development Corporation considers its intent to market this device to be company confidential information per 21 CFR 807.95. Knowledge of this project and product line has been restricted to Ortho Development's employees, suppliers, and agents only.

Please find included one paper copy of the submission and one disc containing an electronic copy per instructions provided on the FDA website.

The Regulatory Affairs Manager of Ortho Development is the official contact and correspondent for this submission. Please direct any correspondence to my attention at:

Tom Haueter
Regulatory Affairs Manager
Telephone: (801) 553-9991
Facsimile: (801) 553-9993
Email: thaueter@orthodevelopment.com

Should you have any immediate questions regarding this submission, please feel free to contact me at your convenience.

Sincerely,

Tom Haueter
Regulatory Affairs Manager
Ortho Development

Questions? Contact FDA/CDRH/OCE/DID at CDRH-FOISTATUS@fda.hhs.gov or 301-796-8118

Records processed under FOIA Request #2014-8015; Released by CDRH on 12-8-2015

Section 4
Indications for Use Statement

Questions? Contact FDA/CDRH/OCE/DID at CDRH-FOISTATUS@fda.hhs.gov or 301-796-8118

Records processed under FOIA Request #2014-8015; Released by CDRH on 12-8-2015

Indication for Use Form
Ortho Development
Balanced Knee® System High Flex Vitamin E PS Tibial Insert and Patella 510(k)

510(k) Number (if known): _____

Device Name: Balanced Knee® System High Flex Vitamin E PS Tibial Insert and Patella

Indications for Use:

The Balanced Knee® System High Flex Vitamin E PS tibial insert and patella is intended for use in cemented total knee arthroplasty procedures.

Total knee arthroplasty is indicated for the following conditions:

1. Loss of knee joint configuration and joint function.
2. Osteoarthritis of the knee joint.
3. Rheumatoid arthritis of the knee joint.
4. Post-traumatic arthritis of the knee joint.
5. Valgus, varus, or flexion deformities of the knee joint.
6. Revision procedures where other treatments or devices have failed.

Prescription Use ____X___ (Part 21 CFR 801 Subpart D) AND/OR Over-The-Counter Use _____ (21 CFR 801 Subpart C)

(PLEASE DO NOT WRITE BELOW THIS LINE-CONTINUE ON ANOTHER PAGE IF NEEDED)

Concurrence of CDRH, Office of Device Evaluation (ODE)

Questions? Contact FDA/CDRH/OCE/DID at CDRH-FOISTATUS@fda.hhs.gov or 301-796-8118

Records processed under FOIA Request #2014-8015; Released by CDRH on 12-8-2015

Section 5
510(k) Summary

Questions? Contact FDA/CDRH/OCE/DID at CDRH-FOISTATUS@fda.hhs.gov or 301-796-8118

Records processed under FOIA Request #2014-8015; Released by CDRH on 12-8-2015

510(k) Summary

NAME OF SPONSOR:	Ortho Development Corporation 12187 South Business Park Drive Draper, Utah 84020
510(k) CONTACT:	Tom Haueter Regulatory Affairs Manager Telephone: (801) 553-9991 Facsimile: (801) 553-9993 Email: thaueter@orthodevelopment.com
DATE PREPARED:	April 24, 2013
PROPRIETARY NAME:	Balanced Knee® System High Flex Vitamin E PS Tibial Insert and Patella
COMMON NAME:	Total Knee Replacement Prosthesis
CLASSIFICATION:	21 CFR 888.3560, Knee joint, patellofemorotibial, polymer/metal/polymer semi-constrained cemented prosthesis, Class II device
DEVICE PRODUCT CODE:	JWH
PREDICATE DEVICES:	Balanced Knee® System (K994370), *Ortho Development Corp.* Balanced Knee® System High Flex PS (K123457), *Ortho Development Corp.* Highly Cross-Linked Vitamin E UHMWPE Tibial Insert (K091956), *DJO Surgical/Encore Medical*

Questions? Contact FDA/CDRH/OCE/DID at CDRH-FOISTATUS@fda.hhs.gov or 301-796-8118

Records processed under FOIA Request #2014-8015; Released by CDRH on 12-8-2015

Device Description

The Balanced Knee® System High Flex Vitamin E (High Flex Vit E) PS tibial insert and patella are machined from extensively crosslinked, compression molded, Vitamin E UHMWPE. Both components are single use only. The High Flex Vit E PS tibial insert must be used in conjunction with the High Flex PS femoral component (K123457). Used together, these components are designed to accommodate increased range of motion up to 150° of flexion. The High Flex Vit E patella may be used in conjunction with the Balanced Knee® System (BKS) femoral components (K994370), the BKS modular femoral components (K060569), or the High Flex PS femoral components (K123457). Both the High Flex Vit E PS tibial insert and patella may be used in conjunction with the BKS standard and modular tibial trays, tibial augments, and stems to complete the semi-constrained modular knee prosthesis. The tibial trays, tibial augments, and stems were approved under K994370 and K031201.

Intended Use

The Balanced Knee® System High Flex Vitamin E PS tibial insert and patella are intended for use in cemented total knee arthroplasty procedures with the following indications:

1. Loss of knee joint configuration and joint function.
2. Osteoarthritis of the knee joint.
3. Rheumatoid arthritis of the knee joint.
4. Post-traumatic arthritis of the knee joint.
5. Valgus, varus, or flexion deformities of the knee joint.
6. Revision procedures where other treatments or devices have failed.

Technological Characteristics

Feature	Equivalent Device
Indications for Use and Design	Ortho Development: Balanced Knee® System (K994370) Ortho Development: Balanced Knee® System High Flex PS (K123457)
Material: Extensively Crosslinked Vitamin E Polyethylene UHMWPE (α-tocopherol)	DJO Surgical/Encore Medical: Vit E UHMWPE Tibial Insert (K091956)

There is only one difference between the High Flex Vit E PS insert when compared to the BKS High Flex PS insert: the implementation of a different material, crosslinked Vitamin E UHMWPE. Likewise, the High Flex Vit E patella is identical to the BKS patella except for the crosslinked Vitamin E UHMWPE material. The indications for use for the High Flex Vit E PS tibial insert and patella are identical to the indications for use for the BKS High Flex. The crosslinked Vitamin E UHMWPE for the High Flex Vit E PS insert and patella undergoes substantially equivalent fabrication and final processing as its predicate, DJO/Encore's Vitamin E UHMWPE tibial insert.

Questions? Contact FDA/CDRH/OCE/DID at CDRH-FOISTATUS@fda.hhs.gov or 301-796-8118

Records processed under FOIA Request #2014-8015; Released by CDRH on 12-8-2015

Performance Data

The following non-clinical testing was performed to determined substantial equivalence to the predicate devices:

Property	Result
Range of Motion	Up to 150° flexion; Identical to predicate device, BKS High Flex
Femorotibial Constraint	Identical to predicate device, BKS High Flex
Femorotibial Contact Area	Identical to predicate device, BKS High Flex
Patellofemoral Constraint	Identical to predicate device, BKS High Flex
Patellofemoral Contact Area	Identical to predicate device, BKS High Flex
PS Spine Fatigue	Sufficient strength to survive in-vivo loading
Insert Assembly/ Disassembly	Sufficient strength to survive in-vivo loading
Crosslinking Characterization of High Flex Vit E	Substantially equivalent or better than BKS
Vitamin E Characterization of High Flex Vit E	Substantially equivalent or better than BKS
High Flex Knee Wear	56% decrease in wear over BKS

Basis for Substantial Equivalence

Ortho Development believes that the High Flex Vit E PS tibial insert and patella are substantially equivalent to the previously cleared predicate devices based on similarities in intended use, design, materials, manufacturing methods, packaging, and mechanical performance.

Questions? Contact FDA/CDRH/OCE/DID at CDRH-FOISTATUS@fda.hhs.gov or 301-796-8118

Records processed under FOIA Request #2014-8015; Released by CDRH on 12-8-2015

Section 6
Truthful and Accurate Statement

Questions? Contact FDA/CDRH/OCE/DID at CDRH-FOISTATUS@fda.hhs.gov or 301-796-8118

Records processed under FOIA Request #2014-8015; Released by CDRH on 12-8-2015

Truthful and Accurate Statement

I certify that, in my capacity as Director of Regulatory Affairs/Quality Assurance of Ortho Development, I believe to the best of my knowledge that all data and information submitted in the premarket notification are truthful and accurate and that no material fact has been omitted.

Edwin O. Goodman

(Signature)

Edwin O. Goodman

(Typed Name)

April 25, 2013

(Date)

(Premarket Notification [510(k)] Number)

Questions? Contact FDA/CDRH/OCE/DID at CDRH-FOISTATUS@fda.hhs.gov or 301-796-8118

Records processed under FOIA Request #2014-8015; Released by CDRH on 12-8-2015

Section 7
Class III Summary and Certification

This section does not apply to the current submission.

Questions? Contact FDA/CDRH/OCE/DID at CDRH-FOISTATUS@fda.hhs.gov or 301-796-8118

Records processed under FOIA Request #2014-8015; Released by CDRH on 12-8-2015

Section 8
Financial Certification or Disclosure Statement

This section does not apply to the current submission.

Questions? Contact FDA/CDRH/OCE/DID at CDRH-FOISTATUS@fda.hhs.gov or 301-796-8118

Records processed under FOIA Request #2014-8015; Released by CDRH on 12-8-2015

Section 9
Declarations of Conformity and Summary Reports

Questions? Contact FDA/CDRH/OCE/DID at CDRH-FOISTATUS@fda.hhs.gov or 301-796-8118

Records processed under FOIA Request #2014-8015; Released by CDRH on 12-8-2015

Form Approved: OMB No. 0910-0120; Expiration Date: 12/31/13

Department of Health and Human Services
Food and Drug Administration

STANDARDS DATA REPORT FOR 510(k)s

(To be filled in by applicant)

This report and the Summary Report Table are to be completed by the applicant when submitting a 510(k) that references a national or international standard. A separate report is required for each standard referenced in the 510(k).

TYPE OF 510(K) SUBMISSION

☒ Traditional ☐ Special ☐ Abbreviated

STANDARD TITLE [1]

AAMI TIR30(2011) A compendium of processes, materials, test methods, and acceptance criteria for cleaning reusable medical ...

Please answer the following questions	Yes	No
Is this standard recognized by FDA [2]?	☐	☒
FDA Recognition number [3] # _____		
Was a third party laboratory responsible for testing conformity of the device to this standard identified in the 510(k)?	☒	☐
Is a summary report [4] describing the extent of conformance of the standard used included in the 510(k)? If no, complete a summary report table.	☐	☒
Does the test data for this device demonstrate conformity to the requirements of this standard as it pertains to this device?	☒	☐
Does this standard include acceptance criteria? If no, include the results of testing in the 510(k).	☒	☐
Does this standard include more than one option or selection of tests? If yes, report options selected in the summary report table.	☒	☐
Were there any deviations or adaptations made in the use of the standard?	☐	☒
If yes, were deviations in accordance with the FDA supplemental information sheet (SIS) [5]?	☐	☐
Were deviations or adaptations made beyond what is specified in the FDA SIS? If yes, report these deviations or adaptations in the summary report table.	☐	☒
Were there any exclusions from the standard? If yes, report these exclusions in the summary report table.	☐	☒
Is there an FDA guidance [6] that is associated with this standard?	☐	☒
If yes, was the guidance document followed in preparation of this 510k?	☐	☐

Title of guidance: _____

[1] The formatting convention for the title is: [SDO] [numeric identifier] [title of standard] [date of publication]

[2] Authority [21 U.S.C. 360d], www.fda.gov/cdrh/stdsprog.html

[3] http://www.accessdata.fda.gov/scripts/cdrh/cfdocs/cfStandards/search.cfm

[4] The summary report should include: any adaptations used to adapt to the device under review (for example, alternative test methods); choices made when options or a selection of methods are described; deviations from the standard; requirements not applicable to the device; and the name and address of the test laboratory or certification body involved in conformance assessment to this standard. The summary report includes information on all standards utilized during the development of the device.

[5] The supplemental information sheet (SIS) is additional information which is necessary before FDA recognizes the standard. Found at http://www.accessdata.fda.gov/scripts/cdrh/cfdocs/cfStandards/search.cfm

[6] The online search for CDRH Guidance Documents can be found at www.fda.gov/cdrh/guidance.html

Questions? Contact FDA/CDRH/OCE/DID at CDRH-FOISTATUS@fda.hhs.gov or 301-796-8118

Records processed under FOIA Request #2014-8015; Released by CDRH on 12-8-2015

EXTENT OF STANDARD CONFORMANCE
SUMMARY REPORT TABLE

STANDARD TITLE
AAMI TIR30(2011) A compendium of processes, materials, test methods, and acceptance criteria for cleaning reusable medical ...

CONFORMANCE WITH STANDARD SECTIONS*

SECTION NUMBER	SECTION TITLE	CONFORMANCE?
5.4.2	Markers	☒ Yes ☐ No ☐ N/A

TYPE OF DEVIATION OR OPTION SELECTED ❖
Protein and Endotoxin

DESCRIPTION
n/a

(b)(4) [redacted]

SECTION NUMBER	SECTION TITLE	CONFORMANCE?
		☐ Yes ☐ No ☐ N/A

TYPE OF DEVIATION OR OPTION SELECTED ❖

DESCRIPTION

JUSTIFICATION

SECTION NUMBER	SECTION TITLE	CONFORMANCE?
		☐ Yes ☐ No ☐ N/A

TYPE OF DEVIATION OR OPTION SELECTED ❖

DESCRIPTION

JUSTIFICATION

* For completeness list all sections of the standard and indicate whether conformance is met. If a section is not applicable (N/A) an explanation is needed under "justification." Some standards include options, so similar to deviations, the option chosen needs to be described and adequately justified as appropriate for the subject device. Explanation of all deviations or description of options selected when following a standard is required under "type of deviation or option selected," "description" and "justification" on the report. More than one page may be necessary.

❖ Types of deviations can include an exclusion of a section in the standard, a deviation brought out by the FDA supplemental information sheet (SIS), a deviation to adapt the standard to the device, or any adaptation of a section.

Paperwork Reduction Act Statement

Public reporting burden for this collection of information is estimated to average 1 hour per response, including the time for reviewing instructions, searching existing data sources, gathering and maintaining the data needed, and completing and reviewing the collection of information. Send comments regarding this burden estimate or any other aspect of this collection of information, including suggestions for reducing this burden to:

Department of Health and Human Services
Food and Drug Administration
Office of Chief Information Officer
1350 Piccard Drive, Room 400
Rockville, MD 20850

An agency may not conduct or sponsor, and a person is not required to respond to, a collection of information unless it displays a currently valid OMB control number.

Questions? Contact FDA/CDRH/OCE/DID at CDRH-FOISTATUS@fda.hhs.gov or 301-796-8118

Records processed under FOIA Request #2014-8015; Released by CDRH on 12-8-2015

Form Approved: OMB No. 0910-0120; Expiration Date: 12/31/13

Department of Health and Human Services
Food and Drug Administration

STANDARDS DATA REPORT FOR 510(k)s

(To be filled in by applicant)

This report and the Summary Report Table are to be completed by the applicant when submitting a 510(k) that references a national or international standard. A separate report is required for each standard referenced in the 510(k).

TYPE OF 510(K) SUBMISSION

☒ Traditional ☐ Special ☐ Abbreviated

STANDARD TITLE [1]

ANSI/AAMI ST79(2006) Comprehensive guide to steam sterilization and sterility assurance in health care facilities

Please answer the following questions	Yes	No
Is this standard recognized by FDA [2]?	☒	☐
FDA Recognition number [3]	#14-312	
Was a third party laboratory responsible for testing conformity of the device to this standard identified in the 510(k)?	☒	☐
Is a summary report [4] describing the extent of conformance of the standard used included in the 510(k)? If no, complete a summary report table.	☐	☒
Does the test data for this device demonstrate conformity to the requirements of this standard as it pertains to this device?	☒	☐
Does this standard include acceptance criteria? If no, include the results of testing in the 510(k).	☒	☐
Does this standard include more than one option or selection of tests? If yes, report options selected in the summary report table.	☒	☐
Were there any deviations or adaptations made in the use of the standard?	☐	☒
If yes, were deviations in accordance with the FDA supplemental information sheet (SIS) [5]?	☐	☐
Were deviations or adaptations made beyond what is specified in the FDA SIS? If yes, report these deviations or adaptations in the summary report table.	☐	☒
Were there any exclusions from the standard? If yes, report these exclusions in the summary report table.	☒	☐
Is there an FDA guidance [6] that is associated with this standard?	☐	☒
If yes, was the guidance document followed in preparation of this 510k?	☐	☐

Title of guidance: _____

[1] The formatting convention for the title is: [SDO] [numeric identifier] [title of standard] [date of publication]

[2] Authority [21 U.S.C. 360d], www.fda.gov/cdrh/stdsprog.html

[3] http://www.accessdata.fda.gov/scripts/cdrh/cfdocs/cfStandards/search.cfm

[4] The summary report should include: any adaptations used to adapt to the device under review (for example, alternative test methods); choices made when options or a selection of methods are described; deviations from the standard; requirements not applicable to the device; and the name and address of the test laboratory or certification body involved in conformance assessment to this standard. The summary report includes information on all standards utilized during the development of the device.

[5] The supplemental information sheet (SIS) is additional information which is necessary before FDA recognizes the standard. Found at http://www.accessdata.fda.gov/scripts/cdrh/cfdocs/cfStandards/search.cfm

[6] The online search for CDRH Guidance Documents can be found at www.fda.gov/cdrh/guidance.html

Questions? Contact FDA/CDRH/OCE/DID at CDRH-FOISTATUS@fda.hhs.gov or 301-796-8118

Records processed under FOIA Request #2014-8015; Released by CDRH on 12-8-2015

EXTENT OF STANDARD CONFORMANCE
SUMMARY REPORT TABLE

STANDARD TITLE
ANSI/AAMI ST79(2006) Comprehensive guide to steam sterilization and sterility assurance in health care facilities

CONFORMANCE WITH STANDARD SECTIONS*

SECTION NUMBER	SECTION TITLE	CONFORMANCE?
7	Cleaning and other decontamination processes	☐ Yes ☐ No ☒ N/A

TYPE OF DEVIATION OR OPTION SELECTED ❖
none

DESCRIPTION
n/a

JUSTIFICATION
Cleaning and decontamination is not performed by the contract lab as part of this validation.

(b)(4)
[redacted]

DESCRIPTION
n/a

JUSTIFICATION
n/a

SECTION NUMBER	SECTION TITLE	CONFORMANCE?
		☐ Yes ☐ No ☐ N/A

TYPE OF DEVIATION OR OPTION SELECTED ❖

DESCRIPTION

JUSTIFICATION

* For completeness list all sections of the standard and indicate whether conformance is met. If a section is not applicable (N/A) an explanation is needed under "justification." Some standards include options, so similar to deviations, the option chosen needs to be described and adequately justified as appropriate for the subject device. Explanation of all deviations or description of options selected when following a standard is required under "type of deviation or option selected," "description" and "justification" on the report. More than one page may be necessary.

❖ Types of deviations can include an exclusion of a section in the standard, a deviation brought out by the FDA supplemental information sheet (SIS), a deviation to adapt the standard to the device, or any adaptation of a section.

Paperwork Reduction Act Statement

Public reporting burden for this collection of information is estimated to average 1 hour per response, including the time for reviewing instructions, searching existing data sources, gathering and maintaining the data needed, and completing and reviewing the collection of information. Send comments regarding this burden estimate or any other aspect of this collection of information, including suggestions for reducing this burden to:

Department of Health and Human Services
Food and Drug Administration
Office of Chief Information Officer
1350 Piccard Drive, Room 400
Rockville, MD 20850

An agency may not conduct or sponsor, and a person is not required to respond to, a collection of information unless it displays a currently valid OMB control number.

Questions? Contact FDA/CDRH/OCE/DID at CDRH-FOISTATUS@fda.hhs.gov or 301-796-8118

Records processed under FOIA Request #2014-8015; Released by CDRH on 12-8-2015

Form Approved: OMB No. 0910-0120; Expiration Date: 12/31/13

Department of Health and Human Services
Food and Drug Administration

STANDARDS DATA REPORT FOR 510(k)s

(To be filled in by applicant)

This report and the Summary Report Table are to be completed by the applicant when submitting a 510(k) that references a national or international standard. A separate report is required for each standard referenced in the 510(k).

TYPE OF 510(K) SUBMISSION

☒ Traditional ☐ Special ☐ Abbreviated

STANDARD TITLE [1]

ASTM D638-10(2010) Standard Test Method for Tensile Properties of Plastics

Please answer the following questions	Yes	No
Is this standard recognized by FDA [2]?	☐	☒
FDA Recognition number [3]	#N/A	
Was a third party laboratory responsible for testing conformity of the device to this standard identified in the 510(k)?	☒	☐
Is a summary report [4] describing the extent of conformance of the standard used included in the 510(k)? If no, complete a summary report table.	☐	☒
Does the test data for this device demonstrate conformity to the requirements of this standard as it pertains to this device?	☒	☐
Does this standard include acceptance criteria? If no, include the results of testing in the 510(k).	☐	☒
Does this standard include more than one option or selection of tests? If yes, report options selected in the summary report table.	☒	☐
Were there any deviations or adaptations made in the use of the standard?	☒	☐
If yes, were deviations in accordance with the FDA supplemental information sheet (SIS) [5]?	☐	☒
Were deviations or adaptations made beyond what is specified in the FDA SIS? If yes, report these deviations or adaptations in the summary report table.	☐	☒
Were there any exclusions from the standard? If yes, report these exclusions in the summary report table.	☐	☒
Is there an FDA guidance [6] that is associated with this standard?	☐	☒
If yes, was the guidance document followed in preparation of this 510k?	☐	☐

Title of guidance: _____

[1] The formatting convention for the title is: [SDO] [numeric identifier] [title of standard] [date of publication]

[2] Authority [21 U.S.C. 360d], www.fda.gov/cdrh/stdsprog.html

[3] http://www.accessdata.fda.gov/scripts/cdrh/cfdocs/cfStandards/search.cfm

[4] The summary report should include: any adaptations used to adapt to the device under review (for example, alternative test methods); choices made when options or a selection of methods are described; deviations from the standard; requirements not applicable to the device; and the name and address of the test laboratory or certification body involved in conformance assessment to this standard. The summary report includes information on all standards utilized during the development of the device.

[5] The supplemental information sheet (SIS) is additional information which is necessary before FDA recognizes the standard. Found at http://www.accessdata.fda.gov/scripts/cdrh/cfdocs/cfStandards/search.cfm

[6] The online search for CDRH Guidance Documents can be found at www.fda.gov/cdrh/guidance.html

Questions? Contact FDA/CDRH/OCE/DID at CDRH-FOISTATUS@fda.hhs.gov or 301-796-8118

Records processed under FOIA Request #2014-8015; Released by CDRH on 12-8-2015

EXTENT OF STANDARD CONFORMANCE SUMMARY REPORT TABLE

STANDARD TITLE
ASTM D638-10(2010) Standard Test Method for Tensile Properties of Plastics

CONFORMANCE WITH STANDARD SECTIONS*

SECTION NUMBER	SECTION TITLE	CONFORMANCE?
See extra pages		☐ Yes ☐ No ☒ N/A

TYPE OF DEVIATION OR OPTION SELECTED ❖

DESCRIPTION

JUSTIFICATION

SECTION NUMBER	SECTION TITLE	CONFORMANCE?
		☐ Yes ☐ No ☐ N/A

TYPE OF DEVIATION OR OPTION SELECTED ❖

DESCRIPTION

JUSTIFICATION

SECTION NUMBER	SECTION TITLE	CONFORMANCE?
		☐ Yes ☐ No ☐ N/A

TYPE OF DEVIATION OR OPTION SELECTED ❖

DESCRIPTION

JUSTIFICATION

* For completeness list all sections of the standard and indicate whether conformance is met. If a section is not applicable (N/A) an explanation is needed under "justification." Some standards include options, so similar to deviations, the option chosen needs to be described and adequately justified as appropriate for the subject device. Explanation of all deviations or description of options selected when following a standard is required under "type of deviation or option selected," "description" and "justification" on the report. More than one page may be necessary.

❖ Types of deviations can include an exclusion of a section in the standard, a deviation brought out by the FDA supplemental information sheet (SIS), a deviation to adapt the standard to the device, or any adaptation of a section.

Paperwork Reduction Act Statement

Public reporting burden for this collection of information is estimated to average 1 hour per response, including the time for reviewing instructions, searching existing data sources, gathering and maintaining the data needed, and completing and reviewing the collection of information. Send comments regarding this burden estimate or any other aspect of this collection of information, including suggestions for reducing this burden to:

Department of Health and Human Services
Food and Drug Administration
Office of Chief Information Officer
1350 Piccard Drive, Room 400
Rockville, MD 20850

An agency may not conduct or sponsor, and a person is not required to respond to, a collection of information unless it displays a currently valid OMB control number.

Questions? Contact FDA/CDRH/OCE/DID at CDRH-FOISTATUS@fda.hhs.gov or 301-796-8118

Records processed under FOIA Request #2014-8015; Released by CDRH on 12-8-2015

(b)(4)

[redacted]

Questions? Contact FDA/CDRH/OCE/DID at CDRH-FOISTATUS@fda.hhs.gov or 301-796-8118

Records processed under FOIA Request #2014-8015; Released by CDRH on 12-8-2015

(b)(4)

[redacted]

TEST LABORATORIES INVOLVED WITH CONFORMANCE

(b)(4)

[redacted]

Questions? Contact FDA/CDRH/OCE/DID at CDRH-FOISTATUS@fda.hhs.gov or 301-796-8118

Records processed under FOIA Request #2014-8015; Released by CDRH on 12-8-2015

Form Approved: OMB No. 0910-0120; Expiration Date: 12/31/13

Department of Health and Human Services
Food and Drug Administration

STANDARDS DATA REPORT FOR 510(k)s

(To be filled in by applicant)

This report and the Summary Report Table are to be completed by the applicant when submitting a 510(k) that references a national or international standard. A separate report is required for each standard referenced in the 510(k).

TYPE OF 510(K) SUBMISSION

☒ Traditional ☐ Special ☐ Abbreviated

STANDARD TITLE [1]

ASTM D695-10(2010) Standard Test Method for Compressive Properties of Rigid Plastics

Please answer the following questions	Yes	No
Is this standard recognized by FDA [2]?	☐	☒
FDA Recognition number [3]	#N/A	
Was a third party laboratory responsible for testing conformity of the device to this standard identified in the 510(k)?	☒	☐
Is a summary report [4] describing the extent of conformance of the standard used included in the 510(k)? If no, complete a summary report table.	☐	☒
Does the test data for this device demonstrate conformity to the requirements of this standard as it pertains to this device?	☒	☐
Does this standard include acceptance criteria? If no, include the results of testing in the 510(k).	☐	☒
Does this standard include more than one option or selection of tests? If yes, report options selected in the summary report table.	☒	☐
Were there any deviations or adaptations made in the use of the standard?	☒	☐
If yes, were deviations in accordance with the FDA supplemental information sheet (SIS) [5]?	☐	☒
Were deviations or adaptations made beyond what is specified in the FDA SIS? If yes, report these deviations or adaptations in the summary report table.	☐	☒
Were there any exclusions from the standard? If yes, report these exclusions in the summary report table.	☐	☒
Is there an FDA guidance [6] that is associated with this standard?	☐	☒
If yes, was the guidance document followed in preparation of this 510k?	☐	☐

Title of guidance: _____

[1] The formatting convention for the title is: [SDO] [numeric identifier] [title of standard] [date of publication]

[2] Authority [21 U.S.C. 360d], www.fda.gov/cdrh/stdsprog.html

[3] http://www.accessdata.fda.gov/scripts/cdrh/cfdocs/cfStandards/search.cfm

[4] The summary report should include: any adaptations used to adapt to the device under review (for example, alternative test methods); choices made when options or a selection of methods are described; deviations from the standard; requirements not applicable to the device; and the name and address of the test laboratory or certification body involved in conformance assessment to this standard. The summary report includes information on all standards utilized during the development of the device.

[5] The supplemental information sheet (SIS) is additional information which is necessary before FDA recognizes the standard. Found at http://www.accessdata.fda.gov/scripts/cdrh/cfdocs/cfStandards/search.cfm

[6] The online search for CDRH Guidance Documents can be found at www.fda.gov/cdrh/guidance.html

Questions? Contact FDA/CDRH/OCE/DID at CDRH-FOISTATUS@fda.hhs.gov or 301-796-8118

Records processed under FOIA Request #2014-8015; Released by CDRH on 12-8-2015

EXTENT OF STANDARD CONFORMANCE SUMMARY REPORT TABLE

STANDARD TITLE
ASTM D695-10(2010) Standard Test Method for Compressive Properties of Rigid Plastics

CONFORMANCE WITH STANDARD SECTIONS*

SECTION NUMBER	SECTION TITLE	CONFORMANCE?
See extra pages		☐ Yes ☐ No ☒ N/A

TYPE OF DEVIATION OR OPTION SELECTED ❖

DESCRIPTION

JUSTIFICATION

SECTION NUMBER	SECTION TITLE	CONFORMANCE?
		☐ Yes ☐ No ☐ N/A

TYPE OF DEVIATION OR OPTION SELECTED ❖

DESCRIPTION

JUSTIFICATION

SECTION NUMBER	SECTION TITLE	CONFORMANCE?
		☐ Yes ☐ No ☐ N/A

TYPE OF DEVIATION OR OPTION SELECTED ❖

DESCRIPTION

JUSTIFICATION

* For completeness list all sections of the standard and indicate whether conformance is met. If a section is not applicable (N/A) an explanation is needed under "justification." Some standards include options, so similar to deviations, the option chosen needs to be described and adequately justified as appropriate for the subject device. Explanation of all deviations or description of options selected when following a standard is required under "type of deviation or option selected," "description" and "justification" on the report. More than one page may be necessary.

❖ Types of deviations can include an exclusion of a section in the standard, a deviation brought out by the FDA supplemental information sheet (SIS), a deviation to adapt the standard to the device, or any adaptation of a section.

Paperwork Reduction Act Statement

Public reporting burden for this collection of information is estimated to average 1 hour per response, including the time for reviewing instructions, searching existing data sources, gathering and maintaining the data needed, and completing and reviewing the collection of information. Send comments regarding this burden estimate or any other aspect of this collection of information, including suggestions for reducing this burden to:

Department of Health and Human Services
Food and Drug Administration
Office of Chief Information Officer
1350 Piccard Drive, Room 400
Rockville, MD 20850

An agency may not conduct or sponsor, and a person is not required to respond to, a collection of information unless it displays a currently valid OMB control number.

Questions? Contact FDA/CDRH/OCE/DID at CDRH-FOISTATUS@fda.hhs.gov or 301-796-8118

Records processed under FOIA Request #2014-8015; Released by CDRH on 12-8-2015

(b)(4)

[redacted]

Questions? Contact FDA/CDRH/OCE/DID at CDRH-FOISTATUS@fda.hhs.gov or 301-796-8118

Records processed under FOIA Request #2014-8015; Released by CDRH on 12-8-2015

(b)(4)

[redacted]

TEST LABORATORIES INVOLVED WITH CONFORMANCE

(b)(4)

[redacted]

Questions? Contact FDA/CDRH/OCE/DID at CDRH-FOISTATUS@fda.hhs.gov or 301-796-8118

Records processed under FOIA Request #2014-8015; Released by CDRH on 12-8-2015

Form Approved: OMB No. 0910-0120; Expiration Date: 12/31/13

Department of Health and Human Services
Food and Drug Administration

STANDARDS DATA REPORT FOR 510(k)s

(To be filled in by applicant)

This report and the Summary Report Table are to be completed by the applicant when submitting a 510(k) that references a national or international standard. A separate report is required for each standard referenced in the 510(k).

TYPE OF 510(K) SUBMISSION

☒ Traditional ☐ Special ☐ Abbreviated

STANDARD TITLE [1]

ASTM D1505-10(2010) Standard Test method for Density of Plastics by the Density-Gradient Technique

Please answer the following questions	Yes	No
Is this standard recognized by FDA [2]?	☐	☒
FDA Recognition number [3]	#N/A	
Was a third party laboratory responsible for testing conformity of the device to this standard identified in the 510(k)?	☒	☐
Is a summary report [4] describing the extent of conformance of the standard used included in the 510(k)? If no, complete a summary report table.	☐	☒
Does the test data for this device demonstrate conformity to the requirements of this standard as it pertains to this device?	☒	☐
Does this standard include acceptance criteria? If no, include the results of testing in the 510(k).	☐	☒
Does this standard include more than one option or selection of tests? If yes, report options selected in the summary report table.	☒	☐
Were there any deviations or adaptations made in the use of the standard?	☐	☒
If yes, were deviations in accordance with the FDA supplemental information sheet (SIS) [5]?	☐	☐
Were deviations or adaptations made beyond what is specified in the FDA SIS? If yes, report these deviations or adaptations in the summary report table.	☐	☒
Were there any exclusions from the standard? If yes, report these exclusions in the summary report table.	☐	☒
Is there an FDA guidance [6] that is associated with this standard?	☐	☒
If yes, was the guidance document followed in preparation of this 510k?	☐	☐

Title of guidance: _____

[1] The formatting convention for the title is: [SDO] [numeric identifier] [title of standard] [date of publication]

[2] Authority [21 U.S.C. 360d], www.fda.gov/cdrh/stdsprog.html

[3] http://www.accessdata.fda.gov/scripts/cdrh/cfdocs/cfStandards/search.cfm

[4] The summary report should include: any adaptations used to adapt to the device under review (for example, alternative test methods); choices made when options or a selection of methods are described; deviations from the standard; requirements not applicable to the device; and the name and address of the test laboratory or certification body involved in conformance assessment to this standard. The summary report includes information on all standards utilized during the development of the device.

[5] The supplemental information sheet (SIS) is additional information which is necessary before FDA recognizes the standard. Found at http://www.accessdata.fda.gov/scripts/cdrh/cfdocs/cfStandards/search.cfm

[6] The online search for CDRH Guidance Documents can be found at www.fda.gov/cdrh/guidance.html

Questions? Contact FDA/CDRH/OCE/DID at CDRH-FOISTATUS@fda.hhs.gov or 301-796-8118

EXTENT OF STANDARD CONFORMANCE SUMMARY REPORT TABLE

STANDARD TITLE
ASTM D1505-10(2010) Standard Test method for Density of Plastics by the Density-Gradient Technique

CONFORMANCE WITH STANDARD SECTIONS*

SECTION NUMBER	SECTION TITLE	CONFORMANCE?
See extra pages		☐ Yes ☐ No ☒ N/A

TYPE OF DEVIATION OR OPTION SELECTED ❖

DESCRIPTION

JUSTIFICATION

SECTION NUMBER	SECTION TITLE	CONFORMANCE?
		☐ Yes ☐ No ☐ N/A

TYPE OF DEVIATION OR OPTION SELECTED ❖

DESCRIPTION

JUSTIFICATION

SECTION NUMBER	SECTION TITLE	CONFORMANCE?
		☐ Yes ☐ No ☐ N/A

TYPE OF DEVIATION OR OPTION SELECTED ❖

DESCRIPTION

JUSTIFICATION

* For completeness list all sections of the standard and indicate whether conformance is met. If a section is not applicable (N/A) an explanation is needed under "justification." Some standards include options, so similar to deviations, the option chosen needs to be described and adequately justified as appropriate for the subject device. Explanation of all deviations or description of options selected when following a standard is required under "type of deviation or option selected," "description" and "justification" on the report. More than one page may be necessary.

❖ Types of deviations can include an exclusion of a section in the standard, a deviation brought out by the FDA supplemental information sheet (SIS), a deviation to adapt the standard to the device, or any adaptation of a section.

Paperwork Reduction Act Statement

Public reporting burden for this collection of information is estimated to average 1 hour per response, including the time for reviewing instructions, searching existing data sources, gathering and maintaining the data needed, and completing and reviewing the collection of information. Send comments regarding this burden estimate or any other aspect of this collection of information, including suggestions for reducing this burden to:

Department of Health and Human Services
Food and Drug Administration
Office of Chief Information Officer
1350 Piccard Drive, Room 400
Rockville, MD 20850

An agency may not conduct or sponsor, and a person is not required to respond to, a collection of information unless it displays a currently valid OMB control number.

Questions? Contact FDA/CDRH/OCE/DID at CDRH-FOISTATUS@fda.hhs.gov or 301-796-8118

Records processed under FOIA Request #2014-8015; Released by CDRH on 12-8-2015

(b)(4)

[redacted]

TEST LABORATORIES INVOLVED WITH CONFORMANCE

(b)(4)

[redacted]

Questions? Contact FDA/CDRH/OCE/DID at CDRH-FOISTATUS@fda.hhs.gov or 301-796-8118

Records processed under FOIA Request #2014-8015; Released by CDRH on 12-8-2015

Form Approved: OMB No. 0910-0120; Expiration Date: 12/31/13

Department of Health and Human Services
Food and Drug Administration

STANDARDS DATA REPORT FOR 510(k)s

(To be filled in by applicant)

This report and the Summary Report Table are to be completed by the applicant when submitting a 510(k) that references a national or international standard. A separate report is required for each standard referenced in the 510(k).

TYPE OF 510(K) SUBMISSION

☒ Traditional ☐ Special ☐ Abbreviated

STANDARD TITLE [1]

ASTM D4169-09(2009) Standard Practice for Performance Testing of Shipping Containers and Systems

Please answer the following questions	Yes	No
Is this standard recognized by FDA [2]?	☒	☐
FDA Recognition number [3]	#14-300	
Was a third party laboratory responsible for testing conformity of the device to this standard identified in the 510(k)?	☒	☐
Is a summary report [4] describing the extent of conformance of the standard used included in the 510(k)? If no, complete a summary report table.	☐	☒
Does the test data for this device demonstrate conformity to the requirements of this standard as it pertains to this device?	☒	☐
Does this standard include acceptance criteria? If no, include the results of testing in the 510(k).	☐	☒
Does this standard include more than one option or selection of tests? If yes, report options selected in the summary report table.	☒	☐
Were there any deviations or adaptations made in the use of the standard?	☐	☒
If yes, were deviations in accordance with the FDA supplemental information sheet (SIS) [5]?	☐	☐
Were deviations or adaptations made beyond what is specified in the FDA SIS? If yes, report these deviations or adaptations in the summary report table.	☐	☒
Were there any exclusions from the standard? If yes, report these exclusions in the summary report table.	☐	☒
Is there an FDA guidance [6] that is associated with this standard?	☐	☒
If yes, was the guidance document followed in preparation of this 510k?	☐	☐

Title of guidance: _____

[1] The formatting convention for the title is: [SDO] [numeric identifier] [title of standard] [date of publication]

[2] Authority [21 U.S.C. 360d], www.fda.gov/cdrh/stdsprog.html

[3] http://www.accessdata.fda.gov/scripts/cdrh/cfdocs/cfStandards/search.cfm

[4] The summary report should include: any adaptations used to adapt to the device under review (for example, alternative test methods); choices made when options or a selection of methods are described; deviations from the standard; requirements not applicable to the device; and the name and address of the test laboratory or certification body involved in conformance assessment to this standard. The summary report includes information on all standards utilized during the development of the device.

[5] The supplemental information sheet (SIS) is additional information which is necessary before FDA recognizes the standard. Found at http://www.accessdata.fda.gov/scripts/cdrh/cfdocs/cfStandards/search.cfm

[6] The online search for CDRH Guidance Documents can be found at www.fda.gov/cdrh/guidance.html

Questions? Contact FDA/CDRH/OCE/DID at CDRH-FOISTATUS@fda.hhs.gov or 301-796-8118

Records processed under FOIA Request #2014-8015; Released by CDRH on 12-8-2015

EXTENT OF STANDARD CONFORMANCE SUMMARY REPORT TABLE

STANDARD TITLE
ASTM D4169-09(2009) Standard Practice for Performance Testing of Shipping Containers and Systems

CONFORMANCE WITH STANDARD SECTIONS*

SECTION NUMBER	SECTION TITLE	CONFORMANCE?
All	N/A	☒ Yes ☐ No ☐ N/A

TYPE OF DEVIATION OR OPTION SELECTED ❖
No deviations. All sections of the standard were followed by the testing lab. See below for options selected.

DESCRIPTION
Describes the test method for distribution simulation testing of shipping containers.

(b)(4)

[redacted]

* For completeness list all sections of the standard and indicate whether conformance is met. If a section is not applicable (N/A) an explanation is needed under "justification." Some standards include options, so similar to deviations, the option chosen needs to be described and adequately justified as appropriate for the subject device. Explanation of all deviations or description of options selected when following a standard is required under "type of deviation or option selected," "description" and "justification" on the report. More than one page may be necessary.

❖ Types of deviations can include an exclusion of a section in the standard, a deviation brought out by the FDA supplemental information sheet (SIS), a deviation to adapt the standard to the device, or any adaptation of a section.

Paperwork Reduction Act Statement

Public reporting burden for this collection of information is estimated to average 1 hour per response, including the time for reviewing instructions, searching existing data sources, gathering and maintaining the data needed, and completing and reviewing the collection of information. Send comments regarding this burden estimate or any other aspect of this collection of information, including suggestions for reducing this burden to:

Department of Health and Human Services
Food and Drug Administration
Office of Chief Information Officer
1350 Piccard Drive, Room 400
Rockville, MD 20850

An agency may not conduct or sponsor, and a person is not required to respond to, a collection of information unless it displays a currently valid OMB control number.

Questions? Contact FDA/CDRH/OCE/DID at CDRH-FOISTATUS@fda.hhs.gov or 301-796-8118

Records processed under FOIA Request #2014-8015; Released by CDRH on 12-8-2015

Form Approved: OMB No. 0910-0120; Expiration Date: 12/31/13

Department of Health and Human Services
Food and Drug Administration

STANDARDS DATA REPORT FOR 510(k)s

(To be filled in by applicant)

This report and the Summary Report Table are to be completed by the applicant when submitting a 510(k) that references a national or international standard. A separate report is required for each standard referenced in the 510(k).

TYPE OF 510(K) SUBMISSION

☒ Traditional ☐ Special ☐ Abbreviated

STANDARD TITLE [1]

ASTM D6068-96(1996) Standard Test Method for Determining J-R Curves of Plastic Materials

Please answer the following questions	Yes	No
Is this standard recognized by FDA [2]?	☐	☒
FDA Recognition number [3] # _____		
Was a third party laboratory responsible for testing conformity of the device to this standard identified in the 510(k)?	☒	☐
Is a summary report [4] describing the extent of conformance of the standard used included in the 510(k)? If no, complete a summary report table.	☐	☒
Does the test data for this device demonstrate conformity to the requirements of this standard as it pertains to this device?	☒	☐
Does this standard include acceptance criteria? If no, include the results of testing in the 510(k).	☐	☒
Does this standard include more than one option or selection of tests? If yes, report options selected in the summary report table.	☒	☐
Were there any deviations or adaptations made in the use of the standard?	☐	☒
If yes, were deviations in accordance with the FDA supplemental information sheet (SIS) [5]?	☐	☐
Were deviations or adaptations made beyond what is specified in the FDA SIS? If yes, report these deviations or adaptations in the summary report table.	☐	☒
Were there any exclusions from the standard? If yes, report these exclusions in the summary report table.	☐	☒
Is there an FDA guidance [6] that is associated with this standard?	☐	☒
If yes, was the guidance document followed in preparation of this 510k?	☐	☐

Title of guidance: _____

[1] The formatting convention for the title is: [SDO] [numeric identifier] [title of standard] [date of publication]

[2] Authority [21 U.S.C. 360d], www.fda.gov/cdrh/stdsprog.html

[3] http://www.accessdata.fda.gov/scripts/cdrh/cfdocs/cfStandards/search.cfm

[4] The summary report should include: any adaptations used to adapt to the device under review (for example, alternative test methods); choices made when options or a selection of methods are described; deviations from the standard; requirements not applicable to the device; and the name and address of the test laboratory or certification body involved in conformance assessment to this standard. The summary report includes information on all standards utilized during the development of the device.

[5] The supplemental information sheet (SIS) is additional information which is necessary before FDA recognizes the standard. Found at http://www.accessdata.fda.gov/scripts/cdrh/cfdocs/cfStandards/search.cfm

[6] The online search for CDRH Guidance Documents can be found at www.fda.gov/cdrh/guidance.html

Questions? Contact FDA/CDRH/OCE/DID at CDRH-FOISTATUS@fda.hhs.gov or 301-796-8118

Records processed under FOIA Request #2014-8015; Released by CDRH on 12-8-2015

EXTENT OF STANDARD CONFORMANCE SUMMARY REPORT TABLE

STANDARD TITLE
ASTM D6068-96(1996) Standard Test Method for Determining J-R Curves of Plastic Materials

CONFORMANCE WITH STANDARD SECTIONS*

SECTION NUMBER	SECTION TITLE	CONFORMANCE?
See extra pages		☐ Yes ☐ No ☒ N/A

TYPE OF DEVIATION OR OPTION SELECTED ❖

DESCRIPTION

JUSTIFICATION

SECTION NUMBER	SECTION TITLE	CONFORMANCE?
		☐ Yes ☐ No ☐ N/A

TYPE OF DEVIATION OR OPTION SELECTED ❖

DESCRIPTION

JUSTIFICATION

SECTION NUMBER	SECTION TITLE	CONFORMANCE?
		☐ Yes ☐ No ☐ N/A

TYPE OF DEVIATION OR OPTION SELECTED ❖

DESCRIPTION

JUSTIFICATION

* For completeness list all sections of the standard and indicate whether conformance is met. If a section is not applicable (N/A) an explanation is needed under "justification." Some standards include options, so similar to deviations, the option chosen needs to be described and adequately justified as appropriate for the subject device. Explanation of all deviations or description of options selected when following a standard is required under "type of deviation or option selected," "description" and "justification" on the report. More than one page may be necessary.

❖ Types of deviations can include an exclusion of a section in the standard, a deviation brought out by the FDA supplemental information sheet (SIS), a deviation to adapt the standard to the device, or any adaptation of a section.

Paperwork Reduction Act Statement

Public reporting burden for this collection of information is estimated to average 1 hour per response, including the time for reviewing instructions, searching existing data sources, gathering and maintaining the data needed, and completing and reviewing the collection of information. Send comments regarding this burden estimate or any other aspect of this collection of information, including suggestions for reducing this burden to:

Department of Health and Human Services
Food and Drug Administration
Office of Chief Information Officer
1350 Piccard Drive, Room 400
Rockville, MD 20850

An agency may not conduct or sponsor, and a person is not required to respond to, a collection of information unless it displays a currently valid OMB control number.

Questions? Contact FDA/CDRH/OCE/DID at CDRH-FOISTATUS@fda.hhs.gov or 301-796-8118

Records processed under FOIA Request #2014-8015; Released by CDRH on 12-8-2015

(b)(4)

[redacted]

Questions? Contact FDA/CDRH/OCE/DID at CDRH-FOISTATUS@fda.hhs.gov or 301-796-8118

Records processed under FOIA Request #2014-8015; Released by CDRH on 12-8-2015

(b)(4)

[redacted]

TEST LABORATORIES INVOLVED WITH CONFORMANCE

(b)(4)

[redacted]

Questions? Contact FDA/CDRH/OCE/DID at CDRH-FOISTATUS@fda.hhs.gov or 301-796-8118

Records processed under FOIA Request #2014-8015; Released by CDRH on 12-8-2015

Form Approved: OMB No. 0910-0120; Expiration Date: 12/31/13

Department of Health and Human Services
Food and Drug Administration

STANDARDS DATA REPORT FOR 510(k)s

(To be filled in by applicant)

This report and the Summary Report Table are to be completed by the applicant when submitting a 510(k) that references a national or international standard. A separate report is required for each standard referenced in the 510(k).

TYPE OF 510(K) SUBMISSION

☒ Traditional ☐ Special ☐ Abbreviated

STANDARD TITLE [1]

ASTM E647-08e1(2008) Standard Test Method for Measurement of Fatigue Crack Growth Rates

Please answer the following questions	Yes	No
Is this standard recognized by FDA [2]?	☐	☒
FDA Recognition number [3] # _____		
Was a third party laboratory responsible for testing conformity of the device to this standard identified in the 510(k)?	☒	☐
Is a summary report [4] describing the extent of conformance of the standard used included in the 510(k)? If no, complete a summary report table.	☐	☒
Does the test data for this device demonstrate conformity to the requirements of this standard as it pertains to this device?	☒	☐
Does this standard include acceptance criteria? If no, include the results of testing in the 510(k).	☐	☒
Does this standard include more than one option or selection of tests? If yes, report options selected in the summary report table.	☒	☐
Were there any deviations or adaptations made in the use of the standard?	☒	☐
If yes, were deviations in accordance with the FDA supplemental information sheet (SIS) [5]?	☒	☐
Were deviations or adaptations made beyond what is specified in the FDA SIS? If yes, report these deviations or adaptations in the summary report table.	☐	☒
Were there any exclusions from the standard? If yes, report these exclusions in the summary report table.	☐	☒
Is there an FDA guidance [6] that is associated with this standard?	☐	☒
If yes, was the guidance document followed in preparation of this 510k?	☐	☐

Title of guidance: _____

[1] The formatting convention for the title is: [SDO] [numeric identifier] [title of standard] [date of publication]

[2] Authority [21 U.S.C. 360d], www.fda.gov/cdrh/stdsprog.html

[3] http://www.accessdata.fda.gov/scripts/cdrh/cfdocs/cfStandards/search.cfm

[4] The summary report should include: any adaptations used to adapt to the device under review (for example, alternative test methods); choices made when options or a selection of methods are described; deviations from the standard; requirements not applicable to the device; and the name and address of the test laboratory or certification body involved in conformance assessment to this standard. The summary report includes information on all standards utilized during the development of the device.

[5] The supplemental information sheet (SIS) is additional information which is necessary before FDA recognizes the standard. Found at http://www.accessdata.fda.gov/scripts/cdrh/cfdocs/cfStandards/search.cfm

[6] The online search for CDRH Guidance Documents can be found at www.fda.gov/cdrh/guidance.html

Questions? Contact FDA/CDRH/OCE/DID at CDRH-FOISTATUS@fda.hhs.gov or 301-796-8118

Records processed under FOIA Request #2014-8015; Released by CDRH on 12-8-2015

EXTENT OF STANDARD CONFORMANCE SUMMARY REPORT TABLE

STANDARD TITLE
ASTM E647-08e1(2008) Standard Test Method for Measurement of Fatigue Crack Growth Rates

CONFORMANCE WITH STANDARD SECTIONS*

SECTION NUMBER	SECTION TITLE	CONFORMANCE?
See extra pages		☐ Yes ☐ No ☒ N/A

TYPE OF DEVIATION OR OPTION SELECTED ❖

DESCRIPTION

JUSTIFICATION

SECTION NUMBER	SECTION TITLE	CONFORMANCE?
		☐ Yes ☐ No ☐ N/A

TYPE OF DEVIATION OR OPTION SELECTED ❖

DESCRIPTION

JUSTIFICATION

SECTION NUMBER	SECTION TITLE	CONFORMANCE?
		☐ Yes ☐ No ☐ N/A

TYPE OF DEVIATION OR OPTION SELECTED ❖

DESCRIPTION

JUSTIFICATION

* For completeness list all sections of the standard and indicate whether conformance is met. If a section is not applicable (N/A) an explanation is needed under "justification." Some standards include options, so similar to deviations, the option chosen needs to be described and adequately justified as appropriate for the subject device. Explanation of all deviations or description of options selected when following a standard is required under "type of deviation or option selected," "description" and "justification" on the report. More than one page may be necessary.

❖ Types of deviations can include an exclusion of a section in the standard, a deviation brought out by the FDA supplemental information sheet (SIS), a deviation to adapt the standard to the device, or any adaptation of a section.

Paperwork Reduction Act Statement

Public reporting burden for this collection of information is estimated to average 1 hour per response, including the time for reviewing instructions, searching existing data sources, gathering and maintaining the data needed, and completing and reviewing the collection of information. Send comments regarding this burden estimate or any other aspect of this collection of information, including suggestions for reducing this burden to:

Department of Health and Human Services
Food and Drug Administration
Office of Chief Information Officer
1350 Piccard Drive, Room 400
Rockville, MD 20850

An agency may not conduct or sponsor, and a person is not required to respond to, a collection of information unless it displays a currently valid OMB control number.

Questions? Contact FDA/CDRH/OCE/DID at CDRH-FOISTATUS@fda.hhs.gov or 301-796-8118

Records processed under FOIA Request #2014-8015; Released by CDRH on 12-8-2015

(b)(4)

[redacted]

Questions? Contact FDA/CDRH/OCE/DID at CDRH-FOISTATUS@fda.hhs.gov or 301-796-8118

Records processed under FOIA Request #2014-8015; Released by CDRH on 12-8-2015

(b)(4)

[redacted]

Questions? Contact FDA/CDRH/OCE/DID at CDRH-FOISTATUS@fda.hhs.gov or 301-796-8118

Records processed under FOIA Request #2014-8015; Released by CDRH on 12-8-2015

(b)(4)

[redacted]

TEST LABORATORIES INVOLVED WITH CONFORMANCE

(b)(4)

[redacted]

Questions? Contact FDA/CDRH/OCE/DID at CDRH-FOISTATUS@fda.hhs.gov or 301-796-8118

Records processed under FOIA Request #2014-8015; Released by CDRH on 12-8-2015

Form Approved: OMB No. 0910-0120; Expiration Date: 12/31/13

Department of Health and Human Services
Food and Drug Administration

STANDARDS DATA REPORT FOR 510(k)s

(To be filled in by applicant)

This report and the Summary Report Table are to be completed by the applicant when submitting a 510(k) that references a national or international standard. A separate report is required for each standard referenced in the 510(k).

TYPE OF 510(K) SUBMISSION

☒ Traditional ☐ Special ☐ Abbreviated

STANDARD TITLE [1]

ASTM F648-10a(2010) Standard Specification for Ultra-High-Molecular-Weight Polyethylene Powder and Fabricated Form...

Please answer the following questions	Yes	No
Is this standard recognized by FDA [2]?	☒	☐
FDA Recognition number [3]	#8-208	
Was a third party laboratory responsible for testing conformity of the device to this standard identified in the 510(k)?	☒	☐
Is a summary report [4] describing the extent of conformance of the standard used included in the 510(k)? If no, complete a summary report table.	☐	☒
Does the test data for this device demonstrate conformity to the requirements of this standard as it pertains to this device?	☒	☐
Does this standard include acceptance criteria? If no, include the results of testing in the 510(k).	☒	☐
Does this standard include more than one option or selection of tests? If yes, report options selected in the summary report table.	☒	☐
Were there any deviations or adaptations made in the use of the standard?	☐	☒
If yes, were deviations in accordance with the FDA supplemental information sheet (SIS) [5]?	☐	☐
Were deviations or adaptations made beyond what is specified in the FDA SIS? If yes, report these deviations or adaptations in the summary report table.	☐	☒
Were there any exclusions from the standard? If yes, report these exclusions in the summary report table.	☐	☒
Is there an FDA guidance [6] that is associated with this standard?	☐	☒
If yes, was the guidance document followed in preparation of this 510k?	☐	☐

Title of guidance: _____

[1] The formatting convention for the title is: [SDO] [numeric identifier] [title of standard] [date of publication]

[2] Authority [21 U.S.C. 360d], www.fda.gov/cdrh/stdsprog.html

[3] http://www.accessdata.fda.gov/scripts/cdrh/cfdocs/cfStandards/search.cfm

[4] The summary report should include: any adaptations used to adapt to the device under review (for example, alternative test methods); choices made when options or a selection of methods are described; deviations from the standard; requirements not applicable to the device; and the name and address of the test laboratory or certification body involved in conformance assessment to this standard. The summary report includes information on all standards utilized during the development of the device.

[5] The supplemental information sheet (SIS) is additional information which is necessary before FDA recognizes the standard. Found at http://www.accessdata.fda.gov/scripts/cdrh/cfdocs/cfStandards/search.cfm

[6] The online search for CDRH Guidance Documents can be found at www.fda.gov/cdrh/guidance.html

Questions? Contact FDA/CDRH/OCE/DID at CDRH-FOISTATUS@fda.hhs.gov or 301-796-8118

Records processed under FOIA Request #2014-8015; Released by CDRH on 12-8-2015

EXTENT OF STANDARD CONFORMANCE SUMMARY REPORT TABLE

STANDARD TITLE
ASTM F648-10a(2010) Standard Specification for Ultra-High-Molecular-Weight Polyethylene Powder and Fabricated Form...

CONFORMANCE WITH STANDARD SECTIONS*

SECTION NUMBER	SECTION TITLE	CONFORMANCE?
See extra pages		☐ Yes ☐ No ☒ N/A

TYPE OF DEVIATION OR OPTION SELECTED ❖

DESCRIPTION

JUSTIFICATION

SECTION NUMBER	SECTION TITLE	CONFORMANCE?
		☐ Yes ☐ No ☐ N/A

TYPE OF DEVIATION OR OPTION SELECTED ❖

DESCRIPTION

JUSTIFICATION

SECTION NUMBER	SECTION TITLE	CONFORMANCE?
		☐ Yes ☐ No ☐ N/A

TYPE OF DEVIATION OR OPTION SELECTED ❖

DESCRIPTION

JUSTIFICATION

* For completeness list all sections of the standard and indicate whether conformance is met. If a section is not applicable (N/A) an explanation is needed under "justification." Some standards include options, so similar to deviations, the option chosen needs to be described and adequately justified as appropriate for the subject device. Explanation of all deviations or description of options selected when following a standard is required under "type of deviation or option selected," "description" and "justification" on the report. More than one page may be necessary.

❖ Types of deviations can include an exclusion of a section in the standard, a deviation brought out by the FDA supplemental information sheet (SIS), a deviation to adapt the standard to the device, or any adaptation of a section.

Paperwork Reduction Act Statement

Public reporting burden for this collection of information is estimated to average 1 hour per response, including the time for reviewing instructions, searching existing data sources, gathering and maintaining the data needed, and completing and reviewing the collection of information. Send comments regarding this burden estimate or any other aspect of this collection of information, including suggestions for reducing this burden to:

Department of Health and Human Services
Food and Drug Administration
Office of Chief Information Officer
1350 Piccard Drive, Room 400
Rockville, MD 20850

An agency may not conduct or sponsor, and a person is not required to respond to, a collection of information unless it displays a currently valid OMB control number.

Questions? Contact FDA/CDRH/OCE/DID at CDRH-FOISTATUS@fda.hhs.gov or 301-796-8118

Records processed under FOIA Request #2014-8015; Released by CDRH on 12-8-2015

(b)(4)

[redacted]

Questions? Contact FDA/CDRH/OCE/DID at CDRH-FOISTATUS@fda.hhs.gov or 301-796-8118

Records processed under FOIA Request #2014-8015; Released by CDRH on 12-8-2015

TEST LABORATORIES INVOLVED WITH CONFORMANCE

(b)(4)

[redacted]

Questions? Contact FDA/CDRH/OCE/DID at CDRH-FOISTATUS@fda.hhs.gov or 301-796-8118

Records processed under FOIA Request #2014-8015; Released by CDRH on 12-8-2015

Form Approved: OMB No. 0910-0120; Expiration Date: 12/31/13

Department of Health and Human Services
Food and Drug Administration

STANDARDS DATA REPORT FOR 510(k)s

(To be filled in by applicant)

This report and the Summary Report Table are to be completed by the applicant when submitting a 510(k) that references a national or international standard. A separate report is required for each standard referenced in the 510(k).

TYPE OF 510(K) SUBMISSION

☒ Traditional ☐ Special ☐ Abbreviated

STANDARD TITLE [1]

ASTM F1223-08(2008) Standard Test Method for Determination of Total Knee Replacement Constraint

Please answer the following questions	Yes	No
Is this standard recognized by FDA [2]?	☒	☐
FDA Recognition number [3]	#11-213	
Was a third party laboratory responsible for testing conformity of the device to this standard identified in the 510(k)?	☒	☐
Is a summary report [4] describing the extent of conformance of the standard used included in the 510(k)? If no, complete a summary report table.	☐	☒
Does the test data for this device demonstrate conformity to the requirements of this standard as it pertains to this device?	☒	☐
Does this standard include acceptance criteria? If no, include the results of testing in the 510(k).	☐	☒
Does this standard include more than one option or selection of tests? If yes, report options selected in the summary report table.	☒	☐
Were there any deviations or adaptations made in the use of the standard?	☐	☒
If yes, were deviations in accordance with the FDA supplemental information sheet (SIS) [5]?	☐	☐
Were deviations or adaptations made beyond what is specified in the FDA SIS? If yes, report these deviations or adaptations in the summary report table.	☐	☒
Were there any exclusions from the standard? If yes, report these exclusions in the summary report table.	☐	☒
Is there an FDA guidance [6] that is associated with this standard?	☒	☐
If yes, was the guidance document followed in preparation of this 510k?	☒	☐

Title of guidance: Knee Joint Patellofemorotibial and Femorotibial Metal/Polymer Porous-Coated Uncemented Prostheses

[1] The formatting convention for the title is: [SDO] [numeric identifier] [title of standard] [date of publication]

[2] Authority [21 U.S.C. 360d], www.fda.gov/cdrh/stdsprog.html

[3] http://www.accessdata.fda.gov/scripts/cdrh/cfdocs/cfStandards/search.cfm

[4] The summary report should include: any adaptations used to adapt to the device under review (for example, alternative test methods); choices made when options or a selection of methods are described; deviations from the standard; requirements not applicable to the device; and the name and address of the test laboratory or certification body involved in conformance assessment to this standard. The summary report includes information on all standards utilized during the development of the device.

[5] The supplemental information sheet (SIS) is additional information which is necessary before FDA recognizes the standard. Found at http://www.accessdata.fda.gov/scripts/cdrh/cfdocs/cfStandards/search.cfm

[6] The online search for CDRH Guidance Documents can be found at www.fda.gov/cdrh/guidance.html

Questions? Contact FDA/CDRH/OCE/DID at CDRH-FOISTATUS@fda.hhs.gov or 301-796-8118

Records processed under FOIA Request #2014-8015; Released by CDRH on 12-8-2015

EXTENT OF STANDARD CONFORMANCE
SUMMARY REPORT TABLE

STANDARD TITLE

ASTM F1223-08(2008) Standard Test Method for Determination of Total Knee Replacement Constraint

CONFORMANCE WITH STANDARD SECTIONS*

(b)(4)

[redacted]

* For completeness list all sections of the standard and indicate whether conformance is met. If a section is not applicable (N/A) an explanation is needed under "justification." Some standards include options, so similar to deviations, the option chosen needs to be described and adequately justified as appropriate for the subject device. Explanation of all deviations or description of options selected when following a standard is required under "type of deviation or option selected," "description" and "justification" on the report. More than one page may be necessary.

❖ Types of deviations can include an exclusion of a section in the standard, a deviation brought out by the FDA supplemental information sheet (SIS), a deviation to adapt the standard to the device, or any adaptation of a section.

Paperwork Reduction Act Statement

Public reporting burden for this collection of information is estimated to average 1 hour per response, including the time for reviewing instructions, searching existing data sources, gathering and maintaining the data needed, and completing and reviewing the collection of information. Send comments regarding this burden estimate or any other aspect of this collection of information, including suggestions for reducing this burden to:

Department of Health and Human Services
Food and Drug Administration
Office of Chief Information Officer
1350 Piccard Drive, Room 400
Rockville, MD 20850

An agency may not conduct or sponsor, and a person is not required to respond to, a collection of information unless it displays a currently valid OMB control number.

Questions? Contact FDA/CDRH/OCE/DID at CDRH-FOISTATUS@fda.hhs.gov or 301-796-8118

Records processed under FOIA Request #2014-8015; Released by CDRH on 12-8-2015

Form Approved: OMB No. 0910-0120; Expiration Date: 12/31/13

Department of Health and Human Services
Food and Drug Administration

STANDARDS DATA REPORT FOR 510(k)s

(To be filled in by applicant)

This report and the Summary Report Table are to be completed by the applicant when submitting a 510(k) that references a national or international standard. A separate report is required for each standard referenced in the 510(k).

TYPE OF 510(K) SUBMISSION

☒ Traditional ☐ Special ☐ Abbreviated

STANDARD TITLE [1]

ASTM F1672-95(2011) Standard Specification for Resurfacing Patellar Prosthesis

Please answer the following questions	Yes	No
Is this standard recognized by FDA [2]?	☒	☐
FDA Recognition number [3]	#11-196	
Was a third party laboratory responsible for testing conformity of the device to this standard identified in the 510(k)?	☒	☐
Is a summary report [4] describing the extent of conformance of the standard used included in the 510(k)? If no, complete a summary report table.	☐	☒
Does the test data for this device demonstrate conformity to the requirements of this standard as it pertains to this device?	☒	☐
Does this standard include acceptance criteria? If no, include the results of testing in the 510(k).	☐	☒
Does this standard include more than one option or selection of tests? If yes, report options selected in the summary report table.	☒	☐
Were there any deviations or adaptations made in the use of the standard?	☐	☒
If yes, were deviations in accordance with the FDA supplemental information sheet (SIS) [5]?	☐	☐
Were deviations or adaptations made beyond what is specified in the FDA SIS? If yes, report these deviations or adaptations in the summary report table.	☐	☒
Were there any exclusions from the standard? If yes, report these exclusions in the summary report table.	☐	☒
Is there an FDA guidance [6] that is associated with this standard?	☒	☐
If yes, was the guidance document followed in preparation of this 510k?	☒	☐

Title of guidance: Knee Joint Patellofemorotibial and Femorotibial Metal/Polymer Porous-Coated Uncemented Prostheses

[1] The formatting convention for the title is: [SDO] [numeric identifier] [title of standard] [date of publication]

[2] Authority [21 U.S.C. 360d], www.fda.gov/cdrh/stdsprog.html

[3] http://www.accessdata.fda.gov/scripts/cdrh/cfdocs/cfStandards/search.cfm

[4] The summary report should include: any adaptations used to adapt to the device under review (for example, alternative test methods); choices made when options or a selection of methods are described; deviations from the standard; requirements not applicable to the device; and the name and address of the test laboratory or certification body involved in conformance assessment to this standard. The summary report includes information on all standards utilized during the development of the device.

[5] The supplemental information sheet (SIS) is additional information which is necessary before FDA recognizes the standard. Found at http://www.accessdata.fda.gov/scripts/cdrh/cfdocs/cfStandards/search.cfm

[6] The online search for CDRH Guidance Documents can be found at www.fda.gov/cdrh/guidance.html

Questions? Contact FDA/CDRH/OCE/DID at CDRH-FOISTATUS@fda.hhs.gov or 301-796-8118

Records processed under FOIA Request #2014-8015; Released by CDRH on 12-8-2015

EXTENT OF STANDARD CONFORMANCE SUMMARY REPORT TABLE

STANDARD TITLE
ASTM F1672-95(2011) Standard Specification for Resurfacing Patellar Prosthesis

CONFORMANCE WITH STANDARD SECTIONS*

SECTION NUMBER	SECTION TITLE	CONFORMANCE?
see extra pages		☐ Yes ☐ No ☒ N/A

TYPE OF DEVIATION OR OPTION SELECTED ❖

DESCRIPTION

JUSTIFICATION

SECTION NUMBER	SECTION TITLE	CONFORMANCE?
		☐ Yes ☐ No ☐ N/A

TYPE OF DEVIATION OR OPTION SELECTED ❖

DESCRIPTION

JUSTIFICATION

SECTION NUMBER	SECTION TITLE	CONFORMANCE?
		☐ Yes ☐ No ☐ N/A

TYPE OF DEVIATION OR OPTION SELECTED ❖

DESCRIPTION

JUSTIFICATION

* For completeness list all sections of the standard and indicate whether conformance is met. If a section is not applicable (N/A) an explanation is needed under "justification." Some standards include options, so similar to deviations, the option chosen needs to be described and adequately justified as appropriate for the subject device. Explanation of all deviations or description of options selected when following a standard is required under "type of deviation or option selected," "description" and "justification" on the report. More than one page may be necessary.

❖ Types of deviations can include an exclusion of a section in the standard, a deviation brought out by the FDA supplemental information sheet (SIS), a deviation to adapt the standard to the device, or any adaptation of a section.

Paperwork Reduction Act Statement

Public reporting burden for this collection of information is estimated to average 1 hour per response, including the time for reviewing instructions, searching existing data sources, gathering and maintaining the data needed, and completing and reviewing the collection of information. Send comments regarding this burden estimate or any other aspect of this collection of information, including suggestions for reducing this burden to:

Department of Health and Human Services
Food and Drug Administration
Office of Chief Information Officer
1350 Piccard Drive, Room 400
Rockville, MD 20850

An agency may not conduct or sponsor, and a person is not required to respond to, a collection of information unless it displays a currently valid OMB control number.

Questions? Contact FDA/CDRH/OCE/DID at CDRH-FOISTATUS@fda.hhs.gov or 301-796-8118

Records processed under FOIA Request #2014-8015; Released by CDRH on 12-8-2015

(b)(4)

[redacted]

TEST LABORATORIES INVOLVED WITH CONFORMANCE

(b)(4)

[redacted]

Questions? Contact FDA/CDRH/OCE/DID at CDRH-FOISTATUS@fda.hhs.gov or 301-796-8118

Records processed under FOIA Request #2014-8015; Released by CDRH on 12-8-2015

Form Approved: OMB No. 0910-0120; Expiration Date: 12/31/13

Department of Health and Human Services
Food and Drug Administration

STANDARDS DATA REPORT FOR 510(k)s

(To be filled in by applicant)

This report and the Summary Report Table are to be completed by the applicant when submitting a 510(k) that references a national or international standard. A separate report is required for each standard referenced in the 510(k).

TYPE OF 510(K) SUBMISSION

☒ Traditional ☐ Special ☐ Abbreviated

STANDARD TITLE [1]

ASTM F1886-09(2009) Standard Test Method for Determining Integrity of Seals for Flexible Packaging by Visual Inspection

Please answer the following questions	Yes	No
Is this standard recognized by FDA [2]?	☒	☐
FDA Recognition number [3]	#14-288	
Was a third party laboratory responsible for testing conformity of the device to this standard identified in the 510(k)?	☐	☒
Is a summary report [4] describing the extent of conformance of the standard used included in the 510(k)? If no, complete a summary report table.	☐	☒
Does the test data for this device demonstrate conformity to the requirements of this standard as it pertains to this device?	☒	☐
Does this standard include acceptance criteria? If no, include the results of testing in the 510(k).	☒	☐
Does this standard include more than one option or selection of tests? If yes, report options selected in the summary report table.	☐	☒
Were there any deviations or adaptations made in the use of the standard?	☐	☒
If yes, were deviations in accordance with the FDA supplemental information sheet (SIS) [5]?	☐	☐
Were deviations or adaptations made beyond what is specified in the FDA SIS? If yes, report these deviations or adaptations in the summary report table.	☐	☒
Were there any exclusions from the standard? If yes, report these exclusions in the summary report table.	☐	☒
Is there an FDA guidance [6] that is associated with this standard?	☐	☒
If yes, was the guidance document followed in preparation of this 510k?	☐	☐

Title of guidance: _____

[1] The formatting convention for the title is: [SDO] [numeric identifier] [title of standard] [date of publication]

[2] Authority [21 U.S.C. 360d], www.fda.gov/cdrh/stdsprog.html

[3] http://www.accessdata.fda.gov/scripts/cdrh/cfdocs/cfStandards/search.cfm

[4] The summary report should include: any adaptations used to adapt to the device under review (for example, alternative test methods); choices made when options or a selection of methods are described; deviations from the standard; requirements not applicable to the device; and the name and address of the test laboratory or certification body involved in conformance assessment to this standard. The summary report includes information on all standards utilized during the development of the device.

[5] The supplemental information sheet (SIS) is additional information which is necessary before FDA recognizes the standard. Found at http://www.accessdata.fda.gov/scripts/cdrh/cfdocs/cfStandards/search.cfm

[6] The online search for CDRH Guidance Documents can be found at www.fda.gov/cdrh/guidance.html

Questions? Contact FDA/CDRH/OCE/DID at CDRH-FOISTATUS@fda.hhs.gov or 301-796-8118

EXTENT OF STANDARD CONFORMANCE SUMMARY REPORT TABLE

STANDARD TITLE
ASTM F1886-09(2009) Standard Test Method for Determining Integrity of Seals for Flexible Packaging by Visual Inspection

CONFORMANCE WITH STANDARD SECTIONS*

SECTION NUMBER	SECTION TITLE	CONFORMANCE?
All	N/A	☒ Yes ☐ No ☐ N/A

TYPE OF DEVIATION OR OPTION SELECTED ❖
No deviations. All sections of the standard were followed by the executioner(s). See below for options selected.

DESCRIPTION
Describes the test method for different types of packaging with at least one transparent side.

JUSTIFICATION
Compliant to all sections for blister trays with Tyvek lids.

SECTION NUMBER	SECTION TITLE	CONFORMANCE?
1.	Scope	☒ Yes ☐ No ☐ N/A

TYPE OF DEVIATION OR OPTION SELECTED ❖
Option selected: Packaging type - transparent blisters with Tyvek lids.

DESCRIPTION
Type of package selected for evaluation.

JUSTIFICATION
Standard states it is applicable to packages with at least one transparent side. All seals are visible and subject to visual inspection on a transparent blister with a Tyvek lid.

SECTION NUMBER	SECTION TITLE	CONFORMANCE?
		☐ Yes ☐ No ☐ N/A

TYPE OF DEVIATION OR OPTION SELECTED ❖

DESCRIPTION

JUSTIFICATION

* For completeness list all sections of the standard and indicate whether conformance is met. If a section is not applicable (N/A) an explanation is needed under "justification." Some standards include options, so similar to deviations, the option chosen needs to be described and adequately justified as appropriate for the subject device. Explanation of all deviations or description of options selected when following a standard is required under "type of deviation or option selected," "description" and "justification" on the report. More than one page may be necessary.

❖ Types of deviations can include an exclusion of a section in the standard, a deviation brought out by the FDA supplemental information sheet (SIS), a deviation to adapt the standard to the device, or any adaptation of a section.

Paperwork Reduction Act Statement

Public reporting burden for this collection of information is estimated to average 1 hour per response, including the time for reviewing instructions, searching existing data sources, gathering and maintaining the data needed, and completing and reviewing the collection of information. Send comments regarding this burden estimate or any other aspect of this collection of information, including suggestions for reducing this burden to:

Department of Health and Human Services
Food and Drug Administration
Office of Chief Information Officer
1350 Piccard Drive, Room 400
Rockville, MD 20850

An agency may not conduct or sponsor, and a person is not required to respond to, a collection of information unless it displays a currently valid OMB control number.

Questions? Contact FDA/CDRH/OCE/DID at CDRH-FOISTATUS@fda.hhs.gov or 301-796-8118

Records processed under FOIA Request #2014-8015; Released by CDRH on 12-8-2015

Form Approved: OMB No. 0910-0120; Expiration Date: 12/31/13

Department of Health and Human Services
Food and Drug Administration

STANDARDS DATA REPORT FOR 510(k)s

(To be filled in by applicant)

This report and the Summary Report Table are to be completed by the applicant when submitting a 510(k) that references a national or international standard. A separate report is required for each standard referenced in the 510(k).

TYPE OF 510(K) SUBMISSION

☒ Traditional ☐ Special ☐ Abbreviated

STANDARD TITLE [1]

ASTM F1980-07(2011) Standard Guide for Accelerated Aging of Sterile Barrier Systems for Medical Devices

Please answer the following questions	Yes	No
Is this standard recognized by FDA [2]?	☒	☐
FDA Recognition number [3]	#14-229	
Was a third party laboratory responsible for testing conformity of the device to this standard identified in the 510(k)?	☒	☐
Is a summary report [4] describing the extent of conformance of the standard used included in the 510(k)? If no, complete a summary report table.	☐	☒
Does the test data for this device demonstrate conformity to the requirements of this standard as it pertains to this device?	☒	☐
Does this standard include acceptance criteria? If no, include the results of testing in the 510(k).	☐	☒
Does this standard include more than one option or selection of tests? If yes, report options selected in the summary report table.	☒	☐
Were there any deviations or adaptations made in the use of the standard?	☐	☒
If yes, were deviations in accordance with the FDA supplemental information sheet (SIS) [5]?	☐	☐
Were deviations or adaptations made beyond what is specified in the FDA SIS? If yes, report these deviations or adaptations in the summary report table.	☐	☒
Were there any exclusions from the standard? If yes, report these exclusions in the summary report table.	☐	☒
Is there an FDA guidance [6] that is associated with this standard?	☐	☒
If yes, was the guidance document followed in preparation of this 510k?	☐	☐

Title of guidance: _____

[1] The formatting convention for the title is: [SDO] [numeric identifier] [title of standard] [date of publication]

[2] Authority [21 U.S.C. 360d], www.fda.gov/cdrh/stdsprog.html

[3] http://www.accessdata.fda.gov/scripts/cdrh/cfdocs/cfStandards/search.cfm

[4] The summary report should include: any adaptations used to adapt to the device under review (for example, alternative test methods); choices made when options or a selection of methods are described; deviations from the standard; requirements not applicable to the device; and the name and address of the test laboratory or certification body involved in conformance assessment to this standard. The summary report includes information on all standards utilized during the development of the device.

[5] The supplemental information sheet (SIS) is additional information which is necessary before FDA recognizes the standard. Found at http://www.accessdata.fda.gov/scripts/cdrh/cfdocs/cfStandards/search.cfm

[6] The online search for CDRH Guidance Documents can be found at www.fda.gov/cdrh/guidance.html

Questions? Contact FDA/CDRH/OCE/DID at CDRH-FOISTATUS@fda.hhs.gov or 301-796-8118

Records processed under FOIA Request #2014-8015; Released by CDRH on 12-8-2015

EXTENT OF STANDARD CONFORMANCE
SUMMARY REPORT TABLE

STANDARD TITLE
ASTM F1980-07(2011) Standard Guide for Accelerated Aging of Sterile Barrier Systems for Medical Devices

CONFORMANCE WITH STANDARD SECTIONS*

SECTION NUMBER	SECTION TITLE	CONFORMANCE?
All	N/A	☒ Yes ☐ No ☐ N/A

TYPE OF DEVIATION OR OPTION SELECTED ❖
No deviations. All sections of the standard were followed by the testing lab. See below for options selected.

DESCRIPTION
Describes the method for accelerated aging of packaging systems for medical devices.

(b)(4)
[redacted]

Describes the temperatures used for accelerated aging and the corresponding calculations used to determine the number of days in aging to simulate one year of shelf life.

(b)(4)
[redacted]

SECTION NUMBER	SECTION TITLE	CONFORMANCE?
		☐ Yes ☐ No ☐ N/A

TYPE OF DEVIATION OR OPTION SELECTED ❖

DESCRIPTION

JUSTIFICATION

* For completeness list all sections of the standard and indicate whether conformance is met. If a section is not applicable (N/A) an explanation is needed under "justification." Some standards include options, so similar to deviations, the option chosen needs to be described and adequately justified as appropriate for the subject device. Explanation of all deviations or description of options selected when following a standard is required under "type of deviation or option selected," "description" and "justification" on the report. More than one page may be necessary.

❖ Types of deviations can include an exclusion of a section in the standard, a deviation brought out by the FDA supplemental information sheet (SIS), a deviation to adapt the standard to the device, or any adaptation of a section.

Paperwork Reduction Act Statement

Public reporting burden for this collection of information is estimated to average 1 hour per response, including the time for reviewing instructions, searching existing data sources, gathering and maintaining the data needed, and completing and reviewing the collection of information. Send comments regarding this burden estimate or any other aspect of this collection of information, including suggestions for reducing this burden to:

Department of Health and Human Services
Food and Drug Administration
Office of Chief Information Officer
1350 Piccard Drive, Room 400
Rockville, MD 20850

An agency may not conduct or sponsor, and a person is not required to respond to, a collection of information unless it displays a currently valid OMB control number.

Questions? Contact FDA/CDRH/OCE/DID at CDRH-FOISTATUS@fda.hhs.gov or 301-796-8118

Records processed under FOIA Request #2014-8015; Released by CDRH on 12-8-2015

Form Approved: OMB No. 0910-0120; Expiration Date: 12/31/13

Department of Health and Human Services
Food and Drug Administration

STANDARDS DATA REPORT FOR 510(k)s

(To be filled in by applicant)

This report and the Summary Report Table are to be completed by the applicant when submitting a 510(k) that references a national or international standard. A separate report is required for each standard referenced in the 510(k).

TYPE OF 510(K) SUBMISSION

☒ Traditional ☐ Special ☐ Abbreviated

STANDARD TITLE [1]

ASTM F2003-02(2008) Standard Practice for Accelerated Aging of Ultra-High Molecular Weight Polyethylene after Gamma...

Please answer the following questions	Yes	No
Is this standard recognized by FDA [2]?	☐	☒
FDA Recognition number [3]	#N/A	
Was a third party laboratory responsible for testing conformity of the device to this standard identified in the 510(k)?	☒	☐
Is a summary report [4] describing the extent of conformance of the standard used included in the 510(k)? If no, complete a summary report table.	☐	☒
Does the test data for this device demonstrate conformity to the requirements of this standard as it pertains to this device?	☒	☐
Does this standard include acceptance criteria? If no, include the results of testing in the 510(k).	☐	☒
Does this standard include more than one option or selection of tests? If yes, report options selected in the summary report table.	☐	☒
Were there any deviations or adaptations made in the use of the standard?	☐	☒
If yes, were deviations in accordance with the FDA supplemental information sheet (SIS) [5]?	☐	☐
Were deviations or adaptations made beyond what is specified in the FDA SIS? If yes, report these deviations or adaptations in the summary report table.	☐	☒
Were there any exclusions from the standard? If yes, report these exclusions in the summary report table.	☐	☒
Is there an FDA guidance [6] that is associated with this standard?	☐	☒
If yes, was the guidance document followed in preparation of this 510k?	☐	☐

Title of guidance: _____

[1] The formatting convention for the title is: [SDO] [numeric identifier] [title of standard] [date of publication]

[2] Authority [21 U.S.C. 360d], www.fda.gov/cdrh/stdsprog.html

[3] http://www.accessdata.fda.gov/scripts/cdrh/cfdocs/cfStandards/search.cfm

[4] The summary report should include: any adaptations used to adapt to the device under review (for example, alternative test methods); choices made when options or a selection of methods are described; deviations from the standard; requirements not applicable to the device; and the name and address of the test laboratory or certification body involved in conformance assessment to this standard. The summary report includes information on all standards utilized during the development of the device.

[5] The supplemental information sheet (SIS) is additional information which is necessary before FDA recognizes the standard. Found at http://www.accessdata.fda.gov/scripts/cdrh/cfdocs/cfStandards/search.cfm

[6] The online search for CDRH Guidance Documents can be found at www.fda.gov/cdrh/guidance.html

Questions? Contact FDA/CDRH/OCE/DID at CDRH-FOISTATUS@fda.hhs.gov or 301-796-8118

Records processed under FOIA Request #2014-8015; Released by CDRH on 12-8-2015

EXTENT OF STANDARD CONFORMANCE SUMMARY REPORT TABLE

STANDARD TITLE
ASTM F2003-02(2008) Standard Practice for Accelerated Aging of Ultra-High Molecular Weight Polyethylene after Gamma...

CONFORMANCE WITH STANDARD SECTIONS*

SECTION NUMBER	SECTION TITLE	CONFORMANCE? ☐ Yes ☐ No ☒ N/A
TYPE OF DEVIATION OR OPTION SELECTED ❖		
DESCRIPTION		
JUSTIFICATION		

SECTION NUMBER	SECTION TITLE	CONFORMANCE? ☐ Yes ☐ No ☐ N/A
TYPE OF DEVIATION OR OPTION SELECTED ❖		
DESCRIPTION		
JUSTIFICATION		

SECTION NUMBER	SECTION TITLE	CONFORMANCE? ☐ Yes ☐ No ☐ N/A
TYPE OF DEVIATION OR OPTION SELECTED ❖		
DESCRIPTION		
JUSTIFICATION		

* For completeness list all sections of the standard and indicate whether conformance is met. If a section is not applicable (N/A) an explanation is needed under "justification." Some standards include options, so similar to deviations, the option chosen needs to be described and adequately justified as appropriate for the subject device. Explanation of all deviations or description of options selected when following a standard is required under "type of deviation or option selected," "description" and "justification" on the report. More than one page may be necessary.

❖ Types of deviations can include an exclusion of a section in the standard, a deviation brought out by the FDA supplemental information sheet (SIS), a deviation to adapt the standard to the device, or any adaptation of a section.

Paperwork Reduction Act Statement

Public reporting burden for this collection of information is estimated to average 1 hour per response, including the time for reviewing instructions, searching existing data sources, gathering and maintaining the data needed, and completing and reviewing the collection of information. Send comments regarding this burden estimate or any other aspect of this collection of information, including suggestions for reducing this burden to:

Department of Health and Human Services
Food and Drug Administration
Office of Chief Information Officer
1350 Piccard Drive, Room 400
Rockville, MD 20850

An agency may not conduct or sponsor, and a person is not required to respond to, a collection of information unless it displays a currently valid OMB control number.

Questions? Contact FDA/CDRH/OCE/DID at CDRH-FOISTATUS@fda.hhs.gov or 301-796-8118

Records processed under FOIA Request #2014-8015; Released by CDRH on 12-8-2015

Form Approved: OMB No. 0910-0120; Expiration Date: 12/31/13

Department of Health and Human Services
Food and Drug Administration

STANDARDS DATA REPORT FOR 510(k)s

(To be filled in by applicant)

This report and the Summary Report Table are to be completed by the applicant when submitting a 510(k) that references a national or international standard. A separate report is required for each standard referenced in the 510(k).

TYPE OF 510(K) SUBMISSION

☒ Traditional ☐ Special ☐ Abbreviated

STANDARD TITLE [1]

ASTM F2083-11(2011) Standard Specification for Total Knee Prosthesis

Please answer the following questions	Yes	No
Is this standard recognized by FDA [2]?	☒	☐
FDA Recognition number [3]	#11-244	
Was a third party laboratory responsible for testing conformity of the device to this standard identified in the 510(k)?	☒	☐
Is a summary report [4] describing the extent of conformance of the standard used included in the 510(k)? If no, complete a summary report table.	☐	☒
Does the test data for this device demonstrate conformity to the requirements of this standard as it pertains to this device?	☒	☐
Does this standard include acceptance criteria? If no, include the results of testing in the 510(k).	☐	☒
Does this standard include more than one option or selection of tests? If yes, report options selected in the summary report table.	☒	☐
Were there any deviations or adaptations made in the use of the standard?	☐	☒
If yes, were deviations in accordance with the FDA supplemental information sheet (SIS) [5]?	☐	☐
Were deviations or adaptations made beyond what is specified in the FDA SIS? If yes, report these deviations or adaptations in the summary report table.	☐	☒
Were there any exclusions from the standard? If yes, report these exclusions in the summary report table.	☒	☐
Is there an FDA guidance [6] that is associated with this standard?	☒	☐
If yes, was the guidance document followed in preparation of this 510k?	☒	☐

Title of guidance: Knee Joint Patellofemorotibial and Femorotibial Metal/Polymer Porous-Coated Uncemented Prostheses

[1] The formatting convention for the title is: [SDO] [numeric identifier] [title of standard] [date of publication]

[2] Authority [21 U.S.C. 360d], www.fda.gov/cdrh/stdsprog.html

[3] http://www.accessdata.fda.gov/scripts/cdrh/cfdocs/cfStandards/search.cfm

[4] The summary report should include: any adaptations used to adapt to the device under review (for example, alternative test methods); choices made when options or a selection of methods are described; deviations from the standard; requirements not applicable to the device; and the name and address of the test laboratory or certification body involved in conformance assessment to this standard. The summary report includes information on all standards utilized during the development of the device.

[5] The supplemental information sheet (SIS) is additional information which is necessary before FDA recognizes the standard. Found at http://www.accessdata.fda.gov/scripts/cdrh/cfdocs/cfStandards/search.cfm

[6] The online search for CDRH Guidance Documents can be found at www.fda.gov/cdrh/guidance.html

Questions? Contact FDA/CDRH/OCE/DID at CDRH-FOISTATUS@fda.hhs.gov or 301-796-8118

Records processed under FOIA Request #2014-8015; Released by CDRH on 12-8-2015

EXTENT OF STANDARD CONFORMANCE SUMMARY REPORT TABLE

STANDARD TITLE
ASTM F2083-11(2011) Standard Specification for Total Knee Prosthesis

CONFORMANCE WITH STANDARD SECTIONS*

SECTION NUMBER	SECTION TITLE	CONFORMANCE?
see extra pages		☐ Yes ☐ No ☒ N/A

TYPE OF DEVIATION OR OPTION SELECTED ❖

DESCRIPTION

JUSTIFICATION

SECTION NUMBER	SECTION TITLE	CONFORMANCE?
		☐ Yes ☐ No ☐ N/A

TYPE OF DEVIATION OR OPTION SELECTED ❖

DESCRIPTION

JUSTIFICATION

SECTION NUMBER	SECTION TITLE	CONFORMANCE?
		☐ Yes ☐ No ☐ N/A

TYPE OF DEVIATION OR OPTION SELECTED ❖

DESCRIPTION

JUSTIFICATION

* For completeness list all sections of the standard and indicate whether conformance is met. If a section is not applicable (N/A) an explanation is needed under "justification." Some standards include options, so similar to deviations, the option chosen needs to be described and adequately justified as appropriate for the subject device. Explanation of all deviations or description of options selected when following a standard is required under "type of deviation or option selected," "description" and "justification" on the report. More than one page may be necessary.

❖ Types of deviations can include an exclusion of a section in the standard, a deviation brought out by the FDA supplemental information sheet (SIS), a deviation to adapt the standard to the device, or any adaptation of a section.

Paperwork Reduction Act Statement

Public reporting burden for this collection of information is estimated to average 1 hour per response, including the time for reviewing instructions, searching existing data sources, gathering and maintaining the data needed, and completing and reviewing the collection of information. Send comments regarding this burden estimate or any other aspect of this collection of information, including suggestions for reducing this burden to:

Department of Health and Human Services
Food and Drug Administration
Office of Chief Information Officer
1350 Piccard Drive, Room 400
Rockville, MD 20850

An agency may not conduct or sponsor, and a person is not required to respond to, a collection of information unless it displays a currently valid OMB control number.

Questions? Contact FDA/CDRH/OCE/DID at CDRH-FOISTATUS@fda.hhs.gov or 301-796-8118

SECTION #	SECTION TITLE	CONFORMANCE?
4	Classification	☒ Yes ☐ No ☐ N/A
TYPE OF DEVIATION OR OPTION SELECTED Device is classified as a semi-constrained prosthesis.		
DESCRIPTION The Balanced Knee System High Flex PS is a posterior stabilized total knee prosthesis.		
JUSTIFICATION The Balanced Knee System High Flex PS design best fits the description of the semi-constrained description.		

SECTION #	SECTION TITLE	CONFORMANCE?
6 (subsection 6.2.1.1)	Performance Requirements	☐ Yes ☐ No ☒ N/A
TYPE OF DEVIATION OR OPTION SELECTED Tibial tray testing was not performed.		
DESCRIPTION "Tibial Tray components shall be evaluated in accordance with Test Method ASTM F1800."		
JUSTIFICATION No new Tibial Tray components are introduced for use with the High Flex PS System.		

(b)(4)

[redacted]

Records processed under FOIA Request #2014-8015; Released by CDRH on 12-8-2015

(b)(4)

[redacted]

TEST LABORATORIES INVOLVED WITH CONFORMANCE

(b)(4)

[redacted]

Questions? Contact FDA/CDRH/OCE/DID at CDRH-FOISTATUS@fda.hhs.gov or 301-796-8118

Records processed under FOIA Request #2014-8015; Released by CDRH on 12-8-2015

Form Approved: OMB No. 0910-0120; Expiration Date: 12/31/13

Department of Health and Human Services
Food and Drug Administration

STANDARDS DATA REPORT FOR 510(k)s

(To be filled in by applicant)

This report and the Summary Report Table are to be completed by the applicant when submitting a 510(k) that references a national or international standard. A separate report is required for each standard referenced in the 510(k).

TYPE OF 510(K) SUBMISSION

☒ Traditional ☐ Special ☐ Abbreviated

STANDARD TITLE [1]

ASTM F2096-11(2011) Standard Test Method for Detecting Gross Leaks in Medical Packaging by Internal Pressurization

Please answer the following questions	Yes	No
Is this standard recognized by FDA [2]?	☒	☐
FDA Recognition number [3]	#14-359	
Was a third party laboratory responsible for testing conformity of the device to this standard identified in the 510(k)?	☒	☐
Is a summary report [4] describing the extent of conformance of the standard used included in the 510(k)? If no, complete a summary report table.	☐	☒
Does the test data for this device demonstrate conformity to the requirements of this standard as it pertains to this device?	☒	☐
Does this standard include acceptance criteria? If no, include the results of testing in the 510(k).	☒	☐
Does this standard include more than one option or selection of tests? If yes, report options selected in the summary report table.	☐	☒
Were there any deviations or adaptations made in the use of the standard?	☐	☒
If yes, were deviations in accordance with the FDA supplemental information sheet (SIS) [5]?	☐	☐
Were deviations or adaptations made beyond what is specified in the FDA SIS? If yes, report these deviations or adaptations in the summary report table.	☐	☒
Were there any exclusions from the standard? If yes, report these exclusions in the summary report table.	☐	☒
Is there an FDA guidance [6] that is associated with this standard?	☐	☒
If yes, was the guidance document followed in preparation of this 510k?	☐	☐

Title of guidance: _____

[1] The formatting convention for the title is: [SDO] [numeric identifier] [title of standard] [date of publication]

[2] Authority [21 U.S.C. 360d], www.fda.gov/cdrh/stdsprog.html

[3] http://www.accessdata.fda.gov/scripts/cdrh/cfdocs/cfStandards/search.cfm

[4] The summary report should include: any adaptations used to adapt to the device under review (for example, alternative test methods); choices made when options or a selection of methods are described; deviations from the standard; requirements not applicable to the device; and the name and address of the test laboratory or certification body involved in conformance assessment to this standard. The summary report includes information on all standards utilized during the development of the device.

[5] The supplemental information sheet (SIS) is additional information which is necessary before FDA recognizes the standard. Found at http://www.accessdata.fda.gov/scripts/cdrh/cfdocs/cfStandards/search.cfm

[6] The online search for CDRH Guidance Documents can be found at www.fda.gov/cdrh/guidance.html

Questions? Contact FDA/CDRH/OCE/DID at CDRH-FOISTATUS@fda.hhs.gov or 301-796-8118

Records processed under FOIA Request #2014-8015; Released by CDRH on 12-8-2015

EXTENT OF STANDARD CONFORMANCE SUMMARY REPORT TABLE

STANDARD TITLE
ASTM F2096-11(2011) Standard Test Method for Detecting Gross Leaks in Medical Packaging by Internal Pressurization

CONFORMANCE WITH STANDARD SECTIONS*

SECTION NUMBER	SECTION TITLE	CONFORMANCE?
All	N/A	☒ Yes ☐ No ☐ N/A

TYPE OF DEVIATION OR OPTION SELECTED ❖
No deviations. All sections of the standard were followed by testing lab. See below for options selected.

DESCRIPTION
Describes the test method for different types of packaging (porous and non-porous).

(b)(4) [redacted]

SECTION NUMBER	SECTION TITLE	CONFORMANCE?
9.	Procedure	☒ Yes ☐ No ☐ N/A

TYPE OF DEVIATION OR OPTION SELECTED ❖
Option selected: Test Method B - Procedure for Porous Packaging

DESCRIPTION
Describes the proper procedure to follow when evaluating porous packaging.

JUSTIFICATION
Tyvek, which is porous, was selected as part of the sterile barrier system.

SECTION NUMBER	SECTION TITLE	CONFORMANCE?
		☐ Yes ☐ No ☐ N/A

TYPE OF DEVIATION OR OPTION SELECTED ❖

DESCRIPTION

JUSTIFICATION

* For completeness list all sections of the standard and indicate whether conformance is met. If a section is not applicable (N/A) an explanation is needed under "justification." Some standards include options, so similar to deviations, the option chosen needs to be described and adequately justified as appropriate for the subject device. Explanation of all deviations or description of options selected when following a standard is required under "type of deviation or option selected," "description" and "justification" on the report. More than one page may be necessary.

❖ Types of deviations can include an exclusion of a section in the standard, a deviation brought out by the FDA supplemental information sheet (SIS), a deviation to adapt the standard to the device, or any adaptation of a section.

Paperwork Reduction Act Statement

Public reporting burden for this collection of information is estimated to average 1 hour per response, including the time for reviewing instructions, searching existing data sources, gathering and maintaining the data needed, and completing and reviewing the collection of information. Send comments regarding this burden estimate or any other aspect of this collection of information, including suggestions for reducing this burden to:

Department of Health and Human Services
Food and Drug Administration
Office of Chief Information Officer
1350 Piccard Drive, Room 400
Rockville, MD 20850

An agency may not conduct or sponsor, and a person is not required to respond to, a collection of information unless it displays a currently valid OMB control number.

Questions? Contact FDA/CDRH/OCE/DID at CDRH-FOISTATUS@fda.hhs.gov or 301-796-8118

Records processed under FOIA Request #2014-8015; Released by CDRH on 12-8-2015

Form Approved: OMB No. 0910-0120; Expiration Date: 12/31/13

Department of Health and Human Services
Food and Drug Administration

STANDARDS DATA REPORT FOR 510(k)s

(To be filled in by applicant)

This report and the Summary Report Table are to be completed by the applicant when submitting a 510(k) that references a national or international standard. A separate report is required for each standard referenced in the 510(k).

TYPE OF 510(K) SUBMISSION

☒ Traditional ☐ Special ☐ Abbreviated

STANDARD TITLE [1]

ASTM F2102-06e1(2006) Standard Guide for Evaluating the Extent of Oxidation in Ultra-High-Molecular-Weight Polyethylene...

Please answer the following questions	Yes	No
Is this standard recognized by FDA [2]?	☒	☐
FDA Recognition number [3]	#8-224	
Was a third party laboratory responsible for testing conformity of the device to this standard identified in the 510(k)?	☒	☐
Is a summary report [4] describing the extent of conformance of the standard used included in the 510(k)? If no, complete a summary report table.	☐	☒
Does the test data for this device demonstrate conformity to the requirements of this standard as it pertains to this device?	☒	☐
Does this standard include acceptance criteria? If no, include the results of testing in the 510(k).	☐	☒
Does this standard include more than one option or selection of tests? If yes, report options selected in the summary report table.	☒	☐
Were there any deviations or adaptations made in the use of the standard?	☐	☒
If yes, were deviations in accordance with the FDA supplemental information sheet (SIS) [5]?	☐	☐
Were deviations or adaptations made beyond what is specified in the FDA SIS? If yes, report these deviations or adaptations in the summary report table.	☐	☒
Were there any exclusions from the standard? If yes, report these exclusions in the summary report table.	☐	☒
Is there an FDA guidance [6] that is associated with this standard?	☐	☒
If yes, was the guidance document followed in preparation of this 510k?	☐	☐

Title of guidance: _____

[1] The formatting convention for the title is: [SDO] [numeric identifier] [title of standard] [date of publication]

[2] Authority [21 U.S.C. 360d], www.fda.gov/cdrh/stdsprog.html

[3] http://www.accessdata.fda.gov/scripts/cdrh/cfdocs/cfStandards/search.cfm

[4] The summary report should include: any adaptations used to adapt to the device under review (for example, alternative test methods); choices made when options or a selection of methods are described; deviations from the standard; requirements not applicable to the device; and the name and address of the test laboratory or certification body involved in conformance assessment to this standard. The summary report includes information on all standards utilized during the development of the device.

[5] The supplemental information sheet (SIS) is additional information which is necessary before FDA recognizes the standard. Found at http://www.accessdata.fda.gov/scripts/cdrh/cfdocs/cfStandards/search.cfm

[6] The online search for CDRH Guidance Documents can be found at www.fda.gov/cdrh/guidance.html

Questions? Contact FDA/CDRH/OCE/DID at CDRH-FOISTATUS@fda.hhs.gov or 301-796-8118

EXTENT OF STANDARD CONFORMANCE SUMMARY REPORT TABLE

STANDARD TITLE
ASTM F2102-06e1(2006) Standard Guide for Evaluating the Extent of Oxidation in Ultra-High-Molecular-Weight Polyethylene...

CONFORMANCE WITH STANDARD SECTIONS*

SECTION NUMBER	SECTION TITLE	CONFORMANCE?
See extra pages		☐ Yes ☐ No ☐ N/A

TYPE OF DEVIATION OR OPTION SELECTED ❖

DESCRIPTION

JUSTIFICATION

SECTION NUMBER	SECTION TITLE	CONFORMANCE?
		☐ Yes ☐ No ☐ N/A

TYPE OF DEVIATION OR OPTION SELECTED ❖

DESCRIPTION

JUSTIFICATION

SECTION NUMBER	SECTION TITLE	CONFORMANCE?
		☐ Yes ☐ No ☐ N/A

TYPE OF DEVIATION OR OPTION SELECTED ❖

DESCRIPTION

JUSTIFICATION

* For completeness list all sections of the standard and indicate whether conformance is met. If a section is not applicable (N/A) an explanation is needed under "justification." Some standards include options, so similar to deviations, the option chosen needs to be described and adequately justified as appropriate for the subject device. Explanation of all deviations or description of options selected when following a standard is required under "type of deviation or option selected," "description" and "justification" on the report. More than one page may be necessary.

❖ Types of deviations can include an exclusion of a section in the standard, a deviation brought out by the FDA supplemental information sheet (SIS), a deviation to adapt the standard to the device, or any adaptation of a section.

Paperwork Reduction Act Statement

Public reporting burden for this collection of information is estimated to average 1 hour per response, including the time for reviewing instructions, searching existing data sources, gathering and maintaining the data needed, and completing and reviewing the collection of information. Send comments regarding this burden estimate or any other aspect of this collection of information, including suggestions for reducing this burden to:

Department of Health and Human Services
Food and Drug Administration
Office of Chief Information Officer
1350 Piccard Drive, Room 400
Rockville, MD 20850

An agency may not conduct or sponsor, and a person is not required to respond to, a collection of information unless it displays a currently valid OMB control number.

Questions? Contact FDA/CDRH/OCE/DID at CDRH-FOISTATUS@fda.hhs.gov or 301-796-8118

Records processed under FOIA Request #2014-8015; Released by CDRH on 12-8-2015

(b)(4)

[redacted]

TEST LABORATORIES INVOLVED WITH CONFORMANCE

(b)(4)

[redacted]

Questions? Contact FDA/CDRH/OCE/DID at CDRH-FOISTATUS@fda.hhs.gov or 301-796-8118

Records processed under FOIA Request #2014-8015; Released by CDRH on 12-8-2015

Form Approved: OMB No. 0910-0120; Expiration Date: 12/31/13

Department of Health and Human Services
Food and Drug Administration

STANDARDS DATA REPORT FOR 510(k)s

(To be filled in by applicant)

This report and the Summary Report Table are to be completed by the applicant when submitting a 510(k) that references a national or international standard. A separate report is required for each standard referenced in the 510(k).

TYPE OF 510(K) SUBMISSION

☒ Traditional ☐ Special ☐ Abbreviated

STANDARD TITLE [1]

ASTM F2183-02(2008) Standard Test Method for Small Punch Testing of Ultra-High Molecular Weight Polyethylene...

Please answer the following questions	Yes	No
Is this standard recognized by FDA [2]?	☒	☐
FDA Recognition number [3]	#8-202	
Was a third party laboratory responsible for testing conformity of the device to this standard identified in the 510(k)?	☒	☐
Is a summary report [4] describing the extent of conformance of the standard used included in the 510(k)? If no, complete a summary report table.	☐	☒
Does the test data for this device demonstrate conformity to the requirements of this standard as it pertains to this device?	☒	☐
Does this standard include acceptance criteria? If no, include the results of testing in the 510(k).	☐	☒
Does this standard include more than one option or selection of tests? If yes, report options selected in the summary report table.	☒	☐
Were there any deviations or adaptations made in the use of the standard?	☒	☐
If yes, were deviations in accordance with the FDA supplemental information sheet (SIS) [5]?	☐	☒
Were deviations or adaptations made beyond what is specified in the FDA SIS? If yes, report these deviations or adaptations in the summary report table.	☐	☒
Were there any exclusions from the standard? If yes, report these exclusions in the summary report table.	☐	☒
Is there an FDA guidance [6] that is associated with this standard?	☐	☒
If yes, was the guidance document followed in preparation of this 510k?	☐	☐

Title of guidance: _____

[1] The formatting convention for the title is: [SDO] [numeric identifier] [title of standard] [date of publication]

[2] Authority [21 U.S.C. 360d], www.fda.gov/cdrh/stdsprog.html

[3] http://www.accessdata.fda.gov/scripts/cdrh/cfdocs/cfStandards/search.cfm

[4] The summary report should include: any adaptations used to adapt to the device under review (for example, alternative test methods); choices made when options or a selection of methods are described; deviations from the standard; requirements not applicable to the device; and the name and address of the test laboratory or certification body involved in conformance assessment to this standard. The summary report includes information on all standards utilized during the development of the device.

[5] The supplemental information sheet (SIS) is additional information which is necessary before FDA recognizes the standard. Found at http://www.accessdata.fda.gov/scripts/cdrh/cfdocs/cfStandards/search.cfm

[6] The online search for CDRH Guidance Documents can be found at www.fda.gov/cdrh/guidance.html

Questions? Contact FDA/CDRH/OCE/DID at CDRH-FOISTATUS@fda.hhs.gov or 301-796-8118

Records processed under FOIA Request #2014-8015; Released by CDRH on 12-8-2015

EXTENT OF STANDARD CONFORMANCE SUMMARY REPORT TABLE

STANDARD TITLE
ASTM F2183-02(2008) Standard Test Method for Small Punch Testing of Ultra-High Molecular Weight Polyethylene...

CONFORMANCE WITH STANDARD SECTIONS*

SECTION NUMBER	SECTION TITLE	CONFORMANCE?
See extra pages		☐ Yes ☐ No ☒ N/A

TYPE OF DEVIATION OR OPTION SELECTED ❖

DESCRIPTION

JUSTIFICATION

SECTION NUMBER	SECTION TITLE	CONFORMANCE?
		☐ Yes ☐ No ☐ N/A

TYPE OF DEVIATION OR OPTION SELECTED ❖

DESCRIPTION

JUSTIFICATION

SECTION NUMBER	SECTION TITLE	CONFORMANCE?
		☐ Yes ☐ No ☐ N/A

TYPE OF DEVIATION OR OPTION SELECTED ❖

DESCRIPTION

JUSTIFICATION

* For completeness list all sections of the standard and indicate whether conformance is met. If a section is not applicable (N/A) an explanation is needed under "justification." Some standards include options, so similar to deviations, the option chosen needs to be described and adequately justified as appropriate for the subject device. Explanation of all deviations or description of options selected when following a standard is required under "type of deviation or option selected," "description" and "justification" on the report. More than one page may be necessary.

❖ Types of deviations can include an exclusion of a section in the standard, a deviation brought out by the FDA supplemental information sheet (SIS), a deviation to adapt the standard to the device, or any adaptation of a section.

Paperwork Reduction Act Statement

Public reporting burden for this collection of information is estimated to average 1 hour per response, including the time for reviewing instructions, searching existing data sources, gathering and maintaining the data needed, and completing and reviewing the collection of information. Send comments regarding this burden estimate or any other aspect of this collection of information, including suggestions for reducing this burden to:

Department of Health and Human Services
Food and Drug Administration
Office of Chief Information Officer
1350 Piccard Drive, Room 400
Rockville, MD 20850

An agency may not conduct or sponsor, and a person is not required to respond to, a collection of information unless it displays a currently valid OMB control number.

Questions? Contact FDA/CDRH/OCE/DID at CDRH-FOISTATUS@fda.hhs.gov or 301-796-8118

Records processed under FOIA Request #2014-8015; Released by CDRH on 12-8-2015

(b)(4)

[redacted]

TEST LABORATORIES INVOLVED WITH CONFORMANCE

(b)(4)

[redacted]

Questions? Contact FDA/CDRH/OCE/DID at CDRH-FOISTATUS@fda.hhs.gov or 301-796-8118

Records processed under FOIA Request #2014-8015; Released by CDRH on 12-8-2015

Form Approved: OMB No. 0910-0120; Expiration Date: 12/31/13

Department of Health and Human Services
Food and Drug Administration

STANDARDS DATA REPORT FOR 510(k)s

(To be filled in by applicant)

This report and the Summary Report Table are to be completed by the applicant when submitting a 510(k) that references a national or international standard. A separate report is required for each standard referenced in the 510(k).

TYPE OF 510(K) SUBMISSION

☒ Traditional ☐ Special ☐ Abbreviated

STANDARD TITLE [1]

ASTM F2214-02(2008) Standard Test Method for In Situ Determination of Network Parameters of Crosslinked Ultra High...

Please answer the following questions	Yes	No
Is this standard recognized by FDA [2]?	☒	☐
FDA Recognition number [3]	#8-201	
Was a third party laboratory responsible for testing conformity of the device to this standard identified in the 510(k)?	☒	☐
Is a summary report [4] describing the extent of conformance of the standard used included in the 510(k)? If no, complete a summary report table.	☐	☒
Does the test data for this device demonstrate conformity to the requirements of this standard as it pertains to this device?	☒	☐
Does this standard include acceptance criteria? If no, include the results of testing in the 510(k).	☐	☒
Does this standard include more than one option or selection of tests? If yes, report options selected in the summary report table.	☒	☐
Were there any deviations or adaptations made in the use of the standard?	☐	☒
If yes, were deviations in accordance with the FDA supplemental information sheet (SIS) [5]?	☐	☐
Were deviations or adaptations made beyond what is specified in the FDA SIS? If yes, report these deviations or adaptations in the summary report table.	☐	☒
Were there any exclusions from the standard? If yes, report these exclusions in the summary report table.	☐	☒
Is there an FDA guidance [6] that is associated with this standard?	☐	☒
If yes, was the guidance document followed in preparation of this 510k?	☐	☐

Title of guidance: _____

[1] The formatting convention for the title is: [SDO] [numeric identifier] [title of standard] [date of publication]

[2] Authority [21 U.S.C. 360d], www.fda.gov/cdrh/stdsprog.html

[3] http://www.accessdata.fda.gov/scripts/cdrh/cfdocs/cfStandards/search.cfm

[4] The summary report should include: any adaptations used to adapt to the device under review (for example, alternative test methods); choices made when options or a selection of methods are described; deviations from the standard; requirements not applicable to the device; and the name and address of the test laboratory or certification body involved in conformance assessment to this standard. The summary report includes information on all standards utilized during the development of the device.

[5] The supplemental information sheet (SIS) is additional information which is necessary before FDA recognizes the standard. Found at http://www.accessdata.fda.gov/scripts/cdrh/cfdocs/cfStandards/search.cfm

[6] The online search for CDRH Guidance Documents can be found at www.fda.gov/cdrh/guidance.html

PSC Graphics (301) 443-6740 EF

Questions? Contact FDA/CDRH/OCE/DID at CDRH-FOISTATUS@fda.hhs.gov or 301-796-8118

Records processed under FOIA Request #2014-8015; Released by CDRH on 12-8-2015

EXTENT OF STANDARD CONFORMANCE SUMMARY REPORT TABLE

STANDARD TITLE
ASTM F2214-02(2008) Standard Test Method for In Situ Determination of Network Parameters of Crosslinked Ultra High...

CONFORMANCE WITH STANDARD SECTIONS*

SECTION NUMBER	SECTION TITLE	CONFORMANCE?
See extra pages		☐ Yes ☐ No ☒ N/A

TYPE OF DEVIATION OR OPTION SELECTED ❖

DESCRIPTION

JUSTIFICATION

SECTION NUMBER	SECTION TITLE	CONFORMANCE?
		☐ Yes ☐ No ☐ N/A

TYPE OF DEVIATION OR OPTION SELECTED ❖

DESCRIPTION

JUSTIFICATION

SECTION NUMBER	SECTION TITLE	CONFORMANCE?
		☐ Yes ☐ No ☐ N/A

TYPE OF DEVIATION OR OPTION SELECTED ❖

DESCRIPTION

JUSTIFICATION

* For completeness list all sections of the standard and indicate whether conformance is met. If a section is not applicable (N/A) an explanation is needed under "justification." Some standards include options, so similar to deviations, the option chosen needs to be described and adequately justified as appropriate for the subject device. Explanation of all deviations or description of options selected when following a standard is required under "type of deviation or option selected," "description" and "justification" on the report. More than one page may be necessary.

❖ Types of deviations can include an exclusion of a section in the standard, a deviation brought out by the FDA supplemental information sheet (SIS), a deviation to adapt the standard to the device, or any adaptation of a section.

Paperwork Reduction Act Statement

Public reporting burden for this collection of information is estimated to average 1 hour per response, including the time for reviewing instructions, searching existing data sources, gathering and maintaining the data needed, and completing and reviewing the collection of information. Send comments regarding this burden estimate or any other aspect of this collection of information, including suggestions for reducing this burden to:

Department of Health and Human Services
Food and Drug Administration
Office of Chief Information Officer
1350 Piccard Drive, Room 400
Rockville, MD 20850

An agency may not conduct or sponsor, and a person is not required to respond to, a collection of information unless it displays a currently valid OMB control number.

Questions? Contact FDA/CDRH/OCE/DID at CDRH-FOISTATUS@fda.hhs.gov or 301-796-8118

Records processed under FOIA Request #2014-8015; Released by CDRH on 12-8-2015

(b)(4)

[redacted]

(b)(4)

[redacted]

TEST LABORATORIES INVOLVED WITH CONFORMANCE

(b)(4)

[redacted]

Questions? Contact FDA/CDRH/OCE/DID at CDRH-FOISTATUS@fda.hhs.gov or 301-796-8118

Records processed under FOIA Request #2014-8015; Released by CDRH on 12-8-2015

Form Approved: OMB No. 0910-0120; Expiration Date: 12/31/13

Department of Health and Human Services
Food and Drug Administration

STANDARDS DATA REPORT FOR 510(k)s

(To be filled in by applicant)

This report and the Summary Report Table are to be completed by the applicant when submitting a 510(k) that references a national or international standard. A separate report is required for each standard referenced in the 510(k).

TYPE OF 510(K) SUBMISSION

☒ Traditional ☐ Special ☐ Abbreviated

STANDARD TITLE [1]

ASTM F2381-10(2010) Standard Test Method for Evaluating Trans-Vinylene Yield in Irradiated Ultra-High-Molecular-Weight...

Please answer the following questions	Yes	No
Is this standard recognized by FDA [2]?	☐	☒
FDA Recognition number [3]	#N/A	
Was a third party laboratory responsible for testing conformity of the device to this standard identified in the 510(k)?	☒	☐
Is a summary report [4] describing the extent of conformance of the standard used included in the 510(k)? If no, complete a summary report table.	☐	☒
Does the test data for this device demonstrate conformity to the requirements of this standard as it pertains to this device?	☒	☐
Does this standard include acceptance criteria? If no, include the results of testing in the 510(k).	☐	☒
Does this standard include more than one option or selection of tests? If yes, report options selected in the summary report table.	☒	☐
Were there any deviations or adaptations made in the use of the standard?	☐	☒
If yes, were deviations in accordance with the FDA supplemental information sheet (SIS) [5]?	☐	☐
Were deviations or adaptations made beyond what is specified in the FDA SIS? If yes, report these deviations or adaptations in the summary report table.	☐	☒
Were there any exclusions from the standard? If yes, report these exclusions in the summary report table.	☐	☒
Is there an FDA guidance [6] that is associated with this standard?	☐	☒
If yes, was the guidance document followed in preparation of this 510k?	☐	☐

Title of guidance: _____

[1] The formatting convention for the title is: [SDO] [numeric identifier] [title of standard] [date of publication]

[2] Authority [21 U.S.C. 360d], www.fda.gov/cdrh/stdsprog.html

[3] http://www.accessdata.fda.gov/scripts/cdrh/cfdocs/cfStandards/search.cfm

[4] The summary report should include: any adaptations used to adapt to the device under review (for example, alternative test methods); choices made when options or a selection of methods are described; deviations from the standard; requirements not applicable to the device; and the name and address of the test laboratory or certification body involved in conformance assessment to this standard. The summary report includes information on all standards utilized during the development of the device.

[5] The supplemental information sheet (SIS) is additional information which is necessary before FDA recognizes the standard. Found at http://www.accessdata.fda.gov/scripts/cdrh/cfdocs/cfStandards/search.cfm

[6] The online search for CDRH Guidance Documents can be found at www.fda.gov/cdrh/guidance.html

Questions? Contact FDA/CDRH/OCE/DID at CDRH-FOISTATUS@fda.hhs.gov or 301-796-8118

Records processed under FOIA Request #2014-8015; Released by CDRH on 12-8-2015

EXTENT OF STANDARD CONFORMANCE SUMMARY REPORT TABLE

STANDARD TITLE
ASTM F2381-10(2010) Standard Test Method for Evaluating Trans-Vinylene Yield in Irradiated Ultra-High-Molecular-Weight...

CONFORMANCE WITH STANDARD SECTIONS*

SECTION NUMBER	SECTION TITLE	CONFORMANCE?
See extra pages		☐ Yes ☐ No ☒ N/A

TYPE OF DEVIATION OR OPTION SELECTED ❖

DESCRIPTION

JUSTIFICATION

SECTION NUMBER	SECTION TITLE	CONFORMANCE?
		☐ Yes ☐ No ☐ N/A

TYPE OF DEVIATION OR OPTION SELECTED ❖

DESCRIPTION

JUSTIFICATION

SECTION NUMBER	SECTION TITLE	CONFORMANCE?
		☐ Yes ☐ No ☐ N/A

TYPE OF DEVIATION OR OPTION SELECTED ❖

DESCRIPTION

JUSTIFICATION

* For completeness list all sections of the standard and indicate whether conformance is met. If a section is not applicable (N/A) an explanation is needed under "justification." Some standards include options, so similar to deviations, the option chosen needs to be described and adequately justified as appropriate for the subject device. Explanation of all deviations or description of options selected when following a standard is required under "type of deviation or option selected," "description" and "justification" on the report. More than one page may be necessary.

❖ Types of deviations can include an exclusion of a section in the standard, a deviation brought out by the FDA supplemental information sheet (SIS), a deviation to adapt the standard to the device, or any adaptation of a section.

Paperwork Reduction Act Statement

Public reporting burden for this collection of information is estimated to average 1 hour per response, including the time for reviewing instructions, searching existing data sources, gathering and maintaining the data needed, and completing and reviewing the collection of information. Send comments regarding this burden estimate or any other aspect of this collection of information, including suggestions for reducing this burden to:

Department of Health and Human Services
Food and Drug Administration
Office of Chief Information Officer
1350 Piccard Drive, Room 400
Rockville, MD 20850

An agency may not conduct or sponsor, and a person is not required to respond to, a collection of information unless it displays a currently valid OMB control number.

Questions? Contact FDA/CDRH/OCE/DID at CDRH-FOISTATUS@fda.hhs.gov or 301-796-8118

Records processed under FOIA Request #2014-8015; Released by CDRH on 12-8-2015

(b)(4)

[redacted]

TEST LABORATORIES INVOLVED WITH CONFORMANCE

(b)(4)

[redacted]

Questions? Contact FDA/CDRH/OCE/DID at CDRH-FOISTATUS@fda.hhs.gov or 301-796-8118

Records processed under FOIA Request #2014-8015; Released by CDRH on 12-8-2015

Form Approved: OMB No. 0910-0120; Expiration Date: 12/31/13

Department of Health and Human Services
Food and Drug Administration

STANDARDS DATA REPORT FOR 510(k)s

(To be filled in by applicant)

This report and the Summary Report Table are to be completed by the applicant when submitting a 510(k) that references a national or international standard. A separate report is required for each standard referenced in the 510(k).

TYPE OF 510(K) SUBMISSION

☒ Traditional ☐ Special ☐ Abbreviated

STANDARD TITLE [1]

ASTM F2565-06(2006) Standard Guide for Extensively Irradiation-Crosslinked Ultra-High Molecular Weight Polyethylene...

Please answer the following questions	Yes	No
Is this standard recognized by FDA [2]?	☐	☒
FDA Recognition number [3]	#N/A	
Was a third party laboratory responsible for testing conformity of the device to this standard identified in the 510(k)?	☒	☐
Is a summary report [4] describing the extent of conformance of the standard used included in the 510(k)? If no, complete a summary report table.	☐	☒
Does the test data for this device demonstrate conformity to the requirements of this standard as it pertains to this device?	☒	☐
Does this standard include acceptance criteria? If no, include the results of testing in the 510(k).	☐	☒
Does this standard include more than one option or selection of tests? If yes, report options selected in the summary report table.	☒	☐
Were there any deviations or adaptations made in the use of the standard?	☒	☐
If yes, were deviations in accordance with the FDA supplemental information sheet (SIS) [5]?	☒	☐
Were deviations or adaptations made beyond what is specified in the FDA SIS? If yes, report these deviations or adaptations in the summary report table.	☐	☒
Were there any exclusions from the standard? If yes, report these exclusions in the summary report table.	☐	☒
Is there an FDA guidance [6] that is associated with this standard?	☐	☒
If yes, was the guidance document followed in preparation of this 510k?	☐	☐

Title of guidance: _____

[1] The formatting convention for the title is: [SDO] [numeric identifier] [title of standard] [date of publication]

[2] Authority [21 U.S.C. 360d], www.fda.gov/cdrh/stdsprog.html

[3] http://www.accessdata.fda.gov/scripts/cdrh/cfdocs/cfStandards/search.cfm

[4] The summary report should include: any adaptations used to adapt to the device under review (for example, alternative test methods); choices made when options or a selection of methods are described; deviations from the standard; requirements not applicable to the device; and the name and address of the test laboratory or certification body involved in conformance assessment to this standard. The summary report includes information on all standards utilized during the development of the device.

[5] The supplemental information sheet (SIS) is additional information which is necessary before FDA recognizes the standard. Found at http://www.accessdata.fda.gov/scripts/cdrh/cfdocs/cfStandards/search.cfm

[6] The online search for CDRH Guidance Documents can be found at www.fda.gov/cdrh/guidance.html

Questions? Contact FDA/CDRH/OCE/DID at CDRH-FOISTATUS@fda.hhs.gov or 301-796-8118

EXTENT OF STANDARD CONFORMANCE SUMMARY REPORT TABLE

STANDARD TITLE
ASTM F2565-06(2006) Standard Guide for Extensively Irradiation-Crosslinked Ultra-High Molecular Weight Polyethylene...

CONFORMANCE WITH STANDARD SECTIONS*

SECTION NUMBER	SECTION TITLE	CONFORMANCE?
See extra pages		☐ Yes ☐ No ☒ N/A

TYPE OF DEVIATION OR OPTION SELECTED ❖

DESCRIPTION

JUSTIFICATION

SECTION NUMBER	SECTION TITLE	CONFORMANCE?
		☐ Yes ☐ No ☐ N/A

TYPE OF DEVIATION OR OPTION SELECTED ❖

DESCRIPTION

JUSTIFICATION

SECTION NUMBER	SECTION TITLE	CONFORMANCE?
		☐ Yes ☐ No ☐ N/A

TYPE OF DEVIATION OR OPTION SELECTED ❖

DESCRIPTION

JUSTIFICATION

* For completeness list all sections of the standard and indicate whether conformance is met. If a section is not applicable (N/A) an explanation is needed under "justification." Some standards include options, so similar to deviations, the option chosen needs to be described and adequately justified as appropriate for the subject device. Explanation of all deviations or description of options selected when following a standard is required under "type of deviation or option selected," "description" and "justification" on the report. More than one page may be necessary.

❖ Types of deviations can include an exclusion of a section in the standard, a deviation brought out by the FDA supplemental information sheet (SIS), a deviation to adapt the standard to the device, or any adaptation of a section.

Paperwork Reduction Act Statement

Public reporting burden for this collection of information is estimated to average 1 hour per response, including the time for reviewing instructions, searching existing data sources, gathering and maintaining the data needed, and completing and reviewing the collection of information. Send comments regarding this burden estimate or any other aspect of this collection of information, including suggestions for reducing this burden to:

Department of Health and Human Services
Food and Drug Administration
Office of Chief Information Officer
1350 Piccard Drive, Room 400
Rockville, MD 20850

An agency may not conduct or sponsor, and a person is not required to respond to, a collection of information unless it displays a currently valid OMB control number.

Questions? Contact FDA/CDRH/OCE/DID at CDRH-FOISTATUS@fda.hhs.gov or 301-796-8118

Records processed under FOIA Request #2014-8015; Released by CDRH on 12-8-2015

(b)(4)

[redacted]

Questions? Contact FDA/CDRH/OCE/DID at CDRH-FOISTATUS@fda.hhs.gov or 301-796-8118

Records processed under FOIA Request #2014-8015; Released by CDRH on 12-8-2015

SECTION #	SECTION TITLE	CONFORMANCE?
6	Biocompatibility	☒ Yes ☐ No ☐ N/A

TYPE OF DEVIATION OR OPTION SELECTED

Option: No additional biocompatibility testing

DESCRIPTION

No additional biocompatibility testing was done from the standards and practices listed in Section 6.

JUSTIFICATION

Biocompatibility has been addressed under Section 15 of this 510(k) submission.

TEST LABORATORIES INVOLVED WITH CONFORMANCE

(b)(4)

[redacted]

Questions? Contact FDA/CDRH/OCE/DID at CDRH-FOISTATUS@fda.hhs.gov or 301-796-8118

Records processed under FOIA Request #2014-8015; Released by CDRH on 12-8-2015

Form Approved: OMB No. 0910-0120; Expiration Date: 12/31/13

Department of Health and Human Services
Food and Drug Administration

STANDARDS DATA REPORT FOR 510(k)s

(To be filled in by applicant)

This report and the Summary Report Table are to be completed by the applicant when submitting a 510(k) that references a national or international standard. A separate report is required for each standard referenced in the 510(k).

TYPE OF 510(K) SUBMISSION

☒ Traditional ☐ Special ☐ Abbreviated

STANDARD TITLE [1]

ASTM F2625-10(2010) Standard Test Method for Measurement of Enthalpy of Fusion, Percent Crystallinity, and Melting Point of...

Please answer the following questions	Yes	No
Is this standard recognized by FDA [2]?	☒	☐
FDA Recognition number [3]	#N/A	
Was a third party laboratory responsible for testing conformity of the device to this standard identified in the 510(k)?	☒	☐
Is a summary report [4] describing the extent of conformance of the standard used included in the 510(k)? If no, complete a summary report table.	☐	☒
Does the test data for this device demonstrate conformity to the requirements of this standard as it pertains to this device?	☒	☐
Does this standard include acceptance criteria? If no, include the results of testing in the 510(k).	☐	☒
Does this standard include more than one option or selection of tests? If yes, report options selected in the summary report table.	☒	☐
Were there any deviations or adaptations made in the use of the standard?	☐	☒
If yes, were deviations in accordance with the FDA supplemental information sheet (SIS) [5]?	☐	☐
Were deviations or adaptations made beyond what is specified in the FDA SIS? If yes, report these deviations or adaptations in the summary report table.	☐	☒
Were there any exclusions from the standard? If yes, report these exclusions in the summary report table.	☐	☒
Is there an FDA guidance [6] that is associated with this standard?	☐	☒
If yes, was the guidance document followed in preparation of this 510k?	☐	☐

Title of guidance: _____

[1] The formatting convention for the title is: [SDO] [numeric identifier] [title of standard] [date of publication]

[2] Authority [21 U.S.C. 360d], www.fda.gov/cdrh/stdsprog.html

[3] http://www.accessdata.fda.gov/scripts/cdrh/cfdocs/cfStandards/search.cfm

[4] The summary report should include: any adaptations used to adapt to the device under review (for example, alternative test methods); choices made when options or a selection of methods are described; deviations from the standard; requirements not applicable to the device; and the name and address of the test laboratory or certification body involved in conformance assessment to this standard. The summary report includes information on all standards utilized during the development of the device.

[5] The supplemental information sheet (SIS) is additional information which is necessary before FDA recognizes the standard. Found at http://www.accessdata.fda.gov/scripts/cdrh/cfdocs/cfStandards/search.cfm

[6] The online search for CDRH Guidance Documents can be found at www.fda.gov/cdrh/guidance.html

Questions? Contact FDA/CDRH/OCE/DID at CDRH-FOISTATUS@fda.hhs.gov or 301-796-8118

EXTENT OF STANDARD CONFORMANCE SUMMARY REPORT TABLE

STANDARD TITLE
ASTM F2625-10(2010) Standard Test Method for Measurement of Enthalpy of Fusion, Percent Crystallinity, and Melting Point of...

CONFORMANCE WITH STANDARD SECTIONS*

SECTION NUMBER	SECTION TITLE	CONFORMANCE?
See extra pages		☐ Yes ☐ No ☒ N/A

TYPE OF DEVIATION OR OPTION SELECTED ❖

DESCRIPTION

JUSTIFICATION

SECTION NUMBER	SECTION TITLE	CONFORMANCE?
		☐ Yes ☐ No ☐ N/A

TYPE OF DEVIATION OR OPTION SELECTED ❖

DESCRIPTION

JUSTIFICATION

SECTION NUMBER	SECTION TITLE	CONFORMANCE?
		☐ Yes ☐ No ☐ N/A

TYPE OF DEVIATION OR OPTION SELECTED ❖

DESCRIPTION

JUSTIFICATION

* For completeness list all sections of the standard and indicate whether conformance is met. If a section is not applicable (N/A) an explanation is needed under "justification." Some standards include options, so similar to deviations, the option chosen needs to be described and adequately justified as appropriate for the subject device. Explanation of all deviations or description of options selected when following a standard is required under "type of deviation or option selected," "description" and "justification" on the report. More than one page may be necessary.

❖ Types of deviations can include an exclusion of a section in the standard, a deviation brought out by the FDA supplemental information sheet (SIS), a deviation to adapt the standard to the device, or any adaptation of a section.

Paperwork Reduction Act Statement

Public reporting burden for this collection of information is estimated to average 1 hour per response, including the time for reviewing instructions, searching existing data sources, gathering and maintaining the data needed, and completing and reviewing the collection of information. Send comments regarding this burden estimate or any other aspect of this collection of information, including suggestions for reducing this burden to:

Department of Health and Human Services
Food and Drug Administration
Office of Chief Information Officer
1350 Piccard Drive, Room 400
Rockville, MD 20850

An agency may not conduct or sponsor, and a person is not required to respond to, a collection of information unless it displays a currently valid OMB control number.

Questions? Contact FDA/CDRH/OCE/DID at CDRH-FOISTATUS@fda.hhs.gov or 301-796-8118

Records processed under FOIA Request #2014-8015; Released by CDRH on 12-8-2015

(b)(4)

[redacted]

TEST LABORATORIES INVOLVED WITH CONFORMANCE

(b)(4)

[redacted]

Questions? Contact FDA/CDRH/OCE/DID at CDRH-FOISTATUS@fda.hhs.gov or 301-796-8118

Records processed under FOIA Request #2014-8015; Released by CDRH on 12-8-2015

Form Approved: OMB No. 0910-0120; Expiration Date: 12/31/13

Department of Health and Human Services
Food and Drug Administration

STANDARDS DATA REPORT FOR 510(k)s

(To be filled in by applicant)

This report and the Summary Report Table are to be completed by the applicant when submitting a 510(k) that references a national or international standard. A separate report is required for each standard referenced in the 510(k).

TYPE OF 510(K) SUBMISSION

☒ Traditional ☐ Special ☐ Abbreviated

STANDARD TITLE [1]

ISO 10993-5(2009) Biological evaluation of medical devices - Part 5: Tests for in vitro cytotoxicity

Please answer the following questions	Yes	No
Is this standard recognized by FDA [2]?	☒	☐
FDA Recognition number [3]	#2-153	
Was a third party laboratory responsible for testing conformity of the device to this standard identified in the 510(k)?	☒	☐
Is a summary report [4] describing the extent of conformance of the standard used included in the 510(k)? If no, complete a summary report table.	☐	☒
Does the test data for this device demonstrate conformity to the requirements of this standard as it pertains to this device?	☒	☐
Does this standard include acceptance criteria? If no, include the results of testing in the 510(k).	☒	☐
Does this standard include more than one option or selection of tests? If yes, report options selected in the summary report table.	☒	☐
Were there any deviations or adaptations made in the use of the standard?	☐	☒
If yes, were deviations in accordance with the FDA supplemental information sheet (SIS) [5]?	☐	☐
Were deviations or adaptations made beyond what is specified in the FDA SIS? If yes, report these deviations or adaptations in the summary report table.	☐	☒
Were there any exclusions from the standard? If yes, report these exclusions in the summary report table.	☐	☒
Is there an FDA guidance [6] that is associated with this standard?	☐	☒
If yes, was the guidance document followed in preparation of this 510k?	☐	☐

Title of guidance: _____

[1] The formatting convention for the title is: [SDO] [numeric identifier] [title of standard] [date of publication]

[2] Authority [21 U.S.C. 360d], www.fda.gov/cdrh/stdsprog.html

[3] http://www.accessdata.fda.gov/scripts/cdrh/cfdocs/cfStandards/search.cfm

[4] The summary report should include: any adaptations used to adapt to the device under review (for example, alternative test methods); choices made when options or a selection of methods are described; deviations from the standard; requirements not applicable to the device; and the name and address of the test laboratory or certification body involved in conformance assessment to this standard. The summary report includes information on all standards utilized during the development of the device.

[5] The supplemental information sheet (SIS) is additional information which is necessary before FDA recognizes the standard. Found at http://www.accessdata.fda.gov/scripts/cdrh/cfdocs/cfStandards/search.cfm

[6] The online search for CDRH Guidance Documents can be found at www.fda.gov/cdrh/guidance.html

Questions? Contact FDA/CDRH/OCE/DID at CDRH-FOISTATUS@fda.hhs.gov or 301-796-8118

Records processed under FOIA Request #2014-8015; Released by CDRH on 12-8-2015

EXTENT OF STANDARD CONFORMANCE SUMMARY REPORT TABLE

STANDARD TITLE
ISO 10993-5(2009) Biological evaluation of medical devices - Part 5: Tests for in vitro cytotoxicity

CONFORMANCE WITH STANDARD SECTIONS*

(b)(4)

[redacted]

DESCRIPTION
n/a

JUSTIFICATION
Test is both qualitative and quantitative.

SECTION NUMBER	SECTION TITLE	CONFORMANCE?
4.2.2	Extraction vehicles	☒ Yes ☐ No ☐ N/A

TYPE OF DEVIATION OR OPTION SELECTED ❖
Culture medium with serum

DESCRIPTION
n/a

JUSTIFICATION
This is the preferred extraction vehicle due to it being able to support cellular growth and extract polar and non-polar substances.

(b)(4)

[redacted]

* For completeness list all sections of the standard and indicate whether conformance is met. If a section is not applicable (N/A) an explanation is needed under "justification." Some standards include options, so similar to deviations, the option chosen needs to be described and adequately justified as appropriate for the subject device. Explanation of all deviations or description of options selected when following a standard is required under "type of deviation or option selected," "description" and "justification" on the report. More than one page may be necessary.

❖ Types of deviations can include an exclusion of a section in the standard, a deviation brought out by the FDA supplemental information sheet (SIS), a deviation to adapt the standard to the device, or any adaptation of a section.

Paperwork Reduction Act Statement

Public reporting burden for this collection of information is estimated to average 1 hour per response, including the time for reviewing instructions, searching existing data sources, gathering and maintaining the data needed, and completing and reviewing the collection of information. Send comments regarding this burden estimate or any other aspect of this collection of information, including suggestions for reducing this burden to:

Department of Health and Human Services
Food and Drug Administration
Office of Chief Information Officer
1350 Piccard Drive, Room 400
Rockville, MD 20850

An agency may not conduct or sponsor, and a person is not required to respond to, a collection of information unless it displays a currently valid OMB control number.

Questions? Contact FDA/CDRH/OCE/DID at CDRH-FOISTATUS@fda.hhs.gov or 301-796-8118

Records processed under FOIA Request #2014-8015; Released by CDRH on 12-8-2015

Form Approved: OMB No. 0910-0120; Expiration Date: 12/31/13

Department of Health and Human Services
Food and Drug Administration

STANDARDS DATA REPORT FOR 510(k)s

(To be filled in by applicant)

This report and the Summary Report Table are to be completed by the applicant when submitting a 510(k) that references a national or international standard. A separate report is required for each standard referenced in the 510(k).

TYPE OF 510(K) SUBMISSION

☒ Traditional ☐ Special ☐ Abbreviated

STANDARD TITLE [1]

ISO 10993-6(2007) Biological Evaluation of medical devices - Part 6: Tests for local effects after implantation

Please answer the following questions	Yes	No
Is this standard recognized by FDA [2]?	☒	☐
FDA Recognition number [3]	#2-120	
Was a third party laboratory responsible for testing conformity of the device to this standard identified in the 510(k)?	☒	☐
Is a summary report [4] describing the extent of conformance of the standard used included in the 510(k)? If no, complete a summary report table.	☐	☒
Does the test data for this device demonstrate conformity to the requirements of this standard as it pertains to this device?	☒	☐
Does this standard include acceptance criteria? If no, include the results of testing in the 510(k).	☒	☐
Does this standard include more than one option or selection of tests? If yes, report options selected in the summary report table.	☒	☐
Were there any deviations or adaptations made in the use of the standard?	☐	☒
If yes, were deviations in accordance with the FDA supplemental information sheet (SIS) [5]?	☐	☐
Were deviations or adaptations made beyond what is specified in the FDA SIS? If yes, report these deviations or adaptations in the summary report table.	☐	☒
Were there any exclusions from the standard? If yes, report these exclusions in the summary report table.	☐	☒
Is there an FDA guidance [6] that is associated with this standard?	☐	☒
If yes, was the guidance document followed in preparation of this 510k?	☐	☐

Title of guidance: _____

[1] The formatting convention for the title is: [SDO] [numeric identifier] [title of standard] [date of publication]

[2] Authority [21 U.S.C. 360d], www.fda.gov/cdrh/stdsprog.html

[3] http://www.accessdata.fda.gov/scripts/cdrh/cfdocs/cfStandards/search.cfm

[4] The summary report should include: any adaptations used to adapt to the device under review (for example, alternative test methods); choices made when options or a selection of methods are described; deviations from the standard; requirements not applicable to the device; and the name and address of the test laboratory or certification body involved in conformance assessment to this standard. The summary report includes information on all standards utilized during the development of the device.

[5] The supplemental information sheet (SIS) is additional information which is necessary before FDA recognizes the standard. Found at http://www.accessdata.fda.gov/scripts/cdrh/cfdocs/cfStandards/search.cfm

[6] The online search for CDRH Guidance Documents can be found at www.fda.gov/cdrh/guidance.html

Questions? Contact FDA/CDRH/OCE/DID at CDRH-FOISTATUS@fda.hhs.gov or 301-796-8118

Records processed under FOIA Request #2014-8015; Released by CDRH on 12-8-2015

EXTENT OF STANDARD CONFORMANCE
SUMMARY REPORT TABLE

STANDARD TITLE

ISO 10993-6(2007) Biological Evaluation of medical devices - Part 6: Tests for local effects after implantation

CONFORMANCE WITH STANDARD SECTIONS*

(b)(4)

[redacted]

* For completeness list all sections of the standard and indicate whether conformance is met. If a section is not applicable (N/A) an explanation is needed under "justification." Some standards include options, so similar to deviations, the option chosen needs to be described and adequately justified as appropriate for the subject device. Explanation of all deviations or description of options selected when following a standard is required under "type of deviation or option selected," "description" and "justification" on the report. More than one page may be necessary.

❖ Types of deviations can include an exclusion of a section in the standard, a deviation brought out by the FDA supplemental information sheet (SIS), a deviation to adapt the standard to the device, or any adaptation of a section.

Paperwork Reduction Act Statement

Public reporting burden for this collection of information is estimated to average 1 hour per response, including the time for reviewing instructions, searching existing data sources, gathering and maintaining the data needed, and completing and reviewing the collection of information. Send comments regarding this burden estimate or any other aspect of this collection of information, including suggestions for reducing this burden to:

Department of Health and Human Services
Food and Drug Administration
Office of Chief Information Officer
1350 Piccard Drive, Room 400
Rockville, MD 20850

An agency may not conduct or sponsor, and a person is not required to respond to, a collection of information unless it displays a currently valid OMB control number.

Questions? Contact FDA/CDRH/OCE/DID at CDRH-FOISTATUS@fda.hhs.gov or 301-796-8118

Records processed under FOIA Request #2014-8015; Released by CDRH on 12-8-2015

Form Approved: OMB No. 0910-0120; Expiration Date: 12/31/13

Department of Health and Human Services
Food and Drug Administration

STANDARDS DATA REPORT FOR 510(k)s

(To be filled in by applicant)

This report and the Summary Report Table are to be completed by the applicant when submitting a 510(k) that references a national or international standard. A separate report is required for each standard referenced in the 510(k).

TYPE OF 510(K) SUBMISSION

☒ Traditional ☐ Special ☐ Abbreviated

STANDARD TITLE [1]

ISO 10993-7(2008) Biological evaluation of medical devices - Part 7: Ethylene oxide sterilization residuals

Please answer the following questions	Yes	No
Is this standard recognized by FDA [2]?	☒	☐
FDA Recognition number [3]	#14-335	
Was a third party laboratory responsible for testing conformity of the device to this standard identified in the 510(k)?	☒	☐
Is a summary report [4] describing the extent of conformance of the standard used included in the 510(k)? If no, complete a summary report table.	☐	☒
Does the test data for this device demonstrate conformity to the requirements of this standard as it pertains to this device?	☒	☐
Does this standard include acceptance criteria? If no, include the results of testing in the 510(k).	☒	☐
Does this standard include more than one option or selection of tests? If yes, report options selected in the summary report table.	☐	☒
Were there any deviations or adaptations made in the use of the standard?	☐	☒
If yes, were deviations in accordance with the FDA supplemental information sheet (SIS) [5]?	☐	☐
Were deviations or adaptations made beyond what is specified in the FDA SIS? If yes, report these deviations or adaptations in the summary report table.	☐	☒
Were there any exclusions from the standard? If yes, report these exclusions in the summary report table.	☐	☒
Is there an FDA guidance [6] that is associated with this standard?	☐	☒
If yes, was the guidance document followed in preparation of this 510k?	☐	☐

Title of guidance: _____

[1] The formatting convention for the title is: [SDO] [numeric identifier] [title of standard] [date of publication]

[2] Authority [21 U.S.C. 360d], www.fda.gov/cdrh/stdsprog.html

[3] http://www.accessdata.fda.gov/scripts/cdrh/cfdocs/cfStandards/search.cfm

[4] The summary report should include: any adaptations used to adapt to the device under review (for example, alternative test methods); choices made when options or a selection of methods are described; deviations from the standard; requirements not applicable to the device; and the name and address of the test laboratory or certification body involved in conformance assessment to this standard. The summary report includes information on all standards utilized during the development of the device.

[5] The supplemental information sheet (SIS) is additional information which is necessary before FDA recognizes the standard. Found at http://www.accessdata.fda.gov/scripts/cdrh/cfdocs/cfStandards/search.cfm

[6] The online search for CDRH Guidance Documents can be found at www.fda.gov/cdrh/guidance.html

Questions? Contact FDA/CDRH/OCE/DID at CDRH-FOISTATUS@fda.hhs.gov or 301-796-8118

Records processed under FOIA Request #2014-8015; Released by CDRH on 12-8-2015

EXTENT OF STANDARD CONFORMANCE SUMMARY REPORT TABLE

STANDARD TITLE
ISO 10993-7(2008) Biological evaluation of medical devices - Part 7: Ethylene oxide sterilization residuals

CONFORMANCE WITH STANDARD SECTIONS*

SECTION NUMBER	SECTION TITLE	CONFORMANCE?
All		☒ Yes ☐ No ☐ N/A

TYPE OF DEVIATION OR OPTION SELECTED ❖
n/a

DESCRIPTION
This standard was followed.

JUSTIFICATION
n/a

SECTION NUMBER	SECTION TITLE	CONFORMANCE?
		☐ Yes ☐ No ☐ N/A

TYPE OF DEVIATION OR OPTION SELECTED ❖

DESCRIPTION

JUSTIFICATION

SECTION NUMBER	SECTION TITLE	CONFORMANCE?
		☐ Yes ☐ No ☐ N/A

TYPE OF DEVIATION OR OPTION SELECTED ❖

DESCRIPTION

JUSTIFICATION

* For completeness list all sections of the standard and indicate whether conformance is met. If a section is not applicable (N/A) an explanation is needed under "justification." Some standards include options, so similar to deviations, the option chosen needs to be described and adequately justified as appropriate for the subject device. Explanation of all deviations or description of options selected when following a standard is required under "type of deviation or option selected," "description" and "justification" on the report. More than one page may be necessary.

❖ Types of deviations can include an exclusion of a section in the standard, a deviation brought out by the FDA supplemental information sheet (SIS), a deviation to adapt the standard to the device, or any adaptation of a section.

Paperwork Reduction Act Statement

Public reporting burden for this collection of information is estimated to average 1 hour per response, including the time for reviewing instructions, searching existing data sources, gathering and maintaining the data needed, and completing and reviewing the collection of information. Send comments regarding this burden estimate or any other aspect of this collection of information, including suggestions for reducing this burden to:

Department of Health and Human Services
Food and Drug Administration
Office of Chief Information Officer
1350 Piccard Drive, Room 400
Rockville, MD 20850

An agency may not conduct or sponsor, and a person is not required to respond to, a collection of information unless it displays a currently valid OMB control number.

Questions? Contact FDA/CDRH/OCE/DID at CDRH-FOISTATUS@fda.hhs.gov or 301-796-8118

Records processed under FOIA Request #2014-8015; Released by CDRH on 12-8-2015

Form Approved: OMB No. 0910-0120; Expiration Date: 12/31/13

Department of Health and Human Services
Food and Drug Administration

STANDARDS DATA REPORT FOR 510(k)s

(To be filled in by applicant)

This report and the Summary Report Table are to be completed by the applicant when submitting a 510(k) that references a national or international standard. A separate report is required for each standard referenced in the 510(k).

TYPE OF 510(K) SUBMISSION

☒ Traditional ☐ Special ☐ Abbreviated

STANDARD TITLE [1]

ISO 10993-10(2010) Biological evaluation of medical devices - Part 10: Tests for irritation and skin sensitization

Please answer the following questions	Yes	No
Is this standard recognized by FDA [2]?	☒	☐
FDA Recognition number [3]	#2-152	
Was a third party laboratory responsible for testing conformity of the device to this standard identified in the 510(k)?	☒	☐
Is a summary report [4] describing the extent of conformance of the standard used included in the 510(k)? If no, complete a summary report table.	☐	☒
Does the test data for this device demonstrate conformity to the requirements of this standard as it pertains to this device?	☒	☐
Does this standard include acceptance criteria? If no, include the results of testing in the 510(k).	☒	☐
Does this standard include more than one option or selection of tests? If yes, report options selected in the summary report table.	☒	☐
Were there any deviations or adaptations made in the use of the standard?	☐	☒
If yes, were deviations in accordance with the FDA supplemental information sheet (SIS) [5]?	☐	☐
Were deviations or adaptations made beyond what is specified in the FDA SIS? If yes, report these deviations or adaptations in the summary report table.	☐	☒
Were there any exclusions from the standard? If yes, report these exclusions in the summary report table.	☐	☒
Is there an FDA guidance [6] that is associated with this standard?	☐	☒
If yes, was the guidance document followed in preparation of this 510k?	☐	☐

Title of guidance: _____

[1] The formatting convention for the title is: [SDO] [numeric identifier] [title of standard] [date of publication]

[2] Authority [21 U.S.C. 360d], www.fda.gov/cdrh/stdsprog.html

[3] http://www.accessdata.fda.gov/scripts/cdrh/cfdocs/cfStandards/search.cfm

[4] The summary report should include: any adaptations used to adapt to the device under review (for example, alternative test methods); choices made when options or a selection of methods are described; deviations from the standard; requirements not applicable to the device; and the name and address of the test laboratory or certification body involved in conformance assessment to this standard. The summary report includes information on all standards utilized during the development of the device.

[5] The supplemental information sheet (SIS) is additional information which is necessary before FDA recognizes the standard. Found at http://www.accessdata.fda.gov/scripts/cdrh/cfdocs/cfStandards/search.cfm

[6] The online search for CDRH Guidance Documents can be found at www.fda.gov/cdrh/guidance.html

PSC Graphics (301) 443-6740 EF

Questions? Contact FDA/CDRH/OCE/DID at CDRH-FOISTATUS@fda.hhs.gov or 301-796-8118

Records processed under FOIA Request #2014-8015; Released by CDRH on 12-8-2015

EXTENT OF STANDARD CONFORMANCE SUMMARY REPORT TABLE

STANDARD TITLE
ISO 10993-10(2010) Biological evaluation of medical devices - Part 10: Tests for irritation and skin sensitization

CONFORMANCE WITH STANDARD SECTIONS*

SECTION NUMBER	SECTION TITLE	CONFORMANCE?
5.4	Animal intracutaneous (intradermal) reactivity test	☒ Yes ☐ No ☐ N/A

TYPE OF DEVIATION OR OPTION SELECTED ❖
Intracutaneous reactivity was chosen.

DESCRIPTION
This standard was followed.

JUSTIFICATION
Testing was performed for an implant.

SECTION NUMBER	SECTION TITLE	CONFORMANCE?
7	Skin sensitization tests	☒ Yes ☐ No ☐ N/A

TYPE OF DEVIATION OR OPTION SELECTED ❖
Guinea pig maximization (Magnusson-Kligman) test was chosen.

DESCRIPTION
This standard was followed.

JUSTIFICATION
The guinea pig maximization is the most sensitive of the sensitization tests.

SECTION NUMBER	SECTION TITLE	CONFORMANCE?
		☐ Yes ☐ No ☐ N/A

TYPE OF DEVIATION OR OPTION SELECTED ❖

DESCRIPTION

JUSTIFICATION

* For completeness list all sections of the standard and indicate whether conformance is met. If a section is not applicable (N/A) an explanation is needed under "justification." Some standards include options, so similar to deviations, the option chosen needs to be described and adequately justified as appropriate for the subject device. Explanation of all deviations or description of options selected when following a standard is required under "type of deviation or option selected," "description" and "justification" on the report. More than one page may be necessary.

❖ Types of deviations can include an exclusion of a section in the standard, a deviation brought out by the FDA supplemental information sheet (SIS), a deviation to adapt the standard to the device, or any adaptation of a section.

Paperwork Reduction Act Statement

Public reporting burden for this collection of information is estimated to average 1 hour per response, including the time for reviewing instructions, searching existing data sources, gathering and maintaining the data needed, and completing and reviewing the collection of information. Send comments regarding this burden estimate or any other aspect of this collection of information, including suggestions for reducing this burden to:

Department of Health and Human Services
Food and Drug Administration
Office of Chief Information Officer
1350 Piccard Drive, Room 400
Rockville, MD 20850

An agency may not conduct or sponsor, and a person is not required to respond to, a collection of information unless it displays a currently valid OMB control number.

Questions? Contact FDA/CDRH/OCE/DID at CDRH-FOISTATUS@fda.hhs.gov or 301-796-8118

Records processed under FOIA Request #2014-8015; Released by CDRH on 12-8-2015

Form Approved: OMB No. 0910-0120; Expiration Date: 12/31/13

Department of Health and Human Services
Food and Drug Administration

STANDARDS DATA REPORT FOR 510(k)s

(To be filled in by applicant)

This report and the Summary Report Table are to be completed by the applicant when submitting a 510(k) that references a national or international standard. A separate report is required for each standard referenced in the 510(k).

TYPE OF 510(K) SUBMISSION

☒ Traditional ☐ Special ☐ Abbreviated

STANDARD TITLE [1]

ISO 11135-1(2007) Sterilization of health care products - Ethylene oxide - Part 1: Requirements for development, validation...

Please answer the following questions	Yes	No
Is this standard recognized by FDA [2]?	☒	☐
FDA Recognition number [3]	#14-228	
Was a third party laboratory responsible for testing conformity of the device to this standard identified in the 510(k)?	☒	☐
Is a summary report [4] describing the extent of conformance of the standard used included in the 510(k)? If no, complete a summary report table.	☐	☒
Does the test data for this device demonstrate conformity to the requirements of this standard as it pertains to this device?	☒	☐
Does this standard include acceptance criteria? If no, include the results of testing in the 510(k).	☒	☐
Does this standard include more than one option or selection of tests? If yes, report options selected in the summary report table.	☐	☒
Were there any deviations or adaptations made in the use of the standard?	☐	☒
If yes, were deviations in accordance with the FDA supplemental information sheet (SIS) [5]?	☐	☐
Were deviations or adaptations made beyond what is specified in the FDA SIS? If yes, report these deviations or adaptations in the summary report table.	☐	☒
Were there any exclusions from the standard? If yes, report these exclusions in the summary report table.	☐	☒
Is there an FDA guidance [6] that is associated with this standard?	☐	☒
If yes, was the guidance document followed in preparation of this 510k?	☐	☐

Title of guidance: _____

[1] The formatting convention for the title is: [SDO] [numeric identifier] [title of standard] [date of publication]

[2] Authority [21 U.S.C. 360d], www.fda.gov/cdrh/stdsprog.html

[3] http://www.accessdata.fda.gov/scripts/cdrh/cfdocs/cfStandards/search.cfm

[4] The summary report should include: any adaptations used to adapt to the device under review (for example, alternative test methods); choices made when options or a selection of methods are described; deviations from the standard; requirements not applicable to the device; and the name and address of the test laboratory or certification body involved in conformance assessment to this standard. The summary report includes information on all standards utilized during the development of the device.

[5] The supplemental information sheet (SIS) is additional information which is necessary before FDA recognizes the standard. Found at http://www.accessdata.fda.gov/scripts/cdrh/cfdocs/cfStandards/search.cfm

[6] The online search for CDRH Guidance Documents can be found at www.fda.gov/cdrh/guidance.html

Questions? Contact FDA/CDRH/OCE/DID at CDRH-FOISTATUS@fda.hhs.gov or 301-796-8118

Records processed under FOIA Request #2014-8015; Released by CDRH on 12-8-2015

EXTENT OF STANDARD CONFORMANCE SUMMARY REPORT TABLE

STANDARD TITLE
ISO 11135-1(2007) Sterilization of health care products - Ethylene oxide - Part 1: Requirements for development, validation...

CONFORMANCE WITH STANDARD SECTIONS*

SECTION NUMBER	SECTION TITLE	CONFORMANCE?
all	Sterilization of health care products - Ethylene oxide - Part 1 . . .	☒ Yes ☐ No ☐ N/A

TYPE OF DEVIATION OR OPTION SELECTED ❖
none

DESCRIPTION
This standard was followed.

JUSTIFICATION
n/a

SECTION NUMBER	SECTION TITLE	CONFORMANCE?
		☐ Yes ☐ No ☐ N/A

TYPE OF DEVIATION OR OPTION SELECTED ❖

DESCRIPTION

JUSTIFICATION

SECTION NUMBER	SECTION TITLE	CONFORMANCE?
		☐ Yes ☐ No ☐ N/A

TYPE OF DEVIATION OR OPTION SELECTED ❖

DESCRIPTION

JUSTIFICATION

* For completeness list all sections of the standard and indicate whether conformance is met. If a section is not applicable (N/A) an explanation is needed under "justification." Some standards include options, so similar to deviations, the option chosen needs to be described and adequately justified as appropriate for the subject device. Explanation of all deviations or description of options selected when following a standard is required under "type of deviation or option selected," "description" and "justification" on the report. More than one page may be necessary.

❖ Types of deviations can include an exclusion of a section in the standard, a deviation brought out by the FDA supplemental information sheet (SIS), a deviation to adapt the standard to the device, or any adaptation of a section.

Paperwork Reduction Act Statement

Public reporting burden for this collection of information is estimated to average 1 hour per response, including the time for reviewing instructions, searching existing data sources, gathering and maintaining the data needed, and completing and reviewing the collection of information. Send comments regarding this burden estimate or any other aspect of this collection of information, including suggestions for reducing this burden to:

Department of Health and Human Services
Food and Drug Administration
Office of Chief Information Officer
1350 Piccard Drive, Room 400
Rockville, MD 20850

An agency may not conduct or sponsor, and a person is not required to respond to, a collection of information unless it displays a currently valid OMB control number.

Questions? Contact FDA/CDRH/OCE/DID at CDRH-FOISTATUS@fda.hhs.gov or 301-796-8118

Records processed under FOIA Request #2014-8015; Released by CDRH on 12-8-2015

Form Approved: OMB No. 0910-0120; Expiration Date: 12/31/13

Department of Health and Human Services
Food and Drug Administration

STANDARDS DATA REPORT FOR 510(k)s

(To be filled in by applicant)

This report and the Summary Report Table are to be completed by the applicant when submitting a 510(k) that references a national or international standard. A separate report is required for each standard referenced in the 510(k).

TYPE OF 510(K) SUBMISSION

☒ Traditional ☐ Special ☐ Abbreviated

STANDARD TITLE [1]

ISO 11607-1(2006) Packaging for Terminally Sterilized Medical Devices

Please answer the following questions	Yes	No
Is this standard recognized by FDA [2]?	☒	☐
FDA Recognition number [3]	#14-355	
Was a third party laboratory responsible for testing conformity of the device to this standard identified in the 510(k)?	☒	☐
Is a summary report [4] describing the extent of conformance of the standard used included in the 510(k)? If no, complete a summary report table.	☐	☒
Does the test data for this device demonstrate conformity to the requirements of this standard as it pertains to this device?	☒	☐
Does this standard include acceptance criteria? If no, include the results of testing in the 510(k).	☐	☒
Does this standard include more than one option or selection of tests? If yes, report options selected in the summary report table.	☐	☒
Were there any deviations or adaptations made in the use of the standard?	☐	☒
If yes, were deviations in accordance with the FDA supplemental information sheet (SIS) [5]?	☐	☐
Were deviations or adaptations made beyond what is specified in the FDA SIS? If yes, report these deviations or adaptations in the summary report table.	☐	☒
Were there any exclusions from the standard? If yes, report these exclusions in the summary report table.	☐	☒
Is there an FDA guidance [6] that is associated with this standard?	☐	☒
If yes, was the guidance document followed in preparation of this 510k?	☐	☐

Title of guidance: _____

[1] The formatting convention for the title is: [SDO] [numeric identifier] [title of standard] [date of publication]

[2] Authority [21 U.S.C. 360d], www.fda.gov/cdrh/stdsprog.html

[3] http://www.accessdata.fda.gov/scripts/cdrh/cfdocs/cfStandards/search.cfm

[4] The summary report should include: any adaptations used to adapt to the device under review (for example, alternative test methods); choices made when options or a selection of methods are described; deviations from the standard; requirements not applicable to the device; and the name and address of the test laboratory or certification body involved in conformance assessment to this standard. The summary report includes information on all standards utilized during the development of the device.

[5] The supplemental information sheet (SIS) is additional information which is necessary before FDA recognizes the standard. Found at http://www.accessdata.fda.gov/scripts/cdrh/cfdocs/cfStandards/search.cfm

[6] The online search for CDRH Guidance Documents can be found at www.fda.gov/cdrh/guidance.html

Questions? Contact FDA/CDRH/OCE/DID at CDRH-FOISTATUS@fda.hhs.gov or 301-796-8118

Records processed under FOIA Request #2014-8015; Released by CDRH on 12-8-2015

EXTENT OF STANDARD CONFORMANCE SUMMARY REPORT TABLE

STANDARD TITLE
ISO 11607-1(2006) Packaging for Terminally Sterilized Medical Devices

CONFORMANCE WITH STANDARD SECTIONS*

SECTION NUMBER	SECTION TITLE	CONFORMANCE?
All	N/A	☒ Yes ☐ No ☐ N/A

TYPE OF DEVIATION OR OPTION SELECTED ❖
Option selected: Blister trays with Tyvek Lids.

DESCRIPTION
Requirements for materials, sterile barrier systems and packaging systems.

JUSTIFICATION
Compliant to all sections for blister trays with Tyvek lids.

SECTION NUMBER	SECTION TITLE	CONFORMANCE?
5	Materials and preformed sterile barrier systems	☒ Yes ☐ No ☐ N/A

TYPE OF DEVIATION OR OPTION SELECTED ❖
Option selected: PETG Trays with Tyvek Lids.

DESCRIPTION
Describes the requirements for materials and preformed sterile barrier systems.

JUSTIFICATION
Die cut Tyvek 1073B lids and PETG trays were selected as the sterile barrier system. Components were preformed by (b)(4) [redacted] and are certified to conform the the requirements of ISO 11607 Part 1. (b)(4) [redacted]

SECTION NUMBER	SECTION TITLE	CONFORMANCE?
		☐ Yes ☐ No ☐ N/A

TYPE OF DEVIATION OR OPTION SELECTED ❖

DESCRIPTION

JUSTIFICATION

* For completeness list all sections of the standard and indicate whether conformance is met. If a section is not applicable (N/A) an explanation is needed under "justification." Some standards include options, so similar to deviations, the option chosen needs to be described and adequately justified as appropriate for the subject device. Explanation of all deviations or description of options selected when following a standard is required under "type of deviation or option selected," "description" and "justification" on the report. More than one page may be necessary.

❖ Types of deviations can include an exclusion of a section in the standard, a deviation brought out by the FDA supplemental information sheet (SIS), a deviation to adapt the standard to the device, or any adaptation of a section.

Paperwork Reduction Act Statement

Public reporting burden for this collection of information is estimated to average 1 hour per response, including the time for reviewing instructions, searching existing data sources, gathering and maintaining the data needed, and completing and reviewing the collection of information. Send comments regarding this burden estimate or any other aspect of this collection of information, including suggestions for reducing this burden to:

Department of Health and Human Services
Food and Drug Administration
Office of Chief Information Officer
1350 Piccard Drive, Room 400
Rockville, MD 20850

An agency may not conduct or sponsor, and a person is not required to respond to, a collection of information unless it displays a currently valid OMB control number.

Questions? Contact FDA/CDRH/OCE/DID at CDRH-FOISTATUS@fda.hhs.gov or 301-796-8118

Records processed under FOIA Request #2014-8015; Released by CDRH on 12-8-2015

Form Approved: OMB No. 0910-0120; Expiration Date: 12/31/13

Department of Health and Human Services
Food and Drug Administration

STANDARDS DATA REPORT FOR 510(k)s

(To be filled in by applicant)

This report and the Summary Report Table are to be completed by the applicant when submitting a 510(k) that references a national or international standard. A separate report is required for each standard referenced in the 510(k).

TYPE OF 510(K) SUBMISSION

☒ Traditional ☐ Special ☐ Abbreviated

STANDARD TITLE [1]

ISO 14243-1(2009) Implants for surgery - Wear of total knee-joint prostheses - Part 1: Loading and displacement parameters...

Please answer the following questions	Yes	No
Is this standard recognized by FDA [2]?	☒	☐
FDA Recognition number [3]	#11-222	
Was a third party laboratory responsible for testing conformity of the device to this standard identified in the 510(k)?	☒	☐
Is a summary report [4] describing the extent of conformance of the standard used included in the 510(k)? If no, complete a summary report table.	☐	☒
Does the test data for this device demonstrate conformity to the requirements of this standard as it pertains to this device?	☒	☐
Does this standard include acceptance criteria? If no, include the results of testing in the 510(k).	☐	☒
Does this standard include more than one option or selection of tests? If yes, report options selected in the summary report table.	☐	☒
Were there any deviations or adaptations made in the use of the standard?	☐	☒
If yes, were deviations in accordance with the FDA supplemental information sheet (SIS) [5]?	☐	☐
Were deviations or adaptations made beyond what is specified in the FDA SIS? If yes, report these deviations or adaptations in the summary report table.	☐	☒
Were there any exclusions from the standard? If yes, report these exclusions in the summary report table.	☐	☒
Is there an FDA guidance [6] that is associated with this standard?	☐	☒
If yes, was the guidance document followed in preparation of this 510k?	☐	☐

Title of guidance: _____

[1] The formatting convention for the title is: [SDO] [numeric identifier] [title of standard] [date of publication]

[2] Authority [21 U.S.C. 360d], www.fda.gov/cdrh/stdsprog.html

[3] http://www.accessdata.fda.gov/scripts/cdrh/cfdocs/cfStandards/search.cfm

[4] The summary report should include: any adaptations used to adapt to the device under review (for example, alternative test methods); choices made when options or a selection of methods are described; deviations from the standard; requirements not applicable to the device; and the name and address of the test laboratory or certification body involved in conformance assessment to this standard. The summary report includes information on all standards utilized during the development of the device.

[5] The supplemental information sheet (SIS) is additional information which is necessary before FDA recognizes the standard. Found at http://www.accessdata.fda.gov/scripts/cdrh/cfdocs/cfStandards/search.cfm

[6] The online search for CDRH Guidance Documents can be found at www.fda.gov/cdrh/guidance.html

Questions? Contact FDA/CDRH/OCE/DID at CDRH-FOISTATUS@fda.hhs.gov or 301-796-8118

Records processed under FOIA Request #2014-8015; Released by CDRH on 12-8-2015

EXTENT OF STANDARD CONFORMANCE SUMMARY REPORT TABLE

STANDARD TITLE
ISO 14243-1(2009) Implants for surgery - Wear of total knee-joint prostheses - Part 1: Loading and displacement parameters...

CONFORMANCE WITH STANDARD SECTIONS*

SECTION NUMBER	SECTION TITLE	CONFORMANCE?
All		☒ Yes ☐ No ☐ N/A

TYPE OF DEVIATION OR OPTION SELECTED ❖
No deviations or options

DESCRIPTION
NA

JUSTIFICATION
NA

SECTION NUMBER	SECTION TITLE	CONFORMANCE?
		☐ Yes ☐ No ☐ N/A

TYPE OF DEVIATION OR OPTION SELECTED ❖

DESCRIPTION

JUSTIFICATION

SECTION NUMBER	SECTION TITLE	CONFORMANCE?
		☐ Yes ☐ No ☐ N/A

TYPE OF DEVIATION OR OPTION SELECTED ❖

DESCRIPTION

JUSTIFICATION

* For completeness list all sections of the standard and indicate whether conformance is met. If a section is not applicable (N/A) an explanation is needed under "justification." Some standards include options, so similar to deviations, the option chosen needs to be described and adequately justified as appropriate for the subject device. Explanation of all deviations or description of options selected when following a standard is required under "type of deviation or option selected," "description" and "justification" on the report. More than one page may be necessary.

❖ Types of deviations can include an exclusion of a section in the standard, a deviation brought out by the FDA supplemental information sheet (SIS), a deviation to adapt the standard to the device, or any adaptation of a section.

Paperwork Reduction Act Statement

Public reporting burden for this collection of information is estimated to average 1 hour per response, including the time for reviewing instructions, searching existing data sources, gathering and maintaining the data needed, and completing and reviewing the collection of information. Send comments regarding this burden estimate or any other aspect of this collection of information, including suggestions for reducing this burden to:

Department of Health and Human Services
Food and Drug Administration
Office of Chief Information Officer
1350 Piccard Drive, Room 400
Rockville, MD 20850

An agency may not conduct or sponsor, and a person is not required to respond to, a collection of information unless it displays a currently valid OMB control number.

Questions? Contact FDA/CDRH/OCE/DID at CDRH-FOISTATUS@fda.hhs.gov or 301-796-8118

Records processed under FOIA Request #2014-8015; Released by CDRH on 12-8-2015

Form Approved: OMB No. 0910-0120; Expiration Date: 12/31/13

Department of Health and Human Services
Food and Drug Administration

STANDARDS DATA REPORT FOR 510(k)s

(To be filled in by applicant)

This report and the Summary Report Table are to be completed by the applicant when submitting a 510(k) that references a national or international standard. A separate report is required for each standard referenced in the 510(k).

TYPE OF 510(K) SUBMISSION

☒ Traditional ☐ Special ☐ Abbreviated

STANDARD TITLE [1]

ISO 14243-2(2009) Implants for surgery - Wear of total knee-joint prostheses - Part 2: Methods of measurement

Please answer the following questions	Yes	No
Is this standard recognized by FDA [2]?	☒	☐
FDA Recognition number [3]	#11-223	
Was a third party laboratory responsible for testing conformity of the device to this standard identified in the 510(k)?	☒	☐
Is a summary report [4] describing the extent of conformance of the standard used included in the 510(k)? If no, complete a summary report table.	☐	☒
Does the test data for this device demonstrate conformity to the requirements of this standard as it pertains to this device?	☒	☐
Does this standard include acceptance criteria? If no, include the results of testing in the 510(k).	☐	☒
Does this standard include more than one option or selection of tests? If yes, report options selected in the summary report table.	☒	☐
Were there any deviations or adaptations made in the use of the standard?	☒	☐
If yes, were deviations in accordance with the FDA supplemental information sheet (SIS) [5]?	☐	☒
Were deviations or adaptations made beyond what is specified in the FDA SIS? If yes, report these deviations or adaptations in the summary report table.	☐	☒
Were there any exclusions from the standard? If yes, report these exclusions in the summary report table.	☐	☒
Is there an FDA guidance [6] that is associated with this standard?	☐	☒
If yes, was the guidance document followed in preparation of this 510k?	☐	☐

Title of guidance: _____

[1] The formatting convention for the title is: [SDO] [numeric identifier] [title of standard] [date of publication]

[2] Authority [21 U.S.C. 360d], www.fda.gov/cdrh/stdsprog.html

[3] http://www.accessdata.fda.gov/scripts/cdrh/cfdocs/cfStandards/search.cfm

[4] The summary report should include: any adaptations used to adapt to the device under review (for example, alternative test methods); choices made when options or a selection of methods are described; deviations from the standard; requirements not applicable to the device; and the name and address of the test laboratory or certification body involved in conformance assessment to this standard. The summary report includes information on all standards utilized during the development of the device.

[5] The supplemental information sheet (SIS) is additional information which is necessary before FDA recognizes the standard. Found at http://www.accessdata.fda.gov/scripts/cdrh/cfdocs/cfStandards/search.cfm

[6] The online search for CDRH Guidance Documents can be found at www.fda.gov/cdrh/guidance.html

Questions? Contact FDA/CDRH/OCE/DID at CDRH-FOISTATUS@fda.hhs.gov or 301-796-8118

EXTENT OF STANDARD CONFORMANCE SUMMARY REPORT TABLE

STANDARD TITLE
ISO 14243-2(2009) Implants for surgery - Wear of total knee-joint prostheses - Part 2: Methods of measurement

CONFORMANCE WITH STANDARD SECTIONS*

SECTION NUMBER	SECTION TITLE	CONFORMANCE?
See extra pages		☐ Yes ☐ No ☒ N/A

TYPE OF DEVIATION OR OPTION SELECTED ❖

DESCRIPTION

JUSTIFICATION

SECTION NUMBER	SECTION TITLE	CONFORMANCE?
		☐ Yes ☐ No ☐ N/A

TYPE OF DEVIATION OR OPTION SELECTED ❖

DESCRIPTION

JUSTIFICATION

SECTION NUMBER	SECTION TITLE	CONFORMANCE?
		☐ Yes ☐ No ☐ N/A

TYPE OF DEVIATION OR OPTION SELECTED ❖

DESCRIPTION

JUSTIFICATION

* For completeness list all sections of the standard and indicate whether conformance is met. If a section is not applicable (N/A) an explanation is needed under "justification." Some standards include options, so similar to deviations, the option chosen needs to be described and adequately justified as appropriate for the subject device. Explanation of all deviations or description of options selected when following a standard is required under "type of deviation or option selected," "description" and "justification" on the report. More than one page may be necessary.

❖ Types of deviations can include an exclusion of a section in the standard, a deviation brought out by the FDA supplemental information sheet (SIS), a deviation to adapt the standard to the device, or any adaptation of a section.

Paperwork Reduction Act Statement

Public reporting burden for this collection of information is estimated to average 1 hour per response, including the time for reviewing instructions, searching existing data sources, gathering and maintaining the data needed, and completing and reviewing the collection of information. Send comments regarding this burden estimate or any other aspect of this collection of information, including suggestions for reducing this burden to:

Department of Health and Human Services
Food and Drug Administration
Office of Chief Information Officer
1350 Piccard Drive, Room 400
Rockville, MD 20850

An agency may not conduct or sponsor, and a person is not required to respond to, a collection of information unless it displays a currently valid OMB control number.

Questions? Contact FDA/CDRH/OCE/DID at CDRH-FOISTATUS@fda.hhs.gov or 301-796-8118

Records processed under FOIA Request #2014-8015; Released by CDRH on 12-8-2015

(b)(4)

[redacted]

TEST LABORATORIES INVOLVED WITH CONFORMANCE

(b)(4)

[redacted]

Questions? Contact FDA/CDRH/OCE/DID at CDRH-FOISTATUS@fda.hhs.gov or 301-796-8118

Records processed under FOIA Request #2014-8015; Released by CDRH on 12-8-2015

Form Approved: OMB No. 0910-0120; Expiration Date: 12/31/13

Department of Health and Human Services
Food and Drug Administration

STANDARDS DATA REPORT FOR 510(k)s

(To be filled in by applicant)

This report and the Summary Report Table are to be completed by the applicant when submitting a 510(k) that references a national or international standard. A separate report is required for each standard referenced in the 510(k).

TYPE OF 510(K) SUBMISSION

☒ Traditional ☐ Special ☐ Abbreviated

STANDARD TITLE [1]

ISO 17664(2004) Sterilization of Medical Devices - Information to be provided by the manufacturer for the processing of...

Please answer the following questions	Yes	No
Is this standard recognized by FDA [2]?	☐	☒
FDA Recognition number [3] # _____		
Was a third party laboratory responsible for testing conformity of the device to this standard identified in the 510(k)?	☒	☐
Is a summary report [4] describing the extent of conformance of the standard used included in the 510(k)? If no, complete a summary report table.	☐	☒
Does the test data for this device demonstrate conformity to the requirements of this standard as it pertains to this device?	☒	☐
Does this standard include acceptance criteria? If no, include the results of testing in the 510(k).	☒	☐
Does this standard include more than one option or selection of tests? If yes, report options selected in the summary report table.	☐	☒
Were there any deviations or adaptations made in the use of the standard?	☐	☒
If yes, were deviations in accordance with the FDA supplemental information sheet (SIS) [5]?	☐	☐
Were deviations or adaptations made beyond what is specified in the FDA SIS? If yes, report these deviations or adaptations in the summary report table.	☐	☒
Were there any exclusions from the standard? If yes, report these exclusions in the summary report table.	☐	☒
Is there an FDA guidance [6] that is associated with this standard?	☐	☒
If yes, was the guidance document followed in preparation of this 510k?	☐	☐

Title of guidance: _____

[1] The formatting convention for the title is: [SDO] [numeric identifier] [title of standard] [date of publication]

[2] Authority [21 U.S.C. 360d], www.fda.gov/cdrh/stdsprog.html

[3] http://www.accessdata.fda.gov/scripts/cdrh/cfdocs/cfStandards/search.cfm

[4] The summary report should include: any adaptations used to adapt to the device under review (for example, alternative test methods); choices made when options or a selection of methods are described; deviations from the standard; requirements not applicable to the device; and the name and address of the test laboratory or certification body involved in conformance assessment to this standard. The summary report includes information on all standards utilized during the development of the device.

[5] The supplemental information sheet (SIS) is additional information which is necessary before FDA recognizes the standard. Found at http://www.accessdata.fda.gov/scripts/cdrh/cfdocs/cfStandards/search.cfm

[6] The online search for CDRH Guidance Documents can be found at www.fda.gov/cdrh/guidance.html

Questions? Contact FDA/CDRH/OCE/DID at CDRH-FOISTATUS@fda.hhs.gov or 301-796-8118

EXTENT OF STANDARD CONFORMANCE SUMMARY REPORT TABLE

STANDARD TITLE
ISO 17664(2004) Sterilization of Medical Devices - Information to be provided by the manufacturer for the processing of...

CONFORMANCE WITH STANDARD SECTIONS*

SECTION NUMBER	SECTION TITLE	CONFORMANCE?
all	Sterilization of medical devices - Information to be provided by the...	☒ Yes ☐ No ☐ N/A

TYPE OF DEVIATION OR OPTION SELECTED ❖
none

DESCRIPTION
This standard was followed, but does not list specific acceptance criteria. Refer to AAMI TIR30 for acceptance criteria.

JUSTIFICATION
n/a

SECTION NUMBER	SECTION TITLE	CONFORMANCE?
		☐ Yes ☐ No ☐ N/A

TYPE OF DEVIATION OR OPTION SELECTED ❖

DESCRIPTION

JUSTIFICATION

SECTION NUMBER	SECTION TITLE	CONFORMANCE?
		☐ Yes ☐ No ☐ N/A

TYPE OF DEVIATION OR OPTION SELECTED ❖

DESCRIPTION

JUSTIFICATION

* For completeness list all sections of the standard and indicate whether conformance is met. If a section is not applicable (N/A) an explanation is needed under "justification." Some standards include options, so similar to deviations, the option chosen needs to be described and adequately justified as appropriate for the subject device. Explanation of all deviations or description of options selected when following a standard is required under "type of deviation or option selected," "description" and "justification" on the report. More than one page may be necessary.

❖ Types of deviations can include an exclusion of a section in the standard, a deviation brought out by the FDA supplemental information sheet (SIS), a deviation to adapt the standard to the device, or any adaptation of a section.

Paperwork Reduction Act Statement

Public reporting burden for this collection of information is estimated to average 1 hour per response, including the time for reviewing instructions, searching existing data sources, gathering and maintaining the data needed, and completing and reviewing the collection of information. Send comments regarding this burden estimate or any other aspect of this collection of information, including suggestions for reducing this burden to:

Department of Health and Human Services
Food and Drug Administration
Office of Chief Information Officer
1350 Piccard Drive, Room 400
Rockville, MD 20850

An agency may not conduct or sponsor, and a person is not required to respond to, a collection of information unless it displays a currently valid OMB control number.

Questions? Contact FDA/CDRH/OCE/DID at CDRH-FOISTATUS@fda.hhs.gov or 301-796-8118

Records processed under FOIA Request #2014-8015; Released by CDRH on 12-8-2015

Form Approved: OMB No. 0910-0120; Expiration Date: 12/31/13

Department of Health and Human Services
Food and Drug Administration

STANDARDS DATA REPORT FOR 510(k)s

(To be filled in by applicant)

This report and the Summary Report Table are to be completed by the applicant when submitting a 510(k) that references a national or international standard. A separate report is required for each standard referenced in the 510(k).

TYPE OF 510(K) SUBMISSION

☒ Traditional ☐ Special ☐ Abbreviated

STANDARD TITLE [1]

ISO 17665(2006) Sterilization of health care products - Moist heat - Part 1: Requirements for the development, validation...

Please answer the following questions	Yes	No
Is this standard recognized by FDA [2]?	☐	☒
FDA Recognition number [3]	#14-261	
Was a third party laboratory responsible for testing conformity of the device to this standard identified in the 510(k)?	☒	☐
Is a summary report [4] describing the extent of conformance of the standard used included in the 510(k)? If no, complete a summary report table.	☐	☒
Does the test data for this device demonstrate conformity to the requirements of this standard as it pertains to this device?	☒	☐
Does this standard include acceptance criteria? If no, include the results of testing in the 510(k).	☒	☐
Does this standard include more than one option or selection of tests? If yes, report options selected in the summary report table.	☐	☒
Were there any deviations or adaptations made in the use of the standard?	☐	☒
If yes, were deviations in accordance with the FDA supplemental information sheet (SIS) [5]?	☐	☐
Were deviations or adaptations made beyond what is specified in the FDA SIS? If yes, report these deviations or adaptations in the summary report table.	☐	☒
Were there any exclusions from the standard? If yes, report these exclusions in the summary report table.	☐	☒
Is there an FDA guidance [6] that is associated with this standard?	☐	☒
If yes, was the guidance document followed in preparation of this 510k?	☐	☐

Title of guidance: _____

[1] The formatting convention for the title is: [SDO] [numeric identifier] [title of standard] [date of publication]

[2] Authority [21 U.S.C. 360d], www.fda.gov/cdrh/stdsprog.html

[3] http://www.accessdata.fda.gov/scripts/cdrh/cfdocs/cfStandards/search.cfm

[4] The summary report should include: any adaptations used to adapt to the device under review (for example, alternative test methods); choices made when options or a selection of methods are described; deviations from the standard; requirements not applicable to the device; and the name and address of the test laboratory or certification body involved in conformance assessment to this standard. The summary report includes information on all standards utilized during the development of the device.

[5] The supplemental information sheet (SIS) is additional information which is necessary before FDA recognizes the standard. Found at http://www.accessdata.fda.gov/scripts/cdrh/cfdocs/cfStandards/search.cfm

[6] The online search for CDRH Guidance Documents can be found at www.fda.gov/cdrh/guidance.html

Questions? Contact FDA/CDRH/OCE/DID at CDRH-FOISTATUS@fda.hhs.gov or 301-796-8118

EXTENT OF STANDARD CONFORMANCE SUMMARY REPORT TABLE

STANDARD TITLE
ISO 17665(2006) Sterilization of health care products - Moist heat - Part 1: Requirements for the development, validation...

CONFORMANCE WITH STANDARD SECTIONS*

SECTION NUMBER	SECTION TITLE	CONFORMANCE?
All	Sterilization of health care products - Moist heat - Part 1: Requirements for...	☒ Yes ☐ No ☐ N/A

TYPE OF DEVIATION OR OPTION SELECTED ❖
n/a

DESCRIPTION
This standard was followed, but does not list specific acceptance criteria. Refer to ANSI/AAMI ST79 for acceptance criteria.

JUSTIFICATION

SECTION NUMBER	SECTION TITLE	CONFORMANCE?
		☐ Yes ☐ No ☐ N/A

TYPE OF DEVIATION OR OPTION SELECTED ❖

DESCRIPTION

JUSTIFICATION

SECTION NUMBER	SECTION TITLE	CONFORMANCE?
		☐ Yes ☐ No ☐ N/A

TYPE OF DEVIATION OR OPTION SELECTED ❖

DESCRIPTION

JUSTIFICATION

* For completeness list all sections of the standard and indicate whether conformance is met. If a section is not applicable (N/A) an explanation is needed under "justification." Some standards include options, so similar to deviations, the option chosen needs to be described and adequately justified as appropriate for the subject device. Explanation of all deviations or description of options selected when following a standard is required under "type of deviation or option selected," "description" and "justification" on the report. More than one page may be necessary.

❖ Types of deviations can include an exclusion of a section in the standard, a deviation brought out by the FDA supplemental information sheet (SIS), a deviation to adapt the standard to the device, or any adaptation of a section.

Paperwork Reduction Act Statement

Public reporting burden for this collection of information is estimated to average 1 hour per response, including the time for reviewing instructions, searching existing data sources, gathering and maintaining the data needed, and completing and reviewing the collection of information. Send comments regarding this burden estimate or any other aspect of this collection of information, including suggestions for reducing this burden to:

Department of Health and Human Services
Food and Drug Administration
Office of Chief Information Officer
1350 Piccard Drive, Room 400
Rockville, MD 20850

An agency may not conduct or sponsor, and a person is not required to respond to, a collection of information unless it displays a currently valid OMB control number.

Questions? Contact FDA/CDRH/OCE/DID at CDRH-FOISTATUS@fda.hhs.gov or 301-796-8118

Records processed under FOIA Request #2014-8015; Released by CDRH on 12-8-2015

Section 10
Executive Summary

Questions? Contact FDA/CDRH/OCE/DID at CDRH-FOISTATUS@fda.hhs.gov or 301-796-8118

Records processed under FOIA Request #2014-8015; Released by CDRH on 12-8-2015

Balanced Knee® System High Flex

Vitamin E PS Tibial Insert and Patella

510(k) Submission Executive Summary

1. General Overview

Ortho Development is submitting a 510(k) for its Balanced Knee® System High Flex Vitamin E PS Tibial Insert and Patella. This document provides a summary of the testing completed and standards used to establish a claim of substantial equivalence. The detailed data supporting the claim of substantial equivalence is found within the labeled sections of this submission.

Trade Name:	Balanced Knee® System High Flex Vitamin E PS Tibial Insert and Patella
Device:	Prosthesis, Knee, Patellofemorotibial, Semi-constrained, Cemented, Polymer/Metal/Polymer
Regulation Description:	21 CFR 888.3560, Knee joint, patellofemorotibial, polymer/metal/polymer semi-constrained cemented prosthesis
Regulation Medical Specialty:	Orthopedic
Review Panel:	Orthopedic
Product Code:	JWH
Submission Type:	510(k)
Regulation Number:	888.3560
Device Class:	II

2. System Description

The Balanced Knee® System High Flex Vitamin E (High Flex Vit E) PS tibial insert and patella are machined from extensively crosslinked, compression molded, Vitamin E UHMWPE. Both components are single use only. The High Flex Vit E PS tibial insert must be used in conjunction with the High Flex PS femoral component (K123457). Used together, these components are designed to accommodate increased range of motion up to 150° of flexion. The High Flex Vit E patella may be used in conjunction with the Balanced Knee® System (BKS) femoral components (K994370), the BKS modular femoral components (K060569), or the High Flex PS femoral components (K123457). Both the High Flex Vit E PS tibial insert

Questions? Contact FDA/CDRH/OCE/DID at CDRH-FOISTATUS@fda.hhs.gov or 301-796-8118

and patella may be used in conjunction with the BKS standard and modular tibial trays, tibial augments, and stems to complete the semi-constrained modular knee prosthesis. The tibial trays, tibial augments, and stems were approved under K994370 and K031201. The High Flex Vit E PS system is designed for cemented use only. A basic configuration of the High Flex Vit E PS system is shown below. Table 1 provides a description of each component in the system.

(b)(4)

[redacted]

Table 1. Component Descriptions

High Flex Vitamin E PS Tibial Insert	
Material	Extensively Crosslinked, Vitamin E UHMWPE (b)(4) [redacted]
Sizes	1-7, 7-20mm thicknesses
Sterilization	Ethylene Oxide ISO 11135 SAL 10^{-6}

High Flex Vitamin E Patella	
Material	Extensively Crosslinked, Vitamin E UHMWPE (b)(4) [redacted]
Sizes	5 sizes, 29-41mm diameters
Sterilization	Ethylene Oxide ISO 11135 SAL 10^{-6}

3. Intended Use

The Balanced Knee® System High Flex Vitamin E PS tibial insert and patella are intended for use in cemented total knee arthroplasty procedures with the following indications:

1. Loss of knee joint configuration and joint function.
2. Osteoarthritis of the knee joint.
3. Rheumatoid arthritis of the knee joint.
4. Post-traumatic arthritis of the knee joint.
5. Valgus, varus, or flexion deformities of the knee joint.
6. Revision procedures where other treatments or devices have failed.

4. Predicate Devices

Balanced Knee® System (K994370)
Ortho Development Corp.

Balanced Knee® System High Flex PS (K123457)
Ortho Development Corp.

Highly Cross-Linked Vitamin E UHMWPE Tibial Insert (K091956)
DJO Surgical/Encore Medical

5. Basis for Substantial Equivalence

Table 2. High Flex Vit E PS Tibial Insert

Design Feature	Equivalent Device
Indications for Use	Ortho Development: Balanced Knee® System High Flex (K123457)
Design (size, thickness, dimensions)	Ortho Development: Balanced Knee® System High Flex PS (K123457)
Material: Extensively Crosslinked Vitamin E Polyethylene UHMWPE (α-tocopherol)	DJO Surgical/Encore Medical: Vit E UHMWPE Tibial Insert (K091956)

Table 3. High Flex Vit E Patella

Design Feature	Equivalent Device
Indications for Use	Ortho Development: Balanced Knee® System (K994370) Ortho Development: Balanced Knee® System High Flex PS (K123457)
Design (size, thickness, dimensions)	Ortho Development: Balanced Knee® System (K994370)
Material: Extensively Crosslinked Vitamin E Polyethylene UHMWPE (α-tocopherol)	DJO Surgical/Encore Medical: Vit E UHMWPE Tibial Insert (K091956)

The key features for the High Flex Vit E PS tibial insert and patella are:

1) Accommodation of flexion angles up to 150° (equivalent to High Flex (K123457)), and
2) The addition of an extensively crosslinked, vitamin E UHMWPE material (substantially equivalent to DJO/Encore's Crosslinked Vitamin E UHMWPE (K091956)).

6. Device Comparison Tables

Table 4. *Tibial Insert* Substantial Equivalence Table

	High Flex Vitamin E PS Tib Insert	**High Flex (CM Poly) PS Tib Insert**	**Balanced Knee® System PS Tib Insert**
Manufacturer	Ortho Development	Ortho Development	Ortho Development
510k Number	Pending	K123457	K994370
Application/ Product code	JWH	JWH	JWH
Size Range			
(b)(4) [redacted]			
Size Compatibility with Femoral	One Up, One Down	One Up, One Down	One Up, One Down
(b)(4) [redacted]			
	Ethylene Oxide	Gamma Irradiation in N_2	Gamma Irradiation in N_2
Range of Motion	Flexion up to 150°	Flexion up to 150°	Flexion up to 113°
Femorotibial Constraint	Identical to High Flex PS	See 510(k) K123457	See 510(k) K994370
Femorotibial Contact Area	Identical to High Flex PS	See 510(k) K123457	See 510(k) K994370
(b)(4) [redacted]			
Indications	Loss of joint configuration and joint function	Loss of joint configuration and joint function	Loss of joint configuration and joint function
	Osteoarthritis	Osteoarthritis	Osteoarthritis
	Rheumatoid arthritis	Rheumatoid arthritis	Rheumatoid arthritis
	Post-traumatic arthritis	Post-traumatic arthritis	Post-traumatic arthritis
	Valgus, varus, or flexion deformities	Valgus, varus, or flexion deformities	Valgus, varus, or flexion deformities
	Revision procedures where other treatments or devices have failed	Revision procedures where other treatments or devices have failed	--

Table 5. *Patella* Substantial Equivalence Table

	High Flex Vitamin E Patella	**High Flex PS (used w/patella from K994370)**	**Balanced Knee® System (BKS)**
Manufacturer	Ortho Development	Ortho Development	Ortho Development
510k Number	Pending	K123457	K994370
Application/ Product code	JWH	JWH	JWH
Size Range (diameter)	Sizes 29-41mm	Sizes 29-38mm	Sizes 29-38mm
(b)(4) [redacted]			
	3 peg	3 peg	3 peg
Size Compatibility with Femoral	Compatible with any size femoral, BKS or High Flex	Compatible with any size femoral, BKS or High Flex	Compatible with any size femoral, BKS
(b)(4) [redacted]			
Sterilization	Ethylene Oxide	Gamma Irradiation in N_2	Gamma Irradiation in N_2
Patellofemoral Constraint	Identical to BKS or High Flex PS, depending on mating femoral	See 510(k) K123457	See 510(k) K994370
Patellofemoral Contact Area	Identical to BKS or High Flex PS, depending on mating femoral	See 510(k) K123457	See 510(k) K994370
Indications	Loss of joint configuration and joint function	Loss of joint configuration and joint function	Loss of joint configuration and joint function
	Osteoarthritis	Osteoarthritis	Osteoarthritis
	Rheumatoid arthritis	Rheumatoid arthritis	Rheumatoid arthritis
	Post-traumatic arthritis	Post-traumatic arthritis	Post-traumatic arthritis
	Valgus, varus, or flexion deformities	Valgus, varus, or flexion deformities	Valgus, varus, or flexion deformities
	Revision procedures where other treatments or devices have failed	Revision procedures where other treatments or devices have failed	--

Table 6. *Vitamin E Material* Substantial Equivalence Table

	High Flex Vitamin E PS Tib Insert and Patella	**Crosslinked Vit E Tib Insert**
Manufacturer	Ortho Development	DJO Surgical/Encore Medical
510k Number	Pending	K091956
Application/ Product code	JWH	JWH, OIY, MBH

(b)(4)

[redacted]

7. Performance Testing

(b)(4) Testing

[redacted]

(b)(4) Testing

(b)(4) Testing

(b)(4) Testing

(b)(4) Testing

[redacted]

8. Biocompatibility

The following tests were performed for the Balanced Knee® System High Flex Vitamin E PS tibial insert and patella.

Test	Standard	Results
Cytotoxicity	ISO 10993-5	(b)(4) Testing [redacted]
Implantation	ISO 10993-6	
Irritation	ISO 10993-10	
Sensitization	ISO 10993-10	

9. Other Considerations

Device does not contain software/firmware.

Device does not require EMC and Electrical Safety evaluation.

Device is not an in-vitro diagnostic device (IVD).

Records processed under FOIA Request #2014-8015; Released by CDRH on 12-8-2015

Section 11
Device Description

Questions? Contact FDA/CDRH/OCE/DID at CDRH-FOISTATUS@fda.hhs.gov or 301-796-8118

Records processed under FOIA Request #2014-8015; Released by CDRH on 12-8-2015

Device Description

1. Overview

The Balanced Knee® System High Flex Vitamin E (High Flex Vit E) PS tibial insert and patella are machined from extensively crosslinked, compression molded, Vitamin E UHMWPE. Both components are single use only. The High Flex Vit E PS insert must be used in conjunction with the High Flex PS femoral component (K123457). Used together, these components are designed to accommodate increased range of motion up to 150° of flexion. The High Flex Vit E patella may be used in conjunction with the Balanced Knee® System (BKS) femoral components (K994370), the BKS modular femoral components (K060569), or the High Flex PS femoral components (K123457). Both the High Flex Vit E PS insert and patella may be used in conjunction with the BKS standard and modular tibial trays, tibial augments, and stems to complete the semi-constrained modular knee prosthesis. The tibial trays, tibial augments, and stems were approved under K994370 and K031201. The High Flex Vit E PS system is designed for cemented use only. A basic configuration of the High Flex Vit E PS system is shown below. Part numbers for all implants are found in Appendix A and drawings of representative sizes of each component are found in Appendix B of this section.

(b)(4)

[redacted]

Questions? Contact FDA/CDRH/OCE/DID at CDRH-FOISTATUS@fda.hhs.gov or 301-796-8118

Records processed under FOIA Request #2014-8015; Released by CDRH on 12-8-2015

2. Intended Use

The Balanced Knee® System High Flex Vitamin E PS tibial insert and patella are intended for use in cemented total knee arthroplasty procedures with the following indications:

1. Loss of knee joint configuration and joint function.
2. Osteoarthritis of the knee joint.
3. Rheumatoid arthritis of the knee joint.
4. Post-traumatic arthritis of the knee joint.
5. Valgus, varus, or flexion deformities of the knee joint.
6. Revision procedures where other treatments or devices have failed.

3. Design Requirement

(b)(4) [redacted]

4. High Flex Vit E PS Tibial Insert

High Flex Vit E PS inserts are manufactured from Compression Molded Vitamin E Ultra High Molecular (b)(4) [redacted]

(b)(4) [redacted]

The High Flex Vit E PS inserts are available in identical sizes to the High Flex PS inserts (K123457). The seven insert sizes match each respective size of tibial tray. The insert is symmetric, not left/right specific. It is supplied in thicknesses of 7, 8, 9, 10, 11, 12, 13, 14, 16, 17, 18, and 20mm. Minimum polyethylene thickness, at the thinnest measurement point, is 7mm for every size of tibial insert. The anterior/posterior and medial/lateral dimensions are outlined for each size in the following table.

Questions? Contact FDA/CDRH/OCE/DID at CDRH-FOISTATUS@fda.hhs.gov or 301-796-8118

(b)(4) [redacted]

5. High Flex Vit E Patella

High Flex Vit E patellae are manufactured from Compression Molded Vitamin E Ultra High Molecular Weight Polyethylene (b)(4) [redacted]

(b)(4) [redacted]

The patella is available in five sizes. (b)(4) [redacted] patella will work on either right or left knees; it is not side-specific. It is supplied in diameters of 29, 32, 35, 38 and 41 mm (b)(4) [redacted]

(b)(4)

[redacted]

The diameter and thickness dimensions are outlined for each size in the following table.

(b)(4)

[redacted]

6. Size Compatibility

The High Flex Vit E PS inserts and High Flex PS femoral components (K123457) can be sized together according to the table below. The insert is matched to the tibial tray size, one-to-one.

(b)(4) [redacted]

7. System Compatibility

(b)(4) [redacted]

(b)(4) [redacted]

510(k) Number
K123457
K994370
K031201

(b)(4) [redacted]

(b)(4) [redacted]

510(k) Number
K994370
K123457
K060569

8. Surgical Instruments

All instruments are standard for the placement of total knee implants and do not represent new or novel technologies. Instrumentation is provided with the High Flex Vit E PS insert and patella for trialing the implants and preparing the patella. A summary of new instruments included in the system is provided in the table below. All other necessary instruments used with this system have been cleared in K994370, K031201, K060569, and K123457.

			Patient	Material

(b)(4) [redacted]

(b)(4) [redacted]

Records processed under FOIA Request #2014-8015; Released by CDRH on 12-8-2015

(b)(4)

[redacted]

Questions? Contact FDA/CDRH/OCE/DID at CDRH-FOISTATUS@fda.hhs.gov or 301-796-8118

(b)(4)

[redacted]

Records processed under FOIA Request #2014-8015; Released by CDRH on 12-8-2015

Appendix B, Representative Component Drawings

Questions? Contact FDA/CDRH/OCE/DID at CDRH-FOISTATUS@fda.hhs.gov or 301-796-8118

(b)(4) Drawings

(b)(4) Drawings

(b)(4) Drawings

(b)(4) Drawings

(b)(4) Drawings

(b)(4) Drawings

(b)(4) Drawings

(b)(4) Drawings

(b)(4) Drawings

(b)(4) Drawings

(b)(4) Drawings

(b)(4) Drawings

(b)(4) Drawings

(b)(4) Drawings

(b)(4) Drawings

(b)(4) Drawings

(b)(4) Drawings

(b)(4) Drawings

(b)(4) Drawings

(b)(4) Drawings

(b)(4) Drawings

(b)(4) Drawings

(b)(4) Drawings

(b)(4) Drawings

(b)(4) Drawings

(b)(4) Drawings

(b)(4) Drawings

(b)(4) Drawings

(b)(4) Drawings

(b)(4) Drawings

(b)(4) Drawings

(b)(4) Drawings

(b)(4) Drawings

(b)(4) Drawings

(b)(4) Drawings

(b)(4) Drawings

Records processed under FOIA Request #2014-8015; Released by CDRH on 12-8-2015

Pages 175 through 208 have been removed because they were duplicates of previous pages.

Questions? Contact FDA/CDRH/OCE/DID at CDRH-FOISTATUS@fda.hhs.gov or 301-796-8118

Records processed under FOIA Request #2014-8015; Released by CDRH on 12-8-2015

Section 12
Substantial Equivalence Discussion

Questions? Contact FDA/CDRH/OCE/DID at CDRH-FOISTATUS@fda.hhs.gov or 301-796-8118

Records processed under FOIA Request #2014-8015; Released by CDRH on 12-8-2015

Substantial Equivalence Discussion

For clarity, the Balanced Knee® System High Flex Vitamin E PS tibial insert and patella substantial equivalence discussion has been divided into three sections: 1) PS insert design, 2) patella design, and 3) vitamin E material.

Table 1. Substantial Equivalence Summary for Tibial Insert

Design Feature	Equivalent Device	Section
Indications for Use	Ortho Development: Balanced Knee® System High Flex PS (K123457)	1
Design (size, thickness, dimensions)	Ortho Development: Balanced Knee® System (K994370) Ortho Development: Balanced Knee® System High Flex PS (K123457)	1
Material: Extensively Crosslinked Vitamin E Polyethylene UHMWPE (α-tocopherol)	DJO Surgical/Encore Medical: Vit E UHMWPE Tibial Insert (K091956)	3

Table 2. Substantial Equivalence Summary for Patella

Design Feature	Equivalent Device	Section
Indications for Use	Ortho Development: Balanced Knee® System (K994370) Ortho Development: Balanced Knee® System High Flex PS (K123457)	2
Design (size, thickness, dimensions)	Ortho Development: Balanced Knee® System (K994370)	2
Material: Extensively Crosslinked Vitamin E Polyethylene UHMWPE (α-tocopherol)	DJO Surgical/Encore Medical: Vit E UHMWPE Tibial Insert (K091956)	3

Questions? Contact FDA/CDRH/OCE/DID at CDRH-FOISTATUS@fda.hhs.gov or 301-796-8118

1. Balanced Knee® System High Flex Vitamin E PS Insert Design

Predicate Devices:

Balanced Knee® System (K994370)
Ortho Development Corp.

Balanced Knee® System High Flex PS (K123457)
Ortho Development Corp.

The Balanced Knee® System High Flex Vitamin E (High Flex Vit E) PS tibial insert has substantially the same intended use, indications for use, dimensions, performance, and principles of operation as the predicate devices. A detailed comparison table is found on the following page (b) (4) [redacted]

(b) (4) [redacted]

Table 3. *Tibial Insert* Substantial Equivalence Table

	High Flex Vitamin E PS Tib Insert	**High Flex (CM Poly) PS Tib Insert**	**Balanced Knee® System PS Tib Insert**
Manufacturer	Ortho Development	Ortho Development	Ortho Development
510k Number	Pending	K123457	K994370
Application/ Product code	JWH	JWH	JWH
Size Range	Sizes 1-7, 7-20mm	Sizes 1-7, 7-20mm	Sizes 1-6, 7-14mm
(b)(4) [redacted]			
Size Compatibility with Femoral	One Up, One Down	One Up, One Down	One Up, One Down
(b)(4) [redacted]			
Sterilization	Ethylene Oxide	Gamma Irradiation in N_2	Gamma Irradiation in N_2
Range of Motion	Flexion up to 150°	Flexion up to 150°	Flexion up to 113°
Femorotibial Constraint	Identical to High Flex PS	See 510(k) K123457	See 510(k) K994370
Femorotibial Contact Area	Identical to High Flex PS	See 510(k) K123457	See 510(k) K994370
(b)(4) [redacted]			
Indications	Loss of joint configuration and joint function	Loss of joint configuration and joint function	Loss of joint configuration and joint function
	Osteoarthritis	Osteoarthritis	Osteoarthritis
	Rheumatoid arthritis	Rheumatoid arthritis	Rheumatoid arthritis
	Post-traumatic arthritis	Post-traumatic arthritis	Post-traumatic arthritis
	Valgus, varus, or flexion deformities	Valgus, varus, or flexion deformities	Valgus, varus, or flexion deformities
	Revision procedures where other treatments or devices have failed	Revision procedures where other treatments or devices have failed	--

Tibial Insert Substantial Equivalence Discussion

The High Flex Vit E PS insert is substantially equivalent to the High Flex PS insert. The indications for use of each device are identical. Although the High Flex Vit E PS insert device is nearly identical to the High Flex PS insert, the BKS PS insert is included in this submission because it has been used as a predicate for testing.

(b)(4)

[redacted]

The High Flex Vit E PS inserts are identical to the High Flex PS inserts in the following ways:

1. (b)(4) [redacted]
2. Accommodation of up to 150° of flexion when used as indicated with the High Flex PS femoral component.

The High Flex Vit E PS insert is different from the High Flex PS insert in the following ways:

(b)(4)

[redacted]

2. The High Flex Vit E PS insert is EO sterilized while the High Flex PS insert is gamma sterilized in inert gas packaging.

The key design feature for both the High Flex Vit E PS and High Flex PS inserts is the accommodation of flexion angles up to 150°.

Records processed under FOIA Request #2014-8015; Released by CDRH on 12-8-2015

2. Balanced Knee® System High Flex Vitamin E Patella

Predicate Devices:

Balanced Knee® System (K994370)
Ortho Development Corp.

Balanced Knee® System High Flex PS (K123457)
Ortho Development Corp.

The Balanced Knee® System High Flex Vitamin E (High Flex Vit E) patella has substantially the same intended use, indications for use, dimensions, performance, and principles of operation as the predicate devices. A detailed comparison table is found on the following page. The same predicate patella design is indicated for use with both the Balanced Knee® System and the Balanced Knee® System High Flex, so both systems have been included in the table. The patella was approved under K994370 and described with a new femoral component in K123457.

While the comparison indicates that in certain instances the predicate devices differ slightly in size and material, the High Flex Vit E patella has been thoroughly examined to ensure that no new issues of strength, safety, or effectiveness are raised by the design or material.

Questions? Contact FDA/CDRH/OCE/DID at CDRH-FOISTATUS@fda.hhs.gov or 301-796-8118

Table 4. *Patella* Substantial Equivalence Table

	High Flex Vitamin E Patella	**High Flex PS (used w/patella from K994370)**	**Balanced Knee® System (BKS)**
Manufacturer	Ortho Development	Ortho Development	Ortho Development
510k Number	Pending	K123457	K994370
Application/ Product code	JWH	JWH	JWH
(b)(4) [redacted]			
Peg Design	3 peg	3 peg	3 peg
Size Compatibility with Femoral	Compatible with any size femoral, BKS or High Flex	Compatible with any size femoral, BKS or High Flex	Compatible with any size femoral, BKS
(b)(4) [redacted]			
	Ethylene Oxide	Gamma Irradiation in N_2	Gamma Irradiation in N_2
Patellofemoral Constraint	Identical to BKS or High Flex PS, depending on mating femoral	See 510(k) K123457	See 510(k) K994370
Patellofemoral Contact Area	Identical to BKS or High Flex PS, depending on mating femoral	See 510(k) K123457	See 510(k) K994370
Indications	Loss of joint configuration and joint function	Loss of joint configuration and joint function	Loss of joint configuration and joint function
	Osteoarthritis	Osteoarthritis	Osteoarthritis
	Rheumatoid arthritis	Rheumatoid arthritis	Rheumatoid arthritis
	Post-traumatic arthritis	Post-traumatic arthritis	Post-traumatic arthritis
	Valgus, varus, or flexion deformities	Valgus, varus, or flexion deformities	Valgus, varus, or flexion deformities
	Revision procedures where other treatments or devices have failed	Revision procedures where other treatments or devices have failed	--

Patella Substantial Equivalence Discussion

The High Flex Vit E patella is substantially equivalent to the Balanced Knee® System/High Flex PS patella. Each indication for the High Flex Vit E patella can be found in the indications for both predicates.

(b)(4)

[redacted]

The High Flex Vit E patella is identical to the Balanced Knee® System patella in overall dimensions (size-to-size) for sizes 29-38mm. The High Flex Vit E patella is different from the Balanced Knee® System patella in following ways:

(b)(4)

[redacted]

3. The High Flex Vit E patella is EO sterilized while the Balanced Knee® System patella is gamma sterilized in inert gas packaging.

3. Balanced Knee® System High Flex Vitamin E Material

Predicate Devices:

Highly Cross-Linked Vitamin E UHMWPE Tibial Insert (K091956)
DJO Surgical/Encore Medical

The Balanced Knee® System High Flex Vitamin E PS (High Flex Vit E PS) tibial insert and patella have substantially the same intended use, materials, performance, and principles of operation as the predicate device. A detailed comparison table is found below. While the comparison indicates that in certain instances the predicate devices differ slightly in characteristics, all High Flex Vit E components have been thoroughly examined to ensure that no new issues of strength, safety, or effectiveness are raised by the material.

Table 5. *High Flex Vitamin E Material* Substantial Equivalence Table

	High Flex Vitamin E PS Tib Insert and Patella	**Crosslinked Vit E Tib Insert**
Manufacturer	Ortho Development	DJO Surgical/Encore Medical
510k Number	Pending	K091956
Application/ Product code	JWH	JWH, OIY, MBH
(b)(4) [redacted]		
Sterilization	Ethylene Oxide	Gas plasma
(b)(4) [redacted]		

Vitamin E Material Substantial Equivalence Discussion

The High Flex Vit E PS insert and patella are manufactured from UHMWPE that is substantially equivalent in both raw material and process to the DJO/Encore crosslinked Vit E insert. (b)(4) [redacted]

The material properties of the High Flex Vit E PS insert and patella are substantially equivalent to the material properties of the DJO/Encore crosslinked Vit E insert. (b)(4) [redacted]

Records processed under FOIA Request #2014-8015; Released by CDRH on 12-8-2015

MAR 2 4 2006
K994370

SUMMARY OF SAFETY AND EFFECTIVENESS:

This safety and effectiveness summary for the Ortho Development Balanced Knee™ System is provided as required per Section 513(i)(3) of the Food, Drug, and Cosmetic Act.

1. **Submitter:**
   Ortho Development Corporation
   106 West 12200 South
   Draper, Utah 84020

2. **Contact Person:**
   Carol Freasier
   Telephone: (801) 553-9991
   Fax: (801) 553-9993

3. **Trade Name:** Ortho Development Balanced Knee™ System
   Common Name: Balanced Knee™ System
   Classification Name: Prosthesis, Knee patellofemorotibial, Semi-constrained, Cemented, Polymer/Metal/Polymer (888.3560)

4. **Predicate or legally marketed devices which are substantially equivalent:**
   - Performance Total Knee System (Kirschner)
   - NexGen Total Knee System (Zimmer)
   - PCA Modular Total Knee System (Howmedica)
   - Natural Knee System (Intermedics)
   - AGC Modular Total Knee System (Biomet)
   - Foundation Total Knee System (Encore)

5. **Description of the device:**
   The Ortho Development Balanced Knee™ System is a semi-constrained total knee replacement system, consisting of femoral, tibial and patellar components.

   Materials: The devices are manufactured from CoCr alloy (cast or Wrought), Ti-6Al-4V alloy and Ultra High Molecular Weight Polyethylene (UHMWPE) per ASTM standards.

   Function: The system functions to provide restoration of function as a replacement for diseased and arthritic knees.

6. **Intended Use:**
   The Ortho Development Balanced Knee™ System is indicated for patients suffering from severe knee pain and disability. Specific indications include femoral, tibial and patellar replacement due to degenerative bone disease such as rheumatoid arthritis or osteoarthritis, primary and secondary traumatic arthritis, polyarthritis, collagen disorders, avascular necrosis of the femoral condyles, pseudo-gout, or complications from a previous prosthesis. This device is intended for cemented use only.

7. **Comparison of the technological characteristics of the device to predicate and legally marketed devices:**
   There are no significant differences between the Ortho Development Balanced Knee™ System and the systems currently being marketed which would adversely affect the use of the product. It is substantially equivalent to these other devices in design, function, material and intended use.

Questions? Contact FDA/CDRH/OCE/DID at CDRH-FOISTATUS@fda.hhs.gov or 301-796-8118

Records processed under FOIA Request #2014-8015; Released by CDRH on 12-8-2015

DEPARTMENT OF HEALTH & HUMAN SERVICES
Public Health Service

Food and Drug Administration
9200 Corporate Boulevard
Rockville MD 20850

MAR 24 2000

Ms. Carol Freasier
Regulatory Affairs / Quality Assurance
Ortho Development Corporation
106 West 12200 South
Draper, Utah 84020

Re: K994370
Trade Name: Ortho Development Balanced Knee™ System
Regulatory Class: II
Product Code: JWH
Dated: December 23, 1999
Received: December 27, 1999

Dear Ms. Freasier:

We have reviewed your Section 510(k) notification of intent to market the device referenced above and we have determined the device is substantially equivalent (for the indications for use stated in the enclosure) to devices marketed in interstate commerce prior to May 28, 1976, the enactment date of the Medical Device Amendments, or to devices that have been reclassified in accordance with the provisions of the Federal Food, Drug, and Cosmetic Act (Act). You may, therefore, market the device, subject to the general control provisions of the Act. The general control provisions of the Act include requirements for annual registration, listing of devices, good manufacturing practice, labeling, and prohibitions against misbranding and adulteration.

If your device is classified (see above) into either class II (Special Controls) or class III (Premarket Approval), it may be subject to such additional controls. Existing major regulations affecting your device can be found in the Code of Federal Regulations, Title 21, Parts 800 to 895. A substantially equivalent determination assumes compliance with the current Good Manufacturing Practice requirement, as set forth in the Quality System Regulation (QS) for Medical Devices: General regulation (21 CFR Part 820) and that, through periodic (QS) inspections, the Food and Drug Administration (FDA) will verify such assumptions. Failure to comply with the GMP regulation may result in regulatory action. In addition, FDA may publish further announcements concerning your device in the Federal Register. Please note: this response to your premarket notification submission does not affect any obligation you might have under sections 531 through 542 of the Act for devices under the Electronic Product Radiation Control provisions, or other Federal laws or regulations.

This letter will allow you to begin marketing your device as described in your 510(k) premarket notification. The FDA finding of substantial equivalence of your device to a legally marketed predicate device results in a classification for your device and thus, permits your device to proceed to the market.

Questions? Contact FDA/CDRH/OCE/DID at CDRH-FOISTATUS@fda.hhs.gov or 301-796-8118

Records processed under FOIA Request #2014-8015; Released by CDRH on 12-8-2015

If you desire specific advice for your device on our labeling regulation (21 CFR Part 801 and additionally 809.10 for in vitro diagnostic devices), please contact the Office of Compliance at (301) 594-4659. Additionally, for questions on the promotion and advertising of your device, please contact the Office of Compliance at (301) 594-4639. Also, please note the regulation entitled, "Misbranding by reference to premarket notification" (21 CFR 807.97). Other general information on your responsibilities under the Act may be obtained from the Division of Small Manufacturers Assistance at its toll-free number (800) 638-2041 or at (301) 443-6597, or at its Internet address "http://www.fda.gov/cdrh/dsmamain.html".

Sincerely yours,

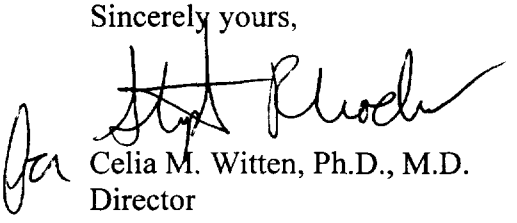

Celia M. Witten, Ph.D., M.D.
Director
Division of General and
Restorative Devices
Office of Device Evaluation
Center for Devices and
Radiological Health

Enclosure

Questions? Contact FDA/CDRH/OCE/DID at CDRH-FOISTATUS@fda.hhs.gov or 301-796-8118

Records processed under FOIA Request #2014-8015; Released by CDRH on 12-8-2015

510(k) Number (if known): K994370

Device Name: Balanced Knee™ System

Indications for Use

The Balanced Knee™ System is intended for single use in primary total knee replacement only. Indications include:

- Loss of joint configuration and joint function;
- Osteoarthritis of the knee joint;
- Rheumatoid arthritis of the knee joint;
- Post-traumatic arthritis of the knee joint;
- Moderate valgus, varus, or flexion deformities.

(PLEASE DO NOT WRITE BELOW THIS LINE-CONTINUE ON ANOTHER PAGE IF NEEDED)

Concurrence of CDRH, Office of Device Evaluation (ODE)

Division Sign-Off)
Division of General Restorative Devices
510(k) Number K994370

Prescription Use X OR Over-The-Counter Use
(Per 21 CFR 801.109) (Optional Format 1-2-96)

Questions? Contact FDA/CDRH/OCE/DID at CDRH-FOISTATUS@fda.hhs.gov or 301-796-8118

(b)(4)

(b)(4)

(b)(4)

(b)(4)

(b)(4)

(b)(4)

(b)(4)

(b)(4)

(b)(4)

(b)(4)

(b)(4)

(b)(4)

(b)(4)

(b)(4)

(b)(4)

(b)(4)

(b)(4)

(b)(4)

(b)(4)

(b)(4)

(b)(4)

(b)(4)

(b)(4)

(b)(4)

(b)(4)

(b)(4)

Records processed under FOIA Request #2014-8015; Released by CDRH on 12-8-2015

K091958 #12

SEP 28 2010

Summary of Safety and Effectiveness

Preparation Date: September 22, 2010

Applicant/Sponsor: Encore Medical (d.b.a. DJO Surgical)
9800 Metric Blvd
Austin, TX 78758

Contact Person: Elizabeth Pugh
Regulatory Affairs Specialist

Device Name: Highly Cross-Linked Vitamin E UHMWPE Tibial Insert

Classification Name: Knee joint patellofemorotibial polymer/metal/polymer semi-constrained cemented prosthesis (888.3560), OIY, JWH, MBH

Legally Marketed Devices to Which Substantial Equivalence is Claimed:

3DKnee	K020114	Encore Medical
E-Poly Tibial Bearings	K080528	Biomet

Device Description:
The Highly Cross-Linked Vitamin E UHMWPE (HXL VE) Tibial Inserts are manufactured from ultra high molecular weight polyethylene (UHMWPE) powder that is blended with pure liquid pharmaceutical grade alpha-tocopheral, compression molded and then highly cross-linked. The tibial inserts are available in 9 sizes (2- 12) and 5 thicknesses (9-19) and are provided in right and left orientations. The HXL VE Tibial Insert design is identical to the 3DKnee Tibial Insert cleared via K020114. This insert is intended to more closely match the kinematics of the knee, allowing some rotation along the medial condyle and increased congruency along the lateral condyle. The baseplate attachment mechanism is the same as the previously cleared 3DKnee System inserts.

Compatible Systems	Clearance	Cemented/Cementless
3DKnee System	K020114	Cemented
3DKnee Porous Coated Femoral Component	K032905	Cementless

Indications for Use:
Total joint replacement is indicated for patients suffering from disability due to:

- degenerative, post-traumatic or rheumatoid arthritis;
- avascular necrosis of the femoral condyle;

Questions? Contact FDA/CDRH/OCE/DID at CDRH-FOISTATUS@fda.hhs.gov or 301-796-8118

Records processed under FOIA Request #2014-8015; Released by CDRH on 02-8-2015

K011956 #2/8

- post-traumatic loss of joint configuration, particularly when there is patellofemoral erosion, dysfunction or prior patellectomy;
- moderate valgus, varus or flexion deformities;

This device may also be indicated in the salvage of previously failed surgical attempts. This device is intended to be used with the 3DKnee System for cemented or uncemented applications.

Intended Use:
DJO Surgical knee devices are intended for treatment of patients who are candidates for knee arthroplasty per the indications for use. While total knee replacements are not intended to withstand activity levels and loads of normal healthy bone, they are a means of restoring mobility and reducing pain for many patients.

Summary of Technologies:

Substantial Equivalence Table

Design Feature	Equivalent Device
Highly Cross-Linked Vitamin E Polyethylene Material UHMWPe (α-tocopherol)	E-Poly Tibial Bearings – Biomet (K080528)
Indications for Use	3DKnee Tibial Insert – Encore Medical (K020114)
Design (size, thickness, configuration, dimensions)	3DKnee Tibial Insert – Encore Medical (K020114)

Non-Clinical Testing:
The following non-clinical laboratory testing was performed to determine substantial equivalence: mechanical material characterization (Tensile, Small Punch, Izod Impact, and crack propagation), physical and chemical characterization (Oxidation Index, Compressive Modulus, Poisson's Ratio, Surface Roughness, Density, Onset Melting Temperature, Peak Melting Temperature, Delta H, Degree of Crystallinity, Crosslink Density, Swell Ratio, Molecular Weight, Polydispersity Index, Lamallae Thickness, Free Radical Concentration, Vitamin E Concentration, Vitamin E Consolidation, Vitamin E Elution/Extraction, Trans-vinylene Index), tibial insert peel-out strength, wear testing, and biocompatibility. All testing has demonstrated the device is substantially equivalent to the predicate devices.

Clinical Testing:
None provided as a basis for substantial equivalence.

Questions? Contact FDA/CDRH/OCE/DID at CDRH-FOISTATUS@fda.hhs.gov or 301-796-8118

Records processed under FOIA Request #2014-8015; Released by CDRH on 12-8-2015

DEPARTMENT OF HEALTH & HUMAN SERVICES

Public Health Service

Food and Drug Administration
10903 New Hampshire Avenue
Document Control Room –WO66-G609
Silver Spring, MD 20993-0002

Encore Medical, L.P.
% Mrs. Beth Pugh
Regulatory Affairs Specialist
9800 Metric Boulevard
Austin, Texas 78758

SEP 28 2010

Re: K091956
Trade/Device Name: Highly Cross-linked Vitamin E UHMWPE Tibial Inserts
Regulation Number: 21 CFR 888.3560
Regulation Name: Knee joint patellofemorotibial polymer/metal/ polymer semi-constrained cemented prothesis
Regulatory Class: Class II
Product Code: OIY, JWH, MBH
Dated: July 29, 2010
Received: July 30, 2010

Dear Mrs. Pugh:

We have reviewed your Section 510(k) premarket notification of intent to market the device referenced above and have determined the device is substantially equivalent (for the indications for use stated in the enclosure) to legally marketed predicate devices marketed in interstate commerce prior to May 28, 1976, the enactment date of the Medical Device Amendments, or to devices that have been reclassified in accordance with the provisions of the Federal Food, Drug, and Cosmetic Act (Act) that do not require approval of a premarket approval application (PMA). You may, therefore, market the device, subject to the general controls provisions of the Act. The general controls provisions of the Act include requirements for annual registration, listing of devices, good manufacturing practice, labeling, and prohibitions against misbranding and adulteration. Please note: CDRH does not evaluate information related to contract liability warranties. We remind you, however, that device labeling must be truthful and not misleading.

If your device is classified (see above) into either class II (Special Controls) or class III (PMA), it may be subject to additional controls. Existing major regulations affecting your device can be found in the Code of Federal Regulations, Title 21, Parts 800 to 898. In addition, FDA may publish further announcements concerning your device in the Federal Register.

Please be advised that FDA's issuance of a substantial equivalence determination does not mean that FDA has made a determination that your device complies with other requirements of the Act or any Federal statutes and regulations administered by other Federal agencies. You must comply with all the Act's requirements, including, but not limited to: registration and listing (21

Questions? Contact FDA/CDRH/OCE/DID at CDRH-FOISTATUS@fda.hhs.gov or 301-796-8118

Records processed under FOIA Request #2014-8015; Released by CDRH on 12-8-2015

CFR Part 807); labeling (21 CFR Part 801); medical device reporting (reporting of medical device-related adverse events) (21 CFR 803); good manufacturing practice requirements as set forth in the quality systems (QS) regulation (21 CFR Part 820); and if applicable, the electronic product radiation control provisions (Sections 531-542 of the Act); 21 CFR 1000-1050.

If you desire specific advice for your device on our labeling regulation (21 CFR Part 801), please go to http://www.fda.gov/AboutFDA/CentersOffices/CDRH/CDRHOffices/ucm115809.htm for the Center for Devices and Radiological Health's (CDRH's) Office of Compliance. Also, please note the regulation entitled, "Misbranding by reference to premarket notification" (21CFR Part 807.97). For questions regarding the reporting of adverse events under the MDR regulation (21 CFR Part 803), please go to http://www.fda.gov/MedicalDevices/Safety/ReportaProblem/default.htm for the CDRH's Office of Surveillance and Biometrics/Division of Postmarket Surveillance.

You may obtain other general information on your responsibilities under the Act from the Division of Small Manufacturers, International and Consumer Assistance at its toll-free number (800) 638-2041 or (301) 796-7100 or at its Internet address http://www.fda.gov/MedicalDevices/ResourcesforYou/Industry/default.htm.

Sincerely yours,

Mark N. Melkerson
Director
Division of Surgical, Orthopedic
and Restorative Devices
Office of Device Evaluation
Center for Devices and
Radiological Health

Enclosure

Questions? Contact FDA/CDRH/OCE/DID at CDRH-FOISTATUS@fda.hhs.gov or 301-796-8118

Records processed under FOIA Request #2014-8015; Released by CDRH on 12-8-2015

SEP 28 2010

510(k) Number (if known): K091956

Device Name: Highly Cross-Linked Vitamin E UHMWPE Tibial Insert

Indications for Use:

Joint replacement is indicated for patients suffering from disability due to:

- degenerative, post-traumatic or rheumatoid arthritis;
- avascular necrosis of the femoral condyle;
- post-traumatic loss of joint configuration, particularly when there is patellofemoral erosion, dysfunction or prior patellectomy;
- moderate valgus, varus or flexion deformities;

This device may also be indicated in the salvage of previously failed surgical attempts. This device is intended to be used with the 3DKnee System for cemented or uncemented applications.

Prescription Use X (Part 21 CFR 801 Subpart D) AND/OR Over-The-Counter Use _____ (21 CFR 801 Subpart C)

(PLEASE DO NOT WRITE BELOW THIS LINE-CONTINUE ON ANOTHER PAGE OF NEEDED)

Concurrence of CDRH, Office of Device Evaluation (ODE)

for MXM

(Division Sign-Off)
Division of Surgical, Orthopedic, and Restorative Devices

510(k) Number K091956

Questions? Contact FDA/CDRH/OCE/DID at CDRH-FOISTATUS@fda.hhs.gov or 301-796-8118

(b)(4)

(b)(4)

(b)(4)

(b)(4)

(b)(4)

(b)(4)

(b)(4)

(b)(4)

(b)(4)

(b)(4)

(b)(4)

(b)(4)

(b)(4)

(b)(4)

(b)(4)

(b)(4)

(b)(4)

(b)(4)

(b)(4)

(b)(4)

(b)(4)

(b)(4)

(b)(4)

(b)(4)

Records processed under FOIA Request #2014-8015; Released by CDRH on 12-8-2015

K123457

MAR 2 2 2013

510(k) Summary

NAME OF SPONSOR:	Ortho Development Corporation 12187 South Business Park Drive Draper, Utah 84020
510(k) CONTACT:	Tom Haueter Regulatory Affairs Manager Telephone: (801) 553-9991 Facsimile: (801) 553-9993 Email: thaueter@orthodevelopment.com
DATE PREPARED:	October 29, 2012
PROPRIETARY NAME:	Balanced Knee System High Flex PS
COMMON NAME:	Total Knee Replacement Prosthesis
CLASSIFICATION:	21 CFR 888.3560, Knee joint, patellofemorotibial, polymer/metal/polymer semi-constrained cemented prosthesis, Class II device
DEVICE PRODUCT CODE:	JWH
PREDICATE DEVICES:	Balanced Knee System (K994370), *Ortho Development Corp.* LPS-Flex Fixed Bearing Femoral and Articular Surface Components (K991581), *Zimmer*

Device Description

The Balanced Knee System High Flex PS (High Flex PS) is designed to accommodate increased range of motion up to 150° of flexion. The High Flex PS includes a highly polished Co-Cr-Mo PS femoral component and a compression molded UHMWPE PS tibial insert component. The High Flex PS femoral and insert components may be used in conjunction with the Balanced Knee System (BKS) standard and modular tibial trays, tibial augments, stems, and patellae to complete the semi-constrained modular knee prosthesis.

Questions? Contact FDA/CDRH/OCE/DID at CDRH-FOISTATUS@fda.hhs.gov or 301-796-8118

Records processed under FOIA Request #2014-8015; Released by CDRH on 12-8-2015

Intended Use

The Balanced Knee System High Flex PS is intended for use in cemented total knee arthroplasty procedures with the following indications:

1. Loss of knee joint configuration and joint function.
2. Osteoarthritis of the knee joint.
3. Rheumatoid arthritis of the knee joint.
4. Post-traumatic arthritis of the knee joint.
5. Valgus, varus, or flexion deformities of the knee joint.
6. Revision procedures where other treatments or devices have failed.

Performance Data

Property	Result
Range of Motion	Up to 150° flexion; Similar to predicate device, LPS-Flex
Femoral Fatigue	Improved Fatigue Strength over predicate device, BKS; Sufficient strength to survive in-vivo loading
Femorotibial Constraint	Similar to predicate device, BKS
Femorotibial Contact Area	Similar to predicate device, BKS
Patellofemoral Constraint	Similar to predicate device, BKS
Patellofemoral Contact Area	Similar to predicate device, BKS
PS Spine Fatigue	Sufficient strength to survive in-vivo loading

Basis for Substantial Equivalence

Ortho Development believes that the Balanced Knee System High Flex PS is substantially equivalent to the previously cleared predicate devices based on similarities in intended use, design, materials, manufacturing methods, packaging, and mechanical performance.

Questions? Contact FDA/CDRH/OCE/DID at CDRH-FOISTATUS@fda.hhs.gov or 301-796-8118

Records processed under FOIA Request #2014-8015; Released by CDRH on 12-8-2015

DEPARTMENT OF HEALTH & HUMAN SERVICES

Public Health Service

Food and Drug Administration
10903 New Hampshire Avenue
Document Control Center – WO66-G609
Silver Spring, MD 20993-0002

March 22, 2013

Ortho Development Corporation
% Mr. Tom Haueter
Regulatory Affairs Manager
12187 South Business Park Drive
Draper, Utah 84020

Re: K123457
Trade/Device Name: Balanced Knee® System High Flex PS
Regulation Number: 21 CFR 888.3560
Regulation Name: Knee joint patellofemorotibial polymer/metal/polymer semi-constrained cemented prosthesis
Regulatory Class: II
Product Code: JWH
Dated: February 8, 2013
Received: February 21, 2013

Dear Mr. Haueter:

We have reviewed your Section 510(k) premarket notification of intent to market the device referenced above and have determined the device is substantially equivalent (for the indications for use stated in the enclosure) to legally marketed predicate devices marketed in interstate commerce prior to May 28, 1976, the enactment date of the Medical Device Amendments, or to devices that have been reclassified in accordance with the provisions of the Federal Food, Drug, and Cosmetic Act (Act) that do not require approval of a premarket approval application (PMA). You may, therefore, market the device, subject to the general controls provisions of the Act. The general controls provisions of the Act include requirements for annual registration, listing of devices, good manufacturing practice, labeling, and prohibitions against misbranding and adulteration. Please note: CDRH does not evaluate information related to contract liability warranties. We remind you, however, that device labeling must be truthful and not misleading.

If your device is classified (see above) into either class II (Special Controls) or class III (PMA), it may be subject to additional controls. Existing major regulations affecting your device can be found in the Code of Federal Regulations, Title 21, Parts 800 to 898. In addition, FDA may publish further announcements concerning your device in the Federal Register.

Please be advised that FDA's issuance of a substantial equivalence determination does not mean that FDA has made a determination that your device complies with other requirements of the Act or any Federal statutes and regulations administered by other Federal agencies. You must comply with all the Act's requirements, including, but not limited to: registration and listing (21

Questions? Contact FDA/CDRH/OCE/DID at CDRH-FOISTATUS@fda.hhs.gov or 301-796-8118

Records processed under FOIA Request #2014-8015; Released by CDRH on 12-8-2015

CFR Part 807); labeling (21 CFR Part 801); medical device reporting (reporting of medical device-related adverse events) (21 CFR 803); good manufacturing practice requirements as set forth in the quality systems (QS) regulation (21 CFR Part 820); and if applicable, the electronic product radiation control provisions (Sections 531-542 of the Act); 21 CFR 1000-1050.

If you desire specific advice for your device on our labeling regulation (21 CFR Part 801), please go to http://www.fda.gov/AboutFDA/CentersOffices/CDRH/CDRHOffices/ucm115809.htm for the Center for Devices and Radiological Health's (CDRH's) Office of Compliance. Also, please note the regulation entitled, "Misbranding by reference to premarket notification" (21CFR Part 807.97). For questions regarding the reporting of adverse events under the MDR regulation (21 CFR Part 803), please go to http://www.fda.gov/MedicalDevices/Safety/ReportaProblem/default.htm for the CDRH's Office of Surveillance and Biometrics/Division of Postmarket Surveillance.

You may obtain other general information on your responsibilities under the Act from the Division of Small Manufacturers, International and Consumer Assistance at its toll-free number (800) 638-2041 or (301) 796-7100 or at its Internet address http://www.fda.gov/MedicalDevices/ResourcesforYou/Industry/default.htm.

Sincerely yours,

Erin D. Keith

Mark N. Melkerson
Director
Division of Orthopedic Devices
Office of Device Evaluation
Center for Devices and
Radiological Health

Enclosure

Questions? Contact FDA/CDRH/OCE/DID at CDRH-FOISTATUS@fda.hhs.gov or 301-796-8118

Records processed under FOIA Request #2014-8015; Released by CDRH on 12-8-2015

Indication for Use Form
Ortho Development
Balanced Knee® System High Flex PS 510(k)

510(k) Number (if known): K123457

Device Name: Balanced Knee® System High Flex PS

Indications for Use:

The Balanced Knee® System High Flex PS is intended for use in cemented total knee arthroplasty procedures.

Total knee arthroplasty is indicated for the following conditions:

1. Loss of knee joint configuration and joint function.
2. Osteoarthritis of the knee joint.
3. Rheumatoid arthritis of the knee joint.
4. Post-traumatic arthritis of the knee joint.
5. Valgus, varus, or flexion deformities of the knee joint.
6. Revision procedures where other treatments or devices have failed.

Prescription Use X (Part 21 CFR 801 Subpart D) AND/OR Over-The-Counter Use _____ (21 CFR 801 Subpart C)

(PLEASE DO NOT WRITE BELOW THIS LINE-CONTINUE ON ANOTHER PAGE IF NEEDED)

Concurrence of CDRH, Office of Device Evaluation (ODE)

Casey L. Hanley, Ph.D.
Division of Orthopaedic Devices

Questions? Contact FDA/CDRH/OCE/DID at CDRH-FOISTATUS@fda.hhs.gov or 301-796-8118

Records processed under FOIA Request #2014-8015; Released by CDRH on 12-8-2015

Section 13
Proposed Labeling

Questions? Contact FDA/CDRH/OCE/DID at CDRH-FOISTATUS@fda.hhs.gov or 301-796-8118

Records processed under FOIA Request #2014-8015; Released by CDRH on 12-8-2015

Ortho Development Label Master

Label Type: 351-1-10429, Product Label 4.75 x 4

Document No.: LM-See Table
Revision: A
CO No.: 8275

Label Format

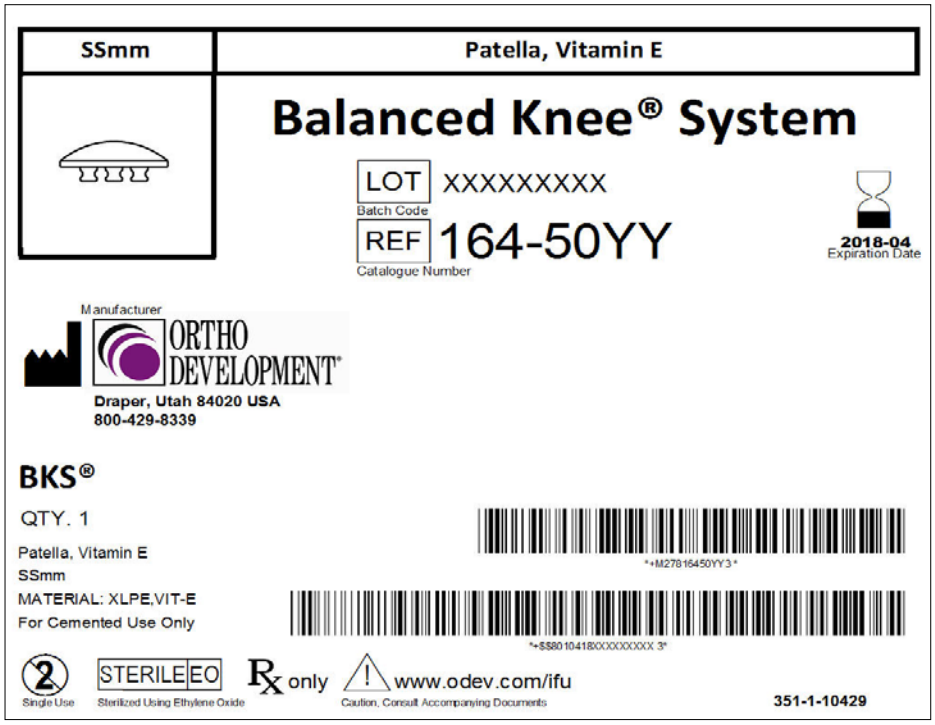

NOTES:

1. Verify label stock P/N is correct.
2. Replace "164-50YY" with the LM Number from table.
3. Replace "SSmm" with the Size from table.
4. Replace "XXXXXXXXX" with the Lot Number.
5. Replace date under Sterile Date Symbol with expiration date.
6. Use (b)(4) [redacted]: **Patella**

TABLE:

LM Number	Size
164-5029	29mm
164-5032	32mm
164-5035	35mm
164-5038	38mm
164-5041	41mm

Questions? Contact FDA/CDRH/OCE/DID at CDRH-FOISTATUS@fda.hhs.gov or 301-796-8118

Records processed under FOIA Request #2014-8015; Released by CDRH on 12-8-2015

Ortho Development Label Master

Label Type: 351-1-10428, St Pd Tyvek/Chart Label

Document No.: LM-See Table
Revision: A
CO No.: 8275

NOTES:

1. Verify label stock P/N is correct.
2. Replace "164-50YY" with the LM Number from table.
3. Replace "SSmm" with the Size from table.
4. Replace "XXXXXXX" with the Lot Number.
5. Replace date next to Sterile Date symbol with expiration date.
6. Use (b)(4) [redacted]

TABLE:

LM Number	Size
164-5029	29mm
164-5032	32mm
164-5035	35mm
164-5038	38mm
164-5041	41mm

Label Format

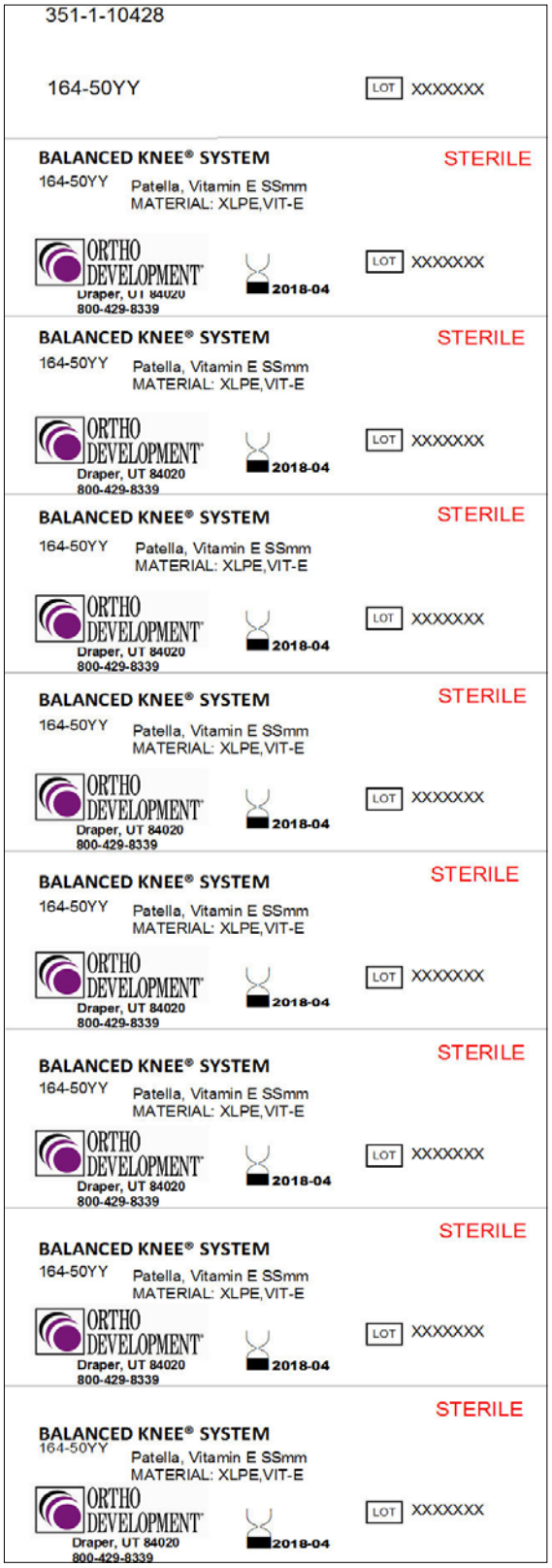

Questions? Contact FDA/CDRH/OCE/DID at CDRH-FOISTATUS@fda.hhs.gov or 301-796-8118

Records processed under FOIA Request #2014-8015; Released by CDRH on 12-8-2015

Ortho Development Label Master

Label Type: 351-1-10429, Product Label 4.75 x 4

Document No.: LM-166-5YYY
Revision: A
CO No.: 8275

Label Format

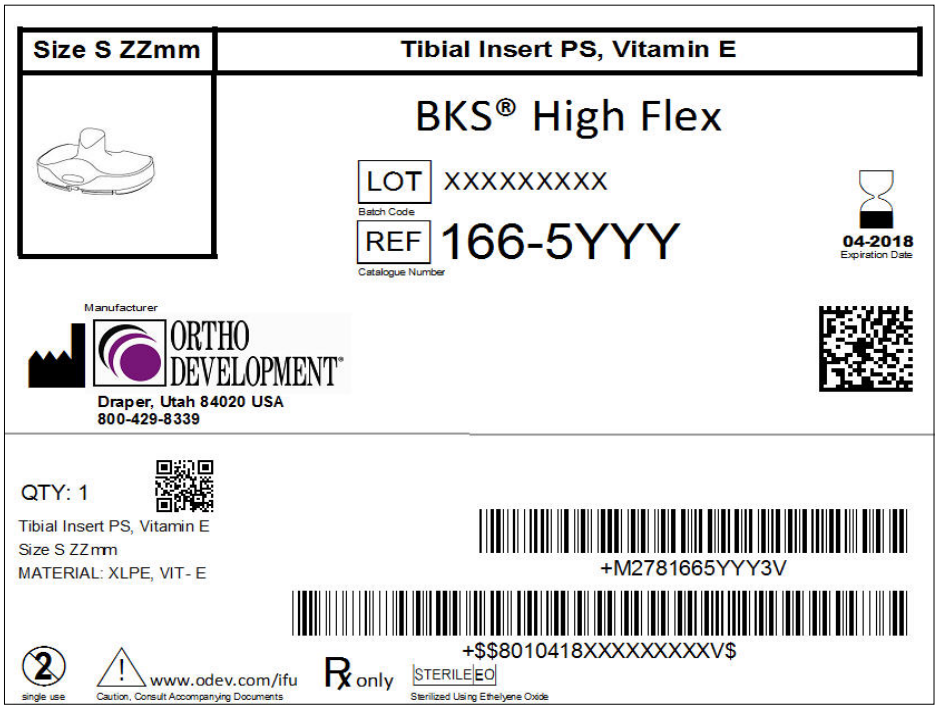

NOTES:

1. Verify label stock P/N is correct.
2. Replace "166-5YYY" with LM Number from Table.
3. Replace "Size S ZZmm" with Size from Table.
4. Replace "XXXXXXXXX" with the Lot Number.
5. Replace date under Sterile Date Symbol with the expiration date.
6. Use (b)(4) [redacted]

TABLE:

LM Number	Size
166-5107	Size 1 7mm
166-5108	Size 1 8mm
166-5109	Size 1 9mm
166-5110	Size 1 10mm
166-5111	Size 1 11mm
166-5112	Size 1 12mm
166-5113	Size 1 13mm
166-5114	Size 1 14mm
166-5116	Size 1 16mm
166-5118	Size 1 18mm
166-5120	Size 1 20mm
166-5207	Size 2 7mm
166-5208	Size 2 8mm
166-5209	Size 2 9mm
166-5210	Size 2 10mm
166-5211	Size 2 11mm

LM Number	Size
166-5212	Size 2 12mm
166-5213	Size 2 13mm
166-5214	Size 2 14mm
166-5216	Size 2 16mm
166-5218	Size 2 18mm
166-5220	Size 2 20mm
166-5307	Size 3 7mm
166-5308	Size 3 8mm
166-5309	Size 3 9mm
166-5310	Size 3 10mm
166-5311	Size 3 11mm
166-5312	Size 3 12mm
166-5313	Size 3 13mm
166-5314	Size 3 14mm
166-5316	Size 3 16mm
166-5318	Size 3 18mm

LM Number	Size
166-5320	Size 3 20mm
166-5407	Size 4 7mm
166-5408	Size 4 8mm
166-5409	Size 4 9mm
166-5410	Size 4 10mm
166-5411	Size 4 11mm
166-5412	Size 4 12mm
166-5413	Size 4 13mm
166-5414	Size 4 14mm
166-5416	Size 4 16mm
166-5418	Size 4 18mm
166-5420	Size 4 20mm
166-5507	Size 5 7mm
166-5508	Size 5 8mm
166-5509	Size 5 9mm
166-5510	Size 5 10mm

Questions? Contact FDA/CDRH/OCE/DID at CDRH-FOISTATUS@fda.hhs.gov or 301-796-8118

Records processed under FOIA Request #2014-8015; Released by CDRH on 12-8-2015

TABLE CONT:

LM Number	Size
166-5511	Size 5 11mm
166-5512	Size 5 12mm
166-5513	Size 5 13mm
166-5514	Size 5 14mm
166-5516	Size 5 16mm
166-5518	Size 5 18mm
166-5520	Size 5 20mm
166-5607	Size 6 7mm
166-5608	Size 6 8mm
166-5609	Size 6 9mm
166-5610	Size 6 10mm
166-5611	Size 6 11mm
166-5612	Size 6 12mm
166-5613	Size 6 13mm
166-5614	Size 6 14mm
166-5616	Size 6 16mm
166-5618	Size 6 18mm
166-5620	Size 6 20mm
166-5707	Size 7 7mm
166-5708	Size 7 8mm
166-5709	Size 7 9mm
166-5710	Size 7 10mm
166-5711	Size 7 11mm
166-5712	Size 7 12mm
166-5713	Size 7 13mm
166-5714	Size 7 14mm
166-5716	Size 7 16mm
166-5718	Size 7 18mm
166-5720	Size 7 20mm

Questions? Contact FDA/CDRH/OCE/DID at CDRH-FOISTATUS@fda.hhs.gov or 301-796-8118

Records processed under FOIA Request #2014-8015; Released by CDRH on 12-8-2015

Ortho Development Label Master

Label Type: 351-1-10428, St Pd Tyvek/Chart Label

Document No.: LM-166-5YYY
Revision: A
CO No.: 8275

NOTES:

1. Verify label stock P/N is correct.
2. Replace "166-5YYY" with LM Number from Table.
3. Replace "Size S ZZmm" with Size from Table.
4. Replace "XXXXXXXXX" with the Lot Number.
5. Replace date under Sterile Date Symbol with the expiration date.
6. Use (b)(4) [redacted]

Table:

LM Number	Size
166-5107	Size 1 7mm
166-5108	Size 1 8mm
166-5109	Size 1 9mm
166-5110	Size 1 10mm
166-5111	Size 1 11mm
166-5112	Size 1 12mm
166-5113	Size 1 13mm
166-5114	Size 1 14mm
166-5116	Size 1 16mm
166-5118	Size 1 18mm
166-5120	Size 1 20mm
166-5207	Size 2 7mm
166-5208	Size 2 8mm
166-5209	Size 2 9mm
166-5210	Size 2 10mm
166-5211	Size 2 11mm
166-5212	Size 2 12mm
166-5213	Size 2 13mm
166-5214	Size 2 14mm
166-5216	Size 2 16mm
166-5218	Size 2 18mm
166-5220	Size 2 20mm
166-5307	Size 3 7mm
166-5308	Size 3 8mm
166-5309	Size 3 9mm
166-5310	Size 3 10mm
166-5311	Size 3 11mm
166-5312	Size 3 12mm
166-5313	Size 3 13mm
166-5314	Size 3 14mm
166-5316	Size 3 16mm
166-5318	Size 3 18mm
166-5320	Size 3 20mm
166-5407	Size 4 7mm
166-5408	Size 4 8mm
166-5409	Size 4 9mm
166-5410	Size 4 10mm
166-5411	Size 4 11mm
166-5412	Size 4 12mm

LM Number	Size
166-5413	Size 4 13mm
166-5414	Size 4 14mm
166-5416	Size 4 16mm
166-5418	Size 4 18mm
166-5420	Size 4 20mm
166-5507	Size 5 7mm
166-5508	Size 5 8mm
166-5509	Size 5 9mm
166-5510	Size 5 10mm
166-5511	Size 5 11mm
166-5512	Size 5 12mm
166-5513	Size 5 13mm
166-5514	Size 5 14mm
166-5516	Size 5 16mm
166-5518	Size 5 18mm
166-5520	Size 5 20mm
166-5607	Size 6 7mm
166-5608	Size 6 8mm
166-5609	Size 6 9mm
166-5610	Size 6 10mm
166-5611	Size 6 11mm
166-5612	Size 6 12mm
166-5613	Size 6 13mm
166-5614	Size 6 14mm
166-5616	Size 6 16mm
166-5618	Size 6 18mm
166-5620	Size 6 20mm
166-5707	Size 7 7mm
166-5708	Size 7 8mm
166-5709	Size 7 9mm
166-5710	Size 7 10mm
166-5711	Size 7 11mm
166-5712	Size 7 12mm
166-5713	Size 7 13mm
166-5714	Size 7 14mm
166-5716	Size 7 16mm
166-5718	Size 7 18mm
166-5720	Size 7 20mm

Label Format

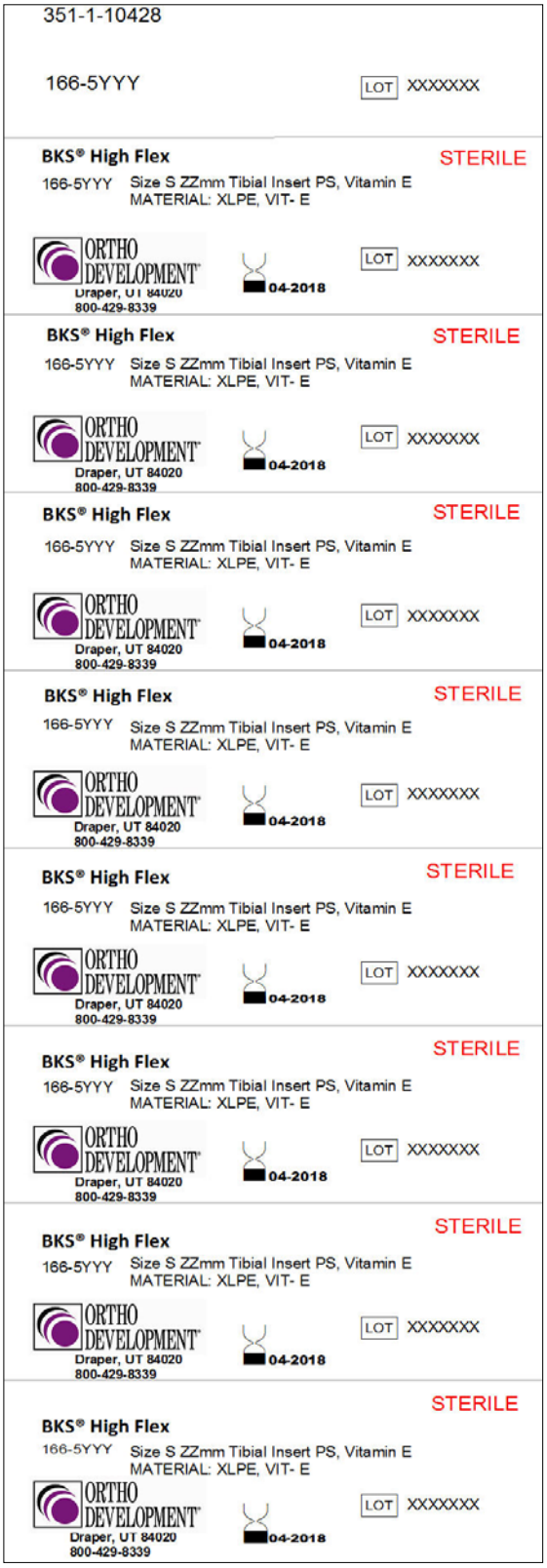

Questions? Contact FDA/CDRH/OCE/DID at CDRH-FOISTATUS@fda.hhs.gov or 301-796-8118

Records processed under FOIA Request #2014-8015; Released by CDRH on 12-8-2015

Instructions for Use

Balanced Knee® System

Manufacturer
Ortho Development® Corporation
12187 South Business Park Drive
Draper, UT 84020
Phone 801-553-9991
Fax 801-553-9993
www.orthodevelopment.com

For cemented use only

DESCRIPTION

The Balanced Knee® System and the Balanced Knee® System Revision are a multi-compartmental total knee replacement providing a system of components for posterior cruciate ligament retaining and substituting procedures. The Balanced Knee® System and the Balanced Knee® System Revision are indicated for cemented use only. Choice of specific femoral and tibial components depends on whether the posterior cruciate ligament is retained or excised, and the extent and nature of anterior/posterior (A/P) and medial/lateral (M/L) stabilization.

Cobalt Chromium Alloy Femoral Component

The femoral components are cobalt chromium (Co-Cr-Mo, ASTM F-75).

Component	*510(k) Number*
BKS Cruciate Retaining (CR)	K994370
BKS Posterior Stabilized (PS)	K994370
High Flex Posterior Stabilized (High Flex PS)	K123457
Modular Femoral	K060569

Femoral components with porous coating are porous coated with cobalt chromium (Co-Cr-Mo, ASTM F-75).

The semi-constrained posterior stabilizing femoral components are designed to provide anterior/posterior (A/P) stability, but rely on collateral ligament balancing techniques for medial/lateral (M/L) stability.

The cruciate retaining femoral components are designed for use with a functional posterior cruciate ligament. These components also rely on collateral ligament balancing techniques for medial/lateral (M/L) stability.

The modular femoral components are posterior stabilized with the option of intramedullary stem extensions and are designed to provide additional anterior/posterior (A/P) and medial/lateral (M/L) stability if needed or desired.

Titanium Tibial Tray

The titanium tibial tray (Ti-6Al-4V ELI, ASTM F-136) is available either with or without porous coating of commercially pure titanium (CP Ti, ASTM F-1580).

Questions? Contact FDA/CDRH/OCE/DID at CDRH-FOISTATUS@fda.hhs.gov or 301-796-8118

Component	*510(k) Number*
BKS Non-Porous Tray	K994370
BKS Porous Tray	K994370
BKS Porous Pegged Tray	K020383
Modular Tray	K031201
Offset Tray	K103837

The porous coated tibial trays are available in two options. The first option is supplied with removable polyethylene screw hole plugs (UHMWPE, ASTM F-648) for optional screw fixation using cancellous bone screws. The second porous coated option is offered with titanium pegs (Ti-6Al-4V ELI, ASTM F-136) instead of screw holes.

The modular tibial trays (Ti-6Al-4V ELI, ASTM F-136) are supplied with a titanium keel cap (Ti-6Al-4V ELI, ASTM F-136) which is removable in cases where a stem extension is needed.

The offset tibial trays (Ti-6Al-4V ELI, ASTM F-136) are used with an offset adapter, offset screw, and stem extension to accommodate various tibial anatomies.

Polyethylene Tibial Insert
The polyethylene tibial inserts are available in five variations:

Component	*510(k) Number*
BKS Cruciate Retaining (CR)	K994370
BKS Posterior Stabilized (PS)	K994370
BKS Ultra Congruent (UC)	K090705
High Flex Posterior Stabilized (HFPS)	K123457
High Flex Crosslinked Vitamin E Posterior Stabilized (HFVPS)	TBD
Semi-Constrained Posterior Stabilized (SCPS)	K060569

The PS, CR, UC, and High Flex PS variations are made of polyethylene (UHMWPE, ASTM F-648) and are to be used with the matching femoral component variation (i.e., PS femoral for PS insert, CR femoral for CR or UC insert, High Flex PS femoral for High Flex PS insert).

The High Flex Vitamin E PS is made of crosslinked Vitamin E polyethylene (Vitamin E UHMWPE, ASTM F-648) and is to be used with the matching femoral component variation (i.e. High Flex PS femoral with High Flex Vitamin E PS insert).

The SCPS variation is made of polyethylene (UHMWPE, ASTM F-648) and includes a titanium (Ti-6Al-4V ELI, ASTM F-136) reinforcement pin for added stability. The SCPS tibial insert is to be used with the matching femoral component (i.e., modular) when additional medial/lateral (M/L) stability is required. The SCPS tibial insert must also be used with the matching modular tibial tray or offset tibial tray.

Patella
The patellae are available in two variations:

Component	*510(k) Number*
Compression Molded Polyethylene Patella	K994370
Crosslinked Vitamin E Polyethylene Patella	TBD

The compression molded polyethylene patella (UHMWPE, ASTM F-648) is a resurfacing patellar prosthesis. 510(k) Number: K994370.

The Crosslinked Vitamin E Polyethylene Patella (Vitamin E UHMWPE, ASTM F-648) is a resurfacing patellar prosthesis. 510(k) Number: TBD.

Titanium Femoral Augments
The titanium femoral augments (Ti-6Al-4V ELI, ASTM F-136) are provided with a locking screw (Ti-6Al-4V ELI, ASTM F-136) and a locking ring (Ti-6Al-4V ELI, ASTM F-136). Femoral augments may only be used with the Balanced Knee® System Revision modular femoral components. 510(k) Number: K060569.

Femoral augments are provided for optional use in order to augment either the distal and/or posterior femur with bony deficiencies. Femoral augments are provided in assorted stepped configurations to facilitate surgeon selection for addressing typical bony defects.

Titanium Tibial Augments
The titanium tibial augments (Ti-6Al-4V ELI, ASTM F-136) are provided with a locking screw (Ti-6Al-4V ELI, ASTM F-136) and a locking ring (Ti-6Al-4V ELI, ASTM F-136). Tibial augments may only be used with the Balanced Knee® System Revision modular or offset tibial tray components. 510(k) Number: K031201.

Tibial augments are provided for optional use in order to augment a tibial plateau with bony deficiencies. Tibial augments are provided in assorted hemispherical stepped and angled configurations to facilitate surgeon selection for addressing typical bony defects.

Titanium Cemented and Fluted Stem Extensions
The titanium cemented and fluted stem extensions (Ti-6Al-4V ELI, ASTM F-136) are provided for optional use with the Balanced Knee® System Revision femoral components and tibial trays to provide increased stability. The stem extensions attach into the modular femoral junction box, the modular tibial tray, or the offset adapter as needed. 510(k) Number: K031201.

Cobalt Chromium Alloy Junction Box
The junction box is manufactured from forged cobalt chromium (Co-Cr-Mo, ASTM F-799) and is used with the modular femoral component when a stem extension is needed. The junction box is available in 5° and 7° options. 510(k) Number: K060569.

Titanium Offset Adapter
The titanium offset adapters (Ti-6Al-4V ELI, ASTM F-136) are provided with one screw (Ti-6Al-4V ELI, ASTM F-136). Offset adapters must be used with the Balanced Knee® System Revision offset tibial tray and stem extension components. One screw is required for sufficient fixation of the offset adapter. 510(k) Number: K103837.

Titanium Offset Screw
The titanium offset screws (Ti-6Al-4V ELI, ASTM F-136) are provided for optional use beyond the single screw that is required with the offset adapter. Offset screws may only be used with the Balanced Knee® System Revision offset tibial tray and offset adapter components. 510(k) Number: K103837.

Records processed under FOIA Request #2014-8015; Released by CDRH on 12-8-2015

INTENDED USE/INDICATIONS

1. Loss of knee joint configuration and joint function.
2. Osteoarthritis of the knee joint.
3. Rheumatoid arthritis of the knee joint.
4. Post-traumatic arthritis of the knee joint.
5. Valgus, varus, or flexion deformities of the knee joint.
6. Revision procedures where other treatments or devices have failed.

The Balanced Knee® System and Balanced Knee® System Revision are intended for total knee arthroplasty procedures.

The Balanced Knee® System is indicated in the salvage of previously failed surgical attempts where femoral bone loss does not require the use of augments or stem extensions and where collateral ligaments may be relied upon for medial/lateral (M/L) stability.

The Balanced Knee® System Revision is indicated in the salvage of previously failed surgical attempts where femoral bone loss may require the use of augments or stem extensions.

The Balanced Knee® System Revision SCPS Tibial Insert is indicated for use with the Balanced Knee® System Revision modular femoral and modular or offset tibial components where collateral ligament may not be relied upon for medial/lateral (M/L) stability.

The Balanced Knee® System Revision Offset Tibia is intended for use in the salvage of previously failed surgical attempts where bone loss may require the use of augments or stem extensions, or in difficult primary surgical cases where a long extension stem is necessary.

CONTRAINDICATIONS

1. Any patient not experiencing a compromised quality of life by loss of joint function and/or joint configuration, or pain from arthritis disease.
2. Any patient whose knee cannot be returned to normal function and normal stability through reconstructive procedures, including ligamentous balancing.
3. Active infection in or near the knee joint, fever and/or local inflammation signs, and elevation of sedimentation rate unexplained by other diseases should not be treated unless preoperative infection is ruled out.
4. Distant foci of infection, such as genitourinary, pulmonary, skin (chronic lesions or ulcerations), and other sites, that may result in hematogenous spread to the implant site.
5. Rapid joint destruction or bone absorption apparent on roentgenograms.
6. Neuromuscular disorders in which the potentially adverse effects on prosthesis function are not outweighed by the benefits gained by the patient from usage of the prosthesis.
7. Mental disorders that would compromise essential patient post-operative care.
8. A painless, stable arthrodesis in a functional position.
9. Allergic reactions to implant materials and/or tissue reactions to the products of corrosion or wear.
10. Skeletal immaturity.

INFORMATION FOR USE

To ensure proper placement and fit, only Balanced Knee® System and the Balanced Knee® System Revision instruments and trials manufactured by Ortho Development® Corporation should only be used to implant the

Questions? Contact FDA/CDRH/OCE/DID at CDRH-FOISTATUS@fda.hhs.gov or 301-796-8118

Records processed under FOIA Request #2014-8015; Released by CDRH on 12-8-2015
Balanced Knee® System and the Balanced Knee® System Revision components.

Components, trials, and instruments from other knee systems must not be used with components, trials, and instruments from the Balanced Knee® System and the Balanced Knee® System Revision and vice versa, unless specifically labeled for such use. Different engineering specifications and dimensional incompatibilities among the various systems may cause premature wear or loosening of the implant.

Components of the Balanced Knee® System and the Balanced Knee® System Revision are not compatible with the components of any other knee system.

Optimal fixation and implant stability are achieved by maximizing bone coverage. Components are provided in a variety of sizes. The largest available components should be chosen that cover, but do not overhang, the femur, tibia, or patella.

Several thicknesses and styles of polyethylene tibial inserts are supplied separately from the tibial tray, but in corresponding sizes to the tibial tray. The surgeon should choose an insert of appropriate thickness and style to restore the original joint line and to achieve proper ligament tension.

PRECAUTIONS

Preoperative:

The surgeon should thoroughly understand all aspects of the surgical procedure and limitations of the device. The surgeon should instruct patients as to the limits of the prosthesis and the impact of excessive loading through patient weight or activity. Patients should also be taught to govern and/or restrict their activities accordingly.

Strict adherence to the indications, contraindications, precautions, and warnings for this product is essential to potentially maximize the success of the procedure and the service life of the implant.

Intraoperative:

If the implant site has been improperly prepared or excessive force is used to seat the implant, fracture of the proximal tibia or femoral condyles may occur.

Polyethylene tibial inserts can be removed after they have been snapped into place. Once removed, however, they must be discarded, as the removal process deforms the plastic and reduces attachment strength. Use trials to determine proper tibial insert sizing.

An implant should never be reused. Any implant, once used, should be discarded. Though it appears undamaged, it may have small defects and internal stress patterns that may eventually lead to failure. Likewise, care must be taken in handling new implants to avoid damage that could compromise the mechanical integrity of the device and cause early failure or loosening, such as marring, nicks, or notches caused by contact with metal or abrasive objects.

The SCPS polyethylene insert can only be used with the modular tibial tray or offset tibial tray. It is not compatible with the primary porous coated, non-coated or pegged tibial trays. The modular femoral component with augments and stem may be used with the primary tibial trays only if a standard tibial insert is used.

If loose fragments of bone cement become detached, they can act as an abrasive on the contact surfaces of

Questions? Contact FDA/CDRH/OCE/DID at CDRH-FOISTATUS@fda.hhs.gov or 301-796-8118

the implant, greatly accelerating the wear rate of the prosthesis. Care should be taken to remove all excess cement from around the implant and its surfaces.

WARNINGS

Components of the Balanced Knee® System and/or the Balanced Knee® System Revision are not compatible with the components of any other knee system. Different specifications and dimensional compatibilities among the various systems may cause premature wear or loosening of the implant.

1. Use only Balanced Knee® System and/or the Balanced Knee® System Revision femoral components with Balanced Knee® System and/or the Balanced Knee® System Revision tibial inserts and tibial trays.
2. Use only Balanced Knee® System and/or the Balanced Knee® System Revision patella prostheses with Balanced Knee® System and/or the Balanced Knee® System Revision femoral components.
3. If optional screw fixation is desired with the porous coated tibial tray, use only Ortho Development® Corporation cancellous bone screws.
4. Components that are labeled as PS should be used only with other PS components. Likewise, CR components should be used only with CR or UC components. In addition components that are marked SCPS should be used only with other SCPS components. If no specification is made, the part can be used with either system.
5. The High Flex femoral component can only be used with the High Flex PS inserts.
6. The correct selection of the implant is extremely important. The potential for success in total joint replacement is increased by the selection of the proper size, shape, and design of the implant. The Balanced Knee® System and the Balanced Knee® System Revision have interchangeable part sizes as described by the following chart, where the number in the shaded box refers to the tibial insert size:

		Femoral Component Size						
		1	2	3	4	5	6	7
Tibial Tray Size	1	1	1					
	2	2	2	2				
	3		3	3	3			
	4			4	4	4		
	5				5	5	5	
	6					6	6	6
	7						7	7

6. The compatibility of the implants vary by what implant is being used. Correct implant choice is crucial in a successful joint replacement. Below is a compatibility chart which refers to the proper implants to be used:

		TIBIAL INSERT AND TRAY									
		BKS Tray				*Modular and Offset Tray*					
		CR	*UC*	*HFPS HFVPS*	*PS*	*CR*	*UC*	*HFPS HFVPS*	*PS*	*SCPS*	←Insert Type
FEMORAL	*BKS CR*	●	●			●	●				
	High Flex PS			●				●			
	BKS PS				●				●		
	Modular Femoral				●				●	●	

● = compatible

ADVERSE EFFECTS

Short-term complication rates may be similar to those occurring with any femoral joint replacement such as:

1. Changes in position and loosening of the implant.
2. Dislocation of implant.
3. Infection.
4. Reduced range of motion.
5. Heterotopic bone formation.
6. Incomplete pain relief.

MAGNETIC RESONANCE (MR)

The Balanced Knee® System and Balanced Knee® System Revision have not been evaluated for safety and compatibility in the MR environment. The Balanced Knee® System and Balanced Knee® System Revision have not been tested for heating or migration in the MR environment.

PACKAGING AND STERILITY

All implants are sterilized to Sterility Assurance Level 10^{-6}. All implants, except for the Vitamin E polyethylene components, are sterilized by a minimum of 25 kGy gamma irradiation. All Vitamin E polyethylene components are ethylene oxide sterilized.

All gamma irradiated polyethylene tibial inserts and polyethylene patellae are sterilized in an oxygen-free/nitrogen-rich environment.

Sterile product packaging should be inspected for flaws before and after opening. In the presence of a flaw, assume the product is non-sterile and do not implant it into a patient.

INSTRUMENT STERILITY

All Instruments should be thoroughly cleaned prior to sterilization. Please refer to Ortho Development Reusable Instrument Care Manual for instrument cleaning and sterilization details.

Unless otherwise indicated on the case labeling, the following Steam Sterilization Cycles must be followed in order to ensure sterility:

	Temperature	Cycle Time (minutes)	Dry Time (minutes)
Prevacuum	270 °F (132°C)	4	60
Gravity	270 °F (132°C)	30	90

Exceptions by Kit Number:

Kit Number	Description	Prevac	Prevac Dry	Gravity	Gravity Dry
261-9301	BKS Femoral 1	6	45	30	90
261-9304(A)	BKS Tibial 1	5	50	30	50

PRODUCT HANDLING

Always store implants unopened in their respective protective packages. Prior to use, inspect the packaging for damage, which may compromise sterility. When removing the implant from its packaging, observe relevant aseptic techniques. Protect the prosthesis from contact with objects that may damage the surface finish. Inspect each implant prior to use for visual damage.

PRODUCT COMPLAINTS

Any complaint or dissatisfaction with product quality, performance, labeling, and/or safety should be reported to Ortho Development® Corporation. If any of the implants or instruments “malfunction” (i.e., do not meet any of their performance specifications or do not perform as intended), and/or are suspected to have caused or

Records processed under FOIA Request #2014-8015; Released by CDRH on 12-8-2015
contributed to the death or serious injury of the patient, Ortho Development Corporation should be notified immediately by phone, fax or written correspondence.

When filing a complaint, please provide the product description, product number, lot number, complainant's name and address, and the nature of the complaint.

CAUTION

Federal Law (USA) restricts this device to sale, distribution, and use by or on the order of a physician.

351-1-10627 04/2013

Questions? Contact FDA/CDRH/OCE/DID at CDRH-FOISTATUS@fda.hhs.gov or 301-796-8118

Records processed under FOIA Request #2014-8015; Released by CDRH on 12-8-2015

Ortho Development Reusable Instrument Care Manual

for Balanced Knee® System, Balanced Knee® System Revision, and Balanced Knee® System High Flex

INSTRUMENT CARE

Considerations

- This guide includes processing instructions for Ortho Development (ODEV) reusable devices only.
- New and used instruments must be thoroughly cleaned per these instructions prior to sterilization and use.

Warnings and Precautions

- Universal precautions should be observed by all hospital personnel that work with contaminated medical devices. Caution should be exercised when handling devices with cutting edges or sharp points.
- Personal protective equipment (PPE) should be worn when handling or working with contaminated or potentially contaminated devices. PPE includes gown, mask, goggles or face shield, gloves and shoe covers.
- Do not place heavy instruments on top of more delicate instruments.
- Do **NOT** use metal brushes or scouring pads during manual cleaning. These will damage the surface and finish of instruments. Only soft-bristled, nylon brushes and pipe cleaners should be used.
- Do **NOT** allow contaminated devices to dry prior to reprocessing. All subsequent cleaning is facilitated by not allowing blood, body fluid, bone and tissue debris, saline or disinfectants to dry on used devices.
- Saline, and cleaning/disinfection agents containing active chlorine, aldehyde, bromide, bromine, chloride, mercury, iodine or iodide are corrosive and should **not** be used.
- Mineral oil or silicone lubricants should not be used because they are difficult to remove, prevent direct contact of the surface with steam during sterilization and coat microorganisms.

Limitations and Restrictions

- Automated cleaning using a washer/disinfector alone may not be effective for cleaning orthopedic instruments. A thorough manual or combination manual/automated cleaning process is recommended.
- Neutral pH enzymatic and cleaning agents are recommended.
- Instrument trays, cases and lids must be cleaned separately. Non-sterile, single use implants are an exception as they may remain in the tray or caddy for reprocessing.
- Repeated processing has minimal effect on ODEV reusable instruments unless otherwise noted. End of life for stainless steel or other metal surgical instruments is normally determined by wear and damage due to the intended use and not reprocessing.
- Use of hard water should be avoided. Softened tap water may be used for initial rinsing. Reverse Osmosis (RO) or Deionized (DI) water should be used for final rinsing of the instruments.

CLEANING INSTRUCTIONS

Point of Use

- Remove excess body fluids and tissue from instruments with a disposable, non-shedding wipe. Place devices in a tray of distilled water or cover with damp towels.
- Instruments should be cleaned within 30 minutes of use to minimize the potential for drying prior to cleaning.
- Used instruments must be transported to the central supply in closed or covered containers to prevent unnecessary contamination risk.

Preparation Before Cleaning

- All cleaning agents should be prepared according to the manufacturer. Softened tap water may be used to prepare cleaning agents. Use of manufacturer recommended temperatures is important for optimal performance of the cleaning agents.
- NOTE: Fresh cleaning solutions should be prepared when the existing solutions become grossly contaminated (turbid and/or bloody).

Questions? Contact FDA/CDRH/OCE/DID at CDRH-FOISTATUS@fda.hhs.gov or 301-796-8118

Table 1. Cleaning/Disinfection Options

Method	Description
Manual (Table 2)	Enzymatic soak and scrub followed by sonication
Combination Manual/Automated (Table 3)	Enzymatic soak and scrub followed by an automated washer/disinfector cycle.
Automated (washer/disinfector)	Automated cycle – Not recommended without manual pre-cleaning.

Manual Cleaning/Disinfection Procedure

Table 2. Manual Cleaning Steps

Step 1	Use a lint-free cloth dampened in tap water to remove gross soil. While wiping, actuate the instrument through the full range of motion.
Step 2	Prepare an enzymatic detergent according to manufacturer's recommendations using lukewarm tap water.
Step 3	Fully immerse the instruments in the detergent and soak for a minimum of 20 minutes. While soaking, the instrument(s) should be actuated to ensure complete penetration of the detergent. Using a soft bristled brush (e.g. M16) and as necessary, lumen brushes (e.g. 45-541, 45-545), remove all visible soil paying attention to crevices and hard to reach areas.
Step 4	Rinse the instrument(s) under running RO/DI water for a minimum of 3 minutes to remove detergent residue. While rinsing, actuate the instrument through its full range of motion.
Step 5	Prepare an enzymatic detergent according to manufacturer's recommendations using lukewarm tap water in an ultrasonic cleaner.
Step 6	Fully immerse the instrument(s) and sonicate for a minimum of 10 minutes.
Step 7	Rinse the instrument(s) under running RO/DI water for a minimum of 5 minutes to remove all evidence of detergent residue. While rinsing, actuate the instrument through its full range of motion.
Step 8	Visually inspect the instrument for soil. Dry using a clean, soft cloth and filtered pressurized air (<40psi). If soil is visible, repeat the process.

NOTE: Use of a sonicator at 45-50 kHz will aid in thorough cleaning of the devices.

NOTE: Use of a syringe or water jet will improve flushing of difficult to reach areas and closely mated surfaces.

Table 3. Combination Manual/Automated Cleaning Steps

Step 1	Use a lint-free cloth dampened in tap water to remove gross soil. Actuate the instrument through the full range of motion.
Step 2	Prepare an enzymatic detergent according to manufacturer's recommendations using lukewarm tap water.
Step 3	Fully immerse the instruments in the detergent and soak for a minimum of 20 minutes. While soaking, the instrument(s) should be actuated to ensure complete penetration of the detergent. Using a soft bristled brush (e.g. M16), remove all visible soil paying attention to crevices and hard to reach areas.
Step 4	Rinse the instruments under running RO/DI water for a minimum of 3 minutes to remove detergent residue. While rinsing, actuate the instrument through its full range of motion.
Step 5	Prepare an enzymatic detergent according to manufacturer's recommendations using lukewarm tap water in an ultrasonic cleaner.
Step 6	Fully immerse the instrument(s) and sonicate for a minimum of 10 minutes.
Step 7	Rinse the instrument(s) under running RO/DI water for a minimum of 5 minutes to remove all evidence of detergent residue. While rinsing, actuate the instrument through its full range of motion.
Step 8	Place instruments into the associated tray, then place into a washer/disinfector with the cover and upper tray(s) separate from the lower tray and main case.
Step 9	Remove from the washer and visually inspect for visible soil. If soil is visible, repeat the process.

NOTE: Use of a sonicator at 45-50 kHz will aid in thorough cleaning of the devices.

NOTE: Use of a syringe or water jet will improve flushing of difficult to reach areas and closely mated surfaces.

Table 4. Recommended Automated Washer/Disinfector Cycle Steps

Step 1	Pre-Wash; Cold Softened Tap Water; 1 minute
Step 2	Enzyme Wash; Hot Softened Tap Water; 1 minute
Step 3	Detergent Wash; Hot Softened Tap Water (66°C set point); 2 minutes
Step 4	Rinse; Hot Softened Tap Water; 1 minute
Step 5	Hot Air Dry (115°C); 7 minutes

Records processed under FOIA Request #2014-8015; Released by CDRH on 12-8-2015

Inspection, Maintenance and Testing

- Carefully inspect each device to ensure all visible contamination has been removed. If contamination is noted, repeat the cleaning/disinfection process.
- Check the action of moving parts to ensure smooth operation throughout the full range of motion.
- Hinged, rotating or articulating instruments should be lubricated with a water soluble product intended for surgical instruments that must be sterilized. Some water-based instrument lubricants contain bacteriostatic agents which are beneficial. Manufacturer's expiration dates should be adhered to for both stock and use-dilution concentrations.

STERILIZATION INSTRUCTIONS

- Trays and cases with lids may be wrapped in standard medical grade, steam sterilization wrap using the AAMI double wrap method or equivalent.
- NOTE: Areas designated for specific devices shall contain only devices specifically intended for these areas.
- NOTE: These validated reprocessing instructions are not applicable to Ortho Development trays that include devices that are not manufactured and/or distributed by Ortho Development. Instrument trays and cases without defined, preconfigured layouts or containing undefined universal spaces or compartments should only be used under the following conditions:
- All devices must be arranged to ensure steam penetration to all instrument surfaces. Instruments should not be stacked or placed in close contact.
- The user must ensure that the instrument case is not tipped or the contents shifted once the devices are arranged in the case. Silicone mats may be used to keep devices in place.
- Only devices manufactured and/or distributed by Ortho Development should be included in Ortho Development instrument trays. Ortho Development validated reprocessing instructions are not applicable to Ortho Development trays that include devices that are not manufactured and/or distributed by Ortho Development.

Sterilization

- Disinfection is only acceptable as a precursor to full sterilization for reusable surgical instruments. Refer to the table below for recommended minimum sterilization parameters that have been validated by Ortho Development to provide a 10^{-6} sterility assurance level (SAL).
- The hospital is responsible for in-house procedures for the reassembly, inspection and packaging of the instruments after they are thoroughly cleaned in a manner that will ensure steam sterilization penetration and adequate drying. Provisions for protection of any sharp or potentially dangerous areas of the instruments should also be recommended by the hospital.
- Moist heat/steam sterilization is the preferred and recommended method for Ortho Development orthopedic instrument sets.
- Sterilizer manufacturer recommendations should always be followed. When sterilizing multiple instrument sets in one sterilization cycle, ensure that the manufacturer's maximum load is not exceeded.
- Instrument sets should be properly prepared and packaged in trays and/or cases that will allow steam to penetrate and make direct contact with all surfaces.
- Ethylene oxide or gas plasma sterilization methods should not be used unless package inserts for the applicable product specifically provide instructions for sterilization using these methods.
- Gravity displacement sterilization cycles are not recommended because cycle times are too long to be practical. However, they are still provided.

Storage

- Sterile, packaged instruments should be stored in a designated, limited access area that is well ventilated and provides protection from dust, moisture, insects, vermin, and temperature/humidity extremes.

Hospital Responsibilities for Ortho Development Loaner Instruments

- Orthopedic instruments generally have a long service life; however, mishandling or inadequate protection can quickly diminish their life expectancy. Instruments which no longer perform properly because of long use, mishandling, or improper case should be returned to Ortho Development to be discarded. Notify your Ortho Development representative of any instrument problems.
- Loaner sets should undergo all steps of decontamination, cleaning, disinfection, inspection, and terminal sterilization before being returned to Ortho Development. Documentation of decontamination should be provided with instruments being returned to Ortho Development.

Questions? Contact FDA/CDRH/OCE/DID at CDRH-FOISTATUS@fda.hhs.gov or 301-796-8118

Records processed under FOIA Request #2014-8015; Released by CDRH on 12-8-2015

All instruments should be thoroughly cleaned prior to sterilization. Unless listed below, the following Steam Sterilization Cycles must be followed to ensure sterility:

	Temperature	Cycle Time (minutes)	Dry Time (minutes)
Prevacuum	270 °F (132°C)	4	60
Gravity	270 °F (132°C)	30	90

Exceptions by Kit Number:

Kit Number	Description	Prevac	Prevac Dry	Gravity	Gravity Dry
261-9301	BKS Femoral 1	6	45	30	90
261-9304(A)	BKS Tibial 1	5	50	30	50

Important Notice

- The instructions provided have been validated by Ortho Development as being capable of preparing orthopedic instruments for use. It is the responsibility of the hospital to ensure that the reprocessing is performed using the appropriate equipment and materials and the personnel in the reprocessing facility have been adequately trained in order to achieve the desired result. Equipment and processes should be validated and routinely monitored. Any deviation by the processor from these instructions should be properly evaluated for effectiveness to avoid potential adverse consequences.

Questions? Contact FDA/CDRH/OCE/DID at CDRH-FOISTATUS@fda.hhs.gov or 301-796-8118

(b)(4)

(b)(4)

(b)(4)

(b)(4)

(b)(4)

(b)(4)

Records processed under FOIA Request #2014-8015; Released by CDRH on 12-8-2015

Section 14
Sterilization and Shelf Life

Questions? Contact FDA/CDRH/OCE/DID at CDRH-FOISTATUS@fda.hhs.gov or 301-796-8118

Records processed under FOIA Request #2014-8015; Released by CDRH on 12-8-2015

Sterilization and Shelf Life

14.1 Sterilization:

14.1.1 Implant Sterility:

The implants are sterilized by ethylene oxide in accordance with ISO 11135-1. Each lot is processed in a validated cycle to achieve a sterility assurance level (SAL) of 10^{-6}.

Residual exposure limits for ethylene oxide and ethylene chlorohydrin comply with

(b)(4) [redacted]

The sterilization validation method is conducted per ISO 11135-1. Sterilization is (b)(4) [redacted] The responsibility of both parties is defined in a signed contract, consistent with FDA guidance on contract sterilization.

Ortho Development does not certify the sterile packaged device as pyrogen-free.

Refer to Section 14.2 for a description of the packaging used to maintain sterility. Refer to Section 13 for a copy of the labels identifying the product as STERILE.

14.1.2 Instrument Sterility:

Surgical instruments will be supplied non-sterile and are intended for sterilization or re-sterilization by the user.

Questions? Contact FDA/CDRH/OCE/DID at CDRH-FOISTATUS@fda.hhs.gov or 301-796-8118

14.1.3 Instrument Kit Sterility:

Surgical instrument kits will be supplied as non-sterile and are intended for sterilization or re-sterilization by the user. The validated steam sterilization cycles given below must be followed in order to ensure sterility.

(b)(4)

[redacted]

Instrument kits pertaining to Balanced Knee® System High Flex Vitamin E have been either revalidated or justified with a steam sterilization cycle, sterility assurance level (SAL) of 10^{-6}. Refer to the re-sterilization instructions in the IFU in Section 13.

14.1.4 Instrument Cleaning:

The IFU contains a statement that "all instruments shall be cleaned prior to sterilization" and provides cleaning instructions for reusable ODEV instruments. All the instruments pertaining to Balanced Knee® System High Flex Vitamin E are similar in material and similar or less complex than other instruments which have been validated for cleaning by Ortho Development and do not present new worst case instruments.

14.2 Implant Packaging:

14.2.1 The packaging configuration used for High Flex Vit E patella is identical to the packaging configuration used for BKS Revision tibial augments (K031201). The packaging configuration used for High Flex Vit E PS tibial inserts is identical to that used for the largest BKS High Flex femoral component (K123457).

(b)(4)

[redacted]

(b)(4)

[redacted]

14.3 Packaging Shelf Life:

(b)(4)

[redacted]

Records processed under FOIA Request #2014-8015; Released by CDRH on 12-8-2015

Section 15
Biocompatibility

Questions? Contact FDA/CDRH/OCE/DID at CDRH-FOISTATUS@fda.hhs.gov or 301-796-8118

Records processed under FOIA Request #2014-8015; Released by CDRH on 12-8-2015

Biocompatibility

The following tests were performed on the Balanced Knee® System High Flex Vitamin E PS tibial insert and patella. Detailed protocols and reports follow this summary.

1. **R-12-0128 Biocompatibility Testing of the High Flex Vitamin E**

Test	Standard	Results
Cytotoxicity	ISO 10993-5	(b)(4) [redacted]
Implantation	ISO 10993-6	
Irritation	ISO 10993-10	
Sensitization	ISO 10993-10	

In accordance with the AAMI/ISO 10993-1 Standard, the contact duration for the implants is designated as permanent (>30 days).

The instrument materials used as part of the High Flex Vitamin E are the same as those for Escalade® Acetabular Cup System (K103384). The contact duration per the AAMI/ISO 10993-1 standard is designated as limited (<24 hours). These materials are stainless steel and Radel®.

Questions? Contact FDA/CDRH/OCE/DID at CDRH-FOISTATUS@fda.hhs.gov or 301-796-8118

(b)(4) Testing

(b)(4) Testing

(b)(4) Testing

(b)(4) Testing

(b)(4) Testing

(b)(4) Testing

(b)(4) Testing

(b)(4) Testing

(b)(4) Testing

Records processed under FOIA Request #2014-8015; Released by CDRH on 12-8-2015

(301) 796 6946
michael.kasser@fda.hhs.gov

Questions? Contact FDA/CDRH/OCE/DID at CDRH-FOISTATUS@fda.hhs.gov or 301-796-8118

Records processed under FOIA Request #2014-8015; Released by CDRH on 12-8-2015

Section 16
Software

This section does not apply to the current submission.

Questions? Contact FDA/CDRH/OCE/DID at CDRH-FOISTATUS@fda.hhs.gov or 301-796-8118

Records processed under FOIA Request #2014-8015; Released by CDRH on 12-8-2015

Section 17
Electromagnetic Compatibility and Electrical Safety

This section does not apply to the current submission.

Questions? Contact FDA/CDRH/OCE/DID at CDRH-FOISTATUS@fda.hhs.gov or 301-796-8118

Records processed under FOIA Request #2014-8015; Released by CDRH on 12-8-2015

Section 18
Performance Testing – Bench

Questions? Contact FDA/CDRH/OCE/DID at CDRH-FOISTATUS@fda.hhs.gov or 301-796-8118

Records processed under FOIA Request #2014-8015; Released by CDRH on 12-8-2015

Performance Testing - Bench

The following tests were performed on the Balanced Knee® System High Flex Vitamin E (High Flex Vit E) PS tibial insert and patella. Each section summarizes the tests performed, results, standards used, and a discussion of the data. Detailed protocols and reports follow this summary.

1. **P-12-0011 Range of Motion Analysis of High Flex Primary Knee System**

   Standards: *ASTM F2083-10 Standard Specification for Total Knee Prosthesis*

(b)(4) Testing

[redacted]

Questions? Contact FDA/CDRH/OCE/DID at CDRH-FOISTATUS@fda.hhs.gov or 301-796-8118

Records processed under FOIA Request #2014-8015; Released by CDRH on 12-8-2015

(b)(4) Testing

[redacted]

Questions? Contact FDA/CDRH/OCE/DID at CDRH-FOISTATUS@fda.hhs.gov or 301-796-8118

2. **P-12-0004 High Flex Knee System Femorotibial Constraint Test**

Standards: *ASTM F2083-11 Standard Specification for Total Knee Prosthesis and ASTM F1223-08 Standard Test Method for Determination of Total Knee Replacement Constraint*

	RESULTS
Rotary/Laxity Test	High Flex PS was substantially equivalent to the benchmark BKS PS
Anterior/Posterior Draw Test	High Flex PS was substantially equivalent to the benchmark BKS PS
Medial/Lateral Shear Test	High Flex PS was substantially equivalent to the benchmark BKS PS

(b)(4) Testing

[redacted]

Records processed under FOIA Request #2014-8015; Released by CDRH on 12-8-2015

3. P-12-0104 High Flex Knee System Femorotibial Contact Area Test

Standards: *ASTM F2083-11 Standard Specification for Total Knee Prosthesis*

RESULTS
High Flex PS was substantially equivalent to the benchmark BKS PS

(b)(4) Testing

[redacted]

Questions? Contact FDA/CDRH/OCE/DID at CDRH-FOISTATUS@fda.hhs.gov or 301-796-8118

Records processed under FOIA Request #2014-8015; Released by CDRH on 12-8-2015

4. P-12-0005 High Flex Knee System Patellofemoral Constraint Test

Standards: *ASTM F1672-95 (2005) Standard Specification for Resurfacing Patellar Prosthesis*

RESULTS
High Flex PS was substantially equivalent to the benchmark BKS PS

(b)(4) Testing

[redacted]

Questions? Contact FDA/CDRH/OCE/DID at CDRH-FOISTATUS@fda.hhs.gov or 301-796-8118

Records processed under FOIA Request #2014-8015; Released by CDRH on 12-8-2015

5. **P-12-0006 High Flex Knee System Patellofemoral Contact Area Test**

Standards: *ASTM F1672-95 (2005) Standard Specification for Resurfacing Patellar Prosthesis*

RESULTS
High Flex PS was substantially equivalent to the benchmark BKS PS

(b)(4) Testing

[redacted]

Questions? Contact FDA/CDRH/OCE/DID at CDRH-FOISTATUS@fda.hhs.gov or 301-796-8118

6. **P-12-0010A BKS High Flex Vitamin E PS Spine Fatigue Test *along with* R-13-0010 Physiologically-Loaded Knee PS Spine Strength Loading Scheme**

   Standards: *FDA Guidance Class II Special Controls Guidance Document: Knee Joint Patellofemorotibial Metal/Polymer Porous-Coated Uncemented Prostheses: Guidance for Industry and FDA*

(b)(4) Testing

[redacted]

[a] D. D'Lima, S. Patil, N. Steklov, S. Chien, C. Colwell Jr., "In vivo knee moments and shear after total knee arthroplasty," *Journal of Biomechanics*, Volume 40 (2007), Pages S11-S17.

7. **P-12-0007 BKS High Flex Vitamin E Tibial Insert Assembly/Disassembly Locking Mechanism**
   Standards: *FDA Guidance Class II Special Controls Guidance Document: Knee Joint Patellofemorotibial Metal/Polymer Porous-Coated Uncemented Prostheses: Guidance for Industry and FDA*

(b)(4) Testing

[redacted]

8. **P-11-0093 Initial process and testing of knee EXLPE, *along with***
   P-12-0098 BKS knee sterilized GUR 1050 UHMWPE material property testing
   Standards:
   ASTM D638, Standard Test Method for Tensile Properties of Plastics

(b)(4) Testing

[redacted]

9. **P-12-0106 Properties of High Flex EXLPE, Part 1, Crosslinking Characterization**

Standards:

ASTM F2565 Standard Guide for Extensively Irradiation-Crosslinked Ultra-High Molecular Weight Polyethylene Fabricated Forms of Surgical Implant Applications

ASTM F648 Standard Specification for Ultra-High-Molecular-Weight Polyethylene Powder and Fabricated Form for Surgical Implants

ASTM F2183 Standard Test Method for Small Punch Testing of Ultra-High Molecular Weight Polyethylene Used in Surgical Implants

ASTM F2102 Standard Guide for Evaluating the Extent of Oxidation in Ultra-High-Molecular-Weight Polyethylene Fabricated Forms Intended for Surgical Implants

ASTM F2381 Standard Test Method for Evaluating Trans-Vinylene Yield in Irradiated Ultra-High-Molecular-Weight Polyethylene Fabricated Forms Intended for Surgical Implants by Infrared Spectroscopy

ASTM F2625 Standard Test Method for Measurement of Enthalpy of Fusion, Percent Crystallinity, and Melting Point of Ultra-High-Molecular Weight Polyethylene by Means of Differential Scanning Calorimetry

ASTM F2003 Standard Practice for Accelerated Aging of Ultra-High Molecular Weight Polyethylene after Gamma Irradiation in Air

(b)(4) Testing

[redacted]

Records processed under FOIA Request #2014-8015; Released by CDRH on 12-8-2015

(b)(4) Testing

[redacted]

Questions? Contact FDA/CDRH/OCE/DID at CDRH-FOISTATUS@fda.hhs.gov or 301-796-8118

10. **P-12-0107 Properties of High Flex EXLPE, Part 2, Crosslinking Characterization**
    Standards:
    ASTM F2565 Standard Guide for Extensively Irradiation-Crosslinked Ultra-High Molecular Weight Polyethylene Fabricated Forms of Surgical Implant Applications
    ASTM E647 Standard Test Method for Measurement of Fatigue Crack Growth Rates
    ASTM D695 Standard Test Method for Compressive Properties of Rigid Plastics
    ASTM D6068 Standard Test Method for Determining J-R curves of Plastic Materials
    ASTM F2214 Standard Test Method for In Situ Determination of Network Parameters of Crosslinked Ultra High Molecular Weight Polyethylene (UHMWPE)
    ASTM D1505 Standard Test Method for Density of Plastics by the Density-Gradient Technique
    ASTM F2003 Standard Practice for Accelerated Aging of Ultra-High Molecular Weight Polyethylene after Gamma Irradiation in Air

(b)(4) Testing

[redacted]

Varadarajan, R., “On the nature of static and cyclic fracture resistance of ultra high molecular weight polyethylenes used in total joint replacements,” Ph.D. Dissertation, Case Western University, 2007.

Haider, H., Weisenburger, J.N., Kurtz, S.M., Rimnac, C.M., Freedman, J., Schroeder, D.W., and Garvin, K.L., “Does vitamin E-stabilized ultrahigh-molecular-weight polyethylene address concerns of cross-linked polyethylene in total knee arthroplasty?” J Arthroplasty, 5(3), p. 461-469, 2011.

(b)(4) Testing

[redacted]

11. **P-12-0117 Properties of High Flex EXLPE, Part 3, Vitamin E Characterization**
    Standards:
    ASTM F648 Standard Specification for Ultra-High-Molecular-Weight Polyethylene Powder and Fabricated Form for Surgical Implants
    ASTM F2102 Standard Guide for Evaluating the Extent of Oxidation in Ultra-High-Molecular-Weight Polyethylene Fabricated Forms Intended for Surgical Implants
    ASTM F2003 Standard Practice for Accelerated Aging of Ultra-High Molecular Weight Polyethylene after Gamma Irradiation in Air

(b)(4) Testing

[redacted]

Gul, R.M., McGarry, F.J., Bragdon, C.R., Muratoglu, O.K., and Harris, W.H., "Effect of consolidation on adhesive and abrasive wear of ultra high molecular weight polyethylene," Biomaterials, 24(19), p. 3193-3199, 2003.

(b)(4) Testing

[redacted]

Records processed under FOIA Request #2014-8015; Released by CDRH on 12-8-2015

(b)(4) Testing

[redacted]

Questions? Contact FDA/CDRH/OCE/DID at CDRH-FOISTATUS@fda.hhs.gov or 301-796-8118

12. **P-12-0103 High Flex Knee System Wear Testing**

    Standards:

    ISO 14243-1 Implants for surgery – Wear of total knee joint prostheses – Part 1: Loading and displacement parameters for wear-testing machines with load control and corresponding environmental conditions for test

    ISO 14243-2 Implants for surgery – Wear of total knee joint prostheses – Part 2: Methods of measurement

    ASTM F2003 Standard Practice for Accelerated Aging of Ultra-High Molecular Weight Polyethylene after Gamma Irradiation in Air

(b)(4) Testing

[redacted]

Records processed under FOIA Request #2014-8015; Released by CDRH on 12-8-2015

(b)(4) Testing

[redacted]

Questions? Contact FDA/CDRH/OCE/DID at CDRH-FOISTATUS@fda.hhs.gov or 301-796-8118

13. **P-12-0118 Properties of High Flex EXLPE, Part 4, Post-wear-test material analysis**
    Standards:
    ASTM F2102 Standard Guide for Evaluating the Extent of Oxidation in Ultra-High-Molecular-Weight Polyethylene Fabricated Forms Intended for Surgical Implants
    ASTM F2003 Standard Practice for Accelerated Aging of Ultra-High Molecular Weight Polyethylene after Gamma Irradiation in Air
    ASTM F2183 Standard Test Method for Small Punch Testing of Ultra-High Molecular Weight Polyethylene Used in Surgical Implants

(b)(4) Testing

[redacted]

Records processed under FOIA Request #2014-8015; Released by CDRH on 12-8-2015

(b) (4)

[redacted]

Questions? Contact FDA/CDRH/OCE/DID at CDRH-FOISTATUS@fda.hhs.gov or 301-796-8118

(b)(4) Testing

(b)(4) Testing

(b)(4) Testing

(b)(4) Testing

(b)(4) Testing

(b)(4) Testing

(b)(4) Testing

(b)(4) Testing

(b)(4) Testing

(b)(4) Testing

(b)(4) Testing

(b)(4) Testing

(b)(4) Testing

(b)(4) Testing

(b)(4) Testing

(b)(4) Testing

(b)(4) Testing

(b)(4) Testing

(b)(4) Testing

(b)(4) Testing

(b)(4) Testing

(b)(4) Testing

(b)(4) Testing

(b)(4) Testing

(b)(4) Testing

(b)(4) Testing

(b)(4) Testing

(b)(4) Testing

(b)(4) Testing

(b)(4) Testing

(b)(4) Testing

(b)(4) Testing

(b)(4) Testing

(b)(4) Testing

(b)(4) Testing

(b)(4) Testing

(b)(4) Testing

(b)(4) Testing

(b)(4) Testing

(b)(4) Testing

(b)(4) Testing

(b)(4) Testing

(b)(4) Testing

(b)(4) Testing

(b)(4) Testing

(b)(4) Testing

(b)(4) Testing

(b)(4) Testing

(b)(4) Testing

(b)(4) Testing

(b)(4) Testing

(b)(4) Testing

(b)(4) Testing

(b)(4) Testing

(b)(4) Testing

(b)(4) Testing

(b)(4) Testing

(b)(4) Testing

(b)(4) Testing

(b)(4) Testing

(b)(4) Testing

(b)(4) Testing

(b)(4) Testing

(b)(4) Testing

(b)(4) Testing

(b)(4) Testing

(b)(4) Testing

(b)(4) Testing

(b)(4) Testing

(b)(4) Testing

(b)(4) Testing

(b)(4) Testing

(b)(4) Testing

(b)(4) Testing

(b)(4) Testing

(b)(4) Testing

(b)(4) Testing

(b)(4) Testing

(b)(4) Testing

(b)(4) Testing

(b)(4) Testing

(b)(4) Testing

(b)(4) Testing

(b)(4) Testing

(b)(4) Testing

(b)(4) Testing

(b)(4) Testing

(b)(4) Testing

(b)(4) Testing

(b)(4) Testing

(b)(4) Testing

(b)(4) Testing

(b)(4) Testing

(b)(4) Testing

(b)(4) Testing

(b)(4) Testing

(b)(4) Testing

(b)(4) Testing

(b)(4) Testing

(b)(4) Testing

(b)(4) Testing

(b)(4) Testing

(b)(4) Testing

(b)(4) Testing

(b)(4) Testing

(b)(4) Testing

(b)(4) Testing

(b)(4) Testing

(b)(4) Testing

(b)(4) Testing

(b)(4) Testing

(b)(4) Testing

(b)(4) Testing

(b)(4) Testing

(b)(4) Testing

(b)(4) Testing

(b)(4) Testing

(b)(4) Testing

(b)(4) Testing

(b)(4) Testing

(b)(4) Testing

(b)(4) Testing

(b)(4) Testing

(b)(4) Testing

(b)(4) Testing

(b)(4) Testing

(b)(4) Testing

(b)(4) Testing

(b)(4) Testing

(b)(4) Testing

(b)(4) Testing

(b)(4) Testing

(b)(4) Testing

(b)(4) Testing

(b)(4) Testing

(b)(4) Testing

(b)(4) Testing

(b)(4) Testing

(b)(4) Testing

(b)(4) Testing

(b)(4) Testing

(b)(4) Testing

(b)(4) Testing

(b)(4) Testing

(b)(4) Testing

(b)(4) Testing

(b)(4) Testing

(b)(4) Testing

(b)(4) Testing

(b)(4) Testing

(b)(4) Testing

(b)(4) Testing

(b)(4) Testing

(b)(4) Testing

(b)(4) Testing

(b)(4) Testing

(b)(4) Testing

(b)(4) Testing

(b)(4) Testing

(b)(4) Testing

(b)(4) Testing

(b)(4) Testing

(b)(4) Testing

(b)(4) Testing

(b)(4) Testing

(b)(4) Testing

(b)(4) Testing

(b)(4) Testing

(b)(4) Testing

(b)(4) Testing

(b)(4) Testing

(b)(4) Testing

(b)(4) Testing

(b)(4) Testing

(b)(4) Testing

(b)(4) Testing

(b)(4) Testing

(b)(4) Testing

(b)(4) Testing

(b)(4) Testing

(b)(4) Testing

(b)(4) Testing

(b)(4) Testing

(b)(4) Testing

(b)(4) Testing

(b)(4) Testing

(b)(4) Testing

(b)(4) Testing

(b)(4) Testing

(b)(4) Testing

(b)(4) Testing

(b)(4) Testing

(b)(4) Testing

(b)(4) Testing

(b)(4) Testing

(b)(4) Testing

(b)(4) Testing

(b)(4) Testing

(b)(4) Testing

(b)(4) Testing

(b)(4) Testing

(b)(4) Testing

(b)(4) Testing

(b)(4) Testing

(b)(4) Testing

(b)(4) Testing

(b)(4) Testing

(b)(4) Testing

(b)(4) Testing

(b)(4) Testing

(b)(4) Testing

(b)(4) Testing

(b)(4) Testing

(b)(4) Testing

(b)(4) Testing

(b)(4) Testing

(b)(4) Testing

(b)(4) Testing

(b)(4) Testing

(b)(4) Testing

(b)(4) Testing

(b)(4) Testing

(b)(4) Testing

(b)(4) Testing

(b)(4) Testing

(b)(4) Testing

(b)(4) Testing

(b)(4) Testing

(b)(4) Testing

(b)(4) Testing

(b)(4) Testing

(b)(4) Testing

(b)(4) Testing

(b)(4) Testing

(b)(4) Testing

(b)(4) Testing

(b)(4) Testing

(b)(4) Testing

(b)(4) Testing

(b)(4) Testing

(b)(4) Testing

(b)(4) Testing

(b)(4) Testing

(b)(4) Testing

(b)(4) Testing

(b)(4) Testing

(b)(4) Testing

(b)(4) Testing

(b)(4) Testing

(b)(4) Testing

(b)(4) Testing

(b)(4) Testing

(b)(4) Testing

(b)(4) Testing

(b)(4) Testing

(b)(4) Testing

(b)(4) Testing

(b)(4) Testing

(b)(4) Testing

(b)(4) Testing

(b)(4) Testing

(b)(4) Testing

(b)(4) Testing

(b)(4) Testing

(b)(4) Testing

(b)(4) Testing

(b)(4) Testing

(b)(4) Testing

(b)(4) Testing

(b)(4) Testing

(b)(4) Testing

(b)(4) Testing

(b)(4) Testing

(b)(4) Testing

(b)(4) Testing

(b)(4) Testing

(b)(4) Testing

(b)(4) Testing

(b)(4) Testing

(b)(4) Testing

(b)(4) Testing

(b)(4) Testing

(b)(4) Testing

(b)(4) Testing

(b)(4) Testing

(b)(4) Testing

(b)(4) Testing

(b)(4) Testing

(b)(4) Testing

(b)(4) Testing

(b)(4) Testing

(b)(4) Testing

(b)(4) Testing

(b)(4) Testing

(b)(4) Testing

(b)(4) Testing

(b)(4) Testing

(b)(4) Testing

(b)(4) Testing

(b)(4) Testing

(b)(4) Testing

(b)(4) Testing

(b)(4) Testing

(b)(4) Testing

(b)(4) Testing

(b)(4) Testing

(b)(4) Testing

(b)(4) Testing

(b)(4) Testing

(b)(4) Testing

(b)(4) Testing

(b)(4) Testing

(b)(4) Testing

(b)(4) Testing

(b)(4) Testing

(b)(4) Testing

(b)(4) Testing

(b)(4) Testing

(b)(4) Testing

(b)(4) Testing

(b)(4) Testing

(b)(4) Testing

(b)(4) Testing

(b)(4) Testing

(b)(4) Testing

(b)(4) Testing

(b)(4) Testing

(b)(4) Testing

(b)(4) Testing

(b)(4) Testing

(b)(4) Testing

(b)(4) Testing

(b)(4) Testing

(b)(4) Testing

(b)(4) Testing

(b)(4) Testing

(b)(4) Testing

(b)(4) Testing

(b)(4) Testing

(b)(4) Testing

(b)(4) Testing

(b)(4) Testing

(b)(4) Testing

(b)(4) Testing

(b)(4) Testing

(b)(4) Testing

(b)(4) Testing

(b)(4) Testing

(b)(4) Testing

(b)(4) Testing

(b)(4) Testing

(b)(4) Testing

(b)(4) Testing

(b)(4) Testing

(b)(4) Testing

(b)(4) Testing

(b)(4) Testing

(b)(4) Testing

(b)(4) Testing

(b)(4) Testing

(b)(4) Testing

(b)(4) Testing

(b)(4) Testing

(b)(4) Testing

(b)(4) Testing

(b)(4) Testing

(b)(4) Testing

(b)(4) Testing

(b)(4) Testing

(b)(4) Testing

(b)(4) Testing

(b)(4) Testing

(b)(4) Testing

(b)(4) Testing

(b)(4) Testing

(b)(4) Testing

(b)(4) Testing

(b)(4) Testing

(b)(4) Testing

(b)(4) Testing

(b)(4) Testing

(b)(4) Testing

(b)(4) Testing

(b)(4) Testing

(b)(4) Testing

(b)(4) Testing

(b)(4) Testing

(b)(4) Testing

(b)(4) Testing

(b)(4) Testing

(b)(4) Testing

(b)(4) Testing

(b)(4) Testing

(b)(4) Testing

(b)(4) Testing

(b)(4) Testing

(b)(4) Testing

(b)(4) Testing

(b)(4) Testing

(b)(4) Testing

(b)(4) Testing

(b)(4) Testing

(b)(4) Testing

(b)(4) Testing

(b)(4) Testing

(b)(4) Testing

(b)(4) Testing

(b)(4) Testing

(b)(4) Testing

(b)(4) Testing

(b)(4) Testing

(b)(4) Testing

(b)(4) Testing

(b)(4) Testing

(b)(4) Testing

(b)(4) Testing

(b)(4) Testing

(b)(4) Testing

(b)(4) Testing

(b)(4) Testing

(b)(4) Testing

(b)(4) Testing

(b)(4) Testing

(b)(4) Testing

(b)(4) Testing

(b)(4) Testing

(b)(4) Testing

(b)(4) Testing

(b)(4) Testing

(b)(4) Testing

(b)(4) Testing

(b)(4) Testing

(b)(4) Testing

(b)(4) Testing

(b)(4) Testing

(b)(4) Testing

(b)(4) Testing

(b)(4) Testing

(b)(4) Testing

(b)(4) Testing

(b)(4) Testing

(b)(4) Testing

(b)(4) Testing

(b)(4) Testing

(b)(4) Testing

(b)(4) Testing

(b)(4) Testing

(b)(4) Testing

(b)(4) Testing

(b)(4) Testing

(b)(4) Testing

(b)(4) Testing

(b)(4) Testing

(b)(4) Testing

(b)(4) Testing

(b)(4) Testing

(b)(4) Testing

(b)(4) Testing

(b)(4) Testing

(b)(4) Testing

(b)(4) Testing

(b)(4) Testing

(b)(4) Testing

(b)(4) Testing

(b)(4) Testing

(b)(4) Testing

(b)(4) Testing

(b)(4) Testing

(b)(4) Testing

(b)(4) Testing

(b)(4) Testing

(b)(4) Testing

(b)(4) Testing

(b)(4) Testing

(b)(4) Testing

(b)(4) Testing

(b)(4) Testing

(b)(4) Testing

(b)(4) Testing

(b)(4) Testing

(b)(4) Testing

(b)(4) Testing

(b)(4) Testing

(b)(4) Testing

(b)(4) Testing

(b)(4) Testing

(b)(4) Testing

(b)(4) Testing

(b)(4) Testing

(b)(4) Testing

(b)(4) Testing

(b)(4) Testing

(b)(4) Testing

(b)(4) Testing

(b)(4) Testing

(b)(4) Testing

(b)(4) Testing

(b)(4) Testing

(b)(4) Testing

(b)(4) Testing

(b)(4) Testing

(b)(4) Testing

(b)(4) Testing

(b)(4) Testing

(b)(4) Testing

(b)(4) Testing

(b)(4) Testing

(b)(4) Testing

(b)(4) Testing

(b)(4) Testing

(b)(4) Testing

(b)(4) Testing

(b)(4) Testing

(b)(4) Testing

(b)(4) Testing

(b)(4) Testing

(b)(4) Testing

(b)(4) Testing

(b)(4) Testing

(b)(4) Testing

(b)(4) Testing

(b)(4) Testing

(b)(4) Testing

(b)(4) Testing

(b)(4) Testing

(b)(4) Testing

(b)(4) Testing

(b)(4) Testing

(b)(4) Testing

(b)(4) Testing

(b)(4) Testing

(b)(4) Testing

(b)(4) Testing

(b)(4) Testing

(b)(4) Testing

(b)(4) Testing

(b)(4) Testing

(b)(4) Testing

(b)(4) Testing

(b)(4) Testing

(b)(4) Testing

(b)(4) Testing

(b)(4) Testing

(b)(4) Testing

(b)(4) Testing

(b)(4) Testing

(b)(4) Testing

(b)(4) Testing

(b)(4) Testing

(b)(4) Testing

(b)(4) Testing

(b)(4) Testing

(b)(4) Testing

(b)(4) Testing

(b)(4) Testing

(b)(4) Testing

(b)(4) Testing

(b)(4) Testing

(b)(4) Testing

(b)(4) Testing

(b)(4) Testing

(b)(4) Testing

(b)(4) Testing

(b)(4) Testing

(b)(4) Testing

(b)(4) Testing

(b)(4) Testing

(b)(4) Testing

(b)(4) Testing

(b)(4) Testing

(b)(4) Testing

(b)(4) Testing

(b)(4) Testing

(b)(4) Testing

(b)(4) Testing

(b)(4) Testing

(b)(4) Testing

(b)(4) Testing

(b)(4) Testing

(b)(4) Testing

(b)(4) Testing

(b)(4) Testing

(b)(4) Testing

(b)(4) Testing

(b)(4) Testing

(b)(4) Testing

(b)(4) Testing

(b)(4) Testing

(b)(4) Testing

(b)(4) Testing

(b)(4) Testing

(b)(4) Testing

(b)(4) Testing

(b)(4) Testing

(b)(4) Testing

(b)(4) Testing

(b)(4) Testing

(b)(4) Testing

(b)(4) Testing

(b)(4) Testing

(b)(4) Testing

(b)(4) Testing

(b)(4) Testing

(b)(4) Testing

(b)(4) Testing

(b)(4) Testing

(b)(4) Testing

(b)(4) Testing

(b)(4) Testing

(b)(4) Testing

(b)(4) Testing

(b)(4) Testing

(b)(4) Testing

(b)(4) Testing

(b)(4) Testing

(b)(4) Testing

(b)(4) Testing

(b)(4) Testing

(b)(4) Testing

(b)(4) Testing

(b)(4) Testing

(b)(4) Testing

(b)(4) Testing

(b)(4) Testing

(b)(4) Testing

(b)(4) Testing

(b)(4) Testing

(b)(4) Testing

(b)(4) Testing

(b)(4) Testing

(b)(4) Testing

(b)(4) Testing

(b)(4) Testing

(b)(4) Testing

(b)(4) Testing

(b)(4) Testing

(b)(4) Testing

(b)(4) Testing

(b)(4) Testing

(b)(4) Testing

(b)(4) Testing

(b)(4) Testing

(b)(4) Testing

(b)(4) Testing

(b)(4) Testing

(b)(4) Testing

(b)(4) Testing

(b)(4) Testing

(b)(4) Testing

(b)(4) Testing

(b)(4) Testing

(b)(4) Testing

(b)(4) Testing

(b)(4) Testing

(b)(4) Testing

(b)(4) Testing

(b)(4) Testing

(b)(4) Testing

(b)(4) Testing

(b)(4) Testing

(b)(4) Testing

(b)(4) Testing

(b)(4) Testing

(b)(4) Testing

(b)(4) Testing

(b)(4) Testing

(b)(4) Testing

(b)(4) Testing

(b)(4) Testing

(b)(4) Testing

(b)(4) Testing

(b)(4) Testing

(b)(4) Testing

(b)(4) Testing

(b)(4) Testing

(b)(4) Testing

(b)(4) Testing

(b)(4) Testing

(b)(4) Testing

(b)(4) Testing

(b)(4) Testing

(b)(4) Testing

(b)(4) Testing

(b)(4) Testing

(b)(4) Testing

(b)(4) Testing

(b)(4) Testing

(b)(4) Testing

(b)(4) Testing

(b)(4) Testing

(b)(4) Testing

(b)(4) Testing

(b)(4) Testing

(b)(4) Testing

(b)(4) Testing

(b)(4) Testing

(b)(4) Testing

(b)(4) Testing

(b)(4) Testing

(b)(4) Testing

(b)(4) Testing

(b)(4) Testing

(b)(4) Testing

(b)(4) Testing

(b)(4) Testing

(b)(4) Testing

(b)(4) Testing

(b)(4) Testing

(b)(4) Testing

(b)(4) Testing

(b)(4) Testing

(b)(4) Testing

(b)(4) Testing

(b)(4) Testing

(b)(4) Testing

(b)(4) Testing

(b)(4) Testing

(b)(4) Testing

(b)(4) Testing

(b)(4) Testing

(b)(4) Testing

(b)(4) Testing

(b)(4) Testing

(b)(4) Testing

(b)(4) Testing

(b)(4) Testing

(b)(4) Testing

(b)(4) Testing

(b)(4) Testing

(b)(4) Testing

(b)(4) Testing

(b)(4) Testing

(b)(4) Testing

(b)(4) Testing

(b)(4) Testing

(b)(4) Testing

(b)(4) Testing

(b)(4) Testing

(b)(4) Testing

(b)(4) Testing

(b)(4) Testing

(b)(4) Testing

(b)(4) Testing

(b)(4) Testing

(b)(4) Testing

(b)(4) Testing

(b)(4) Testing

(b)(4) Testing

(b)(4) Testing

(b)(4) Testing

(b)(4) Testing

(b)(4) Testing

(b)(4) Testing

(b)(4) Testing

(b)(4) Testing

(b)(4) Testing

(b)(4) Testing

(b)(4) Testing

(b)(4) Testing

(b)(4) Testing

(b)(4) Testing

(b)(4) Testing

(b)(4) Testing

(b)(4) Testing

(b)(4) Testing

(b)(4) Testing

(b)(4) Testing

(b)(4) Testing

(b)(4) Testing

(b)(4) Testing

(b)(4) Testing

(b)(4) Testing

(b)(4) Testing

(b)(4) Testing

(b)(4) Testing

(b)(4) Testing

(b)(4) Testing

(b)(4) Testing

(b)(4) Testing

(b)(4) Testing

(b)(4) Testing

(b)(4) Testing

(b)(4) Testing

(b)(4) Testing

(b)(4) Testing

(b)(4) Testing

(b)(4) Testing

(b)(4) Testing

(b)(4) Testing

(b)(4) Testing

(b)(4) Testing

(b)(4) Testing

(b)(4) Testing

(b)(4) Testing

(b)(4) Testing

(b)(4) Testing

(b)(4) Testing

(b)(4) Testing

(b)(4) Testing

(b)(4) Testing

(b)(4) Testing

(b)(4) Testing

(b)(4) Testing

(b)(4) Testing

(b)(4) Testing

(b)(4) Testing

(b)(4) Testing

(b)(4) Testing

(b)(4) Testing

(b)(4) Testing

(b)(4) Testing

(b)(4) Testing

(b)(4) Testing

(b)(4) Testing

(b)(4) Testing

(b)(4) Testing

(b)(4) Testing

(b)(4) Testing

(b)(4) Testing

(b)(4) Testing

(b)(4) Testing

(b)(4) Testing

(b)(4) Testing

(b)(4) Testing

(b)(4) Testing

(b)(4) Testing

(b)(4) Testing

(b)(4) Testing

(b)(4) Testing

(b)(4) Testing

(b)(4) Testing

(b)(4) Testing

(b)(4) Testing

(b)(4) Testing

(b)(4) Testing

(b)(4) Testing

(b)(4) Testing

(b)(4) Testing

(b)(4) Testing

(b)(4) Testing

(b)(4) Testing

(b)(4) Testing

(b)(4) Testing

(b)(4) Testing

(b)(4) Testing

(b)(4) Testing

(b)(4) Testing

(b)(4) Testing

(b)(4) Testing

(b)(4) Testing

(b)(4) Testing

(b)(4) Testing

(b)(4) Testing

(b)(4) Testing

(b)(4) Testing

(b)(4) Testing

(b)(4) Testing

(b)(4) Testing

(b)(4) Testing

(b)(4) Testing

(b)(4) Testing

(b)(4) Testing

(b)(4) Testing

(b)(4) Testing

(b)(4) Testing

(b)(4) Testing

(b)(4) Testing

(b)(4) Testing

(b)(4) Testing

(b)(4) Testing

(b)(4) Testing

(b)(4) Testing

(b)(4) Testing

(b)(4) Testing

Records processed under FOIA Request #2014-8015; Released by CDRH on 12-8-2015

Reference Articles and Literature

Questions? Contact FDA/CDRH/OCE/DID at CDRH-FOISTATUS@fda.hhs.gov or 301-796-8118

Records processed under FOIA Request #2014-8015; Released by CDRH on 12-8-2015

The effects of degree of crosslinking on the fatigue crack initiation and propagation resistance of orthopedic-grade polyethylene

D. A. Baker,[1] A. Bellare,[2] L. Pruitt[1,3]
[1]*Department of Mechanical Engineering, University of California, Berkeley, California 94720*
[2]*Department of Orthopedic Surgery, Harvard Medical School, Brigham and Women's Hospital, Boston, Massachusetts 02115*
[3]*Department of Bioengineering, University of California, Berkeley, California 94720*

Received 14 August 2001; revised 7 October 2002; accepted 11 October 2002

Abstract: Crosslinked ultrahigh molecular weight polyethylene (UHMWPE) has been recently approved by the Food and Drug Administration for use in orthopedic implants. The majority of commercially available UHMWPE orthopedic components are crosslinked using e-beam or gamma radiation. The level of crosslinking is controlled with radiation dose and free radicals are eliminated through heat treatments to prevent long-term degradation associated with chain scission or oxidation mechanisms. Laboratory studies have demonstrated a substantial improvement in the wear resistance of crosslinked UHMWPE. However, a concern about the resistance to fatigue damage remains in the clinical community, especially for tibial components that sustain high cyclic contact stresses. The objective of this study was to investigate both the initiation and propagation aspects of fatigue cracks in radiation crosslinked medical-grade UHMWPE. This work evaluated three levels of radiation, which induced three crosslink densities, on the fatigue crack propagation and total fatigue life behavior. Both as-received UHMWPE, as well as those that underwent an identical thermal history as the crosslinked UHMWPE were used as controls. Fractured crack propagation specimens were examined using scanning electron microscopy to elucidate fatigue fracture mechanisms. The results of this work indicated that a low crosslink density may optimize the fatigue resistance from both a crack initiation and propagation standpoint. © 2003 Wiley Periodicals, Inc. J Biomed Mater Res 66A: 146–154, 2003

Key words: ultrahigh molecular weight polyethylene (UHMWPE); fatigue; crosslinking; initiation; propagation

INTRODUCTION

Crosslinked ultrahigh molecular weight polyethylene (UHMWPE) shows great promise for the improvement of wear resistance and longevity of orthopedic devices.[1–4] Although crosslinked components have been implanted for more than 25 years now,[5] only over the past few years have the crosslinking procedures been performed in a controlled manner. Of the utmost importance in this controlled crosslinking methodology has been the remelting or annealing of the polyethylene to annihilate free radicals.[6] This process results in a crosslinked resin that is not susceptible to long-term oxidation or scission-based degradation. Furthermore, recent studies developed in the orthopedics community show that optimum wear behavior of UHMWPE is obtained using a minimum of 50–150 kGy (5–15 Mrad) of gamma or e-beam radiation; it can also be achieved via chemical crosslinking by a minimum of 0.3–0.5% peroxide.[2] A higher degree of crosslinking results in a restriction of chain mobility in the amorphous region and, as a result, these processes reduce the overall plasticity mechanisms available to the polymer. Plastic deformation has been shown to be the underlying mechanism responsible for stress-induced orientation and concomitant strain hardening behavior observed in non-crosslinked UHMWPE.[7] This microstructural evolution associated with peak stresses acting on the polymer has been termed the "plasticity induced damage layer" by Edidin et al.[4] and has been observed in the subsurface layers of polymer orthopedic devices to depths of several microns. This plasticity induced damage has significant clin-

Correspondence to: L. Pruitt; e-mail: lpruitt@newton
Contract grant sponsor: National Science Foundation
Contract grant sponsor: Office of Naval Research
Contract grant sponsor: Whitaker Foundation

© 2003 Wiley Periodicals, Inc.

Questions? Contact FDA/CDRH/OCE/DID at CDRH-FOISTATUS@fda.hhs.gov or 301-796-8118

Records processed under FOIA Request #2014-8015; Released by CDRH on 12-8-2015

ical relevance in that it has been linked to the wear processes in UHMWPE orthopedic devices.[7] Crosslinking minimizes the texture development through reduced chain mobility and, although these polymers are still susceptible to strain hardening behavior,[8,9] they show substantial improvement in wear resistance when articulated against standard orthopedic alloys such as Co-Cr or Ti-based systems.

Much of the recent focus of crosslinked UHMWPE has been on the optimization of radiation dose rather than optimization of peroxide chemistry. Both processes result in improved wear resistance, but there are concerns about the long-term stability of the peroxide crosslinked polymer.[10] Recent work[11] has shown that accelerated aging (75°C, 10 atm O_2, 21 days) produced an embrittled polymer, and even milder aging conditions have resulted in a reduction in fatigue crack propagation resistance for the chemically crosslinked UHMWPE.[12] Radiation crosslinked UHMWPE, however, did not experience any degradation due to accelerated aging. As a result of the improved resistance to wear and improved long-term stability under *in vitro* conditions, several crosslinking procedures involving ionizing irradiation and annealing have been developed, patented, and used to produce components that are now being implanted in total hip replacements and, more recently, total knee replacements. An overview of some of the processing techniques and resulting commercially available crosslinked polyethylenes have been described in detail elsewhere.[13,14]

Crosslinking of UHMWPE resins has been viewed as a solution to the device failure problem due to improved wear characteristics; however, the fatigue and fracture resistance of the crosslinked polymer in cyclic loading applications remains an area of question. For example, it is well established that crosslinking results in a decrease in strain to failure in the resin. This decreased plasticity in the crosslinked resins which is beneficial to wear resistance has been shown to reduce the toughness[9] and fatigue crack propagation resistance[12] in crosslinked UHMWPE. This creates apprehension in the orthopedics community about the use of crosslinked UHMWPE because of the known propensity for fatigue and delamination wear in total knee components, for example. Fatigue of the polymer used in the tibial plateau is problematic because of the cyclic nature of the physiological loading and the large values of contact stresses acting along the articulating surface.[15] To date, there has been a plethora of studies addressing the beneficial effects of crosslinking on the wear behavior of UHMWPE but studies addressing the role of crosslinking on the fatigue behavior remain limited.[12,16,17] A further complicating factor in the assessment of the fatigue resistance of crosslinked polyethylene lies in the apparent dichotomy of the results reported in the fatigue studies. For example, O'Connor et al.[16] reported that no failures were observed in their crosslinked specimens after 20 million fatigue cycles, whereas Baker et al.[12] reported that crosslinking resulted in a significant decrease in the resistance to fatigue crack propagation. This apparent conflict results from a difference in the philosophical approach used in the assessment of fatigue resistance. The study by O'Connor et al.[16] utilized a total life approach that involved the cyclic loading of specimens without stress concentrations. In this case, no failures were reported at 20 million cycles. However, a lack of failure does not preclude that small flaws could have been generated because of cyclic damage, and such damage remains a clinical concern. The study by Baker et al.[12] applied a defect tolerant philosophy that involved the cyclic loading of notched specimens containing a small mode I crack at the notch tip. This conservative analysis involved a fracture mechanics approach and measured the resistance to fatigue crack propagation. The conflicting results from these two studies are attributable to the differences in methodology: the first is an initiation study that measures the resistance of the material to the initiation of a flaw and the second is a propagation study that measures resistance to crack growth. Both studies contribute to the understanding of the material fatigue resistance; however, the philosophical difference between them is critical to the design and prediction of the performance of the orthopedic device. Life predictions based on the results of a total life study are premised on the assumption that an orthopedic device is initially defect free or that it contains flaws that will spend the majority of their life in the initiation process. A more conservative life prediction is based on a fracture mechanics philosophy that assumes the device contains defects or flaws that are capable of propagation under cyclic loading.

This work examined both the fatigue initiation and propagation resistance of radiation crosslinked orthopedic-grade UHMWPE at varying crosslink doses. The crosslinking was performed with three different dosages of gamma radiation followed by melting to eliminate most of the residual free radicals. Two fatigue evaluation methods were used, a stress-based total life and a fracture mechanics approach to determine how the degree of crosslinking affects resistance to crack initiation and propagation, respectively, in UHMWPE. Electron microscopy was used to examine micromechanisms and microstructural evolution associated with the fatigue processes in the crosslinked polymers. The aim of this work was to assess the role of degree of crosslinking on both the initiation and propagation

Questions? Contact FDA/CDRH/OCE/DID at CDRH-FOISTATUS@fda.hhs.gov or 301-796-8118

Records processed under FOIA Request #2014-8015; Released by CDRH on 12-8-2015

TABLE I
Physical Properties of the Crosslinked UHMWPE

	Control	50 kGy	100 kGy	200 kGy
Crystallinity (%)	50.1 ± 0.5	45.6 ± 0.7	46.3 ± 0.8	47.1 ± 0.4
SAXS long period (nm)	40.0 ± 1.3	39.8 ± 1.1	40.3 ± 1.4	40.6 ± 1.1
Lamellar thickness (nm)	20.0	18.1	18.7	19.1
Modulus (MPa)	495 ± 56	412 ± 50	386 ± 23	266 ± 30
Yield stress (MPa)	20.2 ± 1.0	19.9 ± 0.8	18.9 ± 0.7	20.2 ± 1.0
True stress at break (MPa)	315.5 ± 31.6	237.6 ± 12.3	185.7 ± 7.5	126.0 ± 14.0
Decrease in true stress at break	—	24%	41%	60%

SAXS, small-angle X-ray scattering.

of cracks in UHMWPE, and to provide an assessment of optimized crosslinking level for orthopedic implant design.

MATERIALS AND METHODS

Materials

The base material used in this study was GUR 1050 resin (Hoechst Celanese/Ticona) provided in extruded rod stock from PolyHi Solidur. Crosslinking was performed by Isomedix Inc., using gamma radiation. Subsequent melt stabilization was performed at 170°C for 4 h with addition annealing at 125°C for 2 days. The material was then cooled slowly to room temperature. Three doses of gamma radiation were used to create different levels of crosslink densities in the polymer: 50, 100, and 200 kGy. Two nonirradiated groups were examined as controls. These included both an untreated rod stock and annealed rod stock. The annealed rod stock was subjected to the same thermal history as the crosslinked specimens in order to evaluate the role of heat treatment. In total, five material groups were examined.

Structural characterization

The structural and mechanical properties of the materials used in this study are provided in Table I.[9] Material characterization was performed using differential scanning calorimetry (DSC), small-angle X-ray scattering and quasi-static mechanical testing. DSC was performed using a Perkin-Elmer DSC-7 instrument in order to measure sample crystallinity. Samples of 3-mm diameter and 0.5-mm thickness, sectioned from each rod-stock, were used for all DSC measurements. The degree of crystallinity was calculated using a heat of fusion of 293 J/g for the polyethylene crystal. Small-angle X-ray scattering was performed on 2-mm-thick specimens using a Rigaku CuKα X-ray source at 40 kV and 30 mA to determine the long period. Mechanical properties, including yield stress, true stress at break, and modulus, were determined from tensile tests according to ASTM D638 using an Instron 4201 with a crosshead speed of 500 mm/min. A minimum of five specimens per group were used for all mechanical tests.

Fatigue crack propagation studies

The five material groups were subject to fatigue crack propagation studies (fracture mechanics analysis). All fatigue tests were performed on an Instron 8511 servohydraulic materials testing machine in room temperature air at 5 Hz with sinusoidal loading. Previous work[18] has established that a test frequency of 5 Hz does not result in hysteretic heating or thermal fatigue of the UHMWPE specimens. Compact tension specimens were used to characterize crack propagation resistance. The specimen had the following geometry: width, $W = 15.24$ mm; length, $L = 19.05$ mm; height, $2H = 19.05$ mm; initial notch length, $a = 5.334$ mm; notch width, $t = 1.588$ mm; included notch angle, $\theta = 60$ degrees; notch root radius, $\rho = 0.127$ mm; hole diameter, $d = 3.175$ mm; distance between holes = 10.16 mm; and thickness, $T = 4.76$ mm. A schematic of the compact tension geometry is shown in Figure 1. All specimens were machined such that the crack growth would be perpendicular to the extrusion direction. Sharp cracks were introduced before the tension tests and measured optically with an Olympus BH-2 microscope with a resolution of 0.2 μm. The tension fatigue fracture tests were run with a load ratio $R = 0.1$. Crack length was monitored with number of cycles to determine crack propagation rates, da/dN, as a function of stress intensity range, ΔK. For the crack propagation studies, the stress intensity range necessary to generate crack growth at a rate of 10^{-6} mm/cycle was measured to define ΔK_{incep}. Scanning electron microscopy was performed on the fractured compact tension specimens to examine morphological features associated with the fatigue fracture process. Fractured specimens from each of the five groups were sputter-coated with gold and examined using a JEOL 6500 scanning electron microscope.

Fatigue crack initiation (stress-life analysis)

Stress-life fatigue tests were performed on the five material groups with an Instron 8511 servohydraulic materials testing machine in room temperature air at 5 Hz with sinusoidal loading. Small dogbone specimens were used in the stress-life analysis. The specimens were 31.75 mm in height, 2.7-mm wide through the gage length, and 2-mm thick. A schematic of the dogbone specimen is given in Figure 1. All testing was performed in load control with a load ratio of

Questions? Contact FDA/CDRH/OCE/DID at CDRH-FOISTATUS@fda.hhs.gov or 301-796-8118

Records processed under FOIA Request #2014-8015; Released by CDRH on 12-8-2015

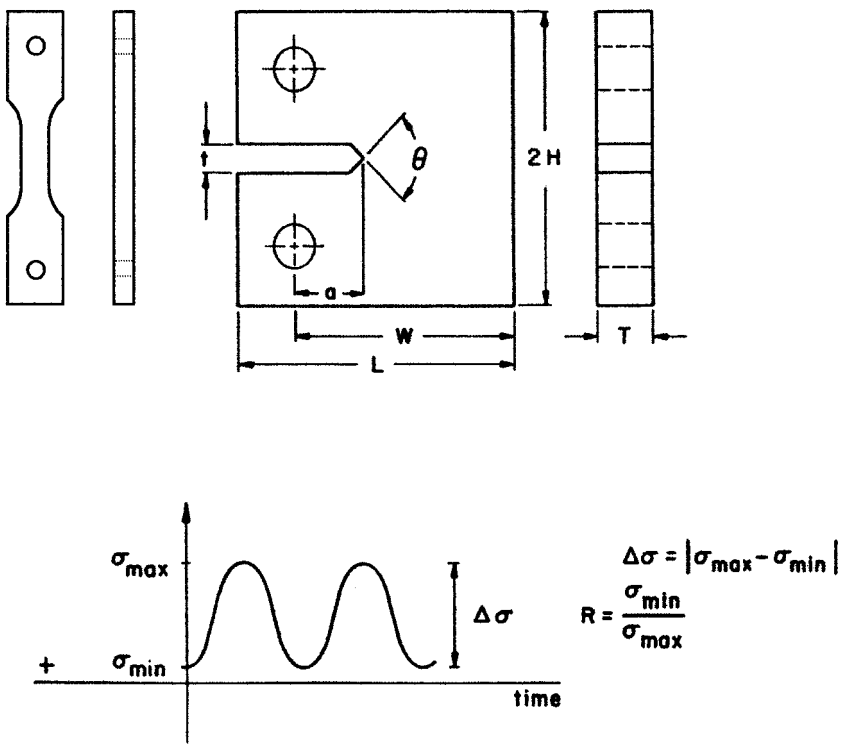

Figure 1. Schematic of the compact tension (top right) and dogbone specimens (top left) used in the fatigue studies. The compact tension specimen had the following geometry: width, $W = 15.24$ mm; length, $L = 19.05$ mm; height, $2H = 19.05$ mm; initial notch length, $a = 5.334$ mm; notch width, $t = 1.588$ mm; included notch angle, $\theta = 60$ degrees; notch root radius, $\rho = 0.127$ mm; hole diameter, $d = 3.175$ mm; distance between holes = 10.16 mm; and thickness, $T = 4.76$ mm. The small dogbones were 31.75 mm in height, 2.7-mm wide through the gage length, and 2-mm thick.

$R = 0.1$. For the stress-life fatigue tests, failure of the specimen was based on plastic deformation associated with the material's yielding criteria. Therefore, the number of cycles to the onset of yield was monitored as a function of nominal stress range to determine the *S-N* curve.

RESULTS

Fatigue crack propagation results for all the material groups are presented in Figure 2(a). It is apparent that radiation crosslinking resulted in decreased crack propagation inception value, ΔK_{incep}, as compared with the nonradiated specimens. Also, the ΔK inception value continued to decrease as radiation dose or crosslink density was increased. Figure 2(b) shows the ΔK_{incep} value plotted as a function of radiation dose. The annealed UHMWPE exhibited a similar ΔK_{incep} as the nonannealed UHMWPE, 1.43 and 1.41 MPa$\sqrt{m}$, respectively, but with slightly different propagation behavior in the Paris regime (the regime where the crack propagation rate is linearly proportional to the stress intensity range on a logarithmic scale). The crosslinking procedures resulted in a decreased ΔK_{incep} to 0.91, 0.69, and 0.55 MPa$\sqrt{m}$ for the 50-, 100-, and 200-kGy specimens, respectively. A summary of the ΔK_{incep} and slope, m, values for all five material groups is given in Table II. For clinical comparison, the ΔK_{incep} and slope, m, values for gamma air sterilized and accelerated aging conditions for a GUR 1050 resin[19] are also included. Note the similar relative decreases in the crack growth inception values for the gamma sterilized and gamma sterilized, aged conditions.

The stress-life results are presented in Figure 3, where life corresponds to cycles to yield. As with the crack propagation tests, the annealed and nonannealed non-crosslinked controls exhibited similar fatigue behavior. An initial crosslink dose of 50 kGy resulted in a reduction in the yield stress range over the two controls. However, the observed trend was that as crosslink radiation dose was increased, the cycles to yield increased for a given stress range. This continued such that the 200-kGy radiation crosslinked specimens exhibited similar stress-life behavior as the nonirradiated specimens. Constants for the Basquin relation, defined as $S = AN_f^B$ where S is the stress range and N_f is the cycles to failure (yield), are given in Table II. Note, for some of the highly crosslinked specimens, early fractures initiated at the pin holes upon loading. These were not included in the total life study, but these findings do stress the importance of

Questions? Contact FDA/CDRH/OCE/DID at CDRH-FOISTATUS@fda.hhs.gov or 301-796-8118

Records processed under FOIA Request #2014-8015; Released by CDRH on 12-8-2015

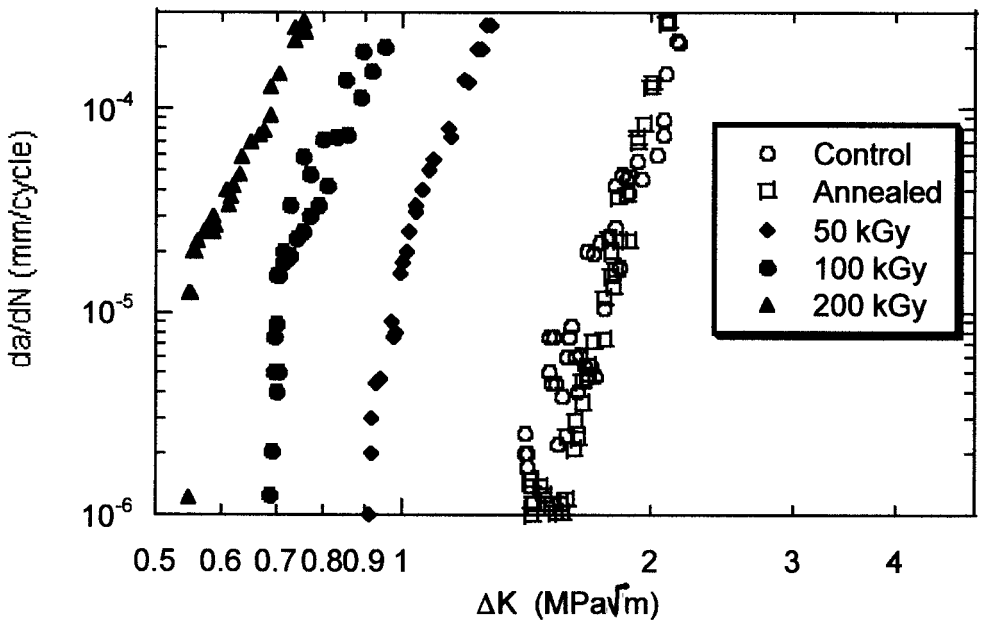

(a)

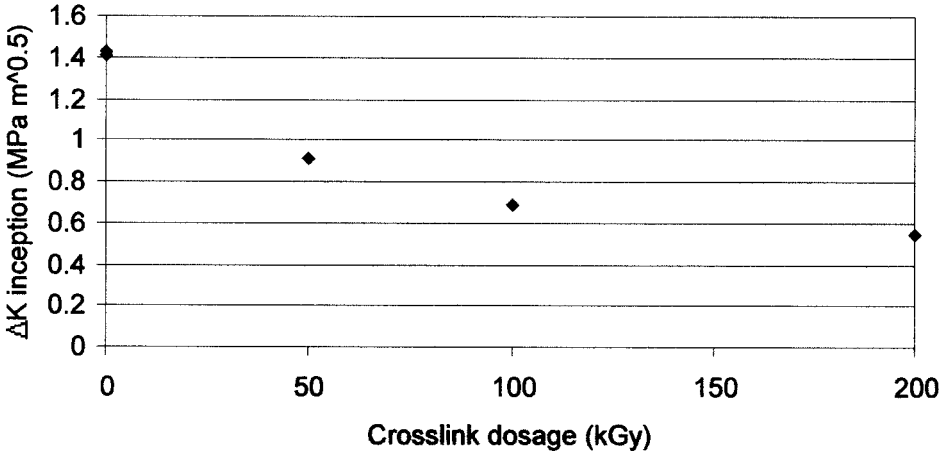

(b)

Figure 2. (a) Fatigue crack propagation results for all five material groups and (b) ΔK_{incep}, value plotted as a function of radiation dose.

stress concentration in the assessment of fatigue resistance.

A representative scanning electron micrograph of the fatigue crack propagation fracture surface for the non-crosslinked controls is shown in Figure 4(a). This image clearly displays the criss-cross patterns associated with ductile tearing in pristine UHMWPE. Figure 4(b) shows the same crack propagation regime for the 50-kGy radiation crosslinked specimen. There was a distinct reduction of ductile features compared with the non-crosslinked controls. This decrease in ductility became more apparent as the degree of crosslinking was increased. Figure 5(a) shows the Paris regime fracture surface for the 100-kGy dose. Note that a five-fold increase in magnification is required to detect the ductile tearing mechanisms in the polymer for the 100 kGy [Fig. 5(b)] as compared with the non-crosslinked control [Fig. 4(a)]. This suggests that a characteristic microstructural length scale associated with fracture is reduced through crosslinking. At 200-kGy radiation, the fracture mechanism was altered and the fracture surface resembled that of a glassy polymer.[20] Figure 6(a,b) shows the Paris regime fracture surface for the 200-kGy specimen. A much higher

Questions? Contact FDA/CDRH/OCE/DID at CDRH-FOISTATUS@fda.hhs.gov or 301-796-8118

Records processed under FOIA Request #2014-8015; Released by CDRH on 12-8-2015

TABLE II
Summary of Fatigue Crack Propagation and Total Life Fatigue Data

(a) Fatigue Crack Inception and Propagation Data for the Crosslinked Resins and Their Control Groups

Paris Regime Fatigue $da/dN = C\ (\Delta K)^m$	Control	Annealed	50 kGy	100 kGy	200 kGy
ΔK_{incep} (MPa$\sqrt{m}$)	1.41	1.43	0.91	0.69	0.55
Decrease in ΔK_{incep} (%)	—	—	35	51	61
Slope, m	11.74	19.40	10.77	9.07	8.92
R^2	0.96	0.99	0.97	0.84	0.98

(b) Fatigue Crack Inception Data for Gamma Radiation Sterilized GUR 1050, Gamma Irradiated GUR 1050 Subjected to Accelerated Aging, and Nonsterile 1050 Control

Paris Regime Fatigue $da/dN = C(\Delta K)^m$	Control[a]	25-kGy Air[a]	25-kGy Aged[a]
ΔK_{incep} (MPa$\sqrt{m}$)	2.01	1.51	0.90
Decrease in ΔK_{incep} (%)	—	24	55
Slope, m	21.4	24.3	—

[a]Note, these data are generated in a previously published article.[19] Data are provided here to show the relative decreases in fatigue resistance caused by gamma radiation sterilization and accelerated aging.

(c) Total Life Fatigue Data for the Crosslinked Resins and Their Control Groups

Basquin Relation $S = AN_f^B$	Control	Annealed	50 kGy	100 kGy	200 kGy
A	26.24	25.81	23.52	25.95	27.54
B	−0.044	−0.039	−0.043	−0.050	−0.050
R^2	0.99	0.97	0.98	0.96	0.96

magnification [Fig. 6(b)] was required to detect any type of tearing mechanism. This suggests that the high dose of crosslinking substantially altered the fracture process to that of a brittle mechanism for the UHMWPE.

DISCUSSION

The results of this study indicate that the high degree of crosslinking (≥100 kGy) is extremely detrimental to fatigue propagation resistance but is seemingly not detrimental to the flaw initiation resistance. Whereas the yield stress did not change substantially for the specimens used in the investigation, the true ultimate stress to fracture (Table I) decreases with increased crosslink density in a similar manner to the decreases observed in ΔK_{incep}. The limited ductility in the highly crosslinked UHMWPE reduces strain to failure and limits the polymer's ability to accommodate plasticity at the crack tip. This is extremely important for fatigue crack propagation as the decreased plasticity at the crack tip enables more of the crack driving force to be utilized in crack advance rather than dissipated through plastic work. The findings from this study show that with increasing crosslink density there is a concomitant decrease in propagation resistance as indicated by the decreasing values of ΔK_{incep}, as shown in Figure 2(b). The ΔK_{incep} is seen to decrease by approximately 35, 50, and 60% below the control (non-crosslinked) UHMWPE with the 50-, 100-, and 200-kGy radiation dosages, respectively.

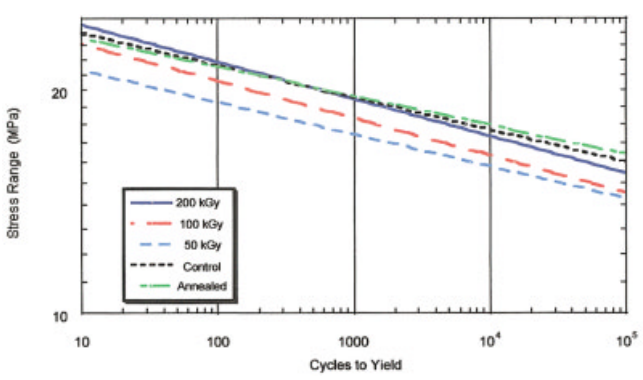

Figure 3. Stress-life fatigue results for all five material groups. [Color figure can be viewed in the online issue, which is available at www.interscience.wiley.com.]

The similar slopes, m, of the crosslinked specimens as reported in Table II indicate that once the crack inception process has occurred, similar mechanisms likely control the fatigue crack growth rate. The crosslinked specimens exhibit a continual reduction in ΔK_{incep} with increased radiation dose. It is expected that the critical stress intensity (fracture toughness) will exhibit a similar reduction as m remains relatively

Questions? Contact FDA/CDRH/OCE/DID at CDRH-FOISTATUS@fda.hhs.gov or 301-796-8118

Records processed under FOIA Request #2014-8015; Released by CDRH on 12-8-2015

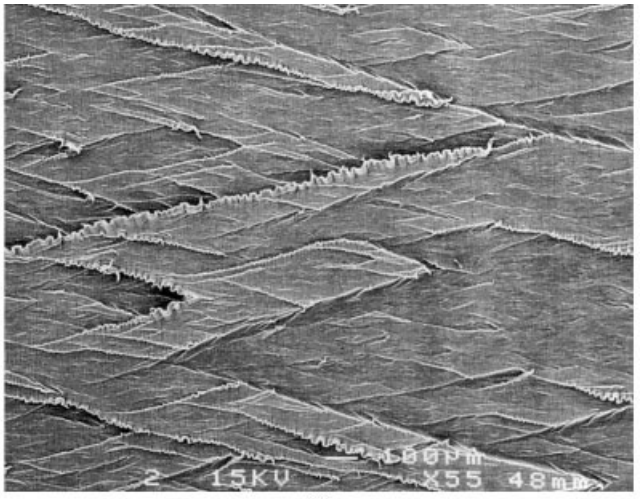

(a)

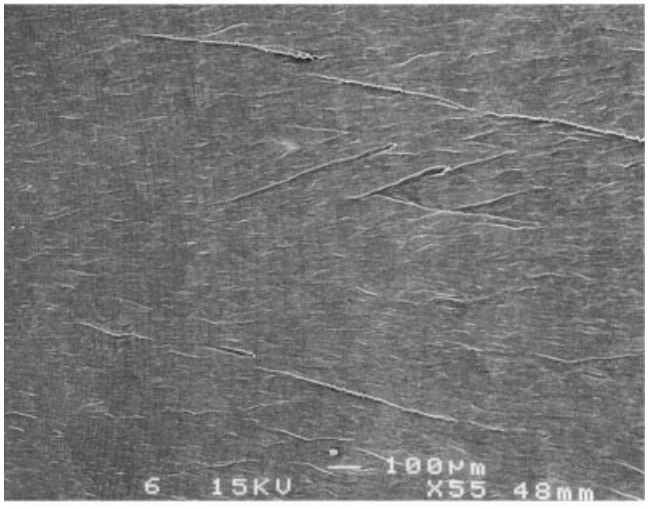

(b)

Figure 4. Representative fracture surface in the (a) Paris regime for the non-crosslinked control, and (b) Paris regime of the 50-kGy crosslinked specimens. Crack growth direction is left to right. Note the degree of ductile tearing is substantially reduced with crosslinking.

constant throughout the Paris regime. This is also predicted by the relation $K_{Ic} \sim \sigma_{ult}\sqrt{l_o}$,[21] where l_o is some characteristic critical flaw size or microstructural length scale associated with the fracture process. For a fixed critical flaw size, it is expected that as the ultimate stress decreases, the fracture toughness will decrease. As seen in Table I, the true ultimate tensile strength, defined as the true stress at break, for the crosslinked UHMWPE, decreases with increased crosslink density. This relationship is corroborated by the reduction in critical stress intensity observed in the fatigue crack propagation analysis.

The scanning electron micrographs provide confirmation of the reduction in ductility responsible for the reduced ΔK_{incep} seen in the crosslinked UHMWPE. The non-crosslinked control, represented in Figure 4(a), exhibited the expected degree of ductile tearing and criss-cross patterns previously reported for pristine UHMWPE.[19,22] Upon exposure to the low level of ionizing radiation to induce crosslinking (50 kGy), the number and size of these ductile features significantly diminished. Substantial increases in magnification were required to detect ductile features as the degree of crosslinking increased. The results of the fractography suggest a scaling effect of microstructural features associated with polymer plasticity. It is believed that the reduction in crystallinity, lamellae size, and ultimate tensile strength brought about through crosslinking is the source of this reduced plasticity and decreased resistance to crack growth (Table I).

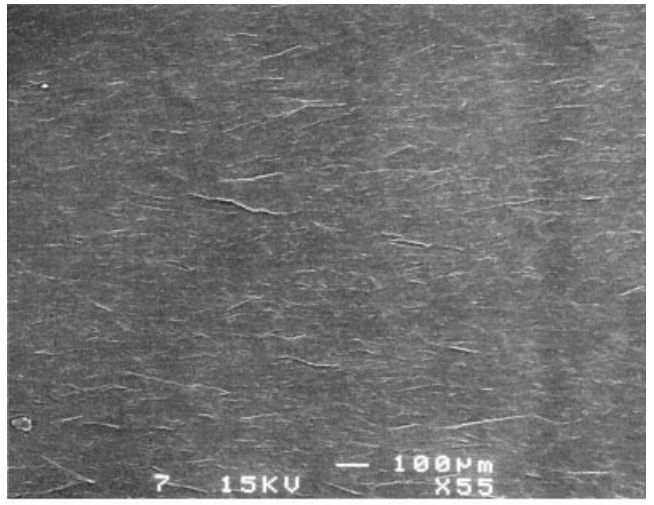

(a)

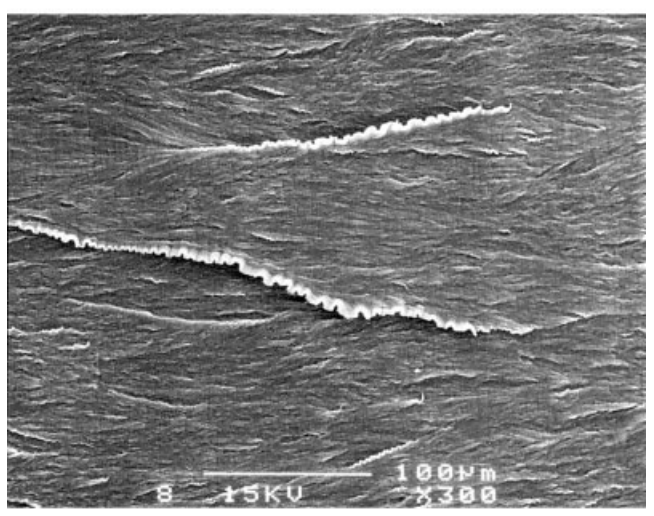

(b)

Figure 5. Representative micrograph of the (a) Paris regime and (b) higher magnification in the Paris regime revealing the limited ductility of the 100-kGy crosslinked specimens. Crack growth direction is left to right.

Questions? Contact FDA/CDRH/OCE/DID at CDRH-FOISTATUS@fda.hhs.gov or 301-796-8118

Records processed under FOIA Request #2014-8015; Released by CDRH on 12-8-2015

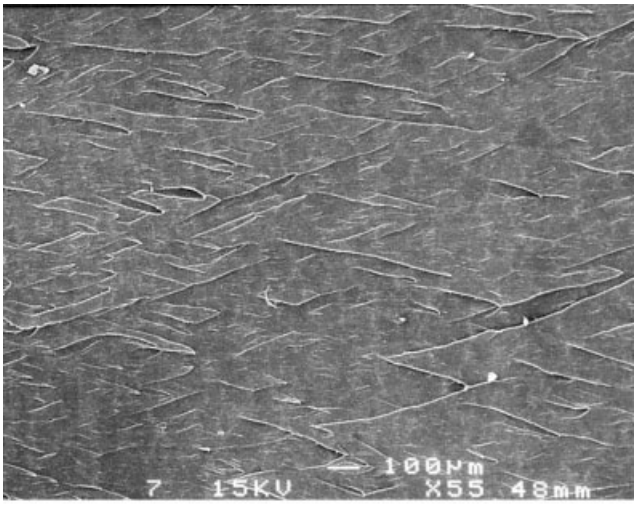

(a)

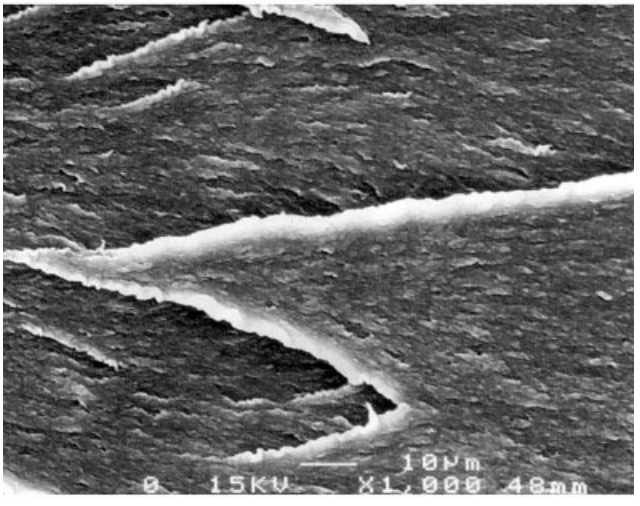

(b)

Figure 6. Scanning electron micrograph of the (a) Paris regime and (b) very high magnification in the Paris regime revealing the very limited ductility of the 200-kGy crosslinked specimens. Crack growth direction is left to right.

The total life analysis presented in this study indicates that increasing the crosslink density will increase the fatigue life to initial yield for a given stress range. As yielding is expected to occur in the polymer crystal, via (100) ⟨001⟩ chain slip, it is expected that the decreased crystallinity associated with crosslinking should result in an accompanying change in cyclic yield stress. It is thought that the crosslinked amorphous region may result in a locking mechanism that induces chain slip at lower strain levels as the crosslink density increases. However, the mechanism that drives the 50-kGy-radiated specimens to yield at a lower cyclic stress range remains unclear and more microstructural studies are needed to determine this micromechanism of deformation. Investigation into this microstructural evolution is currently underway on the total life specimens using ultra-small X-ray scattering analysis.[23]

From a fatigue crack propagation perspective, the primary hindrance to crack growth is lamellae tearing and chain disentanglement. With increasing crosslink density, the mechanisms of lamellae tearing and crystalline plasticity are reduced, resulting in lower stress intensity ranges necessary for crack growth. From an initiation perspective, the crosslinking can be viewed as a strengthening of the amorphous phase. Thus, crosslinking is expected to minimize fatigue-induced void formation that could lead to flaw generation in the polymer.[24] Further microscopy analysis, along with thorough X-ray scattering investigations, are necessary before a theoretical understanding of the micromechanistic processes associated with crack initiation can be provided.

CONCLUSIONS

This study examined the fatigue resistance of UHMWPE at varying crosslink densities. Two fatigue evaluation methods were used, a defect tolerant and a stress-life approach. The defect tolerant approach shows that increasing the crosslink densities in the polymer results in a decreased resistance to crack propagation. This is attributed to the reduction in plastic deformation attained ahead of the crack tip as revealed by fractography. The stress-life analysis results revealed a slight increase in cycles to yield for a given stress range as crosslink density increased. However, because of their increased sensitivity to flaws, caution should be heeded when utilizing the highly crosslinked polyethylenes in cyclic applications where failure could still occur due to a heightened sensitivity to processing defects, stress concentrations, and surface scratches. This suggests that a lower degree of crosslinking may be more optimal when designing for both wear and fatigue in total joint replacements.

This work was funded by National Science Foundation and Office of Naval Research grants to the University of California at Berkeley, and the Whitaker foundation to Brigham & Women's Hospital, Harvard Medical School.

References

1. Jasty M, Bragdon CR, O'Connor DO, Muratoglu OK, Premnath V, Merrill EW, Harris WH. Marked improvement in the wear resistance of a new form of UHMWPE in a physiologic hip simulator. In: Transactions of the 43rd Annual Meeting of the Orthopedic Research Society, San Francisco; 1997. p 785.

Questions? Contact FDA/CDRH/OCE/DID at CDRH-FOISTATUS@fda.hhs.gov or 301-796-8118

Records processed under FOIA Request #2014-8015; Released by CDRH on 12-8-2015

2. Muratoglu OK, Bragdon CR, O'Connor DO, Jasty M, Harris WH, Gul R, McGarry F. Unified wear model for highly crosslinked ultra-high molecular weight polyethylenes (UHMWPE). Biomaterials 1999;20(16):1463–1470.
3. McKellop H, Shen FW, Lu B, Campbell P, Salovey R. Development of an extremely wear-resistant ultra high molecular weight polyethylene for total hip replacements. J Orthop Res 1999;17(2):157–167.
4. Edidin AA, Pruitt L, Jewett CW, Crane DJ, Roberts D, Kurtz SM. Plasticity-induced damage layer is a precursor to wear in radiation-cross-linked UHMWPE acetabular components for total hip replacement. J Arthroplasty 1999;14(5):616–627.
5. Oonishi H, Takayama Y, Tsuji E. Improvement of polyethylene by irradiation in artificial joints. Radiat Phys Chem 1992;39: 495–504.
6. Sun DC, Wang A, Stark C, Dumbleton JH. The concept of stabilization in UHMWPE. In: Transactions of the 5th World Biomaterials Congress; 1996. p 195.
7. Wang A, Sun DC, Yau SS, Edwards B, Sokol M, Essner A, Polineni VK, Stark C, Dumbleton JH. Orientation softening in the deformation and wear of ultra-high molecular weight polyethylene. Wear 1997;203:230–241.
8. Kurtz SM, Pruitt LA, Jewett CW, Foulds JR, Edidin AA. Radiation and chemical crosslinking promote strain hardening behavior and molecular alignment in ultra high molecular weight polyethylene during multi-axial loading conditions. Biomaterials 1999;20(16):1449–1462.
9. Gomoll A, Wanich T, Bellare A. Fracture toughness of ultra-high molecular weight polyethylene used in orthopedic implants. In: Transactions of 11th International Conference on Deformation, Yield, and Fracture of Polymers, Cambridge, UK; 2000. p 254–257.
10. Shen F-W, McKellop H. Long term stability of chemically crosslinked UHMW polyethylene acetabular cups. In: Transactions of 27th Annual Society for Biomaterials Conference, Minneapolis; 2001.
11. Muratoglu OK, Biggs SA, Bragdon CR, O'Connor DO, Merrill EW, Premnath V, Jasty M, Harris WH. Long term stability of radiation and peroxide crosslinked UHMWPE. In: Transactions of 23rd Annual Society for Biomaterials Conference; 1997. p 776.
12. Baker DA, Hastings RS, Pruitt L. Study of fatigue resistance of chemical and radiation crosslinked medical grade ultrahigh molecular weight polyethylene. J Biomed Mater Res 1999;46(4): 573–581.
13. Greenwald AS, Bauer TW, Ries MD. New polys for old: Contribution or caveat. In: Transactions of 68th Annual Meeting of the American Academy of Orthopaedic Surgeons, San Francisco; 2001.
14. Wright T, Goodman S. Implant wear in total joint replacement: Clinical and biologic issues, material, and design considerations. Rosemont, IL: American Academy of Orthopaedic Surgeons; 2002.
15. Bartel DL, Bicknell VL, Wright TM. The effect of conformity, thickness, and material on stresses in ultra-high molecular weight components for total joint replacement. J Bone Joint Surg Am 1986;68(7):1041–1051.
16. O'Connor DO, Muratoglu OK, Bragdon CR, Lowenstein J, Jasty M, Harris WH. Wear and high cycle fatigue of highly crosslinked UHMWPE. In: Transactions of 44th Annual Meeting of the Orthopaedic Research Society, Anaheim, CA; 1999. p 816.
17. Krzypow DJ, Bensusan J, Sevo K, Haggard W, Parr J, Goldberg V, Rimnac C. The fatigue crack propagation resistance of gamma radiation or peroxide crosslinked UHMW polyethylene. In: Transactions of 6th World Biomaterials Congress, Hawaii; 2000. p 382.
18. Pruitt L, Bailey L. Factors affecting near-threshold fatigue crack propagation behavior of orthopedic grade ultra high molecular weight polyethylene. Polymer 1998;39(8–9):1545–1553.
19. Baker DA, Hastings RS, Pruitt L. Compression and tension fatigue resistance of medical grade ultra high molecular weight polyethylene: The effect of morphology, sterilization, aging, and temperature. Polymer 2000;41(2):795–808.
20. Hertzberg RW, Manson JA. Fatigue of engineering plastics. New York: Academic Press; 1980.
21. Kurtz SM, Pruitt L, Jewett CW, Crawford RP, Crane DJ, Edidin AA. The yielding, plastic flow, and fracture behavior of ultra-high molecular weight polyethylene used in total joint replacements. Biomaterials 1998;19(21):1989–2003.
22. Connelly GM, Rimnac CM, Wright TM, Hertzberg RW, Manson JA. Fatigue crack propagation behavior of ultrahigh molecular weight polyethylene. J Orthop Res 1984;2(2):119–125.
23. Baker D, Pruitt L, Bellare A. Ultra-small angle X-ray scattering to detect fatigue damage in polymers. J Mater Sci Lett 2001; 20(12):1163–1164.
24. Kausch HH, Gensler R, Grein C, Plummer CJG, Saramuzzino P. Crazing in semicrystalline thermoplastics. J Macromol Sci Phys 1999;B38(5–6):803–815.

Questions? Contact FDA/CDRH/OCE/DID at CDRH-FOISTATUS@fda.hhs.gov or 301-796-8118

Records processed under FOIA Request #2014-8015; Released by CDRH on 12-8-2015

ELSEVIER

Journal of Biomechanics 40 (2007) S11–S17

JOURNAL OF BIOMECHANICS

www.elsevier.com/locate/jbiomech
www.JBiomech.com

In vivo knee moments and shear after total knee arthroplasty

Darryl D. D'Lima[a,b,*], Shantanu Patil[a], Nikolai Steklov[a], Shu Chien[b], Clifford W. Colwell Jr.[a]

[a]*Shiley Center for Orthopaedic Research and Education at Scripps Clinic, 11025 N. Torrey Pines Road, Suite 140, La Jolla, CA 92037, USA*
[b]*Department of Bioengineering, University of California, San Diego, CA, USA*

Abstract

Tibiofemoral loading is very important in cartilage degeneration as well as in component survivorship after total knee arthroplasty. We have previously reported the axial knee forces in vivo. In this study, a second-generation force-sensing device that measured all six components of tibial forces was implanted in a 74-kg, 83-year-old male. Video motion analysis, ground reaction forces, and knee forces were measured during walking, stair climbing, chair-rise, and squat activities. Peak total force was 2.3 times body weight (BW) during walking, 2.5 × BW during chair rise, 3.0 × BW during stair climbing, and 2.1 × BW during squatting. Peak anterior shear force at the tibial tray was 0.30 × BW during walking, 0.17 × BW during chair rise, 0.26 × BW during stair climbing, and 0.15 × BW during squatting. Peak flexion moment at the tray was 1.9% BW × Ht (percentage of body weight multiplied by height) for chair-rise activity and 1.7% BW × Ht for squat activity. Peak adduction moment at the tray was −1.1% BW × Ht during chair-rise, −1.3% BW × Ht during squatting. External knee flexion and adduction moments were substantially greater than flexion and adduction moments at the tray. The axial component of forces predominated especially during the stance phase of walking. Shear forces and moments at the tray were very modest compared to total knee forces. These findings indicate that the soft tissues around the knee absorbed most of the external shear forces. Our results highlight the importance of direct measurements of knee forces.
© 2007 Elsevier Ltd. All rights reserved.

Keywords: Total knee arthroplasty; Knee forces; In vivo; Knee sheer; Knee moments

1. Introduction

The biomechanics of the knee joint are important in analyzing activities of daily living that primarily involve the lower limbs. The loading of the knee joint correlates with the health of the cartilage, and abnormal loading is associated with the development of cartilage degeneration and osteoarthritis (OA). Patient body weight commonly correlates with OA (Felson et al., 1997). It has been hypothesized that repeated impulse loading leads to the stiffening of bone with concomitant increased stresses at the cartilage (Messier, 1994). Subjects with knee OA walk with a greater than normal peak external knee adduction moment (Baliunas et al., 2002). Another hypothesis is that quadriceps fatigue results in reduced shock absorption of knee forces and is the reason for the higher risk of OA in obese women (Syed and Davis, 2000). Regardless of the precise mechanism, it is commonly believed that knee biomechanics play a major role in the etiology of OA.

Total knee arthroplasty (TKA) is a widely accepted treatment for end-stage arthritis. Knee forces have been shown to affect arthroplasty component survivorship, wear of articular-bearing surfaces, and integrity of the bone–implant interface. Excessive knee forces have been implicated in the breakdown of the cement interface or in the collapse of underlying bone. Knee forces along with component design also determine the contact stresses on the bearing surfaces. Contact stresses have been correlated with the magnitude and distribution of wear. Additionally, high-flexion knee designs are being introduced to permit greater knee flexion. These components will allow patients to engage in common activities that involve deep knee flexion such as kneeling, squatting, and sitting cross-legged.

*Corresponding author. Shiley Center for Orthopaedic Research and Education at Scripps Clinic, 11025 N. Torrey Pines Road, Suite 140, La Jolla, CA 92037, USA. Tel.: +1 858 332 0166; fax: +1 858 332 0140.
E-mail address: ddlima@scripps.edu (D.D. D'Lima).

0021-9290/$ - see front matter © 2007 Elsevier Ltd. All rights reserved.
doi:10.1016/j.jbiomech.2007.03.004

Questions? Contact FDA/CDRH/OCE/DID at CDRH-FOISTATUS@fda.hhs.gov or 301-796-8118

Records processed under FOIA Request #2014-8015; Released by CDRH on 12-8-2015

Studies analyzing these activities have estimated high knee forces (Nagura et al., 2002; Thambyah et al., 2005; Escamilla, 2001). Therefore, existing knee prosthetic designs may have to be modified to withstand increased loading.

Almost all studies relating to knee forces have involved either in vitro measurements (Ellis et al., 1984; Singerman et al., 1999; Kaufman et al., 1996) or estimates using mathematical models (Seireg and Arvikar, 1975; Morrison, 1970; Taylor et al., 2004; Lu et al., 1998). We previously reported the first direct measurement of knee forces in vivo after TKA (D'Lima et al., 2005, 2006). The tibial component used in that study was instrumented with four load cells that measured the axial components of load on the four quadrants of the tibial tray. This instrumented implant measured the total axial force and the location of the center of pressure. However, shear and moments, which are also important components of knee forces, could not be measured in that design.

In collaboration with Zimmer, Inc. (Warsaw, IN), we developed a second-generation, force-sensing device that measured all components of tibial forces (Kirking et al., 2005). The stem of this design was instrumented with strain gauges that measured all six components of forces. In this study, we report on the first in vivo measurements of shear and moments in the knee after TKA.

2. Methods

A custom tibial component was manufactured by Zimmer, Inc., based on the Natural Knee II (NK-II) tibial tray design. The tray and locking mechanism were identical to the standard design for implantation with a standard insert. The stem was instrumented with strain gauges to measure three orthogonal forces and three moments. The stem also housed a microtransmitter, which performed analog-to-digital conversion, filtering, and multiplexing before transmitting data via a hermetic glass-feed-through tantalum antenna. External coil induction was used to power the implant. Details of the implant design, strain gauges, microtransmitter, telemetry system, and accuracy have been previously reported (Kirking et al., 2005).

Appropriate Institutional Review Board approval and patient's consent were obtained before implantation in a 74-kg, 83-year-old male (Fig. 1a). A standard polyethylene insert (NK-II CR Congruent, Zimmer) and a posterior cruciate-retaining femoral component (NK-II CR, Zimmer)

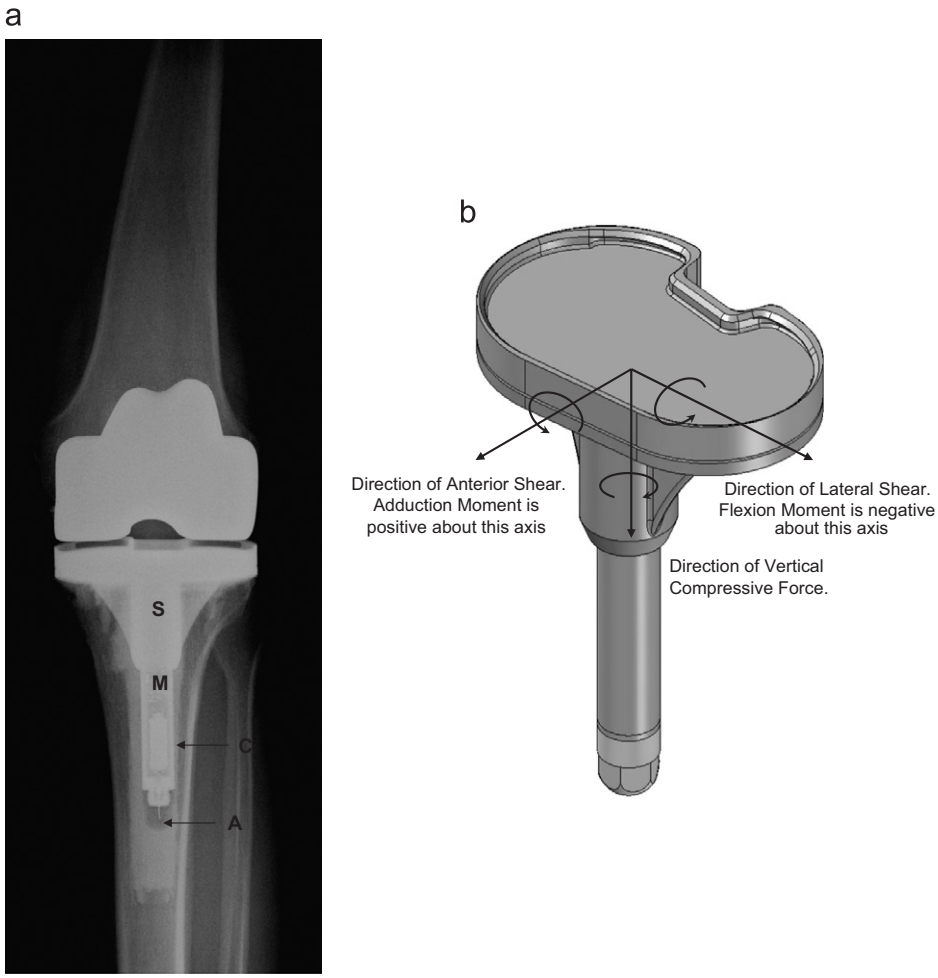

Fig. 1. (a) Postoperative radiograph showing the instrumented tibial prosthesis: S, hollow strain-gaged portion of the stem; M, location of microprocessor; C, internal coil; A, transmitting antenna. (b) The center of the right hand orthogonal coordinate system was located at the level of the top surface of the tray in line with the center of the cylindrical stem of the prosthesis. The forces and moments acting on the tray were recorded in the directions shown here.

Questions? Contact FDA/CDRH/OCE/DID at CDRH-FOISTATUS@fda.hhs.gov or 301-796-8118

Records processed under FOIA Request #2014-8015; Released by CDRH on 12-8-2015

were implanted using a standard anteromedial approach. The tibial bone cut was made at 90° to the long axis in the coronal plane (0° varus) and at 90° in the sagital plane (0° posterior slope). The distal femoral cut was made at 6° valgus to the anatomic axis of the femur. The posterior femoral cut was made at 3° external rotation with reference to the posterior surface of the posterior condyles. Intramedullary alignment was used for femoral and tibial bone preparation. The patella was resurfaced with a standard dome-shaped, all-polyethylene component. All components were cemented. The patient underwent routine postoperative rehabilitation as per a standard primary TKA.

Three months after the surgery, knee kinematics, ground reaction forces, and tibial forces and moments were measured in a motion analysis laboratory (Center for Human Performance, Children's Hospital, San Diego, CA). Knee kinematics were monitored using 6 Vicon cameras and infrared reflective skin markers (Helen Hayes lower limb marker set) (Kadaba et al., 1989, 1990). Ground reaction forces were measured using three force plates (AMTI, Watertown, MA) mounted in the floor of the walkway. Knee kinematics and moments were computed using commercially available software (OrthoTrak, Motion Analysis Corp, Santa Rosa, CA). Data were collected synchronously for the following activities. Walking was studied at a comfortable self-selected pace. Rising from a chair (sit-to-stand) and sitting down in a chair (stand-to-sit) activities were performed with the arms folded across the chest using a chair with a seat height of 44 cm (equal to the joint-to-floor distance of the patient's knee). Stair climbing was conducted on stairs with a 17.8 cm (7 in) riser and with hand-rail support. Squatting was performed with both feet parallel to each other, up to knee flexion angle that was within the patient's tolerance (~80°).

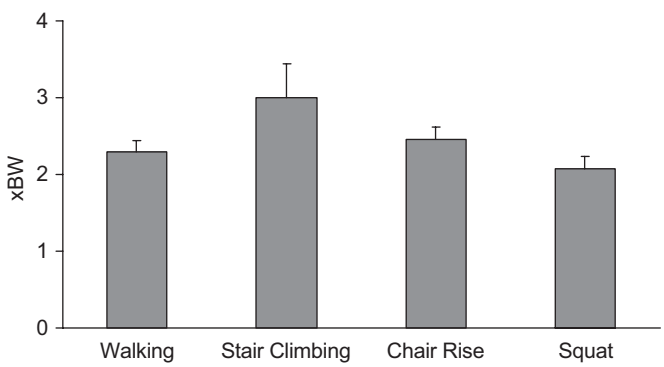

Fig. 2. Peak total tibial forces (mean of six cycles for each activity) measured during activities of daily living (error bars represent standard deviations).

3. Results

Forces are reported as multiples of body weight (× BW) and moments as a percentage of body weight multiplied by height (% BW × Ht). The direction of forces and moments were computed in the coordinate system of the tibial tray (Fig. 1b), which was implanted at 90° to the intramedullary axis of the tibia in the coronal and the sagittal planes. For example, the shear generated at the tibial tray by the femoral component moving in the anterior direction was denoted as anterior shear. Similarly, the moment generated at the tibial tray by adduction of the knee was termed as adduction moment. The peak total tibial forces were between 2 and 3 × BW for the activities studied (Fig. 2).

The vertical component of force predominated in all activities (Figs. 3–6). For example, during walking, the magnitude of the axial component was on average 86% of the magnitude of the total force. During the stance phase of walking, the vertical component averaged 98% of the magnitude of the total force. Peak anteroposterior (AP) and mediolateral (ML) shear forces were substantially lower than the axial component for all the activities studied. Peak anterior shear force was 0.30 × BW during walking, 0.17 × BW during chair rise, 0.26 × BW during stair climbing, and 0.15 × BW during squatting. Overall AP shear was mainly directed anteriorly for all activities.

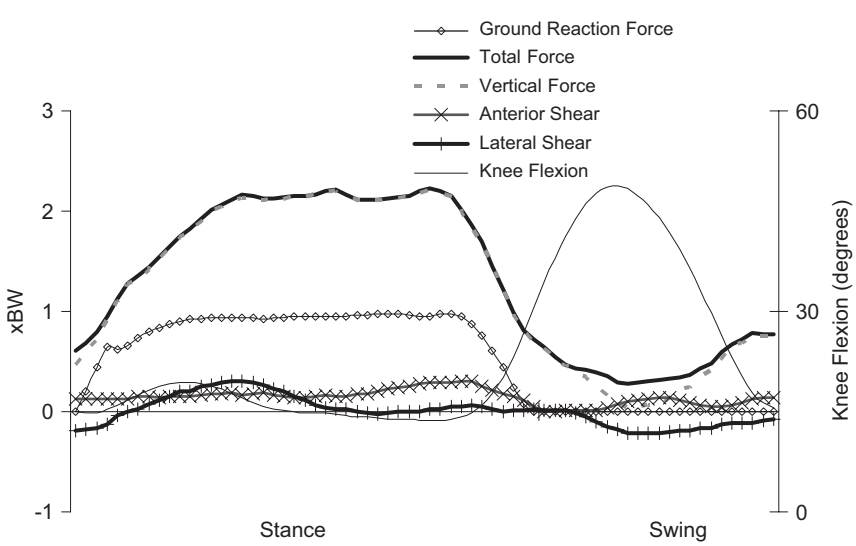

Fig. 3. Knee kinematics and forces during one representative walking cycle are shown. The ground reaction force was used to divide the walking cycle into stance and swing phases. The total force was almost entirely composed of the vertical component of force, especially during the stance phase. Peak anterior shear forces were small (0.3 × BW). Mediolateral shear forces were also in the same range and were laterally directed during most of the stance phase and medially directed during most of the swing phase.

Questions? Contact FDA/CDRH/OCE/DID at CDRH-FOISTATUS@fda.hhs.gov or 301-796-8118

Records processed under FOIA Request #2014-8015; Released by CDRH on 12-8-2015

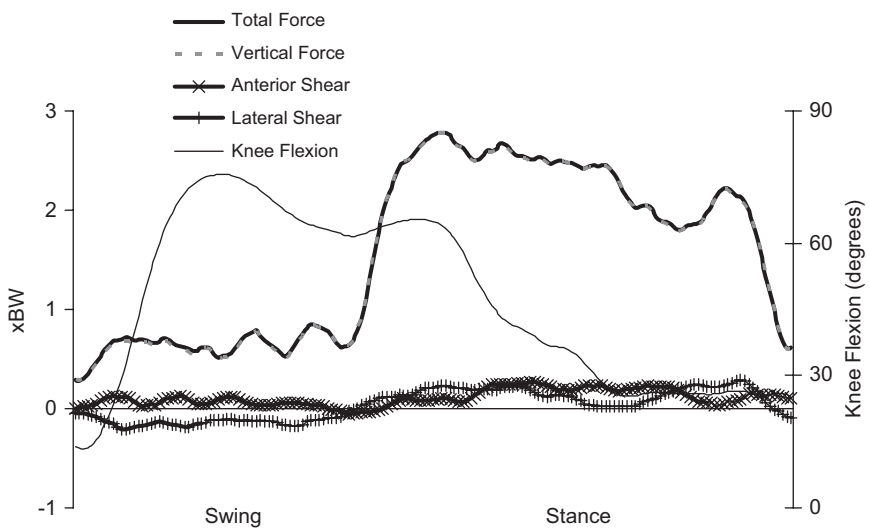

Fig. 4. Knee kinematics and forces measured during one representative stair-climbing cycle are shown. As for walking, the total force was almost entirely composed of the vertical component (the respective plots could not be visually differentiated). Peak anteroposterior shear forces were small (0.26 × BW) and were mainly directed anteriorly. Mediolateral shear forces were laterally directed during most of the stance phase and medially directed during most of the swing phase.

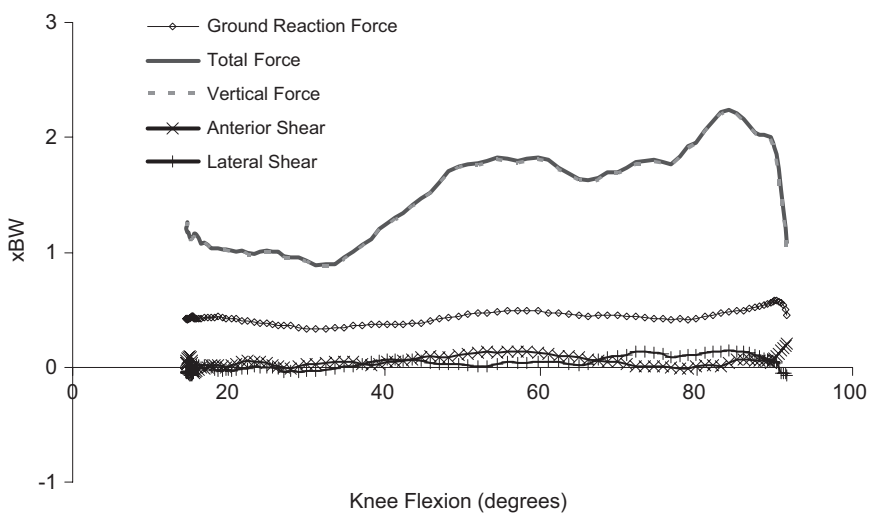

Fig. 5. Knee kinematics and forces were measured during one representative chair-rise cycle. Forces are plotted against knee flexion angle. Total force and vertical force components could not be visually differentiated. Peak shear forces were even smaller than for walking and stair climbing (0.17 × BW). Ground reaction forces under the instrumented limb averaged 44±6% of total ground reaction forces.

During walking and stair climbing, ML shear was medially directed during the swing phase and during heel strike, changing to a lateral direction early in the stance phase (Figs. 3 and 4).

External knee moments were measured using ground reaction forces and inverse dynamics. Moments generated at the tibial tray were measured directly by the instrumented tibial prosthesis (Fig. 7). External knee flexion moments increased with knee flexion angle and peaked at 5.7% BW × Ht (flexion = 90°) during chair rise and 4.3% BW × Ht (flexion = 82°) during squatting. The ground reaction forces under the instrumented side averaged 44±6% of total ground reaction forces for the chair-rise activity and 24±3% for the squat activity. The moment generated by the joint reaction force on the tibial tray peaked at much lower levels: 1.9% BW × Ht for chair-rise activity and 1.7% BW × Ht for squat activity. However, a strong linear correlation was noted between the external knee flexion moment and the flexion moment measured at the tibial tray ($r^2 = 0.81$ for chair rise and $r^2 = 0.87$ for squat activity).

Peak external knee adduction moments were 3.4% BW × Ht for chair-rise activity and 1.8% BW × Ht for squat activity. External adduction moments were higher at low flexion angles and decreased with increased knee flexion (Fig. 7). Adduction moments measured at the tibial

Questions? Contact FDA/CDRH/OCE/DID at CDRH-FOISTATUS@fda.hhs.gov or 301-796-8118

Records processed under FOIA Request #2014-8015; Released by CDRH on 12-8-2015

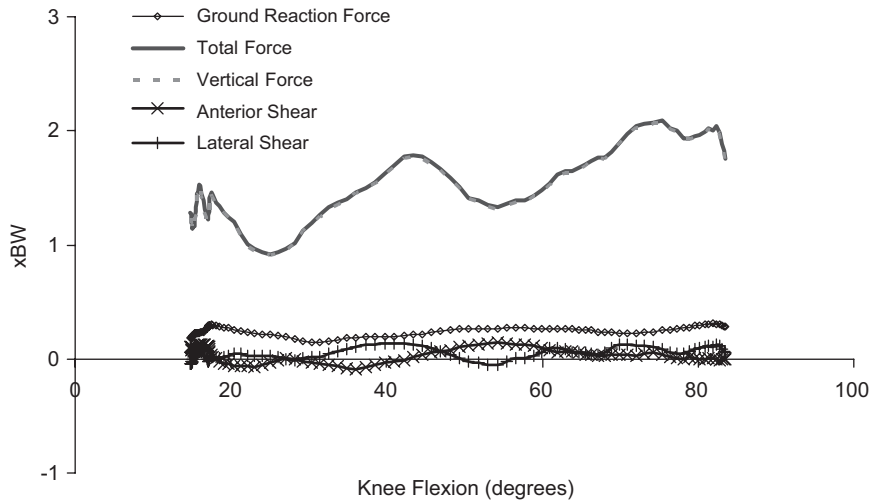

Fig. 6. Knee kinematics and forces were measured during one representative squatting cycle. Forces are plotted against knee flexion angle. Peak shear forces were even smaller than those measuring for walking and stair climbing (0.17 × BW). Ground reaction forces under the instrumented side were lower than for chair activity (24±3% of total ground reaction forces for squat-up and 21±11% for squat-down activities), indicating that the patient was favoring the instrumented knee.

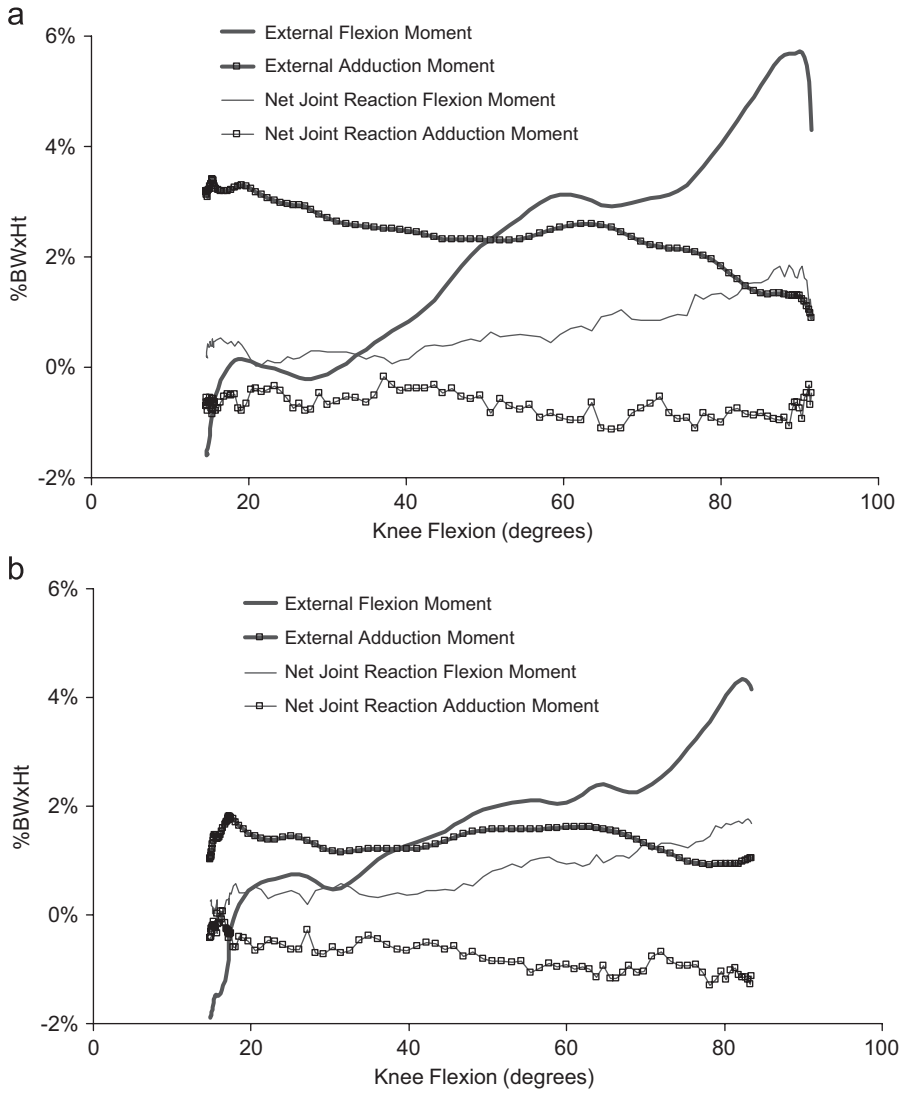

Fig. 7. External knee moments (computed from ground reaction forces and knee kinematic data) were typically high. Moments generated by the joint reaction force at the tibial tray were substantially lower. a: Chair-rise activity; b: squat activity.

Questions? Contact FDA/CDRH/OCE/DID at CDRH-FOISTATUS@fda.hhs.gov or 301-796-8118

Records processed under FOIA Request #2014-8015; Released by CDRH on 12-8-2015

tray were negative and peaked at −1.1% BW × Ht during chair rise and −1.3% BW × Ht during squatting. The external knee adduction moments were poorly correlated with the net moment generated by the joint reaction force at the tibial tray ($r^2 = 0.05$ for chair-rise activity and $r^2 = 0.11$ for squat activity).

4. Discussion

Previously, we measured axial knee forces in vivo after TKA (D'Lima et al., 2005, 2006). However, shear forces and moments are also significant components that affect knee wear and prosthesis survivorship. We therefore developed a second-generation telemetry-enabled tibial prosthesis capable of measuring all six components of force. This is a report of shear and moments measured at the knee joint 3 months after total knee arthroplasty during common activities.

The axial component of forces measured at 3 months peaked between 2 and 3 × BW, which were similar to those measured with the first-generation instrumented tibial prosthesis (D'Lima et al., 2005). The axial component of forces predominated, especially during the stance phase of the activities studied. Shear forces during walking were modest (0.3 × BW) compared to total knee forces. The soft tissues around the knee provide most of the resistance to shear and the intact posterior cruciate ligament may explain the low anterior shear recorded at the tibia tray. Low anteroposterior shear forces during walking (0.40–0.54 × BW) have also been reported at the tibia in a patient with an instrumented distal femoral replacement and a hinged knee design (Taylor et al., 1998). Another study on the lower limb model in patients with instrumented hip arthroplasties reported peak contact shear forces that averaged 0.5 × BW across four patients (Taylor et al., 2004). The knees in those patients were not implanted. These shear forces are in the same range as those reported for younger subjects with normal knees, i.e., peak external shear forces (computed with inverse dynamics) averaged 0.39 × BW (Nagura et al., 2002) and 0.33 × BW (Costigan et al., 2002), while peak joint contact shear forces averaged 0.5 × BW (Costigan et al., 2002). However, knee joint contact shear forces as high as 2 × BW have also been predicted by mathematical models (Seireg and Arvikar, 1975). Shear forces measured in the mediolateral direction were also low, which were similar to earlier estimates (Morrison, 1970).

Peak tibial forces were substantially higher while climbing stairs (averaging 3 × BW) than for the chair-rise and squat activities. This was possibly because the latter two activities involved a double-legged stance throughout the cycle. For the squat activity, the patient appeared to be loading the instrumented limb less than the contralateral side (as evidenced by the distribution of the ground reaction forces under each foot).

Shear forces were also low for the chair-rise and squat activities despite the higher flexion angles achieved (greater than 80° while squatting and greater than 90° during chair rise). Higher peak external anteroposterior shear forces have been computed in young, normal subjects averaging 0.47 × BW for stair climbing and 0.58–0.63 × BW for squatting (Nagura et al., 2002). Even higher peak joint contact shear forces (1.2 × BW) have also been reported during stair climbing (Costigan et al., 2002). Our measurement of low shear forces during these activities again emphasizes the contribution of muscles and ligaments in resisting tibial shear.

We measured moments at the tibial tray for two activities that typically generate high external moments at the knee: rising from a chair and squatting. In young, normal subjects, knee moments were significantly affected by the height of the chair (Rodosky et al., 1989). When compared to normal subjects, osteoarthritic and TKA patients reduced flexion moments by displacing the center of mass anteriorly (Su et al., 1998). This compensation was more pronounced at lower chair heights. At chair seat heights equal to or greater than 100% of the knee joint-to-floor height, the differences in kinetics of the sit-to-stand activity between normal and post-TKA patients cease to exist. We therefore chose a seat height equal to the knee joint-to-floor height. The patient was able to rise from the chair without arm support and demonstrated no significant difficulty. Elderly subjects with chair-rise difficulties typically require a seat height of 120% of the knee joint-to-floor height (Weiner et al., 1993). Patients with unilateral TKA also tend to shift the center of mass to the normal limb as an additional compensatory maneuver (Su et al., 1998). In the present study, the ground reaction forces under the instrumented side averaged 44 ± 6% of total ground reaction forces, indicating that the center of mass was not substantially shifted to the contralateral side.

Peak external knee flexion moment while rising from a chair was moderately high (5.7% BW × Ht). This value was higher than the moments generated by normal, osteoarthritic, or post-TKA subjects of similar age range [3–4% BW × Ht (Su et al., 1998)]. The peak external knee moment calculated during the squat activity (4.3% BW × Ht) was similar to that reported for healthy subjects in the same age range [4.5% BW × Ht (Flanagan et al., 2003)]. However, substantially larger peak flexion moments (13.5% BW × Ht) have been reported for younger, normal subjects (Nagura et al., 2002). This is likely due to the difference in peak flexion angle achieved during the squat activity: 150° for young subjects vs. 100° for older subjects. Peak flexion moment measured at the tibial tray was substantially lower (<2% BW × Ht for both activities).

The peak external adduction moment during chair-rise activity (3.4% BW × Ht) was higher than that for squat activity (1.8% BW × Ht). Low peak external adduction moments have been reported during chair rise for older normal subjects (1.15% BW × Ht) and for subjects with chronic knee pain [1.31% BW × Ht (Amin et al., 2004)]. Adduction moments at the tibial tray were also low (around 1% BW × Ht) and, unlike flexion moments,

Questions? Contact FDA/CDRH/OCE/DID at CDRH-FOISTATUS@fda.hhs.gov or 301-796-8118

Records processed under FOIA Request #2014-8015; Released by CDRH on 12-8-2015

correlated poorly with external adduction moments ($r^2 \leqslant 0.11$ for both activities).

This is a report of knee forces and moments measured in only one patient. Due to patient-to-patient variation and implant design differences, these absolute values cannot be extrapolated to all knee arthroplasty patients. In addition, forces were measured at the 3-month postoperative time point. We have shown that tibial forces can increase up to 2 years postoperative (D'Lima et al., 2005). Finally, only activities of daily living are reported under carefully controlled laboratory conditions. Forces during other activities and during unanticipated events such as stumbling may be substantially higher than those reported here. We are in the process of implanting more patients with this second-generation implant. We are actively following all patients to increase the duration of follow-up, as well as the range of activities analyzed.

Overall, shear forces, as well as moments at the tibial tray, were fairly low. These results indicate that accurate computation of knee contact forces requires appropriate modeling of the passive and active soft tissues. Direct measurements of knee joint reaction forces and moments coupled with robust mathematical models are extremely valuable in increasing our understanding of the loading of the soft tissues, cartilage, and bone of the natural knee, as well as the prosthetic components of the implanted knee.

References

Amin, S., Luepongsak, N., McGibbon, C.A., LaValley, M.P., Krebs, D.E., Felson, D.T., 2004. Knee adduction moment and development of chronic knee pain in elders. Arthritis and Rheumatism 51, 371–376.

Baliunas, A.J., Hurwitz, D.E., Ryals, A.B., Karrar, A., Case, J.P., Block, J.A., Andriacchi, T.P., 2002. Increased knee joint loads during walking are present in subjects with knee osteoarthritis. Osteoarthritis and Cartilage 10, 573–579.

Costigan, P.A., DeLuzio, K.J., Wyss, U.P., 2002. Knee and hip kinetics during normal stair climbing. Gait and Posture 16, 31–37.

D'Lima, D.D., Patil, S., Steklov, N., Slamin, J.E., Colwell Jr., C.W., 2005. The Chitranjan Ranawat Award: in vivo knee forces after total knee arthroplasty. Clinical Orthopaedics and Related Research 440, 45–49.

D'Lima, D.D., Patil, S., Steklov, N., Slamin, J.E., Colwell Jr., C.W., 2006. The HAP Paul Award: tibial forces measured in vivo after total knee arthroplasty. Journal of Arthroplasty 21, 255–262.

Ellis, M.I., Seedhom, B.B., Wright, V., 1984. Forces in the knee joint whilst rising from a seated position. Journal of Biomedical Engineering 6, 113–120.

Escamilla, R.F., 2001. Knee biomechanics of the dynamic squat exercise. Medicine and Science in Sports and Exercise 33, 127–141.

Felson, D.T., Zhang, Y., Hannan, M.T., Naimark, A., Weissman, B., Aliabadi, P., Levy, D., 1997. Risk factors for incident radiographic knee osteoarthritis in the elderly: the Framingham Study. Arthritis and Rheumatism 40, 728–733.

Flanagan, S., Salem, G.J., Wang, M.Y., Sanker, S.E., Greendale, G.A., 2003. Squatting exercises in older adults: kinematic and kinetic comparisons. Medicine and Science in Sports and Exercise 35, 635–643.

Kadaba, M.P., Ramakrishnan, H.K., Wootten, M.E., Gainey, J., Gorton, G., Cochran, G.V., 1989. Repeatability of kinematic, kinetic, and electromyographic data in normal adult gait. Journal of Orthopaedic Research 7, 849–860.

Kadaba, M.P., Ramakrishnan, H.K., Wootten, M.E., 1990. Measurement of lower extremity kinematics during level walking. Journal of Orthopaedic Research 8, 383–392.

Kaufman, K.R., Kovacevic, N., Irby, S.E., Colwell Jr., C.W., 1996. Instrumented implant for measuring tibiofemoral forces. Journal of Biomechanics 29, 667–671.

Kirking, B., Krevolin, J., Townsend, C., Colwell, C.W.J., D'Lima, D.D., 2005. A multiaxial force-sensing implantable tibial prosthesis. Journal of Biomechanics.

Lu, T.W., O'Connor, J.J., Taylor, S.J., Walker, P.S., 1998. Validation of a lower limb model with in vivo femoral forces telemetered from two subjects. Journal of Biomechanics 31, 63–69.

Messier, S.P., 1994. Osteoarthritis of the knee and associated factors of age and obesity: effects on gait. Medicine and Science in Sports and Exercise 26, 1446–1452.

Morrison, J.B., 1970. The mechanics of the knee joint in relation to normal walking. Journal of Biomechanics 3, 51–61.

Nagura, T., Dyrby, C.O., Alexander, E.J., Andriacchi, T.P., 2002. Mechanical loads at the knee joint during deep flexion. Journal of Orthopaedic Research 20, 881–886.

Rodosky, M.W., Andriacchi, T.P., Andersson, G.B., 1989. The influence of chair height on lower limb mechanics during rising. Journal of Orthopaedic Research 7, 266–271.

Seireg, A., Arvikar, R.J., 1975. The prediction of muscular load sharing and joint forces in the lower extremities during walking. Journal of Biomechanics 8, 89–102.

Singerman, R., Berilla, J., Archdeacon, M., Peyser, A., 1999. In vitro forces in the normal and cruciate-deficient knee during simulated squatting motion. Journal of Biomechanical Engineering 121, 234–242.

Su, F.C., Lai, K.A., Hong, W.H., 1998. Rising from chair after total knee arthroplasty. Clinical Biomechanics (Bristol, Avon) 13, 176–181.

Syed, I.Y., Davis, B.L., 2000. Obesity and osteoarthritis of the knee: hypotheses concerning the relationship between ground reaction forces and quadriceps fatigue in long-duration walking. Medical Hypotheses 54, 182–185.

Taylor, S.J., Walker, P.S., Perry, J.S., Cannon, S.R., Woledge, R., 1998. The forces in the distal femur and the knee during walking and other activities measured by telemetry. Journal of Arthroplasty 13, 428–437.

Taylor, W.R., Heller, M.O., Bergmann, G., Duda, G.N., 2004. Tibiofemoral loading during human gait and stair climbing. Journal of Orthopaedic Research 22, 625–632.

Thambyah, A., Goh, J.C., De, S.D., 2005. Contact stresses in the knee joint in deep flexion. Medical Engineering and Physics 27, 329–335.

Weiner, D.K., Long, R., Hughes, M.A., Chandler, J., Studenski, S., 1993. When older adults face the chair-rise challenge. A study of chair height availability and height-modified chair-rise performance in the elderly. Journal of the American Geriatrics Society 41, 6–10.

Questions? Contact FDA/CDRH/OCE/DID at CDRH-FOISTATUS@fda.hhs.gov or 301-796-8118

Records processed under FOIA Request #2014-8015; Released by CDRH on 12-8-2015

ELSEVIER

Power and Sample Size Calculations for Studies Involving Linear Regression

William D. Dupont, PhD and Walton D. Plummer, Jr., BS
Department of Preventive Medicine, Vanderbilt University School of Medicine, Nashville, Tennessee

ABSTRACT: This article presents methods for sample size and power calculations for studies involving linear regression. These approaches are applicable to clinical trials designed to detect a regression slope of a given magnitude or to studies that test whether the slopes or intercepts of two independent regression lines differ by a given amount. The investigator may either specify the values of the independent (x) variable(s) of the regression line(s) or determine them observationally when the study is performed. In the latter case, the investigator must estimate the standard deviation(s) of the independent variable(s). This study gives examples using this method for both experimental and observational study designs. Cohen's method of power calculations for multiple linear regression models is also discussed and contrasted with the methods of this study. We have posted a computer program to perform these and other sample size calculations on the Internet (see http://www.mc.vanderbilt.edu/prevmed/psintro.htm). This program can determine the sample size needed to detect a specified alternative hypothesis with the required power, the power with which a specific alternative hypothesis can be detected with a given sample size, or the specific alternative hypotheses that can be detected with a given power and sample size. Context-specific help messages available on request make the use of this software largely self-explanatory. *Controlled Clin Trials* 1998;19:589–601 © Elsevier Science Inc. 1998

KEY WORDS: *Statistics, regression analysis, linear models, power calculations, sample size calculations, linear regression*

INTRODUCTION

Clinical investigators sometimes wish to evaluate a continuous response measure in a cohort of patients randomized to one of several groups defined by increasing levels of some treatment. In performing sample size and power calculations for such studies, one reasonable approach models patient response as a linear function of dose, and poses power calculations in terms of detecting dose-response slopes of a given magnitude. Alternately, we may wish to evaluate the dose-response curves of two different treatments and test whether slopes of these curves differ. This article provides an easily used, accurate method for power and sample size calculations for such studies. We have

Address reprint requests to: William D. Dupont, PhD, Department of Preventive Medicine, Vanderbilt University School of Medicine, A-1124 Medical Center North, Nashville, TN 37232-2637.
Received 20 June 1996; accepted 2 June 1998.

Controlled Clinical Trials 19:589–601 (1998)
© Elsevier Science Inc. 1998
0197-2456/98/$19.00
655 Avenue of the Americas, New York, NY 10010 PII S0197-2456(98)00037-3

Questions? Contact FDA/CDRH/OCE/DID at CDRH-FOISTATUS@fda.hhs.gov or 301-796-8118

Records processed under FOIA Request #2014-8015; Released by CDRH on 12-8-2015

posted an interactive self-documented program to perform these calculations on the Internet.

Other investigators have reviewed general methods for sample size and power calculations [1–3]. Hintze [4] provided a method for designing studies to detect correlation coefficients of specified magnitudes that uses a computational algorithm of Guenther [5]. This method provides results that are perhaps less easily understood than those based on regression slope parameters, because many investigators can more readily interpret slopes than correlation coefficients. Kraemer and Thiemann [3] provide tables that permit exact sample size calculations for studies designed to detect correlation coefficients of a given magnitude. They also give formulas that permit using these tables for designs involving linear regression. Although accurate, these methods are less convenient than those that we have incorporated into an interactive computer program. Cohen [2] provided more complex methods for designs involving multiple linear regression and correlation analysis. Later in this study we describe these methods, which require expressing the alternative hypothesis in terms of their effect on the multiple correlation coefficient [6]. Hintze [4] has written software for deriving these calculations, but clinical investigators may find his methods somewhat difficult to use and interpret. Goldstein [7] and Iwane et al. [8] have reviewed other power and sample size software packages.

Simple Linear Regression

We study the effect of one variable on another by estimating the slope of the regression line between these variables. For example, we might compare the effects of a treatment at several dose levels. Suppose that we treat n patients, that the jth patient has response y_j after receiving dose level x_j, and that the expected value of y_j given x_j is $\gamma + \lambda x_j$. To test the null hypothesis that $\lambda = 0$ against a two-sided alternative hypothesis with type I error probability α, we must be able to answer the following three questions:

1. How many patients must we study to detect a specific alternative hypothesis $\lambda = \lambda_a$ with power $1 - \beta$?
2. With what power can we detect a specific alternative hypothesis $\lambda = \lambda_a$ given observations on n study subjects?
3. What alternative values of λ_a can we detect with power $1 - \beta$ if we study n patients?

Either observational or experimental studies may use this design. In the former, both $\{x_j\}$ and $\{y_j\}$ are attributes of the study subjects, and we intend to determine whether these two variables are correlated. In these studies, the investigator must also estimate σ_x, the predicted standard deviation of x_j in the patients under study. In experiments, the investigator determines the values of $\{x_j\}$. Typically, x_j denotes a drug dose given at one of K distinct values $w_1, \ldots, w_K$, with a proportion c_k of the study subjects being assigned dose level w_k.

The degree of dispersion of the response values about the regression line affects power and sample size calculations. A parameter that quantifies this dispersion is σ, the standard deviation of the regression errors. The regression error for the jth observation is the difference between the observed and expected

Questions? Contact FDA/CDRH/OCE/DID at CDRH-FOISTATUS@fda.hhs.gov or 301-796-8118

Records processed under FOIA Request #2014-8015; Released by CDRH on 12-8-2015

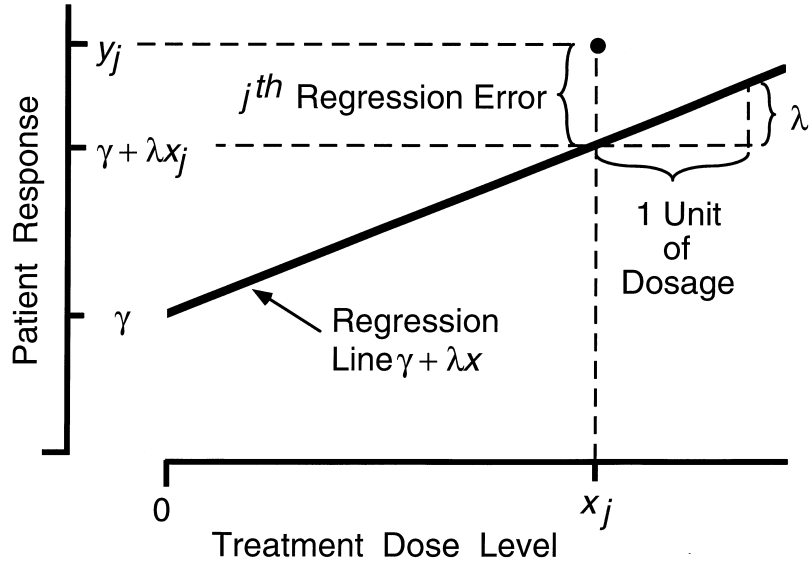

Figure 1 In simple linear regression we obtain n pairs of observations $\{x_j, y_j\}$. We assume that the expected value of the response y_j is given by the linear equation $E(y_j) = \gamma + \lambda x_j$. The jth regression error is the vertical distance between the observed response y_j and its expected value $\gamma + \lambda x_j$.

response value for the jth subject. In other words, the regression error is the vertical distance between the observed response y_j and the true regression line (see Fig. 1); σ is the standard deviation of these vertical distances. The values of σ, σ_x, σ_y, λ, and the correlation coefficient ρ are all interrelated. It is well known [6] that:

$$\lambda = \rho\sigma_y/\sigma_x \tag{1}$$

and it is easily shown that:

$$\sigma = \sigma_y\sqrt{1 - \rho^2} = \lambda\sigma_x\sqrt{1/\rho^2 - 1} = \sqrt{\sigma_y^2 - \lambda^2\sigma_x^2} \tag{2}$$

Thus, when $\rho = 1$, the observations $\{x_j\}$ and $\{y_j\}$ are perfectly correlated and lie on a straight line with slope σ_y/σ_x; the regression errors are all zero because the observed and expected responses are always equal) and hence $\sigma = 0$. When $\rho = 0$, x_j and y_j are uncorrelated, the expected regression line is flat ($\lambda = 0$), and the standard deviation of the regression errors equals the standard deviation of y_j (i.e., $\sigma = \sigma_y$). Figure 2 illustrates the relationship between these parameters when $0 < \rho < 1$. This figure shows simulated data for patients given treatments A and B under the assumption that the two treatments have identical means and standard deviations of the independent and response variables. They differ in that the correlation coefficient between response and independent variables is 0.9 for treatment A (black dots) and 0.6 for treatment B (open circles). Consequently, the response to treatment A are more closely clustered around their (black) regression line than the response to treatment B (gray). Thus, the average regression error is less for treatment A than for treatment B and, hence, σ, the standard deviation of these errors, is less for treatment A than for treatment

Questions? Contact FDA/CDRH/OCE/DID at CDRH-FOISTATUS@fda.hhs.gov or 301-796-8118

Records processed under FOIA Request #2014-8015; Released by CDRH on 12-8-2015

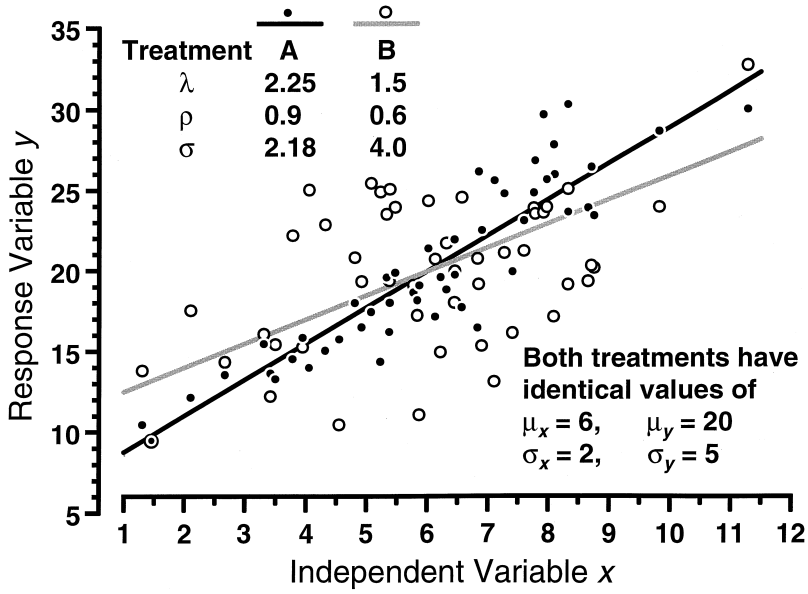

Figure 2 This figure illustrates the relationship in simple linear regression between ρ, the correlation coefficient between the independent and response variables; the regression errors (see Fig. 1); and σ, the standard deviation of the regression errors. Higher values of ρ imply smaller regression errors, which, in turn, imply smaller values of σ (see text).

B. Power or sample size calculations require estimates of σ_x, λ, and σ. It is often difficult to estimate σ directly; however, we can obtain indirect estimates of σ using equation (2) whenever we are able to estimate ρ or σ_y. We derive power and sample size formulas for simple linear regression in the Appendix.

Contrasting Two Linear Regression Lines

Suppose that we want to compare the slopes and intercepts of two independent regression lines. For example, we might wish to compare the effects of two different treatments at several dose levels. Suppose that treatments 1 and 2 are given to n_1 and n_2 patients, respectively, and that the jth subject who receives treatment i (i = 1 or 2) has response y_{ij} to treatment at dose level x_{ij}, where the expected value of y_{ij} is $\gamma_i + \lambda_i x_{ij}$. We want to determine whether the response to the treatments differ. Specifically, we intend to test the null hypotheses that $\gamma_1 = \gamma_2$ and $\lambda_1 = \lambda_2$. In this case, we must answer the three questions given earlier for alternative hypotheses concerning the magnitude of the differences in the y intercept and slope parameters for these two treatments. We derive power and sample size formulas for two treatment linear regression problems in the Appendix.

COMPUTER SOFTWARE

We have written a computer program to implement these and other sample size and power calculations [1] and have posted it, together with program

Questions? Contact FDA/CDRH/OCE/DID at CDRH-FOISTATUS@fda.hhs.gov or 301-796-8118

Records processed under FOIA Request #2014-8015; Released by CDRH on 12-8-2015

documentation, on the Internet. The program runs under either Windows 95 or Windows NT operating systems. To obtain free copies open the http://www.mc.vanderbilt.edu/prevmed/psintro.htm page on the World Wide Web and follow instructions. The program, named *PS*, has a graphical user interface with hypertext help messages that make the use of the program largely self-explanatory. It can answer the three questions given in the Introduction for each study design considered by this software. It can also generate graphs of sample size versus power, sample size versus detectable alternative hypotheses, or power versus detectable alternative hypotheses. It is written in Visual Basic [9] and Fortran 90 [10] and uses the First Impression graphics control [11].

EXAMPLES

Linear Regression in an Observational Study

A dieting program encourages patients to follow a specific diet and to exercise regularly. We want to determine whether the actual average time per day spent exercising is related to body mass index (BMI, in kilograms per square meter) after 6 months on this program. Previous experience suggests that the exercise time of participants has a standard deviation of $\sigma_x = 7.5$ minutes. Kuskowska-Wolk et al. [12] reported that the standard deviation of the BMI for their female study subjects was $\sigma_y = 4.0$ kg/m^2. We have $n = 100$ women willing to follow this program for 6 months. We want to determine the power with which we can detect a true drop of BMI of $\lambda_a = -0.0667$ kg/m^2 per minute of exercise. (This would imply that the average BMI of participants who exercised half an hour a day would be 2 kg/m^2 less than those who did not exercise at all. We use the *PS* program to determine the power with which the alternative hypothesis $\lambda_a = -0.0667$ can be detected with type I error probability $\alpha = 0.05$ as follows: choose linear regression with one treatment; specify that the investigator does not choose the treatment levels; enter $\sigma_x = 7.5$ for the standard deviation of the independent variable; indicate that we want to determine the power of the proposed study and that we will provide an estimate of σ_y; and enter $\alpha = 0.05$, $\lambda_a = -0.0667$, $\sigma_y = 4.0$, and $n = 100$. The *PS* program then calculates that 100 women yield a power of only 0.24 for detecting this alternative hypothesis. Thus, the planned study would be insufficient to detect reliably a true slope of this magnitude. The user may experiment with different values of λ_a, σ_y, and n to determine the sensitivity of the derived power to changes in these parameter values.

The units of measurement of the response variable affect the magnitude of both σ_y and λ_a. Thus, of BMI is measured in grams per square meter, then σ_y becomes 4000 and λ_a becomes -66.7. Substituting these two values into the preceding power calculation, of course, leaves the power unchanged.

Linear Regression in an Experimental Study

Siber et al. [13] studied impaired antibody response to pneumococcal vaccine after treatment for Hodgkin's disease. Seventeen patients treated with subtotal radiation received pneumococcal vaccine from 8 to 51 months later. A linear regression of natural log antibody concentration on the time interval between

Questions? Contact FDA/CDRH/OCE/DID at CDRH-FOISTATUS@fda.hhs.gov or 301-796-8118

Records processed under FOIA Request #2014-8015; Released by CDRH on 12-8-2015

treatment and vaccination suggested that log antibody concentration increased with increasing time interval between treatment and vaccination. Siber's group estimated the slope parameter for this regression to be $\hat{\lambda} = 0.01$ ($p = 0.11$) and the correlation coefficient to be $r = 0.40$.

Suppose that we want to use these results as pilot data for a new study designed to detect the true alternative hypothesis that $\lambda_a = 0.01$ with power $1 - \beta = 0.90$ and type I error probability $\alpha = 0.05$. We might decide to assign patients at random to receive vaccine at either $w_1 = 10$, $w_2 = 30$, or $w_3 = 50$ months after radiation therapy. That is, we consider a study of $K = 3$ treatment levels (vaccination delay times), with equal proportions of patients vaccinated after each delay interval ($c_1 = c_2 = c_3 = 1/3$). To use the *PS* program, we choose linear regression with one treatment; specify equal allocation of the treatment levels to the three times 10, 30, and 50 months; indicate that we intend to determine the sample size and that we will provide an estimate of the correlation coefficient ρ; and enter $\alpha = 0.05$, $1 - \beta = 0.90$, $\lambda_a = 0.01$, and $\rho \cong r = 0.40$. Using these values in the *PS* program gives a sample size of $n = 57$ patients needed to detect a true value of $\lambda = 0.01$ with 90% power, $\alpha = 0.05$, and patients equally allocated to receive vaccinations at 10, 30, and 50 months after radiation therapy.

Comparing Slopes of Two Linear Regression Lines

Armitage and Berry ([6], Table 9.4) gave the age and pulmonary vital capacity for 28 cadmium industry workers with less than 10 years of cadmium exposure and for 44 workers never exposed to cadmium. The standard deviations of the ages of those unexposed and exposed were $\sigma_{x_1} = 12.0$ and $\sigma_{x_2} = 9.19$, respectively. Regressing vital capacity on age in these two groups gives slope estimates of $\hat{\lambda}_1 = -0.0306$ and $\hat{\lambda}_2 = -0.0465$ liters per year of life in unexposed and exposed workers, respectively (i.e., a typical exposed worker loses 46.5 mL of vital capacity per year). The standard errors of $\hat{\lambda}_1$ and $\hat{\lambda}_2$ are 0.00754 and 0.0113, respectively; the residual mean squares from the unexposed and exposed regressions are 0.352 and 0.293, respectively. From equation (9.17) of Armitage and Berry [6], the pooled estimate of the error variance from both groups is $s^2 = 0.329$, and hence $s = 0.574$. The estimated difference in slope estimates, $\hat{\lambda}_2 - \hat{\lambda}_1 = -0.0159$, is not significantly different from zero ($p = 0.26$) {[6] Equation (9.19)}. Suppose that we want to recruit enough workers to detect a true difference of $\lambda_2 - \lambda_1 = -0.0159$ in these two groups, with 80% power, type I error probability $\alpha = 0.05$, and a ratio of unexposed to exposed workers $m = 44/28 = 1.57$. Applying the *PS* program, we choose linear regression with two treatments, specify that the investigator does not choose the treatment levels, enter $\sigma_{x_1} = 12.0$ and $\sigma_{x_2} = 9.19$ for the standard deviation of the independent variable (age) in the control (unexposed) and experimental (exposed) groups, respectively; indicate that we will provide an estimate of the standard deviation of the regression errors, that we wish to calculate sample size, and that we want to compare slopes; and enter $\alpha = 0.05$, $1 - \beta = 0.80$, $\lambda_2 - \lambda_1 = -0.0159$, $\sigma = 0.574$, and $m = 1.57$. The program responds that the required experimental treatment sample size is 166. Hence, if we recruit 427 workers, 166 workers with less than 10 years of cadmium exposure and $1.57 \times 166 = 261$ unexposed

Questions? Contact FDA/CDRH/OCE/DID at CDRH-FOISTATUS@fda.hhs.gov or 301-796-8118

Records processed under FOIA Request #2014-8015; Released by CDRH on 12-8-2015

workers we will have 80% power to detect a difference in the rate of loss of vital capacity with age of −0.0159 L/yr of life.

LINEAR REGRESSION USING THE *PASS* PROGRAM

One of the most popular commercially available power and sample size programs, *PASS 6.0* [4, 8], provides a general approach to power calculations for multiple linear regression using the method of Cohen [2]. Let:

$$y_j = \gamma + \lambda_1 x_{1j} + \lambda_2 x_{2j} + \cdots + \lambda_k x_{kj} + \epsilon_j : j = 1, \ldots, J \tag{3}$$

denote a conventional multiple linear regression model in which the jth patient has a response variable y_j and k covariates $\{x_{1j}, x_{2j}, \cdots x_{kj}\}$. We intend to test the null hypothesis that $\lambda_1 = \lambda_2 = \cdots = \lambda_p = 0$ for some $p \leqslant k$. Under this null hypothesis the regression model, equation (3), reduces to:

$$y_j = \gamma + \lambda_{p+1} x_{p+1,j} + \lambda_{p+2} x_{p+2,j} + \cdots + \lambda_k x_{kj} + \epsilon_j : j = 1, \ldots, J \tag{4}$$

Cohen provides an F statistic to test this null hypothesis that is based on the multiple correlation coefficients R_T and R_0 from equations (3) and (4), respectively. *PASS* [4] uses this test to determine the power with which we are likely to reject the null hypothesis given a true alternative hypothesis that is expressed in terms of $\Delta = R_T^2 - R_0^2$. The next sections describe the applicability of *PASS* to the examples of the present work. Table 1 gives the required input and output for these examples.

Using *PASS* for the BMI and Vaccination Examples

The correlation coefficient module of the *PASS* program is also applicable for simple linear regression when the data have a bivariate normal distribution [4, 5]. In the body mass index example given earlier, we calculated the power to detect $\lambda_a = -0.0667$, given $\sigma_x = 7.5$ and $\sigma_y = 4.0$. From equation (1) we see that this is equivalent to testing the alternative hypothesis that $\rho = \lambda\sigma_x/\sigma_y = 0.125$ against the null hypothesis that $\rho = 0$. Entering this value into the correlation coefficient module of the *PASS* program with a two-tailed type I error probability, $\alpha = 0.05$, a null hypothesis, $\rho_0 = 0$, and a sample size of $n = 100$ gives a power of 0.24 to detect $\rho_a = 0.125$. This is the same power obtained with the *PS* program.

The *PASS* correlation coefficient module is not applicable to the vaccination delay time example because the delay times are not normally distributed. This nonnormality arises from the fact that Hintze–Guenther method [4, 5] used by this program assumes that the independent and dependent variables have a bivariate normal distribution. For experimental data, however, the independent variable is rarely normally distributed. Instead, trials usually assign a fixed, often equal number of patients to, say, low, medium, and high treatment levels as in the vaccine example. In this case, these treatment levels are clearly not normally distributed.

Questions? Contact FDA/CDRH/OCE/DID at CDRH-FOISTATUS@fda.hhs.gov or 301-796-8118

Records processed under FOIA Request #2014-8015; Released by CDRH on 12-8-2015

Table 1 Input and Output Needed by *PS* and *PASS* Programs for Examples Considered in the Present Study

Example	Program	Input[a]	Output
Body mass index	*PS*	$\sigma_x = 7.5$, $\alpha = 0.05$, $\lambda_a = -0.0667$, $\sigma_y = 4$, $n = 100$	Power $1 - \beta = 0.24$
	PASS[b]	$\alpha = 0.05$, $\rho_0 = 0$, $\rho_a = 0.125$, $n = 100$	Power $1 - \beta = 0.24$
Vaccination delay time	*PS*	$w_1 = 10$, $w_2 = 30$, $w_3 = 50$, $c_1 = c_2 = c_3 = 1/3$, $\alpha = 0.05$, $1 - \beta = 0.9$, $\lambda_a = 0.01$, $\rho = 0.4$	Sample size $n = 57$
	PASS	Not applicable	Not applicable
Cadmium exposure	*PS*	$\sigma_{x1} = 12.0$, $\sigma_{x2} = 9.19$, $\alpha = 0.05$, $1 - \beta = 0.80$, $\lambda_2 - \lambda_1 = -0.0159$, $\sigma = 0.574$, $m = 1.57$	Exposed sample size $n = 166$, total sample size $J = 427$
	PASS[c]	$p = 1$, $\Delta = 0.0128$, $k - p = 2$, $R_0^2 = 0.3115$, $J = 427$, $\alpha = 0.05$	Power $1 - \beta = 0.807$

[a] See text for definitions.

[b] *PASS* correlation coefficient module.

[c] *PASS* multiple regression module.

Questions? Contact FDA/CDRH/OCE/DID at CDRH-FOISTATUS@fda.hhs.gov or 301-796-8118

Records processed under FOIA Request #2014-8015; Released by CDRH on 12-8-2015

Using *PASS* for the Cadmium Exposure Example

To use the *PASS* program for the cadmium exposure example just discussed we first combine the data from the unexposed and exposed workers into a single multiple linear regression model. Let

$$x_{2j} = \begin{cases} 1\text{: } j^{th} \text{ worker was exposed} \\ 0\text{: } j^{th} \text{ worker not exposed} \end{cases}$$

also let x_{3j} be the age when the jth patient's vital capacity y_j is measured, and $x_{1j} = x_{2j} \times x_{3j}$. The model:

$$y_j = \gamma + \lambda_1 x_{1j} + \lambda_2 x_{2j} + \lambda_3 x_{3j} + \epsilon_j \tag{5}$$

reduces to $y_j = \gamma + \lambda_3 x_{3j} + \epsilon_j$ and $y_j = (\gamma + \lambda_2) + (\lambda_1 + \lambda_3)x_{3j} + \epsilon_j$ for unexposed and exposed workers, respectively. Hence, in this model, λ_1 represents the difference in the rate of decline in vital capacity between exposed and unexposed workers, and testing whether this rate is the same in both groups is equivalent to testing the null hypothesis that $\lambda_1 = 0$. Analyzing equation (5) with the vital capacity data set gives an estimate of $\lambda_1 = -0.0159$ with $R_T^2 = 0.3243$. (Note that this estimate of λ_1 equals the difference of the slope estimates from the simple linear regressions given earlier). Under the null hypothesis, equation (5) reduces to:

$$y_j = \gamma + \lambda_2 x_{2j} + \lambda_3 x_{3j} + \epsilon_j \tag{6}$$

with a single slope parameter λ_3 for both exposure groups. This model gives $R_0^2 = 0.3115$. Hence the increase in R^2 from equation (6) to equation (5) is $\Delta = 0.3243 - 0.3115 = 0.0128$. Suppose we have access to an additional 427 workers, 166 of whom were exposed for less than 10 years, with the remainder unexposed. Entering $p = 1$, $\Delta = 0.0128$, $k - p = 2$, and $R_0^2 = 0.3115$, $J = 427$, and $\alpha = 0.05$ in the multiple regression module of the *PASS* program gives a power estimate of 0.808, which is comparable to the results of the *PS* program given earlier. (When running the *PASS* program, enter p and Δ in the *Variables to be tested* frame, $k - p$ and R_0^2 in the *Variables controlled for* frame, and zeros in both fields of the *C: Variables removed* frame. Positive values of these last two fields are used in power calculations for certain complex study designs and hypotheses that Cohen refers to as case 2 analyses [2].) Thus, in this example, the *PS* and *PASS* programs produce very similar results; they differ in their requirements for input of parameters. Also, this module of the *PASS* program does not facilitate direct sample size calculations.

DISCUSSION

The chief advantage of Cohen's method of power calculations for multiple linear regression is its flexibility. It may be used to perform power calculations for a very wide range of linear regression problems and null hypotheses. This method, however, has three disadvantages that restrict its use:

1. *The pilot data needed for Cohen's method is often unavailable.* Suppose that the literature provides an estimate of the slope of a linear regression of weight loss against hours of exercise per week for normal (control) subjects. Estimates of the standard deviations of these subjects' weight loss

Questions? Contact FDA/CDRH/OCE/DID at CDRH-FOISTATUS@fda.hhs.gov or 301-796-8118

Records processed under FOIA Request #2014-8015; Released by CDRH on 12-8-2015

and exercise time are also available. You believe that the rate of weight loss per hour of exercise for patients on an experimental treatment will differ from that for control subjects and intend to determine an appropriate sample size for an experimental comparing experimental and control treatments. Our method allows the alternative hypothesis to be naturally specified in terms of a difference in loss-per-hour slope estimates. The user can enter estimates of the control slope and control standard deviations directly into the *PS* program to obtain the sample size needed for the desired power. Cohen's method, however, cannot be used for this example. His method requires estimates of the multiple correlation coefficients R_T and R_0 under equations (5) and (6) of the present study. It is unlikely that these statistics will be published in the literature, For this reason, Cohen's method almost always requires complete pilot data on both experimental and control subjects to calculate R_T and R_0. This was the case in the cadmium example presented in this work. Frequently, however, we want to perform power calculations on the basis of data from the literature or on pilot data that consist of the control data only. In such situations, our method works well but Cohen's is unusable.

2. *It is difficult to interpret the results of Cohen's method.* In Cohen's method the alternative hypothesis is stated in terms of $\Delta = R_T^2 - R_0^2$. This statistic has little intuitive meaning to either clinicians or grant reviewers. In contrast, specifying the alternative hypothesis in terms of a slope difference—say 0.5 kg per hour of exercise—is easier to comprehend.
3. *Some investigators may find Cohen's method difficult to use.* To use Cohen's method, the investigator must first known how to set up equations (3) and (4) and then how to run the linear regressions needed to derive R_T^2 and R_0^2. In contrast, to use our method the investigator need only understand the basic concepts of statistical power and significance, and the simple linear models described in the Introduction.

SOFTWARE ACCURACY

We have written Excel spreadsheets that evaluate Appendix equations (A1) and (A2) for the different cases considered in this study. These spreadsheets provide independent confirmation that the *PS* program has correctly implemented our formulas. The fact that the *PS* and *PASS* programs give very similar answers to the cadmium and body mass index examples using very different methods is evidence that both programs have been coded correctly.

This work was supported by NIH RO1 Grants CA50468, HL19153, and LM06226 and NCI Center Grant CA68485. We thank Drs. W.A. Ray, O.B. Crofford, G.W. Reed, M.D. Decker, G.R. Bernard, M.R. Griffin, and R.I. Shorr for their helpful suggestions.

REFERENCES

1. Dupont WD, Plummer WD. Power and sample size calculations: a review and computer program. *Controlled Clin Trials* 1990;11:116–128.
2. Cohen J. *Statistical Power Analysis for the Behavioral Sciences* 2nd ed. Hillsdale, NJ: Lawrence Erlbaum; 1988.

Questions? Contact FDA/CDRH/OCE/DID at CDRH-FOISTATUS@fda.hhs.gov or 301-796-8118

Records processed under FOIA Request #2014-8015; Released by CDRH on 12-8-2015

3. Kraemer HC, Thiemann S. *How Many Subjects? Statistical Power Analysis in Research*. Newbury Park, CA; 1987.
4. Hintze JL. *PASS 6.0 User's Guide*. Kaysville, UT: NCSS Dr. Jerry L. Hintze; 1996.
5. Guenther W. Desk calculation of probabilities for the distribution of the sample correlation coefficient. *Am Statistician* 1977;31:45–48.
6. Armitage P, Berry G. *Statistical Methods in Medical Research* 3rd ed. Oxford, UK: Blackwell Scientific; 1994.
7. Goldstein R. Power and sample size via MS/PC-DOS computers. *Am Statistician* 1989;43:253–260.
8. Iwane M, Palensky J, Plante K. A user's review of commercial sample size software for design of biomedical studies using survival data. *Controlled Clin Trials* 1997;18:65–83.
9. Microsoft Corporation. *Microsoft Visual Basic Programmer's Guide*. Redmond, WA: Microsoft Corporation; 1995.
10. Microsoft Corporation. *Microsoft Fortran PowerStation Programmer's Guide.* Redmond, WA: Microsoft Corporation; 1995.
11. Visual Components Sybase Inc. *First Impression Active X User's Guide: High Performance Software for Charting Data for Microsoft Visual Basic, Visual C++, and Other Languages* (*Version 5.0*). Overland Park, KS: Visual Components Sybase, Inc.; 1997.
12. Kuskowska-Wolk A, Bergstrom R, Bostrom G. Relationship between questionnaire data and medical records of height, weight and body mass index. *Int J Obes* 1992;16:1–9.
13. Siber GR, Weitzman SA, Aisenberg AC, Weinstein HJ, Schiffman G. Impaired antibody response to pneumococcal vaccine after treatment for Hodgkin's Disease. *N Engl J Med* 1978;299:442–448.

APPENDIX

Generic Power and Sample Size Formulas

Suppose for n patients (or groups of patients) we observe responses that depend on some parameter θ. Let R, a statistic derived from the n responses, have a normal distribution with mean $\sqrt{n}\theta$ and standard deviation σ_R. Let S_R be another statistic independent of R such that vS_R^2/σ_R^2 has a χ^2 distribution with v degrees of freedom. Let $T_v[t]$ be the cumulative probability distribution for a random variable having a t distribution with v degrees of freedom; $t_{v,\alpha} = T_v^{-1}[1 - \alpha]$ denote the critical value that is exceeded by such a t statistic with probability α; θ_0 and θ_α denote the values of θ under the null and a specific alternative hypothesis, respectively; $\delta = (\theta_a - \theta_0)/\sigma_R$; and α and β denote the type I and II error probabilities associated with a two-sided test of the null hypothesis and the alternative hypothesis θ_a, respectively. Then $(R - \sqrt{n}\theta)/S_R$ has a t distribution with v degrees of freedom [6] that can be used to test the null hypothesis that $\theta = \theta_0$. The same argument used to derive equations (2) and (3) of Dupont and Plummer [1] proves that the power to detect alternative hypothesis $\theta = \theta_a$ is:

$$1 - \beta = T_v[\delta\sqrt{n} - t_{v,\alpha/2}] + T_v[-\delta\sqrt{n} - t_{v,\alpha/2}] \tag{A1}$$

and that, for the relevant values of α and β:

Questions? Contact FDA/CDRH/OCE/DID at CDRH-FOISTATUS@fda.hhs.gov or 301-796-8118

Records processed under FOIA Request #2014-8015; Released by CDRH on 12-8-2015

$$n = (t_{v,\beta} + t_{v,\alpha/2})^2/\delta^2 \tag{A2}$$

Equation (A2) must be solved iteratively because both v and δ are themselves functions of n.

Studies Using Simple Linear Regression

Suppose that the error terms $y_j - (\gamma + \lambda x_j)$ are independently and normally distributed with mean 0 and standard deviation σ. Let $\bar{x}$ and $\bar{y}$ denote the means of $\{x_j\}$ and $\{y_j\}$, respectively. Then it is well known [6] that:

$\hat{\lambda} = \Sigma(x_j - \bar{x})(y_j - \bar{y})/\Sigma(x_j - \bar{x})^2$ is an unbiased estimate of λ;
$\hat{\gamma} = \bar{y} - \hat{\lambda}\bar{x}$ is an unbiased estimate of γ; and
$s^2 = \Sigma[y_j - (\hat{\gamma} + \hat{\lambda}x_j)]^2/(n - 2)$ is an unbiased estimate of σ^2 independent of $\hat{\lambda}$.

Also, $(n - 2)s^2/\sigma^2$ has a χ^2 distribution with $n - 2$ degrees of freedom, and $\hat{\lambda}$ has variance $\sigma^2_{\hat{\lambda}} = \sigma^2/\Sigma(x_j - \bar{x})^2$. Let $R = \sqrt{n}\hat{\lambda}$, $\sigma^2_x = \Sigma(x_j - \bar{x})^2/n$ and $S^2_R = s^2/\sigma^2_x$. Then, R has variance $\sigma^2_R = n\sigma^2_{\hat{\lambda}} = \sigma^2/\sigma^2_x$ and $(n - 2)S^2_R/\sigma^2_R = (n - 2)s^2/\sigma^2 \sim \chi^2_{n-2}$. Hence, substituting $v = n - 2$ and $\delta = (\lambda_a - 0)/\sigma_R = \lambda_a\sigma_x/s$ into equations (A1) and (A2) gives power and sample size formulas for simple linear regression. In observational studies the investigator estimates σ^2_x, in experiments, $\bar{x} = \sum_k c_k w_k$ and $\sigma^2_x = \sum_k c_k(w_k - \bar{x})^2$ in the definition of δ given above. We can estimate s indirectly using equation (2) if a direct estimate is unavailable. Thus, if estimates of either r, the sample correlation coefficient, or s_y, the sample standard deviation of y_j, are available then s may be estimated by $\lambda_a s_x \sqrt{1/r^2 - 1}$ or $\sqrt{s^2_y - \lambda^2_a s^2_x}$, respectively.

Studies With Two Linear Regression Lines

Suppose that the errors $y_{ij} - (\gamma_i + \lambda_i x_{ij})$, $i = 1, 2$, are independently and normally distributed with mean 0 and standard deviation σ. Let $\bar{x}_i$, $\bar{y}_i$, $\hat{\lambda}_i$, and $\hat{\gamma}_i$ be the corresponding mean values and regression parameter estimates. Let $s^2 = \Sigma_{ij}[y_{ij} - (\hat{\gamma}_i + \hat{\lambda}_i x_{ij})]^2/(n_1 + n_2 - 4)$. Then s^2 is an unbiased estimate of σ^2 and $(n_1 + n_2 - 4)s^2/\sigma^2 \sim \chi^2_{n_1+n_2-4}$. To test the null hypothesis that $\lambda_2 - \lambda_1 = 0$, we use equation (9.18) of Armitage and Berry [6], which may be rewritten $\mathrm{var}(\hat{\lambda}_2 - \hat{\lambda}_1) = \sigma^2_{\hat{\lambda}_2-\hat{\lambda}_1} = \sigma^2[1/(\sigma^2_{x_1} n_1) + 1/(\sigma^2_{x_2} n_2)]$, where $\sigma^2_{x_i} = \Sigma_j(x_{ij} = \bar{x}_i)^2/n_i$ for $i = 1, 2$. Let $n = n_2$ and let $m = n_1/n_2$ be the ratio of the two group sizes. Let $R = \sqrt{n}\ (\hat{\lambda}_2 - \hat{\lambda}_1)$ and σ^2_R be the variance of R. Then $\sigma^2_R = n\sigma^2_{\hat{\lambda}_2-\hat{\lambda}_1} = \sigma^2[1/(m\sigma^2_{x_1}) + 1/\sigma^2_{x_2}]$. Let $S^2_R = s^2[1/(m\sigma^2_{x_1}) + 1/\sigma^2_{x_2}]$. Then, $[n(1 + m) - 4]S^2_R/\sigma^2_R = (n_2 + n_1 - 4)s^2/\sigma^2 \sim x^2_{n_2+n_1-4}$. Therefore, substituting $v = n(1 + m) - 4$ and $\delta = (\lambda_2 - \lambda_1)/\sigma_R$ into equations (A1) and (A2) gives power and sample size formulas for testing the equality of the dose-response slopes of two treatments.

To test the equality of the y intercepts of the two treatments, we use equation (5.16) or Armitage and Berry [6], which gives $\mathrm{var}(\hat{\gamma}_i) = \sigma^2_{\hat{\gamma}_i} = \sigma^2[1 + \bar{x}^2_i/\sigma^2_{x_i}]/n_i$ for $i = 1, 2$. Therefore, $R = \sqrt{n}\ (\hat{\gamma}_2 - \hat{\gamma}_1)$ has variance

$$\sigma^2_R = \frac{\sigma^2}{m}\left\{1 + \frac{\bar{x}^2_1}{\sigma^2_{x_1}} + m\left[1 + \frac{\bar{x}^2_2}{\sigma^2_{x_2}}\right]\right\}$$

Questions? Contact FDA/CDRH/OCE/DID at CDRH-FOISTATUS@fda.hhs.gov or 301-796-8118

Records processed under FOIA Request #2014-8015; Released by CDRH on 12-8-2015

Let

$$S_R^2 = \frac{s^2}{m}\left\{1 + \frac{\bar{x}_1^2}{\sigma_{x_1}^2} + m\left[1 + \frac{\bar{x}_2^2}{\sigma_{x_2}^2}\right]\right\}$$

Then $[n(1 + m) - 4]S_R^2/\sigma_R^2 = (n_2 + n_1 - 4)s^2/\sigma^2 \sim \chi^2_{n_2+n_1-4}$. Substituting $v = n(1 + m) - 4$ and $\delta = (\gamma_2 - \gamma_1)/\sigma_R$ into equations (A1) and (A2) gives the desired sample size and power formulas.

As in the case for a single regression line, the values of x_{ij} may be either observed attributes of patients or controlled treatment values; s may be estimated from the correlation coefficient or standard deviation of the response variable among control subjects if a direct estimate is unavailable. These terms may be handled in equations (A1) and (A2) in the same way as in the previous section.

Questions? Contact FDA/CDRH/OCE/DID at CDRH-FOISTATUS@fda.hhs.gov or 301-796-8118

Records processed under FOIA Request #2014-8015; Released by CDRH on 12-8-2015

Accelerated aging studies of UHMWPE. I. Effect of resin, processing, and radiation environment on resistance to mechanical degradation

A. A. Edidin,[1,3] M. P. Herr,[2] M. L. Villarraga,[2,3] J. Muth,[1] S. S. Yau,[1] S. M. Kurtz[2,3]
[1]*Stryker Howmedica Osteonics Corporation, 300 Commerce Court, Mahwah, New Jersey 07430*
[2]*Exponent®, Inc., 2300 Chestnut Street, Suite 150, Philadelphia, Pennsylvania 19103*
[3]*Implant Research Center, School of Biomedical Engineering, Science and Health Systems, Drexel University, 3141 Chestnut Street, Philadelphia, Pennsylvania 19103*

Received 20 July 2001; revised 11 October 2001; accepted 2 November 2001

Abstract: The resin and processing route have been identified as potential variables influencing the mechanical behavior, and hence the clinical performance, of ultra-high molecular weight polyethylene (UHMWPE) orthopedic components. Researchers have reported that components fabricated from 1900 resin may oxidize to a lesser extent than components fabricated from GUR resin during shelf aging after gamma sterilization in air. Conflicting reports on the oxidation resistance for 1900 raise the question of whether resin or manufacturing method, or an interaction between resin and manufacturing method, influences the mechanical behavior of UHMWPE. We conducted a series of accelerated aging studies (no aging, aging in oxygen or in nitrogen) to systematically examine the influence of resin (GUR or 1900), manufacturing method (bulk compression molding or extrusion), and sterilization method (none, in air, or in nitrogen) on the mechanical behavior of UHMWPE. The small punch testing technique was used to evaluate the mechanical behavior of the materials, and Fourier transform infrared spectroscopy was used to characterize the oxidation in selected samples. Our study showed that the sterilization environment, aging condition, and specimen location (surface or subsurface) significantly affected the mechanical behavior of UHMWPE. Each of the three polyethylenes evaluated seem to degrade according to a similar pathway after artificial aging in oxygen and gamma irradiation in air. The initial ability of the materials to exhibit post-yield strain hardening was significantly compromised by degradation. In general, there were only minor differences in the aging behavior of molded and extruded GUR 1050, whereas the molded 1900 material seemed to degrade slightly faster than either of the 1050 materials. © 2002 Wiley Periodicals, Inc. J Biomed Mater Res 61: 312–322, 2002

Key words: ultra-high molecular weight polyethylene; UHMWPE; mechanical behavior; small punch test; ultimate properties; failure; degradation

INTRODUCTION

During the past 40 years, clinically successful total joint replacement components have been fabricated from ultra-high molecular weight polyethylene (UHMWPE). UHMWPE is produced as powder or resin, and subsequently converted directly into orthopedic components by direct compression molding, or it may be first converted to stock material by ram extrusion or compression molding, and then subsequently machined into its final form as an implant. As summarized in a recent review,[1] both the resin and processing route have been identified as potential variables influencing the mechanical behavior, and hence the clinical performance, of UHMWPE orthopedic components. More than 90% of the UHMWPE resin used for orthopedic components is produced under the GUR trade name by Ticona (formerly known as Hoechst, Bayport, TX).[1] The remaining UHMWPE used in orthopedics is designated as 1900 grade by Basell (formerly known as Montell, and before that, known as Himont, Wilmington, DE).[1] The nomenclature of the GUR and 1900 UHMWPE resins used in orthopedics has evolved over the years, and a guide to the different grades of UHMWPE used in implants has recently been published.[1]

Researchers have reported that components fabricated from 1900 resin may oxidize to a lesser extent than components fabricated from GUR resin during shelf aging after gamma sterilization in air.[2–7] Furman et al.,[2] Gillis et al.,[3] and Walsh et al.[4] have measured

Correspondence to: A. A. Edidin: e-mail: edidin@warwick.net.com
Contract grant sponsor: Stryker Howmedica Osteonics

© 2002 Wiley Periodicals, Inc.

Questions? Contact FDA/CDRH/OCE/DID at CDRH-FOISTATUS@fda.hhs.gov or 301-796-8118

Records processed under FOIA Request #2014-8015; Released by CDRH on 12-8-2015

density and oxidation in components and stock material fabricated from direct-molded 1900, extruded rods of 1900, and GUR 415, and compression-molded 1900, GUR 412, and 415. The researchers observed that components fabricated from direct-molded 1900 after 1986 exhibited "complete oxidation resistance" at long shelf aging times, and concluded that components fabricated from 1900 resin seemed to be more oxidation resistant than those fabricated from GUR resins, whether processed using compression molding, direct molding, or extrusion.[3] Gsell and colleagues examined the density, crystallinity, and uniaxial mechanical behavior from 16 direct-molded 1900H tibial components and observed no significant changes in properties as a function of aging time for up to 11 years.[5] More recently, Walsh and coworkers[4] hypothesized that the processing method (i.e., direct compression molding) played a greater role than resin in governing the oxidation resistance of a component. Together, this work suggests that both the resin and processing conditions may influence the tendency of UHMWPE components to oxidize after gamma irradiation in air.

Studies in the peer-reviewed orthopedics literature regarding the degradation behavior of 1900 resin are scarce, especially in comparison with GUR resins.[6–8] Grood et al.[8] were among the first to examine the changes in crystallinity of UHMWPE after gamma irradiation in air, but components of both 1900 resin and GUR resin (commercially available as RCH-1000, equivalent to GUR 412[1]) were pooled, precluding an independent analysis of post-irradiation crystallinity changes for the two types of polyethylene. In a comprehensive study of 100 shelf-aged and 68 retrieved tibial bearings, Currier and colleagues[6] observed that both GUR and 1900 resins oxidized during long-term shelf storage after gamma irradiation in air, but the oxidation rate for the GUR implants was reported to be seven times greater than that in components fabricated from 1900. Currier's data further suggested that the mechanical properties of UHMWPE fabricated from 1900 was more susceptible to oxidation than components fabricated from GUR resin. However, fabrication of the bearings was classified by the researchers as either direct molding or machining (from either extruded rod or bulk compression-molded sheet). Thus, Currier's study did not address potential differences between UHMWPE fabricated by extrusion or compression molding.

Because tibial inserts function as mechanical bearing surfaces, the loss of mechanical integrity caused by oxidative degradation can impact the long-term performance of total joint arthroplasty. The conflicting reports of the oxidation resistance for 1900 raise the question of whether resin or manufacturing method, or an interaction between resin and manufacturing method, influences the mechanical behavior of UHMWPE.

Standard methods have been developed to accelerate the oxidation of UHMWPE after gamma irradiation in air,[9] but have not been validated for UHMWPE that has been sterilized in a low-oxygen environment, such as nitrogen. Previous aging studies on polyethylene by Clough and Gillen[10] have suggested that both the irradiation and aging environment, and the synergism between the two, have substantial influences on mechanical degradation. For example, Clough and Gillen showed that either irradiation or aging in a nitrogen environment effectively blocked mechanical degradation of polyethylene, when compared with the effects of irradiation or aging in air.

We have conducted a series of accelerated aging studies to systematically examine the influence of resin, manufacturing method, and sterilization method on the mechanical behavior of UHMWPE. In the first report of this series, we examine the stability of contemporary GUR and 1900 resins that have been converted by bulk compression molding or extrusion. Consequently, in the present study, we addressed the following research question: Does the type of resin (1900 or GUR) or the conversion method (bulk compression molding or extruding) influence the degradation of mechanical behavior for UHMWPE after gamma irradiation in air, or nitrogen followed by accelerated aging in oxygen or nitrogen?

METHODS

Specimen preparation

Test specimens were prepared using the fabrication methods comparable to commercially available orthopedic components. Orthopedic implant-grade UHMWPE was obtained from stock material converters. Compression-molded 1900 (Poly Hi Solidur, Fort Wayne, IN), compression-molded GUR 1050 (Poly Hi Solidur), and ram-extruded GUR 1050 (Perplas Medical Ltd., Bacup England) were obtained from stock material converters. The compression-molded 1900 and GUR 1050 were processed under the same (proprietary) molding conditions as are used to fabricate stock material for orthopedic implants. Extruded 1900 was not evaluated in the present study, because contemporary orthopedic components are fabricated from this resin using compression molding or hot isostatic pressing techniques.[1]

The stock materials were machined into square test samples 30 mm in width and 10 mm in thickness, which corresponded to the approximate dimensions of a tibial insert. One face of the test samples was specified to have a surface finish comparable to the articulating surface of UHMWPE orthopedic components. The average surface roughness (R_a) of each of the materials was 0.58 ± 0.04 μm for the compression-molded 1900, 0.73 ± 0.06 μm for the compression-molded GUR 1050, and 0.82 ± 0.12 μm for the ram-extruded GUR 1050.

Before artificial aging, the materials were subjected to three gamma irradiation conditions: no irradiation (control), irradiation in air (3-MRad dose), and irradiation in nitrogen

Questions? Contact FDA/CDRH/OCE/DID at CDRH-FOISTATUS@fda.hhs.gov or 301-796-8118

Records processed under FOIA Request #2014-8015; Released by CDRH on 12-8-2015

(3-MRad dose). The gamma irradiation in nitrogen condition was intended to represent a contemporary sterilization practice,[1] whereas the nonirradiated and air-irradiated components served as negative and historical positive controls, respectively. The specimens were allowed to equilibrate for 2 months after irradiation to permit the natural decomposition of alkyl to allyl free radicals.[11]

Accelerated aging

The materials were then subjected to three aging conditions: no aging (control), aging in an "oxygen bomb" at 503 kPa (73 psi, 5 atm) O_2 and 70°C for 2 weeks,[9] or aging in a "nitrogen bomb" at 503 kPa N_2 and 70°C for 2 weeks. Aging in oxygen was conducted in accordance with ASTM F2003-00.[9] Aging in nitrogen was performed to control for thermal degradation in the absence of oxygen. Aging was performed concurrently in two wide-mouth 3.8-L, 304 stainless steel pressure vessels (Advantec MFS, Pleasanton CA), each fitted with a pressure gauge, vent relief valve, ball valve, and a fluoroelastomer O-ring (Fig. 1). Test samples for aging were placed in the vessel with the reference surface exposed upwards (i.e., none of the reference surfaces were faced down). The vessels were then filled and purged five times to ensure the purity of the aging environment. The pressure vessel, or "bomb," was placed in an individual air-circulating convection oven with digital (PID) temperature control (Salvis Thermocenter, Cole-Palmer Instrument Company, Vernon Hills, IL). The vessels were placed in the oven at room temperature (24° ± 1°C) and heated to the aging temperature of 70.0° ± 0.1°C at an initial heating rate of 1.0°C/min. Before conducting the aging experiments, the accuracy of the temperature control for each oven was validated to ±0.1°C by thermocouple measurements, and proof testing was conducted with the vessels to confirm that they retained 503 ± 7 kPa (73 ± 1 psi) of pressure without leakage. During the 2-week aging period, the oven door was opened briefly to confirm pressurization of the vessels, but the vessels themselves were never opened.

Small punch testing

The experimental design is summarized in Table I. One sample of each UHMWPE material, irradiation condition, and aging condition was evaluated. Thus, a total of 27 samples were used in this experiment (3 materials × 3 irradiation conditions per aging condition × 3 aging conditions per irradiation condition). From each sample, four cylindrical cores were made and miniature disk-shaped specimens, 0.5 mm in thickness and 6.4 mm in diameter, were prepared within 25 μm of the reference (superior) surface and at a subsurface depth of 1.5 to 2 mm. The subsurface location of the specimens was based on previous natural aging experiments, which showed peak oxidation occurring below the surface at a similar location.[12] Thus, eight disk specimens (four surface and four subsurface) were prepared from each sample, resulting in a total of 216 individual specimens for testing.

Miniature specimen (small punch) mechanical testing was performed in equibiaxial tension using the disk-shaped specimens, as detailed previously.[12–19] The small punch specimens were placed in a custom-built apparatus and deformed against a hemispherical punch moving at a constant displacement rate of 0.5 mm/min. The resulting load-displacement curve was characterized by an initial peak load, an ultimate load, and ultimate displacement. The work to failure, calculated as the area under the load-displacement curve, provided a measure of toughness.

Figure 1. Experimental set-up of the two oxygen pressure vessels.

Oxidation characterization

Fourier transform infrared (FTIR) spectroscopy was used to characterize the oxidation in selected samples of extruded GUR 1050 and molded 1900 to complement the mechanical testing data. Specifically, the samples included in this subset were extruded GUR 1050 specimens that were exposed to the three irradiation (air, nitrogen, none) and aging conditions (air, nitrogen, and none), and molded 1900 samples that were aged in oxygen and unaged, and those irradiated in air or not sterilized. After coring, samples were microtomed normal to the surface, and FTIR spectra (averaged from 32 independent measurements with a scan spacing of 4 cm^{-1}) were obtained in 0.2-mm increments from the reference surface to a depth of 3.4 mm. A Nicolet 840 FTIR bench unit was used with a Nic Plan microscope attachment (Spectratech, Shelton, CT). The oxidation index was calculated as the area ratio of the carbonyl peak (between 1670 and 1850 cm^{-1}) to the 1370 cm^{-1} reference peak (between 1327 and 1394 cm^{-1}) from the FTIR spectra as a function of depth from the reference surface, as described previously.[1,20,21] An average oxidation index was also calculated to correspond with the location where the small punch specimens were machined.

Statistical analyses

Statistical analyses were performed using Statview 5.0 (SAS Institute, Cary, NC) on a personal computer. Analysis

Questions? Contact FDA/CDRH/OCE/DID at CDRH-FOISTATUS@fda.hhs.gov or 301-796-8118

Records processed under FOIA Request #2014-8015; Released by CDRH on 12-8-2015

TABLE I
Summary of Experimental Design of Accelerated Aging Study to Evaluate the Effects of Resin, Processing, and Radiation Environment on Resistance to Mechanical Degradation

Material	Irradiation and Aging Conditions[a] Evaluated for each Material								
	No Irradiation			Gamma-Air (3-MRad dose)			Gamma-Nitrogen (3-MRad dose)		
Molded 1900	No aging	Aging in O_2	Aging in N_2	No aging	Aging in O_2	Aging in N_2	No aging	Aging in O_2	Aging in N_2
Molded GUR 1050	No aging	Aging in O_2	Aging in N_2	No aging	Aging in O_2	Aging in N_2	No aging	Aging in O_2	Aging in N_2
Extruded GUR 1050	No aging	Aging in O_2	Aging in N_2	No aging	Aging in O_2	Aging in N_2	No aging	Aging in O_2	Aging in N_2

A total of 27 sample conditions were evaluated (3 materials × 3 irradiation conditions × 3 aging conditions).
[a]Following ASTM F2003-00.

of variance (ANOVA) was used to examine the influence of the different material groups, irradiation conditions, aging conditions, and specimen location on the mechanical behavior of the UHMWPE characterized by the small punch test. Specifically, during the ANOVA modeling, the material groups (extruded GUR 1050, molded GUR 1050, and molded 1900), irradiation conditions (none, irradiation in air, irradiation in nitrogen), aging conditions (none, aging in oxygen, aging in nitrogen), and specimen location (surface versus subsurface) were treated as independent categorical variables, and the parameters of the small punch test (initial peak load, ultimate load, ultimate displacement, and work to failure) were treated as dependent continuous variables. The ANOVA model included first-order interaction between the categorical variables.

ANOVA was further used to examine the influence of irradiation and aging conditions on the level of oxidation of the UHMWPE. Linear regression was used to evaluate relationships between oxidation index measurements and the mechanical behavior of UHMWPE. For all statistical analyses, a p value of 0.05 was used as the basis for judging statistical significance.

RESULTS

Significant differences were observed in the mechanical behavior of the three UHMWPE materials as a function of irradiation environment, aging condition, and specimen location (Table II; Fig. 2: peak load; Fig. 3: ultimate load; Fig. 4: ultimate displacement; and Fig. 5: work to failure). The sterilization environment had a significant effect ($p < 0.05$) on the peak load, ultimate load, ultimate displacement, and work to failure of UHMWPE. The aging condition and specimen location also significantly affected ($p < 0.05$) the mechanical parameters of UHMWPE, except for the ultimate displacement. Significant interactions between the experimental conditions (irradiation, aging, location) are summarized in Table II.

Regardless of the irradiated conditions, aging in nitrogen did not have a significant effect on the mechanical behavior of the three materials as compared with the unaged controls. Conversely, however, accelerated aging in oxygen degraded the mechanical behavior of all of the UHMWPE materials we examined, no matter how they were sterilized. Degradative changes in the mechanical behavior, most evident in the ultimate load of the small punch test, were observed below the surface in the unirradiated materials that were subjected to the 2 weeks of accelerated aging in oxygen (Fig. 3).

Accelerated aging in oxygen resulted in a significant reduction of all the mechanical parameters of the small punch test with the exception of ultimate displacement. In the irradiated samples, there was a significant increase ($p < 0.05$) in the peak load, but a significant reduction ($p < 0.05$) in the ultimate displacement and work to failure during accelerated aging in oxygen. The specimen location significantly affected the mechanical properties of UHMWPE ($p < 0.05$), with the surface specimens being significantly ($p < 0.05$) more degraded (lower peak load, ultimate

TABLE II
Summary of p Values Showing Significance of the Effect of the Different Experimental Conditions and of the Interaction of These with the Material Groups on the Mechanical Parameters

Experimental Condition	Peak Load	Ultimate Load	Ultimate Displacement	Work to Failure
UHMWPE material group	<0.0001	<0.0001	<0.0001	<0.0001
Irradiation condition	<0.0001	0.0015	<0.0001	<0.0001
Aging environment	<0.0001	<0.0001	0.2384*	<0.0001
Specimen location	<0.0001	0.0003	0.3432*	0.04
Irradiation × material groups interaction	<0.0001	0.0656*	<0.0001	<0.0001
Aging × material groups interaction	0.04	<0.0001	0.0003	<0.0001
Location × material groups interaction	0.0002	0.1518*	0.7396*	0.3428*

*Not significant.

Questions? Contact FDA/CDRH/OCE/DID at CDRH-FOISTATUS@fda.hhs.gov or 301-796-8118

Records processed under FOIA Request #2014-8015; Released by CDRH on 12-8-2015

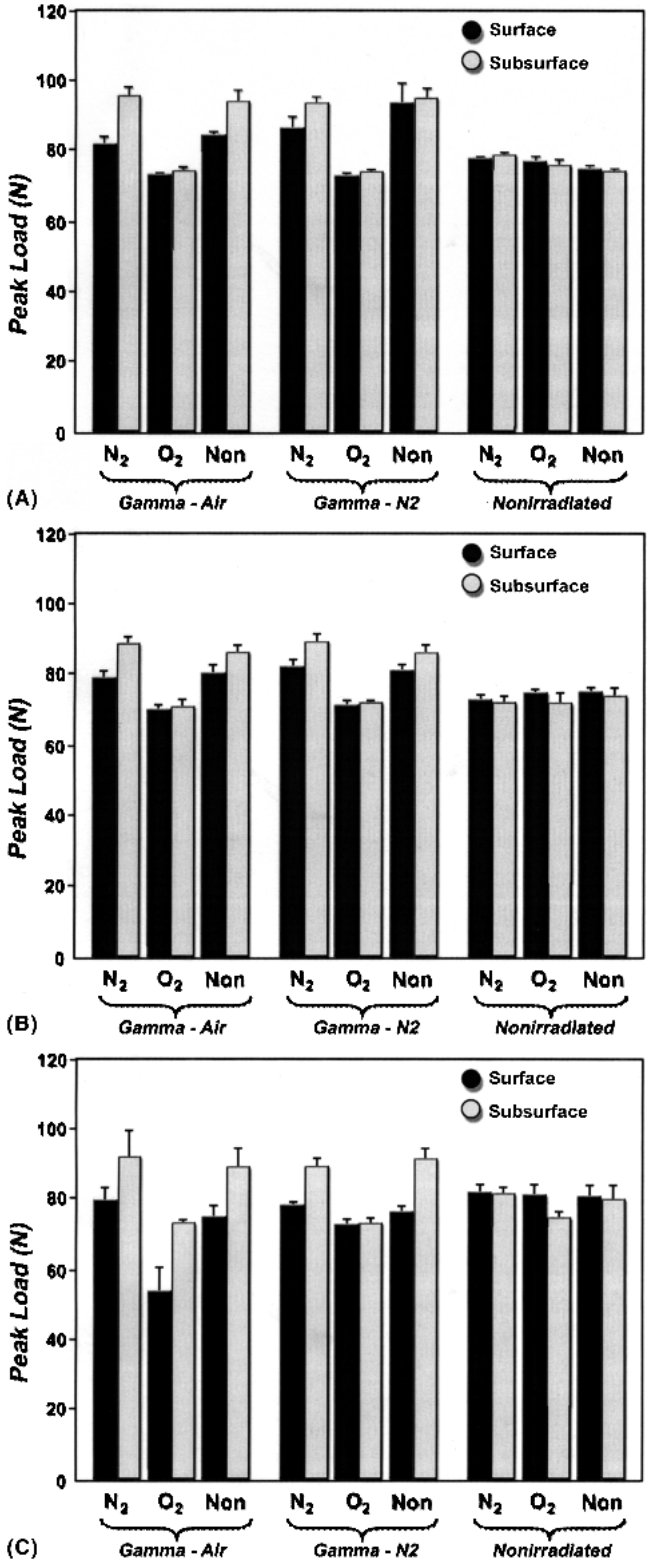

Figure 2. Effect of irradiation state, aging environment, and specimen location on the peak load magnitude for extruded 1050 (A), molded 1050 (B), and molded 1900 (C). Shown are average and standard deviation values.

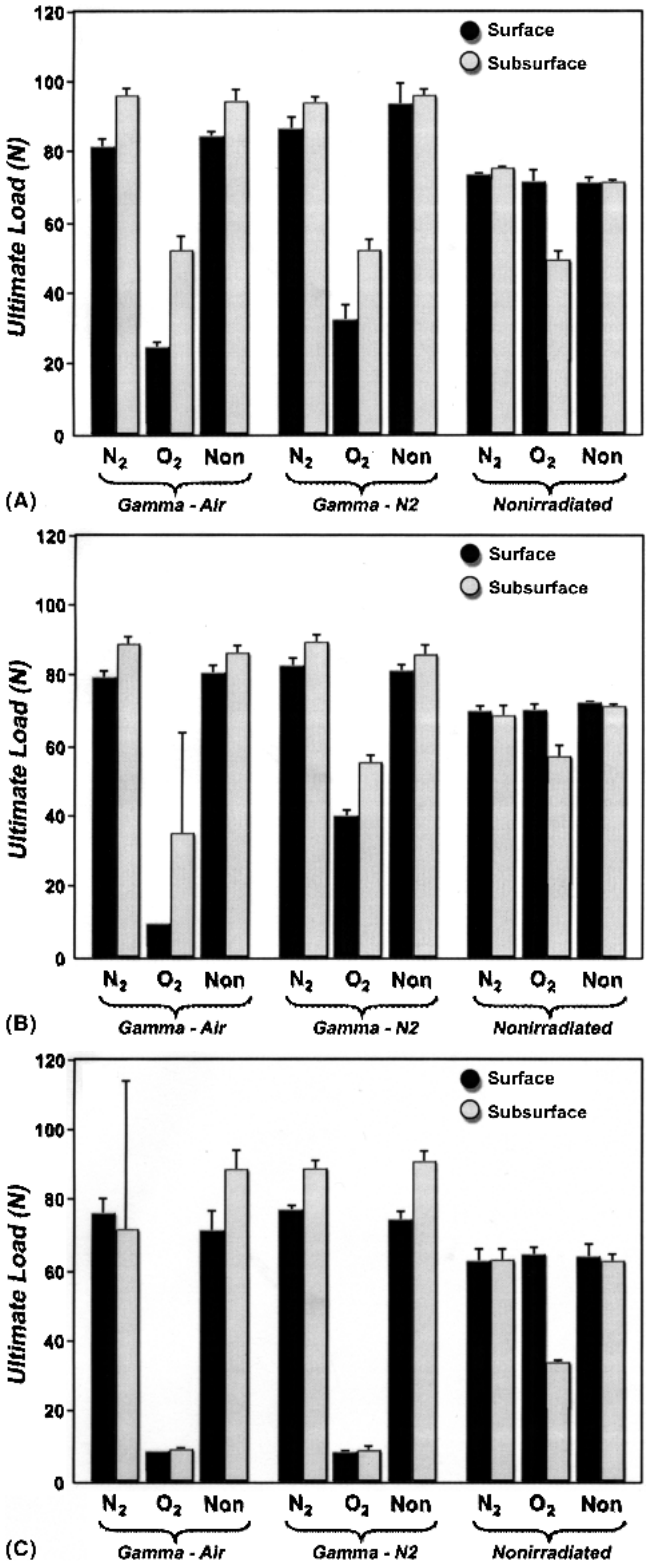

Figure 3. Effect of irradiation state, aging environment, and specimen location on the ultimate load magnitude for extruded 1050 (A), molded 1050 (B), and molded 1900 (C). Shown are average and standard deviation values. Sterilization condition and specimen location did not have a significant effect on the ultimate load of molded 1900 samples ($p > 0.05$).

Questions? Contact FDA/CDRH/OCE/DID at CDRH-FOISTATUS@fda.hhs.gov or 301-796-8118

Records processed under FOIA Request #2014-8015; Released by CDRH on 12-8-2015

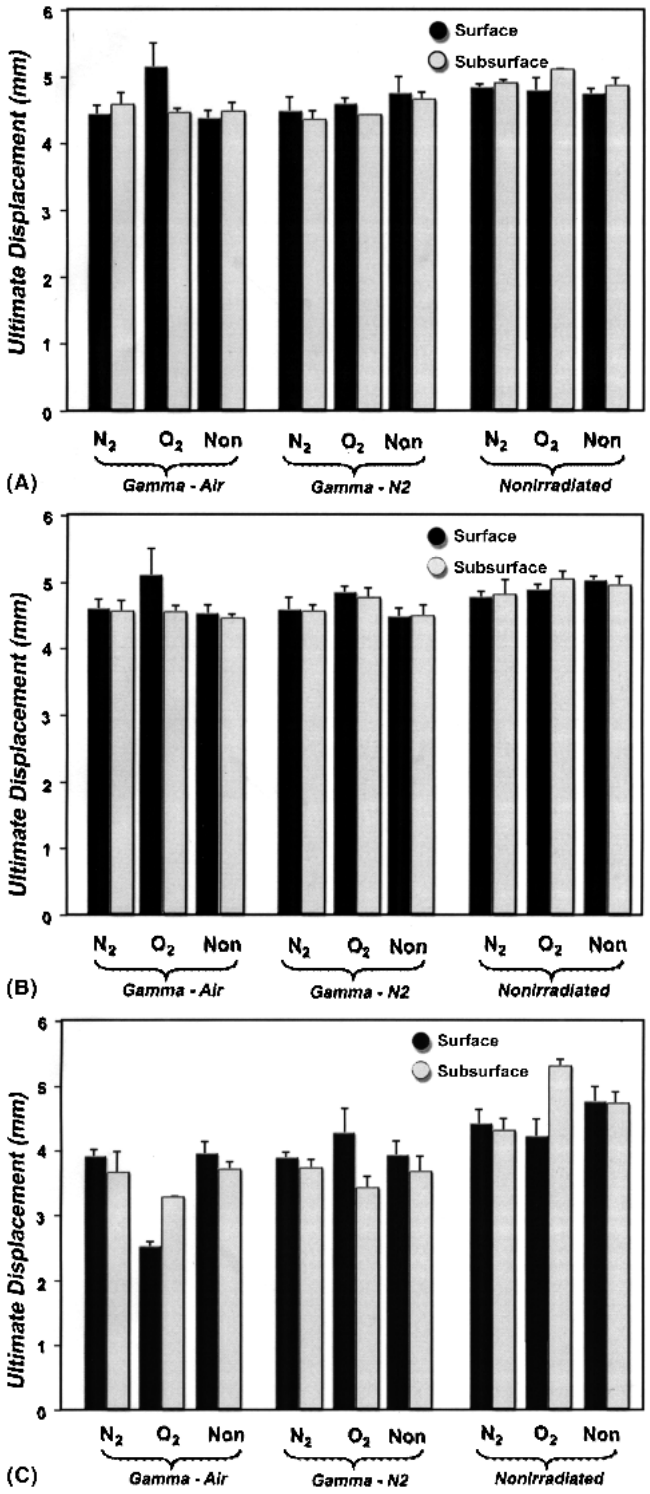

Figure 4. Effect of irradiation state, aging environment, and specimen location on the ultimate displacement magnitude for extruded 1050 (A), molded 1050 (B), and molded 1900 (C). Shown are average and standard deviation values. Specimen location did not have a significant effect on the ultimate displacement of extruded GUR 1050, or molded 1900 samples ($p > 0.05$).

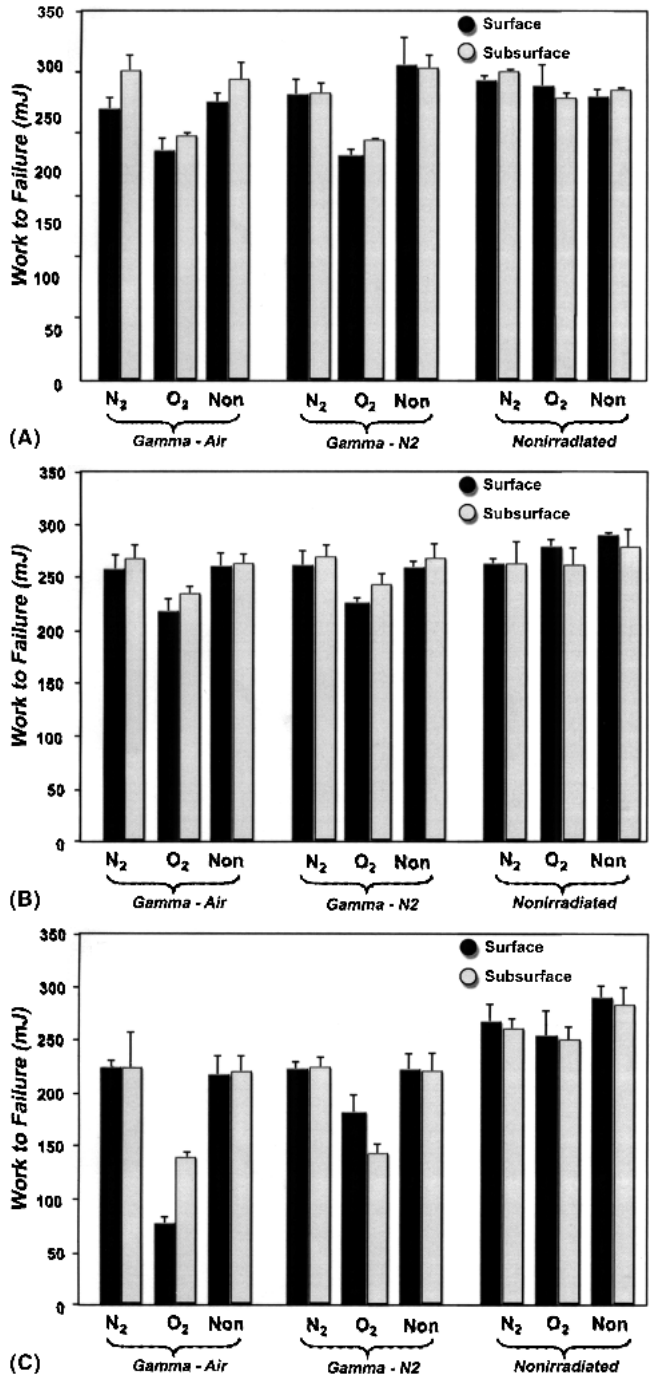

Figure 5. Effect of irradiation state, aging environment, and specimen location on the work-to-failure magnitude for extruded 1050 (A), molded 1050 (B), and molded 1900 (C). Shown are average and standard deviation values. Specimen location did not have a significant effect on the work to failure of molded GUR 1050, or molded 1900 samples ($p > 0.05$).

load, and work to failure) than the subsurface specimens.

Each of the three polyethylenes evaluated seemed to degrade according to a similar pathway after artificial aging in oxygen and gamma irradiation in air. Samples from the surface of each of the three materials

Questions? Contact FDA/CDRH/OCE/DID at CDRH-FOISTATUS@fda.hhs.gov or 301-796-8118

Records processed under FOIA Request #2014-8015; Released by CDRH on 12-8-2015

showed noticeable mechanical degradation as seen in a reduction of the materials' ability to carry load post-peak load (Fig. 6). When comparing the mechanical behavior of the molded and extruded GUR 1050, the differences in the magnitude of the peak load, ultimate displacement, and work to failure ranged from 0.2 to 13% [Figs. 2(A), 4(A), and 5(A), and Figs. 2(B), 4(B), and 5(B)]. The differences in the magnitude of the ultimate load between the molded and extruded GUR 1050 were wider, ranging from 0.6% up to 63% [Figs. 3(A) and (B)]. In contrast, the molded 1900 material seemed to degrade slightly faster than either of the two GUR 1050 materials, with differences in the magnitude of the peak load, ultimate displacement, and work to failure ranging from 0.3 to 65%, when compared with the extruded GUR 1050, and differences of 0.1 to 65%, when compared with the molded GUR 1050. In the ultimate load, the differences between the molded 1900 and either of the two GUR 1050 materials ranged from 1 to 84%. The largest differences between the molded 1900 and either of the 1050 materials always corresponded to the samples irradiated and aged in oxygen [Figs. 2(C), 3(C), 4(C), and 5(C)].

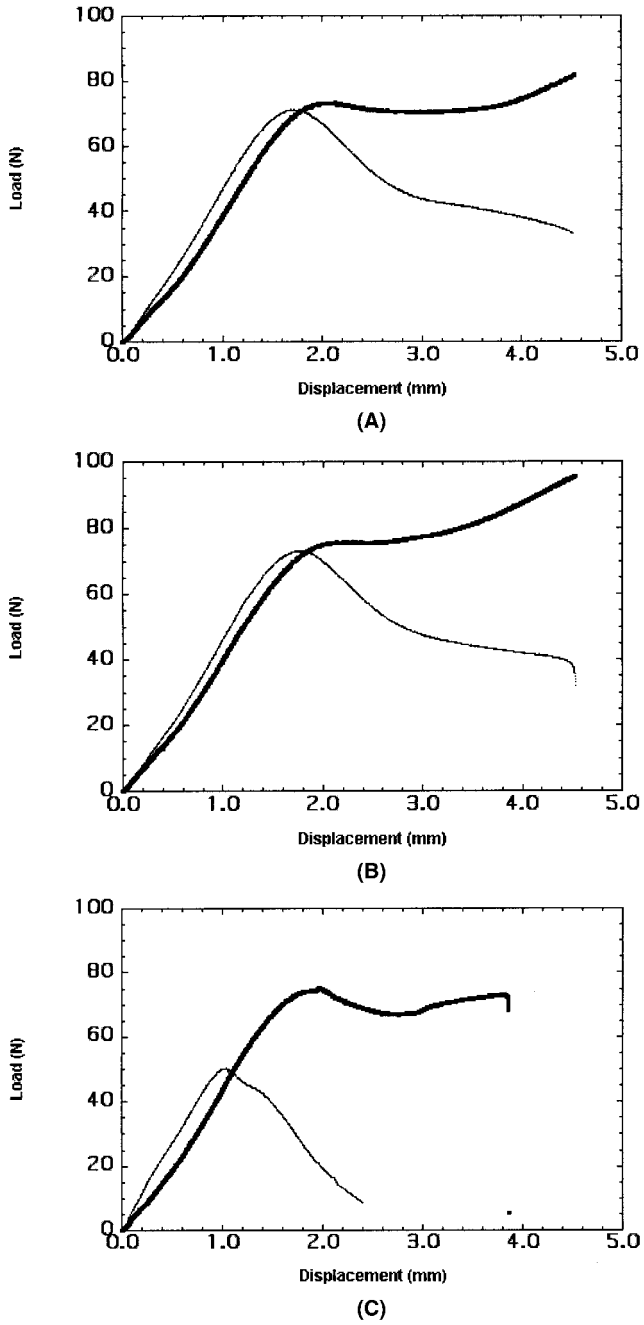

Figure 6. Effect of accelerated aging in oxygen after gamma irradiation in air for compression-molded GUR 1050 (A), extruded GUR 1050 (B), and compression-molded 1900 (C). The degradation pathway (chain scission) appears to be the same for all the materials, but the extent of degradation is more substantial for the 1900 specimens. All of the specimens were obtained from the surface location.

When comparing the oxidation levels of samples that were gamma irradiated in air and aged in oxygen, the molded 1900 samples oxidized significantly ($p < 0.05$) more than the extruded GUR 1050 samples (Table III). Regardless of the irradiation condition, the extruded GUR 1050 samples showed a significant increase ($p < 0.05$) in oxidation when aged in oxygen, and there was no significant difference between those aged in nitrogen and those that remained unaged ($p > 0.05$). Before aging, there was no evidence of carbonyl absorption in the FTIR spectra between 1650 and 1800 cm^{-1} (Fig. 7). In contrast, after 2 weeks of accelerated aging, a carbonyl absorbance peak was observed centered around 1710–1718 cm^{-1} (Fig. 7), consistent with the presence of acid and ketone species in the UHMWPE.[22] In addition, FTIR analysis confirmed that the toughness of the molded 1900 degraded to a greater extent after oxidation than the extruded GUR 1050 (Fig. 8). For example, for a unit increase in oxidation index, the work to failure of the molded 1900 decreased by 29.1 ± 3.7% as compared with a decrease of only 14.2 ± 2.2% for extruded GUR 1050.

Significant correlations between the oxidation index and the mechanical parameters for the extruded GUR 1050 and molded 1900 samples evaluated are summarized in Table IV. Interestingly, whereas all of the irradiated and aged extruded GUR 1050 specimens exhibited peak degradation within the first 1 mm of the surface, the nonirradiated but O_2-aged specimens exhibited *subsurface* peak degradation, with negligible detectable oxidation (Table III).

DISCUSSION

Overall, the compression-molded 1900 exhibited significantly less resistance to mechanical degradation than either the compression-molded or extruded 1050. However, the three materials seemed to mechanically degrade according to a similar mechanism, in that the

Questions? Contact FDA/CDRH/OCE/DID at CDRH-FOISTATUS@fda.hhs.gov or 301-796-8118

Records processed under FOIA Request #2014-8015; Released by CDRH on 12-8-2015

TABLE III
Oxidation and Small Punch Test Data (Mean ± SD)

Material	Conditions	Mean OI	Peak Load (N)	Ultimate Load (N)	Ultimate Displacement (mm)	Work to Fail (mJ)
Extruded GUR 1050	N_2-aged, γ-air, S	0.19	81.5 ± 2.4	81.4 ± 2.4	4.41 ± 0.17	256 ± 11
	N_2-aged, γ-air, SUB-S	0.05	95.9 ± 2.2	95.9 ± 2.2	4.57 ± 0.19	291 ± 16
	N_2-aged, γ-N_2, S	0.07	86.2 ± 3.2	86.2 ± 3.2	4.48 ± 0.20	268 ± 17
	N_2-aged, γ-N_2, SUB-S	0.05	93.8 ± 1.6	93.8 ± 1.6	4.35 ± 0.14	270 ± 11
	N_2-aged, NS, S	0.00	77.7 ± 0.4	73.2 ± 0.4	4.83 ± 0.05	283 ± 5
	N_2-aged, NS, SUB-S	0.00	78.6 ± 0.8	74.8 ± 0.8	4.91 ± 0.05	291 ± 3
	O_2 aged, γ-air, S	1.29	73.2 ± 0.3	25.1 ± 1.6	5.15 ± 0.36	217 ± 12
	O_2 aged, γ-air, SUB-S	1.30	74.5 ± 1.0	51.9 ± 4.2	4.45 ± 0.07	230 ± 3
	O_2 aged, γ-N_2, S	0.86	72.8 ± 0.8	32.5 ± 4.0	4.58 ± 0.09	212 ± 6
	O_2 aged, γ-N_2, SUB-S	0.91	74.0 ± 0.7	52.1 ± 3.1	4.42 ± 0.02	226 ± 2
	O_2 aged, NS, S	0.11	76.8 ± 1.7	71.1 ± 3.7	4.78 ± 0.21	277 ± 21
	O_2 aged, NS, SUB-S	0.00	75.9 ± 1.7	49.2 ± 2.7	5.08 ± 0.03	268 ± 4
	Unaged, γ-air, S	0.37	84.3 ± 1.5	84.2 ± 1.5	4.39 ± 0.11	263 ± 8
	Unaged, γ-air, SUB-S	0.20	94.3 ± 3.1	94.2 ± 3.1	4.48 ± 0.14	284 ± 15
	Unaged, γ-N_2, S	0.29	93.5 ± 5.6	93.4 ± 5.6	4.74 ± 0.26	299 ± 25
	Unaged, γ-N_2, SUB-S	0.01	95.3 ± 2.3	95.3 ± 2.3	4.65 ± 0.11	294 ± 12
	Unaged, NS, S	0.00	74.9 ± 1.0	70.6 ± 1.7	4.74 ± 0.07	268 ± 7
	Unaged, NS, SUB-S	0.00	74.4 ± 0.5	71.3 ± 0.5	4.87 ± 0.12	273 ± 3
Molded 1900	O_2 aged, γ-air, S	2.17	53.7 ± 6.6	8.8 ± 0.0	2.49 ± 0.09	76 ± 7
	O_2 aged, γ-air, SUB-S	1.97	72.7 ± 1.1	9.2 ± 0.6	3.27 ± 0.03	138.5 ± 5
	O_2 aged, NS, S	0.00	80.8 ± 2.8	63.6 ± 2.4	4.18 ± 0.03	251.4 ± 25
	O_2 aged, NS, SUB-S	0.00	74.5 ± 1.4	33.3 ± 0.7	5.25 ± 0.12	248.4 ± 12
	Unaged, γ-Air, S	0.43	74.8 ± 2.8	70.8 ± 6.0	3.92 ± 0.20	215.7 ± 20
	Unaged, γ-Air, SUB-S	0.23	88.9 ± 5.2	88.5 ± 5.4	3.69 ± 0.13	219 ± 16
	Unaged, NS, S	0.03	80.4 ± 3.1	63.4 ± 3.6	4.72 ± 0.27	287 ± 12
	Unaged, NS, SUB-S	0.00	79.6 ± 3.9	62.1 ± 2.1	4.68 ± 0.20	280.2 ± 18

OI, oxidation index; NS, not sterilized; S, surface; SUB-S, sub-surface.

initial ability of the materials to exhibit post-yield strain hardening was significantly compromised by degradation. Evaluation of UHMWPE oxidation resistance is complicated by possible interaction between the resin and the processing method. However, the present study was limited only to evaluation of 1900 resin machined from a bulk compression-molded slab. Further research will be needed to determine the sensitivity of extruded and direct compression-molded 1900 to mechanical degradation. However, the clinical record of components manufactured using Montell 1900 and sterilized in air is excellent, suggesting that results of artificial aging of any polyethylene should ultimately be compared with results of natural (shelf) aged components.

Artificial aging methods have been developed to evaluate the oxidative stability of UHMWPE.[9] How-

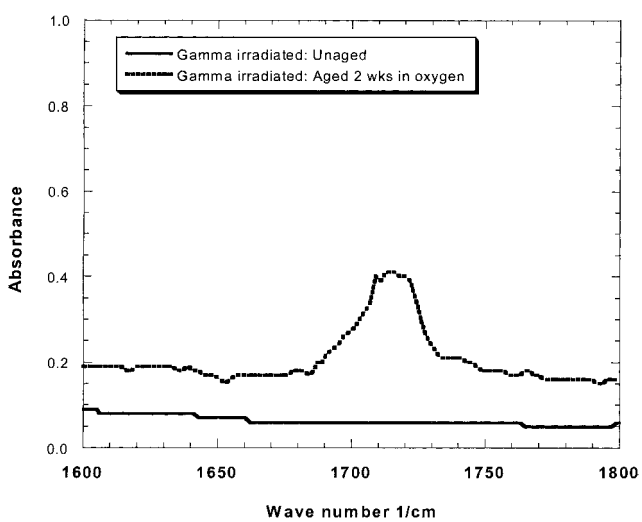

Figure 7. FTIR spectra for gamma-irradiated extruded GUR 1050 after 2 weeks of aging in oxygen and unaged.

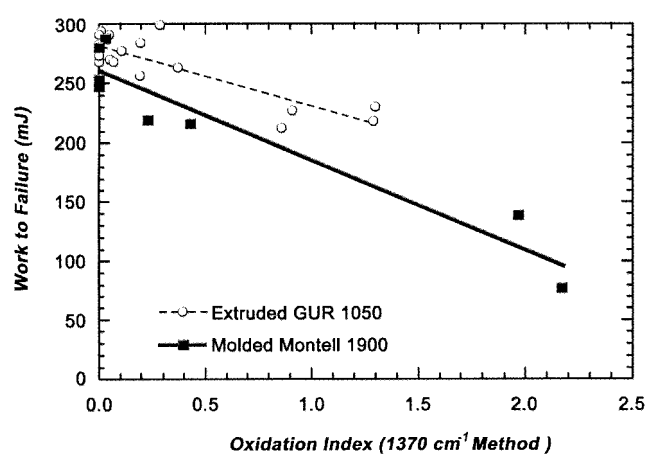

Figure 8. Work to failure versus oxidation index for the extruded GUR 1050 ($r^2 = 0.72$, $p < 0.05$) samples evaluated with FTIR.

Questions? Contact FDA/CDRH/OCE/DID at CDRH-FOISTATUS@fda.hhs.gov or 301-796-8118

Records processed under FOIA Request #2014-8015; Released by CDRH on 12-8-2015

TABLE IV
Significant Correlations Between the Oxidation Index and Mechanical Parameters for the Extruded GUR 1050 and Molded 1900 Samples Evaluated

Material	Peak Load	Ultimate Load	Ultimate Displacement	Work to Failure
Extruded GUR 1050	NS	$r^2 = 0.51$	NS	$r^2 = 0.72$
Molded 1900	$r^2 = 0.59$	$r^2 = 0.64$	$r^2 = 0.75$	$r^2 = 0.91$

NS, not significant.

ever, current accelerated aging methods have been validated by comparing the density, oxidation, and mechanical behavior of artificially aged components with those that were gamma irradiated in air and subjected to long-term shelf aging. Because of the recent shift in sterilization practice by orthopedic manufacturers in the United states to a reduced oxygen environment or sterilization without ionizing radiation, alternative sterilization methods, such as gamma sterilization in nitrogen, have been clinically introduced.[23] As recent as 1998, four of the nine major U. S. orthopedic manufacturers were utilizing gamma sterilization in nitrogen as their sterilization practice.[1] Despite the shift in sterilization method in the manufacturing environment, it still remains unclear to what extent the current accelerated aging protocols used in the laboratory settings replicate the natural shelf aging behavior of UHMWPE sterilized in any environment other than air. Recent experiments conducted on gamma-nitrogen-sterilized components have suggested that UHMWPE exhibits minimal oxidation or degradation of mechanical behavior for up to 10 years.[24]

The results of this study revealed that gamma irradiation in nitrogen had a significant (and similar) effect to that of gamma sterilization in air on the mechanical degradation of all three material groups. Specifically, there was a more noticeable, significant difference in the post-yield strain hardening of molded 1900 specimens when comparing those that underwent gamma sterilization in air with those sterilized in nitrogen. In addition, our study showed that all the UHMWPE samples that were gamma irradiated in nitrogen and subsequently artificially aged in nitrogen exhibited no significant changes in mechanical behavior, analogous to natural aging behavior of nitrogen-sterilized components.[24]

In addition, in the present study, we investigated a new accelerated aging technique in a nitrogen environment to evaluate the stability of extruded- and compression-molded UHMWPE after gamma sterilization in air or nitrogen. In both irradiation conditions, artifical aging in oxygen had similar effects on the degradation of all the material groups evaluated, but aging in nitrogen had no significant effect on their mechanical behavior. Although contemporary aging techniques are an effective tool for accelerating the oxidation of components that were gamma sterilized in air, the results of the present study suggest that the application of such methods to evaluate alternative sterilization techniques may result in excessively degraded, and hence clinically irrelevant, results. Further research, including the evaluation of free-radical concentrations during natural and accelerated aging in nitrogen environments, will be needed to fully validate the nitrogen aging protocols used in the present study. However, an accelerated model for natural aging of nitrogen-sterilized UHMWPE will be a useful tool for exploring the long-term stability of UHMWPE in simulated *in vivo* environments.

Clough and Gillen[10] previously examined the stability of an unspecified grade of polyethylene after aging in air or nitrogen environments, after irradiation in air or nitrogen. Their thermal aging protocol called for an environment at 80°C for 83 days. Elongation data from Clough and Gillen's study, normalized with respect to virgin control polyethylene, is compared with our data for molded 1050 and 1900 UHMWPE in Figure 9. Gamma irradiation in air resulted in a decrease in normalized ductility for both Clough and Gillen's polyethylene, as well as for the molded 1900 samples in our study, irrespective of the aging environment (Fig. 9), with the most noticeable effect seen on the samples aged in air. However, the molded 1050 samples in our study only showed a noticeable decrease in normalized ductility after gamma irradiation in air when aged in a nitrogen environment or when

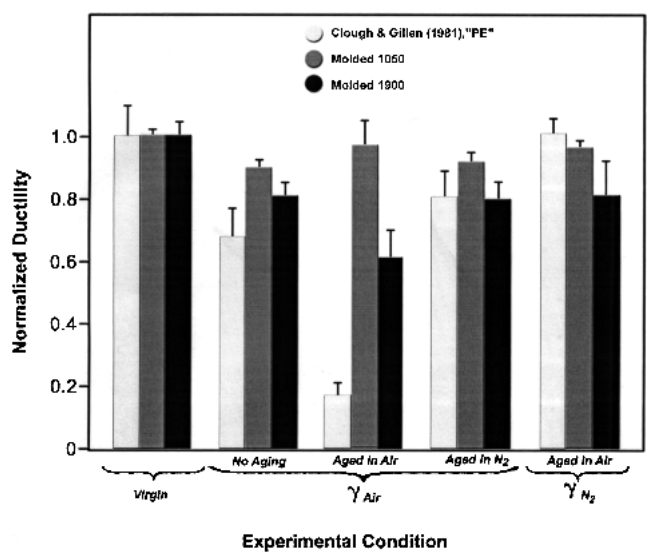

Figure 9. Elongation data from the study of Clough and Gillen,[10] normalized with respect to virgin control polyethylene, is compared with our data for molded 1050 and 1900 UHMWPE for the similar irradiation and aging environments. Note that Clough and Gillen's thermal aging protocol called for an environment at 80°C for 83 days.

Questions? Contact FDA/CDRH/OCE/DID at CDRH-FOISTATUS@fda.hhs.gov or 301-796-8118

Records processed under FOIA Request #2014-8015; Released by CDRH on 12-8-2015

left unaged (Fig. 9). After gamma irradiation in nitrogen and aging in air, Clough and Gillen's polyethylene did not show a decrease in ductility. Conversely, under similar experimental conditions, the molded 1900 samples in our study did show a noticeable decrease in ductility comparable to that of samples gamma irradiated in air, whereas the molded 1050 samples showed only a slight decrease in ductility. Under our experimental conditions, the ductility of both the molded 1050 and 1900 was very similar after aging in nitrogen as compared with the unaged specimens after gamma irradiation in air, as well as with those samples aged in air, after gamma irradiation in nitrogen.

In contrast to what has been reported in the literature for shelf-aged components after gamma sterilization in air,[2–7] our study showed that under conditions of accelerated aging in oxygen, samples of molded 1900 oxidized significantly more than samples from extruded 1050. Under our experimental conditions, the samples obtained from molded 1900 did not seem to be more oxidation resistant than those from GUR 1050. Despite this finding, we cannot conclude if the processing route alone of the 1900 samples had a direct effect on their oxidation resistance because we did not evaluate 1900 resin processed with other methods, such as extrusion.[3]

The results of this study also suggest that measurements of physical and chemical properties, such as density or FTIR, may not accurately characterize completely the extent of mechanical degradation in UHMWPE, particularly when different resins are being compared. A recent article by Currier et al.[6] also showed a similar lack of correspondence between an indirect quantity (FTIR signal) and mechanical performance, reinforcing the concept that tests for mechanical quality should be performed mechanically. Therefore, using FTIR along with mechanical evaluation of specimens provides an improved and complementary evaluation matrix to better understand the effects of changes in physical and mechanical properties of different resins of UHMWPE.

References

1. Kurtz SM, Muratoglu OK, Evans M, Edidin AA. Advances in the processing, sterilization, and crosslinking of ultra-high molecular weight polyethylene for total joint arthroplasty. Biomaterials 1999;20:1659–1688.
2. Furman BD, Ritter MA, Perone JB, Furman GL, Li S. Effect of resin type and manufacturing method on UHMWPE oxidation and quality at long aging times and long implant times. Transactions of the 43rd Orthopedic Research Society, San Francisco, CA; 1997. p 92.
3. Gillis AM, Furman BD, Li S. Influence of ultra high molecular weight polyethylene resin type and manufacturing method on real time oxidation. Transactions of the 44th Orthopedic Research Society, New Orleans, LA; 1998. p 360.
4. Walsh HA, Gillis AM, Furman BD, Li S. Determination of the role of resin type and manufacturing method in the oxidation resistance of directly molded 1900 UHMWPE. Transactions of the 6th World Biomaterials Congress, Kamuela, Hawaii, 2000. p 1120.
5. Gsell RA, Taylor GK, Lin ST. Shelf aging of net shape compression molded 1900H ultra-high molecular weight polyethylene (UHMWPE) components. Transactions of the 44th Orthopedic Research Society, New Orleans, LA; 1998. p 364.
6. Currier BH, Currier JH, Collier JP, Mayor MB. Effect of fabrication method and resin type on performance of tibial bearings. J Biomed Mater Res 2000;53:143–151.
7. Won CH, Rohatgi S, Kraay MJ, Goldberg VM, Rimnac CM. Effect of resin type and manufacturing method on wear of polyethylene tibial components. Clin Orthop 2000;376:161–171.
8. Grood ES, Shastri R, Hopson CN. Analysis of retrieved implants: Crystallinity changes in ultrahigh molecular weight polyethylene. J Biomed Mater Res 1982;16:399–405.
9. ASTM F 2003-00. Standard guide for accelerated aging of ultra high molecular weight polyethylene. West Conshohocken, PA: American Society for Testing and Materials; 2000.
10. Clough RL, Gillen KT. Radiation-thermal degradation of PE and PVC: Mechanism of synergism and dose rate effects. Radiat Phys Chem 1981;18:661–669.
11. Jahan MS, Wang C. Combined chemical and mechanical effects on free radicals in UHMWPE joints during implantation. J Biomed Mater Res 1991;25:1005–1017.
12. Edidin AA, Jewett CW, Kwarteng K, Kalinowski A, Kurtz SM. Degradation of mechanical behavior in UHMWPE after natural and accelerated aging. Biomaterials 2000;21:1451–1460.
13. Edidin AA, Pruitt L, Jewett CW, Crane DJ, Roberts D, Kurtz SM. Plasticity-induced damage layer is a precursor to wear in radiation-cross-linked UHMWPE acetabular components for total hip replacement: Ultra-high-molecular-weight polyethylene. J Arthroplasty 1999;14:616–627.
14. Edidin AA, Kurtz SM. The influence of mechanical behavior on the wear of four clinically relevant polymeric biomaterials in a hip simulator. J Arthroplasty 2000;15:321–331.
15. Edidin AA, Kurtz SM. Development and validation of the small punch test for UHMWPE used in total joint replacements. In: Katsube N, Soboyejo W, Sacks M, editors. Functional biomaterials. Winterthur, Switzerland: Trans Tech Publications; 2001. p 1–40.
16. Kurtz SM, Foulds JR, Jewett CW, Srivastav S, Edidin AA. Validation of a small punch testing technique to characterize the mechanical behavior of ultra-high molecular weight polyethylene. Biomaterials 1997;18:1659–1663.
17. Kurtz SM, Jewett CW, Foulds JR, Edidin AA. A miniature-specimen mechanical testing technique scaled to the articulating surface of polyethylene components for total joint arthroplasty. J Biomed Mater Res 1999;48:75–81.
18. Kurtz SM, Pruitt LA, Jewett CW, Foulds JR, Edidin AA. Radiation and peroxide crosslinking promote strain hardening behavior and molecular alignment in UHMWPE during multiaxial loading conditions. Biomaterials 1999;20:1449–1462.
19. Kurtz SM, Rimnac CM, Pruitt L, Jewett CW, Goldberg V, Edidin AA. The relationship between the clinical performance and large deformation mechanical behavior of retrieved UHMWPE tibial inserts. Biomaterials 2000;21:283–291.

Questions? Contact FDA/CDRH/OCE/DID at CDRH-FOISTATUS@fda.hhs.gov or 301-796-8118

Records processed under FOIA Request #2014-8015; Released by CDRH on 12-8-2015

20. Kurtz SM, Muratoglu OK, Buchanan F, Currier B, Gsell R, Greer K, Gualtieri G, Johnson R, Schaffner S, Sevo S, Spiegelberg S, Shen FW, Yau SS. Interlaboratory reproducibility of standard accelerated aging methods for oxidation of UHMWPE. Biomaterials 2001;22:1731–1737.
21. Kurtz SM, Muratoglu OK, Buchanan F, Currier B, Gsell R, Shen FW, Yau SS. Interlaboratory studies to determine optimal analytical methods for measuring the oxidation index of UHMWPE. Biomaterials 2001;22:2875–2881.
22. Costa L, Brach de Prever EM. UHMWPE for arthroplasty. Turin, Italy: Edizioni Minerva Medica; 2000.
23. Premnath V, Harris WH, Jasty M, Merrill EW. Gamma sterilization of UHMWPE articular implants: An analysis of the oxidation problem. Biomaterials 1996;17:1741–1753.
24. Edidin AA, Muth J, Spiegelberg S, Schaffner SR. Sterilization of UHMWPE in nitrogen prevents oxidative degradation for more than ten years. Transactions of the 46th Orthopedic Research Society, Orlando, FL; 2000. p 1.

Questions? Contact FDA/CDRH/OCE/DID at CDRH-FOISTATUS@fda.hhs.gov or 301-796-8118

Records processed under FOIA Request #2014-8015; Released by CDRH on 12-8-2015

Available online at www.sciencedirect.com
SCIENCE DIRECT®
ELSEVIER
Biomaterials 27 (2006) 1550–1557
Biomaterials
www.elsevier.com/locate/biomaterials

Fatigue crack propagation resistance of virgin and highly crosslinked, thermally treated ultra-high molecular weight polyethylene

Sara J. Gencur[a,*], Clare M. Rimnac[a], Steven M. Kurtz[b,c]

[a]Musculoskeletal Mechanics and Materials Laboratories, Departments of Mechanical and Aerospace Engineering and Orthopaedics, Case Western Reserve University, 10900 Euclid Ave., Cleveland, OH 44106-7222, USA
[b]Exponent, Inc., 3401 Market St., Suite 300, Philadelphia, PA, USA
[c]Implant Research Center, Drexel University, 32nd and Market St., Philadelphia, PA, USA

Received 8 March 2005; accepted 23 August 2005
Available online 21 November 2005

Abstract

To prolong the life of total joint replacements, highly crosslinked ultra-high molecular weight polyethylenes (UHMWPEs) have been introduced to improve the wear resistance of the articulating surfaces. However, there are concerns regarding the loss of ductility and potential loss in fatigue crack propagation (FCP) resistance. The objective of this study was to evaluate the effects of gamma radiation-induced crosslinking with two different post-irradiation thermal treatments on the FCP resistance of UHMWPE. Two highly crosslinked and one virgin UHMWPE treatment groups (ram-extruded, orthopedic grade, GUR 1050) were examined. For the two highly crosslinked treatment groups, UHMWPE rods were exposed to 100 kGy and then underwent post-irradiation thermal processing either above the melt temperature or below the melt temperature (2 h—150 °C, 110 °C). Compact tension specimens were cyclically loaded to failure and the fatigue crack growth rate, da/dN, vs. cyclic stress intensity factor, ΔK, behavior was determined and compared between groups. Scanning electron microscopy was used to examine fracture surface characteristics.

Crosslinking was found to decrease the ability of UHMWPE to resist crack inception and propagation under cyclic loading. The findings also suggested that annealing as a post-irradiation treatment may be somewhat less detrimental to FCP resistance of UHMWPE than remelting. Scanning electron microscopy examination of the fracture surfaces demonstrated that the virgin treatment group failed in a more ductile manner than the two highly crosslinked treatment groups.
© 2005 Published by Elsevier Ltd.

Keywords: Polyethylene; UHMWPE; Fatigue; Crosslinking; Annealing; Remelting

1. Introduction

Ultra-high molecular weight polyethylene (UHMWPE) has been used successfully in orthopedic total joint replacements for four decades [1]. However, concerns regarding wear and oxidative degradation of UHMWPE joint components have led to the development and use of radiation crosslinked and thermally treated UHMWPE in both total hip replacements and total knee replacements [2].

In total joint replacements, "conventional" UHMWPE materials have been defined as UHMWPE that is sterilized by any method, other than ionizing radiation (i.e., uncrosslinked) or following sterilization with up to 40 kGy of gamma radiation (i.e., lightly crosslinked) [3]. "Highly crosslinked" UHMWPEs are those that are manufactured by exposing uncrosslinked UHMWPE to an elevated dose of ionizing radiation (e.g., >40 kGy [1] of gamma radiation), and then typically subjected to post-irradiation thermal processing [4,5]. Thermal processing is conducted on the irradiated UHMWPE to reduce residual free radicals and, thus, minimize the potential for post-irradiation oxidation [4,6]. Post-irradiation thermal processing that occurs below the melt transition is referred to as annealing and thermal processing that occurs above the

*Corresponding author. Tel.: +1 716 456 2326; fax: +1 716 456 2440.
E-mail addresses: sgencur@yahoo.com, sig16@po.cwru.edu (S.J. Gencur).

0142-9612/$ - see front matter © 2005 Published by Elsevier Ltd.
doi:10.1016/j.biomaterials.2005.09.010

Questions? Contact FDA/CDRH/OCE/DID at CDRH-FOISTATUS@fda.hhs.gov or 301-796-8118

Records processed under FOIA Request #2014-8015; Released by CDRH on 12-8-2015

melt transition is referred to as remelting [6]. Post-irradiation thermal processing, regardless of temperature, typically occurs at ambient pressure.

Due to the cyclic nature of the loads applied to joint replacements, the fatigue crack propagation (FCP) resistance of UHMWPE materials is of interest. It has been shown that increasing the radiation dose used for cross-linking causes a decrease in the overall ductility of UHMWPE and also a decrease in FCP resistance [7,8]. In addition, post-irradiation thermal treatments above and below the melting temperature, used primarily to quench residual free radicals to reduce oxidation, have been shown to alter the monotonic mechanical properties of UHMWPE [3].

The objective of this study was to evaluate the effects of gamma radiation-induced crosslinking with two different post-irradiation thermal treatments on the FCP resistance of UHMWPE. In addition, the effect of specimen thickness on FCP behavior was also examined.

2. Materials and methods

Three treatment groups, two highly crosslinked and one virgin (as-received), of ram-extruded, orthopedic grade, GUR 1050 UHMWPE (Ticona, Bayport TX) were examined in this study. For the two highly crosslinked treatment groups, UHMWPE rods were exposed to 100 kGy. After irradiation, the two highly crosslinked treatment groups underwent post-irradiation thermal processing either above the melt temperature (remelted, 150 °C) or below the melt temperature (annealed, 110 °C). To accomplish the post-irradiation thermal processing, the highly crosslinked materials were placed in an air-circulating oven and heated until the center of each stock rod reached the required temperature and were held at that temperature for 2 h. The materials were then cooled to room temperature over a 24-h period. Selected material and monotonic properties of each treatment group have been previously reported (Table 1).

Circular compact tension specimens were machined from transverse cross-sections of the rod stock from all three treatment groups (Fig. 1). Specimen dimensions were selected with guidance from ASTM E 399 [9] and ASTM E 647 [10]. To examine the effect of specimen thickness on FCP behavior, specimens were made with two thicknesses: 10 mm ($n = 5$/material) and 20 mm ($n = 2$/material) (Fig. 1). After notching, specimen surfaces were polished to better visualize crack growth. Immediately prior to testing, the specimens were thawed and razor sharpened at room temperature. A 3 mm long extension of the notch was introduced by slowly and manually pressing a fresh razor blade into the notch of each specimen such that the initial ratio of crack length, a, to width, W, was 0.3 or 0.39 [10].

The compact tension specimens were tested to failure with guidance from ASTM E 647 [10]. Testing was conducted on a servo-hydraulic, closed-loop testing machine (Instron 8874, Canton, MA). Specimens were tested with an R-ratio of 0.1, a sinusoidal waveform, and a frequency of 3 Hz. Specimens were air-cooled during testing to minimize hysteretic heating. Tests were performed at room temperature (22–24 °C).

Fatigue crack growth was monitored with a traveling microscope (10 × objective-Gaertner, Skokie, IL) and the total crack length (a) was recorded (±0.01 mm) approximately every 0.2 mm of growth (0.1 mm when the number of cycles <100). To reduce the influence of the razor-sharpened notch on the crack growth behavior, the first data point was not taken until 0.2 mm of crack growth occurred (>0.2 × notch root radius [11]). The number of cycles (N) for each growth period was also recorded. Specimens were cycled until catastrophic failure occurred or until the specimen deformed such that the crack tip moved past the range of view of the microscope. The crack growth rate (da/dN) was calculated using the secant method [10].

The cyclic stress intensity (ΔK) was calculated according to [10]:

$$\Delta K = \left(\frac{\Delta P}{B\sqrt{W}}\right) f(a/W), \tag{1}$$

where ΔP is the load range, B the specimen thickness, W the specimen width, and $f(a/W)$ is a geometrical correction factor for a circular compact tension specimen.

The cyclic stress intensity (ΔK) and the average crack growth rate (da/dN) for each specimen were plotted. Linear regression analysis was performed on a portion of the Paris region ($10^{-4} < da/dN < 10^{-2}$ mm/cycle) of each resulting curve. The slope and intercept obtained from the linear regression analysis were used to determine the exponent, m, and the coefficient, C, of the Paris relationship for each specimen [12]:

$$da/dN = C(\Delta K)^m. \tag{2}$$

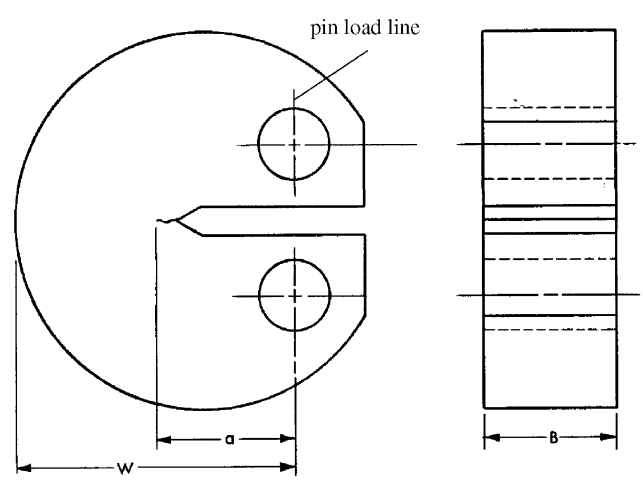

Fig. 1. Circular compact tension specimen used in fatigue crack propagation testing. Dimensions were: $W = 40$ mm, $B = 10$ and 20 mm, $a_n = 12$ and 15.7 mm.

Table 1
Selected material and tensile properties for the three UHMWPE treatment groups (mean ± std. dev., $n = 15$/treatment group)

	Virgin	100 kGy Annealed	100 kGy Remelted
Crystallinity (%)[a]	50.4 ± 3.3	60.8 ± 0.9	45.7 ± 0.3
True ultimate stress (MPa)[a]	238 ± 53	163 ± 12	133 ± 14
True ultimate strain (%)[a]	1.65 ± 0.07	1.25 ± 0.03	1.21 ± .03
True yield strength (MPa)[a]	26.9 ± 0.4	27.94 ± 0.1	24.47 ± 0.24
K_c (MPa $\sqrt{m}$)[b]	4.0 ± 0.5	2.8 ± 0.4	3.0 ± 0.6

Data reported previously [a][3], [b][22].
Note that K_c is an estimated fracture toughness.

Questions? Contact FDA/CDRH/OCE/DID at CDRH-FOISTATUS@fda.hhs.gov or 301-796-8118

Records processed under FOIA Request #2014-8015; Released by CDRH on 12-8-2015

One way analysis of variance (ANOVA) [13] was used to compare the Paris exponent and coefficient of specimens within a treatment group. Data for each treatment group was pooled and ANOVA was conducted between treatment groups for each of the two specimen thicknesses. A value of $p<0.05$ was taken as significant.

The cyclic stress intensity required to produce a crack growth rate of 10^{-6} mm/cycle was recorded as $\Delta K_{\text{inception}}$, when available [7,14,15]. Otherwise, an estimate of $\Delta K_{\text{inception}}$ was made by visual inspection of the da/dN vs. ΔK behavior for each treatment group.

The fracture surface features of each treatment group were examined and compared using scanning electron microscopy. One representative fracture surface from each of the three treatment groups were sputter coated with palladium or gold. Fractographs at $da/dN = 10^{-5}$ and 10^{-3} mm/cycle were taken at low and high magnifications. Fractographs were examined for morphological evidence of differences in fracture mechanisms between the crack growth regions, and in differences between the three treatment groups.

The range of crack growth for which linear elastic fracture mechanics (LEFM) applied was determined for each specimen using [11]:

$$\bar{a}, (W-\bar{a}) \geqslant \frac{4}{\pi}\left(\frac{K_{\max}}{\sigma_y}\right)^2, \tag{3}$$

where $\bar{a}$ is the average crack length, W the specimen width, $K_{\max}$ the maximum calculated stress intensity, and σ_y the yield stress of the material (Fig. 1, Table 1). The maximum stress intensity ($K_{\max}$) was calculated using Eq. (1) by substituting $K_{\max}$ for ΔK and $P_{\max}$ for ΔP. Analysis of the effectiveness of the two specimen geometries for maintaining plane strain loading conditions was also conducted using [11]:

$$B, \bar{a}, (W-\bar{a}) \geqslant 2.5\left(\frac{K_{\max}}{\sigma_y}\right)^2, \tag{4}$$

where B is the specimen thickness. The maximum ΔK (boundary ΔK) and corresponding crack growth rate (boundary da/dN) for which a specimen fulfilled LEFM and plane strain conditions were calculated for each specimen in all material treatment groups.

3. Results

Statistical comparisons of the exponent (m) and coefficient (C) between specimens in a treatment group demonstrated significant differences in some cases and not in others. The virgin treatment group displayed more variability in da/dN vs. ΔK between individual specimens when compared to the highly crosslinked specimens. However, the majority of specimens within a given treatment group were not significantly different from each other so the data from all specimens in a given treatment group for a given specimen thickness were pooled for comparisons with respect to thickness within a treatment group (Table 2, Figs. 2a–c).

Specimen thickness had a significant effect on the FCP resistance for only the annealed UHMWPE (Table 3, Figs. 2a–c). Due to the limited amount of data below 10^{-6} mm/cycle in each treatment group, a single $\Delta K_{\text{inception}}$ was estimated for each treatment group, independent of specimen thickness (Table 2). Because the differences in da/dN vs. ΔK with respect to thickness within a treatment group were small (even when statistically significant), the data for the two thicknesses within each treatment group were pooled for subsequent comparisons between materials.

The highly crosslinked treatment groups demonstrated an overall reduced FCP resistance when compared to the virgin treatment group (Fig. 3). The FCP resistance of the annealed UHMWPE was not significantly different from the remelted UHMWPE (Table 2). The virgin treatment group had the largest estimated $\Delta K_{\text{inception}}$ (2.0 MPa $\sqrt{\text{m}}$), followed by the annealed (1.1 MPa $\sqrt{\text{m}}$), and the remelted (0.9 MPa $\sqrt{\text{m}}$) (Table 2). While the highly crosslinked UHMWPEs had an overall reduced FCP resistance compared with the virgin UHMWPE, there was a trend towards a lower exponent, m, for the Paris relationship (Eq. (2)) for the highly crosslinked materials compared to the virgin material (Table 2, Fig. 3).

Macroscopic examination of the fractured specimens suggested that the virgin treatment group failed in a more ductile manner than the two highly crosslinked treatment groups. The virgin specimens showed an overall rougher fracture surface and more plastic deformation in front of the crack tip as evidenced by the reduction of the cross-section of the specimen on the plane of crack growth. In comparison, the highly crosslinked materials had relatively flat fracture surfaces and sustained less reduction in cross-sectional thickness than was observed in the virgin material. For all treatment groups, there was less plastic deformation (in the form of reduced cross-sectional thickness) for the 20 mm compared with the 10 mm thick specimens, indicating better achievement of plane strain conditions for the thicker specimens.

Scanning electron fractographs showed evidence of similar fracture features for all treatment groups. All fracture surfaces showed characteristic chevron markings

Table 2
Exponent and coefficient for the power law ($da/dN = C(\Delta K)^m$) that describes the Paris region of da/dN vs. ΔK curves for remelted, annealed, and virgin UHMWPE

	Remelted (100 kGy, 150 °C)		Annealed (100 kGy, 110 °C)		Conventional (as-received)	
	10 mm	20 mm	10 mm	20 mm	10 mm	20 mm
Exponent (m)	7.00	8.45	8.04	9.78	11.24	15.72
Coefficient (C) (mm/cycle)/(MPa $\sqrt{\text{m}}$)^m	8.73×10^{-5}	6.68×10^{-5}	1.92×10^{-5}	1.06×10^{-5}	3.07×10^{-8}	2.72×10^{-10}
$\Delta K_{\text{inception}}$ (MPa $\sqrt{\text{m}}$)	0.9		1.1		2.0	

Values for exponent and coefficient are given for both specimen thicknesses (10, 20 mm). The inception stress intensity range ($\Delta K_{\text{inception}}$) was estimated from combined thickness data and was determined for each treatment group.

Questions? Contact FDA/CDRH/OCE/DID at CDRH-FOISTATUS@fda.hhs.gov or 301-796-8118

Records processed under FOIA Request #2014-8015; Released by CDRH on 12-8-2015

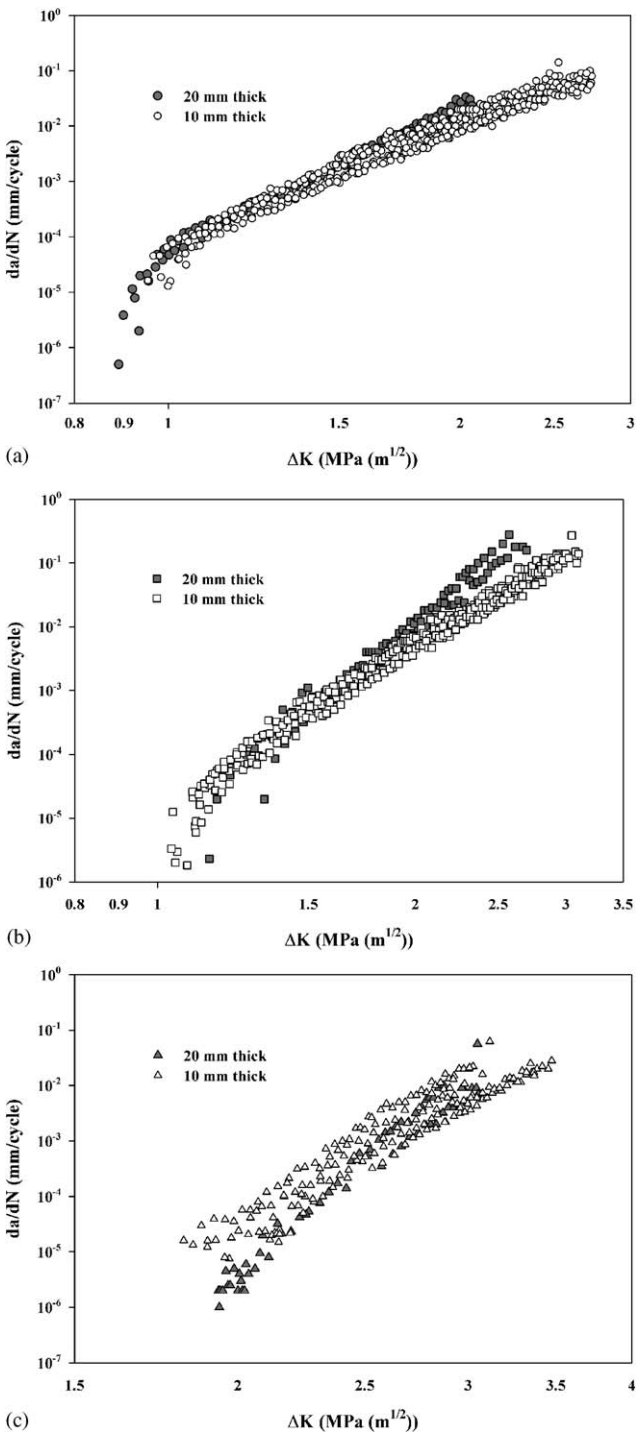

Fig. 2. (a) ΔK vs. da/dN for two specimen thicknesses of remelted UHMWPE (100 kGy, 150 °C). (b) ΔK vs. da/dN for two specimen thicknesses of annealed UHMWPE (100 kGy, 110 °C). (c) ΔK vs. da/dN for two specimen thicknesses of virgin UHMWPE (as-received).

[16] throughout the initiation and Paris regions, with the major axis of each chevron parallel to the direction of crack growth (Fig. 4). In addition, all treatment groups also had characteristic folds perpendicular to the direction of crack growth, spaced approximately 3–6 μm apart, depending on the treatment group (Fig. 5) [7,8,16]. The folds were present

Table 3
p-Values obtained from ANOVA statistical analyses for the effect of radiation crosslinking and post-irradiation thermal treatment on the exponent (*m*) of the Paris region and the coefficient (*C*) for the Paris region for remelted, annealed, and virgin treatment groups

	10 mm FCP	$n = 5$	20 mm FCP	$n = 2$
	Remelted	Annealed	Remelted	Annealed
Exponent (*m*)				
Annealed	0.17		0.09	
Conventional	**0.00**	**0.22**	0.35	0.77
Coefficient (*C*)				
Annealed	0.28		**0.00**	
Conventional	**0.02**	**0.00**	**0.00**	**0.01**

Bold values indicate a significant difference ($p < 0.05$).

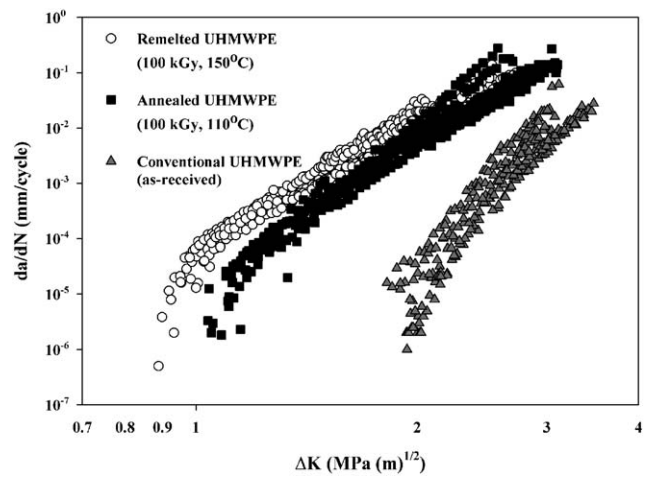

Fig. 3. ΔK vs. da/dN for highly crosslinked remelted, annealed, and virgin UHMWPE. The combined 10 and 20 mm specimen thickness data are presented.

at both low (10^{-5} mm/cycle, initiation region) and high (10^{-3} mm/cycle, Paris region) crack growth rates.

At low magnification the virgin treatment group showed a fracture surface with more chevron markings than the relatively flat highly crosslinked materials (Fig. 4). The edges of the chevrons in the virgin treatment group also showed extensive buckling, often along the entire perimeter of the chevron. Though some buckling was identified in the two highly crosslinked treatment groups, the features were smaller and rarely defined the entire perimeter of a chevron. Folds perpendicular to the direction of crack growth were clearly visible at low magnification in the virgin treatment group; such folds were much less visible in the highly crosslinked treatment groups. At higher magnification, the fracture surfaces of the highly crosslinked treatment groups were almost devoid of the buckling that was prevalent in the virgin group (Fig. 5). In addition, the perpendicular folds were less pronounced and were on the lower end of the spacing range (~3 μm) in the highly crosslinked treatment groups when compared to the virgin group (~6 μm).

Questions? Contact FDA/CDRH/OCE/DID at CDRH-FOISTATUS@fda.hhs.gov or 301-796-8118

Records processed under FOIA Request #2014-8015; Released by CDRH on 12-8-2015

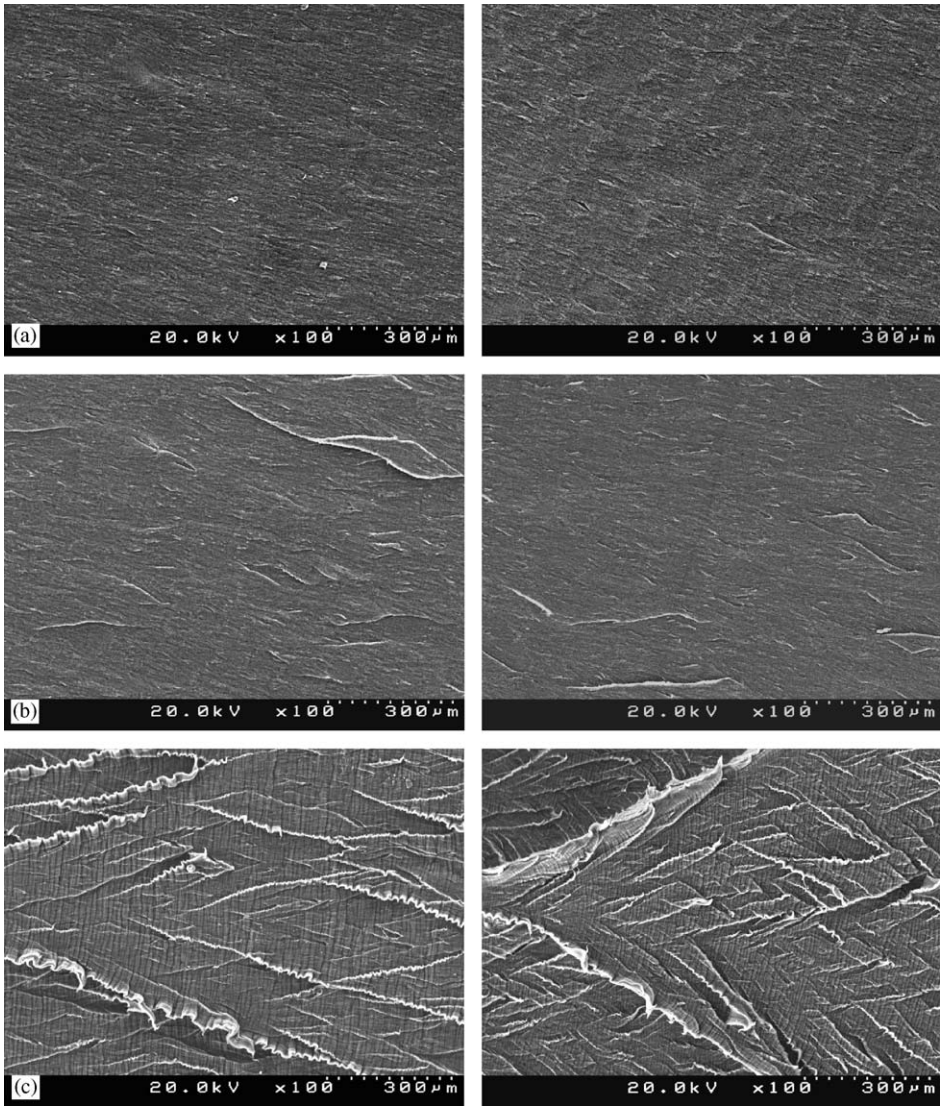

Fig. 4. Low magnification, representative fracture surfaces from the Paris region for: (a) remelted; (b) annealed; and (c) virgin, treatments of UHMWPE for both 10 mm (left) and 20 mm (right) specimen thicknesses. Fractographs, taken at a crack growth rate of 1×10^{-3} mm/cycle, show surface features that are similar in magnitude and prevalence to those seen at a lower crack growth rate (1×10^{-5} mm/cycle) for all three treatment groups. Direction of crack growth is left to right.

Less extreme differences in fracture surfaces were noted between the annealed and the remelted treatment groups, though the remelted material had a somewhat more brittle appearance. Low magnification fractographs of the remelted treatment group showed almost no evidence of ductile buckling, while the annealed material maintained examples of ductile buckling throughout the Paris region (Fig. 4). High magnification fractographs also show limited buckling in the annealed treatment group; no evidence of buckling was found in the remelted treatment group (Fig. 5).

The range of ΔK over which LEFM conditions (Eq. (3)) were maintained was greater for the highly crosslinked treatment groups than the virgin treatment group (Table 4). The specimens met the more severe plane strain conditions (Eq. (4)) for a more limited range of crack growth than the LEFM conditions, as was expected. The 20 mm specimens maintained plane strain conditions to a larger ΔK than the 10 mm specimens in the highly crosslinked treatment groups (Table 4). The virgin treatment group never saw plane strain loading for either specimen thickness (Table 4).

4. Discussion

The results of this study show that in addition to reducing ductility, crosslinking reduces the FCP resistance of UHMWPE. The observed reduction in macroscopic plastic deformation on the fracture plane of the highly crosslinked UHMWPEs is consistent with the reported reduced true ultimate strain in tension for these highly crosslinked UHMWPEs compared with virgin UHMWPE

Questions? Contact FDA/CDRH/OCE/DID at CDRH-FOISTATUS@fda.hhs.gov or 301-796-8118

Records processed under FOIA Request #2014-8015; Released by CDRH on 12-8-2015

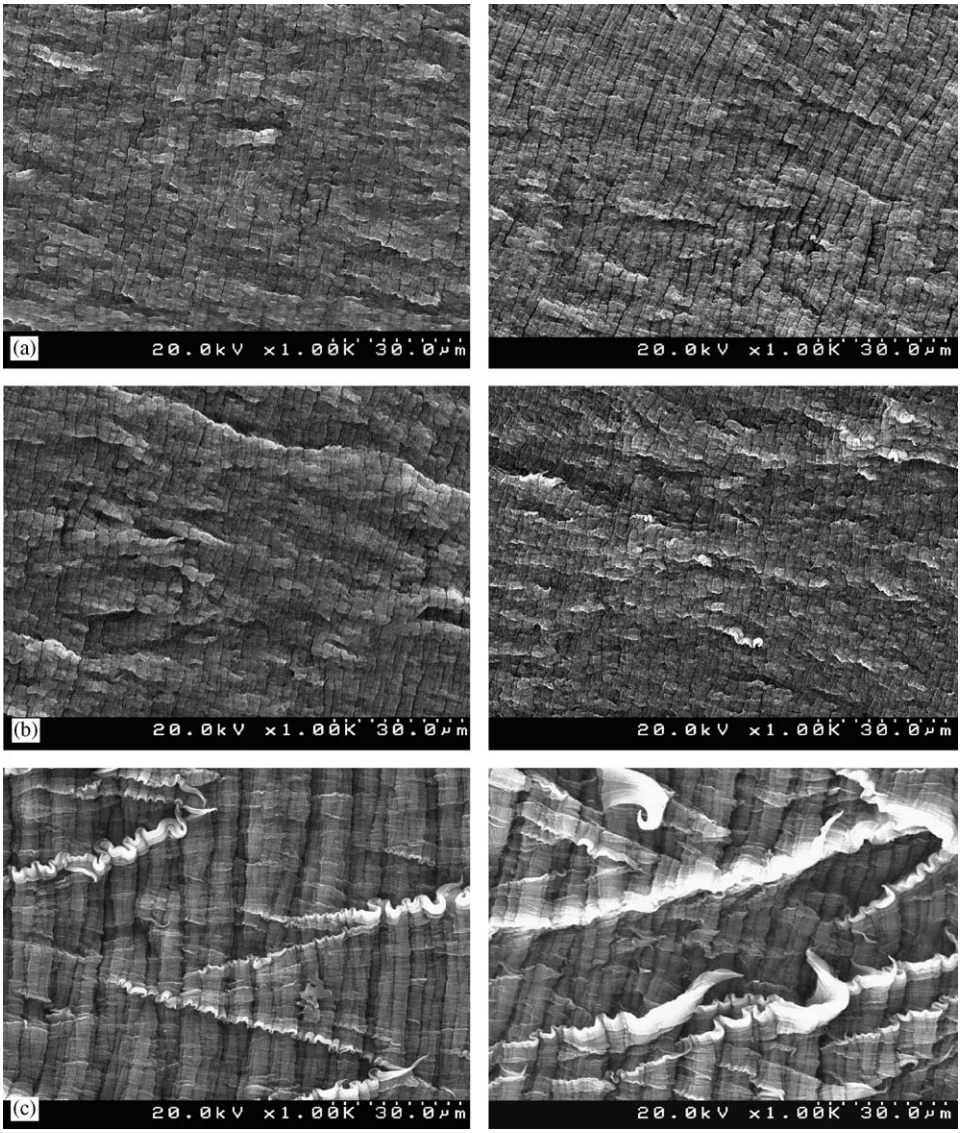

Fig. 5. High magnification, representative fracture surfaces from the Paris region for: (a) remelted; (b) annealed; and (c) virgin, treatments of UHMWPE for both 10 mm (left) and 20 mm (right) specimen thicknesses. Fractographs, taken at a crack growth rate of 1×10^{-3} mm/cycle, show surface features that are similar in magnitude and prevalence to those seen at a lower crack growth rate (1×10^{-5} mm/cycle) for all three treatment groups. Direction of crack growth is left to right.

[3]. The lessening in size and prevalence of the chevron markings for the highly crosslinked treatment groups when compared to the virgin treatment group supports the notion that the crosslinks restrict the relative motion of the chains in the amorphous regions via chain slip [17]. The reduction in the buckling along the edges of the chevrons in the annealed and remelted treatment groups suggests that more limited molecular chain alignment occurs in the highly crosslinked UHMWPEs than in the virgin UHMWPE [18]. Similar embrittlement of the surface fractography has been previously observed in association with an increase in crosslink density [7,8,19].

Connelly et al. [16] have proposed that folds perpendicular to crack growth direction, appearing on fracture surfaces of cyclically fractured UHMWPE (Figs. 4 and 5), are a result of a failure mechanism consisting of repetitive crack-tip blunting and tearing. Throughout the initiation and Paris regions, fold spacing (within a material treatment group) remained constant regardless of crack length or stress intensity range. The qualitatively observed reduction (by almost 50%) in fold spacing as well as the qualitatively lessening distinction of the folds between the virgin and the highly crosslinked treatment groups suggest that the fold depth and spacing are a function of physical structure (Fig. 5). It would be expected that the reduction in ductility due to the addition of crosslinks would modify the tearing behavior of the UHMWPE, resulting in less deformation during crack-tip blunting; less deformation may result in the shorter fold spacing seen in the highly crosslinked treatment groups.

Questions? Contact FDA/CDRH/OCE/DID at CDRH-FOISTATUS@fda.hhs.gov or 301-796-8118

Records processed under FOIA Request #2014-8015; Released by CDRH on 12-8-2015

Table 4
Cyclic stress intensity (ΔK) and crack growth rate (da/dN) values for the limits of LEFM and plane strain applicability for both 10 and 20 mm thick specimens

	LEFM		Plane strain	
	ΔK (MPa$\sqrt{m}$)	da/dN (mm/cycle)	ΔK (MPa$\sqrt{m}$)	da/dN (mm/cycle)
Remelted (100 kGy, 150 °C)				
10 mm	2.14	1.80×10^{-2}	1.22	4.00×10^{-4}
10 mm	2.25	1.80×10^{-2}	1.20	2.20×10^{-4}
10 mm	2.08	1.29×10^{-2}	1.19	1.79×10^{-4}
10 mm	2.08	2.00×10^{-2}	1.21	4.20×10^{-4}
10 mm	2.07	1.00×10^{-2}	1.21	3.86×10^{-4}
20 mm	1.92	1.62×10^{-2}	1.49	1.80×10^{-3}
20 mm	1.93	1.75×10^{-2}	1.49	2.00×10^{-3}
Annealed (100 kGy, 110 °C)				
10 mm	2.15	1.50×10^{-2}	1.20	7.67×10^{-5}
10 mm	2.41	1.67×10^{-2}	1.39	2.10×10^{-4}
10 mm	2.40	1.57×10^{-2}	1.40	2.00×10^{-4}
10 mm	2.41	2.33×10^{-2}	1.40	2.88×10^{-4}
10 mm	2.42	2.00×10^{-2}	1.41	1.67×10^{-4}
20 mm	2.34	4.50×10^{-2}	1.79	2.20×10^{-3}
20 mm	2.29	7.00×10^{-2}	1.77	4.00×10^{-3}
Conventional (as-received)				
10 mm	2.53	2.67×10^{-3}	—	—
10 mm	2.53	3.25×10^{-4}	—	—
10 mm	2.54	6.00×10^{-4}	—	—
10 mm	2.47	1.00×10^{-3}	—	—
10 mm	2.51	9.00×10^{-4}	—	—
20 mm	2.58	3.50×10^{-4}	—	—
20 mm	2.48	6.00×10^{-4}	—	—

Reduced FCP resistance for the highly crosslinked UHMWPEs was also seen in the decrease in $\Delta K_{inception}$ (Table 2). Baker et al. [7] demonstrated a 50% reduction in $\Delta K_{inception}$ for a highly crosslinked, remelted (100 kGy, 170 °C) GUR 1050 UHMWPE compared to a non-irradiated control group. A FCP study by Cole et al. [8] showed a reduction in $\Delta K_{inception}$ of approximately 30% for highly crosslinked, annealed (100 kGy, 110 °C) GUR 1050 UHMWPE compared with a non-irradiated, annealed control group. Bradford et al. [19] compared the FCP resistance of highly crosslinked, remelted (100 kGy, 150 °C) GUR 1050 UHMWPE to a non-crosslinked UHMWPE; $\Delta K_{inception}$ for the highly crosslinked, remelted group was 40% less than the $\Delta K_{inception}$ for the control group. Similar reductions in $\Delta K_{inception}$ and overall shifts of the ΔK vs. da/dN curves towards diminished FCP resistance for remelted and annealed UHMWPEs were seen in the present study (Fig. 3). Loss of chain mobility would be expected to affect the ability of the polymer to plastically deform [20] and, thus, would be reflected in reduced ΔK associated with crack inception.

Examination of the exponent of the Paris relationship for each of the three treatment groups suggests that the highly crosslinked UHMWPEs may be better able to resist FCP following $\Delta K_{inception}$ than the virgin UHMWPE. An increased Paris exponent reflects an increased sensitivity of a material to changes in cyclic stress intensity. The higher exponent of the virgin treatment group (Table 2, Fig. 3) when compared to the highly crosslinked treatment groups suggests that, once a crack has initiated, the number of cycles to failure may be more limited for the virgin UHMWPE. Similar differences between the exponents of highly crosslinked and virgin UHMWPEs have been reported by Baker et al. [7] and Cole et al. [8].

While not statistically significantly different, the annealed UHMWPE had an overall increased cyclic stress intensity for a given da/dN than the remelted UHMWPE. It is possible that annealing as a post-irradiation treatment may be better at preserving the FCP resistance of UHMWPE than remelting (Table 2, Fig. 3). However, annealing UHMWPE after irradiation may not be as effective as remelting at quenching all of the residual free radicals, resulting in a possibly greater potential for oxidation [21].

Though the Paris exponent and coefficient may be considered to be useful for ranking FCP resistance of different UHMWPE formulations, these parameters are somewhat limited as useful indicators of material performance with respect to implant design. Once a fatigue crack enters the Paris regime, the cycles endured by any UHMWPE formulation constitutes a small percentage of component lifetime (Fig. 3).

A more useful property to consider with respect to implant design may be the cyclic stress intensity required for crack inception ($\Delta K_{inception}$), to optimize the life of the component prior to crack inception. The higher estimated $\Delta K_{inception}$ for the annealed UHMWPE suggests that some mitigating effect may be achieved through post-irradiation processing below the melt-transition (annealing) as compared with post-irradiation processing above the melt-transition (remelting) on fatigue crack inception as well as FCP. Little is known about the threshold regime behavior of UHMWPE materials; further study of the effect of material formulation on this stage of fatigue crack growth is warranted.

A limitation of this work may be that neither LEFM nor plane strain conditions were maintained to failure for any of the treatment groups (Table 4). LEFM conditions were met in the $\Delta K_{inception}$ regime for all the treatment groups and were also maintained throughout the region used to calculate the Paris exponent, m, and coefficient, C, for the highly crosslinked treatment groups (Table 1). LEFM conditions were only partially met in the Paris regime for the virgin UHMWPE. However, with respect to FCP, it has been noted that it is generally not necessary to meet the stringent plastic zone size restrictions associated with plane strain or even LEFM conditions that are necessary to be met for static fracture toughness determination [11]. The relatively small differences in FCP behavior between 10 and 20 mm thick specimens, that occurred primarily at high crack growth rates near failure, is consistent with this observation.

Questions? Contact FDA/CDRH/OCE/DID at CDRH-FOISTATUS@fda.hhs.gov or 301-796-8118

Records processed under FOIA Request #2014-8015; Released by CDRH on 12-8-2015

5. Conclusion

In this study, comparison of the FCP behavior of virgin and highly crosslinked UHMWPEs suggest that crosslinking is detrimental to the ability of UHMWPE to resist crack inception and propagation under cyclic loading compared with virgin (non-crosslinked) UHMWPE. The findings also suggest that annealed highly crosslinked UHMWPE may have somewhat better resistance to FCP than remelted highly crosslinked UHMWPE.

Acknowledgements

Supported by NIH Grant AR 47192. Special thanks to J. Bensusan, R. Thomas, J. Berilla, and M. Sobieraj for technical assistance and for helpful discussions.

References

[1] Kurtz SM, Muratoglu OK, Evans M, Edidin AA. Advances in the processing, sterilization, and crosslinking of ultra-high molecular weight polyethylene for total joint arthroplasty. Biomaterials 1999;20(18):1659–88.
[2] Muratoglu OK, Kurtz SM. Alternative bearing surfaces in hip replacement. In: Dekker M, editor. Hip replacement: current trends and controversies. New York: SR; 2002.
[3] Kurtz SM, Villarraga M, Herr M, Bergström J, Rimnac CM, Edidin AA. Thermomechanical behavior of virgin and highly crosslinked ultra-high molecular weight polyethylenes used in total joint replacements. Biomaterials 2002;22(4):3681–97.
[4] McKellop H, Shen F, Lu B, Campbel P, Salovey R. Effect of sterilization method and other modifications on the wear resistance of acetabular cups made of ultra-high molecular weight polyethylene. A hip-simulator study. J Bone Jt Surg Am 2000;82A(12):1708–25.
[5] Duus LC, Walsh HA, Gillis AM, Noisiez E, Li S. A comparison of the fracture toughness of crosslinked UHMWPE made from different resins, manufacturing methods, and sterilization conditions. Transaction on Sixth World Biomaterials Congress, 2000.
[6] Edidin AA, Kurtz SM. Development and validation of the small punch test for UHMWPE used in total joint replacements. In: Sacks M, editor. Functional biomaterials. Winterthur, Swizterland: Trans Tech Publications Ltd.; 2001.
[7] Baker D, Bellare A, Pruitt L. The effects of degree of crosslinking on the fatigue crack initiation and propagation resistance of orthopedic-grade polyethylene. J Biomed Mater Res 2003;66A(1):146–54.
[8] Cole J, Lemons J, Eberhardt A. Gamma irradiation alters fatigue-crack behavior and fracture toughness in 1900 H and GUR 1050 UHMWPE. J Biomed Mater Res 2002;63(5):559–66.
[9] ASTM, E 399-Standard Test Method for Plane-Strain Fracture Toughness of Metallic Materials. In: Annual Book of ASTM Standards. 1990.
[10] ASTM, E 647-Standard Test Method for Measurement of Fatigue Crack Growth Rates. In: Annual Book of ASTM Standards. 1995.
[11] Dowling NE. Mechanical behavior of materials: engineering methods for deformation, fracture, and fatigue. Upper Saddle River, New Jersey: Prentice Hall; 1999.
[12] Paris P, Gomez R, Anderson W. A rational analytic theory of fatigue. Trend Eng 1961;13(1):9–14.
[13] Kleinbaum D, Kupper L, Muller K, Nizam A. Applied regression analysis and other multivariable methods. Pacific Grove, CA: Duxbury Press; 1998. p. 798.
[14] Baker D, Hastings R, Pruitt L. Study of fatigue resistance of chemical and radiation crosslinked medical grade ultrahigh molecular weight polyethylene. J Biomed Mater Res 1999;46(4):573–81.
[15] Baker D, Hastings R, Pruitt L. Compression and tension fatigue resistance of medical grade ultra high molecular weight polyethylene: the effect of morphology, sterilization, aging, and temperature. Polymer 2000;41:795–808.
[16] Connelly G, Rimnac C, Wright T, Hertzberg R, Manson J. Fatigue crack propagation behavior of ultrahigh molecular weight polyethylene. J Orthop Res 1984;2:119–25.
[17] Lin L, Argon A. Review: structure and plastic deformation of polyethylene. J Mater Sci 1994;29:294–323.
[18] Rimnac C, Wright T, Klein R. The effect of waveform on the fatigue crack propagation behavior of ultrahigh molecular weight polyethylene. Transaction on 7th International Conference on Fracture (ICF7). Houston, TX: Pergamon Press; 1989.
[19] Bradford L, Baker D, Ries MD, Pruitt LA. Fatigue crack propagation resistance of highly crosslinked polyethylene. Clin Orthop TRelat Res 2004(429):68–72.
[20] Butler MF, Donald AM, Ryan AJ. Time resolved simultaneous small- and wide-angle X-ray scattering during polyethylene deformation-II. Cold drawing of linear polyethylene. Polymer 1998;39(1):39–52.
[21] Bhattacharyya S, Spiegelberg S, Harris W, Muratoglu O. Mechanical elimination of free radicals in UHMWPE after radiation. San Francisco: Trans. Orthopaedic Research Society; 2004.
[22] Gencur SJ, Rimnac CM, Kurtz SM. Failure micromechanisms during uniaxial tensile fracture of conventional and highly crosslinked ultra-high molecular weight polyethylenes used in total joint replacements. Biomaterials 2003;24(22):3947–54.

Questions? Contact FDA/CDRH/OCE/DID at CDRH-FOISTATUS@fda.hhs.gov or 301-796-8118

Questions? Contact FDA/CDRH/OCE/DID at CDRH-FOISTATUS@fda.hhs.gov or 301-796-8118

Records processed under FOIA Request #2014-8015; Released by CDRH on 12-8-2015

Keith W. Greer,[1] *Richard S. King,*[1] *and Frank W. Chan*[1]

The Effects of Raw Material, Irradiation Dose, and Irradiation Source on Crosslinking of UHMWPE

REFERENCE: Greer, K. W., King, R. S., and Chan, F. W., **"The Effects of Raw Material, Irradiation Dose, and Irradiation Source on Crosslinking of UHMWPE,"** *Crosslinked and Thermally Treated Ultra-High Molecular Weight Polyethylene for Joint Replacements, ASTM STP 1445,* S. M. Kurtz, R. Gsell, and J. Martell, Eds., ASTM International, West Conshohocken, PA, 2003.

ABSTRACT: Four Ultra-High Molecular Weight Polyethylene (UHMWPE) materials were evaluated after various irradiation crosslinking processes to determine the effects of the materials and processes on their properties for orthopaedic applications. The materials and processes included two molecular weight materials (GUR 1020 and GUR 1050), two fabricated forms (ram extruded bar and compression-molded sheet), two irradiation sources (gamma and e-beam) and multiple irradiation doses ranging from 30-120 kGy. Increasing irradiation dose led to increased crosslinking, decreased wear, and decreased toughness. The molecular weight of the starting material and the irradiation source both had effects on the final properties while the fabricated form did not. Wear testing of selected groups indicated that there was a direct correlation with irradiation dose but not with the crosslink density (as calculated from the swell ratio).

KEYWORDS: ultra-high molecular weight polyethylene, gamma irradiation, e-beam irradiation, crosslinking, Fourier-Transform infrared analysis, density, tensile properties, Izod impact, wear testing, orthopaedic medical devices, total joint replacement

Introduction

"Highly crosslinked" Ultra-High Molecular Weight Polyethylene (UHMWPE) is currently being sold for total hip and total knee replacement bearings with the expectation of reduced clinical wear and thus improved clinical outcomes. The crosslinking of these materials has been achieved by either gamma or e-beam irradiation with increased irradiation dose leading to increased crosslinking and reduced wear [*1,2*]. However, increased crosslinking also reduces mechanical properties, particularly toughness, thus there is a trade-off between wear and mechanical properties [*1-5*]. Much of the debate in the orthopaedic community has been about the proper level of crosslinking for a given application that will reduce wear while maintaining mechanical properties necessary for proper *in vivo* function.

[1]Principal Scientist, Principal Scientist, and Team Leader, respectively, Research Department, DePuy Orthopaedics, 700 Orthopaedic Drive, Warsaw, IN, 46581.

Currently manufacturers are using different raw materials, different irradiation processes, and different irradiation doses to produce these "highly crosslinked" UHMWPE products [*1-2, 6-9*]. It was the objective of this study to determine the effects of irradiation source (gamma vs. e-beam) and irradiation dose on the mechanical, physical, and wear properties of UHMWPE materials produced from two molecular weight resins (GUR 1020 and GUR 1050) and by two fabrication methods (ram extrusion and compression molding).

Materials and Methods

Materials

The four materials chosen for this investigation were GUR 1020 compression-molded sheet (CMS) from Perplas (Bacup, UK), GUR 1020 ram extruded bar (REB) from Perplas, GUR 1050 CMS from Poly Hi (Fort Wayne, IN), and GUR 1050 REB from Poly Hi. The 1020 material is reported to have an average molecular weight of 3-4 million while the 1050 is reported to have a molecular weight of 5-6 million. A single lot of each material was used throughout the study.

Gamma irradiated groups were produced by starting with 76 mm diameter bars of each of the four materials. For the two molded sheet materials, the bars were machined from the molded sheet. Five bars of each material (0.76 m long) were vacuum packaged in foil bag and subjected to gamma irradiation (Steris Isomedix, Whippany, NJ) in five groups (four materials per group). The nominal irradiation doses were 40, 50, 60, 80, and 120 kGy.

The e-beam irradiated groups were produced by starting with blocks that were 64 mm by 152 mm by 40 mm thick. The blocks were vacuum packaged in foil and subjected to e-beam irradiation using a 10 MeV source (Titan Scan Systems, San Diego, CA). In order to obtain an even irradiation dose through each bar, the blocks were first irradiated from one side and then irradiated from the second side in a second pass through the e-beam. The 1050 REB and 1050 CMS materials were irradiated at nominal doses of 30, 50, 60, 80, and 120 kGy. The 1020 REB and 1020 CMS materials were irradiated only at 60 kGy.

After irradiation, all bars and blocks were heated in argon to a temperature of 155° C and held for 24 hours to quench free radicals by crosslinking, then held for 24 hours at 120° C and cooled to room temperature. As-received samples of all four materials were also evaluated for comparison.

Mechanical Testing

Tensile and impact tests were conducted to evaluate the mechanical properties and toughness of all the groups. Tensile testing was performed on five samples per group per ASTM Test Method for Tensile Properties of Plastics (D 638) using a Type 4 tensile bar and a crosshead speed of 5.08 cm/min. Double-notched Izod impact tests were performed on five samples per group per ASTM Specification for Ultra-High-Molecular-Weight Polyethylene Powder and Fabricated Form for Surgical Implants (F 648).

Physical Properties

The physical properties evaluated included density, swell ratio, and trans-vinylene index (TVI). Density was evaluated on at least three samples from each material using a density gradient column per ASTM Test Method for Density of Plastics by the Density-Gradient Technique (D 1505). The swell ratio was evaluated on at least two samples per group using an SRT-1™ swell ratio tester (Cambridge Polymer Group, Somerville, MA) at 130° C. Samples were 6 mm diameter by 6 mm high cylinders. The swell ratio was subsequently converted to crosslink density [*10*]. A Nicolet Magna 550 Fourier Transform Infrared (FTIR) spectrometer (Thermo Nicolet, Madison, WI) with a Spectra-Tech IR-Plan microscope (Thermo Spectra-Tech, Shelton, CT) and a 50 μm by 200 μm aperture was used for the TVI evaluation. Cross-sections were taken from each of the bars or blocks. From these, 200 μm thin sections were microtomed. Each thin section was then evaluated in 1 mm steps to a depth of either 30 mm (e-beam samples) or 38 mm (gamma samples) starting at the outside edge to determine if there was a trans-vinylene gradient. The TVI was calculated by taking the area under the trans-vinyl vibration at 964 cm^{-1} and dividing it by the area under the 1900 cm^{-1} peak as has been reported in the literature [*11*]. The average TVI was calculated by averaging the individual TVI measurements through the depth of each sample.

Wear Properties

Hip simulator wear testing was performed on seven of the gamma-irradiated groups to determine if the wear rate was a function of the irradiation dose or the swell ratio (an indication of crosslink density). These seven groups were chosen to include all four materials at 80 kGy, the 1050 CMS material at 40 kGy which had the same swell ratio/crosslink density as the 1020 REB at 80 kGy, a second material at 40 kGy (1020 REB), and a 1020 material with an intermediate dose and swell ratio/crosslink density (1020 CMS at 60 kGy). Either two or three samples per group were tested.

Wear testing was carried out for eight million cycles using an eight-station hip simulator (MTS, Eden Prairie, MN). Test specimens were mounted in the inverted orientation (cup below the head) at 23° to the horizontal plane and rotated about a vertical axis. A load simulating normal gait was applied axially through the acetabular cup base assembly with a peak load of 2000 N [*12*]. Both the load and rotation were synchronized at approximately 0.95 Hz. The lubricant was 90% bovine serum (HyClone Laboratories, Inc., Logan, UT), with 20 mM EDTA and 0.2% NaN_3 added. The serum was changed every quarter million cycles and gravimetric wear was measured every half million cycles with correction for fluid absorption from soak controls. Wear rates were determined by linear regression and compared using a non-parametric ANOVA.

Results

Irradiation Doses

The actual irradiation doses received by the groups are shown in Table 1. The average dose for the gamma irradiated groups came from the average of ten dosimeters

Records processed under FOIA Request #2014-8015; Released by CDRH on 12-8-2015

per bar. The average dose for the e-beam groups was based on the average of the maximum (center of block) and minimum (front of block) doses as calculated from 3-6 dosimeters and a correlation run on a block where dosimeters were placed both on the front and in the middle of the block. The correlation run showed that the inside of a block would receive a 30% higher dose than the front of the block.

Table 1-*Average Irradiation Doses and Dose Ranges*

	Gamma Irradiation		e-beam Irradiation	
Nominal Dose (kGy)	Average Dose (kGy)	Dose Range (kGy)	Average Dose (kGy)	Dose Range (kGy)
30	NA	NA	30	26-34
40	43	40-45	NA	NA
50	51	49-53	50	44-57
60	63	60-66	61	53-69
80	83	78-88	81	70-92
120	124	120-130	121	104-137

Tensile Properties

Even though the yield strength and ultimate tensile strength of the as-received materials were decreased by crosslinking, all groups maintained values above the ASTM F 648 minimums of 19 and 27 MPa respectively (Table 2).

The effects of irradiation dose on the elongation to break are shown in Figure 1 for the gamma materials and in Figure 2 for the e-beam materials. While all four materials showed decreases in elongation with increasing irradiation dose, the two lower molecular weight 1020 materials (CMS and REB) have similar elongation at the same dose, and for gamma irradiation they have about 15% higher elongation for all doses compared to both 1050 materials (CMS and REB). This difference was significant (student's t-test, $p<0.05$). For equal materials and doses, the e-beam process gave higher elongation than the gamma process, although there was more variation for most groups. All the tensile data are given in Table 2.

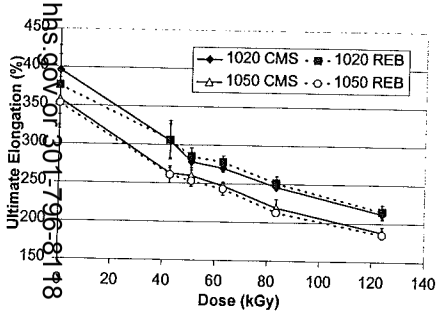

Figure 1-*Ultimate elongation of gamma irradiated materials*

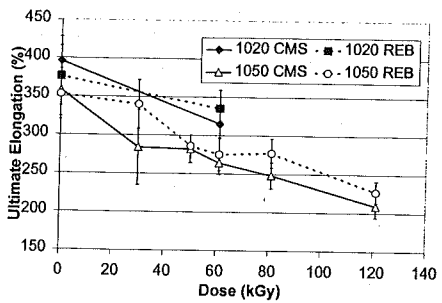

Figure 2-*Ultimate elongation of e-beam irradiated materials*

Table 2-*Tensile Properties*

Nominal Dose (kGy)	Irradiation Source	Material	Form	Yield Strength (MPa)		UTS (MPa)		Ultimate Elongation (%)	
				Avg.	StDev	Avg.	StDev	Avg.	StDev
0	None	1020	CMS	23.6	0.1	42.1	2.7	396	20
			REB	23.6	0.1	37.2	6.4	376	52
		1050	CMS	22.5	0.1	43.8	3.5	358	20
			REB	22.3	0.4	40.0	5.0	353	33
30	e-beam	1050	CMS	20.4	0.1	36.7	5.8	284	49
			REB	21.0	0.1	43.6	6.8	340	32
40	gamma	1020	CMS	21.4	0.1	38.9	4.2	305	22
			REB	21.3	0.2	36.5	4.1	306	25
		1050	CMS	20.0	0.2	32.4	1.5	263	7
			REB	20.8	0.3	32.5	1.1	261	11
50	gamma	1020	CMS	21.1	0.2	35.1	2.6	278	11
			REB	21.4	0.2	33.4	2.3	285	11
	e-beam	1050	CMS	20.4	0.1	37.6	3.3	282	18
			REB	21.1	0.1	35.4	1.0	286	3
	gamma	1050	CMS	20.2	0.3	34.5	2.1	260	10
			REB	22.3	0.1	33.5	1.0	253	7
60	e-beam	1020	CMS	21.3	0.0	41.6	3.7	315	18
			REB	23.5	0.2	45.3	5.0	335	24
	gamma	1020	CMS	23.1	0.1	36.7	0.7	270	5
			REB	23.1	0.2	35.4	0.8	278	8
	e-beam	1050	CMS	20.4	0.1	36.9	3.8	264	15
			REB	21.2	0.2	39.5	3.1	275	21
	gamma	1050	CMS	20.1	0.1	33.2	1.2	247	5
			REB	20.6	0.1	31.6	1.0	243	8
80	gamma	1020	CMS	22.9	0.0	35.5	0.4	246	3
			REB	23.2	0.1	34.0	1.2	251	9
	e-beam	1050	CMS	20.5	0.1	35.6	3.2	248	17
			REB	22.8	0.2	42.5	5.1	277	19
	gamma	1050	CMS	20.3	0.1	32.3	1.4	219	11
			REB	20.8	0.1	30.2	0.6	213	5
120	gamma	1020	CMS	21.4	0.1	33.3	1.7	212	7
			REB	21.3	0.3	31.1	2.1	215	9
	e-beam	1050	CMS	20.6	0.2	34.1	4.0	209	15
			REB	21.2	0.2	36.6	3.2	227	14
	gamma	1050	CMS	20.0	0.1	30.2	1.6	188	7
			REB	21.0	0.1	29.2	1.0	185	5

Questions? Contact FDA/CDRH/OCE/DHT-ERR-CSA/TUS@fda.hhs.gov or 301-796-8118
Records processed under FOIA Request #2014-8015; Released by CDRH on 12-8-2015

Impact Properties

The effects of irradiation dose on impact strength are shown in Figures 3 and 4 for the gamma and e-beam materials respectively. The lower molecular weight 1020 material generally showed higher toughness at the same dose compared to the higher molecular weight 1050 material, although the differences were small from 60-80 kGy for the gamma materials. The fabrication method (i.e. REB vs. CMS) had little effect on the impact strength for either 1020 or 1050. Under the same conditions, the e-beam process showed higher impact strength than the gamma process (except for 1050 REB at 60 kGy). The differences were significant ($p<0.05$) for 1050 REB and for 1050 CMS at all doses except 60 kGy. The impact data are included in Table 3.

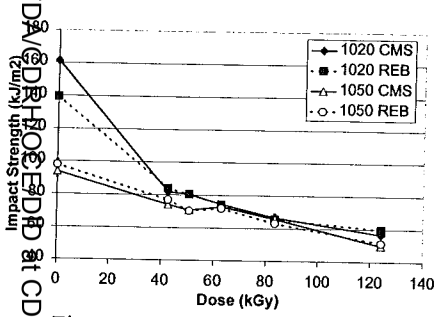

Figure 3-*Impact strength of gamma irradiated materials*

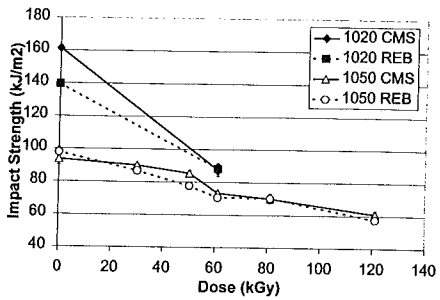

Figure 4-*Impact strength of e-beam irradiated materials*

Density Evaluation

The density values as a function of dose are shown in Figures 5 and 6 for gamma and e-beam materials, respectively. The as-received materials have the highest densities while doses of 30-60 kGy produce the lowest densities for all materials with densities slightly increasing at the higher doses (80-120 kGy). The lower molecular weight 1020 materials have the higher densities at all doses.

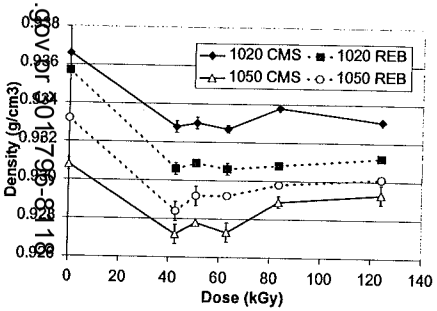

Figure 5-*Density values for gamma irradiated materials*

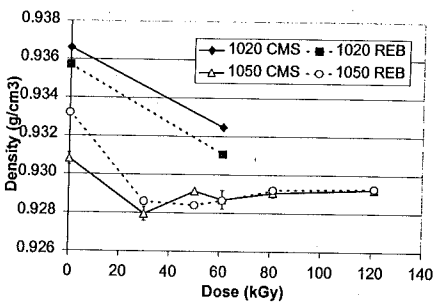

Figure 6-*Density values for e-beam irradiated materials*

Guest 3 (Guest) On Behalf Of CDRH-FOI STATUS (CDRH) at CDRH-FOI STATUS (CDRH) at FDA/CDRH-OEDD at cdrh-foi@mail.fda.gov 2017-08-18 10:00 EDT
Delivery method: Secure Download
Page 215 of 215
Page Count: 215
Tracking ID: FOI-2017-7799

Table 3-*Impact and Swelling Properties*

Nominal Dose (kGy)	Irradiation Source	Material	Form	Impact (kJ/m^2)		Swell Ratio		Apparent XLD	
				Avg.	StDev	Avg.	StDev	Avg.	StDev
0	None	1020	CMS	161.3	1.9	NA	NA	NA	NA
			REB	139.5	1.4	NA	NA	NA	NA
		1050	CMS	93.7	3.4	NA	NA	NA	NA
			REB	97.9	2.9	NA	NA	NA	NA
30	e-beam	1050	CMS	90.1	1.2	3.38	0.00	0.130	0.000
			REB	86.8	1.0	3.41	0.03	0.129	0.002
40	gamma	1020	CMS	81.8	0.8	3.85	0.26	0.105	0.011
			REB	84.0	0.3	3.83	0.12	0.106	0.006
		1050	CMS	74.1	1.1	3.28	0.04	0.137	0.003
			REB	77.0	0.4	3.80	0.31	0.108	0.013
50	gamma	1020	CMS	80.5	1.4	3.77	0.08	0.109	0.004
			REB	80.4	1.5	3.88	0.13	0.105	0.007
	e-beam	1050	CMS	85.4	1.6	3.07	0.12	0.154	0.010
			REB	77.7	2.2	3.18	0.01	0.144	0.001
	gamma	1050	CMS	70.8	1.4	3.31	0.06	0.135	0.005
			REB	70.4	0.5	3.39	0.10	0.130	0.006
60	e-beam	1020	CMS	87.4	3.6	3.27	0.02	0.138	0.001
			REB	88.1	3.2	3.28	0.05	0.138	0.004
	gamma	1020	CMS	74.6	2.0	3.37	0.01	0.131	0.000
			REB	74.3	1.0	3.52	0.02	0.122	0.001
	e-beam	1050	CMS	73.3	1.2	2.88	0.04	0.172	0.004
			REB	70.6	1.5	2.91	0.18	0.170	0.019
	gamma	1050	CMS	73.0	1.6	3.02	0.06	0.158	0.006
			REB	72.0	0.4	3.33	0.05	0.134	0.004
80	gamma	1020	CMS	66.6	2.4	3.10	0.05	0.152	0.005
			REB	65.7	0.9	3.28	0.03	0.137	0.003
	e-beam	1050	CMS	70.1	2.9	2.77	0.23	0.189	0.023
			REB	70.4	2.6	2.81	0.05	0.181	0.006
	gamma	1050	CMS	65.6	0.5	2.94	0.05	0.166	0.004
			REB	63.1	1.2	3.01	0.04	0.160	0.004
120	gamma	1020	CMS	56.7	0.2	3.08	0.29	0.156	0.024
			REB	59.6	1.2	3.17	0.19	0.146	0.015
	e-beam	1050	CMS	60.9	2.0	2.47	0.03	0.234	0.005
			REB	57.5	2.1	2.58	0.00	0.214	0.001
	gamma	1050	CMS	49.9	1.7	2.65	0.01	0.202	0.001
			REB	51.4	0.6	2.79	0.03	0.183	0.004

Swell Ratio/Crosslink Density

The swell ratio, which is expected to be an indicator of crosslink density (XLD), is shown as a function of dose for the gamma materials in Figure 7 and for the e-beam materials in Figure 8. In general, increasing irradiation dose led to decreased swell ratio for all materials. The 1050 materials have a lower swell ratio than the 1020 materials for almost all doses while for the same dose and material, the e-beam materials have a lower swell ratio. This appears to indicate that the 1050 materials have higher crosslink densities than the 1020 materials at the same doses; however, the swell ratio may also be affected by chain entanglements, which are directly related to molecular weight [*13*]. If so, the 1050 materials, with their higher molecular weight, will have more entanglements that may produce a lower swell ratio than 1020 materials, even if their actual crosslink density is the same. Because of the possible contribution of entanglements to the swell ratio, the crosslink density was not plotted as a function of dose. However, the crosslink density was calculated and labeled as apparent XLD and is given in Table 3.

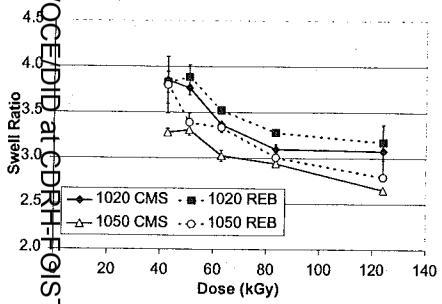

Figure 7-*Swell Ratio for gamma irradiated materials*

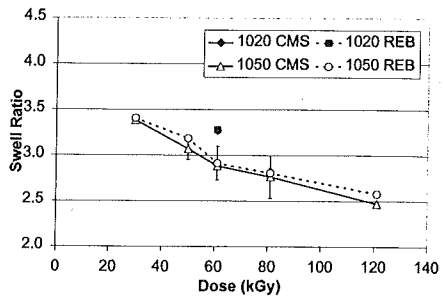

Figure 8-*Swell Ratio for e-beam irradiated materials*

Trans-Vinylene Index

The effect of irradiation dose on the trans-vinylene index (TVI) is shown in Figure 9 for the gamma materials and in Figure 10 for the e-beam materials.

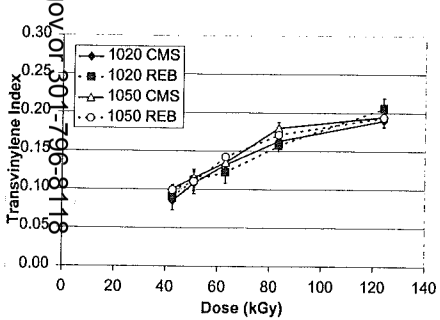

Figure 9-*TVI for gamma irradiated materials*

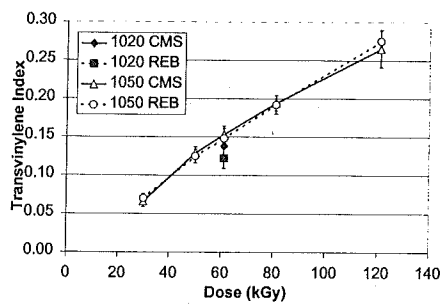

Figure 10-*TVI for e-beam irradiated materials*

The gamma materials show similar levels of trans-vinylene formation for both 1020 and both 1050 materials at all doses, although in many cases the differences are statistically significant. When compared to the gamma 1050 materials, the e-beam 1050 materials show a more linear response with a similar TVI at lower doses (30-50 kGy) and a higher TVI at higher doses (60-120 kGy). Muratoglu et al. [*11*] found similar responses for 1050 REB. One characteristic of the e-beam samples was a gradient in TVI through the thickness as shown in Figure 11 with the lowest TVI at the surface and a higher TVI in the center of the irradiated block. For the 1050 CMS material at 121 kGy, the center was about 48% higher than the surface.

Wear Properties

Wear test results for the seven groups are shown in Figure 12. Figure 13 (wear vs. swell ratio) shows there is no correlation between wear and swell ratio because the two groups with the same swell ratio (1050 CMS at 43 kGy and 1020 REB at 83 kGy) have significantly different wear rates ($p=0.01$). Figure 14 shows that there is a very good linear correlation ($R = -0.98$) between wear rate and dose, despite differences in materials and processing conditions. It also shows that the 1020 REB samples had the same wear rate as the 1050 CMS samples at both 43 kGy ($p=0.999$) and 83 kGy ($p=0.99$). These

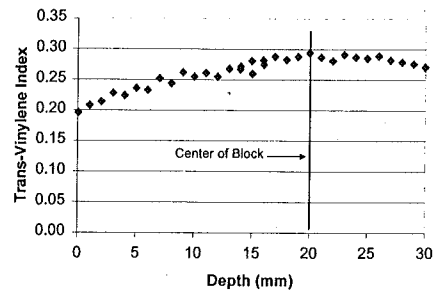

Figure 11-*TVI through the thickness for 1050 CMS e-beam irradiated material at 121 kGy.*

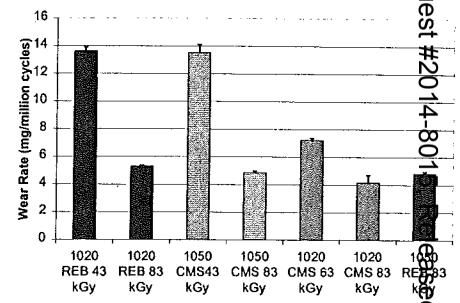

Figure 12-*Hip simulator wear rates for gamma irradiated groups*

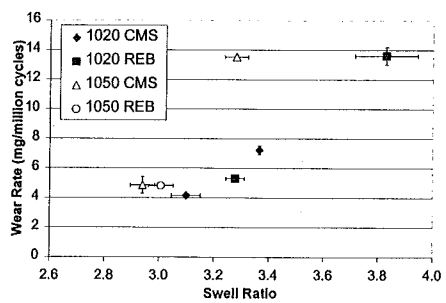

Figure 13-*Wear rate as a function of swell ratio*

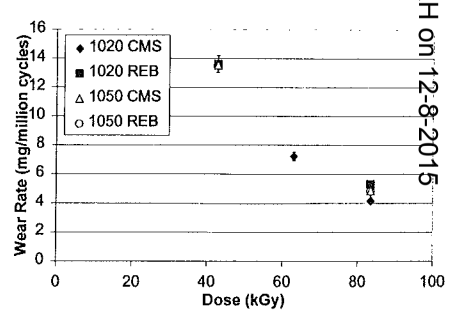

Figure 14-*Wear rate as a function of dose*

Records processed under FOIA Request #2014-801 on behalf of CDRH on 12-8-2015
Customer Contact: DAVIS-BRH/OCE/DID at CDRH-FOISTATUS@fda.hhs.gov or 301-796-8110

results suggest that the wear rate is a function of dose for 1020 and 1050 material fabricated as either CMS or REB.

Discussion

This study indicates that the choice of starting material, fabrication form and irradiation method can affect the crosslinking and subsequent mechanical properties of UHMWPE in the range of doses from 30-120 kGy.

Because irradiation of UHMWPE causes crosslinking of the material, the range of doses evaluated produced major changes in most of the properties. These dose effects were irrespective of the molecular weight of the starting material (e.g., 1020 or 1050), fabricated form (CMS or REB), or irradiation source (gamma or e-beam). In particular, increasing the dose increased the crosslinking level (as noted by the decrease in swell ratio), reduced the tensile elongation, reduced the impact strength, increased the trans-vinylene index, and ultimately reduced the wear rate.

The choice of fabricated form, either CMS or REB, had very little effect on most of the properties reported here while the molecular weight of the resin did. When compared under the same irradiation conditions, the lower molecular weight 1020 material had higher tensile elongation, higher impact strength, and higher swell ratio. However, for the gamma irradiated groups, the trans-vinylene index and hip simulator wear rates were similar for the 1020 and 1050 materials.

The choice of e-beam or gamma irradiation also affected the final properties of the crosslinked material. When the same materials, forms and doses were compared, the e-beam material had higher elongation, higher impact strength, and lower swell ratio and higher TVI. However, there was generally more variation in properties for the e-beam materials, which probably is a result of the uneven irradiation dose through the thickness as shown by the TVI results and the irradiation dosimeters. With regard to reporting on the toughness of irradiation crosslinked materials, it should be noted that the higher impact toughness of e-beam materials reported here is in contrast to the lower fracture toughness of e-beam irradiated materials reported by Duus et al. [*4*].

The finding of this study that wear of irradiated UHMWPE is not solely a function of the crosslink density appears to be in conflict with previous reports [*1-3*]. However, these reports were based only on GUR 4150 REB and did not compare different raw materials. If the gamma irradiated 1020 and 1050 materials are considered separately, then wear rate is directly related to swell ratio as can be seen in Figure 13. However, when the materials are considered together, it is the dose that determines the wear rate as shown in Figure 14.

One explanation for why the wear results are not correlated with crosslink density is that the swell ratio is not just a measure of crosslink density but also includes the effects of chain entanglements in the material. Since chain entanglements in a material increase as molecular weight increases, 1050 materials would have more entanglements than 1020 materials [*13*]. The hypothesis would be that when 1020 and 1050 are irradiated at the same dose, the amount of crosslinking is essentially the same while the swell ratio is different because the higher molecular weight 1050 material has more entanglements that inhibit the swelling of the material.

Questions? Contact DAVIDRH@CDRH.FDA.GOV or call the DRH-CSA at 301-796-5800

Acknowledgment

Thanks to David Warner, Mark Sharp, Charles Frisinger, Travis Hamill, Tom Matthews and Jim Ritchie for their work on this project.

References

[1] McKellop, H., Shen, F., Lu, B., Campbell, P., and Salovey, R., "Development of an Extremely Wear-Resistant Ultra High Molecular Weight Polyethylene for Total Hip Replacements," *Journal of Orthopaedic Research*, Vol. 17, No. 2, 1999, pp. 157-167.

[2] Muratoglu, O. K., Bragdon, C. R., O'Connor, D. O., Jasty, M., and Harris, W. H., "A Novel Method of Cross-Linking Ultra-High-Molecular-Weight Polyethylene to Improve Wear, Reduce Oxidation, and Retain Mechanical Properties," *The Journal of Arthroplasty*, Vol. 16, No. 2, 2001, pp. 149-160.

[3] Muratoglu, O. K., Bragdon, C. R., O'Connor, D. O., Jasty, M., Harris, W. H, Gul, R., and McGarry, F., "Unified Wear Model for Highly Crosslinked Ultra-High Molecular Weight Polyethylenes (UHMWPE)," *Biomaterials*, Vol. 20, 1999, pp. 1463-1470.

[4] Duus, L. C., Walsh, H. A., Gillis, A. M., Noisiez, W., and Li, S., "The Effect of Resin Grade, Manufacturing Method, and Cross Linking on the Fracture Toughness of Commercially Available UHMWPE," *Transactions of the Orthopaedic Research Society,* Vol. 25, 2000, p. 544.

[5] DiMaio, W. G., Saum, K. A., Lilly, W. B., and Moore, W. C., "Effect of Radiation Dose on the Physical Properties of Crosslinked UHMWPE," *Transactions of the Orthopaedic Research Society*, Vol. 24, 1999, p. 100.

[6] Greenwald, A. S., Bauer, T. W., and Ries, M. D., "New Polys for Old: Contribution or Caveat?" *69th Annual meeting of the American Academy of Orthopedic Surgeons*, Dallas, Texas, 2002.

[7] Manley, M. T., Capello, W. N., D'Antonio, J. A., and Edidin, A. A., "Highly Crosslinked Polyethylene Acetabular Liners for Reduction in Wear in Total Hip Replacement," Scientific Exhibit SE022, *67th Annual Meeting of the American Academy of Orthopaedic Surgeons*, Orlando, Florida, 2000.

[8] Furman, B. D., Bhattacharyya, S., Hernoux, C., Ranawat, C. S., and Li, S., "Independent Evaluation of Wear Properties of Commercially Available Cross Linked UHMWPE," *Transactions of the Society for Biomaterials*, Vol. 24, 2001, p. 33.

[9] Furman, B., Agner, S., and Li, S., "Is There a Difference in Wear Properties of Commercially Available Crosslinked UHMWPE?," *Transactions of the Orthopaedic Research Society*, Vol. 27, 2002, p. 1038.

Records processed under FOIA Request #2014-8015; Released by CDRH on 12-8-2015

[10] Spiegelberg, S. H., Kurtz, S. M., and Edidin, A. A., "Effects of Molecular Weight Distribution on the Network Properties of Radiation- and Chemically-Crosslinked Ultra High Molecular Weight Polyethylene," *Transactions of the Society for Biomaterials*, Vol. 22, 1999, p. 215.

[11] Muratoglu, O. K., and Harris, W. H., "Identification and Quantification of Irradiation in UHMWPE Through Trans-Vinylene Yield," *Journal of Biomedical Materials Research*, Vol. 56, 2001, pp. 584-592.

[12] Paul, J.P., "Forces Transmitted by Joints in the Human Body," *Proceedings of the Institution of Mechanical Engineers*, Vol. 181F, 1967, pp. 8-15.

[13] Ferry, J.D., *Viscoelastic Properties of Polymers*, 3rd Edition, John Wiley and Sons, New York, 1980, pp 241-247.

Questions? Contact FDA/CDRH/OCE/DID at CDRH-FOISTATUS@fda.hhs.gov or 301-796-8118

Kenneth R. St. John[1] and Robert A. Poggie[2]

Characterization of the Wear Performance of Crosslinked UHMWPE and Relationship to Molding Procedures

Reference: St. John, K. R., and Poggie, R. A., **"Characterization of the Wear Performance of Crosslinked UHMWPE and Relationship to Molding Procedures,"** Crosslinked and Thermally Treated Ultra-High Molecular Weight Polyethylene for Joint Replacements, *ASTM STP 1445,* S. M. Kurtz, R. Gsell, and J. Martell, Eds., ASTM International, West Conshohocken, PA, 2003.

Abstract: Using an eight-station hip wear simulator, radiation-crosslinked polyethylenes were tested for their resistance to wear-related weight loss and the results compared to results for studies conducted on the same machine using polyethylene that was being implanted at the time. The testing results showed that the wear rate of crosslinked (60 kGy) Slab Compression Molded (SCM) polymer was about 63% lower than standard (30 kGy) SCM cups and 69% less than Ram Extruded 4150 (30 kGy) cups. The Near-net Final Shape molded (NFS) crosslinked (60 kGy) specimens had an 89% reduction in wear rate over the standard (30 kGy) NFS cups, regardless of whether GUR 1020 or GUR 1050 crosslinked cups were tested. All wear rates for nitrogen packaged materials were significantly superior to those for cups sterilized in air and for earlier generation GUR 4150 products sterilized and stored in contact with oxygen.

The results confirm that both the SCM and NFS molding processes produce acetabular cups with excellent wear properties as compared to previous processes. The additional crosslinking process, described herein, provided a major improvement in the wear resistance with either molding process with greater improvement occurring in the NFS specimens.

Keywords: wear, crosslink, compression molding, extrusion, orthopaedics, tribology, final shape molding

Introduction

Over the last 10 to 15 years, there has been a continuous effort in many research laboratories around the country to improve the wear properties of ultra-high molecular weight polyethylene. Improvements in manufacturing, packaging, and sterilization techniques have yielded as much as a 90% reduction in the wear rates of polyethylene bearing components [*1*]. The objectives of this research were to evaluate the effects of raw

[1] Associate Professor, Department of Orthopaedics and Rehabilitation, University of Mississippi Medical Center, 2500 North State Street, Jackson, MS 39216-4505.

[2] Director, Applied Research, Implex Corp., 80 Commerce Drive, Allendale, NJ 07401-1600.

Records processed under FOIA request #2014-3015 Released by CDRH on 12-8-2015

Records processed under FOIA Request #2014-8015; Released by CDRH on 12-8-2015

Available online at www.sciencedirect.com
SCIENCE DIRECT®
ELSEVIER
Biomaterials 24 (2003) 3193–3199
Biomaterials
www.elsevier.com/locate/biomaterials

Effect of consolidation on adhesive and abrasive wear of ultra high molecular weight polyethylene

Rizwan M. Gul[a], Frederick J. McGarry[b], Charles R. Bragdon[c], Orhun K. Muratoglu[c,*], William H. Harris[c]

[a] *Faculty of Metallurgy and Materials Engineering, GIK Institute of Engineering Sciences and Technology, Topi 23460, District Swabi, Pakistan*
[b] *Department of Materials Science and Engineering, Massachusetts Institute of Technology, Cambridge, MA, USA*
[c] *Orthopaedic Biomechanics and Biomaterials Laboratory, Massachusetts General Hospital, GRJ 1206, 55 Fruit Street Jackson, Boston, MA 02114, USA*

Received 25 November 2002; accepted 9 March 2003

Abstract

Total hip replacement (THR) is widely performed to recover hip joint functions lost by trauma or disease and to relieve pain. The major cause of failure in THR is the wear of the ultra high molecular weight polyethylene (UHMWPE) component. The dominant wear mechanism in THR occurs through adhesion and abrasion. While poor consolidation of UHMWPE is known to increase the incidence of a different damage mode, delamination, which is the dominant wear mechanism in tibial inserts but uncommon in THR, the effect of consolidation on adhesive and abrasive wear of UHMWPE is not clear. In this study UHMWPE resin was subjected to hot isostatic pressing under a pressure of 138 MPa at different temperatures (210°C, 250°C, and 300°C) to achieve varying degrees of consolidation. The extent of consolidation was determined by optical microscopy using thin sections, and by scanning electron microscopy using cryofractured and solvent etched specimens. Wear behavior of the samples with varying degree of consolidation was determined using a bi-directional pin-on-disc machine simulating conditions in a hip joint. Increasing the processing temperature decreased the incidence of fusion defects and particle boundaries reflecting the powder flakes of the virgin resin, improving the consolidation. However, the bi-directional pin-on-disc wear rate did not change with the processing temperature, indicating that adhesive and abrasive wear is independent of the extent of consolidation in the range of parameters studied here.
© 2003 Elsevier Science Ltd. All rights reserved.

Keywords: Ultra high molecular weight polyethylene; Wear; Total joint replacement; Processing temperature; Consolidation; Fusion defects

1. Introduction

Total hip and total knee arthroplasty are widely performed to recover joint functions when lost by trauma or disease and to relieve pain. Ultra high molecular weight polyethylene (UHMWPE) has been the material of choice for the fabrication of one side of the load bearing surface used in both total hip and total knee replacements. Damage to UHMWPE in vivo is an important factor that adversely affects the long-term performance of the reconstructed joint. Two primary damage mechanisms, namely delamination and adhesive/abrasive wear, are commonly observed in surgically explanted UHMWPE components. Delamination is initiated by sub-surface cracks, which propagate to the articulating surface, leading to the removal of relatively large (>0.5 mm) flake-like debris. Adhesive/abrasive wear generally follows the orientation and strain hardening of the implant surface and subsequent implant motion results in the removal of small wear debris, usually on the order of a few micrometers or less in size. Abrasive wear occurs through the rubbing action of the hard asperities on the surface of the femoral component. It is also accentuated by hard third body particles, such as bone chips or bone cement particles, within the articulation. Abrasive wear progresses by the cutting and removal of the polyethylene articular surface.

Peri-prosthetic osteolysis secondary to particulate debris is the major cause of long-term failure in total

*Corresponding author. Tel.: +1-617-726-3869; fax: +1-617-726-3883.
E-mail address: omuratoglu@partners.org (O.K. Muratoglu).

0142-9612/03/$ - see front matter © 2003 Elsevier Science Ltd. All rights reserved.
doi:10.1016/S0142-9612(03)00103-0
Questions? Contact FDA/CDRH/OCE/DID at CDRH-FOISTATUS@fda.hhs.gov or 301-796-8118

Records processed under FOIA Request #2014-8015; Released by CDRH on 12-8-2015

Table 1
Wear rate (mg/million cycles) of the test samples

Sample ID	Resin type	Temperature (°C) of hot isostatic pressing	Wear rate (mg/million cycles)
Ram Extruded	GUR 415	Not applicable	9.88 (±0.48)
H1-GUR	GUR 405	210	7.87 (±0.05)
H2-GUR	GUR 405	250	8.75 (±0.54)
H3-GUR	GUR 405	300	9.36 (±0.27)
H1-1900	Himont 1900	210	9.87 (±0.57)
H2-1900	Himont 1900	250	9.10 (±0.80)
H3-1900	Himont 1900	300	8.68 (±1.06)

hip replacements, leading to component loosening and in many cases resulting in revision surgery. The particulate debris is predominantly generated by the adhesive/abrasive wear of UHMWPE articular surface [1–4]. Therefore, research efforts have been concentrated on understanding the structure-property relations pertaining to UHMWPE and improving both forms of its damage resistance.

UHMWPE is synthesized through a Zieglar-Natta catalyst in the form of resin flakes [5]. The average molecular weight is typically 4–6 million grams per mole, which results in a high entanglement density and high melt viscosity. As a result, large-scale melt processing of the resin is not possible. Most UHMWPE articles are machined from consolidated stock. The consolidation is commonly carried out by either ram extrusion or compression molding, both of which rely on sintering the resin flakes at an elevated temperature and pressure. Consolidation fuses the resin flakes but generates distinct boundaries between the flakes [6]. The high entanglement density of the UHMWPE molecules is thought to prevent self-diffusion and result in the formation of these flake boundaries. In addition to the ubiquitous flake boundaries, fusion defects are found in the consolidated UHMWPE as well [7–10]. Fusion defects have been attributed to the agglomerated calcium stearate additive and poor consolidation [6].

It has been proposed that the in vivo UHMWPE damage may be a function of the degree of consolidation, and should decrease with the elimination of fusion defects or flake boundaries. There is clinical evidence for an increase in delamination type wear in tibial knee inserts with decreasing degree of consolidation. For instance, Mayor et al. [11] found a statistically significant correlation between fusion defects and delamination and cracking in a UHMWPE tibial knee insert used in total knee arthroplasty. Landy and Walker [12] also related the occurrence of delamination type wear in a knee joint to fusion defects in the material. Similarly, Walker et al. [13] and Blunn et al. [14] proposed that fusion defects serve as initiation sites for cracks, which under repeated loading results in the release of wear particles. While the detrimental effect of poor consolidation on the delamination resistance of UHMWPE is well documented, its effects on adhesive and abrasive wear are not known.

The aim of the present study was to investigate the adhesive and abrasive wear behavior of UHMWPE with varying degrees of consolidation. Two different types of UHMWPE resins, namely Himont 1900 and GUR 405, were included in the present investigations. These resins are surgical grade resins used in the fabrication of both tibial inserts and acetabular liners. The degree of consolidation was varied by changing the processing temperature during hot isostatic pressing. The wear tests were carried out using a bi-directional pin-on-disk machine capable of producing adhesive and abrasive wear mechanisms [15] (Table 1).

2. Methods and materials

Two types of UHMWPE resins were studied, namely GUR 405 (Hoechst Celanese, League city, TX) and Himont 1900 (Himont USA, Wilmington, DE), which were obtained in their powder form. The Himont 1900 resin contained no added calcium stearate. The resins were stored for less than 5 months prior to consolidation and testing. The virgin resins were consolidated by hot isostatic pressing at different temperatures to achieve varying degrees of consolidation. Hot isostatic pressing involves the application of hydrostatic gas pressure at elevated temperatures as opposed to uniaxial force used in ram extrusion and compression molding. The resins were first compacted in the form of a cylinder and subjected to cold isostatic pressing at 276 MPa at room temperature. The compacted specimens were then packaged and hermetically sealed under vacuum. The specimens to be processed at 210°C were enclosed in a laminated foil bag made of Mil-b-131H Class 1 Type 1 sheet, and those specimens to be processed at 250°C and 300°C were enclosed in a thin stainless steel sheet can. The hot isostatic pressing was performed at Industrial Materials Technology, Andover, MA.

The processing temperatures included 210°C (H1), 250°C (H2), and 300°C (H3). Samples of both groups of

Questions? Contact FDA/CDRH/OCE/DID at CDRH-FOISTATUS@fda.hhs.gov or 301-796-8118

Records processed under FOIA Request #2014-8015; Released by CDRH on 12-8-2015

resins, GUR 405 and Himont 1900, were consolidated at 210°C, 250°C, and 300°C under a hydrostatic pressure of 138 MPa. During hot isostatic pressing the heat soak time and cooling rate were kept constant for all three processing temperatures at 2 h and 3°C/min, respectively. A commercially available ram extruded bar stock (Westlake Plastics, Lenni, PA) processed from GUR 415 resin was also included as a reference material.

Thin sections (20 μm) of the consolidated specimens were prepared by using a sledge microtome. These sections were analyzed using an Olympus BH2 (Olympus Optical Co., Tokyo, Japan) under transmitted polarized light. The presence of fusion defects and sphereulites were noted when present.

To visualize the boundaries of the virgin resin flakes, specimens were fractured after being submerged in liquid nitrogen for 1 h. The cryofractured specimens were gold coated and analyzed using a Stereoscan 240 (Cambridge Instruments, Cambridge, England) scanning electron microscope (SEM). Solvent-etching was used to qualitatively assess the extent of consolidation at the virgin resin flake boundaries as follows. Specimens were mounted in epoxy, polished with SiC paper and alumina powder of 0.05 μm particle size. After cleaning in an ultrasound bath of water, the epoxy mounted specimens were dipped in 98% Decalin at 150°C for 45 s. The etched surfaces were gold coated for SEM analysis.

A bi-directional pin on disc wear testing machine modeling the multidirectional motion of the hip joint was used to characterize the wear behavior of the consolidated specimens [15]. The bi-directional pin-on-disk machine rubbed a UHMWPE pin against a cobalt-chrome disk counterface with implant surface finish ($Ra = 0.38 \pm 0.005$ μin). The rubbing action followed a rectangular path (5×10 mm). The tests were conducted with 100% bovine serum (JRH Biosciences, Lenexa, KS) as lubricating medium. A Paul type load curve was used with a peak load of 267 N which resulted in a normal peak contact stress of 4.2 MPa [15]. The test frequency was 2 Hz. The polyethylene pins used for wear testing were cleaned and weighed at the beginning of the test, after 0.5 million cycles and at the end of the test after 1 million cycles. Two pins, 9 mm in diameter and 13 mm in height, of each series of both consolidated resins and the ram extruded GUR 415 bar stock were wear tested. The incremental wear rates measured at two intervals for the samples of each group were used to carry out an ANOVA two-factor with replication analysis. *P*-values less than 0.05 were considered significant.

3. Results

The analysis by optical microscopy confirmed the presence of fusion defects and some unconsolidated flakes in both the reference material (the ram extruded bar stock) and in the GUR 405 resin processed at 210°C. Himont 1900 resin processed at 210°C exhibited relatively fewer number of fusion defects as compared to GUR 405 resin processed at the same temperature. Consolidation improved for both resins as the processing temperature increased to 250°C and 300°C, as was observed with the decrease in the number of fusion defects and unconsolidated flakes.

The Himont 1900 samples processed at 250°C showed clusters of spherulites. The same resin consolidated at 300°C was completely spherulitic as shown in Fig. 1a. None of the GUR 405 samples exhibited spherulites as shown in Fig. 1b.

Fig. 2 shows representative SEM micrographs of the cryofractured surfaces of the materials studied. The reference material and the GUR 405 sample processed at 210°C exhibited a similar appearance on the cryofractured surfaces, a star-burst morphology. The fracture lines that border the star-burst features are thought to coincide with the borders of the powder flakes of the virgin resin. As the processing temperature of GUR 405 resin was increased to 250°C and 300°C, the star-burst pattern became less apparent, indicating an improvement in consolidation. The start-burst

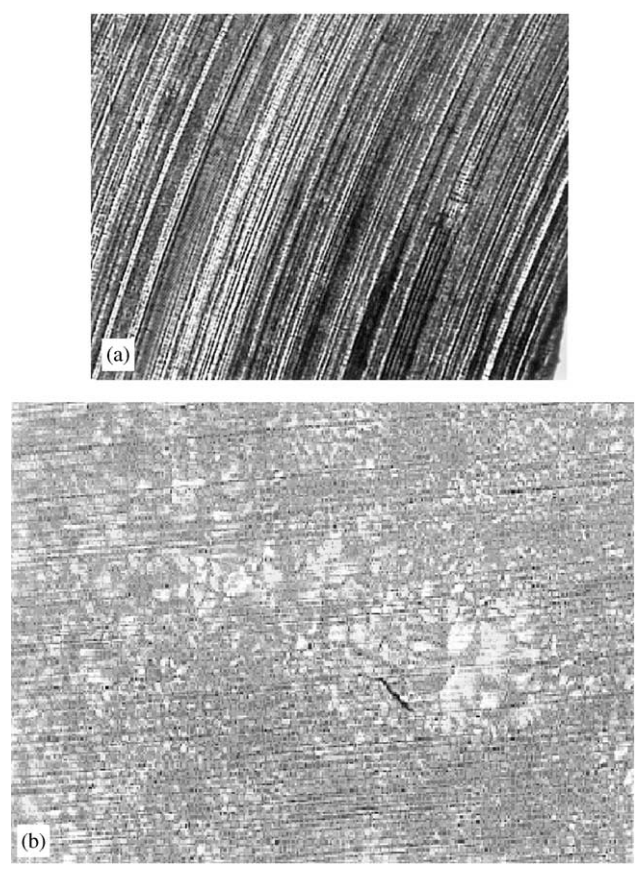

Fig. 1. Polarized light micrographs of the (a) Himont 1900 resin (b) GUR 405 resin hot isostatically pressed at 300°C and 138 MPa for 2 h, then cooled at a rate of 3°C/min. Clusters of spherulites can be observed in Himont 1900 sample (a).

Questions? Contact FDA/CDRH/OCE/DID at CDRH-FOISTATUS@fda.hhs.gov or 301-796-8118

Records processed under FOIA Request #2014-8015; Released by CDRH on 12-8-2015

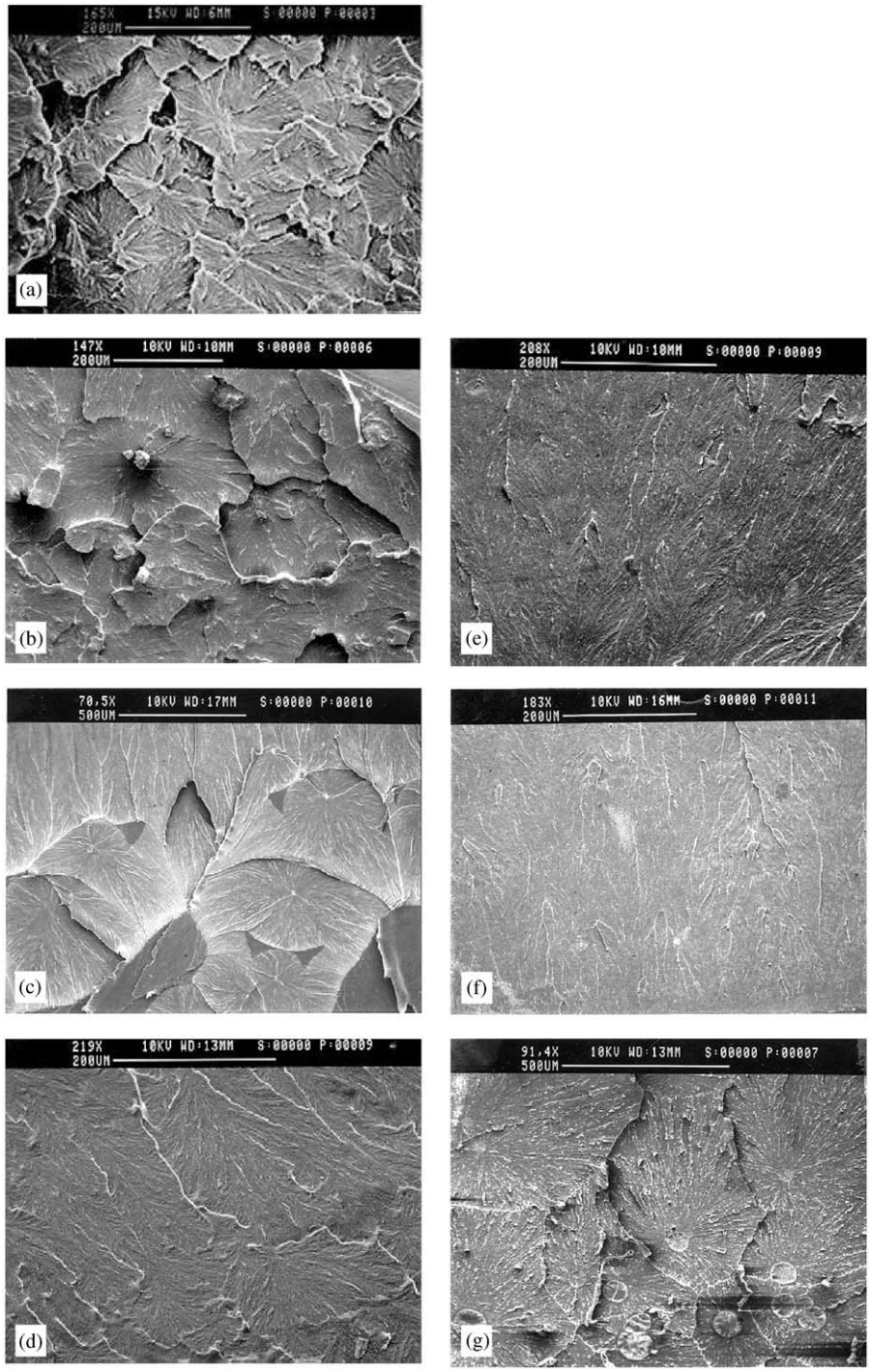

Fig. 2. Typical SEM micrographs of cryofractured surfaces of: (a) Ram extruded material (GUR 415 resin), GUR 405 resin that was hot isostatically pressed at (b) 210°C, (c) 250°C, (d) 300°C, and Himont 1900 resin that was hot isostatically pressed at (e) 210°C, (f) 250°C, (g) 300°C. The GUR 405 and Himont 1900 specimens were hot isostatically pressed at 138 MPa for 2 h, then cooled at a rate of 3°C/min.

morphology was not observed in the Himont 1900 resin processed at 210°C and 250°C, indicating better consolidation. The Himont 1900 resin consolidated at 300°C showed a spherulitic morphology (about 50 μm in diameter) on the cryofractured surface.

Fig. 3 shows representative micrographs of the solvent etched surfaces of the materials studied. The SEM analysis indicated extraction of material near the virgin resin powder boundaries. The particle structure was evident in both the ram extruded material and the GUR 405 sample processed a 210°C (Fig. 3a and b). At the processing temperature of 250°C, GUR 405 resin showed a more diffuse particle structure, indicating improvement in consolidation (Fig. 3c). At 300°C, there

Questions? Contact FDA/CDRH/OCE/DID at CDRH-FOISTATUS@fda.hhs.gov or 301-796-8118

Records processed under FOIA Request #2014-8015; Released by CDRH on 12-8-2015

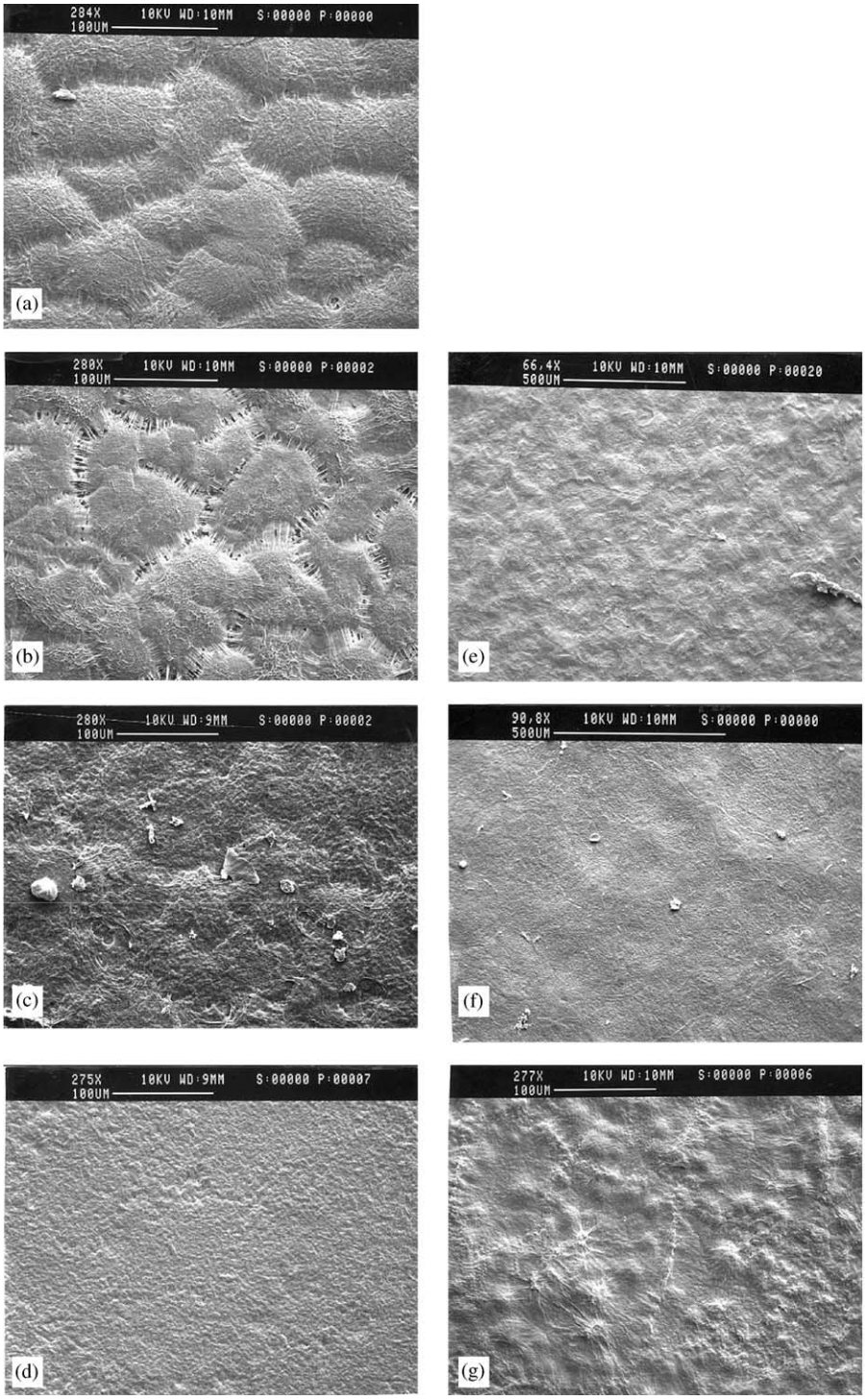

Fig. 3. Typical SEM micrographs of the solvent etched surfaces of all: (a) Ram extruded material (GUR 415 resin), GUR 405 resin that was hot isostatically pressed at (b) 210°C, (c) 250°C, (d) 300°C, and Himont 1900 resin that was hot isostatically pressed at (e) 210°C, (f) 250°C, and (g) 300°C. Etching was by immersion of a polished surface Decalin at 150°C for 45 s. The GUR 405 and Himont 1900 specimens were hot isostatically pressed at 138 MPa for 2 h, then cooled at a rate of 3°C/min.

was no evidence of particle structure, confirming significant improvement in consolidation. The solvent etched surface of the Himont 1900 resin processed at 210°C showed thinner particle boundaries as compared to the GUR 405 resin consolidated at the same temperature. At 250°C, the particle boundaries were no longer visible, indicating a well consolidated material. The solvent etched surface of Himont 1900 resin processed at 300°C showed a bumpy surface attributed to the presence of spherulites.

Questions? Contact FDA/CDRH/OCE/DID at CDRH-FOISTATUS@fda.hhs.gov or 301-796-8118

Records processed under FOIA Request #2014-8015; Released by CDRH on 12-8-2015

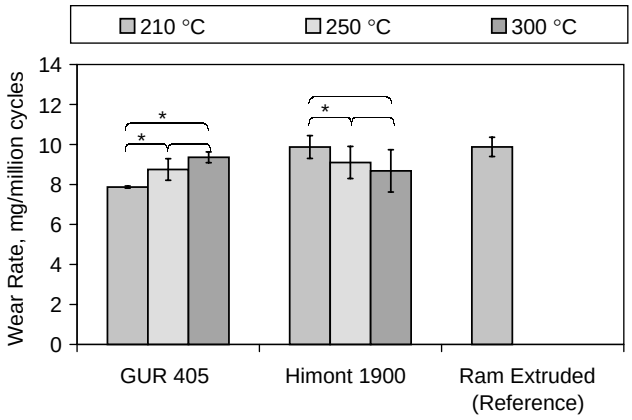

Fig. 4. Effect of processing temperature on the bi-directional pin on disc wear rate (mg/million cycles) of the GUR 405 and Himont 1900 resin. The ram extruded material is also shown for comparison.

Fig. 4 shows the effect of processing temperature on the wear rate of the various preparations of the GUR 405 and Himont 1900 resin. Ram extruded GUR 415 material is also shown for comparison. The ANOVA analysis showed that wear rate did not differ by resin type ($p = 0.19$). Similarly, the effect of consolidation temperature on wear rate was not significant ($p = 0.35$). The wear rate of GUR 405 resin increased with the processing temperature while the wear rate of Himont 1900 resin decreased with processing temperature. This interaction between the two factors was not significant ($p = 0.05$). The wear rate of the ram extruded material with its fusion defects and visible flake boundaries was comparable to those of the hot isostatically pressed GUR 405 and Himont 1900 resins even with varying degrees of consolidation.

4. Discussion

The degree of consolidation of both hot isostatically pressed type of specimens appeared to increase with increasing processing temperature. This improvement in increasing degree of consolidation is attributed to the increased chain mobility at higher processing temperatures. The Himont 1900 resin showed better consolidation than the GUR 405 resin at all consolidation temperatures studied. The number of fusion defects present in samples processed at 210°C was reduced by increasing the pressing temperature. Similarly, the extent of hot Decalin etching of the interparticle boundaries was reduced with increasing pressing temperature. The particle boundaries reflecting the powder flakes of the virgin resin were completely eliminated in the Himont 1900 resin at a consolidation temperature of 250°C. With GUR 405, the same level of consolidation was only achieved at the highest consolidation temperature, namely 300°C. The improved consolidation of the Himont 1900 resin over the GUR 405 may have been the result of lower average molecular weight and wider molecular weight distribution with the former. In addition, no spherulites were seen in the GUR 405 resin, while in the Himont 1900 resin spherulites were present at 250°C and 300°C. The formation of spherulites is an indication of increased chain mobility with the Himont 1900 resin when compared to GUR 405. The formation of spherulites might also be attributed to degradation in the Himont 1900 resin at higher processing temperatures, but, a preliminary infrared analysis of the consolidated resins showed no detectable carbonyl formation and hence no detectable degradation.

There were no significant changes with resin type and consolidation temperature on the adhesive/abrasive wear rate of UHMWPE. Overall the adhesive/abrasive wear resistance of all of the specimens of UHMWPE appeared to be independent of the processing temperature and was not a function of the degree of consolidation. This observation suggests that the adhesive/abrasive wear is a local surface process and is not affected by the bulk inhomogeneities in the material. It has been postulated that adhesive and abrasive wear takes place by the formation of a surface layer that is highly oriented in the direction of sliding induced by the uncoiling of the polymer molecules [16,17]. This oriented surface layer easily breaks up when the direction of sliding changes.

The present study showed that increasing the processing temperature of UHMWPE is accompanied by a marked improvement in its consolidation which was manifested by reduction in the number of fusion defects and visibility of flake boundaries upon extraction with hot Decalin. The adhesive/abrasive wear rate was independent of this improvement in the consolidation. Therefore, improving consolidation by increasing the processing temperature with hot isostatic pressing does not improve the wear behavior in total hip replacements.

Acknowledgements

The financial support for this project is provided by William H. Harris Foundation, Boston, MA.

References

[1] Wright TM, Bartel DL. The problem of surface damage in polyethylene total knee components. Clin Orthop Relat Res 1986;205:67–74.
[2] Kurth M, Eyerer P, Ascherl R, Dittel K, Holz U. An evaluation of retrieved UHMWPE hip joint cups. J Biomater Appl 1988;3:33–51.
[3] McKellop HA, Campbell P, Park SH, Schmalzried TP, Grigoris P, Amstutz HC, Sarmiento A. The origin of submicron

Questions? Contact FDA/CDRH/OCE/DID at CDRH-FOISTATUS@fda.hhs.gov or 301-796-8118

Records processed under FOIA Request #2014-8015; Released by CDRH on 12-8-2015

polyethylene wear debris in total hip arthroplasty. Clin Orthop Relat Res 1995;311:3–20.

[4] Wang A, Stark C, Dumbleton JH. Mechanistic and morphological origins of ultra-high molecular weight polyethylene wear debris in total joint replacement prostheses. Proc Inst Mech Eng Part H, J Eng Med 1996;210(3):141–55 [see comments].

[5] Muratoglu OK, Kurtz S. Alternate bearing surfaces in hip replacement. In: Sinha R, editor. Hip replacement. Current trends and controversies. New York, NY, 2002. p. 1–46.

[6] Kurtz SM, Muratoglu OK, Evans M, Edidin AA. Advances in the processing, sterilization, and crosslinking of ultra-high molecular weight polyethylene for total joint arthroplasty. Biomaterials 1999;20(18):1659–88.

[7] Rose R, Nusbaum H, Schneider H, Ries M, Paul I, Crugnola A, Simon S, Radin E. On the true wear rate of ultra high-molecular-weight polyethylene in the total hip prosthesis. J Bone Joint Surg 1980;62-A:537–49.

[8] Rose R, Radin E. A prognosis for ultra high molecular weight polyethylene. Biomaterials 1990;11(64–67.).

[9] Li S, Burstein AH. Ultra-high molecular weight polyethylene The material and its use in total joint implants. J Bone Joint Surg, Am 1994;76(7):1080–90.

[10] Olley RH, Hosier IL, Bassett DC, Smith NG. On morphology of consolidated UHMWPE resion in hip cups. Biomaterials 1999;20:2037–46.

[11] Mayor MB, Wrona M, Collier J, Jensen JW. The role of polyethylene quality in the failure of tibial knee components. In: Proceedings of the 39th Orthopaedic Research Society, San Francisco, CA, 1993.

[12] Landy MM, Walker PS. Wear of ultra-high-molecular-weight polyethylene components of 90 retrieved knee prostheses. J Arthroplasty 1988;3(Suppl.):S73–85.

[13] Walker P, Blunn G, Joshi A, Sathasivam S. Modulation of delamination by surface wear in total knees. In: Proceedings of the 39th Annual Orthopaedic Research Society. San Francisco, CA, 1993.

[14] Blunn G, Joshi A, Walker P. Performance of ultra-high molecular weight polyethylene in knee replacement. In: Proceedings of the 39th Annual Orthopaedic Research Society. San Francisco, CA, 1993.

[15] Bragdon CR, O'Connor DO, Lowenstein JD, Jasty M, Biggs SA, Harris WH. A new pin-on-disk wear testing method for simulating wear of polyethylene on cobalt-chrome alloy in total hip arthroplasty. J Arthroplasty 2001;16(5):658–65.

[16] Edidin AA, Pruitt L, Jewett CW, Crane DJ, Roberts D, Kurtz SM. Plasticity-induced damage layer is a precursor to wear in radiation-cross-linked UHMWPE acetabular components for total hip replacement. Ultra-high-molecular-weight polyethylene. J Arthroplasty 1999;14(5):616–27.

[17] Jasty MJ, Goetz DD, Lee KR, Hanson AE, Elder JR, Harris WH. Wear of polyethylene acetabular components in total hip arthroplasty An analysis of 128 components retrieved at autopsy or revision operation. J Bone Joint Surg 1997;79(A): 349–58.

Questions? Contact FDA/CDRH/OCE/DID at CDRH-FOISTATUS@fda.hhs.gov or 301-796-8118

Records processed under FOIA Request #2014-8015; Released by CDRH on 12-8-2015

Chapter 26

Tribological Assessment of UHMWPE in the Knee

Hani Haider, PhD

26.1 Introduction
26.2 Pin-on-disc Testing of UHMWPE Destined for Knee Replacements
26.3 Testing UHMWPE within Whole TKR Systems
26.3.1 Degrees of Freedom and a Suitable Joint Coordinate System
26.3.2 Brief History of Knee Wear Simulators
26.3.3 Contemporary Knee Wear Simulators and the Much-Debated Force- versus Displacement-Control Paradigms
26.3.4 Force-Control TKR Simulation for UHMWPE Wear Testing
26.3.5 Soft Tissue Simulation in the Force-Control Test Method
26.3.6 TKR Kinematics Measured from the Force-Control Wear Testing Method
26.3.7 Standardization of the Displacement-Control TKR Simulation Method for Wear Testing
26.4 Considerations and Pitfalls in Knee Wear Testing of UHMWPE
26.4.1 Variable Control and the Number of TKR/UHMWPE Samples to Test
26.4.2 Soaking UHMWPE Prior to Testing and Soak Controls during Testing
26.4.3 Symmetry of Applied Inputs and Simulator Tuning
26.4.4 Choice of Lubricant in Testing UHMWPE Wear in Knee Replacements
26.5 Concluding Remarks and Future Directions in UHMWPE and TKR Longevity Test Methods
References

26.1 INTRODUCTION

The era of mass users of total knee replacement (TKR) is quickly approaching, and virtually all current TKR designs use UHMWPE as a bearing component. With rising demand for TKR from a significant part of the aging population, more manufacturers and more types of prostheses continue to emerge, and the number of surgeons who carry out TKR and revision operations is probably increasing fastest of all. Testing of such variety of implants poses a challenge. Testing itself needed to be standardized to help the industrial design process and to help the regulatory bodies (e.g., FDA in the United States and CE in Europe) in the screening of implants prior to their use clinically.

Testing of implants can be generally categorized into *in vivo* and *in vitro* testing. The former is described in Chapters 23 and 28. In this chapter we are concerned with *in vitro* tests. The obvious main benefit of such tests is that the evaluation can be made at the TKR design and prototyping stage and thus can not only screen risks prior to clinical use but can aid with useful feedback to the design process. Also, most variables can be more easily, systematically, and precisely controlled *in vitro*, almost to the level of elimination, for highly useful comparisons between implants prior, during, and after their design. Uncontrolled variables can, on the other hand, greatly complicate *in vivo* testing and results interpretation (see Section 26.4.1 for examples of such errors).

Durability testing is only a subset of a wide and growing range of possible other *in vitro* TKR motion tests [1]. These include early lower limb simulators for testing knee implants in cadaveric specimens [2], the Oxford Rig [3, 4],

UHMWPE Biomaterials Handbook
Copyright © 2009, Academic Press, Inc. All rights of reproduction in any form reserved.

Questions? Contact FDA/CDRH/OCE/DID at CDRH-FOISTATUS@fda.hhs.gov or 301-796-8118

Records processed under FOIA Request #2014-8015; Released by CDRH on 12-8-2015

variations of it for 3-D motion of the knee to investigate ligament length patterns [5], and continuing upgrades such as with the Purdue Simulator [6, 7], and even later versions to assess deep knee flexion [8]. There are also special simulators with multiple muscle actuators to measure cruciate ligament strain [9], multiaxial freedoms and actuators to assess TKR constraint [10], or the robotic type of simulators for studying the role of ligaments in cadaveric knees [11] and lately robotic simulators [12, 13] for studying high knee flexion too. Wear testing of UHMWPE in a TKR is typically done on what is commonly referred to as a "knee simulator," but wear testing should be viewed in the correct perspective of all those other types of tests, on machines that are also called sometimes called by the same name. This chapter contrasts and critiques the most common methods and simulators for wear testing of UHMWPE bearings in TKR.

It is clear to those who regularly perform knee wear testing, and especially those who try hard to do testing well, that the "devil is in the detail". With the exception of some specialist workshops (e.g., by ASTM) even scientific conferences appear lately to be more focused on results; they leave little room for detailed discussion, especially on methodological detail where most of the variability in results emanate, in the author's view. Nevertheless, this chapter is still not a detailed how-to manual. International standards (where available) are cited instead. Published international standards typically describe such methods in sufficient detail. Nor is this text a review of the results of TKR tests from the literature, as useful as that may be. The results are too many and varied; only some are cited here to illustrate specific points. The main emphasis here is on matters of rationale and know-how to avoid pitfalls in the choice of test methods, in their implementation, and in the interpretation of results. This emphasis should help engineers in the orthopedic industry and in the research community who hunger for the type of detail they cannot usually find in published research papers, usually for lack of space in such result-oriented research articles.

Standardized test methods and international standards are neither yet sufficiently mature nor are they rigorously or uniformly applied. The evolution of standards is naturally slow because of their almost consensus-based nature, having to be unambiguously clear, very doable, and inclusive of sometimes conflicting styles and constraints.

Four categories of durability wear tests are typically done for UHMWPE destined for a TKR application: (1) pin-on-disk material screening tests, (2) force-control knee simulator tests, (3) displacement-control simulator tests, and (4) special damage mode simulation tests. The other (first three) categories will be described at varying levels of detail in this chapter. The second and third test methods will be preceded by describing some general considerations of the biomechanics of the knee, coordinate systems, and the physical variables involved. This will set the scene for a brief portrayal of the history of knee wear simulator development, not surprisingly setting the scene also for the much debated force- and displacement-control testing approaches. The difference between those will be critically highlighted. The final category of testing wear of UHMWPE in TKR relates to variances of these methods to screen for special failure modes, such as on TKR stabilizing posts, high flexion, and those specific for mobile bearing TKRs. This category of testing is not dealt with here because it is typically custom designed to address suspected particular design-related failure modes. Reference to standardized testing techniques is frequently made in the text, elaborating wherever possible on the rationale behind such methods.

26.2 PIN-ON-DISC TESTING OF UHMWPE DESTINED FOR KNEE REPLACEMENTS

Pin-on-disk (POD) is essentially a materials tribology test that is frequently used to screen materials rather than whole TKR systems. Because it is only marginally within the scope of the chapter, this category of tests will be only briefly visited here to highlight special considerations required for TKR testing applications.

In POD testing of UHMWPE for TKR systems, a single station or multistation machine is configured to articulate the end of a pin onto a flat disk to measure frictional and wear characteristics of the given material pair. The setup usually provides for a constant or dynamically varying compressive force on the pin to induce a simulated stress level that would occur in the TKR *in vivo*. POD in general engineering testing (outside orthopedics) typically provides a reciprocating linear motion or curvilinear motion where a disk is rotated under a stationary pin with some compression applied. Resisting force to the pin is measured as well as the compressive force to estimate the coefficient of friction. In orthopedics, conventional UHMWPE or one of the many improved alternatives are tested in a POD configuration as a bearing material for TKR, or what is tested is an alternative metal, ceramic, or coated metal versus UHMWPE (e.g., a nanostructured diamond on a titanium alloy [14]). Among the many complications required here is whether to simulate just sliding, as in simply reciprocating pin or disk articular motion; or gliding [15], such as a metal pin translating relative to a UHMWPE disk, thus producing fatigue type loading and wear as well as adhesive wear of the polymer; or rolling, which is more like the latter but with less friction; or any combination of those effects.

Which one or combination of these motions are actually simulated (or occur) depends on whether the UHMWPE acts as a pin or disc, the shape of each, and whether either pin and/or the disk moves and how. A wide spectrum of POD test machines have therefore been used in a multitude of configurations from the very simple (e.g., linear reciprocal) to the highly sophisticated and flexible, such as

Questions? Contact FDA/CDRH/OCE/DID at CDRH-FOISTATUS@fda.hhs.gov or 301-796-8118

Records processed under FOIA Request #2014-8015; Released by CDRH on 12-8-2015

with two-axis computer driven motions for programmable cross paths (Figures 26.1 and 26.2).

What drove POD testing of UHMWPE for TKR to become exceedingly more complex is that UHMWPE wear is highly accelerated with multidirectional articular paths and cross-shear [16–19], as would occur in knee replacement implants. In one experimental pin-on-disk study [19], only 15 degrees of crossing motion in sliding increased wear over 10 times. Some studies suggested little reason to exaggerate angles of motion crossings beyond this angle. A recent study on *in vivo* kinematics of one TKR design and thorough postprocessing analysis of the crossing motion found the included angle of bidirectional crossing motion not to exceed 10 degrees [20].

FIGURE 26.1 The AMTI OrthoPOD. An example of a six-station computer controlled pin-on-disk test machine, programmable for two dimensional paths, environmentally controlled specimen chambers and with friction force measuring capability. This machine has variable dynamic compressive force and planetary gear pin rotations over a rotating disc platform with six specimen disk holders. Both motions are servo motor controlled and programmable for any two-dimensional paths, with frictional measuring capability.

FIGURE 26.2 MAX-Shear wear experimental testing system. Another example of a six-station computer controlled pin-on-disk test machine. Here a computer driven X-Y stage motor is used with static compressive force on each station [22].

There is a standard test method, ASTM F732 [21], for POD testing, which is comprehensive enough to provide guidance to delineate the motions previously described and attempt to map them to suitable UHMWPE applications across knee, hip, and other implants. This ASTM standard also gives sufficiently detailed procedures to simulate, actuate, measure, and document such POD testing.

The following are some technical considerations that are useful to remember when screening UHMWPE for a TKR application:

- Surface finish: It is obvious, but worth remembering, that when comparing alternatives of bearing couple materials (e.g., against UHMWPE), the surface finish, especially of the metallic material, has to be kept constant as a controlled variable. Sometimes the different surface finish is inherent in the alternative material (e.g., a surface that is difficult to polish, or much easier/cheaper to polish to achieve a superior smoother finish), and therefore the surface finish becomes one of the surrogate variables of interest. In POD tests of materials simulating orthopedic joint replacement conditions, the wear factor was found to rapidly increase for Ra>50 nm values [23]. Considering this level is about the highest (roughest) used in polished metallic articulating surfaces for implants, it is wise to have surfaces polished well below this value in POD tests.
- Edge effects: It is unlikely that full alignment can be achieved and maintained for good control of contact area (and stress) with a flat metal pin articulating on a flat UHMWPE surface. The edge effects would dominate and can be highly complicated with reversing and crossing motions. Metal pins need to be spherical or highly convex, with the contact areas then approximated using "Hertzian" contact [24]. UHMWPE pins can be flat; with reasonable alignment and some deformation, good predictable contact area can be maintained.
- Wear versus wear rate or wear factor: Attention should be given to expressing or interpreting the results from POD tests. In some cases, wear is presented as a wear factor, typically the volumetric wear per unit load and (per unit) distance of articular motion. This implies some dependence on stress, which is itself disputed and adds confusion (discussed later).
- Stress level: Care should be taken in selecting a combination of load and pin contact area to reproduce the

Questions? Contact FDA/CDRH/OCE/DID at CDRH-FOISTATUS@fda.hhs.gov or 301-796-8118

Records processed under FOIA Request #2014-8015; Released by CDRH on 12-8-2015

stress levels expected in the knee. TKR stresses are typically higher than for hips and span a wider range (e.g., 2–50 MPa) depending on the TKR design [25]. The dependence of wear of UHMWPE on contact stress and apparent contact area is inconsistent in the published literature [26–31]. Wear was found not to (necessarily) rise with stress in the loading regime of TKR according to some of these studies. Wear of UHMWPE in the stress range for orthopedic implant applications is as (or even more) sensitive to the contact area [28]. The wear factor in one study was even found to decrease with rising stress at the low stress levels in the range above [31]. At low stress, higher contact areas engage more of the surface asperities, giving more opportunities for material removal. Therefore, the combination as well as the contact area and stress individually need to be physiologically realistic or take account of the worst case scenarios in the design of a POD UHMWPE screening test for TKR.

- Constant or dynamic load: To simulate the loading of a convex TKR femoral component surface with sliding, gliding, and rolling against UHMWPE, the compressive load in a POD test needs to be dynamic and intermittent to induce dynamic UHMWPE stresses with reasonable representation of lubrication replenishment of the articulating surfaces. This is typically achieved through dynamic varying of the load on the pin (for example in the system of Figure 26.1). With a UHMWPE pin, articulation on a smaller area of the poly is maximized, and wear measurements of UHMWPE weight loss are relatively more accurate given small weight pins. Alternatively, the UHMWPE material can be configured as the larger area (disk) bearing material, with a metallic pin having a spherical articulating surface, mimicking more directly TKR bearing systems (e.g., the system of Figure 26.2 [22]). In the latter situation, the actual contact area has frequently been approximated using a simple Hertzian ball-on-flat contact mechanics model [24]. Such estimates have, in the past, provided reasonable approximations when cross-validated with finite element analysis computations and static pressure sensitive film experiments [32]. Care should still be taken because the TKR loading is complex in that it is dynamic, noting that Hertzian contact theory relies on several assumptions, among which are small, frictionless, and continuous contact surfaces, which both deform [24]. A typically metallic femoral component is almost infinitely rigid in most designs compared to a UHMWPE tibial bearing insert.
- Direct volumetric measurement of UHMWPE wear: Wear estimates that rely on thickness (or surface scanning) measurements are plagued with creep and recovery errors associated with viscoelastic deformation and some shape memory properties in UHMWPE [33]. Where possible, such techniques should be avoided, in the author's opinion, or the creep and recovery errors should be comprehensively accounted for, with great difficulty.

26.3 TESTING UHMWPE WITHIN WHOLE TKR SYSTEMS

26.3.1 Degrees of Freedom and a Suitable Joint Coordinate System

The intact knee joint, or one with an installed TKR implant, has 6 degrees of freedom. Because there is no rigid linkage between the bones, the femur exercises three displacements and three rotations (relative to the tibia), and vice versa, to varying levels. Any structure with components capable of rotation and translation in three dimensions can be greatly complicated without a suitable choice of axes for these motions. Typically, the final position/orientation of the structure is influenced by the order (sequence) of motions along and rotations about these axes. A Cartesian coordinate system fixed in space would obviously not be a good choice for the knee. It is much more efficient to fix such an axis system to one bony segment (typically the tibia, based on defined anatomical landmarks) and have the other bone(s), defined similarly, move relative to the first. With simple Cartesian axes, the kinematic position would depend on the order in which the rotations (usually termed Eulerian angles) occur, and it would therefore be complex to describe the knee motions, let alone simulate, actuate, and control them in a wear testing machine. The sequence of rotations, which in reality need to occur simultaneously, would influence the desired kinematic state, compromising both accuracy and speed of response of a simulator.

Various schemes have been published to characterize the natural knee motion, including estimates of the effective axis of flexion by relating it to known anatomical landmarks, such as the transepicondylar line [34]. Various medial pivoting themes [34, 35] have attempted to model the apparent coupling between AP translation with IE rotation and flexion. The posterior femoral rollback onto the proximal tibia, combined with the internal rotation of the tibia with higher flexion, was approximated to a simpler rotation around a proximal-distal axis fixed at the center of the medial compartment of the tibia. Some themes went further to ascribe a helical motion [36] (more widely known as screw motion) to the knee. These comprehensive studies with astute observations have contributed to our understanding of how the knee moves. It is however important to remember that they mostly represented unloaded (passive) knee motion, and it was not clear how they could provide quantitative and unambiguous coordinate axes around which practical knee wear simulators could be built.

The main desire is to have a system that precisely and unambiguously describes the relative position between the femur and tibia and their relative motions in time. The coordinate

Questions? Contact FDA/CDRH/OCE/DID at CDRH-FOISTATUS@fda.hhs.gov or 301-796-8118

Records processed under FOIA Request #2014-8015; Released by CDRH on 12-8-2015

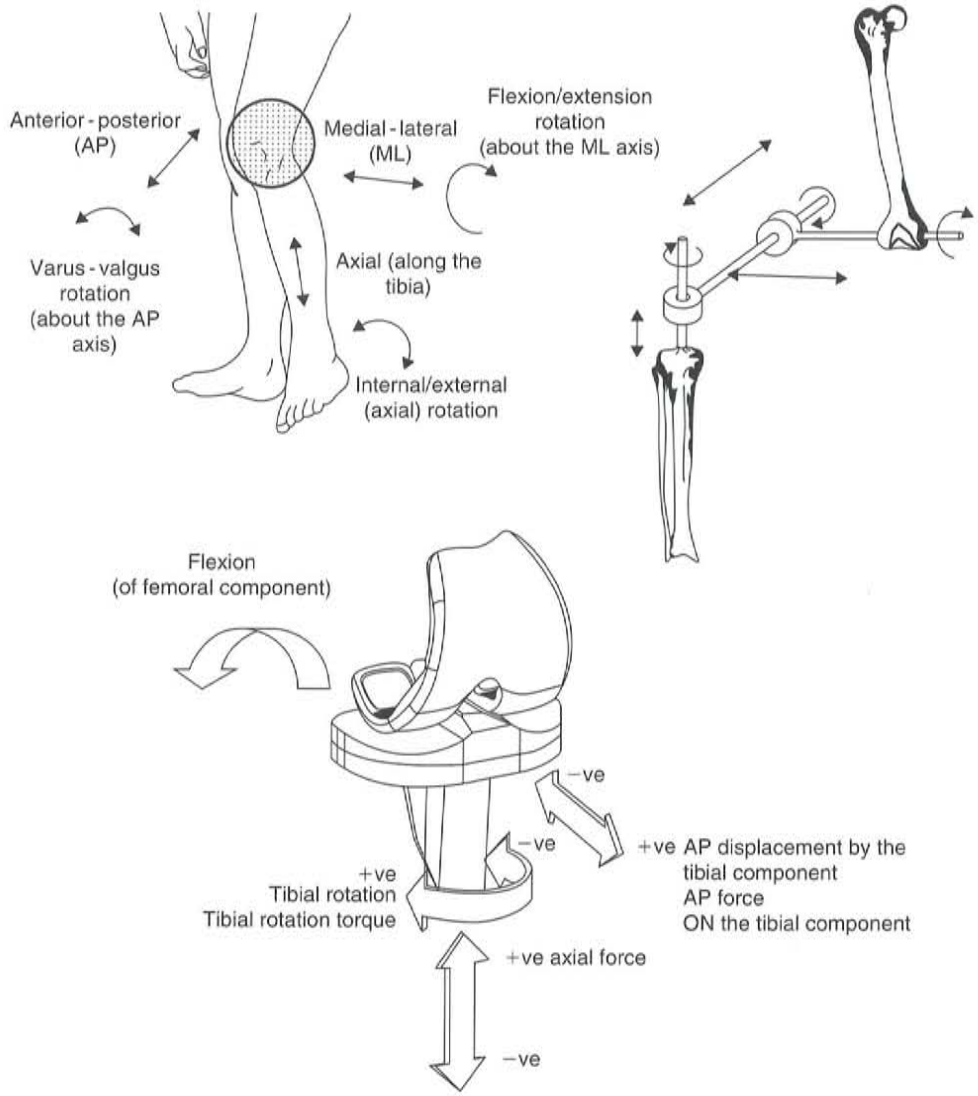

FIGURE 26.3 Top left: Anatomically-based axis system and degrees of freedom of the human knee joint. Top right: Schematic depicting the Grood and Suntay [37] knee coordinate system with a ML (flexion) axis, which floats in the AP direction. Bottom: Application to a left TKR. Note: External forces and torques ON which components, and motion BY which component. (This sign convention is consistent with ISO 14243-1 [38], and a version of this diagram has been suggested for insertion into a revision of this standard.)

system most typically approximated in knee simulators, to varying degrees of success, was proposed by Groot and Suntay [37], illustrated in Figure 26.3. It conceptualizes a four-link kinematic chain, of which the tibia and femur are the first and last, each along an axis fixed to the tibia and femur respectively (as body-fixed axes). Two imaginary links are placed between the body fixed axes; these are not fixed to either bone. Abduction or varus-valgus occurs around one, and flexion around the other, the latter being a "floating" axis which is allowed to translate in the anterior-posterior direction. In the way it was defined, this system provided a set of independent generalized coordinates that harnessed commonly employed clinical terminology and permitted precise definitions of clinical descriptions of knee motion. It allows unambiguous measurements and control of flexion-extension (FE), varus-valgus (VV), and internal-external (IE) (sometimes called axial) rotations, and anterior-posterior (AP), medial-lateral (ML), and proximal-distal (axial) displacements. Note that in this system, within realistic physiological ranges of knee motion, the rotations actually appear to commute. This means that the net final position of the femur relative to the tibia becomes independent of the sequence of the individual rotations. When understood and applied well, this system brought a much needed simplification for knee simulators.

Literally (loosely!) resembling a mechanical hinge, the knee joint mainly provides FE rotation with an angle range of approximately −5 degrees to 140 degrees. Very moderate ranges of axial (lift-off), medial-lateral displacement, and varus-valgus rotation occur. These three degrees of freedom are highly constrained by a mixture of some surface congruency of the tibia-femoral interfaces, the cruciate and collateral ligaments, and other soft tissue. While also moderately

Questions? Contact FDA/CDRH/OCE/DID at CDRH-FOISTATUS@fda.hhs.gov or 301-796-8118

Records processed under FOIA Request #2014-8015; Released by CDRH on 12-8-2015

constrained by the same mechanisms, the knee is relatively more lax on the remaining two degrees of freedom. The AP translation (approximately ±10 mm) helps adjust the effective torque arm length of the quadriceps muscles to balance the flexion/extension moment due to gravity of the body, and it prevents bony impingement at high flexion angles. While the knee joint is flexed, the center of mass of the body above the knee acts with a moment arm (about the ML axis) of many inches in length, whilst the moment arm of either muscle (quadriceps or hamstrings) group is a fraction of this distance. Large muscle forces and joint reactions result, which reach multiples of human body weight.

The flexion moments themselves are of central interest in many biomechanic texts and clinical gait studies [39]. However, our interest in them in TKR testing is indirect only, as the flexional frictional resistance is modest in simulators when testing very low friction TKR bearings. Nevertheless, those large muscle forces also produce large joint reaction forces in a TKR, which have major components axially and significant components in the AP direction [25, 40]. These axial and AP knee joint reaction forces need to be reproduced in TKR and UHMWPE wear testing, and they are usually reproduced by actuating them as forces or reproducing the expected motions from them.

A simple qualitative observation of a human while walking shows the body swinging left and right a little as well undulating up and down a little (typically 50 mm amplitude). The continuous acceleration/deceleration of the body center of mass adds modest perturbations to the joint reaction forces (typically reaching 15%). The slight twisting of the body over the load bearing foot necessitates transmission of a time varying axial torque (and rotation) between the tibia and femur, with an angular range of up to approximately ±30 degrees. The AP translation and IE rotation motions, superimposed on flexion extension, while the knee doubles in function as a hinge and a thrust bearing, are crucial factors on wear and durability of UHMWPE in TKR implants.

A wide range of TKR designs has emerged over the years (see Chapters 7 and 8), all aiming to cater for this complexity. Some are generically different from the anatomically shaped bicondylar type. In one extreme, various early implants were simple hinge designs with essentially one degree of freedom. On the other extreme, mobile bearing TKRs are extremely lax; they have different translational and rotational degrees of freedom provided by separate bearing mechanisms within. Rotating hinge revision TKRs are an example where a simple hinge design rotates on a secondary thrust bearing so the whole TKR assembly offers unconstrained relative rotation about two axes and effectively infinite stiffness rotationally in varus-valgus and translationally in AP. Some mobile bearing TKRs offer all six degrees of freedom with highly nonlinear and highly discontinuous stiffness because of unconstrained axial rotation and/or AP translation limited sometimes by rigid mechanical stops.

26.3.2 Brief History of Knee Wear Simulators

The earliest wear simulator that the author has read about was a 1973 knee and hip machine that provided flexion with axial force only, in which knees were tested in Ringer solution [41]. The first machine designed to specifically simulate and measure TKR wear was developed in Leeds in the mid- to late-1970s [42]. It was a single station hydraulic machine through which axial compressive and anterior-posterior forces were applied in synchrony with flexion, using drip-fed distilled water as lubricant. The AP was force controlled between 66 N in the anterior and 220 N in the posterior directions (respectively) in a (busy!) waveform that reversed the force direction seven times. The VV and IE were allowed to freely rotate. In a later study [43] published on this simulator, wear (and of course creep) was estimated from the penetration of the metallic femoral component into the polyethylene as measured optically by reflective dual-index holography. The UHMWPE bearing insert was coated with a 0.1 nm thick pure aluminum coating (by vacuum vapor deposition) to improve the quality of the optical contouring process, before and after the test (the coating was removed during the actual testing!). That simulator was reported to capture both adhesive and abrasive wear, and the wear factors that resulted were similar to those of pin-on-disk studies (with water also).

Motivated by the need to test the (then) revolutionary new concepts in rotating platform mobile bearing knee designs, the New Jersey simulator provided flexional rotation, axial compressive force, AP motion, and IE rotation [44, 45].

Both the Leeds and the New Jersey knee machines must have been pioneers of their time in wear simulators because, even as late as 1992, knee wear simulator designs were being published, which provided for only axial force varying with flexion [46]. Such simulators had IE free to rotate, and ML and VV were locked but adjustable during setup for alignment. AP displacement was coupled mechanically with flexion to provide "partial constraint of the centroid path" [46].

The preceding were all single (test) station machines. The need for multiple stations in a knee simulator was soon felt. It is important to note that wear is a gradual damage accumulation process that results from highly repetitive gait activities, such as walking. TKR implants *in vivo* need to survive tens of years in service, and thus millions of cycles of walking at least. Considering the polymeric nature of UHMWPE and its viscoplastic behavior (see Chapter 35), there would be a speed limit on experimental simulation of loading, and this is typically chosen to be about 1 Hz and should not exceed 1.5–2 Hz at most. Considering that a typical TKR patient would walk 1–2 million cycles (MC) per year, reasonable simulations should therefore last at least 5 million cycles or more to represent a reasonable duty period *in vivo*. With those low frequencies, a typical TKR wear test with overheads of setup time, breakdown

Questions? Contact FDA/CDRH/OCE/DID at CDRH-FOISTATUS@fda.hhs.gov or 301-796-8118

Records processed under FOIA Request #2014-8015; Released by CDRH on 12-8-2015

for maintenance, and wear measurements would last a minimum of 2.5 months but typically up to 6–9 months. Therefore, a knee simulating machine for wear testing has to have many stations to be practical and usefully test, compare, and screen TKR designs. The earliest multichannel knee simulator was a 12-station machine that provided flexion and axial force only for testing tibial fixation [47].

In 1997 work on the Durham simulator was published, which was specifically designed as a TKR wear simulator, with six test stations [48]. This actuated and controlled flexion, axial force, and AP motion under displacement control (range ±15.6 mm), with fixed ML position and passive rotations allowed for IE and VV. This study ran an 8 million cycle test on one of this simulator's stations and highlighted the importance of long wear tests. Diluted bovine serum was used for lubricant. Only a very modest wear rate of 2.62 mg/MC resulted in that study, presumably because of the absence of actuated IE or torque or rotation, and therefore cross-paths of UHMWPE must have been undersimulated.

Almost at the same time, 1997, early work to develop the Stanmore knee simulator was published in preliminary concept on one prototype station [51]. This simulator allowed dynamic flexion and axial force variation like all the others, with ML and VV freedoms, but also provided for dynamic servo control of AP *force* and IE *torque* as inputs and physically simulated some restraint to the AP and IE motions with simple elastomeric bumpers. However, besides being single station, soft elastomeric bumpers of course could not provide a consistent stiffness between tests or even a constant stiffness within a test for millions of simulator cycles. A full-fledged later implementation of the same concept from Stanmore/England was the four-station force-controlled knee simulator (Figure 26.4 and Figures 26.8–26.10) with springs instead of bumpers [49, 50]. It also featured AP force and IE torque actuations that were more decoupled and provided more precise freedoms in ML and VV. This configuration provided the basis for a TKR wear testing methodology [38, 49, 50, 52–55] known as force control, which continues to be refined even at the present day, and more of it will be described later in this chapter (see Section 26.3.4).

Meanwhile, displacement-controlled knee simulators continued to be developed in a variety of configurations and used for TKR testing. Examples of those machines are the early version of the AMTI knee simulator (Figure 26.5), the Shore Western knee simulator (Figure 26.15), and the ProSim knee simulator (Figure 26.16). The test method used on those machines will be described in detail later in Section 26.3.8.

In capping the above brief summary of the development history of knee simulators, we note the emergence of two general trends, force-control and displacement-control knee simulators. The control refers to the way AP force/translation and IE torque/rotation were imposed on the TKR. These two trends have been much debated and

FIGURE 26.4 Lower left and right: First version of the Stanmore Knee Simulator [49, 50]. The electronics of this simulator have been upgraded by the Instron Corporation, and the mechanics have been upgraded in Nebraska as shown in Figure 26.8.

FIGURE 26.5 Hydraulic six-station displacement-control Knee Wear Simulator by AMTI, Watertown, Massachusetts, USA.

Questions? Contact FDA/CDRH/OCE/DID at CDRH-FOISTATUS@fda.hhs.gov or 301-796-8118

Records processed under FOIA Request #2014-8015; Released by CDRH on 12-8-2015

continue to be the subject of exciting discussions to the present day. The two approaches have themselves evolved and gradually converged into two well-known standard test methods; the first is the force-control method, described in detail in ISO 14243-1 [38], and the second is displacement control, described in ISO 14243-3 [56]. They both specify the relative flexional angular movement between the articulating femoral and tibial components of a TKR, the pattern of the applied axial force synchronized with flexion, speed and duration of testing, sample configuration, and test environment to be used for the wear testing of UHMWPE. The two methods differ in how AP forces and displacement are controlled and how tibial torques or rotation angles are controlled. In choosing which method to use, or in using either, it is important to realize the subtle but important differences and their implications. The two approaches are therefore described in more detail and more critically contrasted in the following sections.

26.3.3 Contemporary Knee Wear Simulators and the Much-Debated Force- versus Displacement-Control Paradigms

In durability testing of UHMWPE bearings in whole TKR systems, a simulating machine must inherently energize as many of the failure modes as can result from continual use of the TKR *in vivo*. To reproduce the wear mechanisms the correct combinations of loading and relative motion between the parts of the TKR must be actuated. Therefore, knee simulator machines, as well as provide multitest stations, correct temperature and lubrication environments; allow disassembly during testing to measure wear; perform repetitive cyclic actuations which best approximate to a realistic human activity such as walking; should importantly provide passive ML and VV freedoms; and actuate the important motions of flexion/extension, AP translation and rotation while the joint is fully loaded and undergoing

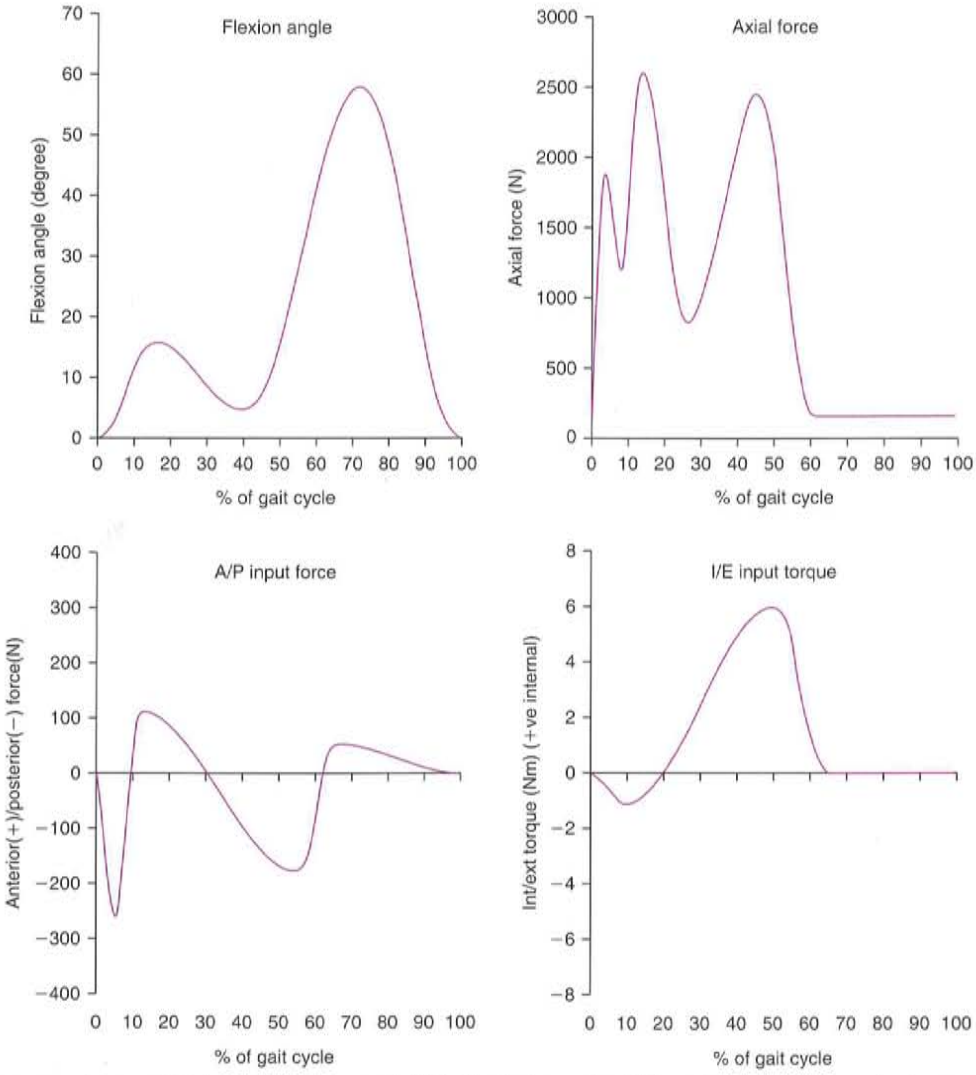

FIGURE 26.6 Input waveforms of ISO 14243-1 (force control) [38]. The flexion and axial force (top two plots) are also the same for ISO 14243-3 (displacement control) [56].

Questions? Contact FDA/CDRH/OCE/DID at CDRH-FOISTATUS@fda.hhs.gov or 301-796-8118

Records processed under FOIA Request #2014-8015; Released by CDRH on 12-8-2015

physiologically realistic joint reaction contact forces. It is almost a prerequisite, therefore, for any standardized TKR wear testing method that it should have predefined, clearly communicated, and easily implemented test conditions to ensure that an appropriate, physiologically realistic movement of the TKR parts in the AP plane occur throughout the test. As will be seen in the following discussion, this latter requirement presents the major difference between the two standardized knee wear test methods [38, 56].

Most current knee simulators treat the flexion angle as an independent variable to which all other variables are synchronized in time in a simulated dynamic gait activity (e.g., walking). Flexion/extension is the kinematic variable with the largest dynamic range within the knee and is easiest to measure externally on a moving human. Flexion has also been abundantly and accurately characterized for different human activities, so it yields itself as efficient in characterizing the phases of any cyclic human activity (or actuation waveform) on a simulator. Figure 26.6 (top left) shows the familiar two-peaked shape curve of flexion angle during walking used in both ISO test methods [38, 56].

Most TKR simulator studies apply the axial compressive component of the joint contact force in synchrony with flexion/extension. This is the largest external force in amplitude resulting from the body weight and its inertia, and compounded upon both are the significant quadriceps and hamstring muscle forces (depending on stance) at all flexion angles above zero. Figure 26.6 (top right) shows the force waveform typically used as input. These waveforms were based on the results of quasi-static analyses of a geometric model of the knee, with electro-myographic (EMG) measured data, ground-to-foot force, and kinematic data [57, 58].

Note the familiar triple peaks of force reaching multiple body weights during the stance phase (0–60% of the walking gate cycle between heel strike and toe off). Notice the modest flexion peak of only 15 degrees reached during the stance phase and the highest flexion peak reached at 58 degrees in the swing phase with nominal (but not zero) forces during the latter.

FIGURE 26.7 The EndoLab knee simulator. This four-station machine is servo-hydraulically actuated for full force-control testing with soft tissue simulation. One of the test stations can be optionally used as a loaded soak control station.

TKR wear is a complex function of the integral of the joint reaction forces and the rolling/sliding and crossing path motions between the implant articulating surfaces. The ratio of distances and velocities between rolling and sliding and the degree to which the motion paths cross are largely influenced by the anterior-posterior (AP) motion and internal-external (IE) rotation kinematics. Displacement-controlled simulation directly actuates input waveforms for the anterior posterior (AP) motion and internal external (IE) rotation of the tibial component relative to the femoral component in synchrony with axial force and flexion angle during walking. This type of dynamic position control allows for robust simulator mechanisms with prolonged wear simulation runs without excessive maintenance. It does, however, require prior and precise knowledge of the actual AP translations and IE rotations expected with ideal insertion *in vivo* for that particular TKR. For example, in a displacement-controlled simulator wear study [59] on a widely-used TKR design with a long clinical history, a normal walking gait was found to have a reasonable wear rate of 17 mg/Mc with a realistic AP displacement range, peaking at under 5.2 mm and a modest IE rotation range of 8 degrees. This wear rate dropped by a staggering 90% and 95% in the absence of AP motion and IE rotation in turn, respectively.

Even in the same (theoretically) assumed average patient with a (theoretically) ideal surgical installation, with a well defined/simulated repetitive gait activity, such motions would primarily depend on the detailed design (shape, materials, and surface finish) of the TKR's articular bearing surfaces, which actually govern its AP and IE laxity.

For example, there would be less AP displacement and IE rotation in highly constrained designs than for low constrained designs, and those kinematics may be much curtailed, or one could become zero for hinge-type revision TKR. Therefore, for simulation in a displacement-controlled regime, the precise kinematics need to be known beforehand, which has not been possible with new designs, except recently with unconfirmed degrees of accuracy using finite element analysis computation [60–62].

Importantly and as briefly explained elsewhere [63], even with a known clinically used design with presumably accurate kinematic data from *in vivo* tests (e.g., using fluoroscopy), displacement-control wear testing would be prone to a major flaw, in the opinion of the author, for the following reason: Some wear, or in some cases most of the wear, may occur in those regions of high compressive or shear stress interaction or impacts between the harder metallic femoral component and the softer UHMWPE bearing insert. Examples of those are impingements onto the posterior stabilizing posts or climbs over steep anterior or posterior ridges of the UHMWPE. The polyethylene deforms viscoelastically

Questions? Contact FDA/CDRH/OCE/DID at CDRH-FOISTATUS@fda.hhs.gov or 301-796-8118

Records processed under FOIA Request #2014-8015; Released by CDRH on 12-8-2015

FIGURE 26.8 Upgraded design of the Instron-Stanmore Knee Simulator. Three machines are located at the University of Nebraska Medical Center. Lower: Upgraded designs of flexion brackets, femoral component holders, and tibial component dishes, which are now stainless steel, round, and much larger to provide higher range of TKR motion and can accommodate optional serum bags to increase the amount of lubricant per station and extend the simulator for use with larger and different TKR designs. Middle left: Custom made femoral component holders as one-piece stainless steel jigs, which are precisely manufactured to fix to the main simulator femoral brackets and are directly cemented with an exact fit to a femoral component. Middle: Holder with femoral component cemented. Top left: Stations running without serum bags. Middle right: One specimen station viewed from the proximal anterior perspective.

in those regions under high stress contact. In force-control testing, the stresses in each cycle would continue to be physiologically realistic as the motions would self-adjust (minutely but automatically) to keep the forces and torque reactions as desired/assumed. In displacement-control testing, the motions are repeated by the simulator actuators precisely without any such adjustments. Imperfect alignment causes either exaggerated stresses from slight (e.g., a few micron) overimpingement, or it causes superficially attenuated stresses in those regions where the motions run minutely short of the physiologically realistic/assumed values. The viscoelastic deformation of an anterior ridge or stabilizing post in the early cycles also grossly alters the impact for later cycles. This would cause the wear during the majority of the test to be undersimulated.

Until 2004, there was no published standard nor agreed inputs for the displacement-control TKR testing. The nearest such document was a set of gradually evolving guidelines in an ASTM draft standard document, which has since been discontinued. The current ISO standard displacement-control test method [56] was based on the earlier developed force-control method [38] but prescribed new displacement-control inputs instead, and these inputs will be described later (see Section 26.3.7).

26.3.4 Force-Control TKR Simulation for UHMWPE Wear Testing

In force-controlled simulation, the knee is treated as a generalized joint required to transmit a deterministic AP force and IE torque across the knee to allow quasi-static equilibrium at each phase/instant of a slow ambulatory gait activity, such as walking. It is assumed here that for such equilibrium to occur, on an average simulated patient, at each posture within a repeated walking gait activity, the external forces acting on the knee joint as a full system (i.e., treated like a black box or surrounded by its own free body diagram) are independent of the design of the TKR implanted. With good estimates based on comprehensive studies, these forces and torques can then be treated as standard inputs and applied to any knee design during simulation of walking. The force-controlled simulation was thus intended to automatically replicate (*in vitro*) the kinematics and kinetics appropriate for that particular TKR design to simulate its wear.

The input waveforms for the force-control method (Figure 26.6) were originally adapted for the (then draft, now published) ISO 14243-1 standard [38] from the rich studies presented in the early 1970s by Morrison [58] and later results from other studies [57]. Morrison derived a comprehensive "quasi-static" theoretical model of the knee joint and computed knee forces based on ground-to-foot reaction force and kinematic data from gait studies and electro-myographic data with assumed/simplified anatomic geometric muscle insertion points. He also assumed zero coefficient of friction of the articulating surfaces, among many other assumptions. The force-control ISO standard itself [38] did not explain the process of how the input curves were devised. The curves were devised through a collaborative research study [50] that proposed and used the input waveforms without elaboration of how the curves were interpreted from the original cited studies.

Many investigators have had to check this validity themselves by reverting to the original studies cited because some have questioned the accuracy of the AP and IE torques and even their sign convention. Those attempts, to the knowledge of the author, verified those interpretations to be good approximations, including the sometimes disputed sign/sense of the AP force. Further, the waveforms continued to prove harmonious with other findings since. They were also verified to be physiologically realistic

Questions? Contact FDA/CDRH/OCE/DID at CDRH-FOISTATUS@fda.hhs.gov or 301-796-8118

Records processed under FOIA Request #2014-8015; Released by CDRH on 12-8-2015

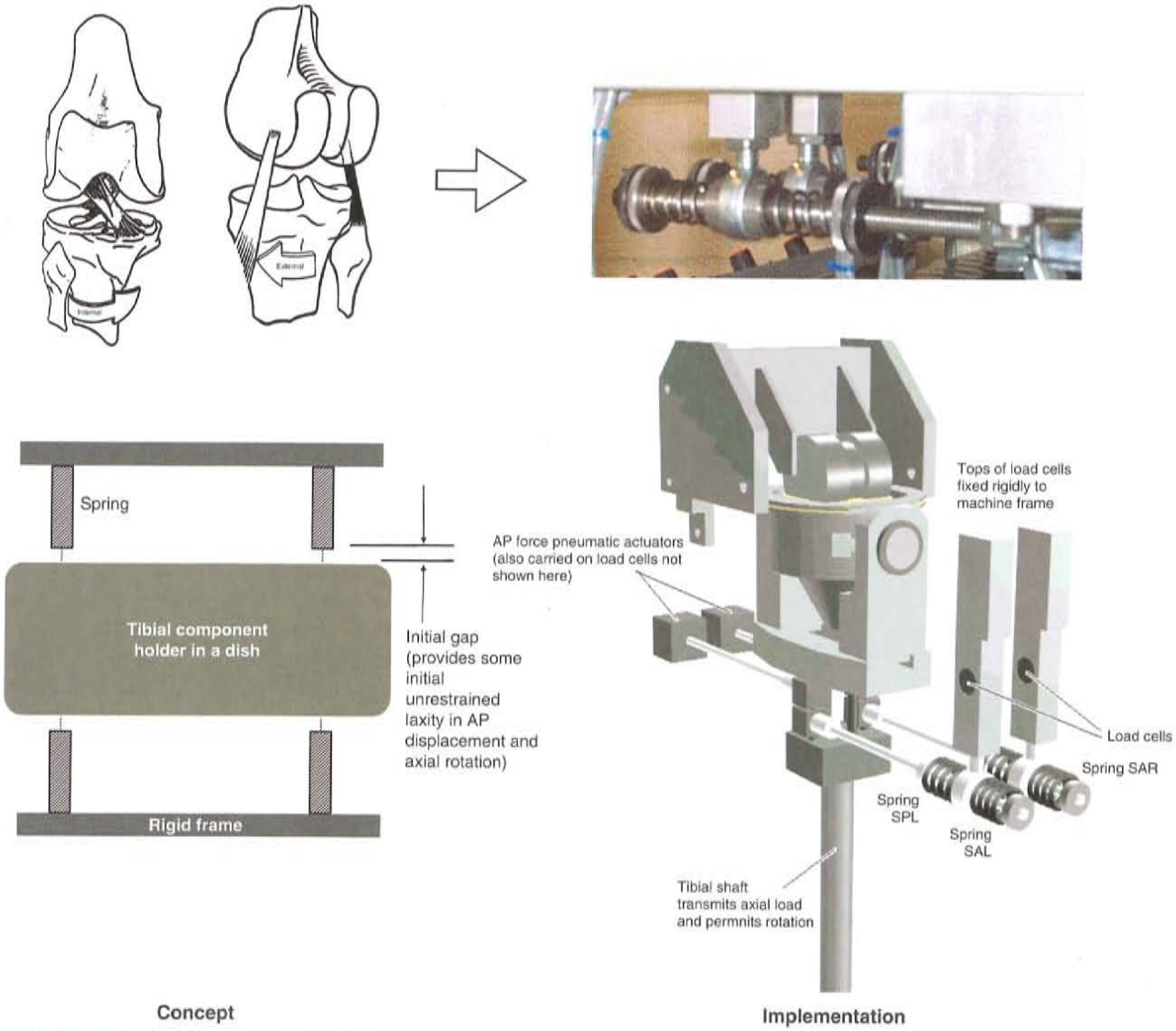

FIGURE 26.9 Basic illustration of the soft tissue restraint simulation system concept and implementation in the Instron-Stanmore Knee Simulator. Top right: The actual spring assembly. Bottom right: The configuration of the main AP force actuators and soft-tissue restraint springs on one station of the first design of the Instron-Stanmore Knee Simulator.

with direct telemetry data from a distal femoral knee replacement [64, 65] and were found to be compatible with and within the range of more recent theoretically modeled/predicted forces [66] and more recent *in vivo* telemetry data from studies with an instrumented TKR [67].

26.3.5 Soft Tissue Simulation in the Force-Control Test Method

For physiologically realistic motions to follow in a simulation where the external (to the knee) AP force and IE torque are (force) controlled, the system requires additional simulation of the ligament and other soft tissue constraints that would occur *in vivo*. This soft tissue restraint would act to attenuate/limit the motions *in vivo* in response to those forces. The restraint of ligaments after TKR surgery and other stabilizing soft tissue depends on the instantaneous AP position and IE angle. In the force-control method, these were initially intended to be simulated with springs, which were desired to modulate the restraint forces and torques based on the actual instantaneous distances and angles moved. Figure 26.9 shows schematically how such a spring configuration was implemented in the force-controlled Instron-Stanmore Knee Simulator.

The initial design, which was adopted in the ISO standard [38], was for the springs to be precompressed such that they would never become loose. Alternatively, the springs can be loose with a gap, such that compression only starts (or ends) when the motion exceeds the gap. It can be shown that the stiffness of this whole assembly with given

Questions? Contact FDA/CDRH/OCE/DID at CDRH-FOISTATUS@fda.hhs.gov or 301-796-8118

Records processed under FOIA Request #2014-8015; Released by CDRH on 12-8-2015

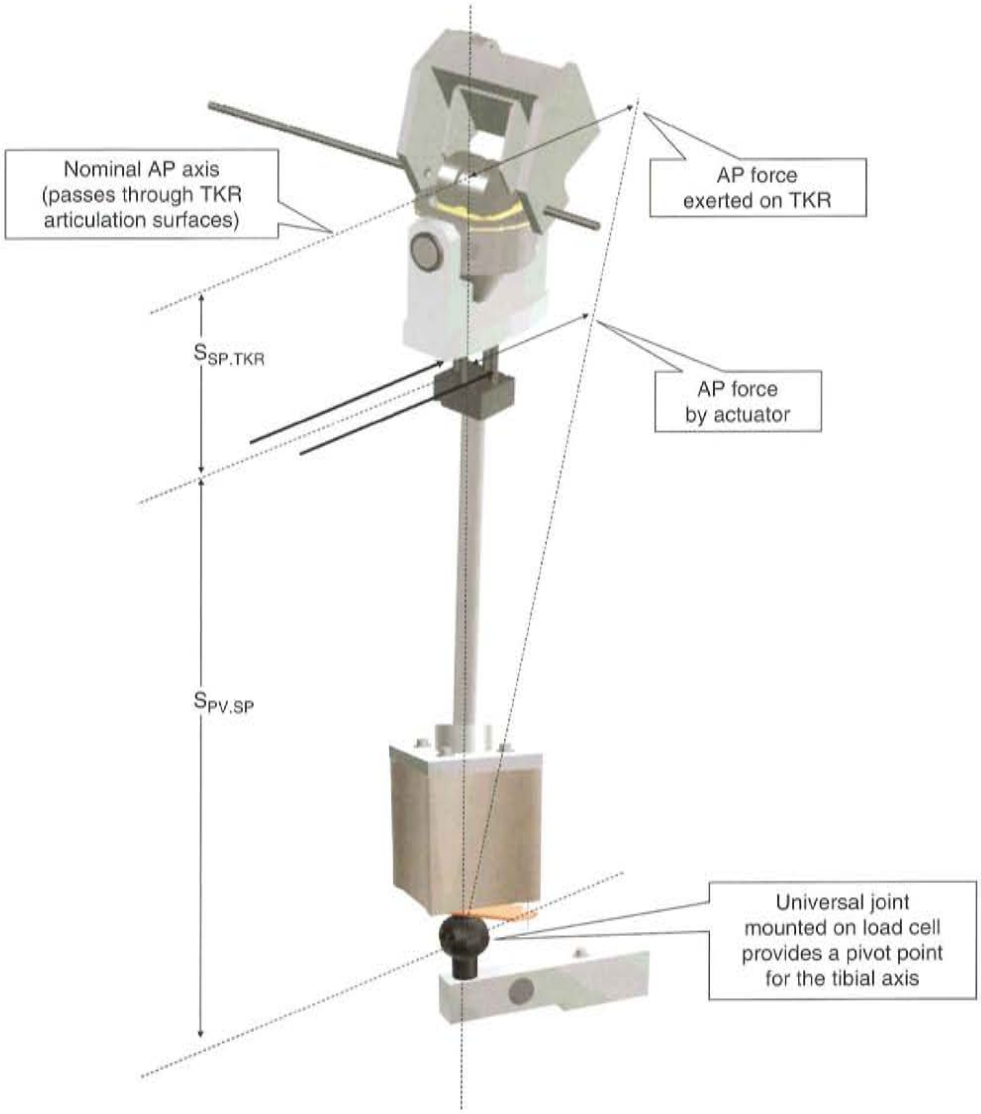

FIGURE 26.10 Schematic illustrating the leverage between where the AP actuators exert forces versus the position of the tibial component on the Instron-Stanmore Knee Simulator.

symmetrical springs set with two-sided precompression drops by 50% when any gap occurs on either side (i.e., two-sided compression becomes one-sided). This situation can easily occur even with moderate motion of the TKR specimen and should preferably be prevented by avoiding precompression altogether.

The stiffness of the springs used and their detailed configuration and settings (i.e., precompression or gap and gap distance) all affect the restraint and thus affect the TKR specimen kinematics [55], which in turn influence the wear. As will be seen later, the *non*-precompressed springs (i.e., with gaps) would also more realistically simulate the physiological soft tissue situation.

In descriptions and results from the force control simulation method [49, 50], initial kinematic studies [53] and wear studies using this simulator, and even in the version of the ISO standard [38] published at the time of this edition of this book, there has not been a definite specification of the details of how the soft tissue restraint springs were set up, all of which would strongly influence the restraint. The standard specified only overall net linear and rotational stiffness to be achieved. However, the detailed spring configuration that affects the stiffness greatly (e.g., precompressed springs double the stiffness, and intermittent freeing of one compressive spring by it reaching its natural length abruptly drops the stiffness) has limited the ability for consistency within each lab and limited the opportunity for reliable data comparison between different laboratories. The way this soft tissue simulation was specified even shed doubts on the credibility of the methodology itself. For example, no differences in spring stiffness nor their configuration were specified to distinguish testing

Questions? Contact FDA/CDRH/OCE/DID at CDRH-FOISTATUS@fda.hhs.gov or 301-796-8118

Records processed under FOIA Request #2014-8015; Released by CDRH on 12-8-2015

posterior cruciate ligament sparing from sacrificing TKRs. A series of later studies [54, 68] had, however, been conducted to address these issues and recommended the stiffness and gap settings for the two most common situations, a resected ACL with retained PCL and a TKR with both cruciates resected, which would approximate how the soft-tissue restraint acts *in vivo*. Those findings are summarized here because they have formed the technical basis for a revision effort to update the force-control ISO 14243-1 [38] standard (being carried out at the time of writing of this chapter).

A mathematical model was developed using the stiffness values of each of the four springs, their settings (level of precompression or gap), and the detailed geometry of the simulator to calculate AP restraint force curves versus AP displacement and how these change with any IE rotation superimposed. Various coupling effects between AP motion and IE rotation and discontinuities resulted from mathematically simulating the behavior of the configuration/assembly of Figure 26.9. These coupling effects affected the net overall AP translational and IE rotational stiffness of the whole assembly and the ranges of motion. For example, the range of restrained linear translation was found to be curtailed by a sudden effectively infinite increase in stiffness when a spring reaches its minimum length when its coils are fully compressed and touching or when a simulator actuator reaches its limit of range of motion. This range of motion is curtailed further if there is some simultaneous IE rotation that eliminates part or all of a spring gap or starts compressing one spring before any net linear translation occurs for the whole assembly (see Figure 26.9).

TABLE 26.1 The Current and Planned Revisions of Soft Tissue Restraint Characteristics for Wear Testing under Force Control

Linear AP restraint		
Current (2005 edition) ISO setting (no gap, and same for PCL retained and resected)	30 N/mm	
Proposed revision and settings used in Nebraska since 2000	Within ± 2.5 mm of the neutral position	Beyond
PCL sacrificing TKR	0	9.3 N/mm
PCL retaining TKR	0	44 N/mm
Rotational IE restraint		
Current (2005 edition) ISO setting (no gap, and same for PCL retained and resected)	0.6 Nm/degree	
Proposed revision and settings used in Nebraska since 2000	Within ± 6 degrees of the neutral position	Beyond
PCL sacrificing TKR	0	0.13 Nm per degree
PCL retaining TKR	0	0.36 Nm per degree

The same analysis was done for rotational restraint with simultaneous linear displacement superimposed. The most optimum spring values, settings, and gaps were chosen in those studies [54, 68] to approximate to published data on the contribution of ligaments to the laxity of the natural knee [69]. The results further confirmed that the behavior of the system was as sensitive to the gap or level of precompression as to the stiffness of the springs [54, 68]. The configuration with the best match between the spring characteristics and the experimentally measured laxity curves for knee joints [69] for the preserved PCL case recommended, for the Instron-Stanmore Knee Simulator, soft (7.24 N/mm) springs on the ACL side and harder (33.8 N/mm) springs on the PCL side, with a 2.5 mm gap on each to simulate the flat horizontal section of the typical anatomical S-shaped laxity curve [54]. For both resected ACL and PCL, the soft (7.24 N/mm) springs for both sides were found to be best, provided that a 2.5 mm gap was set on each side [68]. These values are dependent on the simulator design, and extreme care needs to be taken when extrapolating the preceding values to other types of simulators.

In the Instron-Stanmore Knee Simulator, the location at which these spring forces were applied to the shaft assembly carrying the tibial component was subject to leverage, as shown in Figure 26.10. This simulator-specific leverage was accounted for based on the machine's exact geometry. A similar distance magnification correction was also made to relate the AP distance moved in the plane of the spring system to the actual distance moved by the TKR specimen.

When these restraint settings are generalized (for any simulator) into one linear net restraint (and not two parallel springs), and when the leverage issue is corrected for, the desired net stiffness values recommended for soft tissue restraint are as detailed in Table 26.1. These generalized settings have been proposed as part of a major revision of the force-control ISO standard 14243-1 [38].

How these recommended settings compare to the current ISO standard settings, and how both compare to the physiological functions of the soft tissue restraint from the literature, are shown in Figures 26.11 and 26.12. Note in Figure 26.11 how the physiological soft tissue restraint [69] also shows some coupling between AP linear and IE rotational laxities. The AP laxity was curtailed if no rotation was allowed and vice versa [69].

It is important to note that the physiological knee restraint as measured from the cadaveric study [69] included the restraint from the shape of the anatomical articulating surfaces (joint conformity restraint) as well as the contribution

Questions? Contact FDA/CDRH/OCE/DID at CDRH-FOISTATUS@fda.hhs.gov or 301-796-8118

Records processed under FOIA Request #2014-8015; Released by CDRH on 12-8-2015

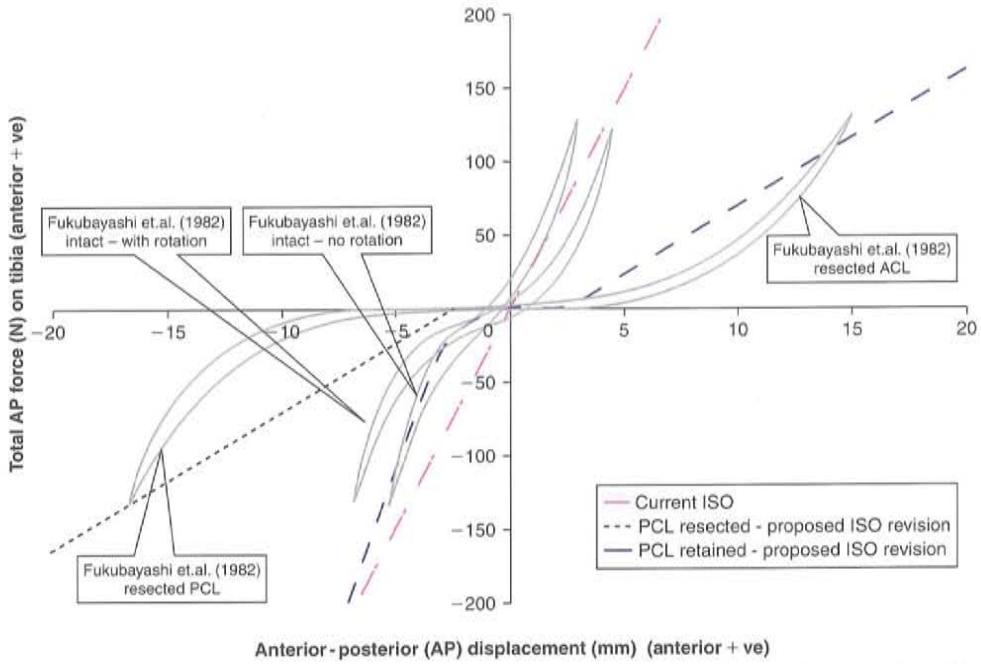

FIGURE 26.11 Anterior-posterior (linear) soft tissue restraint stiffness settings of the current ISO 14243-1 [38] standard and the proposed stiffness revisions, all superimposed on the physiological restraint of an intact knee or with PCL or ACL resected (from the work of Fukubayashi et al., 1982 [69]).

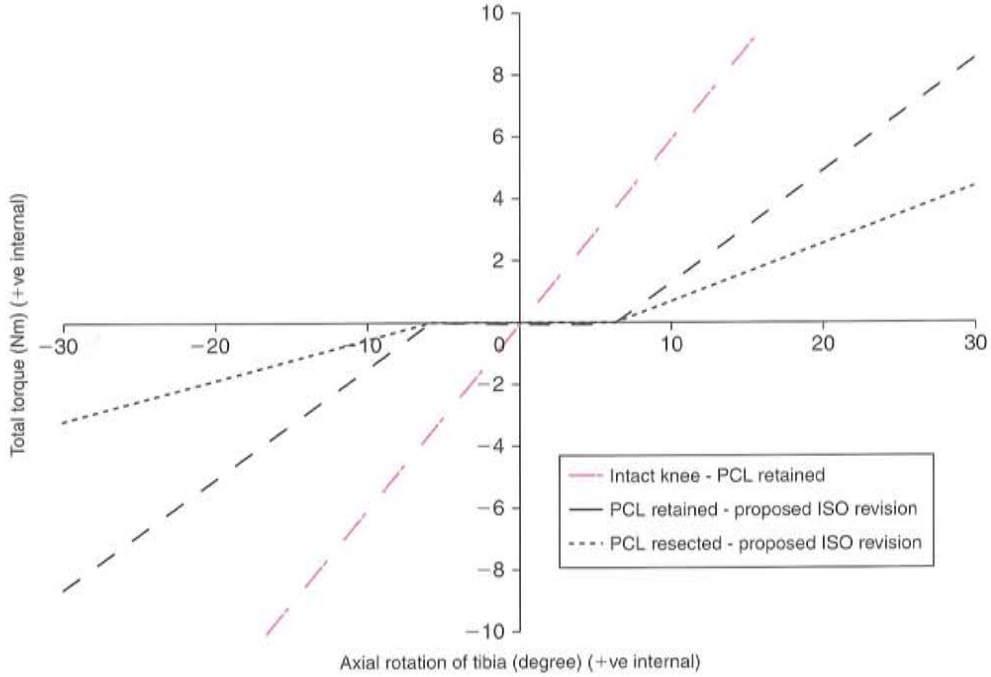

FIGURE 26.12 Internal-external (rotational) soft tissue restraint stiffness settings of the current ISO 14243-1 [38] standard and the proposed stiffness revisions.

from the soft tissue. Therefore, the actual pure soft tissue contribution must be even less *in vivo*. Now observe in Figure 26.11 the straight line simulated restraint currently in the 14243-1 ISO standard [38]. It far exceeds any physiological value when the ACL is resected (which is virtually every time in TKR surgery), and it certainly exceeds the *in vivo* PCL retaining constraint, let alone the PCL resected case from [69]. This means that all tests done strictly according

Questions? Contact FDA/CDRH/OCE/DID at CDRH-FOISTATUS@fda.hhs.gov or 301-796-8118

Records processed under FOIA Request #2014-8015; Released by CDRH on 12-8-2015

to the current ISO settings have excessively restrained TKR motion, and therefore it is not surprising that they typically produce little wear. Since 2000 in the author's laboratory in Nebraska, the soft tissue restraint springs on the knee simulator have *on all tests* been set according to the new proposed ISO revision version shown in Table 26.1 and as shown in Figures 26.11 and 26.12.

There was some initial fear that the gaps would cause impact loading and the springs would fatigue with multimillion cycle use of the machine. With specially designed and made plastic protective collars/bushes, these configurations have been tried on over 10 separate 5-million cycle tests and the spring assemblies proved durable, with the gaps remaining accurate when they were properly set and locked into those settings. It is clear from Figure 26.11 that the stiffness and settings found from the analysis of [54, 68] for the two surgical/ligament situations are obviously very different from each other and are different from the tests with this simulator, which have been published thus far by several laboratories [50–53, 70, 71]. As mentioned earlier, the use of consistent as well as physiologically realistic settings are a precursor for valid comparison of wear and kinematics between TKRs and laboratories.

The 2.5 mm gap in the springs attenuates the simulated ligamentous constraint very close to the neutral position, which has a zero value *in vivo* too near the knees' neutral position. This gap, and the stiffer ligamentous restraint with a PCL-retaining TKR, compared to the sacrificing have made TKR kinematics under force control more like what is expected from their designs [55] and has produced higher and more discriminating wear results.

Regardless of the desired spring settings, it has proven to be (doable but) difficult to accurately implement the restraint physically on a simulator, which requires intricate setting, tuning, and checks throughout a testing period. The nonlinearity and coupling effects between linear and rotational restraint add to those difficulties. A new concept of virtual soft tissue simulation was envisaged, which is simpler and more accurate in implementation. The soft tissue restraint could be modeled in software utilizing the real-time feedback signals of the kinematics and soft-tissue restraint look-up tables, incorporating their effects within the AP force and IE torque actuators. This allows any non-linear and more accurate representation.

This concept takes advantage of measured real-time feedback of AP and IE rotation from sensors on board the knee simulator. Based on those instantaneous AP and IE implant positions/motions, a real-time (or strictly, semi-real-time) computation is made of the influence/contribution of the desired soft tissue springs or any virtual mathematical restraint models. The computed AP force and IE torque contributions are added (vectorially, mathematically) to the electronic command signals for the externally actuated AP and IE torques of the simulator.

The bandwidth of TKR dynamics is well contained in less than 50 Hz (i.e., no physiologically meaningful force spikes or drastic kinematic position changes can occur in less than 20 ms in time, or strictly 40 ms, when considering aliasing sampling errors). Even modest modern electronic data acquisition and control systems can reach at least 1 kHz data sampling, processing, and control loop closure frequency. Therefore, the process of incorporating a soft tissue control correction to the external simulator actuators can be made to occur at least 10–20 times before a TKR changes its kinematic position, therefore, the correction can be considered virtually instantaneous.

This concept is now termed "virtual soft tissue" simulation and has been elegantly implemented in the latest models of the AMTI knee simulator (Figure 26.18). This implementation was combined with adaptive control in this simulator, allowing the electronics to gradually exaggerate or attenuate the cyclic actuation waveforms until the resulting measured forces and torques are closely, cycle by cycle, made to match the desired input forces and torques with the desired soft tissue model. Comprehensive quantitative studies and formal presentations of this novel system are yet to be published.

26.3.6 TKR Kinematics Measured from the Force-Control Wear Testing Method

With the same standardized repeatable external forces, and approximated soft tissue restraint physically simulated as described in the previous section, different TKR designs under the force-control test method would experience different kinematics of motion as governed by their individual design details.

Depending on the simulator, with suitable calibrated sensors (Figure 26.13), this force-control concept could therefore facilitate assessment of the dynamic performance of a TKR implant by measuring its kinematics *in vitro* during a simulated walking activity.

Various studies comparing a wide range of measured TKR kinematics under identical standardized conditions had been carried out in this way. An early one of these studies [53] tested a set of generically different TKR designs of highly different constraint, including fixed, mobile-bearing, and hinged designs. Those TKRs indeed produced expectedly different kinematics; some moved less than half of what others did in the stance phase of walking.

Another study compared four fixed and three mobile bearing TKRs of different designs, all PCL cruciate-retaining (CR), but those produced different kinematics, too, and again reflected the expected variation from their difference in constraint [72]. For example, rotating platform bearings rotated more than fixed bearings, and highly dished fixed bearings translated less than shallower fixed bearings.

Questions? Contact FDA/CDRH/OCE/DID at CDRH-FOISTATUS@fda.hhs.gov or 301-796-8118

Records processed under FOIA Request #2014-8015; Released by CDRH on 12-8-2015

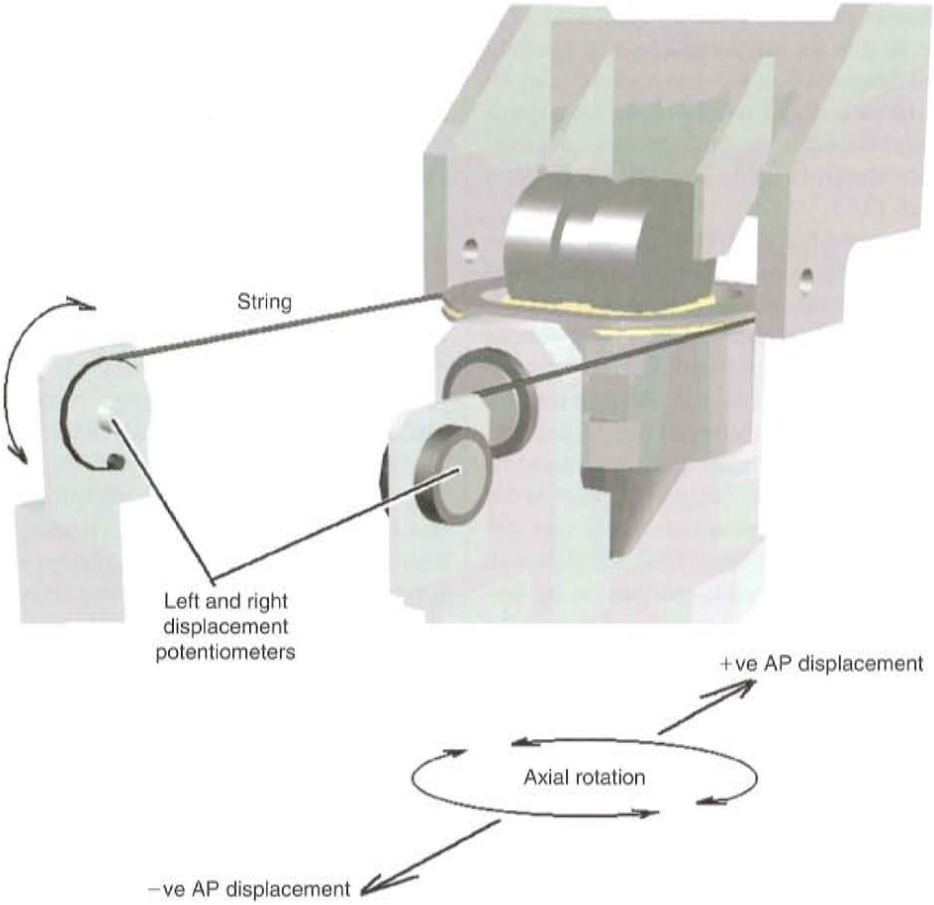

FIGURE 26.13 The configuration of two potentiometer sensors with strings that allow measurement of two parallel motions from which a net AP displacement and a net IE rotation angle were calculated. This configuration allows very accurate measurement of the TKR kinematics, yet it minimizes influence of the sensors or their strings on the freedom of the tibial component to translate proximally-distally and in AP, ML, or rotate in IE and VV. The TKR flexion occurs through rotation of the femoral component holder, so it does not affect and is unaffected by these AP and IE motion sensor measurements.

If the small frictional and inertial forces of the simulator implant holders were neglected, then the external actuated (and measured) simulator input forces, then the soft tissue (spring) restraint forces (also measured on the simulator) and the TKR articulating surface (joint reaction) forces should all balance in a quasi-steady-state equilibrium at each phase of the walking gait cycle. Therefore the latter (TKR joint reaction forces) were computed from the force measurements at each phase of the simulator cycles in both of the previously mentioned studies [53, 72]. As expected, some (the highly constrained) TKRs relied mainly on their inherent conforming surfaces or constraint in limiting their motions, yet the motion of other TKRs were limited mostly by the simulated soft tissue (springs).

It is interesting to note that the TKRs of the [72] study were supposedly indicated for the same type of patient conditions (all CR), yet their function through their measured kinematics varied markedly between the TKR designs, even between fixed-bearing types. The fact that the TKRs' kinematic behavior varied was not surprising considering their slightly different sagittal profile/radii and design philosophies. The wise conclusion from that study [72] was not to expect different TKR clinical products to behave the same way even if they were (through device manufacturer marketing) indicated for the same patient conditions. This conclusion should further extend to the use and durability of UHMWPE in TKR. The real wear and durability of UHMWPE will strongly depend on the detailed design of the TKR system, as well as the generic type of TKR and to which patient indications it is intended.

The same different fixed and mobile cruciate retaining TKR designs in [72] were also tested under the same force-control conditions but with various patient and surgical variability imposed as could occur clinically to establish how sensitive the test method was and how forgiving each TKR design was for such misalignments [55]. An enhanced duty cycle was also applied to simulate a heavier patient or one with more vigorous activities. It was found that the differences in kinematics between TKR became higher, and in some cases, the relative values between designs changed.

Questions? Contact FDA/CDRH/OCE/DID at CDRH-FOISTATUS@fda.hhs.gov or 301-796-8118

Records processed under FOIA Request #2014-8015; Released by CDRH on 12-8-2015

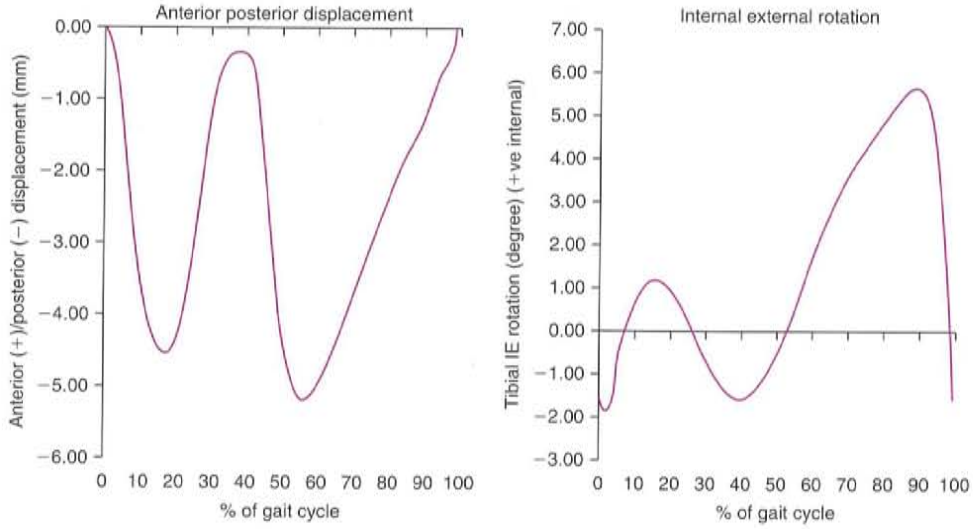

FIGURE 26.14 Input waveforms of ISO 14243-3 (displacement control) [56]. The flexion and axial force (not shown here) are the same as for force control (ISO 14243-1 [38], shown in Figure 26.7).

Different setups were tested to simulate variations in surgical placement equally imposed on all the TKR designs.

Changing the line of action of the compressive force in the frontal plane, equivalent to a change in the frontal varus-valgus angle, did not change the kinematics. Rotating the tibial component about a vertical axis in either direction shifted the internal and external rotational curves (offset them) in that same direction of misalignment. The largest affect on kinematics was that of changing the tightness of the PCL. For a tight PCL, the displacements and rotations were reduced greatly; a loose PCL had the opposite affect.

Interesting to note was that in all of the previously mentioned tests [55], the resulting displacements and rotations of the mobile-bearing knee replacements were in the same general range as for the fixed-bearing designs, or even less in some cases. Good insight was gained from the preceding study about the relative kinematic behavior of different TKR designs and their sensitivity to patient factors and the alignment of the components at surgery.

26.3.7 Standardization of the Displacement-Control TKR Simulation Method for Wear Testing

The kinematics used as inputs in the ISO 14243-3 displacement-control standard [56] are shown in Figure 26.14. The origin of these AP and IE input motion curves in this later standard has been frequently enquired about. Whilst the current author had not contributed to the emergence of this (the displacement-control version) standard, various verbal communications with the originators [73] of this ISO standard and the proposers of its input curves [74] clarified the history of these kinematic waveforms. They originated from a gait laboratory PhD study [75] of *in vivo* measured kinematics extracted using the Point Cluster Technique [76]. Those very curves in ISO 14243-3 [56] were the results from one male patient with a cruciate-retaining Zimmer NexGen CR total knee replacement system.

One related publication that referred to the input curves was also from a Point Cluster Technique study on 10 patients with TKRs of similar design but these were posterior stabilized (PS), where the posterior–cruciate ligament had been substituted [74]. As mentioned earlier, the ISO 14243-3 kinematic curves were from the single patient CR data. It is interesting to note from the study of [74] that the data processing to calculate the surface contact slip velocity profiles had shown marked differences, especially on the knee's medial side between CR and PS knees. Indeed, the conclusion of that study wisely alluded to the need to vary the slip velocities and kinematics when testing different TKR designs. Regardless of how representative these input curves were, they have proven to be useful as part of an ISO standard taking tests with displacement control some way toward conversion of methodology, especially on many simulators still operating today that are not capable of the force-control scheme.

The preceding detailed discussion should render obvious some of the pros and cons of both the force- and displacement-control methods. As mentioned earlier, the displacement control is simpler in concept and more robust in implementation on simulators. However, what displacement inputs should be used for each TKR? One encouraging study demonstrated that if the standard forces in a force-control test were used and suitably chosen displacements in a displacement-control test were also employed, similar wear rates would result for the same implant design

Questions? Contact FDA/CDRH/OCE/DID at CDRH-FOISTATUS@fda.hhs.gov or 301-796-8118

Records processed under FOIA Request #2014-8015; Released by CDRH on 12-8-2015

[77]. In that particular study [77], the knee implant tested in both methods was the very cruciate-retaining TKR design for which the displacement-control inputs (kinematics) were originally devised [74, 75].

How wise is it to use the same AP and IE rotations for different TKR designs in a standardized test? Even in the same TKR design, how would UHMWPE deformations relieve or accentuate stresses under identical displacements and rotations in later cycles of the same test? In the previously mentioned study [77], not only the *in vivo* kinematics of that very TKR design were used, but also the TKR was a relatively lax cruciate-retaining design, so similar wear resulted. It is for the preceding reasons that an important limitation was included, perhaps understated, in the opening "Scope" section of the ISO 14243-3 [56] (the displacement-control standard). It brought attention to its questionable applicability to knee designs with a high degree of constraint, which could result in damage to the articulating components in the early stages of the test that would not be representative of clinical service. The author questions further here: What is a high degree of constraint, and how much damage would be considered unrealistic? Constraint is a function of the detailed design of a TKR and thus varies within a continuum ranging from zero laxity of fully constrained hinged knee systems to the highly lax mobile bearing knee systems [10]. TKR kinematics were found to vary even with slight differences among generically similar TKR designs that had only subtle changes in the sagittal and frontal profiles/radii reflecting various design philosophies [55, 72].

In turn, there have been a variety of criticisms of the force-control method in both concept and in implementation. Among the most profound relate to the complexity and difficulty of implementation in a simulator. Force control is naturally a challenge with fast, dynamically changing forces and torques (lower plots of Figure 26.6). It becomes especially more difficult to physically implement when the target load (usually the tibial component of a TKR in this case) is itself moving fast in complex ways against fast-changing and wide-ranging resistance to motion, coupled in a way such that IE rotation somewhat affects the resistance to AP motion and vice versa. Added to this are the intricacies required in the soft-tissue simulation system. None of the simulators to date have managed to implement force control accurately enough and independently across multiple stations with sufficient ease to make this technique and its technology conveniently transferable across TKR test laboratories. It has been noticed, however, that due to the highly cyclic and repetitive nature of simulating a walking gait up to millions of cycles, a thorough (sometimes seemingly exaggerated) investment of tuning and retuning at the start of a test does bring adequate rewards in sufficient accuracy.

Another fundamental criticism goes to the heart of the concept of force-control and soft-tissue simulation. "In order to specify the correct spring stiffness" (for soft tissue simulation), early critics argued that "some estimate of sensible anterior-posterior translation would be required. Hence, since an estimate of deflection is needed to implement load control, why not control displacement in the first place?" [48]. The answer to this should be clear from the earlier description of the force-control concept (Section 26.3.4) and the soft-tissue simulation (Section 26.3.5). In summary, in force control the simulated soft tissue will not be chosen to suit individual TKR designs but would be the same and is fixed for all designs, except for whether to simulate the PCL action or not for CR and PS TKR designs, respectively. Unless the soft-tissue simulation is widely out of the physiological range, the effects of a wrongly standardized simulated restraint model would be of a secondary level in its influence, especially in comparing the wear of varying TKR designs. If the displacement and rotation are made constant (displacement control) in testing all designs, those kinematics are of a primary order in affecting wear, and they do need to be customized for each TKR design. Further, in Section 26.3.3, it was argued that even with the appropriate kimematics for a given TKR design, the impacts/impingements on UHMWPE posts and viscoelastic stresses will be self-tuned/adjusted in force control but might not be in rigidly implemented displacement control.

26.4 CONSIDERATIONS AND PITFALLS IN KNEE WEAR TESTING OF UHMWPE

26.4.1 Variable Control and the Number of TKR/UHMWPE Samples to Test

26.4.1.1 Variable Control

Consider the requirement for testing a TKR system with a different (say, improved) version of UHMWPE material. Typically, TKR samples with the new material are compared with others of the same TKR design, size, and everything else but with a standard or previous version of UHMWPE as a control. It is obvious that the best control would be one with good clinical history and success. Testing on a knee simulator takes time (e.g., typically a 5 million cycle test takes 6–9 months, including setup and downtime) and is highly costly. In this situation, it is frequently asked how many TKR samples of each material should be tested. The general answer, of course, is that if a significant difference (or absence of it) is to be proven statistically, then the level of that difference should be chosen sensibly such that it would be of clinical significance too. Also, the study/test should secure sufficient "statistical power" [78]. Both of these will depend on the variability (sometimes expressed as variance or standard deviation in the variable of interest) inherent in the results of any testing process, so it is worth examining the potential sources of variability in some detail.

In vitro TKR wear tests can, in principle at least, be much more variable controlled than *in vivo* studies and

Questions? Contact FDA/CDRH/OCE/DID at CDRH-FOISTATUS@fda.hhs.gov or 301-796-8118

Records processed under FOIA Request #2014-8015; Released by CDRH on 12-8-2015

therefore require less sample numbers. Clinical TKR wear or retrieval studies are subject to variability from:

1. Patient anatomy
2. Surgical installation, implant alignment, and soft tissue/ligament tuning
3. Capsule and lubricant conditions
4. Patient daily activities and type of long-term use
5. Duration of duty *in vivo*
6. Limitations in the method of measurements of *in vivo* wear
7. Other factors, including the ones listed in the following discussion for *in vitro* wear tests

Some of the preceding sources of variability are serious in their affects on UHMWPE wear, which is influenced by the TKR kinematics and stresses. An interesting study [61] developed a probabilistic finite element (FE) analysis TKR model to evaluate the effects of two levels of parameter variability with standard deviations of TKR component alignment. The study predicted modest variability of less than 10% (1.66 MPa) in peak contact pressure but up to 226% (3.44 mm) in resulting anterior-posterior (AP) translation and up to 169% (4.30 degrees) in internal-external (IE) rotation. The critical alignment parameters were the tilt of the tibial insert and the IE rotational alignment of the femoral component. The authors commented that the observed variability in kinematics and, to a lesser extent, contact pressure, obviously had the potential to impact UHMWPE wear.

All of the surgical and alignment variables previously listed can be more precisely controlled or eliminated with hardware and detailed experimental procedure in knee simulator testing of UHMWPE wear. Many factors can be more precisely set during installation, alignment, and tuning in a simulator, especially with the relative ease of monitoring and retuning of simulator conditions (for example, see Section 26.4.3). Having eliminated *in vitro* the vast majority of the typically uncontrollable variables *in vivo*, a typical knee simulator test would typically leave the following three remaining or new sources of error and variability:

- Manufacturing tolerances between specimens: These are typically minute because testing standards generally prescribe that TKR test samples should all have passed quality control checks by the manufacturer. Manufacturing tolerances are of the order of microns in dimensions. These are orders of magnitude less in influence than any of the *in vivo* variables previously listed.
- Errors in gravimetric measurements of UHMWPE wear: At each stage/interval of the test, gravimetric weight measurements of UHMWPE should be carried out with advanced instruments (scales) with preferably 10 millionths of a gram resolution or better. The gravitational approach to measure wear of UHMWPE is fundamentally weak, if not flawed. In experimentation and instrumentation theory, subtracting two similar large quantities to determine the required variable being the small difference between them is riddled with errors, especially when the two larger quantities are analog and not digital in their nature and measurement. UHMWPE wear at each testing interval may be as low as a fraction of a milligram or may reach 50 mg at most, yet the UHMWPE component weight is hundreds of times heavier.

  An example is given here to illustrate this. A typical UHMWPE TKR bearing insert component may weigh 22 g with some small *absolute* experimental uncertainty in each weighing measurement (of, say, ± 0.1 mg, thus $<0.0005\%$ relative error). The weight measurements are subtracted to determine a net interim weight loss and thus wear of typically a few milligrams (say, weight loss due to an interim wear interval $= 1.5$ mg). This result is naturally subject to the sum of the absolute errors of the two measurement constituents, therefore the net interval wear result is (1.5 ± 0.2 mg), hence the uncertainty progresses up to a $\pm 13\%$ *relative* error in the final result [79]. Until methods evolve to track and quantitatively measure the amount (weight or volume) of the actual wear particles, the gravimetric technique remains the most accurate and offers the best compromise.

  In the author's own laboratory, the wear of each TKR sample, at each interval of the test, is measured hundreds of times (quickly and automatically by computer) and averaged until statistical stability is reached each time. With a running average continuously updated, more data continue to be taken until the running average ceases to change beyond the 10 μg resolution of the instrument. Such techniques added to the stringent protocol requirements of testing standards (ISO 14243-2) [80] can minimize those errors. The gravitational weighing errors naturally become more significant in screening implant wear as the wear becomes smaller with improved materials. It is therefore fortunate that at some future stage wear may become so small that it loses clinical relevance, and then those tiny errors in wear measurements *in vitro* become unimportant. Some argue that this is the situation now with highly crosslinked UHMWPE whose wear may not exceed the uncertainty level in gravimetric wear measurements and liquid absorption levels.
- Temporal variability in UHMWPE wear during a test: A change in the wear rate may result at different stages/intervals of a prolonged multimillion cycle TKR wear test: In a typical study, measurements are taken at 11–12 stages of (say) a 5 million cycle test, representing 10–11 different intervals of wear for each specimen. A linear regression analysis (least square error method) is typically used to average the results from all those intervals resulting with the (mathematically) best fitting linear wear rate for each test sample. Therefore, the 11

Questions? Contact FDA/CDRH/OCE/DID at CDRH-FOISTATUS@fda.hhs.gov or 301-796-8118

Records processed under FOIA Request #2014-8015; Released by CDRH on 12-8-2015

interval/stage measurements of wear average out this third source of variability/error, which happens to be the most serious, in the author's view. Sometimes the temporal variability may stem from liquid absorption rate changes, and, of course, they have to be corrected. Some temporal variability relates to the environment (temperature and humidity) or a change/drift in testing conditions. Ambiguity may arise in recognizing such phenomena because some temporal variability may actually represent a true physical result. For example, "bedding in," "wearing in," "run in," and "run-away" wear are terms frequently used in total hip replacements (see Chapter 5), but similar effects can actually occur in TKR tests, too. For example, when a lax TKR wears, the conformity of the articulating surfaces may gradually increase, and this may slightly diminish the kinematics range and also the stress, and thus could alter the wear rates between the start and end of a long test. This phenomenon was reported in [50] where AP and especially the rotational laxities were observed to reduce with time over a long wear test. This was attributed to the formation of a more congruent wear track because of wear and deformation. Another possible explanation was that the coefficient of friction increased with time because of embedded particles or slight roughening of the articulating metallic surfaces [50].

26.4.1.2 Number of TKR/UHMWPE Samples to Test

Because the variables *in vitro* can be more controlled as previously outlined, sometimes as few as two TKR samples versus another two would suffice in comparing UHMWPE wear in TKR systems. In the author's laboratory, two TKR samples were compared to another two, with a slightly different (incrementally changed) design to improve the geometry to reduce wear, where retrievals showed it had locally occurred. The results showed a threefold improvement (reduction) in wear, which was statistically significant ($p < 0.05$). In another example from the same lab, the wear was tested of two different TKR mobile bearing designs. Four samples of each TKR were tested, one design type tested to 5 million cycles, the other to 7 million cycles, but both had identical test methods. Although the wear rates of each showed the usual scatter, a statistically significant difference in wear rates resulted ($p < 0.05$) between these two mobile bearing TKR designs.

The same has been echoed in TKR wear studies from other labs. In a recently published study [81], highly crosslinked UHMWPE for TKR was proven in a displacement-controlled test of three TKR samples of each kind to wear statistically significantly less ($P = 0.034$) than conventional UHMWPE. In a force-controlled TKR wear study [70], a fivefold increase in wear rate ($p = 0.002$) was found under different simulator input conditions comparing pure walking to a 70:1 combination of walking with stair climbing. This test compared four samples of a clinically used TKR in each loading condition, with the TKR designs being slightly different. Finally, in an another force-controlled knee simulator test, two different fixed bearing TKR designs were compared, where four samples of each were tested at a time, and the wear rates for one of them was shown to be 10 times less than the other [62]. In that study, the two implant designs were tested in separate setups at different times, at different frequencies of walking cycle (1 Hz versus 1.4 Hz), and the results of wear were retrospectively compared.

The preceding examples showed statistically significant differences in wear rates between designs when such differences existed. Sometimes such differences are smaller or do not exist, and it becomes more difficult to choose how many samples to test and whether to demonstrate the differences or to verify their absence. A good *in vitro* TKR wear study, where possible, should be well designed in terms of sample numbers and criteria for assessing the results prior to the actual simulator testing. The choice of sample numbers to test should ensure sufficient statistical power [78] for the study. The following is an example as a recently published case study [63].

To compare the UHMWPE wear of rotating platform (RP) TKR to a fixed bearing (FB) one of the same design, a recently published study compared the wear of mobile to fixed bearing total knees of identical design in other aspects [63]. The knees had the same femoral components and were tested with identical force-control inputs. Valid justification was needed for choosing a sample number of TKRs to test from each group. The sample numbers chosen were justified based on a previously published study [82] (by a different lab), which compared the wear rates of the same two implant designs with the displacement-control method. That study [82] reported a mean wear rate of 4.86 ± 3.55 mg/million cycles (Mc) for the RP versus a mean of 21.3 ± 5.52 mg/Mc for the FB. These results showed over 75% reduction in wear with the RP, and therefore such reduction was of high clinical interest. Both wear values were in the range of what TKRs produce with conventional UHMWPE, and the difference (75% reduction in wear) was highly worthy for an alternative design to reduce the risk of osteolysis and increase longevity *in vivo*. Those results from the cited study [82] were used as the effect size in a statistical power analysis [78] for the later study [63]. A two-sided t-test was performed with a two-sided alpha level of $p = 0.05$. Those parameters yielded 40% power (probability of correctly rejecting the null hypothesis of no difference between the two groups [78]) by testing two implants in each group, 85% with three implants in each group, and 97% power with four implants in each group. In the case study [63], four samples of each group were chosen and thus approximated to 97% statistical power based on the aforementioned assumptions and the effect size

Questions? Contact FDA/CDRH/OCE/DID at CDRH-FOISTATUS@fda.hhs.gov or 301-796-8118

Records processed under FOIA Request #2014-8015; Released by CDRH on 12-8-2015

published in the study that was cited [82]. Typically, 80% or higher statistical power is deemed acceptable in this field, and so three samples could have also sufficed. Please see any good statistical text [78] for a comprehensive explanation of how a type II (β) error (statistical power = $1-\beta$) interacts with a type I (α) error (level of statistical significance, or p value), and their implications on the required sample numbers (n) in trying to detect a meaningful difference between two groups. Remember, a meaningful difference in the UHMWPE wear in the context of TKR testing is that of clinical significance, and this invariably relates to the potential onset of osteolysis and risk of TKR failure by loosening (see Chapter 8).

26.4.2 Soaking UHMWPE Prior to Testing and Soak Controls during Testing

In the previous section, the principal weakness of estimating UHMWPE gravimetrically was highlighted. Relatively large errors are unfortunately inherent in having to subtract an UHMWPE bearing component weight before and after wear. The example given showed how an interim/interval weight loss in UHMWPE of, say, 1.5 mg may be subject to an overall uncertainty of over 10% due to error progression alone in simple weight measurements, each made to better than 0.001% resolution. Therefore, any other seemingly negligible sources of uncertainty in gravimetric UHMWPE wear measurements can have disproportionate effects on the final wear results and need to be avoided or corrected for.

Soaking of liquid into the UHMWPE material is the most important source of such uncertainty. UHMWPE is essentially porous, and both *in vivo* and during testing *in vitro*, it is submerged and saturated with liquid lubricant. Wear testing measurements are done when the UHMWPE is supposedly, at least nominally, dry, to reduce as far as possible the weight of residual liquid as a source of uncertainty. The first measure to reduce the soaking effect is to presoak the UHMWPE specimens prior to the test for 2–3 weeks in deionized water or in the same diluted serum lubricant used for later testing. This would ensure that the UHMWPE has stabilized and saturated with liquid as it would later be during testing. In the author's own laboratory, a minimum of 2 weeks pretest soaking is continued until the weight rise on any specimen in any extra 24 hour period becomes less than 10% of the overall amount soaked up to that point.

Various cleaning protocols have been used prior to wear measurements, usually ending in some rigorous drying process. Some involve drying with modest heating for long hours and some under vacuum (desiccation) or a combination of both. In the author's lab, the rigorous cleaning and drying protocol described in ISO 14243-2 [80] is usually followed. This involves a well-defined multi-time-step sequence of cleaning and rinsing with detergent and deionized water in an ultrasonic bath, then drying for at least 30 min in a vacuum chamber to a pressure of below 13.3 Pa (approximately 100 mTorr) under ambient temperature.

To correct for any remaining liquid absorption, one or more control UHMWPE specimens are included in the test as prescribed in ISO 14243-1 [38]. These are placed in an identical diluted serum lubricant medium as the actual test specimens so they soak similarly and are cleaned, dried, and weighed similarly. Any changes in the control specimens weight are considered to have occurred only due to the soaking process under the same conditions in that test interval. Those weight changes are used as corrections to the actual weight losses due to wear. Such control specimens are commonly referred to as passive soak controls.

Alternatively, loaded or active soak control specimens can be used. These are not only placed in the same lubricant medium but are also subjected to the same dynamic compressive loads (axial forces of a TKR) during testing without any other motions. The idea here is that the compression/decompression may accelerate or in some way alter the soaking process, and this is suspected to occur more with the highly crosslinked UHMWPE materials. In a prospective revised version of the ISO standards, 14243-1 and 2 [38, 80], whether to use passive or loaded soak controls is expected to be made optional.

How much soaking is expected and typically corrected during a typical TKR wear test? In the author's own laboratory, passive soak controls are more frequently used for conventional UHMWPE, and active controls are used for highly-crosslinked UHMWPE unless there are special requirements otherwise. Each test has its own controls, but if the results from over 20 tests with different UNMWPE lots, different TKR designs, and different levels of crosslinking are averaged, the overall correction from passive soak controls has averaged 0.89 ± 0.85 mg/Mc. From active soak controls, the overall average was higher, 1.65 ± 0.88 mg/Mc. In both cases, the soaking correction increased the net wear rate from the apparent gravimetric measurements. Obviously, the significance of these amounts depends on the wear rate of the actual tested TKR specimens and also depends on the initial presoaking process. The intricacy of those corrections assume a larger importance with the very modern very low wearing highly-crosslinked UHMWPE in TKRs, which explains the early reports of negative wear rates. In screening tests of large contact area TKR implants with conventional UHMWPE with high wear rates reaching tens of mg/Mc, whether a passive or active soak control is used does not really affect the relative ranking between different TKR designs or materials under test.

In the author's opinion, this whole liquid soaking and correction process is riddled with mystery and has evolved in a pseudo-scientific fashion. The reader is reminded that the drying and desiccation under vacuum process is supposedly leaving the specimen consistently dry before each

Questions? Contact FDA/CDRH/OCE/DID at CDRH-FOISTATUS@fda.hhs.gov or 301-796-8118

Records processed under FOIA Request #2014-8015; Released by CDRH on 12-8-2015

weight measurement. Therefore, it is rather unknown how dry should be dry, and therefore liquid soaking data results are inherently noisy to say the least, but as usual, these methods are used until better methods are developed and are demonstrated to improve reliability.

26.4.3 Symmetry of Applied Inputs and Simulator Tuning

Useful results have begun to flow from different research laboratories on the kinematics and wear of TKR implants using the force-control method. A crucial ingredient in the reliability of results is the consistency of the input force waveforms. The standard ISO TKR simulation test of UHMWPE wear (of, say, 14243-1 [38]) is based on defined inputs for simulating a walking cycle originating as mentioned (Section 26.3.4) from theoretical, empirical, and *in vivo* studies. However good or inexact, the waveform inputs are largely assumed to be (actually) input in the same way across simulator stations, throughout long tests, across simulators, and across laboratories. How closely these standard control inputs are physically actuated on the simulator is very important. Comparison of durability can only be valid between implants and studies of consistent inputs. In this section, natural discrepancies of this kind are shown in a case study and shows how they could be reduced from the unacceptable to the negligible.

In this case study, the TKRs were two rotating and translating mobile bearing knees and two fixed-condylar types by the same manufacturer, both with conventional UHMWPE. After appropriate installation and initial mechanical alignment and intricate setting of the soft-tissue restraint springs on a force-controlled Instron-Stanmore Knee Simulator, the measured input forces were symmetrical between stations of identical TKR designs. The solid curves of Figure 26.17 show the intended (at the time, an early 1999 draft) ISO force input waveforms in synchrony with flexion angle for level walking. These inputs produced the (symbol) traces on the same graphs (Figure 26.17) as actuated by the simulator and measured by its calibrated and well-zeroed sensors. The output kinematics were also found to be consistent between each pair of identical specimens. However, for wear testing, the load-bearing stance phase is very important, and the measured curves did not follow the desired command waveforms. For example, during the stance phase (i.e., less than 60% of the cycle) there should have been two distinct peaks of axial force, a distinct peak of positive AP force, and virtually no rotational torque.

Even at 1 Hz, the most popular testing frequency, the results in Figure 26.17 showed a mismatch in magnitude and a more serious one in phase lag (approximately 18 degrees, equivalent to 50 ms) due to the inertia and slower motor-driven flexion actuator compared to the lighter and faster pneumatic force actuators. At the load bearing stance, where any wear mechanism would be strongest, the forces were sometimes 50% less due to the phase mismatch. Note also from Figure 26.17 the flexion did not reach below 7–8

FIGURE 26.15 Hydraulic six-station displacement-control Knee Wear Simulator by Shore Western Manufacturing Inc., Monrovia, California, USA.

FIGURE 26.16 Six-station displacement-controlled Knee Wear Simulator by ProSim, United Kingdom. This machine has force-control capability for AP and IE torque but no soft tissue simulation.

Questions? Contact FDA/CDRH/OCE/DID at CDRH-FOISTATUS@fda.hhs.gov or 301-796-8118

Records processed under FOIA Request #2014-8015; Released by CDRH on 12-8-2015

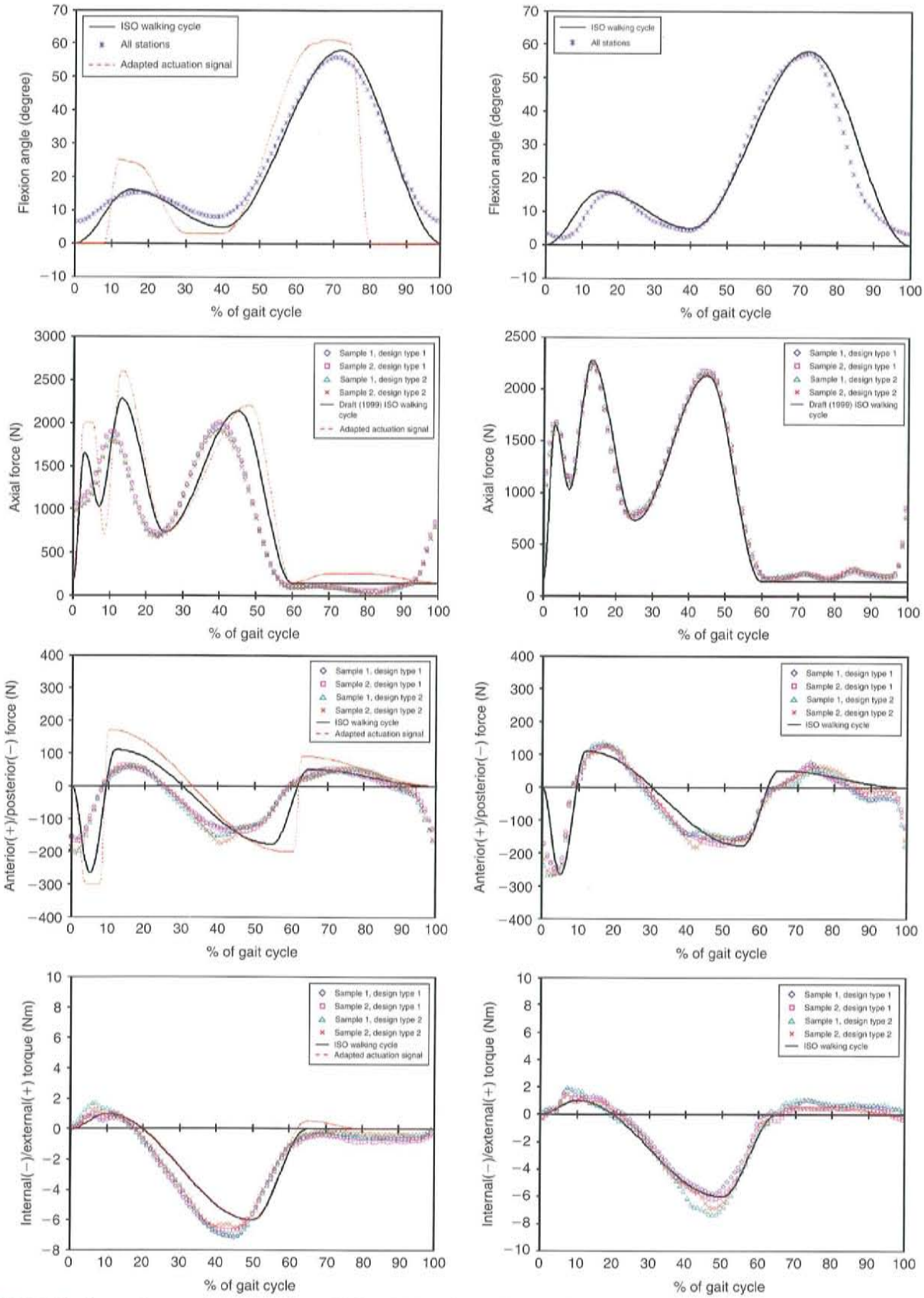

FIGURE 26.17 Traces of measured input actuations with four TKR specimens. Two samples of one design and two of another design were tested on a four-station Instron-Stanmore simulator. The left column shows the input waveforms as measured without adaptation of the command waveforms. The right column shows the measured signals after the command waveforms have been adapted to approximate to the desired waveforms. The right column plots show an example after a set of iterative tuning steps (adaptations of the command signals), which could be improved upon further, such as further tuning of the flexion angle. (Note that the desired waveform of axial force shown here was an early 1999 version of the then-draft ISO standard, with axial forces peaking at about 2300 N. The forces were elevated slightly in the actual published standard to peak at about 2600 N.)

Questions? Contact FDA/CDRH/OCE/DID at CDRH-FOISTATUS@fda.hhs.gov or 301-796-8118

Records processed under FOIA Request #2014-8015; Released by CDRH on 12-8-2015

FIGURE 26.18 AMTI Six-Station knee simulator capable of displacement control and force control with two sets of three identical TKR specimens in each. Each bank of three runs independently with its own programmable virtual soft tissue restraint system.

degrees when it should have been zero. Note lastly the absence of the first of the three axial load peaks at heel strike. All this pointed to the need of applying a correction to each input waveform.

Eleven iterative tuning processes were carried out until the inputs shown in the dotted lines of the left column of Figure 26.17 produced the response of the right column plots.

Measurement with sensors of the (actually) actuated input waveforms, thorough data processing, critical observation of the results, and repeated adaptation of those waveforms until they are at least symmetrical on all stations and follow the desired waveforms in phase and magnitude are therefore recommended as crucial but admittedly arduous steps for accurate wear simulation and testing of UHMWPE wear in TKR. It is the force-motion combinations at the load bearing stance that mostly govern wear, and so any substantial mismatches in that phase must be minimized. The corrections presented here are naturally frequency dependent and to some extent machine and specimen dependent. The verification and correction procedure to the inputs in wear testing of TKR implants with UHMWPE should be implemented to make results comparison within and across different laboratories more reliable. Indeed, the process of verification of the actuated input signals by measurement should be formally reported in the test results.

Only a machine with independent closed-loop control on each station would (attempt to) prevent this effect, resulting in double the complexity and cost of the simulator machine itself. Some modern and advanced simulators feature the so-called "adaptive control" in their driver software. In those simulators, adaptation is made automatically during running tests.

26.4.4 Choice of Lubricant in Testing UHMWPE Wear in Knee Replacements

In TKR simulation and wear testing, a substitute for the synovial fluid is needed as a lubricant. The primary functions of the knee's synovial fluid are lubrication and a medium to carry nutrition to the articular cartilage and waste products back to the blood vessels. Obviously, the lubrication and cooling functions and the stability against deterioration in the lubricant with time are needed in the *in vitro* testing situation. Therefore, however complex synovial fluid may be biologically, its simulant *in vitro* need not be that complex if it provides cooling and lubrication steady enough for test intervals long enough between convenient and economical lubricant changes. The purpose of this section is to attempt to draw from the literature and wealth of experience of others what is thought to be important and how to invite convergence in the types and dilution levels of lubricants used in wear testing.

As with most body fluids, the synovial fluid consists primarily of a high percentage of water. It is, however, a complex lubricant with protein content and hyaluronic acid, among other constituents. After knee joint replacement, the synovial fluid is expected to continue to be secreted into the joint space to lubricate the articulation of a typical CoCr metallic alloy femoral component with a UHMWPE tibial bearing and patellar component. However, its nature and content would vary between patients, their ages, activities, and the state of their joints. In wear testing, the lubricant is treated as one of the (supposedly!) controlled variables, assuming a simulated lubricant of an average TKR patient. Historically and for very good economical and practical reasons, there appears to be agreement in most of the published literature that bovine blood serum diluted with deionized water has more or less similar biological content, especially in terms of proteins, and is thus a good stimulant in TKR wear testing.

Nevertheless, the source, detailed composition and dilution level of the bovine serum has been considered an important factor influencing *in vitro* tested wear results [83–86]. The most consistently discussed, important, and mostly agreed upon of those factors is the concentration of proteins, which act as boundary lubricants on the UHMWPE. The interplay between the source/initial composition of the serum, its dilution level with deionized

Questions? Contact FDA/CDRH/OCE/DID at CDRH-FOISTATUS@fda.hhs.gov or 301-796-8118

Records processed under FOIA Request #2014-8015; Released by CDRH on 12-8-2015

water, and the heat generation/removal from the articulated surfaces affects protein precipitation onto the articulating surfaces, degradation of the proteins, and even calcification, which all affect the resulting wear processes.

One common pitfall in writing and interpreting published studies on this topic is to quote a percentage dilution of the protein in bovine serum. The percentages of dilution in published studies have varied widely. Among the reasons is the initial concentration of proteins in the serums used themselves, which depends on the source, processing, supplier, and even individual lot/batch used. Another difficulty in interpreting the literature is the emphasis of early studies on hip implants, assuming applicability on knee and general pin-on-disc studies. This may be so, but there is the extra difficulty in that the literature findings can be inconsistent or even incoherent sometimes.

From various published studies (such as [83–86] and others cited therein and elsewhere), the protein concentration in human synovial fluid centers around 20 g/l for healthy joints and rises to 30 g/l for some joint replacement patients and can reach even 55 g/l for some osteoarthritic knees. The ISO standard 14243-1 [38] (at the time of writing this chapter) had specified a percentage dilution (which is not useful for the reasons previously described), and it also specified for the protein concentration to *exceed* 17 g/l. Having not specified an exact value, various laboratories gathered data for 3–4 years with their different chosen protein concentrations. In an effort to target one value for the prospective revision of the ISO standard, and without much expertise on serum lubricant content, the author surveyed many orthopedic company and academic laboratory experts in an ASTM forum about what they thought and used and found the average to be around 20 g/l. This also happens to coincide with the protein concentration of normal knee synovial fluid, and it coincides with many test results that already exist on many implants across some laboratories. One popular other concentration used in TKR testing on many implant designs was actually 30 g/l from a very active lab in Germany. The two values were not that different in the author's view, and the literature [83–86] tends to suggest that 20 g/l may be expected to produce higher wear in testing than 30 g/l (see the end of this section for a specific citation of [87] to this end). Knee simulator testing is frequently accused of not being harsh enough to produce physiologically realistic wear levels that are seen *in vivo* or from UHMWPE bearing retrievals. Also, vitamin E doped or sequentially processed modern highly crosslinked UHMWPEs are increasingly advocated for TKR use. Their wear is so small that it makes them hardly measurable in simulator tests. Therefore, in the author's own laboratory, a protein concentration of 20 g/l has been used consistently throughout, and this is the value proposed after long discussion for the forthcoming ISO standard revision.

More variability may perhaps occur in UHMWPE wear testing results due to inconsistent volumes (per station) of diluted serum lubricant used, its cleanliness, consistency of serum replacement, and regular replenishment with deionized water and the onset of deterioration, protein deposits, and calcification. Attention to those areas may be more rewarding in achieving more consistent results. For this reason, additives are typically used to attempt to overcome such problems or delay their influence until a serum batch is due to be replaced (e.g., after nearly 1 week of, say, 0.5 millions walking cycles at 1 Hz simulator frequency). In the author's laboratory and many others, 2 g/l of sodium azide is usually added to the lubricant solution to slow bacterial growth, and 20 mM (7.45 g/l) of ethylenediaminetetraacetic acid (EDTA) is added to reduce calcification and protein precipitation.

The debate about lubricant serum type, content, and dilution for UHMWPE wear tests in knee simulators continues in earnest. More and more clinically relevant recipes for serum lubricant continue to emerge, partly divergent and sometimes convergent, in conclusions. For example, the importance of adding hylauronic acid was stressed and found to multiply simulator wear rates by nearly seven times [86]. Another recent study compared sera of different protein subconstituents from alpha calf and newborn and bovine sources, which were all found to be different and produced different TKR wear rates [87]. In the latter study, wear was found to increase with protein degradation and with more water dilution and decrease particularly with more albumin and α-1 globulin proteins in combination. Such studies continue to be useful and add to the much-needed knowledge in this field. However, caution is advised against prematurely standardizing methodologies based on early results. For example, sodium azide as well as hylauronic acid were used in the [86] study, where they were added to the lubricant in an anodized aluminum tibial dish holder in the knee simulator. That anodized aluminum surface is known to corrode, adding unaccounted-for third body debris particles (a possible serious multiplier of wear based on the author's own experience with this simulator and that very tibial dish holder that had to be upgraded with a stainless steel version very early on). Although statistical significance ($P<0.05$) was quoted for the findings in [87], only three TKR samples were tested for each effect for only 1.5–3 million cycle test stages. The differences in resulting wear rates in those intervals were approximately 20–50% only, which brings into question the statistical power of the findings. More test samples, more prolonged studies, and more variable control can only help extend such efforts to bring more consistent *in vitro* test lubricants with better isolated and more understood variable effects. Until then, in the humble opinion of the author, the more consistent and simply defined the serum lubricant for UHMWPE wear testing is, the more data comparison it will facilitate across laboratories.

Questions? Contact FDA/CDRH/OCE/DID at CDRH-FOISTATUS@fda.hhs.gov or 301-796-8118

Records processed under FOIA Request #2014-8015; Released by CDRH on 12-8-2015

26.5 CONCLUDING REMARKS AND FUTURE DIRECTIONS IN UHMWPE AND TKR LONGEVITY TEST METHODS

As a recap, this tour of tribological testing of UHMWPE destined for TKR started with pin-on-disk (POD) testing, where preliminary screening of *materials* is needed. POD testing was described and could not take any consideration of the TKR design in the planning of the test, except for choices of articular contact area of the pin and the stress levels through suitable choices of loading. POD is relatively simple, economical, and fast (typically <2 million cycles) and can be highly informative whenever new materials are to be assessed. Edge effects and other pitfalls were discussed, and wear was shown to be highly sensitive to the motion paths.

An abridged version of the history of knee simulators was outlined, as well as their use to evaluate whole TKR systems for functional performance and longevity. Knee *wear* simulators were shown to be a subset of other types of TKR simulators. They facilitate the testing of UHMWPE and other materials in combination with the individual TKR design and in combination with the implant installation/alignment factors. The reader should now be aware and hopefully able to contribute to the seemingly perpetual debate about the merits of force-control versus displacement-control testing methodologies, which were delved into in some detail here. Various pitfalls and areas of focus and attention in UHMWPE wear testing were discussed, hopefully convincing the reader that the process of TKR wear testing is typically highly costly and time consuming, especially if done well and with a critical eye for detail.

The future will carry exciting further developments into more sophisticated virtual soft-tissue simulation for the force-control methodology. More daily activities beyond walking will be simulated and in programmed sequential combinations with strenuous and rest periods. Testing will take the TKR systems to extremes of their motion and possibly reveal more UHMWPE failure modes in regions previously unconsidered *in vitro*. A new debate emerges as to whether there should be UHMWPE test methods dedicated especially for mobile bearing knee replacements. The answer is obvious for potential special damage modes that relate to the mobility, deformation, and potential subluxation of the UHMWPE bearing insert. Thus a stream of new test methods continue to be proposed and discussed (e.g., at ASTM). It is less clear what modifications are needed in testing UHMWPE wear during simulated walking with a mobile bearing knee.

There are other pressing needs for standardized testing methods, for example, testing of the UHMWPE in the patella. The forces and stresses there are equal if not higher than in the tibial bearings. Also, patella failures have been rife in the historical literature and do need the testing community's attention. The future may also carry exciting possibilities for new simulators to emerge or for current simulators and methods to be adapted to test implants for partial resurfacing of joints that share loads and contribute to the native articular surfaces of the knee.

In vitro testing of full artificial joint *systems* will remain a serious and costly endeavor, especially for total knee replacement. Perhaps *the* most important thing to stress in conclusion is the *importance of testing* itself as an integral part of the implant design process. The rest of the messages in this chapter pertain to how to do the testing well.

REFERENCES

1. Walker PS, Haider H. Characterizing the motion of total knee replacements in laboratory tests. *J Clin Orthop Relat Res* 2003;**410**:54–68.
2. Shaw JA, Murray MD. Knee joint simulator. *Clin Orthop Relat Res* 1973;**94**:15–23.
3. Harding ML, Harding L, Goodfellow JW. A preliminary report of a simple rig to aid study of the functional anatomy of the cadaver human knee joint. *J Biomech* 1977;**10**:517–21.
4. Zavatsky AB. A kinematic-freedom analysis of a flexed-knee-stance testing rig. *J Biomech* 1997;**30**:277–80.
5. Rovick JS, Reuben JD, Schrager RJ, Walker PS. Relation between knee motion and ligament length patterns. *J Clin Biomech* 1991;**6**:213–20.
6. Zachman NJ, Hillbery BM, Kettlekamp DB. Design of a load simulator for the dynamic evaluation of prosthetic knee joints. ASME 1978:78-DET-59.
7. Maletsky LP, Hillberry BM. Simulating dynamic activities using a five-axis knee simulator. *J Biomech Eng* 2005;**127**(1):123–33.
8. Maletsky LP, Clary CW, Guess TM, Mane AM, Reeve AN. In vitro simulation of deep knee flexion using static and dynamic machines. *Proc. ASME 2008; Summer Bioengineering Conference (SBC2008).* Marco Island, Florida, USA.
9. Dürselen L, Cales L, Kiefer H. The influence of muscle forces and external loads on cruciate ligament strain. *Am J Sports Med* 1995; **23**(1):129–36.
10. Haider H, Walker PS. Measurements of constraint of total knee replacement. *J Biomech* 2005;**38**(2):341–8.
11. Darcy SP, Kilger RHP, Woo SL-Y, Debski RE. Estimation of ACL forces by reproducing kinematics between sets of knees, a novel non-invasive methodology. *J Biomech* 2006;**39**(13):2371–7.
12. Li G, Most E, Sultan PG, Schule S, Zayontz S, Park SE, Rubash HE. Knee kinematics with a high-flexion posterior stabilized total knee prosthesis: an in vitro robotic experimental investigation. *J Bone Joint Surg [Am]* 2004;**86-A**(8):1721–9.
13. Most E, Li G, Sultan PG, Park SE, Rubash HE. Kinematic analysis of conventional and high-flexion cruciate-retaining total knee arthroplasties: an in vitro investigation. *J Arthroplasty* 2005;**20**(4):529–35.
14. Hill MR, Catledge SA, Konovalov V, Clem WC, Chowdhury SA, Etheridge BS, Stanishevsky A, Lemons JE, Vohra YK, Eberhardt AW. Preliminary tribological evaluation of nanostructured diamond coatings against ultra-high molecular weight polyethylene. *J Biomed Mater Res Part B, Appl Biomater* 2008;**85B**:140–8.
15. Cornwall GB, Bryant JT, Hansson CM. The effect of kinematic conditions on the wear of ultrahigh molecular weight polyethylene (UHMWPE) in orthopaedic bearing applications. *Proc Inst Mech Eng, Part H* 2000;**215**:95–106.
16. Bragdon CR, O'Connor DO, Lowenstein JD, Jasty M, Syniuta WD. The importance of multidirectional motion on the wear of polyethylene. *Proc Inst Mech Engrs, Part H: J Eng Med* 1996;**210**(H3):157–65.

Questions? Contact FDA/CDRH/OCE/DID at CDRH-FOISTATUS@fda.hhs.gov or 301-796-8118

Records processed under FOIA Request #2014-8015; Released by CDRH on 12-8-2015

17. Muratoglu OK, Bragdon CR, O'Conner DO, Jasty M, Harris WH, Gul R, McGarry F. Unified wear model for highly crosslinked ultra-high molecular weight polyethylenes (UHMWPE). *J Biomater* 1999;**20**:1463–70.
18. Burroughs BR, Blanchet TA. Factors affecting the wear of irradiated UHMWPE. *Tribol Trans* 2001;**44**:215–23.
19. Wang A. A unified theory of wear for ultra-high molecular weight polyethylene in multi-directional sliding. *J Wear* 2001;**248**:38–47.
20. Hamilton MA, Sucec MC, Fregly BJ, Banks SA, Sawyer WG. Quantifying multidirectional sliding motions in total knee replacements. *J Tribol* 2005;**127**:280–6.
21. ASTM F732-00. Standard test method for wear testing of polymeric materials used in total joint prostheses. *ASTM Int* 2006. West Conshohocken, PA.
22. Gevaert MR, LaBerge M, Gordon JM, DesJardins JD. The quantification of physiologically relevant cross shear wear phenomena on orthopaedic bearing materials using a novel wear testing machine. *J Tribol* 2005;**127**(4):740–9.
23. Fisher J, Dowson D, Hamdzah H, Lee HL. The effect of sliding velocity on the friction and wear of UHMWPE for use in total artificial joints. *J Wear* 1994;**175**:219–25.
24. Lewis G. Contact stress at articular surfaces in total joint replacements. Part II: analytical and numerical methods. *Bio-Med Mater Eng* 1998;**8**:259–78.
25. Walker PS. Biomechanics of total knee replacement designs, chapter 15. In: Mow V, Huiskes R, editors. *Basic orthopaedic biomechanics and mechano-biology*. 3rd ed: Lippincott, Williams and Wilkins; 2004. p. 657–702.
26. Walker PS, Blunn GW, Lilley PA. Wear testing of materials and surface for total knee replacement. *J Biomed Mater Res (Appl Biomater)* 1996;**33**:159–75.
27. Sathasivam S, Walker PS, Campbell PA, Rayner K. The effect of contact area on wear in relation to fixed bearing and mobile bearing knee replacements. *J Biomed Mater Res* 2001;**58**(3):382–90.
28. Mazzucco D, Spector M. Effects of contact area and stress on the volumetric wear of ultrahigh molecular weight polyethylene. *J Wear* 2003;**254**(5-6):514–22.
29. Mazzucco D, Spector M. Contact area as a critical determinant in the tribology of metal-on-polyethylene total joint arthroplasty. *J Tribol* 2006;**128**(1):113–21.
30. Saikko V. Effect of contact pressure on wear and friction of ultra-high molecular weight polyethylene in multidirectional sliding. *Proc Inst Mech Eng, Part H: J Eng Med* 2006;**220**(7):723–31.
31. Vassiliou K, Unsworth A. Is the wear factor in total joint replacements dependent on the nominal contact stress in ultra-high molecular weight polyethylene contacts? *Proc Inst Mech Eng, Part H: J Eng Med* 2004;**218**:101–7.
32. Bartel DL, Bicknell VL, Wright TM. The effect of conformity, thickness and material on stresses in ultra-high molecular weight components for total joint replacement. *J Bone Joint Surg (A)* 1986;**68-A**:1041–52.
33. Lee K-Y, Pienkowski D. Viscoelastic recovery of creep-deformed ultra-high molecular weight polyethylene (UHMWPE). In: Gsell RA, editor. Chapter in *Characterization and properties of ultra-high molecular weight polyethylene*. STP1307-EB ASTM Publications.
34. Churchill DL, Incavo SJ, Johnson CC, Beynnon BD. The transepicondylar axis approximates the optimal flexion axis of the knee. *J Clin Orthop* 1998;**356**:111–8.
35. Iwaki H, Pinskerova V, Freeman MAR. Tibiofemoral motion 1: the shapes and relative movements of the femur and tibia in the unloaded cadaver knee. *J Bone Joint Surg (B)* 2000;**82B**:1189–95.
36. Blankevoort L, Huiskes R, De Lange A. Helical axes of passive knee joint motions. *J Biomech* 1990;**23**:1219–29.
37. Grood ES, Suntay WJ. A joint coordinate system for the clinical description of three-dimensional motions: application to the knee. *J Biomech Eng* 1983;**105**:136–44.
38. ISO 14243-1. Implants for surgery—wear of total knee-joint prostheses —Part 1: loading and displacement parameters for wear-testing machines with load control and corresponding environmental conditions for test, International Organization for Standardization; 2002.
39. Andriacchi TP, Johnson TS, Hurwitz DE, Natarajan RN. Musculosleletal dynamics, locomotion and clinical applications, chapter 3. In: Mow V, Huiskes R, editors. *Basic orthopaedic biomechanics and mechano-biology*. 3rd ed. Lippincott, Williams and Wilkins; 2004. p. 91–121.
40. Nordin M, Frankel VH. Biomechanics of the knee, chapter 7. In: Nordin M, Frankel VH, editors. *Basic biomechanics of the musculoskeletal system*. 3rd ed. Lippincott, Williams & Wilkins; 2001.
41. Swanson SAV, Freeman MAR, Heath JC. Laboratory tests on total joint replacement prosthesis. *J Bone Joint Surg [B]* 1973;**55B**:759–73.
42. Dowson D, Jobbins B, O'Kelly J, Wright V. A knee joint simulator, chapter 7. *Evaluation of artificial hip joints*. UK: Biological Engineering Society; 1977. p. 79–90.
43. Dowson D, Gillis BJ, Atkinson JR. Penetration of metallic femoral components into polymeric tibial components observed in a knee joint simulator. American Chemical Society Symposium Series No. 287, Polymer Wear Contr 1985; p. 215–28.
44. Pappas MJ, Buechel FF. New Jersey knee simulator. *Trans of the 11th Annu Int Biomater Symp* 1979;**3**:101.
45. Pappas MJ, Buechel FF. On the use of a constraint radius femoral component in meniscal bearing knee replacement. *J Orthop Rheum* 1994;**7**:27–9.
46. DiAngelo DJ, Harrington IJ. Design of a dynamic multi-purpose joint simulator. *Adv Bioeng* 1992;**22**:107–11. ASME Bioeng Div Publ BED.
47. Walker PS, Hsieh HH. Conformity in condylar replacement knee prostheses. *J Bone Joint Surg* 1977;**59B**:222–8.
48. Burgess IC, Kolar M, Cunningham JL, Unsworth A. Development of a six station knee wear simulator and preliminary wear results. *Proc Inst Mech Eng, Part H: J Eng Med* 1997;**211**:37–47.
49. Haider H, Walker PS, Blunn GW, Perry J, DesJardins J. A four channel force control knee simulator: from concept to production. *Proceedings of the 11th Annual Symposium, International Society for Technology in Arthroplasty [ISTA]*, Marseille, France; 1998. p. 213–14.
50. Walker PS, Blunn GW, Perry JP, Bell CJ, Sathasivam S, Andriacchi TP, Paul JP, Haider H, Campbell PA. Methodology for long-term wear testing of total knee replacements. *Clin Orthop Relat Res* 2000;**372**:290–301.
51. Walker PS, Blunn GW, Broome DR, Perry J, Watkins A, Sathasivam S, Dewar ME, Paul JP. A knee simulating machine for performance evaluation of total knee replacements. *J Biomech Tech Note* 1997;**30**:83–9.
52. Blunn GW, Bell CJ, Walker PS, Chaterjee S, Perry J, Cambell P, Haider H, Paul JP. Simulator testing of total knee replacements, chapter 9. In: Hutchings IM, editor. *Friction, lubrication and wear of artificial joints*. Professional Engineering Publishing; 2003. p. 113–25. ISBN 1 86058 363 6.
53. DesJardins JD, Walker PS, Haider H, Perry J. The use of a force-controlled dynamic knee simulator to quantify the mechanical performance of total knee replacement designs. *J Biomech* 2000;**33**:1231–42.

Questions? Contact FDA/CDRH/OCE/DID at CDRH-FOISTATUS@fda.hhs.gov or 301-796-8118

Records processed under FOIA Request #2014-8015; Released by CDRH on 12-8-2015

54. Haider H, Walker PS. Analysis and recommendations for the optimum spring configurations for soft tissue restraint in force-control knee simulator testing. *Trans Orthop Res Society, 48th Annual Meeting*; 2002.
55. Haider H, Walker P, DesJardins J, Blunn G. Effects of patient and surgical alignment variables on kinematics in TKR simulation under force-control. *J ASTM Int (JAI)* 2006;**3**(10).
56. ISO 14243-3. Implants for surgery—wear of total knee-joint prostheses—Part 3: loading and displacement parameters for wear-testing machines with displacement control and corresponding environmental conditions for test, International Organization for Standardization; 2004.
57. Mikosz RP, Andriacchi TP, Andersson GBJ. Model analysis of factors influencing the prediction of muscle forces at the knee. *J Orthop Res* 1988;**6**:205–14.
58. Morrison JB. The mechanics of the knee joint in relation to normal walking. *J Biomech* 1970;**3**:51–61.
59. Johnson TS, Laurent MP, Yao JQ, Gilbertson LN. The effect of displacement control input parameters on tibiofemoral prosthetic knee wear. *Wear* 2001;**250**:222–6.
60. Knight LA, Pal S, Coleman JC, Bronson F, Haider H, Levine DL, Taylor M, Rullkoetter PJ. Comparison of long-term numerical and experimental total knee replacement wear during simulated gait loading. *J Biomech* 2007;**40**(7):1550–8.
61. Laz P, Pal S, Halloran J, Petrella J, Rullkoetter PJ. Probabilistic finite element prediction of knee wear simulator mechanics. *J Biomech* 2006;**39**(12):2303–10.
62. Rawlinson JJ, Furman BD, Li S, Wright TM, Bartel DL. Retrieval, experimental, and computational assessment of the performance of total knee replacements. *J Orthop Res* 2006;**24**(7):1384–94.
63. Haider H, Garvin K. Rotating platform versus fixed-bearing total knees—an in vitro study of wear. *Clin Orthop Relat Res* 2008;**466**:2677–85.
64. Taylor SJG, Walker PS, Perry JS, Cannon SR, Woledge R. The forces in the distal femur and the knee during walking and other activities measured by telemetry. *J Arthroplasty* 1998;**13**:428–37.
65. Taylor SJG, Walker PS. Force and moments telemetered from two distal femoral replacements during various activities. *J Biomech* 2001;**34**:839–48.
66. Taylor WR, Heller MO, Bergmann G, Duda GN. Tibio-femoral loading during human gait and stair climbing. *J Orthop Res* 2004;**22**:625–32.
67. D'Lima DD, Patil S, Steklov N, Chien S, Colwell Jr. C. In vivo knee moments and shear after total knee arthroplasty. *J Biomech* 2007;**40**:S11–7.
68. Haider H, Sekundiak TD, Garvin KL. Simulation of the spring-based soft tissue restraint in testing knee wear under force control. *Proceedings of the First International Conference on Mechanics of Biomaterials & Tissues*. Hawaii, USA; 2005 December.
69. Fukubayashi T, Torzilli PA, Sherman MF, Warren RF. An in-vitro biomechanical evaluation of anterior-posterior motion of the knee. *JBJS* 1982;**64-A**:258–64.
70. Benson LC, DesJardins JD, Harman MK, LaBerge M. Effect of stair descent loading on UHMWPE wear in a force-controlled knee simulator. *Proc Inst Mech Engrs (Part. H, J Eng Med)* 2002;**216**(6): 409–18.
71. DesJardins JD, Banks SA, Benson LC, Pace T, Laberge M. A direct comparison of patient and force-controlled simulator total knee replacement kinematics. *J Biomech* 2007;**40**(15):3458–66.
72. Haider H, Walker PS, Blunn GW. Are the kinematics of different TKR designs targeted for the same patient the same? *Trans Orthop Res Society, 48th Annual Meeting*. Dallas, TX; 2002.
73. Verbal communication with Drs. Todd. S. Johnson and Les Gilbertson of Zimmer Inc. between 2001 and 2008.
74. Johnson TS, Andreacchi T, Laurent M. Development of a knee wear test method based on prosthetic in vivo slip velocity profiles. *Trans Orthop Res Society, 46th Annual Meeting*. FL; 2000.
75. Johnson TS. *PhD Thesis*. University of Minnesota; 1999.
76. Andriacchi TP, Alexander EJ, Toney MK, Dyrby CO, Sum J. A point cluster method for in vivo motion analysis: applied to a study of knee kinematics. *J Biomech Eng* 1998;**120**:743–9.
77. Haider H, Alberts LR, Laurent MP, Johnson TS, Yao J, Gilbertson LN, Walker PS, Neff JR, Garvin KL. Comparison between force-controlled and displacement-controlled in-vitro wear testing on a widely used TKR implant. *Trans Orthop Res Society, 48th Annual Meeting*. Dallas, TX; 2002 February.
78. Anderson DR, Sweeney DJ, Williams TA. Chapter 8. In: *Introduction to Statistics, Concepts and Applications*. 3rd ed. St. Paul, MN: West Publishing Co. ISBN: 0-314-02813-7.
79. Taylor JR. *An introduction to error analysis—the study of uncertainties in physical measurements*: University Science Books, Oxford University Press; 1982 ISBN 0-935702-10-5.
80. ISO 14243-2. Implants for surgery—wear of total knee-joint prostheses—Part 2: methods of measurement, International Organization for Standardization; 2006.
81. Muratoglu OK, Rubash HE, Bragdon CR, Burroughs BR, Huang A, Harris WH. Simulated normal gait wear testing of a highly cross-linked polyethylene tibial insert. *J Arthroplasty* 2007;**22**(3):435–44.
82. Fisher J, McEwen HMJ, Tipper JL, Jennings LM, Farrar R, Stone MH, Ingham E. Wear-simulation analysis of rotating-platform mobile bearing knees. *Orthop* 2006;**29**:36–41.
83. Clarke C, Chan FW, Essner A, Good V, Kaddick C, Lappalainen R, Laurent M, McKellop H, McGarry W, Schroeder D, Selenius M, Shen MC, Ueno M, Wang A, Yao JQ. Multi-laboratory simulator studies on effects of serum proteins on PTFE cup wear. *J Wear* 2001;**250**:188–98.
84. Liao YS, Benya PD, McKellop HA. Effect of protein lubrication on the wear properties of materials for prosthetic joints. *J Biomed Mater Res, Appl Biomater* 1999;**48**:465–73.
85. Yao JQ, Laurent MP, Johnson TS, Blanchard CR, Crowninshield RD. The influences of lubricant and material on polymer/CoCr sliding friction. *J Wear* 2003;**255**:780–4.
86. DesJardins JD, Aurora A, Tanner SL, Pace TB, LaBerge DM. Increased total knee arthroplasty ultra-high molecular weight polyethylene wear using a clinically relevant hyaluronic acid simulator lubricant. *Proc Inst Mech Eng, Part. H, J Eng Med* 2006;**220**(5): 609–23.
87. Brandt JM, Charron K, Zhao L, Medley JB, MacDonald SJ, Bourne RB, McCalden, RW. Development of a clinically relevant lubricant for in-vitro wear testing of total knee replacements. *Proc. 75th Annual Meeting AAOS, Poster* 137;477.

Questions? Contact FDA/CDRH/OCE/DID at CDRH-FOISTATUS@fda.hhs.gov or 301-796-8118

Records processed under FOIA Request #2014-8015; Released by CDRH on 12-8-2015
The Journal of Arthroplasty Vol. 27 No. 3 2012

Does Vitamin E–Stabilized Ultrahigh-Molecular-Weight Polyethylene Address Concerns of Cross-Linked Polyethylene in Total Knee Arthroplasty?

Hani Haider, PhD,* Joel N. Weisenburger,* Steven M. Kurtz, PhD,† Clare M. Rimnac, PhD,‡ Jordan Freedman,§ David W. Schroeder,§ and Kevin L. Garvin, MD*

Abstract: Concerns about reduced strength, fatigue resistance, and oxidative stability of highly cross-linked and remelted ultrahigh-molecular-weight polyethylene (UHMWPE) have limited its clinical acceptance for total knee arthroplasty. We hypothesized that a highly cross-linked UHMWPE stabilized with vitamin E would have less oxidation and loss of mechanical properties. We compared the oxidation, in vitro strength, fatigue-crack propagation resistance, and wear of highly cross-linked UHMWPE doped with vitamin E to γ-inert–sterilized direct compression-molded UHMWPE (control). After accelerated aging, the control material showed elevated oxidation, loss of small-punch mechanical properties, and loss of fatigue-crack propagation resistance. In contrast, the vitamin E–stabilized material had minimal changes and exhibited 73% to 86% reduction in wear for both cruciate-retaining and posterior-stabilized total knee arthroplasty designs. Highly cross-linked vitamin E–stabilized UHMWPE performed well in vitro.
Keywords: TKA, UHMWPE, vitamin E, durability, wear, fatigue.
© 2012 Elsevier Inc. All rights reserved.

Highly cross-linked ultrahigh-molecular-weight polyethylene (UHMWPE) is associated with reduced wear of total hip arthroplasty inserts [1-7]. Compared with conventional, γ-inert–sterilized UHMWPE, in vitro simulator studies suggest that highly cross-linked bearing liners in the hips result in more than 90% reduction in wear rates [1-4]. This is supported by reduced femoral head penetration in intermediate-term radiographic studies [5-7].

However, there have been concerns about reduced strength, fatigue resistance, and in vivo oxidation of a highly cross-linked UHMWPE [8,9]. Case studies of liner rim fracture in the hip have highlighted this concern [9-11]. Much higher stresses (eg, up to 60 MPa) and more complex stress patterns are involved in total knee arthroplasty (TKA) bearings compared with hips, and this has been associated with surface damage [12]. Highly cross-linked UHMWPE has not been widely used in TKA because of clinical concern about the compromise in its mechanical properties, especially its ductility and fatigue-crack propagation resistance as a result of the loss of molecular mobility that accompanies the cross-linking process itself [4,13,14]. After radiation cross-linking, unstabilized residual free radicals in the material also have the potential to oxidize, which decreases the molecular weight of the material and may compromise its strength [15,16].

Highly cross-linked UHMWPEs have been produced by radiation and postprocessed by either remelting or annealing. Remelting reduces free radicals to undetectable levels, which may prevent in vivo oxidation [1,17]. However, the crystallinity is reduced, and this compromises the mechanical properties [18]. Annealing the polymer (heating to below melting point) after irradiation [19,20] is also a compromise because it eliminates some but not all of the free radicals and, thus, may lead to in vivo oxidation [21,22].

*From the *Department of Orthopaedic Surgery and Rehabilitation, University of Nebraska Medical, Center, Omaha, Nebraska; †Exponent Inc, Philadelphia, Pennsylvania; ‡Department of Mechanical and Aerospace Engineering, Case Western Reserve University, Cleveland, Ohio; and §Biomet Inc, Warsaw, Indiana.*
Submitted May 12, 2010; accepted March 11, 2011.
The Conflict of Interest statement associated with this article can be found at doi:10.1016/j.arth.2011.03.024.
Reprint requests: Hani Haider, PhD, Department of Orthopaedic Surgery and Rehabilitation, University of Nebraska Medical Center, 985360 Nebraska Medical Center–Scott Technology Center, Omaha, NE 68198.
© 2012 Elsevier Inc. All rights reserved.
0883-5403/2703-0021$36.00/0
doi:10.1016/j.arth.2011.03.024

Questions? Contact FDA/CDRH/OCE/DID at CDRH-FOISTATUS@fda.hhs.gov or 301-796-8118

Records processed under FOIA Request #2014-8015; Released by CDRH on 12-8-2015

Several processes have been attempted to address the limitations introduced by remelting and annealing after irradiation [23,24]. One approach to reduce the potential for oxidation has been to add α-tocopherol (vitamin E) to UHMWPE as an antioxidant [25]. Improvement in delamination fatigue resistance was demonstrated in irradiated UHMWPE with vitamin E in severe 2-dimensional sliding tests [26]. In this and in later studies [27], vitamin E was blended with the UHMWPE powder before compression molding. This vitamin E blending at the powder stage reduces the efficiency of subsequent radiation cross-linking [27]. More recently, researchers have doped UHMWPE with vitamin E after highly cross-linking the polymer, and as demonstrated in a series of studies, this proved to be more promising in the preservation of strength and fatigue properties [18,28-32]. *Doping* here refers to impregnation by soaking the molded UHMWPE in warm vitamin E, followed by further prolonged diffusion at temperatures below the melting point of the cross-linked UHMWPE.

We hypothesized that highly cross-linked UHMWPE stabilized with vitamin E (E1®; Biomet Orthopedics, Warsaw, Ind) would improve the oxidation resistance compared with γ-sterilized direct compression-molded (conventional; hereafter termed the *DCM* or *control*) UHMWPE, maintain mechanical properties after aging, and secure the improved wear performance associated with its elevated level of cross-linking. To test this hypothesis, we sought to address 3 research questions: (1) Does E1 UHMWPE preserve its static mechanical properties after accelerated aging? (2) Does E1 UHMWPE preserve its fatigue-crack growth resistance after accelerated aging? (3) Does E1 UHMWPE exhibit lower wear than the control UHMWPE in cruciate-retaining (CR) and posterior-stabilized (PS) designs evaluated in a knee simulator?

Materials and Methods

In this experimental study, we explored the main effects of bearing material (E1 UHMWPE and γ-inert–sterilized UHMWPE as controls) and accelerated aging (0, 2, and 4 weeks of aging). For each experimental condition, outcomes were measured for oxidation index, as determined by Fourier transform infrared spectroscopy; static mechanical properties, as determined by the small punch test; fatigue-crack propagation resistance, as determined by the notched fatigue test; and wear, as determined by in vitro knee simulator testing. Expected effect differences, confidence limits, statistical power, and the required sample sizes were based on similar statistical considerations as detailed in previous studies [24,33]. For the oxidation and small punch tests, the expected effect size for the power calculations for accelerated aging and small punch testing was a 20% relative difference in the outcome measure of interest from its baseline (unaged) condition. A power analysis was not conducted for the fatigue-crack propagation tests. For the wear tests, a 2-sided (α level) P value of .05 yielded more than 85% statistical power for a sample size of 3 and more than 93% power for a sample size of 4.

Material Preparation

The E1 material for this experiment (Fig. 1) was manufactured from isostatically compression-molded UHMWPE bar stock (GUR 1020 resin from Ticona, Germany). The material was irradiated with a dose of 100 ± 10 kGy (Steris, Libertyville, Ill) and infused with vitamin E in a 2-step process. The specimens were soaked in vitamin E for 0.3 to 1.5 hours at 122°C, and vitamin E was allowed to diffuse through the thickness of the polyethylene in an inert gas oven for 64 to 164 hours at 130°C. Each category of E1 specimen was compared, using its respective testing method, with its corresponding control specimens from DCM GUR 1050 UHMWPE packaged in inert gas with γ-radiation sterilization at 32 kGy (range, 25-40 kGy).

The specimens for the small punch tests were machined from the E1 material into rectangular blocks (about 1 in. square and 0.25 in. thick) (Fig. 1A). The specimens for the oxidation index measurements and fatigue-crack propagation testing were similarly made and sized but were round-notched disks, as shown in Fig. 1B. All these specimens were then cleaned in isopropyl alcohol and γ-sterilized in barrier film packaging (25-40 kGy; Steris).

Both the E1 and control DCM materials were evaluated in the nonaged and 2- and 4-week accelerated aged conditions. The aging was accelerated according to the American Society for Testing and Materials (ASTM) F2003-02 [34], in which the specimens were removed from their packaging and placed in a pure oxygen chamber heated to 70°C ± 1°C and pressurized to 503 ± 7 kPa for the prescribed period.

Oxidation

The extent of oxidation was determined for each of the nonaged and aged material groups. For this purpose, an oxidation index was determined by infrared spectroscopy in accordance with ASTM F2102-06 [35].

Static Mechanical Properties

To determine static mechanical strength, small punch tests were conducted on 36 samples divided into 6 groups (n = 6 in each) based on the 2 material types and the accelerated aging periods of 0, 2, and 4 weeks. The small punch tests were carried out according to ASTM F2183-02 [36], which is essentially an equi-biaxial tension test (to failure). Peak load, ultimate load, ultimate displacement, and energy to failure were determined.

Questions? Contact FDA/CDRH/OCE/DID at CDRH-FOISTATUS@fda.hhs.gov or 301-796-8118

Records processed under FOIA Request #2014-8015; Released by CDRH on 12-8-2015

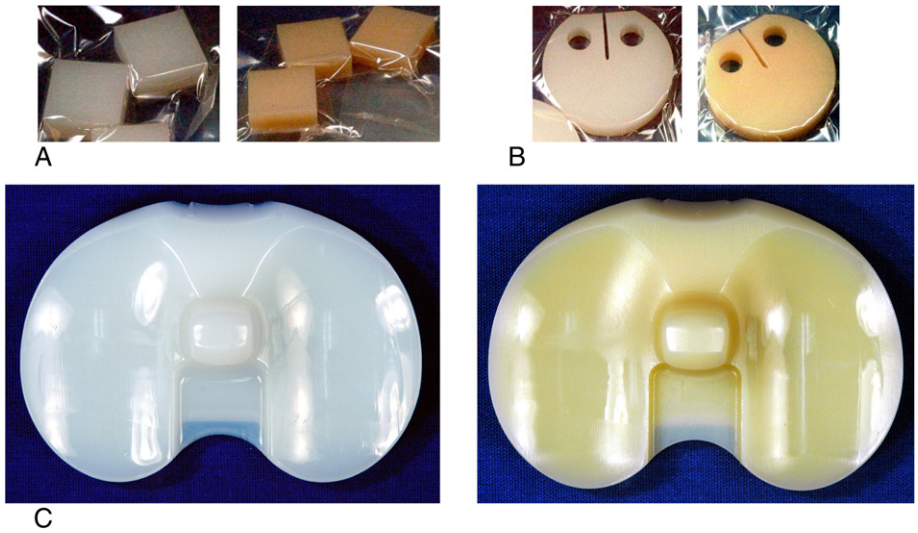

Fig. 1. (A-C) UHMWPE specimens for small punch testing (A), specimens for fatigue-crack propagation (B), and PS tibial bearing insert specimens for simulator wear testing (C). The DMC UHMWPE specimens (left) are usually white, but the vitamin E–doped samples (right) show a distinct light brown color because of the vitamin E content.

Fatigue-Crack Propagation Tests

Fatigue-crack propagation tests were conducted to examine the differences in fatigue-crack propagation resistance between E1 and the control materials (DCM) in the nonaged and 2- and 4-week aged conditions. Two to 3 specimens were tested of each material type (E1 UHMWPE and DCM) and aging condition (0, 2, and 4 weeks). The fatigue tests were performed using ASTM E647-05 [37] as a guide on an Instron closed-loop servohydraulic test system (Instron, Norwood, Mass). Specimens were cycled with a sinusoidal waveform at a test frequency of 3 Hz, with an R ratio of 0.1 (ratio of minimum load to maximum load). Specimens were cooled with an air jet to minimize specimen heating during cycling. Crack growth from the razor-sharpened notch was followed using a traveling microscope at 0.01-mm resolution, recording crack length (a), and number of cycles (n) initially every 0.2 mm. When 0.2 mm of crack growth was reached in less than 100 cycles, the measurements were taken at 0.1-mm intervals. The fatigue-crack growth rate, da/dn (mm/cycle), and the cyclic stress intensity factor, ΔK (MPa $m^{0.5}$), were calculated according to ASTM E647-05 [37]. The data for specimens in each material group were pooled, and linear regression analysis of the log-log–transformed da/dn vs ΔK data was used to determine the exponent (m) and coefficient (C) of the Paris relationship ($da/dn = C\Delta K^m$). For this purpose, data in the fatigue-crack growth rate (da/dn) ranging from 1×10^{-4} to 1×10^{-2} mm/cycle were used.

Knee Simulation Tests

For knee simulator wear testing, Vanguard® TKA CR and PS system designs (Biomet Orthopedics, Warsaw, Ind) were used. The E1 tibial bearings (an example of a PS version is shown in Fig. 1C) were processed similarly to the earlier described E1 test specimens. However, because the tibial bearing inserts were generally larger, the soaking period in vitamin E was lengthened to 4.5 hours, and the diffusion time in inert gas was more than doubled to 360 hours. The finished tibial bearings were also cleaned, γ-sterilized, and packaged for clinical use (25-40 kGy; Steris). For wear testing, 10 whole TKA systems with E1 inserts were compared with 10 corresponding controls of DCM UHMWPE in 4 separate full-knee simulator tests, simulating walking gait for 5 million cycles each.

The wear testing method used was exactly as detailed in a previous study [33] and according to the ISO 14243-1:2009 and 14243-2:2009 standard testing methodology under the force-control regime [38,39]. Eight posterior-cruciate–sacrificing PS TKAs of the largest size (87/91-mm bearings against 80-mm femoral components) with 4 E1 and 4 DCM UHMWPE (control) specimens (n = 4 in each) were staggered on identical stations of two 4-station Instron-Stanmore knee simulators (originally made by Instron in Norwood, MA, then comprehensively upgraded in-house in Omaha, Neb). For soft-tissue restraint, spring settings simulating both anterior cruciate ligament and posterior cruciate ligament as sacrificed were set for this PS TKA implant [39]. The largest size of TKA was chosen for this test so that maximal wear would result, expecting wear, in the regime of loading for a simulated walking gate cycle, to increase faster with the larger contact area (of a big-size implant) than with increased contact stresses (in a small-size implant). Twelve CR knees were tested on a single AMTI knee simulator (Watertown, Mass), with 6 test stations operating under the force-control testing

Questions? Contact FDA/CDRH/OCE/DID at CDRH-FOISTATUS@fda.hhs.gov or 301-796-8118

Records processed under FOIA Request #2014-8015; Released by CDRH on 12-8-2015

regime [39]. Six specimens of the largest size (same as previously mentioned) and 6 of the smallest size (59-mm CR bearings against 55-mm femoral components) were again chosen to cover the maximum contact stress situation. The 12 CR specimens on the AMTI knee simulator tests were divided into 4 subgroups (n = 3 in each) based on bearing material (E1 vs DCM) and size (largest vs smallest). The E1 bearing and DCM control bearing tests were ran in series.

Statistical Modeling

For the oxidation index analyses and small punch tests, comparisons between materials and aging conditions were performed using a step-forward multivariate analysis of variance (ANOVA). An interaction term between materials and aging was incorporated into the ANOVA model. Comparisons between specific aging/-material conditions were performed using post hoc Tukey tests, with $P < .05$ established for significance. Statistical modeling was performed using the JMP software (version 7.0; JMP, Cary, NC). For the fatigue-crack propagation tests, the exponent, m, and the coefficient, C, for the pooled data for each material test group were compared between materials using the linear test method on the log-log–transformed da/dn vs ΔK behavior in the Paris regime, with $P < .05$ established for significance. For the wear tests, we compared the effect of material type (E1 UHMWPE vs control) accounting for design (CR vs PS design) and size (small vs large) as covariates. The least-squares error method was used to calculate the best-fit linear regression line through the wear curve (wear vs cycles) for each specimen and thus compute a "wear rate" from its slope. The wear curves from each subgroup were statistically compared using a random regression coefficient model to infer the statistical significance of the equality of the wear rates (ie, to estimate a P value to test a null hypothesis of no difference in wear rates) using a PROC MIXED procedure (SAS/STAT software, version 9.1.3; SAS Institute, Cary, NC).

Results

The oxidation index results (Table 1) showed an increase from 0 to 1.9 ± 0.1 in 4 weeks for the DCM material, but that for the E1 material increased to only 0.1 ± 0.1. The vitamin E–stabilized material exhibited 12% and 541% higher ultimate strength than did the control ($P < .0001$ for ANOVA material effect, $P < .0001$ for material × aging interaction, $P < .05$ for post hoc Tukey test) after 0 and 4 weeks of accelerated aging, respectively (Figs. 2 and 3). The peak load was sensitive to changes in the material ($P = .004$) but not in the aging condition ($P = .49$); however, a material × aging interaction was observed ($P = .01$) (Fig. 3). For the E1 material, ultimate load, displacement, and energy to failure were insensitive to aging (Figs. 3 and 4). In contrast, these parameters decreased for the DCM UHMWPE ($P < .0001$ for aging effect).

The E1 material showed no significant difference in fatigue-crack propagation behavior (C and m of the Paris relationship; Table 2) between the nonaged and 2-week aged conditions ($P = .219$ and $P = .117$, respectively). There also was no difference between the nonaged and 4-week aged conditions in C and m ($P = .2660$ and .120, respectively). With the DCM control material, there was a significant difference in C but not in m between the nonaged and 2-week aged conditions ($P < .001$ and $P = .450$, respectively), such that there was an apparent improvement in fatigue-crack propagation resistance, as evidenced by a lower C value (Table 2). There was a significant difference in both C and m between the DCM nonaged and 4-week aged conditions and also between the 2- and 4-week aged conditions ($P < .001$), such that the 4-week aged condition demonstrated reduced fatigue-crack propagation resistance, as evidenced by a higher C value. There was a significant difference in both C and m ($P < .001$) between the nonaged E1 and DCM materials, such that the E1 material was less resistant to fatigue-crack growth (higher C value). There was no difference in C ($P = .721$) but a significant difference in m ($P < .001$) between the E1 and DCM materials in the 4-week aged condition. During the fatigue-crack propagation tests, some material bridging was observed to occur between the crack faces in the DCM-aged groups; this made it more difficult to identify the crack tip during testing. Hence, there was more scatter in the fatigue-crack propagation data for the DCM tests in the 2- and 4-week aged conditions than for the E1 tests.

The vitamin E–stabilized material exhibited a significant reduction of 86%, 85%, and 73% ($P = .0003$, $<.0001$, and .0002) in wear for both the PS and the largest and smallest CR designs, respectively (Figs. 5 and 6). Wear of the smallest (59-mm size) CR DCM bearing inserts was less than a third ($P < .0001$) of that of the largest (87/91 mm) CR bearings of the same DCM control material. In the highly cross-linked E1 material, although the wear was smaller overall as mentioned previously, that of the smallest CR bearing was half ($P = .054$) that of the largest. No gross delamination or fracture of the tibial inserts was observed on any of the knee simulator wear tests, and this was expected because none of the UHMWPE

Table 1. Average Oxidation Index Results by Study Group

Study Group	Material	Accelerated Aging (wk)	Average Oxidation Index
1	DCM	None	0.0 ± 0.00
2	DCM	2	0.3 ± 0.02
3	DCM	4	1.9 ± 0.10
4	E1	None	0.0 ± 0.00
5	E1	2	0.1 ± 0.02
6	E1	4	0.1 ± 0.01

Questions? Contact FDA/CDRH/OCE/DID at CDRH-FOISTATUS@fda.hhs.gov or 301-796-8118

Records processed under FOIA Request #2014-8015; Released by CDRH on 12-8-2015

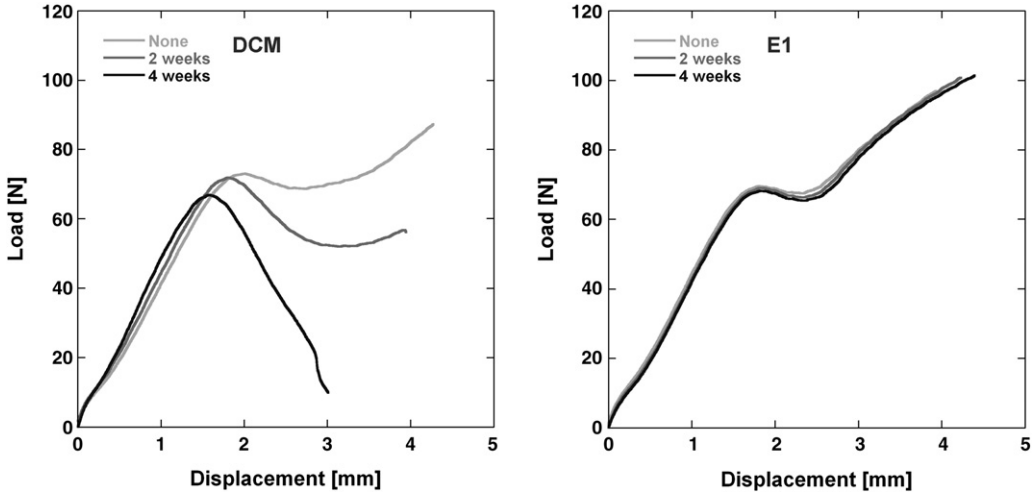

Fig. 2. Representative results of the small punch test for aged and nonaged specimens from the conventional DCM UHMWPE (left) and E1 UHMWPE (right) groups. The curves for both materials were almost identical except for the E1 UHMWPE preserving its strength much better with aging.

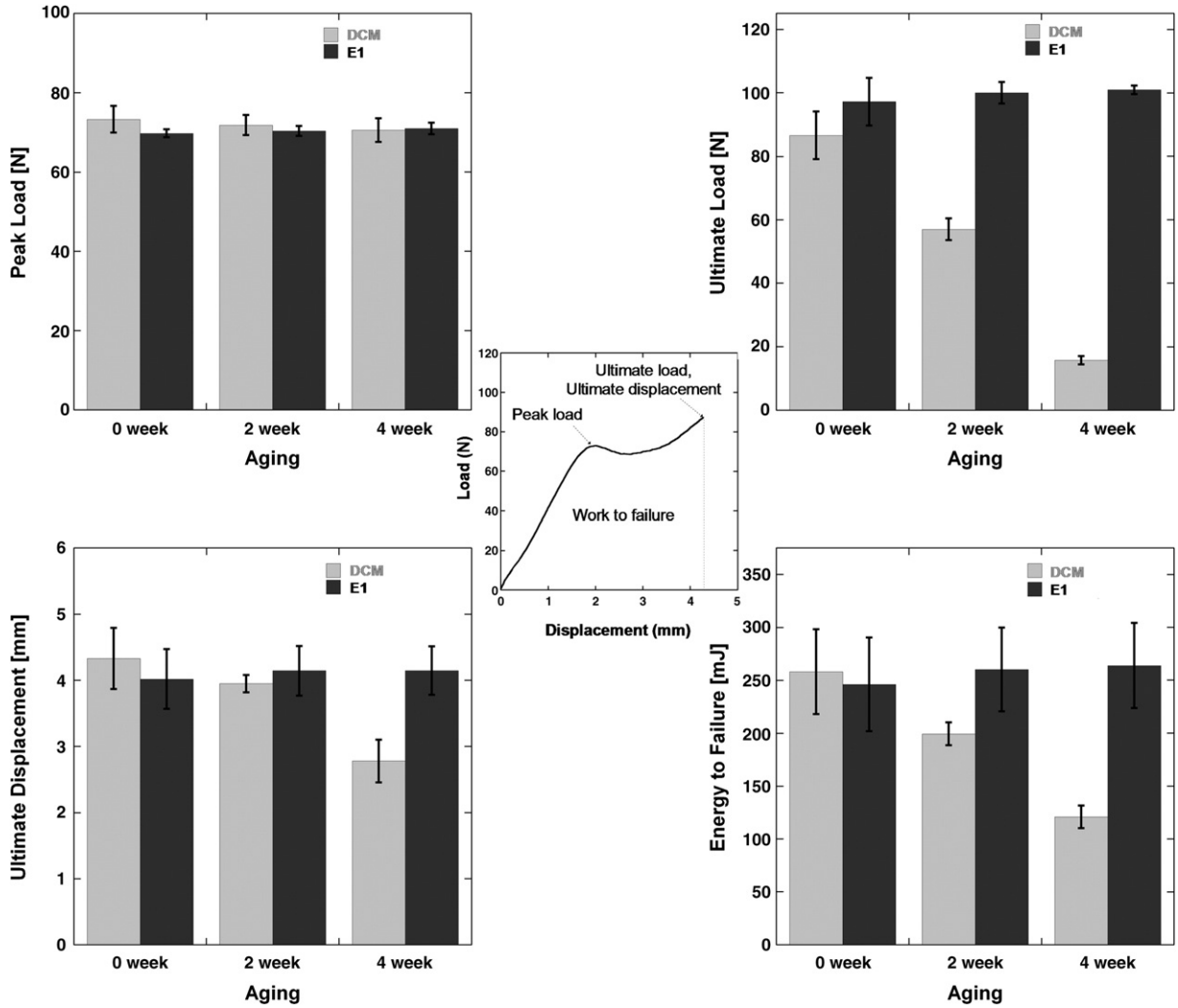

Fig. 3. Average mechanical properties for the E1 material compared with the DCM controls and how these properties varied with aging time. Peak load (top left), ultimate load (top right), ultimate displacement (lower left), energy to failure (lower right), and parameter key (center).

Questions? Contact FDA/CDRH/OCE/DID at CDRH-FOISTATUS@fda.hhs.gov or 301-796-8118

Records processed under FOIA Request #2014-8015; Released by CDRH on 12-8-2015

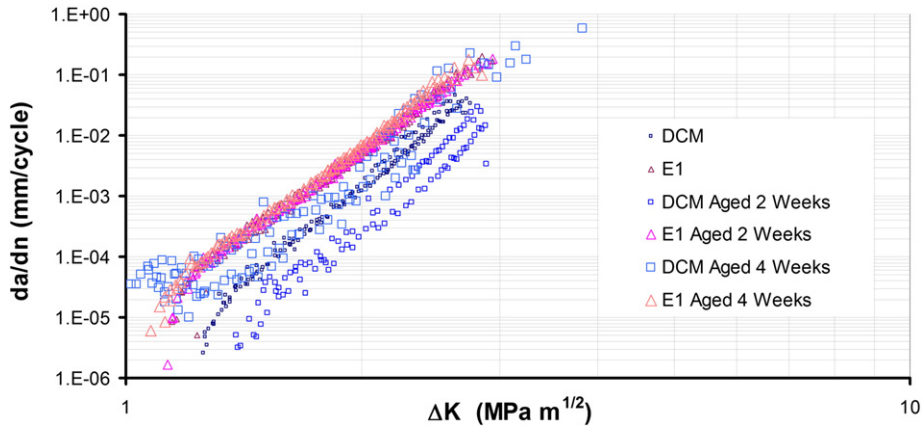

Fig. 4. Fatigue testing results shown for both the DCM and the E1 study groups. Fatigue-crack growth rate (da/dn) is plotted against cyclic stress intensity factor (ΔK).

bearing inserts were aged and all were sterilized in inert gas packaging.

Discussion

The results of this study supported our hypothesis that the E1 UHMWPE would exhibit improved wear performance and oxidation resistance without unduly compromising its mechanical properties. We found that the E1 UHMWPE preserved its static mechanical properties and fatigue-crack growth behavior after accelerated aging. We also found that the E1 UHMWPE exhibited lower wear than did the control UHMWPE in PS and CR designs evaluated in a knee wear simulator.

Our study design was complicated by differences in resin between the E1 and control materials. The E1 and control materials originated from GUR 1020 and 1050 UHMWPE resins, respectively. The E1 specimens in this study were made from GUR 1020 because its high-impact strength is well suited for knee applications. The control materials were fabricated from GUR 1050 resin, which is currently used in the Vanguard TKA design. Overall, differences in resin between the control and E1 materials were not considered to have influenced the wear resistance and oxidation resistance findings from our study, which were governed by radiation cross-linking and vitamin E stabilization (respectively) rather than resin type, as explained further below.

In some parts of our study, we subjected the UHMWPE to a severe in vitro oxidative challenge, which is considered to be an acceleration of real-time shelf aging for historic materials that were γ-radiation sterilized in air [40-42]. The aging method should not be interpreted as a model of real-time aging of UHMWPE sterilized by methods other than γ-radiation in air, nor could it, or any other in vitro experiment, totally simulate long-term oxidation in vivo. Despite these limitations, the protocol we used has been standardized by ASTM International and is widely used by the UHMWPE biomaterial community to evaluate the relative oxidative stability of highly cross-linked materials.

Long-term diffusion of vitamin E out of the UHMWPE and loss of protection have been raised as a potential concern. The long-term clinical effects of any material cannot be completely proven in vitro, so this has been a limitation of this and any in vitro study. Based on the first principles, we do not expect substantial elution of vitamin E, a hydrophobic fat-soluble macromolecule, into a polar, water-based in vivo environment. Several studies have been conducted to experimentally simulate the long-term behavior of vitamin E in UHMWPE [29,43]. The diffusion was found to closely follow Fick's second law

Table 2. Fatigue-Crack Propagation Results

Study Group	Material	Accelerated Aging (wk)	Exponent, m	Coefficient, C
1 (n = 3)	DCM control	None	10.31	1.15×10^{-6}
2 (n = 2)	DCM control	2	10.62	2.03×10^{-7}
3 (n = 2)	DCM control	4	7.42	1.06×10^{-5}
4 (n = 3)	E1	None	8.88	1.06×10^{-5}
5 (n = 2)	E1	2	9.00	9.66×10^{-6}
6 (n = 2)	E1	4	9.09	1.16×10^{-5}

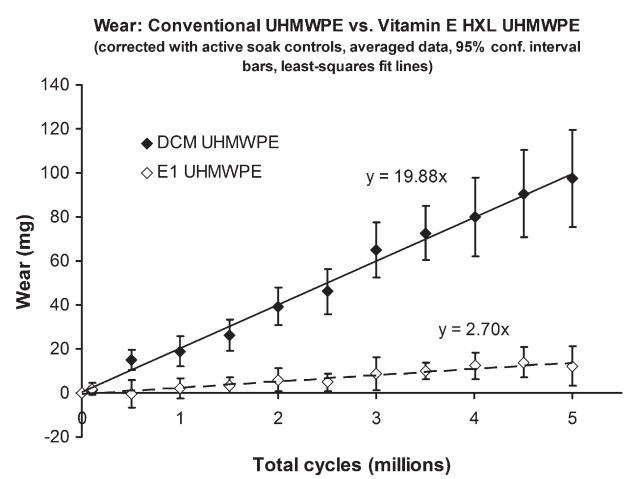

Fig. 5. Sample-corrected and sample-averaged 5-million-cycle test wear results for the PS TKA design, with n = 4 in each curve.

Questions? Contact FDA/CDRH/OCE/DID at CDRH-FOISTATUS@fda.hhs.gov or 301-796-8118

Records processed under FOIA Request #2014-8015; Released by CDRH on 12-8-2015

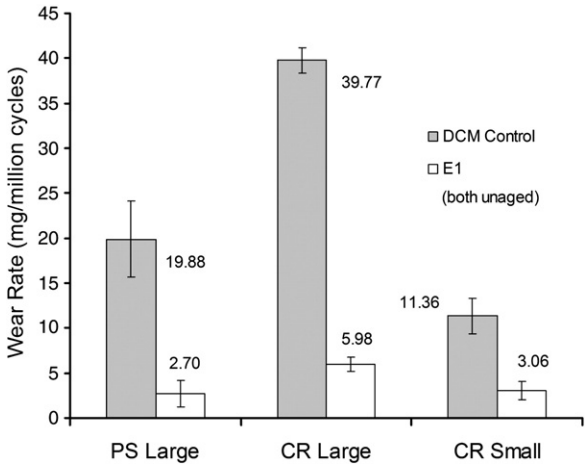

Fig. 6. The averaged wear results and 95% confidence limits for all the knee simulator tests. "Large" represents the largest TKA size of 87/91-mm bearing inserts, and the "small" represents the smallest (59 mm in size), with the highest contact stress.

[29]. Early (7 months) experimental results on elution found no change in the oxidative stability of vitamin E–doped highly cross-linked UHMWPE after 5-million-cycle hip simulator testing with a normal gait, indicating minimal elution [43]. More recent and extensive studies [44] completed 3 years of real-time aging on 100-kGy irradiated, vitamin E–stabilized, and γ-sterilized blocks (40°C water). When the vitamin E index was 0.1, the same as in the TKAs tested in our study, the vitamin E concentration profiles measured as a function of time showed that the solubility of vitamin E in UHMWPE and the surrounding environment had come to an equilibrium and that the driving force for the vitamin E to diffuse out was minimized. After this, not much elution was expected. In another study [45], hip acetabular liners that were 85 kGy irradiated, vitamin E diffused, and γ-sterilized had the vitamin E forcefully extracted with hexane to below detectable levels. These liners were accelerated in aging after extraction of all detectable amounts of vitamin E, and no oxidation was found. This prompted the authors of those studies to postulate that minute (undetectable) quantities of vitamin E had still remained and sufficed, and/or were not extractable, or were perhaps grafted (chemically bonded) to the polyethylene chains. That study [45] was the nearest to a worst-case scenario of in vitro testing reported thus far, short of waiting for tens of years. Analysis of long-term future clinical retrievals will be the only way to ultimately determine the extent of vitamin E elution if any, but this was not the focus of the current study nor was it particularly addressed in measurements here.

Our aging experiments showed that vitamin E is an effective antioxidant for UHMWPE. The stabilizing effect of vitamin E has been observed in several other studies [18,28,46] with similar methodologies and from similar recent tests [47] on UHMWPE cross-linked with 75 kGy of γ-radiation (both GUR 1020 and 1050 resins). Unstabilized UHMWPE showed higher oxidation indices, subsequent oxidative embrittlement, and lower ultimate strength when aged compared with the same polymers with vitamin E [47].

The fatigue-crack propagation results support that fatigue-crack propagation resistance is maintained in E1 UHMWPE after 2 and 4 weeks of accelerated aging. Aging for either 2 or 4 weeks did not significantly alter the fatigue-crack propagation behavior of the E1 material, as determined by comparing the Paris regime parameters of each treatment group. This finding is consistent with the lack of significant difference in the oxidative index values for the aged E1 UHMWPE groups vs the nonaged condition.

Aging had an unexpected effect on the DCM UHMWPE, with the 2-week aged condition showing apparently improved fatigue-crack propagation behavior and the 4-week aged condition showing reduced fatigue-crack propagation behavior compared with the nonaged DCM condition. It is not clear at this time why the 2-week aged condition showed improved fatigue-crack propagation behavior because it would be expected that aging would reduce the fatigue-crack propagation behavior of the control UHMWPE.

The fatigue-crack propagation results support the finding that nonaged E1 UHMWPE has less fatigue-crack propagation resistance relative to nonaged DCM UHMWPE. This finding is consistent with a report by Oral et al [30] on highly cross-linked UHMWPE containing vitamin E. The fatigue-crack propagation behavior of UHMWPE is influenced both by the extent of cross-linking of the polymer and by the percent crystallinity. Generally, there is a loss of resistance to fatigue-crack growth with an increase in cross-linking; this loss can be somewhat offset by maintaining crystallinity [48]. Studies of first-generation-type highly cross-linked UHMWPE materials and retrieved acetabular hip components suggest that they may be more susceptible to fracture under challenging clinical conditions such as impingement compared with unaged conventional UHMWPE [48]. At present, however, the clinical significance of the comparative reduction in fatigue-crack propagation performance of the unaged E1 vs unaged DCM UHMWPE materials in this study cannot be definitively stated.

The clinical performance can also be expected to be influenced by component design. In a separate study [49], the fatigue resistance of one of the TKR bearing component designs of the current study was evaluated to determine if the difference in fatigue-crack propagation resistance of the material would affect the fatigue strength of the PS post in that design. The PS posts for E1 and DCM Vanguard tibial bearings were subjected to cyclic loading at the highest point of their post. This was

Questions? Contact FDA/CDRH/OCE/DID at CDRH-FOISTATUS@fda.hhs.gov or 301-796-8118

Records processed under FOIA Request #2014-8015; Released by CDRH on 12-8-2015

accomplished by orienting the bearing at a 30° angle from the table and the femoral at a 45° angle to the bearing and by applying a 1300-lb force cyclic load through the femoral component. This study demonstrated that the fatigue resistance of the PS post on the E1 bearings was similar to that of the PS post of the DCM Vanguard tibial bearings. It is important to investigate not only material properties such as fatigue-crack propagation resistance but also component design and its effects on fatigue performance.

The vitamin E–stabilized highly cross-linked UHMWPE tibial bearings reduced overall wear by 73% to 86% when compared with tibial bearings of the same design made of the control material when tested under the force-control regime [39]. Several previous studies [4,50-52] have noted improved in vitro wear resistance after elevated doses of radiation cross-linking after knee simulator wear testing under the displacement-control regime [39].

In summary, in this in vitro study, this highly cross-linked UHMWPE stabilized with vitamin E was able to maintain mechanical strength after accelerated aging, maintain fatigue-crack propagation resistance upon accelerated aging, and produce 73% to 86% lower wear compared with the control UHMWPE. Highly cross-linked UHMWPE stabilized with vitamin E performed well in vitro for TKA applications. These results are hoped to translate to clinically meaningful improvements in longevity in vivo, which can only be determined through clinical evaluation.

References

1. Muratoglu OK, Bragdon CR, O'Connor DO, et al. HAP Paul Award: a novel method of crosslinking UHMWPE to improve wear, reduce oxidation, and retain mechanical properties. J Arthroplasty 2001;16:149.
2. Muratoglu OK, Bragdon CR, O'Connor D, et al. Larger diameter femoral heads used in conjunction with a highly cross-linked ultra-high molecular weight polyethylene: a new concept. J Arthroplasty 2001;16:24.
3. Muratoglu OK, O'Connor DO, Bragdon CR, et al. Gradient crosslinking of UHMWPE using irradiation in molten state for total joint arthroplasty. J Biomaterials 2002;23:717.
4. Harris WH, Muratoglu OK. A review of current crosslinked polyethylenes used in total joint arthroplasty. Clin Orthop Relat Res 2005;430:46.
5. Garvin KL, Hartman CW, Mangla J, et al. Wear analysis in THA utilizing oxidized zirconium and crosslinked polyethylene. Clin Orthop Relat Res 2009;467:141.
6. Roerhl S, Nivbrant B, Mingguo L, et al. In vivo wear and migration of high cross linked poly cups: a RSA study. J Arthroplasty 2005;20:409.
7. Digas G, Karrholm J, Thanner J, et al. 5-Year experience of highly cross-linked polyethylene in cemented and uncemented sockets: two randomized studies using radiostereometric analysis. Acta Orthop 2007;78:746.
8. Pruitt L, Koo J, Rimnac CM, et al. Cyclic compressive loading results in fatigue cracks in ultra high molecular weight polyethylene. J Orthop Res 1994;13:143.
9. Gillis AM, Schmieg JJ, Bhattacharyya S, et al. An independent evaluation of the mechanical, chemical, and fracture properties of UHMWPE cross linked by 34 different conditions. Trans Orthop Res Soc 1999;45:908.
10. Tower SS, Currier JH, Currier BH, et al. Rim cracking of the cross-linked longevity polyethylene acetabular liner after total hip arthroplasty. J Bone Joint Surg Am 2007;89:2212.
11. Furmanski J, Anderson M, Bal S, et al. Clinical fracture of cross-linked UHMWPE acetabular liners. Biomaterials 2009;30:5572.
12. Bartel DL, Rawlinson JJ, Burstein AH, et al. Stresses in polyethylene components of contemporary total knee replacements. Clin Orthop 1995;317:76.
13. Gomoll A, Wanich T, Bellare A. J-intergral fracture toughness and tearing modulus measurement of radiation cross-linked UHMWPE. J Orthop Res 2002;20:1152.
14. Muratoglu OK, Oral EO, Valhi A, et al. Limitations of crosslinked polyethylenes and two potential second generation solutions. Presented at the Annual Meeting. AAOS: American Academy of Orthopaedic Surgeons; 2005.
15. Sutula LC, Collier JP, Saum KA, et al. The Otto Aufranc Award: impact of gamma sterilization on clinical performance of polyethylene in the hip. Clin Orthop Relat Res 1995;319:28.
16. Collier JP, Sperling DK, Currier JH, et al. Impact of gamma sterilization on clinical performance of polyethylene in the knee. J Arthroplasty 1996;11:377.
17. McKellop H, Shen FW, Lu B, et al. Development of an extremely wear resistant ultra-high molecular weight polyethylene for total hip replacements. J Orthop Res 1999;17:157.
18. Oral E, Wannomae KK, Hawkins N, et al. Alpha-tocopherol doped irradiated UHMWPE for high fatigue resistance and low wear. Biomaterials 2004;25:5515.
19. Bergström JS, Rimnac CM, Kurtz SM. Molecular chain stretch is a multiaxial failure criterion for conventional and highly crosslinked UHMWPE. J Orthop Res 2005;23:367.
20. Sobieraj MC, Kurtz SM, Rimnac CM. Notch strengthening and hardening behavior of conventional and highly crosslinked UHMWPE under applied tensile loading. Biomaterials 2005;26:3411.
21. Kurtz SM, Hozack W, Turner J, et al. Mechanical properties of retrieved highly crosslinked crossfire liners after short term implantation. J Arthroplasty 2005;20:840.
22. Kurtz SM, Hozack WJ, Purtill JJ, et al. 2006 Otto Aufranc Award paper: significance of in vivo degradation for polyethylene in total hip arthroplasty. Clin Orthop 2006;453:47.
23. Wang A, Zeng H, Yau SS, et al. Wear, oxidation, and mechanical properties of a sequentially irradiated and annealed UHMWPE in total joint replacement. J Phys D Appl Phys 2006;39:3213.
24. Kurtz SM, Mazzucco D, Rimnac CM, et al. Anisotropy and oxidative resistance of highly crosslinked UHMWPE after deformation processing by solid-state ram extrusion. Biomaterials 2006;27:24.

Questions? Contact FDA/CDRH/OCE/DID at CDRH-FOISTATUS@fda.hhs.gov or 301-796-8118

Records processed under FOIA Request #2014-8015; Released by CDRH on 12-8-2015

25. Berzen J, Luketic D. Stabilised polyethylene moulding materials, esp for implants containing polyethylene with molecular wt. 10^5-10^7, antioxidant, and tocopherol, esp. alpha-tocopherol or vitamin E, as stabilizer. European Patent 1994;613:923.
26. Tomita N, Kitakura T, Onmori N, et al. Prevention of fatigue cracks in ultrahigh molecular weight polyethylene joint components by the addition of vitamin E. J Biomed Mater Res 1999;48:474.
27. Shibata N, Tomita N. The antioxidative properties of alpha-tocopherol in gamma-irradiated UHMWPE with respect to fatigue and oxidation resistance. Biomaterials 2005;26:5755.
28. Oral E, Greenbaum ES, Malhi AS, et al. Characterization of irradiated blends of alpha-tocopherol and UHMWPE. Biomaterials 2005;26:6657.
29. Oral E, Wannomae K, Rowell S, et al. Diffusion of vitamin E in ultra-high molecular weight polyethylene. Biomaterials 2007;28:5225.
30. Oral E, Christensen S, Malhi A, et al. Wear resistance and mechanical properties of highly cross-linked ultra-high molecular weight polyethylene doped with vitamin E. J Arthroplasty 2006;21:580.
31. Parth M, Aust N, Lederer K. Studies on the effect of electron beam radiation on the molecular structure of ultra-high molecular weight polyethylene under the influence of alpha-tocopherol with respect to its application in medical implants. J Mater Sci Mater Med 2002;13:917.
32. Wolf C, Maninger J, Lederer K, et al. Stabilization of ultra-high molecular weight polyethylene (UHMW-PE) acetabular components with alpha-tocopherol. J Mater Sci Mater Med 2006;17:1323.
33. Haider H, Garvin K. Rotating platform versus fixed-bearing total knees: an in vitro study of wear. Clin Orthop Relat Res 2008;466:2677.
34. ASTM Standard F2003-02, 2008. Standard practice for accelerated aging of ultra-high molecular weight polyethylene after gamma irradiation in air. Conshohocken (Pa): ASTM International, West; 2008; doi:10.1520/F2003-02R08.
35. ASTM Standard F2102-06, 2006. Standard guide for evaluating the extent of oxidation in ultra-high-molecular-weight polyethylene fabricated forms intended for surgical implants. West Conshohocken (Pa): ASTM International; 2008; doi:10.1520/F2102-06.
36. ASTM Standard F2183-02, 2008. Standard test method for small punch testing of ultra-high molecular weight polyethylene used in surgical implants. West Conshohocken (Pa): ASTM International; 2008; doi:10.1520/F2183-02R08.
37. ASTM Standard ASTM E647 – 05, 2005. Standard test method for measurement of fatigue crack growth rates. West Conshohocken (Pa): ASTM International; 2008; doi:10.1520/E0647-05.
38. ISO 14243;2009. Implants for surgery—wear of total knee-joint prostheses—part 1: loading and displacement parameters for wear-testing machines with load control and corresponding environmental conditions for test and part 2: methods of measurement. International Organization for Standardization, Geneva, Switzerland.
39. Haider H. Tribological assessment of UHMWPE. In: Kurtz SM, editor. UHMWPE Biomaterials Handbook. 2nd ed. Academic Press; 2009; p. 381.
40. Costa L, Bracco P, Brach del Prever EM, et al. Oxidation and oxidation potential in contemporary packaging for polyethylene total joint replacement components. J Biomed Mater Res B Appl Biomater 2006;78:20.
41. Crowninshield RD, Muratoglu OK. Implant Wear Symposium 2007 Engineering Work Group. How have new sterilization techniques and new forms of polyethylene influenced wear in total joint replacement? J Am Acad Orthop Surg 2008;16(Suppl 1):S80.
42. Currier BH, Currier JH, Mayor MB, et al. In vivo oxidation of gamma-barrier sterilized ultra-high-molecular-weight polyethylene bearings. J Arthroplasty 2007;22:721.
43. Oral E, Wannomae KK, Rowell SL, et al. Migration stability of alpha-tocopherol in irradiated UHMWPE. Biomaterials 2006;27:2434.
44. Rowell S, Oral E, Muratoglu O. Three-year real-time aging of vitamin E–diffused, radiation cross-linked UHMWPE. Presented at the Annual Meeting. Orthopaedic Research Society 55th Annual Meeting; 2009.
45. Oral E, Rowell SL, Muratoglu O. Oxidation resistance of vitamin E–doped, irradiated UHMWPE for total joints following forceful extraction of vitamin E. Presented at the Annual Meeting: Orthopaedic Research Society 52nd Annual Meeting; 2006.
46. Oral E, Malhi AS, Wannomae KK, et al. Highly cross-linked ultrahigh molecular weight polyethylene with improved fatigue resistance for total joint arthroplasty. J Arthroplasty 2008;23:1037.
47. Kurtz SM, Dumbleton J, Siskey RS, et al. Trace concentrations of vitamin E protect radiation crosslinked UHMWPE from oxidative degradation. J Biomed Mater Res A 2008.
48. Rimnac C, Pruitt L. How do material properties influence wear and fracture mechanisms? J Am Acad Orthop Surg 2008;16(Suppl 1):S94.
49. Freedman J, Schroeder D. Performance of tibial bearings manufactured from highly-crosslinked, vitamin E infused, UHMWPE. Presented at the Annual Meeting. Translational Research Symposium, Society for Biomaterials, Atlanta, GA; 2008.
50. Muratoglu OK, Bragdon CR, Jasty M, et al. Knee-simulator testing of conventional and cross-linked polyethylene tibial inserts. J Arthroplasty 2004;19:887.
51. Muratoglu OK, Rubash HE, Bragdon CR, et al. Simulated normal gait wear testing of a highly cross-linked polyethylene tibial insert. J Arthroplasty 2007;22:435.
52. Wang A, Yau SS, Essner A, et al. A highly crosslinked UHMWPE for CR and PS total knee arthroplasties. J Arthroplasty 2008;23:559 [Epub ahead of print 2008 Feb 13].

Questions? Contact FDA/CDRH/OCE/DID at CDRH-FOISTATUS@fda.hhs.gov or 301-796-8118

Records processed under FOIA Request #2014-8015; Released by CDRH on 12-8-2015

Society For Biomaterials

Macrophage reactivity to different polymers demonstrates particle size- and material-specific reactivity: PEEK-OPTIMA® particles versus UHMWPE particles in the submicron, micron, and 10 micron size ranges

Nadim James Hallab,[1,2] Kyron McAllister,[1] Mark Brady,[3] Marcus Jarman-Smith[3]

[1]Department of Orthopedic Surgery, Rush University Medical Center, Chicago, Illinois 60612
[2]BioEngineering Solutions Inc., Oak Park, Illinois 60304
[3]Invibio Biomaterial Solutions, Lancashire FY5 4QD, UK

Received 12 January 2011; revised 8 June 2011; accepted 12 July 2011
Published online 21 November 2011 in Wiley Online Library (wileyonlinelibrary.com). DOI: 10.1002/jbm.b.31974

Abstract: Biologic reactivity to orthopedic implant debris is generally the main determinant of long-term clinical performance where released polymeric particles of Ultra-high molecular weight polyethylene (UHMWPE) remain the most prevalent debris generated from metal-on-polymer bearing total joint arthroplasties. Polymeric alternatives to UHMWPE such as polyetherether-ketone (PEEK) may have increased wear resistance but the bioreactivity of PEEK-OPTIMA particles on peri-implant inflammation remains largely uncharacterized. We evaluated human monocyte/macrophage responses (THP-1s and primary human) when challenged by PEEK-OPTIMA, UHMWPE, and X-UHMWPE particles of three particle sizes (0.7 um, 2 um, and 10 um) at a dose of 20 particles-per-cell at 24- and 48-h time points. Macrophage responses were measured using cytotoxicity assays, viability assays, proliferation assays and cytokine analysis (IL-1b, IL-6, IL-8, MCP-1, and TNF-α). In general, there were no significant differences between PEEK-OPTIMA, UHMWPE, and X-UHMWPE particles on macrophage viability or proliferation. However, macrophages demonstrated greater cytotoxicity responses to UHMWPE and X-UHMWPE than to PEEK-OPTIMA at 24 and 48 h, where 0.7 μm-UHMWPE particles produced the highest amount of cytotoxicity. Particles of X-UHMWPE more than PEEK-OPTIMA and UHMWPE induced IL-1β, IL-6, MCP-1, and TNF-α at 24 h, $p < 0.05$ (no significant differences at 48 h). On average, cytokine production was more adversely affected by larger 10 μm particles than by 0.7 and 2 μm sized particles. While limitations of *in vitro* analysis apply to this study, PEEK-OPTIMA particles were more biocompatible than UHMWPE particles, in that they induced less inflammatory cytokine responses and thus, in part, demonstrates that PEEK-OPTIMA implant debris does not represent an increased inflammatory risk over that of UHMWPE. © 2011 Wiley Periodicals, Inc. J Biomed Mater Res Part B: Appl Biomater 100B: 480–492, 2012.

Key Words: MG-63 osteoblasts, THP-1 macrophages, fibroblasts, particles, PEEK, UHMWPE

How to cite this article: Hallab NJ, McAllister K, Brady M, Jarman-Smith M. 2012. Macrophage reactivity to different polymers demonstrates particle size- and material-specific reactivity: PEEK-OPTIMA® particles versus UHMWPE particles in the submicron, micron, and 10 micron size ranges. J Biomed Mater Res Part B 2012:100B:480–492.

INTRODUCTION

Biologic reactivity to implant particulate debris is the main determinant of long term performance.[1] Aseptic osteolysis accounts for over 75% of total joint arthroplasties (TJA) of all implant failures and is the central factor limiting the longevity of current TJAs; other reasons for failure include infection (7%), recurrent dislocation (6%), periprosthetic fracture (5%), and surgical error (3%).[2] Wear and corrosion products are attributed with these local inflammatory responses leading to aseptic failure.[3–11]

Polymeric debris from TJA generated through wear mechanisms induce untoward effects in the peri-implant space, usually through the macrophage-mediated formation of inflammatory foreign-body reactions forming granulation tissue. This has the ability to compromise the integrity of the bone-implant interface and contribute to the pathophysiology of peri-implant bone loss (i.e., osteolysis).[12,13] In human studies of loose implants, granulomatous epithelioid membranes coating the metal implants have been associated with loose total hip replacements,[14–17] where bone radiolucency or osteolysis was associated with the locations responsible for implant debris production. While peri-implant cells like osteoblasts and fibroblasts have been shown to be negatively affected by implant debris, macrophages are professionally dedicated to phagocytosing debris, initiating a local immune response and are more commonly known in orthopedics as the major cell type responsible for mediating the proinflammatory response to debris that leads to inflammation and device loosening over time. Particles induce macrophages to secrete inflammatory mediators

Correspondence to: N. J. Hallab; e-mail: nhallab@rush.edu

 © 2011 WILEY PERIODICALS, INC.

Questions? Contact FDA/CDRH/OCE/DID at CDRH-FOISTATUS@fda.hhs.gov or 301-796-8118

Records processed under FOIA Request #2014-8015; Released by CDRH on 12-8-2015

including TNF-α, IL-1β, IL-6, MCP-1, IL-8, and PGE2, stimulating differentiation of osteoclast precursors into mature osteoclasts resulting in increased periprosthetic bone resorption.[18] Although metallic implant debris has been reported to cause a multitude of reactions such as activation of the adaptive immune system (T-cells and B-cells) through antigen presentation,[19] release of proinflammatory mediators,[20–24] cytotoxicity,[25] DNA damage,[25–27] and oxidative stress,[28] polymeric implant debris has not. General effects of all wear debris particles include interruption of mesenchymal stem cell differentiation into functional osteoblasts,[29] and particles can directly inhibit osteoblast[30] synthesis of collagen and induce osteoblast apoptosis.[31] Of these many possible types of responses, it is the subtle persistent proinflammatory responses to wear debris in the local environment, alone that has been correlated with polymeric implant performance.[32] Exactly which materials and which sizes of particles are most reactive remains controversial, especially among materials of similar chemistry/material type, for example, polymers. Some studies suggest that phagocytosable size particles are the most stimulatory in a dose dependent manner (often up to a saturation level).[21,33–35] There is growing consensus that particles need to be less than 10 μm, that is, within a phagocytosable range to produce an *in vitro* inflammatory response,[23,36–38] where particles with a mean size of 0.24 μm to 7.2 μm are more proinflammatory.[23,36,37,39,40] However, there is disagreement as to which specific size(s) and/or dose of particles (particles/cell or particles/tissue volume) are most inflammatory.[23,35–37,41–43] It has been suggested that the internalization of small particles in the nanometer sizes (< 150 nm) occurs by endocytosis or pinocytosis for particles,[35,44,45] whereas larger particles (> 150 nm to 10 μm) are phagocytosed in the traditional manner inside phagosomes/lysosomes by a range of peri-implant cells types including osteoblasts, fibroblasts, endothelial cells, and macrophages.

Newer polymeric materials, such as polyetherether-ketone (PEEK), with promising wear resistance characteristics[46] are potential alternatives to polyethylene in metal-on-polymer bearing surfaces. However, the proinflammatory potential of PEEK-OPTIMA particles of various sizes compared with similar UHMWPE has not been well characterized. Without this information, it is difficult to assess the relative potential for PEEK-OPTIMA to contribute to poor implant performance and/or peri-implant tissue pathology. PEEK-OPTIMA particles are more hydrophilic than UHMWPE. Previous results have indicated that the more hydrophilic nature of polyurethane particles may result in less inflammatory responses, when compared with UHMWPE both *in vitro* and *in vivo*.[47,48] Thus, to characterize the effects of PEEK-OPTIMA particles *in vitro*, we hypothesized that PEEK-OPTIMA particles will be less inflammatory to macrophages than UHMWPE particles on a particle per cell basis. We tested this hypothesis by measuring the effect of PEEK-OPTIMA and UHMWPE, and crosslinked-UHMWPE (X-UHMWPE) particles on primary and THP-1 human macrophages. The degree to which particles affected cell function was assessed using toxicity assays, viability assays, proliferation assays, and cytokine analysis. In this fashion, we determined which material and particle sizes of PEEK-OPTIMA and UHMWPE were more proinflammatory and thus more likely to interfere with the homeostasis of the implant tissue interface.

MATERIALS AND METHODS

Cells

Differentiated human macrophages (THP-1; ATCC, Rockville, MD) and primary human monocytes were used as a measure of innate immune response to particle challenge. The cells were cultured in Dulbecco's modified Eagle medium, DMEM (Sigma, St Louis, MO) at 37°C and 0.5% CO_2, containing 10% fetal bovine serum (FBS; Hyclone Laboratories, Logan, UT). THP-1 monocytes were differentiated into macrophages by culturing 2.0×10^5 monocytes in 48 well plates or 0.60×10^5 in a 96-well plate with a phorbol ester (TPA) for 18–24 h then washed with DMEM 24 h before particle challenge. A total of 10% ethanol was used as a positive control for toxicity assays.

Blood samples were obtained intravenously from healthy volunteers ($n = 3$) with Institutional Review Board approved, informed consent. Peripheral blood mononuclear cells (PBMCs) were isolated by Ficol gradient. Peripheral blood CD14+ monocytes were isolated from PBMCs by negative selection with a specific magnetic bead antibody cocktail to CD3, CD7, CD16, CD19, CD56, CD123, and Glycophorin A (Miltenyi Biotec). Isolated human primary monocytes were assessed for >90% purity using FACS. Lipopolysaccharide (5 ng/mL final concentration) was used as a positive control for primary human monocyte/macrophages.

Challenge particles

Peri-implant cells were challenged with implantable grade PEEK-OPTIMA particles (PEEK-OPTIMA; Invibio Biomaterial Solutions, Lancashire, UK) and UHMWPE (Enduron) and highly crosslinked UHMWPE (X-UHMWPE, Marathon) particles of three particle sizes, ~0.3–0.7 μm, ~2 μm, and ~10 μm, at a dose of 20 particles per cell, at 24 and 48 h time points, (see Figures 1 and 2). The particles were produced from implant grade nonsterilized PEEK-OPTIMA bar stock (PEEK-OPTIMA-LT1, Invibio Biomaterial Solutions), and sterilized and boxed commercially available UHMWPE acetabular cups (Enduron, Cat 1241-12-526, DePuy) and sterile commercially available X-UHMWPE acetabular cups (Marathon, Cat 1219-36-056, DePuy). Commercially available particles (BioEngineering Solutions, Oak Park, IL) were produced using proprietary techniques involving custom cryo-milling and cryo-pulverization in liquid nitrogen followed by size exclusion separation using ultrasound-facilitated filtration through polystyrene membrane filters. The exact mean sizes and distribution of the particles are provided in Figure 2 and are shown to be similar for each size ranges where >80% of particles of 0.3–0.7 μm average sized particles were less than 1 um, and >95% were < 2 um; for the 2 μm average sized particles for all materials >95% of the particles were >1 μm and <10 μm; for the

Questions? Contact FDA/CDRH/OCE/DID at CDRH-FOISTATUS@fda.hhs.gov or 301-796-8118

Records processed under FOIA Request #2014-8015; Released by CDRH on 12-8-2015

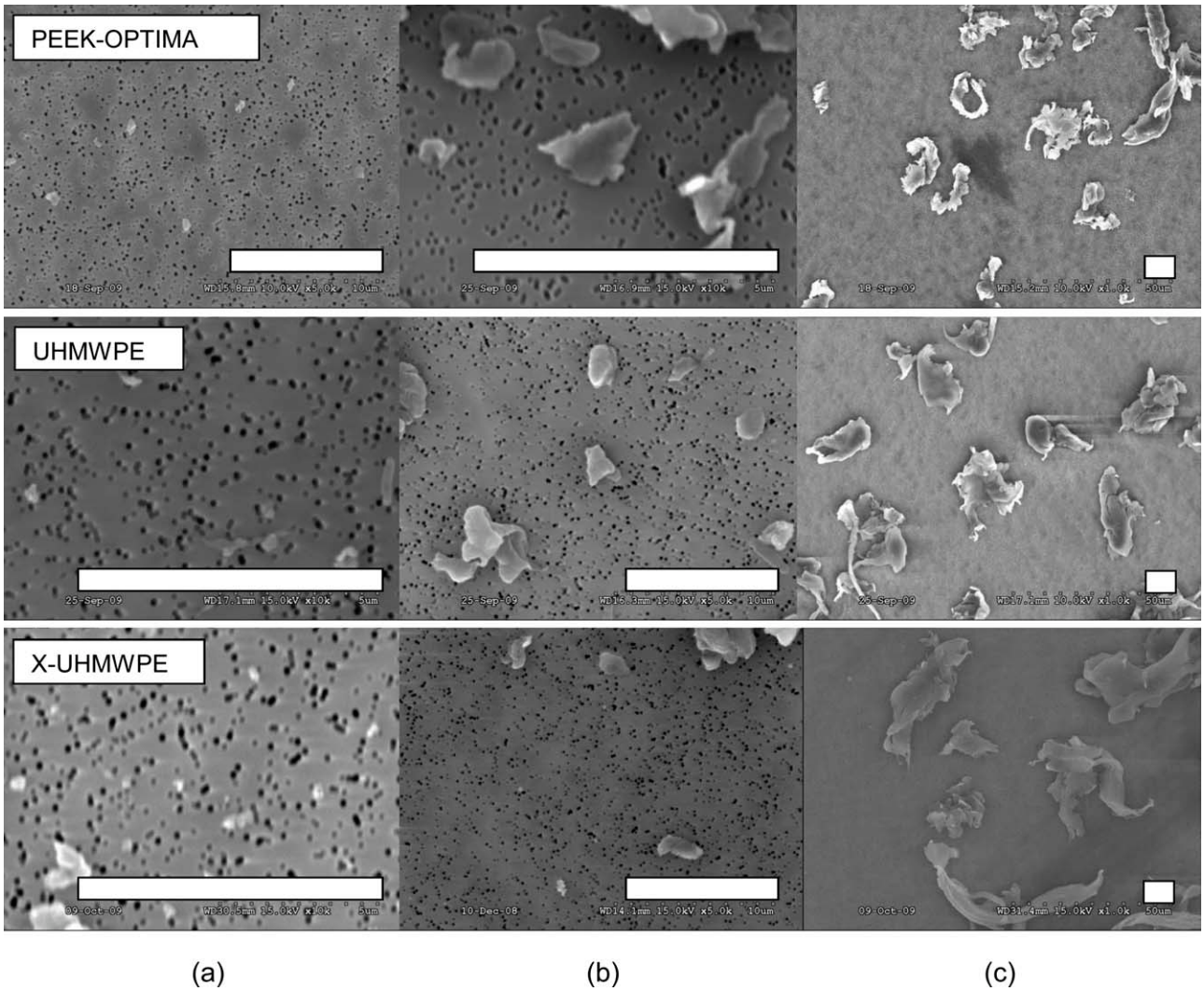

FIGURE 1. SEM photographs showing each material (PEEK-Optima, UHMWPE, and X-UHMWPE) at (a) 0.3–0.7 um, (b) 2 micron, and (c) 10 micron size ranges. Note: Bar = 10 um.

10–13 μm average sized particles >95% were larger than 5 μm and >90% were < 25um. Particles in the 0.7 μm and 2 μm size range and had the same granular to flake-like particle shape with average aspect ratios from 1.1–1.5 (i.e., round to oval). Particles >10 μm were fiber-like with aspect ratios between 2 and 4. PEEK-OPTIMA and UHMWPE particles were sterilized using ethylene oxide sterilization (>2000 mg/L-hours at 72F: Indicated by AN87 Dosimeter) and cleaned of endotoxin (using serial incubation with PyroClean™ and ethanol) and verified to be endotoxin free (<0.01 uE using Kinetic QCL assay). Because UHMWPE and X-UHMWPE particles have a density of 0.96 gm/cc, they tend to float when placed in DMEM or cell culture. Thus, particles of PEEK-OPTIMA and UHMWPE were electrostatically bound to the bottom of the culture plates before addition of cells and media using a proprietary process (BioEngineering Solutions, Oak Park, IL). This method of keeping particles bound to the surface and available for phagocytosis was tested to 6 days in DMEM and shown to maintain over 95% of the original particles (Figure 3).

Proliferation assays

Proliferation of cells was measured using [^{3}H]-thymidine (Amersham International, Arlington Heights, IL) incorporation into DNA. Proliferation assays were performed using monocytes rather than terminally differentiated macrophages because terminally differentiated THP-1 macrophages do not proliferate. Thus, THP-1 monocytes were cultured in 96-well cell-culture plates (Sigma), at a density of approximately 0.6 $\times$ 10^6 cells/well for 24 and 48 h in 450 μL of DMEM/well, 10% FBS at 37°C and 5% CO_2, with or without particle treatments. [^{3}H]-thymidine (1 μCi/well) was added during the last 12 h of the 24- and 48-h culture period. Radioactivity was measured using liquid scintillation Beta plate analysis (Wallac 1450, Gatesburg, MD). The amount of [^{3}H]-thymidine incorporation for each particle treatment was normalized to that of media alone (controls) producing a proliferation index

Questions? Contact FDA/CDRH/OCE/DID at CDRH-FOISTATUS@fda.hhs.gov or 301-796-8118

Records processed under FOIA Request #2014-8015; Released by CDRH on 12-8-2015

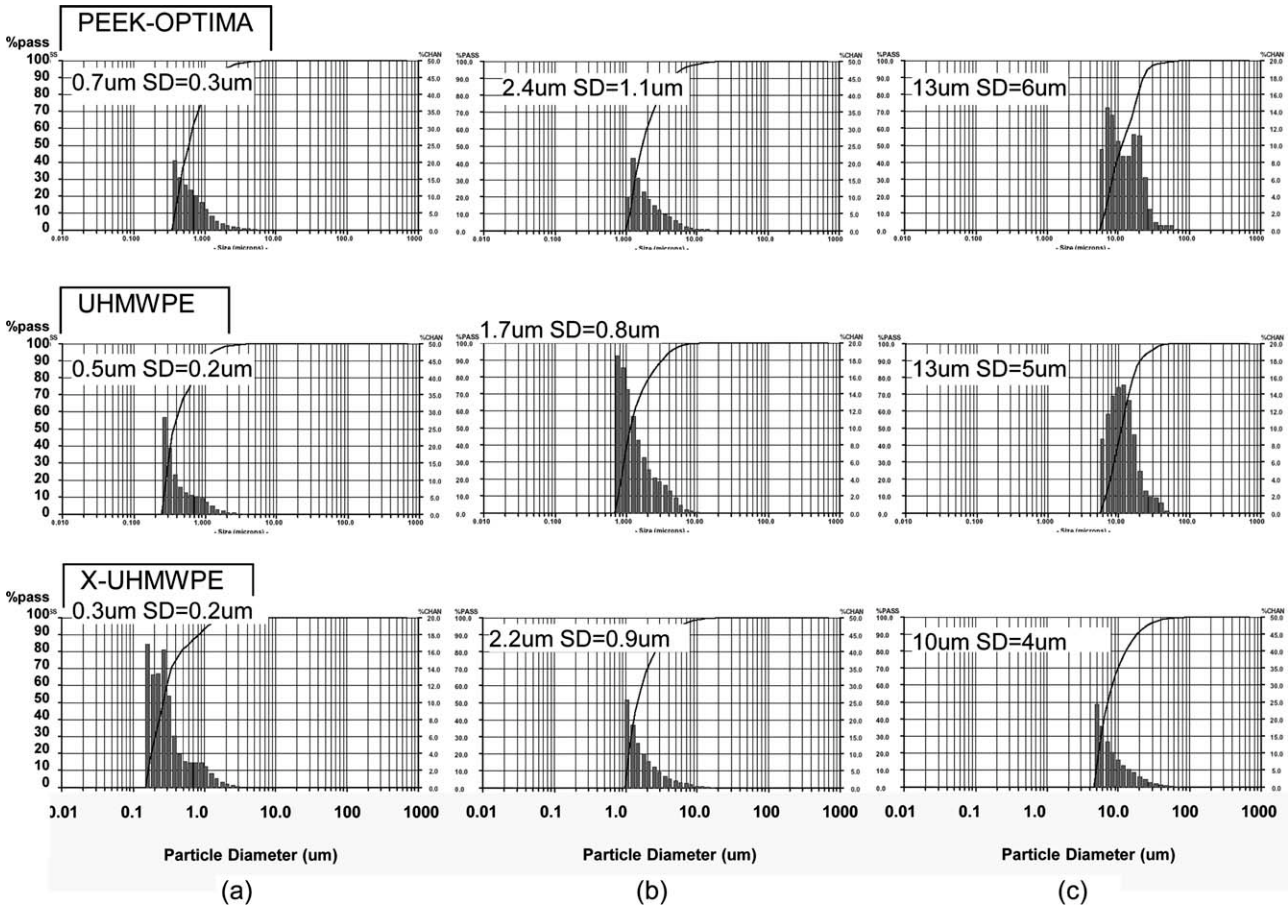

FIGURE 2. Number distributions (mn) from LALLS showing each material (PEEK-OPTIMA, UHMWPE, and XUHMWPE) at (a) 0.3–0.7 μm, (b) 2 μm, and (c) 10–13 μm size ranges. The actual mean (average) size for each if the three size ranges for each material is indicated with the associated standard deviation calculated. The distribution of the particles shown are granular and flake-like in shape (ASTM 1877-05), with average aspect ratios from 1.1 to 1.5 (i.e., round to oval) for particles in the 0.7 μm and 2 μm size ranges. Particles >10 μm were more elongated with aspect ratios of 2–4.

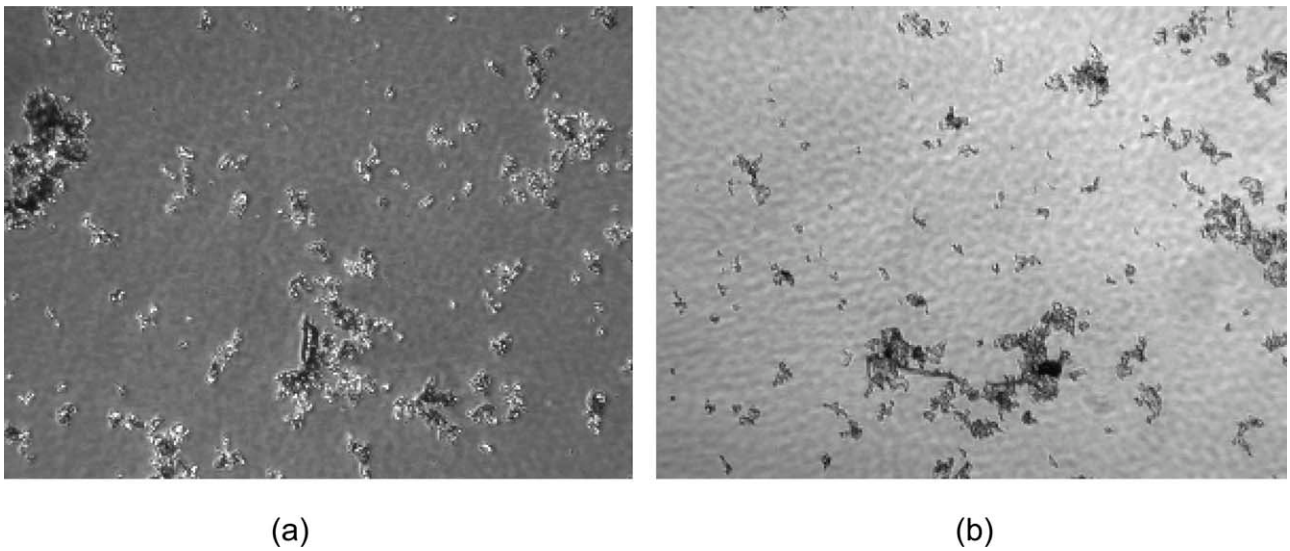

FIGURE 3. Light microscopy of 2 μm UHMWPE particles electrostatically bound to the bottom of standard tissue culture treated polystyrene 96-well plates: (a) dry UHMWPE particles bound to the surface and (b) UHMWPE particles still bound to the well bottom in cell culture media (DMEM) after 6 days incubation at 37°C (without any cells). Original magnification 400×.

Questions? Contact FDA/CDRH/OCE/DID at CDRH-FOISTATUS@fda.hhs.gov or 301-796-8118

Records processed under FOIA Request #2014-8015; Released by CDRH on 12-8-2015

or stimulation index, SI: Stimulation Index, SI = (mean cpm with treatment)/(mean cpm media alone). Radioactive [^{3}H]-thymidine incorporation is used as a highly accurate measure of proliferation, because the incorporation of thymidine into cellular DNA on mitosis does detect viable yet nondividing cells. Viability and toxicity assays were conducted to measure any toxicity responses.

Viability assays

Cell viability was determined by ATP-chemiluminescence, using the luciferase-containing reagent CellTiter Glo (Promega, Madison, WI). Luciferase based cell viability measurement is a method based on the quantitation of ATP present, which measures the presence of metabolically active cells. The process contains detergents and stabilizers to rupture cells which release ATP as well as ATPase inhibitors to stabilize released ATP. 24 and 48 h following particle treatment, 96-well assay plates containing 2.5×10^4 cells/well were treated with 100 μL/well of CellTiter-Glo Assay reagent after equilibration to room temperature. Plates were shaken for 5 min to mix the contents of the wells (MTS5 IKA Works). Following a 10–15-min incubation at ambient temperature, luminescence was determined using a luminometer (Wallac MicroBeta 1450). Cell number linearly correlated with luminescent output in a range from 1 to $> 5 \times 10^4$ cells/well. All viability tests were conducted in triplicate.

Cytotoxicity assays

Cytotoxicity was measured using a lactate dehydrogenase (LDH) detection kit (LDH Cytotoxicity Assay, Cayman Chemical Company, Ann Arbor, MI). The LDH released from dead cells can be measured without damaging membranes of the viable cells using an enzymatic assay that detects a fluorescent signal proportional to dead cell release of lactate and NAD1. The LDH assay was allowed to proceed at room temperature for 10 min prior to addition of 25 μL/well stop solution containing 10% sodium dodecyl sulfate. The contents of the wells were mixed by shaking the plates for 10 s before measuring fluorescence (560 nm excitation, 590 nm emission) using a Wallac Microbeta 1450 fluorescence plate reader.

Cytokine analysis luminex assays

Particle-induced IL-1β, IL-6, IL-8, MCP-1, and TNF-α secretion by THP-1 monocytes and primary macrophages were analyzed with Luminex suspension multiplex array technology. Supernatants from particle-challenged monocytes were collected 24 and 48 h after initial particle challenge and frozen at −80°C. Monocyte/macrophage supernatants were then thawed and analyzed for IL-1β, IL-6, IL-8, MCP-1, and TNF-α concentrations with a proinflammatory-plex cytokine array kit (INVITROGEN). All Luminex assays were analyzed in triplicates with manufacturer's provided buffers and protocols.

Microscopic examination

Microscopic examination of material-induced changes in cell morphology was conducted using phase contrast (Eclipse C1, Nikon, Mississauga, Ontario). Images were captured using monochrome digital photography with image processing limited to brightness and contrast enhancement.

Statistical analysis

Normally distributed data (proliferation and viability data) were subjected to statistical analysis using Student's *t*-tests. Student's *t*-tests for independent samples with unequal or equal variances were used to test equality of the mean values ($p < 0.05$). Comparisons between groups are limited to individual comparison of reactivity for each material concentration. Treatment specific reactivity measurements were normally distributed.

Cytokine analysis

By convention, to calculate group means, cytokine concentrations below the detection limit were assigned a value of one-half the method detection limit. Intergroup comparisons, independent of these means, were made using Kruskall–Wallis nonparametric analysis of variance. The Wilcoxon–Mann–Whitney test was then used if the Kruskall–Wallis test revealed significant differences at $p < 0.05$.

RESULTS

Microscopic morphologic analysis

Microscopically visible toxicity responses of the cells to the particles were not evident after 24 h of cell culture (Figure 4), as was qualitatively assessed by microscopically identifiable decreases in the number of cells per well or changes in the morphology of the cell. Larger particles of < 15 μm were confirmed as phagocytosable by sampling and examination using scanning electron microscopy (SEM) (data not shown). However, larger particles than 15 μm or clumps of particles with effective particle sizes greater than 15 μm were not verified as phagocytosed and likely were not able to be phagocytosed. Thus, the effective number of particles available for phagocytosis with the larger sizes (10–13 um) was likely less than that used for challenging cells and the reported dose represents an upper limit. Particles of submicron size were below the detection limit of light microscopy used, while 2 μm particles of PEEK-OPTIMA were visibly identifiable and 10 μm particles of all materials were readily observable and at a concentration of 20 particles per cell start to obscure imaging of cells.

Viability assays (ATP-chemiluminescence)

The viability of differentiated THP-1 macrophages treated with PEEK-OPTIMA, UHMWPE, and X-UHMWPE particles of 0.5–0.7 μm, ∼2μm, and ∼10μm in size were measured using luminometer measurement of total cell number (ATP-chemiluminescence) after 24 and 48 h of challenge. Both PEEK-OPTIMA and UHMWPE particles induced a significant decrease in viability (Figure 5). However, this decrease in viability was limited to PEEK-OPTIMA and UHMWPE particles 13 μm in size after 24 h of exposure [Figure 5(a)]. After 48 h of exposure, the all three sizes of UHMWPE particle induced a significant decrease in viability. However, only the 13 μm PEEK-OPTIMA particles resulted in decreased viability [Figure 5(b)]. It is important to note that while there were significant decreases in viability due to particle challenge, none of the particle challenge agent reduced the amount of viable cells below 20% of the control values, as opposed to

Questions? Contact FDA/CDRH/OCE/DID at CDRH-FOISTATUS@fda.hhs.gov or 301-796-8118

Records processed under FOIA Request #2014-8015; Released by CDRH on 12-8-2015

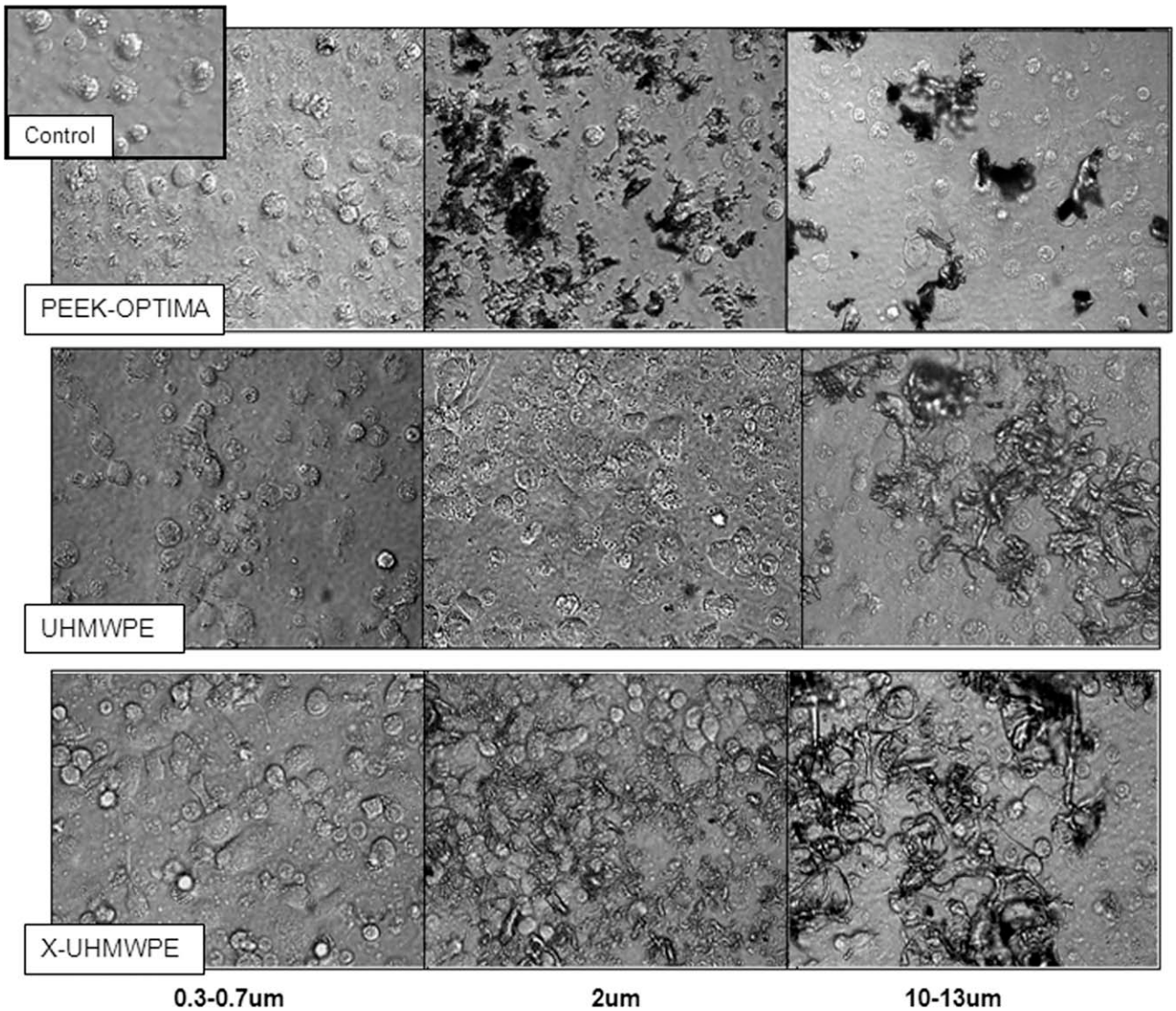

FIGURE 4. Light microscopy images of PEEK-OPTIMA, UHMWPE, and X-UHMWPE) at 0.3–0.7 μm, 2 μm, and 10–13 μm size ranges with differentiated THP-1 human macrophages at a dose of 20 particles/cell after 24 hours of culture show that cell morphology did not change significantly. Inset shows unchallenged control cells. Original magnification 400×.

10% ethanol positive control that reduced viability as measured by ATP-chemiluminescence by >95%.

Cytotoxicity assays (LDH)

The cytotoxicity of THP-1 differentiated macrophages challenged with PEEK-OPTIMA and UHMWPE particles were tested at three particle sizes at a dose of 20 particles per cell by measuring the amount of LDH released from membrane rupture. UHMWPPE particles generally demonstrated significantly increased cell toxicity responses to particle challenge compare with untreated controls, PEEK-OPTIMA and X-UHMWPE (Figure 6).

Material effects

PEEK-OPTIMA versus *PE:* Macrophages demonstrated less cytotoxicity at 48 h than at 24 h, demonstrating increased membrane instability/permeability associated with initial phagocytosis during the first 24 h of exposure.

Particle size effects

At 24 h, only the largest (13 μm) particles of PEEK-OPTIMA resulted in significantly increased LDH. However, UHMWPE induced significantly increased LDH at 0.5 μm, 1.6 μm, and 13 μm sizes, where the greatest amounts of LDH release were at the 0.5 μm size at 24 h. At 48 h, the only material and size to result in significant LDH release ($p < 0.05$) was that of 0.5 μm UHMWPE (Figure 6), which exceeded the level of LDH induced by the 10% ethanol positive control.

Proliferative cell adhesion assays ([H]-thymidine incorporation)

Proliferation responses of proliferating undifferentiated THP-1 monocytes were measured by [^{3}H]-thymidine incorporation and analysis of monocytes after challenge with particles for 24 and 48 h. There was a distinct difference in

Questions? Contact FDA/CDRH/OCE/DID at CDRH-FOISTATUS@fda.hhs.gov or 301-796-8118

Records processed under FOIA Request #2014-8015; Released by CDRH on 12-8-2015

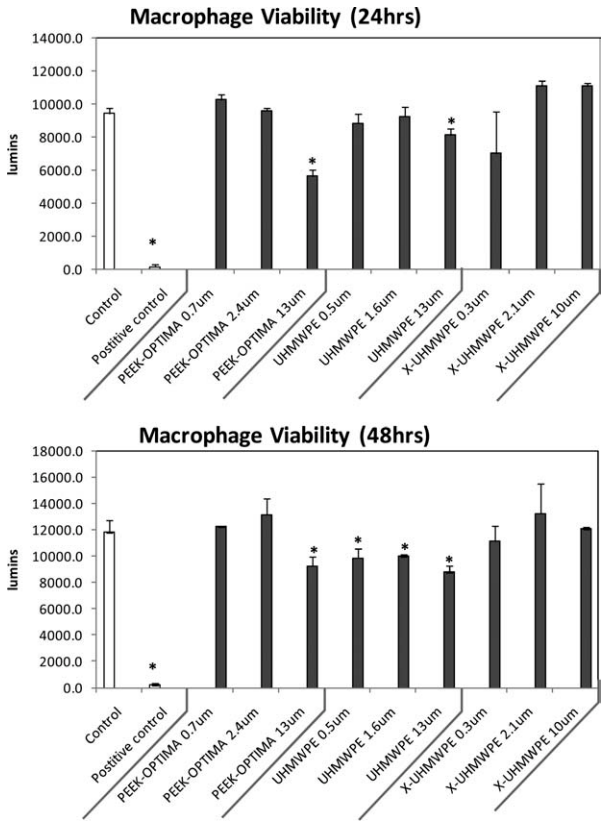

FIGURE 5. The viability of differentiated human THP-1 macrophages challenged with PEEK-OPTIMA, UHMWPE, and X-UHMWPE particles of 0.5–0.7 μm, ~2 μm, and ~10 μm in sizes. Viability was measured using luminometry of total cell number (ATP-chemiluminescence) after 24 h and 48 h of challenge. Positive control was 10% ethanol. Note: $*p < 0.05$, compared with controls (medium alone).

proliferation responses at 24 and 48 h (Figure 7). At 24 h, the smallest (0.5–0.7 μm) particles of both PEEK-OPTIMA and UHMWPE and larger X-UHMWPE particles (2 μm and 10 μm) induced a 30% increase in proliferation ($p < 0.05$). However, at 48 h, the trend reversed itself and PEEK-OPTIMA, UHMWPE, and X-UHMWPE all induced a significant decrease in proliferation of monocytes, except for 0.5 μm UHMWPE and 2.1 μm and 10 μm X-UHMWPE which remained mildly stimulatory ($p < 0.05$). Similar to viability assays, the limited proliferation changes induced by particles (<30%) were comparable decreases in proliferation, when compared with 10% ethanol positive controls. There was no clear size-dependent trend among the particle types at either 24 or 48 h. Thus, there was no one type or size of particle that resulted in significantly decreased proliferation to a greater extent than that of another material of similar size, for example, PEEK-OPTIMA at 0.5 μm and X-UHMWPE at 0.3 μm (Figure 7).

Cytokine assays

THP-1 monocyte/macrophages. PEEK-OPTIMA and UHMWPE particles induced significant increases in IL-1β, IL-6, IL-8, TNF-α, and MCP-1 compared with unchallenged controls at 24 h (Figure 8). The cytokine response to X-UHMWPE was significantly greater than the response to any other type of material with generally a 4- to 100-fold increase in cytokine production over that of PEEK-OPTIMA. The highest response to IL-1β, IL-6, IL-8, TNF-α, and MCP-1 was ~50 pg/ml, 1000 pg/ml, 8000 pg/mL, 2000 pg/mL, and 10,000 pg/mL, respectively, to that of 2.1-μm sized X-UHMWPE particles. The greatest increase of any cytokine was observed with the 13 μm UHMWPE and X-UHMWPE particles, which induced increases ~10,000 pg/mL MCP-1; an increase ~5000-fold that induced by untreated controls and PEEK-OPTIMA particles of similar size (Figure 8). Larger particle sizes of X-UHMWPE (2 μm and 10 μm dia.) resulted in increased cytokine expression of all cytokines assayed. However, while both 2 μm and 10 μm X-UHMWPE particles resulted in the greatest responses, 0.7 μm X-UHMWPE particles did not induce significantly increased production of any of the cytokines. Similarly, high amounts of IL-6, IL-8, and MCP-1 were produced by 13,μm UHMWPE particles.

Primary cells. PEEK-OPTIMA and UHMWPE particles induced significant increases in IL-1β, IL-6, IL-8, and TNF-α

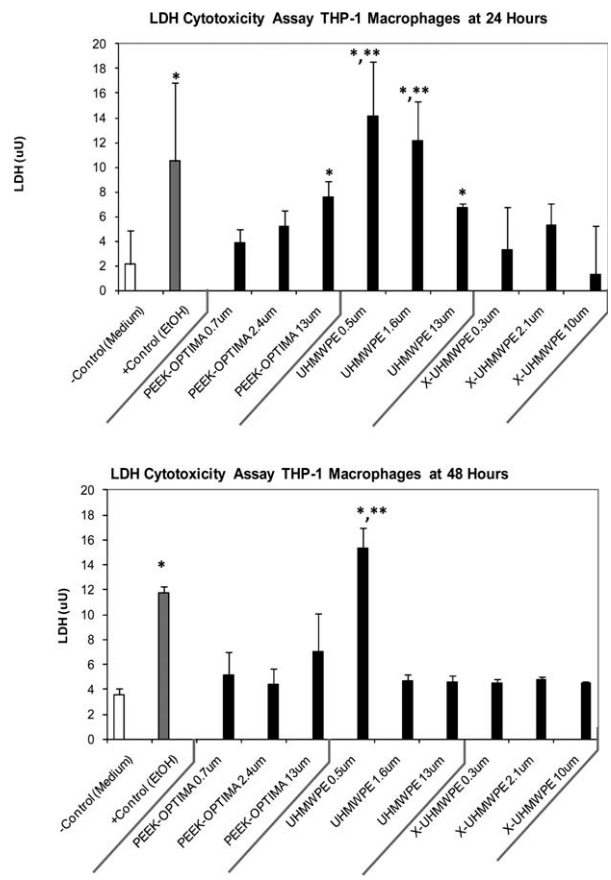

FIGURE 6. Cytotoxicity of human THP-1 differentiated macrophages challenged with PEEK-OPTIMA, UHMWPE, and X-UHMWPE particles of three particle sizes at a dose of 20 particles per cell. Cytotoxicity was measured by the amount of LDH released from membrane rupture. UHMWPE particles generally demonstrated significantly increased cell toxicity responses to particle challenge compare with untreated controls, PEEK-OPTIMA and X-UHMWPE. Note: $*p < 0.05$, compared with controls (medium alone) and $**p < 0.05$ compared with PEEK-OPTIMA at an equal particle size.

Questions? Contact FDA/CDRH/OCE/DID at CDRH-FOISTATUS@fda.hhs.gov or 301-796-8118

Records processed under FOIA Request #2014-8015; Released by CDRH on 12-8-2015

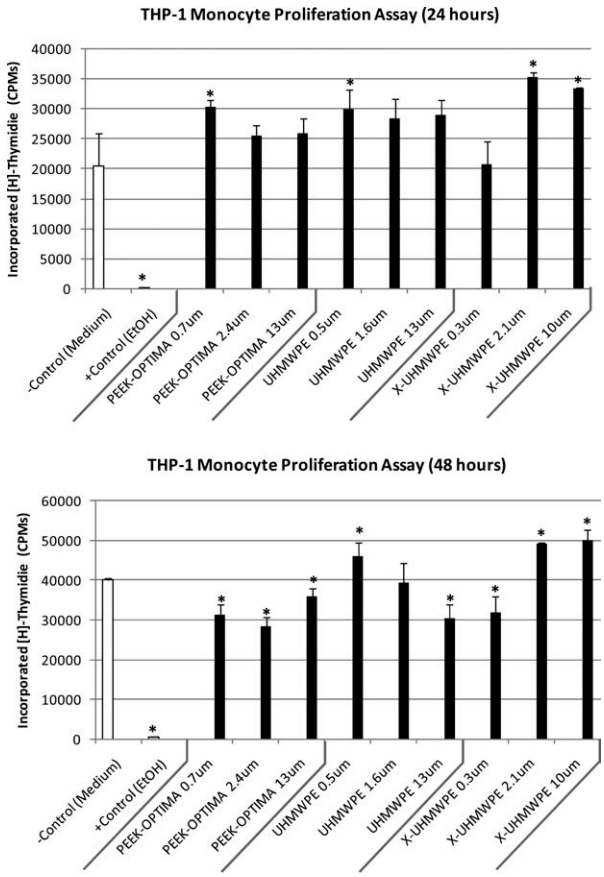

FIGURE 7. Proliferation responses of proliferating undifferentiated THP-1 monocytes/were measured by [3H]-thymidine incorporation and analysis of monocytes after challenge with particles for 24 and 48 h. There was a distinct difference in proliferation responses at 24 and 48 h. Note: $*p < 0.05$, compared with controls (medium alone).

compared with unchallenged controls in all three subjects tested at 24 h (Figure 9). However, there was little difference between PEEK-OPTIMA and UHMWPE cytokine profiles. All three subjects demonstrated roughly similar ranges of IL-1β, IL-6, IL-8, and TNF-α cytokine responses to PEEK-OPTIMA and UHMWPE particles. However, the IL-1β response to X-UHMWPE was greater than to PEEK-OPTIMA in two of three subjects (Figure 9). Additionally, endotoxin free particles of PEEK-OPTIMA and particles induced significantly ($p < 0.05$) greater IL-1β compared with LPS challenge, consistent with and supporting the inflammasome activation model of particle induced bioreactivity.[49–51] The chemokine MCP-1 demonstrated the greatest variability in response to particle challenge in subjects 1 and 3. There was a significantly greater IL-1β cytokine response to X-UHMWPE compared with PEEK-OPTIMA particles in subject 1 and a significantly greater response in MCP-1 (chemokine) to X-UHMWPE compared with PEEK-OPTIMA particles in subject 3 (Figure 9). The cytokines, IL-6, IL-8, and MCP-1 demonstrated the greatest increase in responses compared with unchallenged monocytes for all subjects. The responses to endotoxin free PEEK-OPTIMA and UHMWPE particles rivaled that of high dose LPS (positive control) and in fact demonstrated a greater IL-1β and/or TNF-α response ($p < 0.05$) in all three subjects.

DISCUSSION

The results of this study show that in general neither PEEK-OPTIMA nor UHMWPE particles substantially suppressed macrophage viability and thus were minimally toxic compared with positive controls. However, PEEK-OPTIMA particles were on the whole less inflammatory than UHMWPE and X-UHMWPE particles of the same size and dose after 24 h of exposure. While these findings support our hypothesis that PEEK-OPTIMA particles are less inflammatory than UHMWPE particles of similar size, they do not make a strong case for superiority of biologic response from a magnitude perspective. In other words, while this difference was statistically significant within the different *in vitro* assays tested, the overall difference between PEEK-OPTIMA and UHMWPE was not likely substantial enough to indicate reactivity differences *in vivo*. It does, however, suggest that polymeric material type does affect biologic response. The degree to which surface chemistry-dependent properties between PEEK-OPTIMA and UHMWPE and X-UHMWPE differed was not quantified in this investigation and thus biologic differences attributable to surface chemistry differences remains beyond the scope of this investigation. However, it is likely that the central difference in chemistry-dependent surface properties between PEEK-OPTIMA and UHMWPE is their hydrophilic versus hydrophobic surfaces, respectively (where the approximate PEEK contact angle with water is 62–71° vs. an UHMWPE-water contact angle of 91°).[52,53] Other investigators have reported a decrease in bioreactivity associated with an increase in polymer surface chemistry hydrophilicity (polyurethane versus UHMWPE), that is, consistent with the results found in this investigation.[48] However, despite the growing number of reports confirming this relation between polymer particle hydrophilicity and biocompatibility, it remains unestablished as a consensus opinion.

Particle size effects

Increasing size of the PEEK-OPTIMA and UHMWPE particles generally did not induce >20% changes in proliferation or viability. There was a dramatic increase in cytotoxicity of UHMWPE particles at 0.5 μm at both 24 and 48 h that rivaled the positive control. This was not apparent for PEEK-OPTIMA 0.7μm particles. In fact, PEEK-OPTIMA only induced cytotoxicity at the largest size (13μm). However, because these results were not mirrored in the proliferation and viability assays, it may be that these toxicity results reflect an artifact of the LDH assay in which "floating" submicron UHMWPE particles released from the bottom of the wells during processing were unable to be removed from the media before LDH detection. This phenomenon was not observed in the submicron X-UHMWPE particles that were similarly buoyant to UHMWPE. There was a distinct bias of larger sized particles to elicit an increase in cytokine response at 24 h, where 13 μm sized UHMWPE particles and 2.1 μm and 10 μm X-UHMWPE particles demonstrated a significant >2- to

Questions? Contact FDA/CDRH/OCE/DID at CDRH-FOISTATUS@fda.hhs.gov or 301-796-8118

Records processed under FOIA Request #2014-8015; Released by CDRH on 12-8-2015

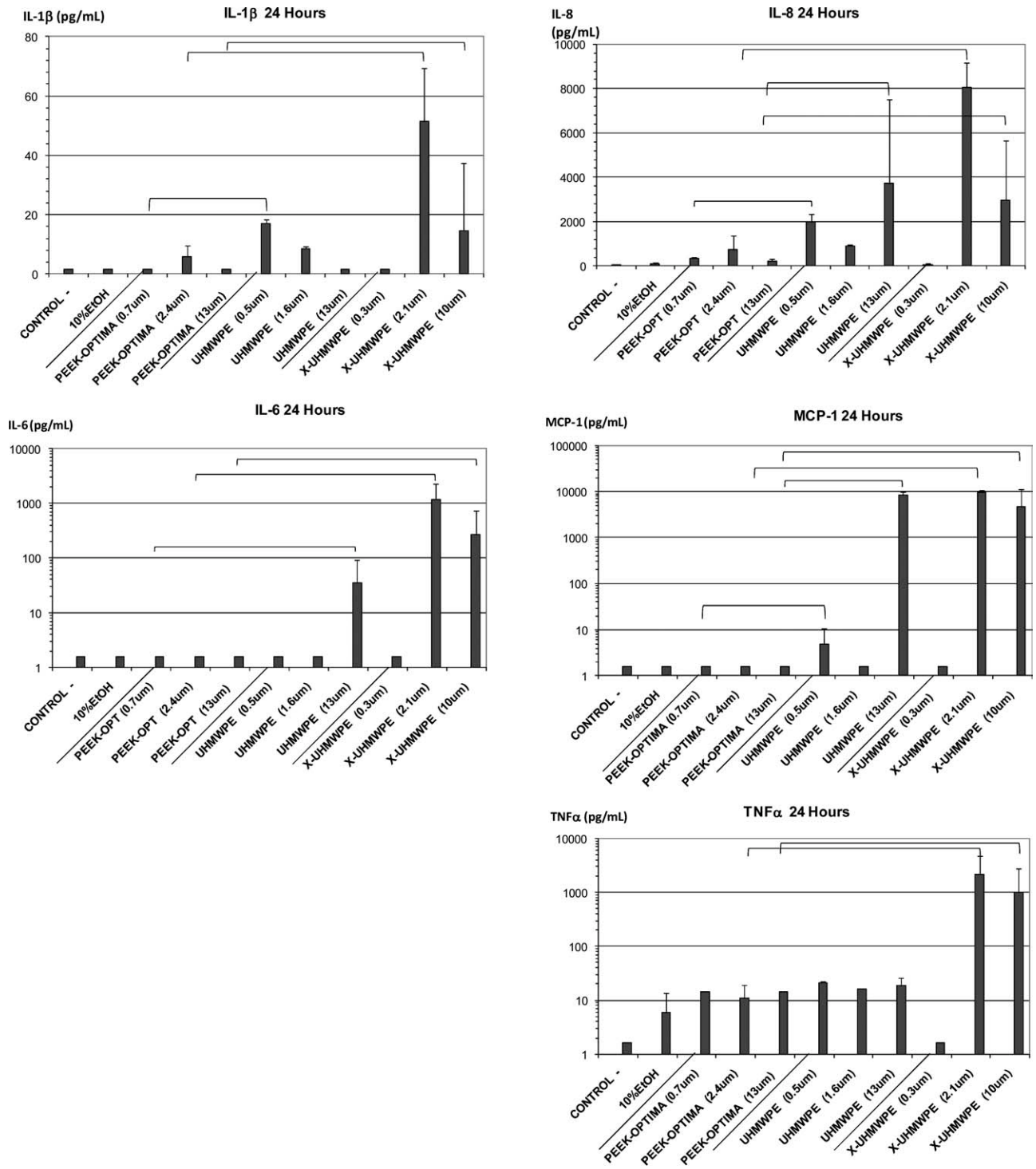

FIGURE 8. THP-1 monocyte/macrophages: PEEK-OPTIMA and UHMWPE particles induced significant ($p < 0.05$) increases in IL-1β, IL-6, IL-8, TNF-α, and MCP-1 compared with unchallenged controls at 24 h (bars). The cytokine response to X-UHMWPE was significantly greater than the response to any other type of material with generally a 4- to 100-fold increase in cytokine production over that of PEEK-OPTIMA.

100-fold increases in IL-1β, IL-6, IL-8, MCP-1, and TNF-α over that of PEEK-OPTIMA particles at 24 h.

This work is in agreement with past investigations, where clinically relevant UHMWPE particles have been found to produce IL-1β, IL-6, PGE2, and TNF-α in response to 0.45 μm and 1.7 μm particles[23,36] but not to particles > 7 μm.[23,36] However, in this previous work, dosing was made on an equal volume (or mass) basis, where there are far fewer large particles (dose) than smaller particles for a given challenge volume. This "smaller is worse" is partially

Questions? Contact FDA/CDRH/OCE/DID at CDRH-FOISTATUS@fda.hhs.gov or 301-796-8118

Records processed under FOIA Request #2014-8015; Released by CDRH on 12-8-2015

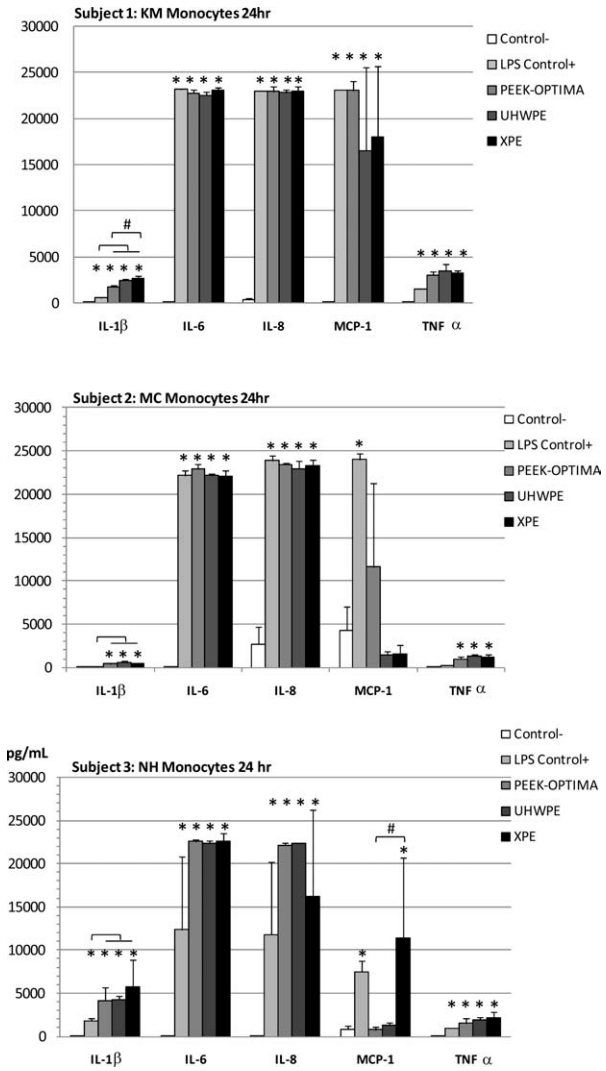

FIGURE 9. PEEK and PE particles induced significant increases in IL-1β, IL-6, IL-8, and TNF-α compared with unchallenged controls in all three subjects tested at 24 h. All three subjects demonstrated roughly similar ranges of increased IL-6, IL-8, and TNF-α cytokine responses to LPS, PEEK particles, and PE particles. However, all particles induced significantly ($p < 0.05$) greater IL-1β compared with LPS (bars). Note: *$p < 0.05$, compared with controls (medium alone) and #$p < 0.05$ compared with PEEK-OPTIMA at an equal particle size.

a misconception, because in these studies the challenge doses generally contained >1000× more small particles per cell than larger particles. Conversely, in this investigation, the sizes of particles were compared on a particle per cell basis which may also be biased since the mass of one large particle (e.g., 100 μm) is equal to the mass of >10,000 smaller particles (e.g., 1 μm). Thus, it may be more accurate to conclude that any ensuing particle-induced inflammatory response is proportional to the particle load, which is the concentration of phagocytosable particles per tissue volume, characterized by both the size and total debris volume. In contrast to some of these past investigations[23,36] and in agreement with others,[54] we found that the most inflammatory particles were not the smallest particles tested (i.e., 0.3–0.7 μm), rather they were the larger 10–13 μm particles barely able to be phagocytosed by the cells. It should be noted that the inability of a cell to engulf a particle does not preclude an attempt by a cell to phagocytose larger particles and result in proinflammatory reactions, see Figure 10.

Are these larger sized particles clinically relevant? Previous investigations have reported that hard-on-hard material couples such as metal-on-metal articulations generally produce smaller sized (nanometer and submicron), fairly round debris whereas traditional metal-on-polymer bearings produce larger (submicron and micron sized) debris that are more elongated in shape.[55–62] Thus, the particles produced from metal-on-polymer bearing surfaces that are predominantly polymeric, generally fall into the range from 0.23 to 2 μm with an average size ~0.6μm.[63–65] Other investigations of UHMWPE particle isolates from peri-implant tissues have shown that UHMWPE particulate debris to be a little smaller with 70%–90% of recovered particulates submicron, with the mean size being ~0.2–1 μm.[66–68] However, the range of particles are well established at 0.2 to 300 μm in size.[63,66–69] Similarly obtained particles of X-UHMWPE were found to be a little smaller and more rounded than UHMWPE, with particles as small as 0.1 μm in size.[56,70] However, the techniques used in the bulk of these past investigations were limited to either SEM or transmission electron microscopy, by necessity because of the limited availability of debris for analysis. These microscopy techniques facilitate a relatively small sample size for the counting of particles within high magnification fields and typically statistically sample < 0.000001% of the total debris generated and are thus accordingly limited.[71,72] So, while the average particles generated from metal-on-polymer bearing surfaces are typically in the smaller ranges (<1 um), larger size particles in the 10 μm range remain clinically relevant

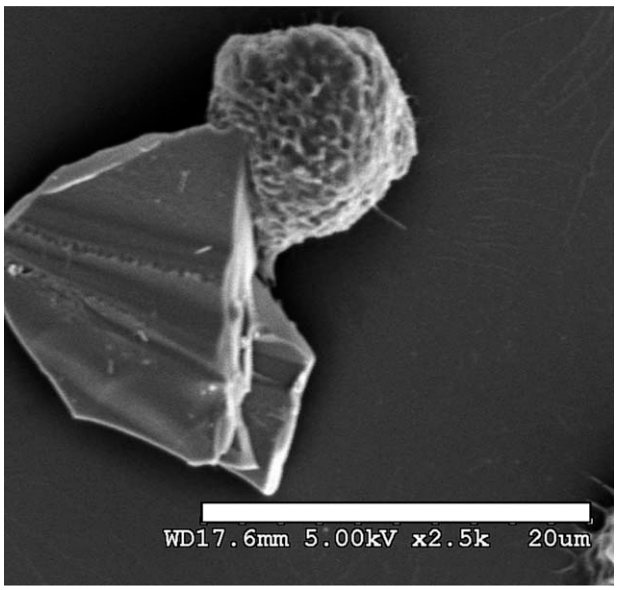

FIGURE 10. Scanning electron micrograph of ~10 μm diameter THP-1 macrophage in the process of trying to phagocytose a 20 μm diameter UHMWPE particle despite the large size difference, (Bar = 20 um).

Questions? Contact FDA/CDRH/OCE/DID at CDRH-FOISTATUS@fda.hhs.gov or 301-796-8118

Records processed under FOIA Request #2014-8015; Released by CDRH on 12-8-2015

and important to the comparison of PEEK-OPTIMA and UHMWPE particles.

Particle-induced proinflammatory responses

Implant debris-induced responses in peri-implant tissues[73] disrupts bone homeostasis through a number of proinflammatory cytokine responses. Particles induce macrophages to secrete TNF-α, IL-1β, IL-6, and PGE2, stimulating further immune chemokine attraction of other cells and maturation of osteoclast precursors. This has been shown to act through the inflammasome pathway and others, which leads to the release of IL-1β, and other powerful proinflammatory cytokines.[49] Inflammatory activation of macrophages in this study was not limited to IL-1β (the result of inflammasome danger signaling pathways). However, the only particles that induced highly elevated IL-1β responses in Human THP-1 macrophages were X-UHMWPE at 2 μm in size and not at 0.3 μm or at 10 μm. This suggests that there may be particularly high phagosomal distress resulting in relatively high IL-1β to X-UHMWPE particles, and that something about this particular size may induce intracellular stress such as lysosomal destabilization that is well known to lead to inflammasome activation and IL-1β production. This hypothesis is supported by increased amounts of the other inflammatory cytokines associated with X-UHMWPE at 2 μm and 10 μm (see Figure 8). These distinct differences between UHMWPE and PEEK-OPTIMA were not as pronounced in primary human macrophages. Only one of three individuals demonstrated a statistical increase in one particle type over another to IL-1β (X-UHMWPE over that of PEEK-OPTIMA, subject 1, Figure 9). It is unknown at this time which of the cytokines released (Figure 9) play a more important role in long-term particle-induced inflammation (e.g., IL-1β or TNF-α). Primary monocytes demonstrated little to no IL-1β response to LPS challenge (5 ng/mL) that was significantly lower than endotoxin free particles of PEEK-OPTIMA and UHMWPE, which is consistent with current paradigms of inflammasome pathway involvement in nonpathogen-derived proinflammatory stimuli.[49]

Clinical relevance of PEEK-OPTIMA versus UHMWPE particle challenge

The growing applications of PEEK-OPTIMA include load-bearing surfaces in orthopedic implants. Although historically there has been a dearth of information regarding the performance of PEEK in general, recent articles have shown that particles within the small-medium-and large size ranges tested in this investigation are produced from the wear of PEEK implants.[74,75] The clinical relevance of the findings in this investigation (that PEEK-OPTIMA is generally less inflammatory to macrophages than UHMWPE particles of similar size, shape, and dose) are critically important in the assessment of PEEK-OPTIMA as a material that aims to improve implant performance. In this *in vitro* study of particle-induced innate immune responses to implant debris, the results of multiassay assessment seem to indicate that PEEK-OPTIMA meets, if not exceeds, the biocompatibility of similar UHMWPE particles. This consistent with the results of other *in vivo* studies using similarly sized PEEK particles where equivalent (to less) inflammatory responses were found in rabbits dosed with PEEK or UHMWPE particles.[76,77]

Study limitations and future efforts

Two major limitations inherent to this line of investigation include: (1) the appropriateness of the challenge conditions, that is, *in vitro* and (2) an incomplete understanding of what specific mechanism(s) mediate particle-induced cytokine responses. Whether the complex environment of the peri-implant milieu ultimately mitigates or makes cells more susceptible to the effects of particle exposure *in vivo* remains unknown. Thus, the results of this study are put forward as an initial guideline and a basis for further examination using more sophisticated conditions, for example, mixed cell populations, direct *in vivo* osteolysis models.

CONCLUSIONS

The results of this study that compare PEEK-OPTIMA and UHMWPE particles ~0.3–0.7 μm, 2 μm, and 10 μm in size demonstrated that PEEK-OPTIMA particles were significantly less inflammatory than UHMWPE and X-UHMWPE after 24 h of exposure. These results support our hypothesis that PEEK-OPTIMA particles are less inflammatory than UHMWPE particles of similar size and shape. Both PEEK-OPTIMA and UHMWPE did not drastically affect the viability or induce toxicity in human THP-1 macrophages, where the viability ranges of particle challenged cells were similar to those of nontreated control macrophages. Although some of the PEEK-OPTIMA and UHMWPE particles induced significant decreases in viability/cell number these changes did not induce >20% changes in proliferation or viability. There was a distinct trend of larger sized particles to elicit a cytokine response at 24 h, where 13 μm sized UHMWPE particles and 2.1 μm and 10 μm X-UHMWPE particles demonstrated a significant >2- to 100-fold increases in IL-1β, IL-6, IL-8, MCP-1, and TNF-α over that of PEEK-OPTIMA particles at 24 h. This *in vitro* study of innate immune responses to implant debris using viability, proliferation, cytotoxicity, and cytokine production assays indicated that PEEK-OPTIMA particles were more biocompatible than UHMWPE particles, mostly by producing less inflammatory cytokines and in part demonstrating that PEEK-OPTIMA implant debris does not represent an increased inflammatory risk over that of UHMWPE.

REFERENCES

1. Willert HG, Semlitsch M. Reactions of the articular capsule to wear products of artificial joint prostheses. J Biomed Mater Res 1977;11:157–164.
2. Holt G, Murnaghan C, Reilly J, Meek RM. The biology of aseptic osteolysis. Clin Orthop Relat Res 2007;460:240–252.
3. Fritz EA, Glant TT, Vermes C, Jacobs JJ, Roebuck KA. Chemokine gene activation in human bone marrow-derived osteoblasts following exposure to particulate wear debris. J Biomed Mater Res A 2006;77:192–201.
4. Goodman SB. Wear particles, periprosthetic osteolysis and the immune system. Biomaterials 2007;28:5044–5048.

Questions? Contact FDA/CDRH/OCE/DID at CDRH-FOISTATUS@fda.hhs.gov or 301-796-8118

Records processed under FOIA Request #2014-8015; Released by CDRH on 12-8-2015

5. Hallab NJ, Anderson S, Stafford T, Glant T, Jacobs JJ. Lymphocyte responses in patients with total hip arthroplasty. J Orthop Res 2005;23:384–391.
6. Jacobs JJ, Hallab NJ. Loosening and osteolysis associated with metal-on-metal bearings: A local effect of metal hypersensitivity? J Bone Joint Surg Am 2006;88:1171–1172.
7. Ren W, Wu B, Peng X, Hua J, Hao HN, Wooley PH. Implant wear induces inflammation, but not osteoclastic bone resorption, in RANK(−/−) mice. J Orthop Res 2006;24:1575–1586.
8. Roebuck KA, Vermes C, Carpenter LR, Fritz EA, Narayanan R, Glant TT. Down-regulation of procollagen alpha1[I]] messenger RNA by titanium particles correlates with nuclear factor kappaB (NF-kappaB) activation and increased rel A and NF-kappaB1 binding to the collagen promoter. J Bone Miner Res 2001;16:501–510.
9. Shanbhag AS, Kaufman AM, Hayata K, Rubash HE. Assessing osteolysis with use of high-throughput protein chips. J Bone Joint Surg Am 2007;89:1081–1089.
10. Skipor AK, Campbell PA, Patterson LM, Anstutz HC, Schmalzried TP, Jacobs JJ. Serum and urine metal levels in patients with metal-on-metal surface arthroplasty. J Mater Sci Mater Med 2002; 13:1227–1234.
11. Xing Z, Schwab LP, Alley CF, Hasty KA, Smith RA. Titanium particles that have undergone phagocytosis by macrophages lose the ability to activate other macrophages. J Biomed Mater Res B Appl Biomater 2008;85:37–41.
12. Goodman SB. Wear particles, periprosthetic osteolysis and the immune system. Biomater 2007;28:5044–5048.
13. Jacobs J, Goodman S, Sumner DR, Hallab N. Biologic response to orthopedic implants. In: Buckwalter J, Einhorn T, Simon S, editors. Orthopedic Basic Science. Chicago: American Academy of Orthopedic Surgeons; 1999. pp 402–426.
14. Doorn PF, Mirra JM, Campbell PA, Amstutz HC. Tissue reaction to metal on metal total hip prostheses. Clin Orthop 1996;329: S187–S205.
15. Hallab NJ, Cunningham BW, Jacobs JJ. Spinal implant debris-induced osteolysis. Spine 2003;28:S125–S138.
16. Inoue S, Kubo T, Suehara H, Yamazoe S, Nakamura M, Miyaoka H, Hirasawa Y. A 10- to 13-year follow-up study of Harris-Galante type prosthesis in total hip arthroplasty. J Orthop Sci 2000;5:561–566.
17. Jacobs JJ, Roebuck KA, Archibeck M, Hallab NJ, Glant TT. Osteolysis: Basic science. Clin Orthop 2001;393:71–77.
18. Sabokbar A, Kudo O, Athanasou NA. Two distinct cellular mechanisms of osteoclast formation and bone resorption in periprosthetic osteolysis. J Orthop Res 2003;21:73–80.
19. Hallab N, Merritt K, Jacobs JJ. Metal sensitivity in patients with orthopaedic implants. J Bone Joint Surg Am 2001;83-A:428–436.
20. Cunningham BW, Orbegoso CM, Dmitriev AE, Hallab NJ, Sefter JC, McAfee PC. The effect of titanium particulate on development and maintenance of a posterolateral spinal arthrodesis: An in vivo rabbit model. Spine 2002;27:1971–1981.
21. Glant TT, Jacobs JJ. Response of three murine macrophage populations to particulate debris: Bone resorption in organ cultures. J Orthop Res 1994;12:720–732.
22. Ingham E, Green TR, Stone MH, Kowalski R, Watkins N, Fisher J. Production of TNF-alpha and bone resorbing activity by macrophages in response to different types of bone cement particles. Biomaterials 2000;21:1005–1013.
23. Matthews JB, Besong AA, Green TR, Stone MH, Wroblewski BM, Fisher J, Ingham E. Evaluation of the response of primary human peripheral blood mononuclear phagocytes to challenge with in vitro generated clinically relevant UHMWPE particles of known size and dose. J Biomed Mater Res 2000;52:296–307.
24. Shanbhag AS, Jacobs JJ, Black J, Galante JO, Glant TT. Macrophage/particle interactions. Effect of size, composition and surface area. J Biomed Mater Res 1994;28:81–90.
25. Hallab NJ, Anderson S, Caicedo M, Brasher A, Mikecz K, Jacobs JJ. Effects of soluble metals on human peri-implant cells. J Biomed Mater Res A 2005;74:124–140.
26. Nagaya T, Ishikawa N, Hata H. Sister chromatid exchange analysis in lymphocytes of workers exposed to hexavalent chromium. Br J Ind Med 1989;46:48–51.
27. Savarino L, Stea S, Granchi D, Visentin M, Ciapetti G, Donati ME, Rollo G, Zinghi G, Pizzoferrato A, Montanaro L, Toni A. Sister chromatid exchanges and ion release in patients wearing fracture fixation devices. J Biomed Mater Res 2000;50:21–26.
28. Soloviev A, Schwarz EM, Darowish M, O'Keefe RJ. Sphingomyelinase mediates macrophage activation by titanium particles independent of phagocytosis: A role for free radicals, NFkappaB, and TNFalpha. J Orthop Res 2005;23:1258–1265.
29. Wang ML, Nesti LJ, Tuli R, Lazatin J, Danielson KG, Sharkey PF, Tuan RS. Titanium particles suppress expression of osteoblastic phenotype in human mesenchymal stem cells. J Orthop Res 2002;20:1175–1184.
30. Vermes C, Chandrasekaran R, Jacobs JJ, Galante JO, Roebuck KA, Glant TT. The effects of particulate wear debris, cytokines, and growth factors on the functions of MG-63 osteoblasts. J Bone Joint Surg Am 2001;83:201–211.
31. Pioletti DP, Leoni L, Genini D, Takei H, Du P, Corbeil J. Gene expression analysis of osteoblastic cells contacted by orthopedic implant particles. J Biomed Mater Res 2002;61:408–420.
32. Kerboull L, Hamadouche M, Courpied JP, Kerboull M. Long-term results of Charnley-Kerboull hip arthroplasty in patients younger than 50 years. Clin Orthop 2004;3:112–118.
33. Glant TT, Jacobs JJ, Mikecz K, Yao J, Chubinskaya S, Williams JM, Urban RL, Shanbhag AS, Lee S-H, Sumner DR. Particulate-induced, prostaglandin- and cytokine-mediated bone resorption in an experimental system and in failed joint replacements. Am J Ther 1996;3:27–41.
34. Glant TT, Jacobs JJ, Molnar G, Shanbhag AS, Valyon M, Galante JO. Bone resorption activity of particulate-stimulated macrophages. J Bone Miner Res 1993;8:1071–1079.
35. Shanbhag AS, Jacobs JJ, Black J, Galante JO, Glant TT. Human monocyte response to particulate biomaterials generated in vivo and in vitro. J Orthop Res 1995;13:792–801.
36. Green TR, Fisher J, Matthews JB, Stone MH, Ingham E. Effect of size and dose on bone resorption activity of macrophages by in vitro clinically relevant ultra high molecular weight polyethylene particles. J Biomed Mater Res 2000;53:490–497.
37. Green TR, Fisher J, Stone M, Wroblewski BM, Ingham E. Polyethylene particles of a "critical size" are necessary for the induction of cytokines by macrophages in vitro. Biomaterials 1998;19: 2297–2302.
38. Matthews JB, Green TR, Stone MH, Wroblewski BM, Fisher J, Ingham E. Comparison of the response of primary murine peritoneal macrophages and the U937 human histiocytic cell line to challenge with in vitro generated clinically relevant UHMWPE particles. Biomed Mater Eng 2000;10:229–240.
39. Daniels AU, Barnes FH, Charlebois SJ, Smith RA. Macrophage cytokine response to particles and lipopolysaccharide in vitro. J Biomed Mater Res 2000;49:469–478.
40. Skoglund B, Larsson L, Aspenberg PA. Bone-resorptive effects of endotoxin-contaminated high-density polyethylene particles spontaneously eliminated in vivo. J Bone Joint Surg Br 2002;84: 767–773.
41. Ingram J, Matthews JB, Tipper J, Stone M, Fisher J, Ingham E. Comparison of the biological activity of grade GUR 1120 and GUR 415HP UHMWPE wear debris. Biomed Mater Eng 2002;12: 177–188.
42. Rader CP, Sterner T, Jakob F, Schutze N, Eulert J. Cytokine response of human macrophage-like cells after contact with polyethylene and pure titanium particles. J Arthroplasty 1999;14: 840–848.
43. von KM, Jewison DE, Sibonga JD, Sprecher C, Morrey BF, Loer F, Berry DJ, Scully SP. The effectiveness of polyethylene versus titanium particles in inducing osteolysis in vivo. J Orthop Res 2004; 22:237–243.
44. Shanbhag AS, Hasselman CT, Jacobs JJ, Rubash HE. Biological Response to Wear Debris. In: Callaghan JJ, Rosenberg AG, Rubash H, editors. The Adult Hip. Philadelphia: Lippincott-Raven Publishers; 1998. pp 279–288.
45. Shukla R, Bansal V, Chaudhary M, Basu A, Bhonde RR, Sastry M. Biocompatibility of gold nanoparticles and their endocytotic fate inside the cellular compartment: A microscopic overview. Langmuir 2005;21:10644–10654.
46. Scholes SC, Unsworth A. Pitch-based carbon-fibre-reinforced poly (ether-ether-ketone) OPTIMA assessed as a bearing material in a mobile bearing unicondylar knee joint. Proc Inst Mech Eng H 2009;223:13–25.

Questions? Contact FDA/CDRH/OCE/DID at CDRH-FOISTATUS@fda.hhs.gov or 301-796-8118

Records processed under FOIA Request #2014-8015; Released by CDRH on 12-8-2015

47. Smith RA, Hallab NJ. In vitro macrophage response to polyethylene and polycarbonate-urethane particles. J Biomed Mater Res A 2010;93:347–355.
48. Smith RA, Maghsoodpour A, Hallab NJ. In vivo response to cross-linked polyethylene and polycarbonate-urethane particles. J Biomed Mater Res A 2010;93:227–234.
49. Caicedo MS, Desai R, McAllister K, Reddy A, Jacobs JJ, Hallab NJ. Soluble and particulate Co-Cr-Mo alloy implant metals activate the inflammasome danger signaling pathway in human macrophages: A novel mechanism for implant debris reactivity. J Orthop Res 2008;27:847–854.
50. Dostert C, Petrilli V, Van BR, Steele C, Mossman BT, Tschopp J. Innate immune activation through Nalp3 inflammasome sensing of asbestos and silica. Science 2008;320:674–677.
51. Hornung V, Bauernfeind F, Halle A, Samstad EO, Kono H, Rock KL, Fitzgerald KA, Latz E. Silica crystals and aluminum salts activate the NALP3 inflammasome through phagosomal destabilization. Nat Immunol 2008;9:847–856.
52. Comyn J, Mascia L, Xiao G, Paraker BM. Corona-discharge treatment of polyetheretherketone (PEEK) for adhesive bonding. Int J Adhes Adhes 1996;16:301–304.
53. Zhang M, King R, Hanes M, James SP. A novel ultra high molecular weight polyethylene-hyaluronan microcomposite for use in total joint replacements. I. Synthesis and physical/chemical characterization. J Biomed Mater Res A 2006;78:86–96.
54. Tomazic-Jezic VJ, Merritt K, Umbreit TH. Significance of the type and the size of biomaterial particles on phagocytosis and tissue distribution. J Biomed Mater Res 2001;55:523–529.
55. Callaghan JJ, Rosenberg A, Rubash H. The Adult Hip. New York: Lippincott Willaims & Wilkins; 2007.
56. Catelas I, Medley JB, Campbell PA, Huk OL, Bobyn JD. Comparison of in vitro with in vivo characteristics of wear particles from metal-metal hip implants. J Biomed Mater Res B Appl Biomater 2004;70:167–178.
57. Heisel C, Silva M, la Rosa MA, Schmalzried TP. Short-term in vivo wear of cross-linked polyethylene. J Bone Joint Surg Am 2004; 86-A:748–751.
58. Kurtz SM, Hozack W, Turner J, Purtill J, MacDonald D, Sharkey P, Parvizi J, Manley M, Rothman R. Mechanical properties of retrieved highly cross-linked crossfire liners after short-term implantation. J Arthroplasty 2005;20:840–849.
59. Minoda Y, Kobayashi A, Iwaki H, Miyaguchi M, Kadoya Y, Ohashi H, Takaoka K. Polyethylene wear particle generation in vivo in an alumina medial pivot total knee prosthesis. Biomaterials 2005;26:6034–6040.
60. Saikko V, Calonius O, Keranen J. Wear of conventional and cross-linked ultra-high-molecular-weight polyethylene acetabular cups against polished and roughened CoCr femoral heads in a biaxial hip simulator. J Biomed Mater Res 2002;63:848–853.
61. Tipper JL, Hatton A, Nevelos JE, Ingham E, Doyle C, Streicher R, Nevelos AB, Fisher J. Alumina-alumina artificial hip joints. Part II: Characterisation of the wear debris from in vitro hip joint simulations. Biomaterials 2002;23:3441–3448.
62. Wroblewski BM, Siney PD, Dowson D, Collins SN. Prospective clinical and joint simulator studies of a new total hip arthroplasty using alumina ceramic heads and cross-linked polyethylene cups. J Bone Joint Surg Br 1996;78:280–285.
63. Doorn PF, Campbell PA, Amstutz HC. Metal versus polyethylene wear particles in total hip replacements. A review. Clin Orthop Relat Res 1996;329:S206–S216.
64. Margevicius KJ, Bauer TW, McMahon JT, Brown SA, Merritt K. Isolation and characterization of debris in membranes around total joint prostheses. J Bone Joint Surg 1994;76-A:1664–1675.
65. Shanbhag AS, Jacobs JJ, Glant TT, Gilbert JL, Black J, Galante JO. Composition and morphology of wear debris in failed uncemented total hip replacement. J Bone Joint Surg [Br] 1994;76: 60–67.
66. Campbell P, Ma S, Yeom B, McKellop H, Schmalzried TP, Amstutz HC. Isolation of predominantly submicron-sized UHMWPE wear particles from periprosthetic tissues. J Biomed Mater Res 1995;29: 127–131.
67. Jacobs JJ, Shanbhag A, Glant TT, Black J, Galante JO. Wear debris in total joint replacements. J Am Acad Orthop Surg 1994;2: 212–220.
68. Maloney WJ, Smith RL, Castro F, Schurman DJ. Fibroblast response to metallic debris in vitro. Enzyme induction cell proliferation, and toxicity. J Bone Joint Surg Am 1993;75:835–844.
69. Savio JAI, Overcamp LM, Black J. Size and shape of biomaterial wear debris. Clin Mater 1994;15:101–147.
70. Scott M, Morrison M, Mishra SR, Jani S. Particle analysis for the determination of UHMWPE wear. J Biomed Mater Res B Appl Biomater 2005;73:325–337.
71. Hallab NJ. A review of the biologic effects of spine implant debris: Fact from Fiction. SAS J 2009;3:143–160.
72. Hallab NJ, Khandha A, Malcolmson G, Timm JP. In Vitro Assessment of Serum-Saline Ratios for Fluid Simulator Testing of Highly Modular Spinal Implants With Articulating Surfaces. J Spine Arthroplasty Soc 2008;2:171–183.
73. Jacobs JJ, Hallab NJ, Urban RM, Wimmer MA. Wear particles. J Bone Joint Surg Am 2006;88(Suppl 2):99–102.
74. Borruto A. A new material for hip prosthesis without considerable debris release. Med Eng Phys 2010;32:908–913.
75. Brown T, Bao QB, Agrawal CM, Hallab NJ. An in vitro assessment of wear particulate generated from NUBAC, a PEEK on PEEK articulating nucleus replacement device. methodology and results from a series of wear tests using different motion profiles, test frequencies and environmental conditions. Spine (Phila Pa 1976). (2011 epub) online not in journal vol yet.
76. Rivard CH, Rhalmi S, Coillard C. In vivo biocompatibility testing of peek polymer for a spinal implant system: A study in rabbits. J Biomed Mater Res 2002;62:488–498.
77. Utzschneider S, Becker F, Grupp TM, Sievers B, Paulus A, Gottschalk O, Jansson V. Inflammatory response against different carbon fiber-reinforced PEEK wear particles compared with UHMWPE in vivo. Acta Biomater 2010;6:4296–4304.

Questions? Contact FDA/CDRH/OCE/DID at CDRH-FOISTATUS@fda.hhs.gov or 301-796-8118

Records processed under FOIA Request #2014-8015; Released by CDRH on 12-8-2015

Chapter 29

ESR Insights into Macroradicals in UHMWPE

M. Shah Jahan, PhD

29.1 Introduction
29.2 Basic Principle of ESR
29.3 Free Radicals in UHMWPE
29.3.1 Alkyl Radical
29.3.2 Allyl Radical
29.3.3 Polyenyl Radical
29.3.4 Peroxy Radical
29.3.5 ESR Evidence of the Peroxy Radical in UHMWPE
29.3.6 Half-Life of the Peroxy Radical in UHMWPE
29.4 Long-lived Oxygen-Induced Radical in UHMWPE
29.4.1 ESR Evidence of the Long-Lived Radicals in UHMWPE
29.4.2 Growth and Decay of the Oxygen-induced Radicals
29.4.3 Identification of the Oxygen-induced Radicals by ESR
29.5 Intermediate Radicals
29.6 ESR of Vitamin E-doped UHMWPE
29.7 Quantitative ESR in UHMWPE
References

29.1 INTRODUCTION

Electron spin resonance or ESR is a technique that can directly detect and quantify unpaired or odd electrons in atomic or molecular systems. The materials that contain unpaired electrons are known as paramagnetic materials because they exhibit a net magnetic moment in an external magnetic field. For this reason, ESR is also known as EPR or electron paramagnetic resonance. While both names are used in practice, a third name has been introduced to replace them. In line with NMR or nuclear magnetic resonance, the new name is EMR or electron magnetic resonance because the magnetic resonance in ESR/EPR results from the electron magnetic moment. In this chapter, the term ESR is used.

ESR is the only technique that is particularly suitable, not only for direct detection, but also for quantitative analyses of free radicals in a solid or fluid. In polymers, free radicals are generally formed as a result of the unpairing of electrons from a particular molecular site (chain, side, or ring) by mechanical or chemical means, or by irradiation with ionizing radiation. The possession of an unpaired electron makes the free radical a good candidate for ESR study. Soon after the ESR instruments became available in mid-1950, free radical measurements in polymers, including polyethylene (PE), began. Most of the early works on PE radicals are compiled by Malcolm Dole in two volumes entitled *The Radiation Chemistry of Macromolecules* [1]. Readers are referred to Chapters 9, 13, and 14 in Volume I, and Chapters 1 and 13 through 16 in Volume II. In 1995, Jan F. Rabek also published a large volume of works, including ESR results, on polymer degradation [2]. In the latter publication, particular attention should be given to Chapters 3 and 10 because of their relevance to the subject of this chapter.

In low density PE, radicals are unstable at room temperature. This low density PE, linear or stretched, was the primary material under study in the aforementioned works of Dole and Rabek. ESR measurements in these early works were therefore conducted at liquid nitrogen temperature. Nevertheless, the results of these measurements on relatively simple PE can help in understanding the macroradical processes in more complex matrix of ultrahigh molecular weight polyethylene (UHMWPE).

UHMWPE has gained its importance in orthopedic science and technology for more than 5 decades as a material of choice for total hip- and knee-joint components. However, the physical and chemical properties of UHMWPE are adversely affected by free radicals that are generated in the polymer matrix as a result of radiation sterilization or crosslinking [3–13]. Consequently, the

UHMWPE Biomaterials Handbook
Copyright © 2009, Academic Press, Inc. All rights of reproduction in any form reserved.

Questions? Contact FDA/CDRH/OCE/DID at CDRH-FOISTATUS@fda.hhs.gov or 301-796-8118

Records processed under FOIA Request #2014-8015; Released by CDRH on 12-8-2015

ESR technique serves as an important diagnostic/research tool for testing irradiated UHMWPE.

Keeping in mind that ESR knowledge can be useful for the orthopedic or biomaterials community, this chapter starts with the basic principle of ESR and provides ESR data on the radicals generated, propagated, and terminated in UHMWPE. Emphasis is given on the short- and long-term oxidation results and on identification of the peroxy and oxygen-induced radicals. ESR results on vitamin E-doped UHMWPE and quantitative ESR are also presented.

29.2 BASIC PRINCIPLE OF ESR

ESR spectroscopy is based on the fundamental properties of electrons. They are mass ($m_e = 9.11 \times 10^{-31}$ kg), charge ($e = -1.6 \times 10^{-19}$ coulomb), and spin(s). Therefore, an unpaired electron in atoms or molecules (for example, hydrogen atoms, transition metal ions, free radicals), possesses both magnetic moment and angular momentum. The ratio between magnetic moment and the angular momentum is known as gyromagnetic ratio. The net magnetic moment of a material (solid, liquid, or gas) can be zero because of the random nature of the spinning electrons. In an external magnetic field (H) the spin magnetic moment aligns parallel or antiparallel to the field, and the spinning electrons are split or divided into high (+) and low (−) energy states. The energy separation ΔE between the states is known as Zeeman energy and is given by $\Delta E = g\beta H$, where H is the external steady magnetic field, β is the electron Bohr magneton ($\beta = 9.27 \times 10^{-24}$ J/T), and g is the spectral splitting factor, commonly known as the g-value. Transitions between these states can be stimulated by an oscillating magnetic field of frequency f when and only when its energy equals ΔE; that is, $hf = \Delta E = g\beta H$, where h is Planck's constant ($h = 6.63 \times 10^{-34}$ J.s). The condition $hf = g\beta H_r$ is known as resonance condition, where H_r is the external magnetic field at resonance. The g-value is related to gyromagnetic ratio (γ) as $\gamma = g\beta/\hbar$, where β is the Bohr magneton (previously given), and $\hbar = h/2\pi$. *Free electrons have a g-value of 2.0023. The g-value of a radical species can be used as an identifying mechanism of the radical type.* The ESR resonance condition is similar to that of the well-known NMR (nuclear magnetic resonance) where g is replaced by g_N (nuclear g-value) and β is replaced by β_N (nuclear magneton). While ESR operates at microwave frequency (GHz), NMR operates at radio frequency (MHz).

The g-value, therefore, is expressed as

$$g = hf/\beta H_r \quad (1)$$

and the resonance magnetic field position is expressed by

$$H_r = hf/g\beta. \quad (2)$$

For electrons, the frequency f falls within the microwave regions. Because g is a constant, or a characteristic value, of a species (free radical, for example), resonance field is directly proportional to microwave frequency. The ESR spectrometer operates at the frequency band $\sim 9 \times 10^9$ Hz, or 9 GHz, and is known as an X-band spectrometer; it is most commonly used to study organic or polymeric materials, including biomaterials. The g-value for organic or polymeric radicals varies only slightly from the free electron value of g = 2.0023. The corresponding magnetic field for g = 2.0 is 3000 Gauss (G) or 0.3 Tesla (T).

NMR (nuclear magnetic resonance) signal intensity is recorded as a function of frequency at a constant magnetic field. Unlike NMR spectrometers, an ESR spectrometer requires a resonator (a microwave cavity) that operates at a fixed frequency, and it records the resonance absorption signal as a function of external magnetic field. The resonance magnetic field of an L-band (f = 1 GHz) spectrometer is 357 G, an S-band (f = 4 GHz) is 1430 G, a K-band (f = 24 GHz) is 8570 G, and a Q-band (f = 35 GHz) is 12,500 G. There are yet other special purpose ESR spectrometers that operate at very low or high frequencies.

At resonance, absorption of microwave energy by the lower energy state (−) spins produces an absorption signal that is generally very weak and may not be directly recorded or displayed. Therefore, an ESR spectrometer, unlike NMR, FTIR (Fourier transformed infrared) or optical spectrometers, records a first derivative of the absorption signal, which results from the modulation of the external magnetic field at 100 kHz (at X-band). A spectrometer may also have the option to produce a second-derivative absorption signal. An unpaired electron formed as a result of a broken covalent bond in a molecule, for example, creates a radical (by definition), and the ESR will most likely produce a single line, or a singlet (see Figure 29.1), provided there is no net nuclear magnetic moment coupled to the unpaired spin or no resolvable hyperfine coupling. Figure 29.1A shows the energy states of an unpaired electron in a magnetic field H with separation $\Delta E = g\beta H$. The transition between the (+) and (−) states is detected as the first-derivative of absorption at resonance $\Delta E = g\beta H_r = hf$, where H_r is the resonance magnetic field and f is the resonance frequency. Figure 29.1B shows an experimentally recorded ESR spectrum due to a stable organic radical, 2, 2-Diphenyl-1-picrylhydrazyl (DPPH). The corresponding absorption curve, shown in Figure 29.1C, is obtained by integrating the first-derive curve or spectrum; the shaded area under the curve is proportional to radical concentration. For computational purposes, resonance magnetic field position H_r (the crossover point in the first-derivative curve, or the peak of the absorption curve, $H_r = 3515.824$ G) and the line width, $\Delta H_{pp} = 1.33$ G, can be measured visually by zooming into the experimental spectrum. As shown in the Figure 29.1C, the magnetic field position of the peak equals H_r-value. The resonance frequency is automatically

Questions? Contact FDA/CDRH/OCE/DID at CDRH-FOISTATUS@fda.hhs.gov or 301-796-8118

Records processed under FOIA Request #2014-8015; Released by CDRH on 12-8-2015

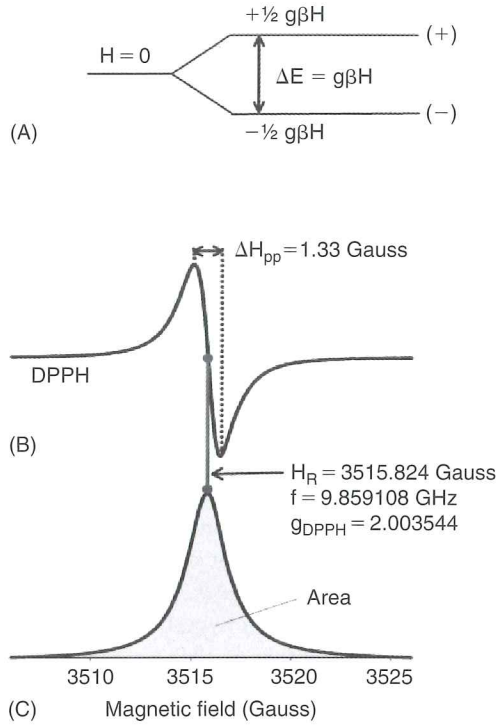

FIGURE 29.1 (A) Zeeman energy ΔE between the high (+) and low (−) energy states of an unpaired electron spin in an externally-applied magnetic field H. (B) Experimentally recorded first-derivative ESR spectrum of 2, 2-Diphenyl-1-picrylhydrazyl (DPPH). (C) absorption curve obtained by integrating the first-derivative spectrum.

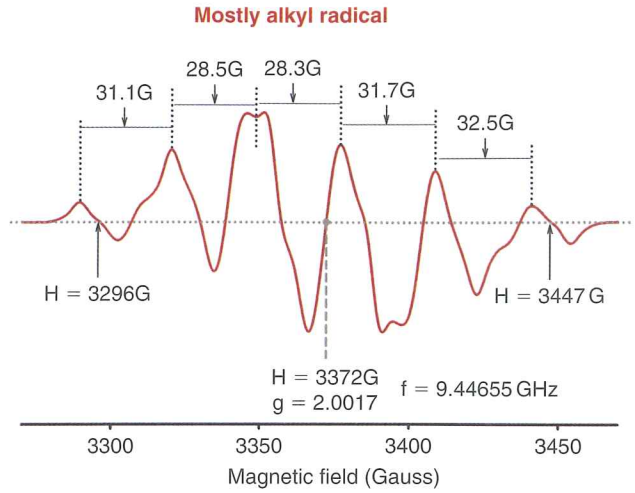

FIGURE 29.2 First derivative ESR spectrum of an alkyl radical —CH_2—$^{\bullet}CH$—CH_2—. Also shown in the figure are the separation between the lines, magnetic field positions of the first line (H = 3296 G) and the sixth line (H = 3447 G), the center of resonance H = 3372 G, frequency f = 9.4465 GHz, and the g-value for the radical g = 2.0017.

recorded at the time of measurement (Bruker EMX). Using f = 9.859108 GHz in the resonance formula (1), the g-value is calculated as g = 2.003544. A more accurate g-value was obtained by taking the average of five measurements. The calculated g-value was g = 2.00360 ± 0.00005, which is same as the textbook value of 2.0036 ± 0.0006. DPPH is frequently used as a standard for quantitative ESR or as a g-marker. The shaded area under the absorption curve is proportional to the radical concentration.

Although structural information about the radical may not be found from a singlet, ESR parameters such as g-value and the line-width or peak-to-peak separation ΔH_{pp} can provide a basic idea about the radical. Additional discussion about the singlet is presented later.

If a proton is situated near the unpaired spin (at the broken site of a molecule), each electron Zeeman energy state will split into two (for nuclear spin I = 1/2) or three (for nuclear spin I = 1) states. For each nuclear spin, electron spin energy level splits into 2I + 1 levels. The magnetic field positions of the resonance lines for I = 1/2 are given by

$$H = H_r \pm 1/2\, a \qquad (3)$$

where H_r is the resonance field position for the radical and 'a' is the hyperfine coupling constant, or hyperfine constant. In this case, two lines are obtained: one at $H_1 = H_r - 1/2\ a$; the other at $H_2 = H_r + ½\ a$. Therefore, the separation $(H_2 - H_1 = (H_r + 1/2\ a) - (H_r - 1/2\ a) = a)$ between the two lines is 'a.' In a multiline spectrum, the hyperfine constant can be determined by measuring the hyperfine separation or, simply, the separation between the lines. For g-value calculation, the value of the magnetic field position H_r is used, although there may not be any real signal at that position.

For a radical containing five equivalent protons in its neighborhood, each of I = 1/2, six resonance lines are observed in its ESR spectrum (2 × 5/2 + 1=6); the six-line spectrum of the alkyl radical in UHMWPE is a good example (see Figure 29.2). One α-proton and four β-protons in the alkyl radical (—$CH_{2,\beta}$—$^{\bullet}CH\alpha$—$CH_{2,\beta}$) effectively act like five equivalent protons because of random orientation of the molecule in a heterogeneous polymer matrix. Intensity ratios (theoretical) of the lines are 1:5:10:10:5:1. The intensity of, and the separation between, the first derivative lines in Figure 29.2 cannot provide accurate results because of the overlapping side lines (or doublets). However, for g-value calculation, the magnetic field positions of the first line (H = 3296 G), the sixth line (H = 3447 G), and the center of resonance H_r = 3372 G are recorded. Using the operational frequency f = 9.4465 GHz in the formula (3), the g-value for the radical was calculated to be g = 2.0017, approximately. Measuring the separation between the lines, the approximate value for the hyperfine constant was found to be a_{alkyl} = 30.4 G. If, however, nonequivalent or different protons of nuclear spin I = 1/2 or 1, are coupled to the same unpaired electron of the radical, line positions and/or intensity ratios can get complicated because of the combined or overlapping effects of different hyperfine couplings. For background

Questions? Contact FDA/CDRH/OCE/DID at CDRH-FOISTATUS@fda.hhs.gov or 301-796-8118

Records processed under FOIA Request #2014-8015; Released by CDRH on 12-8-2015

of ESR, readers are referred to Chapter 6, *Basic Principle of Spectroscopy* by Chang [14] and Chapter 1, *Electron Paramagnetic Resonance* by Weil et al. [15].

29.3 FREE RADICALS IN UHMWPE

The main or primary radicals frequently reported in the literature are: the alkyl —CH_2 —$^{\bullet}CH$ —CH_2—, the allyl —CH_2—CH = CH— $^{\bullet}CH$—CH_2— or —CH_2— $^{\bullet}CH$—CH = CH—CH_2—, and the polyenyl —$HC^{\bullet}$ —$H(CH = CH)_n$—. The secondary or tertiary radicals are: peroxy, —$CHO_2^{\bullet}$—, alkoxy, —$CHO^{\bullet}$—, vinyl >CH=$^{\bullet}CH_2$—, and oxygen-induced radicals (OIR). In simpler terms, a main polymer radical is denoted as $P^{\bullet}$ or $R^{\bullet}$, the peroxy radical as $PO_2^{\bullet}$, $POO^{\bullet}$, $RO_2^{\bullet}$, or $ROO^{\bullet}$, and the alkoxy radical as $PO^{\bullet}$ or $RO^{\bullet}$. A brief discussion of each one of these radicals is given in the following sections. Note that the presence of an unpaired electron at the broken site of a molecule is conventionally denoted with a superlative dot symbol (•), such as —$^{\bullet}CH$—.

29.3.1 Alkyl Radical

The alkyl radical is formed as a result of abstraction of a hydrogen atom from the —CH_2— group in the PE chain. The site of the molecule or group (—$^{\bullet}CH\alpha$—, for example) with one less hydrogen has, therefore, one unpaired electron. The hydrogen atom at the unpaired electron site is known as α-hydrogen, and the four nearest (two on the left and two on the right) are known as β-hydrogen atoms. The molecular structure of the alkyl radical is expressed as —$CH_{2,\beta}$ —$^{\bullet}CH\alpha$ — $CH_{2,\beta}$—. These β-hydrogen atoms are considered as equivalent atoms insofar as their interaction with the unpaired electron is concerned. Of course, orientation difference of each β-hydrogen atom with respect to the molecular chain can make them nonequivalent. The next-nearest hydrogen atoms in the chain of —CH_2—s are known as γ-hydrogens, and they can have an effect on an ESR signal as well. As previously presented, one unpaired electron produces one single line in the ESR signal (or ESR spectrum). The single resonance line splits into two equally intense lines (known as hyperfine lines) with a separation "a" (known as hyperfine separation or coupling constant) when it is coupled with a nearby unpaired proton, such as hydrogen nucleus. Further splitting of the hyperfine lines, with different coupling constant, can occur if the same unpaired electron is also coupled to additional nearby protons (β-hydrogen atoms in polyethylene (PE) chains, for example). In UHMWPE, however, the effects of α-hydrogen and β-hydrogen atoms on the ESR spectrum cannot be distinguished because of random orientation of the molecular chains within the polymer matrix. The typical six-line pattern in the ESR spectrum of the alkyl radical is due to an average coupling of the five hydrogen atoms, one α- and four β-hydrogen atoms (see Figure 29.2). The line separation "a" varies between 23 and 30 Gauss. Each of the lines in Figure 29.2 are broad and exhibit additional features, such as side or satellite lines, or doublets. These additional features in the spectrum may arise from the complex nature of UHMWPE, possessing crystalline, amorphous and interfacial regions in any given matrix. Additional features in the ESR spectrum may arise due to different operating parameters as well such as microwave power, modulation amplitude, temperature, time constant, etc. As a result, attribution of an ESR signal to a particular radical species in UHMWPE becomes nontrivial. One needs to pay careful attention to all of these variables before attributing a signal or spectrum to a particular species. In the early 1960s a number of investigators made very thorough investigations of the irradiated PE and made a precise structural assignment to each radical species based on the ESR spectrum. For example, Dole (see Chapter 14 [1]) observed five hyperfine lines with a separation of 28 G between them (a_β=28 G) due to four equivalent β-hydrogen atoms in the alkyl radical in oriented molecules in a stretched PE sample at 77 K. Additionally, each hyperfine line was found to split in two with a separation of 13 G ($a\alpha$=13 G) produced by one α-hydrogen atom.

29.3.2 Allyl Radical

Shown in Figure 29.3 is an approximate molecular diagram of the allyl radical —CH_2—CH = CH—$^{\bullet}CH$—CH_2—↔—CH_2—$^{\bullet}CH$—CH = CH—CH_2—. As previously mentioned, precise structural analyses of the PE radicals were conducted in the early 1960s (see Chapter 14 [1]). For example, using oriented linear PE at temperature 77–293 K, Ohnishi identified a seven-line ESR spectrum due to four β-hydrogen and two α-hydrogen atoms [16, 17]. The separation between the lines was found to be approximately 21 G. Effects of C_1-Hα and C_3-Hβ bond angles (see Figure 29.3) on the ESR spectrum were also measured at different temperatures. Concentration of the allyl radical at low temperatures was determined by subtracting the alkyl radical concentration at that temperature, or at room temperature when the alkyl radical had decayed. In UHMWPE, a clean seven-line (ESR) fingerprint of the allyl radical is obtained at room temperature following gamma irradiation at the same temperature in nitrogen or vacuum. Figure 29.4A shows a first-derivative

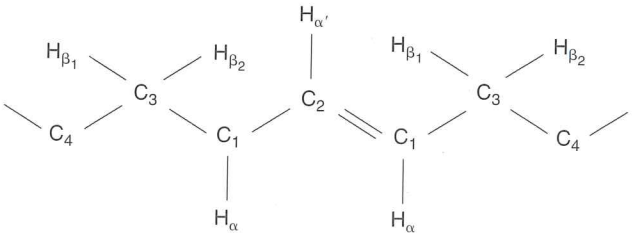

FIGURE 29.3 Molecular structure of the allyl radical showing approximate orientation of the α- and β-hydrogen atoms.

Questions? Contact FDA/CDRH/OCE/DID at CDRH-FOISTATUS@fda.hhs.gov or 301-796-8118

Records processed under FOIA Request #2014-8015; Released by CDRH on 12-8-2015

ESR spectrum of the radical with hyperfine coupling constant a_{allyl} = 13.6 G, and the g-value, g = 2.0016, approximately. Note that the g-value for the radical corresponds to the resonance magnetic field (H_r = 3372 G) of the entire spectrum, which is the crossover point of the middle line. If alkyl radicals are also present, side lines will appear on both ends (right and left) of the spectrum. The weak broad lines, one on the left and one on the right, shown on the magnified y-scale in Figure 29.4B, are the members of the six-line spectrum due to the alkyl radical; the other four lines are overlapped by the strong lines due to the allyl radical. The center or the resonance magnetic field (H_r = 3508 G) of the alkyl radical can be approximately calculated by measuring the magnetic field positions (3433 G and 3583 G) of the two lines. The g-value for the radical was calculated as 2.0025, which is slightly greater than the g-value (g = 2.0017) obtained from the predominantly alkyl ESR spectrum (Figure 29.2). Although each radical has its own characteristic a- and g-value, differences like this can occur due to experimental errors. In practice, therefore, any g-value between 2.001 and 2.003 is acceptable for the alkyl, allyl, and polyenyl radicals. However, to obtain statistically significant results, one needs to make a large number of measurements and compare with the theoretical values.

Two important observations are made at this point: (1) a spectrum like this can be a good indicator of the presence of both alkyl and allyl radicals, and (2) by following any changes in one of these two lines, at extreme right or left, and one of the center lines (due to allyl) one could follow the reaction process of one radical in presence of the other. Subtraction methods may also be used to find the concentration of the alkyl and allyl radicals; however, the presence of di-, tri-, or polyenyl, or vinyl radicals, should be considered as well. To get a good estimate of the constituent radicals, one could deconvolute the experimental spectrum by applying a simulation method (see Section 29.3.3).

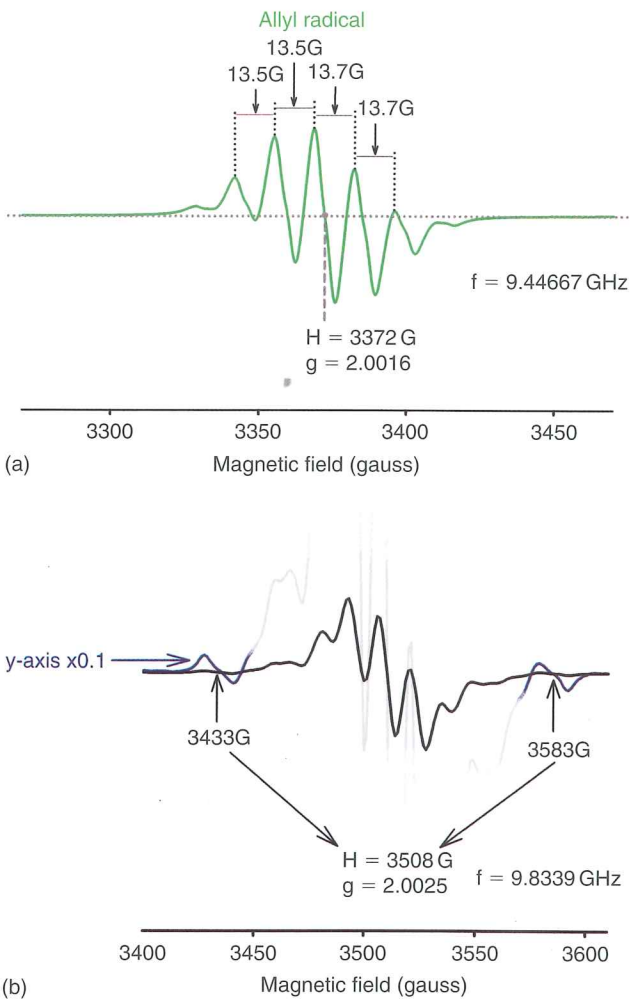

FIGURE 29.4 (A) First derivative ESR spectrum due to allyl radical. (B) First-derivative ESR spectrum due to the alkyl and allyl radicals present in the same sample (GUR 1050, γ-irradiated in nitrogen and then exposed to air before measurements. The presence of the alkyl radical is shown by the weak lines (magnified) at the extreme left and right ends of the spectrum. The seven-line pattern of the allyl radical appears at the central part of the spectrum.

29.3.3 Polyenyl Radical

Ohnishi et al. provides a good discussion on polyenyl radicals, CH_2—$^{\bullet}CH$(—CH = CH)$_n$—CH_2— [17], produced as a result of the migration of the alkyl radical. The polyenyl radicals are quite stable due to the formation of conjugated double bonds. According to Ohnishi et al., polyenyl radicals are produced at high doses (>1000 kGy), while the allyl radical is formed at intermediate doses (100–1000 kGy) and the alkyl is formed at low doses (<10 kGy). Nonetheless, low-level polyenyl radicals are formed at low doses as well but may not be directly observed because of the presence of strong resonance lines of other radicals having very similar g-values. Using the WinSim-2002 (Bruker) simulation program, we found concentration of the allyl (n = 1), dienyl (n = 2), trienyl (n = 3), and higher order polyenyl (n > 3) radicals. A simulation of an ESR spectrum due predominantly to the allyl is shown in Figure 29.5A and to the alkyl in Figure 29.5B. Table 29.1 lists the abundance and hyperfine coupling constants of these split radicals. One should note that the simulation of the allyl spectrum may not include alkyl and that the alkyl may not include allyl. Therefore, these simulations are not perfect, but they provide a means to get a general estimate.

29.3.4 Peroxy Radical

The peroxy radical (—H_2C—$HCO_2^{\bullet}$—CH_2—) is the precursor to the oxidation process in UHMWPE. It leads to the production of hydroperoxide and carbonyl specie (>CO), including esters, aldehydes, alcohols, etc. These nonradical or neutral by-products or end products in UHMWPE can be detected or quantified by FTIR technique. In practice, the FTIR absorption band near 1680–1720 cm^{-1} due to

Questions? Contact FDA/CDRH/OCE/DID at CDRH-FOISTATUS@fda.hhs.gov or 301-796-8118

Records processed under FOIA Request #2014-8015; Released by CDRH on 12-8-2015

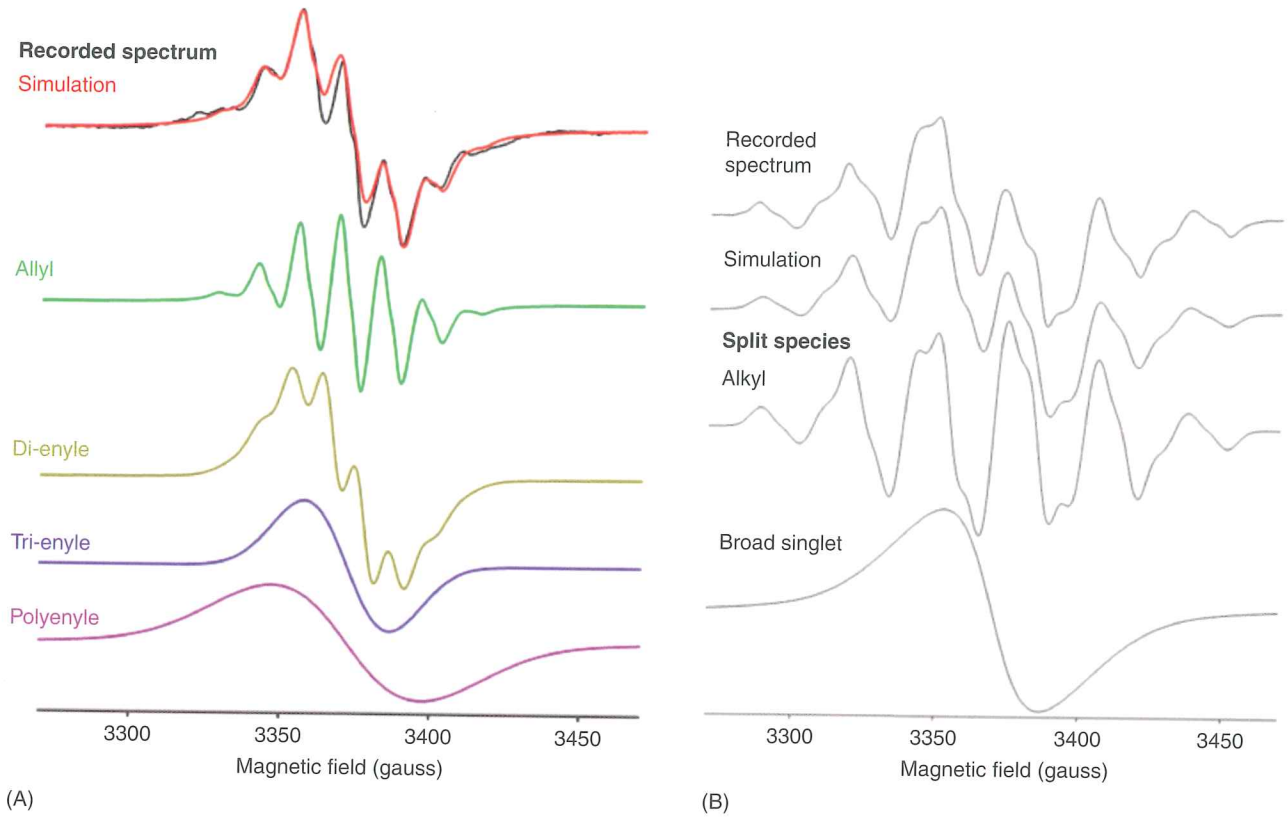

FIGURE 29.5 Spectral simulation for a predominantly allyl radical (A) and alkyl radical (B).

TABLE 29.1 Abundance, Spin 1/2 Hyperfine Coupling Constants, Percentage Lorentzian and Line Width Used for Spectral Simulations in Simulations 1 and 2

	Simulation 1				Simulation 2	
	Allyl	Dienyl	Trienyl	Singlet	Alkyl	Singlet
Abundance	23%	17.70%	26.70%	32.60%	25.70%	74.30%
a-α	2@13.3 G	3@8.9 G	4@7.7 G	NA	1@22.1 G	NA
a-β1	1@4.0 G	2@1.9 G	3@0.7 G	NA	4@31.6 G	NA
a-β2	4@13.3 G	4@8.9 G	4@7.7 G	NA	NA	NA
a-anisotropy	NA	NA	NA	NA	1@7.2 G	NA
% Lorentzian	87.4	100	88.3	29	0	59.2
Line width (G)	4.3	6	7.4	18.8	4.28	23.4

the carbonyl group is used to measure oxidation levels in UHMWPE and is known as the oxidation index (OI). ESR is the only technique that can directly detect peroxy radicals in solid or liquid, but such detection is challenging when applied to UHMWPE due to the overlapping signals from different radicals present in the complex polymer matrix. Furthermore, each individual signal changes due to the ongoing reactions of the radicals from the surface to the core of a given test sample in the presence or absence of oxygen.

Discussions and speculations based on experimental data have been made about the peroxy radical in UHMWPE, but

Questions? Contact FDA/CDRH/OCE/DID at CDRH-FOISTATUS@fda.hhs.gov or 301-796-8118

Records processed under FOIA Request #2014-8015; Released by CDRH on 12-8-2015

to our knowledge, no clear ESR evidence has been reported. Many investigators have attributed the so-called single-line spectrum to peroxy [8, 17–20]. However, as presented in the next section, the single line was found to be made of two separate overlapping spectra, each due to a different radical, neither of which was a peroxy. In this section, we present an ESR method for successful detection of the peroxy radical in UHMWPE made recently in our laboratory.

29.3.5 ESR Evidence of the Peroxy Radical in UHMWPE

Because of the unique orientation of the oxygen molecule-with-unpaired spin (—$O_2^{\bullet}$—) with respect to the PE molecular axis, the peroxy radical produces (theoretically) asymmetric lines in the ESR spectrum with two g-values, $g_{\parallel}$ and $g_{\perp}$. Ranby and Rabek presented a discussion on the dependence of the ESR spectrum on the orientation of the peroxy end in polytetrafluoroethylene (PTFE) radical [21]. "Rabek provides an ESR spectrum of the peroxy radical in polypropylene and also in polyethylene (Chapter 3 [2]). The polypropylene-peroxy radical presented is a clear ESR spectrum, which can be considered as the fingerprint for the peroxy radical; the ESR spectrum of the polyethylene-peroxy (low density polyethylene) is not as well defined."For a better understanding, readers are referred to a survey of the mechanisms for production, propagation, and termination of the peroxy radicals in polyolefins, including PE, compiled by J. F. Rabek (Chapter 3 [2]) and by Dole (Chapter 13 [1]).

Direct detection of the primary peroxy radical in UHMWPE was made in our laboratory in 2004 [22]. We used 200-μm thick sample (GUR 1050) and irradiated it with X-rays in nitrogen or vacuum. Immediately after irradiation the sample was transferred to the ESR cavity, which was continuously purged with nitrogen. In conjunction with microwave power saturation technique (PST), ESR spectra were recorded at and below room temperature. At different time intervals, the flow of nitrogen was stopped to allow oxygen (air) to react with the radicals. As shown in Figure 29.6, when the sample was exposed to air for 1 minute and the microwave power increased to 32 mW (Figure 29.6B), the resonance lines due to the alkyl and the allyl were suppressed (saturated), and a broad asymmetric signal (one line) was formed (Figure 29.6C). Although this is not a fingerprint of a peroxy radical, it was an indication of the formation of one. The fingerprint was obtained when the temperature of the sample was decreased to 118 K by maintaining a flow of cold nitrogen gas through the cavity (airflow was stopped). The unambiguous peroxy structure in the ESR signal is evidenced by its well-defined $g_{\parallel}$ and $g_{\perp}$ positions ($g_{\parallel}$ = 2.032 and $g_{\perp}$ = 2.003) as shown in Figure 29.6D. When the temperature was increased to

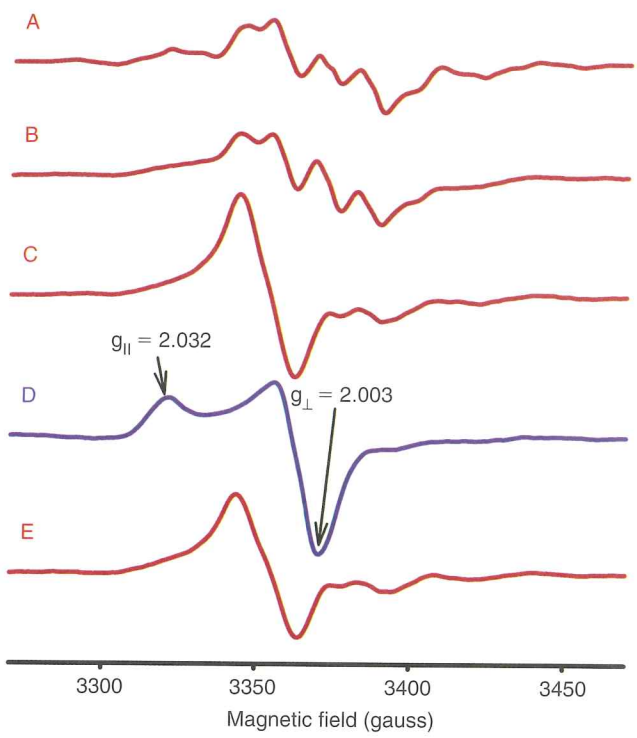

FIGURE 29.6 Various ESR spectra of one GUR 1050 film sample, x-irradiated for 1 hr in a vacuum at 293 K (room temperature). The sample was transported in nitrogen to the ESR cavity, which had nitrogen flowing through it. The film did get exposed to air for a couple of seconds during the transfer. (A) and (B) were recorded at 8 mW and 32 mW of power, respectively. The sample was then exposed to air for 1 min, and (C) was recorded at 32 mW. The temperature was then lowered to 118 K, and (D) was recorded. (E) was recorded after the sample was brought back to room temperature (293 K) again.

293 K (room temperature) and the nitrogen flow was maintained, the spectrum (Figure 29.6E) returned to its original structure (Figure 29.6C), as expected. The result of these measurements suggests that the asymmetric broad single line at room temperature can serve as an indicator of the presence of peroxy radical; however, confirmation should be made by recording ESR signal at low temperature.

Shown in Figure 29.7 is a similar result obtained when the test was performed on a sample containing predominantly alkyl radical (1−mW scan). At 100 mW microwave power, the alkyl radical signal was saturated and the peroxy signal was revealed. As indicated by the decrease in intensity of the signal, recorded at 15 min, 30 min, and 76 min (1 h and 16 min), the peroxy radical concentration decreased in a nitrogen environment at room temperature by recombination. When the sample was opened to air after 76 min in nitrogen, the peroxy-signal intensity increased, indicating the production of the new peroxy radical. Keep in mind that the alkyl radical may not produce an ESR signal at a high microwave power, but it can react with oxygen that is present in the system and form a peroxy radical.

Questions? Contact FDA/CDRH/OCE/DID at CDRH-FOISTATUS@fda.hhs.gov or 301-796-8118

Records processed under FOIA Request #2014-8015; Released by CDRH on 12-8-2015

As shown in Figure 29.8, production of the peroxy radical by the allyl was demonstrated by first allowing the alkyl radical to decay to allyl in 124 hours in nitrogen and then allowing the latter to react with oxygen (air). The corresponding ESR spectra are shown in Figure 29.8.

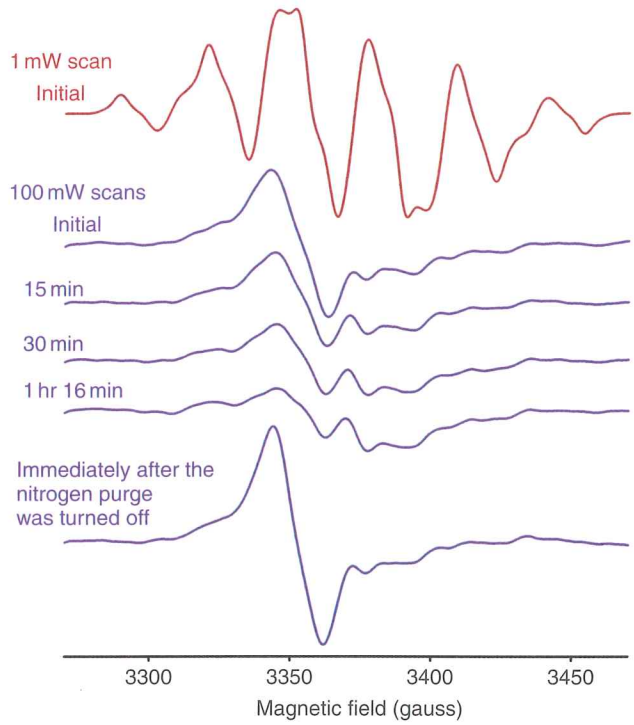

FIGURE 29.7 ESR spectra of the peroxy radical in a 200-μm GUR 1050 film, x-irradiated for 2 hours in a vacuum (10^{-6} torr) and subsequently opened to air. The first spectrum shown was taken 6 minutes after quickly being opened to air and subsequently put in a nitrogen flow. The nitrogen flow was turned back off after 1 hr 16 min.

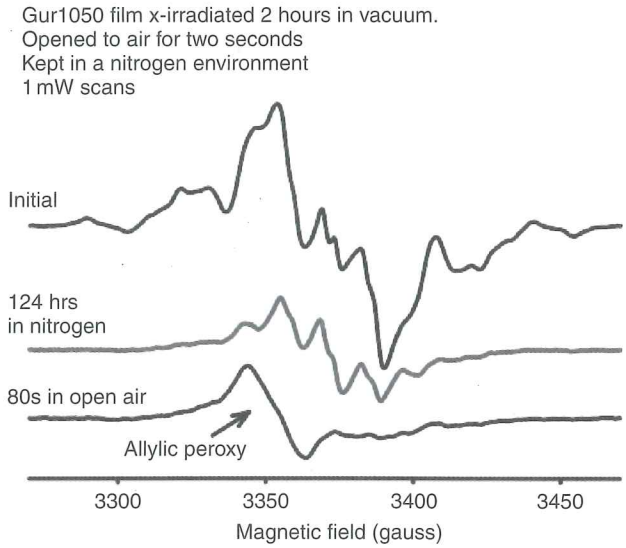

FIGURE 29.8 ESR spectra of GUR 1050, x-irradiated for 2 hr in vacuum and subsequently transported to the ESR cavity, which had a continuous flow of nitrogen running through it. Measurements were taken at 1 mW of microwave power and 1 G modulation amplitude.

29.3.6 Half-Life of the Peroxy Radical in UHMWPE

The decay (in nitrogen) and production (in air) of the peroxy radical was monitored by measuring the normalized peak-to-peak height of the corresponding ESR spectrum.

The decay in nitrogen was greater than that in the open air, possibly due to existing peroxy radicals continuing to decay while little or no generation of new peroxy radicals occurred in the absence of oxygen. In open air, however, generation of new peroxy radicals can occur while others decay. When most of the peroxy radicals decayed in the time interval 80–100 min, subsequent exposure of the same sample to oxygen (air) resulted in the production of a few more peroxy radicals, as indicated by the positive trend in the intensity-time curve. The peroxy radical in UHMWPE is, therefore, very short lived with a half-life of 10–20 min. From the work of Auerbach and Sanders [23], Dole concluded that the half-life of the peroxy radical in linear PE at room temperature was 20 min, which is very close to our result in UHMWPE [1].

29.4 LONG-LIVED OXYGEN-INDUCED RADICAL IN UHMWPE

In addition to the short-lived peroxy radical (previously discussed), growth of a long-lived radical becomes evident in the ESR spectrum of an irradiated UHMWPE when the primary radicals decay. Because this long-lived radical is produced only in the presence of oxygen, it is known as an oxygen-induced radical (OIR), for lack of a better term. While we have been observing the OIR in a large number of samples for more than 20 years, its lifetime is yet to be known. Being a terminal species in the polymer system, the OIR is also known as a "terminal" or "residual" radical. However, distinction must be made between the long-lived OIR and the "residual primary" radicals found in UHMWPE following a long-term postirradiation aging in an inert environment (>10 years in this laboratory). Only a small fraction of the primary radicals survive the long-term aging in an inert environment; the longer the aging time, the lower the concentration (see Section 29.4.1). They are also labeled as "residual" or "residual primary" radicals.

29.4.1 ESR Evidence of the Long-Lived Radicals in UHMWPE

The growth of the OIR following the decay of the primary radicals in the presence of oxygen is illustrated in Figure 29.10 in which the ESR spectrum is recorded as a function of time at room temperature in air for two different samples, A (GUR 4150) and B (GUR 4120). Sample A was irradiated with X-rays at room temperature in air, and its

Questions? Contact FDA/CDRH/OCE/DID at CDRH-FOISTATUS@fda.hhs.gov or 301-796-8118

Records processed under FOIA Request #2014-8015; Released by CDRH on 12-8-2015

ESR tests began immediately after irradiation. Notice that the initial ESR spectrum of the sample A resembles that of the alkyl radical shown in Figure 29.2. Sample B was aged at 75°C for 6 years in vacuum following gamma irradiation in vacuum at room temperature and was subsequently opened to air for oxidation to occur. The ESR spectrum of the sample B, recorded before the sample was open to air, is very weak, but it exhibits the characteristic features of that of the primary alkyl/allyl radicals (see Figures 29.4A and 29.4B). It is important to note that the primary radicals in the sample B decayed significantly, most likely via radical-radical recombination as evidenced by the weak ESR spectrum, but did not transform to other species during the aging period. In the presence of oxygen, these long-lived primary radicals ("residual primary" radicals) in the sample B decayed, and the OIR grew in the same manner as those in the sample A; the growth time for the OIR is approximately 35 days. The growth of the OIR is evidenced by the appearance of the broad line in the ESR spectrum near 3500 G and disappearance of the initial resonance lines as shown in Figure 29.10. From these and similar results obtained from the ESR measurements on a large number of UHMWPE samples, GUR 4120, GUR 4150, GUR 1020, GUR 1050, and Himont 1900, following x-, gamma-, or e-beam irradiation, we make the following observations:

1. OIR can form in the presence of oxygen in UHMWPE resin following irradiation with X-rays, gamma rays, or electron beam.
2. OIR is detectable by ESR in about 35 days after an irradiated sample is exposed to oxygen (air).
3. The concentration of the OIR is directly proportional to that of the primary radicals present at the time of initial oxidation.

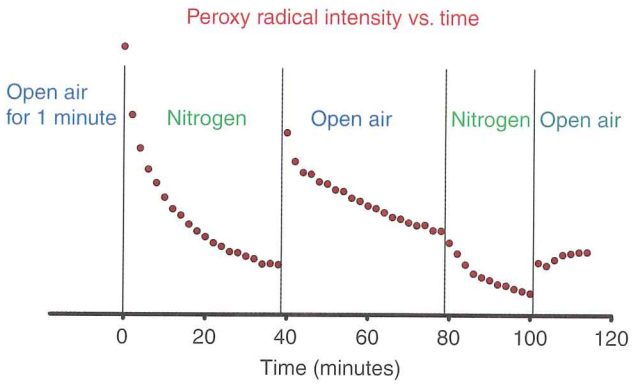

FIGURE 29.9 Relative peak-to-peak height of the ESR signal due to the peroxy radical in a 200-μm GUR 1050 film, x-irradiated for 1 hr in a vacuum (10^{-6} torr) and subsequently opened to air. The spectra were recorded at 100 mW. When opened to air, the nitrogen flow was turned on and off a couple of times.

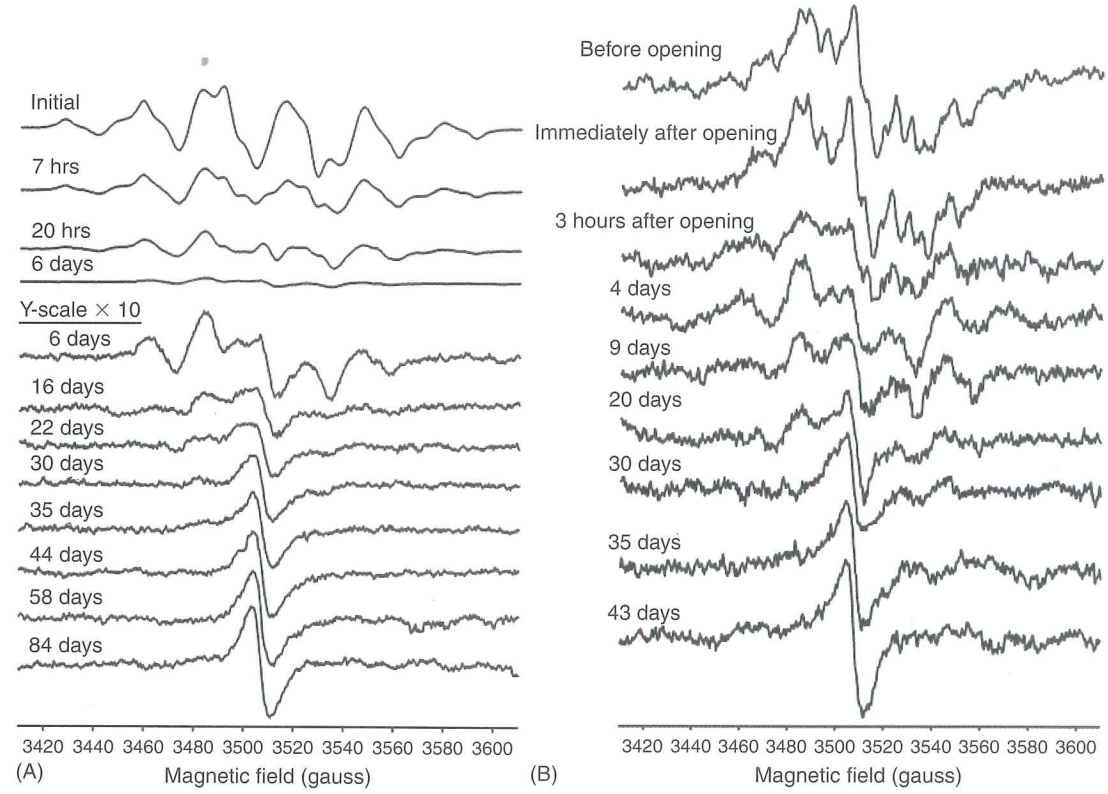

FIGURE 29.10 ESR spectrum recorded as a function of time at room temperature to monitor the growth of the oxygen-induced radical. (A) GUR 4150 bar irradiated with X-ray for 1.3 hours in air and stored in air at room temperature. (B) GUR 4120 was gamma irradiated in an evacuated quartz tube and then stored for 6 years at 75°C in a vacuum. The sample was then removed from the tube to allow oxidation to occur at room temperature.

Questions? Contact FDA/CDRH/OCE/DID at CDRH-FOISTATUS@fda.hhs.gov or 301-796-8118

Records processed under FOIA Request #2014-8015; Released by CDRH on 12-8-2015

29.4.2 Growth and Decay of the Oxygen-induced Radicals

Figure 29.11 shows the growth pattern of the OIR for three samples, GUR 4150, GUR 4120 and Himont 1900, following gamma irradiation in vacuum or nitrogen at room temperature and subsequently exposing them to air. In this figure, peak-to-peak height of the ESR line due to the OIR is plotted as a function of time. As shown in the figure, the OIR reaches its maximum in about 200 days and then decays very slowly, and thus it has a very long life. It is not clear why GUR 4150 has consistently higher concentration (intensity of the ESR line) than GUR 4120 or Himont 1900.

The presence of the long-lived OIR in the shelf-aged or retrieved hip- or knee-joint components can be demonstrated by ESR. Figure 29.12 shows ESR data on the gamma-irradiated tibial plateau inserts (TPI). Figure 29.12A shows images of two TPIs (GUR 4120): a clinically retrieved TPI (GCR) on the left and a shelf-aged TPI (GSS) on the right. The holes in each TPI are the locations from where samples were punched out, and they were numbered for identification (not shown). Figure 29.12B shows a representative ESR spectrum of a clinically retrieved sample from position 5 (GCR5). As shown in the inset, the weak line on the shoulder of the main spectrum is an indication of the presence of a trace amount of primary radical. The bar graph in Figure 29.12C shows the distribution of radical concentration (OIR) as a function of the position in a TPI. The average concentration and the standard deviation (error bar) were determined by measuring 3–5 samples in a given region. For comparison, a gamma-irradiated control (GRM), a nonirradiated control (URM), and an ethylene-oxide-sterilized shelf-aged (ESS) TPI were also included in this study. The ESS sample did not show the presence of any radicals, and the gamma-irradiated control (GRM) had a concentration of an order of magnitude higher. In both GCR and GSS samples, random distribution of the radicals is evident, though the concentration in the GCR samples is, on the average, slightly less than that in the GSS samples. The lower concentration in the GCR samples could possibly be a result of annealing of the radicals due to a rise in temperature during articulation. Temperature rise on the articulating surfaces of the TPIs and acetabular cups was discussed by Davidson et al. [24].

In another example, the OIR were detected in a retrieved acetabular cup following 6–8 years of use *in vivo*. The cup (GUR 4150) was gamma-sterilized (30 kGy, 60 Co) in air before implantation. As shown in Figure 29.13A, samples were prepared from around the periphery of the articulating surface of the cup. Figure 29.13B shows the radical concentration (peak-to-peak height of the ESR line due to the OIR) as a function of the sample position at retrieval and after 13 years of shelf age following the retrieval. Two observations are made from this study: (1) OIR concentration was reduced by an order of magnitude in 13 years of postretrieval aging in air, and (2) the distribution pattern of the concentration over the articulating surface, showing the low- and high-wear areas, did not change. It is reported by Jahan et al. [5] that the low-radical concentration region corresponds to high-wear areas and the high-radical concentration corresponds to low-wear areas.

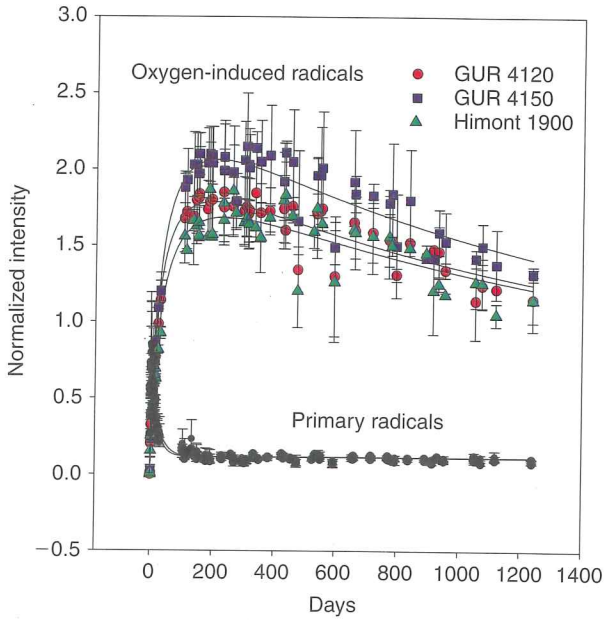

Growth and decay of oxygen induced radicals and decay of primary radicals.

FIGURE 29.11 Growth of the OIR as the primary radical decays in UHMWPE, GUR 4120, GUR 4150, and Himont 1900.

29.4.3 Identification of the Oxygen-induced Radicals by ESR

As shown in Figures 29.10 and 29.12, the ESR spectrum due to OIR is a broad single line, ΔH_{pp}, is 9 G, and its g-value varies between 2.001 and 2.005, approximately. Many reports can be found in the literature about the OIR [8, 17–20]. Most of the reports suggest that it is a peroxy ($POO^{\bullet}$), but others say that it is an alkoxy ($PO^{\bullet}$) or a polyenyl ($P^{\bullet}$) species. Some of these reported works were conducted on low density polyethylene, and the oxidation reaction was investigated by exposing the test samples to oxygen at less than room temperature.

Since 2002, our laboratory (Biomaterials Research Laboratory at the University of Memphis) has been exploring the possibility of determining the structure of the OIR in UHMWPE [22, 25, 26]. Using a high-sensitive ESR spectrometer (Bruker EMX300), microwave power saturation technique (PST) was applied at low temperature (118 K) to demonstrate that the single line was made of two overlapping spectra due to two different radical species, R1 and R2. Further discrimination between these species

Questions? Contact FDA/CDRH/OCE/DID at CDRH-FOISTATUS@fda.hhs.gov or 301-796-8118

Records processed under FOIA Request #2014-8015; Released by CDRH on 12-8-2015

was made by thermal treatment at 130–140°C at very low (for R1) or high (for R2) microwave power. For this study a high-dose (1000 kGy, 60 Co) sample was used to obtain a strong ESR signal. The sample (GUR 4150) was irradiated in 1988 in room temperature air, and this particular study was conducted from 2004 to 2006. Figure 29.14B shows a typical single-line ESR spectrum detected at room temperature (23°C) under standard operating conditions (1.0 mW microwave power and 1.0 G modulation amplitude). This figure further illustrates that the room-temperature signal becomes a well-defined symmetric single line at microwave power 0.01 mW (see Figure 29.14A). The peak-to-peak width of the line $\Delta H_{pp} = 5.5$ G and the g-value, $g = 2.0044 \pm 0.0003$ were also determined. This resonance

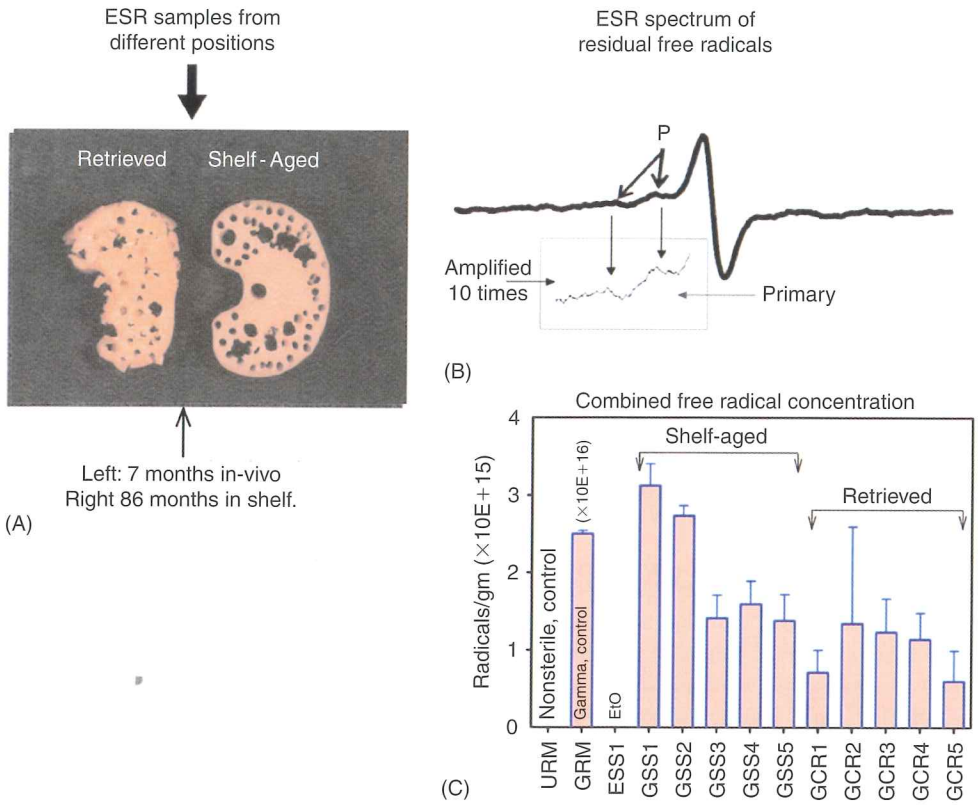

FIGURE 29.12 (A) Retrieved (left) and shelf-aged (right) TPIs. (B) Representative ESR spectrum of one sample showing a strong signal due to OIR and the presence of a trace amount of the primary radical (P). (C) Radical concentration in all TPI samples. Note that the concentration in the gamma-irradiated control (GRM) is an order of magnitude higher.

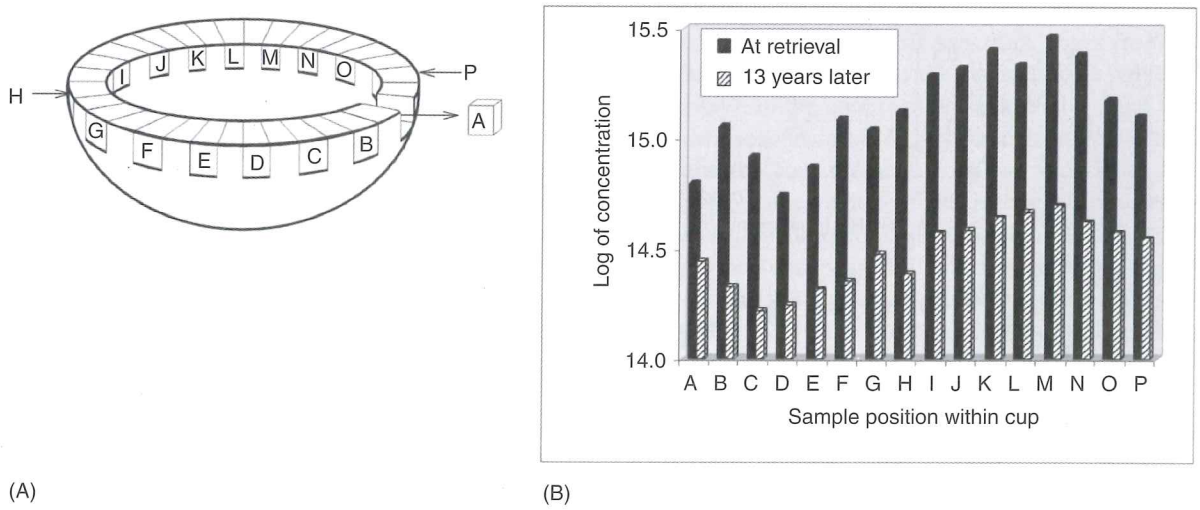

FIGURE 29.13 (A) Schematic diagram of an acetabular cup showing ESR sample locations (periphery of the articulating surface). (B) Concentration of the OIR plotted as a function of the sample position.

Questions? Contact FDA/CDRH/OCE/DID at CDRH-FOISTATUS@fda.hhs.gov or 301-796-8118

Records processed under FOIA Request #2014-8015; Released by CDRH on 12-8-2015

signal was attributed to a carbon-centered radical R1 (discussed later). When microwave power was increased to 160 mW, the signal due to R1 was reduced, and the weak shoulder shown in Figure 29.14B increased (see Figure 29.14C). The broad signal exhibited six hyperfine lines, and the signal due to R1 was further reduced to a nondetectable level at low temperature (−133°C) and 10 mW microwave power (see Figure 29.14D). The second signal (first-derivative spectrum with the six hyperfine lines) is attributed to a second type radical R2. Microwave power saturation tests suggest that R2 is an oxygen-centered radical and R1 is a carbon-centered radical because the former saturates at a higher microwave power than the latter (see Figure 29.15).

Discussion about the dependency of the ESR signal intensity of oxygen-centered radicals on microwave power can be found in [10]. Further discrimination of these radicals was performed by heating the sample at 75°C, 100°C, 130°C, and 140°C. Figures 29.16A and 29.16B show the ESR spectra due to the radicals R1 and R2, respectively, recorded as a function of time at 130°C. At this temperature, R2 suffered more loss (decayed) than did R1, and when heated for 90 min, the signal due to R2 fell below the detection limit of the spectrometer. At 140°C both R1 and R2 decayed completely in about 18 min. This result suggests that both R1 and R2 may have been trapped within crystalline regions; R1 resides completely and R2 is partially inside crystalline regions—a dangling radical. Therefore, the most likely species for R1 is a polyenyl radical (—˙CH—[CH = CH—]m—), a radical having a large number (m) of conjugated double bonds. A radical of this type can produce a single-line ESR spectrum with no resolvable proton splitting due to delocalization of the unpaired spin. Radical 2 could be a similar radical, but it is stretching out of, or dangling at, the crystalline regions because it can be annealed at slightly lower than melting temperature.

The ESR signal due to R2 exhibits proton coupling (~6 lines, $a_H = 4.8$ G), which is more pronounced when the delocalization is frozen at a lower temperature (−133°C), suggesting that the number of conjugated bonds for R2 is less than that for R1. That means R2 could be a dienyl or trienyl (m = 2 or 3) radical, whereas R1 could be a polyenyl (m > 3). Table 29.2 lists the ESR parameters of R1 and R2.

While the details of this investigation can be found in the literature [22, 25, 26], the important findings about the OIR can be highlighted as follows:

1. In presence of oxygen, two radicals (R1 and R2) remain trapped in the irradiated UHMWPE for a very long time (>20 years in this laboratory).
2. One of them (R1) is a polyenyl P˙ (—˙CH— [CH = CH—]$_m$— with m>3).

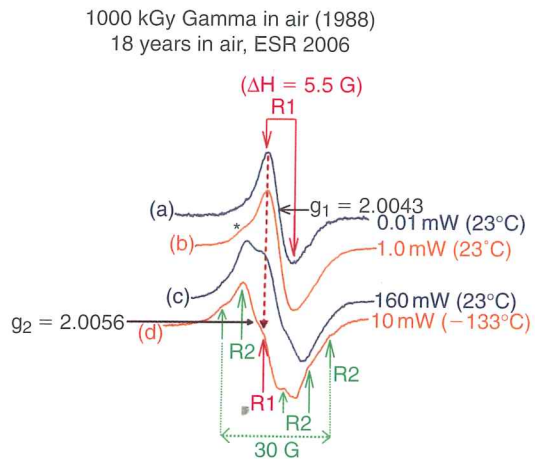

FIGURE 29.14 First derivative ESR spectrum recorded as a function of microwave power at different temperatures. UHMWPE (GUR 4150) was gamma-irradiated (1000 kGy, 60 Co) in 1988 and spectra recorded in 2006. The spectral features due to the radicals R1 and R2 are shown with arrows.

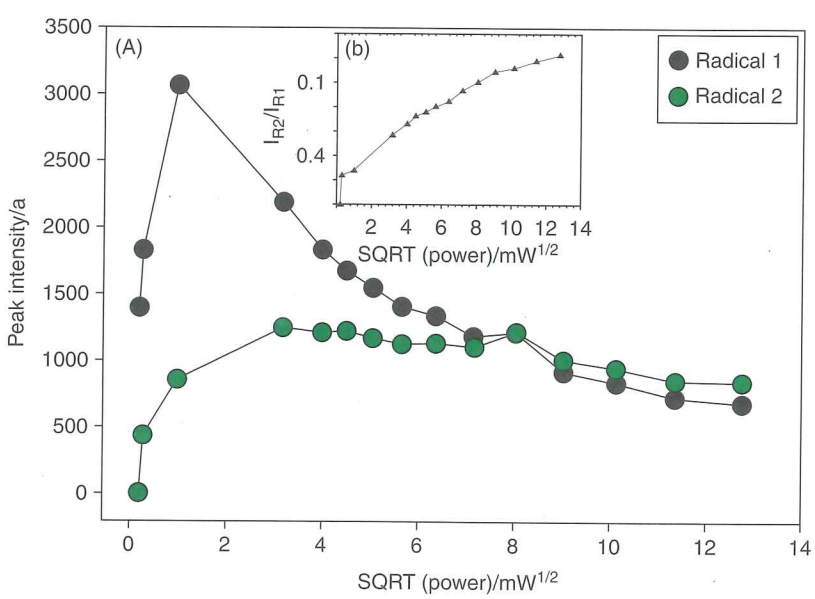

FIGURE 29.15 Microwave power saturation technique (PST). (A) Signal intensity as a function of the square root of the microwave power for the radicals R1 and R2. (B) Ratio of the signal intensities of R1 and R2 plotted as a function of the square root of the microwave power (see inset).

Questions? Contact FDA/CDRH/OCE/DID at CDRH-FOISTATUS@fda.hhs.gov or 301-796-8118

Records processed under FOIA Request #2014-8015; Released by CDRH on 12-8-2015

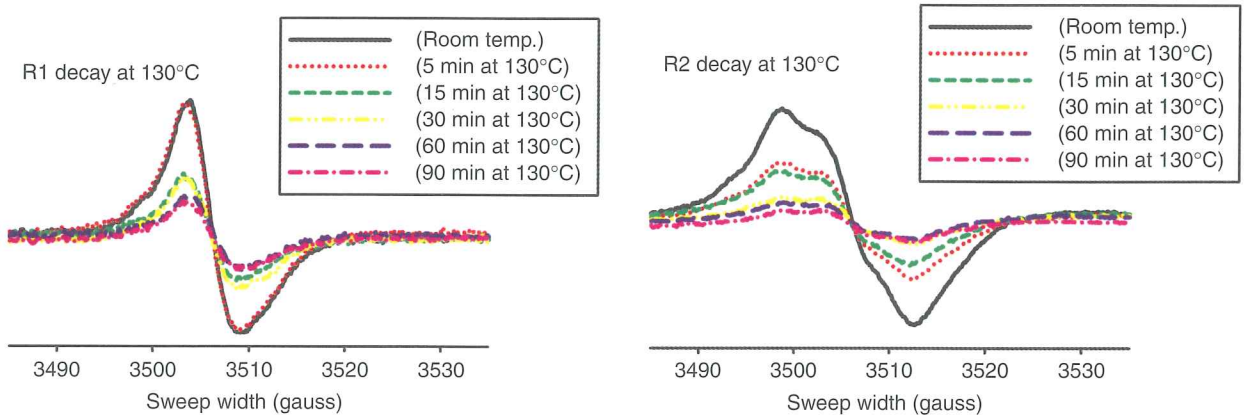

FIGURE 29.16 First-derivative ESR spectrum of radical R1 (A) and R2 (B) are recorded as a function of time at 130°C.

TABLE 29.2 ESR Parameters of Radical-1 (R1) and Radical-2 (R2)

Radical	g-value	Number of lines	Line width	Hyperfine constants, aH
R1	2.0044 ± 0.0003	1	5.5 G	-
R2	~2.0056	6	9.4 G	4.8 G

3. The second radical R2 is an oxygen-centered polyenyl PO•(—•OCH— [CH = CH—]$_m$— with m = 2 or 3).
4. R2 is a dangling radical; it resides in a less crystalline region than R1.
5. There is no ESR evidence of the presence of a long-lived *peroxy* radical.

29.5 INTERMEDIATE RADICALS

In recent years, ESR work on UHMWPE has been limited to investigations of the peroxy (POO•) and the long-lived OIR because of their potential damaging effects (oxidative degradation). Consequently, intermediate radical processes remain significantly unexplored. Of course, chemical models or schemes describing the processes for generation, propagation, and termination of the PE radicals can be found in the literature [1, 2, 27, 28]. This section presents ESR evidence of certain intermediate radical reaction in irradiated UHMWPE.

As shown in Figure 29.10, it takes 30–45 days for the OIR to grow as the primary radicals decay in air. Interestingly, the "primary residual" radicals present in a vacuum-sealed sample following heating at 75°C for 6 years also produces OIR within the same length of time when opened to air. The signal intensity in the latter case is, however, very weak because of the low primary radical concentration at the time of reaction with oxygen (air). This scenario suggests that the oxidation potential of the irradiated UHMWPE components can be reduced, but not eliminated, by heating at a temperature of 75°C in a vacuum or inert environment. Heating or annealing at a near-melting temperature may eliminate all radicals or reduce their concentration to a nondetectable limit of ESR. Another important observation is that the polyenyl radicals that constitute the terminal OIR (previously discussed) are not the primary or initial polyenyl; rather, they are generated as a result of the reaction of the primary radicals in the presence of oxygen.

During the initial 30–45 days when the primary radicals decay in the presence of oxygen, the ESR spectrum changes as a function of time and becomes very complex. The complexity in the ESR spectrum arises from the fact that the radicals at or near the surface (OIR polyenyl and/or peroxy), in the core (primary alkyl/allyl), and the other unknown secondary or tertiary radicals in between the surface and the core produce their own individual spectrum within the same region of the resonance magnetic field. Therefore, unambiguous identification of the radical type or types becomes very difficult. In one of our studies, we recorded an ESR signal and attributed it to a vinyl-type radical. The vinyl feature in the spectrum became clear right before the appearance of the OIR signal, at which time the signal due to the alkyl/allyl decayed or disappeared. For verification, a computer simulation of the spectrum was performed (see Figure 29.17).

In another study, we measured radical concentration (RC) in a series of samples (1.20 ± 0.05 mm thick) prepared from the surface to the core of a 1-inch cube of

Questions? Contact FDA/CDRH/OCE/DID at CDRH-FOISTATUS@fda.hhs.gov or 301-796-8118

Records processed under FOIA Request #2014-8015; Released by CDRH on 12-8-2015

UHMWPE (GUR 4150). The cubes were aged for 1 year in Ringer solution, bovine serum, ethyl alcohol, or air at room temperature following gamma irradiation (30 kGy, 60 Co) in air at room temperature. Each surface sample showed the presence of the surface radical (OIR), and the core sample showed the primary radicals. The remaining samples showed the presence of a combination of different radicals. At about 5-mm depth at that particular time of measurements, RC was minimal or none (see Figure 29.18). Following these measurements, the samples were kept in air at room temperature and measured again after 10 months. To our expectation, each sample showed the presence of identical OIRs. Figure 29.18 also shows the representative ESR spectra. This study concluded that a nonradical region could be found between the surface and the core of an irradiated UHMWPE solid during the time of decay of the primary and growth of the OIR. It was further suggested that the *nonradical region* could possibly be the region of hydroperoxy species, which cannot be detected by ESR [29].

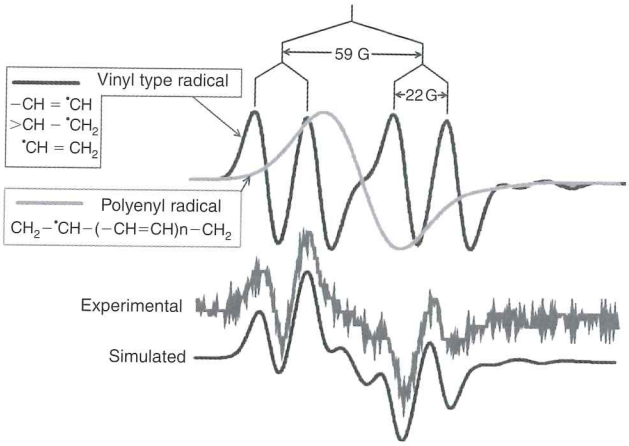

FIGURE 29.17 First-derivative ESR spectrum of gamma-irradiated UHMWPE (GUR 4150) recorded during the decay of the primary radical but before the appearance of the OIR. Experimental, simulated, and the split spectra of the vinyl and polyenyl radicals are also shown.

29.6 ESR OF VITAMIN E-DOPED UHMWPE

Vitamin E (α-tocopherol, α-T) has been found to improve oxidation resistance of UHMWPE [30–32] by scavenging free radicals. Most of the reports on the antioxidation behavior of α-T are, however, based on the FTIR data or mechanical test results; ESR data are minimal at best, to

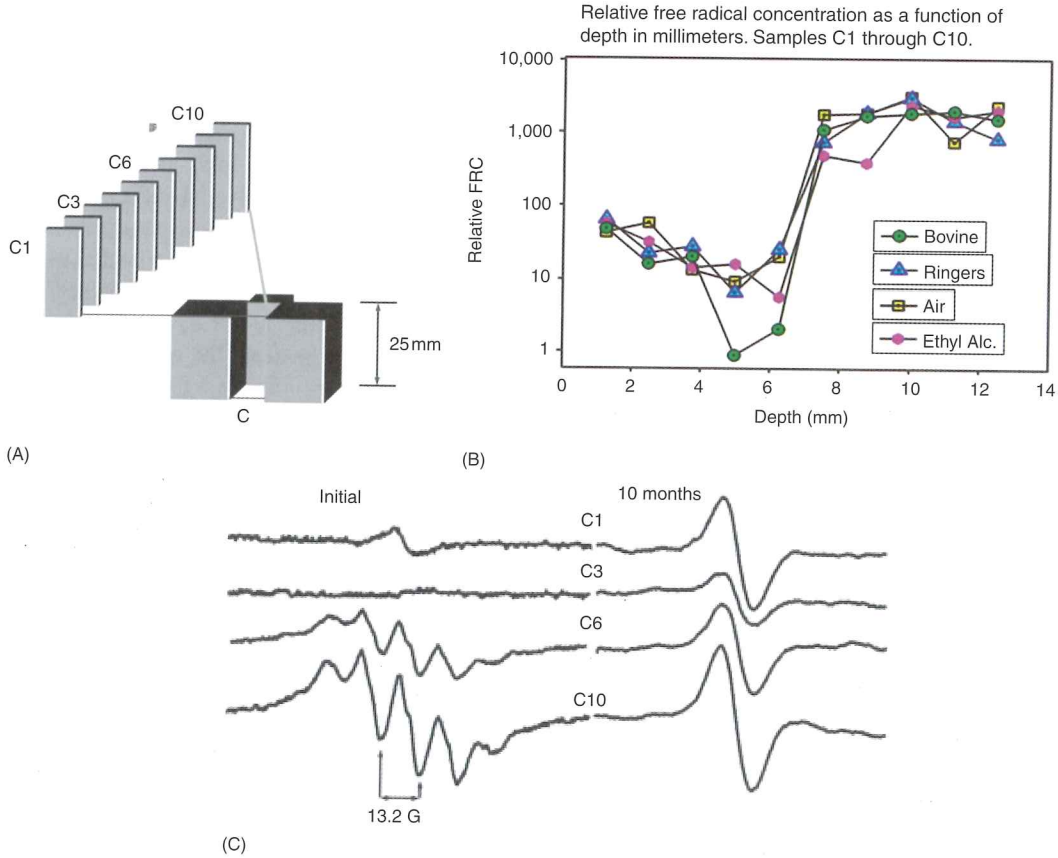

FIGURE 29.18 ESR depth profile of gamma-irradiated UHMWPE (GUR 4150). (A) Samples C1–C10 from the surface to the core were prepared following postgamma aging for 120 days in air, bovine serum, Ringer solution, or ethyl alcohol. (B) Relative free radical concentration as a function of depth. (C) ESR spectrum of representative samples recorded immediately after they were prepared (left) and 10 months later (right).

Questions? Contact FDA/CDRH/OCE/DID at CDRH-FOISTATUS@fda.hhs.gov or 301-796-8118

Records processed under FOIA Request #2014-8015; Released by CDRH on 12-8-2015

our knowledge. While a short summary of the recent ESR works is provided in this section, details can be found in the publications by Ridley and Jahan [33, 34]. More knowledge about the ESR of the antioxidants (tocopherols or Irganox®) can be gained from the reports on the reactions of vitamin E with lipids by Chen et al. [35] and Walker et al. [36] and on low density polyethylene (LDPE) by Jaworska et al. [37] and Yamazaki and Seguchi [38].

As previously mentioned, we reported ESR results on α-T-doped UHMWPE powder resin (labeled as "α-T-resin") and compression molded solid [33]. In practice, less than 1.0 wt% α-T is blended with UHMWPE to avoid plasticization [39], but we used concentrations up to 25% v/v to allow detection of α-T radicals in the presence of strong resonance signals of the primary or secondary PE radicals. Jaworska et al. [37] used 10% Irganox® in low density PE (LDPE) for detection of the antioxidant radicals at liquid nitrogen temperature (77 K).

Vitamin E produces its own radical (tocopheroxyl, α—T— O•) when exposed to room light or ionizing radiation. The molecular structure of vitamin E, and of its radical, are shown in Figure 29.19A. The ESR spectrum of the vitamin E radical is shown in Figure 29.19B (as received) and 29.19C (after gamma irradiation). As shown in Figure 29.19C, the first-derivative ESR spectrum consists of seven resonance lines with separation between the lines $\Delta H = 5\,G$, the line width $\Delta W = 2\,G$, and the intensity ratios 1:6:15:20:15:6:1 (shown by the stick diagram in Figure 29.19D). The characteristic spectral splitting factor, g-value, of the radical is $g \approx 2.0044$ (shown by an arrow). These data are consistent with the reports found in the literature [35, 40, 41].

According to our recent report [33], vitamin E (α-tocopherol) was found to quench the primary PE radicals in the powder sample (GUR 1050) when gamma irradiation (30 kGy, 60 Co) was performed in air, but it did not quench any radicals in the nitrogen environment. When the irradiated powder was removed from nitrogen and placed in air, radical reactions occurred, and the OIR formed as detected by ESR. So far as the decay of the radicals in the presence of oxygen (air) is concerned, no detectable difference was found between the powder samples with or without vitamin E. The good fit between the experimental and the computer-generated ESR spectra shown in Figure 29.20A for the initial measurements, and in Figure 29.20B for the final measurements (71 days later), confirm the fact that the vitamin E (αTO•) and the resin (primary or OIR) radicals decay independently.

Three observations are made in this study.

1. So far as the postirradiation ESR in air is concerned, no detectable difference is found between the nitrogen-packaged and the open-air α-T-resin samples.
2. A high concentration of α-T allows vitamin E radicals (ESR signal of αTO•) to be monitored in the presence of the relatively strong signal due to PE radicals. This is potentially useful for comparison of the radical-radical reaction [37].
3. Although UHMWPE resin powder has no clinical relevance, a powder sample provides a better means for investigation of free radical reaction in presence of oxygen (air) because it has a large effective surface area, which is easily accessible to oxygen.

Similar postirradiation oxidation behavior was also observed in compression-molded solids (UHMWPE, GUR 1050) containing 0.0% (control), 1.0%, or 10.0% α-T. No detectable difference was found in the subsequent decay pattern between the control (0% α-T) and vitamin-E containing UHMWPE. However, one important observation was made in this study. Compared to the control (0% α-T), all UHMWPE-α-T samples were found to contain about an order of magnitude less primary radicals (see Figure 29.21).

Because of lack of initial data points, it is speculated that the quenching of radicals by α-T must occur during

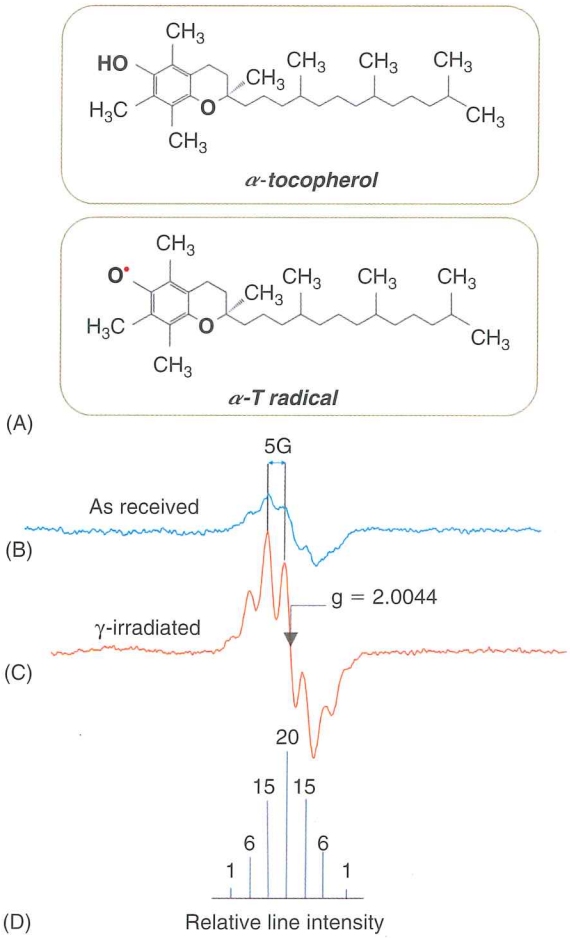

FIGURE 29.19 (A) Molecular structure of the α-tocopherol molecule and the α-tocopheroxyl radical (αTO•). (B) ESR spectrum of the αTO• radical present in as-received vitamin E. (C) Fingerprint of the αTO• with g-value g = 2.0044 and line separation $\Delta H = 5\,G$. (D) The relative intensities of the seven lines are shown by stick diagram.

Questions? Contact FDA/CDRH/OCE/DID at CDRH-FOISTATUS@fda.hhs.gov or 301-796-8118

Records processed under FOIA Request #2014-8015; Released by CDRH on 12-8-2015

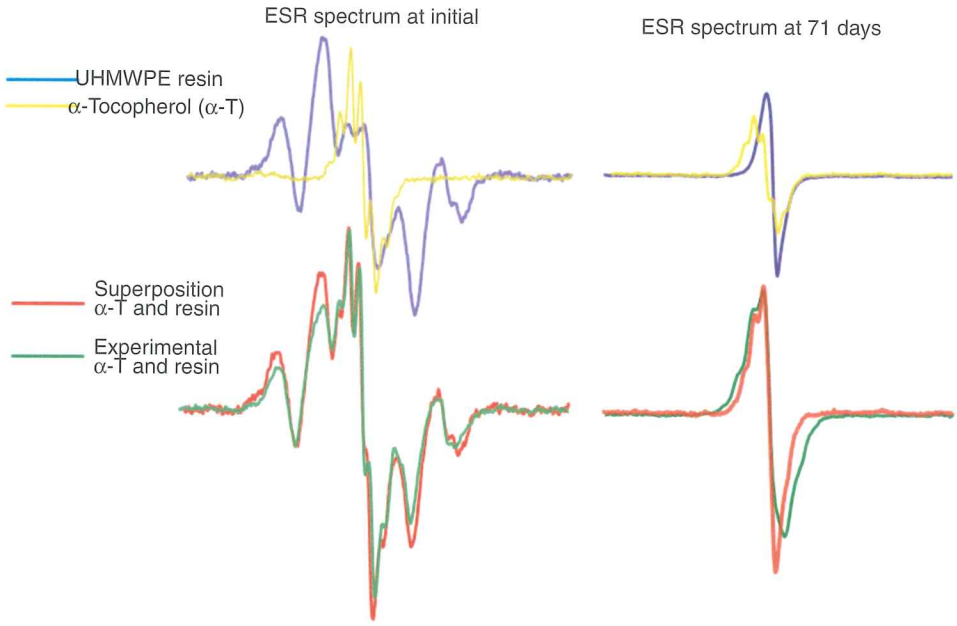

FIGURE 29.20 (A) The ESR spectrum due to the primary/initial radical in vitamin E (αTO˙) and UHMWPE (top). Bottom figure illustrates the fit between the experimental and the computer-generated spectra. (B) The ESR spectrum due to the OIR and the radical in vitamin E (αTO˙) and UHMWPE (top). Bottom figure illustrates the fit between the experimental and the computer-generated spectra.

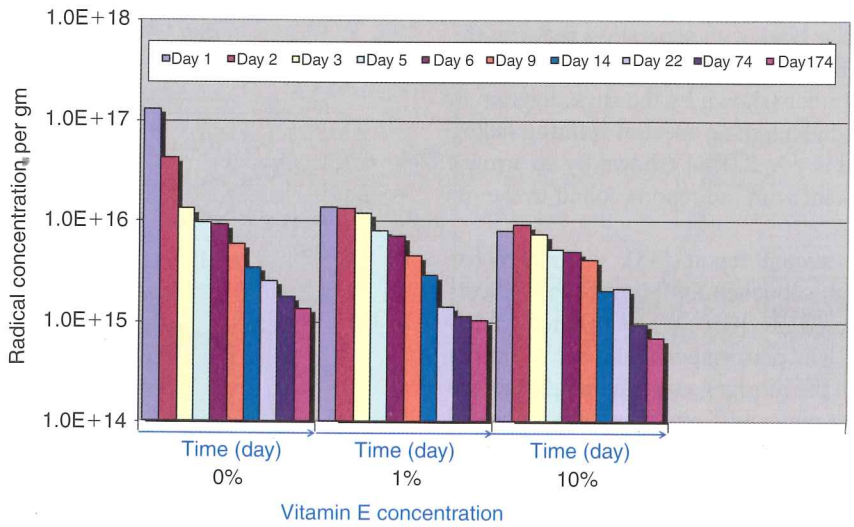

FIGURE 29.21 Free radical concentration plotted as a function of % α-T in compression molded UHMWPE. Gamma irradiation (30 kGy, 60 Co) was performed in air or nitrogen.

or immediately after irradiation. The time taken (3–5 days) in receiving the irradiated samples from the vendor is the main delay between the irradiation and the ESR measurements. Further study is needed to address this issue.

29.7 QUANTITATIVE ESR IN UHMWPE

ESR has been in use for more than 5 decades. During that time, high-sensitive ESR spectrometers have been designed and built to detect low level paramagnetic ions, ionic impurities, and free radicals in a host material. Still, quantitative measurement to determine the "absolute" number of spins or radicals remains a challenge to the ESR community. As pointed out by Mazur [42], careful operational procedures might reduce potential errors to within 2–5% within a given laboratory; however, quantitative analyses of the same sample in different laboratories may vary between 100 and 400%. He listed a number of sources of errors

Questions? Contact FDA/CDRH/OCE/DID at CDRH-FOISTATUS@fda.hhs.gov or 301-796-8118

Records processed under FOIA Request #2014-8015; Released by CDRH on 12-8-2015

that could lead to such a wide variation in the results. The following list shows the ones that are particularly important for UHMWPE work:

- Sample related: Sample volume and shape, sample tube, sample positioning into the microwave cavity
- Microwave cavity: Microwave field profile, cavity Q-factor, modulation field profile
- Spectrometer: Spectrometer calibration, signal-to-noise ratio, and mechanical and electronic stability of spectrometer
- Reference standard: Selection of a standard, absolute spin concentration, storage, and handling of the standard
- Environment: Laboratory temperature, temperature variation inside the cavity, relative humidity, moisture or condensation inside the cavity, and moisture in the "sample" and the "standard"
- Computational: Limits of integration, base-line correction, noise correction, double integration, and formula for final number

For reliable test results, it is essential to have a standard protocol that addresses most or all of the previously mentioned sources of errors and to demonstrate consistency and reproducibility of the results for a long period of time. The most common standards used for quantitative ESR are: (1) the stable organic free radical 2-2-diphenyl-1-picrylhydrazyl (DPPH); (2) Mn2+ in MgO; (3) ruby; (4) vanadyl (V) in K2SO4 or NaCl; and (5) K3CrO8 in K3NbO8. The fifth standard, K3CrO8 in K3NbO8, was recently employed by Cage et al. for g-factor, spin concentration, and field calibration at high field [43]. Ruby is Cr3+-doped aluminum oxide (Al2O3). It is suitable for use with UHMWPE because its anisotropic resonance lines do not interfere with those of the PE radicals. For "alanine dosimetry," Nagy et al. [44] used ruby as an "adjacent reference" by permanently fixing it inside the cavity wall.

The importance of the cavity Q-factor for sample and standard has been discussed by Blakley et al. [45]. Q-factor is given by: $Q=f_0/\Delta f_0$, where $h\Delta f_0$ is the amount of dissipative energy at resonance frequency f_0 (h is Planck's constant). Less dissipation, or loss in microwave energy, results in a higher Q-factor and better sensitivity of the system. The Bruker EMX spectrometer, equipped with a high sensitive cavity (ER4119HS), registers the Q-factor at the time of measurement.

ESR theory for determination of the number of spins or radicals in a given sample is described in detail by Poole [46]. The theory, however, does not fall within the scope of this chapter. Nonetheless, to gain knowledge about the selection of standard reference materials and experimental variables, additional references are cited [47–50].

REFERENCES

1. Dole M. Radiation chemistry of macromolecules Vol. 1. New York; 1972. Vol. 2. New York, 1973.
2. Rabek J. *Polymer photodegradation: mechanisms and experimental methods*: Springer; 2007.
3. Eyerer P. Property changes of UHMW polyethylene during implantation—first hints for the development of an alternative polyethylene. In: Lee SM, editor. *Advances in biomaterials Vol. 1*: CRC Press; 1987.
4. Igarashi M. Free radical identification by ESR in polyethylene and nylon. *J Polym Sci: Polym Chem* 1983;**21A**:2405–25.
5. Jahan MS, Wang C, Schwartz G, Davidson JA. Combined chemical and mechanical effects on free radicals in UHMWPE joints during implantation. *J Biomed Mater Res* 1990;**25**(8):1005–17.
6. Jahan MS, Thomas DE, Banerjee K, Trieu H, Haggard W, Parr JE. Effects of radiation-sterilization on medical implants. *Radiat Phys Chem* 1998;**51**:93–594.
7. Nausbaum HJ, Rose RM. The effects of radiation sterilization on the properties of ultra-high molecular weight polyethylene. *J Biomed Mater Res* 1979;**13**:557–76.
8. O'Neill P, Birkinshaw C, Leahy J, Barklie R. The role of long lived free radicals in the ageing of irradiated ultra high molecular weight polyethylene. *Polym Degrad Stab* 1999;**63**:31–9.
9. Streicher RM. Influence of ionizing radiation in air and nitrogen for sterilization of surgical grade polyethylene for implants. *Radiat Phys Chem* 1988;**31**:693–8.
10. Seguchi T, Tamura N. Mechanism of decay of alkyl radicals in irradiated polyethylene on exposure to air as studied by electron spin resonance. *J Phys Chem* 1973;**77**:40–4.
11. Sun DC, Stark C. *U.S. Patent No. 414,049*; 1995.
12. Kurtz SM, Muratoglu OK, Evans M, Edidin AA. Advances in the processing, sterilization, and crosslinking of UHMWPE for total joint arthroplasty. *Biomaterials* 2000;**20**:1659.
13. Buchanan FJ, White JR. The influence of gamma irradiation and ageing on degradation mechanisms of ultra-high molecular weight polyethylene (UHMWPE). *J Mater Sci Mater Med* 2001;**12**(1):29.
14. Chang R. *Basic principles of spectroscopy*. New York: Robert Krieger Publishing Company; 1978. 104–129.
15. Weil JA, Bolton JR, Wertz JE. *Electron paramagnetic resonance*. New York: John Wiley and Sons, Inc.; 1994. 1–32.
16. Ohnishi S, Sugimoto S, Nitta I. Electron spin resonance study of radiation oxidation of polymers. Results for polyethylene and some general remarks. *Polymer* 1962;**2**:119.
17. Ohnishi S, Sugimoto S, Nitta I. Electron spin resonance study of radiation oxidation of polymers. IIIA. Results for polyethylene and some general remarks. *J Polym Sci* 1963;**1A**:605–23.
18. Nakamura K, Ogata S, Ikada Y. Assessment of heat and storage conditions on γ-ray and electron beam irradiated UHMWPE by electron spin resonance. *Biomaterials* 1998;**19**:2341–6.
19. Costa L, Luda MP, Trossarelli L, Brach del Prever EM, Crova M, Gallinaro P. Oxidation in orthopaedic UHMWPE sterilized by gamma-radiation and ethylene oxide. *Biomaterials* 1998;**19**: 659–68.
20. Ohnishi S, Ikeda Y, Sugimoto S, Nitta I. On the ESR singlet spectra frequently observed in irradiated polymers at a large dose. *J Poly Sci* 1960;**47**(149):503–7.
21. Ranby B, Rabek JF. *Photodegradation, photooxidation and photostabilization of polymers, principles and applications*. New York: John Wiley; 1975 60–71.

Questions? Contact FDA/CDRH/OCE/DID at CDRH-FOISTATUS@fda.hhs.gov or 301-796-8118

Records processed under FOIA Request #2014-8015; Released by CDRH on 12-8-2015

22. Jahan MS, Durant J. Investigation of the oxygen-induced radicals in ultra-high molecular weight polyethylene. *Nucl Instr Meth Phys Res* 2005;**B 236**:166–71.
23. Auerbach I, Sanders LH. *Polymer* 1969;**10**:579.
24. Davidson JA, Schwartz G, Lynch G, Gir S. Wear, creep and frictional heating of femoral implant articulating surfaces and the effect of long-term performance—Part II, friction, heating and torque. *J Biomed Mater Res: Appl Biomater* 1988;**22**:69–91.
25. Durant J, Jahan MS. EPR power saturation techniques and spectral differentiation are used to isolate and simulate radical species in UHMWPE. *Nucl Instr Meth Phys Res* 2005;**B 236**:160–5.
26. Jahan MS, Fuzail M. Examination of the long-lived oxygen-induced radicals in irradiated ultra-high molecular weight polyethylene. *Nucl Instr Meth Phys Res* 2007;**B 265**:67–71.
27. Costa L, Bracco P. Mechanism of croslinking and oxidative degradation of UHMWPE. In: Kurtz SM, editor. *The UHMWPE handbook: ultra-high molecular weight polyethylene in total joint replacement*. New York: Academic Press; 2004 chapter 11. p. 235–50.
28. Khelidj N, Colin X, Audouin L, Verdu J, Monchy-Leroy C, Prunier V. Oxidation of polyethylene under irradiation at low temperature and low dose rate. Part I: The case of pure radiochemical initiation. *Polym Degrad Stab* 2006;**91**:1593–7. Part II. Low temperature thermal oxidation. *Polymer Degradation Stability*; 2006, 91, 1598–605.
29. Jahan MS, Stovall JC, King MC. Observation of a non-radical intermediate in the oxidation pathway of free radicals in gamma-irradiated medical grade polyethylene. *Nucl Instr Meth Phys Res* 2001;**B 185**:323–7.
30. Oral E, Wannomae KK, Hawkins N, Harris WH, Muratoglu OK. α-Tocopherol-doped irradiated UHMWPE for high fatigue resistance and low wear. *Biomaterials* 2004;**25**:5515–22.
31. Shibata N, Tomita N. The anti-oxidative properties of α-tocopherol in α-irradiated UHMWPE with respect to fatigue and oxidation resistance. *Biomaterials* 2005;**26**:5755–62.
32. Tomita N, Kitakura T, Onmori N, Ikada Y, Aoyama E. Prevention of fatigue cracks in ultra high molecular weight polyethylene joint components by the addition of vitamin E. *J Biomed Mater Res (Appl Biomater)* 1999;**48**(1999):474–8.
33. Ridley MD, Jahan MS. Measurements of free radical in vitamin E-doped ultra-high molecular weight polyethylene: dependence of materials processing and irradiation environments. *Nucl Instr Meth Phys Res* 2007;**B 265**:62–6.
34. Ridley MD, Jahan MS. Effects of packaging environments on free radicals in γ-irradiated UHMWPE resin powder blend with vitamin E. *J Biomed Mater Res A* 2009 March 15;**88**(4):1097–103.
35. Chen Z. Biology and life sciences. In: Kawamori A, Yamauchi J, Ohta H, editors. EPR in the 21st Century; 2002.
36. Walker M, Beckert D, Lash J. Interaction of UV light-induced α-tocopherol radicals with lipids detected by an electron spin resonance prooxidation effect. *Photochem Photobiol* 1998;**68**(4):502–10.
37. Jaworska E, Kaluska I, Strzelczak-Burlinkska G, Michalik J. Irradiation of polyethylene in the presence of antioxidants. *Radiat Phys Chem* 1991;**37**(2):285–90.
38. Yamazaki T, Seguchi T. ESR study on chemical crosslinking reaction mechanisms of polyethylene using a chemical agent-II. The effect of phenolic antioxidants. *J Polym Sci, Part A: Polym Chem* 1997;**35**(12):2431–9.
39. Oral E, Greenbaum ES, Malhia AS, Harris WM, Muratoglu OK. Characterization of irradiated blends of α-tocopherol and UHMWPE. *Biomaterials* 2005;**26**:6657–63.
40. Boguth W, Nieman H. Electron spin resonance of chromanoxy free radicals from $\alpha-,\varepsilon^2-,\beta-,\gamma-,\delta-$tocopherol and Toco*. *Biochimica et Biophysica Acta* 1997 April 27;**BBA 55931**(248):121–30.
41. Maguire JJ, Wilson DS, Packer L. Mitochondrial electron transport-linked tocopheroxyl radical reduction. *J Biol Chem Commun* 1989;**264**(36):21462–5.
42. Mazur M, Valco M. Error sources in quantitative EPR spectroscopy. *EPR Newsletter* 2003;**13**:27.
43. Cage B, Weekley A, Brunel LC, Dalal N. K_3CrO_8 in K_3NbO_8 as a proposed standard for g-factor, spin concentration, and field calibration in high-field EPR spectroscopy. *Anal Chem* 1999;**71**:1951–7.
44. Nagy V, Sleptchonok OF, Desrosiers MF, Weber RT, Heiss AH. Advancements in accuracy of the alanine EPR dosimetery sysytem, Part III: usefulness of an adjacent reference sample. *Rad Phy Chem* 2000;**59**:429–41.
45. Blakley RL, Henry DD, Morgan WT, Clapp WL, Smith CJ, Barr D. Quantitative electron paramagnetic resonance: the importance of matching the Q-factor of standards and samples. *Appl Spectrosc* 2001;**55**(10):1375–81.
46. Poole CP. *In Electron spin resonance, a comprehensive treatise on experimental techniques*. 2nd ed.: John Wiley & Sons, Inc.; 1983 chapter 11D, 400–409.
47. Nagy V. Choosing reference samples for EPR concentration measurements: Part 1, general introduction and systems of S=1/2. *Anal Chim Acta* 1997;**339**(1–2):1–11.
48. Madej A, Dyrek K, Mattusch J. Preparation and evaluation of the quality of standards for quantitative EPR measurements of spin concentration. *Fresenius J Anal Chem* 1991;**341**:707–8.
49. Burns D, Flockhart BD. Application of quantitative EPR. *Phil Trans R Soc London* 1990;**333A**:37–48.
50. Chang T, Kahn AH. Standard reference materials: electron paramagnetic resonance intensity standards: SRM 2601, description and use. NIST's special publication 1978: 260-59, 38–45.

Questions? Contact FDA/CDRH/OCE/DID at CDRH-FOISTATUS@fda.hhs.gov or 301-796-8118

Records processed under FOIA Request #2014-8015; Released by CDRH on 12-8-2015

ELSEVIER

Biomaterials 23 (2002) 3681–3697

Biomaterials

www.elsevier.com/locate/biomaterials

Thermomechanical behavior of virgin and highly crosslinked ultra-high molecular weight polyethylene used in total joint replacements

S.M. Kurtz[a,b,*], M.L. Villarraga[a,b], M.P. Herr[a,b], J.S. Bergström[a], C.M. Rimnac[c], A.A. Edidin[b,d]

[a] *Exponent, Inc., 2300 Chestnut Street, Suite 150, Philadelphia, PA 19103, USA*
[b] *Implant Research Center, School of Biomedical Engineering, Science, and Health Systems, Drexel University, 3141 Chestnut St., Philadelphia, PA, USA*
[c] *Departments of Mechanical and Aerospace Engineering and Orthopaedics, Case Western Reserve University, Cleveland, OH, USA*
[d] *Howmedica Osteonics Corp, 300 Commerce Ct., Mahwah, NJ, USA*

Received 27 September 2001; accepted 12 March 2002

Abstract

Three series of uniaxial tension and compression tests were conducted on two conventional and two highly crosslinked ultra-high molecular weight polyethylenes (UHMWPEs) all prepared from the same lot of medical grade GUR 1050. The conventional materials were unirradiated (control) and gamma irradiated in nitrogen with a dose of 30 kGy. The highly crosslinked UHMWPEs were gamma irradiated at room temperature with 100 kGy and then thermally processed by either annealing below the melt transition at 110°C or by remelting above the melt transition at 150°C. The true stress–strain behavior of the four UHMWPE materials was characterized as a function of strain rate (between 0.02 and 0.10 s^{-1}) and test temperature (20–60°C). Although annealing and remelting of UHMWPE are primarily considered as methods of improving oxidation resistance, thermal processing was found to significantly impact the crystallinity, and hence the mechanical behavior, of the highly crosslinked UHMWPE. The crystallinity and radiation dose were key predictors of the uniaxial yielding, plastic flow, and failure properties of conventional and highly crosslinked UHMWPEs. The thermomechanical behavior of UHMWPE was accurately predicted using an Arrhenius model, and the associated activation energies for thermal softening were related to the crystallinity of the polymers. The conventional and highly crosslinked UHMWPEs exhibited low strain rate dependence in power law relationships, comparable to metals. In light of the unifying trends observed in the true stress–strain curves of the four materials investigated in this study, both crosslinking (governed by the gamma radiation dose) and crystallinity (governed by the thermal processing) were found to be useful predictors of the mechanical behavior of UHMWPE for a wide range of test temperatures and rates. The data collected in this study will be used to develop constitutive models based on the physics of polymer systems for predicting the thermomechanical behavior of conventional and crosslinked UHMWPE used in total joint replacements. © 2002 Elsevier Science Ltd. All rights reserved.

Keywords: Ultra-high molecular weight polyethylene (UHMWPE); Temperature; Irradiation; Strain rate; Crosslinking; Mechanical properties

1. Introduction

Ultra-high molecular weight polyethylene (UHMWPE) has been the material of choice for orthopedic bearing materials for nearly four decades [1]. In the past two years, radiation crosslinked and thermally treated UHMWPE materials have been increasingly used in hip bearings and are currently being considered for total knee replacements. During the fabrication of conventional UHMWPE, resin powder is consolidated by a combination of elevated pressure and thermal processing above the melt transition at 135°C [1]. To fabricate contemporary radiation crosslinked UHMWPE, conventional consolidated UHMWPE is first subjected to gamma or electron beam radiation, followed by post-irradiation thermal processing [1,2]. Depending upon the orthopedic

*Corresponding author. Exponent, Inc., 2300 Chestnut Street, Suite 150, Philadelphia, PA 19130, USA. Tel.: +1-215-751-0973; fax: +1-215-751-0660.
E-mail address: skurtz@exponent.com (S.M. Kurtz).

0142-9612/02/$ - see front matter © 2002 Elsevier Science Ltd. All rights reserved.
PII: S0142-9612(02)00102-3
Questions? Contact FDA/CDRH/OCE/DID at CDRH-FOISTATUS@fda.hhs.gov or 301-796-8118

Records processed under FOIA Request #2014-8015; Released by CDRH on 12-8-2015

manufacturer, thermal processing may take place either above or below the melt transition [2]. Post-irradiation thermal processing below the melt transition is referred to as annealing, whereas processing above the melt transition results in remelting [3]. In contrast with the initial melting and recrystallization of conventional UHMWPE, which occurs under elevated pressure, post-irradiation thermal processing takes place at ambient pressure.

The mechanical behavior of UHMWPE will be influenced both by the method of crosslinking as well as by any modifications in crystalline microstructure that may arise during subsequent thermal processing. The effect of irradiation on the properties of UHMWPE has been well documented in the literature, as noted in recent reviews [1,2,4,5]. Numerous hip simulator studies, for example, have demonstrated that radiation crosslinking can improve the wear resistance of UHMWPE by over 90% [1]. In this context, thermal processing has been considered primarily as a method to reduce residual free radicals and to improve the oxidation resistance of UHMWPE [6–9]. However, because thermal processing takes place near the melt transition for UHMWPE, it may also be associated with modifications of the crystallinity, and hence the mechanical behavior of the polymer. The influence of post-irradiation thermal processing on the mechanical behavior of UHMWPE has received comparatively little attention in previous studies [4], and consequently the separate effects of irradiation and thermal processing on the physical and mechanical behavior of crosslinked UHMWPE remain poorly understood.

The application of highly crosslinked and thermally treated UHMWPE to orthopedic bearings has been hindered by the lack of a validated constitutive model for the material that captures its viscoelastic–viscoplastic behavior. Such a material model, if it were developed, would enable the prediction of mechanical behavior not only for simple loading conditions, such as uniaxial tension or compression, but also for more physiologically relevant, complex multiaxial loading conditions. That is, once validated, the constitutive model could be used to predict the mechanical behavior of orthopedic implant geometries subjected to in vivo loading conditions. The validated constitutive model could also serve as the basis for fatigue, wear, and damage models for UHMWPE. Recently, a family of constitutive models for polymers, based on the physics of polymer systems, has been identified that enable accurate prediction of the mechanical response for conventional UHMWPE under uniaxial, multiaxial, and cyclic loading conditions [10,11]. However, sufficient data have not yet been reported in the literature for calibration and validation of these new constitutive theories for highly crosslinked and thermally stabilized UHMWPE materials.

The tensile yield and ultimate properties for highly crosslinked UHMWPE are typically reported in terms of engineering stress and strain for the purposes of comparison with minimum values set forth in national and international standards for conventional, uncrosslinked UHMWPE [5,7–9]. While useful for comparison with historical control UHMWPE materials, engineering stress and strain values provide an incomplete picture of the mechanical behavior of a semi-crystalline polymer. As researchers have previously noted, the entire true stress–strain curve is needed to accurately characterize the yielding and plastic flow behavior of UHMWPE [12], as well as of other semi-crystalline polymers [13–16]. True stress–strain relationships, therefore, form the foundation upon which future constitutive models, as well as fatigue and wear models, will ultimately depend.

Although standard in vitro mechanical testing of UHMWPE is conducted at room temperature, little is known about the changes in mechanical behavior of UHMWPE at elevated temperatures in vivo. Recent measurements using telemeterized hip implants have documented in vivo implant temperatures of up to 43°C during walking [17,18]. In addition, during in vitro hip simulation, the surface temperatures for UHMWPE have been predicted to exceed 60°C, depending upon the femoral head material [19]. Thus, to predict damage at the articulating surface, where local thermal gradients arise in UHMWPE components due to frictional heating, it is important to understand the effects of temperature on the large deformation mechanical behavior of the polymer in the range of 20–60°C.

Furthermore, little information is available regarding the strain rates that UHMWPE components are subjected to in vivo. Based on finite element simulations, the maximum effective (von Mises) strains near the articulating surface of conventional UHMWPE components are about 0.01 in total hip replacements and up to 0.12 or 0.15 for total knee replacements during the peak stance phase of gait [20,21]. It should be noted that the strain predictions from these simulations were obtained assuming a rate-independent constitutive model based on classical isotropic plasticity, which has important limitations with regard to predicting the multiaxial behavior of UHMWPE [11]. If we consider that the typical gait cycle from total joint replacements patients has recently been measured to be 1.67 s [22], then the average strain rate ranges between 0.006 and $0.09\,s^{-1}$, based on our current understanding of the maximum effective strains in hip and knee replacements. In actuality, the maximum strain rate during the gait cycle may be 5–10 times higher than the average because of the short time interval during which the joint forces increase after heel strike [23].

The primary goal of this research was to investigate the true stress–strain behavior of contemporary and

Questions? Contact FDA/CDRH/OCE/DID at CDRH-FOISTATUS@fda.hhs.gov or 301-796-8118

Records processed under FOIA Request #2014-8015; Released by CDRH on 12-8-2015

highly crosslinked UHMWPEs as a function of temperature and strain rate. A secondary goal was to compare the effects of annealing vs. remelting on the mechanical behavior of highly crosslinked UHMWPE. We hypothesized that the post-irradiation annealing or remelting effect on crystallinity would significantly affect the elastic, yielding, and plastic flow behavior of the crosslinked UHMWPE materials. Because the range of temperatures associated with in vitro testing and in vivo loading conditions (20–60°C) is below the onset of melting, we further hypothesized that the effects of temperature on the mechanical behavior of UHMWPE may be described by a thermally activated (Arrhenius) relationship.

2. Methods

Four UHMWPE materials were prepared from GUR 1050 resin (Ticona, Bayport TX), which is fabricated without added calcium stearate [1]. The UHMWPE was obtained from a single lot of ram extruded, 60 mm diameter rods and were certified by the converter as compliant with the ASTM standard for medical grade UHMWPE (ASTM F-648 [24]). The conventional UHMWPE used in this study was therefore suitable for fabrication into orthopedic components.

The four UHMWPE materials investigated in the present study were: (1) as-received (control); (2) gamma radiation sterilized in nitrogen with 30 kGy; (3) highly crosslinked with 100 kGy of gamma radiation and remelted at 150°C; and (4) highly crosslinked with 100 kGy of gamma radiation and annealed at 110°C (Fig. 1). Specific details on the processing of the materials are

(1) The as-received material was the baseline control (uncrosslinked) condition.
(2) To process the sterilized material, 12 extruded rods of 75 cm length were individually packaged in metallic foil pouches, which were evacuated and backfilled with nitrogen three times prior to heat sealing. The nitrogen-packaged rods were then gamma irradiated with a dose of 30 kGy, corresponding to a standard sterilization dose of 25–40 kGy typically used for orthopedic devices [1].
(3) To produce the highly crosslinked and remelted material, 12 extruded rods of 75 cm length were gamma irradiated in air with a dose of 100 kGy, corresponding to the dose previously associated with a 90% reduction of wear in previous hip simulator experiments [3,25,26]. The rods were subsequently thermally processed by heating until the center of the bars reached 150°C for 2 h (as confirmed by thermocouple measurements) in an air circulating oven. The rods were then slow cooled in the oven to ambient temperature over a period of 24 h.
(4) To produce the highly crosslinked and annealed material, 12 extruded rods of 75 cm length were initially crosslinked by 100 kGy of gamma radiation

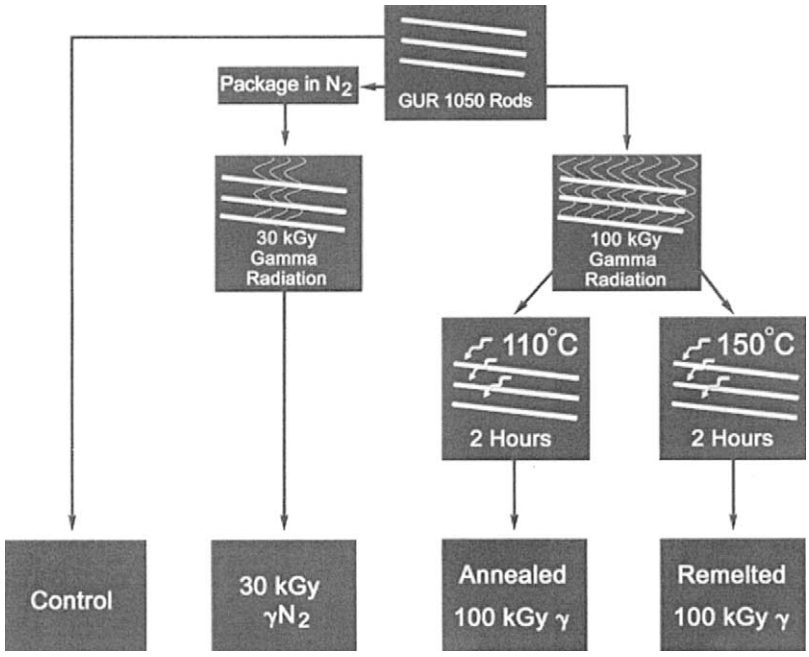

Fig. 1. Schematic of processing routes for the four UHMWPE (GUR 1050) materials examined in this study, including the unirradiated (control), 30 kGy γ-N_2, 100 kGy 110°C, and the 100 kGy 110°C materials.

Questions? Contact FDA/CDRH/OCE/DID at CDRH-FOISTATUS@fda.hhs.gov or 301-796-8118

Records processed under FOIA Request #2014-8015; Released by CDRH on 12-8-2015

at the same time as the rods used to produce the remelted material (see Material No. 3, above). The rods were then heat treated until the center temperature reached 110°C for 2 h, and then cooled as described for Material No. 3.

All of the gamma irradiation was performed by a commercial vendor at ambient temperature. The UHMWPE materials (and subsequent specimens) were consequently stored in a subzero freezer (−40°C) until use, to minimize any potential post-processing oxidative degradation.

The physical properties of the four UHMWPE materials were characterized using the density gradient column technique (to determine bulk density) and differential scanning calorimetry (to determine degree of crystallinity) to quantify changes in crystallinity resulting from irradiation and thermal processing. Density measurements were performed using a gradient column of isopropanol and water in accordance with ASTM D1505 [27]. Differential scanning calorimetry was performed using established methods [28]. For each material, three samples were heated in nitrogen from 30°C to 170°C at a rate of 10°C/min.

Cylindrical tensile specimens (10 mm in diameter and 25 mm in gage length) and cylindrical compression specimens (10 mm in diameter, and 15 mm in height) were machined from each of the materials by a commercial vendor who specializes in the fabrication of orthopedic components. A surface finish comparable to the articulating surface of orthopedic implants was specified for the test specimens. The specimen geometry was the same as that used in a previous study of the tensile and compressive large deformation mechanical behavior of UHMWPE [12].

The UHMWPE materials were subjected to three series of mechanical tests to evaluate the thermal and rate dependence of their mechanical behavior. In the first series of tests, the materials were subjected to uniaxial tension to failure at three rates and at room temperature, thereby characterizing the entire true stress–strain curves to failure. In the second series, the materials were tested in uniaxial compression at three strain rates to moderate true strains (up to 0.63), followed by unloading, at room and body temperature. In the third series, uniaxial compression testing was performed for a single rate up to a true strain of 0.14, followed by unloading, in a temperature range of 20–60°C. The three series of tests, detailed below, were intended to provide characterization of the true stress–strain behavior under a variety of loading, unloading, and thermal conditions, and were judged to be sufficient for future validation of a thermomechanical constitutive model for conventional and crosslinked UHMWPE materials.

2.1. Series I: room temperature, uniaxial tension to failure

Uniaxial testing was conducted using a 4204 Instron electromechanical load frame, equipped with a 5 kN load cell (Canton, MA). Specimens were tested under displacement control at rates of 30, 75, and 150 mm/min at room temperature (22 ± 1°C) in accordance with ASTM D638 [29]. An Instron non-contacting video extensometer (Canton, MA), fitted with a 350 mm FOV lens was used to measure uniaxial strain. The extensometer determined strain by tracking the position of the center of the two contrasting marks that were applied to the test specimen. The video extensometer was calibrated prior to testing with a calibration strip (10 calibration marks) provided by the manufacturer. Digital calipers were used to measure the initial diameter of all samples and the video extensometer measured the initial gage length between the two contrasting marks on the samples. A total of 60 tensile specimens were tested (5 specimens per material × 4 materials × 3 testing rates).

Due to the uncertainty associated with video extensometry at low strains [12], the uniaxial tensile tests to failure were not used to characterize elastic modulus, but rather the yielding, plastic flow, and failure behavior of the UHMWPE materials. The nominal (engineering) strain (ε_N), true strain (ε), nominal (engineering) stress (σ_N), and true stress (σ) were defined as follows [12]:

$$\varepsilon_N = \frac{l - l_0}{l_0}, \tag{1a}$$

$$\varepsilon = \ln(1 + \varepsilon_N), \tag{1b}$$

$$\sigma_N = \frac{P}{A_0}, \tag{1c}$$

$$\sigma = \sigma_N(1 + \varepsilon_N), \tag{1d}$$

where l_0 and l are the initial and final lengths of the gage region, P is the load, and A_0 is the initial undeformed cross-sectional area. The definitions of true stress and strain (in Eqs. (1b) and (1d)) are based on the incompressibility assumption and the absence of necking during the tensile test [12]. The tensile tests were videotaped using a camcorder to document overall changes in the shape of the specimens and to confirm the presence or absence of necking during testing. The camcorder was set up in the same location for all of the tests, so that the field of view could be compared between tests, and such that the gage regions remained in the field of view for the duration of the testing [12].

The engineering and true stress–strain curves were used to calculate the polymer yield strength/strain (defined as the local maximum in the engineering stress–strain curve) and the ultimate stress/strain based on Eqs. (1a)–(1d). The tensile properties at yield and

Questions? Contact FDA/CDRH/OCE/DID at CDRH-FOISTATUS@fda.hhs.gov or 301-796-8118

Records processed under FOIA Request #2014-8015; Released by CDRH on 12-8-2015

failure were statistically analyzed to quantify the significance of changing the testing rate and to assess the differences between the UHMWPE materials. Analysis of covariance (ANCOVA) of the tensile properties was performed using Statview software (SAS Institute, Cary, NC) with the UHMWPE material treated as a categorical variable and the testing rate as a covariate. Relationships were also sought between the tensile properties, irradiation dose, and crystallinity of the UHMWPE. A p-value of 0.05 was taken as significant.

2.2. Series II: room and body temperature, uniaxial compression

Uniaxial compression testing was performed using a 858 Mini Bionix II servohydraulic load frame (MTS: Minneapolis, MN), equipped with a 5 kN load cell and an environmental chamber (Fig. 2). In previous compression tests of UHMWPE, strain was measured by a compressometer spanning the parallel platens [12]. However, initial validation tests with the current system demonstrated the accuracy of platen displacement for the purpose of calculating compressive strain. To characterize the greatest extent of the compressive stress–strain curves on the current system, testing was conducted to a maximum load of –4800 N (96% of the load cell capacity), corresponding to a maximum compressive engineering stress of 61 MPa. Specimens were deformed at constant strain rate to the maximum load, and then unloaded at the same rate. The ends of the specimens were lubricated with liquid soap to minimize end effects (barelling) under the prescribed loading conditions.

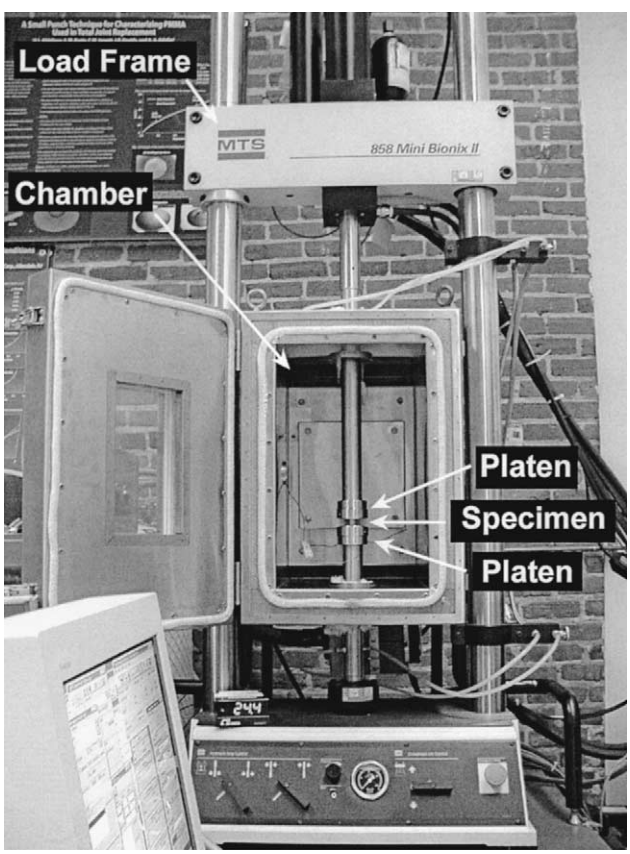

Fig. 2. Load frame and environmental chamber set up for uniaxial compression tests.

Testing was performed at 20°C and 37°C. Constant temperature conditions during compression testing were maintained by a tabletop MTS Series 651 environmental chamber (Fig. 2). Instead of using liquid nitrogen, the environmental chamber was cooled to 20°C using forced air from a custom-built Peltier cooling system (Melcor, Trenton, NJ). Although the chamber was configured with a factory installed thermocouple which monitored the air temperature, a second calibrated thermocouple (Omega Engineering, Stamford, CT) was attached to the lower platen to provide an additional, independent temperature reading. A voltage signal from the second thermocouple was wired into the servohydraulic control module, so that testing would commence automatically as soon as the local temperature was within 1°C of the target test temperature. Specimens were preconditioned at the test temperature for at least 24 h prior to testing. At each test temperature, five specimens of the four materials were tested under strain control at engineering strain rates of 0.02, 0.05, and 0.10 s^{-1}. Thus, a total of 120 tests were performed for this series of tests (5 specimens per material $\times 4$ materials $\times 3$ testing rates $\times 2$ test temperatures).

Engineering and true stress vs. strain were calculated using Eqs. (1a)–(1d), and the resulting compressive true stress–strain curves were corrected for initial toe-in, as described in ASTM D695 [30]. The offset method (using a 0.002 strain) was used to define the onset of plastic deformation (yielding) for the UHMWPE materials in compression. A strain offset of 0.002 was found in previous studies to be an effective yield criterion for conventional UHMWPE in compression [12]; preliminary tests also confirmed the suitability of the offset method for the highly crosslinked UHMWPEs developed for the present study. Mathematica 4.0 (Wolfram Research, Champaign, IL) was used to post-process the data and to calculate the elastic modulus, the maximum true stress/strain, as well as the plastic true strain immediately after unloading. The area under the true stress curve was computed to determine the energy density during loading, unloading, and the hysteresis under the combined loading and unloading curves.

Regression analyses, as well as analyses of (co)variance were performed on the compressive properties to examine the influence of strain rate and testing temperature on the mechanical behavior. G'Sell and colleagues [13] proposed a constitutive relation for

Questions? Contact FDA/CDRH/OCE/DID at CDRH-FOISTATUS@fda.hhs.gov or 301-796-8118

Records processed under FOIA Request #2014-8015; Released by CDRH on 12-8-2015

semi-crystalline polymers in which the true stress at large deformations is related to the true strain rate according to a power law relationship. Consequently, at both test temperatures, elastic modulus, offset yield strength, and maximum compressive true stress were fitted to a power law model

$$A_0\dot{\varepsilon}_N^m, \tag{2}$$

where A_0 is a constant, $\dot{\varepsilon}_N$ is the engineering strain rate, and m is the strain rate sensitivity coefficient. Analysis of variance and regression analyses were conducted to determine whether the rate sensitivity coefficient, m, was influenced by the density and irradiation dose of the UHMWPEs, as well as by the test temperature. For all statistical analyses, Statview software (SAS Institute, Cary, NC) was used and a p-value of 0.05 was taken as significant.

2.3. Series III: 20–60°C, uniaxial compression

To evaluate the thermomechanical behavior of UHMWPE for a broader temperature range, a third series of uniaxial compression tests was conducted using the servohydraulic testing system (Fig. 2) at six different temperatures between 20°C and 60°C. As in Series II, specimens were preconditioned at the test temperature for at least 24 h prior to testing. Specimens were loaded at $0.02\,s^{-1}$ to an engineering strain of 0.15 and unloaded at the same rate (3 specimens per temperature condition $\times$ 6 temperature conditions/material $\times$ 4 materials = 72 specimens). True stress–strain curves and compressive properties were calculated as described for Series II, above.

Step forward multiple linear regression was used to model the influence of test temperature and crystallinity on elastic modulus, yield strength, and maximum true stress with Statview software (SAS Institute, Cary, NC). Young's modulus, compressive yield strength, and the maximum true stress during the compression test were also fitted with Arrhenius models for each material

$$B_0 e^{-Q/RT}, \tag{3}$$

where B_0 is a constant, Q is the activation energy, R is the gas constant ($R = 8.3145\,J/(mol\,K)$), and T is the temperature (K). Confidence intervals (95%) were used as the basis for comparisons of the activation energy between materials.

3. Results

The density and DSC measurements confirmed that the four UHMWPE materials were each associated with unique physical properties (Table 1). During the DSC experiments, a single prominent melting peak between 137°C and 142°C was observed, depending upon the material (Table 1), thereby confirming 110°C and 150°C as processing conditions consistent with annealing and remelting of the UHMWPE. The remelted and annealed highly crosslinked UHMWPE exhibited the lowest and highest average crystallinity of the four materials (45.7% and 60.8%, respectively, Table 1).

3.1. Series I: room temperature, uniaxial tension to failure

All of the conventional and highly crosslinked UHMWPE materials deformed homogeneously, with no evidence of necking or strain localization within the gage region up to the point of tensile failure (Fig. 3). In general, the highly crosslinked materials exhibited less ductility in tension when compared with the two conventional materials (Figs. 3 and 4, Table 2). For all three-displacement rates, the engineering stress–strain curves for each material showed a local maximum, characteristic of the polymer yield point, followed by large-scale deformation and strain hardening. Significant differences were found in the tensile yielding and ultimate properties between all four UHMWPE materials (Table 2).

There was no evidence of a local maximum in the true stress–strain curves for any of the materials, regardless of the displacement rate (Figs. 4A–C). The true stress–strain curves showed subtle evidence of slightly increased hardening with increasing rate of the test as seen by the increase in true ultimate stress (Table 2). Displacement rate had a significant effect on all of the yielding and failure properties in uniaxial tension, with the exception of true ultimate strain (Fig. 4, Table 2).

Significant relationships were observed between the crystallinity, the absorbed dose and the yielding and

Table 1
Irradiation and thermal processing conditions for ram-extruded GUR 1050, with resulting density, crystallinity, and melt transitions (mean ± SD)

Radiation method	Radiation environment	Thermal processing	Density (g/cm^3)	Crystallinity (%)	Peak melt transition (°C)
None (control)	None	None	0.933 ± 0.001	50.4 ± 3.3	136.5 ± 0.8
30 kGy-γ	Nitrogen	None	0.933 ± 0.001	51.3 ± 1.0	138.5 ± 0.2
100 kGy-γ	Air	110°C/2 h	0.934 ± 0.001	60.8 ± 0.9	141.6 ± 0.4
100 kGy-γ	Air	150°C/2 h	0.927 ± 0.001	45.7 ± 0.3	137.5 ± 0.7

Questions? Contact FDA/CDRH/OCE/DID at CDRH-FOISTATUS@fda.hhs.gov or 301-796-8118

Records processed under FOIA Request #2014-8015; Released by CDRH on 12-8-2015

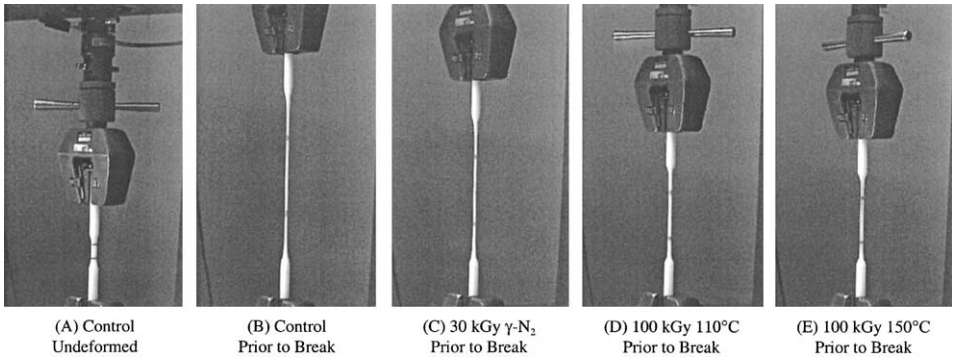

Fig. 3. Digital video frames of the uniaxial tension tests (30 mm/min), contrasting the initial undeformed geometry of the test specimen with the deformed geometry just prior to failure for the four UHMWPE materials.

ultimate behavior of the UHMWPE. For each testing rate, a non-linear (quadratic) relationship was fit between crystallinity and the true yield strength of the polymers (Fig. 5A). No correlation was found between the irradiation dose and the true stress at yield. However, the irradiation dose was significantly related to the true ultimate stress and strain of the UHMWPE (Figs. 5B and C).

3.2. Series II: room and body temperature, uniaxial compression

For the uniaxial compression tests conducted at room and body temperature, significant differences were found in the mechanical behavior of the four UHMWPE materials as a function strain rate, and temperature (Table 3, Figs. 6 and 7). The material, strain rate, and temperature had a significant effect on the compressive properties of UHMWPE (Table 4). In general, for all materials, an increase in testing temperature or a decrease in strain rate resulted in a decrease in the elastic modulus, in the yield and maximum true stresses, but caused an increase in the maximum strain and hysteresis (Table 3). The control and 30 kGy γ-N_2 UHMWPE materials showed comparable true stress–strain behavior under all temperature and strain rate experimental conditions. The crosslinked and remelted material (100 kGy/150°C) had the lowest elastic modulus and yield and ultimate stress values, but higher strains and hysteresis as compared to the other materials (Table 3). When comparing the effects of temperature and strain rate, an increase in temperature from 20°C to 37°C had more effect in increasing the maximum true strain of the materials, with an increase of up to 12%, as compared to a change of up to only 5% with a fivefold decrease in strain rate from 0.1 to $0.02\,s^{-1}$.

Power law behavior was observed between the strain rate and the elastic modulus, offset yield strength, and maximum compressive true stress for each of the UHMWPE materials (Fig. 8). The strain rate sensitivity coefficients for the conventional and crosslinked UHMWPE were all low, ranging between 0.01 and 0.03 for elastic modulus, between 0.02 and 0.09 for offset yield strength, and between 0.01 and 0.03 for the maximum compressive true stress (Fig. 9). There was no significant difference in the strain rate sensitivity between the different conventional and highly crosslinked UHMWPEs. However, increasing the test temperature was found to be significantly increasing the rate sensitivity for all of the UHMWPE materials (Fig. 9).

3.3. Series III: 20–60°C, uniaxial compression

Increasing the test temperature from 20°C to 60°C resulted in systematic decreases in the true stress–strain curves, as shown for the annealed crosslinked UHMWPE in Fig. 10. The compressive properties, such as the elastic modulus, offset yield strength, and maximum compressive stress progressively softened with increasing test temperature (Fig. 11). The 40°C increase in test temperature was associated with substantial (up to 51%) reduction in the compressive properties for UHMWPE. Multiple linear regression analysis indicated that both test temperature and crystallinity were significant predictors of elastic modulus, yield strength, and ultimate stress, accounting for 93–94% of the total variation in the data (based on r^2).

For each individual material, an Arrenhius relationship accurately modeled the effects of temperature on the compressive properties ($0.92 < r^2 < 0.97$, Table 5). In general, the activation energies for the remelted material were significantly greater than the annealed and control materials (Table 5), corresponding to an increased temperature dependence for crosslinked UHMWPE after remelting. Significant relationships were observed between the activation energy and the crystallinity of the UHMWPE materials ($0.96 < r^2 < 0.99$, Fig. 12).

Questions? Contact FDA/CDRH/OCE/DID at CDRH-FOISTATUS@fda.hhs.gov or 301-796-8118

Records processed under FOIA Request #2014-8015; Released by CDRH on 12-8-2015

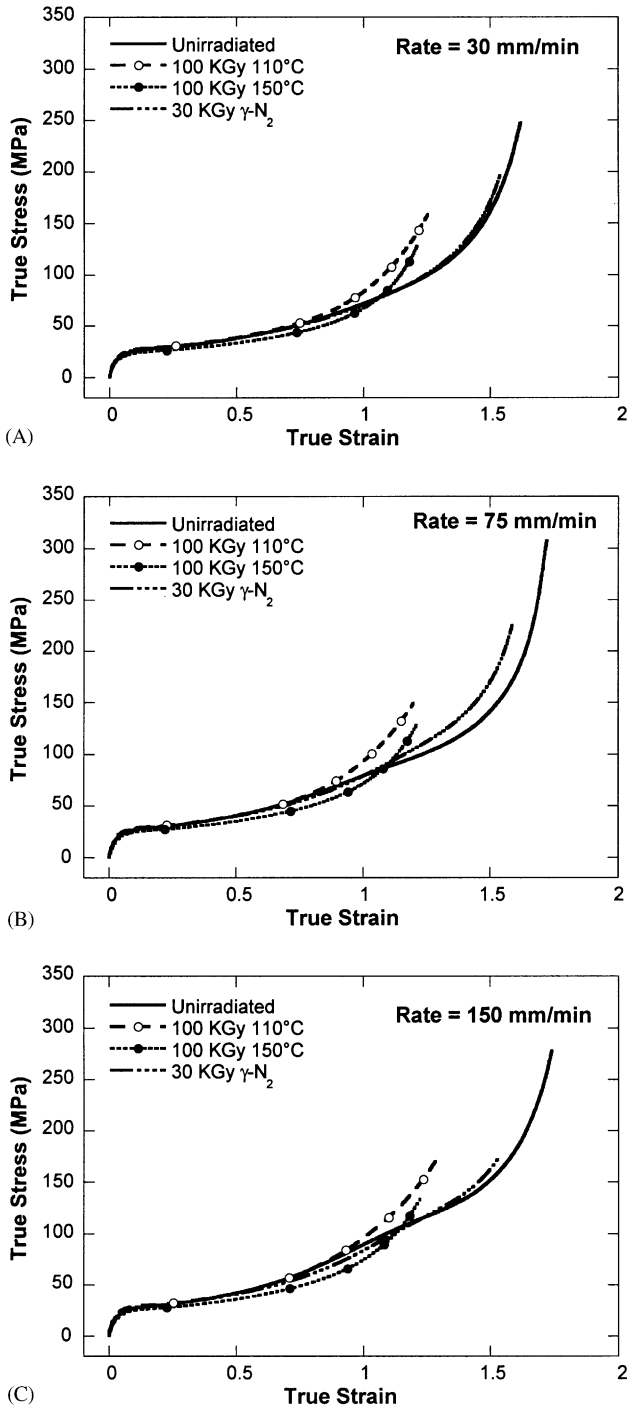

Fig. 4. Effect of material on true stress-strain curves for UHMWPE: (A) 30 mm/min; (B) 75 mm/min; (C) 150 mm/min.

4. Discussion

The results of this study support the hypothesis that large deformation mechanical behavior of the conventional and highly crosslinked UHMWPEs depends not only on the processing of the material, but also on the rate and temperature of the test conditions. Fabrication of highly crosslinked UHMWPE involves

Table 2
Uniaxial tensile properties (mean ±SD) for control GUR 1050, radiation sterilized (30 kGy-γ N2), highly crosslinked and annealed (100 kGy 110°C), and remelted (100 kGy 110°C) UHMWPE as a function of testing rate (30, 75, and 150 mm/min)

	Control GUR 1050			30 kGy-γ N2			100kGy 110°C			100 kGy 150°C		
	30 mm/min	75 mm/min	150 mm/min	30 mm/min	75 mm/min	150 mm/min	30 mm/min	75 mm/min	150 mm/min	30 mm/min	75 mm/min	150 mm/min
Yield strength (MPa)	23.5±0.30	24.25±0.15	24.78±0.16	24.11±0.14	24.93±0.14	25.34±0.12	24.79±0.12	25.76±0.15	26.12±0.12	21.36±0.13	22.20±0.15	22.74±0.08
Yield strain (%)	14.4±0.6	13.9±0.7	14.6±0.4	13.4±0.6	12.7±1.0	12.2±0.4	12.7±0.6	11.9±0.4	11.4±0.7	14.5±0.9	14.1±0.2	12.6±0.7
Ultimate stress (MPa)	50.2±1.6	44.8±9.9	40.0±7.0	47.1±4.2	44.3±3.2	37.7±3.1	46.4±3.4	46.3±1.0	47.0±2.2	37.1±3.2	41.5±2.1	39.8±3.3
Ultimate strain (%)	421±11	429±36	423±56	373±8	385±19	355±51	248±11	242±10	256±12	232±8	244±8	232±11
True yield strength (MPa)	26.9±0.4	27.6±0.2	28.4±0.12	27.35±0.24	28.09±0.24	28.44±0.18	27.94±0.10	28.82±0.13	29.11±0.18	24.47±0.24	25.32±0.15	25.61±0.16
True yield strain	0.134±0.005	0.130±0.006	0.136±0.004	0.126±0.005	0.120±0.009	0.115±0.004	0.120±0.005	0.112±0.004	0.108±0.006	0.136±0.008	0.132±0.002	0.119±0.007
True ultimate stress (MPa)	262±12	240±69	212±57	223±22	216±23	173±31	162±16	159±8	168±12	123±13	143±8	133±14
True ultimate strain	1.65±0.02	1.66±0.07	1.65±0.11	1.55±0.02	1.58±0.04	1.51±0.12	1.25±0.03	1.23±0.03	1.27±0.03	1.20±0.02	1.23±0.02	1.20±0.03

Five specimens were tested for each experimental condition.

Questions? Contact FDA/CDRH/OCE/DID at CDRH-FOISTATUS@fda.hhs.gov or 301-796-8118

Records processed under FOIA Request #2014-8015; Released by CDRH on 12-8-2015

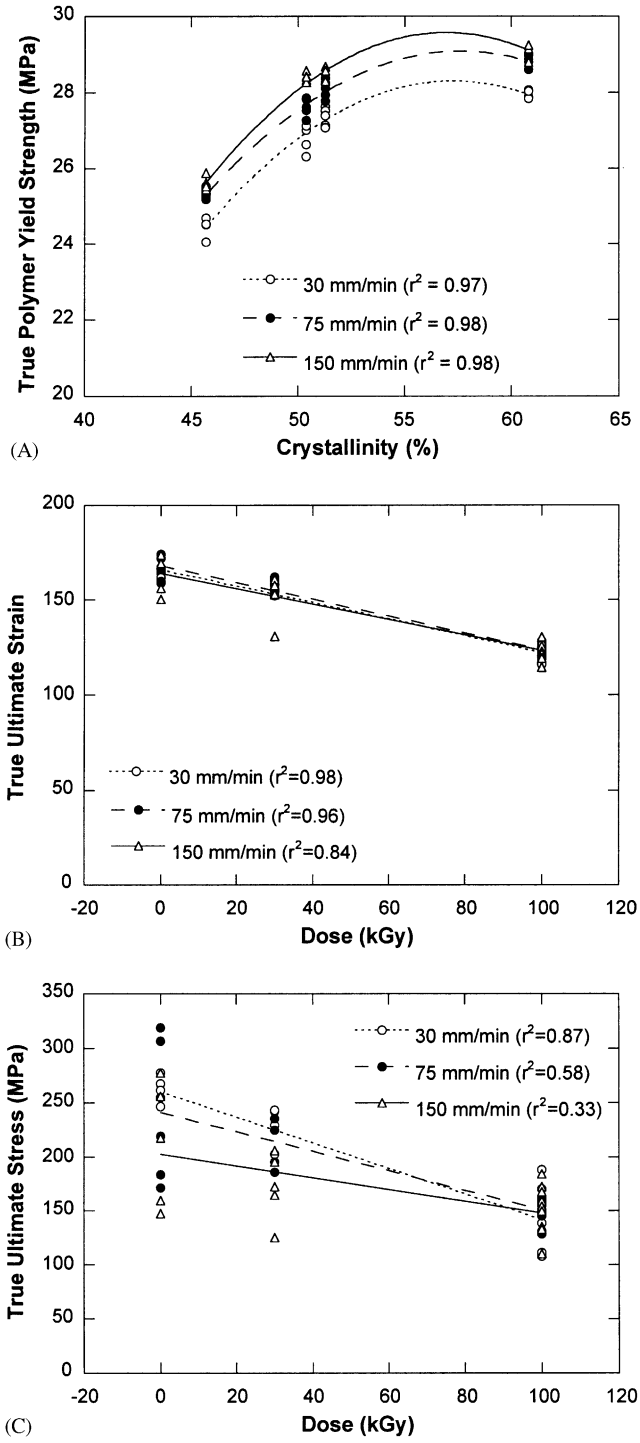

Fig. 5. (A) Effects of crystallinity on the true yield strength of the polymer at different testing rates. Effect of gamma radiation dose on true ultimate strain (B) and true ultimate stress (C) at different testing rates. All of the relationships shown here are statistically significant ($p<0.05$).

both irradiation and thermal processing, and both steps influence the yielding, plastic flow, and fracture behavior of the polymer. As has been discussed previously [12,16,25], the yielding and plastic flow of UHMWPE is accommodated by a number of mechanisms within both the amorphous and crystalline regions of the polymer. At small strains, below the polymer yield point, which for the UHMWPEs in the present study occurred at true strains in the range of 0.11–0.14 (Table 2), plastic deformation is initially accommodated in the amorphous regions [31]. However, at intermediate and large strains, the resistance to deformation is governed increasingly by the plasticity of the crystalline lamellae [31]. The irradiation step, on one hand, results in crosslinking of the UHMWPE primarily in the amorphous regions, and in the present study decreased the true stress and strain at failure. Thermal processing, on the other hand, influences the yielding and plastic flow behavior of UHMWPE by modifying the crystallinity of the polymer. Post-irradiation thermal treatments are intended to improve the oxidation resistance of UHMWPE [1]. However, thermal processing may also result in a trade-off in mechanical behavior due to changes in crystallinity.

The rate and temperature dependence for a wide range of amorphous polymers can be predicted in the vicinity of the glass transition temperature using the time–temperature superposition theory developed by Williams, Landel, and Ferry (WLF) [32,33]. The UHMWPEs examined in the present study exhibited thermomechanical behavior consistent with the basic principles of the WLF theory, namely that decreasing temperature and increasing the rate of testing tended to increase the deformation resistance of the polymers. Although the temperature and rate dependence of linear polyethylenes, such as high-density polyethylene (HDPE), have been well established [13,32–35], data on the thermomechanical behavior of UHMWPE are scarce in the scientific literature, limiting our ability to compare our results with previous studies.

The true stress–strain behavior in uniaxial tension for ram-extruded, unirradiated GUR 4150 HP has been reported [12], which aside from the presence of calcium stearate has a comparable molecular weight to the GUR 1050 employed in the current experiment [1]. The previously reported true stress–strain relationship for GUR 4150 HP [12] was comparable to the true stress–strain relationship found in the present study for conventional GUR 1050 (Fig. 13), with the exception of the ultimate true stress and strain, which were greater for the GUR 1050 than GUR 4150 HP. When tested under conditions identical to those employed in the present study, the ultimate true strain and stress for GUR 4150 HP were previously found to be 1.57 ± 0.04 and 199 ± 24 MPa, respectively [12]. For the GUR 1050 in the current experiment, the ultimate true strain and stress were found to be 1.65 ± 0.02 and 262 ± 12 MPa, respectively. The differences suggest that the presence of calcium stearate, which is added as a processing aid, primarily affects the failure mechanisms rather than the yielding and plastic flow behavior of UHMWPE.

Questions? Contact FDA/CDRH/OCE/DID at CDRH-FOISTATUS@fda.hhs.gov or 301-796-8118

Records processed under FOIA Request #2014-8015; Released by CDRH on 12-8-2015

Table 3
Uniaxial compressive properties (mean ± SD) for Control GUR 1050, radiation sterilized (30 kGy-γ N_2), highly crosslinked and annealed (100 kGy 110°C), and remelted (100 kGy 110°C) UHMWPE as a function of testing strain rate (0.02, 0.05, and 0.10 1/s)

	Control GUR 1050			30 kGy-γ N_2			100 kGy 110°C			100 kGy 150°C		
	0.02 1/s	0.05 1/s	0.10 1/s	0.02 1/s	0.05 1/s	0.10 1/s	0.02 1/s	0.05 1/s	0.10 1/s	0.02 1/s	0.05 1/s	0.10 1/s
(a) *At 20°C*												
Elastic modulus (MPa)	833.0 ± 9.1	932.1 ± 21.2	994.3 ± 29.2	932.1 ± 21.2	940.3 ± 7.9	946.8 ± 12.5	994.3 ± 29.2	1006.3 ± 8.7	1021.7 ± 25.6	778.9 ± 6.8	798.6 ± 7.5	804.3 ± 5.5
Offset yield strength (MPa)	12.0 ± 0.2	12.8 ± 0.1	13.2 ± 0.1	12.8 ± 0.1	13.3 ± 0.2	13.5 ± 0.2	13.2 ± 0.1	13.7 ± 0.2	13.8 ± 0.1	11.6 ± 0.1	12.1 ± 0.1	12.4 ± 0.2
Offset Yield Strain	0.014 ± 0.0	0.014 ± 0.0	0.013 ± 0.0	0.014 ± 0.0	0.014 ± 0.0	0.014 ± 0.0	0.013 ± 0.0	0.014 ± 0.0	0.014 ± 0.0	0.015 ± 0.0	0.015 ± 0.0	0.015 ± 0.0
Maximum true stress (MPa)	39.6 ± 0.1	39.8 ± 0.1	40.3 ± 0.1	39.8 ± 0.1	40.5 ± 0.0	40.8 ± 0.0	40.3 ± 0.1	40.7 ± 0.1	41.1 ± 0.1	37.2 ± 0.1	37.8 ± 0.1	38.2 ± 0.3
Maximum true strain	0.446 ± 0.002	0.444 ± 0.003	0.431 ± 0.002	0.444 ± 0.003	0.429 ± 0.002	0.422 ± 0.002	0.431 ± 0.002	0.422 ± 0.002	0.413 ± 0.003	0.507 ± 0.004	0.495 ± 0.003	0.486 ± 0.008
Maximum plastic true strain	0.251 ± 0.002	0.255 ± 0.002	0.254 ± 0.001	0.255 ± 0.002	0.247 ± 0.001	0.243 ± 0.001	0.254 ± 0.001	0.249 ± 0.002	0.243 ± 0.002	0.280 ± 0.002	0.275 ± 0.002	0.271 ± 0.005
Hysteresis (mJ/mm^3)	11.1 ± 0.0	11.5 ± 0.1	11.5 ± 0.1	11.5 ± 0.1	11.3 ± 0.1	11.2 ± 0.1	11.5 ± 0.1	11.5 ± 0.1	11.3 ± 0.1	12.0 ± 0.1	12.0 ± 0.1	12.0 ± 0.3
(b) *At 37°C*												
Elastic modulus (MPa)	648.2 ± 23.5	660.6 ± 33.4	681.0 ± 16.5	737.2 ± 15.8	764.5 ± 9.0	764.0 ± 4.9	771.4 ± 30.6	822.7 ± 15.3	804.1 ± 19.8	570.0 ± 15.2	595.2 ± 10.4	599.5 ± 14.5
Offset yield strength (MPa)	9.7 ± 0.2	10.6 ± 0.4	10.6 ± 0.3	10.3 ± 0.1	11.1 ± 0.2	11.5 ± 0.2	10.8 ± 0.2	11.4 ± 0.1	12.2 ± 0.2	8.8 ± 0.1	9.5 ± 0.2	10.2 ± 0.2
Offset yield strain	0.015 ± 0.0	0.016 ± 0.0	0.016 ± 0.0	0.014 ± 0.0	0.015 ± 0.0	0.015 ± 0.0	0.014 ± 0.0	0.014 ± 0.0	0.015 ± 0.0	0.016 ± 0.0	0.016 ± 0.001	0.017 ± 0.0
Maximum true stress (MPa)	35.7 ± 0.1	36.8 ± 0.2	37.6 ± 0.1	35.6 ± 0.4	36.7 ± 0.4	37.4 ± 0.3	36.4 ± 0.2	37.7 ± 0.1	38.4 ± 0.2	32.7 ± 0.3	33.8 ± 0.2	34.5 ± 0.3
Maximum true strain	0.548 ± 0.002	0.518 ± 0.005	0.501 ± 0.002	0.551 ± 0.011	0.516 ± 0.005	0.503 ± 0.007	0.529 ± 0.005	0.496 ± 0.003	0.482 ± 0.004	0.631 ± 0.006	0.603 ± 0.004	0.587 ± 0.006
Maximum plastic true strain	0.298 ± 0.001	0.283 ± 0.002	0.275 ± 0.001	0.307 ± 0.007	0.294 ± 0.008	0.285 ± 0.005	0.294 ± 0.001	0.281 ± 0.002	0.277 ± 0.002	0.334 ± 0.008	0.321 ± 0.005	0.312 ± 0.008
Hysteresis (mJ/mm^3)	12.3 ± 0.1	11.9 ± 0.1	11.7 ± 0.1	12.9 ± 0.3	12.7 ± 0.4	12.4 ± 0.3	12.6 ± 0.1	12.3 ± 0.1	12.2 ± 0.2	13.2 ± 0.4	13.0 ± 0.3	12.9 ± 0.2

Five specimens were tested to a maximum engineering stress of −61 MPa and subsequently unloaded for each experimental condition.

Questions? Contact FDA/CDRH/OCE/DID at CDRH-FOISTATUS@fda.hhs.gov or 301-796-8118

Records processed under FOIA Request #2014-8015; Released by CDRH on 12-8-2015

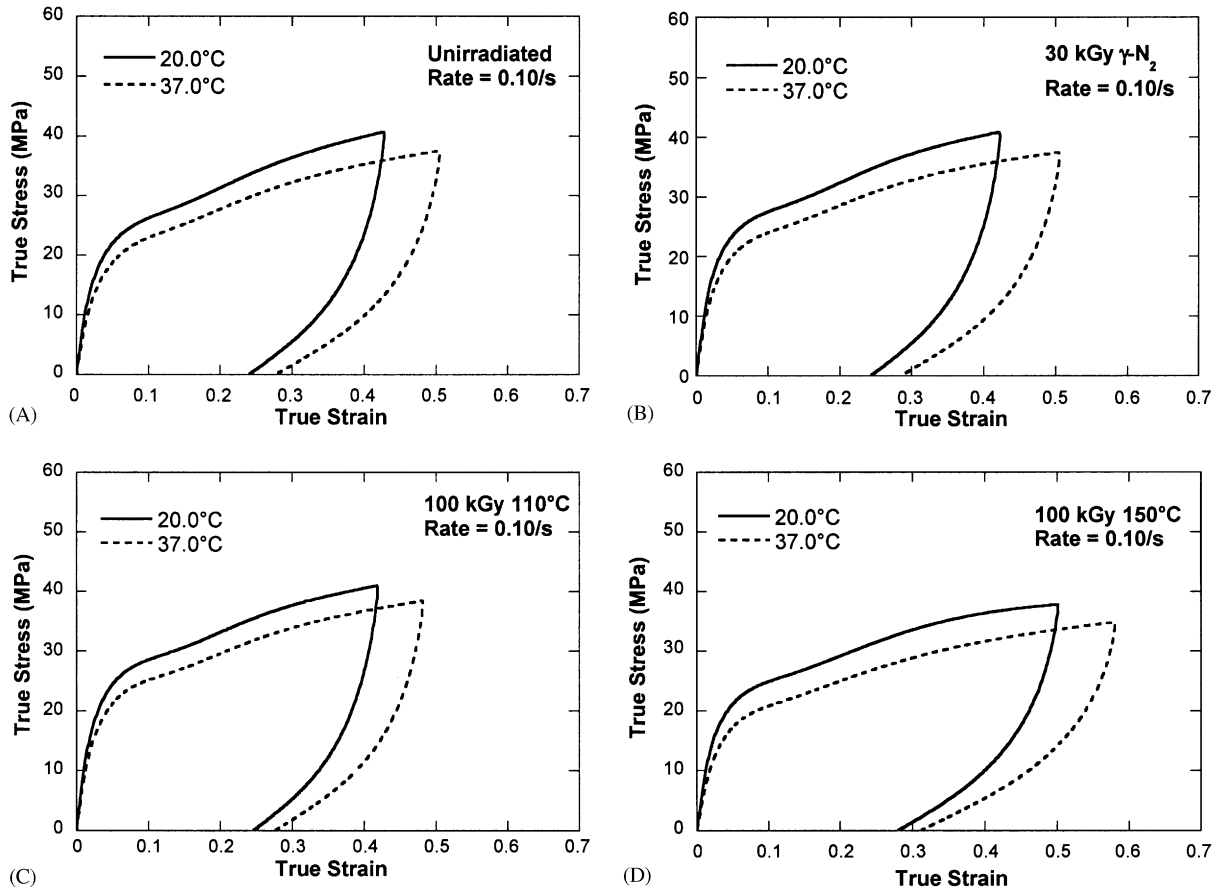

Fig. 6. Effect of temperature (20°C, 37°C) on true stress–strain curves in uniaxial compression for UHMWPE at a strain rate of 0.10 1/s: (A) unirradiated; (B) 30 kGy γ-N_2; (C) 100 kGy 110°C; (D) 100 kGy 150°C.

In the range of temperatures examined, test temperature had a significant affect on the yielding and plastic flow behavior of conventional and highly crosslinked UHMWPE. These findings are consistent with previous studies by Pampillo and Davis [34], who investigated the tensile behavior of an industrial UHMWPE (Allied Chemical Resin AC1220, $M_w = 2.5 \times 10^6$) as a function of temperature between 100 and 375 K (−173°C to 102°C). Pampillo and Davis observed a nearly constant rate of thermal softening for UHMWPE between 0°C and 60°C [34]. The graphical data presented by Pampillo and Davis [34] for yield strength, within the temperature range of interest, were associated with an activation energy of 1.6 ± 0.1 kJ/mol. For the yield strength of the unirradiated UHMWPE in the present study, the activation energy ranged between 1.6 and 1.9 kJ/mol (95% confidence interval, Table 5), consistent with the results of Pampillo and Davis. Thus, our findings support the hypothesis that the thermomechanical behavior of conventional and crosslinked UHMWPE can be predicted based on the physics of a thermally activated (Arrhenius) model in the temperature range of 20–60°C. Negative correlations were observed between the activation energies for thermal softening and the crystallinity of the UHMWPEs, consistent with thermal activation being associated with the amorphous regions within the polymer. If the thermal activation of crystalline regions were responsible for the thermal sensitivity of UHMWPE, one would have expected a positive correlation between crystallinity and activation energy. Our findings suggest that a unified, Arrhenius-based thermomechanical model may be applicable to both conventional and highly crosslinked UHMWPEs, with crystallinity as the controlling state variable. Because of the limited amount of information in the literature regarding the temperature dependence of large deformation mechanical properties in conventional and crosslinked UHMWPE, further research will be needed to clarify the precise molecular mechanisms responsible for thermal activation of these polymers within the clinically relevant temperature range of 20–60°C.

The temperature of UHMWPE in vivo does not remain constant, and can be expected to increase due to frictional heating between the femoral head and the polymer surface, reaching a steady state after 1 h of continuous walking activity, as shown by the recent telemeterized hip measurements by Bergmann and associates [17]. The surface temperature of an

Questions? Contact FDA/CDRH/OCE/DID at CDRH-FOISTATUS@fda.hhs.gov or 301-796-8118

Records processed under FOIA Request #2014-8015; Released by CDRH on 12-8-2015

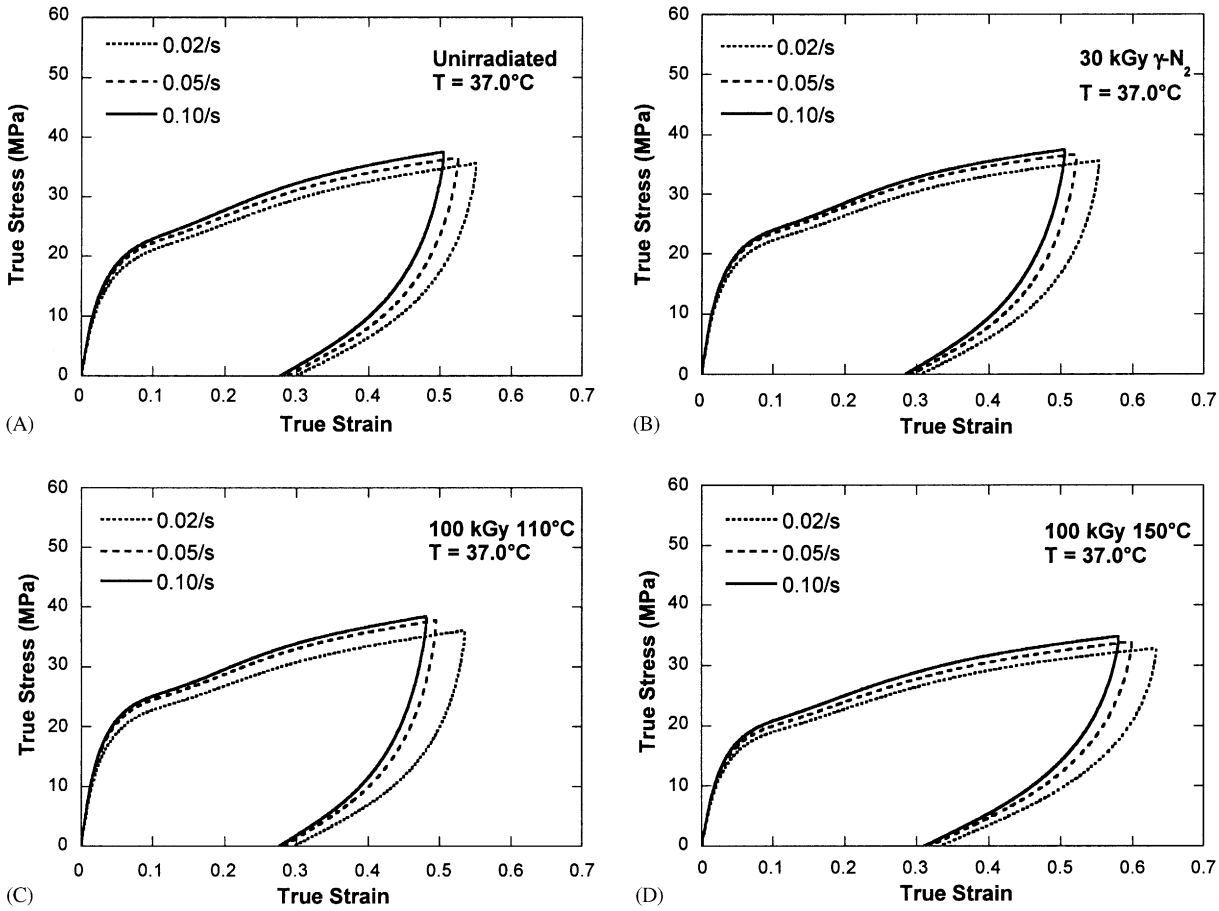

Fig. 7. Effect of strain rate (0.02, 0.05, and 0.10 1/s) on true stress–strain curves in uniaxial compression for UHMWPE at 37.0°C: (A) unirradiated; (B) 30 kGy γ-N_2; (C) 100 kGy 110°C; (D) 100 kGy 150°C.

Table 4
Summary of p values showing significance of the effect of the different experimental conditions and of the interaction of these with the material groups on the mechanical parameters in uniaxial compression

Experimental condition	Elastic modulus	Yield strength	Ult. true stress
Material	<0.0001	<0.0001	<0.0001
Temperature (°C)	<0.0001	<0.0001	<0.0001
Strain rate (1 1/s)	<0.0001	<0.0001	<0.0001
Material × Temperature (°C)	0.0229*	<0.0001	<0.0001
Material × Strain rate (1 1/s)	0.6080*	0.0741*	0.9894*
Material × Temperature (°C) × Strain rate (1 1/s)	0.2329*	<.0001	<0.0001

*Not significant.

Table 5
Activation energies, Q (in kJ/mol) for Arrhenius relationships for the Young's modulus (Q_E), yield strength (Q_{YS}), and maximum stress (Q_{MS}) of the four materials (with the range in 95% CI)

Material	Q_E	Q_{YS}	Q_{MS}
Control	1.88 (1.69–2.07)*	1.75 (1.62–1.88)*	1.22 (1.11–1.33)
30 kGy-γ N_2	1.73 (1.50–1.96)*	1.74 (1.61–1.87)*	1.14 (1.03–1.26)
100 kGy-γ/110°C	1.74 (1.57–1.91)*	1.63 (1.46–1.80)*	1.12 (1.02–1.22)*
100 kGy-γ/150°C	2.30 (2.09–2.51)	2.11 (1.92–2.30)	1.36 (1.22–1.49)

*Significant difference ($p<0.05$) when compared with 100 kGy-γ/150°C.

Questions? Contact FDA/CDRH/OCE/DID at CDRH-FOISTATUS@fda.hhs.gov or 301-796-8118

Records processed under FOIA Request #2014-8015; Released by CDRH on 12-8-2015

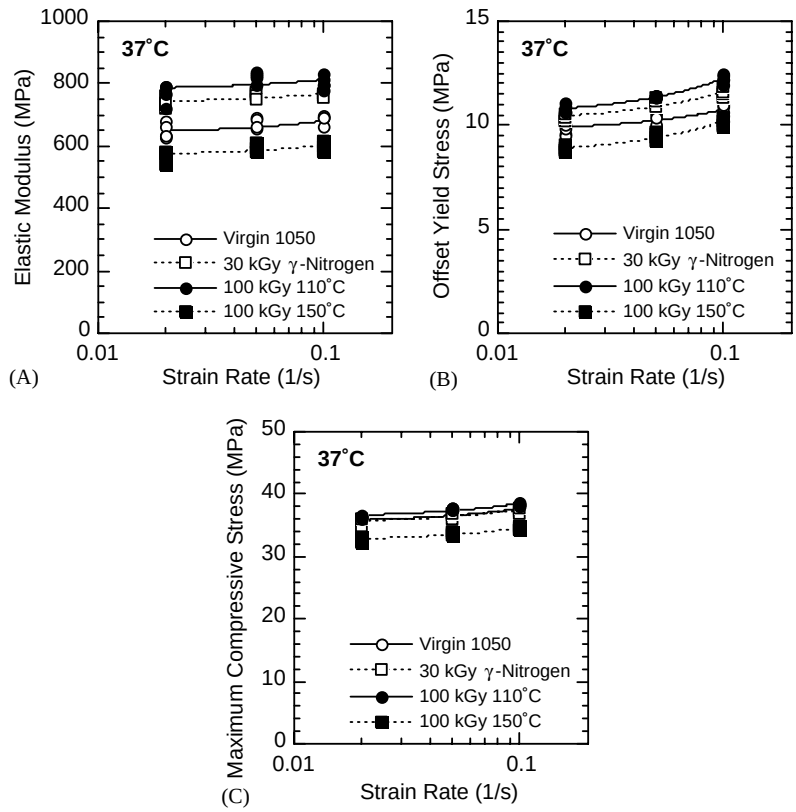

Fig. 8. Power law curves between the compressive mechanical properties and strain rate at 37°C: (A) elastic modulus; (B) offset yield strength; (C) maximum compressive stress.

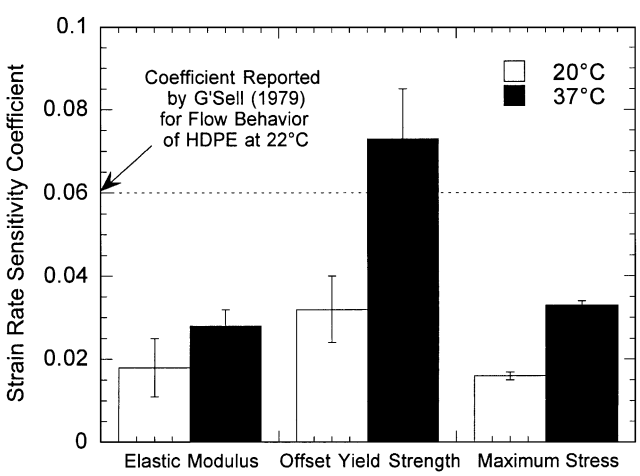

Fig. 9. Average strain rate sensitivity coefficients (±SD) associated with the power law relationships, depicted in Fig. 8, compared with the value reported by G'Sell and Jonas for HDPE [13]. There was no significant difference in the rate sensitivity between the four UHMWPE materials ($p > 0.05$).

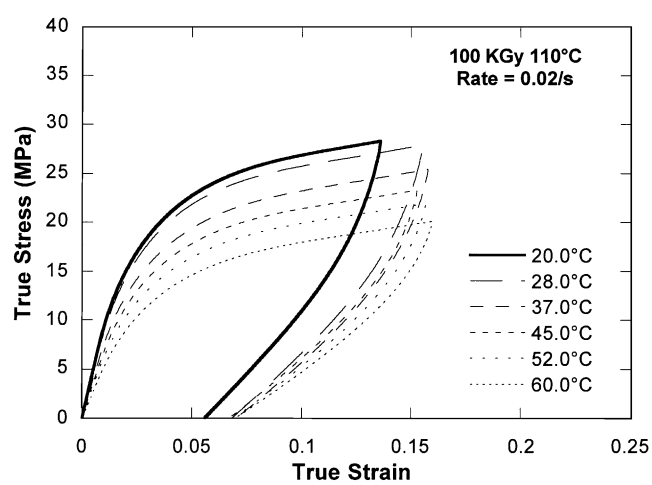

Fig. 10. Effect of temperature between 20°C and 60°C on the compressive true stress–strain curves for 100 kGy 110°C UHMWPE at $0.02\,s^{-1}$.

UHMWPE component will depend upon a number of factors, including the choice of femoral head material [18,19]. Surface temperatures for the UHMWPE will be lower when articulating against conductive metallic femoral heads, which can dissipate heat from the articulating surface, as opposed to articulations against insulating ceramic components. From a bioengineering perspective, elevated surface temperatures in UHMWPE are undesirable due to their adverse influence on the proteins in synovial fluid, which lubricate the artificial joint surfaces [18,19]. From a biomaterial perspective, the elevated surface temperatures are also undesirable

Questions? Contact FDA/CDRH/OCE/DID at CDRH-FOISTATUS@fda.hhs.gov or 301-796-8118

Records processed under FOIA Request #2014-8015; Released by CDRH on 12-8-2015

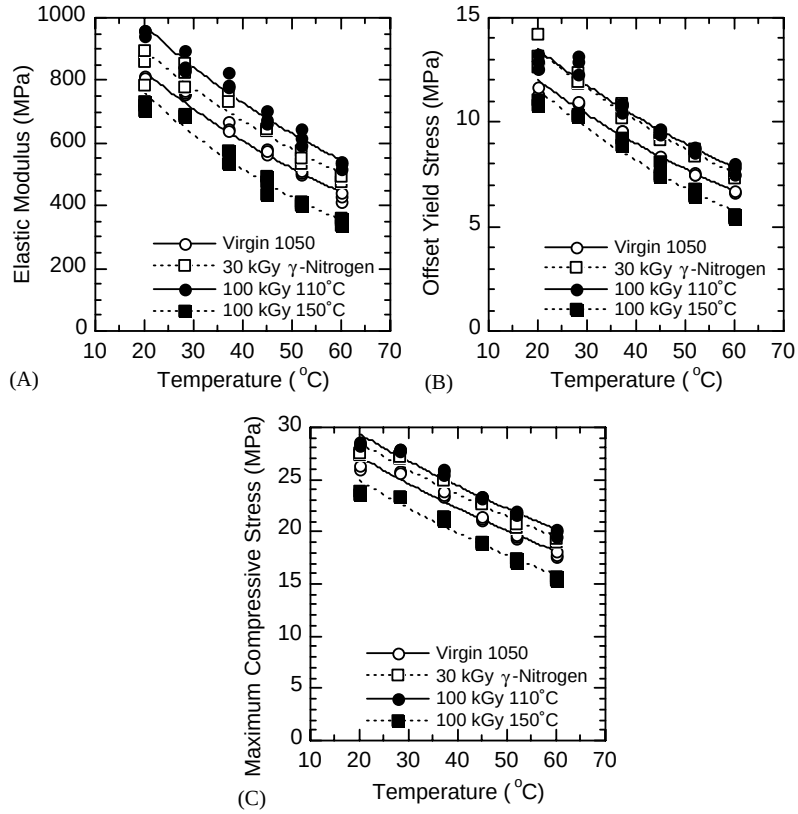

Fig. 11. Effect of temperature between 20°C and 60°C on the compressive properties of conventional and highly crosslinked UHMWPE: (A) elastic modulus; (B) offset yield strength; (C) maximum compressive stress.

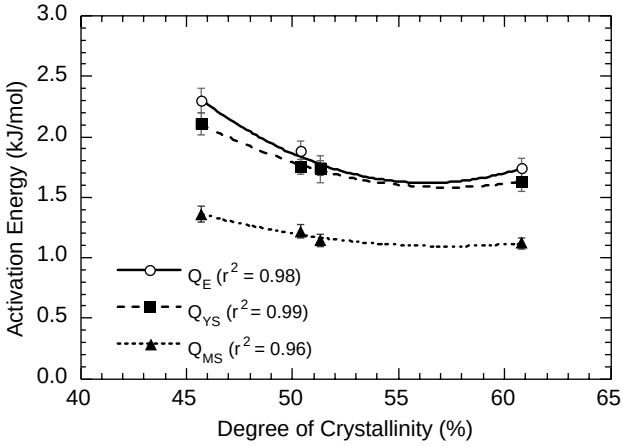

Fig. 12. Effect of crystallinity on the activation energies associated with thermal softening of the elastic modulus (Q_E), offset yield strength (Q_{YS}), and maximum stress during the compression tests (Q_{MS}).

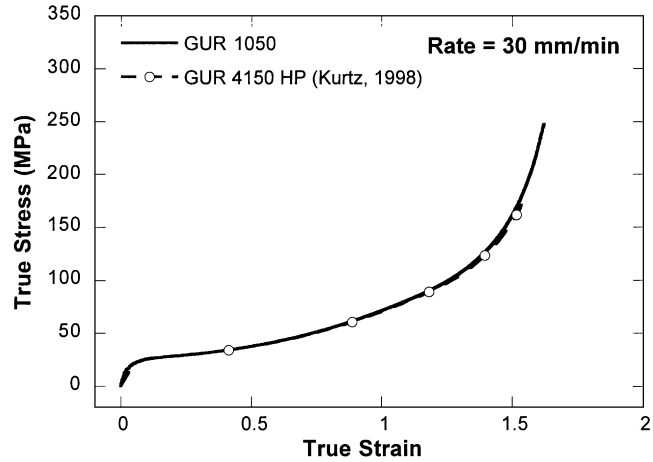

Fig. 13. Comparison of true stress–strain of unirradiated GUR 1050 (control) with previously reported data for GUR 4150 HP [12]. Tests were performed using specimens of identical geometry at room temperature and at 30 mm/min.

because the resistance of UHMWPE to the plastic deformation is lowered. It has been shown that the plasticity-induced damage layer near the articulating surface precedes wear in acetabular and tibial components [25,36,37]. Due to the strong temperature dependence of the mechanical behavior for conventional and crosslinked UHMWPE, accounting for thermal effects is expected to be important for accurate simulations of in vivo mechanical performance.

In the range of strain rates examined, the conventional and highly crosslinked UHMWPEs were all comparably insensitive to changes in strain rate. G'Sell

Questions? Contact FDA/CDRH/OCE/DID at CDRH-FOISTATUS@fda.hhs.gov or 301-796-8118

Records processed under FOIA Request #2014-8015; Released by CDRH on 12-8-2015

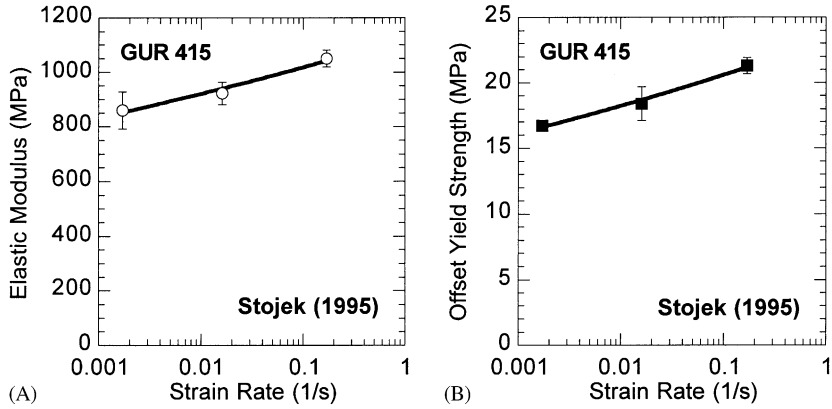

Fig. 14. Power law relationships between the compressive mechanical properties and strain rate for GUR 415 at room temperature: (A) elastic modulus; (B) 1.5% offset yield strength, plotted from previously tabulated data [38].

and Jonas [13] proposed the following constitutive law for the large deformation, plastic flow region of the true stress strain curve of semi-crystalline polymers:

$$\sigma(\varepsilon, \dot{\varepsilon}) = K \exp\left(\frac{\gamma_\varepsilon}{2}\varepsilon^2\right)\dot{\varepsilon}^m, \tag{4}$$

where K, γ_ε, and m are material constants. For a constant strain, Eq. (4) yields a power law relationship shown previously in Eq. (2). G'Sell and Jonas determined the strain rate sensitivity coefficient, m, for HDPE to be 0.06 at room temperature [13], whereas in the present study, m for UHMWPE ranged from 0.01 to 0.03 at 20°C, as shown in Fig. 9. In a conference abstract, Stojek and Li [38] reported on the effect of strain rate on the elastic and 1.5% offset yield strength of GUR 415 in tension at an unspecified (presumably ambient) temperature. GUR 415 is an earlier UHMWPE designation for GUR 4150 HP by Hoechst [1]. Stojek and Li's data, presented originally in tabular form, are accurately represented by power law models ($0.98 < r^2 < 0.99$, Figs. 14A and B), with rate sensitivity coefficients of 0.04 and 0.05 for the elastic modulus (Fig. 14A) and offset yield strength (Fig. 14B), respectively. The low rate sensitivity observed in polyethylenes has been compared with metals [13,16]. The available data would suggest that conventional and highly crosslinked UHMWPE can be modeled using the same low strain rate sensitivity coefficient. Our data further suggest that the rate sensitivity coefficient may be temperature dependent, although further experiments will be needed to fully characterize the effect of temperature on rate sensitivity.

Crosslinking of orthopedic components is currently achieved using gamma or electron beam radiation [1,2]. Gamma radiation at room temperature was chosen as the method of crosslinking in the present study, because of its more widespread use among different orthopedic manufacturers. Four of the six current manufacturers of highly crosslinked orthopedic components (67%) employ room temperature gamma irradiation with dose levels ranging between 50 and 105 kGy [2]. The two remaining manufacturers achieve crosslinking by electron beam radiation at elevated temperatures (ranging between 45°C and 125°C) [2]. Based on measurements of trans-vinylene unsaturation using Fourier transform infrared spectroscopy, Muratoglu and colleagues [39] have recently shown that electron beam irradiation at elevated temperatures influences the extent of crosslinking as a function of dose when compared with room temperature gamma irradiation. Consequently, the relationships between true ultimate tensile properties and gamma radiation dose at room temperature observed in the present study may not be applicable to the commercially available crosslinked UHMWPE fabricated using electron beam irradiation at elevated temperatures. However, the methodology outlined in the present study can be readily extended to investigate the combined effects of any radiation method, post-irradiation thermal stabilization method, and temperature on mechanical behavior of UHMWPE.

5. Summary and conclusions

Three series of uniaxial tension and compression tests were conducted on two conventional and two highly crosslinked UHMWPEs. The highly crosslinked UHMWPEs were gamma irradiated at room temperature with 100 kGy and thermally processed by either annealing below the melt transition at 110°C or by remelting above the melt transition at 150°C. The true stress–strain behavior of the four UHMWPE materials was characterized as a function of strain rate and temperature. The following conclusions may be drawn based on the current series of experiments:

- Although annealing and remelting of UHMWPE are considered primarily as methods of improving

Questions? Contact FDA/CDRH/OCE/DID at CDRH-FOISTATUS@fda.hhs.gov or 301-796-8118

Records processed under FOIA Request #2014-8015; Released by CDRH on 12-8-2015

oxidation resistance, thermal processing also significantly alters the crystallinity, and hence the mechanical behavior, of highly crosslinked UHMWPE.

- The crystallinity and radiation doses are key predictors of the uniaxial yielding, plastic flow, and failure properties of conventional and highly crosslinked UHMWPEs.
- Between 20°C and 60°C, the thermomechanical behavior of conventional and highly crosslinked UHMWPE materials are accurately predicted using an Arrhenius model, and the associated activation energies for thermal softening are related to the crystallinity of the polymer.
- Conventional and highly crosslinked UHMWPEs exhibit low strain rate dependence in power law relationships, comparable to metals. The rate dependence of the UHMWPEs may be sensitive to test temperature, but is apparently not sensitive to gamma irradiation or thermal processing.

In light of the unifying trends observed in the true stress–strain curves of the four materials investigated in this study, both crosslinking (governed by the gamma radiation dose) and crystallinity (governed by the thermal processing) were found to be useful predictors of the mechanical behavior of UHMWPE for a wide range of test temperatures and rates. The data collected in this study will be used to develop and validate constitutive models based on the physics of polymer systems for predicting the thermomechanical behavior of conventional and crosslinked UHMWPE used in total joint replacements.

Acknowledgements

Supported by NIH Grant R01 AR 47192 and by a research grant from Stryker Howmedica Osteonics. Special thanks to Lauren Ciccarelli and Charles Jewett, Exponent Inc., for performing the compression and tension testing, and to Chuck Fox, Temple University, for performing the DSC measurements.

References

[1] Kurtz SM, Muratoglu OK, Evans M, Edidin AA. Advances in the processing, sterilization, and crosslinking of ultra-high molecular weight polyethylene for total joint arthroplasty. Biomaterials 1999;20:1659–88.

[2] Muratoglu OK, Kurtz SM. Alternative bearing surfaces in hip replacement. In: Sinha R, editor. Hip replacement: current trends and controversies. New York: Marcel Dekker, 2002.

[3] McKellop H, Shen FW, Lu B, Campbell P, Salovey R. Development of an extremely wear-resistant ultra-high molecular weight polyethylene for total hip replacements. J Orthop Res 1999;17:157–67.

[4] Edidin AA, Kurtz SM. Development and validation of the small punch test for UHMWPE used in total joint replacements. In: Katsube N, Soboyejo W, Sacks M, editors. Functional biomaterials. Winterthur, Switzerland: Trans Tech Publications Ltd., 2001.

[5] Lewis G. Properties of crosslinked ultra-high-molecular-weight polyethylene. Biomaterials 2001;22:371–401.

[6] Sun DC, Wang A, Stark C, Dumbleton JH. The concept of stabilization in UHMWPE. Transactions of the Fifth World Biomaterials Congress, vol. 1, 1996. p. 195.

[7] McKellop H, Shen FW, Salovey R. Extremely low wear of gamma-crosslinked/remelted UHMW polyethylene acetabular cups. Transactions of the 44th Orthopedic Research Society, vol. 23, 1998. p. 98.

[8] Muratoglu OK, Bragdon CR, O'Connor DO, Jasty M, Harris WH. A novel method of cross-linking ultra-high-molecular-weight polyethylene to improve wear, reduce oxidation, and retain mechanical properties. Recipient of the 1999 HAP Paul Award. J Arthroplasty 2001;16:149–60.

[9] Muratoglu OK, Bragdon CR, O'Connor DO, Jasty M, Harris WH, Gul R, McGarry F. Unified wear model for highly crosslinked ultra-high molecular weight polyethylenes (UHMWPE). Biomaterials 1999;20:1463–70.

[10] Bergström JS, Kurtz SM, Rimnac CM, Edidin AA. Constitutive modeling of ultra-high molecular weight polyethylene under large-deformation and cyclic loading conditions. Biomaterials 2002;23:2329–43.

[11] Kurtz SM, Bergström JS, Rimnac CM, Edidin AA. Multiaxial validation of constitutive theories for UHMWPE. Transactions of the 27th Annual Meeting of the Society for Biomaterials, vol. 24, 2001. p. 310.

[12] Kurtz SM, Pruitt L, Jewett CW, Crawford RP, Crane DJ, Edidin AA. The yielding, plastic flow, and fracture behavior of ultra-high molecular weight polyethylene used in total joint replacements. Biomaterials 1998;19:1989–2003.

[13] G'Sell C, Jonas JJ. Determination of the plastic behaviour of solid polymers at constant true strain rate. J Mater Sci 1979;14:583.

[14] G'Sell C, Hiver JM, Dahoun A, Souahi A. Video-controlled tensile testing of polymers and metals beyond the necking point. J Mater Sci 1992;27:5031–9.

[15] G'Sell C, Paysant-Le Roux B, Dahoun A, Cunat C, von Stebut J, Mainard D. Plastic behaviour and resistance to wear of ultra-high molecular weight polyethylene. Deformation, Yield Fracture Polym 1997;10:57–60.

[16] Lin L, Argon AS. Review: structure and plastic deformation of polyethylene. J Mater Sci 1994;29:294–323.

[17] Bergmann G, Graichen F, Rohlmann A, Verdonschot N, van Lenthe GH. Frictional heating of total hip implants, Part 1: measurements in patients. J Biomech 2001;34:421–8.

[18] Bergmann G, Graichen F, Rohlmann A, Verdonschot N, van Lenthe GH. Frictional heating of total hip implants. Part 2: finite element study. J Biomech 2001;34:429–35.

[19] Lu Z, McKellop H. Frictional heating of bearing materials tested in a hip joint wear simulator. Proc Inst Mech Eng [H] 1997;211:101–8.

[20] Kurtz SM, Bartel DL, Rimnac CM. Post-irradiation aging affects the stresses and strains in UHMWPE components for total joint replacement. Clin Orthop 1998;350:209–20.

[21] Bartel DL, Rawlinson JJ, Burstein AH, Ranawat CS, Flynn Jr. WF. Stresses in polyethylene components of contemporary total knee replacements. Clin Orthop 1995;317:76–82.

[22] Morlock M, Schneider E, Bluhm A, Vollmer M, Bergmann G, Muller V, Honl M. Duration and frequency of every day activities in total hip patients. J Biomech 2001;34:873–81.

[23] Paul JP. Forces transmitted by joints in the human body. Proc Inst Mech Eng 1966;Pt 3F:8:.

Questions? Contact FDA/CDRH/OCE/DID at CDRH-FOISTATUS@fda.hhs.gov or 301-796-8118

Records processed under FOIA Request #2014-8015; Released by CDRH on 12-8-2015

[24] ASTM F 648-96. Standard specification for ultra-high-molecular-weight polyethylene powder and fabricated form for surgical implants. West Conshohocken, PA: American Society for Testing and Materials, 1996.
[25] Edidin AA, Pruitt L, Jewett CW, Crane DJ, Roberts D, Kurtz SM. Plasticity-induced damage layer is a precursor to wear in radiation-cross-linked UHMWPE acetabular components for total hip replacement. Ultra-high-molecular-weight polyethylene. J Arthroplasty 1999;14:616–27.
[26] Wang A, Essner A, Polineni VK, Stark C, Dumbleton JH. Lubrication and wear of ultra-high molecular weight polyethylene in total joint replacements. Tribol Int 1998;31:17–33.
[27] Rimnac CM, Klein RW, Burstein AH, Wright TM, Santner TJ. In vitro chemical and mechanical degradation of UHMWPE: one year results. Transactions of the 44th Orthopedic Research Society, vol. 19, 1994. p. 175.
[28] Kurtz SM, Jewett CW, Foulds JR, Edidin AA. A miniature-specimen mechanical testing technique scaled to the articulating surface of polyethylene components for total joint arthroplasty. J Biomed Mater Res (Appl Biomater) 1999;48:75–81.
[29] ASTM D 638-98. Standard test method for tensile properties of plastics. West Conshohocken, PA: American Society for Testing and Materials, 1998.
[30] ASTM D 695-96. Standard test method for compressive properties of rigid plastics. West Conshohocken, PA: American Society for Testing and Materials, 1996.
[31] Butler MF, Donald AM, Ryan AJ. Time resolved simultaneous small- and wide-angle X-ray scattering during polyethylene deformation—II. Cold drawing of linear polyethylene. Polymer 1998;39:39–52.
[32] Young RJ. Introduction to polymers. London: Chapman & Hall Ltd., 1983.
[33] Ward IM, Hadley DW. An introduction to the mechanical properties of solid polymers. Chichester: Wiley, 1993.
[34] Pampillo CA, Davis LA. Temperature dependence of the yield and flow stresses of linear high-molecular-weight polyethylene. J Appl Phys 1972;42:4277–85.
[35] Boyd RH. Relaxation processes in crystalline polymers: experimental behavior—a review. Polymer 1985;26:323–47.
[36] Cooper JR, Dowson D, Fisher J. Macroscopic and microscopic wear mechanisms in ultra-high molecular weight polyethylene. Wear 1993;162–164:378–84.
[37] Kurtz SM, Rimnac CM, Pruitt L, Jewett CW, Goldberg V, Edidin AA. The relationship between the clinical performance and large deformation mechanical behavior of retrieved UHMWPE tibial inserts. Biomaterials 2000;21:283–91.
[38] Stojek MD, Li S. The effect of strain rate on the tensile properties of ultra high molecular weight polyethylene. Transactions of the 21st Society of Biomaterials, vol. 18, 1995. p. 112.
[39] Muratoglu OK, Harris WH. Identification and quantification of irradiation in UHMWPE through trans-vinylene yield. J Biomed Mater Res 2001;56:584–92.

Questions? Contact FDA/CDRH/OCE/DID at CDRH-FOISTATUS@fda.hhs.gov or 301-796-8118

Records processed under FOIA Request #2014-8015; Released by CDRH on 12-8-2015

Available online at www.sciencedirect.com
SCIENCE DIRECT®
ELSEVIER
Biomaterials 27 (2006) 24–34
Biomaterials
www.elsevier.com/locate/biomaterials

Anisotropy and oxidative resistance of highly crosslinked UHMWPE after deformation processing by solid-state ram extrusion

Steven M. Kurtz[a,b,*], Dan Mazzucco[a,b], Clare M. Rimnac[c], Dave Schroeder[d]

[a]Exponent, Inc., 3401 Market St., Suite 300, Philadelphia, PA 19104, USA
[b]School of Biomedical Engineering, Science, and Health Systems, Drexel University, 3141 Chestnut St., Philadelphia, PA 19104, USA
[c]Musculoskeletal Mechanics and Materials Laboratories, Departments of Orthopaedics and Mechanical and Aerospace Engineering, Case Western Reserve University, Cleveland, OH, USA
[d]Biomet Inc., 56 East Bell Drive, Warsaw, IN 46582, USA

Received 23 February 2005; accepted 27 May 2005
Available online 8 August 2005

Abstract

Solid-state deformation processing is a promising technique for modifying the physical and mechanical properties of highly crosslinked ultra-high molecular weight polyethylene (UHMWPE) beyond simple thermal treatment cycles that have been employed previously. This study evaluates anisotropy and oxidative resistance in a novel, radiation crosslinked (50 kGy) UHMWPE material (ArComXL: Biomet, Inc., Warsaw, IN), incorporating solid-state, deformation processing by extrusion below the melt transition for application in total hip arthroplasty. Tensile, compression, and small punch tests were conducted to evaluate the material properties in the three principal axes of the resulting material. Furthermore, short-term oxidative resistance was evaluated using Fourier transform infrared spectroscopy and the small punch test in conjunction with accelerated shelf aging protocols. The results of this testing indicate that the material is anisotropic, with significantly enhanced strength oriented along the long axis of the rod. For certain other properties, the magnitude of the anisotropy was relatively slight, especially in the elastic regime, in which only a 20% difference was noted between the long axis of the rod and the orthogonal, radial direction. The highly crosslinked material contains detectable free radicals, at a concentration that is 90% less than control, gamma inert sterilized UHMWPE. An unexpected finding of this study was evidence of oxidative stability of the deformation-processed material, even after 4 weeks of accelerated aging in a pressure vessel containing five atmospheres of oxygen (ASTM F2003), which resulted in macroscopic embrittlement of the control material. The oxidative stability observed in ArComXL suggests that the deformation-processed material may be suitable for air-permeable packaging and gas sterilization, which has thus far been reserved for remelted highly crosslinked UHMWPE.
© 2005 Elsevier Ltd. All rights reserved.

Keywords: UHMWPE; Ultra-high molecular weight polyethylene; Radiation crosslinking; Gamma radiation; Mechanical properties; Oxidation; Anisotropy; Solid-state extrusion; Deformation processing

1. Introduction

Highly crosslinked, wear-resistant ultra-high molecular weight polyethylene (UHMWPE) is now widely used in acetabular components for total hip replacements [1,2]. There remains great interest by members of the orthopedic community in alternate methods for processing of radiation crosslinked UHMWPE to improve mechanical properties while still retaining wear resistance and oxidative stability. Current highly crosslinked UHMWPE materials have not yet gained widespread acceptance for total knee arthroplasty, due in part to concerns about the reduced fatigue and fracture resistance relative to conventional UHMWPE [3–5].

Mechanical deformation is a well-established general method of enhancing the strength of polymers, including

*Corresponding author. Exponent, Inc., 3401 Market St., Suite 300, Philadelphia, PA 19104, USA. Tel.: +1 215 594 8800; fax: +1 215 594 8899.
E-mail address: skurtz@exponent.com (S.M. Kurtz).

0142-9612/$ - see front matter © 2005 Elsevier Ltd. All rights reserved.
doi:10.1016/j.biomaterials.2005.05.102

Questions? Contact FDA/CDRH/OCE/DID at CDRH-FOISTATUS@fda.hhs.gov or 301-796-8118

Records processed under FOIA Request #2014-8015; Released by CDRH on 12-8-2015

linear polyethylenes [6,7]. A variety of mechanical deformation processes, including cold drawing, unaxial or confined compression, and die drawing are used in the industrial production of fibers, films, sheets, pipes, and extruded forms of polyethylene [6–10]. Mechanical deformation enhances strength of polyethylene by orienting crystalline planes with respect to the principal deformation axes [9]. Mechanical deformation also increases the alignment of molecular chains, as well as the density of tie molecules, within the amorphous phase of polyethylene [11]. Further modification of the properties may be obtained by deformation processing polyethylene either above or below the melt transition, and by radiation crosslinking the polyethylene, either before or after deformation processing [8–11].

Deformation processing of UHMWPE for orthopedic implants is uniquely complicated by the high melt viscosity of the polymer, as well as by the physical size requirements of hip and knee components. Of the previously mentioned methods, compression molding, die drawing, and extrusion are among the most practical candidates for processing of UHMWPE for implants. Ohta et al. [12–14] have reported the successful enhancement of crosslinked UHMWPE mechanical properties by deformation processing above the melt temperature. In Ohta's previous experiments, crosslinked and oriented UHMWPE were prepared by uniaxial compression of radiation-crosslinked blocks between flat plates [12,13]. Die drawing is another deformation processing method that has been used successfully with UHMWPE [7,15]. During die drawing, a rectangular sheet of UHMWPE is heated below the melt temperature (110 °C) and pulled through a rectangular slotted die [15]. Slot-drawn virgin, non-crosslinked UHMWPE was found to exhibit anisotropic material properties, but the wear resistance of the material biaxially oriented in this manner was not affected [15].

Anisotropy in a material is of little value unless it can be exploited by and harmonized with design. For example, the ultra-high modulus and strength achieved by drawing or spinning of UHMWPE fibers is appropriate for applications that require resistance to uniaxial tension. In UHMWPE components for joint replacement, on the other hand, the stresses at the bearing surface are typically multiaxial, and the magnitude of the stresses further depends on the conformity of the joint, which differ in hip versus knee arthroplasty [16]. Hence, the extreme anisotropy achieved by very high draw ratios ($\gg 2$) in UHMWPE, which result in a trade-off in strength and modulus in orthogonal directions [15], may not be universally suited for all total joint applications.

Solid-state extrusion is a novel method for deformation processing of radiation crosslinked UHMWPE rods on a commercially relevant scale for the manufacture of orthopedic implants. In this study, we hypothesized that deformation-processed, radiation crosslinked UHMWPE would exhibit anisotropic mechanical behavior. We further hypothesized that deformation processing would influence the oxidative stability of the UHMWPE. The primary purpose of this study was to quantify the extent of anisotropy in the static and fatigue mechanical properties of highly crosslinked UHMWPE that was deformation processed by solid-state extrusion. A secondary purpose of this study was to evaluate the effect of accelerated aging on the small punch and oxidative properties of the deformation-processed UHMWPE.

2. Materials and methods

2.1. UHWMPE formulation and physical property characterization

Two UHMWPE formulations were evaluated, both starting from isostatically molded bar stock that was consolidated from GUR 1050 resin (Ticona, Inc., Bishop, TX). As a control, specimens machined from isostatically molded GUR 1050 were packaged in an argon environment and gamma sterilized with 25–40 kGy (ArCom: Biomet, Inc., Warsaw, IN). Since this material was consolidated by isostatic molding, it was assumed that the material properties were isotropic.

Anisotropy was evaluated in radiation crosslinked, deformation-processed UHMWPE (ArCom XL: Biomet, Inc., Warsaw, IN). The ArCom XL was produced using the following five steps:

(1) *Radiation crosslinking*: The isostatically molded rods were gamma radiation crosslinked with a nominal dose of 50 kGy. This level of crosslinking has previously been shown to result in a substantial reduction of wear, both in a hip simulator and in clinical studies, as compared with conventional UHMWPE [2,17].
(2) *Preheating*: Prior to deformation processing, the radiation crosslinked UHMWPE was raised to 130 °C. Heating of the UHMWPE facilitates the subsequent deformation processing step. Maintaining the UHMWPE below the melt transition also reduces the concentration of free radicals and maintains the crystalline microstructure prior to deformation processing [18].
(3) *Solid-state, hydrostatic extrusion*: The heated bar was then ram extruded through a circular die, with a diametral compression ratio of 1.5. This processing step induces plastic deformation and orientation of the molecules in the UHMWPE [7].
(4) *Stress relief, annealing*: The deformed bar went through a final annealing step at 130°, to relieve residual stresses [19]. The annealing also improves dimensional stability in the material [19]. The extruded rod retains 90–95% of its initial diameter after the stress relief step.
(5) *Gas plasma sterilization*: The UHMWPE was gas sterilized; this does not further modify the chemical or physical properties of the polymer [20].

Questions? Contact FDA/CDRH/OCE/DID at CDRH-FOISTATUS@fda.hhs.gov or 301-796-8118

Records processed under FOIA Request #2014-8015; Released by CDRH on 12-8-2015

2.2. Specimen preparation and orientation

Test specimens were milled from the rod stock parallel or perpendicular to the long axis of the processed rods of UHMWPE (Fig. 1). For compression tests and accelerated aging in our study, right rectangular prism specimens were evaluated. These specimens measured 12.7 mm × 12.7 mm × 25.4 mm (0.50 in × 0.50 in × 1.00 in) as per the ASTM Standard Test Method for Compressive Properties of Rigid Plastics (ASTM D 695-02a). In addition to being a preferred specimen size in the standard for determining stress–strain behavior, a similar size specimen has been used previously to calculate elastic modulus of conventional and highly crosslinked UHMWPE in compression [21,22].

One pair of faces of each rectangular specimen was perpendicular to the long axis of the rod stock (Fig. 1). It was possible to obtain specimens oriented with the long axis of the rod stock; these specimens were assigned the label "Long Axis 1." It was also possible to obtain specimens oriented radially in at least one axis perpendicular to the long axis. This axis was assigned the label "Radial Axis 3." The axis mutually perpendicular to Axes 1 and 3 was assigned the label "Radial Axis 2."

For tensile tests, dumbbell-shaped tensile specimens consistent with the Type IV and V specimen description provided in ASTM D638-02a were tested. Specimens were 3.2 ± 0.1-mm-thick. Specimens were oriented parallel or perpendicular to the long axis (Fig. 1).

2.3. Compression testing

A total of 20 specimens were tested in uniaxial compression. Fifteen specimens were ArCom XL, and five were controls. A group of five ArCom XL specimens whose long axis was coincident with the long axis of the UHMWPE rod stock (i.e., Long Axis 1; see Fig. 1) and a group of 10 specimens was oriented in two configurations along Radial Axis 3 (see Fig. 1).

The prism specimens were placed between two parallel platens in an MTS MiniBionix II servo-hydraulic test system (MTS, Eden Prairie, MN; see Fig. 1) and tested at 1.3 mm/min in unconfined compression at 21 ± 1 °C in accordance with ASTM D 695-02a. Specimens were cyclically loaded for 10 cycles within the elastic regime to determine elastic modulus and Poisson's ratio. Axial strain and lateral strains were simultaneously measured using extensometers with a gauge length of 10 mm (Epsilon Technology Corporation; Jackson, WY).

In all, two moduli of elasticity and four Poisson's ratios were calculated for ArCom XL. Since the control material was assumed to be isotropic, one modulus of elasticity and one Poisson's ratio was calculated for this material. To maintain uniformity of testing, and to verify our ability to detect anisotropy, each GUR 1050 specimen was tested twice; the extensometers were reconfigured between tests to measure ν on two different faces.

After characterization of the small-strain elastic behavior, the extensometers were removed and the specimens were tested at 1.3 mm/min at large strains to the limit of the load cell, which was reached as a maximum compressive load of −29.5 kN, or until the specimen fell off the platens. During testing, the specimens were videotaped using a digital video camera recorder (Model DCR-TRV900; Sony Corporation, Tokyo, Japan) to enable later evaluation of failure mechanisms during large-strain compression. Engineering and true stress–strain curves were generated from each of the 20 tests. Additionally, 0.2% offset compressive yield stress and percent compressive strain at 0.2% offset yield were calculated.

2.4. Tension testing

A total of 25 test specimens were tested in uniaxial tension. One group of five specimens were control; the remaining 20 were ArComXL specimens, divided into four groups based upon their orientation. One group included five Type V ArCom XL specimens whose long axis was coincident with the long axis of the UHMWPE rod stock (i.e., Long Axis 1; see Fig. 1B), a group of five Type IV specimens whose long axis was coincident with Radial Axis 2 (see Fig. 1C), and two groups of five Type V specimens oriented in two configurations along Radial Axis 3 (see Fig. 1D and E).

Testing was performed at a temperature of 21 ± 1 °C and a relative humidity of 46 ± 6%. The specimens were placed in an Instron 4204 electro-mechanical test machine (Instron, Canton, MA) and pulled apart at a rate of 10 mm/min (Type V

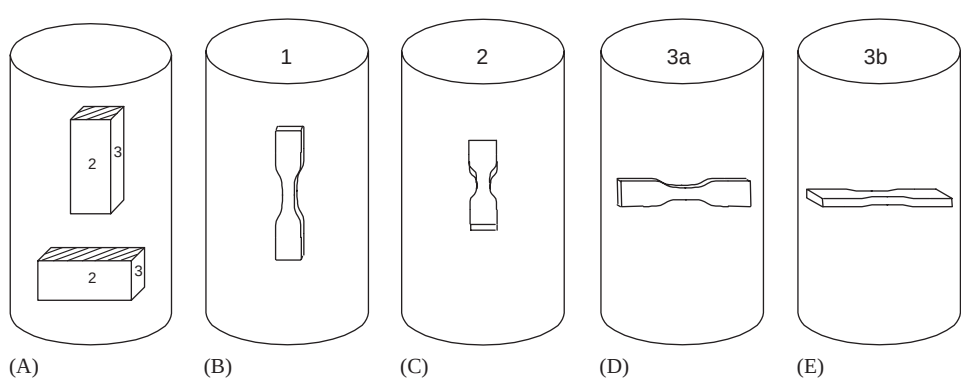

Fig. 1. Orientation of rectangular and tensile specimens with respect to the long axis (Axis 1) of the rod. (A) For rectangular specimens, Axis 1 (the long axis of the rod) is identified with diagonal stripes. Radial Axes 2 and 3 are identified according to the schematic. (B–E) For tensile specimens, the long axis of the specimen is identified as shown. (D,E) Specimens grouped "3a" and "3b" shared the same long axis, but their secondary axes were swapped.

Questions? Contact FDA/CDRH/OCE/DID at CDRH-FOISTATUS@fda.hhs.gov or 301-796-8118

Records processed under FOIA Request #2014-8015; Released by CDRH on 12-8-2015

specimens) or 50 mm/min (Type IV specimens), which resulted in approximately 5 min to rupture, as recommended by ASTM D638-02a. During tensile testing, axial strain was measured using a video extensometer.

The resulting load–displacement outputs were converted to both engineering stress–strain and true stress–strain curves. True strain was calculated from engineering strain using the formulas $\varepsilon_T = \ln(1+\varepsilon_E)$ and $\sigma_T = \sigma_E(1+\varepsilon_E)$, where ε is strain, σ is stress, and the subscripts T and E represent "true" and "engineering," respectively, as described previously [22].

The curves were characterized by an initial elastic region, followed by yielding, strain hardening, and eventual rupture. From the stress–strain curves, engineering and true yield stress, engineering and true percentage elongation at yield, engineering and true tensile strength, and engineering and true percentage elongation at break were calculated for each specimen as per ASTM D638-02a.

2.5. Fatigue crack propagation testing

Fatigue crack propagation tests were conducted on an Instron closed-loop servohydraulic test system using ASTM E647 as a guide [23]. Eight specimens of the compact tension type were evaluated, including two of the control material and six of ArCom XL material (two specimens were tested in each of the three reference axes, as indicated in Fig. 1).

The notch was razor sharpened at least 24 h prior to testing and the specimen thickness was recorded. A sinusoidal waveform was used with a frequency of 3 Hz and an R-ratio of 0.1 (ratio of minimum load to maximum load). Specimens were cooled with an air jet to minimize specimen heating during cycling. Crack growth was followed using a traveling microscope with a resolution of 0.01 mm. The crack length and the number of cycles were initially recorded approximately every 0.2 mm. When the 0.2 mm of crack growth was reached in less than 100 cycles the measurements were taken at 0.1 mm intervals. Crack length measurements were taken with the specimen at the mean load. Specimens were cycled until the crack opening displacement was too large to obtain useful fatigue crack growth data (i.e., the specimens did not fracture catastrophically).

Calculations of the fatigue crack growth rate, da/dn, and the cyclic stress intensity factor, ΔK, were made following ASTM E 647 [23]. The data for each specimen were examined using linear regression to determine the exponent (m) and coefficient (C) of the Paris relationship ($da/dn = C\,\Delta K^m$). The Paris regime was defined as the data in the crack growth rate (da/dn) range of 1×10^{-4}–1×10^{-2} mm/cycle. Statistical comparisons were conducted between test groups with respect to both C and m. Statistical significance was determined at $p<0.05$.

The cyclic stress intensity required to produce a crack growth rate of 10^{-6} mm/cycle was used to determine as $\Delta K_{\text{inception}}$, when available [3]. When this value was not available, an estimate of $\Delta K_{\text{inception}}$ was made by visual inspection of the da/dn versus ΔK curves for each treatment group. The lower estimated $\Delta K_{\text{inception}}$ of the two specimens in a treatment group was determined. As defined by Baker et al. [3], $\Delta K_{\text{inception}}$ is the upper bound of the near-threshold regime. As such, it defines the initial crack growth rate at the onset of the Paris region. Thus, $\Delta K_{\text{inception}}$ indicates the resistance to fatigue crack initiation from a pre-existing crack or defect or stress concentration.

2.6. Swell ratio

Swelling experiments were conducted to evaluate the anisotropy of the radiation crosslinking, to complement the mechanical testing results. The swell ratio (SR) of the UHMWPE materials ($n=3$) was characterized using a custom-built SR tester in accordance with ASTM F2215 in o-xylene at 130 °C. The SR of UHMWPE at equilibrium with an appropriate solvent is related to its average crosslink density; the higher the SR, the lower the density of crosslinking and the higher the molecular weight between crosslinks. The SR for an isotropic material is defined as the ratio of the final (V_f) to initial (V_i) volumes of the sample:

$$\mathrm{SR} = V_f/V_i = (h_f/h_i)^3,$$

where h_f and h_i are the final (swollen) and initial heights of the sample, respectively. For an anisotropic material, the anisotropic SR is defined as

$$\mathrm{SR} = (h_{f,\text{axis }1}\,h_{f,\text{axis }2}\,h_{f,\text{axis }3})/(h_{i,\text{axis }1}\,h_{i,\text{axis }2}\,h_{i,\text{axis }3}),$$

where h_f and h_i are now measured with respect to three orthogonal axes (axis 1, axis 2, axis 3). Crosslink density was calculated based on the equations listed in ASTM F2215.

2.7. Accelerated aging

A total of 35 ArCom XL and control rectangular blocks were tested before or after accelerated aging to evaluate the oxidative stability of the materials (Table 1). Twelve specimens were not aged. Twenty-three specimens were aged in five atmospheres of oxygen accordance with ASTM F 2003-00. Twelve specimens were aged for 2 weeks according to this standard, and 11 were aged for 4 weeks, rather than 2. Aging

Table 1
Accelerated aging experimental matrix

Material	Test axis	Sterilization	Number of prisms tested as received	Number of prisms aged 2 weeks, then tested	Number of prisms aged 4 weeks, then tested
ArCom XL	Long 1	GP	3	3	3
ArCom XL	Radial 2	GP	3	3	3
ArCom XL	Radial 3	GP	3	3	3
Control	N/A	γ Inert	3	3	2

γ Inert = gamma sterilization in an inert environment; GP = gas plasma

Questions? Contact FDA/CDRH/OCE/DID at CDRH-FOISTATUS@fda.hhs.gov or 301-796-8118

Records processed under FOIA Request #2014-8015; Released by CDRH on 12-8-2015

was performed in a stainless steel pressure vessel, as described previously [24,25]. The specimens were chosen and oriented such that the tested axis was vertical. Thus, the top and bottom faces were perpendicular to the test axis. The top face was labeled for later identification. The vessels were then filled with oxygen and purged five times to ensure the purity of the aging environment. The prisms rested on a flat surface inside the pressure vessel; thus each prism's bottom face was not exposed to oxygen, but each of its other faces were exposed to oxygen throughout the aging period. It is important to note that the blocks were not placed within barrier packaging during aging. Thus, the control blocks were aged in a way not representative of the normal shelf aging of ArCom, which is barrier packaged to protect it from exposure to oxygen. The aging method utilized in this study was intended to represent a more aggressive mode of aging that has been used historically to represent unprotected shelf aging.

The vessel was placed in the oven at room temperature (24 ± 2 °C), and the oven was heated to the aging temperature of 70.0 ± 0.1 °C at a rate of 0.1 °C/min. Prior to conducting the aging experiments, the accuracy of the temperature control for the oven was validated to ± 0.1 °C by thermocouple measurements, and proof testing was conducted with the vessel to confirm that it retained 503 ± 7 kPa (73 ± 1 psi) of pressure without leakage. All specimens from each aging group were aged simultaneously.

2.8. Small punch testing

Before and after aging, two cylindrical cores were extracted from each rectangular specimen, and from each core, two disc-shaped specimens measuring 0.5 mm in thickness and 6.4 mm in diameter were machined. One specimen was machined from the exposed surface of the block (0–0.5 mm) and the other from the subsurface region (1.5–2.0 mm). The subsurface location of the specimens was based on previous natural aging experiments, which showed greater degradation of mechanical properties occurring below the surface at similar locations [26]. Thus, four disk specimens (two surface and two subsurface) were prepared from each sample, resulting in a total of 140 individual specimens for testing (35 samples $\times$ 2 cores $\times$ 2 specimens).

Miniature specimen (small punch) mechanical testing was performed in equibiaxial tension using the disk-shaped specimens, in accordance with F 2183-02. The small punch specimens were placed in a custom-built apparatus attached to an MTS MiniBionix II servo-hydraulic test system (MTS, Eden Prairie, MN) and deformed against a hemispherical punch moving at a constant displacement rate of 0.5 mm/min [27]. The resulting load–displacement curve was characterized by initial peak load, ultimate load, and ultimate displacement. The work to failure, calculated as the area under the load–displacement curve, provided a measure of toughness.

2.9. FTIR and ESR analysis of chemical stability

The chemical properties of the control and ArCom XL were evaluated by Fourier transform infrared spectroscopy (FTIR) in transmission (Excalibur series FTS3000 with a UMA-500 microscope attachment; Bio-Rad Laboratories, Hercules, CA) using 200 μm-thick specimens. Both materials were evaluated before and after accelerated aging. FTIR profiling was conducted perpendicular to Radial Axis 2. Radial Axis 2 was chosen because it was the only axis that showed evidence of mechanical changes after accelerated aging, as described below in the "Results: Small Punch Testing" section. Each material and aging condition was tested with ($n = 3$), for a total of 12 samples evaluated by FTIR.

Oxidation index and *trans*-vinylene index calculations were based on ASTM F 2102-01 and ASTM F 2381-04, respectively. The FTIR utilized an aperture size of 200 μm and a continuous nitrogen purge; 32 scans were performed at each step, and there was a step size of 200 μm though the thickness of the block. In these calculations, oxidation peak area is the integrated area below the carbonyl peak between 1650 and 1850 cm^{-1}. *Trans*-vinylene peak area is the integrated area below the vinyl peak between 950 and 980 cm^{-1}. As this area is often influenced by Fourier rippling at 965 cm^{-1}, the samples were lightly sanded before being scanned. Both oxidation peak area and *trans*-vinylene peak area are normalized by the integrated area below the methylene stretch between 1330 and 1396 cm^{-1}. Oxidation index was calculated by dividing the oxidation peak area by the normalization peak area. The *trans*-vinylene index is calculated by dividing the *trans*-vinylene peak by the normalization peak area.

To aid in the interpretation of oxidative stability behavior during accelerated aging, the concentration of free radicals in the unaged UHMWPE materials was characterized using an ESR spectrometer (Bruker EMX), as described previously [28]. This spectrometer operated at 9.8 GHz (X Band) microwave frequency and 100 kHz modulation/detection frequency, and it was fitted with a high-sensitivity resonator cavity. For a good spectral resolution and/or signal-to-noise ratio, modulation amplitude was varied between 0.5 and 5.0 G, and microwave power between 0.5 and 2.0 mW. Three control and three ArComXL specimens were tested. Three tests were conducted on each sample.

2.10. Statistical analysis and power calculations

When appropriate, statistically significant differences ($p < 0.05$) between axes and between the ArCom XL and the control UHMWPE were evaluated with JMP Statistical Discovery Software (SAS Institute, Cary, NC) using analysis of variance. When appropriate, effects of material, axis, and aging and depth on various mechanical parameters were also evaluated using a least-squares model.

For tension and compression tests, sample sizes of $n = 5$ and 6 were used. These sample sizes are sufficient to determine 24% and 21% or greater differences, respectively, in a mechanical parameter (with $\alpha = 0.05$ and $\beta = 0.1$) between two groups having a 10% coefficient of variation. In some cases, mechanical parameters were measured more than once from the same specimen; in these cases, the mean value was determined and considered a single test article for the purposes of analysis.

For small punch tests, the use of four specimens from each prism enabled a sample size of $n = 12$ for most comparisons (surface versus subsurface used $n = 6$). Using a two-tailed unpaired Student's t-test, $n = 12$ is sufficient to determine a

Questions? Contact FDA/CDRH/OCE/DID at CDRH-FOISTATUS@fda.hhs.gov or 301-796-8118

Records processed under FOIA Request #2014-8015; Released by CDRH on 12-8-2015

14% or greater difference in any given small punch parameter (with $\alpha = 0.05$ and $\beta = 0.1$) between two groups having a 10% coefficient of variation. A sample size of six is sufficient to determine a 21% or greater difference between two groups having a 10% coefficient of variation.

3. Results

3.1. Compression testing

Overall, the compressive mechanical behavior of the control material and ArCom XL was qualitatively similar. The control material had a significantly higher compressive modulus (1220 ± 50 MPa) than ArCom XL, in both Long Axis 1 (930 ± 70 MPa) and Radial Axis 3 (1060 ± 60) ($p \leqslant 0.002$, Table 2). The ArCom XL had a lower compressive modulus in Axis 1 than in Axis 3 ($p \leqslant 0.004$). Poisson's ratio was virtually identical in GUR 1050 (0.38 ± 0.03) and ArCom XL in the 3–1 (0.36 ± 0.07) and 3–2 (0.38 ± 0.06) directions. Poisson's ratio was slightly higher in the 1–2 (0.40 ± 0.04) and 1–3 (0.42 ± 0.05) directions for the ArCom XL, but due to the small difference between the groups for this parameter, these comparisons did not reach statistical significance. The only significant difference found in ν was that ν_{31} was less than ν_{13} ($p = 0.01$).

The offset yield behavior of the control material and ArCom XL material was also very similar. GUR 1050 specimens exhibited the highest offset yield stress (15.3 ± 2.2 MPa), followed by Radial Axis 3 of the ArCom XL (12.8 ± 1.1 MPa). Long Axis 1 specimens exhibited the lowest offset yield stress (9.5 ± 0.4 MPa).

3.2. Tension testing

For all specimens, the stress–strain curves were similar, and demonstrated an elastic region, followed by yielding behavior, and, eventually, failure (Table 2). Although all specimens exhibited yield, four of the five specimens oriented along Long Axis 1 did not exhibit an increase in strain without a concomitant increase in stress (a traditional yield point). Thus, the yield data calculated for these four specimens group were calculated using the Considére construction [29].

Significant differences in tensile behavior were found between the control and ArCom XL, and between Axis 1 and Axis 3 of the ArCom XL (Table 2). Specifically, ArCom XL exhibited a higher yield strain than control in both axes. In Axis 1, the ArCom XL specimens also exhibited higher yield stress, whereas in Axis 3, the yield stress was lower than in control. All these differences were statistically significant ($p < 0.05$) except for true yield stress, which was not found to be significantly different when comparing control to Axis 3b of ArCom XL. Long Axis 1 specimens exhibited a greater engineering tensile strength at break than any of the other groups; the control exhibited the greatest true tensile strength at break, though it was not significantly greater than that exhibited by Axis 3b. With regard to ultimate strain, control elongated the most before fracture, followed by Axis 3b, then Axis 3a of the ArCom XL. The Long Axis 1 specimens elongated the least before rupture.

3.3. Fatigue crack propagation testing

ArCom XL, evaluated in all three directions, had reduced fatigue crack propagation resistance compared to the control (Table 3, Fig. 2), as evidenced in a higher coefficient C, of the Paris regime and in a lower estimated $\Delta K_{\text{inception}}$ for the ArCom XL groups compared with the control (Table 3). The higher coefficient, C, indicates that, at a given ΔK (e.g., $\Delta K = 1.0\,\text{MPa}\sqrt{m}$), cracks grow faster in ArCom XL specimens than in control specimens. The lower $\Delta K_{\text{inception}}$ for these groups indicates that it would be easier to get a crack to grow by cyclic loading from a defect or stress

Table 2
Mean and standard deviation tensile properties for control and ArCom XL materials

	Control	ArCom XL			
Axis:	N/A (isotropic)	Axis 1	Axis 2	Axis 3a	Axis 3b
Sample size:	$n = 5$	$n = 5$	$n = 5$	$n = 5$	$n = 5$
Modulus (MPa)	1290 ± 190	920 ± 100	1330 ± 280	1350 ± 500	1030 ± 110
Tensile stress at yield (MPa)	23.9 ± 0.1	24.2 ± 0.4[a]	26.9 ± 0.3	21.5 ± 0.3	22.0 ± 0.2
Percent elongation at yield (%)	8.6 ± 0.5	12.4 ± 3.5[a]	15.4 ± 0.7	12.6 ± 0.8	13.2 ± 1.0
True tensile stress at yield (MPa)	26.0 ± 0.1	27.2 ± 1.1[a]	31.1 ± 0.5	24.2 ± 0.4	24.8 ± 0.4
True strain at yield (%)	8.3 ± 0.4	11.6 ± 3.1[a]	14.3 ± 0.7	11.9 ± 0.7	12.4 ± 0.9
Tensile strength at break (MPa)	46.8 ± 2.0	64.7 ± 4.5	63.4 ± 3.0	46.1 ± 3.5	46.4 ± 2.7
Percent elongation at break (%)	362 ± 12	207 ± 11	221 ± 16	294 ± 14	295 ± 8
True tensile strength at break (MPa)	216 ± 15	198 ± 11	203 ± 15	182 ± 19	183 ± 14
True strain at break (%)	153 ± 3	112 ± 4	117 ± 5	137 ± 4	137 ± 2

[a]For four of five specimens, yield point was determined using the Considére construction.

Questions? Contact FDA/CDRH/OCE/DID at CDRH-FOISTATUS@fda.hhs.gov or 301-796-8118

Records processed under FOIA Request #2014-8015; Released by CDRH on 12-8-2015

Table 3
Paris regime and $\Delta K_{inception}$ for each treatment group ($n = 2$)

Material	m	C	$\Delta K_{inception}$, MPa$\sqrt{m}$ (est.)
Control (GUR 1050)	11.89	3.88×10^{-9}	1.79
ArCom XL, Long Axis 1	9.44	7.13×10^{-7}	1.29
ArCom XL, Radial Axis 2	9.76	1.68×10^{-7}	1.30
ArCom XL, Radial Axis 3	10.62	1.39×10^{-7}	1.41

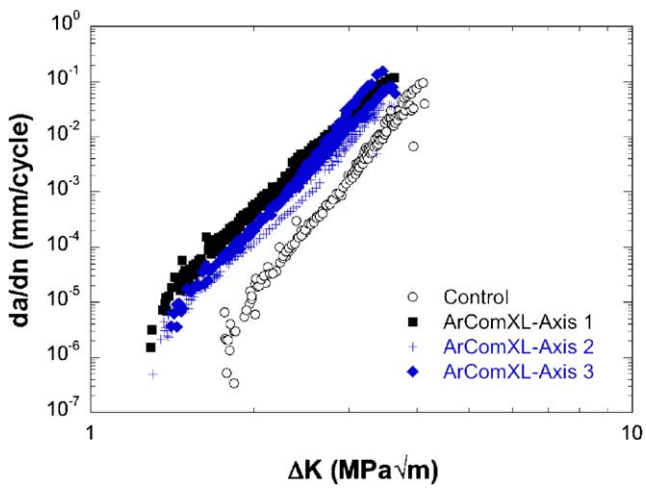

Fig. 2. Fatigue crack growth behavior, da/dn versus ΔK, for the control and ArCom XL materials ($n = 2$/group).

concentration for the ArCom XL, in all three orientations, as compared with the control (Table 3).

The fatigue crack propagation resistance of the ArCom XL was similar in all three specimen orientations (Fig. 2). Statistical analysis of the Paris regime data suggests that Long Axis 1 is less resistant to fatigue crack growth than Radial Axes 2 and 3 in the Paris regime, and that Radial Axes 2 and 3 have comparable Paris regime fatigue crack growth resistance (based on significant differences in the Coefficient C). Within the ability to estimate this variable, $\Delta K_{inception}$ appears to be similar for the three groups.

3.4. Swell ratio

The swelling measurements in o-xylene at 130 °C revealed anisotropic swell behavior for ArCom XL. The longitudinal axis and one of the radial axes exhibited comparable changes in dimension during swelling; the ratio of final to initial heights for these two axes ranged between 1.55 and 1.57. For one of the orthogonal radial directions (Fig. 1), the height ratio was 1.29 ± 0.01. The overall SR of the control and ArComXL materials was 3.33 ± 0.03 and 3.12 ± 0.04, respectively. These SRs corresponded with calculated crosslink densities of 0.172 ± 0.003 mol/dm^3 for the control material and 0.194 ± 0.005 mol/dm^3 for ArComXL.

3.5. Small punch testing

For all control and ArCom XL specimens, the load–displacement curve was consistent with that typically demonstrated by UHMWPE specimens [24], including an initial peak load, displacement by drawing, and failure. Preliminary statistical analyses revealed no significant difference between surface and subsurface specimens for any of the small punch parameters among ArCom XL specimens. Consequently, all subsequent statistical analyses considered surface and subsurface specimens together.

Significant differences in mechanical behavior were found between the control and ArCom XL prior to aging. Overall, the ArCom XL material behaved like the control in Axis 1, but was tougher and more ductile than the control in Axes 2 and 3 (Table 4). Specifically, ArCom XL exhibited a lower peak load than the control in all but one axis (Radial Axis 3, $p = 0.8$; Radial Axis 2, $p = 0.003$; Long Axis 1, $p < 0.0001$). ArCom XL exhibited a higher ultimate load than the control in all but one axis (Long Axis 1, $p = 0.9$; Radial Axis 2, $p < 0.0001$; Radial Axis 3, $p < 0.0001$). ArCom XL exhibited a higher ultimate displacement than the control in all but one axis (Long Axis 1, $p = 0.1$; Radial Axis 2, $p = 0.004$; Radial Axis 3, $p < 0.0001$). Finally, ArCom XL required more work to failure than the control in all but one axis (Long Axis 1, $p = 0.4$; Radial Axis 2, $p = 0.01$; Radial Axis 3, $p < 0.0001$).

Differences were also found among the axes of the non-aged ArCom XL material. Specimens tended to be tougher and more ductile in Axis 3 than in Axis 2, and the least tough and ductile in Axis 1. All comparisons in these groups were significantly different ($p < 0.05$) with the following exceptions: for peak load, Radial Axis 2 and Radial Axis 3 did not differ significantly; and for ultimate displacement, Radial Axis 2 did not differ significantly from either of the other axes.

After 4 weeks of accelerated aging, the ArCom XL specimens appeared grossly no different than when they were placed in the vessel. The control specimens, however, had obviously undergone degradation. When cores were removed from the control prisms, brittle

Questions? Contact FDA/CDRH/OCE/DID at CDRH-FOISTATUS@fda.hhs.gov or 301-796-8118

Records processed under FOIA Request #2014-8015; Released by CDRH on 12-8-2015

fracture was evident. The cores obtained from the ArCom XL prisms were each a single unbroken cylinder, but those obtained from the control GUR 1050 exhibited significant subsurface cracks. These cracks were sufficient to break the cylinder into two pieces. From these prisms, it was only possible to machine subsurface specimens. Thus, only four specimens were available from the two control prisms aged for 4 weeks.

The load–displacement curves of all specimens after 2 weeks of accelerated aging were consistent with those typically demonstrated by UHMWPE specimens, and consistent with those determined from specimens that were not aged. Among the control specimens, accelerated aging significantly reduced the fracture toughness (ultimate load, $p<0.0001$) and work to failure ($p=0.02$), and increased the peak load ($p<0.0001$) and ultimate displacement ($p=0.01$) (see Tables 4 and 5). These results are shown to be statistically significant when fit to a model for each parameter including the effect of depth from the surface as well as the effect of aging. Additionally, among aged control specimens, surface specimens demonstrated reduced toughness and work to failure and higher ultimate displacement relative to subsurface specimens (ultimate load and displacement, $p<0.0001$; work to failure, $p<0.002$). These results are consistent with degeneration due to oxidative degradation [24].

For ArCom XL specimens, the load–displacement curve was consistent with those reported for ArCom XL specimens aged for zero or 14 days, including an initial peak load, displacement by drawing, and fracture. Two of the four GUR 1050 specimens, however, exhibited brittle fracture, based upon both evaluation of their small punch curves and examination of the specimens themselves after testing. The ArCom XL material responded less to accelerated aging than GUR 1050 did. Since models including the effects of sterilization, axis, depth, and aging did not find any effect of specimen depth, this parameter was dropped from the model. Considering the effects of axis and aging only, the data indicated significant effects of 2 weeks of aging on the ArCom XL specimens. Overall, there was a small but significant increase in peak load ($p=0.045$), and there were decreases in ultimate displacement ($p<0.0001$) and work to failure ($p=0.0013$). The ArCom XL material still showed relatively few changes after 28 days of accelerated aging. Long Axis 1 exhibited no statistically significant changes in material properties after 28 days of aging. In Radial Axes 2 and 3, ultimate displacement was reduced, and, in Radial Axis 3, ultimate load and work to failure were reduced. These changes were statistically significant ($p<0.05$). Even though the properties in Radial Axes 2 and 3 had declined somewhat during aging, the ultimate load and work to failure for both axes were still greater than those

Table 4
Mean and standard deviation small punch parameters for aged and non-aged specimens

Small punch test parameter	Control (γ inert, isotropic)			ArCom XL (Axis 1)			ArCom XL (Axis 2)			ArCom XL (Axis 3)		
	Non-aged ($n=12$)	2 weeks ($n=12$)	4 weeks ($n=4$)	Non-aged ($n=12$)	2 weeks ($n=12$)	4 weeks ($n=12$)	Non-aged ($n=12$)	2 weeks ($n=12$)	4 weeks ($n=12$)	Non-aged ($n=12$)	2 weeks ($n=12$)	4 weeks ($n=11$)
Peak load (N)	72.2±1.8	75.6±1.1**	44.2±25.2	61.1±5.7	70.0±5.8*	64.3±5.6	67.8±6.7	64.9±2.2	66.2±8.1	71.8±1.8	75.7±2.6*	71.5±1.9
Ultimate load (N)	75.4±5.3	42.6±16.0**	23.1±1.0	75.7±8.1	90.4±13.2*	75.5±13.2	88.7±12.5	78.2±7.9*	84.6±13.9	98.4±3.9	106.8±3.7**	92.6±4.0
Ultimate disp. (mm)	3.96±0.15	4.16±0.28*	3.01±2.04	4.17±0.21	3.91±0.14*	4.17±0.33	4.37±0.33	3.69±0.22**	4.12±0.17	4.56±0.51	4.00±0.24*	3.98±0.14
Work to failure (N mm)	223±12	211±10*	101±97.2	211±16	232±27*	220±46	258±46	194±24*	228±32	298±47	267±25	239±11

Statistically significant differences between non-aged and two-week aged specimens are noted with asterisks. *$p<0.05$, **$p<0.0001$.

Questions? Contact FDA/CDRH/OCE/DID at CDRH-FOISTATUS@fda.hhs.gov or 301-796-8118

Records processed under FOIA Request #2014-8015; Released by CDRH on 12-8-2015

Table 5
Change in mean values for small punch parameters after 2 weeks accelerated aging

Small punch test parameter	Control, isotropic ($n = 12$) (%)	ArCom XL, Axis 1 ($n = 12$) (%)	ArCom XL, Axis 2 ($n = 12$) (%)	ArCom XL, Axis 3 ($n = 12$) (%)
Peak load (N)	+4.6	+14.6	NS	+5.5
Ultimate load (N)	−43.6	+19.5	−11.9	+8.6
Ultimate disp. (mm)	+5.2	−6.3	−15.6	−12.4
Work to failure (N mm)	−5.4	+9.7	−24.8	NS

Changes that were not significant are indicated by NS.

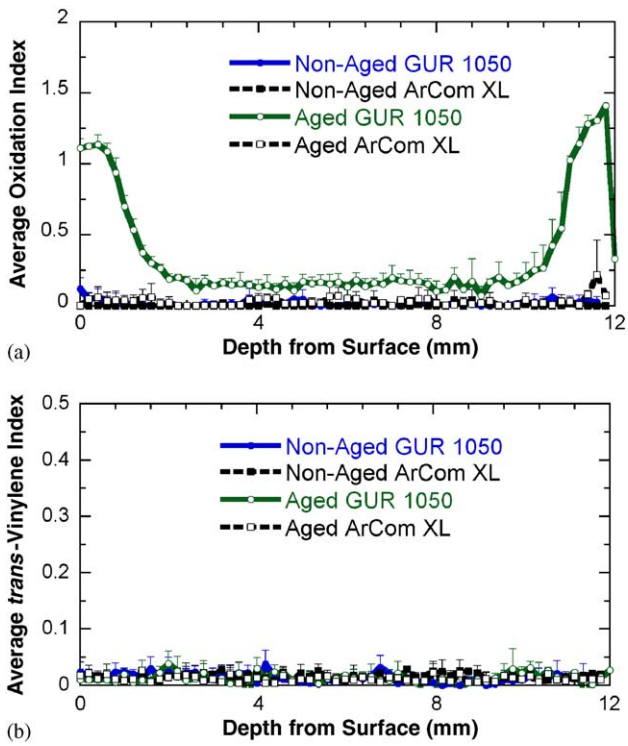

Fig. 3. ASTM oxidation index and *trans*-vinylene index for four groups of specimens.

properties exhibited by GUR 1050 prior to accelerated aging.

3.6. FTIR and ESR analysis of chemical stability

Oxidation index and *trans*-vinylene index were measured in aged and non-aged specimens of both ArCom XL (sterilized by GP) and control GUR 1050 (sterilized by gamma irradiation). The results from all four groups are summarized in Fig. 3. These curves represent the average oxidation index and *trans*-vinylene index measured for three specimens from each group. The aged control material shows oxidation near its surface. None of the other groups indicate measurable oxidation, including the aged ArCom XL. This result supports the small punch results, which indicated that ArCom XL retains its mechanical properties better than GUR 1050 after accelerated aging. There is little evidence of *trans*-vinylene groups in any of the samples.

Free radicals were detected in both the control and the ArComXL materials; however, the concentration in the ArComXL was over 90% lower than the control. This difference was significant ($p < 0.0001$). The average free radical concentration was 3.82×10^{15} spins/g in the control and 0.22×10^{15} spins/g in ArComXL.

4. Discussion

The anisotropy in ArComXL was apparent in the SR and associated network properties, as well as in the mechanical properties. However, the magnitude of the anisotropy was found to be relatively small due to the final stress relaxation step, which relieved much of the deformation and molecular orientation imparted by the previous solid-state extrusion. It is clear that ArComXL retains some memory of its previously oriented state, but the variation in properties was much less than previously observed with slot-drawn unirradiated GUR 1020 UHMWPE, having a draw ratio of 2, but which was not subjected to stress relief thermal treatment [15]. In contrast with Dharmastiti's experiment, for the present study, we evaluated radiation crosslinked GUR 1050, which was subsequently thermally relaxed from an oriented state. Notwithstanding the differences in resin and crosslinking between Dharmastiti's experiment and our study, which complicate the comparison of results, the absolute property variations we observed were generally much smaller, and more subtle, than in the previous slot drawing process. With the exception of the work to failure parameter of the small punch test, which varied by 37% (367 mJ along Axis 3 as compared with 211 mJ along Axis 1, Table 4), the remaining uniaxial, biaxial static and fatigue properties of ArComXL varied by less than 30% when compared with the different axes of testing. In terms of the compressive elastic modulus, e.g., the modulus parallel to the draw direction was 0.9 GPa, as compared with 1.1 GPa in the radial direction (e.g., a 20% difference between axes). Furthermore, we also

Questions? Contact FDA/CDRH/OCE/DID at CDRH-FOISTATUS@fda.hhs.gov or 301-796-8118

Records processed under FOIA Request #2014-8015; Released by CDRH on 12-8-2015

found evidence that the ultimate properties were not isotropic in the radial plane. Ultimate properties measured in radial direction 3 showed greater ductility (e.g., elongation to failure, resistance to crack initiation, small punch toughness) as compared with radial direction 2 and long axis 1. These results are consistent with the SR tests, which also showed a slightly greater extent of swelling in one of the radial axes.

The elastic modulus, yield stress, and ultimate stress data observed in this study all fell within the range of previously reported mechanical properties for conventional and highly crosslinked UHMWPE [18,21,30–32]. Within that broad range of previously reported mechanical properties, ArComXL shows greater similarity to annealed highly crosslinked UHMWPE materials, which exhibit a higher yield stress, resistance to plastic deformation, and ultimate strength by virtue of their higher crystalline content, relative to remelted materials [21].

Like previous studies of annealed highly crosslinked UHMWPE [18], ArComXL also contains detectable free radicals, but the concentration was reduced by over 90% relative to the gamma sterilized control material. Consequently, an unexpected finding of this study was that ArComXL showed little evidence of oxidation even after 4 weeks of accelerated aging, similar to previous aging studies of remelted UHMWPE materials [30,33]. The clinical relevance of accelerated aging studies remains controversial because the standardized protocol has only been shown to reproduce certain oxidation trends of UHMWPE materials that were gamma irradiated in air and that were stored in air—a packaging technique that is no longer used by major orthopedic manufacturers. Furthermore, the oxidizing environment associated with the standardized aging protocol employed in this study is so severe that virgin, unirradiated UHMWPE, containing no free radicals, can exhibit significant degradation [25]. Despite these shortcomings, the accelerated aging method we employed has been accepted as an international standard by both ASTM and ISO for evaluating the oxidative stability [34]. Based on the oxidation resistance displayed in the accelerated aging, which was comparable to remelted UHMWPE materials [30,33], the manufacturer has decided to use air-permeable packaging and terminally sterilize ArComXL using gas plasma. Real-time shelf aging studies are planned to test the hypothesis that ArComXL does not oxidize during shelf aging.

As mentioned previously in the introduction, anisotropy can be useful if harmonized with design. In contrast with the high-strength fibers discussed in the introduction, ArComXL is produced with a relatively low draw ratio (1.5) and is intended for total hip applications, in which the polar axis of the cup is aligned with the longitudinal axis of the extruded rod, corresponding to Axis 1 in the present study. The wall of the cup, at the equator and rim, is parallel to the long axis of the rod, and may benefit from the enhanced strength in this direction during eccentric and rim loading scenarios. Further functional fatigue testing and finite element analyses will be needed to elucidate the more subtle, complex effects of anisotropy on the mechanical behavior of acetabular components fabricated from ArComXL.

5. Conclusions

Solid-state extrusion below the melt transition was found to be a promising deformation processing technique, suitable for highly crosslinked UHMWPE on a commercially relevant scale. The deformation-processed, highly crosslinked UHMWPE was anisotropic, with enhanced ultimate tensile strength parallel to the long axis of the rod. However, relative to drawn fibers, the magnitude of the anisotropy was relatively small, especially for the elastic properties, which only varied by 20% between the longitudinal and radial axes. By comparison of our results with previous experiments with slot-drawn UHMWPE that did not undergo a final stress-relief thermal cycle, we hypothesize that the stress relaxation step in our study had the effect of reducing molecular alignment and decreasing the anisotropy in the final material. It was clear, nonetheless, that the final material retained some memory and benefits, in the form of enhanced ultimate strength, from its previously oriented state.

The deformation-processed, highly crosslinked UHMWPE contained residual free radicals, but the concentration was 90% less than the control. An unexpected finding of this study was that, despite the presence of detectable free radicals, the deformation-processed, highly crosslinked material was oxidatively stable, even after 4 weeks in a pressure vessel containing 5 atm of oxygen at 70 °C, which macroscopically embrittled gamma inert sterilized, control UHMWPE. It is unclear from the results of this study whether the free radicals in the deformation-processed UHMWPE are inherently highly stabilized (and hence inherently resistant to oxidative degradation) or whether they are trapped within crystalline regions, and hence merely unavailable to participate in the oxidation process.

Acknowledgments

Supported by a Research Grant from Biomet, Inc. Fatigue crack propagation testing was conducted by Jay Bensusan.

Questions? Contact FDA/CDRH/OCE/DID at CDRH-FOISTATUS@fda.hhs.gov or 301-796-8118

Records processed under FOIA Request #2014-8015; Released by CDRH on 12-8-2015

References

[1] Martell JM, Verner JJ, Incavo SJ. Clinical performance of a highly cross-linked polyethylene at two years in total hip arthroplasty: a randomized prospective trial. J Arthroplasty Oct 2003;18(7 Suppl 1):55–9.

[2] Heisel C, Silva M, dela Rosa MA, Schmalzried TP. Short-term in vivo wear of cross-linked polyethylene. J Bone Jt Surg Am Apr 2004;86-A(4):748–51.

[3] Baker D, Hastings RS, Pruitt L. Study of fatigue resistance of chemical and radiation crosslinked medical grade ultrahigh molecular weight polyethylene. J Biomed Mater Res 1999;46(4): 573–81.

[4] Bradford L, Baker DA, Graham J, Chawan A, Ries MD, Pruitt LA. Wear and surface cracking in early retrieved highly cross-linked polyethylene acetabular liners. J Bone Jt Surg Am Jun 2004;86-A(6):1271–82.

[5] Halley D, Glassman A, Crowninshield RD. Recurrent dislocation after revision total hip replacement with a large prosthetic femoral head. A case report. J Bone Jt Surg Am Apr 2004;86-A(4):827–30.

[6] Porter RS, Kanamoto T, Zachariades AE. Property opportunities with polyolefins: a review. Preparations and applications of high stiffness and strength by uniaxial draw. Polymer 1994;11, 35(23): 4979–84.

[7] Ward IM. Recent developments in oriented polymers for biomedical and engineering applications. Macromol Symp 2003; 195:293–6.

[8] Kitamaru R. The properties of transparent film made from linear polyethylene by irradiation cross-linking. Macromolecules 1973; 6:337–43.

[9] Kitamaru R. Size and orientation of cristallites in lightly cross-linked polyethylene, crystallized from the melt under unaxial compression. Die Makromoek Chem 1974;175:255–75.

[10] Kitamaru R. Structure and properties of lightly crosslinked crystalline polymers crystallized or processed under molecular orientation. J Polym Sci: Macromol Rev 1979;14:207–64.

[11] Josefsson J, Delin M. Molecular orientation of crosslinked polyethylene. ANTEC; 2000.

[12] Ohta M, Hyon S, Oka M, Tsutsumi S. Wear resistance of lightly cross-linked ultrahigh-molecular-weight polyethylene crystallized from the melt under uniaxial compression. Wear 1999; 225–229:312–8.

[13] Ohta M, Hyon S, Kang Y, et al. Effect of the compression ratio on wear properties of slightly cross-linked ultra-high molecular weight polyethylene, crystallized under uniaxial compression. Wear 2001;250:145–51.

[14] Ohta M, Hyon S, Tsutsumi S. Control of crystalline orientation to enhance the wear resistance of ultra-high molecular weight polyethylene crystallization cups for artificial joints. Wear 2003; 255:1045–50.

[15] Dharmastiti R, Barton DC, Fisher J, Edidin A, Kurtz S. The wear of oriented UHMWPE under isotropically rough and scratched counterface test conditions. Biomed Mater Eng 2001;11(3): 241–56.

[16] Bartel DL, Bicknell VL, Wright TM. The effect of conformity, thickness, and material on stresses in ultra-high molecular weight components for total joint replacement. J Bone Jt Surg [Am] 1986;68(7):1041–51.

[17] McKellop H, Shen FW, Lu B, Campbell P, Salovey R. Development of an extremely wear-resistant ultra high molecular weight polyethylene for total hip replacements. J Orthop Res 1999;17(2):157–67.

[18] Kurtz SM, Manley M, Wang A, Taylor S, Dumbleton J. Comparison of the properties of annealed crosslinked (Cross-fire) and conventional polyethylene as hip bearing materials. Bull Hosp Jt Dis 2002–2003;61(1–2):17–26.

[19] Miller K, Ramani K. Process-induced residual stresses in compression molded UHMWPE. Polym Eng Sci 1999;39(1): 110–8.

[20] Kurtz SM. The UHMWPE handbook: ultra-high molecular weight polyethylene in total joint replacement. New York: Academic Press; 2004.

[21] Kurtz SM, Villarraga ML, Herr MP, Bergstrom JS, Rimnac CM, Edidin AA. Thermomechanical behavior of virgin and highly crosslinked ultra-high molecular weight polyethylene used in total joint replacements. Biomaterials 2002;23(17):3681–97.

[22] Kurtz SM, Pruitt L, Jewett CW, Crawford RP, Crane DJ, Edidin AA. The yielding, plastic flow, and fracture behavior of ultra-high molecular weight polyethylene used in total joint replacements. Biomaterials 1998;19(21):1989–2003.

[23] ASTM E 647-95a. Standard test method for measurement of fatigue crack growth rates. West Conshohocken, PA: American Society for Testing and Materials; 1996.

[24] Edidin AA, Herr MP, Villarraga ML, Muth J, Yau SS, Kurtz SM. Accelerated aging studies of UHMWPE. I. Effect of resin, processing, and radiation environment on resistance to mechanical degradation. J Biomed Mater Res 2002;61(2):312–22.

[25] Edidin AA, Villarraga ML, Herr MP, Muth J, Yau SS, Kurtz SM. Accelerated aging studies of UHMWPE. II. Virgin UHMWPE is not immune to oxidative degradation. J Biomed Mater Res 2002;61(2):323–9.

[26] Edidin AA, Jewett CW, Kwarteng K, Kalinowski A, Kurtz SM. Degradation of mechanical behavior in UHMWPE after natural and accelerated aging. Biomaterials 2000;21(14):1451–60.

[27] Edidin AA, Kurtz SM. Development and validation of the small punch test for UHMWPE used in total joint replacements. In: Katsube N, Soboyejo W, Sacks M, editors. Functional Biomaterials. Winterthur, Switzerland: Trans Tech Publications Ltd.; 2001. p. 1–40.

[28] Jahan MS, Wang C. Combined chemical and mechanical effects on free radicals in UHMWPE joints during implantation. J Biomed Mater Res 1991;25:1005–17.

[29] Ward IM, Hadley DW. An introduction to the mechanical properties of solid polymers. Chichester: Wiley; 1993.

[30] Muratoglu OK, Bragdon CR, O'Connor DO, Jasty M, Harris WH. A novel method of cross-linking ultra-high-molecular-weight polyethylene to improve wear, reduce oxidation, and retain mechanical properties. Recipient of the 1999 HAP Paul Award. J Arthroplasty 2001;16(2):149–60.

[31] Abt NA, Schneider W. Influence of irradiation on the properties of UHMWPE. In: Kurtz SM, Gsell R, Martell J, editors. Highly crosslinked and thermally treated ultra-high molecular weight polyethylene for joint replacements. Vol ASTM STP 1445. West Conshohoken: American Society for Testing and Materials; 2003.

[32] Greer K, King R, Chan FW. Effects of raw material, irradiation dose, and irradiation source on crosslinking of UHMWPE. In: Kurtz SM, Gsell R, Martell J, editors. Highly crosslinked and thermally treated ultra-high molecular weight polyethylene for joint replacements. Vol ASTM STP 1445. West Conshohoken: American Society for Testing and Materials; 2003.

[33] McKellop H, Shen FW, Lu B, Campbell P, Salovey R. Development of an extremely wear-resistant ultra high molecular weight polyethylene for total hip replacements. J Orthop Res 1999;17:157–67.

[34] Kurtz SM, Muratoglu OK, Buchanan F, et al. Interlaboratory reproducibility of standard accelerated aging methods for oxidation of UHMWPE. Biomaterials 2001;22(13):1731–7.

Questions? Contact FDA/CDRH/OCE/DID at CDRH-FOISTATUS@fda.hhs.gov or 301-796-8118

Records processed under FOIA Request #2014-8015; Released by CDRH on 12-8-2015

Trace concentrations of vitamin E protect radiation crosslinked UHMWPE from oxidative degradation

S. M. Kurtz,[1,2] J. Dumbleton,[3] R. S. Siskey,[1,2] A. Wang,[4] M. Manley[5]
[1]*Exponent, Inc., 3401 Market St., Suite 300, Philadelphia, Pennsylvania 19104*
[2]*School of Biomedical Engineering, Science, and Health Systems, Drexel University, 3141 Chestnut St., Philadelphia, Pennsylvania 19104*
[3]*Consultancy in Medical Devices, Ridgewood, New Jersey*
[4]*Stryker Orthopedics, Mahwah, New Jersey*
[5]*Homer Stryker Center for Orthopedic Education, Mahwah, New Jersey*

Received 11 September 2007; revised 9 December 2007; accepted 11 December 2007
Published online 18 June 2008 in Wiley InterScience (www.interscience.wiley.com). DOI: 10.1002/jbm.a.32122

Abstract: The effect of very low concentrations of Vitamin E on the stability and mechanical behavior of UHMWPE remains unknown. We tested the hypothesis that the oxidation resistance of Vitamin E-blended UHMWPE would be influenced by trace doses of antioxidant, resin, and radiation treatment. Trace concentrations (≤500 ppm w/w%) of α-tocopherol (Vitamin E) were blended separately with GUR 1020 and 1050 resins and molded into disks. From each disk, three groups of 10 mm thick blocks were machined: (1) no irradiation (control); (2) 30 kGy of gamma irradiation in nitrogen; and (3) 75 kGy of gamma irradiation in air. Specimens were subjected to three aging protocols: (a) no aging (control); (b) two weeks and (c) four weeks of accelerated aging in accordance with ASTM F 2003 (i.e., 70°C and 5 atm oxygen). The minimum concentration of Vitamin E needed to stabilize UHMWPE during our accelerated tests depended upon the method of radiation processing. For the 30 and 75 kGy irradiated materials, the addition of 125 ppm or more Vitamin E was sufficient to maintain baseline mechanical and chemical properties through two weeks of accelerated aging. For these groups, the addition of 375 ppm or 500 ppm, respectively, was necessary to maintain baseline mechanical and chemical properties throughout the four-week accelerated aging period. UHMWPE resin molecular weight did not have an effect on oxidation behavior. The results of this experiment therefore supported our hypotheses that trace concentrations of Vitamin E, coupled with radiation treatment—but not resin grade—influence the mechanical and oxidative degradation behavior of UHMWPE. © 2008 Wiley Periodicals, Inc. J Biomed Mater Res 90A: 549–563, 2009

Key words: UHMWPE; ultra-high molecular weight polyethylene; radiation crosslinking; gamma radiation; mechanical properties; oxidation; α-tocopherol; vitamin E

INTRODUCTION

Oxidation of ultra-high molecular weight polyethylene (UHMWPE) has been recognized as a potential limiting factor for the longevity of total joint replacements.[1,2] The highest levels of oxidation have been found for polyethylene gamma sterilized in air.[3–9] Low oxygen barrier packaging was introduced to protect gamma-sterilized components during shelf storage.[10–12] Implants stored in first-generation, polymeric barrier packaging have also been found to exhibit substantial oxidation when tested beyond their expiration date.[13]

Correspondence to: S. M. Kurtz; e-mail: skurtz@exponent.com
Contract grant sponsor: Stryker Orthopedics, Inc

© 2008 Wiley Periodicals, Inc.

Regardless of how they are packaged, gamma sterilized UHMWPE components contain free radicals and oxidize in the presence of oxygen. In vivo oxidation of UHMWPE occurs, not only for gamma air materials,[14–17] but also for gamma inert and highly crosslinked UHMWPE materials as well.[18] Although its clinical significance is still the subject of scientific debate, *in vivo* oxidation is regarded as undesirable. Over the past decade, several measures to reduce free radical levels, broadly referred to as "stabilization," have been proposed for irradiated UHMWPE, including thermal stabilization above the melt transition (remelting)[19,20]; thermal stabilization below the melt transition (annealing)[21,22]; solid state deformation processing[23]; and chemical stabilization using α-tocopherol (Vitamin E).[24–26] The general mechanism of Vitamin E stabilization of UHMWPE is by now well established,[25,27–31] although many

Questions? Contact FDA/CDRH/OCE/DID at CDRH-FOISTATUS@fda.hhs.gov or 301-796-8118

Records processed under FOIA Request #2014-8015; Released by CDRH on 12-8-2015

details regarding the by-products of anti-oxidant stabilization of free radicals continue to be closely examined.[29]

Tocopherol compounds were first proposed as "hygienically safe" stabilizers for polyolefins in the early 1980s[32] and techniques were developed for blending Vitamin E with UHMWPE powder prior to consolidation for implant applications.[33] Blending 1000–3000 ppm (0.1–0.3%) of Vitamin E with UHMWPE improved the fatigue wear resistance of the material following gamma sterilization[34] and gamma-sterilized, Vitamin E-blended UHMWPE implants were introduced clinically starting in 2006 (Nakashima Medical Division, Nakashima Propeller Co., Ltd., Okayama, Japan).[28] Recent studies, employing 1000–8000 ppm (0.1–0.8%) of Vitamin E, have determined that blending the stabilizer with the powder prior to consolidation may decrease the efficiency of radiation crosslinking.[31,35] Other researchers doped highly crosslinked UHMWPE with 16,000 ppm to 400,000 ppm (1.6–40%) Vitamin E via diffusion after irradiation.[30,36] However, it may be challenging to achieve uniformity and the desired level of Vitamin E concentration when doping thick components by diffusion.[26,30,36,37]

In the food packaging industry, very low concentrations (100–300 ppm) of Vitamin E are sufficient to protect polyethylene from shelf oxidation.[38] However, the effect of such concentrations of Vitamin E on the stability and mechanical behavior of UHMWPE remains unknown. The objective of the present study was to determine the minimum Vitamin E concentration necessary to protect conventional and highly crosslinked UHMWPE from a severe, *in vitro* oxidative challenge. We tested the hypothesis that the oxidation resistance of Vitamin E blended UHMWPE would be influenced by trace levels of antioxidant (<500 ppm), resin, and radiation treatment.

MATERIALS AND METHODS

Compression molded disks

Consolidated disk samples of UHMWPE were provided by Ticona GmbH (Oberhausen, Germany). Trace concentrations (0, 125, 250, 375, and 500 ppm by weight) of α-tocopherol (Vitamin E) were blended separately with GUR 1020 (ASTM nominal 3.5 MM g/mol) and 1050 (ASTM nominal 5.5 MM g/mol) resins. A certified pharmaceutical grade of D,L-α-tocopherol was employed, and the purity of the Vitamin E was verified by the manufacturer using HPLC. Blended polymer samples were consolidated using the standardized compression molding cycle specified in ISO 11542-2. Each disk was ~20 cm in diameter, 2 cm in thickness, and was labeled as containing a unique combination of resin and Vitamin E concentration (Table I). Specimens were milled from these disks for mechanical and chemical characterization.

TABLE I
Summary of As-Received Compression Molded Disks

Resin	Vitamin E Concentration (ppm)[a]	Resin	Vitamin E Concentration (ppm)[a]
GUR 1020	0	GUR 1050	0
GUR 1020	125	GUR 1050	125
GUR 1020	250	GUR 1050	250
GUR 1020	375[b]	GUR 1050	375
GUR 1020	500	GUR 1050	500

[a]Nominal concentration reported by the manufacturer.
[b]When analyzed using FTIR, the Vitamin E concentration in this sample was not significantly different than 500 ppm.

The α-tocopherol levels reported in this study were nominal values based on the manufacturer's certification. We investigated the accuracy of the trace concentrations with FTIR, using a method similar to that reported by Oral et al.[31] We confirmed the concentrations of 250, 375, and 500 ppm GUR 1050 samples; as well as the 250 and 500 ppm GUR 1020 samples using FTIR (Personal Communication, Pierangiola Bracco, Ph.D., University of Torino, Italy). However, we were unable to detect a significant difference in α-tocopherol concentration between the 375 and 500 ppm GUR 1020 samples. The 125 ppm GUR 1020 and 1050 samples fell below the detection limit of the FTIR technique.

Tensile behavior of as-molded disks

Tensile properties were measured by testing dumbbell-shaped specimens according to the ASTM Standard Test Method for Tensile Properties of Plastics (ASTM D638-02a). For tensile tests, 50 dumbbell-shaped tensile specimens consistent with the Type V specimen description provided in ASTM D638-02a were tested. At least five specimens were machined from each of the 10 disks described above (Table I).

The specimens were placed in an Instron test system with a screw-driven load frame (Model 4505; Instron, Canton, MA) equipped with a 30 kN load cell. Specimens were pulled apart at a rate of 10 mm/min. Axial strain was measured by the relative displacement of the gauge lines using a laser extensometer (Model LE-05, Electronic Instrument Research, Irwin, PA).

Experimental design

Oxidative resistance was evaluated by aging specimens from each of the supplied disks according to the ASTM Standard Guide for Accelerated Aging of Ultra-High Molecular Weight Polyethylene (F 2003-00). From each disk, 36 blocks were machined and divided into three groups: (1) no irradiation (control); (2) 30 kGy of gamma irradia-

Questions? Contact FDA/CDRH/OCE/DID at CDRH-FOISTATUS@fda.hhs.gov or 301-796-8118

Records processed under FOIA Request #2014-8015; Released by CDRH on 12-8-2015

TABLE II
Oxidative Resistance Test Matrix

Parameter	Test Groups	Values				
Resin	2	GUR 1020			GUR 1050	
Vitamin E (ppm)	5	0	125	250	375	500
Processing	3	None		30 kGy in nitrogen	75 kGy + machining	
Aging Time	3	None		2 weeks	4 weeks	

Each combination of resin, Vitamin E concentration, processing condition, and aging time has been tested in triplicate.

tion in nitrogen (conventional sterilized UHMWPE); and (3) 75 kGy of gamma irradiation in air (highly crosslinked UHMWPE). For the highly crosslinked UHMWPE material (Group 3), 3 mm of material was removed from the surface of each block subsequent to processing in order to achieve the final 10 mm thickness. The final dimensions of all specimens were 20 mm by 15 mm by 10 mm thickness.

Each specimen was preconditioned in room air for 28 days from the start of processing. Preconditioned specimens were stored in a cryogenic freezer at −80°C until preconditioning of all specimens was completed.

From each subset of nine blocks of a given resin, Vitamin E concentration, and processing combination, three were not aged and six were aged for two weeks according to ASTM F 2003-00. After this aging period, three of the aged specimens were evaluated, and the remaining three blocks were aged for two additional weeks according to ASTM F 2003-00 (for a total of four weeks) prior to evaluation.

This test design is a full factorial design, and made it possible to evaluate the interactions among all of the test parameters. For a sample size of $n = 3$, this experimental design required a total of 270 specimens. The test matrix for the full factorial design is provided in Table II. Oxidation resistance specimens were characterized using both the small punch test and FTIR.

Accelerated aging apparatus and protocol

Aging was conducted in accordance with the ASTM F2003.[39] Aging was performed in three wide-mouth 3.8 L, 304 stainless steel pressure vessels (Advantec MFS, Dublin, CA), each fitted with a pressure gauge, vent relief valve, ball valve, and a fluoroelastomer O-ring. The bottom face of each block was labeled for later identification during subsequent evaluation. In the case of specimens that had been machined as part of their processing, the top (exposed) face was the freshly machined 20 mm by 15 mm surface. The vessels were then filled with oxygen and purged five times to ensure the purity of the aging environment. The blocks rested on flat surfaces inside the pressure vessel; thus each block's bottom face was not exposed to oxygen, but each of its other five faces was exposed to oxygen throughout the aging period. Each pressure vessel was placed in an air circulating convection oven with digital (PID) temperature control (Salvis Thermocenter: Cole-Palmer Instrument Company, Vernon Hills, IL).

The vessels were placed in the ovens at room temperature, and the ovens were heated to the aging temperature of 70°C at a rate of 0.1°C/min. During the aging experiments, the accuracy of the oven temperature controls was validated to ±0.1°C by thermocouple measurements. Proof testing was conducted with the vessel to confirm that it retained 503 ± 7 kPa (73 ± 1 psi) of pressure without leakage. During the aging period, the oven door was opened daily for a few seconds to confirm pressurization of the vessel, but the vessel itself was not opened.

All blocks were aged simultaneously. Specimens were assigned randomly to one of three ovens to minimize the ovens as confounding factors. After two weeks of aging, all specimens were removed from the aging vessels. Specimens designated to be aged four weeks in total were randomly reassigned to one of two aging vessels for the final two weeks of aging. The ovens and pressure vessels were allowed to cool to room temperature between aging experiments.

Small punch apparatus and protocol

Before and after two to four weeks of aging, one cylindrical core was extracted from each sample. From each core, one disk-shaped specimen measuring 0.5 mm in thickness and 6.4 mm in diameter was machined from the exposed surface of the block (0–0.5 mm). Miniature specimen (small punch) mechanical testing was performed according to the guidelines established in ASTM F2183.[40] Specimens were placed in a custom-built apparatus attached to an Instron test system with a screw-driven load frame (Model 4505; Instron, Canton, MA). Testing was performed at a rate of 0.5 mm/min. The resulting load-displacement curve was characterized by initial peak load, ultimate load, and ultimate displacement. The work to failure, calculated as the area under the load-displacement curve, provided a measure of toughness.

FTIR apparatus and protocol

Fourier Transform Infrared spectroscopy (FTIR) was performed on each of the block specimens to a depth of 3 mm to determine oxidation profile and *trans*-vinylene levels. To prepare the samples for FTIR microscopy, a 200-μm slice was microtomed perpendicular to the surface of the aged blocks. The section was taken at least 3 mm from the end of the sample to minimize the effects of the adjacent surfaces.

The microtomed samples were then placed under the microscope portion of a model 6700 Nicolet FTIR with a

Questions? Contact FDA/CDRH/OCE/DID at CDRH-FOISTATUS@fda.hhs.gov or 301-796-8118

Records processed under FOIA Request #2014-8015; Released by CDRH on 12-8-2015

Nicolet Continuum FT-IR microscope attachment (Thermo Electron Corporation, Madison, WI). Since the FTIR utilized an aperture size of 120 μm, the specimens were initially placed under the microscope such that the aperture covered approximately the first 120 μm down from the surface of the sample. After the initial reading was taken, the microscope stepped across the specimen in a direction perpendicular to the top surface, taking readings in 100 μm increments until the specimen had been sampled to a depth of 3 mm. A background scan was performed for each specimen and polystyrene was used to verify the machine weekly.

The resulting absorbance spectra were analyzed to determine the oxidation and *trans*-vinylene indices in accordance with ASTM F2102[41] and F 2381,[42] respectively. The maximum oxidation index (OI) and *trans*-vinylene index (TVI) were calculated for a given specimen by determining the maximum normalized peak area through the depth of the specimen. As specified in ASTM F2102, oxidation peak area was the integrated area below the carbonyl peak between 1650 and 1850 cm^{-1}.[41] The TVI peak area was the integrated area below the peak between 950 and 980 cm^{-1} as specified in ASTM F2381.[42] The peak areas were then normalized by the integrated area below the methylene peak between 1330 and 1396 cm^{-1}.

Statistical analysis

Results of the tensile testing (yield and post-yield properties) were analyzed using single factor analysis of variance (with post-hoc Tukey tests) to determine whether Vitamin E concentration significantly affected the mechanical properties of either resin type. The results of the small punch testing were analyzed using two factor analysis of variance (with post-hoc Tukey tests) to determine whether age, Vitamin E concentration, or interactions thereof significantly affected the mechanical or chemical properties of polyethylene comprised of a given resin type or processing procedure. SigmaStat V. 3.0 (Systat Software, Inc., Port Richmond, CA) and $\alpha = 0.05$ were used for all statistical tests.

RESULTS

The compression molded disks containing no added Vitamin E appeared white. The addition of Vitamin E resulted in yellowing of the disks, although increasing nominal Vitamin E concentration was not completely associated with increasing discoloration (Fig. 1). Discoloration of the specimens was also attributed to slight variation in degradation products during the ISO compression molding cycle.

The uniaxial tensile stress–strain curves of the as-received compression molded disks demonstrated a typical elastic region, followed by yielding behavior, and, eventually, rupture (Fig. 2). All groups exhibited comparable yield properties; no significant differences were detected in stress or strain magnitude at yield point with Vitamin E concentration. Ultimate stress and strain magnitudes were comparable among all combinations of resin type and Vitamin E concentration, though the failure properties of specimens with 125 ppm Vitamin E differed from some of the other groups ($p < 0.05$; Fig. 3).

Small punch behavior before and after aging

The load-displacement curves for each specimen were consistent with that typically demonstrated by UHMWPE specimens[10] including an initial peak load, displacement by drawing, and fracture. Certain specimens, discussed below, were sufficiently oxidized to exhibit brittle fracture. The addition of Vitamin E had little effect on the baseline small punch properties of the PE. Interactions were observed between aging and Vitamin E concentration for all combinations of processing and resin types ($p < 0.001$; Figure 4 through Figure 12). These effects are described below for each of the three processing methods.

In the absence of Vitamin E, nonirradiated GUR 1020 and GUR 1050 specimens exhibited evidence of mechanical degradation with aging, particularly with respect to postyield properties (Fig. 4). The addition of Vitamin E, even at a nominal concentration of only 125 ppm, brought the ultimate load back to baseline levels (Fig. 5). Embrittlement was best quantified by ultimate load: without Vitamin E, both resins exhibited significantly reduced ultimate load after four weeks of aging ($p < 0.05$). Specimens with 125–500 ppm Vitamin E exhibited higher ultimate load than those without Vitamin E ($p < 0.05$; Fig. 6).

For GUR 1020 and GUR 1050 irradiated with 30 kGy in nitrogen, detectable oxidation in the absence of Vitamin E was evident in the mechanical properties after two weeks of aging. After four weeks, the specimens were highly embrittled, and fractured after less than half a millimeter of displacement (Fig. 7). The addition of Vitamin E lessened the effects of aging (Fig. 8). Ultimate load decreased significantly with aging for specimens with less than 375 ppm Vitamin E ($p < 0.05$), while aging had no significant effect on the ultimate load of specimens with 375 ppm Vitamin E or greater ($p > 0.05$). At weeks two and four, specimens without Vitamin E had significantly lower ultimate strength compared to all other concentrations of Vitamin E. By week four, specimens with higher concentrations of Vitamin E (375 and 500 ppm) had higher ultimate load than specimens with lower concentrations of Vitamin E (125 and 205 ppm, Fig. 9).

Like the 30 kGy condition, specimens irradiated at 75 kGy exhibited oxidative embrittlement when aged

Questions? Contact FDA/CDRH/OCE/DID at CDRH-FOISTATUS@fda.hhs.gov or 301-796-8118

Records processed under FOIA Request #2014-8015; Released by CDRH on 12-8-2015

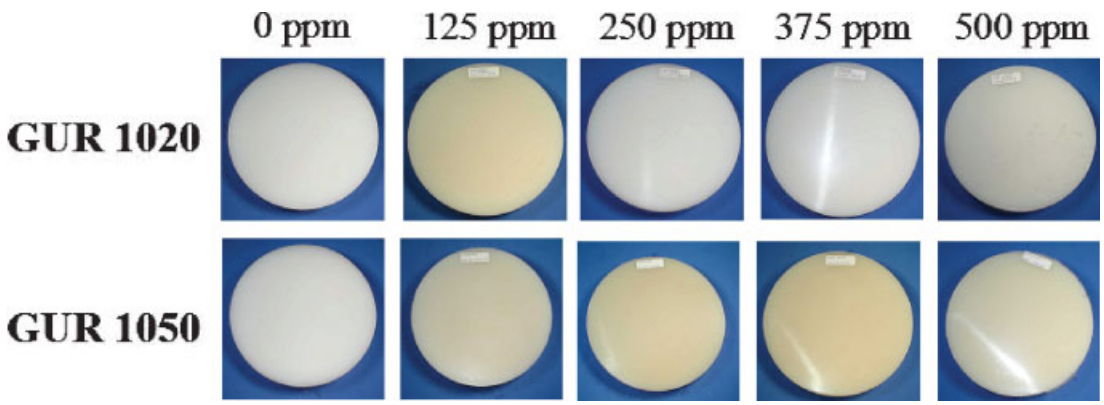

Figure 1. Photographs of GUR 1020 disks (top) and GUR 1050 disks (bottom), with Vitamin E concentration increasing from left to right. [Color figure can be viewed in the online issue, which is available at www.interscience.wiley.com.]

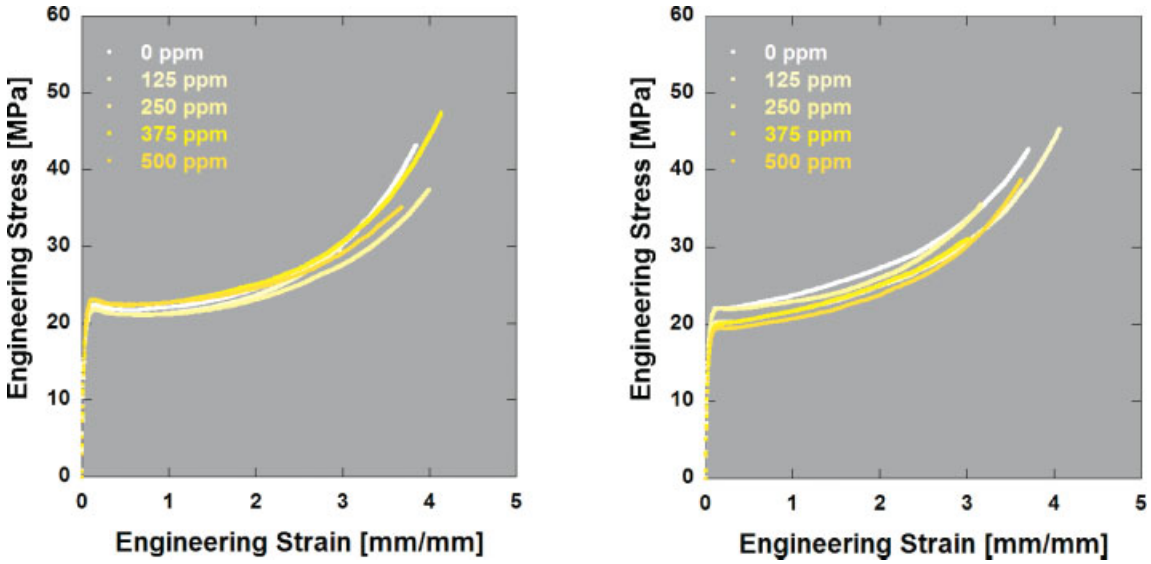

Figure 2. Engineering stress-strain curves of representative specimens from each of the five GUR 1020 (left) and GUR 1050 (right) materials. [Color figure can be viewed in the online issue, which is available at www.interscience.wiley.com.]

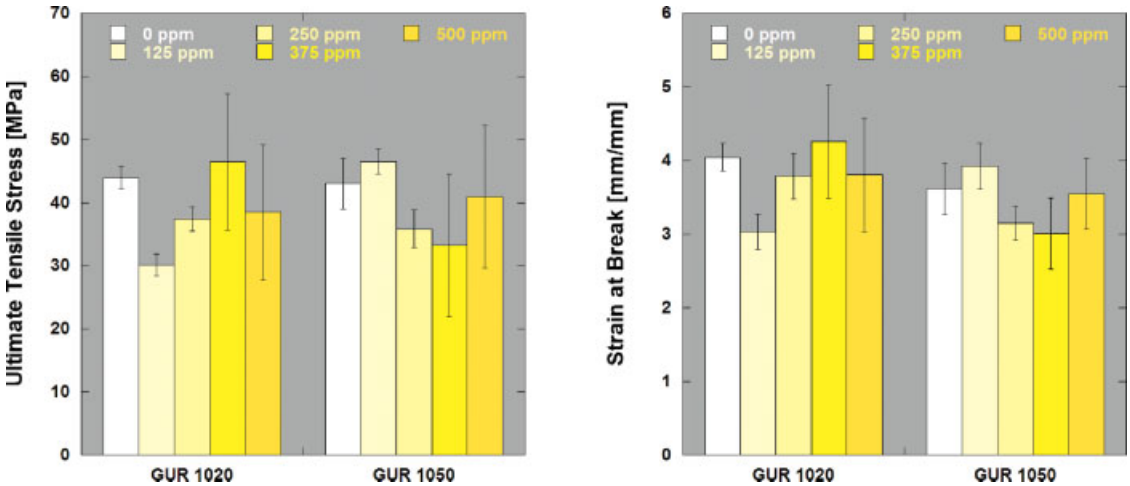

Figure 3. Ultimate strength (left) and strain (right) for each combination of resin type and Vitamin E concentration. [Color figure can be viewed in the online issue, which is available at www.interscience.wiley.com.]

Questions? Contact FDA/CDRH/OCE/DID at CDRH-FOISTATUS@fda.hhs.gov or 301-796-8118

Records processed under FOIA Request #2014-8015; Released by CDRH on 12-8-2015

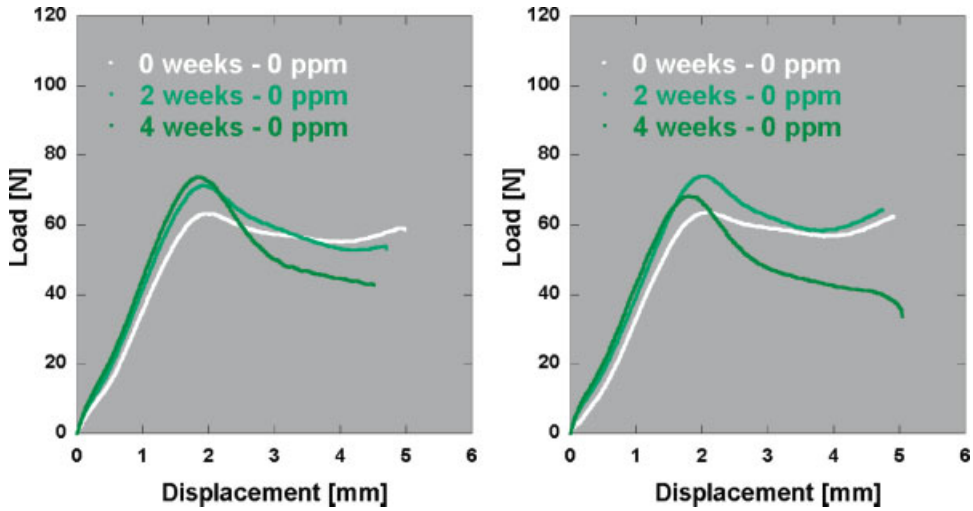

Figure 4. Representative small punch curves at all aging times for non-irradiated GUR 1020 (left) and GUR 1050 (right) without Vitamin E. [Color figure can be viewed in the online issue, which is available at www.interscience.wiley.com.]

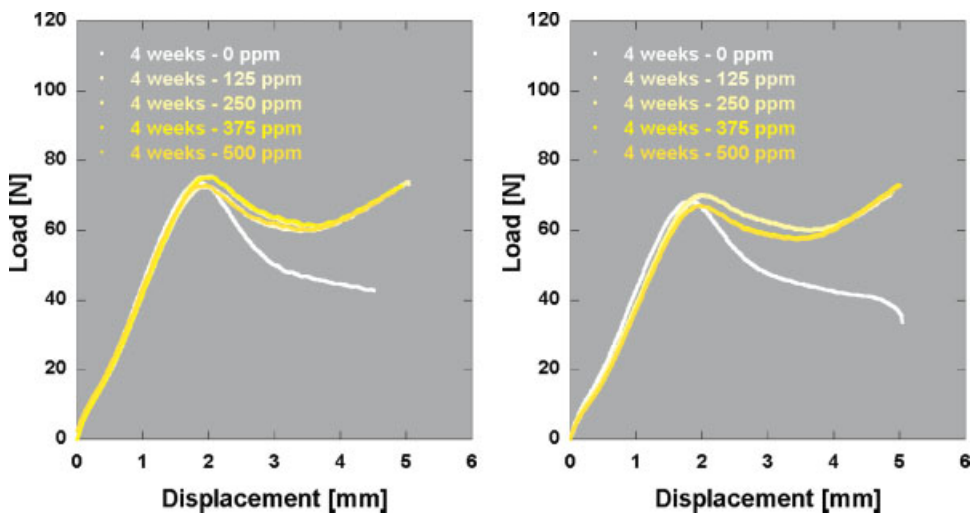

Figure 5. Representative small punch curves for non-irradiated GUR 1020 (left) and GUR 1050 (right) with 0-500 ppm Vitamin E aged 4 weeks. [Color figure can be viewed in the online issue, which is available at www.interscience.wiley.com.]

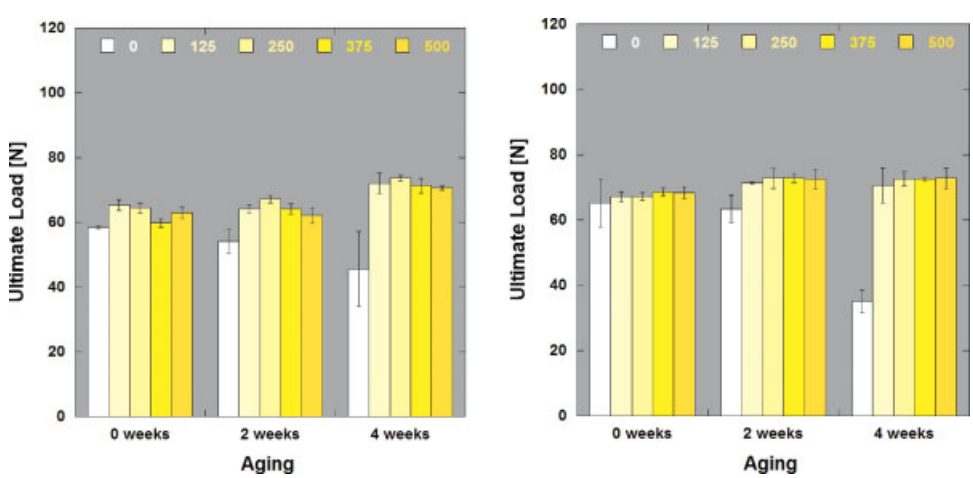

Figure 6. Ultimate load for non-irradiated GUR 1020 (left) and GUR 1050 (right) specimens with 0-500 ppm Vitamin E aged 0-4 weeks. [Color figure can be viewed in the online issue, which is available at www.interscience.wiley.com.]

Questions? Contact FDA/CDRH/OCE/DID at CDRH-FOISTATUS@fda.hhs.gov or 301-796-8118

Records processed under FOIA Request #2014-8015; Released by CDRH on 12-8-2015

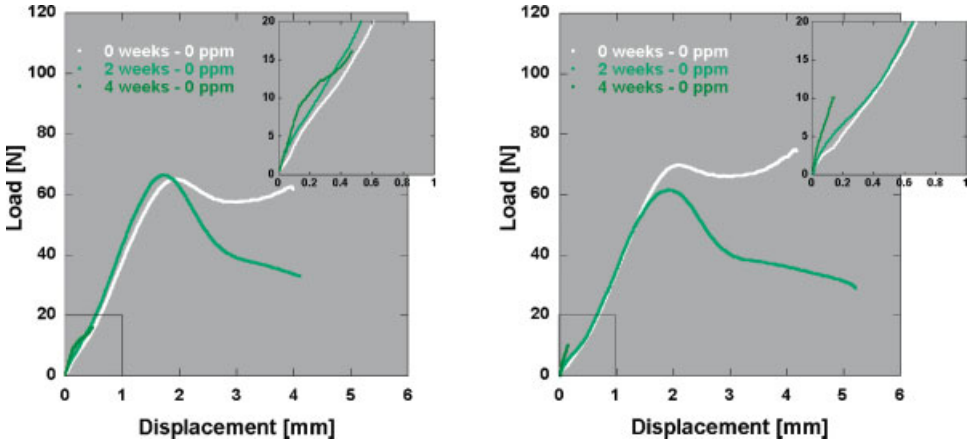

Figure 7. Representative small punch curves at all aging times for 30 kGy in nitrogen GUR 1020 (left) and GUR 1050 (right) without Vitamin E. [Color figure can be viewed in the online issue, which is available at www.interscience.wiley.com.]

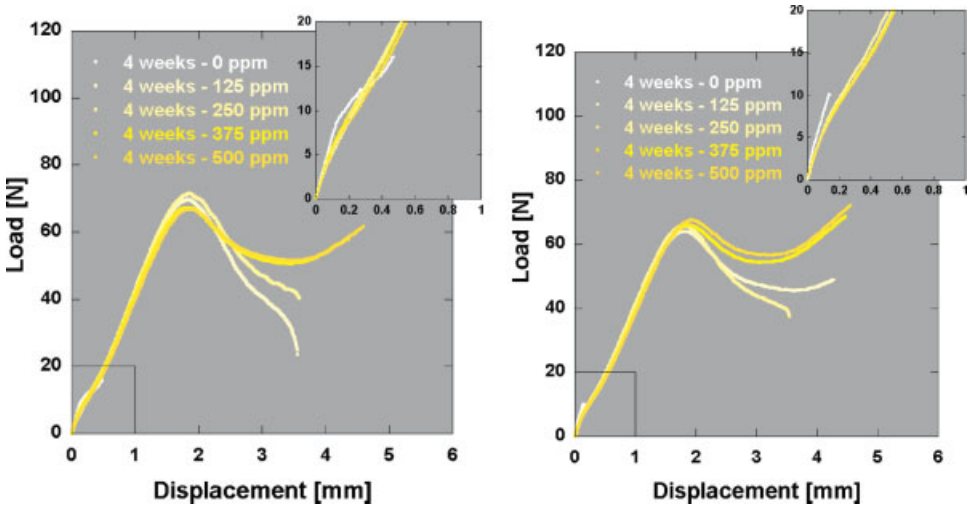

Figure 8. Representative small punch curves for 30 kGy in nitrogen GUR 1020 (left) and GUR 1050 (right) with 0-500 ppm Vitamin E aged 4 weeks. [Color figure can be viewed in the online issue, which is available at www.interscience.wiley.com.]

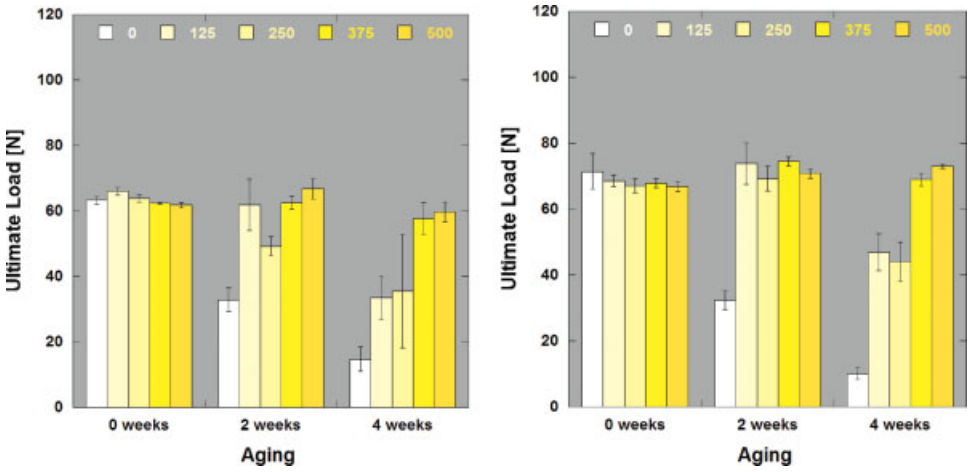

Figure 9. Ultimate load for 30 kGy in nitrogen GUR 1020 (left) and GUR 1050 (right) specimens with 0-500 ppm Vitamin E and aged 0-4 weeks. [Color figure can be viewed in the online issue, which is available at www.interscience.wiley.com.]

Questions? Contact FDA/CDRH/OCE/DID at CDRH-FOISTATUS@fda.hhs.gov or 301-796-8118

Records processed under FOIA Request #2014-8015; Released by CDRH on 12-8-2015

in the absence of Vitamin E (Fig. 10). Again, the addition of Vitamin E lessened the effects of aging (Fig. 11). Specifically, the ultimate strength of GUR 1020 and GUR 1050 specimens without Vitamin E and processed by 75 kGy irradiation + machining decreased significantly with aging time (Fig. 12). Specimens with smaller concentrations of Vitamin E (125 or 250 ppm) exhibited lower ultimate strength after four weeks of aging, while the ultimate strength of specimens with higher concentrations of Vitamin E (375 and 500 ppm) did not decrease significantly ($p > 0.05$). After two and four weeks of aging, specimens without Vitamin E had significantly lower ultimate strength compared to specimens with Vitamin E ($p < 0.05$).

Oxidation and *trans*-vinylene content before and after aging

The FTIR spectra of differently processed materials had different characteristic signatures. In the absence of Vitamin E, 30 kGy in nitrogen, and 75 kGy + machining specimens exhibited the near-surface oxidation peaks characteristic of irradiated and aged PE. The addition of Vitamin E did not change the nature of these peaks, but substantially reduced their magnitude. Figure 13 shows an example of the FTIR spectra of aged UHMWPE after 30 kGy in nitrogen, with and without Vitamin E. Representative, through thickness distribution of oxidation index after aging are shown in Figure 14, and demonstrate the subsurface oxidation peak characteristic of shelf-aged material.

Unprocessed specimens exhibited moderate oxidation without Vitamin E, and no measurable oxidation in the presence of Vitamin E, even after 4 weeks of aging [Fig. 15(A,B)]. Radiation dose had a substantial effect on the amount of oxidation that occurred, particularly in specimens that did not contain Vitamin E. Nonirradiated GUR 1020 and GUR 1050 specimens without Vitamin E had significantly higher maximum OI at four weeks aging compared to zero and two weeks aging ($p < 0.05$). At four weeks aging, GUR 1020 and GUR 1050 specimens without Vitamin E had significantly higher maximum OI compared to all other concentrations of Vitamin E ($p < 0.05$).

There were significant interactions in oxidation index between Vitamin E concentration and aging time in irradiated specimens. ($p < 0.001$; Fig. 15). Specimens without Vitamin E had substantial increases in oxidation after four weeks of aging, whereas specimens with higher concentrations of Vitamin E (375 and 500 ppm) did not have any significant increases in oxidation. After four weeks of aging, specimens without Vitamin E had significantly more oxidation compared to those with Vitamin E; this pattern was more consistent and less variable for specimens with higher concentrations of Vitamin E (i.e., 375 and 500 ppm Vitamin E). These patterns were exhibited by 30 kGy in nitrogen specimens [Fig. 15(C,D)] and 75 kGy + machining specimens [Fig. 15(E,F)].

TVI depended strictly on the absorbed dose, not the Vitamin E content (Fig. 16). Nonirradiated specimens exhibited little to no *trans*-vinylene (Fig. 16(A,B)], and the amount of *trans*-vinylene increased progressively from 30 kGy in nitrogen specimens [Fig. 16(C,D)] to 75 kGy + machining [Fig. 16(E,D)]. There were few statistically significant interactions between Vitamin E concentration and age in TVI among combinations of processing and resin types.

DISCUSSION

The results of this experiment supported our hypothesis that trace concentrations of Vitamin E influence the mechano-oxidative degradation behavior of UHMWPE. Although many previous studies have established that elevated concentrations of Vitamin E will stabilize irradiated UHMWPE,[28] to the authors' knowledge, this study represents the first attempt to establish the lower concentration limits of the antioxidant's effectiveness. We found that the minimum concentration of Vitamin E needed to stabilize UHMWPE during our accelerated tests depended upon the method of radiation processing. For the 30 and 75 kGy irradiated materials, the addition of 125 ppm or more Vitamin E was sufficient to maintain baseline mechanical and chemical properties through two weeks of accelerated aging. For these groups, the addition of 375 ppm or 500 ppm, respectively, was necessary to maintain baseline mechanical and chemical properties throughout the four-week accelerated aging period.

Although trace levels of Vitamin E were observed to substantially influence the oxidative stability of virgin and irradiated UHMWPE, for the 125–500 ppm concentrations evaluated in this study, there was little impact on the mechanical behavior of the unaged samples. Previous authors have reported that Vitamin E, at concentrations exceeding 1000 ppm, may improve the fatigue resistance of UHMWPE by acting as a plasticizer.[24,26] We were unable to detect a substantial plasticizing effect of trace levels of Vitamin E in our small punch mechanical test results of unaged samples. It may be that plasticization has a more marked effect on fatigue as opposed to static properties of UHMWPE; however, an evaluation of dynamic mechanical behavior was beyond the scope of the current study.

Questions? Contact FDA/CDRH/OCE/DID at CDRH-FOISTATUS@fda.hhs.gov or 301-796-8118

Records processed under FOIA Request #2014-8015; Released by CDRH on 12-8-2015

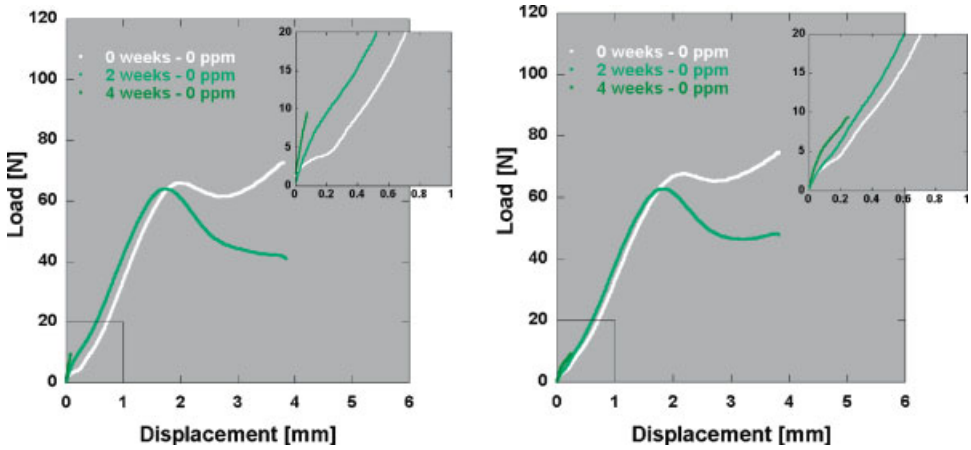

Figure 10. Representative small punch curves at all aging times for 75 kGy irradiated + machined GUR 1020 (left) and GUR 1050 (right) without Vitamin E. [Color figure can be viewed in the online issue, which is available at www.interscience.wiley.com.]

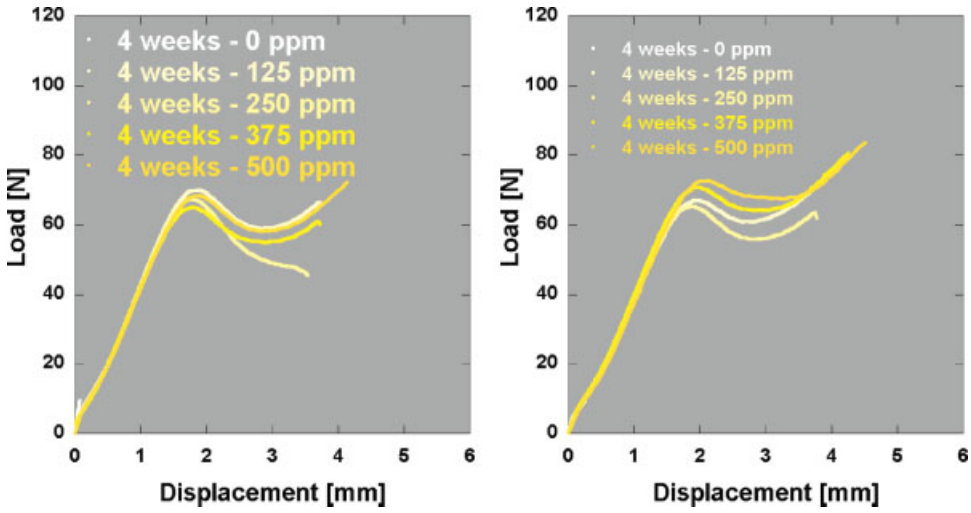

Figure 11. Representative small punch curves for 75 kGy irradiated + machined GUR 1020 (left) and GUR 1050 (right) with 0-500 ppm Vitamin E aged 4 weeks (right). [Color figure can be viewed in the online issue, which is available at www.interscience.wiley.com.]

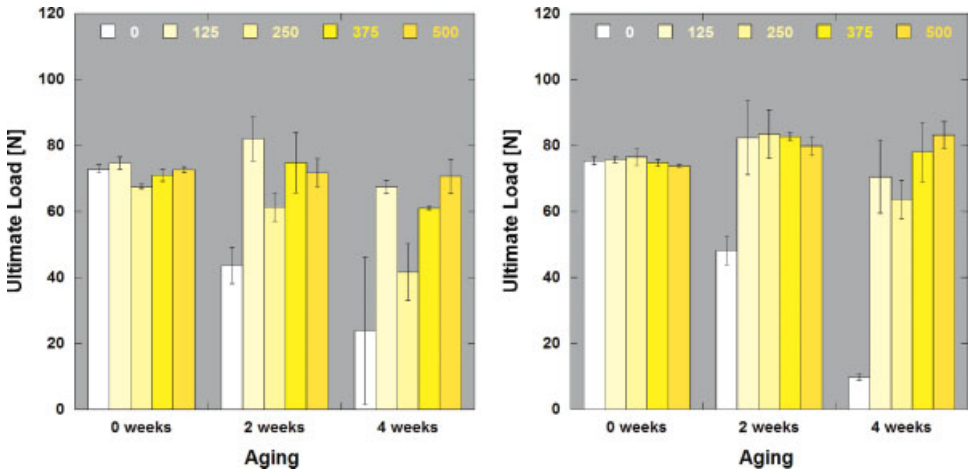

Figure 12. Ultimate load for 75 kGy irradiated + machined GUR 1020 (left) and GUR 1050 (right) specimens with 0-500 ppm Vitamin E and aged 0-4 weeks. [Color figure can be viewed in the online issue, which is available at www.interscience.wiley.com.]

Questions? Contact FDA/CDRH/OCE/DID at CDRH-FOISTATUS@fda.hhs.gov or 301-796-8118

Records processed under FOIA Request #2014-8015; Released by CDRH on 12-8-2015

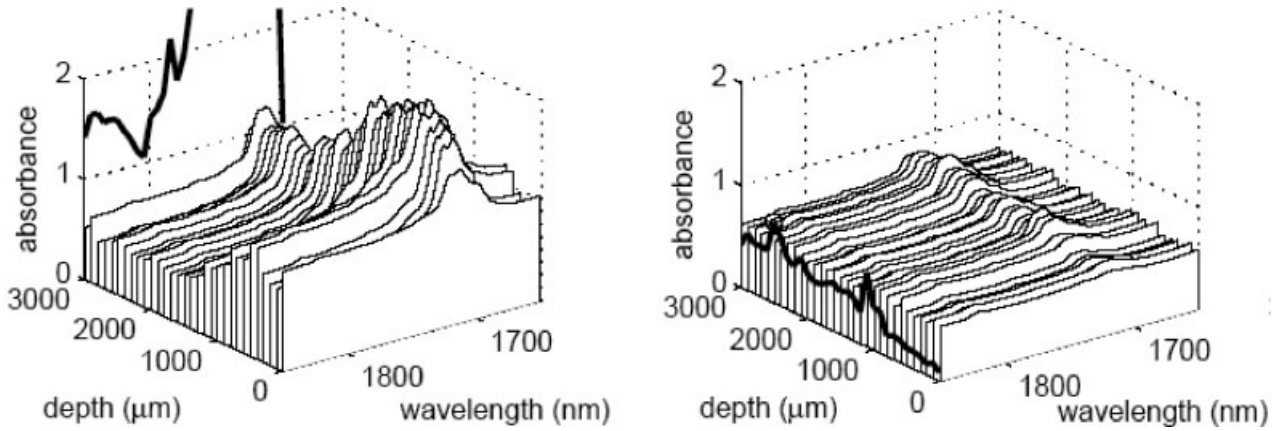

Figure 13. Example oxidation profies of 30 kGy in nitrogen GUR 1020 after four weeks of accelerated aging, without Vitamin E (left) and with 250 ppm Vitamin E (right). The profile on the depth axis represents OI. On the left, OI exceeds the scale of the graph.

Our general findings are supported by the current practices of the food packaging industry, which also employs trace concentrations of Vitamin E to stabilize polyolefins from degradation during shelf storage.[38,43,44] Trace concentrations of blended Vitamin E are currently used to stabilize food packaging because the natural anti-oxidant is highly cost-effective, has established international regulatory acceptance, and has a positive perception among public consumers.[44] By studying HDPE stabilized with as low as 160 ppm (0.016%) for beverage bottle applications, Mallegol et al.[43] showed that the blended material retained "residual anti-oxidant" properties after the initial Vitamin E was consumed by gamma irradiation in air. Specifically, the oxidation products of Vitamin E include dimers, trimers, quinones, and aldehydes.[38] Thus, not only Vitamin E, but also its complex degradation products are themselves effective anti-oxidants for polyolefins.[38,43] Apart from producing cosmetic alteration in UHMWPE, resulting in a yellowish color, as demonstrated in Figure 1, the degradation products generated by irradiating UHMWPE blended with up to 8000 ppm of Vitamin E has been shown to be otherwise biocompatible during *in vitro* studies and recent animal experiments.[45–49]

The accelerated aging protocol employed in this study was used to provide a severe but standardized oxidative challenge. Although this ASTM protocol is widely used to compare the oxidation resistance of UHMWPE materials, accelerated aging does not replicate real-time or clinically relevant aging conditions.[30] Indeed, accelerated aging will consistently oxidize virgin UHMWPE, which does not occur during real-time aging.[50] Nevertheless, this *in vitro* aging model is well-accepted in the orthopedic community for quickly comparing oxidation resistance of historical materials[50,51] as well as second-generation highly crosslinked materials,[22,23] including UHMWPE that has been blended[25] or doped[30] with Vitamin E.

Using FTIR, we did not observe a substantial influence of trace levels of Vitamin E, or aging, on the *trans*-vinylene yield of UHMWPE by irradiation of up to 75 kGy. The *trans*-vinylene yield in irradiated UHMWPE has been found to be proportional to dose, serving as an "internal dosimeter" for the material.[52] Accordingly, this methodology was subsequently adopted as a test method for ASTM.[42] As expected, the *trans*-vinylene content for the 75 kGy material was greater than that for the 30 kGy material, which in turn was greater than the low levels observed in the unirradiated controls.

Previous studies of radiation crosslinked UHMWPE have demonstrated a highly linear reduction in crosslinking efficiency after blending with Vitamin E between 1000 and 3000 ppm (r^2 = 0.99, Fig. 17).[31] With 1000 ppm Vitamin E, Oral et al.[31] have reported an average reduction of 17% in crosslink density following a dose of 100 kGy. For the range of 125–500 ppm blended Vitamin E in the present study, a 2–8% reduction of crosslinking density would be expected by interpolation of Oral's previous data (Fig. 17). This reduction also falls within the experimental uncertainty of the measurement technique, as illustrated by the SD bars for unstabilized material (0 ppm, Fig. 17). Thus, previous studies[31,35] reporting a reduction of crosslinking when UHMWPE is blended with $\geq$1000 ppm are consistent with the findings of the present study. Previous data, when interpolated in the trace concentration range of 125–500 ppm, demonstrates minimal ($\sim$2–8%) impact on crosslinking efficiency, falling within the detection limits of current methodology. Even if this minimal loss of crosslinking

Questions? Contact FDA/CDRH/OCE/DID at CDRH-FOISTATUS@fda.hhs.gov or 301-796-8118

Records processed under FOIA Request #2014-8015; Released by CDRH on 12-8-2015

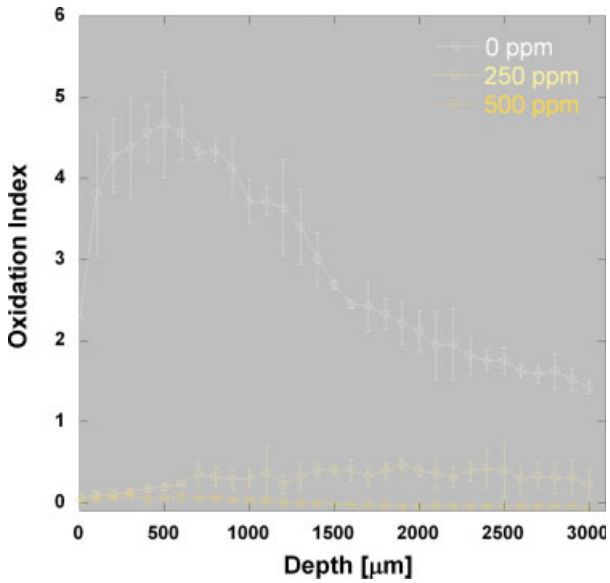

Figure 14. Example oxidation profiles for 30 kGy in nitrogen GUR 1020 after four weeks of aging. [Color figure can be viewed in the online issue, which is available at www.interscience.wiley.com.]

efficiency were judged to be meaningful, it can easily be corrected by slightly increasing the specified dose for sterilization or radiation crosslinking.

The small punch test data from the current study further suggest that when trace concentrations are employed, crosslinking is little affected. The hardening, post-yield phase of the punch test has been associated with crosslinking in UHMWPE.[53] Trace levels of Vitamin E were found to have negligible effects on the small punch behavior in unaged, radiation crosslinked UHMWPE, suggesting that at these low concentrations, radiation crosslinking may not be substantially compromised.

With the exception of the 375 ppm GUR 1020 disk, which appeared to be similar in concentration to the 500 ppm GUR 1020 disk, and the 125 ppm samples, which fell below the detection limit using FTIR, we were able to confirm the nominal Vitamin E concentrations reported by the manufacturer. Our findings for 375 ppm UHMWPE are, strictly speaking, limited to GUR 1050, which could be verified using FTIR. Because we did not find a significant difference in the anti-oxidant behavior of Vitamin E in GUR 1020 and 1050, the uncertainty in the concentration for the 375 ppm GUR 1020 disk can be addressed by relying on findings for GUR 1050 at 375 ppm.

The two radiation crosslinked conditions, 30 kGy in nitrogen and 75 kGy in air + machining, were selected to represent different types of UHMWPE materials. The 30 kGy in nitrogen samples were irradiated using the same techniques to produce conventional UHMWPE hip and knee components. The 75 kGy in air + machining condition, on the other hand, was chosen to replicate the techniques used to produce the feedstock for a first-generation, annealed highly crosslinked UHMWPE.[10] For irradiated feedstock, the outer 3 mm of the consolidated form is typically machined away, because the surface layer has the highest oxidation levels. Thus, the results of the 30 and 75 kGy conditions are not directly comparable, even though the samples had the same final thickness.

Highly crosslinked UHMWPEs in clinical use today receive a total dose of 90–105 kGy.[10] Thus, it remains unclear from the results of this study whether trace doses of Vitamin E will be sufficient to stabilize UHMWPE receiving a dose greater than 75 kGy. Because the actual effectiveness of Vitamin E not only depends on the anti-oxidant levels, but also on the consolidation conditions, the irradiation conditions, and the aging method used to produce oxidation. We are unable to recommend a universal minimum effective dose of Vitamin E for all UHMWPE formulations used in joint replacements based on the current study. To address questions about the stabilization of specific commercial formulations of highly crosslinking UHMWPE, it will be necessary to conduct fully scaled up manufacturing trials, in addition to the pilot scale experimentation reported here.

An interesting observation from our research was that the color changes in the compression-molded disks did not correspond to their Vitamin E concentration. Studies on polyolefin stability for the food packaging industry have demonstrated that color change in polyolefins following the addition of Vitamin E is a function not only of the anti-oxidant concentration, but also the processing conditions, and the evolution of tocopherol oxidation products within the sample.[38] All of the disk samples in this study were compression molded using a standardized compression molding cycle. If the color changes in UHMWPE associated with elevated Vitamin E content are judged aesthetically undesirable, they may be mitigated by reducing the concentration of anti-oxidant; by more precise control of the molding cycle; and/or by excluding oxygen during thermal processing of the polymer (e.g., by compression molding in a low-oxygen environment, such as nitrogen).

The standard processing conditions used for the disks were judged to be reasonable for the purposes of evaluating changes in oxidative stability in UHMWPE. The mechanical properties for the virgin GUR 1020 and 1050 exceeded the current guidelines for yield strength, ultimate strength, and elongation to failure specified for Type 1 and 2 materials in ASTM F648.[54] Nonetheless, our uniaxial tensile data were somewhat lower than what has been reported by commercial converters.[10] Based on our encourag-

Questions? Contact FDA/CDRH/OCE/DID at CDRH-FOISTATUS@fda.hhs.gov or 301-796-8118

Records processed under FOIA Request #2014-8015; Released by CDRH on 12-8-2015

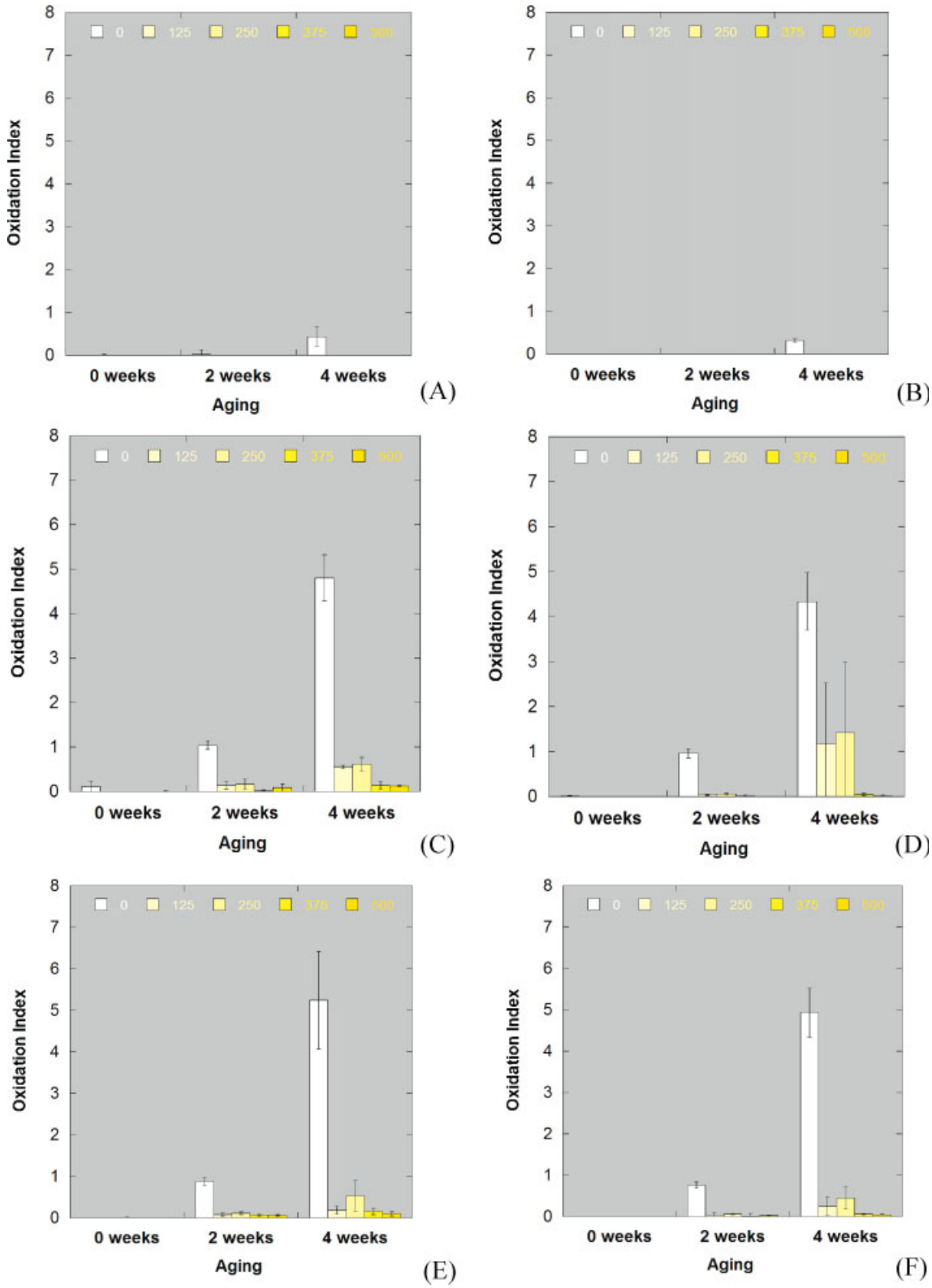

Figure 15. Summary of oxidation index results for unirradiated GUR 1020/1050 (A&B); 30 kGy irradiated in nitrogen GUR 1020/1050 (C&D); and 75 kGy irradiated + machined GUR 1020/1050 (E&F). Specimens with 0-500 ppm Vitamin E and aged 0-4 weeks. [Color figure can be viewed in the online issue, which is available at www.interscience.wiley.com.]

ing initial findings at a pilot experimental scale, further research is currently underway with large-scale blending techniques and commercial conversion processes to study the effects of trace concentrations of Vitamin E on irradiated UHMWPE at a commercial scale.

Questions? Contact FDA/CDRH/OCE/DID at CDRH-FOISTATUS@fda.hhs.gov or 301-796-8118

Records processed under FOIA Request #2014-8015; Released by CDRH on 12-8-2015

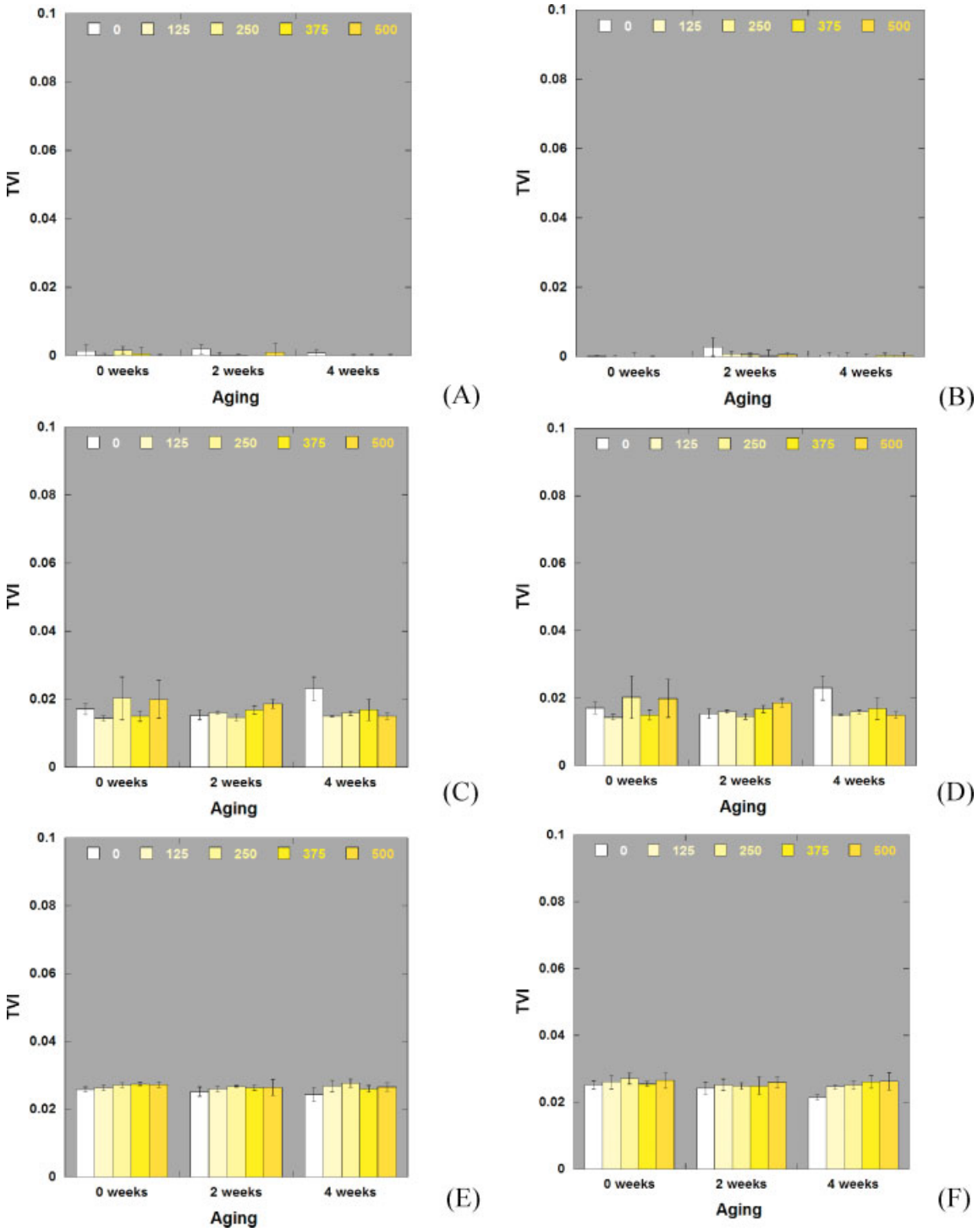

Figure 16. Summary of trans-vinylene index (TVI) results for unirradiated GUR 1020/1050 (A&B); 30 kGy irradiated in nitrogen GUR 1020/1050 (C&D); and 75 kGy irradiated + machined GUR 1020/1050 (E&F). Specimens with 0-500 ppm Vitamin E and aged 0–4 weeks. [Color figure can be viewed in the online issue, which is available at www.interscience.wiley.com.]

CONCLUSIONS

Our study demonstrates that elevated concentrations of Vitamin E are not necessary for the oxidative stability of radiation crosslinked UHMWPE. The minimum concentration necessary to stabilize irradiated UHMWPE was found to depend on the processing conditions, but not the resin. When blended with UHMWPE powder prior to consolidation, 500 ppm was found to stabilize both conventional and highly crosslinked UHMWPE materials investi-

Questions? Contact FDA/CDRH/OCE/DID at CDRH-FOISTATUS@fda.hhs.gov or 301-796-8118

Records processed under FOIA Request #2014-8015; Released by CDRH on 12-8-2015

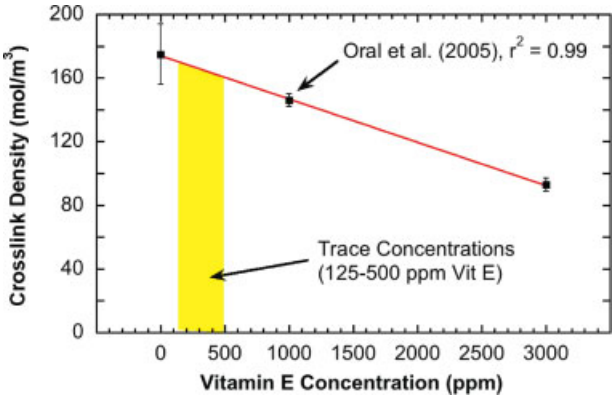

Figure 17. Crosslink density of vacuum packaged, 100 kGy-irradiated UHMWPE blended with Vitamin E, adapted from previously published data from Oral et al.[31] The range of trace concentrations employed in the current study is superimposed on the graph. For 125–500 ppm blended Vitamin E, a 2–8% reduction of crosslinking density is expected by interpolation of Oral's data. This reduction also falls within the experimental uncertainty of the measurement technique, as illustrated by the SD bars for unstabilized material (0 ppm). [Color figure can be viewed in the online issue, which is available at www.interscience.wiley.com.]

gated in this study for up to 4 weeks of exposure in an oxygen bomb, representing a severe oxidative challenge. Trace concentrations of Vitamin E had no significant effect on small punch hardening behavior or on *trans*-vinylene content, consistent with minimal impact on crosslinking efficiency. Based on previous crosslink density measurements,[31] only a reduction of 2–8% of crosslink density is expected for the range of trace Vitamin E concentrations investigated in the present study. Although gamma sterilized UHMWPE blended with higher levels of Vitamin E is currently in clinical trials,[28] the results of the present study suggest that only trace levels of Vitamin E may be needed for oxidative stability.

Special thanks to Ticona for preparing the material samples, as well as to Shi-Shen Yau, Stryker Orthopedics, and to Dan Mazzucco and Allyson Ianuzzi, Exponent, for their contributions. We also extend our grateful thanks to Pierangiola Bracco from the University of Turin, Italy, for her assistance with verifying the Vitamin E concentrations in the compression molded discs using FTIR.

References

1. Rimnac CM, Klein RW, Betts F, Wright TM. Post-irradiation aging of ultra-high molecular weight polyethylene. J Bone Joint Surg A 1994;76:1052–1056.
2. Premnath V, Harris WH, Jasty M, Merrill EW. Gamma sterilization of UHMWPE articular implants: An analysis of the oxidation problem. Biomaterials 1996;17:1741–1753.
3. Costa L, Jacobson K, Bracco P, Brach del Prever EM. Oxidation of orthopaedic UHMWPE. Biomaterials 2002;23:1613–1624.
4. Costa L, Luda MP, Trossarelli L, Brach del Prever EM, Crova M, Gallinaro P. Oxidation in orthopaedic UHMWPE sterilized by gamma-radiation and ethylene oxide. Biomaterials 1998;19(7–9):659–668.
5. Collier JP, Sperling DK, Currier JH, Sutula LC, Saum KA, Mayor MB. Impact of gamma sterilization on clinical performance of polyethylene in the knee. J Arthroplasty 1996; 11:377–389.
6. Sutula LC, Collier JP, Saum KA, Currier BH, Currier JH, Sanford WM, Mayor, MB, Wooding, RE, Sperling, DK, Williams, IR. Impact of gamma sterilization on clinical performance of polyethylene in the hip. Clin Orthop 1995; 319:28–40.
7. Collier MB, Engh CA Jr, Engh GA. Shelf age of the polyethylene tibial component and outcome of unicondylar knee arthroplasty. J Bone Joint Surg Am A 2004;86:763–769.
8. McGovern TF, Ammeen DJ, Collier JP, Currier BH, Engh GA. Rapid polyethylene failure of unicondylar tibial components sterilized with gamma irradiation in air and implanted after a long shelf life. J Bone Joint Surg Am A 2002;84:901–906.
9. Bohl JR, Bohl WR, Postak PD, Greenwald AS. The Coventry Award. The effects of shelf life on clinical outcome for gamma sterilized polyethylene tibial components. Clin Orthop 1999;367:28–38.
10. Kurtz SM. The UHMWPE Handbook: Ultra-High Molecular Weight Polyethylene in Total Joint Replacement. New York: Academic Press; 2004.
11. Greer K. A prospective study of the effects of five years shelf aging on the properties of UHMWPE following gamma sterilization in air or in a vacuum foil pouch. Transactions of the 28th Society for Biomaterials; 2003. p 378.
12. Buchanan FJ, Sim B, Downes S. Influence of packaging conditions on the properties of gamma-irradiated UHMWPE following accelerated ageing and shelf ageing. Biomaterials 1999;20:823–837.
13. Costa L, Bracco P, Brach del Prever EM, Kurtz SM, Gallinaro P. Oxidation and oxidation potential in contemporary packaging for polyethylene total joint replacement components. J Biomed Mater Res B Appl Biomater 2006;78:20–26.
14. Eyerer P, Ke YC. Property changes of UHMW polyethylene hip cup endoprostheses during implantation. J Biomed Mater Res 1984;18:1137–1151.
15. Bostrom MP, Bennett AP, Rimnac CM, Wright TM. The natural history of ultra high molecular weight polyethylene. Clin Orthop 1994;309:20–28.
16. Kurtz SM, Hozack W, Marcolongo M, Turner J, Rimnac C, Edidin A. Degradation of mechanical properties of UHMWPE acetabular liners following long-term implantation. J Arthroplasty 2003;18(7 Suppl 1):68–78.
17. Kurtz SM, Rimnac CM, Hozack WJ, Turner J, Marcolongo M, Goldberg VM, Kraay MJ, Edidin AA. In vivo degradation of polyethylene liners after gamma sterilization in air. J Bone Joint Surg Am A 2005;87:815–823.
18. Kurtz SM, Hozack WJ, Purtill JJ, Marcolongo M, Kraay MJ, Goldberg VM, Sharkey PF, Parvizi J, Rimnac CM, Edidin AA. 2006 OTTO AUFRANC AWARD PAPER: Significance of in vivo degradation for polyethylene in total hip arthroplasty. Clin Orthop Relat Res 2006;453:47–57.
19. McKellop H, Shen FW, Salovey R. Extremely low wear of gamma-crosslinked/remelted UHMW polyethylene acetabular cups. Transactions of the 44th Orthopedic Research Society; 1998 February 21–24; New Orleans, LA; 1998. p 98.
20. Muratoglu OK, Bragdon CR, O'Connor DO, Jasty M, Harris WH. A novel method of cross-linking ultra-high-molecular-weight polyethylene to improve wear, reduce oxidation, and retain mechanical properties. Recipient of the 1999 HAP Paul Award. J Arthroplasty 2001;16:149–160.

Questions? Contact FDA/CDRH/OCE/DID at CDRH-FOISTATUS@fda.hhs.gov or 301-796-8118

Records processed under FOIA Request #2014-8015; Released by CDRH on 12-8-2015

21. Kurtz SM, Manley M, Wang A, Taylor S, Dumbleton J. Comparison of the properties of annealed crosslinked (Crossfire) and conventional polyethylene as hip bearing materials. Bull Hosp Jt Dis 2002– 2003;61(1–2):17–26.
22. Dumbleton JH, D'Antonio JA, Manley MT, Capello WN, Wang A The basis for a second-generation highly crosslinked UHMWPE. Clin Orthop Relat Res 2006;453:265–271.
23. Kurtz SM, Mazzucco D, Rimnac CM, Schroeder D. Anisotropy and oxidative resistance of highly crosslinked UHMWPE after deformation processing by solid-state ram extrusion. Biomaterials 2006;27:24–34.
24. Tomita N, Kitakura T, Onmori N, Ikada Y, Aoyama E. Prevention of fatigue cracks in ultrahigh molecular weight polyethylene joint components by the addition of Vitamin E. J Biomed Mater Res 1999;48:474–478.
25. Wolf C, Krivec T, Blassnig J, Lederer K, Schneider W. Examination of the suitability of alpha-tocopherol as a stabilizer for ultra-high molecular weight polyethylene used for articulating surfaces in joint endoprostheses. J Mater Sci 2002;13:185–189.
26. Oral E, Wannomae KK, Hawkins N, Harris WH, Muratoglu OK. Alpha-tocopherol-doped irradiated UHMWPE for high fatigue resistance and low wear. Biomaterials 2004;25:5515–5522.
27. Wolf C, Macho C, Lederer K. Accelerated ageing experiments with crosslinked and conventional ultra-high molecular weight polyethylene (UHMW-PE) stabilised with alpha-tocopherol for total joint arthroplasty. J Mater Sci 2006;17:1333–1340.
28. Shibata N, Kurtz SM, Tomita N. Advances of mechanical performance and oxidation stability in ultrahigh molecular weight polyethylene for total joint replacement: Highly crosslinked and α-tocopherol doped. J Biomed Sci Eng 2006;1:107–123.
29. Oral E, Rowell SL, Muratoglu OK. The effect of alpha-tocopherol on the oxidation and free radical decay in irradiated UHMWPE. Biomaterials 2006;27:5580–5587.
30. Oral E, Christensen SD, Malhi AS, Wannomae KK, Muratoglu OK. Wear resistance and mechanical properties of highly cross-linked, ultrahigh-molecular weight polyethylene doped with Vitamin E. J Arthroplasty 2006;21:580–591.
31. Oral E, Greenbaum ES, Malhi AS, Harris WH, Muratoglu OK. Characterization of irradiated blends of alpha-tocopherol and UHMWPE. Biomaterials 2005;26:6657–6663.
32. Dolezel B, Adamirova L. Method of hygienically safe stabilization of polyolefins against thermooxidative and photoxidative degradation. Czechoslovakian Socialist Republic Pat 1982;221:403.
33. Berzen J, Luketic D. Stabilised polyethylene moulding materials, esp. for implants containing polyethylene with molecular wt. 10^5–10^7, antioxidant, and tocopherol, esp. alpha- tocopherol or Vitamin E, as stabiliser. Eur Pat 1994;613:923.
34. Shibata N, Tomita N The anti-oxidative properties of alpha-tocopherol in gamma-irradiated UHMWPE with respect to fatigue and oxidation resistance. Biomaterials 2005;26:5755–5762.
35. Parth M, Aust N, Lederer K. Studies on the effect of electron beam radiation on the molecular structure of ultra-high molecular weight polyethylene under the influence of alpha-tocopherol with respect to its application in medical implants. J Mater Sci 2002;13:917–921.
36. Wolf C, Maninger J, Lederer K, Fruhwirth-Smounig H, Gamse T, Marr R. Stabilisation of crosslinked ultra-high molecular weight polyethylene (UHMW-PE)-acetabular components with alpha-tocopherol. J Mater Sci 2006;17:1323–1331.
37. Oral E, Wannomae KK, Rowell SL, Muratoglu OK. Migration stability of alpha-tocopherol in irradiated UHMWPE. Biomaterials 2006;27:2434–2439.
38. Al-Malaika S. Perspectives in stabilization of polyolefins. Adv Polym Sci 2004;169:121–150.
39. ASTM F 2003–02. Standard guide for accelerated aging of ultra high molecular weight polyethylene. West Conshohocken, PA: American Society for Testing and Materials, 2002.
40. ASTM F 2183–02. Standard test method for small punch testing of ultra-high molecular wieght polyethylene used in surgical implants. West Conshohocken, PA: American Society for Testing and Materials, 2002.
41. ASTM F 2102–01. Standard guide for evaluating the extent of oxidation in ultra-high molecular weight polyethylene fabricated forms intended for surgical implants. West Conshohocken, PA: American Society for Testing and Materials, 2001.
42. ASTM F 2381–04. Standard test method for evaluating trans-vinylene yield in irradiated ultra-high-molecular-weight polyethylene fabricated forms intended for surgical implants by infrared spectroscopy West Conshohocken, PA: American Society for Testing and Materials, 2004.
43. Mallégol J, Carlsson DJ, Deschêne L. Antioxidant effectiveness of Vitamin E in HDPE and tetradecane at 32°C. Polym Degrad Stab 1991;73:269–280.
44. LaCoste A, Schaich KM, Zumbrunnen D, Yam KL. Advancing controlled release packaging through smart blending. Packag Technol Sci 2005;18:77–87.
45. Wolf C, Lederer K, Muller U. Tests of biocompatibility of alpha-tocopherol with respect to the use as a stabilizer in ultrahigh molecular weight polyethylene for articulating surfaces in joint endoprostheses. J Mater Sci 2002;13:701–705.
46. Reno F, Bracco P, Lombardi F, Boccafoschi F, Costa L, Cannas M The induction of MMP-9 release from granulocytes by Vitamin E in UHMWPE. Biomaterials 2004;25:995–1001.
47. Reno F, Cannas M. UHMWPE and Vitamin E bioactivity: An emerging perspective. Biomaterials 2006;27:3039–3043.
48. Wolf C, Lederer K, Bergmeister H, Losert U, Bock P. Animal experiments with ultra-high molecular weight polyethylene (UHMW-PE) stabilised with alpha-tocopherol used for articulating surfaces in joint endoprostheses. J Mater Sci 2006; 17:1341–1347.
49. Wolf C, Lederer K, Pfragner R, Schauenstein K, Ingolic E, Siegl V. Biocompatibility of ultra-high molecular weight polyethylene (UHMW-PE) stabilized with alpha-tocopherol used for joint endoprostheses assessed in vitro. J Mater Sci Mater Med 2007;18:1247–1252.
50. Edidin AA, Villarraga ML, Herr MP, Muth J, Yau SS, Kurtz SM. Accelerated aging studies of UHMWPE. II. Virgin UHMWPE is not immune to oxidative degradation. J Biomed Mater Res 2002;61:323–329.
51. Edidin AA, Herr MP, Villarraga ML, Muth J, Yau SS, Kurtz SM. Accelerated aging studies of UHMWPE. I. Effect of resin, processing, and radiation environment on resistance to mechanical degradation. J Biomed Mater Res 2002;61:312–322.
52. Muratoglu OK, Harris WH. Identification and quantification of irradiation in UHMWPE through trans-vinylene yield. J Biomed Mater Res 2001;56:584–592.
53. Kurtz SM, Pruitt LA, Jewett CW, Foulds JR, Edidin AA. Radiation and chemical crosslinking promote strain hardening behavior and molecular alignment in ultra high molecular weight polyethylene during multi-axial loading conditions. Biomaterials 1999;20:1449–1462.
54. ASTM F 648–07. Standard Specification for Ultra-High-Molecular-Weight Polyethylene Powder and Fabricated Form for Surgical Implants. West Conshohocken, PA: American Society for Testing and Materials, 2007.

Questions? Contact FDA/CDRH/OCE/DID at CDRH-FOISTATUS@fda.hhs.gov or 301-796-8118

Records processed under FOIA Request #2014-8015; Released by CDRH on 12-8-2015

For submission: Convert to PDF and email abstract with contact information to skurtz@exponent.com

Homogeneity and Grafting of Small and Large Quantities of Vitamin E in Ultra High Molecular Weight Polyethylene

Reto Lerf[1], Daniel Zurbrügg[2], Daniel Delfosse[1].
[1]Mathys Ltd. Bettlach, Switzerland; [2] Niutec AG Winterthur, Switzerland.

Statement of Purpose: The further improvement of UHMWPE for joint replacement application is topical. The reduction of the wear rate may be achieved by cross-linking and by an increase in the oxidative stability trough the addition of vitamin E (Kurtz SM, 2009). Although the stabilising effect of vitamin E is undisputed, the physical and chemical state of vitamin E in cross-linked UHMWPE is still under investigation. On the one hand, it was found that migration of vitamin E out of the polymer is unlikely (Oral E, 2006). On the other hand, grafting of vitamin E molecules to the polyethylene backbone was postulated (Wolf C, 2011). The purpose of the current investigation is to quantify the amount of grafting of vitamin E in UHMWPE in concentrations, 0.1 % and 1.0% blended and an E-Poly® product by Biomet.

Methods: UHMWPE powder GUR 1020 and two different concentrations of vitamin E (0.1 wt % and 1.0 wt%) were mixed and sintered. The samples with vitamin E addition of 0.1 % correspond to the pre-forms of vitamys® hip cups by Mathys Ltd Bettlach, i.e. hemispheres of diameter 68 mm. The experimental 1.0 % vitamin E samples were discs (Ø: 110 mm, H: 22 mm). Cross-linking was done at a gamma dose of 96.5 kGy. To be sure that the amount of grafting was not influenced by an inhomogeneous distribution of vitamin E, profiles in the as sintered condition were analysed by Fourier transform infrared spectroscopy (FTIR) before sampling the cross-linked specimens. Two profiles were analysed in each sample. 0.3 mm sections were cut in two directions perpendicular to each other by a microtom HM 350 (Microm GmbH, Germany). From the E-Poly sample by Biomet (E-Poly liner Ringloc-X by Biomet, size 66/36), a vitamin E profile in the pole region and another one close to the rim were established. The spectra of all sections were recorded by a Bio-Rad FTS-45 (Bio-Rad Laboratories, United Kingdom) in transmission with an aperture size of 1x1 cm at a resolution of 4 cm-1. The vitamin E index (VEI) was calculated as the ratio of the area of a characteristic vitamin E peak (1275 -1245 cm-1) to the polyethylene reference peak at 1985-1850 cm-1. The relative vitamin E index (RVEI) was calculated by subtracting the background of a pure UHMWPE.
To assess the extent of vitamin E grafting, three 0.3 mm sections were cut from the centre of both, the non-irradiated and the cross-linked 0.1 % and 1.0 % experimental samples. From the E-Poly implant, such sections were taken from the middle of the liner wall. VEI was determined as described above. Then the sections were extracted for 48 h in heptane at 98 °C and finally dried at room temperature. Again, FTIR was used to calculate VEI as described above.

Results: The control of the homogeneity of the vitamin E distribution in the as sintered condition yielded a very uniform and equal VEI over both perpendicular profiles in the samples of both vitamin E concentrations, of 0.1 % and 1.0 %. The mean relative vitamin E index (RVEI) of all sections analysed by FTIR was 0.0227 ± 0.0006 in the 0.1 % material. In the 1.0 % vitamin E sample, RVEI was 0.2786 ± 0.0067. Figure 1 illustrates these vitamin E profiles for both concentrations, for the 0.1 % vitamys® pre-form material and for experimental 1.0 %, respectively. The vitamin E content in the E-Poly liner exhibits a gradient. Minimum RVEI analysed by FTIR is 0.082 at the articulation surface at the pole and the maximum value RVEI 0.208 at the outer surface on the rim. The mean relative vitamin E index (RVEI) of the pole profile is 0.137 and 0.159 in the rim profile, respectively. Figure 2 depicts the two vitamin E profiles, pole and rim, as relative vitamin E index in the E-Poly product by Biomet.

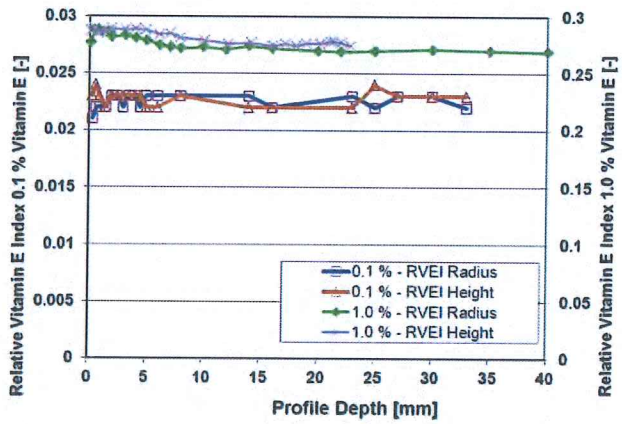

Figure 1. Concentration profiles trough the 0.1 % vitamin E sample (left scale) and the 1.0 % sample (right scale)

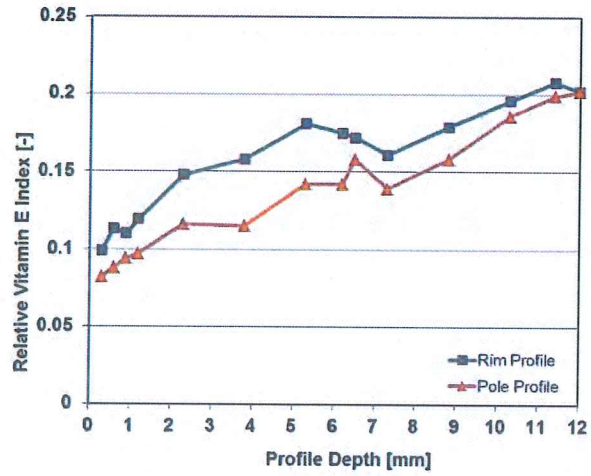

Figure 2: Concentration of vitamin E as pole profile and rim profile trough the E-Poly liner by Biomet.

There is a marked disparity in the amount of vitamin E extracted in the as sintered and the cross-linked state.

Questions? Contact FDA/CDRH/OCE/DID at CDRH-FOISTATUS@fda.hhs.gov or 301-796-8118

Records processed under FOIA Request #2014-8015; Released by CDRH on 12-8-2015

Vitamin E of the non-irradiated samples is completely extracted. After extraction, RVEI of both samples is below the detection limit of 0.001. Besides cross-linking, an effect of irradiation is the (at least partial) bonding of vitamin E to the polymer. These grafted molecules of anti-oxidant can no longer be extracted. The extracted amount of vitamin E is 23 % for the 0.1 % vitamys® sample and reaches 87 % in the experimental 1.0 % material. From the E-Poly liner, 95 % could be extracted. Hence, bonding of vitamin E is not proportional to the vitamin E concentration. At low concentrations, the majority of the vitamin E remains in the polymer, whereas at high concentration the majority can be extracted. However, at high and low concentrations a certain amount of vitamin E remains in the polymer, most likely grafted to the polymer chains. Figure 3 depicts RVEI before and after extraction and lists the percentages of vitamin E extracted.

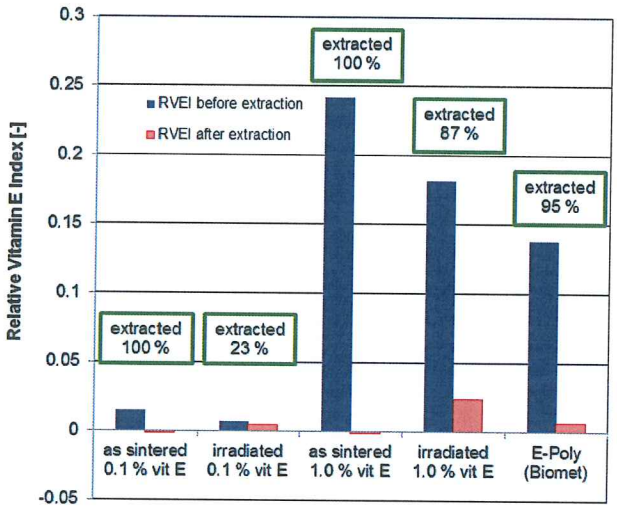

Figure 3. RVEI before and after extraction. The percentage of decrease in RVEI is indicated for each sample.

Conclusions: The production route of mixing vitamin E to UHMWPE powder results in a homogenous distribution of this anti-oxidant in the whole consolidated PE body. Therefore, artefacts in gauging the vitamin E concentration by FTIR due to inhomogeneity can be excluded. Irradiation of UHMWPE blended with vitamin E induces grafting of the α-tocopherole to the polymer macromolecules. The amount of vitamin E remaining in the polymer is not proportional to the initial concentration. It seems rather that there is a saturation of the absolute amount of vitamin E grafted for a given dose of irradiation. A dependence of the percentage grafted on the irradiation dose is reported by Wolf et al. (Wolf C, 2011). The grafting of the anti-oxidant has shown to reduce the amount of vitamin E which can be leached out. Therefore, protection of the UHMWPE against oxidation remains high (Lerf R, 2010). However, more experimental data with variable concentrations of vitamin E and different irradiation doses are required to understand the phenomenon of vitamin E grafting in irradiated UHMWPE.

References:

Kurtz SM et al, in: Kurtz SM, editor. UHMWPE biomaterials handbook 2nd ed. Amsterdam: Elsevier; 2009 p. 237–46

Oral E et al., Biomaterials 2006;27: 2434-2439

Wolf C et al., ORS 2011 Annual Meeting, poster 1178

Lerf R et al., Biomaterials 2010;31: 3643–3648

Records processed under FOIA Request #2014-8015; Released by CDRH on 12-8-2015

CLINICAL ORTHOPAEDICS AND RELATED RESEARCH
Number 340, pp 257–266
© 1997 Lippincott–Raven Publishers

Patellofemoral Joint Kinematics and Contact Pressures in Total Knee Arthroplasty

Thay Q. Lee, MS,**,†; Andrew P. Gerken, MD**; Francis E. Glaser, MD**; William C. Kim, MD**; and Sanford H. Anzel, MD***

Patellofemoral joint kinematics, contact areas, and contact pressures were measured concomitantly before and after total knee arthroplasty in 10 fresh frozen human cadaver knees using an Instron machine, a custom patellofemoral joint testing jig, axial bone markers, a continuous video digitizing system, and Fuji pressure sensitive film. The implant used in this study was the Kirschner Performance Knee System with an all polyethylene, domed patellar component. For all tests, the patella was aligned in its anatomically neutral position. Patellofemoral joint contact areas decreased as much as 19-fold after total knee arthroplasty. Mean patellofemoral joint contact pressures increased as much as 32-fold, and peak patellofemoral joint contact pressures increased as much as 22-fold after total knee arthroplasty. No statistically significant differences between preoperative and postoperative specimens were observed with respect to the patellofemoral, patellotibial, or patellar tilt angles from 30° to 120° knee flexion. Thus, the elevated patellofemoral joint contact pressures observed after total knee arthroplasty in vitro are not a primary consequence of iatrogenically altered patellofemoral kinematics.

From the *Orthopaedic Biomechanics Laboratory, Department of Physical Medicine and Rehabilitation, Long Beach Veterans Affairs Medical Center, Long Beach, CA; **Department of Orthopaedic Surgery, University of California, Irvine, Orange, CA; and †Department of Biomaterials/Handicap Research, Gothenberg University, Gothenburg, Sweden.

Supported by a grant from the Department of Veterans Affairs. Specimen radiographs were provided by the Radiology Service at the Long Beach Veterans Affairs Medical Center, implants were donated by Kirschner Medical Corporation, and the video digitizing system was provided by the California Orthopaedic Research Institute.

Reprint requests to Thay Q. Lee, MS, Orthopaedic Biomechanics Laboratory, Long Beach Veterans Affairs Medical Center (151), 5901 East Seventh Street, Long Beach, CA 90822.

Received: August 31, 1995.

Revised: July 10, 1996; October 28, 1996; December 6, 1996.

Accepted: December 20, 1996.

Modern total knee arthroplasty procedures attempt to restore the functional mechanics of the normal knee.[11,14] Many modifications during the past 25 years have resulted in a substantial decrease in complications such as component loosening and joint instability.[6,33] However, complications involving the patellofemoral joint continue to be reported after 1.5% to 12% of all total knee arthroplasties and are the cause of as many as 50% of all total knee revisions.[5,7,29] These complications, which include patellar subluxation and dislocation, uneven wear, deformation and failure of the prosthetic components, patellar fracture, and anterior knee pain, are caused largely by increased contact pressures and altered kinematics at the patellofemoral joint.[34]

The increase in patellofemoral contact pressures after total knee arthroplasty is well docu-

Questions? Contact FDA/CDRH/OCE/DID at CDRH-FOISTATUS@fda.hhs.gov or 301-796-8118

Records processed under FOIA Request #2014-8015; Released by CDRH on 12-8-2015

mented. This is especially true when domed, rather than congruent, patellar prostheses are used. Several authors have reported patellofemoral contact stresses exceeding the yield strength of the polyethylene patellar components after total knee arthroplasty.[8,17,30] Although creep and wear of the patellar component may contribute to decreased contact stresses at the patellofemoral joint, domed patellar prostheses removed from patients at the time of revision continue to exhibit substantially elevated contact stresses at the patellofemoral joint in vitro.[30]

Altered patellofemoral joint kinematics also has been associated with complications in total knee arthroplasty.[6,10,19,31] This is largely because of the resultant increased patellofemoral contact pressures. Yoshii et al[37] experimented with altered component positioning to determine the most anatomic positioning with the least patellar tilt. Singerman et al[36] reported increased patellofemoral contact stresses with varied Q angles in vitro. Meyer et al[32] reported altered patellofemoral joint contact areas with experimentally induced patellar baja in vitro.

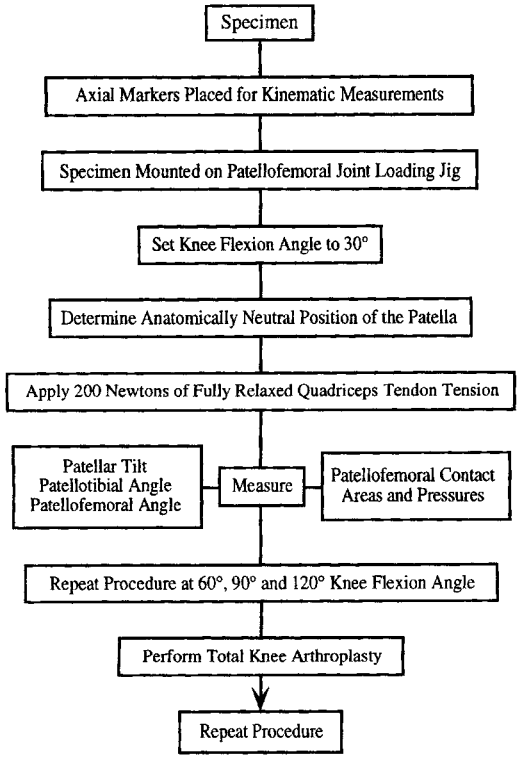

Fig 1. Flow chart describing the experimental protocol. Patellofemoral joint kinematics, contact pressures, and contact areas were assessed concurrently using the same specimens for preoperative and postoperative measurements to control for interspecimen variability.

Although altered contact pressures and kinematics are major sources of patellofemoral joint complications after total knee arthroplasty, these two interdependent variables have not been studied concurrently before and after total knee arthroplasty. The objective of this study was to measure simultaneously the patellofemoral joint kinematics (patellar tilt, patellofemoral angle, and patellotibial angle) and patellofemoral contact areas and pressures in human cadaver knees before and after total knee arthroplasty. This information provides additional detail for total knee arthroplasty procedures using the Kirschner Performance Knee System and subsequently may aid in the better understanding and prevention of patellofemoral complications.

MATERIALS AND METHODS

Patellofemoral kinematics, contact areas, and contact pressures were measured concurrently before and after total knee arthroplasty (Fig 1). Ten fresh frozen human cadaver knees were used as control (preoperative) and experimental (postoperative) specimens. All knees were macroscopically intact with radiographically normal bone structure and no history of knee surgery. The ages were estimated to be between 60 and 80 years. The femurs were 69 ± 7 mm (mean ± standard deviation) in the anteroposterior dimension and 84 ± 5 mm in the mediolateral dimension. The tibias were 61 ± 4 mm in the anteroposterior dimension and 79 ± 2 mm in the mediolateral dimension.

Specimen Preparation

The knees were dissected carefully leaving the patellofemoral joint, the tibiofemoral joint, the

Questions? Contact FDA/CDRH/OCE/DID at CDRH-FOISTATUS@fda.hhs.gov or 301-796-8118

Records processed under FOIA Request #2014-8015; Released by CDRH on 12-8-2015

periarticular skin and subcutaneous tissue, and the knee capsule intact. The vasti muscles were excised, but the rectus femoris and the quadriceps tendon were left for clamping. The fibula was removed, and the femur and tibia were cut 25 cm from the tibial plateau. Care was exercised not to violate the cartilaginous structures. The superior part of the synovial pouch was freed to allow placement of the Fuji pressure sensitive film (Fuji Photo Film Co, Ltd, Tokyo, Japan; Fig 2A). The specimens were kept moist throughout the experiment.

Five 2.8-mm threaded Steinmann pins were used to indicate the anatomic axes of each knee (Fig 2B). The first was placed transversely through the distal femur from the medial to the lateral epicondyle. The second was placed through the central longitudinal axis of the patella. The third was placed transversely through the midline of the patella perpendicular to the longitudinal pin. The final two pins were attached to the testing jig to represent the longitudinal axes of the femur and the tibia. Lateral and skyline radiographs of the specimens were taken to determine the difference between the pin placement and the axes they represented. A correction factor was determined and used during the kinematics analysis.

Patellofemoral Joint Testing Jig and Specimen Mounting

A previously described custom testing jig was modified to permit simultaneous measurement of the patellofemoral contact pressure and the quadriceps tendon tension.[18] The tibia and femur of each specimen were positioned in mounting cylinders using 12 fixation pins and rigidly fixed using diaphyseal bolts. An intramedullary alignment guide also was used to ensure that the tibial shaft was concentric within its mounting cylinder. The femur was mounted with its coronal plane parallel to its cylinder and in anatomic valgus. With the aid of a Model 1122 Instron machine (Instron Corporation, Canton, MA), the mounted specimen could be positioned at variable knee flexion angles while allowing translation in the x, y, and z axes and independent rotational freedom for the femur and the tibia. Once the specimen was mounted securely, it was positioned at the desired knee flexion angle. For each knee flexion angle, the patella was oriented in the trochlear groove in a position such that either medial or lateral deviation would result in a measurable increase in the quadriceps tendon tension. This was defined as the anatomically neutral position of the patella for a given knee flexion angle. After this

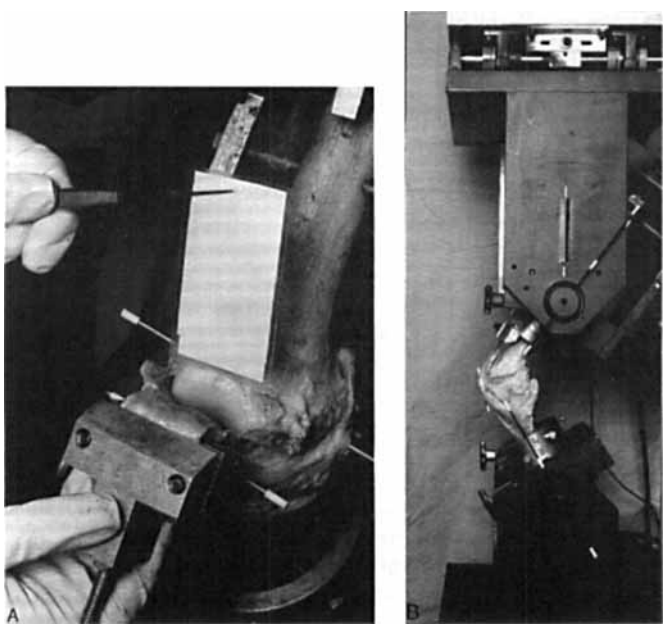

Fig 2A–B. Photographs showing the preparation and mounting of the specimens. (A) The knee was dissected carefully leaving the patellofemoral joint, the tibiofemoral joint, the knee capsule, and the periarticular soft tissues intact. The proximal portion of the patella was freed to allow insertion of the Fuji film. (B) The knee was mounted in a custom testing jig and an Instron machine. This system allows translation in the x, y, and z axes and independent rotation of the femur and tibia. Three threaded Steinmann pins were used to indicate the anatomic axes of the knee. Note that Steinmann pins also were attached to the Instron to represent the femoral and tibial longitudinal axes. The patellofemoral and patellotibial angles are shown in this lateral view.

Questions? Contact FDA/CDRH/OCE/DID at CDRH-FOISTATUS@fda.hhs.gov or 301-796-8118

Records processed under FOIA Request #2014-8015; Released by CDRH on 12-8-2015

position was determined, the quadriceps tendon was tensioned to and maintained at a fully relaxed equilibrated tension of 200 N for the measurement of the patellofemoral joint kinematics, contact areas, and contact pressures.

Patellofemoral Kinematics

The patellofemoral, patellotibial, and patellar tilt angles were measured at knee flexion angles of 30°, 60°, 90°, and 120°. The patellofemoral angle was defined as the angle in the sagittal plane between the longitudinal axis of the femur and the longitudinal axis of the patella. The patellotibial angle was defined as the angle in the sagittal plane between the longitudinal axis of the tibia and the longitudinal axis of the patella (Fig 3A). The patellar tilt angle was defined as the angle in a transverse plane between the epicondylar axis of the femur and the transverse axis of the patella (Fig 3B).

The kinematics measurements were made by tracking reflective markers attached to the Steinmann pins representing the anatomic axes of the specimens. Images of the external markers were recorded and analyzed on a video digitizing system composed of a video camera, a video cassette recorder, a high resolution monitor, a video processor (Motion Analyses VP320 and Expertvision Software, Santa Rosa, CA), and a computer. The camera was centered on the patella and aligned exactly parallel to the transverse axis of the femur for the lateral view and to the longitudinal axis of the patella for the skyline view. This was confirmed using the video digitizing system before each test. The distance from the camera to each specimen was kept constant for the lateral and skyline views. A 10-mm gauge was used to calibrate the two-dimensional coordinates before each test. With the use of the video digitizing system, the centroids of the reflective markers were calculated and tracked in Cartesian coordinates for the determination of the patellofemoral angle, patellotibial angle, and patellar tilt. The precision of this video digitizing system is achieved through subpixel centroid calculations and previously has been established at 0.005 mm for the magnification used in this study.[25,26] This detailed mounting protocol, custom testing jig, and video digitizing system yielded patellofemoral joint kinematics measurements reproducible to within 1° for five repeated trials.

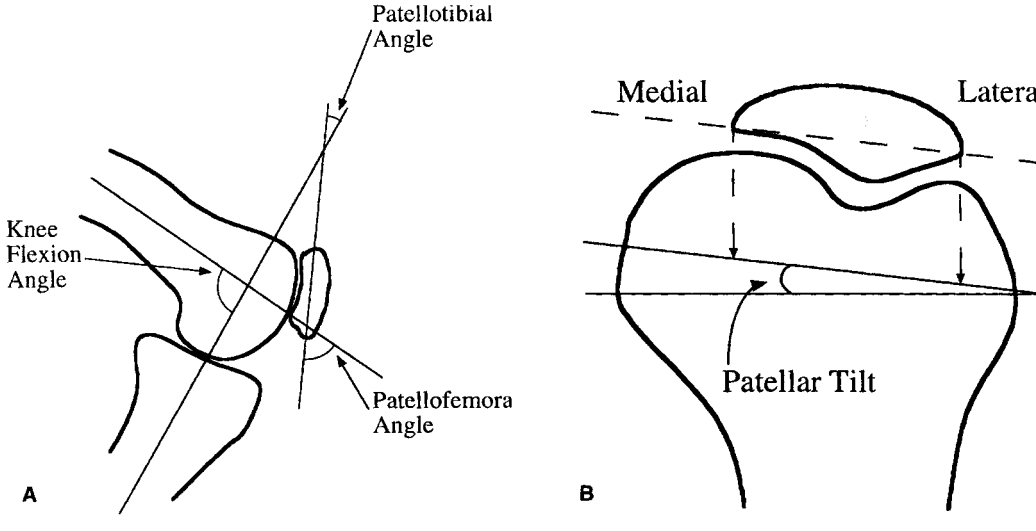

Fig 3A–B. A schematic drawing showing the patellofemoral joint kinematics variables determined using the video digitizing system. (A) The knee flexion, patellofemoral, and patellotibial angles were determined in the sagittal plane with the camera aligned with the transverse axis of the femur. (B) The patellar tilt angle was defined as the angle between the transverse axis of the femur and the transverse axis of the patella. For this skyline view, the camera was aligned with the longitudinal axis of the patella.

Questions? Contact FDA/CDRH/OCE/DID at CDRH-FOISTATUS@fda.hhs.gov or 301-796-8118

Records processed under FOIA Request #2014-8015; Released by CDRH on 12-8-2015

Patellofemoral Contact Areas and Pressures

The intraarticular contact areas and pressures of the patellofemoral joint were measured at 30°, 60°, 90°, and 120° knee flexion using Fuji pressure sensitive film. The film was cut to 5 × 5 cm and sealed within thin polyethylene sheets for use within each saline lubricated patellofemoral joint. The total thickness of the film and polyethylene sheets was approximately 250 μm. This has been shown to have a negligible effect on the measurement of patellofemoral contact areas and pressures.[3] Super low type Fuji film with a range of 0.5 to 2.5 MPa was used preoperatively, and medium type Fuji film with a range of 10 to 50 MPa was used postoperatively. The color density on the Fuji film is proportional to the intraarticular contact pressure.

The quadriceps tendon was tensioned to a constant load of 200 N for a minimum of 2 minutes to obtain the patellofemoral contact pressure patterns. Two measurements were obtained at each knee flexion angle to ensure reproducibility. Films with any evidence of crinkling artifact were discarded and repeated. The Fuji film images were scanned on a Hewlett Packard (Palo Alto, CA) Desk Scan II color scanner and analyzed with the National Institutes of Health (Bethesda, MD) Image Version 1.52 program with a calibrated scale from the manufacturer as a reference. This program converts the Fuji film image into a scaled image with 256 levels of gray. The scanned images were analyzed for total contact area (mm^2), peak contact pressure (MPa), and mean pressure (MPa). The peak contact pressure was defined as the average contact pressure of the 10% of the contact area with the highest contact pressure. The mean contact pressure was defined as the average contact pressure of the entire contact area. Preliminary studies revealed the accuracy of the color scanner to be within 0.5% for area and pressure measurements. The accuracy of Fuji film has been reported to be within 10%.[12,15,27]

Total Knee Arthroplasty

After the preoperative kinematics measurements, contact pressures, and contact areas were determined, the specimens underwent total knee arthroplasty using the Kirschner Performance Knee System (Kirschner Medical Corporation, Timonium, MD). This prosthesis is a modular, tricompartmental, semiconstrained system with a domed, all polyethylene patellar button and a lateral femoral flange. The total knee arthroplasties were performed using the company's recommended surgical protocol by a designer of the knee system (WCK) with the assistance of an orthopaedic surgery resident (APG). Patellar resection criteria based on specific anatomic landmarks were used for the prosthetic patellar resurfacing.[24] After the components were implanted, the knees were taken through a full range of motion to assess soft tissue balance. No soft tissue releases were required after implantation of the components. The knees were closed in anatomic layers. The same anatomically based mounting criteria, fixation pins, and diaphyseal mounting holes were used for preoperative and postoperative testing for reproducible positioning of each specimen. Each specimen was subjected to the same testing procedures as before total knee arthroplasty to determine the patellar tilt, patellofemoral angle, patellotibial angle, contact area, and contact pressure at each knee flexion angle.

Statistical Analysis

Data were analyzed using a multivariate analysis of variance with a significance level of 0.05.

RESULTS

Patellofemoral Kinematics

No statistically significant differences between preoperative and postoperative specimens were observed with respect to the patellofemoral, patellotibial, or patellar tilt angles from 30° to 120° knee flexion (Fig 4). The maximum changes for individual specimens in patellofemoral, patellotibial, and patellar tilt angles after total knee arthroplasty were 14°, 11°, and 11°, respectively (Fig 5).

Patellofemoral Contact Areas and Pressures

Typical patellofemoral contact area and pressure patterns before and after total knee arthroplasty are shown in Figure 6. Of note is the two-point patellofemoral contact seen throughout the range of motion tested in the postoperative specimens.

Questions? Contact FDA/CDRH/OCE/DID at CDRH-FOISTATUS@fda.hhs.gov or 301-796-8118

Records processed under FOIA Request #2014-8015; Released by CDRH on 12-8-2015

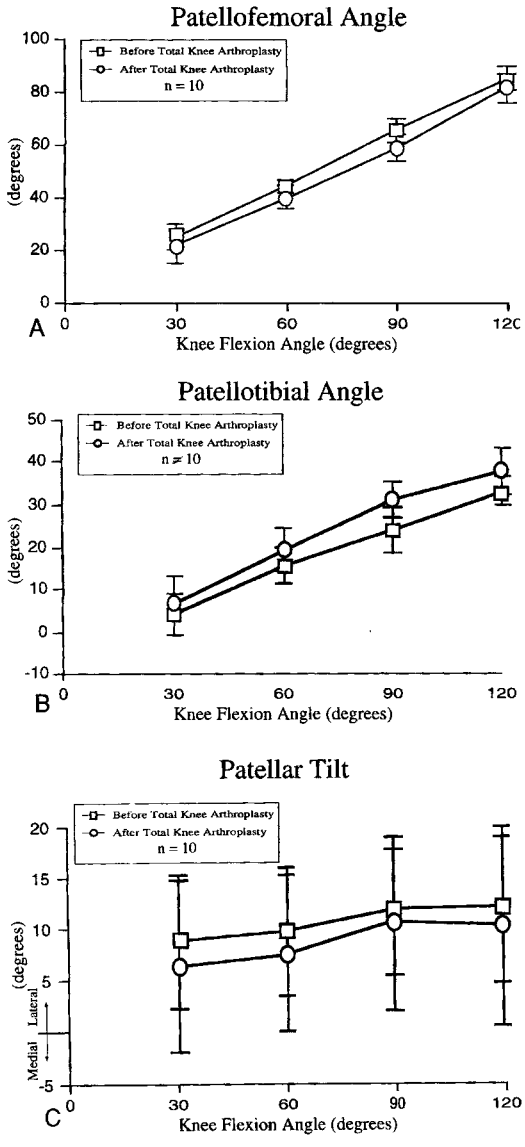

Fig 4A–C. Graphs showing the knee flexion angle versus patellofemoral, patellotibial, and patellar tilt angles before and after total knee arthroplasty. No statistically significant difference was observed between 30° and 120° knee flexion. Error bars indicate standard deviation from the mean. (A) A graph showing knee flexion angle versus patellofemoral angle before and after total knee arthroplasty. (B) A graph showing knee flexion angle versus patellotibial angle before and after total knee arthroplasty. (C) A graph showing knee flexion angle versus patellar tilt angle before and after total knee arthroplasty.

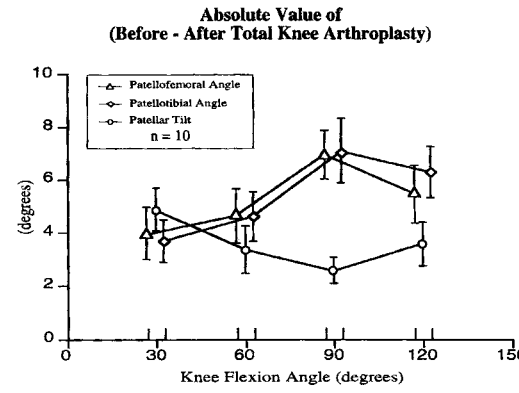

Fig 5. A graph showing the change in patellofemoral, patellotibial, and patellar tilt angles after total knee arthroplasty. The change in patellar tilt angle was minimum at 30° knee flexion.

A statistically significant change in patellofemoral joint contact area was seen after total knee arthroplasty. The average patellofemoral joint contact area before total knee arthroplasty was 189 ± 83 (mean ± standard deviation), 231 ± 80, 232 ± 80, and 191 ± 51 mm^2 at 30°, 60°, 90°, and 120° knee flexion, respectively. The average patellofemoral joint contact area after total knee arthroplasty was 16 ± 5, 17 ± 7, 13 ± 3, and 10 ± 2 mm^2 at 30°, 60°, 90°, and 120° knee flexion, respectively. These data represent 12-, 13-, 18-, and 19-fold reductions in patellofemoral joint contact area after total knee arthroplasty for the respective knee flexion angles. There were no statistically significant differences when medial and lateral facet contact areas were compared.

A statistically significant change in average patellofemoral joint contact pressure also was observed. The average contact pressure before total knee arthroplasty was 0.75 ± 0.18, 0.70 ± 0.17, 0.72 ± 0.16, and 0.79 ± 0.24 MPa at 30°, 60°, 90°, and 120° knee flexion, respectively. The average contact pressure after total knee arthroplasty was 18.2 ± 2.2, 20.2 ± 3.6, 23.2 ± 2.5, and 23.8 ± 3.1 MPa at 30°, 60°, 90°, and 120° knee flexion, respectively. These are increases of 24-,

Questions? Contact FDA/CDRH/OCE/DID at CDRH-FOISTATUS@fda.hhs.gov or 301-796-8118

Records processed under FOIA Request #2014-8015; Released by CDRH on 12-8-2015

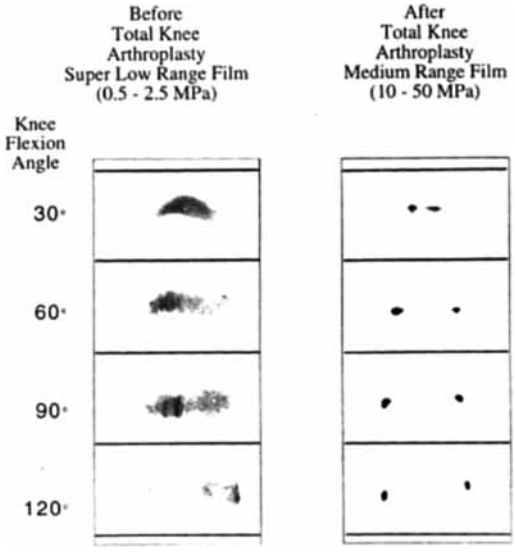

Fig 6. Photographs of the Fuji pressure sensitive film patterns at the patellofemoral joint before and after total knee arthroplasty at 30°, 60°, 90°, and 120° knee flexion. These patterns were scanned with a Hewlett Packard color scanner and analyzed using the National Institutes of Health Image Version 1.52 program to determine the mean and peak contact pressures and total contact areas. The patellofemoral contact areas after total knee arthroplasty using the Kirschner Performance Knee System show the typical two-point contact pattern consistent with its dome shaped patellar prosthesis.

29-, 32-, and 30-fold after total knee arthroplasty for the respective knee flexion angles. The peak contact pressure before total knee arthroplasty was 1.48 ± 0.48, 1.44 ± 0.45, 1.66 ± 0.50, and 1.63 ± 0.64 MPa at 30°, 60°, 90°, and 120° knee flexion, respectively. The peak contact pressure after total knee arthroplasty was 28.9 ± 3.8, 31.4 ± 4.1, 32.7 ± 3.6, and 33.4 ± 5.1 MPa at 30°, 60°, 90°, and 120° knee flexion, respectively. This indicates increases of 20-, 22-, 20-, and 20-fold after total knee arthroplasty for the respective knee flexion angles. As with the contact areas, there were no statistically significant differences when medial and lateral facet contact pressures were compared.

DISCUSSION

It is well established that patellofemoral contact pressures increase significantly after total knee arthroplasty. Not surprisingly, a concomitant decrease in patellofemoral contact areas has been observed. In addition, experimentally altered patellofemoral joint kinematics has been shown to cause increased patellofemoral joint contact pressures.[21] The question remained whether the increase in patellofemoral contact pressures after total knee arthroplasty in vitro is a primary consequence of iatrogenically altered patellofemoral kinematics in vitro. This study specifically addressed the changes in patellofemoral joint contact areas and pressures before and after total knee arthroplasty with simultaneous assessment of the patellofemoral kinematics. An increase in peak and average contact pressures and a decrease in contact areas at the patellofemoral joint has been shown with no associated alteration of patellofemoral joint kinematics.

The method used in this study is unique in that permanent axial markers were strategically placed before testing and were used throughout the experiment. The use of Steinmann pins as fixed, external markers of anatomic axes for the measurement of patellofemoral kinematics offers several advantages over conventional radiographic or skin markers. First, accurate placement is assured between preoperative and postoperative specimens because the pins were not removed. Second, using external markers with consistent and reproducible camera positions, measurements are not distorted by rotation, as would occur with radiographic analysis. This video digitizing system has been used successfully for large and small measurements in bone and soft tissues.[9,16,23,26] Finally, because the Steinmann pins are rigidly fixed, they could move with respect to the bone, as could markers affixed to the skin or soft tissues. To eliminate out of plane errors of angular measurements, the camera was aligned meticulously with the referenced axial Steinmann

Questions? Contact FDA/CDRH/OCE/DID at CDRH-FOISTATUS@fda.hhs.gov or 301-796-8118

Records processed under FOIA Request #2014-8015; Released by CDRH on 12-8-2015

pins at each knee flexion angle. The knees were mounted on the jig following a detailed positioning protocol using the same anatomically based mounting criteria, fixation pins, and diaphyseal drill holes before and after total knee arthroplasty. Following this protocol, reproducible patellofemoral joint kinematics measurements to within 1° could be achieved for five trials with a given knee. Previous studies have found this system to be as accurate as radiographic, manual, and electromagnetic (linearly variable differential transducer) means of positional measurement.[9,23,26]

Patellofemoral kinematics parameters were restored to within a maximum deviation of 14°, 11°, and 11° from the original values for the patellofemoral, patellotibial, and patellar tilt angles, respectively. This was not statistically significant through the range of knee flexion tested. The minimum change in patellar tilt after total knee arthroplasty procedure occurred at 90° knee flexion, where the patella is deeply seated in the intact and prosthetic trochlear grooves. This suggests the importance of the geometric constraints of the patellofemoral joint, especially at higher knee flexion angles. The variability of the patellofemoral joint kinematics parameters observed is likely related to differences in the patellofemoral joint geometry of the preoperative and postoperative knees. The authors do not attribute this variability to the surgical technique because of the detailed procedural controls used during this study. The same cadaveric knees were used for control (preoperative) and experimental (postoperative) measurements to control for interspecimen variability. The same surgeons performed each procedure. Optimal exposure was achieved because implantation of the prosthesis was accomplished in a controlled laboratory setting.

Soft tissue structures have been shown to contribute significantly to the stability of the patellofemoral joint near terminal extension of the knee.[18,28] In the current study, the periarticular soft tissues including the skin were left intact. The rectus femoris in continuity with the quadriceps tendon was loaded with the patella in its anatomically neutral position to simulate the resultant force vector of the knee extensors.[1,2] Because there is interspecimen variability of the patellofemoral joint, this anatomically neutral position is essential for accurate assessment of kinematics, contact areas, and contact pressures.[22] In addition, the quadriceps tendon tension was equilibrated to and maintained at 200 N during all measurements. The constant tension of 200 N, although lower than estimated maximal physiologic values, was used for consistent and even clamping across the width of the quadriceps tendon clamp.

Average patellofemoral joint contact areas decreased as much as 19-fold, mean contact pressures increased as much as 32-fold, and peak contact pressures increased as much as 22-fold after total knee arthroplasty. These findings were statistically significant and are consistent with previously published trends.[8,19,30] The magnitude of increase in mean contact pressures was greater than the magnitude of decrease in contact areas, despite a constant quadriceps tendon tension being maintained. This suggests that the transmission of quadriceps tendon force via soft tissues is more significant preoperatively than postoperatively. Huberti and Hayes[21] found direct evidence for tendofemoral load transmission in the knee at high flexion angles. The retropatellar fat pad and the extensor retinaculum also may contribute to load bearing across the knee. The resection of the retropatellar fat pad and the transection of the patellofemoral ligament during total knee arthroplasty may affect patellofemoral joint contact pressures after total knee arthroplasty in vitro.

Although pressure sensitive Fuji film has been reported to have a maximum measurement error of 10%,[12,15,27] it is unlikely that this has a significant impact on the proportional change in patellofemoral joint contact areas and pressures between the preoperative and postoperative groups. Hale and Brown[15] determined that medium range Fuji film is sufficient for evaluating articular contact pressures. Ateshian et al[3] concluded that analysis of con-

Questions? Contact FDA/CDRH/OCE/DID at CDRH-FOISTATUS@fda.hhs.gov or 301-796-8118

Records processed under FOIA Request #2014-8015; Released by CDRH on 12-8-2015

tact areas with Fuji film yields results comparable with stereophotogrammetric methods and superior to dye staining and rubber casting. Pressure sensitive film has become a well accepted means of investigating articular contact areas and pressures.[8,12,17,21,22,27,30]

Increased patellofemoral joint contact stress after total knee arthroplasty has been implicated as the primary cause of component wear and failure.[2,4,6,10,13,31,35] Although this increased stress may be caused by component malalignment or inadequate soft tissue balancing leading to altered patellofemoral kinematics, this study has shown that the elevated patellofemoral joint contact pressures exist despite the restoration of preoperative patellofemoral kinematics after total knee arthroplasty in vitro. Thus, elevated contact stress in vitro is largely because of the material and structural characteristics of the prosthetic components in a properly done total knee arthroplasty. Clinically, patient characteristics such as weight, activity, and preexisting deformity also contribute to elevated contact pressures. Although the increase in contact stress after patellar resurfacing with domed prostheses has been shown to exceed the yield strength of ultra high molecular weight polyethylene, this does not mean imminent component failure. Creep and wear of the prosthesis and structural remodeling of the underlying bone allow for increased contact area and decreased contact stress after prolonged use.[20,30] The results of this study directly apply to the Kirschner Performance Knee System but may be applicable to other systems.

Acknowledgments

The authors thank Yi-Peng Wang, MD, Guisou Mahmoud, BS, and Michael Danto, MS, for technical assistance.

References

1. Ahmed AM, Burke DL, Yu A: In-vitro measurement of static pressure distribution in synovial joints-Part II: Retropatellar surface. J Biomech Eng 105: 226–236, 1983.
2. Ahmed AM, Shi S, Hyder A, Chan KH: The effects of quadriceps tension characteristics on the patellar tracking pattern. Trans Orthop Res Soc 13:280, 1988.
3. Ateshian GA, Kwak SD, Soslowski LJ, Mow VC: A Stereophotogrammetric method for determining in-situ contact areas in diarthrodial joints: A comparison study. Adv Bioeng ASME 22:35–38, 1992.
4. Berger RA, Rubash HE, Seel MJ, Thompson WH, Crossett LS: Determining the rotational alignment of the femoral component in total knee arthroplasty using the epicondylar axis. Clin Orthop 286:40–47, 1993.
5. Boyd AD, Frederick CE, Thomas WH, Poss R, Sledge CB: Long-term complications after total knee arthroplasty with or without resurfacing of the patella. J Bone Joint Surg 75A:674–681, 1993.
6. Briard JL, Hungerford DS: Patellofemoral instability in total knee arthroplasty. J Arthroplasty 4(Suppl):87–97, 1989.
7. Brick GW, Scott RD: The patellofemoral component of total knee arthroplasty. Clin Orthop 231:163–178, 1988.
8. Collier JP, McNamara JL, Surprenant VA, Jensen RE, Surprenant HP: All polyethylene patellar components are not the answer. Clin Orthop 273: 198–203, 1991.
9. Derwin KA, Soslowsky LJ, Green WDK, Elder SH: A new optical system for the determination of deformation and strains: Calibration characteristics and experimental results. J Biomech 27:1277–1285, 1994.
10. Figgie HE, Goldberg VM, Figgie MP, et al: The effect of alignment of the implant on fractures of the patella after condylar total knee arthroplasty. J Bone Joint Surg 71A:1031–1039, 1989.
11. Figgie HE, Goldberg VM, Heiple KG, Moller HS, Gordon NH: The influence of tibial-patellofemoral location on the function of the knee in patients with the posterior stabilized condylar knee prosthesis. J Bone Joint Surg 68A:1035–1040, 1986.
12. Fukubayashi T, Kurosawa H: The contact area and pressure distribution pattern of the knee. Acta Orthop Scand 51:871–879, 1980.
13. Gomes LSM, Bechtold JE, Gustilo RB: Patellar prosthesis positioning in total knee arthroplasty. A roentgenographic study. Clin Orthop 236:72–81, 1988.
14. Gunston FH: Polycentric knee arthroplasty. Prosthetic simulation of normal knee movement. J Bone Joint Surg 53B:272–277, 1971.
15. Hale JE, Brown TD: Contact stress gradient detection limits of pressensor film. J Biomech Eng 114:352–357, 1992.
16. Harner CD, Xerogeanes JW, Livesal GA, et al: The human posterior cruciate ligament complex: An interdisciplinary study. Ligament morphology and biomechanical evaluation. Am J Sports Med 23: 736–745, 1995.
17. Hayes WC, Lathi VK, Takeuchi TY, et al: Patellofemoral contact pressures exceed the compressive yield strength of UHMWPE in total knee arthroplasty. Trans Orthop Res Soc 39:421, 1993.
18. Heegaard J, Leyvraz PF, Van Kampen A, et al: Influence of soft tissue structures on patellar three-dimensional tracking. Clin Orthop 299:235–243, 1994.

Questions? Contact FDA/CDRH/OCE/DID at CDRH-FOISTATUS@fda.hhs.gov or 301-796-8118

Records processed under FOIA Request #2014-8015; Released by CDRH on 12-8-2015

19. Hoffman GO, Hagena FW: Pathomechanics of the patellofemoral joint following total knee arthroplasty. Clin Orthop 224:251–259, 1987.
20. Hsu HP, Walker PS: Wear and deformation of patellar components in total knee arthroplasty. Clin Orthop 246:260–265, 1989.
21. Huberti HH, Hayes WC: Patellofemoral contact pressures. The influence of Q-angle and tendofemoral contact. J Bone Joint Surg 66A:715–724, 1984.
22. Lee TQ, Anzel SH, Bennett KA, Pang D, Kim WC: The influence of fixed rotational deformities of the femur on the patellofemoral contact pressures in human cadaveric knees. Clin Orthop 302:69–74, 1994.
23. Lee TQ, Danto MI: Application of a continuous video digitizing system for tensile testing of bone-soft tissue-bone complex. Adv Bioeng ASME 22:87–90, 1992.
24. Lee TQ, Kim WC, Di Zio RM, Bass DV, Anzel SH: Geometric characteristics of the patella: Quantitative assessment of a consistent method for patellar resection. Trans Orthop Res Soc 16:562, 1991.
25. Lee TQ, Lewis DA, Kim WC, Anzel SH: Nondestructive Biomechanical Assessment of Intact and Reconstructed Hips. In Vossoughi J (ed). Southern Biomedical Engineering Conference. Vol 13. Washington, DC, University of the District of Columbia 427–429, 1994.
26. Lee TQ, Wang YP, Ishak AM, et al: Assessment of geometry and deformation characteristics of human cadaveric femur. Adv Bioeng ASME 22:39–41, 1992.
27. Lorenz M, Patwardhan A, Vanderby R: Load-bearing characteristics of lumbar facets in normal and surgically altered spinal segments. Spine 8: 122–130, 1983.
28. Luo ZP, Hsu HC, Rand JA, An KN: Importance of soft tissue integrity on biomechanical studies of the patella after TKA. J Biomech Eng 118:130–132, 1996.
29. Lynch AF, Rorabeck CH, Bourne RB: Extensor mechanism complications following total knee arthroplasty. J Arthroplasty 2:135–140, 1987.
30. McNamara JL, Collier JP, Mayor MB, Jensen RE: A comparison of contact pressures in tibial and patellar total knee components before and after service in-vivo. Clin Orthop 299:104–113, 1994.
31. Merkow RL, Soudry M, Insall JN: Patellar dislocation following total knee replacement. J Bone Joint Surg 67A:1321–1327, 1985.
32. Meyer SA, Brown TD, Pedersen DR, Albright JP: The effects of patella infra on patellofemoral contact stress. Trans Orthop Res Soc 18:303, 1993.
33. Murray DG: Total knee arthroplasty. Clin Orthop 192:59–68, 1985.
34. Rand JA: The patellofemoral joint in total knee arthroplasty. J Bone Joint Surg 76A:612–620, 1994.
35. Rhoads DD, Noble PC, Reuben JD, Tullos HS: The effect of femoral component position on the kinematics of total knee arthroplasty. Clin Orthop 286: 122–129, 1993.
36. Singerman R, Daly J, Brazinski M, Davy DT: In vitro measurement of patellofemoral contact forces. Trans Orthop Res Soc 17:609, 1992.
37. Yoshii I, Whiteside LA, Anouchi YS: The effects of patellar button placement and femoral component design on patellar tracking in total knee arthroplasty. Clin Orthop 275:211–219, 1992.

Questions? Contact FDA/CDRH/OCE/DID at CDRH-FOISTATUS@fda.hhs.gov or 301-796-8118

Records processed under FOIA Request #2014-8015; Released by CDRH on 12-8-2015

Bio-Medical Materials and Engineering 11 (2001) 167–183
IOS Press

Effect of crosslinking UHMWPE on its tensile and compressive creep performance

Gladius Lewis [a,*] and Michael Carroll [b]
[a] *Department of Mechanical Engineering, The University of Memphis, Memphis, TN 38152-3180, USA*
[b] *Wright Medical Technology, Inc., Arlington, TN 38002, USA*

Received 21 September 2000

Abstract. The *in vitro* quasi-static tensile and compresssive creep properties of three sets of GUR 1050 ultra-high-molecular-weight polyethylene (UHMWPE) specimens were obtained. These sets were: control (as-received stock); "low-gamma" (specimens were crosslinked using γ radiation, with a minimum dose of 5 Mrad); and "high-gamma" (specimens were crosslinked using γ radiation, with a minimum dose of 15 Mrad). The % crystallinity ($\%C$) and crosslink density (ρ_x) of the specimens in the three sets were also obtained. It was found that, in both tension and compression, crosslinking resulted in a significant depreciation in the creep properties, relative to control. The trend in the creep results is explained in terms of the impact of crosslinking on the polymer's $\%C$ and ρ_x. The present results are in contrast to literature reports that show that crosslinking enhances the wear resistance of the polymer. The implications of the present results, taken together with the aforementioned literature results, are fully discussed *vis-a-vis* the use of crosslinked UHMWPE for fabricating articular components for arthroplasties.

Keywords: Ultra-high-molecular-weight-polyethylene, crosslinking, creep, crystallinity, crosslink density

1. Introduction

There are two main reasons for studying various aspects of the creep performance of ultra-high-molecular-weight-polyethylene (UHMWPE) – such as factors that influence it, magnitude, and mechanism(s) – relative to its use for fabricating articular components for arthroplasties.

First, regardless of the method used to determine the extent of permanent dimensional changes ("aggregate wear") seen in retrieved UHMWPE components – the Livermore radiographic [1] and oil displacement [2] methods, for example – it is agreed that these changes are the result of both creep and wear. On some of these components, it is obvious that creep is the dominant mode; for example, curling reported along the anterior margins of tibial inserts [3]. In the majority of cases, however, the relative contributions of creep and wear are a matter of debate. For example, for one set of retrieved acetabular cup liners, Wroblewski et al. [4] opined that "there is little doubt that wear rather creep is mainly responsible for the dimensional changes", while for another set they attributed the large mean penetration rate (of 0.11 mm/y) seen in the first 2 years to "bedding-in" or creep [5]. This controversy is understandable, as current methods of evaluating retrieved UHMWPE articular components have limited utility for making the distinction between creep and wear [6]. Thus, knowledge of creep values would allow "aggregate wear" results to be corrected.

The second reason for the interest in UHMWPE creep is that, in arthroplasties, creep of the UHMWPE articular component can result in various undesirable phenomena, such as impingement of the femoral

*Corresponding author.

0959-2989/01/$8.00 © 2001 – IOS Press. All rights reserved

Questions? Contact FDA/CDRH/OCE/DID at CDRH-FOISTATUS@fda.hhs.gov or 301-796-8118

Records processed under FOIA Request #2014-8015; Released by CDRH on 12-8-2015

neck on the rim of the acetabular cup liner, in the case of the hip prosthesis, which could culminate in implant loosening [7].

A strong consensus has emerged that particles worn from UHMWPE articular component adversely affect the *in vivo* longevity of the prosthesis through the following pathway: these particles are phagocytosed, resulting in many reactions, notably osteolysis, which, in turn, contributes to or causes aseptic loosening of the implant [8]. In recognition of these postulates, a vast volume of literature on UHMWPE wear exists [9]. In addition, enormous research efforts continue to be expended in developing methods of increasing the wear resistance of UHMWPE components, the most recent being crosslinking the polymer [10]. In contrast to these efforts, UHMWPE creep has attracted much less research attention (Table 1), and, to date, only a few systematic studies have been reported on the effect of crosslinking UHMWPE on its creep performance [18–22]. It is particularly important to both delineate the details of this effect and the factors that influence it, in light of the substantial reduction in wear rate that has been reported for crosslinked UHMWPE [10].

Thus, three research questions are posed: Does crosslinking have a uniformly beneficial effect on all properties of UHMWPE that are germane to its use for fabricating articular components for arthroplasties? Or are some properties enhanced while others are degraded? What accounts for the changes in properties seen? The answers to these questions have important implications for the use of crosslinked UHMWPE articular components.

The present study, therefore, is designed to provide answers to the posed research questions, with reference to quasi-static tensile and compressive creep in laboratory ambient air (at 22 ± 1°C).

2. Materials and methods

The following three sets of specimens were fabricated from ram-extruded GUR 1050 UHMWPE (Poly-Hi Solidlur, Inc., Fort Wayne, IN, USA): "control" (as-received bar stock); "low-γ" [specimens crosslinked by being γ-irradiated in air; minimum dose of 5 Mrad (SteriGenics, Inc., Gurnee, IL, USA)]; and "high-γ" (specimens crosslinked by being γ-irradiated in air; minimum dose of 15 Mrad).

In the quasi-static tensile creep tests, a specimen (Fig. 1) was subjected to an applied load (M, kg) in a bench-top creep tester (Model SM106 Mk 2; TecQuipment, Ltd., Nottingham, England) (Fig. 2(a)) and the longitudinal extension of the specimen ($\square L$) was determined, from the reading of the attached dial gage (R), over a period that varied from 12 to 24 min. The tensile stress applied to the specimen (σ, MPa) was calculated thus: $9.81(2.84 + 8M)/A_{\mathrm{i}}$, where 2.84 kg is the total mass of the weight hanger and pins; 8 is the mechanical advantage of the lever arm; M is the applied mass; and A_{i} is the initial cross-sectional area of the gage section of the specimen (nominally, this is 6.86 mm × 1.40 mm; see Fig. 1). Note that $\square L = R/2$ because the distance from the grooved plate (that attaches the dial gage to the top of the lever arm) (point A) to the pivot is twice that from the center of the specimen (point B) to the pivot (Fig. 2(b)). In the tests, 3 values of M (0.25 kg, 0.50 kg and 0.75 kg) and, hence, three values of σ (4.94 ± 0.08 MPa, 7.06 ± 0.07 MPa and 9.03 ± 0.06 MPa) were used. At each stress level, 2 specimens from each set were tested. Thus, a total of 18 specimens were tested. For each specimen, the following parameters were calculated: (a) tensile creep strain (ε) = $\square L/20$ mm, with 20 mm being the initial gage section length of the specimen; (b) the ε-time, t plot; and (c) the slope of the steady-state or secondary zone of the ε–t plot; this parameter is referred to as the steady-state tensile creep strain rate, $\dot{\varepsilon}_{\mathrm{ss}}$.

From all the results in each set of specimens, the best fits to following relationships were obtained: (a) the Norton equation, which is $\dot{\varepsilon}_{\mathrm{ss}} = B\sigma^n$, where B and n are the material constants [23], (b) tensile creep compliance ($C = \varepsilon/\sigma$) $= \alpha + \beta(\log t)^\gamma$, where α, β, and γ are material constants [24].

Questions? Contact FDA/CDRH/OCE/DID at CDRH-FOISTATUS@fda.hhs.gov or 301-796-8118

Records processed under FOIA Request #2014-8015; Released by CDRH on 12-8-2015

Table 1
Some salient features of literature studies on the creep of UHMWPE

Type of applied loading	State of UHMWPE	Test conditions	Variable(s) studied	Reference
Quasi-static compression	Uncrosslinked; γ-irradiated (2.5 Mrad)	Medium: air at $37 \pm 1°C$	Applied stress (1, 1.5, 2, 3, 4, 5 MPa)	Little [11]
Quasi-static tension	Uncrosslinked	Stress: 4 MPa	Sterilization method (unsterilized vs. γ-irradiated)	Hood et al. [12]
Quasi-static tension	Uncrosslinked; unsterilized	Medium: air σ: 4 MPa	Specimen temperature (23, 38, 57°C)	Crissman [13]
Dynamic compression	Uncrosslinked; unsterilized	Frequency: 1 Hz Medium: bovine serum at $37 \pm 0.3°C$	$\sigma^{a}_{max} = 2$, 4, or 8 MPa; $R^{a} = 0.1$	Lee and Pienkowski [14]
Dynamic compression	Uncrosslinked	Frequency: 1 Hz Medium: bovine serum at $37 \pm 0.3°C$ σ_{max}: 8 MPa; $R = 0.1$	(1) Sterilization method (unsterilized, ram-extruded GUR 4150 vs. γ-irradiated, ram-extruded GUR 4150) (2) Specimen fabrication method (γ-irradiated ram-extruded GUR 4150 vs. γ-irradiated compression-molded GUR 4150) (3) Resin molecular weight (γ-irradiated compression-molded GUR 4150 vs. γ-irradiated slab-molded GUR 1020)	Lee et al. [15]
Quasi-static compression	Uncrosslinked; unsterilized	Medium: bovine serum + sodium azide solution at $36.5 \pm 0.7°C$	Applied stress (2, 4, 8 MPa)	Lee and Pienkowski [7]
Quasi-static compression	Uncrosslinked; unsterilized	Medium: air Stress: 1 MPa	(1) Specimen temperature (37, 42, 47, 52 57, 62°C)	Deng et al. [16]
Quasi-static tension	Uncrosslinked; unsterilized	Medium: air Stress: 1 MPa	(2) Reinforcement of the polymer (none vs. reinforcing with 5 wt. % gel-spun UHMWPE fibers)	
Quasi-static tension	Uncrosslinked; γ-irradiated (2.5–3.0 Mrad)	Medium: air at 20°C Loading rate: 250 $N\,s^{-1}$	Applied stress (1, 2, 4, 6, 8, 10, 15, 20, 25 MPa)	Estupinan et al. [17]

Questions? Contact FDA/CDRH/OCE/DID at CDRH-FOISTATUS@fda.hhs.gov or 301-796-8118

Records processed under FOIA Request #2014-8015; Released by CDRH on 12-8-2015

Table 1
(Continued)

Type of applied loading	State of UHMWPE	Test conditions	Variable(s) studied	Reference
Quasi-static compression	Uncrosslinked; crosslinked[b]	NS[c]	Crosslinking [none (γ-irradiated in N_2) vs. "highly crosslinked"]	Levine et al. [18]
Hip simulator	Uncrosslinked; crosslinked	Medium: bovine serum	(1) Crosslinking [none (γ-irradiated in air) vs. crosslinked, using electron beam radiation at room temperature, and then ethylene oxide (EtO) sterilized vs. crosslinked, using electron beam (with temperature being >120°C prior to and during irradiation), and then EtO sterilized (2) Test frequency (1, 2 Hz)	Bragdon et al. [19]
Hip simulator	Uncrosslinked; crosslinked	Medium: bovine serum at 37°C Frequency: 2 Hz	(1) Crosslinking [none (γ-irradiated in oxygenless packaging) vs. crosslinked, using electron beam radiation (initial temperature >120°C), melted, machined, and then EtO sterilized (2) Acetabular component size (22 mm vs. 28 mm diameter)	Bragdon et al. [20]
Hip simulator	Uncrosslinked; crosslinked	Medium: air or bovine serum Load: double-peaked Paul type Frequency: 2 Hz	Crosslinking [none (γ-irradiated in air) vs. crosslinked, using electron beam radiation at a starting temperature of 125°C, followed by melting, and sterilization with EtO	Estok et al. [21]
NS	Uncrosslinked;	Medium: air	(1) Crosslinking (none vs. crosslinking, using γ radiation, vs. crosslinking, using electron beam radiation) (2) Crosslinking radiation dose (2.5, 5, 10, 20 Mrad) (3) Post-crosslinking treatment (none vs. radical quenching[d]) (4) Test load (1107 N, 2225 N)	Furman et al. [22]
NS	Uncrosslinked; unsterilized	Medium: air Load: 4673 N	(1) Crosslinking (none vs. crosslinking, using γ radiation)	Furman et al. [22]

Questions? Contact FDA/CDRH/OCE/DID at CDRH-FOISTATUS@fda.hhs.gov or 301-796-8118

Records processed under FOIA Request #2014-8015; Released by CDRH on 12-8-2015

Table 1
(Continued)

Type of applied loading	State of UHMWPE	Test conditions	Variable(s) studied	Reference
			(2) Crosslinking radiation dose (2.5, 10 Mrad) (3) Post-crosslinking treatment (none vs. radical quenching)	

[a]Stress ratio, R = minimum stress, $\sigma_{\min}$/maximum stress, $\sigma_{\max}$.
[b]Crosslinking details were not stated in the report.
[c]Conditions were not stated in the report.
[d]At 150°C for 5 h under vacuum.

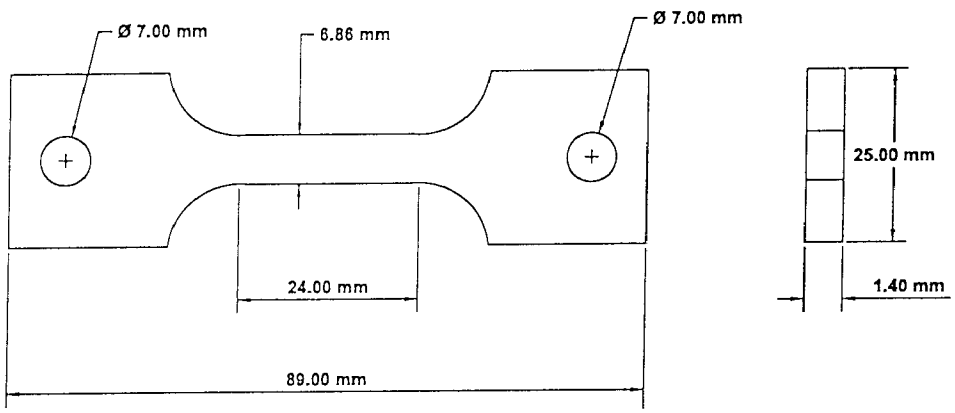

Fig. 1. Dimensioned drawing of the tensile creep test specimen.

The quasi-static compressive tests were conducted in accordance with ASTM D621 [25]. In the tests, a specimen (nominally a cube, measuring 12.7 mm × 12.7 mm × 12.7 mm) was subjected to a stress of 6.89 MPa in a servohydraulically-activated materials testing machine (Model 1321, Instron Corp., Canton, MA, USA) for a period of 1 h. The actuator displacement, □h-versus-time, t, plot was obtained. The height of the specimen after any time was determined as the difference between the initial height of the specimen and □h at that time. The compressive creep strain (ε_{com}) was calculated as $(H_{10\text{s}} - -H_{1\text{h}})/(H_{10\text{s}})$, where $H_{10\text{s}}$ and $H_{1\text{h}}$ are the specimen heights after 10 s and 1 h, respectively, under the stress. 6 control, 4 low-γ, and 6 high-γ specimens were tested. For each specimen, the results were obtained as an ε_{com}–t plot. Best fits were obtained for the compressive creep compliance (C') relation, which is $C' = \delta + \lambda(\log t)^{\eta}$, where δ, λ and η are material constants.

The crosslink density (ρ_x) of a specimen was determined, per ASTM D2765-90 [26], by measuring the relative mass change (δ), due to swelling, of a compression creep test specimen, in 100 ml of xylene at 110°C. ρ_x was then calculated using: (a) the equilibrium volume swell ratio, q, corrected for expansion due to heating and melting [27] (which was calculated from δ); (b) the Flory–Huggins interaction parameter, χ [28]; and (c) the molar volume of xylene, $V_1 (= 136 \times 10^{-6}\ \text{m}^3\ \text{mol}^{-1})$.

The two relevant expressions used to calculate ρ_x are as follows:

$$\text{Flory–Huggins interaction parameter} = \chi = \frac{0.55}{q} + 0.33,$$

Questions? Contact FDA/CDRH/OCE/DID at CDRH-FOISTATUS@fda.hhs.gov or 301-796-8118

Records processed under FOIA Request #2014-8015; Released by CDRH on 12-8-2015

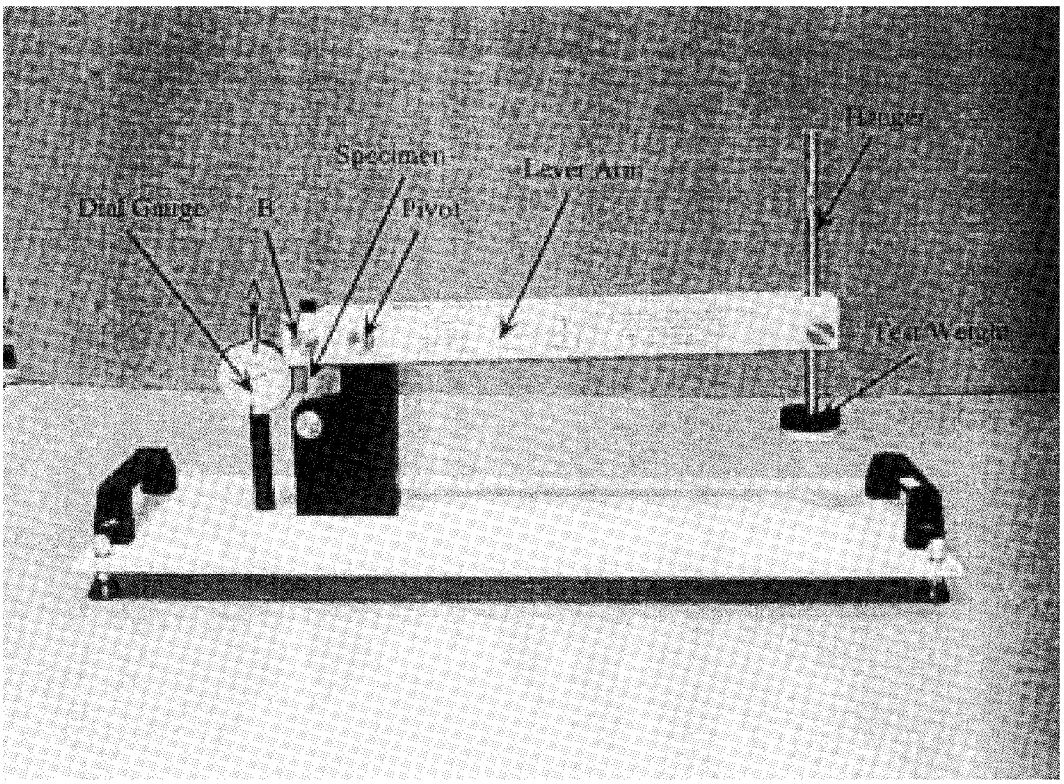

(a)

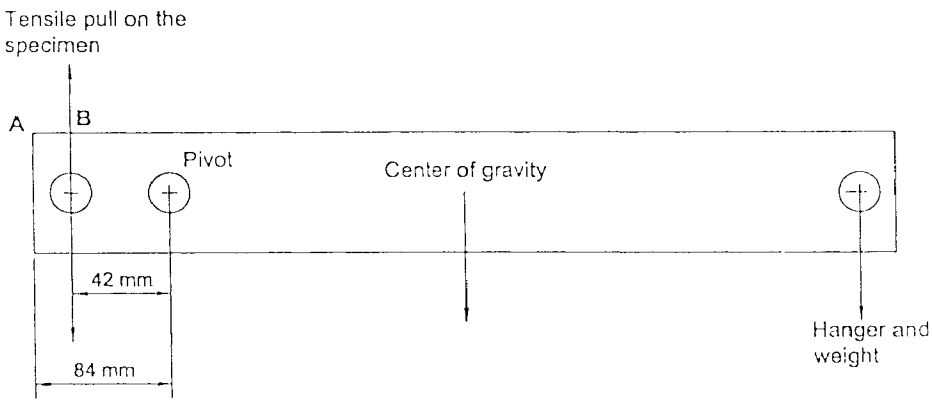

(b)

Fig. 2. Photograph (a) and schematic drawing (b) of the tensile creep test machine.

$$\text{Crosslink density} = \rho_x = \left[\frac{\sqrt[3]{q}}{V_1}\right]\left[\ln\left(1 - \frac{1}{q}\right) + \left(\frac{1}{q}\right) + \left(\frac{\chi}{q^2}\right)\right].$$

The cross-link density tests were conducted in triplicate for each specimen set.

$\%C$ was determined using differential scanning calorimetry on a DSC-7 instrument (Perkin-Elmer Corp., Norwalk, CT, USA) on samples taken from the surface, near-surface region (that is, 2 mm below specimen surface), and core zone (that is, 6.4 mm below the surface) of the specimen. Each such sample, with a mass of 3.5 ± 0.5 mg, was placed in a closed aluminum pan and heated at $10°\text{C min}^{-1}$ from 20

Questions? Contact FDA/CDRH/OCE/DID at CDRH-FOISTATUS@fda.hhs.gov or 301-796-8118

Records processed under FOIA Request #2014-8015; Released by CDRH on 12-8-2015

to 100°C. From the thermogram obtained, $\%C$ was calculated, with the aid of a computer program, as the ratio of the heat of fusion of the specimen to that of fully crystalline UHMWPE, which was taken to be 289.74 J/g [29].

3. Results

A typical specimen extension-versus-time, t plot, obtained for a tensile creep test, is presented in Fig. 3(a). A typical tensile strain-versus-time plot is given in Fig. 3(b). The tensile creep strain results for the three sets of specimens are summarized in Figs 3(c) and 4. Sample Norton and tensile creep compliance plots are given in Figs 5 and 6, respectively, with all the results of the fits being contained in Table 2.

Typical □h–t, h–t and ε_{com}–t, plots, obtained for a compressive creep test, are given in Fig. 7. All the compressive creep strain rate results for the three sets of specimens are summarized in Fig. 8, while a sample compressive compliance plot is presented in Fig. 9. Results of all the compressive compliance fits are given in Table 2. The ρ_x and $\%C$ results are given in Table 3.

From the tensile and compressive creep compliance relations, estimates for creep strains to be expected in an articular component subjected to a stress of 5 MPa for 10 years were obtained and are plotted against $\%C$ and ρ_x in Figs. 10 and 11.

4. Discussion

Prior to the discussion of the specific results of the present work, the case for studying tensile and compressive creep performance of UHMWPE as well as the rationale for utilizing quasi-static loading are presented briefly.

Knowledge about tensile creep performance of UHMWPE is useful because significant tensile stresses are generated in nonconforming articular surfaces, such as in the knee joint. Compressive creep behavior of UHMWPE should be investigated because compressive loading in the direction normal to the bearing surface is the dominant loading mode in highly-conforming articular surfaces, such as in the hip joint.

Creep measurements based on quasi-static loading may be criticized as being very different from those that would be obtained under dynamic loading, which is seen *in vivo*. This observation, while valid, does not undermine the merit of the present study for the following reason. Quasi-static loading does not permit viscoelastic recovery of the UHMWPE specimen as happens during and between load cycles when dynamic loading is imposed. Thus, quasi-static loading may be considered as a "worst-case scenario" and, hence, may be used for testing aimed at discriminating between variants of a given grade of UHMWPE.

Turning now to the results obtained in the present study (Figs. 4, 8, 10 and 11), two key trends are observed. First, crosslinking leads to a statistically significant depreciation in creep performance, relative to the controls (paired Student's t-test; $p = 0.05$). This indications are that this trend is attributable to the decrease in crystallinity induced by crosslinking. Indeed, Wang [30] has referred to crosslinked UHMWPEs with crystallinity as low as 40% as "soft", and stated that these materials "may creep excessively under load...".

Muratoglu et al. [31] have shown that, for electron-beam-crosslinked UHMWPE, there is a positive linear correlation between molecular weight between crosslinks, MW_c, of the polymer and the *in vitro* wear rate of specimens made from it. Since there is an inverse relationship between ρ_x and MW_c ($\text{MW}_\text{c} =$

Questions? Contact FDA/CDRH/OCE/DID at CDRH-FOISTATUS@fda.hhs.gov or 301-796-8118

Records processed under FOIA Request #2014-8015; Released by CDRH on 12-8-2015

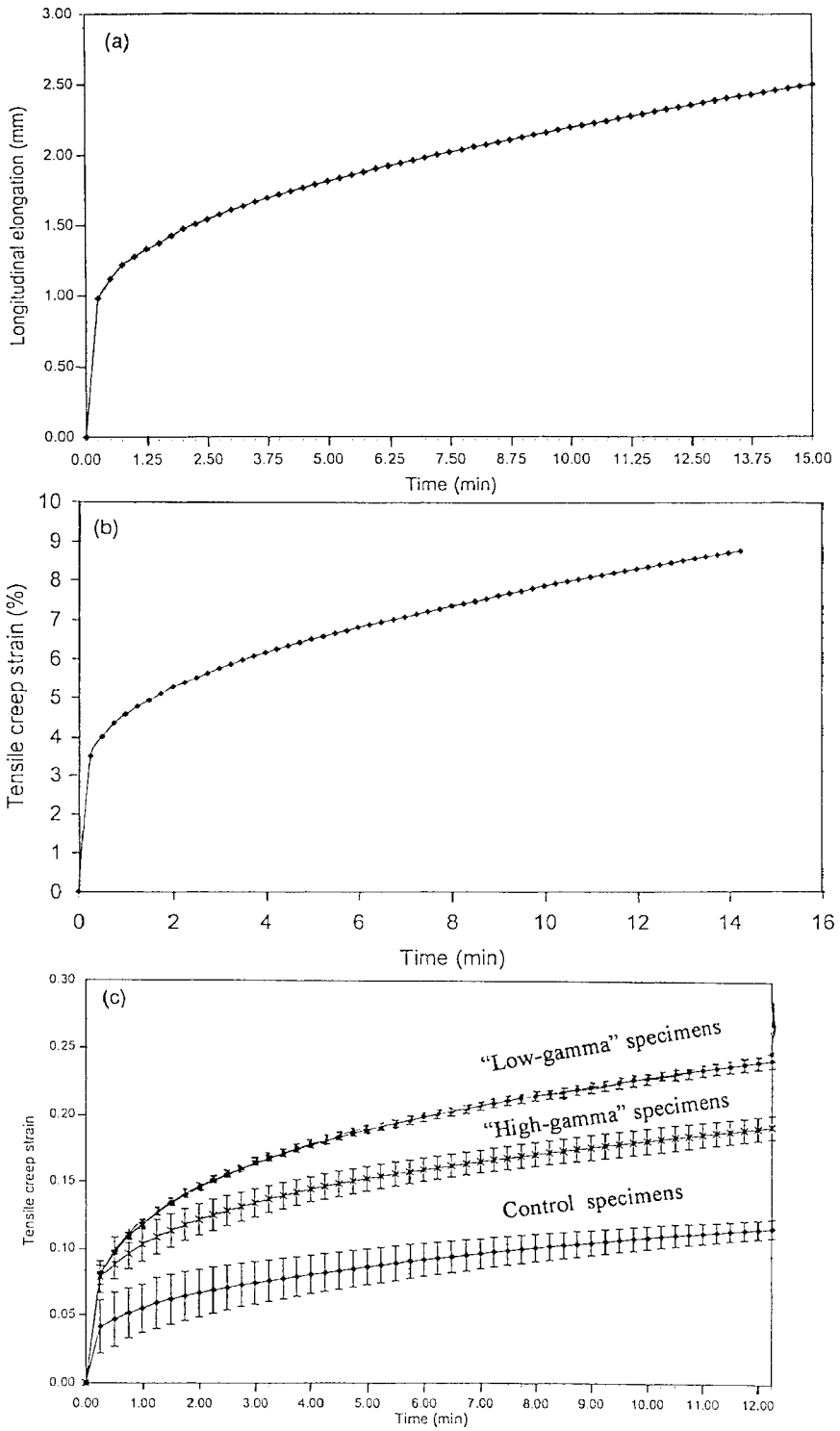

Fig. 3. (a) A typical extension-versus-time plot; (b) a typical tensile creep strain-versus-time plot; (c) summarized presentation of all the tensile creep strain-versus-time results at the three applied stress levels.

Questions? Contact FDA/CDRH/OCE/DID at CDRH-FOISTATUS@fda.hhs.gov or 301-796-8118

Records processed under FOIA Request #2014-8015; Released by CDRH on 12-8-2015

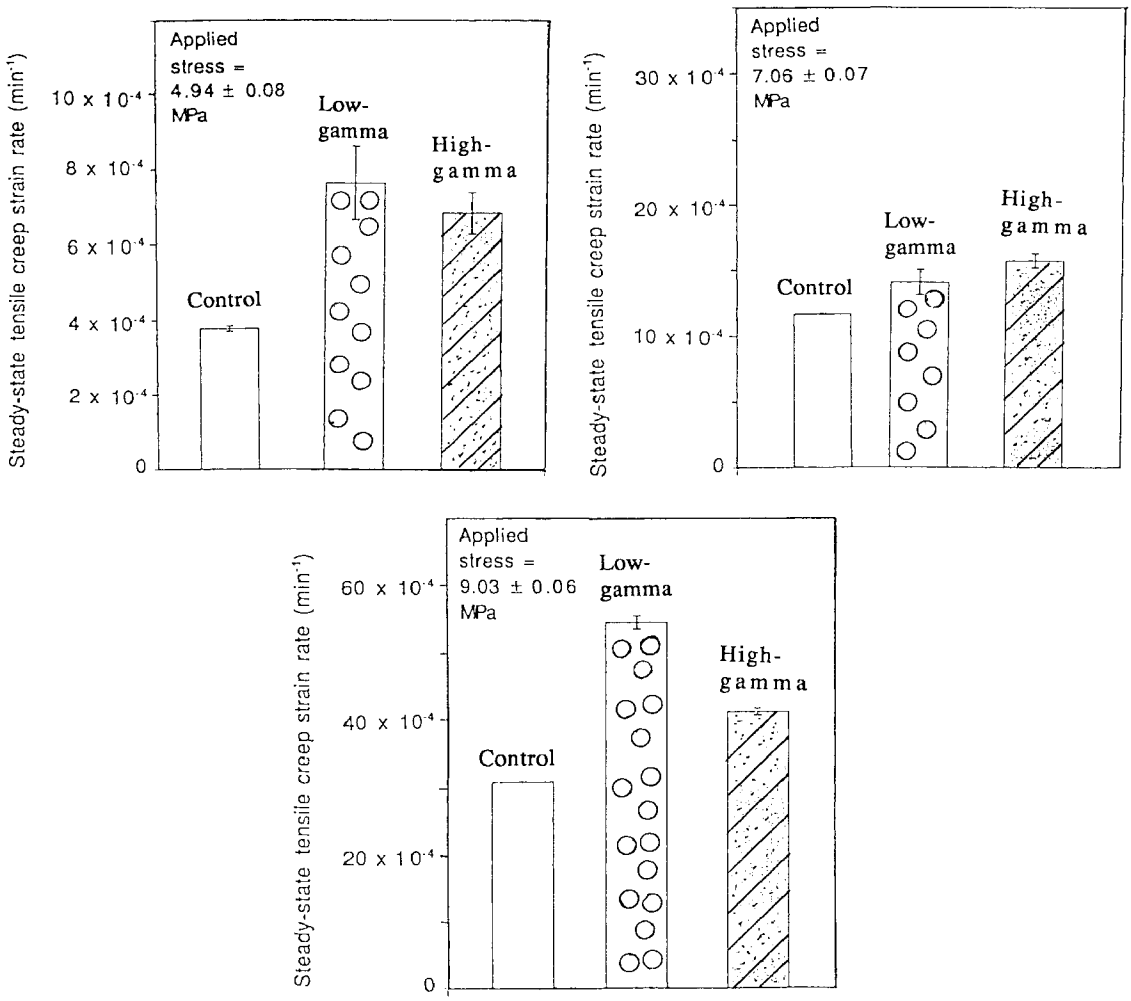

Fig. 4. Summarized presentation of all the tensile steady-state creep strain rate results.

ρ_a/ρ_x, where ρ_a is the density of amorphous UHMWPE, which has a constant value of 855 kg m^{-3}), another way of putting Muratoglu et al.'s [31] conclusion is to say that the higher the polymer's ρ_x is, the lower is the *in vitro* wear rate of components fabricated from it. In the present study, the second trend seen in the results is that, as ρ_x increases, so does the creep strain (Figs. 10(b) and 11(b)), a finding that is in direct opposition to that reported by Muratoglu et al. [31] for wear resistance. This type of conflicting performance of crosslinked UHMWPE in terms of various material properties is not unusual. For example, it is known that, with increase in the gamma radiation dose used in crosslinking UHMWPE, the *in vitro* wear rate decreases [32] – a desirable outcome – but the fracture toughness decreases [33] – an undesirable outcome. Thus, the goal should be to find the crosslinking process and attendant process conditions that produce an optimal mix of the polymer's properties. This issue is well recognized, as evidenced by the remarks of Edidin et al. [34]: "Therefore, from both a biomaterials and a biomechanics perspective, any modification of UHMWPE for total hip replacements must necessarily strike an optimal balance between wear performance, ductility, ultimate strength, fatigue endurance, and fracture resistance".

Questions? Contact FDA/CDRH/OCE/DID at CDRH-FOISTATUS@fda.hhs.gov or 301-796-8118

Records processed under FOIA Request #2014-8015; Released by CDRH on 12-8-2015

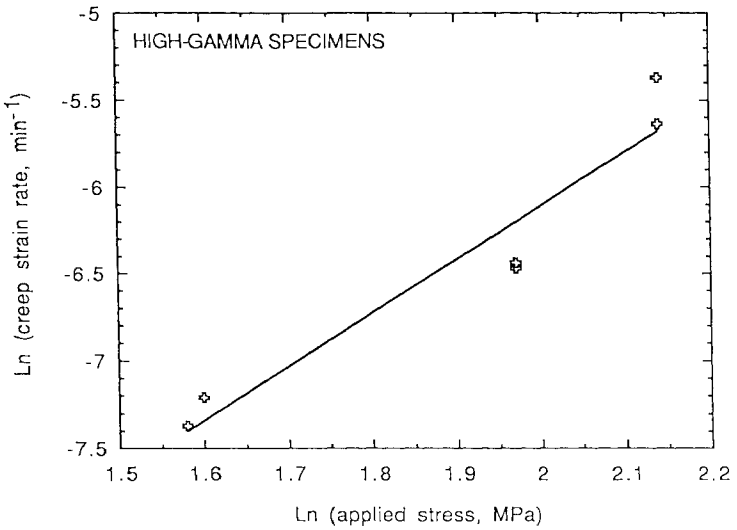

Fig. 5. Sample Norton plot ("high-gamma" specimens).

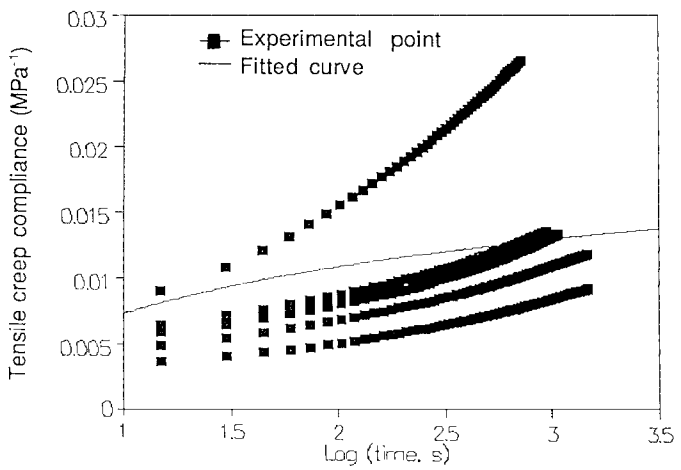

Fig. 6. Sample tensile creep compliance plot ("high-gamma" specimens).

It would have been instructive to compare the trends seen in the present work with those in relevant literature reports; specifically, the five reports that, to date, have focused on the effect of crosslinking on creep of UHMWPE, namely those by Levine et al. [18], Bragdon et al. [19,20], Estok et al. [21], and Furman et al. [22]. However, we are hampered in this exercise by the differences in relevant experimental details between the present study on the one hand and each of the previous reports, on the other hand. These differences are now described.

Levine et al. [18] reported that the compressive creep deformation of a "highly cross-linked" UHMWPE was noticeably lower than that of control ("γ-irradiated in nitrogen") specimens. There are two important differences in the experimental details of the present and Levine et al. [18] studies that severely limits comparison of trends obtained in these studies. First, while the crosslinking method used in the present work was stated, Levine et al. did not provide any details of the crosslinking process they

Questions? Contact FDA/CDRH/OCE/DID at CDRH-FOISTATUS@fda.hhs.gov or 301-796-8118

Records processed under FOIA Request #2014-8015; Released by CDRH on 12-8-2015

Table 2
Summary of material constants obtained from fits of the creep strain results

	Specimen set		
Parameter	Control	Low-γ	High-γ
Tensile creep			
B^{a}	1.93×10^{-6}	3.84×10^{-6}	4.73×10^{-6}
n^{a}	3.32	3.21	3.08
α^{b}	−0.0534	−0.0925	−0.1452
β^{b}	0.0584	0.0979	0.1532
γ^{b}	0.0375	0.0558	0.0344
r^{b}	0.237	0.258	0.278
Compressive creep			
δ^{c}	−0.0103	0.0434	−0.0535
λ^{c}	0.0644	0.0715	0.1104
η^{c}	1.4119	1.3956	1.2307
r'^{c}	0.932	0.840	0.954

[a] $\varepsilon_{ss} = B\sigma^{n}$.
[b] Tensile creep compliance, C (MPa^{-1}) $= \alpha + \beta(\log t, s)^{\gamma}$; r is the correlation coefficient.
[c] Compressive creep compliance, C' (% MPa^{-1}) $= \delta + \lambda(\log t, s)^{\eta}$; r' is the correlation coefficient.

used. Second, the controls used in the present study were unsterilized, while those used by Levine et al. were sterilized.

Bragdon et al. [19,20] have reported on two studies of the plastic deformation (creep) at the articular surfaces of acetabular components, as obtained in a hip simulator. In one case [19], the components were fabricated from 1050 ram extruded bar stock, and the performance of the following three groups was compared: "conventional" (polymer γ-irradiated in air, at 2.5 Mrad); "cold" electron beam-induced crosslinked (polymer exposed to the electron beam at room temperature, 15 Mrad, followed by ethylene oxide, EtO, sterilization); and "warm" electron beam-induced crosslinked (polymer heated to 120°C prior to and during electron beam exposure, followed by EtO sterilization). The creep of the component was determined at 2 test frequencies, 1 and 2 Hz. In the other study [20], the specimens were machined from 1050 ram-extruded UHMWPE, and two groups were compared; namely, "conventional" (polymer γ-irradiated in oxygenless packaging, at 2.5 Mrad); and "warm" electron beam-induced crosslinked (polymer heated to >120°C prior to electron beam exposure, stabilized by melting, and then EtO sterilized). Two acetabular component sizes were used, 22 and 28 mm. In both studies, Bragdon et al. [19, 20] found that creep performance is not affected by crosslinking. In spite of some similarities in the Bragdon et al. and present studies (firstly, in both Bragdon et al. studies [19,20], compressive creep was studied; also, secondly, in one of the Bragdon et al. study [20] and the present work, UHMWPE 1050 ram-extruded polymer was used), the results obtained in the Bragdon et al. and present studies cannot be compared because of one crucial difference; namely, Bragdon et al. [19,20] used acetabular components while cube specimens were utilized in the present work.

In tests conducted in a hip simulator, Estok et al. [21] measured the penetration of the head of the femoral stem into the UHMWPE liners of 12 acetabular cups. Six of the cup liners were fabricated from "conventional UHMWPE" (which the present authors assume to be uncrosslinked polymer) and then gamma sterilized in air. The other six cup liners were "highly cross-linked" using electron beam irradiation at a starting temperature of 125°C, annealed by melting, and then sterilized using ethylene oxide gas. Estok et al. [21] found that, over a span of 750,000 cycles, the level of penetration in the two groups

Questions? Contact FDA/CDRH/OCE/DID at CDRH-FOISTATUS@fda.hhs.gov or 301-796-8118

Records processed under FOIA Request #2014-8015; Released by CDRH on 12-8-2015

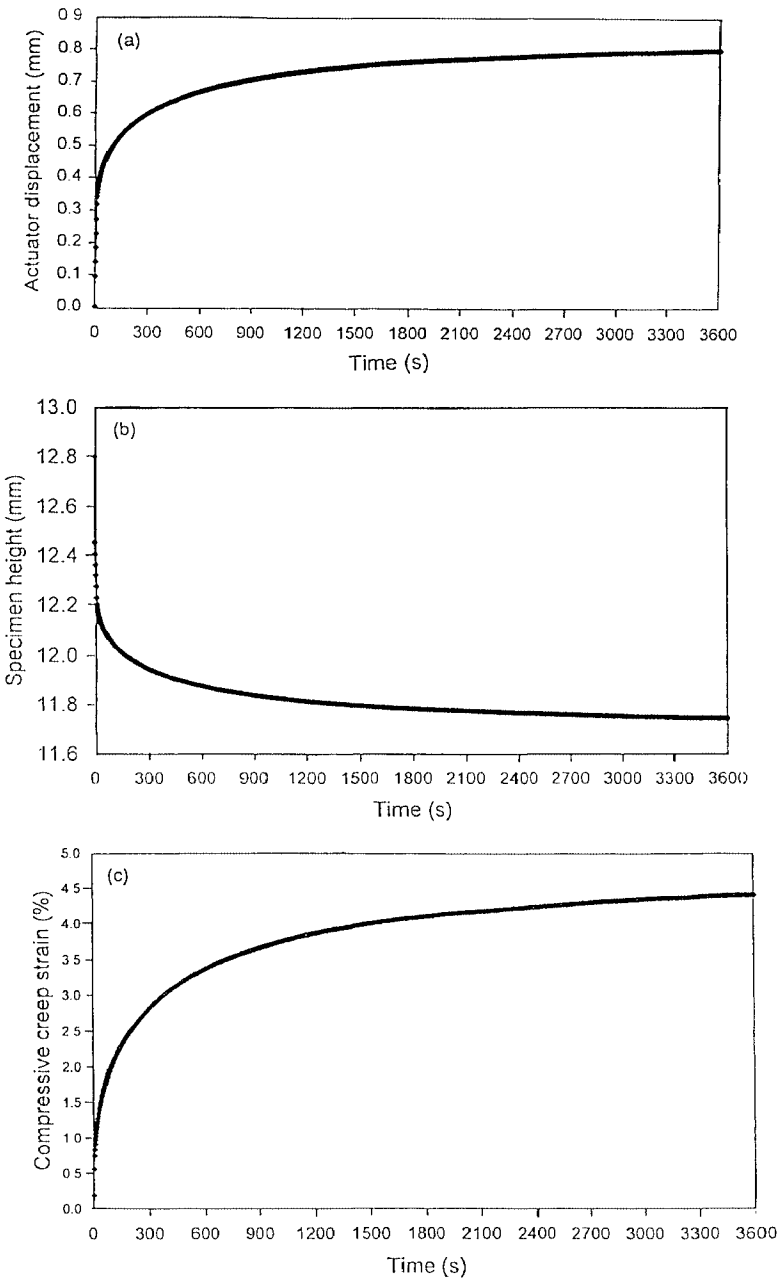

Fig. 7. (a) A typical actuator displacement-versus-time plot; (b) a typical specimen height-versus-time plot; (c) a typical compression strain-versus-time plot.

of cup liners was essentially the same. These workers speculated that this result was the consequence of the balance between the competing mechanisms that account for the creep of the crosslinked polymer; namely, the drop in creep deformation due to the crosslinking being balanced by the rise in creep deformation due to the decrease in the material's modulus. One drawback of the Estok et al. [21] study is that different sterilization methods were used in the two sets of cup liners. This introduced another variable

Questions? Contact FDA/CDRH/OCE/DID at CDRH-FOISTATUS@fda.hhs.gov or 301-796-8118

Records processed under FOIA Request #2014-8015; Released by CDRH on 12-8-2015

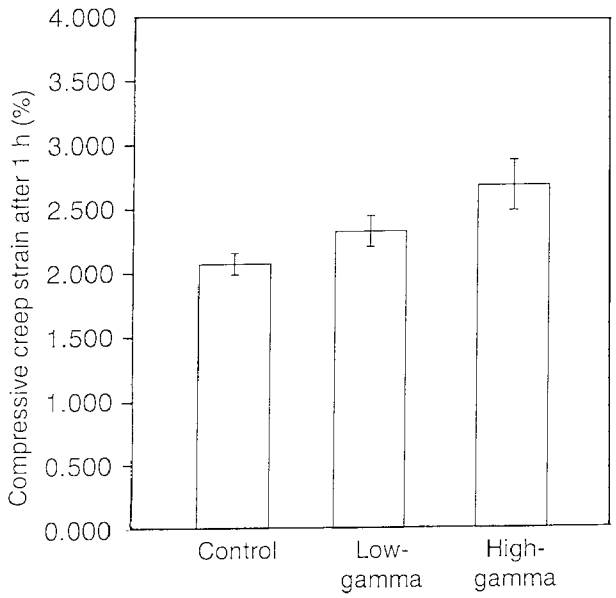

Fig. 8. Summarized presentation of all the compressive creep strain results.

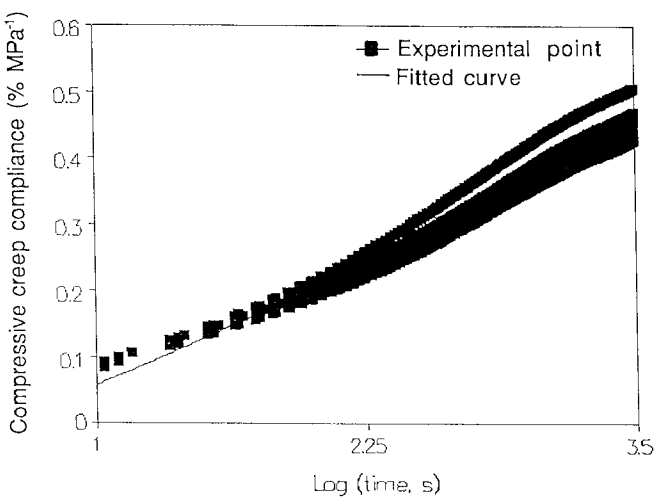

Fig. 9. Sample compressive creep compliance plot ("high-gamma" specimens).

Table 3
Crosslink density, % crystallinity, and strain estimates of UHMWPE in the three test sets

Specimen set	Crosslink density ($mol\,m^{-3}$)	% Crystallinity	Tensile strain estimate ($\sigma = 5$ MPa; $t = 10$ y) [%]	Compressive strain estimate ($\sigma = 5$ MPa; $t = 10$ y) [%]
Control	50 ± 5[a]	52.1 ± 4.34	4.9	6.5
Low-γ	800 ± 80	44.1 ± 6.38	8.9	7.3
High-γ	1150 ± 100	36.3 ± 3.88	9.8	7.4

[a]Results stated as mean $\pm$ standard deviation.

Questions? Contact FDA/CDRH/OCE/DID at CDRH-FOISTATUS@fda.hhs.gov or 301-796-8118

Records processed under FOIA Request #2014-8015; Released by CDRH on 12-8-2015

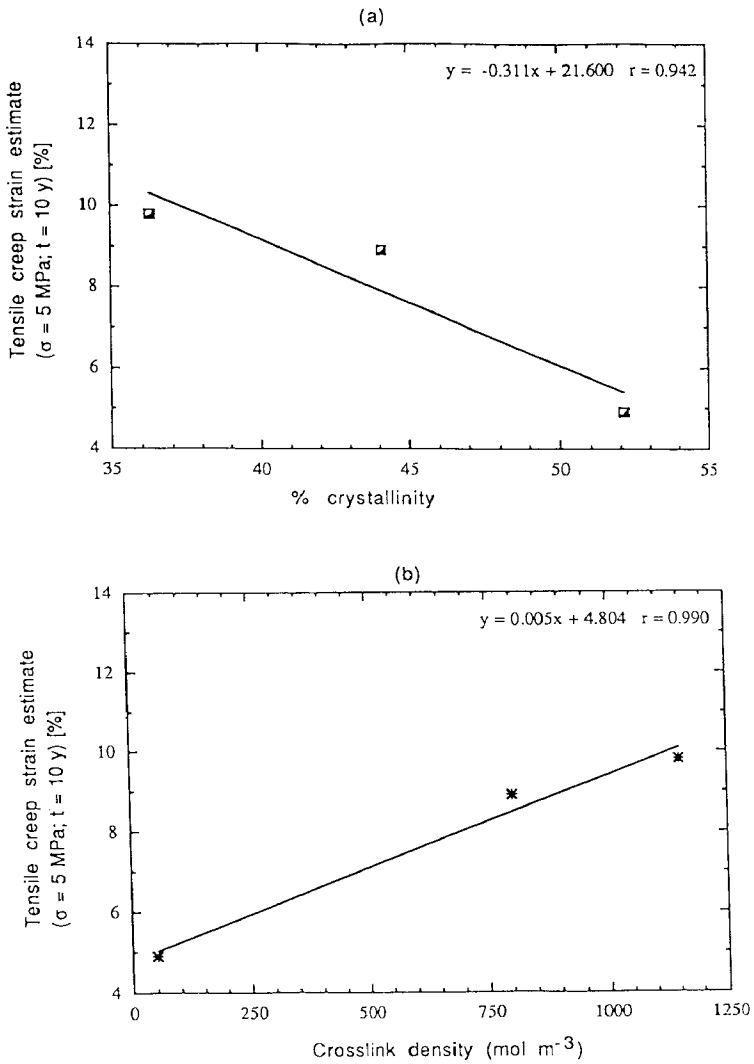

Fig. 10. Variation of tensile creep strain estimate ($\sigma = 5$ MPa; $t = 10$ y) with (a) % crystallinity, and (b) crosslink density.

in the study, thereby confounding the intended comparison between uncrosslinked and crosslinked cup liners. Even without this consideration, a comparison in the trends of the present study and that by Estok et al. [21] may not be appropriate because of the difference in crosslinking methods employed in the two studies.

Furman et al. [22] carried out an extensive study on two groups of specimens ("groups 1 and 2") involving a myriad of variables. In group 1 tests (12.7 mm × 12.7 mm × 12.7 mm specimens), the variables were crosslinking method (gamma versus electron beam irradiation); radiation dose (2, 5, 10 and 20 Mrad); post-crosslinking treatment (none versus radical quenching at 150°C for 5 h under vacuum); and static stress level (6.89 versus 13.78 MPa). In group 2 tests (32 mm acetabular cups), the variables were gamma radiation dose (2.5 and 10 Mrad); post-crosslinking treatment (none versus radical quenching); and test duration (1 d versus 5 d). Although some combination of conditions in group 1 tests were the same as in the present tests (controls were uncrosslinked and unsterilized; gamma-radiation

Questions? Contact FDA/CDRH/OCE/DID at CDRH-FOISTATUS@fda.hhs.gov or 301-796-8118

Records processed under FOIA Request #2014-8015; Released by CDRH on 12-8-2015

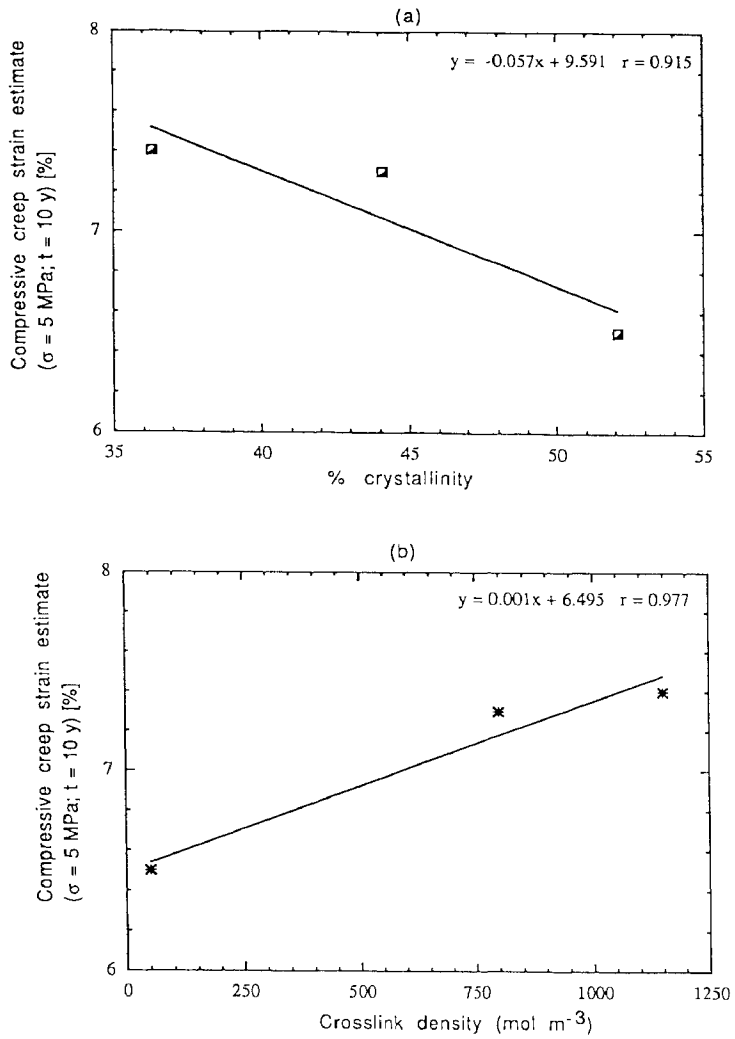

Fig. 11. Variation of compressive strain estimate ($\sigma = 5$ MPa; $t = 10$ y) with (a) % crystallinity, and (b) crosslink density.

crosslinking, at 5 Mrad; no quenching), there were noteworthy differences (specifically, the present tests used 1050 resin and ran for 1 h, while, in the Furman et al. [22] study, 4150 HP resin and a test duration of 24 h were used). Thus, again, no straightforward comparison may be made between the present results and those given by Furman et al. [22].

All the aforementioned observations regarding comparisons between the present and relevant literature results highlight the need for careful study design in future studies on this topic. For example, it must be ensured that all relevant parameters in all the crosslinked group(s) [such as post-crosslinking stabilization method (in the case of radiation-induced crosslinking) and post-crosslinking sterilization conditions] are identical. The only difference between the groups should, therefore, be the details of the crosslinking method used (for example, radiation dose in the case of radiation-induced crosslinking or peroxide concentration in the case of chemical-induced crosslinking).

Questions? Contact FDA/CDRH/OCE/DID at CDRH-FOISTATUS@fda.hhs.gov or 301-796-8118

Records processed under FOIA Request #2014-8015; Released by CDRH on 12-8-2015

5. Conclusions

The following are the main conclusions of the present work:

(1) Crosslinking unsterilized UHMWPE, with the aid of gamma radiation, leads to a depreciation in its tensile and compressive creep performance. This depreciation may be attributed to the concomitant substantial reduction in the polymer's crystallinity.
(2) More studies are needed on the effect of crosslinking on the creep performance of UHMWPE, with care being taken to designing the studies properly; for example, ensuring that all possible confounding variables are eliminated.

Acknowledgements

The authors extend their thanks to the following persons for their contributions to this study: Mr Tuan Nguyen and Mr Bobby McVay (both of the Department of Mechanical Engineering, The University of Memphis, Memphis, TN, USA), and Mr Jim Kershner and Dr Warren Haggard (both of Wright Medical Technology, Inc., Arlington, TN, USA).

References

[1] J. Livermore, D. Ilstrup and B. Morrey, Effect of femoral head size on wear of polyethylene acetabular component, *J. Bone Joint Surg.* **72-A** (1990), 518–528.
[2] S.P. James, K.R. Lee and G.P. Beauregard, Clinical wear of 62 ultrahigh molecular weight polyethylene acetabular components: effect of starting resin and forming method, *J. Biomed. Mater. Res.* **48** (1999), 374–384.
[3] T.M. Wright, R.W. Hood and A.H. Burstein, Analysis of material failures, *Orthop. Clin. North Amer.* **13** (1982), 33–44.
[4] B.M. Wroblewski, Wear and loosening of the socket in the Charnley low-friction arthroplasty, *Orthop. Clin. North Amer.* **19** (1988), 627–630.
[5] B.M. Wroblewski, Low-friction arthroplasty of the hip using alumina ceramic and cross-linked polyethylene: a ten-year follow-up report, *J. Bone Joint Surg.* **81-B** (1999), 54–55.
[6] M.D. McDonald and R.D. Bloebaum, Distinguishing wear and creep in clinically retrieved polyethylene inserts, *J. Biomed. Mater. Res.* **29** (1995), 1–7.
[7] K.-Y. Lee and D. Pienkowski, Compressive creep characteristics of extruded ultrahigh-molecular-weight polyethylene, *J. Biomed. Mater. Res.* **39** (1998), 261–265.
[8] W.H. Harris, The problem is osteolysis, *Clin. Orthop. Rel. Res.* **311** (1995), 46–53.
[9] G. Lewis, Wear of ultra-high-molecular-weight polyethylene, *J. Biomed. Mater. Res. (Appl. Biomater.)* **34** (1997), 34–45.
[10] G. Lewis, Properties of crosslinked ultra-high-molecular-weight polyethylene, *Biomaterials* **22** (2001), 371–401.
[11] E.G. Little, Compressive creep behavior of irradiated ultra-high-molecular-weight poly-ethylene at 37°C, *Eng. Med.* **14** (1985), 85–87.
[12] R.G. Hood, J.M. Courtney, J.P. Paul and J.D. White, The influence of sterilization on the creep properties of ultra high molecular weight polyethylene, *Plast. Med. Surg.* **27** (1979), 1–5.
[13] J.M. Crissman, On the mechanical preconditioning of UHMW-PE at small uniaxial deformations, in: *Ultra-High Molecular Weight Polyethylene as Biomaterial in Orthopedic Surgery*, H.-G. Willert, G.H. Bucchorn and P. Eyerer, eds, Hogrefe & Huber Publishers, Toronto, Canada, 1991, pp. 23–27.
[14] K.-Y. Lee and D. Pienkowski, Dynamic compressive creep of extruded ultrahigh molecular weight polyethylene, in: *Transactions of the Fifth World Biomaterials Congress*, Toronto, Canada, May 29–June 2, 1996, p. 987.
[15] K.-Y. Lee, A. Tesar and D. Pienkowski, Effects of gamma irradiation, processing, and molecular weight on viscoelastic creep and recovery of ultra-high-molecular-weight polyethylene, in: *Transactions of the 44th Annual Meeting, Orthopaedic Research Society*, March 16–19, New Orleans, LA, 1998, p. 780.
[16] M. Deng, R. Latour, A.A. Ogale and S.W. Shalaby, Study of creep behavior of ultra-high-molecular-weight polyethylene systems, *J. Biomed. Mater. Res.* **40** (1998), 214–223.
[17] J.E. Estupinan, T.H. Baldini and D.L. Bartel, Recoverable and irrecoverable creep of ultra-high-molecular-weight polyethylene, in: *Transactions of the 45th Annual Meeting of the Orthopaedic Research Society*, Anaheim, CA, 1–4 February 1999, p. 818.

Questions? Contact FDA/CDRH/OCE/DID at CDRH-FOISTATUS@fda.hhs.gov or 301-796-8118

Records processed under FOIA Request #2014-8015; Released by CDRH on 12-8-2015

[18] D. Levine, S. Lin, L. Kilpatrick, K. Kedward and M. He, Creep/relaxation in ultra-high-molecular-weight polyethylene – applications to design of an acetabular cup, in: *Transactions of the 45th Annual Meeting of the Orthopaedic Research Society*, Anaheim, CA, 1–4 February 1999, p. 837.
[19] C.R. Bragdon, D.O. O'Connor, E.A. Weinberg, H.C. Skehan III and O.K. Muratoglu, The effect of cycle rate on the wear of conventional and highly crosslinked UHMWPE acetabular components using a Boston AMTI hip simulator, in: *Transactions of the 25th Annual Meeting of the Society for Biomaterials,* Providence, RI, USA, April 28–May 2, 1999, p. 211.
[20] C.R. Bragdon, D.O. O'Connor, E.A. Weinberg, H.C. Skehan III, O.K. Muratoglu, J.D. Lowenstein and W.H. Harris, The role of head size on creep and wear of conventional vs. highly cross-linked polyethylene acetabular components, in: *Transactions of the 25th Annual Meeting of the Society for Biomaterials*, Providence, RI, USA, April 28–May 2, 1999, p. 497.
[21] D.M.B. Estok II, C.R. Bragdon, G.R. Plank, W.H. Harris, O.K. Muratoglu and E. Weinberg, Measurement of creep in ultra-high-molecular-weight polyethylene (UHMWPE): comparison of conventional UHMWPE vs. a highly cross-linked polyethylene, in: *Transactions of the 46th Annual Meeting of the Orthopaedic Research Society*, Orlando, FL, March 12–15, 2000, p. 550.
[22] B.D. Furman, M.M. Saunders, E. Potier and S. Li, Effect of sterilization method and dose on the creep properties of cross linked UHMWPE, in: *Transactions of the Sixth World Biomaterials Congress*, Kamuela, HI, USA, May 15–20, 2000, p. 459.
[23] I. LeMay, *Principles of Mechanical Metallurgy*, Edward Arnold, London, 1981.
[24] M.A. Meyers and K.K. Chawla, *Mechanical Behavior of Materials*, Prentice Hall, NJ, USA, 1999.
[25] American Society for Testing and Materials (ASTM), Standard D621-94, Test methods for deformation of plastics under load, in: *1994 Annual Book of ASTM Standards*, Vol. 08.01, ASTM, West Conshohocken, PA, USA, 1994.
[26] American Society for Testing and Materials (ASTM), Standard D2765-95, Standard test method for determination of gel content and swell ratio of crosslinked ethylene plastics, in: *1999 Annual Book of ASTM Standards*, Vol. 08.02, ASTM, West Conshohocken, PA, USA, 1999, pp. 110–116.
[27] J. Brandup and E.H. Immergut, *Polymer Handbook*, Vol. 16–17, Wiley, New York, NY, USA, 1989.
[28] P.J. Flory, *Principles of Polymer Chemistry*, Cornell University Press, Ithaca, NY, USA, 1990.
[29] K. Lee and S. Kim, Effect of crystalline lamellar orientation on the wear of UHMWPE, in: *Transactions of the 46th Annual Meeting of the Orthopaedic Research Society*, Orlando, FL, 12–15 March 2000, p. 557.
[30] A. Wang, "Out of the laboratory and into the patient" – report of a roundtable discussion, T.P. Schmalzried (moderator), *Orthopaedics Today* **20**(2) (February 2000), 50–68.
[31] O.K. Muratoglu, C.R. Bragdon, D.O. O'Connor, M. Jasty, W.H. Harris, R. Gul and F. McGarry, Unified wear model for highly crosslinked ultra-high molecular weight polyethylenes (UHMWPE), *Biomaterials* **20** (1999), 1463–1470.
[32] H. McKellop, F.-W. Shen and R. Salovey, Extremely low wear of gamma-crosslinked remelted UHMW polyethylene acetabular cups, in: *Transactions of the 44th Annual Meeting of the Orthopaedic Research Society*, New Orleans, LA, USA, 16–19 March 1998, pp. 98–17.
[33] A.M. Gillis, J.J. Schmieg, S. Bhattacharyya and S. Li, An independent evaluation of the mechanical, chemical, and fracture properties of UHMWPE cross linked by 34 different conditions, in: *Transactions of the 25th Annual Meeting of the Society for Biomaterials,* Providence, RI, USA, April 28–May 2, 1999, p. 216.
[34] A.A. Edidin, L. Pruitt, C.W. Jewett, D.J. Crane, D. Roberts and S.M. Kurtz, Plasticity-induced damage layer is a precursor to wear in radiation-cross-linked UHMWPE acetabular components for total hip replacement, *The Journal of Arthroplasty* **14** (1999), 616–27.

Questions? Contact FDA/CDRH/OCE/DID at CDRH-FOISTATUS@fda.hhs.gov or 301-796-8118

Records processed under FOIA Request #2014-8015; Released by CDRH on 12-8-2015

EFFECTS OF GAMMA-IRRADIATION ON ULTRA-HIGH-MOLECULAR-WEIGHT POLYTHYLENE

Ching T. Lue
Edward J. Ellis
Aldo Crugnola

Department of Plastics Engineering
University of Lowell
Lowell, Massachusetts 01854

INTRODUCTION

Linear polyethylene with a molecular weight in the 1.5 to 3.0 X 10^6 range is termed ultrahigh molecular weight polyethylene (UHMWPE). This material exhibits a combination of properties which are not found in the lower molecular weight more commercial, high density polyethylene (HDPE) - extreme abrasion resistance, low coefficient of friction and exceptional chemical resistance. These attractive characteristics have led to the widespread acceptance of UHMWPE components in total joint replacement. As with any material implanted in the human body, UHMWPE components must be sterile. This is often accomplished with gamma-irradiation, usually to a level of 2.5 megarads.

It is well known that when high density polyethylene is subjected to gamma-irradiation both crosslinking and chain scission occur at the same time (1-3). This results in great changes in the molecular weight distribution and, as a consequence, the mechanical properties of polyethylene are altered (4). In general, the literature deals only with high dosage levels typically 10 megarads and above. At these levels the shear strength, tensile strength and elongation to break first increase, pass a maximum and then decrease with increasing radiation dose. On the other hand, very little is reported in the literature on the effects of irradiation on the mechanical properties of UHMWPE. This is especially so for the effects of the low level doses of interest in radiation sterilization.

Previous work in our laboratory has established that these sterilization doses do alter the molecular weights and molecular weight distributions of prosthetic devices (5,6). It would reasonably follow that the mechanical properties also would be modified.

To investigate this possibility a study was undertaken to follow the effects of gamma-irradiation on selected mechanical properties of UHMWPE. Two irradiation levels were selected, 2.5 and 5.0 megarads. In addition the effect of atmosphere was determined by alternately irradiating in air and in nitrogen.

EXPERIMENTAL

Material - Commercial 30 mil UHMWPE sheet purchased from DIXON Corporation.

Specimens - Samples in the form of either dog bones or disks were die cut from the UHMWPE sheet.

Irradiation - The specimens were irradiated in a Gamma Cell utilizing a cobalt 60 source at a rate of 200,000 rads per hours. Two atmospheres were employed, air or nitrogen, with specimens irradiated to a total level of 2.5 Megarads and 5.0 Megarads.

Gel and/or High Molecular Weight Fraction - This fraction is defined as that portion of the polymer which was not soluble after 12 hours of extraction with xylene at 135°C. Strictly speaking, insoluble material was either crosslinked or of a molecular weight greater than 6 x 10^6.

Molecular Weight - This determination was made on that portion of the polymer which was soluble in xylene at 135°C. The intrinsic viscosity was determined in decalin at 135°C and the molecular weight calculated from the relationship $\eta = 6.77 \times 10^{-4} M_W^{0.67}$.

Crystallinity Through Density - The gradient column technique (ASTM D1505) was used to determine densities. The liquid system was isopropanol/water with the column calibrated at 23 C with known density standards. Total crystalline content was calculated by assuming a direct proportionality with density.

Crystallinity Through DSC - A Perkin-Elmer SDC model DSC-1B instrument was used with a heating rate of 10°C/min. Indium was the standard (ΔH_f = 6.8 cal/gm) for establishing the magnitude of sample endotherms crystallinity then calculated by assuming a value of ΔH_f = 68 cal/gm for totally crystalline high density polyethylene.

Tensile Properties - Stress/strain curves were generated utilizing an Instron testing machine. A gauge length of 7/8 inch and a crosshead speed of 2.0 inch/min were used.

Wear Resistance - The wear behavior was ascertained using an abrasion test similar to that described by Margolies (7). Circular samples of UHMWPE were mounted on a shaft and rotated at 1735 rpm for 24 hours in sand-water slurry, the abrasive slurry was composed of a 50-50 (by volume) mixture of #40 silicon carbide and water. Wear was reported as the weight lost per unit area of the sample.

Fatigue Endurance - A cyclic fatigue machine was utilized to study the fatigue behavior of UHMWPE in the form of notched (see ASTM D 1693) dog bone samples. Twelve samples were fastened in each of the two chambers of the machine. Water was introduced so that all samples were completely immersed. During operation the samples were loaded in an alternating fashion by a motor/cam/spring arrangement. The stress applied to the samples was determined by the force constant and elongation of the springs. The test conditions were:

Temperature	37°C ± 1.5
Cycle	34 cpm ± 0.5
Max. Stress	2000 psi ± 50
Min. Stress	0 psi

DISCUSSION

Irradiation produced substantial increases in the gel content of the UHMWPE samples. This increase was more evident when the irradiation was carried out in nitrogen. This difference in gel content with atmosphere can be directly attributed to a shift in the relative ratio of cross-linking to chain scission reactions. The average molecular weight of the soluble fraction was found to be dramatically decreased after irradiation and fall into the range of commercial HDPE. These results agree quite well with previously reported work by this group (6).

The crystalline content of the samples, calculated from both density and DSC data, exhibit similar trends. The crystallinity increased slightly with irradiation even though a major portion of the polymer was crosslinked. Lawton suggests that the crosslinking process occurs in the amorphous regions during irradiation (8). Concomitantly, irradiation generates a considerable amount of low molecular polymer. Since the crystallyzation process in polyethylene is hindered by high molecular weight polymer a lowering of molecular weight could promote further crystallization. This hypothesis is supported by the fact that the melting points of all the irradiated samples were higher than the non-irradiated sample. There was an obvious change in the cahracter of the crystals as a consequence of irradiation.

Within the dose range investigated, irradiation resulted in a modest increase in yield strength, more so with the material irradiated in air. In general the yield strength of a polymer is mainly a function of the crystalline content (9). Indeed, when yield strength is plotted as a function of crystallinity a linear relationship is obtained (Figure 1).

The ultimate tensile strength of the irradiated samples was reduced, in all cases, over the value obtained with the control sample. This finding agrees with the work of Lawton in which he studied the effects of irradiation of high density polyethylene (10). It was shown that the ultimate tensile strength of high molecular weight linear polyethylene gradually decreased with increased radiation dosages.

There was a significant increase in the elongation to break with irradiated samples which does not appear to correlate with either dose level or atmosphere. When consulting Lawton's work with high density polyethylene we find a rapid increase in elongation to break, followed by a less rapid decrease, with progressing radiation dosages (10). When comparing the results reported here with Lawton's findings, in the 0 to 10 megarads range, there is general agreement. That is the ultimate elongation is rising with irradiation in this range.

The effects of irradiation on the tensile fatigue endurance of the UNMWPE samples were mixed. When the irradiation was carried out in air the fatigue life increased at the higher 5.0 megarad level. When the irradiation was carried out in nitrogen the fatigue life was observed to first increase (2.5 megarad) and then decrease at 5.0

Questions? Contact FDA/CDRH/OCE/DID at CDRH-FOISTATUS@fda.hhs.gov or 301-796-8118

Records processed under FOIA Request #2014-8015; Released by CDRH on 12-8-2015

When the yield strength was correlated with the gel content of the UHMWPE samples it was observed to first increase with gel content - pass through a maximum - then decrease. This correlation included both samples irradiated in air and nitrogen.

In general irradiation decreased the wear resistance of UHMWPE. This decrease is more pronounced when UHMWPE was irradiated in air.

The abrasion resistance of polyethylene is believed to be a complex property depending on several other mechanical properties (11). For this reason further investigation is necessary before more complete correlations between irradiation conditions and wear behavior can be drawn.

SUMMARY

The use of UHMWPE in total joint replacement stemmed from the exceptional properties of this material. There are, however, problems associated with such use that have been noted with prostheses removed from patients or tested in simulators. One finding is that the wear data are inconsistent, ranging from negligible wear to severe wear.

This study revealed that significant changes in structure and properties of UHMWPE can occur under sterilization levels of irradiation. It is reasonable to assume that these changes will be reflected clinically in the ultimate performance of the total joint system.

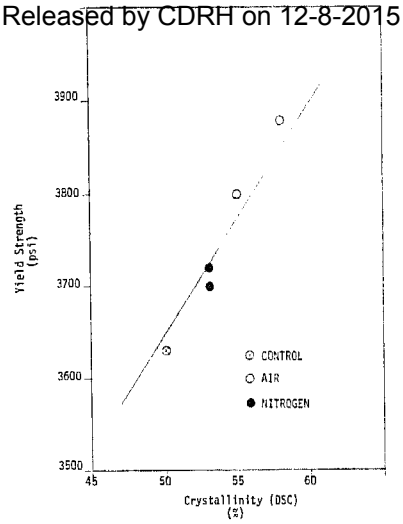

Figure - I
Yield Strength vs Crystallinity

REFERENCES

1. A. Charlesby, Proc. Royal Soc. (London) A222, 60 (1954).
2. A.C. Baskett and C.W. Miller, Nature, 174, 364 (1954).
3. A.C. Baskett, Int. Symp. Macromol. Chem., Milan-Torino, Ricerca Sci, Suppl., A379, (1955).
4. A. Charpiro, Radiation Chemistry of Polymeric Systems, Interscience, Chapter IX, (1962).
5. M.B. Berry et. al., ACS Organic Coatings and Plastics Prepr., 37 (a), 276 (1977).
6. J.Y. Ellis et. al., ACS Organic Coatings and Plastics Prepr., 37 (2), 280 (1977).
7. A.F. Margolies, SPE Journal, 27, 44 (1971).
8. E.J. Lawton et. al., J. Poly. Sci. 32, 257 (1958).
9. E.T. Darden and C.F. Hammer, Material Methods, 44, 94 (1956).
10. E.J. Lawton et. al., Ind. and Eng. Chem., 46, 1703 (1954)
11. R.D. Deanin and L.B. Patel, ACS Organic Coatings and Plastics Prepr., 34 (1), 373 (1974).

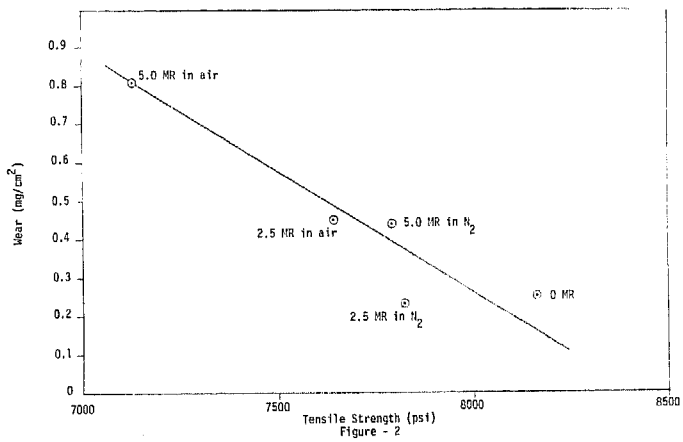

Figure - 2

ABRASION RESISTANCE vs. TENSILE STRENGTH

TABLE II

PHYSICAL PROPERTIES OF UHMWPE

Sample	Yield Str. (psi)	Tensile Str. (psi)	Elongation (%)	Fatigue Life (Normalized)	Wear (mg/cm^2)
OMR	3630	8160	376	1.0	0.25
2.5MR/Air	3800	7640	447	1.0	0.45
5.0MR/Air	3880	7130	420	1.5	0.81
2.5MR/N_2	3700	7820	416	1.3	0.23
5.0MR/N_2	3720	7790	421	0.7	0.44

10^3psi = 6.89MPa = 0.703 Kg/mm^2

Yield Str STD DEV = ± 35

Tensile Str STD DEV = ± 150

Elongation STD DEV = ± 10

TABLE I

STRUCTURAL CHARACTERISTICS OF UHMWPE

Sample	GEL (%)	Soluble (%)	Soluble MW	Density (gm/cm^3)	Chrystallinity (%) from Density	Chrystallinity (%) from DSC	Melting Point (°C)
OMR	10	90	2,991,000	0.939	60	50	134
2.5MR/Air	40	60	399,000	0.943	71	55	136
5.0MR/Air	56	44	227,000	0.945	72	58	137
2/5MR/N_2	72	28	263,000	0.942	71	53	137
5.0MR/N_2	77	23	201,000	0.944	72	53	137

Questions? Contact FDA/CDRH/OCE/DID at CDRH-FOISTATUS@fda.hhs.gov or 301-796-8118

Records processed under FOIA Request #2014-8015; Released by CDRH on 12-8-2015

Comparative Fatigue Behavior and Toughness of Remelted and Annealed Highly Crosslinked Polyethylenes

Francisco J. Medel,[1] P. Peña,[1] José Cegoñino,[2] E. Gómez-Barrena,[3] J. A. Puértolas[1]*

[1] Department of Materials Science and Technology, Centro Politécnico Superior-I3A, Universidad de Zaragoza, E-50018 Zaragoza, Spain

[2] Department of Mechanical Engineering, Centro Politécnico Superior-I3A, Universidad de Zaragoza, E-50018 Zaragoza, Spain

[3] Department of Orthopaedic Surgery and Traumatology, "Fundación Jiménez Díaz" Hospital, Universidad Autónoma de Madrid, E-28040 Madrid, Spain

Received 15 February 2006; revised 16 January 2007; accepted 24 January 2007
Published online 6 August 2007 in Wiley InterScience (www.interscience.wiley.com). DOI: 10.1002/jbm.b.30807

Abstract: Highly cross-linked polyethylenes (HXLPEs) have been incorporated into the hip replacement armamentarium based on their improved wear resistance. However, two different methods of thermal treatment separate the orthopedic community as strategies to control potential long-term oxidation, and controversy remains with problems in the long-term use of acetabular liners (long-term oxidation, rim fracture after impingement, etc.). Meanwhile, the mechanical properties of HXLPEs that may alleviate these problems are still unclear. On the other hand, HXLPEs are scarcely used in knee replacements, as there exists concern about the probably reduced fatigue and fracture performances of these materials. Thus, our aim was to compare the effects of both thermal treatment regimes on mechanical properties and to associate these findings with the material microstructure. The fatigue behavior of annealed and remelted HXLPEs was characterized using short-term cyclic stress–strain, long-term fatigue, and fatigue crack propagation tests. On the other hand, impact tests, tensile experiments, and the *J*-integral multispecimen method allowed us to assess toughness. Microstructure features such as crosslink density, crystallinity percentage, and lamellar thickness were investigated by swelling measurements, differential scanning calorimetry, and transmission electron microscopy, respectively. This study confirms that annealing preserves mechanical properties better than remelting from both fatigue and fracture resistance points of view, and it remarks that a suitable selection of irradiation and stabilization conditions is needed to achieve optimal mechanical performances of ultra high molecular weight polyethylenes for each specific total joint replacement. © 2007 Wiley Periodicals, Inc. J Biomed Mater Res Part B: Appl Biomater 83B: 380–390, 2007

Keywords: UHMWPE; highly crosslinked polyethylenes; annealing; remelting; fatigue resistance; fracture resistance

INTRODUCTION

Highly cross-linked polyethylenes (HXLPEs) were introduced in orthopaedic implants as a promising alternative to conventional, γ-irradiated ultra high molecular weight polyethylenes (UHMWPE).[1,2] As a semicrystalline polymer, a crystalline phase and an amorphous one characterize UHMWPE's microstructure. Changing the polymer chemistry in the two phases can modify its mechanical properties.[3] In this sense, radiative methods, γ or electron beam irradiation, have prevailed over chemical methods in the production of HXLPEs.[2] Thus, high irradiation doses introduce a significant crosslink density in the amorphous phase of the polymer, which is responsible for the relevant improvement in its wear resistance.[2–5] The irradiation processes used to generate commercial HXLPEs are normally carried out at ambient temperature (cold irradiation) or at an elevated temperature (warm irradiation) in an inert atmosphere.[2,6] However, concern remains in the long-term because of the generation of free radicals during irradiation of the polymer in the presence of molecular oxygen.[7] As a consequence, an oxidation process may take place with measurable effects on the polymer's microstructure, therefore affecting

Correspondence to: Prof. J. A. Puértola (e-mail: japr@unizar.es)
Contract grant sponsor: Comisión Interministerial de Ciencia y Tecnología, Spain; Contract grant number: MAT 2003-2340.

© 2007 Wiley Periodicals, Inc.

WILEY InterScience® DISCOVER SOMETHING GREAT

Questions? Contact FDA/CDRH/OCE/DID at CDRH-FOISTATUS@fda.hhs.gov or 301-796-8118

Records processed under FOIA Request #2014-8015; Released by CDRH on 12-8-2015

the material's mechanical and physical properties. This oxidation process turned the conventional UHMWPE, γ sterilized in air, into a brittle polymer in the long-term, with a significant loss of multiple mechanical properties required for satisfactory performance.[8] In addition, the absence of polyethylene oxidation during *in vivo* use has been recently challenged,[9] since unloaded regions of implanted cups undergo oxidation in spite of the characteristic low oxygen concentration of the human body.

In the search for a method that decreases this long-term risk of oxidation, orthopaedic manufacturers combined the irradiation process with a subsequent thermal stabilization step to obtain commercial HXLPEs. Nowadays, polyethylenes treated with warm and cold irradiation, both γ- or electron beam, and subsequent thermal stabilization predominate within the first generation of commercial HXLPEs, such as Crossfire®, Marathon®, Durasul®, Longevity®, etc. In this sense, it is possible to classify HXLPEs into two different groups depending on whether the stabilization temperature falls below (annealing) or above (remelting) the melting transition temperature of the polymer. However, an important controversy still remains regarding the best conditions in which the thermal treatment must be carried out.[10–12] From a wear resistance point of view, both remelted and annealed HXLPEs seem to retain their wear resistance and are virtually equal. Nevertheless, there is a crucial difference as remelting destroys the original crystallinity of the polymer,[13] and therefore it affects some of the polymer's mechanical properties, such as yield stress, secant modulus, and fatigue resistance.[13,14] Recently, fatigue crack propagation resistance has been claimed to be worse in remelted HXLPEs than in annealed HXLPEs.[15,16] This mechanical loss may compromise the performance of HXLPEs, especially in high demanding mechanical situations such as the knee joint or the rim of hip components, which are subjected to impingement.[17] Although annealing preserves better mechanical properties,[18] since it does not imply such a drastic change in the crystallinity of the polymer compared with remelting, it may fail to assure a complete oxidative stability. As original crystals do not completely melt during annealing, some of the free radicals located in the crystalline regions are not able to recombine, and they may be precursors of long-term oxidation.[3] Thus, a potential oxidation threatens the lifespan of annealed HXLPEs in prosthetic components, especially at the rim area where oxidation may be high after long-term *in vivo* use.[9]

In summary, three important questions prevail about HXLPEs: Do remelting and annealing assure the oxidative stability of HXLPEs? Are remelted and annealed HXLPEs equally suitable for hip joints? Are both materials proper candidates for use in other joint prostheses, in particular the knee? The orthopedic community has reached a certain consensus regarding the first question, as mentioned above. Remelting has been shown by McKellop et al.[4] and Wannomae et al.[19] to completely stabilize the polymer against oxidation, whereas annealing may not prevent oxidation in the long-term.[3,20] With regard to the second question, both HXLPEs perform similarly with respect to wear resistance.[2] However, they may have a completely different behavior at the rim area of hip components, since these materials feature very different mechanical properties. These different mechanical features, especially fatigue and fracture resistance, are the key point in the third question, addressing HXLPEs' use in knee joints. Unfortunately, there is a lack of systematic studies comparing different remelted and annealed HXLPEs from a mechanical point of view. Such studies will help to develop a rationale to choose the proper irradiation and thermal stabilization conditions to produce suitable polyethylenes depending on their final requirements.[21] In the context presented above, the current work aims to give a comparison between the effects of postirradiation annealing and remelting on the fatigue behavior and toughness of HXLPEs. In addition, a correlation between microstructural features and the mentioned mechanical properties is proposed.

MATERIALS AND METHODS

In this study, the raw material was GUR 1050 UHMWPE in the form of compression-molded sheets (Perplas Medical, Lancashire, UK). Preforms of mechanical specimens underwent electron beam irradiation in air at different doses: 50, 100, and 150 kGy. A 10-MeV Rhodotron TT 200 accelerator (Ionmed Esterilización S.A., Tarancón, Spain) performed the single side irradiation in 25 kGy-passes. After irradiation, specimens were maintained at $-20°C$ in a subzero freezer before a remelting (150°C) or an annealing (130°C) process was carried out in a vacuum oven (Gallenkamp) for 2 h. All specimens underwent a slow cooling (0.5°C/min) to room temperature as the final stage in both thermal treatments. Thus, the current study involved 10 different material groups, NI, β50, β100, β150, β50R, β100R, β150R, β50A, β100A, and β150A, where NI, β, R, and A mean non-irradiated, electron beam irradiated, remelted, and annealed material, respectively.

Different techniques allowed the characterization of the changes in microstructure caused by irradiation and thermal treatments. Thus, crosslink density measurements were performed per ASTM F2214 (Cambridge Polymer Group; Boston; MA) on the β50, β150, and β150R material groups. Changes in crystallinity content and melting temperature were assessed by heating samples ($n = 3$) from 20 to 170°C at a rate of 10°C/min in a Differential Scanning Calorimeter (Perkin-Elmer). The area below the thermograms from 80 to 160°C, normalized by 290 J/g as the enthalpy of melting of a 100% crystalline polyethylene, gave the crystallinity percentages for each material. In addition, specimens of all materials groups underwent specific preparation, reported elsewhere,[22] to obtain Transmission Electron Microscopy (TEM) images. These images allowed the

DOI 10.1002/jbmb
Questions? Contact FDA/CDRH/OCE/DID at CDRH-FOISTATUS@fda.hhs.gov or 301-796-8118

Records processed under FOIA Request #2014-8015; Released by CDRH on 12-8-2015

measurement of lamellar thickness as well as the detection of changes in morphology caused by irradiation and stabilization.

The fatigue response was investigated by means of three different experimental tests. First, cyclic stress–strain experiments were conducted on tensile specimens (ASTM D638 type M-I) for up to 50 cycles. The experiments had a constant displacement rate of 15 mm/min, which gave an initial nominal strain rate of 0.025 s^{-1}, and a constant maximum nominal stress, σ_{max}, with a stress ratio $R = 0$. For each material group, at least three samples were tested at $\sigma_{max} = 14$ and 16 MPa. Tests were performed in an Instron 5565 machine at (24 ± 1)°C, using an extensometer to measure the strain. These short-term cyclic experiments provided with information about the total plastic strain reached, $\varepsilon(50)$, and the secant modulus values at the first cycle, which are measures of the material softening and stiffness respectively. Secondly, long-term fatigue tests, *S/N* stress–life experiments, were performed on dog bone specimens following ASTM E606 guidelines, in a servohydraulic Instron 8032 machine. These fatigue tests were carried out under load control following a sine waveform at a frequency of 1 Hz and with a stress ratio $R = 0$. An extensometer evaluated the strain continuously and an air jet kept the testing temperature in the range of (23 ± 2)°C. In this test, we did not consider the life, *N*, as the number of cycles to fracture, but the number of cycles when the specimen reached 12% strain. The bases of this failure criterion are the material yield strain, as the maximum expected strain in UHMWPE tibial components is 12%–15%,[23] and the appearance of microscopic defects due to cyclic fatigue damage at a maximum load below the yield stress in monotonic loading, as reported by Baker et al.[24] for UHMWPE, Hristov et al.[25,26] and Li et al.[27] for polycarbonate, and Jones and Lesser for polypropylene.[28] Statistical data analysis was performed using linear regression analysis, with Minitab software, on the long-term fatigue results. Finally, standard compact tension specimens, 8 mm in thickness, 50 mm in width, and with a 10 mm long machined notch, underwent near-threshold fatigue crack propagation tests per ASTM E647. All compact specimens were precracked under cyclic tension. Crack length was measured with the use of a movable microscope. Three specimens were measured for each material group and underwent tension cycling at a frequency of 5 Hz with $R = 0.1$. $\Delta K_{inception}$ values and Paris coefficients were obtained from crack propagation curves, and one-way analysis of variance (ANOVA) was performed to assess significant differences ($p < 0.05$) between annealed and remelted materials with regard to power law fit parameters.

The toughness of HXLPEs was assessed by three different mechanical experiments. Firstly, impact Izod tests were carried out on double-notched specimens following ASTM F648 at room temperature. These experiments provided a measure of the impact toughness for each material group. Secondly, uniaxial tensile tests per ASTM D638 were performed in a Lloyd 1000S machine on specimens type M-I, at $T = (23 \pm 2)$°C, at a displacement rate of 5 mm/min giving an initial nominal strain rate of 0.002 s^{-1}. Thus, works of fracture values were calculated from engineering stress–strain curves as the area below the curve, which are an estimation of the material toughness in a quasi-static situation. In addition to that, results corresponding to maximum yield stress, fracture stress, and fracture strain were extracted from stress–strain curves. Finally, *J*-integral versus crack growth resistance, *J–R*, curves were obtained following ASTM D6068-02 for all material groups. The *J–R* curves characterized the resistance of the HXLPEs to slow stable crack growth after initiation from a pre-existing sharp flaw and served as an index of material toughness. A minimum of seven compact tension specimens were used to build each *J–R* curve. Specimens' geometry complied with ASTM D6068-02 recommendations. Thus, all in-plane dimensions were proportional to specimen width, $W = 20$ mm, so thickness, *B*, was 10 mm and the original crack length, a_0, was also 10 mm. Testing procedure was performed as follows. To obtain the sharpest initial crack, a precrack was induced at the end of the machined notch subjecting specimens to cyclic loading at 3 Hz. After that, specimens were ready to be loaded at a strain rate of 1 mm/min to a selected displacement level, which was judged to produce a suitable crack extension. Load versus displacement curves were recorded, and finally, the specimen was broken to further fracture surface inspection by SEM. All testing was conducted at a temperature $T = (24 \pm 1)$°C. Fracture surfaces were gold coated and observed by means of a Jeol JSM-6400 SEM working at 15 kV in the secondary electron mode. SEM micrographs allowed measuring machined notch and pretest crack lengths, as well as stable crack extensions. In the last case, the crack length was measured at five equally spaced points centered about the specimen and extending near lateral surfaces. *J* values were calculated as the energy required to extend the crack, *U*, multiplied by a geometrical factor,[29] $J = \eta U/(B(W-a_0))$. *U* was calculated as the area under the load–displacement curve minus the work of indentation, which was obtained by loading unnotched calibration specimens up to a load 10% greater than the maximum load used in the *J* tests. Thus, the stable crack extensions and their corresponding *J* values proportioned the data points needed for the *J–R* curves. These data were fit to a power law, $J = C_1 \Delta a_0^{C2}$, and C_1 coefficients, which can be interpreted as the *J* value corresponding to a 1 mm-long crack extension, were registered as a toughness metric already used elsewhere.[2]

It must be mentioned that some of the results corresponding to control, as-irradiated and remelted specimens were already presented in two previous works.[13,23] Those data are also included in the current work to allow a better comparison between remelting and annealing effects on mechanical performance of HXLPEs.

DOI 10.1002/jbmb
Questions? Contact FDA/CDRH/OCE/DID at CDRH-FOISTATUS@fda.hhs.gov or 301-796-8118

Records processed under FOIA Request #2014-8015; Released by CDRH on 12-8-2015

TABLE I. Material Crystallinities and Melting Transition Temperatures Obtained in DSC Measurements, Along With Lamellar Thickness Measured From TEM Micrographs, and Mechanical Parameters Obtained From Stress–Strain Curves

	Work I[23]				Work II[13]			Current Work		
	NI	β50	β100	β150	β50R	β100R	β150R	β50A	β100A	β150A
% Crystallinity	51.3 ± 2.3	55.5 ± 2.2	57.7 ± 1.0	58.6 ± 2.4	43.6 ± 1.9	46.8 ± 1.1	49.7 ± 3.3	59.5 ± 0.3	61.0 ± 0.7	61.0 ± 0.8
Melting temperature (°C)	135.6 ± 0.6	138.0 ± 0.5	139.5 ± 0.4	139.2 ± 0.6	133.3 ± 0.8	133.9 ± 0.5	131.5 ± 0.7	139.0 ± 0.1	141.0 ± 1.1	142.0 ± 0.3
Lamellar thickness (nm)	(30–35)	(35–40)	(40–45)	(40–45)	(20–25)	(20–25)	(17–22)	30–40	30–40	30–40
Max. yield stress (MPa)	19.1 ± 1.3	20.7 ± 0.2	20.6 ± 0.1	20.5 ± 0.2	16.7 ± 0.2	15.8 ± 0.6	15.3 ± 1.3	19.2 ± 0.2	18.9 ± 0.3	19.3 ± 0.3
Fracture stress (MPa)	37.5 ± 4.4	36.9 ± 0.1	42.1 ± 2.0	38.6 ± 4.1	33.1 ± 4.2	32.9 ± 4.0	27.2 ± 4.5	31.9 ± 1.3	29.5 ± 2.6	29.6 ± 2.0
Fracture strain	(3.6 ± 0.7)	(3.5 ± 0.7)	(2.8 ± 0.5)	(2.2 ± 0.4)	3.7 ± 0.6	3.2 ± 0.5	2.2 ± 0.6	3.5 ± 0.1	2.6 ± 0.2	2.2 ± 0.2

Results appearing in round brackets are presented in the current study for the first time.

RESULTS

UHMWPE Microstructure

After electron beam irradiation, the crosslink density of UHMWPE strongly increased with dose from 0.127 ± 0.010 mol/dm^3 to 0.192 ± 0.009 mol/dm^3 for 50 and 150 kGy respectively, i.e. a 51% increment. However, the remelting process supposed a small decrease of 7% in this property, as the measured crosslink density for the samples irradiated at 150 kGy and subsequently remelted was only slightly lesser 0.178 ± 0.003 mol/dm^3.

Irradiation caused an increase in crystallinity and was dose dependent. Thus, the crystallinity content rose from 51.3 ± 2.3 for the virgin polymer to 55.5 ± 2.2 and to 58.6 ± 2.4 for materials irradiated at 50 and 150 kGy, respectively.[23] As for the thermal steps after electron beam irradiation, they had different effects on the polymer's crystallinity depending on the treatment temperature, although both treatments kept the previous influence of the irradiation dose. The remelting step resulted in a notable drop in crystallinity since the measured values ranged from 43.6 ± 1.9 to 49.7 ± 3.3.[13] On the contrary, the annealing process produced a small increase in crystallinity, which ranged from 59.5 ± 0.3 to 61.0 ± 0.8. Table I includes crystallinity data for virgin, as-irradiated, remelted, and annealed UHMWPEs to allow for an easier comparison between the effects of the different processes. As reported in a previous work, TEM images of virgin UHMWPE showed the typical aspect of a semicrystalline polymer with randomly oriented crystal lamellae with a thickness of 30–35 nm and immersed in a dark grey region, which is the amorphous region.[22] TEM micrographs of electron beam irradiated UHMWPE confirmed a thickening of crystal lamellae up to 40–45 nm. On the other hand, both thermal treatments created a decrease in lamellar thickness, although the remelting process provided a stronger slimming of lamellae than the annealing step, as crystal thickness ranged 20–25 nm and 30–40 nm for remelted and annealed materials, respectively [Figure 1(a,b)]. Lamellar thickness results corresponding to the main crystal population appear on Table I for virgin, as-irradiated, remelted, and annealed materials.

Other microstructure changes appear to concern the lamellar configuration. The electron beam irradiation introduced some new crystal organizations that resembled branched structures, which consisted of a central crystal with a few slightly thinner lamellae, around 25 nm thick, emerging from the central one. Figure 1(b) also shows this structure in the typical micrograph of a 100-kGy irradiated and annealed UHWMPE. In addition, the postirradiation remelting process revealed a more chaotic aspect and some lamellae adopted a radial arrangement, especially at low doses. However, the annealed materials showed a thickening of the central crystals that belonged to the branched structures, reaching a thickness up to 60–70 nm, whereas remelting hardly changed them, although it produced a large decrease in thickness.

DOI 10.1002/jbmb
Questions? Contact FDA/CDRH/OCE/DID at CDRH-FOISTATUS@fda.hhs.gov or 301-796-8118

Records processed under FOIA Request #2014-8015; Released by CDRH on 12-8-2015

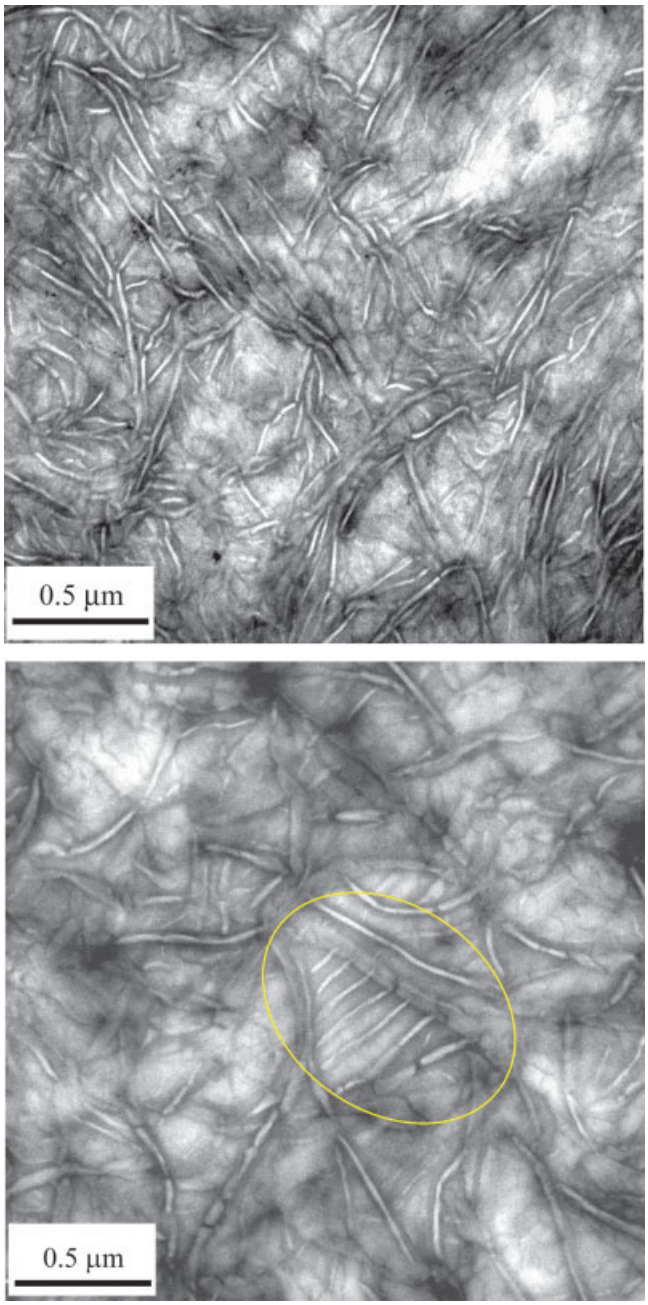

Figure 1. (a) TEM micrograph (60,000×) of β100R, 100 kGy-electron beam irradiated and subsequently remelted UHMWPE. (b). TEM micrograph (60,000×) of β100A, 100 kGy-electron beam irradiated and subsequently annealed UHMWPE. A characteristic branched structure is highlighted. [Color figure can be viewed in the online issue, which is available at www.interscience.wiley.com.]

Mechanical Parameters

As an example, Figure 2 depicts the typical engineering stress–strain tensile curves for 100 kGy-irradiated UHMWPEs, and the main results obtained from uniaxial tests are shown in Table I. As relevant results, it is worth mentioning the decrease in yield stress after both thermal treatments, but especially after remelting, compared to the yield stress values, around 20.6 MPa, found for as-irradiated materials.[23]

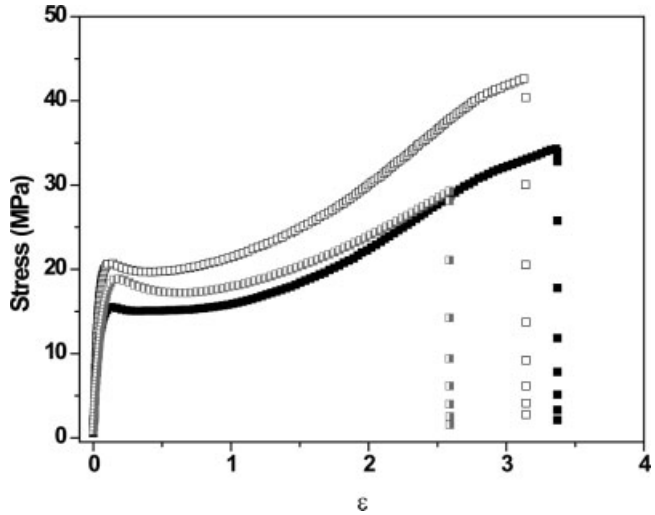

Figure 2. Stress–strain curves in the uniaxial tension test for β100, (□); β100R, (■); and β100A, (◨) materials.

A decreasing trend with irradiation dose characterized fracture stress results, which was not altered after thermal treatments. Similarly, fracture strain values were also lower with higher irradiation doses, and both thermal treatments did not alter them.

Fatigue Behavior

In a previous work, cyclic stress–strain experiments confirmed a small decrease in material softening, $\varepsilon(50)$, with increasing irradiation dose with respect to virgin UHMWPE. At 16 MPa, $\varepsilon(50)$ ranged from 5.9 ± 0.5 to 4.7 ± 0.5 for as-irradiated UHMWPEs.[23] On the contrary, both thermal treatments caused a remarkable increase in softening above of all after remelting stabilization (Figure 3 and Table II). In particular, remelted specimens showed, independently of irradiation dose, $\varepsilon(50)$ values of about 12.2 ± 1.6, which are

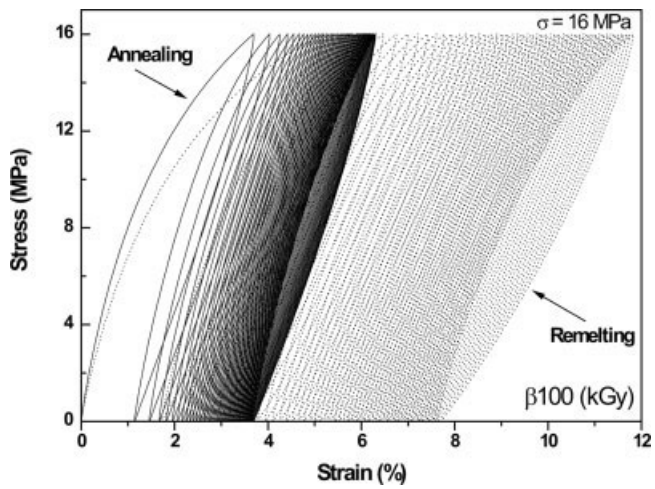

Figure 3. Typical cyclic stress–strain curves for β100R (dotted line) and β100A (solid line) materials. Tests performed at σ_{max}= 16 MPa.

DOI 10.1002/jbmb
Questions? Contact FDA/CDRH/OCE/DID at CDRH-FOISTATUS@fda.hhs.gov or 301-796-8118

Records processed under FOIA Request #2014-8015; Released by CDRH on 12-8-2015

TABLE II. Secant Modulus at the First Cycle and Strain Reached after 50 Cycles at the Cyclic Stress-Strain Test for Virgin, As-Irradiated, Remelted, and Annealed materials

	Work I[23]				Work II[13]			Current work		
	NI	β50	β100	β150	β50R	β100R	β150R	β50A	β100A	β150A
E_s(1c) (MPa)	748 ± 19	803 ± 13	820 ± 5	841 ± 15	642 ± 18	650 ± 25	658 ± 14	764 ± 50	811 ± 14	868 ± 50
ε(50c) (%); $\sigma = 16$ MPa	7.4 ± 0.4	5.9 ± 0.5	5.2 ± 0.5	4.7 ± 0.5	12.2 ± 1.6	11.2 ± 0.9	12.3 ± 1.1	7.1 ± 0.5	6.2 ± 0.2	5.2 ± 0.8

twice as high as those of only irradiated samples. As for the annealed materials, they showed an intermediate softening behavior between as-irradiated and remelted specimens with values ranging from 7.1 ± 0.5 to 5.2 ± 0.8 (Table II). As it regards to secant modulus, E_s(1c), while irradiation introduced a 12% increase in stiffness at the highest dose with respect to NI material, both thermal treatments provoked a drop in this property. Particularly, a remarkable 21% decrease was noticed after remelting with respect to as-irradiated materials. Table II includes secant modulus results for all materials.

Long-term fatigue tests provided stress–life, *S–N* curves for β50A and β150A, plotted in Figure 4 in a semilogarithmic scale along with *S–N* curves obtained previously for virgin, as-irradiated,[23] and remelted specimens.[13] Parallel straight lines fit the logarithmic behavior $S = A \log(N) + B$, with A and B as fitting parameters (Table III). Long-term fatigue results clearly confirmed the trend found in cyclic stress–strain experiments. Thus, stress–life curves point to a small increase in fatigue life with irradiation dose, as reported in a previous work.[13] However, both thermal treatments reduced fatigue life remarkably, especially under remelting conditions (Figure 4). Nevertheless, materials irradiated at higher doses achieve a slightly better fatigue life even after the thermal stabilization.

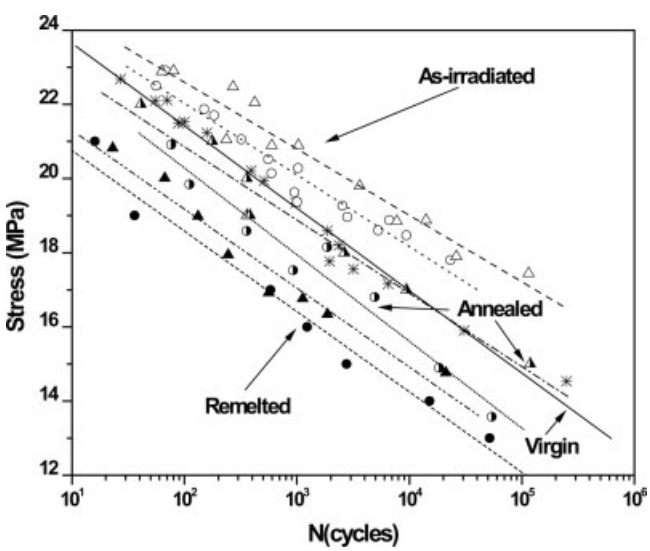

Figure 4. Stress–life curves for NI, (∗); β50, (○); and β150, (△) materials according to,[23] β50R, (●) and β150R, (▲), as presented in,[13] and β50A, (◑) and β150A, (◭), obtained in this work.

Fatigue crack propagation tests allowed characterizing the crack growth resistance of annealed HXLPEs. In all samples, crack propagation results showed two different regions in a log-log scale of the crack growth rate, da/dN, versus the stress intensity range, ΔK (Figure 5). The first region matched the slow crack growth regime, whereas the second one represented the intermediate crack growth or Paris regime, which is described by the Paris equation $da/dN = C(\Delta K)^m$, where C and m are constants. In the first region, a fatigue crack inception stress intensity range ($\Delta K_{inception}$) could be defined as the intersection of the first regime curve with the x-axis, at a value of $da/dN = 10^{-7}$ m/cycle. This approach permits comparison of the initiation of measurable fatigue crack propagation.[30] Non-fast-fracture regime was reached in all the specimens. In a previous work,[13] we showed that the crack propagation resistance suffers a monotonic decrease after irradiation, as the stress intensity factor range at crack inception, $\Delta K_{inception}$, drops with irradiation dose from 1.53 ± 0.06 to 1.16 ± 0.01 for 50 and 150 kGy, respectively. Moreover, remelting has a detrimental effect on $\Delta K_{inception}$ as well, since provokes a decrease of 10% in this property at the highest irradiation dose.[13] On the contrary, the annealing step imparted an improvement between 7% and 11% in fatigue resistance onto notched samples in the current work, since $\Delta K_{inception}$ values ranged from 1.64 ± 0.05 to 1.29 ± 0.04 for 50 and 150 kGy-irradiated and annealed materials (Table IV). Figure 5 displays the fatigue crack propagation plots corresponding to as-irradiated, annealed, and remelted materials irradiated at the lowest and the highest doses to provide a better comparison. Besides our data, data from a different

TABLE III. Fitting Constants of the Equation $S = A \log(N) + B$ in Long-Term Test, Linear Correlation Coefficient, R^2, and 95% Confidence Band for A Parameter

	A	B	R^2	95% CI for A Parameter
Work I[23]				
NI	−2.38	26.3	0.986	−2.21 to −2.56
β50	−1.93	25.9	0.950	−1.68 to −2.19
β150	−1.79	26.3	0.949	−1.50 to −2.09
Work II[13]				
β50R	−2.17	22.9	0.976	−1.87 to −2.47
β150R	−2.13	23.4	0.957	−1.77 to −2.49
Current work				
β50A	−2.34	25.0	0.959	−1.85 to −2.82
β150A	−1.98	24.8	0.950	−1.52 to −2.43

DOI 10.1002/jbmb
Questions? Contact FDA/CDRH/OCE/DID at CDRH-FOISTATUS@fda.hhs.gov or 301-796-8118

Records processed under FOIA Request #2014-8015; Released by CDRH on 12-8-2015

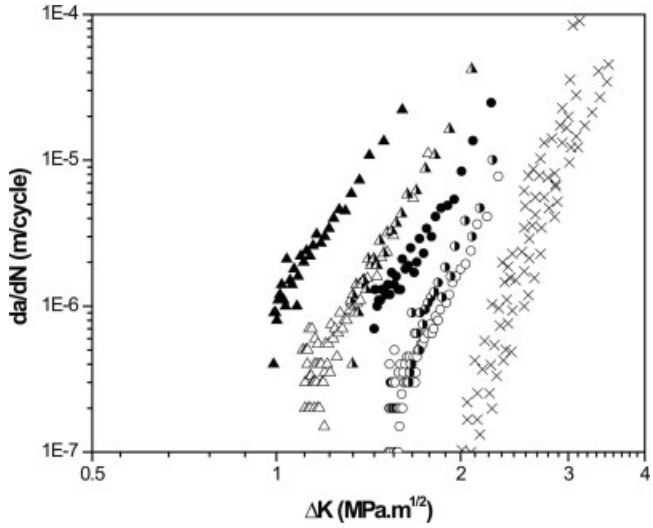

Figure 5. Fatigue crack propagation curves for β50, (○); β50R, (●); β50A (◑); β150, (△); β150R, (▲); and β150A, (◭) materials. Data corresponding to ram-extruded virgin GUR 1050 UHMWPE, (×), were adapted from Gencur et al.[15]

study[15] corresponding to virgin ram-extruded GUR 1050 UHMWPE is included in Figure 5 to account for a reference material. Regarding Paris coefficients, annealed materials exhibited the same values independently of the irradiation dose, and non-significant differences ($p < 0.05$) between Paris coefficients of remelted and annealed materials were found.

Toughness

As impact Izod and work to fracture results pointed out, UHMWPE toughness was clearly lower after irradiation (Table V). The *J*-integral versus crack growth resistance (*J–R*) curves, which characterized the slow stable crack growth resistance of UHMWPE specimens, as well as the *J* values at 1 mm long crack extension, C_1 fitting coefficients, confirmed the trend found in impact and tensile experiments. Even though impact and work to fracture results did not reveal remarkable changes in tough response (Table V), the *J–R* curves showed a clear toughness drop in irradiated specimens after remelting. On the other hand, the *J–R* curves of the annealed materials signaled a small increase in toughness compared with as-irradiated UHMWPEs at low or intermediate doses (Table V). As an example, Figure 6 displays the *J–R* curves for as-irradiated, annealed, and remelted materials that received the intermediate dose.

TABLE IV. Results of $\Delta K_{inception}$ and Paris Coefficients Obtained From Crack Propagation Experiments

	ΔK_{incept}	Paris Coeff.
Work II[13]		
β50	1.53 ± 0.06	8.1 ± 1.0
β100	1.37 ± 0.05	7.5 ± 0.9
β150	1.16 ± 0.01	7.4 ± 0.9
β50R	1.58 ± 0.05	6.8 ± 0.7
β100R	1.36 ± 0.05	6.0 ± 0.7
β150R	1.03 ± 0.07	6.0 ± 0.4
Current Work		
β50A	1.64 ± 0.05	6.7 ± 0.6
β100A	1.49 ± 0.06	6.7 ± 0.3
β150A	1.29 ± 0.04	6.7 ± 0.7

TABLE V. Results Corresponding to Work to Fracture, Impact Toughness and *J*-Integral Tests. *J*-Integral Values at a Crack Extension Equal to 1 mm[a] Are Presented

	Work to Fracture (MPa or MJ/m^3)	Impact Toughness (kJ/m^2)	*J*-Integral (Δa = 1 mm) (kJ/m^2)
NI	92 ± 23	121 ± 7	77 ± 6
β50	80 ± 12	99 ± 7	32 ± 3
β100	68 ± 21	66 ± 2	19 ± 4
β150	50 ± 8	53 ± 3	16 ± 2
β50R	71 ± 20	91 ± 5	22 ± 1
β100R	61 ± 19	70 ± 5	17 ± 2
β150R	29 ± 2	57 ± 8	12 ± 2
β50A	77 ± 4	96 ± 4	35 ± 2
β100A	55 ± 7	61 ± 1	20 ± 3
β150A	40 ± 4	49 ± 3	12 ± 1

[a] Metric used in reference 2.

DISCUSSION

Postirradiation remelting and annealing produced important changes in UHMWPE microstructure. First of all, crosslink density measurements confirmed the increase in the level of crosslinking with irradiation dose, which is responsible for a remarkable improvement in wear resistance, as shown by different studies.[2–5] However, we could say that thermal treatments scarcely affect this property, since after remelting, the most aggressive stabilization treatment, the β150R

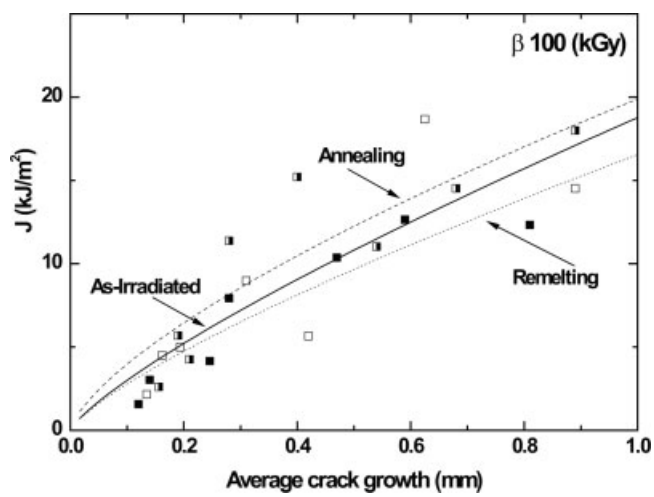

Figure 6. *J*-integral versus crack growth resistance, *J–R*, curves for β100, (□); β100R, (■); and β100A, (◨) materials.

DOI 10.1002/jbmb
Questions? Contact FDA/CDRH/OCE/DID at CDRH-FOISTATUS@fda.hhs.gov or 301-796-8118

Records processed under FOIA Request #2014-8015; Released by CDRH on 12-8-2015

material group had a slightly lower crosslink density than the as-irradiated material. Therefore, the stabilization steps may not significantly alter the crosslinking level in the polymer, at least in the conditions of this study. The increase in lamellar thickness with irradiation dose could be associated with the increase in crystallinity content observed by calorimetric measurements, probably via recrystallization processes and molecular chain rearrangements within crystals.[31] At high doses, the radiolitic cleavage of molecular chains and the molecular mobility are high enough to allow the creation of new crystal morphologies, i.e. branched structures. Comparing both thermal treatments, the remelting process caused the most severe microstructural alterations. In addition to a strong drop in crystallinity content, which is probably correlated to an important decrease in lamellar thickness, the recrystallization after remelting introduced radial configurations, especially in low dose-irradiated UHMWPE. On the other hand, annealing resulted in a small increase in crystallinity, which seems inconsistent with the slight lamellar slimming noted in TEM micrographs. Regarding lamellar thickness, different phenomena such as partial melting, lamellar thickening, and lamellar doubling have been reported to occur during annealing of polyethylene.[32–36] In particular, Matsuda et al. proposed that two competitive rearrangement mechanisms overlap during annealing of polyethylene.[33] The first one would be predominant at low annealing temperatures and involve the gradual thickening of lamellar crystals. On the contrary, partial melting and further rearrangement resulting in lamellar doubling would predominate at high annealing temperatures. Other authors Fischer,[32] Sobieraj et al.,[35] and Cho et al.[36] reported that the annealing of UHMWPE involved two competing processes, namely partial or surface melting and thickening of the original lamellae. The predominance of one process over the other is dependent on molecular weight distribution, crystallization temperature, annealing temperature,[32] and annealing times.[36] In our case, it seemed that the annealing temperature used, 130°C, might correspond to the intermediate-upper region of overlapping of the two competing mechanisms proposed by Matsuda et al. Thus, the surface melting of many of the original lamellae would result in lamellae with a decreased size, and the molten material may take part in lamellar doubling,[33] or even in the creation of new crystals in the interlamellar space.[36] Under appropriate conditions, the previous processes could result in the presence of a predominant population of original lamellae slightly slimmed, few lamellae that experienced doubling, and a few crystals originated in the interlamellar region, as we found in our TEM micrographs [Figure 1(b)]. Besides, the balance between the generalized lamellar slimming and the appearance of doubled and new lamellae would explain the slight increase in crystallinity and melting temperature reported in the current study.

The mechanical behavior of UHMWPE was clearly affected by the crosslinking and stabilization processes, as demonstrated by our results. Even more, there seems to be a direct relation between mechanical behavior and microstructure for HXLPEs. First of all, yield stress and secant modulus results appear to be governed by crystalline parameters, as proposed previously.[13,23] Coherently, the strong drop in crystallinity caused by remelting would be related to the decreased yield stress and stiffness. The combined analysis of the results obtained from remelted and annealed specimens allowed concluding that yield stress appears to be governed by lamellar thickness, which would explain the decreased yield stress even after an increase in crystallinity caused by annealing, and that secant modulus is dictated by crystallinity percentage. Galeski reported similar dependencies in a review article.[37] Regarding fatigue behavior, the main parameters obtained from short-term and long-term tests, final strain reached after 50 cycles, $\varepsilon(50)$, and number of cycles to failure, fatigue life or N_f, followed a similar trend. Hence, both results are discussed together in terms of either fatigue life or fatigue resistance. First of all, irradiation improved fatigue life considerably as the dose increased, which stemmed from either the increase in crystallinity percentage or the lamellar thickening that UHMWPE suffered upon irradiation. A potential influence of crosslink density on fatigue life appears to be less important, as materials with similar crosslink densities, β150 and β150R, showed very different fatigue performances. Contrary to the improvement imparted by irradiation, the fatigue performance of the irradiated and remelted materials declined abruptly. This drop in fatigue life corresponds well with the crystallinity changes detected after remelting, but at this point it is not possible to affirm whether the crystallinity content or the crystal size governs fatigue behavior. Fortunately, the fatigue life results of the irradiated and annealed UHMWPEs offer an answer to this question. Annealed materials required a fewer number of cycles to failure than as-irradiated UHMWPEs, even though after annealing they had higher crystallinity content. Nevertheless, this worse fatigue performance could be explained by the general lamellar slimming that the irradiated UHMWPEs experienced after annealing and remelting. Thus, any process that causes a decrease in the crystal size, such as the thermal treatments in our study, would make the fatigue behavior of HXLPEs worse. Conversely, any process that increased lamellar size would be responsible for an improved fatigue performance, as the one produced by electron beam irradiation in the current study. In this sense, Figure 7 depicts the correlation between the final strain reached in the cyclic stress–strain experiments, $\varepsilon(50)$, and the lamellar thickness for all the materials considered in this study. It becomes clear from Figure 7 that the thicker the lamellae are, the lower the softening is, so then, the better the fatigue life. Similarly, Simis et al.[38] based the analysis of the fatigue crack propagation thresholds of highly crystalline and highly crosslinked UHMWPEs on their corresponding lamellar thickness values. Thus, highly crystalline polymers obtained by high-pressure crystallization

DOI 10.1002/jbmb
Questions? Contact FDA/CDRH/OCE/DID at CDRH-FOISTATUS@fda.hhs.gov or 301-796-8118

Records processed under FOIA Request #2014-8015; Released by CDRH on 12-8-2015

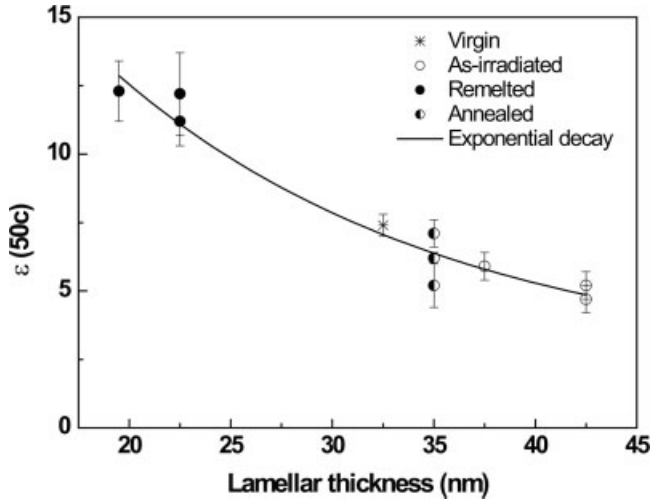

Figure 7. Correlation between final strain reached after 50 cycles of short-term fatigue testing and lamellar thickness for all materials considered in this work.

exhibited an improved fatigue crack propagation resistance, as a consequence of a greatly increased lamellar thickness. Even though fatigue crack experiments and fatigue life tests represent very different stages and approaches to fatigue behavior, this work and the aforementioned one point out the importance of the lamellar thickness through the whole fatigue behavior of HXLPEs.

Crack propagation resistance behavior followed a different pattern in comparison with the cyclic and long-term fatigue performances in this study. In this case, electron beam irradiation resulted in a remarkable dose-dependent drop in the stress intensity factor at crack inception, $\Delta K_{\text{inception}}$. In other words, a pre-existing crack in the irradiated material would start to propagate before than in the virgin UHMWPE. The greater the irradiation dose was, the lower the $\Delta K_{\text{inception}}$ values resulted. Most likely, the increased crosslink density introduced by irradiation prevents UHMWPE from exhibiting ductile behavior, and hence the $\Delta K_{\text{inception}}$ lowers, as crosslinking points reduce the deformation modes of the amorphous region.[39,40] On the other hand, both thermal treatments did not strongly affect the slope of the Paris regime, although they introduced slight variations in $\Delta K_{\text{inception}}$. The remelting step provoked a slight decrease in the crack propagation threshold. On the contrary, the annealing treatment introduced a small but noticeable improvement in the $\Delta K_{\text{inception}}$ of irradiated UHMWPE (Figure 5). In this line, two recent studies[15,16] confirmed an improved fatigue crack propagation resistance of annealed highly crosslinked polyethylenes compared with remelted materials. As regards microstructural interpretation, and in light of the crosslink density and crystallinity content results, the former seems practically to dictate crack propagation behavior. In the aforementioned study by Simis et al.,[38] they detected a negative influence of an elevated crosslink density on fatigue crack propagation thresholds as well. However, they found a direct correlation between the mentioned parameter and the lamellar thickness, but not with crystalline content. Nevertheless, it should be borne in mind that our study involved relatively small variations in lamellar thickness, compared to the bigger variations caused by high-pressure crystallization methods.

Finally, the toughness, or fracture resistance, results exhibited a pattern similar to the crack propagation resistance trends. Impact and tensile experiments detected a clear decrease in toughness that rose with irradiation dose. In addition, *J–R* curves also confirmed this behavior. Previously, Gomoll et al.,[41] Duus et al.,[42] and Cole et al.[30] also reported a similar decrease in *J* with an increase in radiation dose. Again, the crosslink density was responsible via a diminution in the ductile capability that imparts a reduced fracture resistance. Consistently, fracture strain results confirmed the loss of ductility with higher crosslink density, which probably reduces the amorphous deformation modes of the polymer, as mentioned by some authors.[14,40,41] Impact and tensile experiments were not sensitive enough to notice any changes in toughness after either remelting or annealing. However, the multispecimen *J*-integral method was able to detect an improvement in fracture resistance after annealing, and a decrease after remelting of as-irradiated polyethylenes. Lamellar thickness changes, Table I, do not appear to be responsible for those variations in fracture resistance, as both thermally treated materials showed decreased lamellar size compared to as-irradiated materials, but the fracture performance was altered in opposite directions (Table V). Thus, it seems more feasible that a rise in crystallinity content was the cause of a slight fracture resistance enhancement and vice versa.

These different fatigue and toughness behaviors of remelted and annealed HXLPEs, based on different microstructural changes, may have noteworthy consequences to the orthopedic industry. Hip and knee prostheses endure different kinematics patterns. Abrasive and adhesive wear damage is predominant in retrieved acetabular inserts, while pitting and delamination, which are related to subsurface fatigue,[43] appear in explanted tibial components. In addition, the fatigue and fracture resistances play an important role in knee prostheses, as these properties define the period to initial crack growth rate. Thus, HXLPEs are expected to have a suitable articular performance in the hip, since a high crosslink density increases the wear resistance independent of the thermal treatment used to stabilize the polymer.[2] However, our work suggests that cracking associated with impingement may be less frequent with annealed material, as long as oxidation does not occur, in view of the toughness improvement with annealing and the decreased lamellar size with remelting. When looking at HXLPEs use in knee inserts, a decreased fatigue performance may limit the lifespan of the component if they underwent a thermal treatment, particularly under remelting conditions. Nevertheless, the annealing stabilization does not assure a total elimination of free radicals, and therefore tibial inserts, that are made of annealed HXLPEs, may

DOI 10.1002/jbmb
Questions? Contact FDA/CDRH/OCE/DID at CDRH-FOISTATUS@fda.hhs.gov or 301-796-8118

Records processed under FOIA Request #2014-8015; Released by CDRH on 12-8-2015

suffer serious microstructural and mechanical changes in the long-term. Not only do the thermal treatments damage the polymer's mechanical properties, but also a high irradiation dose could also significantly decrease the fracture resistance, making the UHMWPE too weak to use in knee prostheses. Therefore, the criteria to select appropriate crosslinking and stabilization conditions for each kinematics condition, i.e. hip and knee, should be based on the final microstructural, mechanical, and oxidative properties of the modified UHMWPE.

CONCLUSIONS

Fatigue and toughness behavior of highly crosslinked UHMWPEs were analyzed in this study, focusing on the comparison between the effects of the annealing and remelting stabilization processes after a previous irradiation step and their microstructural interpretation. Other mechanical parameters, such as yield stress and secant modulus, were correlated to lamellar thickness and crystallinity percentage, in the light of DSC and TEM results. The stress–life curves showed a loss of fatigue strength after both thermal treatment processes, especially after remelting. This reduced fatigue strength seemed to be also related to the drop in lamellar thickness. On the contrary, the fatigue resistance in the presence of defects was mainly controlled by the crosslinking density, and to a lesser extent, by variations in the crystallinity content. Similarly, the toughness or fracture resistance appears to be dictated by crosslink density as the remarkable decrease suffered by UHMWPE after the irradiation step points out. With respect to this property, annealed HXLPEs also showed a slightly improved toughness. Thus, the current study confirmed that annealing preserves mechanical properties better than remelting. In addition, this study identified lamellar thickness and crosslink density as the relevant microstructural factors that govern the fatigue behavior and toughness of HXLPEs, respectively. Coherently, a suitable selection of irradiation and stabilization conditions is needed to achieve optimal mechanical performance from UHMWPE in specific total joint replacements.

REFERENCES

1. Kurtz SM, Muratoglu OK, Evans M, Edidin AA. Advances in the processing, sterilization, and crosslinking of PEUAPM for total joint arthroplasty. Biomaterials 1999;20:1659–1688.
2. Lewis G. Properties of crosslinked ultra-high-molecular-weight polyethylene. Biomaterials 2001;22:371–401.
3. Ries MD, Pruitt L. Effect of cross-linking on the microstructure and mechanical properties of ultra-high molecular weight polyethylene. Clin Orthop Relat Res 2005;440:149–156.
4. McKellop H, Shen F-W, Lu B, Campbell P, Salovey R. Development of an extremely wear-resistant ultra high molecular weight polyethylene for total hip replacements. J Orthop Res 1999;17:157–167.
5. Muratoglu OK, Bragdon CR, O'Connor DR, Jasty M, Harris WH, Gul R, McGarry F. Unified wear model for highly crosslinked ultra-high molecular weight polyethylenes. Biomaterials 1999; 20:1463–1470.
6. Jacobson K. The crosslinked UHMWPE. In: Trossarelli L, Costa L, editors. UHMWPE for Arthroplasty: From Synthesis to Implant. Torino; 2005.
7. Premnath V, Harris WH, Jasty M, Merrill EW. γ Sterilization of UHMWPE articular implants: An analysis of the oxidation problem. Biomaterials 1996;17:1741–1753.
8. Puértolas JA, Larrea A, Gómez-Barrena E. Fracture behavior of UHMWPE in non-implanted, shelfaged knee prostheses after γ irradiation in air. Biomaterials 2001;2:2107–2114.
9. Kurtz SM, Rimnac CM, Hozack WJ, Turner J, Marcolongo M, Goldberg VM, Kraay MJ, Edidin AA. In vivo degradation of polyethylene liners after γ sterilization in air. J Bone Joint Surg Am 2005;87:815–823.
10. Jasty M, Rubash HE, Muratoglu O. Highly cross-linked polyethylene: The debate is over–in the affirmative. J Arthroplasty 2005;20(4 Suppl 2):55–58.
11. Ries MD. Highly cross-linked polyethylene: The debate is over–in opposition. J Arthroplasty 2005;20(4, Suppl 2):59–62.
12. Harris WH. Highly cross-linked, electron-beam-irradiated, melted polyethylene: Some pros. Clin Orthop Relat Res 2004; 429:63–67.
13. Puértolas JA, Medel FJ, Cegoñino J, Gomez-Barrena E, Ríos R. Influence of the remelting process on the fatigue behavior of electron beam irradiated UHMWPE. J Biomed Mater Res Part B: Appl Biomater 2006;76:346–353.
14. Oral E, Malhi AS, Muratoglu OK. Mechanisms of decrease in fatigue crack propagation resistance in irradiated and melted UHMWPE. Biomaterials 2006;27:917–925.
15. Gencur SJ, Rimnac CM, Kurtz SM. Fatigue crack propagation resistance of virgin and highly crosslinked, thermally treated ultra-high molecular weight polyethylene. Biomaterials 2006; 27:1550–1557.
16. Varadarajan R, Rimnac CM. Compliance calibration for fatigue crack propagation testing of ultra high molecular weight polyethylene. Biomaterials 2006;27:4693–4697.
17. Birman MV, Noble PC, Conditt MA, Li S, Mathis KB. Cracking and impingement in ultra-highmolecular-weight polyethylene acetabular liners. J Arthroplasty 2005;20(7, Suppl 3): 87–92.
18. Kurtz SM, Hozack W, Turner J, Purtill J, MacDonald D, Sharkey P, Parvizi J, Manley M, Rothman R. Mechanical properties of retrieved highly cross-linked crossfire liners after short-term implantation. J Arthroplasty 2005;20:840–849.
19. Wannomae KK, Christensen SD, Freiberg AA, Bhattacharyya S, Harris WH, Muratoglu OK. The effect of real-time aging on the oxidation and wear of highly cross-linked UHMWPE acetabular liners. Biomaterials 2006;27:1980–1987.
20. Muratoglu OK, Merrill EW, Bragdon CR. Effect of radiation, heat, and aging on in vitro wear resistance of polyethylene. Clin Orthop Relat Res 2003;417:253–262.
21. Medel FJ, Buldain D, Schaaff P, Kurtz SM, Puertolas JA. Optimal electron-beam irradiation and thermal treatment conditions for highly crosslinked UHMWPE based on artificial neural network simulations. Submitted for publication to Computational Materials Science.
22. Medel FJ, Garcia-Alvarez F, Gomez-Barrena E Puértolas JA. Microstructure changes of extruded ultra high molecular weight polyethylene after γ irradiation and shelf-aging. Polym Degrad Stab 2005;88:435–443.
23. Urriés I, Medel FJ, Ríos R, Gómez-Barrena E, Puértolas JA. Comparative cyclic stress-strain and fatigue resistance behavior of electron-beam and γ-irradiated ultra-high molecular weight polyethylene. J Biomed Mater Res Part B: Appl Biomater 2004;70:152–160.

DOI 10.1002/jbmb
Questions? Contact FDA/CDRH/OCE/DID at CDRH-FOISTATUS@fda.hhs.gov or 301-796-8118

Records processed under FOIA Request #2014-8015; Released by CDRH on 12-8-2015

24. Baker DA, Pruitt L, Bellare A. Ultra-small angle X-ray scattering to detect fatigue damage in polymers. J Mater Sci Lett 2001;20:1163–1164.
25. Hristov HA, Yee AF, Xie L, Gidley DW. Fatigue craze initiation in polycarbonate—Study by small-angle X-ray-scattering. Polymer 1994;35:4287–4292.
26. Hristov HA, Yee AF, Gidley DW. Fatigue craze initiation in polycarbonate—Study by transmission electron-microscopy. Polymer 1994;35:3604–3611.
27. Li XW, Hristov HA, Yee AF, Gidley DW. Influence of cyclic fatigue on the mechanical-properties of amorphous polycarbonate. Polymer 1995;36:759–765.
28. Jones NA, Lesser AJ. Morphological study of fatigue-induced damage in isotactic polypropylene. J Polym Sci Part B: Polym Phys 1998;36:2751–2760.
29. ASTM D6068–96(2002)e1. Standard test method for determining *J–R* curves of plastic materials. ASTM International, West Conshohocken, 2002.
30. Cole JC, Lemons JE, Eberhardt AW. γ irradiation alters fatigue-crack behavior and fracture toughness in 1900H and GUR 1050 UHMWPE. J Biomed Mater Res 2002;63:559–566.
31. Premnath V, Bellare A, Merril EW, Jasty M, Harris WH. Molecular rearrangements in PEUAPM after irradiation and long-term storage in air. Polymer 1999;40:2215–2229.
32. Fischer EW. Effect of annealing and temperature on the morphological structure of polymers. Pure Appl Chem 1972;31: 113–131.
33. Matsuda H, Aoike T, Uehara H, Yamanobe T, Komoto T. Overlapping of different rearrangement mechanisms upon annealing for solution-crystallized polyethylene. Polymer 2001;42:5013–5021.
34. Rastogi S, Spoelstra AB, Goossens JGP, Lemstra PJ. Chain mobility in polymer system: On the borderline between solid and melt. I. Lamellar doubling during annealing of polyethylene. Macromolecules 1997;30:7880–7889.
35. Sobieraj MC, Kurtz SM, Rimnac CM. Large deformation compression induced crystallinity degradation of conventional and highly crosslinked UHMWPEs. Biomaterials 2005;26:6430–6439.
36. Cho MH, Kyu T, Lin JS, Saijo K, Hashimoto T. Time-resolved small-angle X-ray-scattering and wide angle X-ray-diffraction studies on premelting during annealing of gelation crystallized ultrahigh molecular-weight polyethylene films. Polymer 1992;33:4152–4157.
37. Galeski A. Strength and toughness of crystalline polymer systems. Prog Polym Sci 2003;28:1643–1699.
38. Simis KS, Bistolfi A, Bellare A, Pruitt LA. The combined effects of crosslinking and high crystallinity on the microstructural and mechanical properties of ultra high molecular weight polyethylene. Biomaterials 2006;27:1688–1694.
39. Lin L, Argon AS. Structure and plastic-deformation of polyethylene. J Mater Sci 1994;29:294–323.
40. Pruitt LA. Deformation, yielding, fracture and fatigue behavior of conventional and highly cross-linked ultra high molecular weight polyethylene. Biomaterials 2005;26:905–915.
41. Gomoll A, Wanich T, Bellare A. *J*-integral fracture toughness and tearing modulus measurement of radiation cross-linked UHMWPE. J Orthop Res 2002;20:1152–1156.
42. Duus LC, Walsh HA, Gillis AM, Noisiez E, Li S. The effect of resin grade, manufacturing method and cross-linking on the fracture toughness of commercially available UHMWPE. In: Transactions of the Orthopaedic Research Society at the 46th Annual Meeting of the Orthopaedic Research Society, Orlando, FL; 2000. p 544.
43. Shibata N, Tomita N, Onmori N, Kato K, Ikeuchi K. Defect initiation at subsurface grain boundary as a precursor of delamination in ultrahigh molecular weight polyethylene. J Biomed Mater Res A 2003;67:276–284.

DOI 10.1002/jbmb
Questions? Contact FDA/CDRH/OCE/DID at CDRH-FOISTATUS@fda.hhs.gov or 301-796-8118

Records processed under FOIA Request #2014-8015; Released by CDRH on 12-8-2015
ISSN 0965-545X, Polymer Science, Ser. A, 2012, Vol. 54, No. 5, pp. 343–348. © Pleiades Publishing, Ltd., 2012.

The Effect of High Dose of Gamma-Irradiation on Residual Radicals Concentration in Ultra-High Molecular Weight Polyethylene (UHMWPE) in the Presence of Vitamin E[1]

M. S. Mehmood[a,b], Hafeez-Ullah[b], M. S. Jahan[a], S. Mishra[a], B. M. Walters[a], and M. Ikram[b]

[a] *Biomaterial Research Lab, Physics Department, University of Memphis, Memphis TN 38152, USA*
[b] *Department of Physics and Applied Mathematics, Pakistan Institute of Engineering and Applied Sciences, Nilore, Islamabad 45650, Pakistan*
e-mail: hafeezullah79@gmail.com

Received August 7, 2011;
Revised Manuscript Received November 9, 2011

Abstract—Powder samples of UHMWPE (GUR 1020) containing 0.1% by wt. vitamin E (α-tocopherol, α-T) were irradiated at room temperature in air for doses of 30-kGy, 65-kGy or 100-kGy (^{60}Co). After irradiation, they were stored at −78.5°C (dry ice temperature) for one year and then opened to air at room temperature. Following the decay of the primary alkyl and allyl radicals (at room temperature in air), growth of the carbon-centered polyenyl R1 ($-^{\bullet}CH{+}CH{=}CH{+}_m$, $m \geq 3$), and the oxygen-centered di- or tri-enyl R2 ($-^{\bullet}OCH{+}CH{=}CH{+}_m$, $m \leq 3$) residual radicals were measured for eight weeks. An X-band electron spin resonance (ESR) spectrometer was used for radical measurements. The initial relative radical concentrations (R2/R1) were found to be 10.13, 4.6 and 3.7 for the 65-kGy, 30-kGy and 100-kGy samples, respectively. R1 and R2 were both found to grow significantly in the 65-kGy samples while they grew only slightly in the 30-kGy and 100-kGy samples. In 65-kGy sample, R1 grew faster than R2 and the relative concentration R2/R1 was reduced from 10.13 to 2.9 for the 65-kGy sample while that for the 30-kGy and 100-kGy samples reduced only slightly, from 4.6 to 3.5 and 3.7 to 3.2, respectively. The behavior of the residual radicals can be explained by Raman spectroscopic data which suggest that the 65-kGy samples had a higher percentage of amorphous regions when compared to the 30-kGy or 100-kGy (21.7% compared to 15.7% or 17.9%) and also suggest a lower percentage of inter-phase regions (16.4% compared to 25.6% or 17.5%) and a lower level of structural disorder (0.26% compared to 0.44% or 0.27%).

DOI: 10.1134/S0965545X12040062

INTRODUCTION

Ultra-high molecular weight polyethylene (UHMWPE) is widely used in the applications where enhanced mechanical and physical characteristics are required as compared to conventional Polyethylene (PE) [1]. Free radicals generated by radiation sterilization and/or cross linking are believed to be precursors to oxidation of (UHMWPE) via their decay in air through oxidative reaction. Addition of vitamin E (α-T) as biocompatible and lipophilic anti oxidant and free radical quencher has been shown to effectively stabilize the medical grade UHMWPE from oxidation. There are two methods for the incorporation of vitamin E (α-T) in polyethylene (PE) matrix. One method is by diffusion in sterilized and/or cross-linked UHMWPE, while the other is to blend it into UHMWPE polymer powder and then consolidate this blend for device manufacturing process. The main advantage of α-T blending is the ease of obtaining uniformity throughout the polymer matrix [2]. Also, this blend i.e. "α-T UHMWPE polymer powder" before consolidation provides a better mean for investigation of free radical reactions because of larger exposed surface area to the environment [3].

In our previous report [3] we had used high concentration (20%) of α-T in UHMWPE matrix for the direct detection of tocopheroxyl radical (α-T–O$^{\bullet}$) in the presence of strong PE radicals. It was reported that, when irradiation was performed in open air, observed electron spin resonance (ESR) signals were the characteristics of α-T radicals and there were no indication of residual radicals growth. When irradiation is performed in nitrogen (N_2) environment both PE and α-T radicals were observed, also the growth of residual radicals were evident on sample exposure to air (for 71 days). However, FTIR data which was taken after 85 days of post irradiation ageing in air showed no significant oxidation in either environment [3]. But the recent findings of Costa et al. and Oral et al. [4, 5] suggested that α-T quench free radicals very well in oxygen free environment then open air. Also, high concentrations (0.3% and above) of α-T at low radiation doses caused the cross linking to be suppressed by α-T.

[1] The article is published in the original.

Questions? Contact FDA/CDRH/OCE/DID at CDRH-FOISTATUS@fda.hhs.gov or 301-796-8118

Records processed under FOIA Request #2014-8015; Released by CDRH on 12-8-2015

Most of the studies used concentrations of α-T less than 1.0% to limit the plasticization of UHMWPE [6, 7].

In this study we have investigated the effect of 30, 65 and 100-kGy on the PE residual radicals at low vitamin E concentration (0.1% by wt). The growths of residual radicals were monitored as a function of radiation dose and time after opening the samples from cold environment. Dependence of these radicals growths on three phase morphology was also investigated during the study.

MATERIALS AND METHODS

Material, Irradiation and Storage

UHWMPE samples used in this study were the GUR 1020 (provided by Ticona) polymer powder and 0.1% containing α-T UHMWPE powder. These samples were irradiated with gamma rays using ^{60}Co source for total doses ranging from 30-kGy to 100-kGy. The irradiation was done in open air and nitrogen environment at room temperature in 2009. After irradiation, samples were stored at −78.5°C (dry ice temperature) for one year in their respective environments to minimize the radical reaction. Also, the diffusion of vitamin E (α-T) inside polymer matrix for radical quenching during storage time is another reason for this storage. Irradiation services were provided by Food Technology Service, Inc. (Mulberry, Florida, USA).

ESR Measurements

For free radical measurements, a highly sensitive ESR spectrometer (Bruker) was used. The spectrometer was fitted with a high-sensitive, mixed mode cavity and operates at 9.8 GHz microwave frequency (X-band) and 100 kHz modulation and detection frequencies. The modulation amplitude was kept between 1–5 Gauss (G), while the microwave power was varied from 0.005 to 40 mW. After the initial measurements all samples were stored in open air approximately for eight weeks at room temperature to monitor the residual radicals growth. All measurements were performed at room temperature.

The samples in powder form were taken out from the cold (dry ice) environment and brought to the room temperature. The powder fills approximately 10.0 mm of ESR sample tube with internal diameter of 3.8 mm and weight 4.33 mg. The weight of the powder samples was approximately 65–68 mg.

X-ray Diffraction (XRD) Measurements

The XRD measurements of powder samples were done on a Bruker D8 Advanced X-ray diffractometer with CuK_α radiation ($\lambda = 0.15406$ nm). The data were collected in 2θ range from 5°–60° in steps of the 0.04° with a rate of 4 s per point. The de-convolution of XRD pattern was used to estimate the percent crystallinity of the sample following the approach used by Joo et al. [8].

Differential Scanning Calorimetric (DSC) Measurements

Differential scanning calorimetry of these powder samples were carried out using a 910 differential scanning calorimeter by DU Pont Instruments. The samples were weighed (approximately 5.0 mg) with a highly sensitive microgram scale (GA 110, OHAUS) and placed in aluminum pan. The measurements were performed at a heating rate of 10°C/min from room temperature to 200°C under continues nitrogen purge. Heat flow as a function of time and temperature was recorded. The percent crystallinity was calculated by integrating the enthalpy peak and normalizing it with 100% crystalline polyethylene value, 291 J/g [6].

Raman Spectroscopic Measurements

An EZRamman-M Raman analyzer by Enware Optronics incorporation was used to collect the Raman spectra from 250 to 2350 cm^{-1}. The samples were prepared in the form of pallet for the measurements. The percentage fraction of crystalline, amorphous region was calculated from the Intensity bands at 1416 and 1080 cm^{-1}. The sum of the intensities of 1295 and 1303 cm^{-1} was used as internal standard. Having calculated the crystalline and amorphous contents, the value of interfacial or inter-phase region was obtained as the balance [9, 10]. The value of percentage crystallinity for GUR 1020 sample was found to be 56.98% using Raman method which is in good agreement with the value (55.90%) found for this particular sample using DSC method explains above.

RESULTS AND DISCUSSIONS

Figures 1a and 1b show ESR spectra of α-T polymer powder irradiated in open air and nitrogen sealed packages respectively to 65-kGy radiation dose and allowed for ageing at −78.5°C (dry ice temperature) for approximately one year. The measurements were performed at room temperature immediately after opening. The sample irradiated in air and stored in air shows the single line signal at 1 mW microwave power and 2 Gs modulation amplitude because of significant amount of oxygen induced residual radicals R1 and R2 (R1 is a carbon centered polyenyl ($-{}^{\bullet}CH{+}CH{=}CH{+}_m$, $m \geq 3$) with $\Delta H_{pp} = 5.5$ Gs and $g = 2.0044$ and R2 is an oxygen-centered di- or trienyl radical ($-{}^{\bullet}OCH{+}CH{=}CH{+}_m$, $m \leq 3$) with $a_H = 4.8$ G and $g = 2.0056$) [11] as evident in Fig. 1 by ESR power saturation technique. The samples irradiated in nitrogen sealed packages showed the primary/secondary type radicals along with vitamin E radi-

Questions? Contact FDA/CDRH/OCE/DID at CDRH-FOISTATUS@fda.hhs.gov or 301-796-8118

Records processed under FOIA Request #2014-8015; Released by CDRH on 12-8-2015

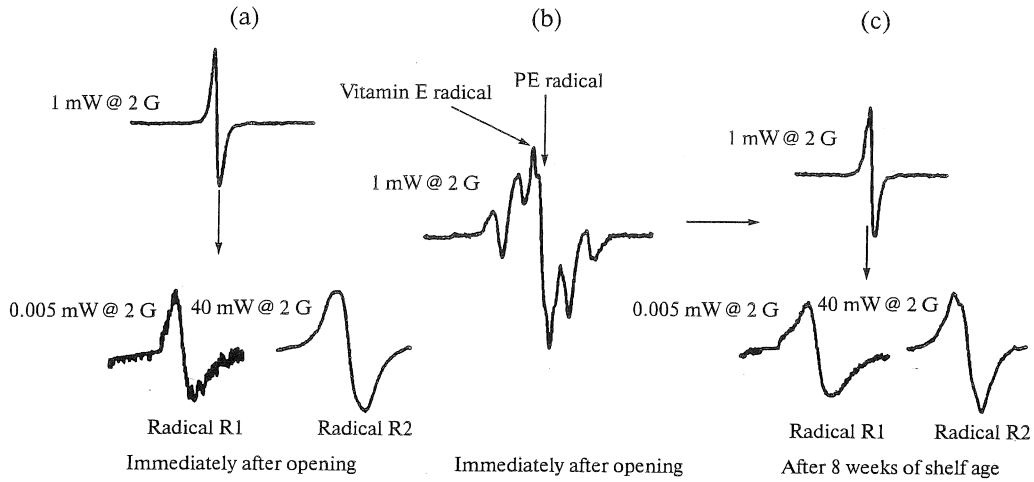

Fig. 1. ESR spectrum of 65-kGy vitamin E blended (a) open air irradiated sample, (b), and (c) nitrogen irradiated samples.

cals signal. There is no indication of radicals R1 and R2 on testing the samples immediately after opening which was confirmed by power saturation behavior of both radicals (not shown in the Fig. 1). This mixed ESR signal reduces to single line in around eight weeks of shelf ageing as shown in the Fig. 1c.

The quenching of free radicals in PE is because of α-T reaction with macro peroxyl [3] or macro-alkyl radicals (due to their high mobility) [4] but the less mobility of macro peroxyl in the main polymer chain cause the former reaction to reduce the efficacy of α-T as free radical quencher at lower concentration. At higher α-T concentrations aforementioned reactions work in parallel because of denser distribution of α-T molecules inside the blend while irradiated in open air. But for the case of nitrogen environment irradiated samples, the possible factors of the presence of PE primary/secondary radicals and their decay to oxygen induced residual radicals are: (1) the less mobility of the macro-allyle (formed via radical migration) in the main polymer chain [4] (2) possibility of minimum or no α-T molecules left behind after irradiation (3) the mobility of α-T which is restricted to amorphous region due to its low diffusion coefficient [3] and (4) the less reactivity of alkoxy type radicals (radicals like R2) to vitamin E [12].

Figure 2 shows the residual radicals R1 and R2 concentration per unit mass after eight weeks of shelf ageing. The radical's concentration was calculated using the peak to peak height of first derivative ESR absorption signal, because we have isolated the radicals with power saturation technique and this height is proportional to the concentration. It is clear from the Fig. 2 that R1 and R2 concentration is significantly less in vitamin E blended N_2 irradiated sample as compared to control (GUR 1020 polymer powder irradiated to 65-kGy dose in air) and vitamin E blended open air irradiated sample as opposite to our previously reported work [3]. The reason may include that in inert environment the macro alkyl radical's reacts with α-T or form cross-links, and only the radicals which are formed and trapped inside the crystalline regions are left behind. But for open air irradiated samples the competitive reaction for macro alkyl radicals increases due to the presence of oxygen which results in larger amount of oxygen induced residual radicals as cleared from ESR results.

A comparative study was also performed on α-T blended samples irradiated in open air with 30-kGy, 65-kGy and 100-kGy samples respectively because of the importance of these values as sterilizing and cross-linking issues of UHMWPE. Figures 3a and 3b show the radicals R1 and R2 concentration per unit mass as a function of radiation dose. The radical's growth as a function of ageing time was also monitored up to eight

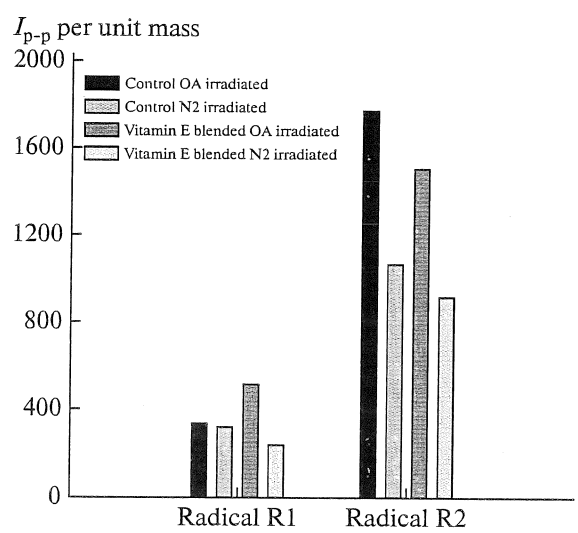

Fig. 2. Residual radical concentration after eight weeks of shelf ageing.

Questions? Contact FDA/CDRH/OCE/DID at CDRH-FOISTATUS@fda.hhs.gov or 301-796-8118

Records processed under FOIA Request #2014-8015; Released by CDRH on 12-8-2015

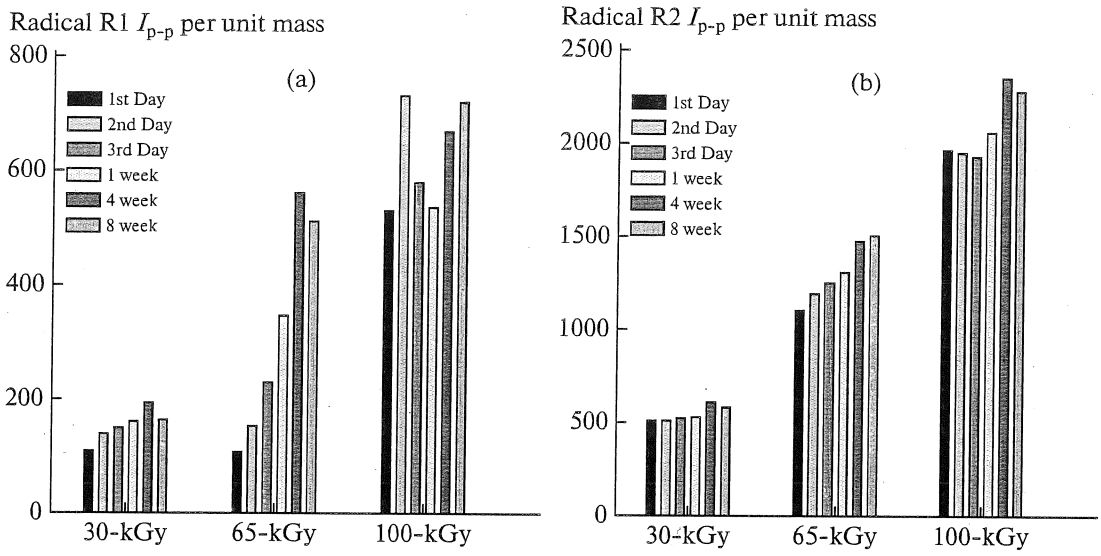

Fig. 3. Residual radical concentration as a function of time and radiation dose: (a) radical R1, (b) radical R2.

weeks. The concentration of both radicals rise for 30-kGy and 65-kGy samples while the sample with 100-kGy the concentration of R1 first decrease then starts rising. The radical's growth can be explained as; there may be some primary/secondary type radicals still there which were produced inside the crystal core as suggested by Fujimura et al. [13] when samples stored in cold environment but not in the detectable range of ESR. These radicals start migrating towards the crystalline/inter-phase boundary at room temperature and react with diffused oxygen. The slight decrease initially and then increase in the 100-kGy is because at higher doses the possibility of formation of crystals with smaller size [9] and increased concentration of radicals results in cross-linking of radicals inside the crystalline regions during their migration process towards crystalline/inter-phase boundary.

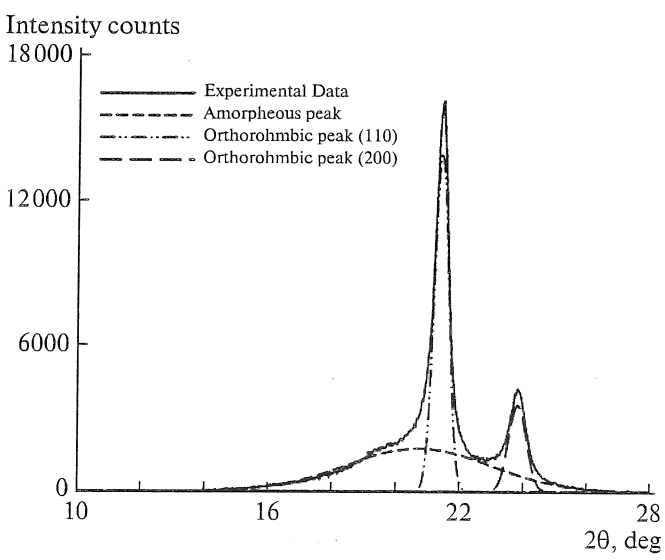

Fig. 4. XRD pattern with de-convoluted peaks of 30-kGy irradiated sample.

There is a general trend of increase in radical R1 and R2 concentration and decrease in the relative radical ratio (R2/R1) as a function of ageing time. The growth of radical R1 (polyenyle type radical trapped inside the crystalline region) as well as decrease in ratio for 65-kGy irradiated sample occurs at higher rate than 30-kGy and 100-kGy (except for initial decrease in concentration for 100-kGy) irradiated samples. There may be two reasons for this; (1) It is possible that the further oxidation of radical R2 occurs at higher rate in 65-kGy samples than 30-kGy and 100-kGy samples and (2) It is also possible that radiation induced changes in polymer may affect the three phase morphological structure depending on the absorbed dose which results in different growth rate for 65-kGy. The more dominant rate of change in radical R1 than radical R2 and slower rate of formation of oxidation products in vitamin E containing samples as suggested by Costa et al. [4] seem to support the later argument here.

A further investigation using XRD (Fig. 4) and Raman spectroscopy was also conducted to address aforementioned later issue. Raman and nuclear magnetic resonance (NMR) are more suitable than XRD for UHMWPE morphological investigation because both techniques can give an estimate about the third phase i.e. inter-phase region [8, 14]. An XRD pattern for 30-kGy irradiated sample with the de-convoluted amorphous and orthorhombic crystalline peaks is shown in Fig. 4. Figure 5a and 5b show the typical Raman spectrums of un-irradiated and 100-kGy vitamin E blended UHMWPE samples respectively. Table 1

Questions? Contact FDA/CDRH/OCE/DID at CDRH-FOISTATUS@fda.hhs.gov or 301-796-8118

Records processed under FOIA Request #2014-8015; Released by CDRH on 12-8-2015

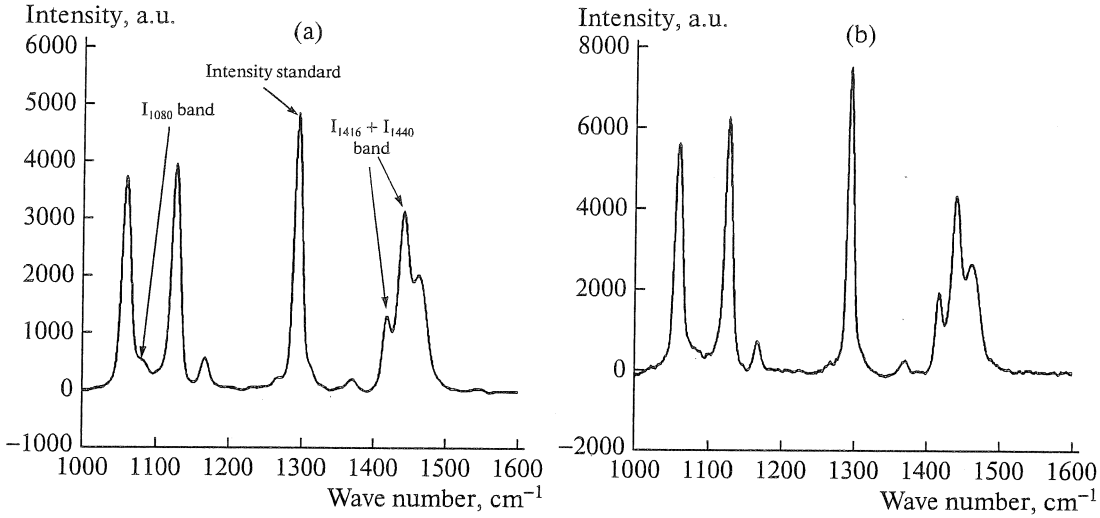

Fig. 5. Typical Raman spectrum (a) un-irradiated UHMWPE, (b) 100-kGy irradiated UHMWPE.

shows the obtained fractions of crystalline, amorphous and inter-phase regions for 30-kGy, 65-kGy and 100-kGy samples respectively. The crystallinity values obtain independently from the DSC and XRD method, are in good agreement with Raman data for nearly all samples studied (Fig. 6). Also increase in the crystallinity values as a function of radiation dose and higher contents of inter-phase regions obtained in this study with Raman method are in accordance with the literature. The relative radical ratio (R2/R1) for these samples at 1st day of opening and after 8 weeks of shelf ageing at room temperature along with the level of structural disorder obtained from Raman data following the approach used by Wang et al. [10] is given in Table 2.

The percentage of inter-phase regions for 65-kGy has the minimum value, while the amorphous region for this particular sample (65-kGy irradiated) has the maximum value as compared to 30-kGy and 100-kGy samples. The reason of this behavior is beyond the scope of this particular paper and still is under investigation. But the general decrease in inter-phase region percentage and increase in percent crystallinity on irradiation (Table 1) is because of lamellae's surface clean up as a result of chain scission close to the inter-phase regions [9]. The growth rate of residual radicals has a linear relation with the percentage of amorphous region [15] (Fig. 7). This rate is mainly dependant on the rate of change of radical R1. Polyethylene free radical decay at initial stage via oxidative reaction due to the diffused oxygen can be used to explain this. As the

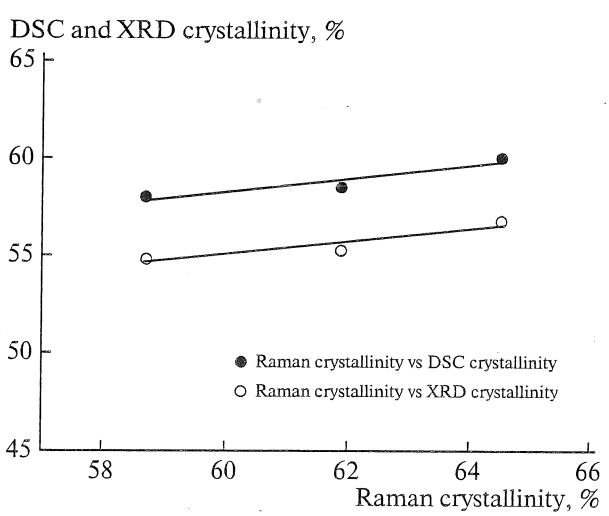

Fig. 6. Relationship between the crystallinity measured by different methods.

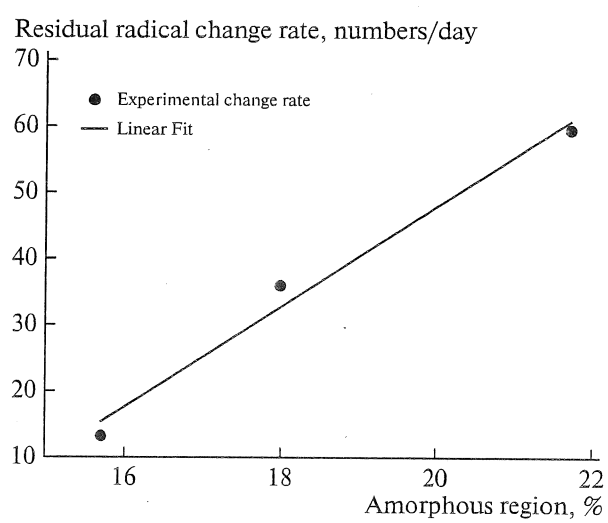

Fig. 7. Residual radical growth rate as a function of % amorphous region obtain from Raman analysis.

Questions? Contact FDA/CDRH/OCE/DID at CDRH-FOISTATUS@fda.hhs.gov or 301-796-8118

Records processed under FOIA Request #2014-8015; Released by CDRH on 12-8-2015

Table 1. UHMWPE three phase fractions obtain from Raman analysis

Sample	% Crystalline	% Amorphous	% Interfacial
30-kGy	58.70	15.70	25.60
65-kGy	61.88	21.68	16.44
100-kGy	64.51	17.98	17.51

Table 2. Relative radical ratio (R2/R1) along with the level of structural disorder

Sample	Relative ratio, at 1st day	Relative ratio, at 8th week	Level of structural disorder
30-kGy	4.56	3.52	0.44
65-kGy	10.13	2.93	0.26
100-kGy	3.73	3.16	0.27

diffusion of oxygen inside the polymer matrix occurs through amorphous region and higher percentage of amorphous phase in 65-kGy irradiated samples than 30-kGy and 100-kGy samples result in higher value of growth rate. However, the relative radical ratio (R2/R1) after eight weeks of ageing found to be dependent on the percentage of inter-phase and the level of structural disorder (Table 2), i.e. higher the structural disorder larger the value of radical R2 and vice versa.

CONCLUSIONS

In this study, both the oxygen-centered polyenyl (R2) and the carbon-centered polyenyl (R1) residual radicals were detected in UHMWPE following post-gamma ageing of 0.1% vitamin E containing UHMWPE. Apparently, vitamin E did not fully quench the primary radicals; the unquenched ones transformed to residual radicals. It has to be emphasized that the final numbers (concentration) of the residual radicals include the initial polyenyl radicals (generated at the time of irradiation) which remained trapped in the crystalline as well as inter-phase regions. The rate of change of the residual radicals, as well as the relative ratio (R2/R1) as a function of time, during the eight-weeks measurement period was significant in the 65-kGy-irradiated powder compared to that in the 30-kGy or 100-kGy powder. Comparing with the Raman spectroscopic data of these irradiated UHMWPE (30-, 65-, and 100-kGy) samples one could suggest that the polyenyl residual radical growth would be high when the percent amorphous region was high, and that the ratio (R2/R1) would also be of higher value for the samples which have larger contents of inter-phase regions and structural disorder.

It is suggested that the results provided here would be useful while considering the long term oxidation degradation problem of UHMWPE because of the trapped radicals inside the crystalline region.

ACKNOWLEDGMENTS

The author M.S. Mehmood would like to acknowledge Higher Education Commission (HEC), Pakistan for the financial support under the international university linkage and indigenous PhD fellowship programs. Work was also supported in parts by the NSF Industry/University Cooperative Center for Biosurfaces (IUCB) at the University of Memphis. The authors also acknowledge the Ticona for providing the UHMWPE samples for this research.

REFERENCES

1. E. Sinevich, V. Aulov, and N. Bakeev, Polymer Science, Ser. A **50**, 893 (2008).
2. E. Oral and O. K. Muratoglu, Nucl. Instr. Methods Phys. Res., Sect. B **265**, 18 (2007).
3. M. D. Ridley and M. S. Jahan, J. Biomed. Mater. Res., Part A **88**, 1097 (2009).
4. L. Costa, I. Carpentieri, and P. Bracco, Polym. Degrad. Stab. **94**, 1542 (2009).
5. E. Oral, C. Godleski Beckos, A. S. Malhi, and O. K. Muratoglu, Biomaterials **29**, 3557 (2008).
6. E. Oral, A. S. Greenbaum, A. S. Malhi, W. H. Harris, and O. K. Muratoglu, Biomaterials **26**, 6657 (2005).
7. E. Oral, S. L. Rowell, and O. K. Muratoglu, Biomaterials **27**, 5580 (2006).
8. Y. L. Joo, O. H. Han, H. K. Lee, and J. K. Song, Polymer **41**, 1355 (2000).
9. D. Barron and C. Birkinshaw, Polymer **49**, 3111 (2008).
10. L. H. Wang, R. S. Porter, H. D. Stidham, and S. L. Hsu, Macromolecules **24**, 5535 (1991).
11. J. M. Shah and M. Fuzail, Nucl. Instr. Methods Phys. Res., Sect. B **265**, 67 (2007).
12. E. Oral, K. K. Wannomae, S. L. Rowell, and O. K. Muratoglu, Biomaterials **28**, 5225 (2007).
13. T. Fujimura, N. Hayakawa, and I. Kuriyama, Polymer **19**, 103 (1978).
14. L. Myasnikova, E. Egorov, V. Zhizhenkov, N. Kvachadze, Y. Boiko, E. Ivan'kova, V. Marikhin, A. Valendo, E. Voronova, and G. Michler, Polymer Science, Ser. A **50**, 640 (2008).
15. M. S. Jahan and B. M. Walters, Radiat. Phys. Chem. **80**, 281 (2011).

Questions? Contact FDA/CDRH/OCE/DID at CDRH-FOISTATUS@fda.hhs.gov or 301-796-8118

Records processed under FOIA Request #2014-8015; Released by CDRH on 12-8-2015
The Journal of Arthroplasty Vol. 27 No. 1 2012

Knee Simulator Wear of Vitamin E Stabilized Irradiated Ultrahigh Molecular Weight Polyethylene

Brad R. Micheli, BS,* Keith K. Wannomae, BS,* Andrew J. Lozynsky, BS,* Steven D. Christensen, BA,* and Orhun K. Muratoglu, PhD*†

Abstract: Wear and damage of ultrahigh molecular weight polyethylene (UHMWPE) tibial inserts used in total knee arthroplasty are accelerated by oxidation. Radiation crosslinking reduces wear but produces residual free radicals adversely affecting stability. One alternative to stabilize radiation-crosslinked UHMWPE is to infuse the material with vitamin E (vit E). We investigated the properties of 100-kGy e-beam–irradiated UHMWPE that was subsequently doped with vitamin E in comparison with conventional UHMWPE. Both polymers were sterilized with gamma irradiation in vacuum packaging. Vitamin E–doped UHMWPE showed lower wear before and after aging (2.4 ± 0.5 and 2.5 ± 0.8 mg/million cycle, respectively, vs 26.9 ± 3.5 and 40.8 ± 3.0 mg/million cycle for conventional UHMWPE). Conventional UHMWPE showed oxidation after accelerated aging, and its mechanical properties were adversely affected, whereas vit E–doped UHMWPE showed no oxidation or changes in its mechanical properties. Vitamin E stabilization of radiation-crosslinked UHMWPE resulted in low wear and high oxidation resistance; it is an alternative load-bearing material for total knee applications. **Keywords:** polyethylene, wear, fatigue, oxidation, vitamin E, knee arthroplasty.
© 2012 Elsevier Inc. All rights reserved.

Contemporary total knee arthroplasty uses metallic and polymeric materials to reconstruct the knee joint, where the tibial insert and the patellar component are made of ultrahigh molecular weight polyethylene (UHMWPE). The UHMWPE components articulate against cobalt-chrome counterfaces, and it is at these articulations where most damage modes are initiated. The damage is mainly in the form of adhesive/abrasive wear and delamination. When the damage is extensive, the performance of the joint deteriorates and eventually leads to revision surgery [1].

Wear typically occurs in the form of adhesive and abrasive wear on both the articular and backside surfaces of the components. These wear mechanisms are a major source of particulate debris that contributes to periprosthetic osteolysis, which is a growing problem in total knees [2]. Osteolysis can lead to and often complicates revision surgery. Delamination occurs on the articular surfaces of UHMWPE components and can lead to adverse circumstances such as fracture of the components or mechanical instability of the reconstructed joint. The extent of delamination increases with the extent of oxidation in these components. Oxidation is primarily induced by the terminal gamma sterilization process, which generates residual free radicals in the material. In the long term, oxygen reacts with these free radicals, and through a reaction, cascade leads to the embrittlement of the material [3-5]. With the reduced mechanical properties, delamination type failure becomes more common. Therefore, an improved UHMWPE material for total knee arthroplasty should have increased wear resistance to reduce the rate of osteolysis and increased oxidation resistance to reduce the extent of delamination.

Crosslinking by ionizing irradiation has been shown to increase the wear resistance of UHMWPE. Irradiation also generates residual free radicals, which are the precursors of long-term oxidative embrittlement [6-9]. Postirradiation melting can be used to eliminate these residual free radicals and achieve oxidative stability [10].

*From the *Harris Orthopaedic Laboratory, Massachusetts General Hospital, Boston, Massachusetts; and †Harvard Medical School, Boston, Massachusetts.*
Submitted May 25, 2010; accepted March 3, 2011.
This study was funded by a research grant from Biomet, Inc.
The Conflict of Interest statement associated with this article can be found at doi:10.1016/j.arth.2011.03.006.
Reprint requests: Orhun K. Muratoglu, PhD, Harris Orthopaedic Laboratory, Massachusetts General Hospital, 55 Fruit Street, GRJ-1206, Boston, MA 02114.
© 2012 Elsevier Inc. All rights reserved.
0883-5403/2701-0016$36.00/0
doi:10.1016/j.arth.2011.03.006

Questions? Contact FDA/CDRH/OCE/DID at CDRH-FOISTATUS@fda.hhs.gov or 301-796-8118

Records processed under FOIA Request #2014-8015; Released by CDRH on 12-8-2015

Radiation crosslinking and melting of polyethylene reduced the adhesive and abrasive wear in acetabular components in hip simulator investigations [11,12], as well as on the articular and backside surfaces of tibial inserts in knee simulator investigations [13,14].

An alternative method to postirradiation melting is to stabilize the irradiated UHMWPE by vitamin E infusion (vit E–doped UHMWPE) [15-17]. Vitamin E is a potent antioxidant and can stabilize the residual free radicals in UHMWPE. It has been shown that doping with vitamin E is an effective method of improving the oxidative stability of irradiated UHMWPE [15]. One advantage of vitamin E stabilization is that, because the irradiated polyethylene is not melted, its crystallinity is not reduced, and as a result, the mechanical properties and fatigue strength of the irradiated UHMWPE are preserved [15,18].

Considering that oxidation-induced delamination of conventional UHMWPE tibial inserts can compromise long-term performance of total knees, we propose the use of vit E–doped UHMWPE as an alternative bearing surface for total knee reconstruction because of its markedly improved oxidation resistance. The potential benefit of vit E–doped UHMWPE is not only the reduction in oxidation-induced delamination but also reduction in adhesive wear. The objective of this study was to investigate the wear behavior, mechanical properties, fatigue resistance, oxidation resistance, and oxidation potential of vit E–doped UHMWPE in comparison with conventional UHMWPE.

Materials and Methods

Conventional and Highly Crosslinked Sample Preparation

All specimens were manufactured from direct compression-molded UHMWPE stock. The UHMWPE resin used was the GUR1050 (Ticona, Bishop, Tex). Three specimens from each of the following groups were tested.

The conventional samples were prepared as follows: cruciate retaining tibial inserts (Vanguard CR Design, size 10 × 87/91 mm; Biomet Inc, Warsaw, Ind) for knee simulator wear testing were direct compression molded. Samples for other tests were machined from direct compression-molded stock material prepared using the same molding process. All specimens were vacuum packaged and gamma sterilized to approximately 25 to 40 kGy.

The vit E–doped UHMWPE samples were prepared as follows: cruciate retaining tibial inserts (Vanguard CR Design, size 10 × 87/91 mm; Biomet Inc) for knee simulator wear testing were direct compression molded (Biomet, Inc). Samples for other tests were machined from direct compression-molded stock material prepared using the same molding process. Specimens were placed in silicone molds, vacuum packaged, and electron beam irradiated to 100 kGy (BeamOne LLC, formerly TitanScan, Lima, Ohio). The irradiated specimens were then doped by soaking the components in pure vitamin E (α-tocopherol) at 120°C and subsequently homogenized in argon gas at 120°C to ensure full vitamin E penetration. Fourier transform infrared spectroscopy (FTIR; Varian FTS2000, Natick, Mass) was performed on a spare piece to verify the full vitamin E penetration through the components. α-Tocopherol index values were calculated by normalizing the absorbance at 1245 to 1275 cm^{-1} to the internal reference absorbance at 1850 to 1985 cm^{-1} after subtracting the corresponding baselines. The specimens were then vacuum packaged and gamma sterilized to 30 to 35 kGy.

Wear Assessment Via Simulated Gait

The wear study was performed at a rate of 1 Hz on an AMTI 6-Station Displacement Controlled Knee Simulator (Advanced Mechanical Technology, Inc., Watertown, Mass). A total of 5 specimens per group were tested: 3 motion tibial bearings were subjected to both load and motion, and 2 load-soak tibial bearings were subjected only to load. The kinematics used was the standard International Standards Organization (ISO) 14243-3 walking gait with a peak load of approximately 3000 N. The lubricant used was 100% bovine serum, with a protein content of 6.6 g/dL, stabilized with 10.7 mmol of ethylenediamine tetraacetate (Fisher Scientific, Pittsburgh, Pa) and 33 mL of penicillin-streptomycin solution (Sigma-Aldrich, St Louis, MO) per 500 mL of serum. All stations were maintained at 37°C. The simulator was interrupted at approximately 1-million cycle intervals for gravimetric assessment of wear. The tibial inserts were cleaned as directed in ISO 14243-2 before weighing. The tibial inserts were weighed 3 times and then averaged using an A-250 balance (Denver Instrument Co, Arvada, CO). The articular and backside surfaces were photographed using an Olympus SZX12 optical microscope and an Olympus DP11 camera (Olympus America, Inc., Center Valley, Pa) at every gravimetric measurement.

The weight loss of each liner was used to calculate a wear rate after correction for fluid absorption. The correction for fluid absorption was done by subtracting the average weight gain of load-soak components from the weight change of the test components. A linear wear rate was calculated by linear regression, excluding the data point at time zero.

The initial (unaged) test was carried out to a total of 5 million cycles of simulated gait. After 5 million cycles of testing, all components were aged for 2 weeks under 5 atm of pure O_2 in a pressure vessel placed in a convection oven at 70°C in accordance with American Society for Testing and Materials (ASTM) F2003. The aged samples were then tested for an additional 2.5

Questions? Contact FDA/CDRH/OCE/DID at CDRH-FOISTATUS@fda.hhs.gov or 301-796-8118

Records processed under FOIA Request #2014-8015; Released by CDRH on 12-8-2015

million cycles using the same protocol as was used in the unaged portion of the test.

At the conclusion of all simulated gait testing, both the unaged and aged segments, the wear scar on the lateral condyle from a representative conventional UHMWPE tibial bearing, and a representative vit E–doped UHMWPE tibial bearing were gold coated and examined with scanning electron microscopy (SEM). Images were collected with a 30-kV beam strength at magnifications between ×1200 and ×25 000.

Tensile Mechanical Properties

Tensile specimens (ASTM D638, type V, n = 6 per group) were tested on an MTS hydraulic testing machine (Eden Prairie, Minn) at a cross-head speed of 10 mm/min. The axial displacement and force were sampled at a rate of 100 Hz. The test was also recorded on videotape to visually determine elongation at break (EAB). For this purpose, a gage length of approximately 6.5 to 7 mm was marked on the specimens. The thickness of the specimens and the width of the specimens in the gage region were measured using calipers before deformation. The separation of the gage marks just before failure was measured from the recorded videos, and the EAB was computed as the ratio of the change in gage length at fracture and the initial gage length. The yield strength (YS) in megapascal and the ultimate tensile strength (UTS) in megapascal were calculated per ASTM D638. Testing was done on the samples before and after ASTM F2003–accelerated aging. Differences between groups were determined with a Student *t* test, with a significance level of $P = .05$.

Fatigue Crack Propagation Resistance

Fatigue crack propagation testing was performed on a MiniBionix 858 (MTS) following ASTM E647. Compact tension (C(T)) specimens (n = 5 per group) were precracked at the notch using a razor blade. Testing was conducted at a sinusoidal load cycle frequency of 5 Hz and a stress ratio of 0.1 in tension. Crack length was monitored optically every 20 000 cycles. The average of the crack length on both sides of the C(T) specimen was used as the representative crack length for the computation of crack growth rates. Stress intensity factor ranges at crack inception (ΔK_{incep}) were reported at a threshold crack growth rate of 10^{-6} mm/cycle. All testing was done in an aqueous bath at 40°C [19] to simulate the physiologic temperature of the joint. Testing was done on the samples before and after ASTM F2003 aging. Differences between groups were determined with a Student *t* test, with a significance level of $P = .05$.

Thermal Properties

Differential scanning calorimetry (TA Instruments Q1000, New Castle, Del) was used to determine the thermal properties of the test samples. The specimens (n = 3 per group) were initially cooled to −20°C and held at that temperature for 2 minutes. They were then heated to 180°C, cooled back to −20°C, and reheated to 180°C. Both the heating and cooling segments of this procedure were done at a rate of 10°C/min. All analyses were based on the thermogram of the first and second heating segments from −20°C to 180°C. The peak melting point and the tangential onset melting point were recorded. Crystallinity was quantified by integrating the thermogram from 20°C to 160°C, and crystallinity was calculated assuming a melting enthalpy of 291 J/g for 100% crystalline UHMWPE. Testing was done on the samples before and after ASTM F2003 accelerated aging. Differences between groups were determined with a Student *t* test, with a significance level of $P = .05$.

Oxidation Potential and Oxidation Resistance

The oxidation potentials of vit E–doped UHMWPE and conventional UHMWPE were determined using a method described by Costa et al [20]. Thin films (n = 3 per group) were microtomed and hung on a "clothesline" suspended inside a 3-neck round bottom flask. The 3-neck flask was purged with nitrogen gas for at least 30 minutes to remove any residual atmospheric gases and was then filled and purged with 100% nitric oxide gas. The samples were exposed to nitric oxide for 16 hours at room temperature. The thin sections were removed from the flask and immediately analyzed using FTIR spectroscopy. The nitrate level was obtained by taking the height of the nitrate absorbance at 1630 cm^{-1} and normalizing to the height of internal reference absorbance at 1895 cm^{-1}, after subtracting the corresponding baselines. As a control comparison, we also included a 100-kGy e-beam–irradiated UHMWPE in the oxidation potential experiments.

The oxidation resistances of the materials were determined using 2 different aging methodologies. Pressure vessel–aged samples were aged for 2 weeks under 5 atm of pure O_2 in a pressure vessel placed in a convection oven at 70°C in accordance with ASTM F2003. Oven-aged samples were aged by placing the samples directly into a mechanical convection oven (Imperial V; Lab-Line Barnstead International, Dubuque, Iowa) set at 80°C for 5 weeks. All aged samples were analyzed by FTIR according to ASTM F2102 within 2 weeks of aging. Oxidation index values were calculated by normalizing the carbonyl absorbance at 1680 to 1780 cm^{-1} to the internal reference absorbance at 1370 to 1390 cm^{-1}, after subtracting the corresponding baselines. The surface oxidation index was calculated as the average of the oxidation indices over the first 3 mm of the sample, whereas the bulk oxidation index was calculated as the average of the oxidation indices of the central 500 μm of the sample.

Questions? Contact FDA/CDRH/OCE/DID at CDRH-FOISTATUS@fda.hhs.gov or 301-796-8118

Records processed under FOIA Request #2014-8015; Released by CDRH on 12-8-2015

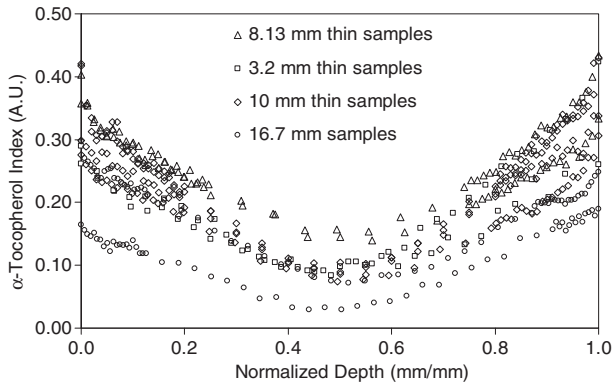

Fig. 1. Vitamin E concentration profiles of the vit E–doped UHMWPE samples used in various tests. Because different tests required samples of different thicknesses, the concentration profiles are shown, with the actual depth of FTIR scan normalized to the total thickness of each sample.

Results

Fourier transform infrared spectroscopy analysis of the vit E–doped UHMWPE samples showed vitamin E penetration through the entire thickness of the test samples used, namely, the tibial bearings, C(T) samples for fatigue propagation resistance, dog-bone specimens for tensile mechanical properties, and differential scanning calorimetry specimens for thermal properties (Fig. 1). Vitamin E was detectable throughout the entire thickness of all test samples with a higher concentration near free surfaces.

The wear rate of vit E–doped UHMWPE inserts was significantly lower than that measured with conventional tibial inserts during the first 5 million cycles of testing (Fig. 2). During testing, 1 conventional station experienced a simulator fixture failure such that the load and kinematics no longer adhered to the ISO standard; the results from that station were subsequently discarded, and thus, only 2 conventional components are reported. The wear rate of the unaged conventional UHMWPE tibial bearings after correction for fluid absorption was 26.9 ± 3.5 mg/million cycle; this rate rose to 40.8 ± 3.0 mg/million cycle after accelerated aging that followed 5 million cycles of simulated gait. The vit E–doped UHMWPE tibial bearings exhibited wear rates of 2.4 ± 0.5 and 2.5 ± 0.8 mg/million cycles before and after aging, respectively. The wear rates measured with vit E–doped UHMWPE inserts were 91% and 94% lower than those measured with conventional inserts before and after aging, respectively. The difference in the wear rate between the conventional and vit E–doped UHMWPE tibial bearings was statistically significant both before and after accelerated aging ($P < .05$).

The fluid uptake in the load-soak components, as measured gravimetrically, was similar in both the conventional UHMWPE and vit E–doped UHMWPE tibial inserts (Fig. 3). The inserts in both groups gained weight with increasing number of cycles in a linear fashion for the first 5 million cycles. The subsequent aging of the inserts after 5 million cycles of simulated normal gait did not change their fluid uptake behavior. Overall, the vit E–doped UHMWPE inserts absorbed slightly less fluid than their conventional counterparts.

Both the conventional and vit E–doped UHMWPE tibial-bearing surfaces that were subjected to both motion and load showed a damage scar in both medial and lateral condyles on the articular surfaces after 0.5 million cycles of simulated normal gait testing (Figs. 4 and 5). During the subsequent 5 million cycles of testing, the damage area on the articular surfaces increased slightly on both condyles. On the back sides of both components, there was no visible damage after

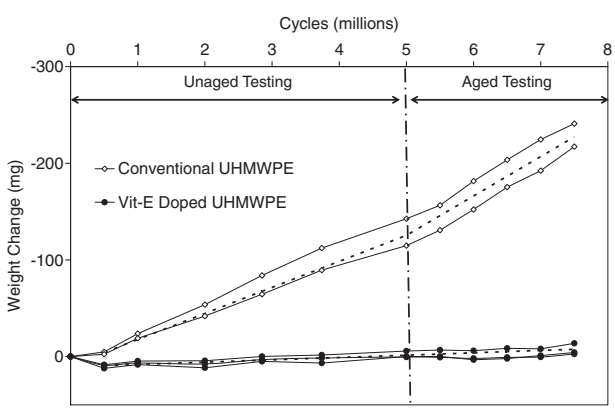

Fig. 2. Weight change of conventional UHMWPE and vit E–doped UHMWPE tibial inserts that were subjected to 5 million cycles of accelerated aging and subsequently tested for an additional 2.5 million cycles. The average linear wear rate, calculated by averaging the linear regressions (from 0.5 to 5 million cycles for unaged and from 5.5 to 7.5 million cycles for aged) of each component is shown as the dashed lines within each group of samples.

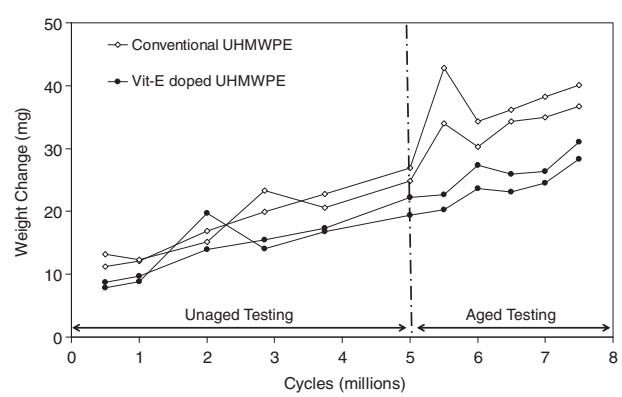

Fig. 3. Fluid uptake of the conventional and vit E–doped UHMWPE load-soak inserts tested on the knee simulator. At 5 million cycles, the test components were subjected to accelerated aging and subsequently tested for an additional 2.5 million cycles.

Questions? Contact FDA/CDRH/OCE/DID at CDRH-FOISTATUS@fda.hhs.gov or 301-796-8118

Records processed under FOIA Request #2014-8015; Released by CDRH on 12-8-2015

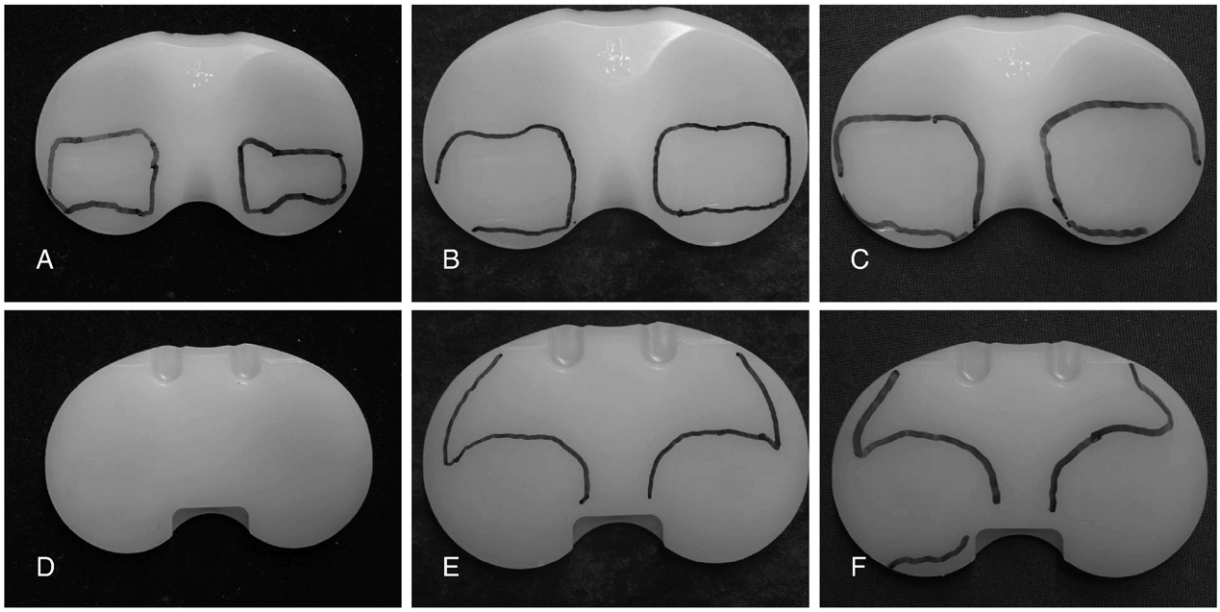

Fig. 4. A representative conventional UHMWPE tibial bearing that was subjected to load and motion on the knee simulator after 0.5 million cycles (A), after 5 million cycles (B), and after accelerated aging (C) and an additional 2.5 million cycles. The backsides of the tibial bearing at these testing intervals are also shown (D-F). The areas outlined in black are the observed damage scars.

0.5 million cycles of testing; however, after 5 million cycles of simulated normal gait, the backside surfaces showed areas of burnishing and damage of comparable size in both types of UHMWPEs. Following the final 2.5 million cycles after the accelerated aging, the size of the damage scar on the articular surfaces grew slightly, and the extent of damage on the backside remained largely unchanged.

The SEM analysis of the conventional tibial bearing showed a burnished surface with a few scratches and abrasions from third-body debris (Fig. 6A, B), typical of conventional UHMWPE. At a higher magnification, a porous nanostructure was observed on the wear scar (Fig. 6C) that was not observed in the unworn region (Fig. 6B). The vit E–doped UHMWPE tibial bearing exhibited more abrasions in the wear scar (Fig. 7A),

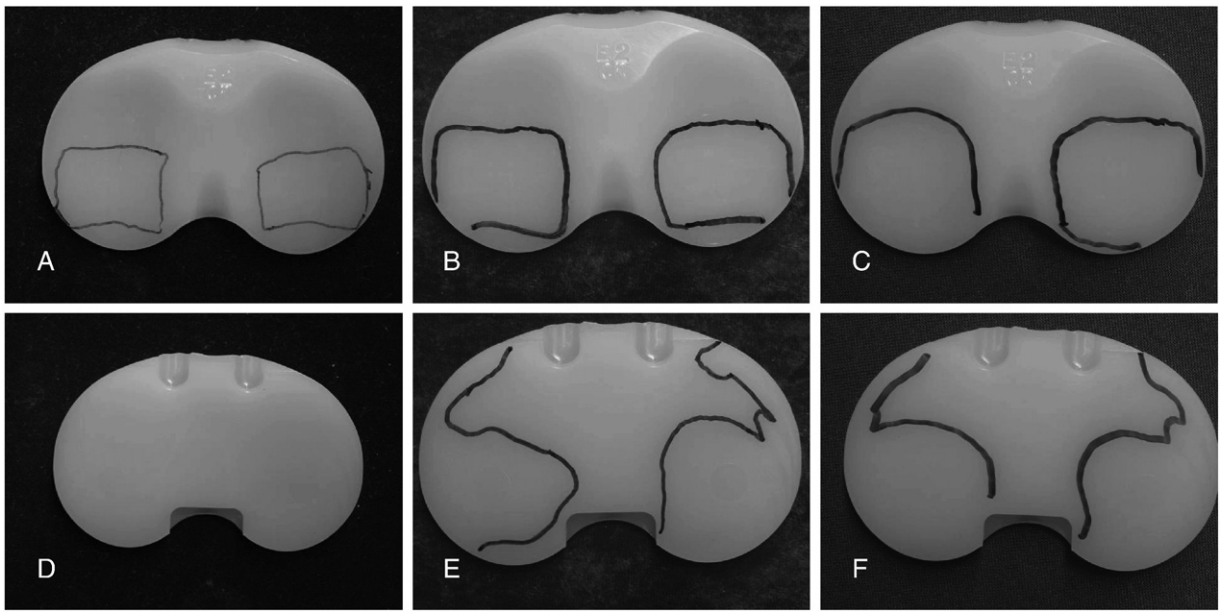

Fig. 5. A representative vit E–doped UHMWPE tibial bearing that was subjected to load and motion on the knee simulator after 0.5 million cycles (A), after 5 million cycles (B), and after accelerated aging (C) and an additional 2.5 million cycles. The backsides of the tibial bearing at these testing intervals are also shown (D-F). The areas outlined in black are the observed damage scars.

Questions? Contact FDA/CDRH/OCE/DID at CDRH-FOISTATUS@fda.hhs.gov or 301-796-8118

Records processed under FOIA Request #2014-8015; Released by CDRH on 12-8-2015

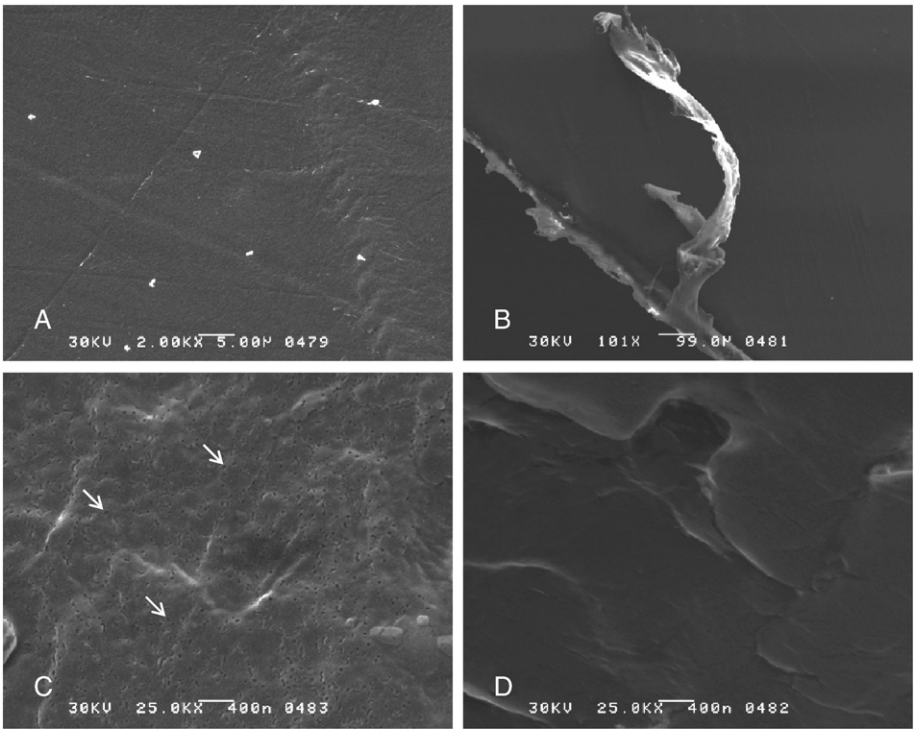

Fig. 6. SEM images of the lateral condyle of a representative conventional UHMWPE tibial bearing after 5 million cycles of knee simulator testing, accelerated aging, and an additional 2.5 million cycles of knee simulator testing. Low magnification images of the wear scar showed, some fibrillar structure formation (A), while high magnification images (B) showed a nanoporous topology in the worn region (C; see arrows) but not in the unworn region (D).

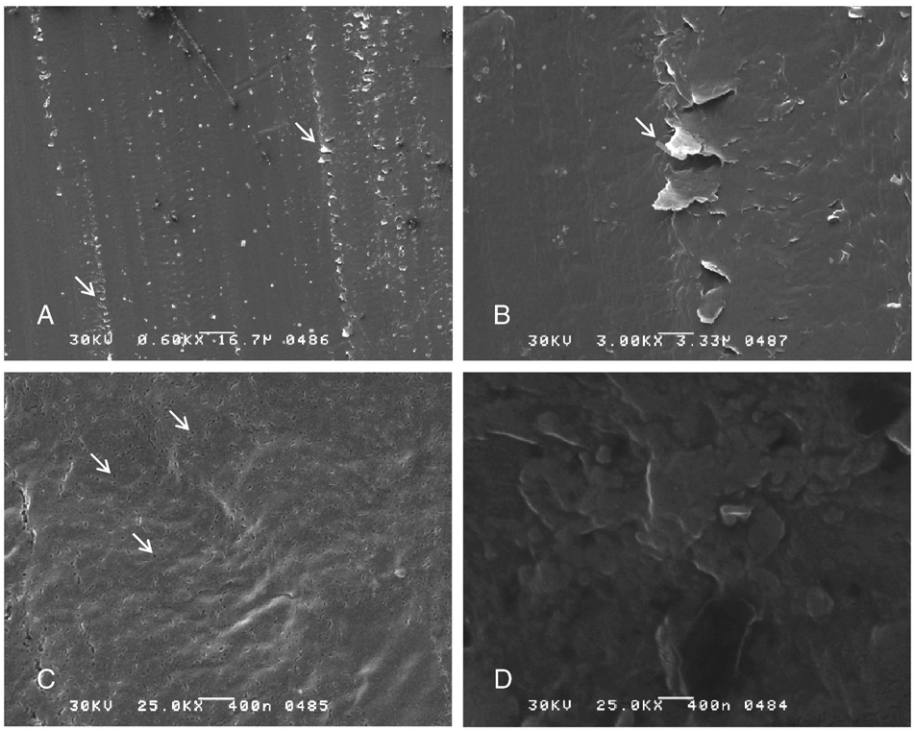

Fig. 7. SEM images of the lateral condyle of a representative vit E–doped UHMWPE tibial bearing after 5 million cycles of knee simulator testing, accelerated aging, and an additional 2.5 million cycles of knee simulator testing.

Questions? Contact FDA/CDRH/OCE/DID at CDRH-FOISTATUS@fda.hhs.gov or 301-796-8118

Records processed under FOIA Request #2014-8015; Released by CDRH on 12-8-2015

Table 1. Oxidation Potential as Measured by Average Nitrate Height After Nitric Oxide Exposure, and Surface and Bulk Oxidation Indices as Measured According to ASTM F2102 After Aging for Both Materials

	Unaged	Oven Aged		Pressure Vessel Aged	
	Oxidation Potential	Surface Oxidation Index	Bulk Oxidation Index	Surface Oxidation Index	Bulk Oxidation Index
Conventional UHMWPE	0.51 ± 0.02	0.34 ± 0.02	0.13 ± 0.00	0.48 ± 0.06	0.27 ± 0.06
Vit E–doped UHMWPE	0.40 ± 0.04	0.01 ± 0.00	0.01 ± 0.00	0.03 ± 0.01	0.01 ± 0.00

For comparison, the nitrate height average for 100-kGy irradiated UHMWPE with no thermal treatment is 0.74 ± 0.07.

which had a flaky appearance at higher magnifications (Fig. 7B). Similar to the observation in the conventional inserts, the vit E–doped UHMWPE tibial bearing had a porous nanostructure in the wear scar (Fig. 7C). The porous nanostructure was not observed in the unworn section of the articular surface (Fig. 7D).

The oxidation potential measured as the nitrate absorbance after nitric oxide reaction was lower with vit E–doped UHMWPE in comparison with the conventional UHMWPE and the 100-kGy irradiated UHMWPE (Table 1). The measured nitrate absorbance in vit E–doped UHMWPE remained unchanged as a function of distance between the articular and backside surfaces of the vit E–doped UHMWPE tibial insert. Both the surface and bulk oxidation indexes of the conventional UHMWPE were higher than vit E–doped UHMWPE after accelerated aging in either the pressure vessel or the oven (Table 1). Accelerated aging in the pressure vessel resulted in higher oxidation levels on the surface and in the bulk of the conventional UHMWPE in comparison with oven aging. The oxidation levels measured in vit E–doped UHMWPE material following either of the accelerated aging methods were below the detection limit for the infrared method.

The tensile mechanical properties, fatigue crack propagation resistance, and thermal properties before and after aging in the pressure vessel are reported in Table 2, and the *P* values comparing the conventional vs vit E–doped UHMWPE and aged vs unaged groups for these properties are reported in Table 3. Accelerated aging decreased the UTS by 32% and fatigue crack propagation resistance (ΔK_{incep}) by 51% with the conventional UHMWPE—both changes were significant (Tables 2 and 3). After accelerated aging, the changes in UTS and fatigue crack propagation resistance in vit E–doped UHMWPE were not significant (Table 3). There was a significant increase in the yield strength (31%) and EAB (35%) for the conventional UHMWPE after accelerated aging, whereas vit E–doped UHMWPE showed no statistically significant difference in these parameters after accelerated aging. The peak melting temperature of either UHMWPE remained unchanged with accelerated aging. There was no statistically significant difference in the crystallinity of the vit E–doped UHMWPE after accelerated aging. The conventional UHMWPE showed a significant increase in its crystallinity after accelerated aging.

Discussion

The general aim of this investigation was to demonstrate the benefits of diffusing α-tocopherol (vitamin E) into irradiated UHMWPE to stabilize it against oxidation for applications in tibial knee inserts. The radiation-crosslinked UHMWPE stabilized by diffused vitamin E showed improved oxidation resistance and improved wear resistance in comparison with conventional UHMWPE.

We used a radiation dose level of 100 kGy for the crosslinking of UHMWPE. Prior studies have used similar [13] or lower radiation doses [14] for the crosslinking of UHMWPE for total knee applications. The lower radiation dose increases the wear rate of UHMWPE in return for better mechanical properties in irradiated and melted UHMWPEs [21]. With vitamin E stabilization, the melting step is eliminated, and the ultimate tensile strength of the polymer is not adversely affected in comparison with conventional UHMWPE—therefore, use of 100-kGy irradiation in conjunction with vitamin E stabilization is justified.

Table 2. Tensile Mechanical Properties, Fatigue Crack Propagation Resistance, and Thermal Properties of Both Conventional UHMWPE and of vit E–doped UHMWPE Before and After ASTM F2003 Aging

	Unaged Conventional UHMWPE	ASTM F2003 Aged Conventional UHMWPE	Unaged Vit E–Doped UHMWPE	ASTM F2003 Aged Vit E–Doped UHMWPE
UTS (MPa)	50.2 ± 2.1	34.7 ± 2.3	43.4 ± 2.3	45.0 ± 1.4
YS (MPa)	20.4 ± 0.6	26.8 ± 1.5	21.4 ± 0.6	21.8 ± 1.6
EAB (%)	346 ± 51	467 ± 24	256 ± 17	282 ± 55
ΔK_{incep} (MPa·m$^{1/2}$)	1.09 ± 0.05	0.53 ± 0.06	0.65 ± 0.04	0.61 ± 0.01
Peak melting temperature (°C)	137.3 ± 0.4	136.2 ± 0.4	138.5 ± 0.3	138.6 ± 0.3
Crystallinity (%)	60.0 ± 1.5	69.7 ± 0.9	58.6 ± 1.4	60.0 ± 0.8

Questions? Contact FDA/CDRH/OCE/DID at CDRH-FOISTATUS@fda.hhs.gov or 301-796-8118

Records processed under FOIA Request #2014-8015; Released by CDRH on 12-8-2015

Table 3. The *P* Values as Determined by a Student *t* Test for the Pairs of Samples Compared Are Listed Here for UTS, YS, EAB, Fatigue Crack Propagation Resistance (ΔK_{incep}), Peak Melting Temperature, and Crystallinity

	P					
Pairs	UTS	YS	EAB	ΔK_{incep}	Peak Melting Temperature	Crystallinity
Conventional vs aged conventional	.0000*	.0000*	.0004*	.0000*	.0022*	.0000*
Conventional vs vit E–doped UHMWPE	.0011*	.0203*	.0145*	.0000*	.0004*	.1748
Conventional vs aged vit E–doped UHMWPE	.0016*	.1083	.2742	.0000*	.0004*	.9399
Vit E–doped UHMWPE vs aged conventional	.0000*	.0000*	.0000*	.0109*	.0000*	.0000*
Vit E–doped UHMWPE vs aged vit E–doped UHMWPE	.2220	.6195	.3397	.0636	.6808	.0835
Aged conventional vs aged vit E–doped UHMWPE	.0000*	.0005*	.0000*	.0461*	.0000*	.0000*

* Indicates significant difference, $P < .05$.

The postirradiation vitamin E doping technology requires each implant thickness to be treated differently to ensure that vitamin E is diffused throughout the entire thickness [15]. In the present study, we tested samples of different thicknesses, and by varying doping and homogenization conditions, we were able to obtain vitamin E concentration profiles that were comparable—they all exhibited high vitamin E concentration on free surfaces and lower concentrations at the center.

We designed the knee simulator testing to investigate the wear rate before and after accelerated aging. The accelerated aging was performed on parts that were tested on the simulator for 5 million cycles to determine the effect of vitamin E elution, if any, from the surfaces on the oxidative stability of the vit E–doped UHMWPE samples. Knee simulator testing after accelerated aging showed no change in the wear behavior of these inserts indicating that there was enough vitamin E on the surface to provide oxidative stability to the polymer. This finding does not rule out any potential elution of vitamin E from the surfaces during loading and articulation. We could not use the infrared method to determine if there was any vitamin E elution because lipid absorption from the bovine serum during testing affected the characteristic infrared absorbance that we used to quantify vitamin E in polyethylene. Currently, we are investigating methods to deconvolute the infrared spectra to separate the absorbance due to absorbed lipids from that of vitamin E to determine if there is any vitamin E elution during loading and articulation.

We used tibial inserts that were only subjected to load without motion to quantify the extent of fluid uptake during testing to correct the gravimetric assessment of wear of the inserts that were subjected to both motion and load. We expected the rate of fluid absorption measured in these load-soak components to slow down with continued testing—instead, we found a linear increase in the weight of these components with no effect from the accelerated aging at 5 million cycles (Fig. 3). The absorption mainly includes the uptake of lipids from the surrounding lubricant [20]. The slight decrease in the fluid absorption with the vit E–doped UHMWPE components was likely because of the presence of vitamin E (itself a lipid) reducing the extent of additional lipid uptake. The fluid absorption we observed with the vit E–doped UHMWPE was comparable with what was previously observed with irradiated and melted UHMWPE tibial knee inserts [13].

One limitation of the study was the use of accelerated aging to study the oxidative stability of the vitamin E–stabilized, irradiated UHMWPE and conventional UHMWPE. We used 2 different methods, one under atmospheric air pressure (1 atm) and the other under high oxygen pressure (5 atm), both at elevated temperatures. There is no conclusive evidence in literature that these aging methodologies can simulate oxidation of UHMWPE that takes place in vivo in the long term. Nevertheless, these methods are often used for comparative oxidation resistance of different UHMWPE formulations, which was our purpose when we compared the oxidative stability of the 2 UHMWPE formulations. Another one of the common limitations of all joint simulator wear studies is the use of bovine serum to lubricate the articulating pairs during testing. Bovine serum is expected to simulate the lubrication provided by synovial fluid in vivo. Whereas some studies use diluted serum in joint simulator wear testing, others use 100% bovine serum, as was the case for the present study. Serum dilution is used to decrease the protein concentration to the levels typically found in synovial fluid. In our laboratory, dilute serum causes pitting-type damage in acetabular liners tested under simulated normal gait, a damage mechanism that is not clinically relevant. Therefore, we chose to use undiluted serum in the present study.

One reason for the accelerated aging during the knee simulator testing was to determine the effect of oxidation on delamination resistance of the tibial inserts. The absence of delamination in the vit E–doped UHMWPE samples was not surprising because there was no detectable oxidation on these components after accelerated aging (Table 1). The conventional tibial inserts did not show any delamination either because the oxidation levels after accelerated aging were not high enough (Table 1). However, the conventional UHMWPE samples showed a significant rise in

Questions? Contact FDA/CDRH/OCE/DID at CDRH-FOISTATUS@fda.hhs.gov or 301-796-8118

Records processed under FOIA Request #2014-8015; Released by CDRH on 12-8-2015

Table 4. Knee Simulator Wear Rates Measured With Irradiated and Melted UHMWPE Formulations With 2 Different Designs in Comparison With the Wear Rates Measured in the Present Study

	65-kGy Irradiated and Melted UHMWPE NexGen CR *	Conventional UHMWPE NexGen CR [14]	95-kGy Irradiated and Melted UHMWPE NK II CR [13] *	Conventional UHMWPE NK II CR	Vitamin E–Stabilized Vanguard CR—Present Study	Conventional UHMWPE Vanguard CR—Present Study
Unaged wear rate (mg/million cycle)	4.6 ± 2	23 ± 6	NT	8.8 ± 1.5	2.4 ± 0.5	26.9 ± 3.5
Aged wear rate (mg/million cycle)	NT	NT	0.7 ± 0.1	9.6 ± 3.6	2.5 ± 0.8	40.8 ± _3.0

Note that the head-to-head comparison of the wear rates is not possible because of the different designs resulting in different contact areas that enhance different mechanics of loading during testing.

* Manufactured by Zimmer, Inc., Warsaw, Ind.

crystallinity likely because of the oxidation-induced chain scission that typically results in recrystallization of the smaller molecules [5] and a decline in ultimate tensile strength as we observed here. The increase in the crystallinity was likely responsible for the increase in the yield strength of conventional UHMWPE. The increase in the EAB with accelerated aging was surprising in that oxidation and chain scission typically reduce the ductility of UHMWPE. We postulate that because the oxidation is typically limited to the surface, the more ductile core of the test samples deformed with an effectively smaller thickness, resulting in a higher EAB.

The oxidation potential as measured by the height of the nitrate absorbance after reacting the hydroperoxides with nitric oxide was about 25% higher with the conventional UHMWPE, yet the difference in the extent of oxidation between the conventional and vit E–doped UHMWPE was much larger. Hydroperoxide decay creates oxidation byproducts and free radicals. The latter continue the oxidation chain reaction. In the case of the conventional UHMWPE, the chain reaction likely resulted in higher oxidation levels during accelerated aging. In contrast, vitamin E must have terminated the free radicals generated during hydroperoxide decay, thus breaking the chain reaction and preventing its progress in vit E–doped UHMWPE samples. As a result, the vit E–doped UHMWPE did not oxidize during the accelerated aging, and the changes in their mechanical properties were not significant.

In another study conducted in this laboratory, we reported the fatigue crack propagation resistance of 100-kGy irradiated UHMWPE as 0.74 ± 0.03 MPa·m$^{1\backslash 2}$, and with subsequent melting, we showed a 32% decline to 0.56 ± 0.02 MPa·m$^{1\backslash 2}$ [22]. In this study, the fatigue crack propagation resistance for vit E–doped UHMWPE was 0.65 ± 0.04 MPa.m$^{1\backslash 2}$, significantly greater than that of 100-kGy irradiated and melted UHMWPE ($P < .05$). The change in the fatigue crack propagation resistance of vit E–doped UHMWPE was not significant with accelerated aging largely due to the antioxidant properties of vitamin E and its protection against oxidation, and the decline in the fatigue crack propagation resistance of conventional UHMWPE was not surprising because of its oxidation during accelerated aging.

Irradiated and melted UHMWPE is the only alternative bearing surface material used in total knees. Previously reported knee simulator testing that was carried under comparable conditions used for the present study showed improved wear resistance with 65- and 95-kGy irradiated and melted UHMWPE in comparison with the conventional UHMWPE tibial inserts (Table 4) [13], [14]. The vitamin E–stabilized radiation-crosslinked UHMWPE tibial inserts also showed an increase in the wear resistance in comparison with the corresponding conventional UHMWPE tibial inserts. The comparison between the irradiated and melted and vitamin E–stabilized tibial inserts in terms of wear rate measured on the knee simulator is not possible because they all used different tibial insert designs. However, one can note that the percent reduction of the wear rates with respect to the corresponding conventional UHMWPE is approximately the same for all 3 highly crosslinked UHMWPEs (Table 4). Therefore, the vitamin E technology presented here is superior to the current alternative bearing surface material in terms of its fatigue strength and wear resistance simultaneously.

Conclusion

The irradiated and vitamin E–stabilized material studied showed decreased adhesive/abrasive wear when tested on a knee simulator for 5 million cycles of normal gait. The vit E–doped UHMWPE material retained its high wear resistance after aging and further testing on the knee simulator. The presence of vitamin E in irradiated UHMWPE did not adversely affect its wear behavior while increasing the oxidation resistance of the irradiated polymer.

Acknowledgments

We acknowledge with thanks the assistance of Dave Schroeder and Jordan Freedman of Biomet, Inc, in the preparation of the test components.

Questions? Contact FDA/CDRH/OCE/DID at CDRH-FOISTATUS@fda.hhs.gov or 301-796-8118

Records processed under FOIA Request #2014-8015; Released by CDRH on 12-8-2015

References

1. Muratoglu O, Mark A, Vittetoe D, et al. Polyethylene damage in total knees and use of highly crosslinked polyethylene. J Bone Joint Surg 2003;85-A(Suppl 1):7.
2. Gupta SK, Chu A, Ranawat AS, et al. Review Article: osteolysis after total knee arthroplasty. J Arthroplasty 2007; 22:787.
3. Costa L, Jacobson K, Bracco P, et al. Oxidation of orthopaedic UHMWPE. Biomaterials 2002;23:1613.
4. Costa L, Luda MP, Trossarelli L, et al. Oxidation in orthopaedic UHMWPE sterilized by gamma radiation and ethylene oxide. Biomaterials 1998;19:659.
5. Sutula L, Collier J, Saum K, Currier B, Currier J, Sanford W, et al. The Otto Aufranc Award. Impact of gamma sterilization on clinical performance of polyethylene in the hip. Clin Orthop 1995;28.
6. Waterman D, Dole M. Radiation chemistry of polyethylene. 10. Kinetics of conversion of alkyl to allyl free radicals. J Phys Chem 1970;74:1913.
7. Dole M. Free radicals in irradiated polyethylene. In: Dole M, editor. The radiation chemistry of macromolecules. New York: Academic Press; 1972. p. 335.
8. Kashiwabara H, Shimada S, Hori Y. Free radicals and crosslinking in irradiated polyethylene. Radiat Phys Chem 1991;37:43.
9. Premnath V, Harris W, Jasty M, et al. Gamma sterilization of UHMWPE articular implants: an analysis of the oxidation problem. Ultra high molecular weight poly ethylene. Biomaterials 1996;17:1741.
10. Wannomae KK, Christensen SD, Freiberg AA, et al. The effect of real-time aging on the oxidation and wear of highly cross-linked UHMWPE acetabular liners. Biomaterials 2006;27:1980.
11. Muratoglu OK, Bragdon CR, O'Connor DO, et al. 1999 HAP Paul Award. A novel method of crosslinking UHMWPE to improve wear, reduce oxidation and retain mechanical properties. J Arthroplasty 2001;16:149.
12. McKellop H, Shen FW, Lu B, et al. Development of an extremely wear resistant ultra-high molecular weight polyethylene for total hip replacements. J Orthop Res 1999;17:157.
13. Muratoglu OK, Bragdon CR, Jasty M, et al. Knee simulator testing of conventional and crosslinked polyethylene tibial inserts. J Arthroplasty 2004;19:887.
14. Muratoglu OK, Rubash HE, Bragdon CR, et al. Simulated normal gait wear testing of a highly cross-linked polyethylene tibial insert. J Arthroplasty 2007;22:435.
15. Oral E, Wannomae KK, Rowell SL. Muratoglu OK. Diffusion of vitamin E in ultra-high molecular weight polyethylene. Biomaterials 2007;28:5225.
16. Bracco P, Brunella V, Zanetti M, et al. Stabilisation of ultra-high molecular weight polyethylene with vitamin. E Polym Degrad Stab 2007;92:2155.
17. Parth M, Aust N, Lederer K. Studies on the effect of electron beam radiation on the molecular structure of ultra-high molecular weight polyethylene under the influence of alpha-tocopherol with respect to its application in medical implants. J Mater Sci: Mater Med 2002;13:917.
18. Oral E, Christensen S, Malhi A, et al. Wear resistance and mechanical properties of highly crosslinked UHMWPE doped with vitamin. E J Arthroplasty 2006; 21:580.
19. Bergmann G, Graichen F, Rohlmann A, et al. Frictional heating of total hip implants. Part I. Measurements in patients. J Biomechanics 2001;34:421.
20. Costa L, Bracco P, Brach del Prever EM, et al. Oxidation and oxidation potential in contemporary packaging for polyethylene total joint replacement components. J Biomed Mater Res B Appl Biomater 2006;78:20.
21. Muratoglu OK, Bragdon CR, O'Connor DO, et al. Unified wear model for highly crosslinked ultra-high molecular weight polyethylenes (UHMWPE). Biomaterials 1999;20: 1463.
22. Oral E, Wannomae KK, Hawkins NE, et al. α-Tocopherol doped irradiated UHMWPE for high fatigue resistance and low wear. Biomaterials 2004;25:5515.

Questions? Contact FDA/CDRH/OCE/DID at CDRH-FOISTATUS@fda.hhs.gov or 301-796-8118

Records processed under FOIA Request #2014-8015; Released by CDRH on 12-8-2015

Evaluation of Sequentially Crosslinked Ultra-High Molecular Weight Polyethylene

M. L. Morrison, S. Jani

Smith and Nephew Orthopaedics, Memphis, Tennessee 38116

Received 26 February 2008; revised 2 July 2008; accepted 20 August 2008
Published online 5 November 2008 in Wiley InterScience (www.interscience.wiley.com). DOI: 10.1002/jbm.b.31257

Abstract: This study was undertaken to investigate the effect of crosslinking ultra-high molecular weight polyethylene (UHMWPE) in a sequential manner to the final desired dose and to compare the results to single-dose crosslinking. To verify these results, an explanted, commercially available, sequentially crosslinked component was characterized. Finally, additional tensile testing was conducted to determine if tensile-sample thickness has a significant effect on the mechanical properties of UHMWPE. Based upon this well-controlled study with the same starting material, there is no apparent benefit of sequential crosslinking over crosslinking by single dose in any of the mechanical, thermophysical, physical, or oxidative properties evaluated in this study. In contrast, the soak temperature of the postirradiation heat treatment was more influential and exhibited statistically significant effects on the stability, structure, and properties of the resultant material. Compared to virgin material, crosslinking always resulted in decreases in tensile strength, elongation, and impact strength. These results were confirmed by characterization of a retrieved, sequentially crosslinked (X3™) cup. All of the metrics derived for the retrieved cup were virtually identical to the sequential- and single-dose-crosslinked materials produced in this study. Examination of the effect of tensile-sample thickness demonstrated that there are significant effects on the resultant properties. In particular, the ultimate tensile strength of UHMWPE can be elevated by conducting tensile tests with thin specimens. © 2008 Wiley Periodicals, Inc. J Biomed Mater Res Part B: Appl Biomater 90B: 87–100, 2009

Keywords: UHMWPE; crosslinking; mechanical properties; oxidation; crystallinity

INTRODUCTION

In vitro studies[1,2] and clinical experience[3–9] have demonstrated that crosslinking of ultra-high molecular weight polyethylene (UHMWPE) with ionizing radiation significantly reduces the volumetric wear of total hip arthroplasties. On the other hand, there is a well-documented, concomitant decrease in mechanical properties with increasing radiation dose and crosslink density.[10–12] Generally, the ultimate tensile strength (UTS), elongation at break (EL), and impact strength all decrease with increasing dose due to the increasing constraint of the crosslinks, which results in decreases in ductility and a reduction of strain-induced, polymer chain reorientation. These decreases in mechanical properties are also exacerbated by the postirradiation heat treatment that is commonly conducted to reduce the residual free-radical concentration (FRC). Postirradiation remelting leads to additional decreases in crystallinity and mechanical properties, but removes all of the measurable free radicals, which stabilizes the material against aging. Submelt annealing maintains or increases the crystallinity and results in smaller decreases in the strength of the crosslinked material, but leaves residual free radicals that could oxidize with time. Consequently, the selection of radiation dose and heat treatment should be made to achieve the proper balance of wear reduction, long-term stability, and maintenance of adequate mechanical properties for a given application.

Notwithstanding these fundamental effects of crosslinking, sequential irradiation and submelt annealing of UHMWPE has been suggested as a novel method to achieve increased wear resistance and long-term stability against oxidation without compromising "strength."[13,14] The exact mechanism of this technique has not been delineated. However, it has been reported that irradiation in small steps, each step followed by submelt annealing, results in a dramatic reduction of the free radicals, dramatically reduced wear, and maintenance of the UTS at the same level as the virgin material.[13] This process is utilized in commercially available hip- and knee-arthroplasty components (X3™, Stryker, Mahwah, NJ).

The first objective of this study was to determine if sequential irradiation and annealing produced a material that

Correspondence to: M. L. Morrison (e-mail: mark.morrison@smith-nephew.com)

© 2008 Wiley Periodicals, Inc.

Questions? Contact FDA/CDRH/OCE/DID at CDRH-FOISTATUS@fda.hhs.gov or 301-796-8118

Records processed under FOIA Request #2014-8015; Released by CDRH on 12-8-2015

was measurably different from the standard single-dose irradiation and annealing process. For direct comparison between the processes, the total, cumulative radiation dose was equivalent between the two processes. The effects of annealing above and below the peak melt temperature in the postirradiation heat treatment were also examined.

To verify the results for the sequentially crosslinked material produced in the first portion of this study, an explanted, commercially available, sequentially crosslinked component (X3™, Stryker, Mahwah, NJ) was received and characterized. These results were compared to the properties reported for X3™ in the literature[13,14] and to the aforementioned materials produced through either single-dose or sequential crosslinking. Because of the limited material available, bulk mechanical properties of the X3™ cup could not be assessed. Thus, the mechanical properties of the retrieved cup were characterized by small-punch testing.

As specified by the American Society for Testing and Materials (ASTM F648-04), the mechanical properties of UHMWPE should be determined according to ASTM D638 with the Type IV sample geometry. However, this standard does not specify a particular thickness for the samples, only a range of 4 mm or less. All mechanical testing in the first part of this study was conducted with tensile-sample thicknesses of 3.0 ± 0.05 mm. On the other hand, tensile testing of sequentially crosslinked materials in the literature was conducted with tensile-sample thicknesses of 1 mm.[15] To clarify the results of these testing differences, the third part of this study was conducted to determine if tensile-sample thickness has a significant effect on the mechanical properties of UHMWPE materials.

MATERIALS AND METHODS

Effects of Sequential Irradiation

Compression-molded GUR1020 UHMWPE rod stock was purchased from MediTECH Medical Polymers (Fort Wayne, IN) with diameters of 7.6 cm. To eliminate batch-to-batch variability, all of the test materials were produced from the same resin and production lots and were subjected to the standard postconsolidation anneal to relieve residual stresses in the as-molded rod stock. The individual rods were processed according to the gamma-radiation doses and heat treatments outlined in Table I. Briefly, the materials were gamma-irradiated (Steris, Libertyville, IL) in air to total doses of 9 Mrad by either (a) single dose, or (b) three sequences of 3 Mrad (SQXL-1). The materials crosslinked with a single-dose were annealed at either 130°C for 8 h (XL-130) or 147°C for 2 h (XL-147). Since the peak melting temperature of UHMWPE is typically in the range of 140–145°C, the 130°C heat treatment is considered to be a submelt anneal, while the 147°C heat treatment is termed remelting. The SQXL-1 material was annealed at 130°C for 8 h after each irradiation sequence, as taught in the publications and patent application for X3™.[16] Unirradiated, virgin GUR1020 (CPE-1) from the same lot was utilized as the control material.

TABLE I. Experimental Materials and Processing Parameters

Sample ID	Resin/ Production Lot	Nominal Radiation Dose (Mrad)	Postirradiation Heat Treatment
CPE-1	A	–	–
SQXL-1	A	3 × 3.0	3 × 130°C for 8 h
XL-130	A	9.0	130°C for 8 h
XL-147	A	9.0	147°C for 2 h
X3™	B	3 × 3.0	3 × 130°C for 8 h
CPE-2	C	–	–
SQXL-2	D	3 × 3.0	3 × 130°C for 8 h

All of these materials were fabricated from compression-molded GUR1020 UHMWPE rod stock.

All heat treatments were monitored with a "control rod" that contained a thermocouple in the core. The time period for the heat treatment was begun when this thermocouple reached 10°C below the nominal heat-treatment temperature. After the specified time period for the heat treatments, the oven was cooled at an average rate of not more than 5.6°C/h until the control rod temperature was at 50°C or below.

Mechanical Properties Characterization. The bulk mechanical properties of the rod stock were characterized by MediTECH. All tensile testing ($n = 5$) was performed following ASTM D638-03 specifications with a displacement rate of 50 mm/min and Type IV samples that were 3.0 ± 0.05 mm thick. Izod impact testing ($n = 5$) was conducted according to ASTM F648-04.

Small-punch testing (SPT) was performed on these materials by Exponent (Philadelphia, PA) according to ASTM F2183-02. Test specimens ($n = 3$) were fabricated by punching cores (Ø 7.14 mm) from the bulk materials. One disc-shaped specimen (Ø 6.35 × 0.5 mm) was machined from each core. Mechanical testing was conducted on a screw-driven load frame (Instron 4505, Canton, MA) at a constant displacement rate of 0.5 mm/min. The applied load and crosshead displacement were recorded during each test and plotted to derive several test metrics.

An illustration of a typical small-punch load–displacement plot is shown in Figure 1. The peak load is analogous to the yield strength (YS) in a standard, uniaxial tensile test and is indicative of the transition from the initial bending phase to the drawing phase in which the specimen is plastically deformed by the head of the punch.[17] The ultimate load is defined as the load at failure and is indicative of the strength of the material. The amount of ductility is indicated by the extent of crosshead displacement at failure (ultimate displacement) and is analogous to the EL. Finally, the area under the load–displacement curve, or the energy to failure, is a measure of the toughness (strength and ductility) of the material. The samples were returned after test-

Questions? Contact FDA/CDRH/OCE/DID at CDRH-FOISTATUS@fda.hhs.gov or 301-796-8118

Records processed under FOIA Request #2014-8015; Released by CDRH on 12-8-2015

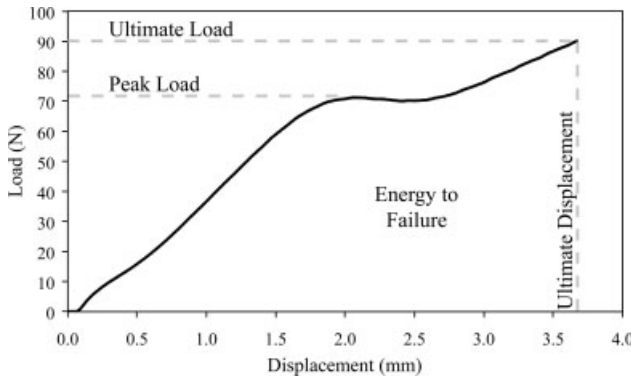

Figure 1. Schematic load–displacement plot from small-punch testing demonstrating the derived mechanical parameters.

ing, sectioned along the fracture plane, sputter-coated with gold, and examined by SEM with a secondary electron detector.

Differential Scanning Calorimetry. Thermal analysis was conducted according to ASTM F2625-07 using a Netzsch 204 F1 Phoenix (Burlington, MA) differential scanning calorimeter (DSC) and Proteus thermal analysis software (Huntersville, NC). Five samples (n = 5) were removed from the core of each rod.

Samples were cut and weighed to a resolution of 0.01 mg and ranged in mass from ~5 to 10 mg. An attempt was made to keep the approximate dimensions of the samples consistent to minimize dimensional effects on the thermogram variability. For all of the thermograms, an empty aluminum crucible was used as the reference. First, an empty aluminum crucible was run as a baseline correction. For each of the materials, the samples were crimped into aluminum crucibles and placed in the DSC chamber, which was continuously flushed with nitrogen gas at a flow rate of ~30 mL/min. The DSC cycle consisted of a 1-min equilibration at 25°C, followed by heating to 180°C at 10°C/min rate. The samples were then cooled to 25°C at 20°C/min. These thermograms were analyzed to determine the extrapolated onset (T_{OM}) and peak melting (T_{PM}) temperatures and the heat of fusion (ΔH_m). For the determination of ΔH_m, the lower limits of the peak-area calculation were systematically placed at 50°C. The upper limit was varied to account for changes in the location of the melting endotherm. The percent crystallinity ($\%X$) for each condition was estimated as:

$$\%X = \frac{\Delta H_m}{291} \times 100 \quad (1)$$

where 291 is the enthalpy (J/g) associated with the melting of 100% crystalline polyethylene.

Molecular Network Parameters. Portions of the rod stock were sent to Cambridge Polymer Group (Boston, MA) for determination of the swell ratio (q_s), percent extract (for CPE-1 only), crosslink density (v_d), and molecular weight between crosslinks (M_c). Three cubes (n = 3) with nominal dimensions of 5 × 5 × 5 mm^3 were prepared from each material by Cambridge Polymer. The CPE-1 sample was evaluated according to ASTM D2765-01, Method C, while the highly crosslinked samples (SQXL-1, XL-130, and XL-147) were evaluated according to ASTM F2214-02. Once q_s was determined according to the pertinent ASTM standard, the crosslink densities and molecular weights between crosslinks were calculated for all materials according to the following equations delineated in ASTM F2214-02:

$$\text{Crosslink density} = v_d = \frac{Ln\left(1 - q_s^{-1}\right) + q_s^{-1} + \chi_1 q_s^{-2}}{\phi_1\left(q_s^{-1/3} - \frac{q_s^{-1}}{2}\right)} \quad (2)$$

$$\text{Molecular weight between crosslinks} = M_c = \left(\bar{v} v_d\right)^{-1} \quad (3)$$

where χ_1 = heat of mixing for the polymer–solvent system (Flory interaction parameter) = $0.33+0.55/q_s$; ϕ_1 = molar volume of the solvent = 136 cm^3/mol = 0.136 dm^3/mol; $\bar{v}^{-1}$ = specific volume of the polymer = 920 g/dm^3.

Electron Spin Resonance. Samples for electron spin resonance (ESR) with diameters of 3 mm and lengths of 10 mm were punched from each of the materials in this study (n = 4). Because the free radicals in these materials are highly reactive and sensitive to exposure to oxygen, care was taken to minimize this exposure prior to analysis. The ESR samples were removed from the center of the rod stock where the material had been effectively shielded from exposure to the atmosphere by the surrounding material. In addition, the time from sample preparation to ESR analysis was minimized and generally maintained at 1–2 days with storage at room temperature in the dark.

The FRC in each sample was determined with an X-band ESR spectrometer (Bruker EMX300) operating at a microwave frequency of ~9.8 GHz and employing a high-sensitivity universal X-band resonator cavity. ESR test parameters were constant for all measurements at 1 mW microwave power, 5 Gauss amplitude modulation, 200 G sweep width, 3500 center field, and a relatively high gain and Q-value. The absolute magnitude of the FRC was analyzed and computed with WinEPR analysis software. The area under the absorption curve of a test specimen was compared to that of the National Institute of Standards and Testing (NIST) intensity standard SRM-2601, and these results were normalized to the specimen's weight.

Oxidation. To assess the oxidation potential of these materials, three specimens (25.4 × 25.4 × 4.76 mm^3) of each material were artificially aged according to ASTM F2003-02. Briefly, the samples were placed in a pressure vessel and heated to 70°C in oxygen at 503 kPa (5 atm) for a total of 14 days. A microtome was used to remove thin,

Questions? Contact FDA/CDRH/OCE/DID at CDRH-FOISTATUS@fda.hhs.gov or 301-796-8118

Records processed under FOIA Request #2014-8015; Released by CDRH on 12-8-2015

through-thickness slices (~200 μm thick) from the artificially aged samples. These films were then briefly cleaned with acetone to remove any oils or other contaminants and dried.

For all oxidation measurements, a Thermo Nexus 670 Fourier-transform infrared (FTIR) spectrometer with a Nicolet Centaurus microscope (Thermo Electron, Waltham, MA) was used in transmission mode with a resolution of 4 cm^{-1} and a triangular apodization function. Each profile was begun ~75 μm below the outer surface of the sample, and spectra were recorded every 200 μm thereafter through the thickness of the sample. Sixty-four spectra were collected and averaged at each step in the profile, and background spectra were collected after every five steps in the profile. The oxidation index (OI) was determined to be the ratio of the area under the peak at 1720 cm^{-1} to the area under the peak between 1330 and 1396 cm^{-1}, as outlined in ASTM F2102-06. Three profiles were measured per sample for a total of nine profiles per material ($n = 9$). The maximum oxidation indices (OI_{max}) were determined for each profile and averaged to produce a mean OI_{max} for each material.

Statistical Analysis. Statistical analyses of the results were performed with Minitab 13.32 software (Minitab, State College, PA). Analysis of variance (ANOVA) was conducted to determine statistically significant differences between all of the treatments. When significant differences were found at a 0.05 level of significance (α), the exact relationships between variables were examined through *post hoc* Tukey or Dunnett's analyses.

Analysis of an Explanted, Sequentially Crosslinked Component

An explanted X3™ acetabular liner (Part #623-00-36E) was obtained after revision for recurrent dislocations. Based upon the identifying information on the component, it appears that this acetabular cup was manufactured in 2005. Since the cup was received in May 2007, it was 29 months old, at most. Upon receiving the retrieved cup, it was stored in air at room temperature in the dark. The durations of preoperative shelf-aging, *in vivo* service, and postretrieval shelf-aging were unknown. According to the literature,[13] X3™ components are also fabricated from compression-molded GUR1020 UHMWPE.

This cup was sectioned into multiple specimens for analysis to directly compare the properties to the materials produced in this well-controlled study. Because of the limited material available, bulk mechanical properties of the X3™ cup could not be assessed. Thus, the retrieved cup was characterized by SPT, DSC, ESR, FTIR, and swelling experiments in the same manner as delineated above. For SPT, three cores (Ø 7.14 mm) were punched from the articular surface of the retrieved cup. One disc-shaped specimen (Ø 6.35 × 0.5 mm) was machined from the middle of each core. For evaluation with DSC, five samples each were removed from the rim and the bearing surface of the cup, for a total of 10 samples. Samples for ESR with diameters of 3 mm and lengths of ~5 mm were punched from the articular region ($n = 3$). The X3™ acetabular cup was not subjected to artificial aging; however, oxidation of the as-received cup was evaluated. Extraction of absorbed lipids from the retrieved cup was not performed because an ester peak was not observed in the FTIR spectra in the region of 1738 cm^{-1}. A microtome was used to remove thin, through-thickness slices (~200 μm thick) at both the rim and the bearing portion of the articular surface of the cup for analysis by FTIR. Finally, three samples for the swelling experiments (ASTM F2214-02) were fabricated from the articular region.

Effects of Tensile-Sample Thickness

In the third part of this study, additional compression-molded GUR1020 materials were purchased from MediTECH. One material remained in the virgin condition (CPE-2) and a second rod was sequentially crosslinked (SQXL-2) in the same manner as previously outlined for the SQXL-1 material. It should be noted that these materials were from different lots; therefore, these results also include lot-to-lot variability.

Again, the tensile tests were conducted by MediTECH following ASTM D638-03 specifications with the Type IV sample at displacement rates of 50 mm/min. However, in this part of the study, the nominal thicknesses of the samples were either 1, 2, or 3 mm with tolerances of ±0.05 mm. Five replicates ($n = 5$) of each material were tested at each thickness.

Statistical Analysis. To evaluate the correlation between a given mechanical property and the sample thickness, various regression models (e.g., linear, power, exponential) were fit to the data and the goodness-of-fit was assessed through the coefficient of determination (r^2). Significant changes in a given mechanical property upon changes in the thickness for a given material were evaluated by ANOVA as previously described.

RESULTS

Effects of Sequential Irradiation

Mechanical and Physical Properties Characterization. The mechanical and physical properties are reported in Table II. A comparison of SQXL-1 and XL-130 demonstrates that, at the tested levels, sequential irradiation had no significant effect on the YS ($p = 0.611$), UTS ($p = 0.9999$), elongation ($p = 0.9999$), or impact strength ($p = 0.8688$). On the other hand, each of these properties, with the exception of YS, decreased by significant amounts ($p \leq 0.0014$) for all forms of crosslinked materials compared to the virgin CPE-1 material (Figures 2–4). Compared to

Questions? Contact FDA/CDRH/OCE/DID at CDRH-FOISTATUS@fda.hhs.gov or 301-796-8118

Records processed under FOIA Request #2014-8015; Released by CDRH on 12-8-2015

TABLE II. Mean ± Standard Deviation Values of the Properties Evaluated

	CPE-1	SQXL-1	XL-130	XL-147	X3™
Yield strength (MPa)	23.0 ± 0.3	23.3 ± 0.2	23.6 ± 0.4	21.0 ± 0.2	–
Ultimate tensile strength (MPa)	57.4 ± 3.1	47.7 ± 1.9	47.3 ± 3.2	42.9 ± 3.1	–
Elongation at break (%)	509 ± 29	267 ± 6	264 ± 17	279 ± 19	–
Izod impact strength (kJ/m^2)	158 ± 3	60 ± 2	59 ± 3	68 ± 1	–
Small-punch test peak load (N)	73.4 ± 1.6	71.6 ± 1.0	73.4 ± 2.4	70.6 ± 1.8	73.1 ± 1.8
Small-punch test ultimate load (N)	62.0 ± 1.0	95.8 ± 6.1	97.8 ± 3.2	91.5 ± 2.0	100.7 ± 4.7
Small-punch test ultimate displacement (mm)	4.4 ± 0.0	3.7 ± 0.4	3.7 ± 0.2	3.8 ± 0.1	3.7 ± 0.1
Small-punch test energy to failure (mJ)	243 ± 5	222 ± 39	229 ± 17	222 ± 8	231 ± 31
Onset melting temperature, T_{OM} (°C)	126.6 ± 0.7	131.1 ± 0.7	130.6 ± 0.6	122.7 ± 0.6	132.4 ± 0.5
Peak melting temperature, T_{PM} (°C)	140.7 ± 1.8	145.8 ± 1.1	144.5 ± 1.1	140.5 ± 1.5	146.3 ± 1.2
Percent crystallinity, $\%X$ (%)	57.3 ± 1.1	61.3 ± 0.9	60.5 ± 1.1	52.3 ± 2.1	62.1 ± 1.1
Free-radical concentration ($\times 10^{15}$ spins/g)	ND	2.4 ± 0.7	1.3 ± 0.2	ND	0.73 ± 0.16
Maximum oxidation index (OI_{max})	0.02 ± 0.00	0.20 ± 0.11	0.31 ± 0.19	0.02 ± 0.00	0.10 ± 0.03[a]
Swell ratio, q_s	15.77 ± 0.76	3.14 ± 0.08	3.12 ± 0.09	2.98 ± 0.01	3.34 ± 0.15
Crosslink density, ν_d (mol/dm^3)	0.013 ± 0.001	0.193 ± 0.010	0.195 ± 0.010	0.213 ± 0.001	0.171 ± 0.014
Extract (%)	21.0 ± 3.5	–	–	–	–
Molecular weight between crosslinks, M_c ($\times 10^3$ g/mol)	78.97 ± 5.72	4.77 ± 0.23	4.72 ± 0.26	4.31 ± 0.03	5.39 ± 0.46

ND, not detectable.
[a] As-received condition with no accelerated aging.

annealing below the melt (SQXL-1 and XL-130), annealing above the melt temperature (XL-147) produced a 10% decrease in the UTS ($p \geq 0.454$), a similar EL ($p \geq 0.485$), and a 13–16% increase in impact strength ($p \leq 0.001$). These statistical differences are summarized in Table III, where, within the derived parameter of interest, materials not connected by the same letter are statistically different.

Similar results were observed with SPT (Table II, Figures 5–9). All of the crosslinked materials were distinctly different from CPE-1 with strain hardening behavior in the load–displacement plots (Figure 5) and higher ultimate loads ($p = 0.000$). The crosslinked materials also exhibited lower ultimate displacements than CPE-1, although only SQXL-1 and the retrieved cup were significantly different ($p = 0.029$) at the tested levels. As found with the bulk mechanical properties, no significant differences between single-dose (XL-130) and sequential-dose (SQXL-1) irradiation were observed in the load–displacement curves or any of the mechanical properties derived through SPT (Table IV). No significant differences were found for the peak load (Figure 6) or the energy to failure (Figure 9) between any of the samples evaluated, at the levels tested in this study.

No statistically significant differences in the small-punch-test metrics were observed between the X3™ retrieval and any of the crosslinked materials produced for this study. In addition, the ultimate load and ultimate displacement for the retrieved cup were significantly different from the virgin material.

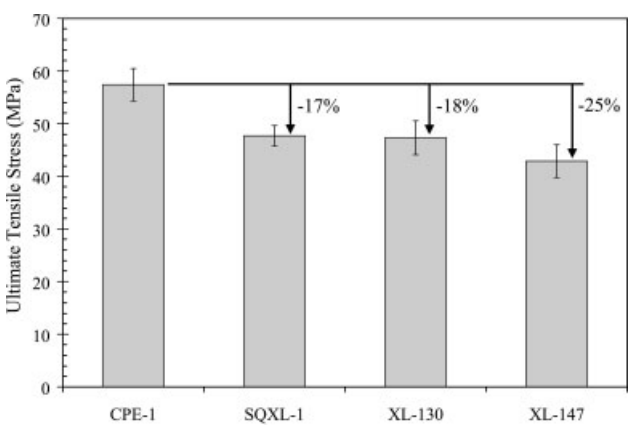

Figure 2. Plot of the ultimate tensile strength (UTS) for the compression-molded GUR1020 UHMWPE samples subjected to various gamma-radiation doses and heat treatments. The error bars represent the standard deviations.

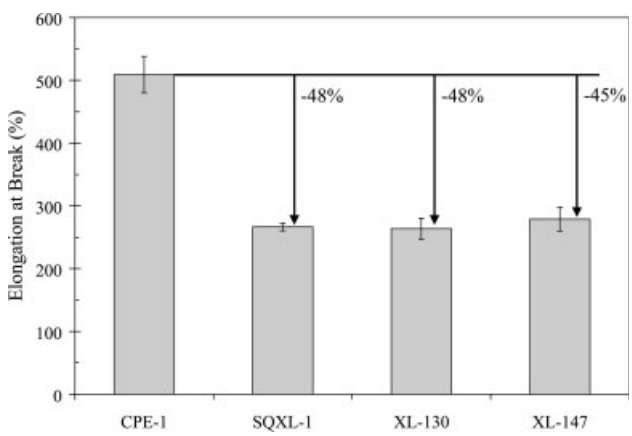

Figure 3. Plot of the elongation at break for the compression-molded GUR1020 UHMWPE samples subjected to various gamma-radiation doses and heat treatments. The error bars represent the standard deviations.

Questions? Contact FDA/CDRH/OCE/DID at CDRH-FOISTATUS@fda.hhs.gov or 301-796-8118

Records processed under FOIA Request #2014-8015; Released by CDRH on 12-8-2015

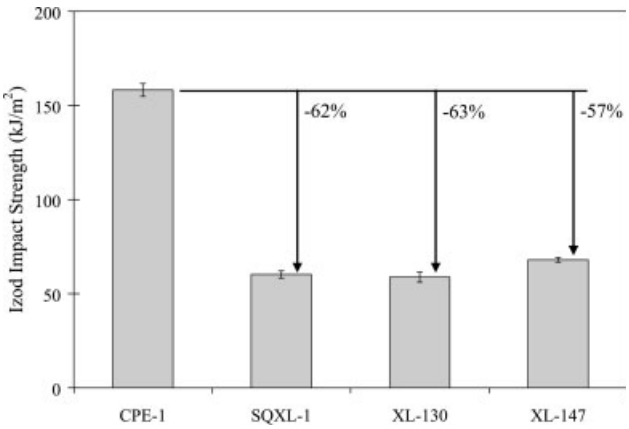

Figure 4. Plot of the Izod impact strength for the compression-molded GUR1020 UHMWPE samples subjected to various gamma-radiation doses and heat treatments. The error bars represent the standard deviations.

Post-test examination of the sample cross-sections (Figure 10) demonstrated that the CPE-1 samples experienced greater amounts of drawing due to their inherent ductility. This behavior was evidenced by the greater extent of thinning of the sample [Figure 10(a)] and the ductile appearance of the fracture surfaces. An attempt was made to measure the cross-section thicknesses of the samples on the fracture planes, but this was complicated by difficulties in assuring that the viewing axis was perpendicular to the fracture surface of interest. Therefore, only estimates of the final thicknesses were possible. The thicknesses for CPE-1 ranged from 20 to 100 μm, while the thicknesses for the remaining samples were on the order of 120–200 μm. Thus, the true stresses at fracture for the thinner, CPE-1 samples were likely higher than those of the thicker, crosslinked materials. As a result, the strain softening behavior for the CPE-1 samples (Figure 5) in the small-punch tests appears to be an artifact of the load–displacement plot.

Differential Scanning Calorimetry. The mean T_{OM}, T_{PM}, and $\%X$ derived from the DSC thermograms are reported in Table II. Again, no statistically significant differences were found within these parameters between the single-dose (XL-130) and sequentially (SQXL-1) irradiated materials ($p \geq 0.365$), at the levels tested (Table IV). On the other hand, the crosslinked, submelt-annealed materials (SQXL-1 and XL-130) exhibited significantly higher T_{OM}, T_{PM}, and $\%X$ compared to the virgin (CPE-1) and crosslinked, remelted (XL-147) materials. However, these changes represented small increases that were ~4% for T_{OM}, 4% for T_{PM}, and 7% for $\%X$, respectively.

At the levels tested in this study, there were no statistically significant differences ($p \geq 0.409$) in the thermophysical properties found between the rim and the bearing surface of the retrieved X3™ cup. Therefore, the values for the cup reported in Table II and in the following statistical analyses are representative of all 10 samples collected at both locations.

The T_{OM} for SQXL-1 and XL-130 were slightly lower (−1%, $p < 0.001$) than for the X3™ cup, while the virgin (CPE-1) and crosslinked, remelted (XL-147) materials were 4–7% lower, respectively. On the other hand, no statistically significant differences were detected for the T_{PM} and $\%X$ between the X3™ cup and either of the crosslinked, submelt-annealed materials. For T_{PM} and $\%X$, only the virgin and crosslinked, remelted materials were significantly lower ($p < 0.001$) than the X3™ cup. The crystallinity of the retrieved X3™ cup was approximately equivalent to values reported for sequentially crosslinked UHMWPE in the literature.[13,14,18,19]

Molecular Network Parameters. The mean swell ratios (q_s), percent extracts, crosslink densities (ν_d), and molecular weights between crosslinks (M_c) are reported in Table II. Again, there were no statistically significant differences ($p > 0.50$) detected between the sequential- and single-dose materials at the levels tested in this study. In contrast, postirradiation remelting increased the crosslink density by a statistically significant amount for the XL-147 samples compared to the submelt-annealed materials. No statistically significant differences in crosslink densities were detected in this study between the X3™ cup, SQXL-1, and XL-130. For comparison of these numerous crosslink densities, the crosslink densities from this study have been plotted as a function of radiation dose in Figure 11. Within this plot, the reported ranges of crosslink densities for various doses in the literature are denoted by the dashed lines.

It should be noted that it appears to be a common practice in the literature to truncate Eq. (2) by ignoring the final term in the denominator ($-0.5q_s^{-1}$), which, according to Flory,[20] is only applicable if the swell ratio is above 10.

TABLE III. Summary of ANOVA Observed Levels of Significance (p) and the Post-Hoc Tukey Tests of the Yield Strength (YS), Ultimate Tensile Strength (UTS), Elongation at Break, and Izod Impact Strength

	YS (p = 0.000)			UTS (p = 0.000)		Elongation (p = 0.000)		Impact (p = 0.000)		
CPE-1		B		A		A		A		
SQXL-1		B	C		B		B			C
XL-130			C		B		B			C
XL-147	A				B		B		B	

Within each of the derived parameters, materials not connected by the same letter are significantly different.

Questions? Contact FDA/CDRH/OCE/DID at CDRH-FOISTATUS@fda.hhs.gov or 301-796-8118

Records processed under FOIA Request #2014-8015; Released by CDRH on 12-8-2015

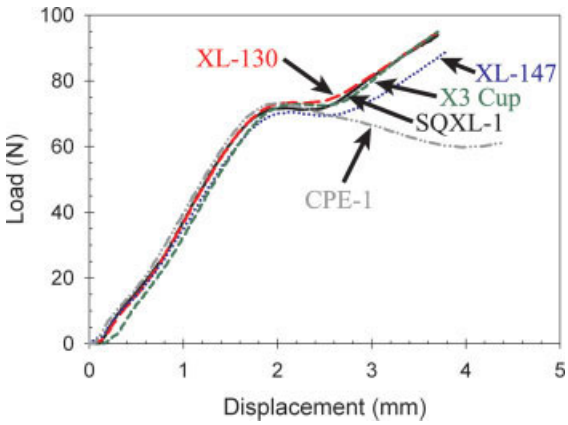

Figure 5. Average load–displacement plots from small-punch testing for the compression-molded GUR1020 UHMWPE samples subjected to various gamma-radiation doses and heat treatments.

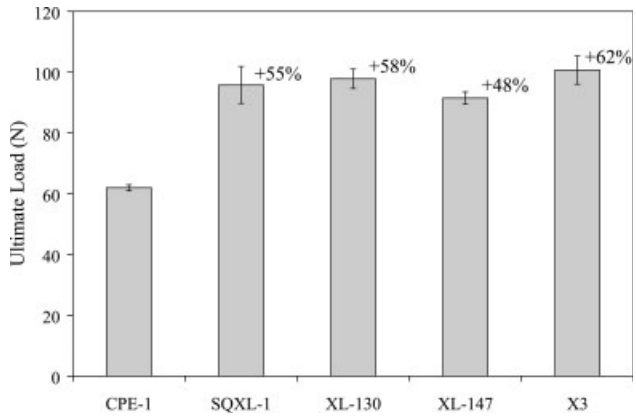

Figure 7. Plot of the ultimate load as determined by small-punch testing for the compression-molded GUR1020 UHMWPE samples subjected to various gamma-radiation doses and heat treatments. The error bars represent the standard deviations, and the percent differences are relative to CPE-1.

For crosslinked UHMWPE, the swell ratio is far below 10; therefore, the full equation should be used. This truncation results in artificially decreased crosslink densities that deviate further from the true value as the swell ratio decreases. For materials with even low levels of crosslinking (e.g., 2 Mrad dose, $q_s \approx 5$), this truncation results in a minimum of a 15% error. Moreover, the error grows dramatically with increases in the irradiation dose. At least two previous studies of sequential crosslinking clearly utilized the truncated equation to calculate the crosslink density.[18,19] Since several of these same values are also reported in other studies[13,14] of X3™, it is assumed that all of the crosslink densities reported by these authors are calculated by the truncated equation. To facilitate meaningful comparisons with the current study, those crosslink densities were converted to the correct value as determined by the full ASTM equation [Eq. (2)].

Electron Spin Resonance. In the evaluation of the FRCs (Table II), the difference between the sequential- and single-dose materials (SQXL-1 and XL-130) was statistically significant ($p = 0.004$); sequential crosslinking was found to result in an 85% greater FRC than single-dose crosslinking to the same dose. Based upon analyses of the spectra for these submelt-annealed samples (Figure 12), the appearance of six lines with hyperfine splitting of about 20 G is indicative of alkyl free radicals.[21] The unirradiated (CPE-1) and melt-annealed (XL-147) materials did not show discernible peaks in the ESR spectra (Figure 12); only system noise was observed for these materials. Therefore, the FRCs for CPE-1 and XL-147 were considered to be not detectable (ND).

For the retrieved cup, the FRC was significantly lower than SQXL-1 and similar to XL-130 and previous studies of sequentially crosslinked materials.[13,14,18,19,22] However, comparison of the ESR spectra (Figure 12) demonstrates that the type of free radicals present in the retrieval is distinctly different from those of the other materials produced for this study and subjected to accelerated aging.

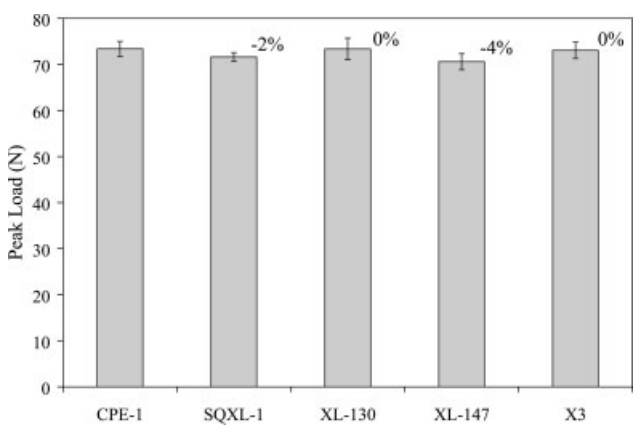

Figure 6. Plot of the peak load as determined by small-punch testing for the compression-molded GUR1020 UHMWPE samples subjected to various gamma-radiation doses and heat treatments. The error bars represent the standard deviations, and the percent differences are relative to CPE-1.

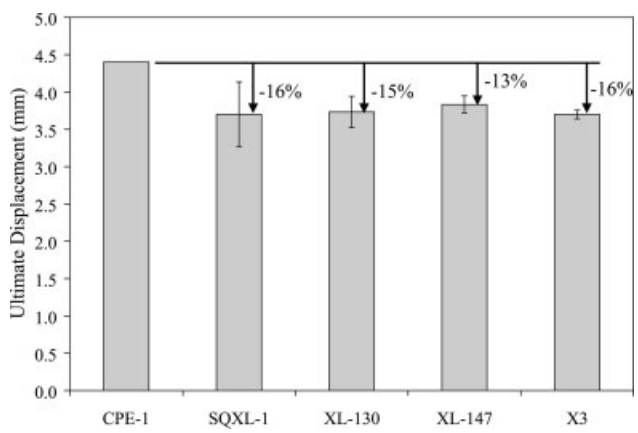

Figure 8. Plot of the ultimate displacement as determined by small-punch testing for the compression-molded GUR1020 UHMWPE samples subjected to various gamma-radiation doses and heat treatments. The error bars represent the standard deviations.

Questions? Contact FDA/CDRH/OCE/DID at CDRH-FOISTATUS@fda.hhs.gov or 301-796-8118

Records processed under FOIA Request #2014-8015; Released by CDRH on 12-8-2015

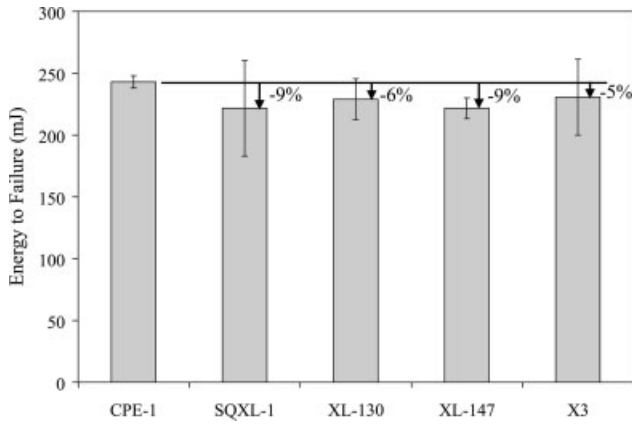

Figure 9. Plot of the energy to failure as determined by small-punch testing for the compression-molded GUR1020 UHMWPE samples subjected to various gamma-radiation doses and heat treatments. The error bars represent the standard deviations.

Oxidation. The mean maximum oxidation indices (OI_{max}) for each material are reported in Table II. Accelerated aging resulted in minimal OI_{max} of 0.02 in the virgin (CPE-1) and remelted (XL-147) materials, which denotes little to no oxidation and is within the range of the uncertainty of the test method.[23] Measurably greater oxidation was observed for both of the submelt-annealed materials (SQXL-1 and XL-130) with no statistically significant difference ($p = 0.140$) between the two, at the levels tested. The OI_{max} for SQXL-1 was much greater than those reported for X3™ (0.05-0.1).[13,14,22,24] On the other hand, the OI_{max} found for XL-130 in this study is 76% lower than that reported previously ($1.1 \leq OI_{max} \leq 1.3$) for a similarly processed material.[13,14,22]

Analysis of the oxidation present in the as-received X3™ cup by FTIR showed that minimal oxidation had occurred in the component. The OI_{max} was 0.10 ± 0.03 (Table II), which is minimal and near the noise level of the measurement technique. In every case, the OI_{max} in each profile was at the exposed surface.

Effects of Tensile-Sample Thickness

The results from tensile testing with Type IV samples of various thicknesses are summarized in Table V. The power regression model was the best fit for all of the materials and mechanical properties (Tables VI and VII), with the exception of EL for CPE-2. For CPE-2, the YS and UTS were found to be inversely correlated with sample thickness; more than 90% of the variability in those properties was explained by the changes in the sample thickness (Table VI). However, none of these trends were found to be statistically significant ($p \geq 0.163$) at the levels tested in this study. For SQXL-2, UTS and elongation were inversely correlated with sample thickness (Table VII). More than 88% of the variabilities in those properties were explained by the changes in sample thickness. Only the UTS for SQXL increased by a statistically significant

TABLE IV. Summary of ANOVA Observed Levels of Significance (*p*) and the Post-Hoc Tukey Tests of the Metrics Derived Through the Small-Punch Tests and DSC Experiments

	Small-Punch Testing				DSC		
	Peak Load ($p = 0.267$)	Ultimate Load ($p = 0.000$)	Ultimate Displacement ($p = 0.029$)	Energy to Failure ($p = 0.797$)	T_{OM} ($p = 0.000$)	T_{PM} ($p = 0.000$)	%X ($p = 0.000$)
CPE-1	A	A	B	A	B	A	B
SQXL-1	A	B	A	A	C	B	C
XL-130	A	B	A B	A	C	B	C
XL-147	A	B	A B	A	A	A	A
X3™	A	B	A	A		D	C

Within each of the derived parameters, materials not connected by the same letter are significantly different.

Questions? Contact FDA/CDRH/OCE/DID at CDRH-FOISTATUS@fda.hhs.gov or 301-796-8118

Records processed under FOIA Request #2014-8015; Released by CDRH on 12-8-2015

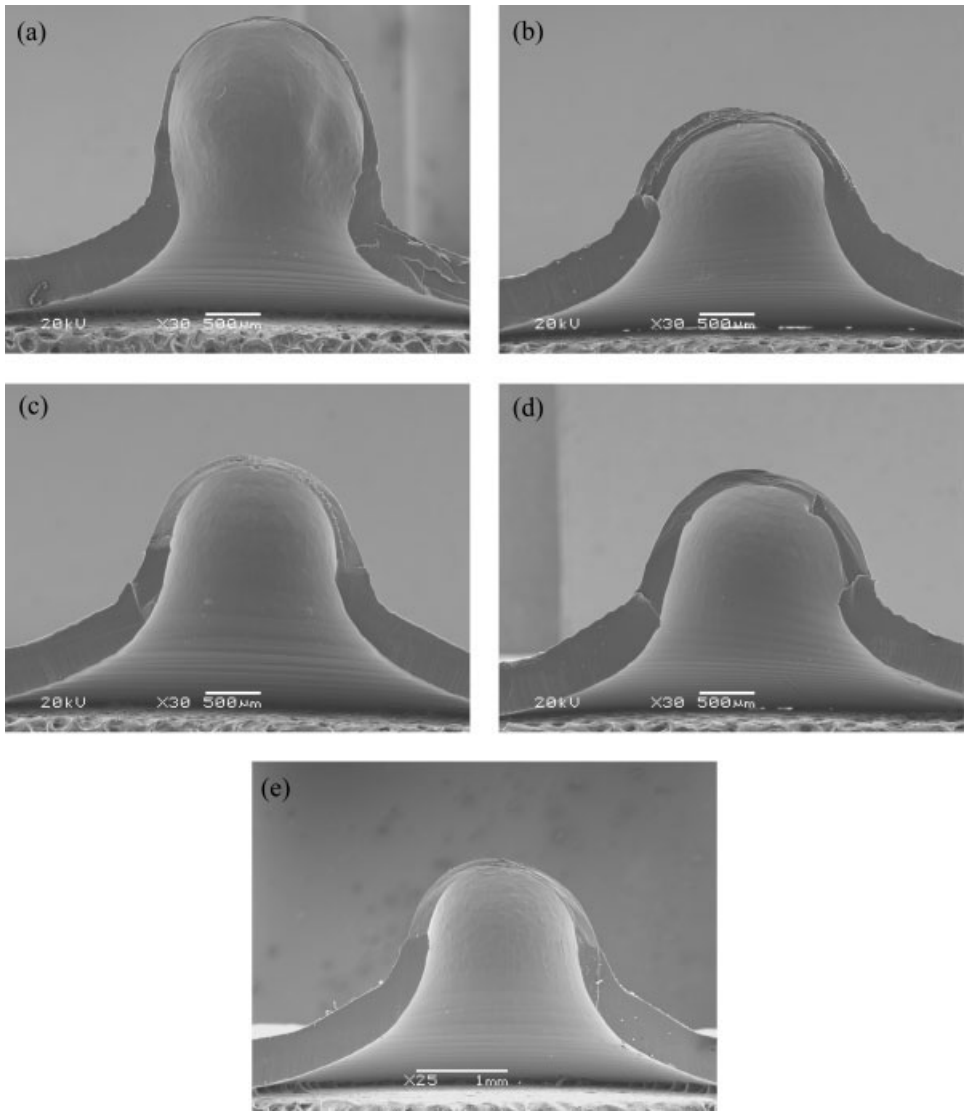

Figure 10. SEM photomicrographs of the cross-sections of the small-punch-test samples after testing. (a) CPE-1, (b) SQXL-1, (c) XL-130, (d) XL-147, and (e) X3™ retrieval.

amount ($p < 0.001$) with a decrease in sample thickness to 1 mm.

Based upon these correlations, the UTS is the primary property that is affected by changes in the sample thickness. A reduction of thickness from 3 to 1 mm resulted in a 21% increase in UTS for SQXL-2, as shown in Figure 13. In contrast, the virgin material (CPE-2) was less sensitive to the reductions in thickness and exhibited a 13% increase ($p = 0.163$) in UTS. Examination of the engineering stress-engineering strain plots demonstrated that the increases in mechanical properties are primarily due to increased strain hardening with decreasing thickness.

DISCUSSION

This study was undertaken to investigate the effect of crosslinking UHMWPE in a stepped sequence to the final desired dose and to compare the results to single-dose crosslinking. Numerous properties were examined, with the exception of wear resistance. The results of this study are summarized below.

The mechanical properties of submelt-annealed UHMWPE derived from bulk and SPT were found to be indifferent to single- or sequential-dose irradiation. None of the mechanical-test metrics showed measurable effects of sequential irradiation. Furthermore, select mechanical properties (i.e., UTS, elongation, and impact strength) were measurably decreased for all forms of crosslinked UHMWPE compared to virgin UHMWPE. These findings are in conflict with previous studies of sequential crosslinking[13,14,18,19,25] and product advertisements[26] for commercially available products that utilize sequential crosslinking methods (X3™, Stryker, Mahwah, NJ). Although the mean YS and elongation determined in the current study are approximately equivalent to those previously published val-

Questions? Contact FDA/CDRH/OCE/DID at CDRH-FOISTATUS@fda.hhs.gov or 301-796-8118

Records processed under FOIA Request #2014-8015; Released by CDRH on 12-8-2015

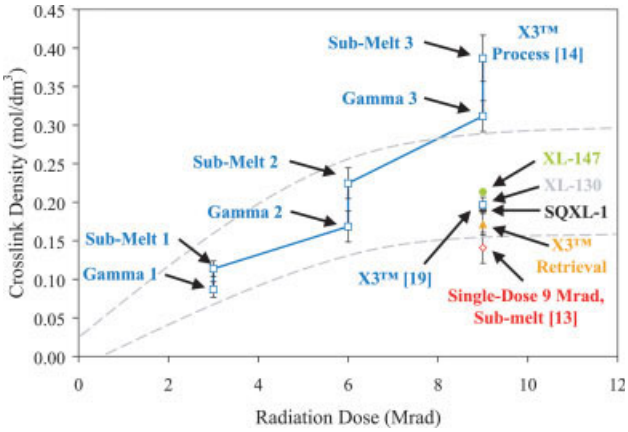

Figure 11. Plot of crosslink density as a function of radiation dose for the retrieved X3™ acetabular cup and the additional materials produced from compression-molded GUR1020 UHMWPE for this study. Data for X3™ reported in the literature (open symbols) are also plotted for comparison.[13,14,18,19] Based upon a survey of the literature, the typical range of crosslink densities is approximated by the dashed lines.

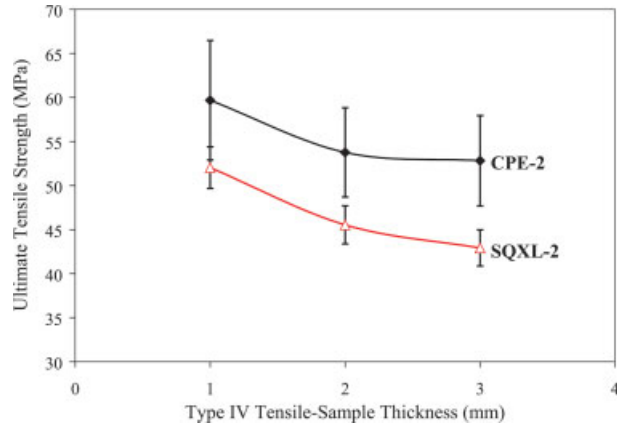

Figure 13. Mean ultimate tensile strengths (UTS) for the virgin GUR1020 (CPE-2) and sequentially crosslinked GUR1020 (SQXL-2) tested with specimen thicknesses of 1, 2, and 3 mm.

ues, the UTS was considerably lower in this study. It is not clear if these previous studies used the same starting virgin UHMWPE in manufacturing the various formulations of crosslinked UHMWPE. In contrast, it should be noted that the present study was conducted with material produced from single resin and production lots, thereby eliminating resin-to-resin and compression-molding variabilities.

The findings of this study are consistent with the understanding that crosslinking and the subsequent properties are primarily dominated by the total, cumulative irradiation dose. Upon crosslinking, the new UHMWPE structure limits the strain-induced chain alignment that accompanies mechanical loading of the material. Because the molecular chains are constrained, applied strains are accommodated by chain fracture, which results in a net decrease of the UTS and EL. The same mechanism is also responsible for the observed reduction of toughness (i.e., impact strength and energy to failure) upon crosslinking. It is important to note that the published studies for X3™ UHMWPE report a reduction in EL that is similar to that found in the present study. Additionally, Lancin et al.[24] reported an Izod impact strength of 78 kJ/m^2 for the X3™ material. This value is measurably lower than the impact strength of virgin, compression-molded GUR1020 UHMWPE ($\geq$140 kJ/m^2).[27,28] Therefore, previously published results of elongation and impact strength for X3™ are consistent with the present study in that these metrics are measurably reduced upon sequential crosslinking of UHMWPE.

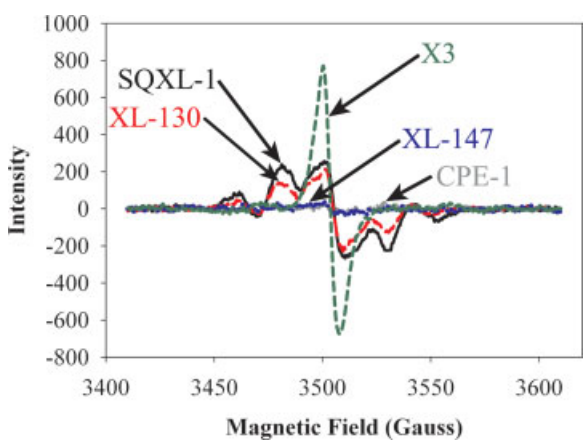

Figure 12. Representative electron spin resonance (ESR) spectra for the compression-molded GUR1020 UHMWPE samples subjected to various gamma-radiation doses and heat treatments and the retrieved X3™ cup.

This study confirmed that certain mechanical properties are affected by the temperature of postirradiation thermal treatments, namely annealing below the melt temperature and remelting above the melt temperature. Remelting showed measurably greater elongation and impact strength, while annealing below the melt showed a trend towards greater YS and UTS.

Because the mechanical properties of UHMWPE are directly influenced by the molecular structure of the material, this study also measured thermophysical and molecular-network parameters for sequential- and single-dose-crosslinked materials. Similar to the mechanical properties discussed above, this study found that the temperatures at the onset of melting (T_{OM}) and at the peak melt (T_{PM}), along with the percent crystallinities (%X), were not different for the sequential- and single-dose-crosslinked materials. Furthermore, T_{OM}, T_{PM}, and %X for both of these materials were measurably different from those of the original, virgin UHMWPE. The crosslink density and molecular weight between crosslinks of sequentially crosslinked material were found to be the same as the submelt-annealed, single-dose material. These observations lend further credence to the mechanical-property results that showed sequential irradiation and annealing had no effect compared to a single-dose process.

Questions? Contact FDA/CDRH/OCE/DID at CDRH-FOISTATUS@fda.hhs.gov or 301-796-8118

Records processed under FOIA Request #2014-8015; Released by CDRH on 12-8-2015

TABLE V. Mean ± Standard Deviation Mechanical Properties of the Virgin GUR1020 (CPE-2) and Sequentially Crosslinked GUR1020 (SQXL-2) Materials Tested With Specimen Thicknesses of 1, 2, or 3 mm

Material	Sample Thickness (mm)	Young's Modulus (MPa)	Yield Strength (MPa)	Ultimate Tensile Strength (MPa)	Elongation at Break (%)
CPE-2	1	472 ± 19	23.2 ± 0.3	59.7 ± 6.8	476 ± 58
	2	525 ± 30	23.0 ± 0.3	53.8 ± 5.1	485 ± 59
	3	475 ± 32	22.9 ± 0.3	52.8 ± 5.1	470 ± 45
SQXL-2	1	502 ± 41	23.0 ± 0.4	52.0 ± 2.4	282 ± 14
	2	524 ± 32	23.3 ± 0.4	45.5 ± 2.2	264 ± 14
	3	493 ± 21	23.0 ± 0.6	42.9 ± 2.1	263 ± 11

Comparison of the crosslink densities determined in this study with those from the literature for similar materials further verifies this study. The crosslink densities for the materials produced in this study (SQXL, XL-130, and XL-147) are within this expected range ($0.150 \leq v_d \leq 0.260$) for materials irradiated to doses of 9 Mrad (Figure 11).[27] The mean crosslink density for the X3™ retrieval was determined to be 0.171 mol/dm^3, which is on the lower end of the range expected for a material crosslinked with a 9 Mrad dose. These values are in reasonably good agreement with the corrected crosslink density of 0.197 mol/dm^3 that is reported in a previous study of sequential crosslinking in the literature.[18] On the other hand, these findings are dramatically different from several other studies[13,14] in which the X3™ process reportedly resulted in a corrected crosslink density (v_d = 0.387 mol/dm^3) that was 2.7 times greater than the value reported for a single-dose material and 38% higher than the crosslink density reported for a material irradiated to 20 Mrad.[29] In these previous studies, the crosslink density of X3™ is compared to that of a 9 Mrad, single-dose material (v_d = 0.141 mol/dm^3), which is slightly lower than expected for a 9 Mrad material and comparable to the values reported in other studies for materials crosslinked with doses of ~3–5 Mrad.[27,29,30] These abnormally high (X3™) and low (single-dose 9 Mrad) crosslink densities result in dramatic differences that the authors attribute directly to the sequential crosslinking process. However, these values are difficult to reconcile based upon comparisons with the majority of the studies in the literature and the results in the current study.

When striving to duplicate previously published experimental results, the results can often be confounded by not knowing the nuances and minute details of all of the experiments and processes. This concern was ameliorated in this study by the commercial availability of the end product of that previous research on sequential crosslinking in the form of X3™ arthroplasty components. An X3™ acetabular cup retrieved from a patient was available for testing, the results of which can be compared directly with the sequentially crosslinked UHMWPE produced in this study. The acetabular cup size is such that it was amenable only to mechanical testing through SPT. The bulk, uniaxial mechanical properties of the SQXL-1 and XL-130 materials were shown to be equivalent to each other and substantially different from both the virgin material (CPE) and the reported values for X3.[13,24] In SPT, the mechanical properties of SQXL-1 and XL-130 were again found to be equivalent to each other and substantially different from the virgin material (CPE). Because the small-punch-test behavior of the retrieved X3™ cup was virtually identical to SQXL-1 and XL-130 (Figure 5), it is reasonable to conclude that X3™ would have bulk deformation behavior similar to these crosslinked materials. In addition, the thermophysical and molecular-network parameters were measured for the retrieved X3™ cup and were virtually identical to the sequential- and single-dose-crosslinked UHMWPE materials produced in this study.

In UHMWPE orthopedic implants, it is desirable not only to have advantageous mechanical and wear properties, but also to retain them over long durations *in vivo*. This stability is typically measured by determining the residual FRC in the material. It is well known that remelting is vastly more effective in quenching the free radicals than annealing below the melt temperature. The present study confirmed this. Furthermore, no advantage was found in se-

TABLE VI. Best-Fit Regression Models and the Associated Coefficients of Determination (r^2) for the Correlations Between Mechanical Properties and Tensile-Sample Thickness for the Virgin GUR1020 (CPE-2)

Mechanical Property	Model	r^2	p
YS	Power	0.905	0.237
UTS	Power	0.944	0.163
EL	Exponential	0.150	0.908

The observed levels of significance (p) were determined by ANOVA.

TABLE VII. Best-Fit Regression Models and the Associated Coefficients of Determination (r^2) for the Correlations Between Mechanical Properties and Tensile-Sample Thickness for the Sequentially Crosslinked GUR1020 (SQXL-2)

Mechanical Property	Model	r^2	p
YS	Power	0.009	0.488
UTS	Power	0.995	<0.001
EL	Power	0.880	0.066

The observed levels of significance (p) were determined by ANOVA.

Questions? Contact FDA/CDRH/OCE/DID at CDRH-FOISTATUS@fda.hhs.gov or 301-796-8118

Records processed under FOIA Request #2014-8015; Released by CDRH on 12-8-2015

quential irradiation and annealing, compared to single-dose irradiation and annealing.

The presence of free radicals at similar levels was also verified in the X3™ retrieval. However, it should be noted that the extent of exposure to oxygen for the retrieved X3™ cup is unknown, and that the effects of this time on the FRC are unknown as well. The ESR spectra for the retrieved cup were distinctly different from those of the other materials analyzed. While the other materials exhibited primary free radicals, the retrieval was found to have a singlet resonance line that is the result of reactions of the primary radicals with oxygen to produce an oxygen-induced radical (OIR). Depending upon the study referenced, this terminal radical has been defined as a polyenyl-type radical,[21] a peroxy radical,[31,32] or multiple radical types that remain undetermined.[33]

Because a measurable FRC was found in all of the submelt-annealed materials (i.e., the sequential- and single-dose UHMWPE materials and the X3™ retrieval), oxidation is possible with time and exposure to oxygen.[34,35] This potential for oxidation was observed in both of the submelt-annealed materials produced for this study, independent of the method of irradiation (i.e., sequential- or single-dose). Limited oxidation was also measured in the retrieved cup. However, conclusions about the extent of oxidation measured in the retrieved cup are difficult, because its exact history of oxygen exposure is unknown. In contrast to these submelt-annealed materials, the remelted material produced for this study exhibited a nondetectable level of free radicals and no measurable oxidation after accelerated aging. As a result, it can be anticipated that this material will remain stable *in vivo*, and the mechanical and tribological properties will not degrade with time.

For some perspective on the clinical implications of these FRCs, the level of free radicals measured in the X3™ cup is comparable to those reported for both gamma-in-air-sterilized materials[36] and Crossfire™,[36,37] another submelt-annealed, highly crosslinked UHMWPE (Stryker, Mahwah, NJ). Oxidation of gamma-in-air-sterilized components has been thoroughly documented as detrimental to the tribological and mechanical properties of knee components in particular.[38,39] With Crossfire, emerging clinical experience[35,40–42] is demonstrating that this level of residual free radicals leads to measurable levels of oxidation in as little as several years *in vivo*.

The metastability of the retrieved X3™ cup with measurable free radicals and the prior history of oxygen exposure have the potential to influence the metrics derived in this study. On the other hand, the low level of oxidation measured in the retrieved cup suggests that few changes had taken place in the relatively short duration of, at most, 29 months between manufacture and revision surgery. Furthermore, the small-punch tests samples were extracted from the core regions of the cup, which are less likely than the near-surface regions to be influenced by the environment. The sum of these findings confirms that the sequentially crosslinked material produced for this study according to the teachings in the literature is a reasonable representation of the commercially available product.

Previous studies[13,14,18,19] reported that sequential irradiation and annealing have a profound, beneficial effect on the mechanical properties, particularly the UTS. The present study was not able to duplicate these results. However, it should be noted that these previous studies reported that sequential crosslinking did indeed result in greatly reduced elongation to break and impact strength. The discrepancy in UTSs between this study and the published literature warrants examination, because UTS is a commonly reported metric of UHMWPE materials for use as a medical implant. Mechanical testing for the determination of UTS is typically conducted according to ASTM D638 utilizing Type IV samples. However, this standard does not specify a particular thickness for the samples, only a range of 4 mm or less. At the same time, this standard acknowledges that variations in the sample thickness "may influence the test results." It has been confirmed that all previous reports on sequential crosslinking utilized samples with thicknesses of 1 mm.[15,43] On the other hand, the materials produced in the present study were tested with sample thicknesses of 3.0 ± 0.05 mm. To elucidate the effect of these differences in sample thickness, additional mechanical testing was conducted with Type IV samples of varying thickness. The UTS of sequentially crosslinked UHMWPE was found to be measurably more sensitive to sample thickness than virgin UHMWPE.

Although this effect is not fully understood, it may be related to a higher probability of critical sized flaws in thicker samples. The additional constraint of more material in the thicker samples may also be influential in these results. However, the large changes in UTS with little to no change in EL suggest that the mechanism is not due to a higher probability of flaws in a thicker sample. If this were the operating mechanism, one would expect both UTS and elongation to decrease with increasing thickness. Notwithstanding these considerations, it is possible that the UTS results reported for X3™ in the literature are confounded by the choice of 1 mm-thick tensile samples.

CONCLUSIONS

Based upon a well-controlled study with the same starting material, there is no apparent benefit of sequential crosslinking over crosslinking by single dose in any of the mechanical, thermophysical, physical or oxidative properties evaluated in this study. In contrast, the soak temperature of the postirradiation heat treatment was more influential and exhibited statistically significant effects on the stability, structure, and properties of the resultant material. This study confirms that irradiation always results in decreases in tensile strength, elongation, and impact strength, as compared to unirradiated, virgin UHMWPE. Furthermore, this study confirmed that submelt annealing leaves residual free radicals in the materials, independent of whether the mate-

Questions? Contact FDA/CDRH/OCE/DID at CDRH-FOISTATUS@fda.hhs.gov or 301-796-8118

Records processed under FOIA Request #2014-8015; Released by CDRH on 12-8-2015

rial was crosslinked by the sequential- or single-dose methods. As a result, oxidation of these materials is possible with time and exposure to oxygen.

These results were confirmed by characterization of a retrieved, sequentially crosslinked (X3^{TM}) retrieval. Evidence of strength preservation, elimination of free radicals, or elevated crosslink density was not observed for this explanted X3^{TM} component.

Examination of the effect of tensile sample thickness on the resultant properties demonstrated that the UTS of UHMWPE can be elevated by conducting tensile tests with thin specimens. Therefore, the purported benefits of sequential crosslinking may, in actuality, be an artifact of the sample thickness.

REFERENCES

1. McKellop H, Shen F, Lu B, Campbell P, Salovey R. Development of an extremely wear-resistant ultra high molecular weight polyethylene for total hip replacements. J Orthop Res 1999;17:157–167.
2. Scott M, Morrison M, Mishra SR, Jani S. Particle analysis for the determination of UHMWPE wear. J Biomed Mater Res B 2005;73:325–337.
3. Wroblewski BM, Siney PD, Dowson D, Collins SN. Prospective clinical and joint simulator studies of a new total hip arthroplasty using alumina ceramic heads and cross-linked polyethylene cups. J Bone Joint Surg Br 1996;78:280–285.
4. Oonishi H, Kadoya Y. Wear of high-dose gamma-irradiated polyethylene in total hip replacements. J Orthop Sci 2000;5: 223–228.
5. Oonishi H, Saito M, Kadoya Y. Wear of high-dose gamma irradiated polyethylene in total joint replacement—Long term radiological evaluation. In: Transactions of the 44th Annual Meeting of the Orthopaedic Research Society, New Orleans, LA, March 16–19, 1998;97:17.
6. Li MG, Zhou ZK, Wood DJ, Rohrl SM, Ioppolo JL, Nivbrant B. Low wear with high-cross linked polyethylene especially in combination with oxinium heads. A RSA evaluation. In: Transactions of the 52nd Annual Meeting of the Orthopaedic Research Society, Chicago, IL, March 19–22, 2006. p 0643.
7. Digas G, Karrholm J, Thanner J, Malchau H, Herberts P. The Otto Aufranc Award. Highly cross-linked polyethylene in total hip arthroplasty: randomized evaluation of penetration rate in cemented and uncemented sockets using radiostereometric analysis. Clin Orthop Relat Res 2004;429:6–16.
8. Dorr LD, Wan Z, Shahrdar C, Sirianni L, Boutary M, Yun A. Clinical performance of a Durasul highly cross-linked polyethylene acetabular liner for total hip arthroplasty at five years. J Bone Joint Surg Am 2005;87:1816–1821.
9. Bragdon CR, Kwon YM, Geller JA, Greene ME, Freiberg AA, Harris WH, Malchau H. Minimum 6-year followup of highly cross-linked polyethylene in THA. Clin Orthop Relat Res 2007;465:122–127.
10. Oral E, Malhi AS, Muratoglu OK. Mechanisms of decrease in fatigue crack propagation resistance in irradiated and melted UHMWPE. Biomaterials 2006;27:917–925.
11. Ries MD, Pruitt L. Effect of cross-linking on the microstructure and mechanical properties of ultra-high molecular weight polyethylene. Clin Orthop Relat Res 2005;440:149–156.
12. Lewis G. Properties of crosslinked ultra-high-molecular-weight polyethylene. Biomaterials 2001;22:371–401.
13. Dumbleton JH, D'Antonio JA, Manley MT, Capello WN, Wang A. The basis for a second-generation highly crosslinked UHMWPE. Clin Orthop Relat Res 2006;453:265–271.
14. Wang A, Zeng H, Yau SS, Essner A, Manley M, Dumbleton J. Wear, oxidation and mechanical properties of a sequentially irradiated and annealed UHMWPE in total joint replacement. J Phys D Appl Phys 2006;39:3213–3219.
15. Dumbleton JH, Manley MT. Sequential irradiation annealed polyethylene: The next generation of highly crosslinked polyethylene. In: 72nd Annual Meeting of the American Academy of Orthopaedic Surgeons, Washington, DC, February 23–27, 2005. p SE052.
16. Wang A, Dumbleton JH, Essner A, Yau SS. Sequentially cross-linked polyethylene. US Patent 20050043431, 2005.
17. Kurtz SM, Pruitt LA, Jewett CW, Foulds JR, Edidin AA. Radiation and chemical crosslinking promote strain hardening behavior and molecular alignment in ultra high molecular weight polyethylene during multi-axial loading conditions. Biomaterials 1999;20:1449–1462.
18. Wang A, Essner A, Yau SS, Manley MT, Dumbleton JH. Sequential irradiation annealing: A process for the next generation of highly crosslinked polyethylenes. In: 5th Annual Meeting of the Combined Orthopaedic Research Society, Banff, Canada, October 10–13, 2004. p 77.
19. Yau SS, Wang A, Essner A, Manley MT, Dumbleton JH. Sequential irradiation and annealing of highly crosslinked polyethylenes: Resist oxidation without sacrificing physical/mechanical properties. In: Transactions of the 51st Annual Meeting of the Orthopaedic Research Society, Washington, DC, February 20–23, 2005. p 1670.
20. Flory PJ. Principles of Polymer Chemistry. Ithaca, NY: Cornell University Press; 1953.
21. Naheed N, Jahan MS, Ridley M. Measurements of free radicals over a period of 4.5 years in gamma-irradiated ultra-high molecular weight polyethylene. Nucl Instrum Methods Phys Res B 2003;208:204–209.
22. Essner A, Wang A, Yau SS, Manley M, Dumbleton J. Sequential irradiation and annealing overcomes drawbacks with current highly crosslinked ultra high molecular weight polyethylenes (UHMWPE). In: 7th Congress of the European Federation of National Associations of Ortopaedics and Traumatology (EFORT), Lisbon, Portugal, June 4–7, 2005. p F90.
23. ASTM. ASTM F2102 Standard Guide for Evaluating the Extent of Oxidation in Ultra-High-Molecular-Weight Polyethylene Fabricated Forms Intended for Surgical Implants. West Conshohocken, PA: ASTM International; 2006.
24. Lancin P, Yau SS, Essner A, Wang A, Schmalzried T. Critical properties and wear performance of 1900 direct compression molded versus crosslinked UHMWPE. In: Transactions of the 53rd Annual Meeting of the Orthopaedic Research Society, San Diego, CA, February 11–14, 2007. p 1876.
25. Essner A, Yau SS, Schmidig G, Wang A, Dumbleton JH, Manley MT. Acetabular liner functional fatigue performance of crosslinked UHMWPE. In: Transactions of the 51st Annual Meeting of the Orthopaedic Research Society, Washington, DC, February 20–23, 2005. p 245.
26. Stryker X3 Advertisement. J Bone Joint Surg Am 2006; 88A(1).
27. Greer KW, King RS, Chan FW. The effects of raw material, irradiation dose, and irradiation source on crosslinking of UHMWPE. In: Kurtz SM, Gsell R, Martell J, editors. Crosslinked and Thermally Treated Ultra-High Molecular Weight Polyethylene for Joint Replacements, ASTM STP 1445. West Conshohocken, PA: ASTM International; 2003. pp 209–220.
28. Wolf C, Krivec T, Blassnig J, Lederer K, Schneider W. Examination of the suitability of alpha-tocopherol as a stabilizer for ultra-high molecular weight polyethylene used for articu-

Questions? Contact FDA/CDRH/OCE/DID at CDRH-FOISTATUS@fda.hhs.gov or 301-796-8118

Records processed under FOIA Request #2014-8015; Released by CDRH on 12-8-2015

lating surfaces in joint endoprostheses. J Mater Sci Mater Med 2002;13:185–189.
29. Muratoglu OK, Bragdon CR, O'Connor DO, Jasty M, Harris WH, Gul R, McGarry F. Unified wear model for highly cross-linked ultra-high molecular weight polyethylenes (UHMWPE). Biomaterials 1999;20:1463–1470.
30. Wang A. A unified theory of wear for ultra-high molecular weight polyethylene in multi-directional sliding. Wear 2001; 248:38–47.
31. Jahan MS, Wang C, Schwartz G, Davidson JA. Combined chemical and mechanical effects on free radicals in UHMWPE joints during implantation. J Biomed Mater Res A 1991;25:1005–1017.
32. Nakamura K, Ogata S, Ikada Y. Assessment of heat and storage conditions on gamma-ray and electron beam irradiated UHMWPE by electron spin resonance. Biomaterials 1998; 19:2341–2346.
33. Jahan MS, Durant J. Investigation of the oxygen-induced radicals in ultra-high molecular weight polyethylene. Nucl Instrum Methods Phys Res B 2005;236:166–171.
34. Currier BH, Currier JH, Mayor MB, Lyford KA, Van Citters DW, Collier JP. In vivo oxidation of gamma-barrier-sterilized ultra-high-molecular-weight polyethylene bearings. J Arthroplasty 2007;22:721–731.
35. Currier BH, Mayor MB, Currier JH, Lyford KA, Collier JP. Crossfire retrievals—What can we learn? In: Transactions of the 51st Annual Meeting of the Orthopaedic Research Society, Washington, DC, February 20–23, 2005. p 1182.
36. Muratoglu OK, Merrill EW, Bragdon CR, O'Connor D, Hoeffel D, Burroughs B, Jasty M, Harris WH. Effect of radiation, heat, and aging on in vitro wear resistance of polyethylene. Clin Orthop Relat Res 2003;(417):253–262.
37. Kurtz SM, Manley M, Wang A, Taylor S, Dumbleton J Comparison of the properties of annealed crosslinked (Crossfire) and conventional polyethylene as hip bearing materials. Bull Hosp Jt Dis 2002;61(1/2):17–26.
38. White SE, Paxson RD, Tanner MG, Whiteside LA. Effects of sterilization on wear in total knee arthroplasty. Clin Orthop Relat Res 1996;(331):164–171.
39. Williams IR, Mayor MB, Collier JP. The impact of sterilization method on wear in knee arthroplasty. Clin Orthop Relat Res 1998;(356):170–180.
40. Bhattacharyya S, Doherty AM, Wannomae KK, Oral E, Freiberg AA, Harris WH, Muratoglu OK. Severe in vivo oxidation in a limited series of retrieved highly-crosslinked UHMWPE acetabular components with residual free radicals. In: Transactions of the 50th Annual Meeting of the Orthopaedic Research Society, San Francisco, CA, March 7–10, 2004. p 0276.
41. Kurtz SM, Hozack WJ, Purtill JJ, Marcolongo M, Kraay MJ, Goldberg VM, Sharkey PF, Parvizi J, Rimnac CM, Edidin AA. 2006 Otto Aufranc Award Paper: Significance of in vivo degradation for polyethylene in total hip arthroplasty. Clin Orthop Relat Res 2006;453:47–57.
42. Wannomae KK, Bhattacharyya S, Freiberg A, Estok D, Harris WH, Muratoglu O. In vivo oxidation of retrieved cross-linked ultra-high-molecular-weight polyethylene acetabular components with residual free radicals. J Arthroplasty 2006;21: 1005–1011.
43. Wang A. Forum discussion. In: Third UHMWPE International Meeting, Madrid, Spain, September 14–15, 2007.

Questions? Contact FDA/CDRH/OCE/DID at CDRH-FOISTATUS@fda.hhs.gov or 301-796-8118

Records processed under FOIA Request #2014-8015; Released by CDRH on 12-8-2015

Available online at www.sciencedirect.com
SCIENCE DIRECT®
ELSEVIER
Biomaterials 25 (2004) 5515–5522
Biomaterials
www.elsevier.com/locate/biomaterials

α-Tocopherol-doped irradiated UHMWPE for high fatigue resistance and low wear

Ebru Oral[a,b], Keith K. Wannomae[a], Nathaniel Hawkins[a], William H. Harris[a,b], Orhun K. Muratoglu[a,b,*]

[a] *Orthopaedic Biomechanics and Biomaterials Laboratory, Department of Orthopaedic Surgery, Massachusetts General Hospital, 55 Fruit Street, GRJ 1206, Boston, MA 02114, USA*
[b] *Harvard Medical School, Boston, MA, USA*

Received 11 September 2003; accepted 19 December 2003

Abstract

Longevity of total joints has been compromised by wear and fatigue of ultrahigh molecular weight polyethylene (UHMWPE) components. Crosslinking reduces UHMWPE wear, but combined with postirradiation melting, also reduces its fatigue strength, therefore limiting its use in high-stress applications. We hypothesized that a lipophilic antioxidant (α-tocopherol, α-T) can protect UHMWPE against oxidation eliminating the need for postirradiation melting of crosslinked UHMWPE and improve its fatigue strength. To test these hypotheses, 65- and 100-kGy irradiated, α-T-doped and subsequently γ-sterilized UHMWPE were used. (I) α-T-doped irradiated UHMWPEs showed significantly lower oxidation levels (0.48 ± 0.25 and 0.44 ± 0.06) compared to 100-kGy irradiated UHMWPE (3.74 ± 0.16) after 5 weeks of accelerated aging at 80°C in air. (II) Wear rate of α-T-doped irradiated UHMWPE (1.9 ± 0.5, and 0.9 ± 0.1 mg/million cycles (MC) for 65- and 100-kGy irradiated UHMWPE, respectively) were comparable to that of 100-kGy irradiated/melted UHMWPE (1.1 ± 0.7 mg/million cycles). (III) The stress intensity factor at crack inception (ΔK_i) of 100-kGy irradiated UHMWPE increased significantly upon doping with α-T from 0.74 to 0.87 MPa m$^{1/2}$ ($p < 0.01$). The ΔK_i for the 100-kGy irradiated and melted UHMWPE, currently in clinical use, was 0.55 MPa m$^{1/2}$. Doping with α-T eliminated the need for postirradiation melting to protect irradiated UHMWPE against long-term oxidation. The fatigue strength was improved by 58% for α-T-doped 100-kGy irradiated UHMWPE compared to irradiated and melted UHMWPE. The increase in oxidative stability of α-T-doped UHMWPE is attributed to the ability of α-T to react with peroxy free radicals on lipid chains and arrest the oxidation reactions. The improved fatigue strength is attributed to the increase in plasticity of UHMWPE due to the lipophilic nature of α-T.
© 2003 Elsevier Ltd. All rights reserved.

Keywords: UHMWPE; Arthroplasty; Fatigue; Antioxidant; Lipid

1. Introduction

Ultrahigh molecular weight polyethylene (UHMWPE) has been the material of choice for the load-bearing, articulating surface for the metal/articular pair used in total joint arthroplasty [1]. Despite high long-term success rates for such reconstructions, wear and fatigue damage of UHMWPE components can limit the in vivo longevity of the joint replacement.

Adhesive/abrasive wear is the primary cause of failure in total hips as it is a source of particulate debris leading to peri-prosthetic osteolysis [2]. In total knees, implant failure is caused primarily by fatigue damage secondary to oxidation of UHMWPE components [3]. Peri-prosthetic osteolysis in total knees is also a growing problem and plays a secondary role in implant failure [4–6].

Radiation crosslinking and melting increases the wear and oxidation resistance of UHMWPE [7–9]. Ionizing radiation creates free radicals that recombine to form crosslinks. Some of these radicals ('residual free radicals') are trapped, mostly in the crystalline domains. The residual free radicals react with diffused oxygen and consequently cause oxidative chain scission and embrittlement. Typically, UHMWPE is melted subsequent to

*Corresponding author. Orthopaedic Biomechanics and Biomaterials Laboratory, Massachusetts General Hospital, 55 Fruit Street, GRJ 1206, Boston, MA 02114, USA. Tel.: +1-617-726-3869; fax: +1-617-726-3883.
E-mail address: orhun@alum.mit.edu (O.K. Muratoglu).

0142-9612/$ - see front matter © 2003 Elsevier Ltd. All rights reserved.
doi:10.1016/j.biomaterials.2003.12.048
Questions? Contact FDA/CDRH/OCE/DID at CDRH-FOISTATUS@fda.hhs.gov or 301-796-8118

Records processed under FOIA Request #2014-8015; Released by CDRH on 12-8-2015

irradiation to recombine the residual free radicals. However, radiation crosslinking and melting reduces the fatigue strength of UHMWPE, thereby limiting the use of highly crosslinked UHMWPE to low-stress applications. Therefore, methods other than postirradiation melting are needed to provide long-term oxidative stability and prevent loss of crystallinity. Also, improvement of the fatigue strength of highly crosslinked UHMWPE would allow its use in high-stress applications.

High toughness and high fatigue strength of polymers are attributed to energy absorbing mechanisms such as cavitation and plastic deformation [10]. A fatigue crack starts and propagates when the localized stress at the crack tip cannot be dissipated through energy absorbing mechanisms in the process zone ahead of the crack tip. Micromechanical processes, such as cavitation and plastic deformation are usually present in this process zone, thereby decreasing the localized stresses at the crack tip and resisting crack growth.

The major energy absorbing mechanism in UHMWPE is the plastic deformation of the crystalline domains (crystal plasticity), which depends on ductility and crystallinity. We postulate that crosslinking and melting decrease fatigue strength of UHMWPE by a combination of two separate factors. First, the crosslinks formed during irradiation reduce the chain mobility of UHMWPE, decreasing its ductility [8]. Second, the postirradiation melting decreases the crystallinity, which is likely caused by the decrease in amorphous content of the polymer available for recrystallization after crosslinking. This decrease in crystallinity might lead to a decrease in fatigue strength [11].

We hypothesized that the incorporation of an antioxidant would prevent oxidation and could be used instead of postirradiation melting to protect UHMWPE against oxidation. We further hypothesized that a lipophilic antioxidant would locally plasticize the irradiated UHMWPE, improving its fatigue strength.

We used α-tocopherol (also called α-T, vitamin E) as the lipophilic antioxidant compound (Fig. 1). α-T is biocompatible and is lipophilic owing to its phytyl tail, providing favorable interactions with UHMWPE. Furthermore, it is an antioxidant which can serve the purpose of eliminating long-term adverse effects of postirradiation oxidation. Kamal-Eldin and Appelqvist [12] described the antioxidant mechanism of α-T on lipids. The alkyl, oxy and peroxy free radicals on the lipid molecules are spared from further reaction by the donation of the phenolic hydrogen on the chroman ring of α-T to the oxidized molecule (Fig. 1). The chroman ring becomes resonance stabilized and subsequently reacts further with free radicals. In the presence of oxygen and oxidized species, the average reduced molecule per molecule of α-T is theoretically 2.0 [13]

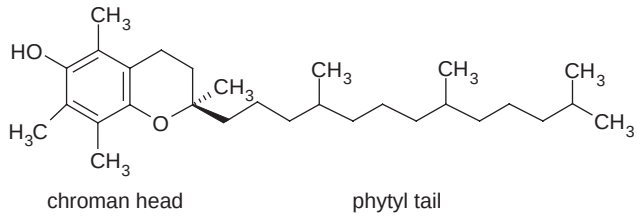

Fig. 1. Chemical structure of α-T is shown. The chroman head is responsible for abstracting free radicals and stabilizing them within the structure. The long lipophilic chain termed the 'phytyl tail' provides compatibility with UHMWPE.

and was reported to be 1.3–1.6 experimentally [14]. Because of its hydrophobic nature, it blends easily with UHMWPE. α-T has been blended with UHMWPE powder before consolidation, and shown to reduce oxidation levels in γ-sterilized UHMWPE after accelerated aging [15]. However, α-T is an efficient free radical scavenger and stabilizes free radicals on alkyl chains even at low concentrations. Therefore, we performed our doping experiments by diffusion of α-T into UHMWPE after irradiation in order to ensure high and reproducible crosslinking. Although it would take a large amount of time to obtain a high and uniform concentration of α-T in UHMWPE, the highly efficient antioxidant nature of α-T should allow us to use low concentrations for improved oxidation resistance.

Irradiated UHMWPE without postirradiation stabilization oxidizes to a large extent because the residual free radicals react with diffusing oxygen molecules, forming one peroxy free radical and one primary carbon free radical, which induces more oxidation. Typically, oxidative stability of irradiated UHMWPE is measured by accelerated aging methods [16,17]. We expected the oxidative stability of irradiated UHMWPE to improve when doped with α-T because of this compound's ability to react with peroxy radicals on the UHMWPE chains. Therefore, α-T would hinder the oxidation reaction from continuing in a cascading manner. The wear behavior of crosslinked UHMWPE should not be affected by α-T doping based on our previous studies showing the effect of lipid absorption on the wear behavior of UHMWPE in a bidirectional pin-on-disc (POD) wear study [18]. α-T was also expected to increase the plasticity of irradiated UHMWPE, thereby increasing energy absorption around a crack tip by increasing the extent of plastic deformation.

Our objectives for this study were to investigate the effect of α-T on: (1) the oxidative stability of irradiated (highly crosslinked) UHMWPE as a means to eliminate postirradiation melting, (2) fatigue strength of irradiated UHMWPE, and (3) the wear behavior of irradiated UHMWPE to prove that low wear exhibited by crosslinked UHMWPE was not compromised in the presence of α-T.

Questions? Contact FDA/CDRH/OCE/DID at CDRH-FOISTATUS@fda.hhs.gov or 301-796-8118

Records processed under FOIA Request #2014-8015; Released by CDRH on 12-8-2015

2. Materials and methods

In the following studies, artificial aging and infrared spectroscopy were used to determine the effect of α-T on the oxidative stability of UHMWPE. Fatigue crack propagation testing was used to measure the fatigue resistance and bidirectional POD testing was used to determine the wear resistance of α-T-doped irradiated UHMWPE.

2.1. Preparation of test samples with α-T

Consolidated GUR 1050 UHMWPE bar stock (Perplas Ltd., Lancashire, UK) was γ-irradiated to 65- and 100-kGy (Steris Isomedix, Northborough, MA). Cubes (2 cm) for diffusion and oxidative stability experiments, cylindrical pins (9 mm diameter, 13 mm length) for POD wear testing and compact tension (CT) specimens (ASTM E-647 A1) for fatigue crack propagation testing were machined from these irradiated UHMWPEs. Samples were then doped with α-T for 16 h at room temperature or 100°C in air. Following doping, the samples were further γ-sterilized at a dose of 27 kGy. These two test groups will be referred to as *α-T-92* and *α-T-127* with a total radiation dose of 92 and 127 kGy, respectively.

The preparation of relevant control materials for each testing condition is detailed in each of the following sections. A summary of test and control samples used in this study are given in Table 1.

α-D,L-Tocopherol was purchased from Fischer Scientific (Houston, TX) and used without further processing.

2.2. Diffusion of α-T into UHMWPE

To measure the extent of α-T diffusion into UHMWPE, 2 cm cubes of 100-kGy γ-irradiated UHMWPE (Steris Isomedix, Northborough, MA) (CI 100) were immersed in α-T at 100°C for 16 h under 0.5–0.6 atm of nitrogen pressure. Pressure was applied by first purging the oven with nitrogen, then applying vacuum and then adjusting the amount of nitrogen.

To measure the diffusion profile, a cross-section was cut out of the immersed cube (100–150 μm) using an LKB Sledge Microtome (Sweden). The thin cross-section was then analyzed using a BioRad UMA 500 infrared microscope (Natick, MA). Infrared spectra were collected with an aperture size of $50 \times 50\,\mu m^2$ as a function of depth away from one of the edges that coincided with the free surface of the cube. The infrared spectra of UHMWPE and α-T are shown in Fig. 2 along with the spectrum of a thin UHMWPE section with a thin layer of α-T spread over it. The absorbance between 1226 and 1295 cm^{-1} is characteristic of α-T and UHMWPE does not absorb near these frequencies. With a selection of internal reference that is proportional to the beam path length, one can accurately calculate the relative composition of the material. For

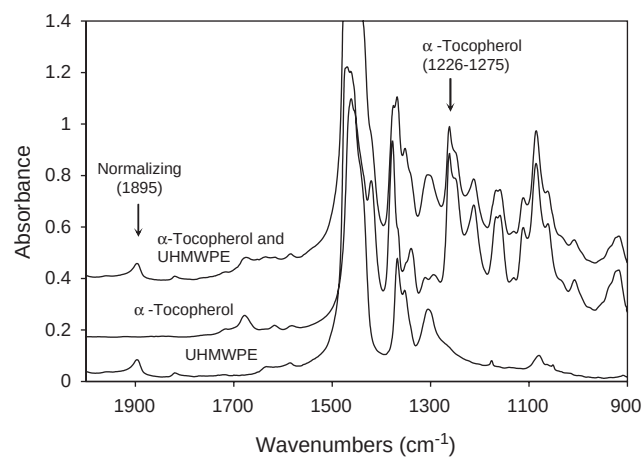

Fig. 2. Infrared spectra of UHMWPE, α-T and UHMWPE with α-T spread on the surface are shown here. The α-T absorbances (1226–1295 cm^{-1}) and the normalizing skeletal vibration of UHMWPE (1895 cm^{-1}) are indicated.

Table 1
A summary of samples used in this study[a]

Sample name	Type of irradiation	Irradiation dose (kGy)	Postirradiation stabilization method
Test samples for accelerated aging, fatigue and wear testing			
α-T-92	Gamma	65	α-T doping followed by 27-kGy γ irradiation
α-T-127	Gamma	100	α-T doping followed by 27-kGy γ irradiation
Control samples for accelerated aging			
CI-100	E-beam	100	—
Control samples for fatigue testing			
Unirradiated	—	—	—
Conventional	Gamma	25	—
CI-100	E-beam	100	—
CISM	E-beam	100	Melting

[a] Starting material was consolidated GUR 1050.

Questions? Contact FDA/CDRH/OCE/DID at CDRH-FOISTATUS@fda.hhs.gov or 301-796-8118

Records processed under FOIA Request #2014-8015; Released by CDRH on 12-8-2015

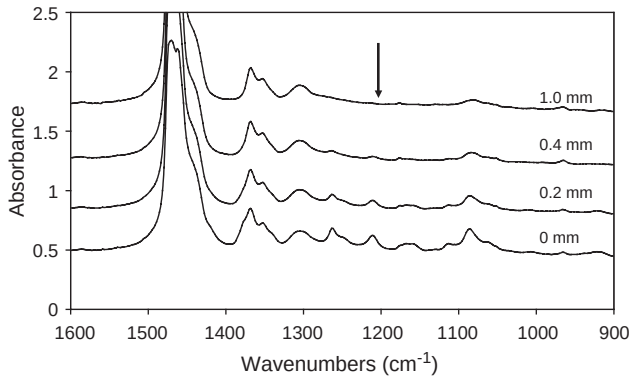

Fig. 3. Infrared spectra of a thin cross-section (100 μm) of a 100-kGy irradiated UHMWPE cube (CI-100) doped with α-T at 100°C for 16 h. The absorbances are shown as a function of distance away from the edge of the thin sections that corresponded to a free surface of the cube.

UHMWPE, the 1895 cm^{-1} wave number for the CH_2 rocking mode is a typical choice as an internal reference [19]. The normalized value, which is the ratio of the integrated absorbances of 1260 and 1895 cm^{-1}, is an index (α-TI) that provides a relative metric of α-T composition in UHMWPE. Spectra of α-T-doped UHMWPE are shown as a function of distance away from the surface in Fig. 3.

2.3. Accelerated aging and oxidation

We studied the protective effects of α-T on the oxidation of irradiated UHMWPE during artificial aging using α-T-92 and α-T-127 samples that had been doped at room temperature. The objective of this study was to show that the oxidation levels of a high-dose irradiated, aggressively aged UHMWPE would be much higher than that of a high-dose irradiated/α-T stabilized and aggressively aged UHMWPE. Therefore, the control used in this study was 100-kGy γ-irradiated UHMWPE (CI 100) without postirradiation stabilization.

Accelerated aging was performed by placing cubes ($n = 3$) in an oven at 80°C in air for 5 weeks. These aggressive conditions for aging were chosen in order to simulate extreme oxidation levels in UHMWPE and to show the protective effects of α-T even under these aggressive conditions. After aging, the cubes were microtomed to thin sections (100–200 μm) using an LKB Sledge Microtome (Sweden). A BioRad UMA 500 infrared microscope (Natick, MA) was used to measure the extent and depth of oxidation. Infrared spectra were collected with an aperture size of $50 \times 50\,\mu m^2$ as a function of depth away from one of the edges that coincided with the free surface of the cube. The infrared spectra were analyzed to calculate an oxidation index, as the ratio of the areas under the 1740 cm^{-1} carbonyl and 1370 cm^{-1} methylene stretching absorbances.

2.4. Fatigue crack propagation testing

Fatigue crack propagation testing was performed on a MiniBionix 858 (MTS, Eden Prairie, MN) following ASTM E-647, the standard method for the measurement of fatigue crack growth rates. We used compact tension (CT) specimens of Type A1, precracked the notch and conducted the tests with a stress ratio of 0.1 in a 40°C water bath to simulate the in vivo temperature of an articulating joint.

Unirradiated, 25-kGy γ-irradiated (*conventional*), accelerated aged conventional, 100-kGy γ-irradiated (*CI 100*) and 100-kGy γ-irradiated/melted UHMWPE (*CISM*) were used as controls. These controls were chosen to investigate the separate effects of irradiation, aging and melting on UHMWPE. The α-T-doped samples (α-T-92 and α-T-127) were tested in two distinct concentration regimes that were observed. First, the stress intensity factor at crack inception was measured within the α-T-rich surface region. Second, the same measurement was repeated after driving the crack tip well into the bulk of the test sample, at least 3 mm from the original notch tip, to measure the fatigue strength of the α-T-poor bulk region.

2.5. Wear testing

POD wear testing was done to determine the wear resistance of high-dose irradiated UHMWPEs subsequently doped with α-T. The wear rates of unaged and accelerated aged α-T-92 and α-T-127 samples that had been doped at room temperature were compared to literature values of unaged and aged conventional 25-kGy γ-irradiated (in N_2), 100-kGy electron beam irradiated and melted and 105-kGy γ-irradiated and -annealed UHMWPEs that we previously reported [20]. These samples were chosen as control material because they provided means of comparing α-T-doped samples to commercially used UHMWPE with different levels of residual free radicals. Unaged samples were compared to accelerated aged ones because aging was used to investigate the wear rates for α-T-doped test samples when compared to samples containing residual free radicals due to oxidative degradation.

Unaged and accelerated aged cylindrical α-T-92 and α-T-127 samples were tested on a custom-built bidirectional POD wear tester at a frequency of 2 Hz before or after accelerated aging as described above [21]. We used undiluted bovine calf serum (JRH Biosciences, Inc., Lenexa, KS) as lubricant with 0.3 wt% of sodium azide as antibacterial agent and 0.1 M ethylenedimainetetraaceticacid as metal chelating agent. Wear was quantified gravimetrically at 0.5 million cycle intervals. Initially, we subjected the pins to 200,000 cycles of POD testing to remove any loosely bound α-T. Thereafter, pins of each group ($n = 3$) were tested for a total of 2 million cycles.

Questions? Contact FDA/CDRH/OCE/DID at CDRH-FOISTATUS@fda.hhs.gov or 301-796-8118

Records processed under FOIA Request #2014-8015; Released by CDRH on 12-8-2015

The wear rate was calculated by a linear regression of weight change versus number of cycles from 0.5 to 2 million cycles.

2.6. Optical microscopy

We qualitatively analyzed the fatigue fracture surface of a CT specimen of α-T-92. The fracture surface of the sample was gold coated using an Edward Sputter Coater S150B and observed under an optical microscope (Olympus SZX12, Melville, NY).

In the following studies, statistical analysis was performed using a Student's *t*-test for two-tailed distributions with equal variance.

3. Results

In order to measure the extent and depth of α-T diffusion, we obtained infrared spectra of 100-kGy irradiated UHMWPE that had been doped with α-T. The change in the α-T absorbance as a function of depth away from the free surface is shown in Fig. 3. Diffusion profiles of α-T in 100-kGy irradiated UHMWPE at 100°C are shown in Fig. 4. This figure demonstrates the α-T-rich and -poor regions. From the surface to as deep as 500 μm, there was a large concentration of α-T whereas beyond this depth, the bulk of the polymer contained no detectable α-T. α-T-rich and -poor regions are also qualitatively observed in the optical micrograph of the fracture surface of a α-T-92 CT specimen (Fig. 5).

The effects of aging on the oxidation of undoped and α-T-doped samples (at room temperature) are shown in Fig. 6. The curves represent averages of three samples. The 100-kGy γ-irradiated control samples (CI 100) showed significantly higher oxidation levels when compared to α-T-92 and α-T-127; maximum oxidation indices were 3.74 ± 0.16, 0.48 ± 0.25 ($p < 0.001$) and

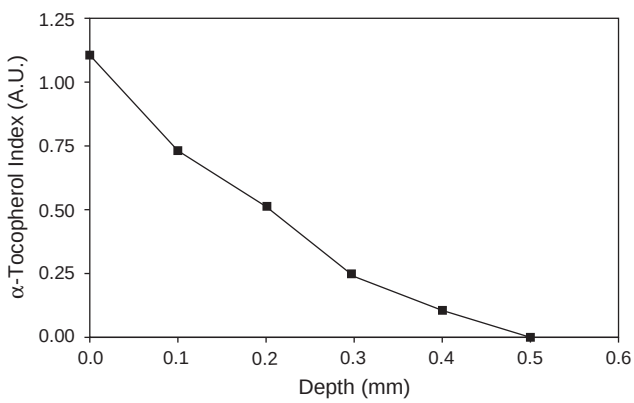

Fig. 4. α-T index as a function of distance away from the surface of a 100-kGy irradiated UHMWPE cube (CI-100). The doping was done at 100°C for 16 h.

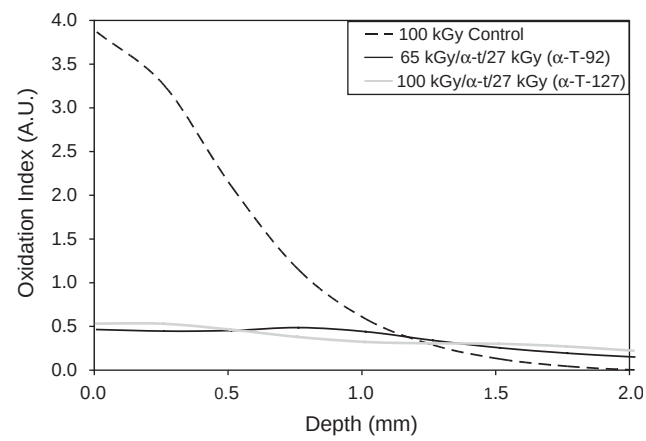

Fig. 6. Oxidation index as a function of distance away from the surface of 5-week accelerated aged (80°C, in air) 100-kGy irradiated UHMWPE (CI-100), α-T-92 and α-T-127 samples doped at room temperature are shown here. The curves represent averages of three test samples.

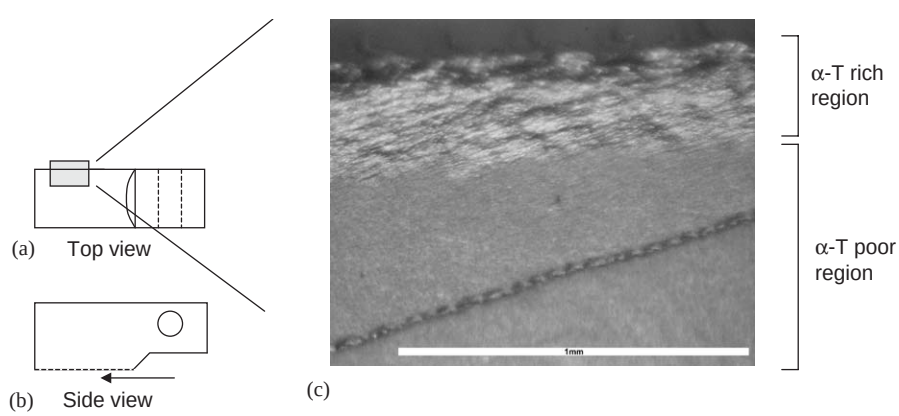

Fig. 5. An optical micrograph of the border region of a representative α-T-doped (α-T-92) CT specimen following complete fatigue fracture. Top (a) and side (b) views of a failed fatigue specimen are shown schematically. The arrow indicates the direction of fatigue crack growth. The micrograph (c) was taken from the edge of the sample. The fracture surface had a rougher appearance near the α-T-rich region presumably due to increased ductility of the crosslinked UHMWPE imparted by α-T. The scale bar represents 1 mm.

Questions? Contact FDA/CDRH/OCE/DID at CDRH-FOISTATUS@fda.hhs.gov or 301-796-8118

Records processed under FOIA Request #2014-8015; Released by CDRH on 12-8-2015

Table 2
Stress intensity factor range at fatigue crack inception (ΔK_i) for unirradiated, sterilized and aged UHMWPE, and crosslinked and crosslinked/melted UHMWPE

Material	Unirradiated	Conventional (25 kGy in air)	100 kGy (CI-100)	100 kGy irradiated/ melted (CISM)	Aged conventional (25 kGy in air)
ΔK_i (MPa m$^{1/2}$)	1.37 ± 0.06 ($n = 3$)	1.29 ± 0.04 ($n = 3$)	0.74 ± 0.01 ($n = 3$)	0.56 ± 0.02 ($n = 3$)	0.18 ± 0.06 ($n = 3$)

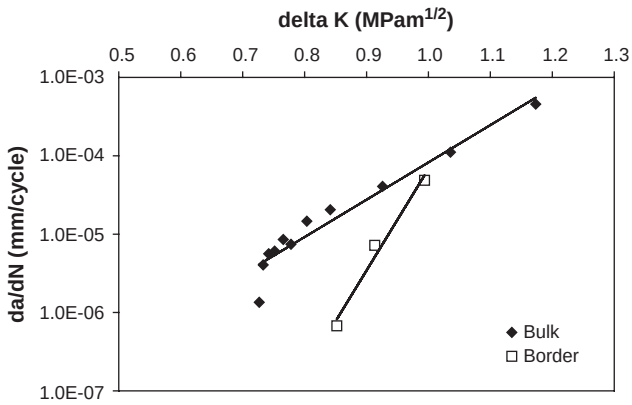

Fig. 7. The rate of fatigue crack length growth as a function of stress intensity factor for a representative α-T-92 sample. Note the two distinct fatigue crack inception and propagation regimes of α-T-rich (border) and α-T-poor (bulk) regions in the doped UHMWPE.

0.44 ± 0.06 ($p < 0.001$), respectively. The presence of α-T protected irradiated UHMWPE against oxidation during 5-week accelerated aging at 80°C in air.

The stress intensity factor range at crack inception (ΔK_i) for undoped samples is shown in Table 2. The decrease in fatigue strength of the GUR 1050 upon γ-sterilization at a low dose of 25 kGy was not significant in the unaged specimens ($p > 0.1$); however, aged conventional UHMWPE showed significantly lower fatigue strength ($p < 0.01$) compared to unaged UHMWPE. Irradiation to 100 kGy (CI-100) significantly reduced the fatigue resistance of UHMWPE ($p < 0.01$). CISM samples that were 100-kGy irradiated and melted had lower fatigue strength than CI-100 that were only irradiated to 100 kGy ($p < 0.001$).

For the α-T-doped samples, there were two different regimes of fatigue crack propagation (Fig. 7) corresponding to different concentration of α-T within the sample. The values obtained from the surface region were higher than the bulk values for both α-T-92 and α-T-127 samples (Table 3). Although the bulk values for α-T-92 and α-T-127 samples prior to α-T doping were similar, the samples with less irradiation (α-T-92) prior to α-T doping had higher fatigue resistance.

The wear rate of the α-T-92 and α-T-127 samples did not change upon aging ($p > 0.05$, Fig. 8). The wear rate of α-T-92 was 111% higher than that of α-T-127.

Table 3
Stress intensity factor range at fatigue crack inception (ΔK_i) in the bulk and at the α-T-rich border for irradiated/α-T-doped polyethylene[a]

Material	α-T-92	α-T-127
Total radiation dose (kGy)	92	127
ΔK_I (MPa m$^{1/2}$) at the α-T-rich border	0.94 ($n = 2$)	0.83 ± 0.02 ($n = 4$)
ΔK_i (MPa m$^{1/2}$) at the bulk with no α-T	0.76 ($n = 2$)	0.70 ($n = 1$)

[a] α-T doping was performed at 100°C for 16 h in air.

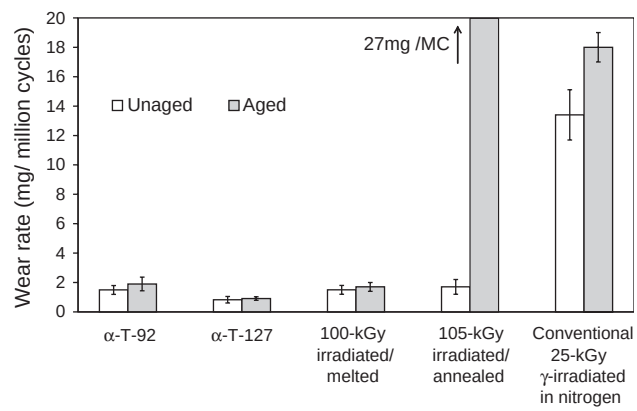

Fig. 8. Bidirectional POD wear rates before and after accelerated aging for α-T-doped α-T-92 and α-T-127 are shown here. For comparison purposes, we also include literature wear rate values for the unaged and aged 100-kGy irradiated and melted, 105-kGy irradiated and annealed, and conventional UHMWPE that was γ-sterilized in nitrogen [20].

4. Discussion

Ionizing radiation and subsequent melting increases the wear resistance of UHMWPE, but decreases its mechanical properties, especially fatigue resistance. Crosslinking that results from irradiation reduces the wear of UHMWPE. Postirradiation melting is necessary to remove the residual free radicals that would otherwise cause oxidative embrittlement in the long term. Our aim was to create a wear-, oxidation- and fatigue-resistant material by the incorporation of α-T (a lipophilic antioxidant) into irradiated UHMWPE, eliminating the need for postirradiation melting. α-T is an antioxidant which can serve the purpose of eliminating long-term adverse effects of postirradiation oxidation. As described above, it acts on alkyl, oxy and peroxy free radicals on lipids to spare them from further reaction with oxygen.

Questions? Contact FDA/CDRH/OCE/DID at CDRH-FOISTATUS@fda.hhs.gov or 301-796-8118

Records processed under FOIA Request #2014-8015; Released by CDRH on 12-8-2015

The presently used doping conditions (16 h and 100°C) resulted in a surface region (<500 μm) that was rich in α-T (Fig. 4). The 16-h duration for α-T doping was chosen to comply with practical considerations for the potential use of this technique in manufacturing. We chose to increase diffusion by using elevated temperatures but elected not to go above 100°C to avoid any decrease in the crystallinity of UHMWPE upon cooling down.

The 100-kGy irradiated UHMWPE (CI-100) oxidized more than the irradiated and α-T-doped UHMWPE (α-T-92 and α-T-127) after accelerated aging. This was presumably a manifestation of the strong antioxidant and scavenging ability of α-T, supporting our hypothesis that α-T can provide oxidative stability to irradiated UHMWPE eliminating the need for postirradiation melting.

We examined the effects of sterilization, sterilization and aging, high-dose irradiation and melting subsequent to irradiation on the fatigue strength of UHMWPE to determine how each of these UHMWPEs compared to α-T-doped test samples. Table 2 shows the fatigue behavior of conventional and highly crosslinked contemporary UHMWPEs.

Although conventional UHMWPE had high fatigue resistance, γ-sterilization in air made it prone to oxidation following accelerated aging, hence significantly lowering its fatigue resistance to values below that for unaged crosslinked material. Compared to conventional material, crosslinked UHMWPE displayed much lower fatigue resistance presumably due to decreases in chain mobility with increased crosslinking as mentioned above. Also, there was a significant decrease in fatigue resistance associated with melting subsequent to irradiation likely due to a decrease in chain mobility and hence amorphous content available for recrystallization after crosslinking.

Our second hypothesis was that α-T would form a blend with UHMWPE to increase its fatigue strength.

The fatigue resistance of crosslinked UHMWPE increased with the addition of α-T as was measured at the border region of the irradiated and α-T-doped UHMWPE. The fatigue strength was lower in the bulk of the α-T-doped samples because the concentration of α-T decreased to undetectable levels. The fracture surface of one of the doped samples supports this observation with a more ductile fracture appearance near the α-T rich surface region (Fig. 5). This ductile surface region also coincided with the measured diffusion profile for α-T (Fig. 4). These observations are in support of our hypothesis that a lipophilic compound compatible with UHMWPE would increase the fatigue resistance of irradiated UHMWPE.

One limitation of the use of diffusion to blend α-T with UHMWPE is the limited depth of α-T distribution. We recognize this limitation and our current studies focus on obtaining deeper penetration of α-T throughout UHMWPE. Preliminary studies are already encouraging in obtaining a uniform distribution through CT specimens.

The incorporation of α-T did not adversely affect the wear resistance of irradiated UHWMPE. The wear rate of the α-T-92 and α-T-127 doped at room temperature were comparable to the wear rates of contemporary highly crosslinked UHMWPEs previously reported by our group [20] (Fig. 8). Muratoglu et al. [20] showed an over 14-fold increase in the wear rate of 105-kGy irradiated and annealed UHMWPE following 3 weeks of 80°C accelerated aging in air. This increase in wear rate was presumably due to oxidation during aging secondary to the large amount of residual free radicals. In contrast, the ~100-kGy irradiated and α-T-doped UHMWPEs of the present study showed no significant increase in the wear rate following 5 weeks of accelerated aging in 80°C in air, similar to what was reported by Muratoglu et al. [20] for the 100-kGy irradiated and melted UHMWPE. This shows that α-T doping can protect irradiated UHMWPE against oxidation without the further need for melting.

Our results supported our hypotheses that an antioxidant molecule, one that is compatible with UHMWPE, would be able to protect it from post-irradiation oxidation and form a blend with improved fatigue resistance. Despite the gradient in concentration of α-T across our samples and a relatively low concentration of α-T, oxidative stability of irradiated UHMWPE was improved. The antioxidant capabilities of α-T on UHMWPE have been investigated here; however, the mechanism by which it provides higher fatigue resistance to UHMWPE is not yet known. We have presumed that the local plasticization effect of such a lipophilic molecule would participate in energy absorbing mechanisms around the fatigue crack. Consequently, the effect of α-T on the morphology and hence the crystal plasticity of UHMWPE warrants further investigation. Our current and future work focus on investigating the morphology around a crack tip of irradiated UHMWPE in the absence and presence of α-T by optical and diffraction methods to quantify plasticization on a local scale.

Future work will also include testing of irradiated and α-T doped UHMWPE test samples on hip and knee simulators. Such experiments are delayed until the optimum radiation dose level, α-T concentration and doping methodology is developed.

5. Conclusion

We have created a highly crosslinked UHMWPE blended with the lipophilic antioxidant α-tocopherol that showed oxidation and wear resistance comparable

Questions? Contact FDA/CDRH/OCE/DID at CDRH-FOISTATUS@fda.hhs.gov or 301-796-8118

Records processed under FOIA Request #2014-8015; Released by CDRH on 12-8-2015

to contemporary highly crosslinked/melted UHMWPEs and fatigue resistance higher than these contemporary crosslinked UHMWPEs. These are encouraging results on the way to creating a novel material that will allow the use of low-wear crosslinked UHMWPE in high-stress orthopedic applications and increase the longevity of joint implants in general.

Acknowledgements

This work was funded by William H. Harris Foundation.

References

[1] Kurtz SM, Muratoglu OK, Evans M, Edidin AA. Advances in the processing, sterilization, and crosslinking of ultra-high molecular weight polyethylene for total joint arthroplasty. Biomaterials 1999;20(18):1659–88.

[2] Harris W. The problem is osteolysis. J Biomed Mater Res 1996;31:19–26.

[3] Collier JP, Sperling DK, Currier JH, Sutula LC, Saum KA, Mayor MB. Impact of γ-sterilization on clinical performance of polyethylene in the knee. J Arthroplasty 1996;11(4): 377–89.

[4] Collier JP, Mayor MB, McNamara JL, Surprenant VA, Jensen RE. Analysis of the failure of 122 polyethylene inserts from uncemented tibial knee components. Clin Orthop Relat Res 1991;273:232–42.

[5] Mikulak SA, Mahoney OM, dela Rosa MA, Schmalzried TP. Loosening and osteolysis with the press-fit condylar posterior-cruciate-substituting total knee replacement. J Bone Joint Surg Am Vol 2001;83-A(3):398–403.

[6] O'Rourke MR, Callaghan JJ, Goetz DD, Sullivan PM, Johnston RC. Osteolysis associated with a cemented modular posterior-cruciate-substituting total knee design: five to eight-year follow-up. J Bone Joint Surg 2002;84-A(8):1362–71.

[7] Muratoglu OK, Bragdon CR, O'Connor DO, Jasty M, Harris WH. A novel method of crosslinking UHMWPE to improve wear, reduce oxidation and retain mechanical properties. J Arthroplasty 2001;16(2):149–60.

[8] Muratoglu OK, Bragdon CR, O'Connor DO, Jasty M, Harris WH, Gul R, et al. Unified wear model for highly crosslinked ultra-high molecular weight polyethylenes (UHMWPE). Biomaterials 1999;20(16):1463–70.

[9] McKellop H, Shen F-W, Lu B, Campbell P, Salovey R. Development of an extremely wear resistant ultra-high molecular weight polyethylene for total hip replacements. J Orthop Res 1999;17(2):157–67.

[10] Argon AS, Bartczak Z, Cohen RE, Muratoglu OK. In: Andersen S, Brondted P, Lillhot H, Lystrup A, Rheinlander J, Sorensen B, et al., editors. Novel mechanisms of toughening semi-crystalline polymers. Denmark, Roskilde: Riso National Laboratory; 1997.

[11] Baker DA, Hastings RS, Pruitt L. Compression and tension fatigue resistance of medical grade ultra high molecular weight polyethylene: the effect of morphology, sterilization, aging and temperature. Polymer 2000;41(2):795–808.

[12] Kamal-Eldin A, Appelqvist L. The chemistry and antioxidant properties of tocopherols and tocotrienols. Lipids 1996;31(7): 671–701.

[13] Burton G, Ingold K. Autoxidation of biological molecules, 1, the antioxidant activity of vitamin E and related chain-breaking phenolic antioxidants in vitro. J Am Achem Soc 1981;103:6472–7.

[14] Winterle J, Mill T. Reactions of vitamin E with alkylperoxy radicals in homgeneous solution and liposomes. In: Rodgers M, Powers E, editors. Oxygen and oxy-radicals in chemistry and Biology. New York: Academic Press; 1981. p. 779–80.

[15] Mori A, Sakuramoto I, Tomita N, Kawano S, Nagata K, Utsumi K, et al., Mechanical behavior of UHMWPE when mixed with vitamin E. Transactions of the 47th Orthopaedic Research Society, 2001. p. 1017.

[16] Sanford W, Saum K. Accelerated oxidative aging testing of UHMWPE. Transactions of the 41st Orthopaedic Research Society, 1995. p. 119.

[17] Sun D, Stark C, Dumbleton J. Development of an accelerated aging method for evaluation of long-term irradiation effects on UHMWPE Implants. In: Meeting of American Chemical Society. Washington, DC: Division of Polymer Chemistry; 1994. p. 969–70.

[18] Greenbaum E, Burroughs B, Harris W, Muratoglu O. Effect of lipid absorption on wear and compressive properties of uni-irradiated and highly crosslinked UHMWPE: an in vitro experimental model. Biomaterials, in press.

[19] Kurtz SM, Muratoglu OK, Gsell R, Greer K, Shen F-W, Cooper C, et al. Interlaboratory validation of oxidation-index measurement methods for UHMWPE after long-term shelf aging. J Biomed Mater Res (Appl Biomater) 2002;63(1):15–23.

[20] Muratoglu OK, Merrill EW, Bragdon CR, O'Connor DO, Hoeffel D, Burroughs B, et al. Effect of radiation, heat, and aging on in vitro wear resistance of polyethylene. Clin Orthop Relat Res 2003;417:253–62.

[21] Bragdon CR, O'Connor DO, Lowenstein JD, Jasty M, Biggs SA, Harris WH. A new pin-on-disk wear testing method for simulating wear of polyethylene on cobalt-chrome alloy in total hip arthroplasty. J Arthroplasty 2001;16(5):658–65.

Questions? Contact FDA/CDRH/OCE/DID at CDRH-FOISTATUS@fda.hhs.gov or 301-796-8118

Records processed under FOIA Request #2014-8015; Released by CDRH on 12-8-2015

Available online at www.sciencedirect.com
SCIENCE DIRECT®
ELSEVIER
Biomaterials 26 (2005) 6657–6663
Biomaterials
www.elsevier.com/locate/biomaterials

Characterization of irradiated blends of α-tocopherol and UHMWPE ☆

Ebru Oral[a,b], Evan S. Greenbaum[a,1], Arnaz S. Malhi[a], William H. Harris[a,b], Orhun K. Muratoglu[a,b,*]

[a]Department of Orthopaedic Surgery, Massachusetts General Hospital, 55 Fruit Street, GRJ 1206, Boston, MA 02114, USA
[b]Harvard Medical School, Harvard, USA

Received 19 November 2004; accepted 7 April 2005
Available online 1 July 2005

Abstract

Adhesive/abrasive wear in ultra-high molecular weight polyethylene (UHMWPE) has been minimized by radiation cross-linking. Irradiation is followed by melting to eliminate residual free radicals and avoid long-term oxidative embrittlement. However, post-irradiation melting reduces the crystallinity of the polymer and hence its strength and fatigue resistance. We proposed an alternative to post-irradiation melting to be the incorporation of the antioxidant α-tocopherol into UHMWPE prior to consolidation. α-Tocopherol is known to react with oxygen and oxidized lipids, stabilizing them against further oxidative degradation reactions. We blended GUR 1050 UHMWPE resin powder with α-tocopherol at 0.1 and 0.3 wt% and consolidated these blends. Then we gamma-irradiated these blends to 100-kGy. We characterized the effect of α-tocopherol on the cross-linking efficiency, oxidative stability, wear behavior and mechanical properties of the blends. (I) The cross-link density of virgin, 0.1 and 0.3 wt% α-tocopherol blended, 100-kGy irradiated UHMWPEs were 175 ± 19, 146 ± 4 and 93 ± 4 mol/m^3, respectively. (II) Maximum oxidation indices for 100-kGy irradiated UHMWPE previously blended with 0, 0.1 and 0.3 wt% α-tocopherol that were subjected to accelerated aging at 80 °C in air for 5 weeks were 3.32, 0.09, and 0.05, respectively. (III) The pin-on-disc wear rates of 100-kGy irradiated UHMWPE previously blended with 0.1 and 0.3 wt% α-tocopherol that were subjected to accelerated aging at 80 °C in air for 5 weeks were 2.10 ± 0.17 and 5.01 ± 0.76 mg/million cycles, respectively. (IV) Both accelerated aged, α-tocopherol-blended 100-kGy irradiated UHMWPEs showed higher ultimate tensile strength, higher yield strength, and lower elastic modulus when compared to 100-kGy irradiated, virgin UHMWPE. These results showed that α-tocopherol-blended 100-kGy irradiated UHMWPEs were not cross-linked to the same extent as the 100-kGy irradiated, virgin UHMWPE.
© 2005 Elsevier Ltd. All rights reserved.

Keywords: Antioxidant; Polyethylene; Wear mechanism; Lipid; Gamma-irradiation; Hip replacement prosthesis

1. Introduction

Adhesive/abrasive wear of ultra-high molecular weight polyethylene (UHMWPE) is the primary source of debris leading to peri-prosthetic osteolysis, compromising the long-term performance of total joint implants [1]. Wear is decreased by radiation cross-linking and melting of UHMWPE [2–5]. Cross-links are imparted between the polyethylene chains by the recombination of free radicals formed by high-dose ionizing radiation. The carbon free radicals formed during radiation ('primary free radicals') in the amorphous region of the semi-crystalline UHMWPE possess enough mobility to recombine to form cross-links in the polymer.

The free radicals formed in the crystalline phases of the polymer network, however, lack the mobility to

☆This study was funded by NIH R01 AR051142-01.
*Corresponding author. Orthopaedic Biomechanics and Biomaterials Laboratory, Massachusetts General Hospital, 55 Fruit Street, GRJ 1206, Boston, MA 02114, USA. Tel.: +1 617 726 3869; fax: +1 617 726 3883.
E-mail address: orhun@alum.mit.edu (O.K. Muratoglu).
[1]Now at Department of Cellular and Integrative Physiology, Indiana University School of Medicine.

0142-9612/$ - see front matter © 2005 Elsevier Ltd. All rights reserved.
doi:10.1016/j.biomaterials.2005.04.026

Questions? Contact FDA/CDRH/OCE/DID at CDRH-FOISTATUS@fda.hhs.gov or 301-796-8118

Records processed under FOIA Request #2014-8015; Released by CDRH on 12-8-2015

recombine and hence are trapped for prolonged periods of time in the lamellae. These 'residual free radicals' can react with diffused oxygen to form peroxy radicals. These peroxy radicals attack other polyethylene chains, which leads to a second generation of free radicals and hence furthers the reactions with oxygen. This cascade of events results in the oxidative embrittlement and reduction in the mechanical properties of UHMWPE.

Post-irradiation melting is used effectively to remove the residual free radicals effectively. Melting releases the trapped free-radicals from the crystalline regions and allows them to recombine in the form of cross-links. Therefore, the irradiated and melted polymer is protected against reactions with diffused oxygen and oxidative embrittlement.

Cross-linking by irradiation reduces the fatigue strength of UHMWPE. Post-irradiation melting leads to a decrease in the crystallinity of the polymer; further decreasing the fatigue strength of irradiated UHMWPE [6]. Fatigue failure of UHMWPE components has been a rare occurrence mostly due to severe oxidation [7,8]. Nevertheless, fatigue damage, especially in components under high cyclic stresses, is a major problem after wear, limiting the longevity of joint implants. Hence, there is a need to find alternative methods of processing UHMWPE to combine decreased wear with higher crystallinity and high fatigue resistance.

Introducing an antioxidant such as α-tocopherol into UHMWPE is an alternative to post-irradiation melting to render it stable against oxidation without further sacrificing its mechanical strength. α-Tocopherol is biocompatible and is lipophilic owing to its phtyl tail, easily blending with UHMWPE. Furthermore, it is an antioxidant, which can serve the purpose of eliminating long-term adverse effects of post-irradiation oxidation. α-Tocopherol spares free radicals on lipid molecules [9,10] from further reactions with oxygen and each other by the donation of the phenolic hydrogen on its chroman ring (Fig. 1).

We have diffused α-tocopherol into UHMWPE after high-dose irradiation and shown that α-tocopherol protected high-dose irradiated UHMWPE against oxidation during in vitro accelerated aging and did not detrimentally affect its wear behavior [6]. These high-dose irradiated and α-tocopherol-doped UHMWPEs showed wear resistance comparable to irradiated and subsequently melted UHMWPE. As described above, α-tocopherol incorporated irradiated UHMWPE is sought as an alternative to irradiated and subsequently melted UHMWPE because of the possibility to avoid the decrease in mechanical properties caused by post-irradiation melting. In our previous study, we showed that 100-kGy irradiated, α-tocopherol diffused UHMWPE had 22% increase in fatigue propagation resistance over irradiated/non-melted UHMWPE and 58% increase over irradiated/melted UHMWPE [6].

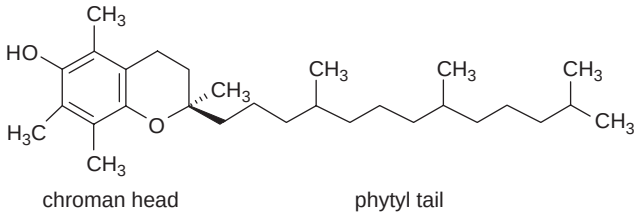

Fig. 1. α-Tocopherol. The chroman head is responsible for abstracting free radicals and stabilizing them within the structure. The long lipophilic chain termed the 'phytyl tail' provides compatibility with UHMWPE.

An alternate way of introducing α-tocopherol into UHMWPE is blending α-tocopherol with UHMWPE resin powder and consolidating the mixture. The blend is then irradiated for cross-linking, machined into components, and packaged. Mori et al. [11] have shown that blending α-tocopherol with UHMWPE and subjecting this blend to 25-kGy gamma-irradiation for sterilization resulted in a more oxidation resistant material than conventional gamma-sterilized UHMWPE. Also, Tomita et al. [12] have shown that α-tocopherol-blended, gamma-sterilized UHMWPE had increased delamination resistance, which they attributed to a decreased hardness in the grain boundaries of the resin.

We hypothesized that α-tocopherol, blended with UHMWPE prior to irradiation, would react with the primary free radicals formed during irradiation; decreasing the cross-linking efficiency of UHMWPE. Parth et al. [13] showed that the gel content of samples taken from α-tocopherol-containing and 10, 17, 22 and 100-kGy irradiated (by e-beam) UHMWPE decreased as the α-tocopherol content increased from 0.1 to 0.8 wt/wt%. A hypothesized decrease in cross-linking density may lead to increase in wear of α-tocopherol-blended and irradiated UHMWPE compared to a virgin, irradiated UHMWPE.

It is also not known if high-dose irradiated and cross-linked UHMWPE has oxidative stability owing to blended α-tocopherol and if this stability is maintained after oxidative aging. We hypothesized that the efficiency of α-tocopherol will be reduced because it will absorb some of the radiation dose intended to cross-link UHMWPE.

To test our hypotheses, we (i) measured the cross-link density in α-tocopherol-blended and high-dose irradiated UHMWPE, and (ii) determined the oxidation and wear resistance and mechanical properties of α-tocopherol-blended high-dose irradiated UHMWPE.

2. Materials and methods

In the following studies, swelling in hot xylene was used to determine cross-link density of blended and virgin

Questions? Contact FDA/CDRH/OCE/DID at CDRH-FOISTATUS@fda.hhs.gov or 301-796-8118

Records processed under FOIA Request #2014-8015; Released by CDRH on 12-8-2015

UHMWPEs. Accelerated aging and infrared spectroscopy were used to determine the effect of blended α-tocopherol on the oxidative stability of polyethylene. Bidirectional pin-on-disc (POD) wear testing was performed to measure the wear rate, thereby, determine the wear resistance. Finally, tensile testing was performed to determine mechanical properties.

2.1. Sample preparation

GUR 1050 powder (Ticona, Houston, TX) was blended with α-tocopherol (Fisher Scientific, Houston, TX) and consolidated (Perplas Technologies, Lancashire, UK). Consolidated GUR 1050 UHMWPE powder was used as virgin material. The concentrations at which α-tocopherol was incorporated in the UHMWPE were 0.1 and 0.3 wt/wt%. The blends were first prepared in 5 wt% for consistency, after which they were diluted down to their respective concentrations by adding UHMWPE powder. These molded blocks were packaged under vacuum and γ-irradiated to 100 kGy (Steris Isomedix, Northborough, MA).

Out of these blocks, cylindrical pins (9 mm diameter, 13 mm length) were machined for oxidative stability experiments and POD wear testing and 3.2 mm thick sections were machined for tensile testing. Dogbone specimens (ASTM D-638) and swelling samples used in measuring cross-link density (approx. 3×3 mm) were cut out from these 3.2 mm thick sections.

2.2. Determination of α-tocopherol content

The presence of α-tocopherol was ascertained by calculating an α-tocopherol index for each sample. A thin section (100–200 μm) was microtomed using a LKB Sledge Microtome (Sweden). A BioRad UMA 500 infrared microscope (Natick, MA) was used to measure the α-tocopherol content. The infrared spectra were analyzed to calculate an 'α-tocopherol index', as the ratio of the areas under the α-tocopherol absorbance at 1276 cm^{-1} and the polyethylene skeletal absorbance at 1895 cm^{-1}. The limits of integration for the α-tocopherol absorbance were adjusted to 1245 and 1275 cm^{-1} to achieve a more sensitive measurement. Therefore, the index reported here is different than our previously published results [6].

2.3. Determination of cross-linking density

Cross-link density measurements were performed with a thermal mechanical analyzer (TMA) (DMA 7e, Perkin Elmer, Wellesley, MA). Thin sections were machined out of virgin, 0.1 and 0.3 wt% α-tocopherol-blended and 100-kGy irradiated UHMWPE (thickness 3.2 mm). These thin sections were melted at 170 °C under flowing nitrogen to remove residual stresses from the consolidation process that might result in additional swelling.

Small sections were cut out by razor blade from these thin sections to be analyzed (approximately $3\,mm \times 3\,mm$). These small pieces were placed under the quartz probe of the TMA and the initial height of the sample was recorded. Then, the probe was immersed in xylene, which was subsequently heated to 130 °C and held for at least 100 min. The UHMWPE samples swelled in hot xylene until equilibrium was reached. The final height was recorded.

The cross-link density of the blends was calculated as described previously [5] and are reported as mol/m^3.

2.4. Accelerated aging and oxidative stability

Accelerated aging was performed on some of the cylindrical samples (9 mm diameter, 13 mm length) to determine the extent of oxidation in blends of α-tocopherol and UHMWPE under adverse conditions.

One cylindrical sample each of irradiated, virgin, and irradiated 0.1 and 0.3 wt% blocks was aged at 80 °C in a convection oven for 5 weeks in air. After aging, the cylinders were microtomed to thin sections (100–200 μm) using a LKB Sledge Microtome (Sweden). A BioRad UMA 500 infrared microscope (Natick, MA) was used to measure the extent and depth of oxidation. Infrared spectra were collected with an aperture size of 50×50 μm as a function of depth away from one of the edges that coincided with the free surface of the sample. The infrared spectra were analyzed to calculate an oxidation index, as the ratio of the areas under the 1740 cm^{-1} carbonyl and 1370 cm^{-1} methylene stretching absorbances.

2.5. Bidirectional pin-on-disc (POD) wear testing

Three cylindrical samples (9 mm in diameter and 13 mm in length) out of each of the three irradiated blocks (virgin, 0.1%, and 0.3 wt%) were used for POD wear testing. These pins were accelerated aged at 80 °C in air for 5 weeks and tested on our custom-built bi-directional POD tester at a frequency of 2 Hz for 2 million cycles (MCs) with gravimetric assessment of wear at every 0.5 MCs. Undiluted bovine serum was used as lubricant with 0.3 wt% sodium azide as antibacterial agent and 1 mM EDTA as chelating agent. The wear rate was determined by linear regression of the weight change of each pin over number of cycles from 0.5 to 2 MCs.

2.6. Determination of percent crystallinity by differential scanning calorimetry (DSC)

The DSC specimens were weighed with a Sartorius CP 225D balance to a resolution of 0.01 mg and placed in aluminum sample pans. The pan was crimped with an aluminum cover and placed in a Q-1000 Differential Scanning Calorimeter (TA Instruments, Newark, DE). The sample and the reference were then heated at a heating rate of 10 °C/min from −20 to 180 °C, cooled to −20 °C at −10 °C/min and subjected to another heating cycle from −20 to 180 °C at 10 °C/min. Heat flow as a function of time and temperature was recorded and the cycles are referred to as 1st heat, 1st cool and 2nd heat.

Crystallinity of the irradiated virgin, 0.1 and 0.3 wt% α-tocopherol-blended UHMWPEs was determined by integrating the enthalpy peak from 20 to 160 °C, and normalizing it with the enthalpy of melting of 100% crystalline polyethylene, 291 J/g.

Questions? Contact FDA/CDRH/OCE/DID at CDRH-FOISTATUS@fda.hhs.gov or 301-796-8118

Records processed under FOIA Request #2014-8015; Released by CDRH on 12-8-2015

2.7. Mechanical testing

Dogbone specimens ($n = 5$ each) were stamped from virgin, 0.1 and 0.3 wt% α-tocopherol-blended and 100-kGy irradiated UHMWPE in accordance with ASTM D638, standard test method for tensile properties of plastics. The dogbone specimens were accelerated aged at 80 °C for 5 weeks in air. These samples were then tested in accordance with ASTM D-638 using a MTS II machine (Eden Prarie, MN) at a crosshead speed of 10 mm/min.

Tensile specimens prepared in the same manner from unirradiated GUR 1050, 100-kGy irradiated GUR 1050 and 100-kGy irradiated and subsequently melted (at 150 °C) GUR 1050 were also tested as control.

In the following studies, where $n \geqslant 3$, statistical analysis was performed using a Student's t-test for two-tailed distributions with unequal variance.

3. Results

The content of α-tocopherol in the 0.1 and 0.3 wt% blended UHMWPE was ascertained by determining α-tocopherol index. α-Tocopherol index was determined to be 0.012 ± 0.003 and 0.030 ± 0.003 for 0.1 and 0.3 wt% blended samples, respectively.

Cross-link density of both 100-kGy irradiated 0.1 and 0.3 wt% α-tocopherol-blended UHMWPE was lower than 100-kGy irradiated virgin UHMWPE. These values for 0.1 and 0.3 wt% blends were 146 ± 4 and 93 ± 4 mol/m^3, respectively, compared to 175 ± 19 mol/m^3 for virgin UHMWPE (Fig. 2).

Neither of the irradiated α-tocopherol blends oxidized when subjected to accelerated aging compared to virgin irradiated UHMWPE. The maximum oxidation levels were 0.09, 0.04 and 3.32 for blends with 0.1, 0.3 wt% α-tocopherol and virgin irradiated polyethylene, respectively. An oxidation profile as a function of depth is shown in Fig. 3 for all three samples.

The POD wear rates of 0.1 and 0.3 wt% blended and irradiated UHMWPE were both higher than the wear rates that our group published for 100-kGy irradiated and melted UHMWPE [14]. The in vitro wear rates obtained from POD testing for 0.1 and 0.3 wt% α-tocopherol-blended, and 100-kGy irradiated UHMWPE following accelerated aging were 2.10 ± 0.17 and 5.01 ± 0.76 mg/MC, respectively (Fig. 4). The wear rate for the 0.3 wt% blended UHMWPE was higher than that for 0.1 wt% blended UHMWPE ($p = 0.018$).

Percent crystallinity of 0, 0.1 and 0.3 wt% α-tocopherol-blended UHMWPE all increased as a result of irradiation and accelerated aging; however, the increase in crystallinity due to aging for the sample containing no α-tocopherol was greater than either blend (Table 1).

The ultimate tensile strength (UTS) of 0.1 and 0.3 wt% α-tocopherol-blended, unirradiated UHMWPEs were comparable to unirradiated GUR 1050 control and to

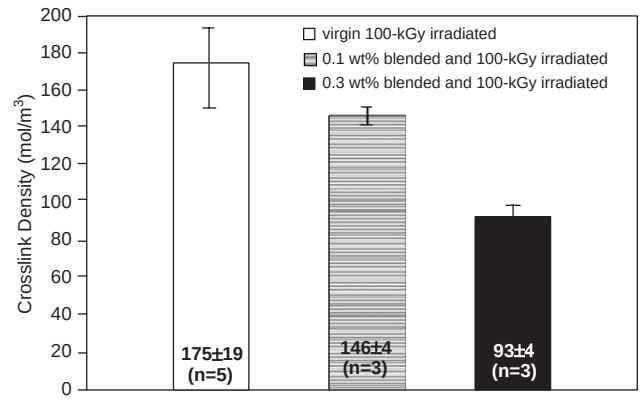

Fig. 2. Cross-link density measurements of virgin, and 0.1 and 0.3 wt% α-tocopherol-blended, 100-kGy irradiated UHMWPE.

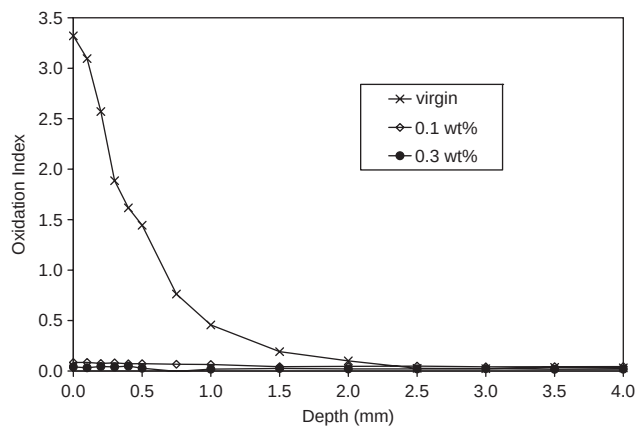

Fig. 3. The oxidation levels of control, 0.1 and 0.3 wt% α-tocopherol-blended UHMWPE post-irradiation and accelerated aging. Aging was done at 80 °C for 5 weeks in air.

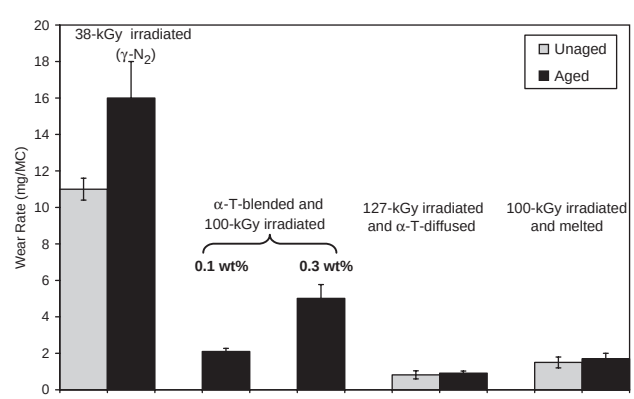

Fig. 4. The wear rates of accelerated aged 0.1 and 0.3 wt% α-tocopherol-blended UHMWPE. Accelerated aging was done at 80 °C for 5 weeks in air. For comparison, 127-kGy irradiated and α-tocopherol-diffused UHMWPE [6], 38-kGy sterilized and 100-kGy irradiated and melted GUR 1050 [14] are also included. Accelerated aging for the 38 and 100-kGy irradiated samples taken from Muratoglu et al. [14] were done at 80 °C for 3 weeks in air.

Questions? Contact FDA/CDRH/OCE/DID at CDRH-FOISTATUS@fda.hhs.gov or 301-796-8118

Records processed under FOIA Request #2014-8015; Released by CDRH on 12-8-2015

Table 1
Percent crystallinity of 0, 0.1 and 0.3 wt% α-tocopherol-blended GUR 1050 UHMWPE before and after irradiation and accelerated aging

	Unirradiated	100-kGy irradiated	100-kGy accelerated aged
No α-tocopherol	60.9±2.0	65.4±1.1	68.4±0.3
0.1 wt% α-tocopherol	63.9±0.1	66.3±0.6	64.2±0.3
0.3 wt% α-tocopherol	63.7±0.4	65.0±0.3	65.7±0.1

Table 2
Mechanical properties of α-tocopherol-blended and 100-kGy irradiated GUR 1050 UHMWPE as compared to unirradiated GUR 1050 and 100-kGy irradiated GUR 1050

	Ultimate tensile strength (MPa)	Yield strength (MPa)	Elongation at break (%)
α-Tocopherol-blended GUR 1050			
Virgin	52±2	23±1	521±16
0.1 wt% α-tocopherol	55±3	23±1	423±8
0.3 wt% α-tocopherol	51±3	23±1	392±16
Accelerated aged 100-kGy irradiated and melted GUR 1050			
Virgin	33±2	21±1	301±18
Unaged 100-kGy irradiated GUR 1050			
Virgin	45±1	24±1	213±33
Accelerated aged 100-kGy irradiated GUR 1050			
Virgin	20±1	19±1	NA
0.1 wt% α-tocopherol	49±2	24±1	282±2
0.3 wt% α-tocopherol	51±2	25±1	349±10

each other (Table 2, $p = 0.25$, 0.60, 0.15, respectively). After irradiation and accelerated aging, their UTS was still not different from unirradiated GUR 1050 ($p = 0.09$, 0.5), whereas the UTS of virgin, 100-kGy irradiated and accelerated aged GUR 1050 was lower than before aging ($p < 0.00001$). The same effect was seen on the yield strength (YS).

4. Discussion

The α-tocopherol content of the samples was established by using the α-tocopherol index. The ratio of the index for 0.3 wt% blended sample was three times that for 0.1 wt% blended sample, showing that an α-tocopherol content of 0.1 wt% could be detected by our technique, and that the ratio of α-tocopherol concentration of the blends was maintained during consolidation.

The first aim of this study was to calculate the cross-link density of α-tocopherol-blended and subsequently irradiated UHMWPE. According to our hypothesis, α-tocopherol would react with the primary free-radicals formed on the UHMWPE chains during irradiation, thereby decreasing the amount of free radicals available for the formation of cross-links.

The 17% and 47% decrease in the cross-link density of 0.1 and 0.3 wt% α-tocopherol-blended and 100-kGy irradiated UHMWPE compared to the virgin material (Fig. 2) supports the hypothesis that α-tocopherol stabilized some of the primary free-radicals required for cross-linking of UHMWPE. As a result, increasing α-tocopherol concentration to 0.1 and 0.3 wt% led to fewer primary free-radicals available for cross-linking UHMWPE and a decrease in overall cross-linking proportional to α-tocopherol concentration. Hence, the efficiency of cross-linking was reduced in 0.1 and 0.3 wt% α-tocopherol-blended UHMWPE.

The interference of α-tocopherol in the cross-linking reaction did not detrimentally affect the oxidation resistance of the two α-tocopherol blends subjected to accelerated aging (Fig. 3). α-Tocopherol was able to react also with the residual free-radicals, stabilizing UHMWPE against oxidation.

Although α-tocopherol is a potent antioxidant at room temperature and ambient pressure, it is heat and light-sensitive. Thus, the effect of high consolidation temperatures and pressures on α-tocopherol's efficiency to stabilize the residual free radicals subsequently caused by ionizing irradiation was not known. The oxidation resistance shown by these blends demonstrated that despite high temperatures and pressures under consolidation conditions, the resulting antioxidant efficiency was not detrimentally affected. Blended α-tocopherol with UHMWPE resin powder prior to irradiation was able to stabilize 100-kGy irradiated UHMWPE against oxidation.

The high oxidation of irradiated and accelerated aged virgin UHMWPE was accompanied by an increase in crystallinity, which was not observed in the two α-tocopherol blends (Table 1). The slight increase in crystallinity due to irradiation in all samples was an expected result since chain scission due to free radical formation and rearranging of these new chains into crystals occurred to some extent in the blends as well as virgin UHMWPE. The increase in crystallinity as a result of accelerated aging, however, is a result of the rearranging of smaller chains formed as a part of the oxidation and chain scission cascade. This effect was observed only in the virgin UHMWPE, which was highly oxidized, and not observed in the α-tocopherol blends, which did not oxidize. Highly oxidized UHMWPE showing high crystallinity was also brittle, whereas the α-tocopherol blends did not show embrittlement.

Questions? Contact FDA/CDRH/OCE/DID at CDRH-FOISTATUS@fda.hhs.gov or 301-796-8118

Records processed under FOIA Request #2014-8015; Released by CDRH on 12-8-2015

The decrease in cross-link density of 0.1 and 0.3 wt% α-tocopherol-blended, 100-kGy irradiated UHMWPE resulted in increased wear rates that were higher than that for 100-kGy irradiated and subsequently melted UHMWPE after accelerated aging [14] (Fig. 4). At the same time, these values were lower than that for gamma-sterilized GUR 1050 (38 kGy) [14]. Since the cross-link density of 0.3 wt% blended UHMWPE was lower than that for 0.1 wt% blended samples, the wear rate was significantly higher with the former.

The wear rate of 100-kGy irradiated, and α-tocopherol-diffused (at room temperature for a duration of 16 h) and gamma-sterilized UHMWPE (27 kGy) [6] was lower than that of 0.1 and 0.3 wt% α-tocopherol-blended UHMWPE in this study. This was because α-tocopherol-diffused samples received 100-kGy irradiation before the introduction of α-tocopherol; hence, there was no decrease in the cross-linking density due to the presence of α-tocopherol during the cross-linking process.

Wear rate of those materials that contain some unstabilized residual free radicals increase due to cascading oxidation and chain scission reactions when subjected to accelerated aging [14]. The difference in the wear rates of unaged and aged gamma-sterilized UHMWPE (Fig. 4) demonstrated this phenomenon since the residual free-radicals caused by 38 kGy of ionizing radiation in this material had not been stabilized. However, this type of increase in wear rate was not expected for α-tocopherol-blended samples, since these UHMWPEs showed very low oxidation indicative of stabilization of residual free-radicals. These results further corroborated the cross-link density measurements and showed that some of the radiation dose was absorbed by α-tocopherol such that the intended cross-link density was not imparted on α-tocopherol-blended UHMWPE.

Tensile testing of 0.1 and 0.3 wt% α-tocopherol-blended UHMWPE showed small changes from their unirradiated state to their irradiated and accelerated aged state (Table 2): a decrease in UTS, an increase in YS; and a decrease in elongation at break (EB).

The effects of oxidation and chain scission caused large decreases in UTS and YS in the accelerated aged, irradiated virgin UHMWPE. The UTS of α-tocopherol-blended, irradiated and accelerated aged UHMWPEs was between that of unirradiated and 100-kGy irradiated virgin material. YS values were similar to that of unirradiated material. There was a decrease in EB of irradiated and accelerated aged α-tocopherol blends compared to unirradiated blends, which can presumably be associated with cross-linking. This measure of mechanical property perhaps provided a more sensitive measurement of the effects of the degree of cross-linking on UHMWPE because of the difference that it showed as a function of α-tocopherol concentration. Since 0.1 and 0.3 wt% α-tocopherol-blended UHMWPE showed very low oxidation after irradiation and accelerated aging and no differences in crystallinity (Table 1), the difference in EB for the two concentrations were attributed to differences in cross-link density.

α-Tocopherol blending with UHMWPE prior to irradiation presents some advantages compared to introducing α-tocopherol after irradiation; very small amounts of α-tocopherol can be introduced into the polymeric material reliably and the concentration, low or high, would be uniform throughout. Based on previous studies, very small concentrations of α-tocopherol are enough to stabilize high-dose irradiated (~100-kGy) UHMWPE against oxidation even when the concentration is not uniform and only the surface is α-tocopherol-rich [6]. In terms of mechanical properties, a concentration of 0.2 wt% has been proposed for optimal results [15].

In this study, we have shown that α-tocopherol can react with the free radicals induced by ionizing radiation during and after irradiation. Therefore, interactions between the free-radicals and α-tocopherol as well as absorbed dose for cross-linking as a function of concentration of α-tocopherol warrant further investigation in order to render UHMWPE more wear resistant by blending with α-tocopherol and cross-linking by irradiation.

5. Conclusion

We have shown that α-tocopherol-blending with UHMWPE prior to irradiation imparts considerable oxidation resistance to irradiated UHMWPE and is a good stabilization method. However, cross-link density measurements and wear testing showed that α-tocopherol hinders cross-linking by reacting with some of the free-radicals during irradiation. Therefore, it is more desirable to diffuse α-tocopherol into previously irradiated UHMWPE to obtain a highly oxidation and wear-resistant cross-linked UHMWPE.

Acknowledgements

This work was funded by National Institutes of Health Grant R01 AR051142-01.

References

[1] Harris W. The problem is osteolysis. Clin Orthop 1995;311:46–53.
[2] McKellop H, Shen F-W, Lu B, Campbell P, Salovey R. Development of an extremely wear resistant ultra-high molecular weight polyethylene for total hip replacements. J Orthop Res 1999;17(2):157–67.
[3] Muratoglu O, Bragdon D, O'Connor D, Jasty M, Harris W. A novel method of crosslinking UHMWPE to improve wear with little or no sacrifice of mechanical properties. Society for biomaterials 25th annual meeting transactions, 1999. p. 496.

Questions? Contact FDA/CDRH/OCE/DID at CDRH-FOISTATUS@fda.hhs.gov or 301-796-8118

Records processed under FOIA Request #2014-8015; Released by CDRH on 12-8-2015

[4] Muratoglu OK, Bragdon CR, O'Connor DC, Jasty M, Harris WH. A unique crosslinking technique to improve the wear resistance of UHMWPE without sacrificing mechanical properties. Annual meeting of Academy of Orthopaedic Surgeons, 1999.

[5] Muratoglu OK, Bragdon CR, O'Connor DO, Jasty M, Harris WH, Gul R, McGarry F. Unified wear model for highly crosslinked ultra-high molecular weight polyethylenes (UHMWPE). Biomaterials 1999;20(16):1463–70.

[6] Oral E, Wannomae KK, Hawkins NE, Harris WH, Muratoglu OK. α-Tocopherol doped irradiated UHMWPE for high fatigue resistance and low wear. Biomaterials 2004;25(24):5515–22.

[7] McGovern TF, Ammeen DJ, Collier JP, Currier BH, Engh GA. Rapid polyethylene failure of unicondylar tibial components sterilized with gamma irradiation in air and implanted after a long shelf life. J Bone Jt Surg 2002;84-A(6):901–6.

[8] Chiu YS, Chen WM, Huang CK, Chiang CC, Chen TH. Fracture of the polyethylene tibial post in a NexGen posterior-stabilized knee prosthesis. J Arthroplasty 2004;19(8):9.

[9] Kamal-Eldin A, Appelqvist L. The chemistry and antioxidant properties of tocopherols and tocotrienols. Lipids 1996;31(7): 671–701.

[10] Burton G, Ingold K. Autoxidation of biological molecules. 1. The antioxidant activity of vitamin E and related chain-breaking phenolic antioxidants in vitro. J Am Chem Soc 1981; 103:6472–7.

[11] Mori A, Sakuramoto I, Tomita N, Kawano S, Nagata K, Utsumi K, Moriya H. Mechanical behavior of UHMWPE when mixed with vitamin E. 47th annual meeting, Orthopaedic Research Society, 2001

[12] Tomita N, Kitakura T, Onmori N, Ikada Y, Aoyama E. Prevention of fatigue cracks in ultrahigh molecular weight polyethylene joint components by the addition of vitamin E. J Biomed Mater Res 1999;48(4):474–8.

[13] Parth M, Aust N, Lederer K. Studies on the effect of electron beam radiation on the molecular structure of ultra-high molecular weight polyethylene under the influence of alpha-tocopherol with respect to its application in medical implants. J Mater Sci—Mater Med 2002;13(10):917–21.

[14] Muratoglu OK, Merrill EW, Bragdon CR, O'Connor DO, Hoeffel D, Burroughs B, Jasty M, Harris WH. Effect of radiation, heat, and aging on in vitro wear resistance of polyethylene. Clin Orthop Relat Res 2003;417:253–62.

[15] Luisetto Y. Degradation mechanism and effects of vitamin E addition in UHMWPE hip implants, PhD Thesis in polymer science and engineering. Lund: Lund Institute of Technology; 2003.

Questions? Contact FDA/CDRH/OCE/DID at CDRH-FOISTATUS@fda.hhs.gov or 301-796-8118

Records processed under FOIA Request #2014-8015; Released by CDRH on 12-8-2015

Biomaterials 29 (2008) 3557–3560

Contents lists available at ScienceDirect

Biomaterials

journal homepage: www.elsevier.com/locate/biomaterials

The effects of high dose irradiation on the cross-linking of vitamin E-blended ultrahigh molecular weight polyethylene

Ebru Oral [a,b], Christine Godleski Beckos [a], Arnaz S. Malhi [a], Orhun K. Muratoglu [a,b,*]

[a] Massachusetts General Hospital, Department of Orthopaedic Surgery, USA
[b] Harvard Medical School, USA

ARTICLE INFO

Article history:
Received 12 March 2008
Accepted 12 May 2008
Available online 2 June 2008

Keywords:
Antioxidant
Arthroplasty
Cross-linking
Gamma irradiation
Joint replacement
Polyethylene

ABSTRACT

Vitamin E-stabilized, highly cross-linked ultrahigh molecular weight polyethylene (UHMWPE) is a promising oxidation and wear resistant UHMWPE with improved mechanical strength in comparison with the first generation, irradiated and melted UHMWPE. One approach of incorporating vitamin E in UHMWPE is through blending of vitamin E in UHMWPE powder followed by consolidation and radiation cross-linking. However, radiation cross-linking efficiency of UHMWPE decreases in the presence of vitamin E. Therefore an optimum vitamin E concentration and radiation dose level need to be determined to achieve a cross-link density comparable to 100-kGy irradiated and melted UHMWPE, which has shown excellent wear properties in vivo. We investigated the cross-link density and mechanical properties of vitamin E-blended UHMWPEs as a function of vitamin E concentration in the blend and gamma irradiation doses up to 200 kGy. We found that 0.3 wt% vitamin E-blended UHMWPE could not be cross-linked above a cross-link density achieved at a radiation dose of 65 kGy for virgin UHMWPE and 1.0 wt% vitamin E-blended UHMWPE could not be cross-linked above a cross-link density achieved at a radiation dose of 25 kGy for virgin UHMWPE even when the these UHMWPEs were irradiated to a radiation dose of 200 kGy. In addition, higher plasticity at vitamin E concentrations at and above 0.3 wt% indicated that increased chain scissioning may be prevalent. Since the wear resistance of this irradiated UHMWPE would be expected to be low, vitamin E concentrations equal to or above 0.3 wt% are not recommended for subsequent irradiation to achieve a wear resistant cross-linked UHMWPE. The long-term oxidative stability of irradiated blends with low vitamin E concentrations has yet to be studied to determine an optimum between cross-link density and long-term oxidative stability.

© 2008 Elsevier Ltd. All rights reserved.

1. Introduction

Ultrahigh molecular weight polyethylene (UHMWPE) is the material of choice for total joint arthroplasty bearings. Wear of UHMWPE bearing surfaces contributes to the particulate debris burden that eventually leads to peri-prosthetic osteolysis in total joints. Radiation cross-linking of UHMWPE has been used to decrease wear successfully in vitro [1,2] and in vivo [3]. In addition, oxidation of cross-linked UHMWPE can decrease the mechanical properties and wear resistance substantially. Oxidation is primarily caused by trapped residual free radicals in the crystalline regions of UHMWPE after irradiation. Currently, thermal annealing below the melting point or melting of the cross-linked material is used to stabilize cross-linked UHMWPE, however, thermally annealed cross-linked UHMWPE has shown oxidation in vivo, presumably, due to the lack of elimination of all free radicals [4]. In contrast, melting subsequent to radiation cross-linking decreases the concentration of residual free radicals to undetectable levels and prevents long-term oxidation. However, melting also reduces crystallinity and mechanical properties of the irradiated polymer [5].

A second generation of cross-linked UHMWPE has been developed by stabilizing irradiated UHMWPE by the incorporation of vitamin E, an antioxidant, without melting the irradiated polymer, thus avoiding the reduction of mechanical properties [6,7]. Vitamin E hinders the cascading oxidation reactions in UHMWPE [8] by donating a hydrogen to the primary alkyl free radicals on polyethylene chains and the peroxy free radicals caused by reactions with oxygen. One approach is to diffuse the antioxidant into virgin UHMWPE after consolidation and radiation cross-linking. Another is to blend the vitamin E into UHMWPE powder and consolidate the blend. This blend subsequently can be irradiated to achieve a desired cross-link density. In addition to cross-linking, main chain scissioning is a mechanism that occurs when polymers are

* Corresponding author. Harris Orthopaedic Biomechanics and Biomaterials Laboratory, Massachusetts General Hospital, 55 Fruit Street, GRJ 1206, Boston, MA 02114, USA. Tel.: +1 617 726 3869; fax: +1 617 643 2521.
E-mail address: omuratoglu@partners.org (O.K. Muratoglu).

0142-9612/$ – see front matter © 2008 Elsevier Ltd. All rights reserved.
doi:10.1016/j.biomaterials.2008.05.004

Questions? Contact FDA/CDRH/OCE/DID at CDRH-FOISTATUS@fda.hhs.gov or 301-796-8118

Records processed under FOIA Request #2014-8015; Released by CDRH on 12-8-2015

irradiated. These mechanisms are characterized by their respective yields, which are defined as the number of newly formed intermolecular linkages, G_x and the number of main chain bonds broken, G_s per 100 eV of absorbed energy. Chain scission in polyethylene is very low with G_s/G_x values of 0.3–0.6 [9], where cross-linking dominates below a ratio of 4.0 [10]. The free radical scavenging ability of vitamin E interferes with cross-linking in UHMWPE [9,11], therefore, vitamin E concentration and radiation dose have to be optimized to achieve a desired cross-link density, comparable to 100-kGy irradiated and melted UHMWPE, which has shown very high wear resistance in vivo [12].

Another concern when considering the vitamin E concentration in blended UHMWPE is long-term oxidative stability. The advantage of vitamin E-stabilized cross-linked UHMWPE is improved mechanical properties over irradiated and melted UHMWPE while maintaining wear and oxidation resistance. However, some of the vitamin E is exhausted during radiation cross-linking of the blend [13]. Although not the topic of this paper, another optimum has to be considered between the cross-link density in the presence of vitamin E and the vitamin E concentration which will be enough to protect irradiated UHMWPE against oxidation in the long term.

The aim of this study was to investigate the effect of vitamin E concentration and radiation dose on cross-linking and mechanical properties. We further aimed to determine the vitamin E concentrations and subsequent radiation doses that could be used to achieve a cross-link density and mechanical properties equivalent to that of 100-kGy irradiated virgin UHMWPE. Since cross-link density has been shown to be directly related to wear [14], it is used as an indicator of wear resistance.

2. Materials and methods

2.1. Sample preparation

Blocks of UHMWPE (5.5 × 10 × 12 cm, GUR1050) containing vitamin E (D,L-α-tocopherol, >98%, Alfa Aesar, Ward Hill, MA) were prepared by mixing UHMWPE powder with vitamin E and consolidating the mixture. The UHMWPE powder was first mixed with vitamin E to obtain a 5 wt% mixture for consistency after which the mixture was adjusted to 0.1, 0.3, and 1.0 wt% vitamin E by diluting with virgin UHMWPE powder (Orthoplastics Ltd, Lancashire, UK). Virgin UHMWPE consolidated without vitamin E was used as control. Samples were irradiated by gamma irradiation to 25, 65, 100, 150 and 200 kGy (Steris Isomedix, Northborough, MA) in air. Thin sections (3.2 mm) were machined from samples for further testing.

2.2. Determination of cross-link density

Cross-link density measurements were performed by thermal mechanical analysis (DMA 7e, Perkin Elmer, Wellesley, MA). Thin sections (thickness 3.2 mm) were melted at 170 °C under nitrogen purge to remove any stresses residual from the consolidation process that might result in additional swelling during cross-link density measurements. Small sections were cut out by razor blade from these thin sections to be analyzed (approximately 3 mm by 3 mm). These pieces were placed under the quartz probe of the DMA (10 mN) and the initial height of the sample was recorded after about 10 min when the creep deformation equilibrated. Then, the probe was immersed in xylene, which was subsequently heated to 130 °C and held for at least 100 min. The UHMWPE samples swelled in hot xylene until equilibrium was reached. The final height was recorded. The cross-link density of the samples was calculated as described previously [14] and are reported as mol/m^3.

2.3. Mechanical testing

Dogbone specimens ($n = 5$ each) were stamped from 3.2 mm-thick sections in accordance with ASTM D638, standard test method for tensile properties of plastics. These samples were then tested in accordance with ASTM D638 using a MTS II machine (Eden Prarie, MN) at a crosshead speed of 10 mm/min. The engineering ultimate tensile strength (UTS) and work-to-failure (WF), calculated as the area under the engineering stress–strain curve are reported here. In addition, the elongation at break (EAB) was determined using an extensometer.

In all studies in which there were at least three samples, statistical analysis was performed using a Student's t-test for two-tailed distributions with unequal variance. Significance was reported if $p < 0.05$.

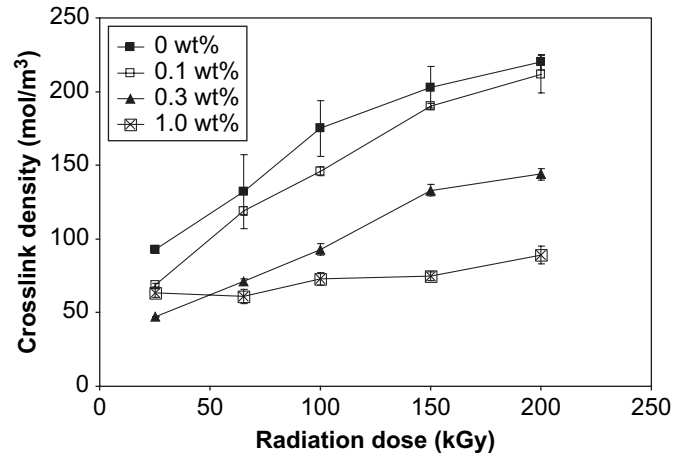

Fig. 1. Cross-link density of vitamin E-blended and subsequently irradiated UHMWPE as a function of vitamin E concentration.

3. Results

The cross-link density of virgin UHMWPE increased from about 90 mol/m^3 at a radiation dose of 25 kGy to about 210 mol/m^3 at 200 kGy (Fig. 1). The cross-link density did not change significantly above 150 kGy as previously shown for electron beam irradiated UHMWPE [14]. Except for 65-kGy irradiated 0.1 wt% vitamin E blend, the cross-link density of vitamin E-blended and irradiated UHMWPE was less than virgin UHMWPE at all radiation doses and decreased with increasing vitamin E concentration (Fig. 1).

Although the gel content increased with increasing radiation dose, except for 0.1 wt% vitamin E-blended UHMWPE, it decreased with increasing vitamin E concentration compared to virgin irradiated UHMWPE; this decrease was significant with the 0.3 wt% blend that was irradiated at a radiation dose of 65 kGy and 1 wt% blend at all radiation doses (Table 1).

The UTS and WF of irradiated virgin UHMWPE did not change significantly at 25 kGy and decreased gradually over the radiation dose range from 25 to 200 kGy compared to virgin, unirradiated UHMWPE (Figs. 2 and 4). The EAB decreased significantly at all doses (Fig. 3). The UTS, EAB and WF of 0.1 wt% vitamin E-blended UHMWPE stayed constant up to 100, 25 and 65 kGy, respectively, after which they decreased significantly (Figs. 2–4).

The UTS for 0.3 and 1 wt% vitamin E-blended UHMWPEs did not change at 25 kGy and increased significantly at 65 kGy compared to their unirradiated counterparts, then decreased significantly at 200 kGy (Fig. 2). The EAB and WF for 0.3 wt% vitamin E-blended UHMWPE increased significantly at 25 and 65 kGy was similar to unirradiated 0.3 wt% blended UHMWPE at 100 kGy and decreased significantly at 150 and 200 kGy. The EAB and WF of 1.0 wt% vitamin E-blended UHMWPE were similar to unirradiated 1.0 wt% blended UHMWPE at 25 kGy, increased significantly at 65 and 100 kGy, were similar to unirradiated 1.0 wt% blended UHMWPE at 150 kGy and decreased significantly at 200 kGy (Figs. 3 and 4).

Table 1
Gel content of vitamin E-blended and irradiated UHMWPEs

Vitamin E concentration (wt%)	Radiation Dose (kGy)				
	25	65	100	150	200
0	NT	97.6 ± 0.3	99.0 ± 0.5	98.2 ± 0.3	97.4 ± 0.1
0.1	NT	98.3 ± 0.8	98.4 ± 0.1	98.6 ± 0.1	98.2 ± 0.1
0.3	NT	95.1 ± 0.5	97.4 ± 1.4	97.4 ± 1.0	97.2 ± 0.4
1.0	NT	92.3 ± 0.4	93.7 ± 0.9	92.8 ± 0.1	93.5 ± 0.1

Questions? Contact FDA/CDRH/OCE/DID at CDRH-FOISTATUS@fda.hhs.gov or 301-796-8118

Records processed under FOIA Request #2014-8015; Released by CDRH on 12-8-2015

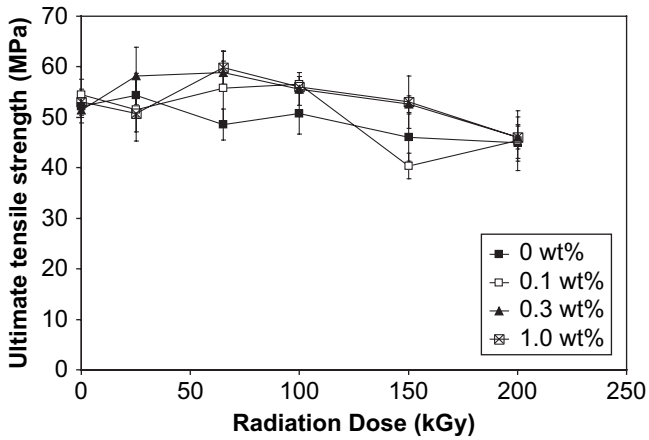

Fig. 2. Ultimate tensile strength (UTS) of vitamin E-blended and subsequently irradiated UHMWPE.

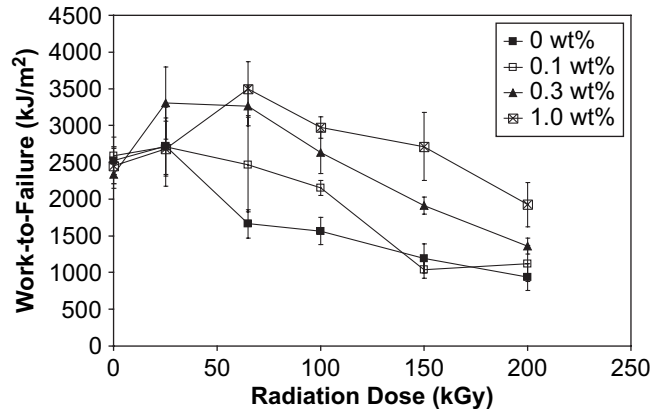

Fig. 4. Work-to-failure (WF) of vitamin E-blended and subsequently irradiated UHMWPE.

4. Discussion

The goal in irradiating vitamin E/UHMWPE blends is to obtain a cross-linked UHMWPE with enough cross-link density to achieve (1) wear properties equivalent to that of 100-kGy irradiated and melted UHMWPE, (2) improved strength to resist cyclic stresses even under adverse conditions and (3) long-term oxidative stability such that the wear and mechanical properties can be maintained in the long term. One disadvantage of blending vitamin E with UHMWPE prior to irradiation is decreasing the potency of vitamin E during irradiation. Since vitamin E is a free radical scavenger, it interacts with the free radicals formed on polyethylene chains during irradiation and sacrifices some of its activity. In addition, we [11] and others [9] have shown that cross-linking efficiency in UHMWPE is decreased with increasing vitamin E concentration due to its activity during irradiation. Therefore, it is proposed that high radiation dose with low vitamin E concentration is required to obtain a desired cross-link density. Although not the topic of this paper, it has to be noted that the vitamin E concentration has to be kept high enough to protect irradiated UHMWPE against oxidation in the long term.

In light of these general goals, the specific aim of this paper was to investigate the effects of vitamin E concentration and radiation dose on the cross-link density and mechanical properties of irradiated blends. The dependence of cross-linking of virgin UHMWPE on radiation dose (Fig. 1) was previously reported [14] and relates directly to increased wear resistance. Similar to the cross-link density of radiation cross-linked virgin UHMWPE, the cross-link density for vitamin E blends reached an equilibrium value above 150 kGy. In contrast, the maximum value of cross-link density reached at 200 kGy was lower than virgin UHMWPE and decreased with increasing vitamin E concentration. Of the vitamin E-blended samples used in this study, 0.3 and 1.0 wt% vitamin E-blended UHMWPEs reached an equilibrium cross-link density of 144 and 89 mol/m^3, respectively, at 200 kGy; this value was lower than that of 100-kGy irradiated virgin UHMWPE (175 mol/m^3; Fig. 1). UHMWPE bearing surfaces cross-linked to approximately 65–100 kGy have been successful in reducing the wear rate of UHMWPE substantially. Ideally, an optimized vitamin E-blended UHMWPE would have a cross-link density and thus a wear rate comparable to or better than 100-kGy irradiated, virgin UHMWPE. Looking at the minimal incremental change in cross-link density of 1 wt% vitamin E-blended UHMWPE over the 25–200 kGy dose range, it appeared that it was not even possible to obtain a substantially cross-linked UHMWPE from stock containing 1 wt% vitamin E (Fig. 1). Moreover, the gel content of 0.3 and 1.0 wt% blends are substantially lower than that of virgin and 0.1 wt% blended UHMWPE, even at the highest radiation dose (Table 1). These results suggest that vitamin E concentrations equal to or above 0.3 wt% prevent achieving desirable cross-link density in UHMWPE for improved wear resistance.

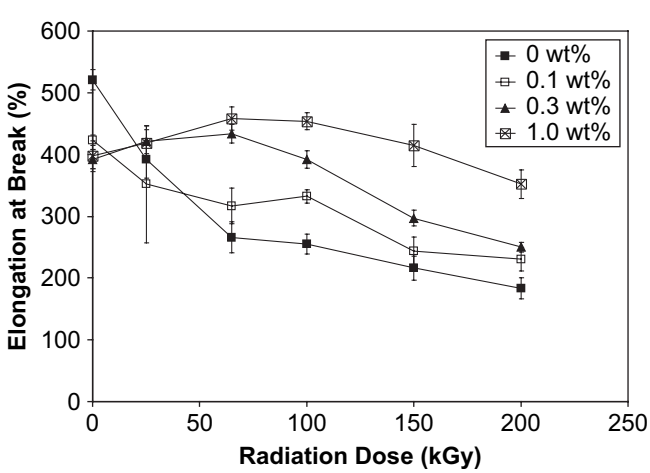

Fig. 3. Elongation at break (EAB) of vitamin E-blended and subsequently irradiated UHMWPE.

Cross-links introduced into the amorphous phase by radiation decrease the mobility of the chains and the overall plasticity of the polymer. While this phenomenon results in a decrease in wear, it also leads to a decrease in mechanical properties of virgin irradiated UHMWPE ([5], Figs. 2–4). The decrease in plasticity is manifested as a dose-dependent decrease in elongation to break (EAB) and work-to-failure (WF). If the mechanical properties were dependent solely on the cross-link density, then we would have expected that EAB, WF and UTS of vitamin E-blended, irradiated UHMWPE to be similar to those of virgin UHMWPE of similar cross-link density and gradually decrease as a function of radiation dose as observed in virgin irradiated UHMWPE. However, the increase and eventual decrease in UTS, EAB and WF of 0.3 and 1.0 wt% blends over the studied radiation dose range suggested that there may be increased chain scissioning affecting the properties despite increasing cross-linking.

We propose that because vitamin E could hinder cross-linking, that chain scissioning became more prominent. Consider that a vitamin E molecule is in the vicinity of a C–C bond, which has been broken and has created two C free radicals due to radiolytic cleavage. It is possible that the recombination probability of these

Questions? Contact FDA/CDRH/OCE/DID at CDRH-FOISTATUS@fda.hhs.gov or 301-796-8118

Records processed under FOIA Request #2014-8015; Released by CDRH on 12-8-2015

two free radicals is decreased because vitamin E can donate a proton to at least one of these free radicals. This would result in increased incidence of chain scission and a decrease in effective molecular weight by an increase in the number of chain ends. This mechanism would also compete with the effect of cross-linking in terms of mechanical properties. While cross-linking creates a less mobile network, chain scissioning would increase local mobility of the chains. We discuss the possibility of increased chain scission through mechanical properties because it was not possible to calculate reliable G_S and G_X values for such highly cross-linked samples, whose gel content did not change substantially with increasing radiation dose within the studied range (Table 1). These values are reliably calculated for irradiated UHMWPEs below or around gelation [15].

Similar to virgin UHMWPE, 0.1 wt% vitamin E-blended UHMWPE showed gradually decreasing mechanical properties as a function of increasing radiation dose. This suggested that cross-linking was the dominating mechanism in this irradiated UHMWPE. In contrast, in 0.3 wt% up to 100 kGy and in 1.0 wt% vitamin E-blended UHMWPE up to 150 kGy, plasticity (as quantified by EAB and WF) increased, suggesting that the effect of chain scissioning may have dominated, despite increasing cross-linking density. We postulate that at radiation doses higher than 150 kGy for 0.3 and 1.0 wt% vitamin E-blended UHMWPE, the activity of vitamin E was substantially decreased and therefore cross-linking became more prominent; as a result, the UTS, EAB and WF decreased.

We determined that not only is the cross-link density at a given radiation dose lower for increasing vitamin E concentration blended into UHMWPE, but also that the limit of cross-link density is lower at higher concentrations of vitamin E, making it impossible to achieve high cross-link density despite high radiation doses for some vitamin E concentrations. In addition, we found that at high vitamin E concentrations and low irradiation doses, chain scissioning in UHMWPE may become prevalent. This study suggests that there is a maximum concentration of vitamin E below 0.3 wt% feasible for use in radiation cross-linking of vitamin E blends as alternative total joint replacement bearing surfaces.

Another concern in considering what vitamin E concentration should be used in highly cross-linked UHMWPE is long-term oxidative stability. Since vitamin E is used up during irradiation, there should also be a lower limit of vitamin E that can be used such that irradiated UHMWPE is protected against oxidation. Our current studies focus on accelerated and real-time aging of vitamin E-blended UHMWPEs of different concentrations irradiated up to 200 kGy to determine this yet unknown limit.

5. Conclusions

The cross-linking density of 100-kGy irradiated virgin UHMWPE could not be achieved by increasing radiation dose for 0.3 and 1.0 wt% vitamin E-blended UHMWPE due to the free radical scavenging activity of vitamin E. Irradiation at this concentration of vitamin E also resulted in higher plasticity over 65–150 kGy irradiation range, suggesting increased chain scissioning in addition to decreased cross-linking compared to virgin, irradiated UHMWPE. Since these will lead to decreased wear resistance, vitamin E concentrations equal to or above 0.3 wt% are not recommended for subsequent irradiation to achieve a wear and oxidation resistant cross-linked UHMWPE.

Acknowledgements

This work was funded by a research grant from the National Institutes of Health (AR051142) and a research grant from Zimmer, Inc.

References

[1] Muratoglu OK, Merrill EW, Bragdon CR, O'Connor DO, Hoeffel D, Burroughs B, et al. Effect of radiation, heat, and aging on in vitro wear resistance of polyethylene. Clinical Orthopaedics and Related Research 2003;417:253–62.
[2] McKellop H, Shen F-W, Lu B, Campbell P, Salovey R. Development of an extremely wear resistant ultra-high molecular weight polyethylene for total hip replacements. Journal of Orthopaedic Research 1999;17(2):157–67.
[3] Digas G, Karrholm J, Thanner J, Herberts P. 5-year experience of highly crosslinked polyethylene in cemented and uncemented sockets – two randomized studies using radiostereometric analysis. Acta Orthopaedica 2007;78(6):746–54.
[4] Wannomae K, Bhattacharyya S, Freiberg A, Estok D, Harris W, Muratoglu O. In vivo oxidation of retrieved crosslinked UHMWPE acetabular components with residual free radicals. Journal of Arthroplasty 2006;21(7):1005–11.
[5] Oral E, Malhi A, Muratoglu O. Mechanisms of decrease in fatigue crack propagation resistance in irradiated and melted UHMWPE. Biomaterials 2006;27:917–25.
[6] Oral E, Wannomae KK, Hawkins NE, Harris WH, Muratoglu OK. α-Tocopherol doped irradiated UHMWPE for high fatigue resistance and low wear. Biomaterials 2004;25(24):5515–22.
[7] Oral E, Christensen S, Malhi A, Wannomae K, Muratoglu O. Wear resistance and mechanical properties of highly crosslinked UHMWPE doped with vitamin E. Journal of Arthroplasty 2006;21(4):580–91.
[8] Oral E, Rowell S, Muratoglu O. The effect of alpha-tocopherol on the oxidation and free radical decay in irradiated UHMWPE. Biomaterials 2006;27:5580–7.
[9] Parth M, Aust N, Lederer K. Studies on the effect of electron beam radiation on the molecular structure of ultra-high molecular weight polyethylene under the influence of alpha-tocopherol with respect to its application in medical implants. Journal of Materials Science: Materials in Medicine 2002;13(10):917–21.
[10] Charlesby A, Pinner SH. Analysis of the solubility behaviour of irradiated polyethylene and other polymers. Proceedings of the Royal Society of London 1958;269A:367–86.
[11] Oral E, Greenbaum E, Malhi A, Muratoglu O. Characterization of blends of α-tocopherol with UHMWPE. Biomaterials 2005;26:6657–63.
[12] Digas G, Karrholm J, Thanner J, Malchau H, Herberts P. Highly cross-linked polyethylene in total hip arthroplasty: randomized evaluation of penetration rate in cemented and uncemented sockets using radiostereometric analysis. Clinical Orthopaedics and Related Research 2004;429:16.
[13] Bracco P, Brunella V, Zanetti M, Luda MP, Costa L. Stabilisation of ultra-high molecular weight polyethylene with vitamin E. Polymer Degradation and Stability 2007;92:2155–62.
[14] Muratoglu OK, Bragdon CR, O'Connor DO, Jasty M, Harris WH, Gul R, et al. Unified wear model for highly crosslinked ultra-high molecular weight polyethylenes (UHMWPE). Biomaterials 1999;20(16):1463–70.
[15] Janik I, Kasprzak E, Al-Zier A, Rosiak J. Radiation cross-linking and scission parameters for poly(vinyl methyl ether) in aqueous solution. Nuclear Instruments and Methods in Physics Research B 2003;208:374–9.

Questions? Contact FDA/CDRH/OCE/DID at CDRH-FOISTATUS@fda.hhs.gov or 301-796-8118

Records processed under FOIA Request #2014-8015; Released by CDRH on 12-8-2015

Crosslinked Vitamin E Blends with Improved Grafting and Wear Resistance

+[1,2]Oral, E; [1]Neils, A; [1]Rowell, SL; [1,2]Muratoglu OK
+[1]Harris Orthopaedic Laboratory, Massachusetts General Hospital, Boston, MA; [2]Department of Orthopaedic Surgery, Harvard Medical School
eoral@partners.org

Statement of Purpose

Vitamin E-stabilization of irradiated UHMWPE for oxidation resistant total joint implants can be done by blending vitamin E into UHMWPE powder, consolidation of the mixture, and irradiation [1]. This method avoids post-irradiation melting, which decreases the fatigue strength of irradiated UHMWPE [2].

Table 1. The radiation doses used to crosslink vitamin E blended UHMWPE.

Vitamin E concentration (wt%)	Radiation Dose (kGy)
-	100
0.05	120
0.1	125
0.2	160
1	198

Free radicals formed on the polymer during irradiation recombine to form cross-links, which impart increased wear resistance [3]. When vitamin E is present in UHMWPE during irradiation, it reacts with the free radicals, decreasing crosslinking compared to virgin UHMWPE at the same radiation dose [4]. At the same time, it is possible that some of the vitamin E gets grafted onto the polymer as previously shown with other antioxidants [5]. This is beneficial as it would localize some of the antioxidant and prevent elution.

In this study, we determined the amount of grafting in vitamin E-blended and irradiated UHMWPE. We hypothesized that increasing irradiation temperature would increase crosslinking despite decreasing vitamin E potency due to degradation at the higher temperature. To test our hypothesis, we determined the vitamin E content, vitamin E grafting, crosslink density and wear properties of vitamin E-blended UHMWPE irradiated at room temperature and at 120°C.

Materials and Methods

Medical grade GUR1050 UHMWPE (Orthoplastics, UK) was blended with 1 wt% vitamin E and consolidated. One group was irradiated using e-beam (2.5 MeV, MIT, MA) to 25, 50, 75, 100, 125 and 150 kGy at room temperature (RT). Another group was pre-heated at 120°C for 2 hours and then irradiated to the same doses (Warm). Thin sections (150 μm-thick) were microtomed from the irradiated blocks. Fourier transform infrared spectroscopy (FTIR) was used to determine a vitamin E index (1245-1275 cm^{-1} normalized to 1850-1985 cm^{-1}) before and after extraction with boiling hexane for 16 hours. Graft percentage was calculated by the ratio of the post-extraction vitamin E index to that before extraction.

Crosslink density was measured by swelling 3 mm cubes in xylene pre-heated to130°C for 2 hours. The gravimetric swell ratio was converted to a volumetric swell ratio using the density of polyethylene as 0.94 g/cc and the density of xylene at 130°C as 0.75 g/cc. The crosslink density was further calculated as previously described [7].

Cylindrical pins (dia. 9 mm, height 13 mm) were machined from virgin UHMWPE and blends of UHMWPE containing 0.05, 0.1, 0.2 and 1 wt% vitamin E. These pins were irradiated as described in Table 1. Pin-on-disc (POD) wear testing was performed as previously described [8] at 2 Hz for 1.2 million-cycles (MC). Wear was determined gravimetrically every ~0.16 MC and the wear rate was determined by the weight change from 0.5 to 1.2 MC.

Results

The goal of this study was to determine the extent of grafting in vitamin E-blended, irradiated UHMWPE. We used 1 wt% vitamin E blends because at this concentration, we could detect vitamin E by FTIR even after irradiation. However, we know from previous studies on the crosslinking of UHMWPE in the presence of vitamin E that radiation behavior as a function of concentration may not be linear; this remains a limitation of our study.

We showed previously that vitamin E decreased crosslinking in UHMWPE, thus at 1 wt% vitamin E, crosslink density is lower than at vitamin E concentrations typically considered for implants, e.g. 0.1 or 0.2 wt% at the equivalent radiation dose [5]. During irradiation used for crosslinking UHMWPE, vitamin E interferes with the free radicals on the polymer chains, which also results in the transformation of vitamin E into other products. Thus, vitamin E concentration decreased with increasing radiation dose (Fig 1). Increasing irradiation temperature resulted in higher vitamin E concentrations after irradiation (Fig 1), suggesting longer post-irradiation oxidative stability.

We also showed that vitamin E was grafted in UHMWPE by irradiation (Fig 2). Grafting may suggest longer term in vivo oxidative stability without elution.

Figure 1. Vitamin E index as a function of radiation dose and temperature.

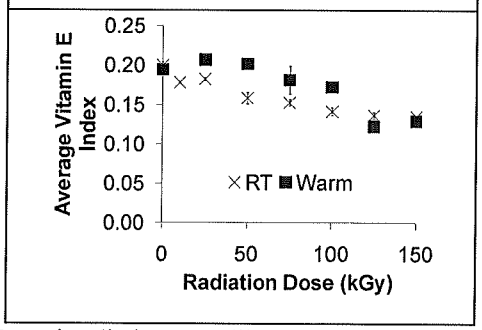

Warm irradiation was likely to cause more thermal degradation of vitamin E and the free radical scavenging of vitamin E was likely faster at higher temperature. It was unexpected not only that vitamin E content was better preserved after warm irradiation but also that increasing

Questions? Contact FDA/CDRH/OCE/DID at CDRH-FOISTATUS@fda.hhs.gov or 301-796-8118

Records processed under FOIA Request #2014-8015; Released by CDRH on 12-8-2015

irradiation temperature increased grafting (Fig 2). The implication of this result is that by controlling irradiation temperature, grafting of antioxidants can be maximized for optimal oxidation resistance.

Figure 2. The extent of vitamin E grafting on UHMWPE as a function of radiation dose and temperature.

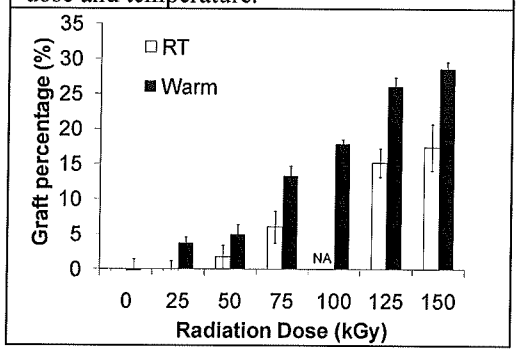

Figure 3. Cross-link density of vitamin E-blended, irradiated UHMWPE as a function of radiation dose and temperature.

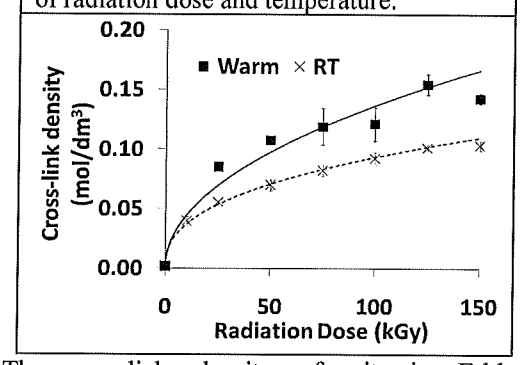

The crosslink density of vitamin E-blended, irradiated UHMWPE was higher than that irradiated at RT (Fig 3), again suggesting that the free radical scavenging activity of vitamin E was less at higher temperature. Since the wear of UHMWPE decreases with increasing crosslinking [4], this suggests that warm irradiation leads to lower wear rate.

This was corroborated by wear testing, where warm irradiation of UHMWPE resulted in lower wear rate than irradiation at room temperature for irradiated vitamin E blends of UHMWPE (Fig 4). The blends were irradiated to different doses to obtain similar crosslink density.

Figure 4. Wear rates of irradiated blends.

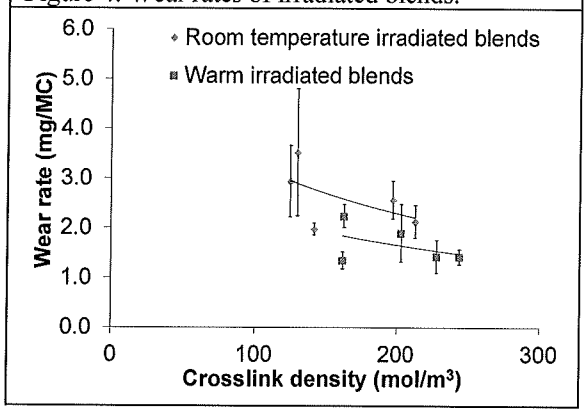

Conclusions

While radiation crosslinking of vitamin E-blended UHMWPE decreases crosslinking compared to virgin UHMWPE and also decreases the vitamin E in UHMWPE for long-term oxidative stability, it also results in increased grafting of the antioxidant on the polymer, presumably resulting in longer-term stability. Moreover, warm irradiation allowed for increased preservation of the antioxidant, increased grafting, increased cross-linking and decreased wear. This result is significant for the wear and oxidation stability of stabilized UHMWPE joint implants.

Acknowledgements

This study was funded by laboratory funds.

References

[1] Kurtz et al. JBMR 90A:549-563 (2009); [2] Oral et al. Biomaterials 27(6):917-925 (2006); [3]Muratoglu et al. Biomaterials 24(8): 1527-1537 (2003); [4]Oral et al. Biomaterials 29(26): 3557-3560 (2008); [5]Allen et al. Radiat. Phys. Chem.. 38(5): 461-465 (1991); [6] Oral et al. Biomaterials 31:7051-7060 (2010); [7] Bragdon et al. JOA 16(5): 658-665 (2001).

Questions? Contact FDA/CDRH/OCE/DID at CDRH-FOISTATUS@fda.hhs.gov or 301-796-8118

Records processed under FOIA Request #2014-8015; Released by CDRH on 12-8-2015

Acta Orthop. Belg., 2011, **77**, 421-431

REVIEW ARTICLE

Basic kinematics and biomechanics of the patello-femoral joint Part 1 : The native patella

Oliver S. Schindler, W. Norman Scott

From Droitwich Spa Hospital, England, UK

The patello-femoral joint (PFJ) enhances our ability of knee flexion and extension and is assumed to have evolved through men's ability of having adopted a bipedal gait. This articulation between patella and femur is relatively complex and displays intricate biomechanical behaviour. Forces in the patello-femoral joint are a function of the quadriceps force, and the angle of flexion of the knee. They are highly dependent on the distance between the patello-femoral joint and the centre of gravity, which explains why different activities despite equivalence in tibio-femoral angle may exert wide variations in patello-femoral reaction forces and contact pressures. During normal daily activities the PFJ becomes exposed to force values between 0.5 to 9.7 × body weight, whilst sporting activities create force values that approach up to 20 × body weight. Those forces are considerable and it is therefore not surprising that the PFJ is particularly susceptible to degenerative disease especially if its mechanical equilibrium is disturbed through injury, muscle weakness and congenital or developmental abnormalities. The clinician must be aware of biomechanical and kinematic specifics, the high patello-femoral load values, small patellofemoral contact areas, and resultant high stress magnitudes when trying to remedy such abnormalities.

Keywords : patellofemoral joint ; kinematics ; biomechanics.

INTRODUCTION

Any clinician contemplating treatment for conditions affecting the patello-femoral joint must possess some basic knowledge of anatomy, biomechanics and kinematics of the knee and the locomotor system. Without such understanding it is difficult to appreciate the implications associated with the various surgical and conservative treatment modalities. This is of particular importance when considering surgical remedies in the treatment of patello-femoral disorders (e.g. localised cartilage defects, chondromalazia) especially if associated with patella mal-tracking, as changes in the relationship between patella and femur may significantly alter the distribution of forces and any overcorrection may potentially hasten the development of degenerative disease. Similar concerns exist with regard to the treatment of the patella in total knee arthroplasty, where surgically imposed changes through resurfacing may have significant effects on performance and behaviour of the patello-femoral joint (*1,11*). Complications arising from patella resurfacing are still considerable and analysis of retrieved patellar components and the significant

■ Oliver S. Schindler, MD, ÖFD, MFSEM, FRCSEd, FRCSE, FRCS (Orth).
Droitwich Spa Hospital, England, UK.
■ W. Norman Scott, MD, FACS.
Insall Scott Kelly Institute of Orthopaedics and Sports Medicine, New York City, NY, USA.
Correspondence : Mr O. Schindler, PO Box 1616, Bristol BS40 5WG, England, UK. E-mail : schindler@doctors.net.uk
© 2011, Acta Orthopædica Belgica.

No benefits or funds were received in support of this study

Questions? Contact FDA/CDRH/OCE/DID at CDRH-FOISTATUS@fda.hhs.gov or 301-796-8118

Records processed under FOIA Request #2014-8015; Released by CDRH on 12-8-2015

failure rate of metal backed patella designs continue to underscore the extreme mechanical environment in which these implants are expected to perform (*8,12,42*).

Kinematics of the patello-femoral joint

Kinematics of knee joint characterises the relative motion that exists between femur, tibia and patella (*53*). The patella is a sesamoid bone implanted within the tendon of the extensor mechanism. Arguably its most important function is its role in facilitating extension of the knee by increasing the efficacy of the quadriceps muscle (*26*). This is achieved through the patella's function as a fulcrum, thus anteriorly displacing the line of pull and increasing the moment arm of the quadriceps muscle force in relation to the centre of rotation of the knee. The patella has shown to enhance the force of extension by as much as 50% throughout the entire range of motion (*53*). The patella also facilitates improved distribution of patello-femoral compressive force on the femur through an increase in contact area during flexion (Fig. 1). In addition the patella acts as a guide for the extensor mechanism by centralising the divergent pull from the four muscles of the quadriceps and transmitting these forces to the patella tendon. Together with the anatomical shape of the patello-femoral articulation this protects the extensor apparatus from dislocating.

When the knee is extended, the tightened quadriceps pulls the patella upwards until the upper border reaches beyond the femoral trochlea groove. So long as the line of gravity falls behind the center axis of the knee joint when standing upright, the quadriceps must contract to neutralize the rotatory effect of gravity on the knee, which would otherwise force the knee into flexion. As soon as the line of gravity falls within or in front of the knee, as seen in full extension or hyperextension, the quadriceps becomes relaxed. The quadriceps apparatus, being oblique in its angulation towards the patella and patellar tendon, creates a line of pull with an outward directed horizontal component when contracted. The angle between the line of pull and the patella tendon is often referred to as the Q-angle, which is responsible for a tendency of the patella to slip outward over the lateral femoral condyle creating a lateral force vector (*18*). To offset this propensity the lateral condyle projects farther forward whilst the fibres of vastus medialis which secure the patella medially extend farther distally compared to those of the vastus lateralis (*53*). The reversal of the 'screw home mechanism' during the initial 30° of knee flexion, essentially derotates the tibia, leading to a reduction in Q-angle and lateral force vector (*7,19,23,40,41*). In the coronal and axial views, this sideways component (lateral vector), which reduces with knee flexion, is balanced by the reaction occurring on the slope of the femoral trochlea (Fig. 2) (*60*). Hence the patella is most vulnerable during the initial degrees of knee flexion, when its engagement into the trochlea may still be incomplete whilst the effect of the Q-angle, albeit reduced, remains present.

Patello-femoral contact areas

The patella is usually out of contact with the trochlea groove in full extension. Depending on the length of the patellar tendon, the patella is drawn into the trochlea from a slight lateral position and gains contact with the femur between 10° to 20° (Fig. 1) (*20,51*). The contact begins with the inferior margin of the patella and moves proximally as flexion proceeds (Fig. 3) (*36*). Beyond 30° the patella settles into the deepening trochlea groove where it is further stabilised by the quadriceps and patellar tendon force.

The patello-femoral contact area extends from the medial margin of the medial facet to the lateral margin of the lateral facet as a broad band of contact moving from distal to proximal (*2,19,22,25,29*). Between 30° to 60° of flexion the contact is across the centre, at 90° of flexion the contact moves towards the superior pole, and beyond 90° the patella is astride the medial and lateral condyles, forming two separate contact areas (Fig. 4). During flexion the patella maintains a lateral shift as well as a subtle degree of rotation around a longitudinal axis, positioning the medial facet more posterior (*47,56,58*). In full flexion the lateral femoral condyle is completely covered by the lateral patella

Questions? Contact FDA/CDRH/OCE/DID at CDRH-FOISTATUS@fda.hhs.gov or 301-796-8118

Records processed under FOIA Request #2014-8015; Released by CDRH on 12-8-2015

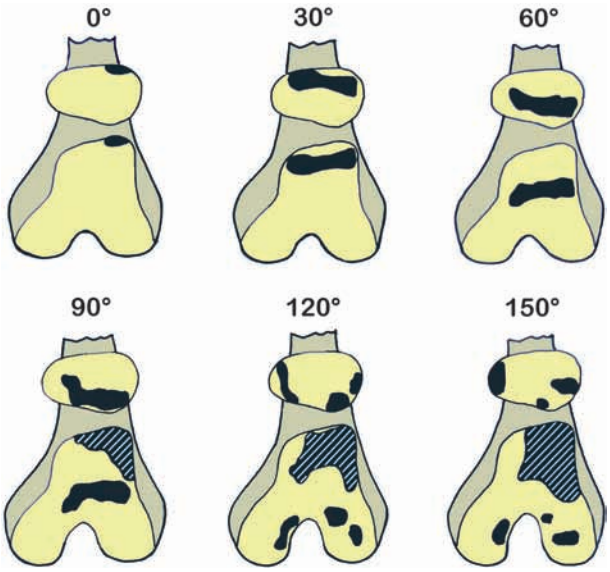

Fig. 1. — Patello-femoral (solid area) and tendo-femoral (shaded area) contact areas at various degrees of knee flexion.

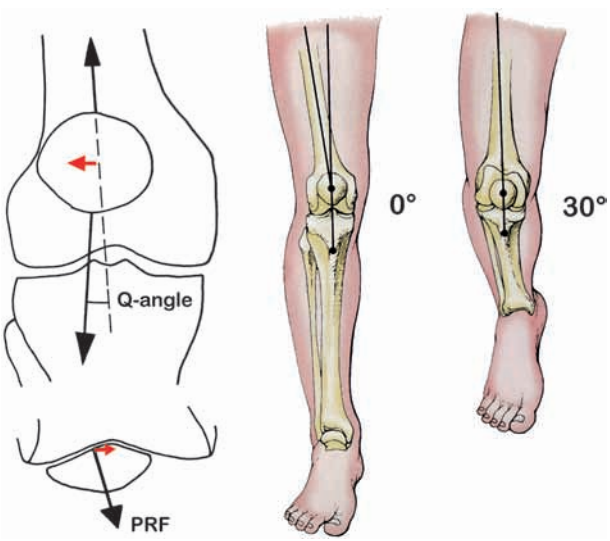

Fig. 2. — Internal rotation of tibia during flexion neutralises Q-angle and reduces lateral patello-femoral vector. In the coronal and axial views, the sideways component is balanced by the reaction occurring on the slope of the femoral trochlea (Adapted from Walker (60), courtesy of Charles C Thomas Publishers Ltd, Springfield, Illinois).*

FIGURES (* where necessary permission has been obtained from publisher).

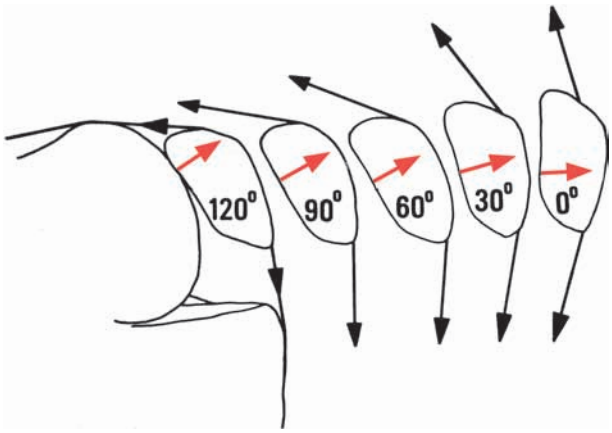

Fig. 3. — Contact points between patella and femur move from proximal to distal on the femur and from distal to proximal on the patella during knee flexion (adapted from Walker (60), courtesy of Charles C Thomas Publishers Ltd, Springfield, Illinois).*

facet whilst the medial condyle is almost completely uncovered being merely in contact with the odd facet. Ficat and Hungerford have described this movement of the patella in the coronal plane during flexion as a 'gentle curve with its concavity facing laterally' (*19*). Studies of the tracking pattern of the natural patella have confirmed that the patella rotates as much as 12° to 15° in relation to the femur, with most of the rotation occurring beyond 50° of knee flexion (*31,47,49,56,57*). Furthermore the patella tilts about a medio-lateral direction in the axial plane, being influenced by knee flexion, the degree of internal or external rotation and the varus/valgus alignment of the tibio-femoral joint (*56,57*). Similarly, the patella undergoes medially directed displacement by as much as 5 mm in the coronal plane, with most of the displacement occurring during the initial 30° of knee flexion.

In the transverse or axial plane, as seen on skyline radiographs, the patella is perfectly congruent with the trochlea, assuring its medial/lateral stability. Longitudinal sectioning of the patella, as performed by Krakow and Hungerford, has confirmed that the patella adopts almost a flat surface in the sagittal plane making it perfectly unconstrained as far as its anatomical form is concerned (*34*). They concluded that the length of the patella tendon and the angle between the patellar tendon and the

Questions? Contact FDA/CDRH/OCE/DID at CDRH-FOISTATUS@fda.hhs.gov or 301-796-8118

Records processed under FOIA Request #2014-8015; Released by CDRH on 12-8-2015

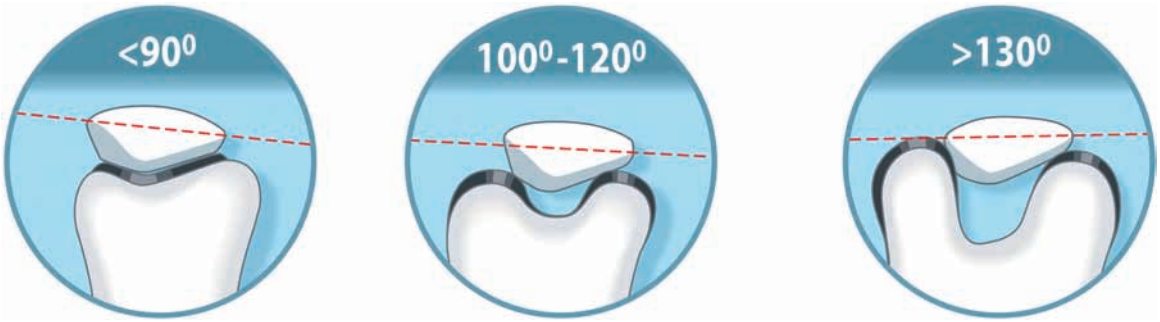

Fig. 4. — Bifurcation of patello-femoral contact area beyond 100° of knee flexion. The odd facet of the patella only makes contact with the medial femoral condyle beyond 125° to 135° of knee flexion.

quadriceps tendon determine the load bearing area of the patella. The patella form, therefore, provides stability against lateral subluxation but does not impede the patella from rocking around its transverse axis to the point at which the resultant of the patello-femoral joint reaction force is perpendicular to the contact surface.

As with the location of patello-femoral contact areas, the size of the contact areas is highly dependent on knee position. From 20° to 60° of flexion the average contact area increases linearly from around 150 mm^2 to 480 mm^2 (*2,28,39,55*). It then remains almost constant up to about 90° of flexion after which a linear reduction occurs (*25,28,39*). At 120° the contact area will have dropped to 360 mm^2 (*55*). Due to the drastically changed contact pattern beyond 100°, when the patella leaves the trochlea straddling the intercondylar notch, contact areas may fall well below 100 mm^2 at full flexion (Fig. 4) (*25*). Matthews *et al* have shown that on average only 19% of the patella bearing surface is engaged at 30° of flexion, 29% at 60°, 28% at 90°, and 13% at 120° (*39*). These values compare favourably with those obtained by Huberti *et al* who measured percentage values of the patello-femoral contact area of between 20.5% to 32.2% (*28*).

Biomechanics

Wide attention has been given to define the force transmission in the patello-femoral joint. For ease of calculation it is sufficiently accurate to consider these forces to lie in a sagittal plane. Reaction forces are equal and opposite forces that exist between adjacent bones at a joint and caused by the weight and inertial forces of the two segments. The term patello-femoral compressive force (PCF), representing the sole load acting on the patella, and patello-femoral reaction force (PRF) may be used interchangeably, although it is conceivable that the resultant (reaction) force produced by the quadriceps mechanism at different angles of flexion may be broken into normal (compressive) and tangential force components. For the purpose of this review however, we may assume equality between PCF and PRF, with the latter acting perpendicular to the articulating surface of the patella and equal and opposite to the resultant of the patellar tendon and quadriceps force, based on the 'Parallelogram of Forces' (Fig. 5) (*60*). With increasing flexion the line of reaction moves upwards leading to an increase in PRF for the following reasons. As the angle between the patella tendon and the quadriceps becomes more acute the resultant force vector increases. With knee flexion effective leaver arms of femur and tibia increase, requiring greater quadriceps power to resist the flexion moment of the body weight. Close to extension the PRF is only about 1/3 of the quadriceps force, whilst beyond 60° of flexion the patella force is about 1 ¼ times the quadriceps force (*60*). The line of pull between the quadriceps and patella tendon when viewed in the coronal plane is affected by the Q-angle, giving a resultant force in the lateral direction (Fig. 2) (*19*). In the axial plane this is balanced by a reaction force which is inclined inwards. Walker conceded

Questions? Contact FDA/CDRH/OCE/DID at CDRH-FOISTATUS@fda.hhs.gov or 301-796-8118

Records processed under FOIA Request #2014-8015; Released by CDRH on 12-8-2015

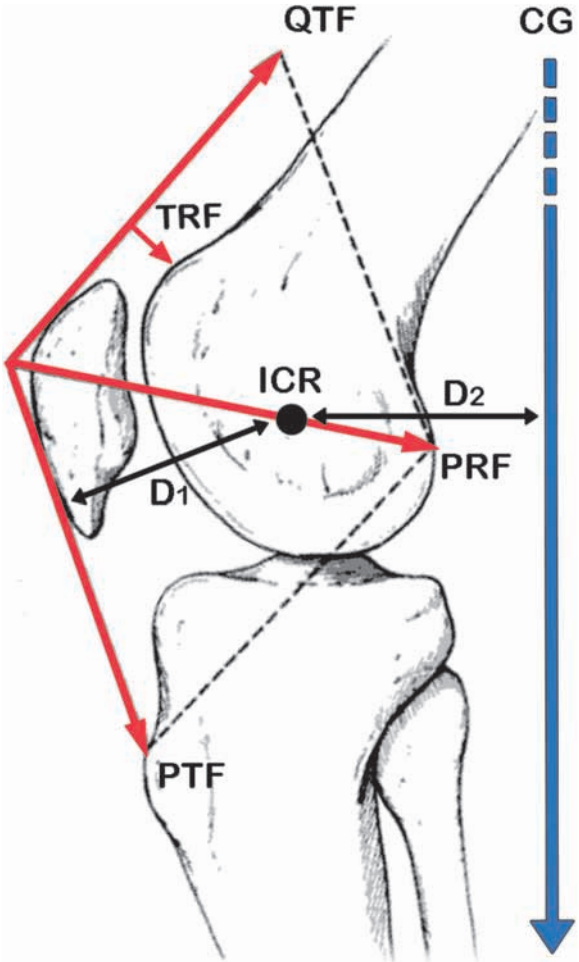

Fig. 5. — Free-body diagram of the patello-femoral joint showing the 'Parallelogram of Forces'. The patella-femoral reaction force (PRF) is the resultant vector of the quadriceps tendon strain force (QTF) and the patellar tendon strain force (PTF). The tendo-femoral reaction force (TRF = force between quadriceps tendon and trochlea) is also shown. CG = centre of gravity. ICR = instant centre of rotation.

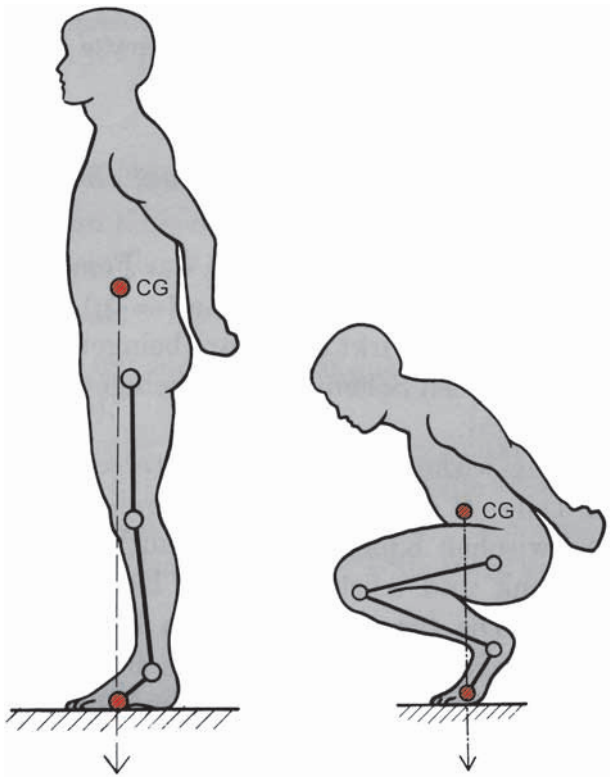

Fig. 6. — Moment arms acting on the patello-femoral joint are depending on body position and the distance between the centre of gravity (CG) and the patello-femoral joint (Adapted from Bandi (5,6), courtesy of Hans Huber Verlag, Bern, Switzerland).*

that in the midrange of flexion up to 60°, the condition for lateral stability of the patella is namely that the angle of inclination of the lateral trochlea groove is larger than the Q-angle (*60,61*).

The most important variable in the calculation of static forces is the distance between the line of body weight (centre of gravity) and the patello-femoral joint. Changes of posture in the sagittal plane (leaning forward or backward) will alter this distance and lead to substantial differences in static force transmission, whilst changes in the coronal plane will exert little influence (Fig. 6) (*5,14*). In full extension the centre of gravity falls anterior to the knee, moment arms become 0, hence no forces acting on the patello-femoral joint (*5*). Whenever the line of body weight is moved posterior and away from the patello-femoral joint, muscle activity and tension in the patellar ligament will increase to maintain position, resulting in higher patello-femoral compressive forces.

During normal activities requiring flexion under load, hip flexion is also present, thus bringing the centre of gravity forward and shortening the femoral lever arm. This relationship is exemplified by the skier, who, by leaning backwards on his skis, has to increase his quadriceps force to prevent a fall. This in turn dramatically increases PRF potentially leading to quadriceps tendon or anterior cruciate ligament rupture (*6*). On the other hand the patient with quadriceps weakness can rise from a

Questions? Contact FDA/CDRH/OCE/DID at CDRH-FOISTATUS@fda.hhs.gov or 301-796-8118

Records processed under FOIA Request #2014-8015; Released by CDRH on 12-8-2015

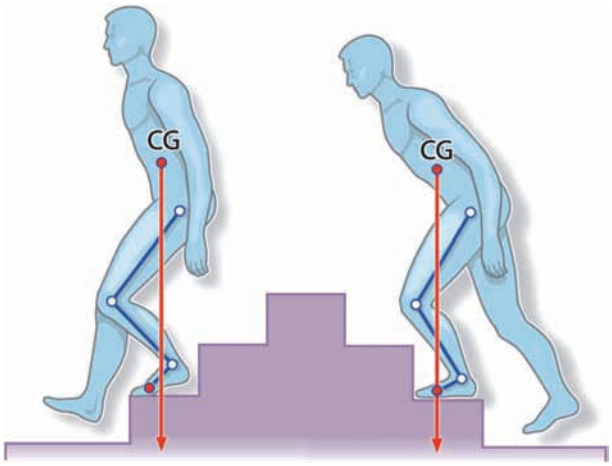

Fig. 7. — During stair ascend the centre of gravity (CG) is positioned almost above the patello-femoral joint, hence moment arm of femur and tibia are relatively short and the patello-femoral reaction force (PRF) is low. During stair descend the CG is positioned further posterior to the patello-femoral joint, creating longer moment arms and a subsequent increase in PRF.

chair by leaning forward, bringing the centre of gravity closer to the knee. Similarly there are significant differences in PRFs in ascending and descending stairs (Fig. 7). Predicted force values for stair ascend range from 1.8 to 2.3 × BW, compared to those for stair descent which are ranging from 2.9 to 6 × BW (*4,45*). The increased values on descending are due to the centre-of-gravity being moved further backward behind the patello-femoral joint in order to maintain balance. Force transmission in the patello-femoral joint is therefore dependent on the relationship between the centre of gravity of the body and the knee flexion angle and calculations should not be based simply on the length of the femur and the position of the hip joint alone (*5*). To demonstrate the calculation of PRF we may use a simplified model of a person standing with both knees flexed to 45° and with half the body weight (0.5 × BW) being transferred through each knee (Fig. 5). In this position the centre of gravity is approx. 42 mm posterior, and the patella tendon 30 mm anterior to the centre of rotation of the knee. Let us further assume that there is no frictional loss at the patello-femoral interface and quadriceps and patellar tendon forces are equal. The patellar tendon force (PTF) = (0.5 × BW) × 42 mm / 30 mm = 0.7 × BW. The parallelogram of forces can now be scaled to obtain a value of approx. 0.8 × BW for the resultant patello-femoral force.

In 1911 Fick first recognised that the quadriceps tendon started to abut onto the proximal aspect of the femoral trochlea in mid range of knee flexion (*20*). As a result the compressive forces become divided between the tendo-femoral and patello-femoral contact areas (*6,21,24,44*). This phenomenon later described by Goymann & Müller as the 'turn-round' of forces, represents an elegant way of main-

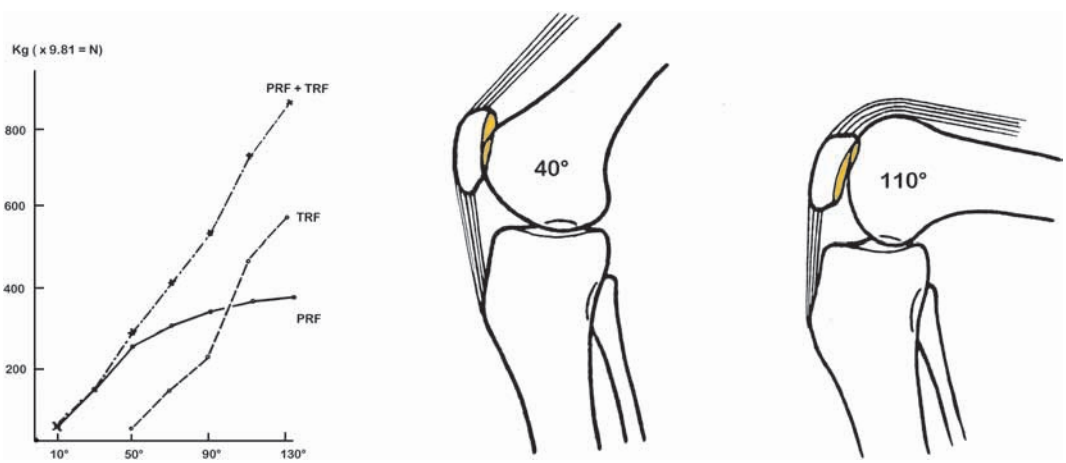

Fig. 8. — Patello-femoral reaction force (PRF) plotted against the tendo-femoral reaction force (TRF). Calculated values for PRF show noticeable tail-off beyond 50° of knee flexion due to the turn-round phenomenon of the quadriceps tendon against the femoral trochlea (adapted from Bandi[6], courtesy of Hans Huber Verlag, Bern, Switzerland).*

Questions? Contact FDA/CDRH/OCE/DID at CDRH-FOISTATUS@fda.hhs.gov or 301-796-8118

Records processed under FOIA Request #2014-8015; Released by CDRH on 12-8-2015

Table I. — Static measurements of patello-femoral joint reaction forces in relation to knee flexion angle. (Values should be viewed with due regard to the complexity of the problem and with the knowledge of the assumptions which must necessarily be made in obtaining them)

Knee flexion angle	Average PF contact area (mm^2)	Percentage of total contact area°	Tendo-femoral compressive force (Newtons)	Peak PRF (Newtons)	Peak PRF (body weight)	Peak PF contact pressure (N/mm^2)
0°	140	10	0	0	-	-
10°	200	15	0	100	0.2	0.5
30°	280	20	0	300	0.5	1.1
50°	320	23	250	860	1.2	2.7
70°	450	32	1300	1810	2.7	4.0
90°	350	25	2200	2860	4.2	8.1
110°	260	19	4500	3300	4.8	12.7
135°	130	9	5800	7500	12.9	57.7

° based on an average total contact area of 1340 mm^2.

taining relatively constant unit load under a mechanical situation where total load is increasing (Fig. 8) (*24,25*). The efficacy of the turn-round of the divided forces is dependent on the length and the altitude of the patella (*24*). The 'turn-round' of forces takes effect between 50° to 90° of flexion (*5,21,25*). According to measurements obtained by Hehne the contact area of the quadriceps tendon is significantly larger compared to the contact area of the patello-femoral joint (*27*). At 90° the quadriceps contact area measures approx. 1 to 2 times, at 120° 2 to 3 times, and at 140° 3 to 4 times that of the patello-femoral contact area (Fig. 1).

Huberti *et al* calculated average tendo-femoral contact forces at 120° of approximately 550N, whilst patello-femoral contact forces at the same degree of knee flexion measured on average 1600N, indicating a ratio of 1:3 between tendo-femoral and patello-femoral contact force (*28*). This may at least to some extent explain the higher frequency of chondromalacia in patella alta, as tendo-femoral contact may be eliminated or substantially decreased, creating an increase in patello-femoral reaction force (*3,28,30,35*).

Static measurements of patello-femoral reaction forces (PRF) have been reported as showing an almost linear increase in force values up to 110° after which they decline (Table I). The first such measurements were performed by Burckhardt in 1924, who disregarded the load sharing function of the quadriceps tendon, hence his results have been flawed (*10*). Furmaier in 1953 and Bandi in 1972 made appropriate adjustments in their force calculations incorporating tendo-femoral contact forces (*5,21*). Calculated PRF values range from 0 × BW at 15° to 12.9 × BW at 135° (*5,21,28,38,46,51*).

Patello-femoral reaction forces (PRF) during activities vary greatly and are essentially dependent on the type of activity performed (Table II). Predicted force values range from 0.6 × BW for level walking to 7.7 × BW for jogging, and 20 × BW for jumping (*9,13,16,17,32,33,43-45,48,52,59,62,63*). For isokinetic exercise Kaufman *et al* found that PFR peaked at around 70° to 75° of knee flexion. Calculated values are dependent on exercise speed and ranged from 3.4 to 6.8 × BW. Ericson and Nisell noted that both patello-femoral and tendo-femoral reaction forces during cycling were generally lower when compared to those generated through daily and most other sporting activities (Fig. 9) (*17*). The magnitude of joint forces was almost independent of body weight, but increased with work load and reduced saddle height. Tendo-femoral reaction force rose to 295N at 108° of knee flexion. Anterior knee pain during cycling may henceforth be associated with compression of the supra-patellar bursa or medial para-patellar plica at higher knee flexion angles if the saddle position is kept low and knee flexion angles are subsequently increased throughout all stages of the revolu-

Questions? Contact FDA/CDRH/OCE/DID at CDRH-FOISTATUS@fda.hhs.gov or 301-796-8118

Records processed under FOIA Request #2014-8015; Released by CDRH on 12-8-2015

Table II. — Patello-femoral joint reaction forces for various activities. (Values should be viewed with due regard to the complexity of the problem and with the knowledge of the assumptions which must necessarily be made in obtaining them)

Author	Year	Activity	Body Weight (kg)	Knee flexion Angle	Peak PRF (N)	Peak PRF (xBW)
Reilly & Martens	1972	Level walking	70	10°	334	0.5
Morra & Greenwald	2006	Walking gait	-	15°	420	0.6
Bresler & Frankel	1950	Level Walking	71	20°	840	1.2
Ericson & Nisell	1987	Cycling	71	83°	905	1.3
Nisell	1985	Lifting (12.8 kg box)	77	90°	1600	2.2
Andriacchi *et al*	1980	Stair ascent Stair descent	71 71	65° 60°	1500 4000	2.1 5.7
Morra & Greenwald	2006	Stair ascent	-	45°	1760	2.5
Reilly & Martens	1972	Stair walking	85	55°	2500	3.3
Smidt	1973	Isometric quads contraction	82	75°	2127	2.6
Morra & Greenwald	2006	Rising from a chair	-	90°	1950	2.8
Ellis *et al*	1979	Rising from a chair	-	120°	-	3.1
Kelley *et al*	1978	Rising from a chair	-	90°	3800	5.5
Kaufman *et al*	1991	Isokinetic exercise	81	70°	-	5.1
Huberti & Hayes	1984	Isometric extension		90°	4600	6.5
Nisell	1985	Isometric extension	72	90°	6900	9.7
Dahlqvist *et al*	1982	Ascending from squat Descending from squat		140° 140°		6.0 7.6
Reilly & Martens	1972	Squatting	85	130°	6375	7.6
Winter	1983	Jogging	72	50°		7.7
Wahrenberg *et al*	1978	Kicking	76	100°	5800	7.8
Smith *et al*	1972	Jumping	-	-		20
Nisell	1985	Quadriceps tendon rupture			10900-18300	14.4-24.2
Zernicke *et al*	1977	Patellar tendon rupture	-	90°		25

tion (*15,50*). Cycling should be considered a preferable activity for most patients recovering from knee surgery, but especially for those who are obese. Proper attention however should be given to appropriate adjustment of work load and saddle height..

When considering the magnitude of patello-femoral compressive force it has to be remembered that this force acts through an area which varies with knee flexion (*37,54,60*). Henceforth an increase in PRF does not necessarily assume an increase in patello-femoral pressure. Patello-femoral contact area is small close to full extension of the knee, indicating that patello-femoral pressure is higher for the same PRF magnitude. From this follows, that the patello-femoral pressure, near extension may be relatively high although the compressive force appears comparatively low (*44*).

To obtain a rough estimate of the resulting contact pressures in the patello-femoral joint, the mean pressure is calculated by dividing patello-femoral force values by the patello-femoral contact area. Patello-femoral contact pressure values are dependent on activity and knee flexion angle, and range from 1.28 to 12.6 N/mm^2 (*28,29*). Accordingly a 696 Newton man climbing stairs would generate a patello-femoral compression force of 1754N equivalent to 2.5 × BW and experience patello-femoral pressures between 3.73 and 6.87 N/mm^2 (*39*).

Questions? Contact FDA/CDRH/OCE/DID at CDRH-FOISTATUS@fda.hhs.gov or 301-796-8118

Records processed under FOIA Request #2014-8015; Released by CDRH on 12-8-2015

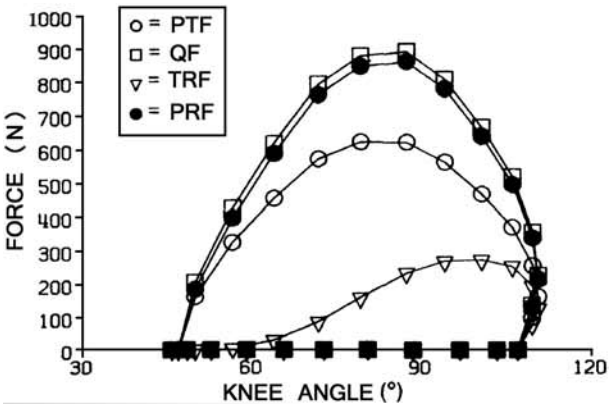

Fig. 9. — Patello-femoral joint forces during cycling motion. Patello-femoral reaction force (PRF), patellar tendon strain force (PTF), quadriceps strain force (QF), and tendo-femoral reaction force (TRF) plotted against the knee flexion angle during a complete revolution (Redrawn and adapted from Ericson & Nisel (17), with permission of the American Physical Therapy Association).*

Women have smaller knees and hence shorter patellar tendon moment arms than men. Subsequently the PRF increases by up to 20% for the same knee extending moment which would explain the somewhat higher frequency of patello-femoral disorders in females (*44*).

Denham and Bishop have shown that the patello-femoral reaction force exceeds the tibio-femoral reaction force in angles above 25°. At near full knee flexion these values rose to almost 150% of the forces passing through the tibio-femoral joint (*14*). It is therefore not surprising that the patello-femoral articulation is covered by a deep and deformable layer of hyaline cartilage. With 4 to 6 mm in depth, this cartilaginous cover is the thickest to be found in the body, and designed to protect the richly innervated subchondral bone in such a way that the pain threshold is not surpassed (*19*).

Articular cartilage carries viscoleastic properties enabling it to adapt to the changing surface contours whilst the patella moves along its irregular pathway. At the same time surface deformation under load will lead to a subsequent increase in pressure transmitting area. This process is time dependent and pressure values will thus be different for short-term and long-term loading. The above mentioned values concerning patello-femoral pressure should hence be regarded as reference values only, as pressure transmitting areas of the patello-femoral joint increase with increasing load and duration of loading (*5,22,28,39,55*). This may explain why peak stresses of up to 20 times body weight can be tolerated without causing lasting damage as they are applied over a relatively large area for only very short periods of time, whilst long term application of such loads would invariably lead to cartilage breakdown.

Acknowledgement

The authors would like to convey their appreciation to Arlen Hanssen MD of the Mayo Clinic in Rochester/Minnesota, and Gil Scuderi MD of the Insall Scott Kelly Institute of Orthopaedics and Sports Medicine in New York for their inspiration and encouragement. Especial gratitude goes to Seth Greenwald DPhil(Oxon) of the Orthopaedic Research Laboratories in Cleveland/Ohio for his scientific advice and friendship.

REFERENCES

1. **Abraham W, Buchanan JR, Daubert H, Greer III RB, Keefer J.** Should the patella be resurfaced in total knee arthroplasty ? Efficacy of patellar resurfacing. *Clin Orthop Relat Res* 1988 ; 236 : 128-134.
2. **Aglietti P, Insall JN, Walker PS, Trent PS.** A new patella prosthesis : Design and application. *Clin Orthop Relat Res* 1975 ; 107 : 175-187.
3. **Aglietti P, Buzzi R, Insall JN.** Disorders of the patellofemoral joint. In : Insall JN, Windsor RE, Scott N, Kelly MA, Aglietti P (eds). *Surgery of the Knee*. 2nd ed, Churchill Livingstone, New York, 1993, pp 241-385.
4. **Andriacchi TP, Andersson GBJ, Fremier RW, Stern D, Galante JO.** A study of lower limb mechanics during stair climbing. *J Bone Joint Surg* 1980 ; 62-A : 749-757.
5. **Bandi W.** [Chondromalacia patellae and arthritis of the patello-femoral joint.] (in German). *Helv Chir Acta*, 1972 ; Suppl. 11 : 1-70.
6. **Bandi W.** *Die retropatellaren Kniegelenksschäden*. [Retropatellar derangement of the knee], 2nd ed, Verlag Hans Huber, Bern, 1982. (In German).
7. **Bousquet G, Dejour H.** [The anatomical and physiological basis in the conception and development of knee arthroplasty.] (in French). *Acta Orthop Belg* 1973 ; 39 : 40-55.
8. **Boyd AD, Ewald FC, Thomas WH, Poss R, Sledge CB.** Long-term complications after total knee arthroplasty with or without resurfacing of the patella. *J Bone Joint Surg* 1993 ; 75-A : 674-681.

Questions? Contact FDA/CDRH/OCE/DID at CDRH-FOISTATUS@fda.hhs.gov or 301-796-8118

Records processed under FOIA Request #2014-8015; Released by CDRH on 12-8-2015

9. **Bresler B, Frankel JP.** The forces and moment in the leg during level walking. *Trans Am Society of Medical Engineers* 1950 ; 72 : 27-36.
10. **Burckhardt H.** [Development of loose bodies and mechanics of the knee joint.] (in German). *Bruns Beitr Klin Chir* 1924 ; 130 : 163-214.
11. **Burnett RSJ, Boone JL, McCarthy KP, Rosenzweig S, Barrack RL.** A prospective randomised clinical trial of patellar resurfacing and nonresurfacing in bilateral TKA. *Clin Orthop Relat Res* 2007 ; 464 : 65-72.
12. **Collier JP, McNamara JL, Surprenant VA, Jensen RE, Surprenant HP.** All-polyethylene components are not the answer. *Clin Orthop Relat Res* 1991 ; 273 : 198-203.
13. **Dahlqvist NJ, Mayo P, Seedhom BB.** Forces during squatting and rising from a deep squat. *Eng Med* 1982 ; 11 : 69-76.
14. **Denham RA, Bishop RED.** Mechanics of the knee and problems in reconstructive surgery. *J Bone Joint Surg* 1978 ; 60-B : 345-352.
15. **Dickson Jr. TB.** Preventing overuse cycling injuries. *Phys Sportsmed* 1985 ; 13 : 116-123.
16. **Ellis MI, Seedhom BB, Amis AA, Dowson D, Wright V.** Forces in the knee joint whilst rising from normal and motorised chairs. *Eng Med* 1979 ; 8 : 33-40.
17. **Ericson MO, Nisell R.** Patellofemoral joint forces during ergometer cycling. *Phys Ther* 1987 ; 67 : 1365-1369.
18. **Ficat P.** *Pathologie Fémoro-Patellaire*. [Pathology of the patello-femoral joint], Masson & Cie, Paris, 1970.
19. **Ficat P, Hungerford DS.** *Disorders of the Patello-femoral Joint*. Williams & Wilkins, Baltimore, 1977.
20. **Fick R.** *Handbuch der Anatomie und Mechanik der Gelenke*. Vol. III : Spezielle Gelenk- und Muskelmechanik. Gustav Fischer Verlag, Jena, 1911.
21. **Furmaier A.** [Contribution to the mechanics of patella and knee joint.] (in German). *Arch Orthop Unfallchir* 1953 ; 46 : 78-90.
22. **Goodfellow JW, Hungerford DS, Zindel M.** Patello-femoral joint mechanics and pathology. *J Bone Joint Surg* 1976 ; 58-B : 287-290.
23. **Goodsir J.** On the mechanism of the knee joint. In : Turner W (ed). *The Anatomical Memoirs of John Goodsir.* Vol. 2. Adams and Charles Black, Edinburgh, 1868, pp 231-245.
24. **Goymann V, Haasters J, Heller W.** [Current studies on the biomechanics of the patella.] (in German). *Z Orthop* 1974 ; 112 : 623-625.
25. **Goymann V, Müller HG.** New calculations of the biomechanics of the patellofemoral joint and its clinical significance. In : Ingwersen OS, Van Linge B, Van Rens ThJG, Rösingh GE, Veraart BEEMJ, Le Vay D (eds). *The Knee Joint : Recent Advances in Basic Research and Clinical Aspects*. American Elsevier Publishing, New York, 1974, pp 16-21.
26. **Haxton H.** The function of the patella and the effects of its excision. *Surg Gyn Obst* 1945 ; 80 : 389-395.
27. **Hehne HJ.** *Das Patellofemoralgelenk*. [The patello-femoral joint], Enke, Stuttgart, 1983.
28. **Huberti HH, Hayes WC.** Patellofemoral contact pressures : The influence of Q-angle and tendofemoral contact. *J Bone Joint Surg* 1984 ; 66-A : 715-724.
29. **Hungerford DS, Goodfellow JW.** [Patello-femoral contact areas and their relationship to chondomalacia.] (in German). *Z Orthop* 1975 ; 113 : 784-786.
30. **Insall JN, Goldberg V, Salvati E.** Recurrent dislocation of the high-riding patella. *Clin Orthop Relat Res* 1972 ; 88 : 67-69.
31. **Kaltwasser P, Uematsu O, Walker PS.** The patello-femoral joint in total knee replacement. *Trans Orthop Res Soc* 1987 ; 12 : 292.
32. **Kaufman KR, An KN, Litchy WJ, Morrey BF, Chao EYS.** Dynamic joint forces during knee isokinetic exercise. *Am J Sports Med* 1991 ; 19 : 305-316.
33. **Kelley DL, Dainis A, Wood GK.** Mechanics and muscular dynamics of rising from a seated position. In : Komi PV (ed). *International Series on Biomechanics. Proceedings of the 5th International Congress on Biomechanics*. Biomechanics V-B. University Park Press, Baltimore, 1976, pp 127-134.
34. **Krackow KA, Hungerford DS.** Anatomy and kinematics of the normal knee. In : Hungerford DS, Krackow KA, Kenna RV (eds). *Total Knee Arthroplasty. A Comprehensive Approach*. Williams & Wilkins, Baltimore, 1984, pp 5-19.
35. **Lancourt JE, Christini JA.** Patella alta and patella infera : The etiological role in patella dislocation, chondromalacia, and apophysitis of the tibial tubercle. *J Bone Joint Surg* 1975 ; 57-A : 1112-1115.
36. **Leszko F, Sharma A, Komistek RD *et al.*** Comparison of in vivo patellofemoral kinematics for subjects having high-flexion total knee arthroplasty implant with patients having normal knees. *J Arthroplasty* 2010 ; 25 : 398-404.
37. **Maquet P, Van de Berg A, Simonet J.** Femoro-tibial weight bearing areas. *J Bone Joint Surg* 1975 ; 57-A : 766-771.
38. **Maquet P.** *Biomechanics of the Knee*. Springer, Berlin, 1984.
39. **Matthews LS, Sonstegard DA, Henke JA.** Load bearing characteristics of the patello-femoral joint. *Acta Orthop Scand* 1977 ; 48 : 511-516.
40. **Menschik A.** [Knee joint mechanics : Screw-home.] (In German). *Z Orthop* 1975 ; 113 : 388-400.
41. **Meyer H.** [Knee joint mechanics.] (in German). *Arch Anat Physiol Wiss Med* (Müllers Archiv) 1853 ; 497-547.
42. **Moreland JR.** Mechanisms of failure in total knee arthroplasty. *Clin Orthop Relat Res* 1988 ; 226 : 49-64.
43. **Morra EA, Greenwald AS.** Patello-femoral replacement polymer stress during daily activities : A finite element study. Presented at the *56th Annual Meeting of the AAOS*, Chicago, 2006.
44. **Nisell R.** Mechanics of the knee : A study of joint and muscle load with clinical applications. *Acta Orthop Scand* 1985 ; 56 (Suppl. 216) : 1-42.
45. **Paul JJ.** Force actions transmitted in the knee of normal subjects and by prosthetic joint replacements. In : The

Questions? Contact FDA/CDRH/OCE/DID at CDRH-FOISTATUS@fda.hhs.gov or 301-796-8118

Records processed under FOIA Request #2014-8015; Released by CDRH on 12-8-2015

Medical Engineering Working Party (ed). *Total Knee Replacement*. Mechanical Engineering Publications Limited, London, 1974, pp 126-131.

46. **Perry J, Antonelli D, Ford W.** Analysis of knee-joint forces during flexed-knee stance. *J Bone Joint Surg* 1975 ; 57-A : 961-967.
47. **Reider B, Marshall JL, Ring B.** Patellar tracking. *Clin Orthop Relat Res* 1981 ; 157 : 143-148.
48. **Reilly DT, Martens M.** Experimental analysis of the quadriceps muscle force and patello-femoral joint reaction force for various activities. *Acta Orthop Scand* 1972 ; 43 : 126-137.
49. **Rhoads DD, Nobel PC, Reuben JD, Mahoney OM, Tullos HS.** The effect of femoral component position on patella tracking after total knee arthroplasty. *Clin Orthop Relat Res* 1990 ; 260 : 43-51.
50. **Schindler OS.** Synovial plicae of the knee. *Current Orthopaedics* 2004 ; 18 : 210-219.
51. **Smidt GL.** Biomechanical analysis of knee flexion and extension. *J Biomech* 1973 ; 6 : 79-92.
52. **Smith AJ.** *A study of force on the body in athletic activities with particular reference to jumping*. PhD thesis. England, Leeds, 1972.
53. **Steindler A.** *Kinesiology of the Human Body under Normal and Pathological Conditions*. 2nd print. Charles C Thomas, Springfield, 1964.
54. **Townsend PR, Rose RM, Radin EL, Raux P.** The biomechanics of the human patella and its implications for chondromalacia. *J Biomech* 1977 ; 10 : 403-407.
55. **Trent PS.** The patello-femoral joint. In : Walker PS (ed). *Human Joints and their Artificial Replacement*. Charles C. Thomas, Springfield, 1977, pp 181-182.
56. **Van Kampen A, Huiskes R, Blankevoort L, Van Rens ThJG.** The three-dimensional tracking pattern of the patella in the human knee joint and its effects on surgical intervention. In : Müller W, Hackenbroich W (eds). *Surgery and Arthroscopy of the Knee*. Springer, Heidelberg, 1988, pp 434-445.
57. **Van Kampen A, Huiskes R.** The three-dimensional tracking pattern of the human patella. *J Orthop Res* 1990 ; 8 : 372-382.
58. **Veress SA, Lippert FG, Hou MCY, Takamoto T.** Patellar tracking patterns measurement by analytical x-ray photogrammetry. *J Biomech* 1979 ; 12 : 639-650.
59. **Wahrenberg H, Lindbeck L, Ekholm J.** Knee muscular moment, tendon tension force and EMG during a vigorous movement in man. *Scand J Rehab Med* 1978 ; 10 : 99-106.
60. **Walker PS.** *Human Joints and their Artificial Replacement*. Charles C. Thomas, Springfield, 1977.
61. **Walker PS.** Contact areas and load transmission in the knee. *In* American Academy of Orthopaedic Surgeons : *Symposium on Reconstructive Surgery of the Knee*. Mosby Company, Saint Louis, 1978, pp 26-36.
62. **Winter DA.** Moments of force and mechanical power in jogging. *J Biomech* 1983 ; 16 : 91-97.
63. **Zernicke RF, Garhammer J, Jobe FW.** Human patellar-tendon rupture. A kinetic analysis. *J Bone Joint Surg* 1977 ; 59-A : 179-183.

Questions? Contact FDA/CDRH/OCE/DID at CDRH-FOISTATUS@fda.hhs.gov or 301-796-8118

Records processed under FOIA Request #2014-8015; Released by CDRH on 12-8-2015

Acta Orthop. Belg., 2012, **78**, 11-29

REVIEW ARTICLE

Basic kinematics and biomechanics of the patellofemoral joint Part 2 : The patella in total knee arthroplasty

Oliver S. Schindler

From St Mary's Hospital, Bristol, England, UK

Patellar and femoral component in total knee arthroplasty are inextricably linked as a functional unit. The configuration of this unit has been a matter of ongoing debate, and the myriad of different patellar and femoral components currently available reflect the lack of consensus with respect to the ideal design. One of the major challenges is to overcome the biomechanical disadvantages of a small contact area through which high contact pressures are transferred, making this mechanical construct the weakest part of the prosthetic knee. Contact areas are highly dependent on the congruency of the patellofemoral joint articulation, and are significantly smaller for dome shaped patellar components compared to those of more anatomic designs. However, when exposed to 3-dimensional movements, the contact areas of the dome shaped patella are significantly greater, indicating enhanced forgiveness regarding patellar malpositioning. Although contact stresses, a function of implant design and surface conformity, can reach levels far beyond the yield strength of UHMWPE, catastrophic failure of resurfaced patellar components, commonly seen in metal backed patellae, fashionable in the 1980s, has rarely been observed since. Although plastic deformation and wear of UHMWPE continue to represent a problem, in the absence of suitable alternatives polyethylene remains the bearing surface of choice. The appreciation of the consequences of the mechanical environment on the behaviour of the patellofemoral joint is of particular importance in the endeavour to develop knee replacement systems which provide satisfactory function together with clinical long-term success.

Keywords : TKA ; patella ; patellofemoral joint ; kinematics ; biomechanics ; contact area ; UHMWPE.

INTRODUCTION

The articulation between patella and femur is relatively complex and displays intricate biomechanical behaviour. Concerns exist with regard to the treatment of the patella in total knee arthroplasty, as surgically imposed changes through resurfacing may have significant effects on kinematic behaviour and clinical performance of the patello-femoral joint (*28*). Although symptoms originating from the patello-femoral joint, following knee arthroplasty, are rarely severe enough to justify revision, they may be sufficient to spoil an otherwise satisfactory result.

Matthews and associates, who investigated the load bearing characteristics of the patello-femoral joint, remarked that *'High patello-femoral load values, small patello-femoral contact areas, and resultant high stress magnitudes indicate the need for caution in the design and development of a patello-femoral component for total joint replacement prostheses'* (*61*). Analysis of retrieved patellar components and the significant failure rate of metal

■ Oliver S. Schindler, MD, FMH, OFD, MFSEM, FRCSEd, FRCSEng, FRCS (Orth).
St Mary's Hospital, Clifton, Bristol, England, UK.
Correspondence : Mr O. Schindler, PO Box 1616, Bristol, BS40 5WG, England, UK. E-mail : schindler@doctors.net.uk
© 2012, Acta Orthopædica Belgica.

No benefits or funds were received in support of this study

Questions? Contact FDA/CDRH/OCE/DID at CDRH-FOISTATUS@fda.hhs.gov or 301-796-8118

Records processed under FOIA Request #2014-8015; Released by CDRH on 12-8-2015

backed patellar designs continue to underscore the extreme mechanical environment in which these implants are expected to perform (*20*). Complications arising from patellar resurfacing are still considerable and include patellar component deformation, wear, fracture and loosening (*49,64,67,76*). It is therefore not surprising that patellar resurfacing remains controversial (*49,52,87,88*).

Patellar tracking, contact area, and pressure distribution differ quite significantly between native and prosthetic knee (*47,100*). Mechanical features to be considered in the creation of a prosthetic patello-femoral joint should include functional range of motion in multi-axial planes, stability, fixation, dimensions, load transfer areas, and materials. A successful patello-femoral articulation must be designed to function under high stress conditions, and over a long period of time, as ground reaction, gravitational, ligamentous, and muscular forces all act to produce significant compressive, shear, and torsional loads (*38,69,92*). Hence both design and materials used must be at least compatible with the mechanical forces of up to 5 × body weight (BW), as encountered during activities of daily living (*87*).

PATELLAR COMPONENT DESIGN

The multitude of patellar components currently available reflects the lack of consensus with respect to the ideal design (Fig. 1). Articular surface geometries of patellar components vary greatly but can be classified into five basic shapes : convex or dome shaped ; modified dome shaped, also known as sombrero hat ; anatomically shaped ; cylindrical or saddle shaped ; mobile bearing (Fig. 2) (*51*). Every implant design bears particular advantages regarding conformity, stability, forgiveness and wear pattern, with none being ultimately superior. Advantages attributed to a particular design should however not be generalized to all designs of similar shape as the behaviour of a particular patellar component is directly dependent on a number of variables with the surface geometry of the mating femoral component probably being the most important (*18,25,63,102,104,116*). Apart from component positioning and alignment other factors such as patient's demographics (e.g. body mass index, mechanical leg-alignment, range of motion) will also influence the performance of the patello-femoral joint (*41*).

Dome shaped patella

The majority of currently available patellar components belongs to the all-polyethylene dome shaped type ; its prevalence today is itself an off-shoot of its practicality. The mating geometries between patella and femur are simple spherical shapes, which usually provide congruency only in the early flexion range up to 70° (Fig. 2 & 3). At higher flexion angles the convex patellar surface contacts the convex inner surfaces of the femoral condyles, exposing the patella to high stresses and point contact. Some of these problems have been addressed successfully through design adaptation of femoral condylar and trochlear geometries. Extension of the trochlear groove concavity onto the inner portion of the femoral condyles has provided for an increase of patello-femoral congruency in flexion. The principal advantage of dome shaped components compared to all other designs is their ability to allow for flexion to occur in various planes, hence avoiding edge loading, a problem associated with modified-dome and anatomic patellar devices (Fig. 4). Because of the spherical shape, rotatory alignment of the implant is less critical, highlighting the relative forgiveness of dome shaped patellae regarding minor degrees of malpositioning and making it easy to implant. Despite their excellent clinical results however, failure of cemented all-polyethylene dome shaped patellar components is not uncommon and is attributed to the exposure to high contact stresses (*4,24,32,33,45,89, 113*).

Modified dome shaped patella or sombrero hat

In an attempt to increase the contact area in flexion, the standard dome patella was modified to include a concave surface near the circumference, allowing it to more closely match the curve of the femoral condyles in the axial plane (*9*). The modified dome shaped patella, also known as 'sombrero hat', improves the articulation with the convexities

Questions? Contact FDA/CDRH/OCE/DID at CDRH-FOISTATUS@fda.hhs.gov or 301-796-8118

Records processed under FOIA Request #2014-8015; Released by CDRH on 12-8-2015

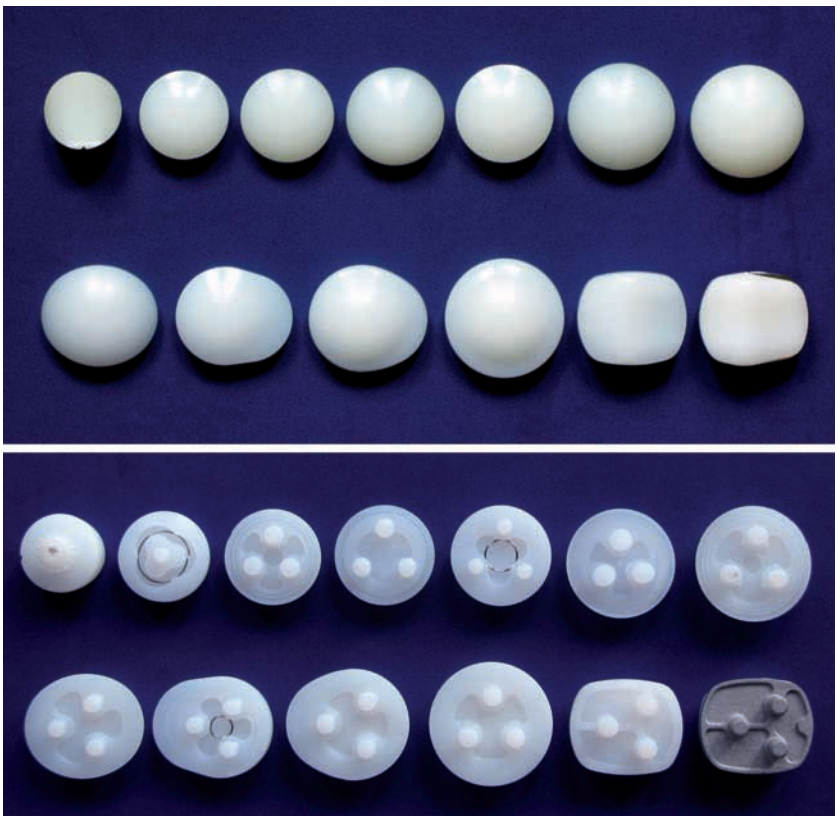

Fig. 1. — Commercially available patellar components. Articulating surface (top), retro-patellar surface (bottom). Top row from left to right : MEDIAL ROTATION KNEE®, Finsbury ; GENESIS® II (biconvex), Smith&Nephew ; VANGUARD®, Biomet ; OPTETRAK®, Exactech ; GENESIS® II dome, Smith&Nephew ; ADVANCE® Medial-Pivot, Wright Inc. ; AGC®, Biomet Inc. Bottom row : PFC-Sigma®, DePuy ; JOURNEY® (off-set dome) Smith&Nephew ; TRIATHLON® (off-set dome), Stryker Inc. ; TRIATHLON® (sombrero), Stryker ; LCS® (all poly), DePuy ; LCS® (rotating platform), DePuy.

of the femoral condyles especially at higher flexion angles (Fig. 2). Wear simulator studies confirmed that the increased conformity enhances the life of the component by more than 20 times when compared to a standard dome component (*44*). Concerns however remain, since the amount of conformity that is acceptable must be considered in relation to patellar motion.

Anatomically shaped patella

Prostheses with anatomical surface profile (Fig. 2) have distinct lateral and medial facets. They provide a more conforming articulation with an increased contact area and reduced contact stresses between patellar and femoral component, thereby decreasing the risk of subluxation (*10,12,46*). A variety of anatomically shaped patellar implants have been available over the years, including a mobile bearing variant. Although anatomic patellar implants make the most sense theoretically, they have introduced a number of complexities into the instrumentation and surgical technique. Due to their high level congruency with the femoral component they are more sensitive to mal-positioning and hence more difficult to implant (*56*).

Cylindrical or saddle shaped patella

The cylindrical or saddle shaped patellar component (Fig. 1 & 2) occupies a fringe position in total knee arthroplasty. The initial idea was developed by

Questions? Contact FDA/CDRH/OCE/DID at CDRH-FOISTATUS@fda.hhs.gov or 301-796-8118

Records processed under FOIA Request #2014-8015; Released by CDRH on 12-8-2015

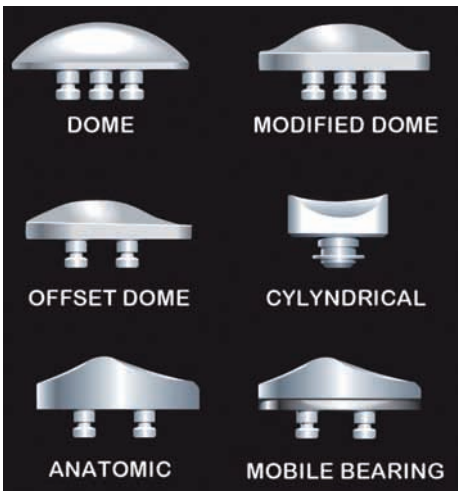

Fig. 2. — Common types of patellar component surface configuration (Copyrights of illustration remain with author).

Freeman and Swanson in the late 1970s, who attempted to combine a high level of congruency with relatively large contact areas throughout flexion of up to 110° (*34,35*). Due to design specifics, the patella becomes highly dependent on a close matching geometry of the femoral component in the sagittal plane, requiring a femoral trochlea with a single radius (*35,53*). The diameter of the patellar component is reduced to 25-30 mm, allowing the implant to be recessed into the patella, similar to an inlay technique. Subsequently the remaining patellar rim participates in articulating with the femoral component and in further assisting stress dissipation. The patellar implant possesses a central peg with a collar and can be used with or without cement. If left uncemented the implant retains the ability to self-centre and to rotate as has been observed in revision situations for reasons unrelated to the patella (*2,53*). Although fibrous in-growth may eventually halt this process, the implant is likely to have already adopted favourable alignment (*107*). Despite concerns of being rotationally constrained, the design concept has provided for satisfactory function and pain relief, with 10 year survival rates of 96 to 98.4% (*35,53,57,108*).

Mobile bearing patella

A different biomechanical concept has been conceived with the anatomically shaped mobile bearing metal backed patella (Fig. 1 & 2) (*11,12,13*). The design is based on the same principle as rotating platform tibial components. The clinical performance record of mobile bearing patellae has been surprisingly good and has not been characterized by the complications generally associated with metal backed prostheses. Reported survival rates of up to 99.5% at 12 years have been attributed to the high conformity and low stresses permitted by the mobile bearing articulation (*48*). The absence of significant back-side wear in mobile patellar bearings has led some clinicians to believe that these devices may not actually rotate in service. It has therefore

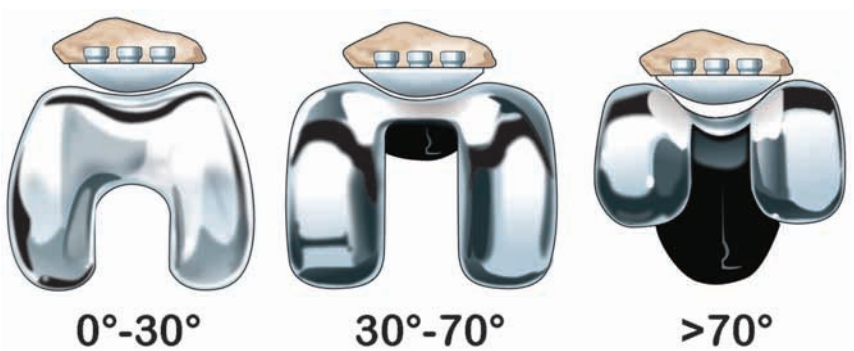

Fig. 3. — Contact position between patellar implant and femoral component at various degrees of knee flexion. Point contact in extension and early flexion, due to limited conformity between patellar implant and femoral flange ; line contact in mid-flexion (30°-70°), due to increasing conformity between patellar implant and trochlea ; bifurcation of contact area beyond 70° (Copyrights of illustration remain with author).

Questions? Contact FDA/CDRH/OCE/DID at CDRH-FOISTATUS@fda.hhs.gov or 301-796-8118

Records processed under FOIA Request #2014-8015; Released by CDRH on 12-8-2015

Fig. 4. — Dome-shaped patellar components when articulating with a designated femoral component may compensate for limited degrees of patellar tilt and rotation by maintaining acceptable contact congruency, especially in the mid-flexion range.

been speculated that the advantages of mobile bearing patellae may in fact be their ability to compensate for variations in surgical alignment by rotating into a preferential position after engagement with the femoral component and simply to stay there (*14,63*).

PATELLAR CONTACT AREA AND KINEMATICS

The contact area of the prosthetic patello-femoral joint measures, at best, no more than 40% of the contact area established for the native knee (*40,51,59,*

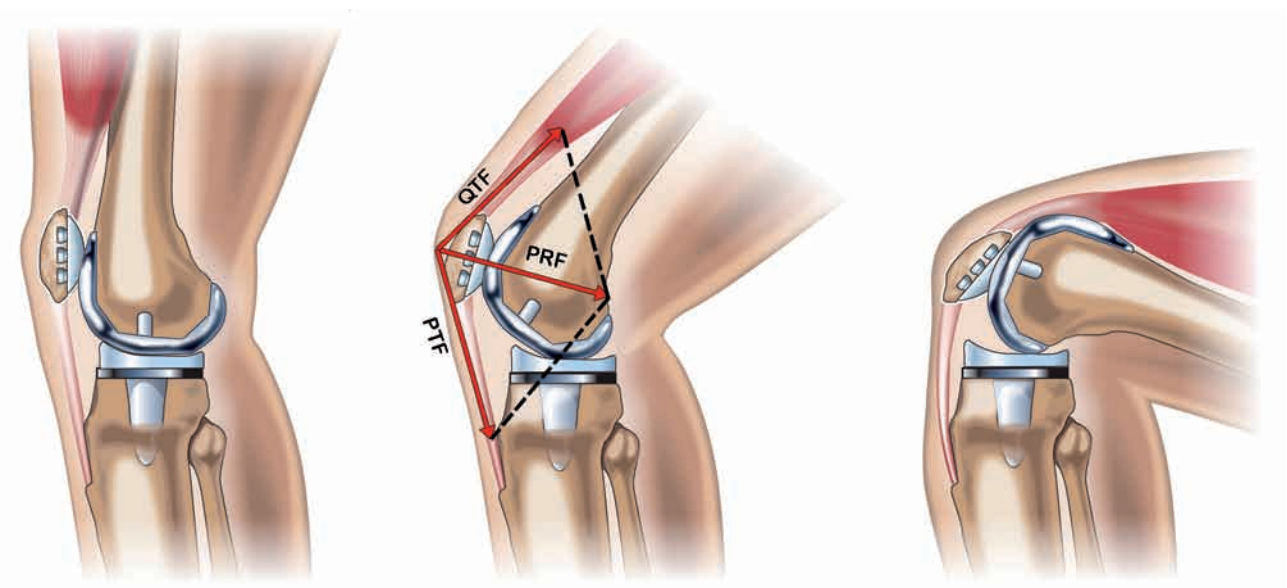

Fig. 5. — Changes of patellar position in relation to the femoral component during extension, mid-flexion and full flexion in the sagittal plane. With increasing flexion the patella declines and moves in a posterior direction with the femur, whilst the patellar contact area moves proximally. The centre image also shows the force vectors acting on the patellofemoral joint (Copyrights of illustration remain with author).

Questions? Contact FDA/CDRH/OCE/DID at CDRH-FOISTATUS@fda.hhs.gov or 301-796-8118

Records processed under FOIA Request #2014-8015; Released by CDRH on 12-8-2015

68,103,115). Measurements obtained experimentally vary widely and depend on the technical set-up and the level of compression force applied during testing. For dome shaped designs contact areas range from 13 to 162 mm^2, with highest values usually observed between 30° and 90° degrees of knee flexion (*68*). Values for modified dome shaped, anatomic, and cylindrical patellar components may vary, but due to the increased level of conformity are generally higher with contact areas of up to 270 mm^2 (*59,68,94,97*).

Up to 75° of flexion the contact area between prosthetic patella and femur is relatively large and contact pressures are generally low. As with the native patella the area of contact on the patellar component moves proximally with increasing flexion reaching the superior patellar pole between 60° to 90° depending on trochlea design (Fig. 5). Beyond this point the patella leaves the trochlea in most arthroplasty designs, leading to bifurcation of the patello-femoral contact area (Fig. 3). The transition from a one-area to a two-area contact is associated with a significant decrease in contact surface, whilst patello-femoral compressive force continues to rise. The direct influence of this transition in contact area on wear pattern can be observed in retrieved patellar components, which demonstrate deformation and development of characteristic facets at the margin of the polyethylene surface (Fig. 6) (*29,44, 62,63,114*).

As with the native patella the motion path of the resurfaced patella is complex and influenced by extrinsic stability, provided by muscle and soft tissue support, and intrinsic stability, provided by implant design. Intrinsic design stability is defined as the capacity of the implant alone, with or without patellar resurfacing, to resist interaction between implant and muscular, capsular, or ligamentous structures.

The geometry of the prosthetic components, as well as surgically imposed changes, will bring with them a plethora of variables, which all have the potential to influence patellar tracking. However, even in a well aligned and balanced total knee prosthesis the resurfaced patella will present a complex three-dimensional movement pattern broadly similar to the native knee, and predominantly consisting

Fig. 6. — Focal area of polyethylene deformation (cold-flow) at the periphery of a retrieved patellar component, created through bifurcation of contact at flexion > 70°. Changes considered to accommodate non-conformity between patellar implant and femoral condyle by creeping in ways to reduce contact stress . Component courtesy of Prof. W. Plitz, Ludwig-Maximilian-University, Munich.

of rotation in both sagittal (flexion-extension) and axial (medio-lateral tilt) planes, as well as rotation and translation in the coronal plane (Fig. 7) (*82*). Studies have shown that the patella may rotate as much as 15° with respect to the femur, with most of the rotation occurring beyond 50° of knee flexion (*82*). The patella may translate medially in the coronal plane during the initial 30° of knee flexion, returning to neutral at about 60° after which it moves laterally by as much as 8° (*70*). Finally, for every 30° of knee flexion, 20° of patello-femoral flexion occur, defined as rotation in the sagittal plane (Fig. 5) (*55*).

Stiehl *et al* (*99*) assessed patellar kinematic patterns and were able to demonstrate that patellar axis rotation, which compares the angle between the patellar tendon and the sagittal axis of the patella, increases with flexion in TKA (Fig. 5 & 7) beyond the levels observed in normal knees. Contact position of dome-shaped and anatomically shaped patellar components showed greater variability compared to the normal knee, with the average contact position for the resurfaced patellae lying more superior, and tilt angles being significantly increased. However, the kinematic behaviour of an anatomically shaped or an unresurfaced patella

Questions? Contact FDA/CDRH/OCE/DID at CDRH-FOISTATUS@fda.hhs.gov or 301-796-8118

Records processed under FOIA Request #2014-8015; Released by CDRH on 12-8-2015

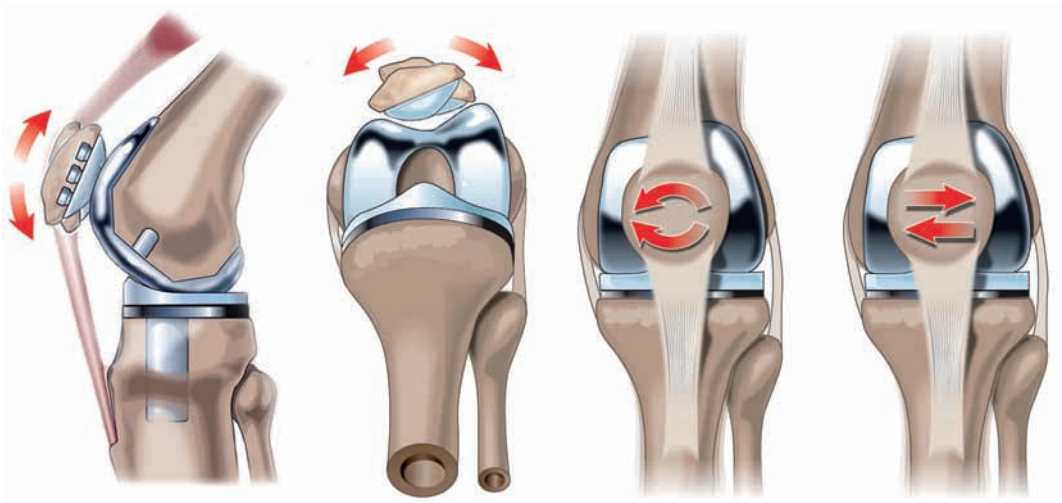

Fig. 7. — Various types of patellar movement known to occur in both resurfaced and un-resurfaced patellae when articulating with a prosthetic femoral component. From left to right : rotation in the sagittal plane (flexion-extension), in the axial plane (medio-lateral tilt), and in the coronal plane ; translation in the coronal plane (Copyrights of illustration remain with author).

more closely resembled normal knee kinematics, compared to those observed with dome shaped designs.

The complexities of the patello-femoral movement pattern highlight the difficulties in reproducing natural patellar kinematics when resurfacing the patello-femoral joint. Although an unconstrained patello-femoral articulation would allow the patella to move relatively unrestrictedly, it requires a low level of conformity between the mating surfaces, which in turn would lead to an increase in contact stresses. In contrast, a highly conforming articulation will constrain patellar movement, imparting unwanted shear forces which may increase the risk of patellar subluxation and component loosening.

In a cadaver study Kim *et al* (*51*) assessed the effect of patellar kinematics on the contact area of dome, modified dome, anatomic and rotating patellar designs. Under optimal tracking conditions the contact areas of the dome shaped patella were significantly smaller compared to the modified dome and anatomic designs. When exposed to 3-dimensional movements however, the contact area of the dome shaped patella was significantly greater, indicating enhanced forgiveness regarding patellar mal-positioning, whilst modified dome and anatomic components appeared more sensitive to patellar mal-alignment.

PATELLO-FEMORAL FORCES

The mechanical environment of the replaced patello-femoral joint differs quite significantly from the natural knee and is biomechanically disadvantaged by having smaller contact areas through which high contact stresses are transferred. Anterior patellar strain, a measure of the effect of external forces on the geometric configuration of the patella, has shown a threefold increase following TKA (*62*). Contact stress, measured in megapascal (1 MPa = 1 N/mm^2), is defined as force divided by the area over which the force is applied. It will increase with a rise in reaction force, but decrease with an increase in contact area. As we know from the native knee, the increase in patello-femoral contact area with flexion up to 90° together with the 'turn-round' phenomenon of the quadriceps tendon beyond 90°, help to dissipate the patello-femoral reaction force (PRF) over a larger area (*37,38*). Despite these compensatory mechanisms however, we observe a net increase in contact stress during

Questions? Contact FDA/CDRH/OCE/DID at CDRH-FOISTATUS@fda.hhs.gov or 301-796-8118

Records processed under FOIA Request #2014-8015; Released by CDRH on 12-8-2015

flexion in TKA as reaction forces increase disproportionately compared to the contact area.

The forces transmitted by the patella originate from the pull of the quadriceps, resulting in a tension force in the patellar tendon and a contact pressure force between the patella and the trochlea. In a practical simplified model, these forces act coplanar (in the sagittal plane) and even concurrent, in such a way that it is permissible to consider them as a single resultant force (Fig. 5). Experimental *in vitro* studies have been able to show that these forces can be quite considerable, with PFR values of 1.2 × body weight (BW) for simple activities such as walking on level ground, 5.7 × BW for descending stairs or rising from a chair and 7.7 × BW for jogging (*87*). *In vivo* studies have so far only looked at peak forces generated within the replaced tibio-femoral joint, which confirmed approximate values of 1.3 × BW for biking, 2.7 × BW for walking, 3.8 × BW for tennis and up to 4.5 × BW for golf (*21*). The level of contact stresses is directly influenced by the magnitude of the contact force (PRF). The magnitude of PRF is a function of implant design. Certain patient demographics like younger age, above average BMI, and increased post-operative flexion, especially in those patients of high demand, are likely to further increase the level of compressive and shear forces on the patellar component during knee flexion (*29,64,72*).

The fixation surface of all-polyethylene onlay patellar components has also been subject to biomechanical investigations. Large single central fixation lugs, which were popular in the 1970s and 80s, required significant bone removal leaving only a relatively shallow bone bridge below the lug. This created focal stress raisers leading to an increased risk of patellar fracture close to the fixation site (*9,19*). Single lug patellar components have hence been largely abandoned in favour of three smaller fixation lugs placed more peripherally. Such an arrangement is subject to less stress compared to lugs placed centrally, especially if lugs are oriented in a transverse direction (*17*). The construct of three smaller and peripherally placed lugs has been shown to avoid precarious bone weakening and provides better resistance against tilt and rotational forces (*54,58*). Inlay patellar components of convex, biconvex or cylindrical configuration are inset into the retropatellar surface and continue to use single peg fixation. These pegs are usually quite small in size and the low rate of complication with this technique may be due to the additional strength gained through peripheral bone preservation. In addition the particular geometry of the patellar component and the moving centre of loading produced by knee mechanics and interaction with the femoral trochlea impose peculiar stresses on the patellar fixation site. The resulting strains are compressive, shear, and tensile in character and presumed to be relatively small. They are often referred to as 'micromotion' and implicated as a mechanical contribution to loosening (*8*).

MATERIAL SCIENCE AND PERFORMANCE OF PATELLAR IMPLANTS

Owing to the great disparity between moduli and strength of cobalt-chrome alloys on the one hand and ultra high molecular weight polyethylene (UHMWPE) on the other, *wear* is primarily observed on the polymeric side of the prosthetic patello-femoral articulation. Notwithstanding its limitations, UHMWPE has evolved as the material of choice for the patellar component based on the low friction principle (*16*). Mechanical properties of UHMWPE are far from being ideal, with *yield* strength affected by the level of molecular weight, degree of cross linking and sterilisation method.

Uniaxial yield strength of UHMWPE, which equals the lowest stress at which the material undergoes plastic deformation, is estimated at around 23 MPa (*3,20,39,83,96*). Concerns have been raised if such stresses are applied continually. For industrial applications repeated maximum contact stresses of 10 MPa are hence recommended, a value which incidentally is identical to the yield strength estimated for articular cartilage (*80*). Buechel *et al* (*12*) have even suggested that for long-term human use maximum contact stresses of 5 MPa may be more appropriate, as body temperature further reduces the strength of UHMWPE by almost 25%. *In vitro* contact stress analysis has confirmed that all-polyethylene dome shaped patellar components produced contact pressures between 20 to 30 MPa in

Questions? Contact FDA/CDRH/OCE/DID at CDRH-FOISTATUS@fda.hhs.gov or 301-796-8118

Records processed under FOIA Request #2014-8015; Released by CDRH on 12-8-2015

extension, rising to between 36 and 100 MPa at 90° to 120° of knee flexion, therefore exceeding the yield strength of UHWMPE (23 MPa) by up to 400% (*20,47,51,63,115*). Anatomically shaped rotating platform patellar components produced significantly lower values, mostly staying below the yield strength of UHMWPE (*20,63*). *Wear* simulator studies further confirmed that congruent patellar components (modified dome and anatomic) exhibited significantly lower rates of creep and wear than dome shaped designs, again indicating that conformity is critical to wear resistance and protection against post-*yield* deformation (*20,43,44*).

Viscoelastic properties of surface cartilage allow for its deformation under load and subsequent increase in pressure transmitting area. Due to differences in elastic modulus between cartilage and UHMWPE, the prosthetic patella however has limited ability to change its surface contact area through variations in patello-femoral load (*6,42,44,63*).

Xu *et al* (*115*) and associates were able to demonstrate the effect of patellar resurfacing on contact area and pressure in cadaveric knees. The mean contact area between 30° to 120° of flexion in the non-resurfaced patello-femoral joint ranged from 70 to 150 mm^2, whilst peak patellar contact pressures did not exceed 12 MPa (*115*). Once resurfaced the mean contact area decreased almost 10 fold to 10 to 15 mm^2, creating a dramatic increase in patellar contact pressure values of 50 to 100 MPa. Greenwald *et al* (*15,68,98*) performed biomechanical studies assessing patellar surface contact area, compression force, and contact pressure using a variety of different prosthetic models. These authors (*15*) found that patello-femoral contact pressure values at knee flexion angles beyond 45° exceeded polyethylene yield strength in all tested components with peak measurement of up to 75 N/mm^2 (= 75MPa) (Fig. 8). The authors postulate that contemporary component designs should provide for congruent patellar contact throughout flexion and extension, which seeks to minimise surface and sub-surface stresses.

Steubben *et al* (*97,98*) measured the distribution of patello-femoral surface stresses by mapping areas above and below the tensile *yield* strength of polyethylene. All implants whether of dome, modified-dome, or anatomic shape demonstrated material yielding over their range of flexion. Their results indicated the importance in appreciating the location of the yield areas within a given patellar component, as rim loaded contact areas above yield are more likely to deform and *wear*. It has hence been suggested that polymer integrity does not rest primarily with the size of the contact area, but rather with the extent of the surface within this region which exceeds yield condition.

Subsequently, contact stresses above the *yield* strength do not necessarily lead to catastrophic failure as demonstrated by the large number of relatively undamaged retrievals. As highest values of contact stress are experienced during flexion, variations in patient's activity may not expose the patellar component to large cyclic loads frequently enough to accumulate damage. McNamara (*63*) considered the constraining effect of surrounding polyethylene responsible for this phenomenon. *Yield* in polyethylene is characterized by plastic deformation (creep) rather than brittle failure, which explains why non-conforming patellar components are capable of 'wearing-in' (*6*). Retrieval studies (*32,114*) have shown that creep of polyethylene occurs independent of *wear*, which permits adaptation to the tracking position. Such surface adaptation produces characteristic facets at the margin of spherical patellar components, increasing the contact area particularly in flexion where there is least congruency between patella and femur (Fig. 6) (*19,44,63*). Although reduction in contact stresses of 23% to 58% through increased conformity have been reported, contact stress values remain above the UHMWP yield strength (*20,29,40*). Elbert *et al* (*29*) were surprised that, despite artificial "wearing in" of a polyethylene patellar surface into a concave shape, the von Mises stress (a criterion used in predicting the onset of *yield* in ductile materials) was at or near the polyethylene yield stress in most of the contact areas, which suggested that the deformation might continue anyway. Williams (*112*) found, via analysis of von Mises stress, that most stresses above yield strength occurred 1-2 mm below the articulating surface area in the newly manufactured component, whilst in retrieved com-

Questions? Contact FDA/CDRH/OCE/DID at CDRH-FOISTATUS@fda.hhs.gov or 301-796-8118

Records processed under FOIA Request #2014-8015; Released by CDRH on 12-8-2015

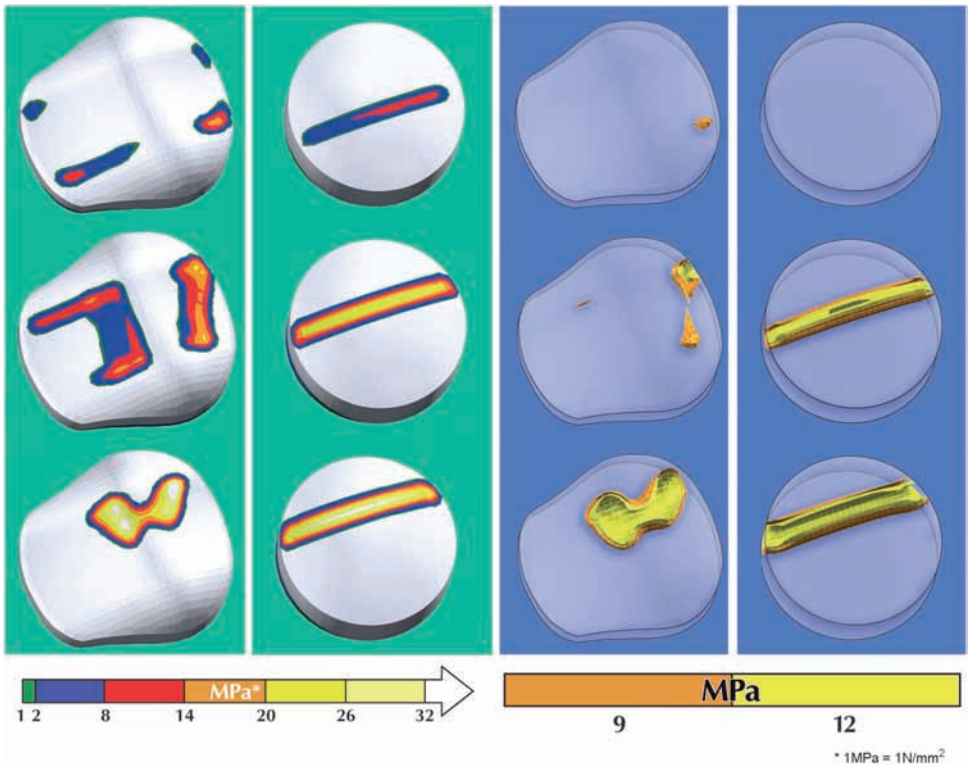

Fig. 8. — Green background : contact areas and contact stress images, simulating walking gait (15°, PRF = 420N, top row), stair ascend (45°, PRF = 1760N, middle row), and chair raise (90°, PRF = 1950N, bottom row) for anatomic and dome shaped patellar components. Purple background : von Mises subsurface stress images for the same activities, illustrating the volume of polymer stressed above 9 MPa (*68*). Illustration courtesy of Seth Greenwald of the Orthopaedic Research Laboratories, Cleveland/OH, USA.

ponents von Mises stress remained near yielding through the depth of the implant (*112*) (Fig. 8). Due to sub-surface stresses, permanent deformation may henceforth be expected to continue even when the component has 'worn-in' (*29*). Although Collier *et al* (*20*) conceded that "*all-polyethylene patellar components are not the answer as an ideal bearing surface*", in the absence of a suitable alternative, UHMWPE is likely to remain the material of choice at least in the foreseeable future (*20*).

FEMORAL COMPONENT DESIGN

The patella, whether native or prosthetic, cannot be considered in separation as it works in direct partnership with the femoral component. Contact areas are highly dependent on the congruency of the patello-femoral joint articulation at all angles of knee flexion, whilst motion constraints of the patella are determinated by the surface geometry of the femoral component (intrinsic stability) and by the balance of soft-tissue forces (extrinsic stability). Following on from the disappointing results of early arthroplasty designs which frankly ignored the patello-femoral joint, Seedhom suggested an array of design changes to the femoral component in order to improve patello-femoral kinematics and function (Fig. 9) (*91*). It is generally believed that a more congruent patello-femoral articulation with a deepened trochlear groove that extends both proximally and distally together with a build-up lateral trochlear wall is likely to provide for improved patellar tracking and enhance patellar stability during flexion and extension (Fig. 10) (*18,91,104, 116*).

Bartel *et al* (*3*) demonstrated the importance of conformity in prosthetic design to increase contact area and to decrease contact stress. Current femoral prosthesis designs display a wide variation in

Questions? Contact FDA/CDRH/OCE/DID at CDRH-FOISTATUS@fda.hhs.gov or 301-796-8118

Records processed under FOIA Request #2014-8015; Released by CDRH on 12-8-2015

length, depth and orientation of the trochlear groove, sagittal radius, and axial geometry (*25,104*). Anatomically shaped femoral component designs appear to be particularly suitable when articulating against the non-resurfaced patella, and hence referred to as 'patella-friendly (Fig. 11). They provide increased conformity between native patella and femoral component and require minimal biological patellar remodelling (*12,49*). Non-anatomical designs are those where the trochlear groove is concave spherical and designed to accommodate a non-anatomical patella usually of dome-shaped design.

The group of Freeman (*30,36,53*) believes that the design of the trochlea is the key feature in provid-

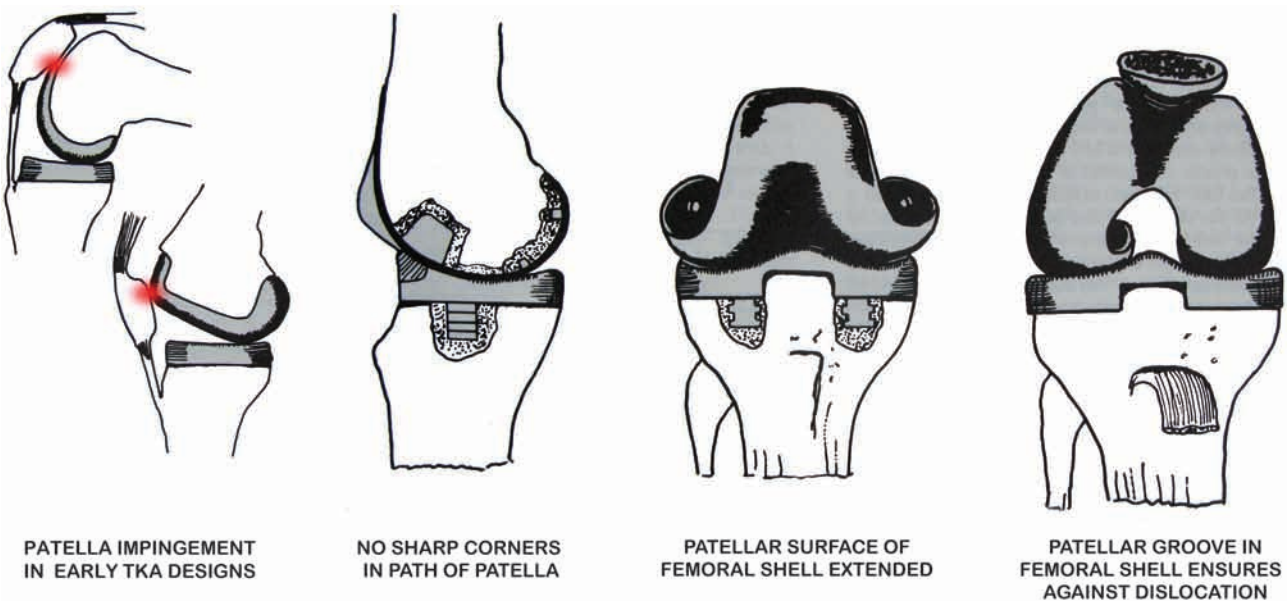

Fig. 9. — Failure to accommodate the patella in early arthroplasty designs resulted in patello-femoral impingement (areas denoted in red) and anterior knee pain. The 3 images on the right denote design alterations suggested by Seedhom in 1974 to overcome problems of impingement and to improve patello-femoral kinematics and function (*91*).

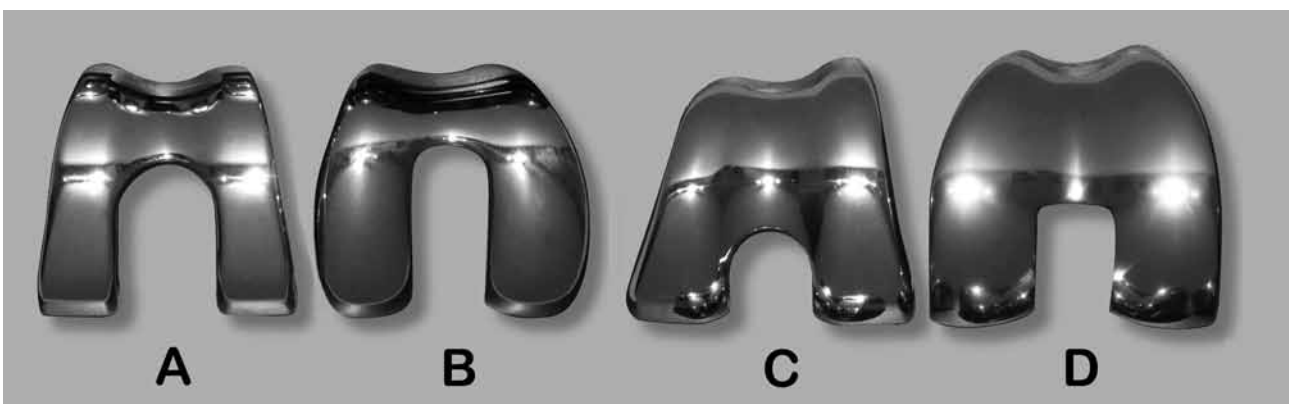

Fig. 10. — Characteristic design features of various femoral components which have shown to exert significant effects on patellar kinematics and biomechanics. Femoral components with relatively 'patella-unfriendly' design features usually provide a symmetric, shallow and short trochlear groove (A = unmodified Ortholoc®, Dow Corning Wright ; B = Townley®, Biopro). Femoral components with relatively 'patella-friendly' design features usually provide an asymmetric, deepened central femoral groove, elevated lateral trochlear flange, and distal extension of trochlear groove (C = modified Ortholoc®, Wright Medical ; D = Buechel-Pappas®, Endotec). Ortholoc implants courtesy of Leo Whiteside of the Missouri Bone & Joint Research Foundation, St. Louis, MO.

Questions? Contact FDA/CDRH/OCE/DID at CDRH-FOISTATUS@fda.hhs.gov or 301-796-8118

Records processed under FOIA Request #2014-8015; Released by CDRH on 12-8-2015

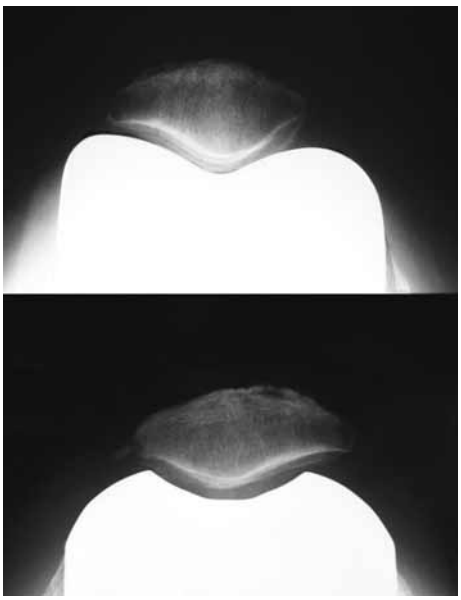

Fig. 11. — Postoperative radiographs (Merchant's view) showing a 'patellar-friendly' anatomic femoral component (top) and a patellar unfriendly femoral component (bottom), both articulating against the native patella.

ing satisfactory clinical results. They postulate that the floor of the prosthetic trochlea, viewed from the side, should be circular (single radius), similar to the native knee, extending from 0° to 110° of flexion. Furthermore it should be recessed to an anatomical extent in order to restore the patello-femoral joint line, a feature not to be confused with the height of the patella in relation to the tibio-femoral joint. In a large cohort study using such a design the same authors found no clinical differences between resurfaced and native patellae at a mean follow-up of 10 years. Based on this observation it has generally been accepted that increasing the radius of curvature and deepening of the trochlear groove reduces patello-femoral shear and compressive forces (*15,18,74,104*). Some experimental evidence also exists that the depth of the trochlear groove may be a more important variable in the prevention against patellar subluxation than the shape of the articulating surface itself (*15*). Excessive deepening of the trochlea groove however will decrease the moment arm of the quadriceps muscle force as the patella is brought closer to the centre of rotation of the knee.

The importance of femoral component design and its influence on patello-femoral performance has been highlighted by Theiss *et al* (*104*), based on clinical results of two arthroplasty designs with distinct differences in trochlear geometry. A 14-fold decrease in patellar related complications was observed when using a patellar friendly design. Similar results have been reported by Yoshii *et al* (*116*) in an experimental study. These authors were able to demonstrate that specific femoral design changes (e.g. 1 mm deepening of the trochlear groove, elevation of the lateral trochlear flange) improved patellar tracking compared to an unmodified femoral component (Fig. 10).

Proximal extension of the femoral flange will help to capture the patella during early flexion whilst extension of the concave shape of the trochlear groove onto the intercondylar surface will allow for increased metal-to-plastic contact at higher flexion angles (*85,90,116*).

The effect of valgus alignment of the trochlear groove on shear stresses, compared to symmetrical designs, has been investigated with mixed results. Asymmetric trochlear groove designs are thought to provide for earlier patellar capture through prominence of the lateral flange and to decrease the predominant valgus force vector thus reducing patellar shear (*25*). In some reports reduction in lateral shear forces of up to 10% was observed, whilst others saw either no effect or even a shift toward the generation of medial shear forces (*18,25,74,104*). The exact clinical advantages of asymmetric designs have remained largely theoretical, lacking compelling clinical proof of their effectiveness (*18,111*).

Lateral subluxation. Compressive and lateral forces acting at the patello-femoral articulation increase with knee flexion (*110*). The magnitude of the lateral forces, which are depending on valgus alignment, Q-angle and soft tissue balance may, if excessive, cause patellar subluxation and contribute to component failure. Steubben, Postak and Greenwald (*98*) investigated the resistance offered to lateral subluxation of the resurfaced patella by defining the intrinsic lateral stability of various patello-femoral designs. They disregarded surgical variables such as component placement, alignment and correction of varus and valgus deformity, but

Questions? Contact FDA/CDRH/OCE/DID at CDRH-FOISTATUS@fda.hhs.gov or 301-796-8118

Records processed under FOIA Request #2014-8015; Released by CDRH on 12-8-2015

recognized their importance in assisting this process. They found that the medio-lateral component of force was highly dependent on the interaction of condylar and patellar surface geometry. All tested implants presented force values required to produce lateral subluxation at or above those measured for the native knee. Force values of up to 2250 N at 90° were generated by some designs representing a 6 fold increase compared to the native patella, highlighting that appropriate design changes, e.g. deepening of the trochlear groove, can significantly increase resistance to patellar subluxation (*97,98*).

Conformity or non-conformity between femoral and patellar components (*82,99,101,109*) ? The level of conformity between femoral and patellar components influences the joint's ability to tolerate natural variations in motion. Conformity increases contact area and stability, whilst non-conformity allows the patella to establish an 'equilibrium of forces', and avoids excessive shear forces from arising. Potential advantages of conforming designs may hence be offset by an increase in constraint, potentially resulting in deleterious effects on patellar tracking and fixation. This typically leads to a compromise whereby conformity and subsequently contact areas are reduced to avoid over-constraining the joint. The question however, of how much contact area to sacrifice and how to best achieve this compromise remains unanswered. As a general trend most clinicians favour spherical patellar implants over anatomic patellar designs for ease of application, since they are less prone to surgical malalignment (*79,84*). Especially in combination with a mobile bearing TKA, dome patellar components have provided improved tracking and reduction in patello-femoral contact stress (*86*).

EFFECT OF CRUCIATE RETENTION OR SUBSTITUTION

Moment arms affecting the patella are dependent on the distance between the patello-femoral joint to the axis of rotation (flexion and extension) of the femoral component. They are increased if the axis is deviated posteriorly from its physiologic position. Femoral rollback facilitates this process and represents a characteristic feature of normal knee kinematics. Increased rollback effectively lengthens the patellar moment arm, thus increasing the efficacy of the extensor mechanism. D'Lima *et al* (*25*) investigated the influence of various degrees of posterior femoral rollback on patellofemoral compressive force. Femoral rollback resulting from PCL preservation produced reductions in patellofemoral compressive force of up to 7% throughout knee flexion, whereas the effect in PCL-substituting devices only became noticeable after cam-post engagement, with maximum effect recorded at 85 degrees of knee flexion. Miller *et al* (*66*), in an earlier study comparing PCL-retaining with PCL-substituting arthroplasties, failed to note femoral rollback when the PCL was retained. They stipulated that the absence of the anterior cruciate ligament may render the PCL ineffective, which may explain the appearance of paradoxical movements (reverse rollback) observed on fluoroscopic investigation (*22,23,25*). Although PCL substitution kept patellofemoral forces close to the level of the native knee, a lateral release became necessary in 50% of knees, raising potential concerns about an increase in patellofemoral stress through ligamentous tension. This notion has also been expressed by Ranawat and Sculco (*75,76*), who raised concern that femoral rollback either through a cam and post mechanism, as in posterior-stabilizing designs, or through a functional posterior cruciate ligament (PCL) may increase tensile forces across the patella in flexion. Overall, patellar thickness following resurfacing should therefore not exceed preoperative values, particularly in posterior-stabilized designs, as this will tighten the extensor mechanism, create loss of flexion, and increase both anterior patellar strain and PRF (*27,65,81,95,106*).

THE UNRESURFACED (NATIVE) PATELLA

Due to differences in the modulus of elasticity, the articular surface of the patella, if left un-resurfaced, must adapt to the geometry of the opposing surface by bedding-in. This process of remodelling, also known as 'stress contouring', produces gradual adaptation of the retro-patellar surface and subchondral bone plate to the trochlear shape (*93*).

Questions? Contact FDA/CDRH/OCE/DID at CDRH-FOISTATUS@fda.hhs.gov or 301-796-8118

Records processed under FOIA Request #2014-8015; Released by CDRH on 12-8-2015

Keblish *et al* (*50*) noted that minimal remodelling was required if the patella was exposed to an anatomical design with constant radius of curvature and uniform femoral geometry, whilst excessive remodelling was observed in non-anatomical designs. The remodelling process is time dependent and not displayed on axial radiographs much before two years after implantation.

Matsuda *et al* (*59*) assessed patellofemoral contact stress and contact area following TKA by comparing a non-conforming dome patella, a conforming anatomic patella and an unresurfaced patella with those values obtained in the native knee. In the un-resurfaced patella, peak contact stress and contact area remained almost at the level of the native knee. Following patellar resurfacing patello-femoral contact stress rose beyond yield strength for UHMWPE, with an average increase of 200%, whilst patello-femoral contact area decreased on average by 60%. The authors concluded that although the effect of metal action on cartilage was uncertain, the option of leaving the patella without a prosthetic component remains an attractive one. This is thought to apply especially to those cases where the patella is not severely worn, as peak stresses are known to be closer to normal if the patella is left unresurfaced.

Tanzer *et al* (*102*) looked at the effect of femoral component designs on contact and tracking characteristics of the unresurfaced patella in total knee arthroplasty. The authors noted substantial alterations in patellofemoral contact areas, contact pressures and tracking at higher flexion angles when the native patella was articulating with a prosthetic femoral component. The percentage of patellofemoral contact area compared to the native knee reduced markedly with increasing knee flexion, with measured values of 79%, 69% and 65% at 60°, 90° and 105° respectively.

The surface geometries of some prosthetic femoral components, particularly those of posterior-stabilized design, appear incompatible with the native patella, as the apex of the retropatellar ridge may impinge on the prosthetic intercondylar notch beyond 90° of knee flexion. Patellar deformation and wear are likely consequences and in the case of significant patellar tilt, displacement of the patella into the notch becomes possible (*62*). Whiteside's group (*116*) was able to show that distal extension of the trochlea and shortening of the intercondylar notch safeguard patellar support beyond 90° of knee flexion. Such design modifications are hence important if one considers leaving the patella unresurfaced. Most current femoral components present a surface geometry designed to articulate with a designated patellar component but are ill equipped to accommodate the native patella (Fig. 11) (*60*). Specific efforts are required to improve patellar kinematics and biomechanics by creating a femoral component which not only conforms to the normal trochlea and intercondylar notch topography, but which also takes the movement pattern of the native patella into account. Only then would we be in a position to offer prostheses dedicated to be used with the native patella, compared to the mostly inadequate femoral designs currently available.

SURGICAL EFFECT ON PATELLAR TRACKING

Despite major contributions through geometrical specifics of the replacement, performance and function, the resurfaced patella remains highly dependent on the surgical technique safeguarding correct placement of the components (*52,77,78,88*). Decisions made by the surgeon can compensate for implant design limitations, but conversely may also exacerbate such limitations (*26*). Any digression from the ideal position may affect the proper function and lead to deviation from the ideal tracking pattern. If mal-tracking is not corrected it may increase shear stresses at the fixation site which are likely to increase wear and affect the long-term survival of the patellar component (*49,105,107*). Intraoperative assessment of component positioning is unable to account for the effect of muscles and tendons on the kinematic behaviour of the replacement. Despite careful surgical technique patellar tilt often occurs, as intraoperative tests are static while postoperative function is dynamic (*7,73*).

Mistakes that are known to detrimentally affect patellar tracking are manifold and relate to component mismatch and sizing errors (e.g. undersized

Questions? Contact FDA/CDRH/OCE/DID at CDRH-FOISTATUS@fda.hhs.gov or 301-796-8118

Records processed under FOIA Request #2014-8015; Released by CDRH on 12-8-2015

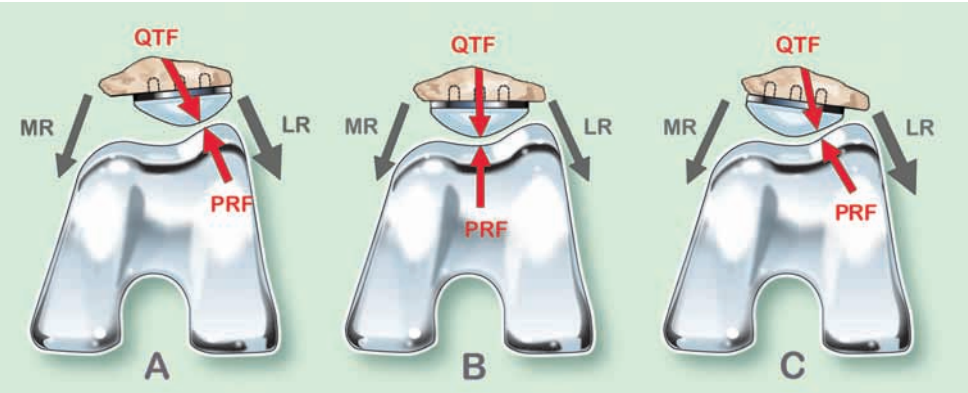

Fig. 12. — Left knee : lateral positioning of the patellar implant on the retro-patellar surface (A) will tighten the lateral retinacular structures (LR) and may provoke lateral subluxation. Overzealous medial positioning of the patellar implant (C) may create lateral patellar tilt through off centre positioning of the quadriceps tendon force (QTF). Moderate medialisation (B) will re-create the asymmetrical contour of the native retropatellar high point, centralise both, QTF and patello-femoral reaction force (PRF), and improve patellar tracking (Copyrights of illustration remain with author).

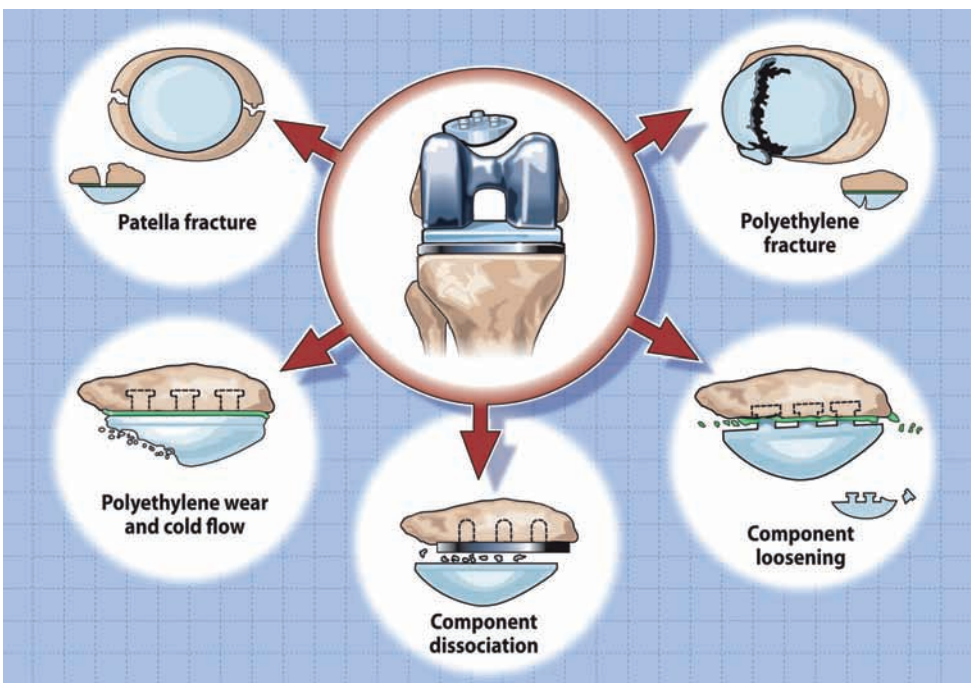

Fig. 13. — Potential complications, commonly associated with patellar mal-tracking, following patellar resurfacing (Copyrights of illustration remain with author).

patella, overstuffing), component malpositioning (e.g. lateralisation of patellar component, internal rotation and medialisation of femoral component, internal rotation of tibial component, excessive joint line elevation > 8 mm), overall leg mal-alignment (e.g. excessive valgus or varus), and ligamentous imbalance (*1,5,31,66,71,79,81,85*). Even minor alterations, such as patellar component placement on the retropatellar surface, have been shown to influence intra-articular force distribution (Fig. 12) (*1*). Any of the aforementioned surgical improprieties may exert a cumulative effect on patellar tracking and stability, potentially leading to disastrous results (Fig. 13). The author would like to

Questions? Contact FDA/CDRH/OCE/DID at CDRH-FOISTATUS@fda.hhs.gov or 301-796-8118

Records processed under FOIA Request #2014-8015; Released by CDRH on 12-8-2015

refer the reader to other publications on this subject matter as this aspect remains outside the realm of this article (*73,78,79,88*).

Acknowledgement

The author conveys his appreciation to Seth Greenwald of Cleveland for his scientific advice, to Leo Whiteside and staff of the Missouri Bone & Joint Research Foundation in St Louis for the provision of research material, to W Norman Scott of New York for his guidance and to Roger Lemaire and the co-editors of Acta Orthopaedica Belgica for their support and patience during the editing process. Special thanks are extended to Lesley Greig and her team at Southmead Medical Library in Bristol for their overwhelming kindness and successful endeavours in unearthing the most elusive of scientific literature.

REFERENCES

1. **Anglin C, Brimacombe JM, Wilson DR *et al.*** Biomechanical consequences of patellar component medialization in total knee arthroplasty. *J Arthroplasty* 2010 ; 25 : 793-802.
2. **Arora J, Ogden AC.** Osteolysis in a surface-cemented, primary, modular Freeman-Samuelson total knee replacement. *J Bone Joint Surg* 2005 ; 87-B : 1502-1506.
3. **Bartel DL, Bicknell VL, Wright TM.** The effect of conformity, thickness and material on stresses in ultra-high molecular weight components for total joint replacement. *J Bone Joint Surg* 1986 ; 68-A : 1041-1051 (see also letters : *J Bone Joint Surg* 1987 ; 69-A : 471-474.
4. **Bayley JC, Scott RD, Ewald FC, Holmes GB Jr.** Failure of the metal-backed patellar component after total knee replacement. *J Bone Joint Surg* 1988 ; 70-A : 668-674.
5. **Berger RA, Crossett LS, Jacobs JJ, Rubash HE.** Malrotation causing patellofemoral complications after total knee arthroplasty. *Clin Orthop Relat Res* 1998 ; 356 : 144-153.
6. **Bergström JS, Kurtz SM, Rimnac CM, Edidin AA.** Constitutive modeling of ultra-high molecular weight polyethylene under large deformation and cyclic loading conditions. *Biomaterials* 2002 ; 23 : 2329-2343.
7. **Bindelglass DF, Cohen JL, Dorr LD.** Patellar tilt and subluxation in total knee arthroplasty. Relationship to pain, fixation and design. *Clin Orthop Relat Res* 1993 ; 286 : 103-109.
8. **Black J.** Requirements for successful total knee replacement. Material considerations. *Orthop Clin North Am* 1989 ; 20 : 1-13.
9. **Brick GW, Scott RD.** The patellofemoral component of total knee arthroplasty. *Clin Orthop Relat Res* 1988 ; 231 : 163-178.
10. **Buechel FF, Pappas MJ.** New Jersey low contact stress knee replacement system. Ten year evaluation of meniscal bearings. *Orthop Clin North Am* 1989 ; 20 : 147-177.
11. **Buechel FF, Rosa RA, Pappas MJ.** A metal-backed, rotating-bearing patellar prosthesis to lower contact stress. An 11-year clinical study. *Clin Orthop Relat Res* 1989 ; 248 : 34-49.
12. **Buechel FF, Pappas MJ, Makris G.** Evaluation of contact stress in metal-backed patellar replacements. A predictor of survivorship. *Clin Orthop Relat Res* 1991 ; 273 : 190-197.
13. **Buechel FF.** Rotating patella. In : Scuderi JR, Tria Jr AJ (eds). "*Surgical Techniques in Total Knee Arthroplasty*". Springer, New York, 2002, pp 310-314.
14. **Cameron HU.** The patella in total knee arthroplasty. In : Laskin RS (ed). *Total Knee Replacement*. Springer, London, 1991, pp 199-210.
15. **Cepulo AJ, Stahurski TM, Black JD *et al.*** Mechanics of patello-femoral replacement. Presented at the *38th Annual Meeting of the American Academy of Orthopaedic Surgeons*, Las Vegas, NV, 1989.
16. **Charnley J.** *Low Friction Arthroplasty of the Hip*. Springer-Verlag, Berlin, 1979.
17. **Cheal EJ, Hayes WC, Harry JD, Gerhart TN, Page D.** Influence of component orientation on peg failure of patellar surface replacements. Presentation at the *32nd Annual Orthopaedic Research Society Meeting*, New Orleans, Feb. 17-20, 1986.
18. **Chew JT, Stewart NJ, Hanssen AD *et al.*** Differences in patellar tracking and knee kinematics among three different total knee designs. *Clin Orthop* 1997 ; 345 : 87-98.
19. **Clayton ML, Thirupathi R.** Patellar complications after total condylar arthroplasty. *Clin Orthop Relat Res* 1982 ; 170 : 152-155.
20. **Collier JP, McNamara JL, Surprenant VA, Jensen RE, Surprenant HP.** All-polyethylene patellar components are not the answer. *Clin Orthop Relat Res* 1991 ; 273 : 198-203.
21. **Colwell Jr CW, D'Lima DD, Patil S, Steklov N, Chen PC.** In vivo knee forces during recreational activities after total knee arthroplasty. Presented at the *75th annual meeting of the AAOS*. March, 2008 ; American Academy of Orthopaedic Surgeons ; San Francisco, USA.
22. **Dennis DA, Komistek RD, Hoff WA, Gabriel SM.** In vivo knee kinematics derived using an inverse perspective technique. *Clin Orthop Relat Res* 1996 ; 331 : 107-117.
23. **Dennis DA, Komistek RD, Colwell CE Jr *et al.*** In vivo anteroposterior femorotibial translation of total knee arthroplasty : a multicentre analysis. *Clin Orthop* 1998 ; 356 : 47-57.
24. **DeSwart RJ, Stulberg BN, Gaisser DM, Reger SI.** Wear characteristics of all-polyethylene patellar components : A retrieval analysis. *Trans Orthop Res Soc* 1989 ; 14 : 367.
25. **D'Lima D, Chen PC, Kester MA, Colwell CW Jr.** Impact on patellofemoral design on patellofemoral forces and polyethylene stresses. *J Bone Joint Surg* 2003 ; 85-A : suppl 4, 85-93.

Questions? Contact FDA/CDRH/OCE/DID at CDRH-FOISTATUS@fda.hhs.gov or 301-796-8118

Records processed under FOIA Request #2014-8015; Released by CDRH on 12-8-2015

26. **Doerr TE, Eckhoff DG.** Lateral patellar burnishing in total knee arthroplasty following medialization of the patellar button. *J Arthroplasty* 1995 ; 10 : 540-542.
27. **Dorr LD, Boiardo RA.** Technical considerations in total knee arthroplasty. *Clin Orthop Relat Res* 1986 ; 205 : 5-11.
28. **Doolittle KH 2nd, Turner RH.** Patellofemoral problems following total knee arthroplasty. *Orthop Rev* 1988 ; 17 : 696-702.
29. **Elbert K, Bartel D, Wright T.** The effect of conformity on stresses in dome-shaped polyethylene patellar components. *Clin Orthop Relat Res* 1995 ; 317 : 71-75.
30. **Elias SG, Freeman MA, Gokcay EI.** A correlative study of the geometry and anatomy of the distal femur. *Clin Orthop Relat Res* 1990 ; 260 : 98-103.
31. **Figgie HE 3rd, Goldberg VM, Heiple KG, Moller HS 3rd, Gordon HN.** The influence of tibial-patellofemoral location on function of the knee in patients with the posterior stabilized condylar knee prosthesis. *J Bone Joint Surg* 1986 ; 68-A : 1035-1040.
32. **Figgie MP, Wright TM, Santner T, Fisher D, Forbes A.** Performance of dome shaped patellar components in total knee arthroplasty. *Trans Orthop Res Soc* 1989 ; 14 : 531.
33. **Francke EI, Lachiewicz PF.** Failure of a cemented all-polyethylene patellar component of a press-fit condylar total knee arthroplasty. *J Arthroplasty* 2000 ; 15 : 234-237.
34. **Freeman MA, Samuelson KM, Bertin KC.** Freeman-Samuelson total arthroplasty of the knee. *Clin Orthop* 1985 ; 192 : 46-58.
35. **Freeman MA, Samuelson KM, Elias SG *et al.*** The patellofemoral joint in total knee prostheses. Design considerations. *J Arthroplasty* 1989 ; 4 (Suppl.) : S69-74.
36. **Freeman MAR, Kulkarni SK, Poal Manresa J.** Patellofemoral Joint. In : Sculco TP, Martucci EA (eds). *"Knee Arthroplasty"*, Springer, Wien, 2001, pp 61-70.
37. **Goymann V, Müller HG.** New calculations of the biomechanics of the patellofemoral joint and its clinical significance. In : Ingwersen OS, Van Linge B, Van Rens ThJG, Rösingh GE, Veraart BEEMJ, Le Vay D (eds). *"The Knee Joint : Recent Advances in Basic Research and Clinical Aspects"*. American Elsevier Publishing, New York, 1974, pp 16-21.
38. **Greenwald AS, Black JD, Matejczyk MB *et al.*** Total knee replacement. *Instr Course Lect* 1981 ; 30 : 301-341.
39. **Greenwald AS.** Personal communication.
40. **Hassenpflug J.** Das Patellofemoralgelenk beim künst - lichen Kniegelenksersatz, Springer, Berlin, 1989.
41. **Healy WL, Wasilewski SA, Takei R, Oberlander M.** Patellofemoral complications following total knee arthroplasty. Correlation with implant design and patient risk factors. *J Arthroplasty* 1995 ; 10 : 197-201.
42. **Hehne HJ.** *The Patello-Femoral Joint*. Enke, Stuttgart, 1983.
43. **Hood RW, Wright TM, Burstein AH.** Retrieval analysis of total knee prostheses : a method and its application to 48 total condylar prostheses. *J Biomed Mater Res* 1983 ; 17 : 829-842.
44. **Hsu HP, Walker PS.** Wear and deformation of patellar components in total knee arthroplasty. *Clin Orthop Relat Res* 1989 ; 246 : 260-265.
45. **Huang CH, Lee YM, Lai JH, Liau JJ, Cheng CK.** Failure of the all-polyethylene patellar component after total knee arthroplasty. *J Arthroplasty* 1999 ; 14 : 940-944.
46. **Hungerford DS, Kenna RV.** Preliminary experience with a total knee prosthesis with porous coating used without cement. *Clin Orthop Relat Res* 1983 ; 176 : 95-107.
47. **Innocenti B, Follador M, Salerno M *et al.*** Experimental and numerical analysis of patello-femoral contact mechanics in TKA. In : Vander Sloten J, Verdonk P, Nyssen M, Haueisen J (eds). *"ECIFMBE 2008, IFMBE Proceedings 22"*, Springer, Berlin, 2009, pp 1789-1793.
48. **Jordan LR, Dowd JE, Olivio JL, Voorhorst PE.** The clinical history of mobile-bearing patella components in total knee arthroplasty. *Orthopedics* 2002 ; 25 (Suppl. 2) : s247-250.
49. **Keblish PA, Greenwald SA.** Patellar retention vs patellar resurfacing in total knee arthroplasty. The patella : The unresolved problem in TKA. Presented at the *41st Annual Meeting of the American Academy of Orthopaedic Surgeons*, Anaheim, California, 1991.
50. **Keblish PA, Varma AK, Greenwald AG.** Patellar resurfacing or retention in total knee arthroplasty. A prospective study of patients with bilateral replacement. *J Bone Joint Surg* 1994 ; 76-B : 930-937.
51. **Kim W, Rand JA, Chao EYS.** Biomechanics of the knee. In Rand JA (ed) : *"Total Knee Arthroplasty"*, Raven Press, New York, 1993, pp 9-58.
52. **Krackow KA.** *The Technique of Total Knee Arthroplasty*. Mosby, Saint Louis, 1990.
53. **Kulkarni SK, Freeman MAR, Poal-Manresa JC, Asencio JI, Rodriguez JJ.** The patellofemoral joint in total knee arthroplasty. Is the design of the trochlea the critical factor ? *J Arthroplasty* 2000 ; 15 : 424-429.
54. **Larson CM, McDowell CM, Lachiewicz PF.** One-peg versus three-peg patella component fixation in total knee arthroplasty. *Clin Orthop Relat Res* 2001 ; 392 : 94-100.
55. **Lee TQ, Gerken AP, Glaser FE, Kim WC, Anzel SH.** Patellofemoral joint kinematics and contact pressures in total knee arthroplasty. *Clin Orthop Relat Res* 1997 ; 340 ; 257-266.
56. **MacCollum MS 3rd, Karpman RR.** Complications of the PCA anatomic patella. *Orthopedics* 1989 ; 12 : 1423-1428.
57. **Mannan K, Scott G.** The medial rotating total knee replacement ; a clinical and radiologic review at a mean follow-up of six years. *J Bone Joint Surg* 2009 ; 91-B : 750-756.
58. **Mason MD, Brick GW, Scott RD, Thornhill TS, Ewald FC.** Three peg all-polyethylene patella : 2-6 year results. *Orthop Trans* 1994 ; 17 : 991-992.

Questions? Contact FDA/CDRH/OCE/DID at CDRH-FOISTATUS@fda.hhs.gov or 301-796-8118

Records processed under FOIA Request #2014-8015; Released by CDRH on 12-8-2015

59. **Matsuda S, Ishinishi T, White SE, Whiteside LA.** Patellofemoral joint after total knee arthroplasty. Effect on contact area and contact stress. *J Arthroplasty* 1997 ; 12 : 792-797.
60. **Matsuda S, Ishinishi T, Whiteside LA.** Contact stresses with an unresurfaced patella in total knee arthroplasty : the effect of femoral component design. *Orthopedics* 2000 ; 23 : 213-218.
61. **Matthews LS, Sonstegard DA, Henke JA.** Load bearing characteristics of the patello-femoral joint. *Acta Orthop Scand* 1977 ; 48 : 511-516.
62. **McLain RF, Bargar WF.** The effect of total knee design on patellar strain. *J Arthroplasty* 1986 ; 1 : 91-98.
63. **McNamara JL, Collier JP, Mayor MB, Jensen RE.** A comparison of contact pressures in tibial and patellar total knee components before and after service in vivo. *Clin Orthop Relat Res* 1994 ; 299 : 104-113.
64. **Meding JB, Fish MD, Berend ME, Ritter MA, Keating EM.** Predicting patellar failure after total knee arthroplasty. *Clin Orthop Relat Res* 2008 ; 466 : 2769-2774.
65. **Merkow RL, Soudry M, Insall JN.** Patellar dislocation following total knee replacement. *J Bone Joint Surg* 1985 ; 67-A : 1321-1327.
66. **Miller MC, Berger RA, Petrella AJ, Karmas A, Rubash HE.** Optimizing femoral component rotation in total knee arthroplasty. *Clin Orthop Relat Res* 2001 ; 392 : 38-45.
67. **Moreland JR.** Mechanisms of failure in total knee arthroplasty. *Clin Orthop Relat Res* 1988 ; 226 : 49-64.
68. **Morra EA, Greenwald AS.** Patellofemoral replacement polymer stress during daily activities : a finite element study. *J Bone Joint Surg* 2006 ; 88-A : suppl 4, 213-216.
69. **Morrison JB.** The mechanics of the knee joint in relation to normal walking. *J Biomech* 1970 ; 3 : 51-61.
70. **Nagamine R, Whiteside LA, White SE, McCarthy DS.** Patellar tracking after total knee arthroplasty. The effect of tibial tray malrotation and articular surface configuration. *Clin Orthop Relat Res* 1994 ; 304 : 262-271.
71. **Nagamine R, Whiteside LA, Otani T, White SE, McCarthy DS.** Effect of medial displacement of the tibial tubercle on patellar position after rotational malposition of the femoral component in total knee arthroplasty. *J Arthroplasty* 1996 ; 11 : 104-110.
72. **Ortiguera CJ, Berry DJ.** Patellar fracture after total knee arthroplasty. *J Bone Jont Surg* 2002 ; 84-A : 532-540.
73. **Pagnano MW, Kelly MA.** The intraoperative assessment of patellar tracking. In : Scuderi GR, Tria Jr AJ (eds) : *"Surgical techniques in Total Knee Arthroplasty"*. Springer, New York, 2002, pp 317- 325.
74. **Petersilge WJ, Oishi CS, Kaufman KR, Irby SE, Colwell CW Jr.** The effect of trochlea design on patellofemoral shear and compressive forces in total knee arthroplasty. *Clin Orthop Relat Res* 1994 ; 309 : 124-130.
75. **Ranawat CS, Sculco TP.** History and development of the total knee prosthesis at the Hospital for Special Surgery. In : Ranawat CS (ed). *"Total-Condylar Knee Arthroplasty"*, Springer, New York, 1985, pp 3-6.
76. **Ranawat CS.** The patellofemoral joint in total condylar knee arthroplasty. Pros and cons based on five- to ten-year follow-up observation. *Clin Orthop Relat Res* 1986 ; 205 : 93-99.
77. **Rand JA.** Patellar resurfacing in total knee arthroplasty. *Clin Orthop Relat Res* 1990 ; 260 : 110-117.
78. **Rand JA.** The patello-femoral joint in total knee arthroplasty. *J Bone Joint Surg* 1994 ; 76-A : 612-620.
79. **Rand JA.** Failures in patellar replacement in total knee arthroplasty. In : Bellemans J, Ries MD, Victor JMK (eds). *"Total Knee Arthroplasty"*, Springer, Berlin, 2005, pp 57-64.
80. **Repo RU, Finlay JB.** Survival of articular cartilage after controlled impact. *J Bone Joint Surg* 1977 ; 59-A : 1068-1076.
81. **Reuben JD, McDonald CL, Woodard PL, Hennington LJ.** Effect of patella thickness on patella strain following total knee arthroplasty. *J Arthroplasty* 1991 ; 6 : 251-258.
82. **Rhoads DD, Nobel PC, Reuben JD, Mahoney OM, Tullos HS.** The effect of femoral component position on patellar tracking after total knee arthroplasty. *Clin Orthop Relat Res* 1990 ; 260 : 43-51.
83. **Rimnac CM, Wright TM.** The fracture behavior of UHMWPE. In : Willert HG, Buchorn GH, Eyerer P (eds). *"Ultra-High Molecular Weight Polyethylene as Biomaterial in Orthopaedic Surgery"*. Hogrefe & Huber, Toronto, 1991, pp 28-31.
84. **Ritter MA.** The anatomical graduated component total knee replacement : a long-term evaluation with 20-year survival analysis. *J Bone Joint Surg* 2009 ; 91-B : 745-749.
85. **Robie BH, Rosenthal DE.** Prosthetic design and patellofemoral function. In : Sculco TP, Martucci EA. (eds). "*Knee Arthroplasty"*, Springer, Wien, 2001, pp 27-36.
86. **Sawaguchi N, Majima T, Ishigaki T *et al.*** Mobile-bearing total knee arthroplasty improves patellar tracking and patellofemoral contact stress. In vivo measurements in the same patients. *J Arthroplasty* 2010 ; 25 : 920-925.
87. **Schindler OS, Scott WN.** Basic kinematics and biomechanics of the patello-femoral joint. Part 1. The native patella. *Acta Orthop Belg* 2011 ; 77 : 421-431.
88. **Schindler OS.** Patellar resurfacing in total knee arthroplasty. In : Scott WN (ed). *"Insall and Scott Surgery of the Knee"*. 5th edition, Elsevier/Churchill-Livingstone, Philadelphia, 2012, pp 1161-1190.
89. **Schwartz O, Aunallah J, Levitin M, Mendes DG.** Wear pattern of retrieved patellar implants. *Acta Orthop Belg* 2002 ; 68 : 362-369.
90. **Scott RD.** *Total Knee Arthroplasty*. Saunders, Philadelphia, 2006.

Questions? Contact FDA/CDRH/OCE/DID at CDRH-FOISTATUS@fda.hhs.gov or 301-796-8118

Records processed under FOIA Request #2014-8015; Released by CDRH on 12-8-2015

91. **Seedhom BB.** The patellar surface of femoral components. In : The Medical Engineering Working Party : *"Total Knee Replacement"*. Mechanical Engineering Publications Limited, London, 1975, pp 176-178.
92. **Seireg A, Arvikar RJ.** The prediction of muscular load sharing and joint forces in the lower extremities during walking. *J Biomech* 1975 ; 8 : 89-102.
93. **Smith SR, Stuart P, Pinder IM.** Nonresurfaced patella in total knee arthroplasty. *J Arthroplasty* 1989 ; 4 (Suppl.) : S81-86.
94. **Spreckelsen von L, Hahne HJ, Hassenpflug J.** [Patellofemoral contact zones in knee endoprostheses.] (in German). *Z Orthop Ihre Grenzgeb* 1998 ; 136 : 560-565.
95. **Star MJ, Kaufman KR, Irby SE, Colwell CW Jr.** The effects of patellar thickness on patellofemoral forces after resurfacing. *Clin Orthop Relat Res* 1996 ; 322 : 279-284.
96. **Stein HL.** Ultra-high molecular weight polyethylenes (UHMWPE). In : "*Engineering Plastics. Engineering Materials Handbook. Vol. 2"*, ASM International, Metals Park OH, 1988, pp 167-171.
97. **Steubben CM, Postak PD, Greenwald AS.** Mechanical characteristics of patello-femoral replacements. Presented at the *42nd Annual Meeting of the American Academy of Orthopaedic Surgeons*, Washington, DC, 1992.
98. **Steubben CM, Postak PD, Greenwald AS.** Mechanical characteristics of patello-femoral replacements. Presented at the *43rd Annual Meeting of the American Academy of Orthopaedic Surgeons*, San Francisco, CA, 1993.
99. **Stiehl JB, Komistek RD, Dennis DA, Paxson RD, Hoff WA.** Fluoroscopic analysis of kinematics after posterior-cruciate-retaining knee arthroplasty. *J Bone Joint Surg* 1995 ; 77-B : 884-889.
100. **Stiehl JB, Komistek RD, Dennis DA.** Detrimental kinematics of a flat on flat total condylar knee arthroplasty. *Clin Orthop Relat Res* 1999 ; 365 : 139-148.
101. **Stiehl JB, Komistek RD, Dennis DA, Keblish PA.** Kinematics of the patellofemoral joint in total knee arthroplasty. *J Arthroplasty* 2001 ; 16 : 706-714.
102. **Tanzer M, McLean CA, Laxer E, Casey J, Ahmed AM.** Effect of femoral component designs on the contact and tracking characteristics of the unresurfaced patella in total knee arthroplasty. *Canadian J Surg* 2001 ; 44 : 127-133.
103. **Takeuchi T, Lathi VK, Khan AM, Hayes WC.** Patellofemoral contact pressures exceed the compressive yield strength of UHMWPE in total knee arthroplasties. *J Arthroplasty* 1995 ; 10 : 363-368.
104. **Theiss SM, Kitziger KJ, Lotke PS, Lotke PA.** Component design affecting patellofemoral complications after total knee replacement. *Clin Orthop Relat Res* 1996 ; 326 : 183-187.
105. **Toksvig-Larsen S, Ryd L, Stentström A *et al.*** The porous-coated anatomic total knee experience. Special emphasis on complications and wear. *J Arthroplasty* 1996 ; 11 : 11-17.
106. **Tria AJ, Klein KS.** *An Illustrated Guide to the Knee*. Churchill Livingstone. New York, 1992.
107. **Tsao A, Mintz L, McRae CR, Stulberg SD, Wright T.** Failure of the porous-coated anatomic prosthesis in total knee arthroplasty due to severe polyethylene wear. *J Bone J Surg* 1993 ; 75-A : 19-26.
108. **Valdivia GG, Dunbar MJ, Jenkinson RJ *et al.*** Press-fit versus cemented all-polyethylene patellar component : midterm results. *J Arthroplasty* 2002 ; 17 : 20-25.
109. **van Kampen A, Huiskes R.** The tree-dimensional tracking pattern of the human patella. *J Orthop Res* 1990 ; 8 : 372-382.
110. **Walker PS.** *Human Joints and their Artificial Replacement*. Charles C. Thomas, Springfield, 1977.
111. **Walker PS.** Requirements for successful total knee replacements. Design considerations. *Orthop Clin North Am* 1989 ; 20 : 15-29.
112. **Williams JG.** *Stress Analysis of Polymers*. John Wiley & Sons, Halstead Press, 1984.
113. **Wright TM, Bartel DL.** The problem of surface damage in polyethylene total knee components. *Clin Orthop Relat Res* 1986 ; 205 : 67-74.
114. **Wright, TM.** Design considerations in patellar replacement. In : Goldberg VM (ed). "*Controversies of Total Knee Arthroplasty"*, Raven Press, New York, 1991, pp 145-154.
115. **Xu C, Chu X, Wu H.** Effects of patellar resurfacing on contact area and contact stress in total knee arthroplasty. *Knee* 2007 ; 14 : 183-187.
116. **Yoshii I, Whiteside LA, Anouchi YS.** The effect of patellar button placement and femoral component design on patellar tracking in total knee arthroplasty. *Clin Orthop Relat Res* 1992 ; 275 : 211-219.

Questions? Contact FDA/CDRH/OCE/DID at CDRH-FOISTATUS@fda.hhs.gov or 301-796-8118

Records processed under FOIA Request #2014-8015; Released by CDRH on 12-8-2015

Structural Changes of UHMWPE After e-Beam Irradiation and Thermal Treatment

Miroslav Slouf,[1] Hana Synkova,[1] Josef Baldrian,[1] Antonin Marek,[1] Jana Kovarova,[1] Pavel Schmidt,[1] Helmut Dorschner,[2] Michael Stephan,[2] Uwe Gohs[3]

[1] Institute of Macromolecular Chemistry of the Academy of Sciences of the Czech Republic, Heyrovsky Sq. 2, 162 06 Prague, Czech Republic

[2] Leibniz-Institute of Polymer Research Dresden, Hohe Strasse 6, 01069 Dresden, Germany

[3] Fraunhofer-Institute of Electron and Plasma Technology, Winterbergstrasse 28, D-01277 Dresden, Germany

Received 28 August 2006; revised 2 July 2007; accepted 3 July 2007
Published online 12 September 2007 in Wiley InterScience (www.interscience.wiley.com). DOI: 10.1002/jbm.b.30942

Abstract: Ultra-high molecular weight polyethylene (UHMWPE) was irradiated with accelerated electrons (1 MeV in air) using high dose rates (> 25 kGy/min) and thin specimens (thickness 1 mm). Parts of the specimens were remelted (200°C for 10 min; 150°C for 0, 2, 10, 30, 60 min). All specimens were stored in nitrogen in the dark at 5°C. Supermolecular structure, extent of crosslinking, oxidative degradation, and macroradical content were studied by a number of methods (SAXS, WAXS, SEM, DSC, FTIR, ESR, TGA, solubility experiments, image analysis). The results obtained with irradiated samples were compared with those obtained with irradiated and remelted samples. It was confirmed that crosslinking predominates over chain scission at very high dose rates, even if the irradiation is performed in air. Discrepancies concerning supermolecular structure changes in UHMWPE after irradiation and thermal treatment, found in various studies in the literature, are discussed. A simple model, which describes and explains all supermolecular structure changes, is introduced. An effective way of eliminating residual macroradicals in UHMWPE is proposed.
© 2007 Wiley Periodicals, Inc. J Biomed Mater Res Part B: Appl Biomater 85B: 240–251, 2008

Keywords: UHMWPE supermolecular structure; e-beam irradiation; thermal treatment; oxidative degradation; macroradicals

INTRODUCTION

Ultra-high molecular weight polyethylene (UHMWPE) is used in arthroplasty as a bearing component of total joint replacements (TJR).[1] Despite the development of metal-on-metal and ceramic-on-ceramic replacements, UHMWPE is still regarded as one of the best materials for TJR, both for total hip replacements (THR, Ref. 2) and total knee replacements (TKR, Ref. 3). However, the UHMWPE component of TJR articulates with metallic or ceramic parts of TJR, which leads to release of tiny wear particles, whose dimensions range from 0.1 μm to 10 μm (e.g., Ref. 4). Several studies report that the wear particles are even smaller[5] or larger.[6] The wear of UHMWPE is considered to be one of the most important life-limiting factors of TJRs. A reduced thickness polymer layer may lead to mechanical failure of the TJR, and the wear debris causes complex inflammatory reactions that may lead to osteolysis of bone and, consequently, to implant loosening.[7] Therefore, it is desirable to prepare UHMWPE with increased wear resistance, while keeping all other relevant mechanical properties at sufficient level.

The wear resistance of UHMWPE can be increased by crosslinking with ionizing radiation, such as γ-rays or accelerated electrons.[1,8] The irradiation causes homolytic cleavage of C—C and C—H bonds.[9] The resulting alkyl radicals are not stable and enter a complex system of reactions, which lead to crosslinking, but also to chain scissions, oxidation, formation of C=C double bonds and transformations to more stable allyl and peroxy radicals.[10] In the presence of oxygen, the radicals in UHMWPE survive for up to 30 months.[11] Crosslinking improves wear resistance but it leads to certain reductions in mechanical properties.[12] The formation of C=C bonds is not assumed to have a significant effect, but all other reactions influence wear and mechanical properties adversely. Chain scission leads to lower-molecular-weight-polyethylene, whose wear and mechanical performance is worse than that of the origi-

Correspondence to: M. Slouf (e-mail: slouf@imc.cas.cz)
Contract grant sponsor: Grant Agency of the Czech Republic (GACR); contract grant number: 106/04/1118
Contract grant sponsor: Ministry of Education, Youth and Sports of the Czech Republic (MSMT); contract grant number: 2B06096

© 2007 Wiley Periodicals, Inc.

Questions? Contact FDA/CDRH/OCE/DID at CDRH-FOISTATUS@fda.hhs.gov or 301-796-8118

Records processed under FOIA Request #2014-8015; Released by CDRH on 12-8-2015

nal UHMWPE.[13] Oxidation of UHMWPE during irradiation, that is, immediate oxidative degradation, is always associated with chain scissions.[14] Transformation to more stable radicals leads to long-term oxidative degradation, which also results in chain scissions, and which occurs both during the UHMWPE shelf-life and *in vivo*.[9] Immediate oxidative degradation is minimized by irradiation in an inert atmosphere[12,15] or vacuum.[16,17] Long-term oxidative degradation is minimized by destroying the residual radicals by thermal treatment.[12,15] Hence, the preparation of commercial crosslinked UHMWPEs includes remelting (i.e., thermal treatment above 140°C), annealing (thermal treatment below 140°C), and/or irradiation of UHMWPE in its molten state.[8]

Both irradiation and thermal treatment influence the supermolecular structure of UHMWPE, which impacts on mechanical properties.[1,18,19] A number of articles on supermolecular structure changes in UHMWPE exist,[11,12,15–31] but the majority concentrate on irradiation-induced changes[11,17,18,20,21,25–27,29,31,32] and do not take into account thermal treatment, which means that the very important aspect of residual radical elimination is not taken into account. Studies of residual macroradicals in UHMWPE have also been performed,[10,33–36] but only a small number of them[33,35,36] deal with thermal treatment and mostly they are focused on macroradical transformations after irradiation.[10,34] Moreover, the results in the literature are often contradictory. For instance, in some studies[15,21] a peak in the dose-crystallinity curve was found around 25 kGy, whereas in other studies this was not observed.[18,17] In the present study, a number of methods (small- and wide-angle X-ray scattering, differential scanning calorimetry, thermogravimetric analysis, scanning electron microscopy, infrared spectroscopy, electron spin resonance (ESR), solubility experiments, image analysis of light micrographs) were employed to study the influence of both e-beam irradiation and thermal treatment on the supermolecular structure, oxidation and elimination of residual radicals in UHMWPE. A simple and reliable model is introduced, which explains all the observed changes of the supermolecular structure. In addition, we discuss various discrepancies, connected with supermolecular structure changes. Finally, we propose an efficient way of eliminating residual macroradicals, which minimizes oxidative degradation of UHMWPE.

EXPERIMENTAL

Materials and Preparation of Samples

Ultra-high molecular weight polyethylene (UHMWPE) Chirulen 1020 (PolyHi Solidur, Germany), prepared by compression molding, was used in all experiments. Thin samples ($50 \times 50 \times 1$ mm^3) were cut from the virgin UHMWPE to assure homogeneous radiation dose distribution in the material. During cutting the material was intensively cooled to prevent changes of internal structure: The speed of cutting and the flow of cooling liquid were set in such a way that UHMWPE did not melt and the final plates were perfectly flat and noncrooked.

Irradiation, Thermal Treatment and Shelf Life of the Samples

Irradiation with Accelerated Electrons. This was performed by using an electron beam accelerator ELV-2 (Budker Institute of Nuclear Physics, Novosibirsk, Russia) at the Leibniz Institute of Polymer Research Dresden (IPF Dresden e.V.), Germany.[37] The electron beam irradiation was carried out in air. The electron energy was 1.0 MeV. Application of high dose rates (> 25 kGy/min) should minimize oxidation during the irradiation process.[11] Two series of samples were generated with irradiation doses of 0, 15, 25, 35, 50, 100, and 200 kGy. The third series of samples was irradiated under the same conditions as described above but using an irradiation dose of 50 kGy only.

Thermal Treatment. The first series of samples was left at room temperature. The second series of samples was remelted (RM): they were placed in a hot press (200°C, 10 min, zero pressure) and then cooled to room temperature (cooling rate ~5°C/min). The samples from the third series were remelted for 0, 2, 10, 30, and 60 min at 150°C as described above.

Shelf Life. After irradiation and between all experiments, the samples were kept in the dark (in a paper box), in nitrogen atmosphere (small PE bags filled with N_2), and at low temperature (refrigerator, 5°C).

Notation and Number of Samples. The nonirradiated and nonremelted samples are denoted as 0 kGy in the following text. The irradiated samples are denoted as 15 kGy, 25 kGy, 35 kGy, etc. The remelted samples are referred to as 0 kGy_RM, 15 kGy_RM, 25 kGy_RM, etc. Total number of samples was 18 (1 nonirradiated sample + 1 nonirradiated, remelted sample + 6 irradiated samples + 6 irradiated, and remelted samples + 4 different thermal treatments for sample 50 kGy).

Characterization of Structural Changes

Small-Angle X-ray Scattering. SAXS curves were measured using a Kratky camera (A. Paar, Austria). After background subtraction, the scattering curves were desmeared and Lorentz correction was applied. Peak positions q_m were employed to obtain long periods (LP) according to Bragg's law, LP = $2\pi/q_m$, where $q = (4\pi/\lambda)\sin\theta$, λ = CuKα = 1.54 Å, and 2θ is the scattering angle.

Wide-Angle X-ray Scattering. Wide-Angle X-ray Scattering (WAXS) patterns were obtained with a powder diffractometer HZG/4A (Freiberger Praezisionsmechanik

Questions? Contact FDA/CDRH/OCE/DID at CDRH-FOISTATUS@fda.hhs.gov or 301-796-8118

Records processed under FOIA Request #2014-8015; Released by CDRH on 12-8-2015

Freiberg GmbH, Germany). The total integral intensity I and integral intensity diffracted by crystalline part I_{CR} of samples were used for determination of crystallinity CR $= I_{CR}/I_{ALL}$.

Scanning Electron Microscopy. SEM was used to observe amorphous and crystalline parts of the samples directly. Before scanning electron microscopy (SEM) observation, the crystalline lamellae were visualized as described elsewhere.[38] Briefly, small pieces of the samples ($\sim 3 \times 3 \times 3$ mm^3) were cut out, smooth surfaces of the samples were prepared by microtoming at room temperature and etched with permanganic mixture (a 1:1 mixture of conc. H_2SO_4 and conc. H_3PO_4, containing 1 wt % of $KMnO_4$). It is worth mentioning here that washing of the samples is crucial to the success of the procedure. In this study, the samples were washed immediately after etching with four solutions: (i) mixture H_2SO_4:H_2O (2:7 vol., cooled in refrigerator at 5°C), (ii) conc. H_2O_2 (cooled in refrigerator at 5°C), (iii) H_2O, and (iv) acetone. In each step, a sample was placed in 2 mL of the wash solution in an ultrasonic bath. The etched and washed samples were fixed to copper supports, sputtered with platinum ($\sim$5 nm; Vacuum sputter coater SCD 050, Balzers) to avoid charging, decrease sample damage due to electron beam, and increase resolution. Finally, the samples were observed in scanning electron microscope (Vega Plus TS 5135, Tescan) in the secondary electron mode at 30 kV. Image analysis of SEM micrographs was performed with our own program MDFT.[39]

Differential Scanning Calorimetry. Differential scanning calorimetry (DSC) was measured using the Pyris 1 DSC apparatus (Perkin-Elmer, USA), in nitrogen at a heating rate of 10°C/min. T_m was determined from the position of the peak maximum, and crystallinity (CR_{DSC}) was calculated as the area under the melting peak.

Solubility Experiments. Determination of insoluble fraction (gel content), soluble fraction (extract percentage), and mass swell ratio was based on a modified procedure described in ASTM D 2765-95. Samples (1 mm thick, weight $\sim$0.5 g) were submerged in 100 mL of xylene in a 250-mL flask. Commercial antioxidant (BHT; 1 wt %) was added to prevent degradation of the sample. The xylene solution was boiled under reflux (138°C) for 8 h. Separate experiments showed that after 8 h the decrease in insoluble fraction is less than 1%. Three measurements were performed per sample: (i) initial mass of the sample, m_0, was measured before the experiment, (ii) mass of the sample swollen with xylene, m_X, was measured immediately after taking out the specimen from xylene and fast removal of the liquid on the surface by means of nitrogen flow, and (iii) mass of the dried sample, m_D, was measured after vacuum drying at 60°C, which was carried out to constant weight. All measurements were made on a balance with an accuracy of 0.1 mg. The insoluble fraction, g, soluble fraction, e, and mass swell ratio, q_m, were calculated as follows:

$$g = m_D/m_0 \times 100, \quad (1)$$

$$e = (m_0 - m_D)/m_0 \times 100, \quad (2)$$

$$q_m = m_X/m_D. \quad (3)$$

The crosslinking density according to Flory-Rehner expression was not calculated as the crosslinking was not homogeneous because more irradiation-induced crosslinks were formed in the amorphous phase.

Infrared Spectroscopy. This was employed to determine the oxidation index and vinylene index.[38] Infrared spectroscopy (IR) spectra of the samples (1 mm thick and 4–12 mm in diameter) were measured in transmission mode, using the FTIR spectrometer Bruker IFS-55 with DTGS detector. Oxidation index (OI, Refs. 33 and 40) and *trans*-vinylene index (VI, Ref. 33) were defined as follows:

$$\mathrm{OI} = \frac{\mathrm{absorption_area}_{1720\mathrm{cm}^{-1}}}{\mathrm{absorption_area}_{2022\mathrm{cm}^{-1}}}, \quad (4)$$

$$\mathrm{VI} = \frac{\mathrm{absorption_area}_{965\mathrm{cm}^{-1}}}{\mathrm{absorption_area}_{2022\mathrm{cm}^{-1}}}, \quad (5)$$

where absorption_area$_{1720}$ is the absorbance of C=O bonds in aldehydes, ketones, and carboxyls; absorption_area$_{965}$ is the absorbance of C=C bonds (mostly *trans*-vinylene, —CH=CH—); and absorption_area$_{2022}$ is the absorbance of the reference peak corresponding to vibrations of both amorphous and crystalline parts of virgin polyethylene.[40]

Electron Spin Resonance. ESR was used for the detection and quantitative identification of free radical intermediates occurring in chemical reactions of the polymer degradation. A sample tube (internal diameter = 4 mm) was filled with thin 1-cm long strips of UHMWPE, which were cut out of the original plates. Electron spin resonance (ESR) spectra were recorded using continuous X-band (9 GHz) ESR spectrometer Bruker ELEXSYS E-540 in the usual form of the first derivative of the microwave absorption curve. A double integral of the spectra, which is the area under the absorption peaks, is proportional to the number of detected spins. A standard calibration procedure using a sample of known spin concentration (DPPH 10^{-3} M in benzene) allows for estimation of absolute spin concentration. A sufficient signal/noise ratio for determination of the radical concentration in irradiated UHMWPE samples was typically obtained for $\sim$50 mg of sample. ESR spectra were measured at 6 mW microwave power, 1 G modulation width at 100 kHz frequency, Q-value about 4000, and accumulation time about 3 min.

Thermogravimetric Analysis. Thermogravimetric Analysis (TGA) curves were obtained with Perkin Elmer TGA

Questions? Contact FDA/CDRH/OCE/DID at CDRH-FOISTATUS@fda.hhs.gov or 301-796-8118

Records processed under FOIA Request #2014-8015; Released by CDRH on 12-8-2015

7 apparatus equipped with Pyris 1 software. The measurements were performed in air using a longer-term isothermal mode at different temperatures, ranging from 120°C up to 200°C in 10°C intervals. The mass increase due to the absorption of oxygen by the sample was monitored and the respective induction period of oxidation at a given temperature was evaluated.

Image Analysis of Light Micrographs. Small sections of 1-mm thick samples were placed on a light box LP 310 (Fomei) and light micrographs were made with a digital camera DXM 1200 (Nikon) with macroobjective (Nikon), which allowed all samples to be photographed at once. This guaranteed recording of all samples at constant illumination. Image analysis was performed with the program Lucia (Laboratory Imaging, Czech Republic). The goal of the image analysis was to quantify slight changes in color, which were observable even with the naked eye. Nonirradiated samples appeared white and with increasing radiation dose the samples became slightly yellow. Two image analysis parameters were evaluated: *HueTypical* and *MeanSaturation*. The first parameter, *HueTypical*, gives the hue (color) value with maximum frequency in a hue value histogram; red, green, and blue color correspond to 0, 120, and 240 value of hue, respectively. The second parameter, *MeanSaturation*, is a statistical mean of the saturation values of pixels; generally speaking, it determines how much the color of the sample differs from white.

RESULTS

Small- and Wide-Angle X-Ray Scattering

UHMWPE long periods (LPs) and crystallinities (CRs) were determined from SAXS and WAXS, respectively. The results are summarized in Figure 1. The CR and LP of nonirradiated and nonremelted samples were within usual limits.[15,16,18,24] The CR of nonremelted samples monotonically increased with radiation dose. This is usually attributed to irradiation induced chain scissions of loops and tie molecules, followed by additional crystallization of released chain segments.[11,15,17,18,25–27] Also, the LPs of the nonremelted samples grew slightly with increasing dose. As the LP corresponds to average distance between amorphous and crystalline regions, the only possible explanation is that some lamellae must disappear or merge. We assume that both disappearing and merging of lamellae took place as discussed below. After remelting, both CR and LP values went down. The drop in CR and LP results from different thermal history of the samples: the original bulk material is consolidated from the UHMWPE resin at elevated temperatures and pressures followed by several-hour annealing,[19,41] whereas our remelting procedure consisted of relatively fast heating and cooling without any annealing. Further decrease in CR and LP of the irradiated and remelted samples with radiation dose was caused by the fact that the crosslinking partially prevents crystallization.

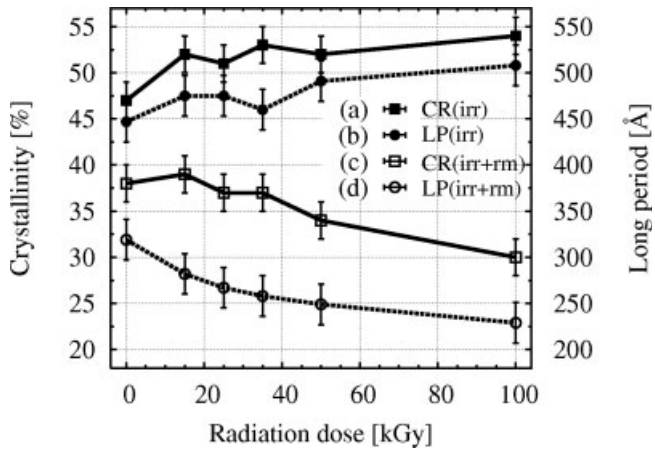

Figure 1. Small- and wide-angle scattering results. CR(irr) and LP(irr) denote the crystallinity and long period of UHMWPE after irradiation, whereas CR(irr+rm) and LP(irr+rm) represent crystallinity and long period of UHMWPE after irradiation and remelting. Error bars give 95% confidence limits, which were calculated as $1.96 \times \sigma/\sqrt{n}$, where σ is the estimated standard deviation calculated from all n measurements.

Scanning Electron Microscopy

SAXS and WAXS (or SWAXS) experiments yielded useful but indirect pieces of information on supermolecular structure of UHMWPE. SEM micrographs of smoothed and etched surfaces showed the supermolecular structure directly (Figure 2, upper row). Crystalline lamellae were etched more slowly than amorphous regions and, consequently, the crystalline phase appeared light and the amorphous phase appeared dark in SEM micrographs taken in the secondary electron mode. *Qualitative information* contained in the images is evident: sample 0 kGy exhibited relatively coarse structure, the structure in sample 0 kGy_RM was much finer, sample 100 kGy seemed to show the coarsest structure while the structure in sample 100 kGy_RM was destroyed by the etching. *Quantitative information* concerning structure coarseness can be extracted from the SEM micrographs only by image analysis. Standard image analysis of the micrographs, based on setting the threshold and further PC-assisted image processing, would be very laborious, time-consuming and hard to reproduce. Therefore, we have developed an automatic image analysis technique, based on our program MDFT.[39] In the first step, program MDFT calculates the two-dimensional discrete Fourier transform of the images (Figure 2, lower row). The two-dimensional Fourier transform (2D-FT) is calculated as:

$$F(k,l) = \sum_{x=0}^{N-1}\sum_{y=0}^{N-1} f(x,y) \times \exp[2\pi i(kx/N + ly/N)], \qquad (6)$$

where (x,y) are coordinates of the pixel in the input image, (k,l) are coordinates of the pixel in the output image, $f(x,y)$

Questions? Contact FDA/CDRH/OCE/DID at CDRH-FOISTATUS@fda.hhs.gov or 301-796-8118

Records processed under FOIA Request #2014-8015; Released by CDRH on 12-8-2015

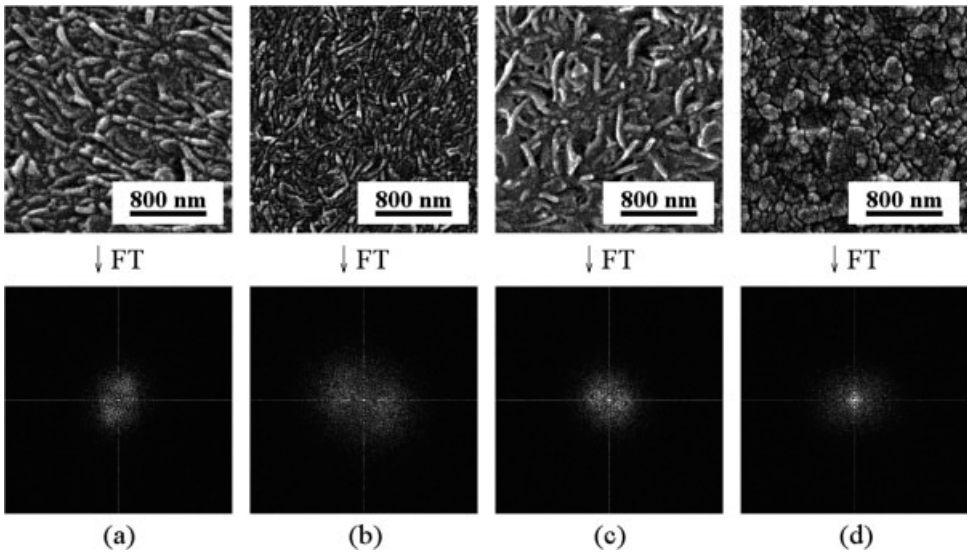

Figure 2. SEM micrographs (upper row) and their two-dimensional Fourier transforms (lower row): (a) virgin UHMWPE, sample 0 kGy; (b) remelted UHMWPE, sample 0 kGy_RM; (c) irradiated UHMWPE, sample 100 kGy; (d) irradiated and remelted UHMWPE, sample 100 kGy_RM. Fourier transforms were calculated according to Eq. (6).

and $F(k,l)$ represent the grayscale intensity of the pixel in input and output image, respectively, N is the dimension of the (square) input image and the double summation runs through the whole picture. In the second step, MDFT converts two-dimensional Fourier transform to one-dimensional Fourier transform (1D-FT), which is the grayscale intensity as a function of distance from the centre of the image. This is achieved by a simple averaging process. In the third step, long period (LP) is calculated from the position of the first peak on the 1D-FT curve using modified Bragg's Law:

$$\mathrm{LP} = 1/S_{\mathrm{MAX}} \times \mathrm{RWI}, \tag{7}$$

where S_{MAX} is the position of the first local maximum on the calculated 1D-FT curve and RWI is the real width of the analyzed SEM micrograph. The use of Bragg's Law follows from the analogy between Fourier transform of a SEM micrograph and small-angle X-ray scattering by the sample itself.[39] The results of calculation for samples 0 kGy, 0 kGy_RM, 100 kGy, and 100 kGy_RM are summarized in Figure 3. It is worth noting that sample 100 kGy_RM, whose SEM micrograph did not show the correct structure, exhibited no peak on 1D-FT curve. The other values of LPs calculated from SEM micrographs, LP(SEM), exhibit the same trend as the LPs determined from SAXS curves, LP(SAXS). Both LP(SAXS) and LP(SEM) decreased in the order 100 kGy > 0 kGy > 0 kGy_RM. Nevertheless, the values of LP(SEM) differed from those of LP(SAXS), which may have been caused by several facts: (i) the thinnest lamellae are below the SEM resolution, which makes the values from SEM systematically higher. (ii) In SAXS, we investigate quite a large part of the sample while in SEM we see just a small region. (iii) The position of the first peak on 1D-FT curve must be estimated by the user, which may not be absolutely precise. (iv) SAXS determines the LP from 3D sample, while in SEM we investigate a 2D section of the sample. To conclude, SEM micrographs allowed the direct qualitative look at the supermolecular structure and MDFT program extracted semiquantitative information from the micrographs, which confirmed and verified the SAXS results.

Differential Scanning Calorimetry

DSC results, which were used to supplement and verify SWAXS measurements, are summarized in Figure 4 and

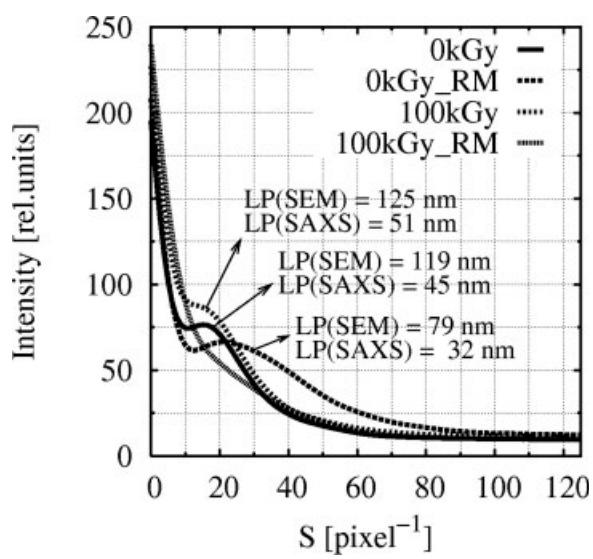

Figure 3. One-dimensional Fourier transforms of SEM micrographs with calculated values of long periods, LP(SEM), which were calculated according to Eq. (7).

Questions? Contact FDA/CDRH/OCE/DID at CDRH-FOISTATUS@fda.hhs.gov or 301-796-8118

Records processed under FOIA Request #2014-8015; Released by CDRH on 12-8-2015

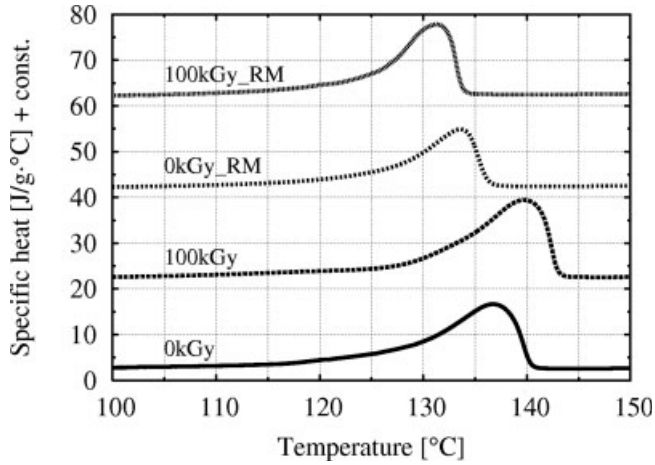

Figure 4. Differential scanning calorimetry curves for: virgin sample (0 kGy), remelted sample (0 kGy_RM), irradiated sample (100 kGy), and irradiated+remelted sample (100 kGy_RM).

Table I. Both melting points (T_m) and crystallinities (CR_{DSC}) were determined from DSC curves and decreased in the following order: 100 kGy > 0 kGy > 0 kGy_RM > 100 kGy_RM. As for crystallinities, the trend in DSC was exactly the same as in WAXS. The increase in melting points after irradiation was in agreement with the concept of additional crystallization, which results in thicker lamellae. The decrease in T_m after remelting agreed with the drop in CR and LP indicated by SWAXS: this means that a higher number of thinner lamellae were formed during the remelting process. Further decrease in T_m observed in the irradiated and remelted sample 100 kGy_RM results from the fact that the thickness of the lamellae in this sample was further limited due to crosslinks. In other words, the new lamellae that were formed after remelting in the irradiated sample were thinner not only because of faster cooling, but also due to space constraints as they had to fit in among the existing crosslinks.

Solubility Measurements

Insoluble fractions, soluble fractions, and swell ratios of selected samples are summarized in Table II. Insoluble fraction (or gel fraction, g) is given in weight percent and increases with both molecular weight of polymer due to entanglements (physical crosslinks) and crosslinking density (chemical crosslinks). Soluble fraction (or extract percentage, e) gives the dissolved fraction of the sample in weight percent. The value of e represents a fraction of shorter, nonentangled, and noncrosslinked polymer chains. Mass swell ratio, q_m, gives a measure of how tightly the polymer is crosslinked. Higher crosslinking density results in lower swelling and lower values of q_m. The data in Table II showed that (i) irradiation crosslinking predominated over chain scission in all studied samples, (ii) the difference between samples irradiated at 50 kGy and 100 kGy was almost negligible from the point of view of solubility measurements, and (iii) remelting did not significanlty influence crosslinking and chain scission in the polymer. The irradiation procedure (very fast e-beam irradiation of thin samples in air) led to crosslinking rather than to chain scission because the insoluble fraction of all irradiated samples was more than 40% higher than the insoluble fraction of virgin UHMWPE. The extract percentage was very small. Similar results were obtained in the study of Premnath et al.,[11] in which a zero extract percentage was found in e-beam-irradiated samples for radiation doses higher than 25 kGy. The remelting procedure (remelting of thin samples at 200°C for 10 min) did not influence crosslinking density, because no solubility parameter changed significantly.

TABLE I. Comparison of X-ray Scattering and Differential Scanning Calorimetry Results

Sample	LP (SAXS)[a] (Å)	CR (WAXS)[b] (%)	CR (DSC)[c] (%)	T_m (DSC)[d] (°C)
0 kGy	447(27)	47(2)	56(2)	136(1)
0 kGy_RM	319(12)	38(2)	44(2)	133(1)
100 kGy	508(35)	54(3)	64(2)	140(1)
100 kGy_RM	229(6)	30(3)	38(2)	131(2)

Estimated standard deviations of each measurement are given in brackets.
[a] LP(SAXS), long period determined by small-angle X-ray scattering.
[b] CR(WAXS), crystallinity determined by wide-angle X-ray scattering.
[c] CR(DSC), crystallinity determined by differential scanning calorimetry.
[d] T_m(DSC), melting point determined from differential scanning calorimetry.

TABLE II. Results of Solubility Measurements: Values of *g* and *e* Give Insoluble and Extract Fraction of UHMWPE After 8 h in Boiling Xylene, Respectively, Value of q_m Gives Swell Ratio (Dimensionless)

Sample	g (%)	e (%)	q_m ( )
0 kGy	54.37	45.63	7.31
50 kGy	95.57	4.43	2.81
100 kGy	96.04	3.96	2.40
50 kGy_RM	95.02	4.98	2.58
100 kGy_RM	96.69	3.31	2.15

All values are averages of two independent measurements; maximum absolute differences between corresponding measurements were less than 1 % (for g and e) and 0.3 (for q_m).

Infrared Spectroscopy

Oxidation index, OI, is widely accepted as a measure of oxidation of UHMWPE.[40] *Trans*-vinylene index, VI, might be used as an estimate of crosslinking, because it increases with radiation dose almost linearly[33,42] and higher radiation doses result in higher crosslinking density, if the doses are smaller than 100 kGy.[11,17,18,33] FTIR measurements are shown in Figure 5. OI increased with radiation dose, suggesting that the oxidation took place in spite of the very high dose rate. This was confirmed by ESR measurements. Further increase in OI was observed after remelting of both nonirradiated and irradiated samples, indicating that the

Questions? Contact FDA/CDRH/OCE/DID at CDRH-FOISTATUS@fda.hhs.gov or 301-796-8118

Records processed under FOIA Request #2014-8015; Released by CDRH on 12-8-2015

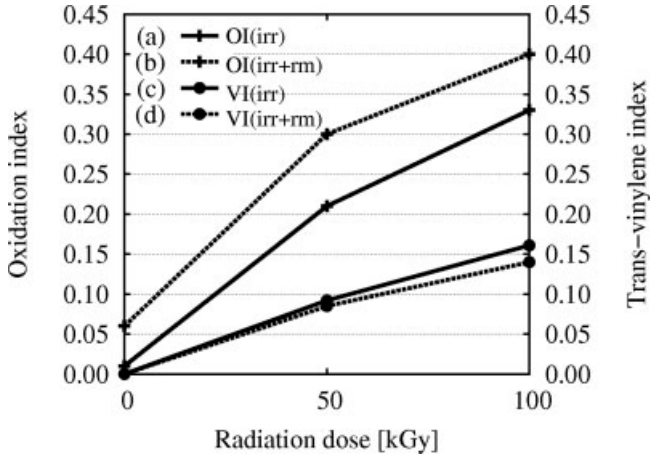

Figure 5. Oxidation index (OI) and *trans*-vinylene index (VI) as a function of radiation dose.

selected remelting procedure was not optimal, as oxidation is usually associated with undesired chain scissions. This was confirmed by thermogravimetric analysis (TGA). VI increased with irradiation dose and did not change after remelting, which was in agreement with our assumption that the remelting procedure did not impact on crosslinking significantly. This was also confirmed by solubility measurements.

Thermogravimetric Analysis

Medical grade UHMWPE is very sensitive to oxidation because it must not contain stabilizers and/or antioxidants, although the use of α-tocopherol (vitamin E) is being considered.[9] IR measurements signaled that some oxidation occurred during the remelting procedure at 200°C for 10 min. Consequently, a set of TGA experiments was performed to quantify the stability of virgin UHMWPE at elevated temperatures (Figure 6). To our knowledge and surprise, such a study has not been published so far. Figure 6 shows that UHMWPE oxidation was quite slow if the temperature was below T_m. At 120°C the mass change of the sample was almost unobservable. At 130°C the sample was also stable but, after ~100 min, its weight slightly increased, indicating that oxidation products inside the polymer started to form. At 140°C the observable oxidation started after ~50 min, at 150°C after ~10 min and at 160°C it started almost immediately. At higher temperatures the rate of oxidation increased as evidenced by steeper and steeper slopes of the curves. For the temperatures higher than 150°C the TGA curves exhibited a peak, indicating that after a certain amount of oxygen was consumed, the polymeric hydroperoxides formed in the sample underwent decomposition: volatile oxidation products were released and thus the weight of the sample decreased. In accord with the expectations, the peak occurred after shorter time periods with increasing temperature, being 330, 180, 70, 40, and 15 min for 160, 170, 180, 190, and 200°C, respectively. The peak height decreased with the growing temperature, which indicated that the release of low-molecular-weight oxidation products was faster as the temperature went up. It should be noted, however, that our remelting procedure was performed in a closed hot press, which could be regarded as a low-oxygen atmosphere. Therefore the oxidation rate during our remelting procedure may have been lower.

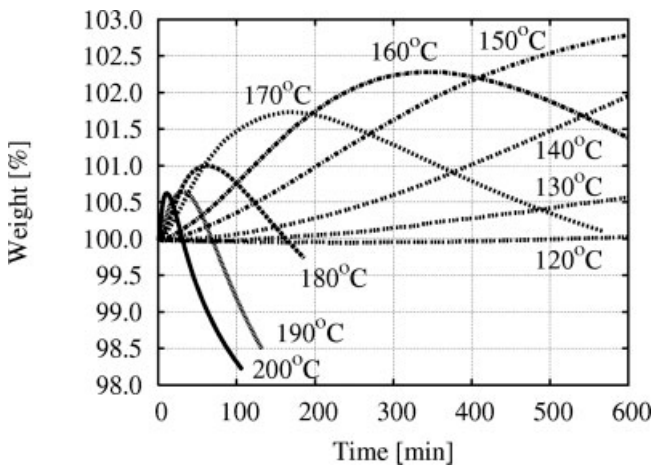

Figure 6. Thermogravimetric analysis (TGA) curves of virgin UHMWPE at various temperatures.

Image Analysis of Light Micrographs

The irradiated samples exhibited yellowing that is associated with oxidation and can be estimated at a semiquantitative level using image analysis (Figure 7). The yellowing indicated that oxidation occurred even if very high dose rates and correspondingly short irradiation times were used. Oxidation of the 200 kGy sample, whose yellow color was

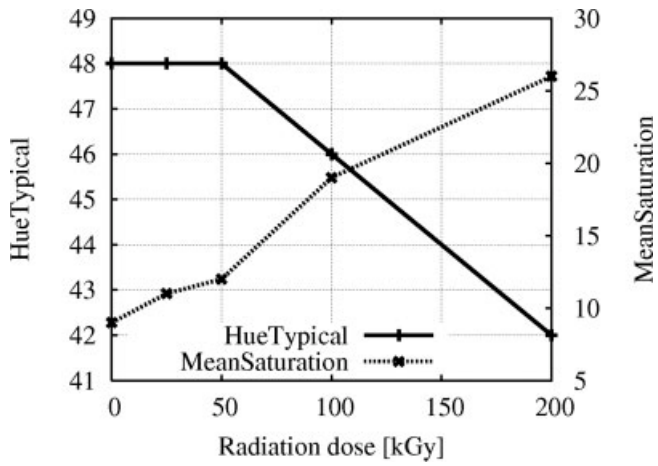

Figure 7. Image analysis of light micrographs of irradiated UHMWPE. *HueTypical* and *MeanSaturation* are image analysis parameters giving hue and saturation of a color image as explained in the Experimental section.

Questions? Contact FDA/CDRH/OCE/DID at CDRH-FOISTATUS@fda.hhs.gov or 301-796-8118

Records processed under FOIA Request #2014-8015; Released by CDRH on 12-8-2015

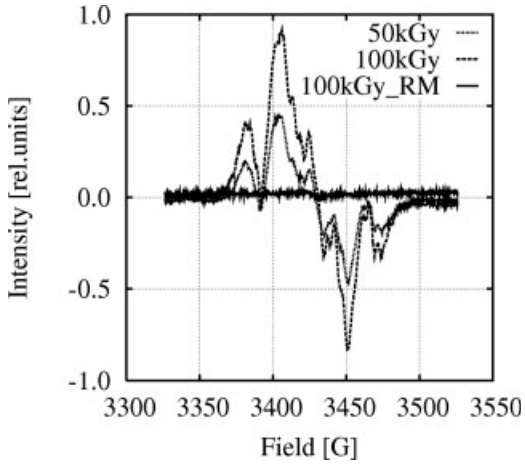

Figure 8. Electron spin resonance spectra of irradiated samples before and after remelting (10 min at 200°C).

observable even with naked eye, was too high and so it was excluded from further experiments. The parameters of supermolecular structure of the 200 kGy sample differed significantly from all other samples and were completely off all trends observed by SAXS, WAXS, and SEM. This was caused by the elevated temperature during irradiation: each 10 kGy increases the temperature of the irradiated sample by ~7°C, which gives the temperature inside the sample at around 165°C. Such a high temperature leads to fast oxidative degradation as evidenced by TGA (Figure 6).

Electron Spin Resonance

ESR spectroscopy was employed in the investigation of both oxidation and radical content after irradiation and remelting. The samples 0 kGy and 0 kGy_RM did not contain any detectable amount of radicals. The spectra of samples 50 kGy and 100 kGy (Figure 8, dashed lines) were measured immediately after irradiation. The number of radicals in sample 50 kGy and 100 kGy was 2.61×10^{-8} mol/g and 5.30×10^{-8} mol/g, respectively. This corresponded to a linear increase in macroradical concentration with radiation dose. The ESR spectrum of sample 100kGy_RM (Figure 8, full line) proved that our remelting procedure removed all radicals. The noncentrosymmetric shape of ESR spectra in Figure 8 (and OI measurements summarized in Figure 5) indicated that the samples suffered from oxidation despite the extremely high dose rates and storage under nitrogen. Primary products of irradiation are alkyl radicals ($—CH_2—CH^*—CH_2—$), which undergo crosslinking, chain scission, oxidation, double bond formation, or transformation to more stable radicals such as allyl ($—CH_2—CH^*—CH{=}CH—$) and peroxy ($—CH_2—C(OO)^*—CH_2—$) radicals.[10,11,34,35,36] The peroxy radicals are the primary product of oxidation; the final oxidation products are alcohols, aldehydes, ketones, carboxylic acids, and esters. The overall reaction is known as the Bolland's cycle[43]; during this cyclic reaction the peroxy radical abstracts hydrogen from the same or another polymer chain with the formation of hydroperoxide and of further alkyl radical, which reacts with oxygen forming again the peroxy radical. Hydroperoxide transforms into more stable, final oxidation products and peroxy radical reenters the Bolland's cycle; this is the chemical principle of UHMWPE oxidative degradation.[9] The somewhat irregular shapes of the spectra of the 50 kGy and 100 kGy samples in Figure 8 indicated the presence of allyl and peroxy radicals.[10,34] The ESR spectra of the 50 kGy sample that was held in a hot press at 150°C for 0, 2, 10, 30, and 60 min are shown in Figure 9. The single peak corresponding to the nonremelted 50 kGy sample results from the fact that this set of experiments was performed several weeks after irradiation, and indicated that the alkyl and allyl radicals formed after irradiation transformed into oxidized species.[11,35] The total disappearance of the peak in Figure 9 for the 50 kGy sample, which was remelted for 2 min, proved that all macroradicals were removed in a very short period of time on the condition that the specimen was thin (here 1 mm) and the RM temperature (here 150°C) slightly exceeded the T_m of UHMWPE.

DISCUSSION

Changes of Supermolecular Structure

UHMWPE supermolecular structure changes after irradiation and remelting can be summarized as follows: (i) after irradiation, both CR and LP increased slightly in comparison with virgin polymer; (ii) after remelting, both CR and LP markedly decreased and this drop in CR and LP amplified with increasing radiation dose (Figure 1). We propose a simple model explaining the observed changes (Figure 10). The model is based on the assumption that three different phases—amorphous, crystalline, and crosslinked—exist in the UHMWPE.

The small increase in CR after irradiation [Figure 10(a,b)] is well established in the literature. It is usually

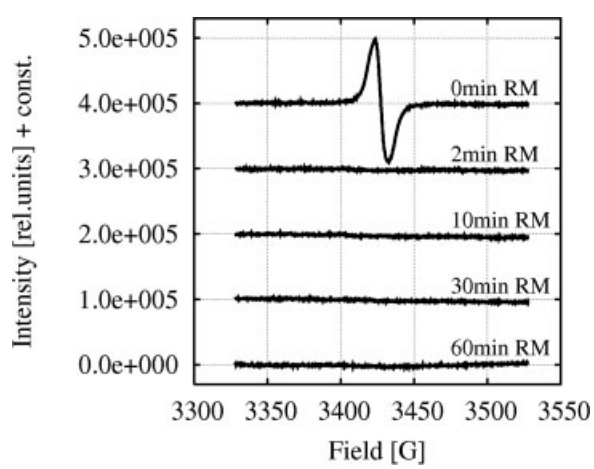

Figure 9. Electron spin resonance spectra of 50 kGy samples, which were remelted for 0, 2, 10, 30, and 60 min at 150°C.

Questions? Contact FDA/CDRH/OCE/DID at CDRH-FOISTATUS@fda.hhs.gov or 301-796-8118

Records processed under FOIA Request #2014-8015; Released by CDRH on 12-8-2015

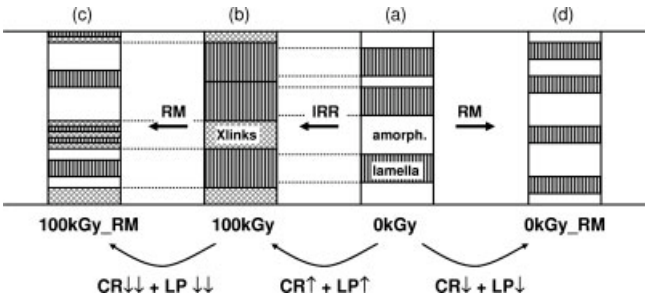

Figure 10. Proposed model of supermolecular structure changes in: (a) virgin UHMWPE, (b) UHMWPE after irradiation, (c) UHMWPE after irradiation and remelting, (d) UHMWPE after remelting. CR, LP, IRR, and RM stand for crystallinity, long period, irradiation and remelting, respectively.

attributed to preferential scission of highly constrained entanglements,[21] tie molecules,[15,17] and the loops on the surface of crystallites.[17,26] These chain scissions are followed by crystallization of freed molecular fragments as shown schematically in Figure 11.

The small increase in LP after irradiation [Figure 10(a,b)] is more difficult to explain. LP represents average distance between amorphous and crystalline regions and, consequently, it can increase only if some lamellae disappear or merge. Disappearance of lamellae is practically impossible unless the polymer is heated. The smallest lamellae start to melt when the temperature rises above 60–90°C.[44] Our e-beam irradiation increases the temperature inside the sample by ~7°C per 10 kGy. Thus, the approximate temperature in the 100 kGy sample should be 95°C. The temperature in the 50 kGy sample (60°C) is just at the lower limit of lamellar melting. Therefore, in the samples irradiated at more than 50 kGy, a fraction of the smallest lamellae can melt, increasing the final LP value. In the samples irradiated with doses lower than 50 kGy, the only possible way to increase LP is the merging of existing lamellae. However, full merging of the lamellae is highly improbable due to tie molecules, whose parts are anchored in different lamellae. It is possible that some small lamellae do not merge fully, but the amorphous region between them may become so thin that it is not visible with X-rays. Moreover, this partial merging of the lamellae might be easier due to preferential chain scissions of the tie molecules.[15,17] To conclude, limited partial merging of the lamellae takes place at all radiation doses, whereas melting of the smallest lamellae may be due to increased temperature at higher radiation doses. Both effects lead to an increase in LP.

The drop in both CR and LP after remelting [Figure 10(a,d)] is caused by the change in the thermal history of the sample. It has been shown that different thermal treatments result in different supermolecular structures.[15,16,19,23,29] Virgin bulk UHMWPE is consolidated from resin at elevated pressures and temperatures, which is usually followed by annealing to remove residual stresses.[19] In contrast, our remelting procedure comprised fast heating, only 10 min remelting and fast cooling. Fast cooling results in thinner lamellae, whereas annealing and slow cooling leads to thicker lamellae.[19] Therefore, after our remelting procedure both CR and LP are lowered.

Further decrease in CR and LP after both irradiation and remelting [compare Figure 10(c) with Figure 10(d)] results from two facts: (i) our remelting procedure leads to lower CR and LP as explained in the previous paragraph and (ii) the crystallization in the irradiated samples is further constrained due to crosslinks in the polymer. The crosslinks are formed preferentially in the amorphous region [Figure 10(b), Refs. 15, 17, 21, and 26] and so the lamellae in the crosslinked phase are especially thin. The lamellae grown at sites that were occupied by a crystalline phase before remelting are also thinner in comparison with nonremelted samples. This is caused both by faster cooling in our remelting procedure, and a limited amount of crosslinks formed in the crystalline phase.

Although the model in Figure 10 is based mostly on SWAXS results, it should be emphasized that all the other techniques confirm its correctness and, consequently, reproducibility and reliability of our irradiation and remelting procedures. Image analysis of SEM micrographs showed that remelting resulted in significantly smaller lamellae (Figures 2 and 3). DSC curves confirmed the increase in CR and formation of thicker lamellae after irradiation as well as the decrease in CR and formation of thinner lamellae after irradiation and remelting (Table I, Figure 4). Solubility experiments indicated the presence of crosslinks in irradiated samples (Table II). FTIR and ESR measurements, together with analysis of light micrographs, confirmed oxidation in irradiated samples (Figures 5, 7, and 8), which is usually associated with additional crystallization.[27,31]

Oxidative Degradation and Macroradicals

Medical grade UHMWPE must be a pure polyethylene because of biocompatibility; it must not contain any stabilizers and, as a result, it is more prone to oxidative degradation than the common, stabilized polymers. As already

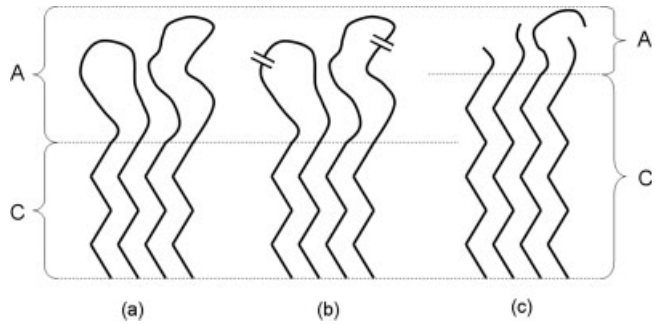

Figure 11. Additional crystallization: (a) edge of a lamella with loops, (b) chain scissions due to irradiation, (c) additional crystallization due to increased mobility of UHMWPE chains. Capital letters C and A denote crystalline and amorphous regions, respectively.

Questions? Contact FDA/CDRH/OCE/DID at CDRH-FOISTATUS@fda.hhs.gov or 301-796-8118

Records processed under FOIA Request #2014-8015; Released by CDRH on 12-8-2015

mentioned in the introduction and section on ESR results, oxidation may take place during irradiation (immediate oxidative degradation), shelf life, and *in vivo* (long-term oxidative degradation). In this study, immediate oxidative degradation was minimized by using a very high dose rate, although the irradiation was performed in air. Long-term oxidative degradation was limited by storing the samples in the dark, at 5°C and in nitrogen atmosphere. Moreover, we investigated elimination of macroradicals, which are the cause of long-term oxidative degradation.

In spite of all efforts, the FTIR and ESR methods revealed that our methods of irradiation, storage, and remelting did not prevent oxidation completely. IR spectra measured immediately after e-beam irradiation showed an increase in oxidation index (Figure 5) and ESR spectra indicated the presence of some peroxy radicals (Figure 8). ESR spectra measured after several weeks of shelf-life (samples in a box, in a refrigerator at 5 °C, in polyethylene bags filled with nitrogen) exhibited even more peroxy radicals (compare Figures 8 and 9 with Refs. 10, 34, 35, and 36). IR spectra of samples after our remelting procedure (10 min at 200°C) showed further increases in oxidation index (Figure 5), which indicates that the remelting procedure is far from ideal. All these facts confirm extreme sensitivity of UHMWPE to oxidation.

In the next step, we investigated the rate of UHMWPE oxidative degradation by means of thermogravimetric analysis (Figure 6). It was demonstrated that the temperature of the thermal treatment played a crucial part in oxidation. During annealing (thermal treatment below T_m(UHMWPE) = 140°C) the oxidation rate is slow but not all radicals are removed.[33] During remelting (treatment above 140°C) it is possible to destroy all radicals (Figure 8), but the oxidative degradation proceeds much faster (Figure 6). TGA experiments prove that longer remelting times in combination with temperatures slightly above 140°C lead to lower oxidation damage than shorter remelting time at higher temperatures. This knowledge was employed in the second ESR experiment (Figure 9), which revealed that a surprisingly short time (2 min) is sufficient to scavenge all radicals. However, our sample was rather thin (1 mm) in comparison with commercially produced crosslinked UHMWPEs (irradiated bars with diameter > 50 mm). On the other hand, the producers of crosslinked polyethylene use several-hour-long remelting[8] to remove all radicals and remove residual stresses in the material.[19,41] This may impact on supermolecular structure and, consequently, slightly improve mechanical properties of UHMWPE such as modulus and yield stress.[1,19]

Differences Among Various Studies of UHMWPE Structure

Our proposed model of supermolecular structure changes (Figure 10) is in agreement with all experimental results. However, some problems with reproducibility of the results were experienced. Moreover, some other studies dealing with changes of UHMWPE supermolecular structure lead to different conclusions. Below we summarize possible sources of discrepancies and errors.

As to the reproducibility, the biggest problems were with SWAXS and DSC data. SWAXS measurements are very sensitive to preferred orientation of polymer chains. Preferred orientation may be introduced into the structure during UHMWPE consolidation.[45] DSC measurements are sensitive to residual stresses, which can be caused by cutting the thin specimens from the bulk.[46] Moreover, cutting the thin specimens results in preferred orientation on the surface. SWAXS experiments should always be performed in transmission mode to minimize the surface effects. Reproducibility of DSC results improves if the measurements are performed with three-dimensional samples cut from inside of the material, rather than from thin sections close to the surface. In this study, some measurements were performed several times, using different locations and/or orientations on the same specimen. The following variability in the measured data was observed: up to 5% in CR(WAXS), up to 30 Å in LP(SAXS), up to 4°C in T_m(DSC) and up to 5% in CR(DSC).

As to the different results obtained in various studies, there are several possible explanations. Structural changes of UHMWPE after irradiation are strongly influenced not only by total dose, but also by dose rate, which is rarely taken into consideration.[15,22] Structural changes of UHMWPE after thermal treatment are significantly affected not only by temperature, but also by the rate of cooling.[19] Two other important factors are variation of radiation dose with depth[11] and aging associated with oxidative degradation.[11,33] Nevertheless, in this study the variation of radiation dose with depth was reduced by using 1 mm-thin specimens and the effect of long-term oxidative degradation was limited by characterizing the specimens in a few days after irradiation and thermal treatment. The importance of an inert atmosphere during both irradiation and thermal treatment has already been widely accepted and in this study it was reconfirmed. We believe that most of the different results found in the literature are due to the extreme sensitivity of UHMWPE to oxidative degradation, which is linked with the majority of the effects listed above.

CONCLUSION

Several facts concerning UHMWPE irradiation and remelting have been shown and/or confirmed.

1. It has been shown that crosslinking predominates over chain scission in medical grade UHMWPE if the e-beam irradiation dose rates are high. This holds even if the irradiation is performed in air, although some oxidation products were detected in this case.
2. A model of UHMWPE supermolecular structure changes after irradiation and remelting was proposed. Despite its simplicity the model describes all the

Questions? Contact FDA/CDRH/OCE/DID at CDRH-FOISTATUS@fda.hhs.gov or 301-796-8118

Records processed under FOIA Request #2014-8015; Released by CDRH on 12-8-2015

observed effects in a consistent way. The reliability of the model has been verified by a number of microscopic, diffraction, thermal, and other methods.

3. The importance of inert atmosphere during both irradiation and remelting was re-confirmed. This study has shown that the temperatures higher than 160°C result in severe oxidation in a low oxygen atmosphere, whereas longer remelting times are acceptable if the temperature is just slightly above the T_m.
4. In addition, a new program MDFT, which calculates long periods, LP(SEM), directly from SEM micrographs of etched UHMWPE, was introduced. It was demonstrated that the values of LP(SEM) agree qualitatively with the corresponing values of long periods, LP(SAXS), obtained in a standard way from SAXS measurements.

REFERENCES

1. Lewis G. Properties of crosslinked ultra-high-molecular-weight polyethylene. Biomaterials 2001;22:371–401.
2. Kurtz SM, editor. Alternatives to conventional UHMWPE for hip arthroplasty. The UHMWPE Handbook. Amsterdam: Elsevier; 2004. chapter 6, p 93.
3. Kurtz SM, editor. The clinical performance of UHMWPE in knee replacements. The UHMWPE Handbook. Amsterdam: Elsevier; 2004. chapter 8, p 182.
4. Howling GI, Barnett PI, Tipper JL, Stone MH, Fisher J, Ingham E. Quantitative characterization of polyethylene debris isolated from periprosthetic tissue in early failure knee implants and early and late failure Charnley hip implants. J Biomed Mater Res 2001;58:415–420.
5. Scott M, Widding K, Jani S. Do current wear particle isolation procedures underestimate the number of particles generated by prosthetic bearing components? Wear 2001;250(Part 2):1213–1217.
6. Tipper JL, Firkins PJ, Besong AA, Barbour PSM, Nevelos J, Stone MH, Ingham E, Fisher J. Characterisation of wear debris from UHMWPE on zirconia ceramic, metal-on-metal and alumina ceramic-on-ceramic hip prostheses generated in a physiological anatomical hip joint simulator. Wear 2001; 250(Part 1):120–128.
7. Wright TM, Goodman SB, editors. Implant Wear in Total Joint Replacement. Rosemont: American Academy of Orthopaedic Surgeons; 2001.
8. Kurtz SM, editor. Compendium of highly crosslinked and thermally treated UHMWPEs. The UHMWPE handbook. Amsterdam: Elsevier; 2004. chapter 15, pp 337–361.
9. Costa L, Bracco P. Mechanism of crosslinking and oxidative degradation of UHMWPE. In: Kurtz SM, editor. The UHMWPE Handbook. Amsterdam: Elsevier; 2004. chapter 11, pp 245–261.
10. Durant J, Jahan MS. EPR power saturation techniques and spectral differentiation are used to isolate and simulate radical species in UHMWPE. Nucl Instrum Methods Phys Res Sect B 2005;236:160–165.
11. Premnath V, Bellare A, Merrill EW, Jasty M, Harris WH. Molecular rearrangements in ultra high molecular weight polyethylene after irradiation and long-term storage in air. Polymer 1999;40:2215–2229.
12. McKellop H, Shen FW, Lu B, Campbell P, Salovey R. Development of an extremely wear-resistant ultra high molecular weight polyethylene for total hip replacements. J Orthop Res 1999;17:157–167.
13. Edidin AA, Kurtz SM. Influence of mechanical behavior on the wear of 4 clinically relevant polymeric biomaterials in a hip simulator. J Arthroplasty 2000;15:321–331.
14. Costa L, Luda MP, Trossarelli L, del Prever EMB, Crova M, Gallinaro P. Biomaterials 1998;19:659–668.
15. Nevoralova M, Baldrian J, Pospisil J, Chodak I, Horak Z. Structure modification of UHMWPE used for total joint replacements. J Biomed Mater Res B Appl Biomater 2005;74: 800–807.
16. Andjelic S, Richard RE. Crystallization behavior of ultrahigh molecular weight polyethylene as a function of in vacuo gamma-irradiation. Macromolecules 2001;34:896–906.
17. Zhao Y, Luo YX, Jiang BZ. Effect of irradiation on crystallinity and mechanical-properties of ultrahigh molecular-weight polyethylene. J Appl Polym Sci 1993;50:1797–1801.
18. Lee SM, Choi SW, Nho YC, Song HH. Modification of microstructures and physical properties of ultra high molecular weight polyethylene by electron beam irradiation. J Polym Sci Part B: Polym Phys 2005;43:3019–3029.
19. Turell MB, Bellare A. A study of the nanostructure and tensile properties of ultra-high molecular weight polyethylene. Biomaterials 2004;25:3389–3398.
20. Deng M, Shalaby SW. Effects of gamma-irradiation, gas environments, and postirradiation aging on ultrahigh molecular-weight polyethylene. J Appl Polym Sci 1995;58:2111–2119.
21. Kamel I, Finegold L. A model for radiation-induced changes in ultrahigh-molecular weight polyethylene. J Polym Sci Part B: Polym Phys 1985;23:2407–2409.
22. Stephen CP, Benson RS, Martinez-Pardo ME, Barker ED, Walker JB, Stephens TP. The effect of dose rate on the crystalline lamellar thickness distribution in gamma-radiation of UHMWPE. Nucl Instrum Methods Phys Res Sect B 2005; 236:540–545.
23. Nevoralova M, Mikesova J, Baldrian J, Horak Z. The modification of ultra-high-molecular-weight polyethylene supramolecular structures induced by irradiation and thermal treatment. Polym Adv Technol 2003;14:802–806.
24. Ohta M, Hyon SH, Tsutumi S. Control of crystalline orientation to enhance the wear resistance of ultra-high molecular weight polyethylene crystallization cups for artificial joints. Wear 2003;255:1045–1050.
25. Goldman M, Gronsky R, Long GG, Pruitt L. The effects of hydrogen peroxide and sterilization on the structure of ultra high molecular weight polyethylene. Polym Degrad Stab 1998;62:97–104.
26. Goldman M, Gronsky R, Pruitt L. The influence of sterilization technique and ageing on the structure and morphology of medical-grade ultrahigh molecular weight polyethylene. J Mater Sci Mater Med 1998;9:207–212.
27. Goldman M, Gronsky R, Ranganathan R, Pruitt L. The effects of gamma radiation sterilization and ageing on the structure and morphology of medical grade ultra high molecular weight polyethylene. Polymer 1996;37:2909–2913.
28. Bellare A, Schnablegger H, Cohen Re. A small-angle X-ray-scattering study of high-density polyethylene and ultrahigh molecular-weight polyethylene. Macromolecules 1995;28: 7585–7588.
29. Medel JF, Garcia-Alvarez F, Gomez-Barrena E, Pertolas JA. Microstructure changes of extruded ultra high molecular weight polyethylene after gamma irradiation and shelf-aging. Polym Degrad Stab 2005;88:435–443.
30. Medel F, Gomez-Barrena E, Garcia-Alvarez F, Rios R, Gracia-Villa L, Puertolas JA. Fractography evolution in accelerated aging of UHMWPE after gamma irradiation in air. Biomaterials 2004;25:9–21.
31. Lee K-Y, Lee KH. Wear of shelf-aged UHMWPE acetabular liners. Wear 1999;229:728–733.

Questions? Contact FDA/CDRH/OCE/DID at CDRH-FOISTATUS@fda.hhs.gov or 301-796-8118

Records processed under FOIA Request #2014-8015; Released by CDRH on 12-8-2015

32. Uehara H, Nakae M, Kanamoto T, Ohtsu O, Sano A, Matsuura K. Structural characterization of ultrahigh-molecular-weight polyethylene reactor powders based on fuming nitric acid etching. Polymer 1998;39:6127–6135.
33. Kim S, Kang PH, Nho YC, Yang OB. Effect of electron beam irradiation on physical properties of ultrahigh molecular weight polyethylene. J Appl Polym Sci 2005;97:103–116.
34. Ikada Y, Nakamura K, Ogata S, Makino K, Tajima K, Endoh N, Hayashi T, Fujita S, Fujisawa A, Masuda S, Oonishi H. Characterization of ultrahigh molecular weight polyethylene irradiated with gamma-rays and electron beams to high doses. J Polym Sci Part A: Polym Chem 1999;37:159–168.
35. Nakamura K, Ogata S, Ikada Y. Assessment of heat and storage conditions on gamma-ray and electron beam irradiated UHMWPE by electron spin resonance. Biomaterials 1998;19:2341–2346.
36. O'Neill P, Birkinshaw C, Leahy JJ, Barklie R. The role of long lived free radicals in the ageing of irradiated ultra high molecular weight polyethylene. Polym Degrad Stab 1999;63: 31–39.
37. Dorschner H, Lappan U, Lunkwitz K. Electron beam facility in polymer research: radiation induced functionalisation of polytetrafluorethylenen. Nucl Instrum Methods Phys Res Sect B 1998;139:495–501.
38. Olley RH, Bassett DC. An improved permanganic etchant for polyolefines. Polymer 1982;23:1707–1710.
39. Slouf M, Synková H, Baldrian J. MDFT program: Calculation of 2D and 1D diffraction patterns from electron micrographs. Mater Struct 2005;12:85–89.
40. Kurtz SM, Muratoglu OK, Gsell R, Greer K, Shen FW, Cooper C, Buchanan FJ, Spiegelberg S, Yau SS, Edidin AA. Interlaboratory validation of oxidation-index measurement methods for UHMWPE after long-term shelf aging. J Biomed Mater Res 2002;63:15–23.
41. Mark A. UHMWPE processing: Techniques and problems. In Proceedings of UHMWPE for Arthroplasty: Past, Present and Future, Torino 2003, Italy, pp 30.
42. Tretinnikov ON, Fujita SI, Ogata S, Ikada Y. Surface studies of ultra-high molecular weight polyethylene irradiated with high-energy pulsed electron beams in air. J Polym Sci Part B: Polym Phys 1999;37:1503–1512.
43. Bolland JL. Kinetics of olefin oxidation. Q Rev Chem Soc 1949;3:1–21.
44. Kurtz SM, editor. A primer on UHMWPE. The UHMWPE Handbook. Amsterdam: Elsevier; 2004. chapter 1, p 6.
45. Bellare A, Cohen RE. Morphology of rod stock and compression moulded sheets of ultra-high molecular-weight polyethylene used in orthopaedic implants. Biomaterials 1996;17:2325–2333.
46. Costa L, Jacobson K, Brunella V, Bracco P. Effects of microtomy on the material properties of ultra high molecular weight polyethylene. Polym Test 2001;20:649–659.

Questions? Contact FDA/CDRH/OCE/DID at CDRH-FOISTATUS@fda.hhs.gov or 301-796-8118

Records processed under FOIA Request #2014-8015; Released by CDRH on 12-8-2015

Chapter 27

Characterization of UHMWPE Wear Particles

Joanne L. Tipper, PhD, Laura Richards, PhD, Eileen Ingham, PhD and John Fisher, PhD

27.1 Introduction
27.2 Rationale for Wear Particle Isolation
27.3 Delipidization of Samples
27.4 Alkali Digestion of Periprosthetic Tissues and Simulator Lubricants
27.5 Acid Digestion of Periprosthetic Tissues and Simulator Lubricants
27.6 Enzyme Digestion of Periprosthetic Tissues and Simulator Lubricants
27.7 Centrifugation of Samples
27.8 Filtering to Recover Particles
27.9 Polarized Light Microscopy of Tissue Samples
27.10 Scanning Electron Microscopy Analysis
27.11 Image Analysis of UHMWPE Wear Particles
27.12 Automated Particle Analysis
27.13 Standards
27.14 Particle Measurements (size/shape Descriptors)
27.15 Predicting Functional Biological Activity
27.15.1 Materials
27.15.2 Methods
27.15.3 Results
27.16 Conclusion
References

27.1 INTRODUCTION

Although most total joint prostheses remain stable for many years, a significant proportion of patients experience loosening, with about 10% requiring revision 10 years after primary arthroplasty [1–3]. It is generally accepted that osteolysis is initiated by the biological response to wear particles, which are released from ultrahigh molecular weight polyethylene (UHMWPE) acetabular liners and tibial trays [4–6]. Wear particles up to 10 μm in size are predicted to be phagocytosed by resident macrophages and cause the release of inflammatory cytokines and chemokines, including tumour necrosis factor alpha (TNF-α), interleukin-1beta (IL-1β), IL-6, and IL-8 [7–10]. These cytokines stimulate the release of other mediators and the ensuing inflammatory cascade results in the formation of a periprosthetic granulomatous tissue reaction [3, 5]. Histopathological studies have revealed that these inflammatory cytokines facilitate osteoclastogenesis, which results in resorption of bone and a painfully loose implant. Revision surgery is the only option for patient and surgeon [11].

Insights into failure modes of total joint prostheses have been gained by analyzing the particulate wear debris present in periprosthetic tissues from around failed joint replacements [12–19]. In addition, the response of various cell types, including macrophages [7–9, 20–22], fibroblasts [23, 24], and osteoblasts [25, 26], has been investigated *in vitro*. Animal models of particle-induced osteolysis have been developed [27, 28] and the molecular mechanisms of osteolysis have been explored [29].

27.2 RATIONALE FOR WEAR PARTICLE ISOLATION

Particle size, volume, morphology, and composition have been shown to be critical determinants of the biological response to wear particles [7, 8, 20, 21]. In recent years orthopedic manufacturers have focused on improving the wear properties of UHMWPE and improving the design of joint prostheses, which has resulted in an increase in the number of new devices coming to the market. Preclinical testing of new devices and materials has become more stringent recently, and it is recognized that quantification of the wear particles and the ability to predict osteolytic potential of the wear debris released is a valuable marketing

Copyright © 2009, Academic Press. Inc. All rights of reproduction in any form reserved.

Questions? Contact FDA/CDRH/OCE/DID at CDRH-FOISTATUS@fda.hhs.gov or 301-796-8118

Records processed under FOIA Request #2014-8015; Released by CDRH on 12-8-2015

tool. It is therefore important that investigations into the *in vivo* and *in vitro* cellular response to particles should be underpinned by accurate and comprehensive particle characterization techniques.

It is essential that proteins are removed from tissues and simulator lubricants so that only purified particles are recovered for analysis. Any lipids and proteins that are not removed may mask the true particle sizes and morphologies. Many of the particle isolation techniques reported to date utilize strong acids [30, 31], alkalis [13, 17, 32, 33], or enzymes [19] to digest tissues or protein-containing lubricants from *in vitro* joint simulators, followed by filtration to isolate the particles from the digested suspension. Individual particle information is then gained from scanning electron microscopy analysis, which can be time consuming and expensive. More recently, techniques using automated particle sizers, for example, the Malvern Mastersizer and Zetasizer [34, 35] and the Nanosight particle sizer [36], or automated analysis of scanning electron micrographs [37] have been reported, which attempt to speed up the process of particle characterization while removing observer bias. Details of the different procedures for the isolation and characterization of UHMWPE particles from periprosthetic tissues and joint simulator lubricants are outlined in the following discussion.

27.3 DELIPIDIZATION OF SAMPLES

Delipidization of tissues and simulator lubricants is necessary to achieve recovery of purified particles. Contaminating lipids from tissues or those produced by the breakdown of bacteria in serum lubricants of simulator samples, if not removed, will form a layer over the particles during the subsequent filtration steps. Complete removal of lipids is therefore important. This is generally achieved by incubation with chloroform:methanol (2:1) at room temperature for 12–72 h, either before [12, 37] or after [13, 17] digestion with strong alkali, concentrated acids, or enzymes. Tissues delipidized before digestion can be removed from the solvents directly into the chosen digestion solution. Tipper et al. [13] found more complete lipid removal was possible when repeated extraction with chloroform:methanol was performed after the tissues had been digested. However, because the combination of strong alkali with these solvents evokes an exothermic reaction, care should be taken to ensure that tissue digests are cooled to 4°C prior to combining with chloroform:methanol. Chlorofom: methanol extraction results in contaminating lipids and proteins partitioning at the interface between the digested tissue solution (upper layer) and the solvent layer (lower layer). When extraction is combined with centrifugation at 2000 g, the upper layer containing UHMWPE particles can be removed to a clean tube, leaving the unwanted cellular debris behind at the interface. The process is usually repeated until the upper layer containing the UHMWPE particles has visibly cleared of lipids.

27.4 ALKALI DIGESTION OF PERIPROSTHETIC TISSUES AND SIMULATOR LUBRICANTS

Several methods for the digestion of tissues and simulator lubricants have been described, which usually involve incubation with either potassium or sodium hydroxide at concentrations between 4 M and 12M, at temperatures above 55°C, for 1 to 7 days. Shanbhag et al. [18] digested periprosthetic tissues with 4 M potassium hydroxide (KOH) at 56°C for 48 h, while Campbell et al. [12] digested periprosthetic tissues using 5 M sodium hydroxide (NaOH) for 1–5 h at 65°C in a shaking water bath. Many of the subsequently published protocols are based upon the latter method. Tipper et al. [13] found that the higher concentration of 12M KOH was more effective for the complete digestion of formalin-fixed retrieval tissues at 60°C over 5 to 7 days. More recently, Baxter et al. [38] compared digestion of porcine and human capsular tissue with sodium hydroxide and potassium hydroxide at concentrations of 5 M, 10M, and 15M over 24 h at 65°C. These authors found that 5 M KOH followed by 5 M NaOH produced the best results in terms of most complete tissue digestion.

27.5 ACID DIGESTION OF PERIPROSTHETIC TISSUES AND SIMULATOR LUBRICANTS

Margevicius et al. [30] found that digestion of periprosthetic tissue samples with concentrated nitric acid at room temperature over 48 h was more effective than digestion with hydrochloric acid for the isolation of UHMWPE, cobalt chromium, and titanium alloy wear particles. In contrast, Niedzwiecki et al. [39] found that using concentrated hydrochloric acid (37% by volume) to digest simulator serum at a 5:1 volume ratio at 60°C for 45 minutes removed serum proteins effectively and produced UHMWPE particles that were comparable in size and shape to those produced by digestion with 5 M NaOH. Slouf et al. [37] also reported on a method that used 65% nitric acid to digest periprosthetic tissues at room temperature over 24 h. This technique incorporated repeated washing of the upper layer of the digest with nitric acid, neutralization with 12M KOH, and washing with water until the sample was purified.

While strong alkalis and acids do not appear to have an adverse affect on the size and shape of UHMWPE wear particles [39], it is not recommended that these reagents are used when isolating metal wear particles, particularly

Questions? Contact FDA/CDRH/OCE/DID at CDRH-FOISTATUS@fda.hhs.gov or 301-796-8118

Records processed under FOIA Request #2014-8015; Released by CDRH on 12-8-2015

cobalt chrome alloy particles, because it has been shown that these reagents have an affect on the size and composition of cobalt chromium particles [40]. Gentler enzymatic methods of digestion are recommended for isolation of metal wear particles from periprosthetic tissues and simulator lubricants [41, 42].

27.6 ENZYME DIGESTION OF PERIPROSTHETIC TISSUES AND SIMULATOR LUBRICANTS

Campbell et al. [32] evaluated the ability of various enzymes, including crude and pure papain, collagenase, and protease, to digest fresh and formalin fixed capsular tissues compared to sodium hydroxide. This study revealed that crude papain introduced particulates that masked UHMWPE particles during scanning electron microscopy analysis and that the protease and collagenase enzymes were ineffective against fixed tissues. Pure papain was able to digest fresh tissues effectively but was sensitive to changes in pH brought about by the formalin preservative in the fixed tissues. This could be overcome by extensive washing of the fixed tissues prior to digestion. There may also be issues of cost associated with pure papain. In contrast, concentrations of sodium hydroxide above 5 M were effective in digesting both fresh and fixed tissue samples. Maloney et al. [19] utilized papain to digest periprosthetic tissues at 65°C over 24 h to recover UHMWPE, titanium, and cobalt chrome alloy particles. If the tissue was not completely digested, then a further aliquot of papain was added, and it was subjected to an additional 24 h digestion time. Other enzymes used to digest periprosthetic tissues include pronase used for 72 h at 37°C followed by collagenase at 37°C for 72 h [37]. However, both enzymes were subject to self-digestion and had to be replenished regularly over the digestion period. In addition, Proteinase K has been used to digest hip simulator lubricants at 37°C for 45 minutes with stirring at 350 rpm [39].

27.7 CENTRIFUGATION OF SAMPLES

Whether alkali or acid digestion is used, various centrifuge steps or separation by density gradient centrifugation are the preferred methods used to remove biological contaminants and limit the agglomeration of particles. UHMWPE has a density of around 0.94 g/cc and will easily separate from heavier elements, such as metal and ceramic, when centrifuged in the correct medium; however, removing all biological material is often very challenging. In addition, some authors have suggested that centrifugation or ultracentrifugation causes particle loss and deformation [43]. It has been recognized that loss of UHMWPE particles occurs at each stage of the digestion and centrifugation protocol, and Visentin et al. [43] remarked that the average particle retrieval rate using the method of Campbell et al. [12] was just 40%.

Campbell et al. [12] employed sucrose density gradient centrifugation at 40,000 rpm over 3 h to separate UHMWPE particles from contaminating cellular debris and metal wear particles. Using this method the UHMWPE particles remain at the top of the gradient, the cellular debris will collect toward the middle, and any metal or ceramic particles that may be present in the tissue sample will sediment to the bottom of the gradient. Thus the particles of interest are spatially removed from contaminating proteins and may be harvested, washed, and purified using isopropanol density gradients before undergoing further analysis. However, this method relies on collecting particles banded diffusely at interfaces or particular locations in the centrifuge tube used for the gradient, making it difficult to ensure that all isolated particles have been collected. This may account for the poor particle retrieval rate of this method [43].

Other methods utilize ethanol precipitation combined with high-speed centrifugation (up to 20,000 g) for 2 h to remove contaminating proteins before filtration of the whole tissue or simulator lubricant digest [13, 17, 44]; particle recovery rate of this method has been determined to be in the region of 70–75% [45].

27.8 FILTERING TO RECOVER PARTICLES

Initially filter membranes with a pore size of 0.1–0.2 μm were utilized to collect all the particles isolated [12]. However, the diverse size range of UHMWPE particles generated both *in vivo* and *in vitro* quickly became apparent, and samples have been sequentially filtered through filter membranes with progressively smaller pore sizes, such as 10 μm, 1 μm, and 0.1 μm [13].

More recently, as UHMWPE particles in the nanoscale have been identified [15, 17, 46, 47] additional filters with pore sizes in the range of 0.01–0.015 μm are now being utilized.

27.9 POLARIZED LIGHT MICROSCOPY OF TISSUE SAMPLES

Initial attempts to characterize UHMWPE wear particles released into the periprosthetic tissues around failing implants used histological staining and polarized light microscopy to identify UHMWPE [48, 49]. When observed using polarized light, particles of UHMWPE have a characteristic birefringent "glow" [49, 50]. However, it was soon recognized that submicron-sized individual particles could not be observed due to the limited resolution of the light microscope (approximately 0.5–1 μm). Intracellular particles were described in association with macrophages and giant cells, and particles were identified in the range of "less than one micrometre" to 100 μm. Most of the intracellular particles were <10 μm in length. Particle shape and morphology were described as shard or needle-shaped,

Questions? Contact FDA/CDRH/OCE/DID at CDRH-FOISTATUS@fda.hhs.gov or 301-796-8118

Records processed under FOIA Request #2014-8015; Released by CDRH on 12-8-2015

granular, and flakelike [19, 49]. This technique could be used to semiquantitatively grade the amount of wear debris present within the tissue sections but did not attempt to estimate actual numbers or volumes of particles. Schmalzried et al. [6] investigated the use of oil red O staining to identify UHMWPE quantitatively within tissue sections; however, two "no particle" control specimens stained positive for UHMWPE. Neither of these techniques distinguishes agglomerates of particles, and therefore the size ranges of particles identified by polarized light microscopy are likely to be overestimated.

27.10 SCANNING ELECTRON MICROSCOPY ANALYSIS

Scanning electron microscopy (SEM) has been used extensively to analyze particles isolated from periprosthetic tissue samples or simulator lubricants that have been digested and isolated onto filter membranes. The resolution of a standard SEM is approximately 0.1 μm. Campbell et al. [12] used magnification ranges up to 10,000× to observe particles from tissues down to 0.07 μm in size. Using this higher resolution analysis, more detailed particle shape descriptors were reported, and particle size was measured more accurately using digital image analysis systems. Campbell reported on two distinct morphologies of particles: rounded and elongated particles; the elongated particles were further separated into fibrils (short and thin, <3 μm long and <0.25 μm thick) and shreds (up to 12 μm long and up to 1 μm thick). Also around this time the first particle size distributions were published, which revealed that the majority of the particles (>90%) were less than one micrometer in size [19]. However, particle frequency distributions were similar for all patients regardless of implant type, with the mode of the distribution typically falling in the submicron size range [22, 30, 51].

Tipper et al. [13] digested 18 samples of periprosthetic tissue that had been isolated from failed Charnley hip prostheses. These authors reported particles ranging from 0.1 μm to 1000 μm in size, using magnification ranges up to 25,000×. In addition to particle frequency distributions, which showed the mode of the distribution to be in the 0.1–0.5 μm size range, these authors reported mass distributions for all patients. Using the mass distributions, the wear particles from different patients were successfully differentiated, with each patient demonstrating an individual distribution of particles. This study was the first to recognize the importance of the particles above 10 μm in size. Up until this time many studies had concentrated on the smaller submicron-sized particles because they had been shown to be the most biologically active in terms of causing the release of osteolytic cytokines from macrophages [21]. Indeed, several studies showed that particles >10 μm in size exhibited minimal biological activity. However, the study by Tipper et al. [13] recognized that a relatively small number of larger particles could account for a large proportion of the total wear volume, and consequently the total wear volume of particles would have lower biological activity.

More recently, mass distributions have been replaced by volume [35] or area distributions [15, 17]; the latter approach takes the two-dimensional area of the wear particles and converts it to volume assuming a constant particle thickness [45].

Scott et al. [31, 47] analyzed hip simulator debris from conventional, 50 kGy, and 100 kGy crosslinked UHMWPE at magnifications of 10,000× and 20,000×. Particles with equivalent circle diameters (ECD) of 0.19, 0.11, and 0.08 were observed for the conventional, 50 kGy, and 100 kGy UHMWPE samples, respectively. Scott et al. [31, 47] was one of the first authors to report on the isolation of particles in the nanometer size range from *in vitro* hip simulator lubricants.

Galvin et al. [46] and Tipper et al. [15] used high-resolution field emission gun-scanning electron microscopy (FEG-SEM) to analyze particles of UHMWPE from hip and knee simulator lubricants. FEG-SEM can achieve magnifications over 200,000×. With these advances in technology, these authors identified particles as small as 10 nm in size, with the mode of particles isolated from the hip simulator lubricant lying in the nanometer size range (<0.1 μm). More recently, Richards et al. [17] used alkaline digestion, filtration, and FEG-SEM analysis to isolate and analyze UHMWPE from periprosthetic tissues from around failed Charnley hip prostheses. Using this high-powered technique, *in vivo* generated UHMWPE particles in the nanometer size range were observed for the first time in all tissue samples examined. Other authors have also recently reported the presence of nanometer-sized UHMWPE particles in some periprosthetic tissue samples [52].

27.11 IMAGE ANALYSIS OF UHMWPE WEAR PARTICLES

Digital image analysis software represents a useful tool to assist with particle size analysis. Particles can be sized automatically by the software, with multiple measurements of maximum width, maximum length, area, and perimeter being recorded simultaneously. Alternatively, particles can be sized manually, with each individual particle being traced with a cursor. There are drawbacks associated with both methods. One of the limitations of automatic sizing is that the system can count clumped or agglomerated particles as one large particle. This can be overcome by manual manipulation of the images prior to automatic sizing. However, particle isolation can be subject to contamination, either with biological or environmental contaminants. Biological

Questions? Contact FDA/CDRH/OCE/DID at CDRH-FOISTATUS@fda.hhs.gov or 301-796-8118

Records processed under FOIA Request #2014-8015; Released by CDRH on 12-8-2015

contaminants might be lipids or proteins that originate from the tissue or simulator lubricant sample or salt crystals that originate from the isolation procedure. Common environmental contaminants encountered include silicon dust from the atmosphere. Automatic sizing procedures do not discriminate between particles of UHMWPE and contaminating particles, leaving this technique open to overestimation of the number of particles. However, this method is quickly executed and lends itself to accurately sizing large numbers of particles.

Manual sizing allows each individual particle to be assessed for inclusion into the size distribution, making it simple to identify and exclude contaminants. However, manual sizing is very time consuming and tedious and may be less accurate because it relies on the operator's accuracy to trace large numbers of particles.

However, both methods have the following further limitations associated with SEM observation: observer bias toward a particular particle size (may be overcome with random sampling techniques; see Richards et al. [17]); only a small number of sample micrographs are taken from across the filter membrane representing analysis of a very small area of the filter, which introduces the possibility of misrepresentative sampling; and small numbers of particles analyzed can introduce systematic and observer bias, which can be compounded by sampling errors. Elfick et al. [34] reasoned that image analysis techniques improved upon the sampling statistics of these methods by increasing the numbers of particles analyzed, but the accuracy of the size distribution is dependent upon resolution of discrete particles.

27.12 AUTOMATED PARTICLE ANALYSIS

Given the problems associated with image analysis of wear particles previously described, automated particle size analysis by Coulter counter seemed like an obvious way forward. Maloney et al. [19] and Margevicius et al. [30] analyzed tissue membranes using a Coulter Multisizer, which employed electrical impedance technology. These authors reported the mean diameter of particles to be 0.63 μm and 0.40 μm, respectively. This method meets a number of pitfalls; firstly, particles are assumed to be spheroids. Secondly, the minimum detection range is 0.4 μm to 0.5 μm; and lastly, agglomerated particles would result in particle size overestimation, which would be included in the analysis. Various studies have utilized automated sizing equipment. Elfick et al. [34, 35] used laser diffraction particle analysis (LDPA) to analyze particles from both hip simulator samples [34] and periprosthetic tissue samples [34, 35]. LDPA uses Mie theory to predict the volume distribution of the debris in suspension by the scattering of light from two laser beam sources, where the smallest particles diffract light by a larger angle. The lower detection limit of the Malvern Multisizer 2000 used in this study was 0.02 μm according to the manufacturers; however, the minimum particle size detected in tissue samples was 0.113 μm, almost tenfold larger than the smallest particle detected by FEG-SEM analysis of periprosthetic hip tissues [17]. The authors concluded that particles smaller than 0.113 μm were not produced *in vivo*, but they go on to speculate on the relationship between small particle size and the increased propensity for particle transport away from the implant site.

More recently, automated particle sizers with improved lower detection thresholds have become available commercially, such as the Malvern Zetasizer (detection range 0.006–6 μm) and the Nanosight particle sizer (detection range 0.01–800 μm). These may be useful for sizing particles with a limited size range in the nanoscale, such as metal or ceramic wear particles, but have limited applicability to sizing UHMWPE particles due to the large size range of particles (0.01–1000 μm). However, all automated sizing suffers from the inability to visualize the particles directly and determine the degree of agglomeration accurately.

Slouf et al. [37] reported a novel automated quantitative analysis technique, SEMq, which was based on a light scattering theory. In this method automated image analysis of electron micrographs is used to determine the total amount of wear particles released into the tissues around total joint replacements. This technique was shown to provide rapid, reliable, and reproducible results, which indicated that the distribution of wear particles around TJRs is nonhomogeneous [37]. However, this technique does not calculate absolute numbers of wear particles but rather determines relative numbers of wear particles in one sample compared to another. The technique may also be sensitive to errors introduced by particle clumping and protein contamination of filters used for SEM analysis.

27.13 STANDARDS

It has been recognized that a standardized method of particle retrieval from the tissues and simulator lubricants, followed by debris characterization and quantification, is required for a uniform approach to debris response investigations. However, there are a number of different standards available from the British Standards Institution (BSI), International Organization for Standardization (ISO), and the American Society for Testing and Materials (ASTM), which currently offer conflicting advice for isolation of wear particles from periprosthetic tissues and simulator lubricant samples.

The British standard (BS ISO 17853:2003 Wear of implant materials—Polymer and metal wear particles—Isolation, characterization and quantification) [53], and

Questions? Contact FDA/CDRH/OCE/DID at CDRH-FOISTATUS@fda.hhs.gov or 301-796-8118

Records processed under FOIA Request #2014-8015; Released by CDRH on 12-8-2015

the ISO standard (ISO 17853 Wear of implant materials—Polymer and metal wear particles—Isolation, characterization and quantification) [53] are identical documents. Both current standards, issued in 2003, recommend the use of 5 M sodium hydroxide to digest tissue and simulator lubricants to recover both polymer and metal wear particles. As discussed in Section 27.5, strong acids and alkalis are not suitable reagents for use in the recovery of metal wear particles from tissue or simulator lubricants due to adverse effects on particle size and shape. Enzymatic digestion protocols are recommended for use to recover metal wear particles to avoid these effects. The BSI and ISO standards recommend purification of particles by sucrose density gradient centrifugation followed by filtration through filter membranes with pore sizes of 0.1 μm, followed by observation of particles using SEM analysis at magnifications between 1000× and 5000×. Since the publication of this standard, a number of studies have identified UHMWPE particles in the nanometer size range [15, 17, 46, 47, 52], and filters with pore sizes in the range of 0.01–0.05 μm are commonly employed to isolate particles in this size range. In addition, UHMWPE fibrils up to 1 mm in length are generated both *in vivo* (13) and *in vitro* (15) and magnifications of 1000× would be too high to observe particles of this size. Magnifications between 150× and 100,000× may be more appropriate to capture images of all sizes of particles after sequential filtration through 10, 1, and 0.015 μm filters or similar [17]. The ISO standard is currently being updated to incorporate recent advances in technology, that is, increased magnification range achievable with FEG-SEM and to ensure that particles in the nanometer size range are isolated and observed.

The ASTM standard (F561-05a Standard Practice for Retrieval and Analysis of Medical Devices, and Associated Tissues and Fluids) [54] is also currently being revised to reflect similar changes. The current standard is very detailed, giving four recommended methods of tissue digestion (papain, 4 M KOH and pronase, concentrated nitric acid and 5 M sodium hydroxide) and two recommended methods for digestion of protein containing simulator lubricants (12M sodium hydroxide and concentrated hydrochloric acid). However, there is no indication of which methods are suited to particular types of materials, and the overall effect is one of confusion rather than guidance. Filtration is the recommended method for the recovery of wear particles and sequential filtration, and the need for smaller pore size filters to recover particles in the nanometer size range are discussed. All the standards recommend that chemical analysis by energy dispersive X-ray analysis (EDX) or Fourier transform infrared spectroscopy (FTIR) analysis are performed to eliminate contaminating particles or verify the identification of UHMWPE particles, respectively.

In addition, all the particle isolation standards previously referred to recommend that particle morphology should be characterized using a series of predefined descriptions, such as length, width, equivalent circle diameter, area, perimeter, aspect ratio, form factor, elongation, and roundness, as described in detail in ASTM F1877-05 (Standard Practice for Characterization of Particles) [55]. These parameters are described in more detail in Section 27.14.

27.14 PARTICLE MEASUREMENTS (SIZE/SHAPE DESCRIPTORS)

Many different shape descriptors have been employed over the past 15 years; these include spherical, spheroidal, granular, angulated, globular, floret, flakes, shards, needle-like, fibrillar, and ribbons. Particles of UHMWPE generated *in vitro* and *in vivo* tend to exhibit many different morphologies over a number of size ranges, that is, fibrils isolated from periprosthetic tissues have been described up to 1 mm in length, but also smaller fibrils of around 1 μm were also observed by SEM at higher magnifications [13]. A detailed description of the nomenclature used for particle morphology description can be found in the ASTM Standard Practice for Characterization of Particles (F1877-05) [55].

Simple measurements are shown in Table 27.1.

TABLE 27.1 Simple Measurements

Area of particle: This does not include any holes within the object.	
Perimeter of particle: The outline of the object.	
Maximum diameter (d_{max}): Defined as the length of the longest line joining two points of the object outline and passing through the centroid.	
Minimum diameter (d_{min}): Defined as the length of the shortest line joining two points of the object outline and passing through the centroid.	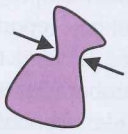
Size (length, L): Defined as the Feret diameter (i.e., caliper length) along major axis of the object.	
Size (width, W): Defined as the Feret diameter (i.e., caliper length) along minor axis of the object.	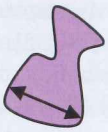

Questions? Contact FDA/CDRH/OCE/DID at CDRH-FOISTATUS@fda.hhs.gov or 301-796-8118

Records processed under FOIA Request #2014-8015; Released by CDRH on 12-8-2015

In addition, more detailed measurements of equivalent circle diameter (ECD), which is defined as the diameter of a circle with an area equivalent to the area of the particle, and has units of length:

$$ECD = (4 \times A/\pi)^{1/2}$$

Aspect ratio (AR) is defined as the ratio of maximum diameter to minimum diameter:

$$AR = d_{max}/d_{min}$$

Elongation (E) is similar to the aspect ratio but is a more suitable measure for long fibril-type particles, where the major axis line does not stay within the boundaries of the particle. It is given as a ratio of particle length to width:

$$E = L/W$$

Roundness (R) is a measure of how closely a particle resembles a circle. A perfect circle has a value of one:

$$R = (4A)/(\pi\, d_{max}{}^2)$$

Form factor (FF) is similar to roundness but is based on the perimeter (p) of the particle outline rather than the major diameter:

$$FF = (4\,\pi A)/p^2$$

These measurements provide a more complex analysis of particle shape and morphology.

27.15 PREDICTING FUNCTIONAL BIOLOGICAL ACTIVITY

Traditionally, prediction of the clinical performance of different materials or devices has been assessed by wear testing using laboratory simulators prior to clinical implantation, which allows measurement of the total wear volume produced in mm^3 and wear rate of a particular type of material/device in mm^3/million cycles of simulation. This enables materials or devices to be ranked using their wear performance. Such measurements are useful when assessing the performance of new materials against existing ones and have led to the introduction of newer materials with improved wear resistance into clinical practice, for example, crosslinked UHMWPEs have been shown to have significantly lower wear rates compared to noncrosslinked UHMWPEs [56, 57]. However, differences in the wear particle characteristics can lead to altered biological responses and a different potential for the development of osteolysis. It has been shown that the biological response to different types of UHMWPE wear debris will vary depending on the kinematic conditions [58], oxidative state [45], and level of crosslinking [59, 60]. Therefore, it is desirable to combine information on both the wear volume of a material with its wear particle characteristics, in terms of size, volume, and biological activity, to give a clearer indication of the osteolytic potential of the material or joint replacement device.

Fisher et al. [61] devised a novel method for predicting the osteolytic potential of UHMWPE wear particles generated in hip or knee simulators from different UHMWPEs or different device designs, using functional biological activity (FBA). This approach integrates the volumetric concentration of wear particles in three different size ranges (<0.1–1.0 μm, 1.0–10 μm, >10 μm), with the biological activity index for wear particles in each of the three size ranges (as determined in previous studies) [7]. The percentage volumetric concentration of wear as a function of particle size, $C(r)$, can be determined by isolating the particles from the bovine serum lubricant from laboratory wear simulations using one of the methods previously described. Using the particle area distributions, and assuming a constant particle thickness, a volume distribution can be determined, giving the volumetric concentration of wear particles in each of the three size ranges: <0.1–1 μm, 1–10 μm, >10 μm.

The biological activity function $B(r)$ for UHMWPE wear debris was determined as a function of particle size, r, at fixed volumetric concentrations. The wear particles were used to stimulate primary human macrophages obtained from six human donors in triplicate [7]. Tumor necrosis factor-alpha (TNF-α) was used as a marker of biological activity because it has previously been shown to correlate with bone resorption [62]. Biological activity, $B(r)$, of the particles in the different size ranges was normalized with respect to particle in the smallest size range, which was assigned a value of unity (Figure 27.1). Normalization was carried out on each donor with the mean from at least three replicates to eliminate donor-to-donor variability. The index of specific biological activity (SBA) of UHMWPE wear debris is defined as the relative biological activity per unit volume. It is calculated by integrating the biological activity function, $B(r)$, and the volumetric concentration function, $C(r)$, over the size range of the wear particles:

$$SBA = \int C(r)B(r)$$

The total size range studied was <0.1–100 μm.

Determining the volumetric concentration of wear particles in each size range for each material or device and then integrating these values with the biological activity function for UHMWPE allows the SBA for each material or device tested to be determined. The SBA can then be integrated with the volumetric wear rate (in mm^3/million cycles) to give a measure of functional biological activity (FBA),

$$FBA = V \times SBA$$

where V has units of $mm^3/10^6$ cycles or mm^3/year. The values of SBA and FBA can be compared for the wear

Questions? Contact FDA/CDRH/OCE/DID at CDRH-FOISTATUS@fda.hhs.gov or 301-796-8118

Records processed under FOIA Request #2014-8015; Released by CDRH on 12-8-2015

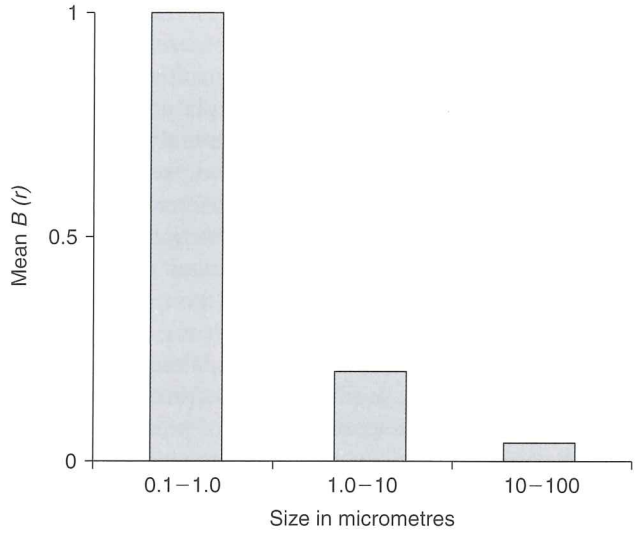

FIGURE 27.1 Biological activity $B(r)$ as a function of particle size derived from *in vitro* cell culture studies.

particles from all materials or devices. To illustrate the use of this predictive methodology, the following example compares the wear, wear debris, and specific and functional biological activity of two different UHMWPEs, GUR 1020 GVF and GUR 1050 (sterilized with 25 and 50 kGy gamma radiation) in the hip and the knee.

27.15.1 Materials

GUR 1020 was irradiated with 25–40 kGy of gamma radiation in a vacuum and then foil packed (GVF), and hence was moderately crosslinked. GUR 1050 was either gamma irradiated in air with 25 kGy of radiation or was moderately crosslinked with 50 kGy of gamma radiation, followed by remelting above 155°C for 24 h to eliminate residual free radicals. The GUR 1020 40 kGy GVF UHMWPE acetabular cups and tibial trays were off-the-shelf clinical products supplied by DePuy International, a Johnson & Johnson company. All other UHMWPE acetabular cups and tibial trays were manufactured specifically for these studies.

In the hip GUR 1020 25–40 kGy (GVF) UHMWPE acetabular cups were compared to GUR 1050 25 kGy UHMWPE acetabular cups in a 10-station ProSim hip simulator against 28 mm diameter cobalt chromium femoral heads, which were highly polished, with R_a values of $<0.02\,\mu m$. Fixed bearing and mobile bearing total knee replacements (TKRs) were investigated in the Leeds knee simulator [63]. Three press fit condylar (PFC) Sigma Rotating Platform (DePuy International, UK) mobile bearing knees (GUR 1020 25–40 kGy GVF) were compared to three PFC Sigma fixed bearing knees (GUR 1020 25–40 kGy GVF; DePuy International, UK). In addition, three PFC Sigma fixed bearing TKRs with UHMWPE inserts manufactured from GUR 1050 50 kGy were investigated.

27.15.2 Methods

The methodologies for both the hip and knee simulator tests are described below together with details of the particle isolation technique employed in this study.

27.15.2.1 Hip Simulator

A minimum of three 28 mm prosthesis pairs of each UHMWPE material were studied under standard simulation conditions in a 10-station Leeds ProSim hip joint simulator for 5 million cycles [64]. The cups were positioned superiorly and inclined at 35 degrees to the horizontal plane in an anatomical configuration. The simulator applied two independently controlled motions. The head underwent flexion extension (+30 degrees and −15 degrees), and the acetabular insert underwent ±10 degrees rotation. A twin peak time-dependent loading curve was applied with a peak load of 3 kN at heel strike and toe off, and a swing phase load of 50N was also applied.

Tests were carried out in 25% (v/v) newborn calf serum (Harlan Seralabs, UK) with 0.1% (w/v) sodium azide to retard bacterial growth. The lubricant was changed every 330,000 cycles and stored frozen at −20°C until required for wear debris analysis. Wear was determined volumetrically every million cycles. The three-dimensional geometry of the cups was determined before the test and every million cycles using a coordinate measuring machine (Kemco 400 3D, Keeley Measurement Co., UK).

27.15.2.2 Knee Simulator

In the fixed bearing PFC Sigma TKR, 10 mm thick tibial inserts were assembled by snap fit into size three titanium alloy (Ti-6Al-4 V) tibial trays. The 10 mm thick PFC Sigma RP bearings freely rotated within size three, polished cobalt chrome alloy (CoCrMo) tibial trays. All PFC Sigma and PFC Sigma RP components articulated with size three posterior cruciate retaining, right cobalt chrome alloy femoral components. All devices were tested in the Leeds six-station ProSim force/displacement controlled knee simulator under ISO conditions. All components were tested using "high" kinematic inputs, which closely reproduce those found in the natural knee and were chosen because they represent a normal walking gait cycle [65]. The knee prostheses were subjected to ±5 degrees internal/external (IE) rotation and 0–10 mm anterior-posterior translation. Fixed bearing knees were simulated under displacement control, whereas the rotating platform mobile bearing knees were simulated under force control (ISO 14243) in the AP direction due to RP design constraints, which restrict movement in this axis. Testing was performed at 1 Hz using 25% (v/v) newborn calf serum plus 0.1% (w/v) sodium azide to retard bacterial growth. The lubricant was changed every 330,000 cycles. Knee components were tested to 5 million cycles.

Questions? Contact FDA/CDRH/OCE/DID at CDRH-FOISTATUS@fda.hhs.gov or 301-796-8118

Records processed under FOIA Request #2014-8015; Released by CDRH on 12-8-2015

Wear measurements were determined gravimetrically every million cycles using unloaded soak controls as a comparison. Serum lubricants were stored frozen at −20°C until required for wear debris analysis.

UHMWPE wear particles were isolated according to the methods of Tipper et al. [15]. Three replicates were analyzed for each prosthesis type. Particles were isolated from each lubricant by alkaline digestion and sequential filtration onto 10, 1.0, and 0.1 μm filters. Filter samples were coated with 5 nm of platinum for analysis by field emission gun-scanning electron microscopy (FEG-SEM) and image analysis using Image Pro Plus (Media Cybernetics, USA). Maximum diameter and area measurements were taken for a minimum of 150 particles in each size range to generate size and area distributions for the particles from the different materials. Percentage data were arcsine transformed, and the transformed data were analyzed by two-way ANOVA. The minimum significant difference ($p < 0.05$) between group means was calculated using the T-method.

The osteolytic potential of the wear particles generated in the hip and knee simulators was predicted using the method of Fisher et al. [61] to calculate functional biological activity (FBA) as previously described. The values of SBA and FBA were compared for the wear particles from the two UHMWPEs in both the hip and knee simulations.

27.15.3 Results

The wear rates, sizes and morphologies of the wear particles together with the predicted biological activity indices for both the hip and knee prostheses are reported below.

27.15.3.1 Volumetric Wear Rates

The wear rates for the two UHMWPEs in the hip and knee are shown in Figure 27.2. In the hip, the GUR 1020 GVF material exhibited a lower wear rate (35 ± 9 mm^3/million cycles) compared to the GUR 1050 25 kGy (46 ± 9 mm^3/million cycles); however, this difference was not significant. In the knee in the PFC Sigma fixed bearing, the GUR 1020 had a significantly higher ($p < 0.05$) wear rate than the moderately crosslinked GUR 1050 50 kGy UHMWPE, at 22.8 ± 6 mm^3/million cycles compared to 13 ± 4 mm^3/million cycles [66]. Thus, the introduction of moderate levels of crosslinking into the UHMWPE component improved the wear resistance of the UHMWPE and the performance of the TKR device. However, the PFC Sigma RP mobile bearing knee (GUR 1020 GVF) exhibited a much lower wear rate of 5.2 ± 4 mm^3/million cycles. This represented a fourfold reduction in wear compared to the PFC Sigma fixed bearing with GUR 1020 UHMWPE and a 2.5-fold reduction in wear compared to the PFC Sigma fixed bearing with GUR 1050 50 kGy UHMWPE.

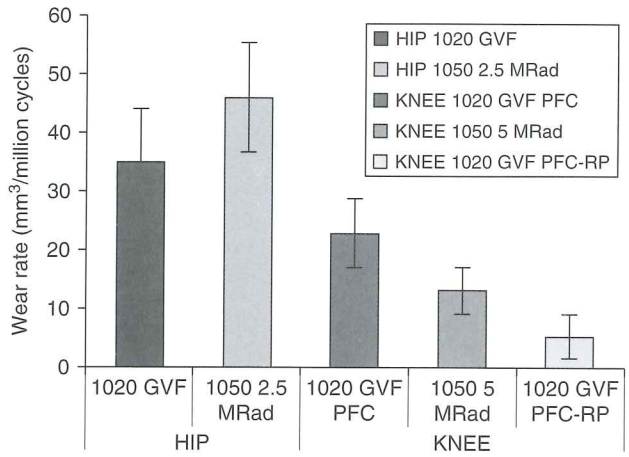

FIGURE 27.2 Mean volumetric wear rates (±95% confidence limits) for GUR 1020 and GUR 1050 UHMWPEs in the hip and the knee.

27.15.3.2 Wear Particles

The wear particles isolated from the lubricants of both the TKR and the THR prostheses were predominantly less than 1.0 μm in size (Figure 27.3). However, a small number of larger particles >1 μm in size were also observed (Figure 27.4). The mode of the frequency distribution for the particles from both the THR and TKR prostheses was in the <0.1–1 μm size range, indicating that the majority of the wear particles were submicrometer in size (Figure 27.5). There were no significant differences in the particle size distributions between the fixed bearing and the Rotating Platform TKR designs or between the TKR and THR prostheses (Figure 27.5). The mode of the distribution for the volumetric concentration of particles as a function of size was in the <0.1–1.0 μm size range for the two different UHMWPEs in the THRs (Figure 27.6); however, the GUR 1020 GVF UHMWPE had approximately 40% of the wear volume comprised of submicrometer-sized wear particles, compared to almost 90% for the GUR 1050 25 kGy UHMWPE. In the knee prostheses the mode of the volume distribution for the GUR 1020 GVF UHMWPE components, fixed and mobile bearing designs, was in the 1.0–10 μm (Figure 27.6). However, for the PFC Sigma fixed bearing with the GUR 1050 50 kGy UHMWPE components, the mode of the volume distribution was in the smaller particle size range (<0.1–1 μm), with over 60% of the wear volume comprised of submicrometer wear particles.

The volumetric concentrations of wear particles in the different size ranges had a marked effect on the biological activity indices for the different UHMWPEs and the prostheses. In the hip, the SBA of the GUR 1050 25 kGy UHMWPE was markedly higher than the GUR 1020 GVF UHMWPE, at 0.89 compared to 0.51 (Table 27.2). This increase in SBA can be accounted for by the much higher volumetric concentration of wear particles in the more

Questions? Contact FDA/CDRH/OCE/DID at CDRH-FOISTATUS@fda.hhs.gov or 301-796-8118

Records processed under FOIA Request #2014-8015; Released by CDRH on 12-8-2015

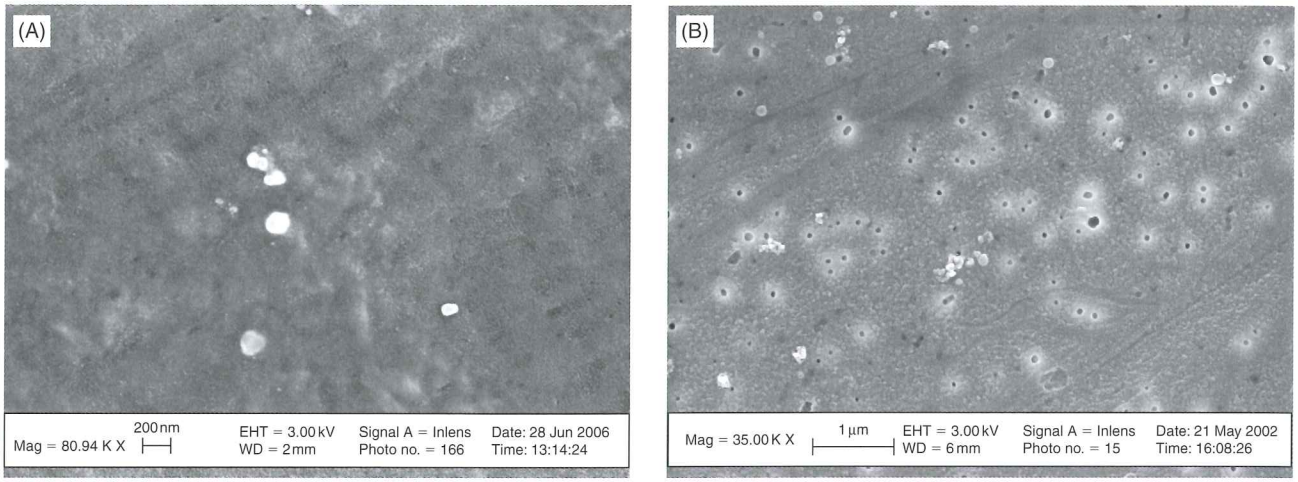

FIGURE 27.3 Scanning electron micrographs of (A) submicrometer-sized UHMWPE particles from the hip (magnification 80,940x, size bar 200 nm) and (B) submicrometer-sized UHMWPE particles from the knee (magnification 35,000x, size bar 1 μm).

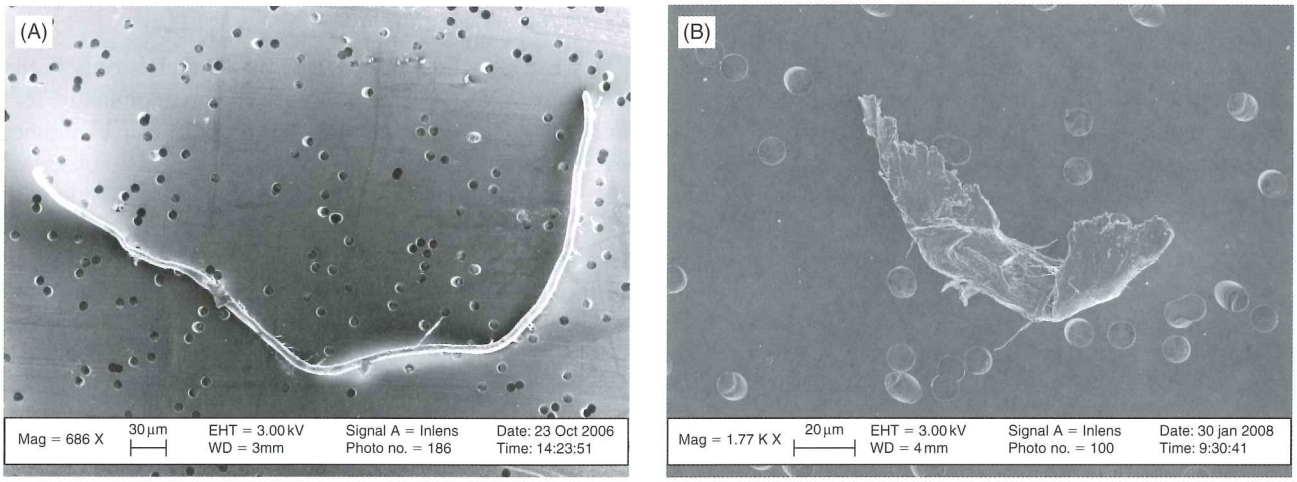

FIGURE 27.4 Scanning electron micrographs of (A) larger UHMWPE wear particles from the hip (magnification 686x, size bar 30 μm) and (B) larger UHMWPE wear particles from the knee (magnification 1770x, size bar 20 μm).

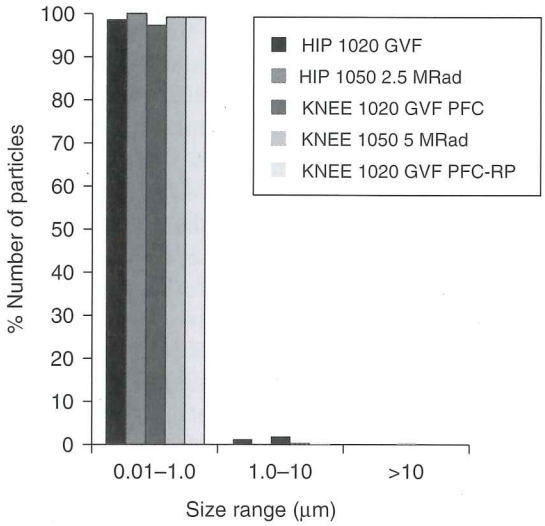

FIGURE 27.5 Frequency distributions as a function of particle size for GUR 1020 and GUR 1050 UHMWPEs in the hip and knee.

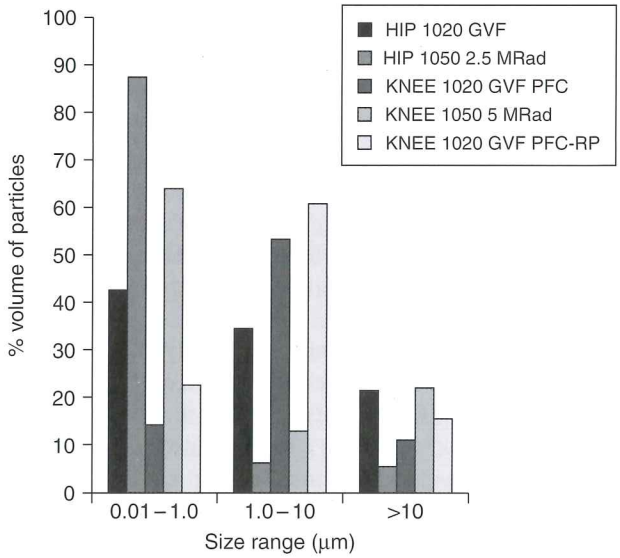

FIGURE 27.6 Volume distributions as function of particle size for GUR 1020 and GUR 1050 UHMWPEs in the hip and knee.

Questions? Contact FDA/CDRH/OCE/DID at CDRH-FOISTATUS@fda.hhs.gov or 301-796-8118

Records processed under FOIA Request #2014-8015; Released by CDRH on 12-8-2015

TABLE 27.2 Specific Biological Activity and Functional Biological Activity Values for GUR 1020 and GUR 1050 under Different Simulation Conditions

Material/implant design	Specific biological activity (SBA)	Functional biological activity (FBA)
HIP GUR 1020 GVF	0.51	17.81
HIP GUR 1050 25 kGy	0.89	41.1
KNEE PFC Sigma fixed GUR 1020 GVF	0.26	5.9
KNEE PFC Sigma RP GUR 1020 GVF	0.36	1.86
KNEE PFC Sigma fixed GUR 1050 50 kGy	0.68	8.83

biologically active size range (<0.1–1 μm) for the GUR 1050 material. In the fixed bearing knee design, again the GUR 1020 GVF UHMWPE had a lower SBA value compared the GUR 1050 50 kGy UHMWPE, at 0.26 compared to 0.68 (Table 27.2). Once again, this increase in SBA for the GUR 1050 material can be explained by a much higher volumetric concentration of particles in the smaller and more biologically active size range (<0.1–1 μm). The Rotating Platform mobile bearing TKR had an SBA somewhere between the two (Table 27.2). In the hip, high SBA coupled with a higher wear rate for the GUR 1050 25 kGy UHMWPE meant that the FBA for this material was more than twice as high as the GUR 1020 GVF UHMWPE material (Table 27.2). In the fixed bearing PFC Sigma knee, although the GUR 1050 50 kGy material had a higher SBA than the GUR 1020 GVF UHMWPE, the reduction in wear rate conferred by the introduction of moderate levels of crosslinking led to similar FBA values. The PFC Sigma rotating platform TKR design had the lowest FBA or osteolytic potential, and in general the TKR designs exhibited lower FBA values or osteolytic potential than the THRs (Table 27.2).

27.15.3.3 Discussion

In the hip there was no significant difference in the wear rates of the two UHMWPE materials; however, in the PFC Sigma fixed bearing knee the introduction of moderate levels of crosslinking into the GUR 1050 UHMWPE caused a significant reduction in the wear rate. Changing the design to a mobile bearing rotating platform knee, but keeping the UHMWPE constant (GUR 1020 GVF) caused a fourfold, highly significant reduction in the wear. Rotating Platform mobile bearing TKR devices have been shown to redistribute the motions between the femoral-insert and tray-insert articulating surfaces and translate complex input motions into more unidirectional motions. The majority of the rotation occurs at the tibial-articulating interface, and as a result the motion at the femoral-insert interface is predominantly unidirectional. This results in reduced cross-shear forces and, hence, reduced wear rates compared with fixed bearing TKR devices [67]. In contrast, rotation of the knee with the PFC Sigma fixed bearing occurs entirely at the femoral-insert articulation. The resulting multidirectional wear path at this interface increases the amount of cross-shear on the UHMWPE bearing and therefore produces a greater polymer wear rate when subjected to high kinematic inputs [67,68].

Consideration of the wear debris size and morphology and its resulting specific biological activity is important, and this is illustrated by the wide range of values determined for the two materials under different kinematic conditions and with different methods of sterilization. In general, the knee prostheses had lower specific biological activity values than the hip, and the lower molecular weight GUR 1020 GVF had lower values of SBA than the GUR 1050 UHMWPE in both the knee and the hip. In the hip, the SBA value for the GUR 1020 UHMWPE was 40% lower than the GUR 1050 UHMWPE, and in the fixed bearing knee it was 60% lower. This is due to the high volumetric concentrations of smaller, more biologically active wear particles generated by the GUR 1050 material in both the hip and the knee. These results were confirmed when the wear rates were taken into consideration, where the GUR 1020 GVF material had lower FBA values in the hip and knee compared to the GUR 1050 UHMWPE materials. However, the limitations of this study were that the materials chosen differed in both their molecular weight and methods of sterilization and therefore were not strictly comparable, that is, GUR 1050 25 kGy UHMWPE was studied in the hip, whereas in the knee the GUR 1050 was irradiated with 50 kGy gamma radiation.

In the studies reported here, lower wear rates were recorded in the knee for rotating platform mobile bearing knee designs and moderately crosslinked UHMWPE. The increase in the biological activity of the wear particles from crosslinked UHMWPE was predicted from analysis of debris size, volume, and morphology. Of equal importance is the observation that GUR 1020 GVF (irradiated in an inert atmosphere), which has become standard, produces wear particles with lower biological activity in both the knee and the hip compared to the GUR 1050 UHMWPEs investigated in this study. Relatively low wear rates in TKR prostheses, coupled with the low biological activity of particles produced indicates that current designs and materials could provide adequate osteolysis-free *in vivo* implant service times for the majority of patients. In the hip, the introduction of highly crosslinked GUR 1050 100 kGy UHMWPE has been shown to cause an 80% reduction in wear rate (46). Although the wear particles have a high

Questions? Contact FDA/CDRH/OCE/DID at CDRH-FOISTATUS@fda.hhs.gov or 301-796-8118

Records processed under FOIA Request #2014-8015; Released by CDRH on 12-8-2015

SBA, the reduction in wear rate is so great that the FBA value for this material is reduced almost sixfold [69]. Highly crosslinked UHMWPE has not yet been introduced clinically in the knee, and therefore the effects on wear and particle distributions remain to be determined.

27.16 CONCLUSION

This chapter clearly shows that there are many published methods suitable for separating and characterizing UHMWPE wear particles from tissues and simulator lubricants. Many of these methods successfully remove proteins and lipids from particles, preserve particle morphology, and yield similar particle size distributions. Clearly, advances in technology are continually being employed, for example the use of high-resolution FEG-SEM has allowed increasingly smaller particles to be observed and characterized. In addition, the limitations of each method are now widely recognized. Particle characterization, in terms of size and volume distributions and particle contribution to the osteolytic potential of new and existing UHMWPE materials, has been recognized by academic and industrial stakeholders as being an important step in the preclinical assessment of total joint replacements. However, there is no one standard method for isolation or characterization of UHMWPE particles that can be applied to both tissues and simulator lubricant samples, and this would clearly be advantageous.

REFERENCES

1. Amstutz HC, Campbell P, Kossovsky N, Clarke IC. Mechanism and clinical significance of wear debris-induced osteolysis. *Clin Orthop Relat Res* 1992 March;**1**(276):7–18.
2. Ingham E, Fisher J. Biological reactions to wear debris in total joint replacement. *Proc Inst Mech Eng Part H, J Eng Med* 2000 January 1;**214**(1):21–37.
3. Jacobs JJ, Roebuck KA, Archibeck M, Hallab NJ, Glant TT. Osteolysis: basic science. *Clin Orthop Relat Res* 2001 December; **1**(393):71–7.
4. Goldring SR, Schiller AL, Roelke M, Rourke CM, O'Neil DA, Harris WH. The synovial-like membrane at the bone-cement interface in loose total hip replacements and its proposed role in bone lysis. *J Bone Joint Surg Am Vol* 1983 June 1;**65**(5):575–84.
5. Ingham E, Fisher J. The role of macrophages in osteolysis of total joint replacement. *Biomaterials* 2005 April 1;**26**(11):1271–86.
6. Schmalzried TP, Jasty M, Harris WH. Periprosthetic bone loss in total hip arthroplasty. Polyethylene wear debris and the concept of the effective joint space. *J Bone Joint Surg Am Vol* 1992 July 1;**74**(6):849–63.
7. Matthews JB, Besong AA, Green TR, Stone MH, Wroblewski BM, Fisher J, Ingham E. Evaluation of the response of primary human peripheral blood mononuclear phagocytes to challenge with in vitro generated clinically relevant UHMWPE particles of known size and dose. *J Biomed Mater Res* 2000 November 1;**52**(2):296–307.
8. Matthews JB, Green TR, Stone MH, Wroblewski BM, Fisher J, Ingham E. Comparison of the response of primary human peripheral blood mononuclear phagocytes from different donors to challenge with model polyethylene particles of known size and dose. *Biomaterials* 2000 October 1;**21**(20):2033–44.
9. Horowitz SM, Gonzales JB. Effects of polyethylene on macrophages. *J Orthop Res* 1997 January 1;**15**(1):50–6.
10. Shanbhag AS, Jacobs JJ, Black J, Galante JO, Glant TT. Human monocyte response to particulate biomaterials generated in vivo and in vitro. *J Orthop Res* 1995 September 1;**13**(5):792–801.
11. Willert HG. Reactions of the articular capsule to wear products of artificial joint prostheses. *J Biomed Mater Res* 1977 March 1;**11**(2):157–64.
12. Campbell P, Ma S, Yeom B, McKellop H, Schmalzried TP, Amstutz HC. Isolation of predominantly submicron-sized UHMWPE wear particles from periprosthetic tissues. *J Biomed Mater Res* 1995 January;**29**(1):127–31.
13. Tipper JL, Ingham E, Hailey JL, Besong AA, Fisher J, Wroblewski BM, Stone MH. Quantitative analysis of polyethylene wear debris, wear rate and head damage in retrieved Charnley hip prostheses. *J Mater Sci Mater Med* 2000 February;**11**(2):117–24.
14. Tipper JL, Firkins PJ, Ingham E, Fisher J, Stone MH, Farrar R. Quantitative analysis of the wear and wear debris from low and high carbon content cobalt chrome alloys used in metal on metal total hip replacements. *J Mater Sci Mater Med* 1999 June;**10**(6):353–62.
15. Tipper JL, Galvin AL, Williams S, McEwen HM, Stone MH, Ingham E, Fisher J. Isolation and characterization of UHMWPE wear particles down to ten nanometers in size from in vitro hip and knee joint simulators. *J Biomed Mater Res A* 2006 September 1;**78**(3):473–80.
16. Tipper JL, Hatton A, Nevelos JE, Ingham E, Doyle C, Streicher R, et al. Alumina-Alumina artificial hip joints. Part II: characterisation of the wear debris from in vitro hip joint simulations. *Biomaterials* 2002 August;**23**(16):3441–8.
17. Richards L, Brown C, Stone MH, Fisher J, Ingham E, Tipper JL. Identification of nanometre-sized ultra-high molecular weight polyethylene wear particles in samples retrieved in vivo. *J Bone Joint Surg Br* 2008 August;**90**(8):1106–13.
18. Shanbhag AS, Jacobs JJ, Glant TT, Gilbert JL, Black J, Galante JO. Composition and morphology of wear debris in failed uncemented total hip replacement. *J Bone Joint Surg Br* 1994 January;**76**(1):60–7.
19. Maloney WJ, Smith RL, Schmalzried TP, Chiba J, Huene D, Rubash H. Isolation and characterization of wear particles generated in patients who have had failure of a hip arthroplasty without cement. *J Bone Joint Surg Am* 1995 September;**77**(9):1301–10.
20. Ingram JH, Stone M, Fisher J, Ingham E. The influence of molecular weight, crosslinking and counterface roughness on tnf-alpha production by macrophages in response to ultra high molecular weight polyethylene particles. *Biomaterials* 2004 August;**25**(17):3511–22.
21. Green TR, Fisher J, Stone M, Wroblewski BM, Ingham E. Polyethylene particles of a 'critical size' are necessary for the induction of cytokines by macrophages in vitro. *Biomaterials* 1998, December; **19**(24):2297–302.
22. Shanbhag AS, Jacobs JJ, Black J, Galante JO, Glant TT. Macrophage/particle interactions: effect of size, composition and surface area. *J Biomed Mater Res* 1994 January;**28**(1):81–90.
23. Yao J, Glant TT, Lark MW, Mikecz K, Jacobs JJ, Hutchinson NI, et al. The potential role of fibroblasts in periprosthetic osteolysis: fibroblast response to titanium particles. *J Bone Miner Res* 1995 September;**10**(9):1417–27.

Questions? Contact FDA/CDRH/OCE/DID at CDRH-FOISTATUS@fda.hhs.gov or 301-796-8118

Records processed under FOIA Request #2014-8015; Released by CDRH on 12-8-2015

24. Maloney WJ, Smith RL, Castro F, Schurman DJ. Fibroblast response to metallic debris in vitro. Enzyme induction cell proliferation, and toxicity. *J Bone Joint Surg Am* 1993 June;**75**(6):835–44.
25. Dean DD, Schwartz Z, Blanchard CR, Liu Y, Agrawal CM, Lohmann CH, et al. Ultrahigh molecular weight polyethylene particles have direct effects on proliferation, differentiation, and local factor production of MG63 osteoblast-like cells. *J Orthop Res* 1999 January;**17**(1):9–17.
26. Vermes C, Chandrasekaran R, Jacobs JJ, Galante JO, Roebuck KA, Glant TT. The effects of particulate wear debris, cytokines, and growth factors on the functions of MG-63 osteoblasts. *J Bone Joint Surg Am* 2001 February;**83-A**(2):201–11.
27. Dowd JE, Schwendeman LJ, Macaulay W, Doyle JS, Shanbhag AS, Wilson S, et al. Aseptic loosening in uncemented total hip arthroplasty in a canine model. *Clin Orthop Relat Res* 1995 October(319):106–21.
28. Howie DW, Vernon-Roberts B, Oakeshott R, Manthey B. A rat model of resorption of bone at the cement-bone interface in the presence of polyethylene wear particles. *J Bone Joint Surg Am* 1988 February;**70**(2):257–63.
29. Clohisy JC, Hirayama T, Frazier E, Han SK, Abu-Amer Y. Nf-Kb signaling blockade abolishes implant particle-induced osteoclastogenesis. *J Orthop Res* 2004 January;**22**(1):13–20.
30. Margevicius KJ, Bauer TW, McMahon JT, Brown SA, Merritt K. Isolation and characterization of debris in membranes around total joint prostheses. *J Bone Joint Surg Am* 1994 November;**76**(11):1664–75.
31. Scott M, Widding K, Jani S. Do current wear particle isolation procedures underestimate the number of particles generated by prosthetic bearing components?. *Wear* 2001 October;**251**:1213–17.
32. Campbell P, Ma S, Schmalzried T, Amstutz HC. Tissue digestion for wear debris particle isolation. *J Biomed Mater Res* 1994 April;**28**(4):523–6.
33. Mabrey JD, Afsar-Keshmiri A, Engh GA, Sychterz CJ, Wirth MA, Rockwood CA, Agrawal CM. Standardized analysis of UHMWPE wear particles from failed total joint arthroplasties. *J Biomed Mater Res* 2002;**63**(5):475–83.
34. Elfick AP, Green SM, Pinder IM, Unsworth A. A novel technique for the detailed size characterization of wear debris. *J Mater Sci Mater Med* 2000 May;**11**(5):267–71.
35. Elfick AP, Green SM, Krikler S, Unsworth A. The nature and dissemination of UHMWPE wear debris retrieved from periprosthetic tissue of THR. *J Biomed Mater Res A* 2003 April 1;**65**(1):95–108.
36. Kinbrum A, Unsworth A, Kamali A. The wear of high carbon metal on metal bearings. *Transactions of the 54th Annual Meeting of the Orthopeadic Research Society*; 2008:1905.
37. Slouf M, Eklova S, Kumstatova J, Berger S, Synkova H, Sosna A, et al. Isolation, characterization and quantification of polyethylene wear debris from periprosthetic tissues around total joint replacements. *Wear* 2007 April 10;**262**:1171–81.
38. Baxter R, Steinbeck M, Tipper J, Rimnac C, Parvvizi J, Marcolongo M, Kurtz S. Evaluation of methods for periprosthetic tissue digestion and polyethylene wear particle analysis. *Transactions of the 54Th Annual Meeting of the Orthopaedic Research Society*; 2008:58.
39. Niedzwiecki S, Klapperich C, Short J, Jani S, Ries M, Pruitt L. Comparison of three joint simulator wear debris isolation techniques: acid digestion, base digestion, and enzyme cleavage. *J Biomed Mater Res* 2001 August;**56**(2):245–9.
40. Catelas I, Bobyn JD, Medley JB, Krygier JJ, Zukor DJ, Petit A, Huk OL. Effects of digestion protocols on the isolation and characterization of metal-metal wear particles. I. Analysis of particle size and shape. *J Biomed Mater Res* 2001 June 5;**55**(3):320–9.
41. Doorn PF, Campbell PA, Worrall J, Benya PD, McKellop HA, Amstutz HC. Metal wear particle characterization from metal on metal total hip replacements: transmission electron microscopy study of periprosthetic tissues and isolated particles. *J Biomed Mater Res* 1998 October;**42**(1):103–11.
42. Brown C, Williams S, Tipper JL, Fisher J, Ingham E. Characterisation of wear particles produced by metal on metal and ceramic on metal hip prostheses under standard and microseparation simulation. *J Mater Sci Mater Med* 2007 May;**18**(5):819–27.
43. Visentin M, Stea S, Squarzoni S, Antonietti B, Reggiani M, Toni A. A new method for isolation of polyethylene wear debris from tissue and synovial fluid. *Biomaterials* 2004 November;**25**(24):5531–7.
44. Galvin AL, Tipper JL, Jennings LM, Stone MH, Jin ZM, Ingham E, Fisher I. Wear and biological activity of highly crosslinked polyethylene in the hip under low serum protein concentrations. *Proc Inst Mech Eng [H]* 2007 January;**221**(1):1–10.
45. Besong AA, Tipper JL, Ingham E, Stone MH, Wroblewski BM, Fisher J. Quantitative comparison of wear debris from UHMWPE that has and has not been sterilised by gamma irradiation. *J Bone Joint Surg Br* 1998 March;**80**(2):340–4.
46. Galvin AL, Williams S, Hatto P, Thompson J, Isaac G, Stone M, et al. Comparison of wear of ultra high molecular weight polyethylene acetabular cups against alumina ceramic and chromium nitride coated femoral heads: 15th international conference on wear of materials. *Wear* 2005;**259**:972–6.
47. Scott M, Morrison M, Mishra SR, Jani S. Particle analysis for the determination of UHMWPE wear. *J Biomed Mater Res B Appl Biomater* 2005 May;**73**(2):325–37.
48. Gruen TA, Amstutz HC. A failed vitallium/stainless steel total hip replacement: a case report with histological and metallurgical examination. *J Biomed Mater Res* 1975 September;**9**(5):465–77.
49. Schmalzried TP, Callaghan JJ. Wear in total hip and knee replacements. *J Bone Joint Surg Am* 1999 January;**81**(1):115–36.
50. Savio JA, Overcamp LM, Black J. Size and shape of biomaterial wear debris. *Clin Mater* 1994;**15**(2):101–47.
51. McKellop HA, Campbell P, Park SH, Schmalzried TP, Grigoris P, Amstutz HC, Sarmiento A. The origin of submicron polyethylene wear debris in total hip arthroplasty. *Clin Orthop Relat Res* 1995 February(311):3–20.
52. Lapcikova M, Slouf M, Dybal J, Zolotarevova E, Entlicher G, Pokorny D, et al. Nanometer size wear debris generated from ultra high molecular weight polyethylene in vivo. *Wear* 2009 January(266):349–55.
53. Wear of implant materials, polymer and metal wear particles. Isolation, characterisation and quantification. ISO Standard 17853; 2003.
54. Standard practice for retrieval and analysis of medical devices and associated tissues and fluids. ASTM Standards Committee F561-05A; 2005.
55. Standard practice for characterisation of particles. ASTM Standards Committee F1877-05; 2005.
56. Endo M, Tipper JL, Barton DC, Stone MH, Ingham E, Fisher J. Comparison of wear, wear debris and functional biological activity of moderately crosslinked and non-crosslinked polyethylenes in hip prostheses. *Proc Inst Mech Eng [H]* 2002;**216**(2):111–22.
57. Galvin A, Kang L, Tipper J, Stone M, Ingham E, Jin Z, Fisher J. Wear of crosslinked polyethylene under different tribological conditions. *J Mater Sci Mater Med* 2006 March;**17**(3):235–43.
58. Besong AA, Tipper JL, Mathews BJ, Ingham E, Stone MH, Fisher J. The influence of lubricant on the morphology of ultra-high molecular

Questions? Contact FDA/CDRH/OCE/DID at CDRH-FOISTATUS@fda.hhs.gov or 301-796-8118

Records processed under FOIA Request #2014-8015; Released by CDRH on 12-8-2015

weight polyethylene wear debris generated in laboratory tests. *Proc Inst Mech Eng [H]* 1999;**213**(2):155–8.

59. Endo MM, Barbour PS, Barton DC, Fisher J, Tipper JL, Ingham E, Stone MH. Comparative wear and wear debris under three different counterface conditions of crosslinked and non-crosslinked ultra high molecular weight polyethylene. *Biomed Mater Eng* 2001;**11**(1):23–35.
60. Yamamoto K, Clarke IC, Masaoka T, Oonishi H, Williams PA, Good VD, Imakiire A. Microwear phenomena of ultrahigh molecular weight polyethylene cups and debris morphology related to gamma radiation dose in simulator study. *J Biomed Mater Res* 2001 July;**56**(1):65–73.
61. Fisher J, Bell J, Barbour PS, Tipper JL, Matthews JB, Besong AA, et al. A novel method for the prediction of functional biological activity of polyethylene wear debris. *Proc Inst Mech Eng [H]* 2001;**215**(2):127–32.
62. Green TR, Fisher J, Matthews JB, Stone MH, Ingham E. Effect of size and dose on bone resorption activity of macrophages by in vitro clinically relevant ultra high molecular weight polyethylene particles. *J Biomed Mater Res* 2000 September;**53**(5):490–7.
63. Barnett PI, McEwen HM, Auger DD, Stone MH, Ingham E, Fisher J. Investigation of wear of knee prostheses in a new displacement/force-controlled simulator. *Proc Inst Mech Eng [H]* 2002;**216**(1):51–61.
64. Barbour PS, Stone MH, Fisher J. A hip joint simulator study using simplified loading and motion cycles generating physiological wear paths and rates. *Proc Inst Mech Eng [H]* 1999;**213**(6):455–67.
65. Lafortune MA, Cavanagh PR, Sommer HJ, Kalenak A. Three-Dimensional kinematics of the human knee during walking. *J Biomech* 1992 April;**25**(4):347–57.
66. Fisher J, McEwen HM, Tipper JL, Galvin AL, Ingram J, Kamali A, et al. Wear, debris, and biologic activity of cross-linked polyethylene in the knee: benefits and potential concerns. *Clin Orthop Relat Res* 2004 November(428):114–19.
67. McEwen HM, Barnett PI, Bell CJ, Farrar R, Auger DD, Stone MH, Fisher J. The influence of design, materials and kinematics on the in vitro wear of total knee replacements. *J Biomech* 2005 February; **38**(2):357–65.
68. Wang A, Stark C, Dumbleton JH. Mechanistic and morphological origins of ultra-high molecular weight polyethylene wear debris in total joint replacement prostheses. *Proc Inst Mech Eng [H]* 1996; **210**(3):141–55.
69. Tipper JL, Galvin AL, Ingham E, Fisher J. Estimation of the osteolytic potential of noncrosslinked and crosslinked polyethylenes and ceramic total hip prostheses. *J Am Soc Test Mater Int* 2006;**3**:1–17.

Questions? Contact FDA/CDRH/OCE/DID at CDRH-FOISTATUS@fda.hhs.gov or 301-796-8118

Records processed under FOIA Request #2014-8015; Released by CDRH on 12-8-2015

Available online at www.sciencedirect.com

ScienceDirect

Acta Biomaterialia 5 (2009) 2495–2502

Acta BIOMATERIALIA

www.elsevier.com/locate/actabiomat

Influence of design and bearing material on polyethylene wear particle generation in total knee replacement

S. Utzschneider [a,*], A. Paulus [b], J.-C. Datz [b], C. Schroeder [b], B. Sievers [b], B. Wegener [a], V. Jansson [a]

[a] *Orthopedic Department, Ludwig-Maximilians-University, Großhadern Medical Center, Marchioninistr. 15, 81377 Munich, Germany*
[b] *Orthopedic Department, Laboratory for Biomechanics and Experimental Orthopedics, Ludwig-Maximilians-University, Großhadern Medical Center, Marchioninistr. 23, 81377 Munich, Germany*

Received 21 August 2008; received in revised form 5 March 2009; accepted 11 March 2009
Available online 24 March 2009

Abstract

Periprosthetic osteolysis is one of the main reasons for revision of arthroplasty. The osteolytic reaction is influenced by the dose, size and shape of the wear particles. For arthroplasty, a low number and biologically less active particles are required. This is the first study which analyzes the impact of different knee designs, combined with crosslinked polyethylenes (sequentially irradiated and annealed as well as remelted techniques), on the amount, size and shape of particles. Overall, six material combinations, four of them with crosslinked polyethylene (XPE) and two of them with ultra-high molecular weight polyethylene (UHMWPE) inserts, including fixed and mobile bearings, were tested in a knee joint simulator. After isolation nearly 100,000 particles were analyzed in size, shape and number by scanning electron microscopy and image analysis. For all the designs, the wear was predominantly smooth and granular with few fibrillar particles. The Scorpio® design with the X3™ insert, the Natural Knee® II design with the Durasul™ insert and the LCS® design, also combined with a crosslinked polyethylene insert, generated statistically significant ($P < 0.05$) lower particle numbers. The particle size was independent of the radiation dose. The wear generated by the LCS® knee design (XPE and UHMWPE) had a higher percentage fraction of particles >1 μm in size (equivalent circle diameter). The NexGen® design, tested with the Prolong™ insert, showed a high number of particles in the biologically active size range compared with the other crosslinked designs, which could be a predictor for higher biological reactivity.
© 2009 Acta Materialia Inc. Published by Elsevier Ltd. All rights reserved.

Keywords: Arthroplasty; Polyethylene; Wear debris; Knee replacement

1. Introduction

Prosthetic wear plays a central role in the initiation and development of osteolysis, which leads to the loosening of total joint replacements [1–3]. Numerous factors can influence the cellular response to wear particles, including the size, dose, volume, shape and composition of the particles [1–3].

For total knee arthroplasty, conventional ultra-high molecular weight polyethylene (UHMWPE) is the material of choice for tibial inserts [4,5]. However, UHMWPE is now widely perceived as the most significant factor in wear-induced bone resorption [6–8]. The characteristics of polyethylene particles associated clinically with an osteolytic response by histiocytes have been shown and detailed in the literature [3,9,10]. Crosslinked polyethylene (XPE) was developed to reduce volumetric wear in both total hip and knee prostheses [11–16]. Furthermore, some studies have shown that XPE wear particles could be different from UHMWPE particles in size and volume [2,17,18].

Principally, there are two ways of crosslinking UHMWPE which may reduce the mechanical properties of polyethylene [19]. Annealing after irradiation creates free

* Corresponding author. Tel.: +49 8970950; fax: +49 8970958881.
E-mail address: sandra.utzschneider@med.uni-muenchen.de (S. Utzschneider).

1742-7061/$ - see front matter © 2009 Acta Materialia Inc. Published by Elsevier Ltd. All rights reserved.
doi:10.1016/j.actbio.2009.03.016

Questions? Contact FDA/CDRH/OCE/DID at CDRH-FOISTATUS@fda.hhs.gov or 301-796-8118

Records processed under FOIA Request #2014-8015; Released by CDRH on 12-8-2015

radicals or highly energized unpaired electrons, which may lead to late oxidation of the polyethylene [19,20]. Otherwise, remelting the polyethylene after irradiation removes the free radicals but also reduces fatigue strength [20].

In addition, in the knee a range of design and kinematic variables have to be considered, as they can markedly influence wear, regardless of the type of polyethylene used [21]. Current tibial component designs in total knee arthroplasty can be subdivided into two different groups: fixed bearing and mobile bearing. The mobile-bearing knee implant was designed to minimize contact stress on the bearing surface and to reduce polyethylene wear [22,23]. Although the mobile-bearing design has theoretical advantages over the fixed-bearing implant, there is little evidence that mobile-bearing implants lead to better clinical results [24].

In considering the benefits of using XPE in the knee, the nature of the debris has to be considered. Therefore, the purpose of this study was to determine the size, morphology and number of polyethylene particles for six different current knee designs. Different XPE, including fixed- and mobile-bearing inserts, made by remelting as well as by sequential irradiation and annealing, were compared.

2. Materials and methods

2.1. Materials

Six different types of tibial inserts (four XPE inserts and two UHMWPE inserts; shown in Table 1) were used with the appropriate femoral and tibial component recommended from the particular manufacturer. Whereas the material combinations A–C, E and F are actual product devices, D is an experimental combination and not a commercially available product.

2.2. Knee simulator testing

The experimental knee designs (three inserts/material) were tested on a knee simulator (Stallforth/Ungethuem, Germany), involving three simultaneously running test stations over 5×10^6 cycles. Before the measurements, the inserts were left at 37 °C for 30 days to reach thermal equilibrium and dimensional stability [25]. The physiologic load, flexion/extension (0–60°) motion, anterior/posterior translation waveforms were taken from the recommended ISO kinematics of the knee during normal gait [26]. The compressive load applied to each knee was offset 5 mm medially from the tibial axis [26], and the simulator was run at a frequency of 1 Hz. The lubricant was changed every 6 days. This lubricant used for testing was 25% (v/v) newborn calf serum (Heraeus Kulzer, Berlin, Germany) with 0.1% (m/v) sodium azide solution (Sigma–Aldrich, Munich, Germany) in sterile water [26]. Wear was determined gravimetrically at every 0.5 million cycles, for up to 5 million cycles of testing, by the technique outlined by the ISO [27]. Volumetric wear of the bearings was calculated from weight loss data converted to volumetric data (by material density).

One load-soaked insert was used to correct for fluid absorption in the polyethylene inserts. The load-soaked inserts were subjected to the same cyclic load profile without motion and with the femoral component flexed by 10° to coincide with the peak load during gait. All other test conditions were the same for the load-soak inserts. The load-soak corrected weight loss data were fitted with a linear regression in the steady-state weight increase region (steady state occurred between 0.5 and 2 million cycles). The slope of the regression was recorded as the gravimetric wear rate.

2.3. Isolation of the particles

The particles were separated from the lubricant using the acid digestion method [28]. Then, 10 ml of each serum sample were added to 50 ml of hydrochloric acid (37% v/v; Merck, Darmstadt, Germany) and mixed with a magnetic stir bar at 60 °C for ~1 h. Then, 3 ml of this digestion solution was added to 150 ml of methanol (Merck, Darmstadt, Germany) and filtered through a 0.02-μm polycarbonate membrane (Anodisc 47, Whatman plc, Maidstone, Kent, UK). The filter membrane was then dried for at least 6 h and sputter-coated with gold.

Table 1
Types of knee designs including tibial inserts that were tested in the knee simulator.

Material combination	Knee design	Type of polyethylene	Manufacturing process
A	Scorpio® (Stryker)	XPE (crosslinked polyethylene) (X3™)	Fixed-bearing *CR* 24 mm, GUR 1020, 3 × 30 kGy gamma irradiation, annealed and sequential irradiated, Gasplasma sterilized
B	Natural Knee® II (Zimmer)	XPE (Durasul™)	Fixed-bearing *ultra-congruent* 19 mm, GUR 1050, 95 kGy E-beam, remelted, EtO sterilized
C	NexGen® (Zimmer)	XPE (Prolong™)	Fixed-bearing *CR* 14 mm, GUR 1050, 65 kGy E-beam, remelted, Gasplasma sterilized
D	LCS® (DePuy)	XPE	Mobile-bearing (rotating platform) 15 mm, GUR 1020, 50 kGy gamma irradiation, remelted, gas plasma sterilized (experimental combination: not a commercially available product)
E	LCS® (DePuy)	Conventional UHMWPE	Mobile-bearing (rotating platform) 15 mm, GUR 1020, 25–40 kGy gamma irradiation under vacuum in foil (GVF)
F	Natural Knee® II (Zimmer)	Conventional UHMWPE	Fixed-bearing congruent 13 mm, GUR 1050, gamma sterilized

Questions? Contact FDA/CDRH/OCE/DID at CDRH-FOISTATUS@fda.hhs.gov or 301-796-8118

Records processed under FOIA Request #2014-8015; Released by CDRH on 12-8-2015

2.4. Determination of particle size, morphology and number

The particles recovered on the filter membranes were imaged by scanning electron microscopy (SEM; Leica Stereoscan 420, Leica Microsystems, Wetzlar, Germany). The particles that were >1.0 μm in size were analyzed at a magnification of 5000 diameters, and the particles that were <1.0 μm at a magnification of 10,000 diameters. A minimum of 20 random, non-overlapping fields of view and 200 particles were analyzed at each magnification. Overall, nearly 100,000 particles were analyzed using SEM. Images of each field of view were captured, and the particles were measured using a digital image analysis program (Leica QWin, Image Processing and Analysis Application, Leica Microsystems, Wetzlar, Germany).

The boundary of each particle was defined on the basis of a gray-scale level threshold.

The following parameters were recorded: mean diameter, perimeter, area, equivalent circle diameter (ECD), aspect ratio (AR) and the roundness (R) of the wear particles [29]. AR was calculated using the Leica software by dividing the length of the major axis by the length of the minor axis. According to Sieving et al., particles with an AR 1–2.39 were defined as having a globular/circular shape, whereas particles with an AR 2.4–5 were defined as having a fibular/elongated shape [30]. The percentage of particles was calculated for the size ranges (ECD) <0.25 μm, 0.25–0.5 μm, >0.5–1 μm and >1 μm.

Assuming a constant particle thickness and a spherical shape, the number of particles was determined by the particle volume as a function of size by the following formula:

$$N_{(p)} = \frac{n_{(p)} \times G_{(v)}}{\sum_{k=1}^{n} \left(\frac{\pi \times d_{(m)}^3}{6} \right)}$$

The absolute number of particles $N_{(p)}$ is defined as the division of the number of the measured particles $n_{(p)}$ multiplied by the determined volumetric wear rate $G_{(v)}$ by the sum of all calculated particle volumes as a function of size $d_{(m)}$.

2.5. Statistical analysis

Statistical analysis was performed to analyze the significance of variance between two groups using a 2-way analysis of variance (ANOVA) and the Tukey–Kramer method as an adjustment for multiple comparisons. The differences were considered significant at P-values < 0.05.

3. Results

3.1. Wear particle size and morphology

\For all the groups, >85% (mean diameter) of the particles were submicron. The analyses of the wear debris determined by the particle size distribution for particles produced from the six knee designs are shown in Fig. 1 and Table 2. All types of knee designs used in this study showed similar size distributions of polyethylene wear, with a mean ECD of 0.39 ± 0.37 and 0.42 ± 0.44 μm for the knee designs tested with UHMWPE, and a mean ECD from 0.33 ± 0.23 up to 0.46 ± 0.46 μm for the designs tested with XPE. However, all difference values shown in Fig. 1 and Table 2 are statistically significantly ($P < 0.05$).

There was a tendency for the UHMWPE as well as the XPE mobile-bearing knee designs to create larger particles (Fig. 1). The morphology of the submicron-sized wear particles can be seen in the SEM micrographs (Fig. 2). The majority of the particles generated from all six knee designs were approximately round in shape, smooth, granular, irregular and had similar AR percentage values (Table 3).

3.2. Number of particles

A histogram of the mean number of particles calculated is shown in Fig. 3. For all test intervals combined,

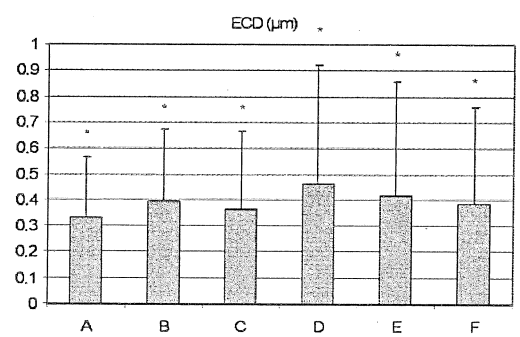

Fig. 1. ECD in micrometers of the analyzed wear particles from six current knee designs (*$P < 0.05$).

Table 2
Parameters of size and shape description of analyzed wear particles.

Knee design	Mean diameter (μm)	Perimeter (μm)	Area (μm²)	Roundness	Aspect ratio
A	0.37 ± 0.30*	1.32 ± 1.16*	0.13 ± 0.25*	0.69 ± 0.23*	1.44 ± 0.50*
B	0.44 ± 0.37*	1.56 ± 1.51*	0.18 ± 0.41*	0.68 ± 0.21*	1.46 ± 0.57*
C	0.40 ± 0.36*	1.39 ± 1.37*	0.18 ± 0.45*	0.72 ± 0.20*	1.39 ± 0.52*
D	0.52 ± 0.55*	1.89 ± 2.32*	0.33 ± 0.88*	0.67 ± 0.22*	1.48 ± 0.60*
E	0.48 ± 0.56*	1.72 ± 2.29*	0.29 ± 0.89*	0.66 ± 0.21*	1.49 ± 0.52*
F	0.44 ± 0.48*	1.57 ± 1.94*	0.23 ± 0.82*	0.66 ± 0.22*	1.50 ± 0.60*

* $P < 0.05$.

Questions? Contact FDA/CDRH/OCE/DID at CDRH-FOISTATUS@fda.hhs.gov or 301-796-8118

Records processed under FOIA Request #2014-8015; Released by CDRH on 12-8-2015

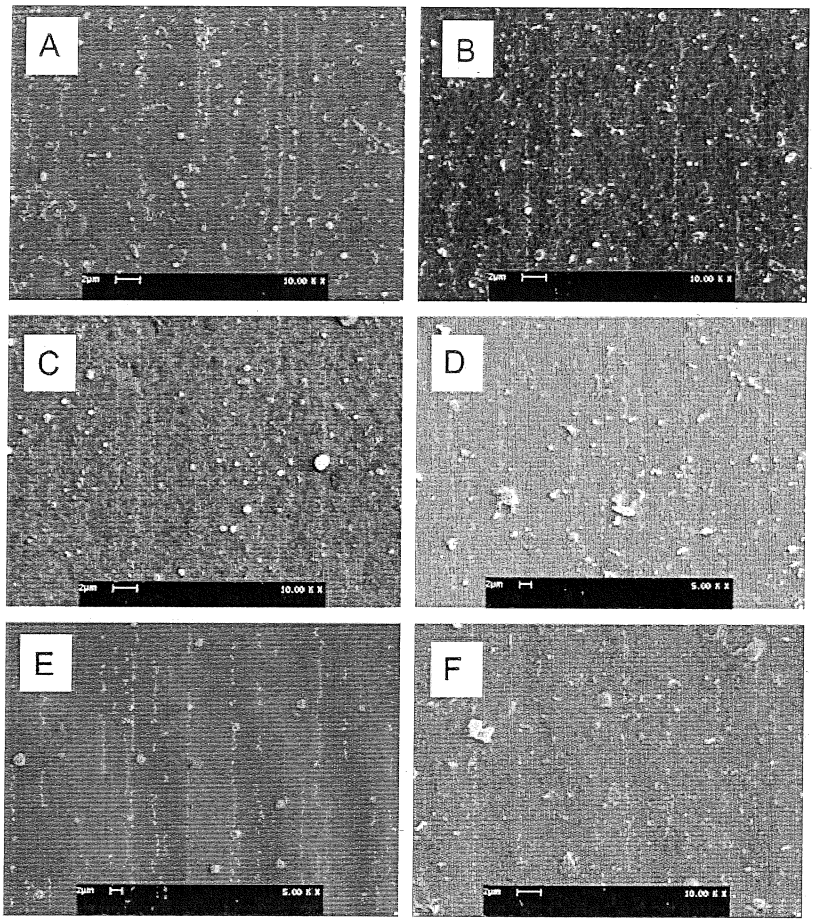

Fig. 2. SEM micrographs of polyethylene wear particles generated from knee designs using XPE (A–D) and UHMWPE (E and F) (original magnifications, 5000 and 10,000×).

Table 3
AR values (according to Sieving et al. [30]) for shape description of analyzed wear particles.

Knee design	Aspect ratio	
	1–2.39 (%)	⩾2.4 (%)
A	95.4	4.6
B	94.9	5.1
C	95.8	4.2
D	93.2	6.8
E	94.3	5.8
F	93.4	6.6

the mean particle generation rates (expressed in 10^9 particles per 10^6 cycles) were lower for knee designs A, B and D ($P < 0.05$).

For each group, the total number of particles partitioned by the size intervals is shown in Fig. 4. The particles generated by designs A and B were mostly distributed in the size range <0.5 μm (ECD). However, design A still produced the lowest number of particles <0.5 μm owing to the very low number of particles produced overall.

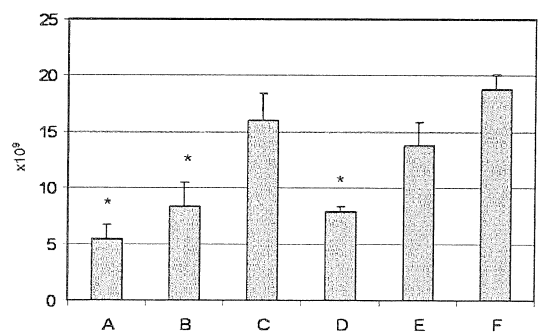

Fig. 3. Calculated number of particles per 10^6 cycles of knee designs using XPE (A–D) and UHMWPE (E and F) ($^*P < 0.05$).

4. Discussion

The size, shape and total number of polyethylene wear particles have been reported to affect the biological response to these particles, which can cause osteolysis [1–3]. Joint simulators allow preclinical evaluation of wear of artificial joints in a controlled environment [2]. The results of knee

Questions? Contact FDA/CDRH/OCE/DID at CDRH-FOISTATUS@fda.hhs.gov or 301-796-8118

Records processed under FOIA Request #2014-8015; Released by CDRH on 12-8-2015

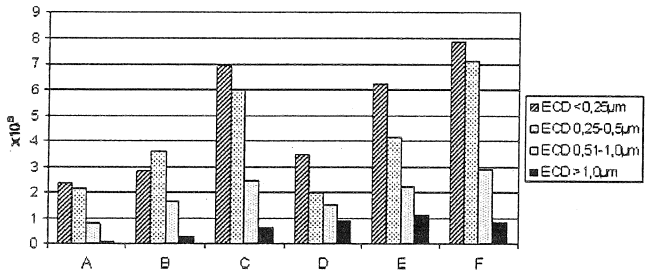

Fig. 4. Total number of analyzed particles partitioned by the size intervals (ECD < 0.25 μm, 0.25–0.5 μm, >0.5–1 μm and >1 μm).

wear simulator studies, in terms of wear volume and size of debris produced, have been shown to be similar to those found in early retrieved knee prostheses [21,31,32]. However, there is a dependence of wear on kinematic conditions in vitro [21,33,34]. Therefore, in this study the knee joint wear simulator was considered to be suitable to compare the wear of different polyethylene materials and designs under the same simulator conditions.

The size of the particles of UHMWPE vary from nanometer to millimeter [35,36], but the majority of the particles are in the submicron range [9,10,37]. In addition, the debris from conventional polyethylene (UHMWPE) in the total knee replacements has been found to be slightly larger than debris found in total hip replacements [32,35,37].

The morphology of the wear particles of all knee designs and their appropriate tibial inserts reported in this study were similar to those reported elsewhere in the literature. The predominance of submicron, round wear debris is consistent with other studies both in vitro and in vivo [6,10,17,18,38].

It is currently known that XPE leads to a reduction in wear of hip and knee prostheses [11–16]. However, little is known about the characteristics of XPE wear particles of the knee. Minoda et al. reported a wear particle analysis of failed XPE hip arthroplasty [39]. In this case, XPE generated fewer, smaller and rounder particles compared with the corresponding reported values for particles generated from UHMWPE. All the particles were round, and fibrils or shreds were not detected. Particle size (ECD) was 0.66 ± 0.40 μm (mean ± standard error). AR and R were 1.37 ± 0.26 and 1.44 ± 0.67 μm. In a recent study, Laurent et al. reported that XPE produced a > 90% reduction in the number of wear particles in all size ranges, and statistically significant ($P < 0.0001$) smaller average size particles than the conventional UHMWPE in the hip [40].

Fisher et al. isolated wear debris from fixed- and mobile-bearing knees and demonstrated that the moderately crosslinked material had a larger percentage volume of particles <1 μm compared with conventional polyethylene for the fixed-bearing prostheses [2]. Whereas the conventionally used polyethylene had only 17% of the volume of the debris <1 μm in size, the moderately crosslinked material had 50% of the volume of the debris <1 μm in size [2]. The overall wear volumes were 23 ± 6 mm^3/10^6 cycles for the conventional GUR 1020, 13 ± 4 mm^3/10^6 cycles for the moderately (5 Mrad) crosslinked fixed-bearing and 2 ± 1 mm^3/10^6 cycles for the moderately (5 Mrad) crosslinked mobile-bearing insert.

Essner at al. analyzed wear particles of, on the one hand, conventional and, on the other hand, sequentially irradiated and annealed polyethylene (X3™) from a knee joint simulator with a trend towards smaller AR of the XPE material, which indicates a slightly more rounded particle [41]. They could not find any differences in the particle length between the conventional and the XPE particles; however, XPE showed a greater width and ECD (0.43 ± 0.22 μm; 0.38 ± 0.10 μm for the conventional UHMWPE). However, those results were based on measurements of ~100 wear particles.

To the authors' knowledge, this study is the first direct comparison of six different knee designs (fixed and mobile bearings) including four XPE and two conventional UHMWPE. Nearly 100,000 particles of six different knee designs were analyzed, which seems to be a representative number of particles. Statistical analysis of comparisons of such high numbers of particles gives significant differences for all parameters, even if the difference is very small.

Currently, it is known that the pore size of the filter could influence the results of the particle analysis. Scott et al. [18,42] demonstrated that filtration through 0.05 μm is necessary to isolate a greater number of submicron wear particles. A filter with a pore size of 0.02 μm was used, and therefore it is noted that a majority of the particles could be isolated.

The results show similar mean diameters and ECD for all the knee designs tested (Table 2). It could not be confirmed that "crosslinking" itself leads to smaller wear particles. Furthermore, the trend of decreasing ECD with increasing radiation dose which is described in other reports in the literature [2,17] could not be found in this study. Knee design C, tested with a moderately crosslinked insert, shows relatively smaller particles than knee design B, tested with a highly crosslinked insert. This might be due to the different knee designs or to the different manufacturing processes of the tibial inserts.

But it is evident that the LCS® design tends towards larger mean diameters, ECD and areas for XPE as well as for the UHMWPE inserts (Table 2). The combination of the Scorpio® design with the X3™ insert tended towards smaller particles, even if the difference was only a few nanometers in size.

In synovial fluids of patients one year after implantation of 22 well-functioning total knee prostheses (11 mobile-bearing type, 11 posterior-stabilized type; 2.5 Mrad irradiation), Minoda et al. found a particle size (ECD) of 0.81 ± 0.12 μm in mobile-bearing types and 0.78 ± 0.08 μm in posterior-stabilized types [43]. The differences in these parameters between the two groups were not statistically significant.

The role of particulate debris in cellular response and ultimately osteolysis appears to be a complex cascade [1].

Questions? Contact FDA/CDRH/OCE/DID at CDRH-FOISTATUS@fda.hhs.gov or 301-796-8118

Records processed under FOIA Request #2014-8015; Released by CDRH on 12-8-2015

In vitro and in vivo studies found stronger response to submicron-size than to larger particles [44–46], to elongated than to globular particles [30,47], and to large numbers of particles [48,49].

Green et al. reported that already small differences in the size range (mean size 0.24 μm vs 0.45 μm and 1.71 μm) lead to a different reaction of the macrophages [50]. The particles with a mean size of 0.24 μm were the most reactive [50]. It remains unclear whether the extremely small differences in the size distributions in the present study are indicative of different biological activities in vivo.

Revell et al. found that the number of UHMWPE particles released into the joint space is linked to the presence and severity of osteolysis [51]. It is important to note that the number of particles in a given total volume increases as the particle size decreases. These findings suggest the possibility that the particle generation rate in numbers may be an equally critical parameter in the osteolytic cascade.

In the present study, the combination of the Scorpio® design with the X3™ insert, the Natural Knee® II design with the Durasul™ insert, and the LCS® design with the 5 Mrad crosslinked insert (which is not an actual product and is never intended to be) showed statistically significant ($P < 0.05$) reduced numbers of particles (Fig. 3). The combination of the Scorpio® design with the X3™ insert seems to lead to a slightly higher percentage of small particles, but with a marked reduction in the total number of generated wear particles. Therefore, the total number of particles <0.5 μm (ECD) is still very low compared with the other knee designs tested.

Although SEM is a traditionally used method of characterizing wear particles [18,29], the height of particulate debris cannot be conveniently measured by SEM. Therefore, the wear particles were assumed to be spherical in shape [52]. However, this approximation may influence the results, especially the calculation of the total number of particles.

A complex network of cellular pathogenesis is implicated in the development of periprosthetic osteolysis in response to wear debris [1]. Other factors, including particle surface texture as well as surface chemistry, could influence the cellular response. Therefore, further investigation in adequate in vivo models is mandatory to clarify the biological activity of the wear debris isolated in this study.

In contrast to THA, there are only few clinical data available in TKA using crosslinked polyethylene [53]. In a recent study, Hodrick et al. reviewed retrospectively the clinical and radiographic outcomes of 200 patients (100 Natural Knee® II designs with Durasul™ inserts and 100 Natural Knee® II designs with standard UHMWPE) with a 5-year follow-up [53]. Compared with the standard group, there were no reoperations related to osteolysis in the XPE group. Owing to the lack of clinical data in TKA, especially because there are no clinical data available for the annealed variety (X3™), further studies are needed.

5. Conclusion

The number, shape and size of conventional UHMWPE and XPE particles isolated from six different knee designs running in a knee joint simulator were examined. The particles for all knee designs were approximately round and few fibrillar. A higher radiation dose in itself did not lead to smaller particles. The LCS® design showed slightly larger particles than the other designs for the XPE as well as for the UHMWPE inserts. Overall, the NexGen® design with the Prolong™ insert showed a high number of particles in a small size which could be, according to the literature [1,44,46,48,51], a predictor for a higher biological reactivity. The Scorpio® design with the X3™ insert produced the lowest number of particles in the biologically active size range.

Acknowledgements

This study was supported by the private foundation for medical research "Dr.-Auguste-Schaedel-Dantscher" and Stryker Orthopedics.

References

[1] Purdue PE, Koulouvaris P, Potter HG, Nestor BJ, Sculco TP. The cellular and molecular biology of periprosthetic osteolysis. Clin Orthop Relat Res 2007;454:251–61.

[2] Fisher J et al. Wear, debris, and biologic activity of cross-linked polyethylene in the knee: benefits and potential concerns. Clin Orthop Relat Res 2004;428:114–9.

[3] Campbell P, Doorn P, Dorey F, Amstutz HC. Wear and morphology of ultra-high molecular weight polyethylene wear particles from total hip replacements. Proc Inst Mech Eng [H] 1996;210(3):167–74.

[4] Muratoglu OK, Ruberti J, Melotti S, Spiegelberg SH, Greenbaum ES, Harris WH. Optical analysis of surface changes on early retrievals of highly cross-linked and conventional polyethylene tibial inserts. J Arthroplasty 2003;18(7 Suppl 1):42–7.

[5] Wright TM. Polyethylene in knee arthroplasty: what is the future? Clin Orthop Relat Res 2005;440:141–8.

[6] Amstutz HC, Campbell P, Kossovsky N, Clarke IC. Mechanism and clinical significance of wear debris-induced osteolysis. Clin Orthop Relat Res 1992;276:7–18.

[7] Howie DW, Vernon-Roberts B, Oakeshott R, Manthey B. A rat model of resorption of bone at the cement-bone interface in the presence of polyethylene wear particles. J Bone Joint Surg Am 1988;70(2):257–63.

[8] Schmalzried TP, Jasty M, Harris WH. Periprosthetic bone loss in total hip arthroplasty. Polyethylene wear debris and the concept of the effective joint space. J Bone Joint Surg Am 1992;74(6):849–63.

[9] Shanbhag AS, Jacobs JJ, Glant TT, Gilbert JL, Black J, Galante JO. Composition and morphology of wear debris in failed uncemented total hip replacement. J Bone Joint Surg Br 1994;76(1):60–7.

[10] Campbell P, Ma S, Yeom B, McKellop H, Schmalzried TP, Amstutz HC. Isolation of predominantly submicron-sized UHMWPE wear particles from periprosthetic tissues. J Biomed Mater Res 1995;29(1):127–31.

[11] Digas G, Karrholm J, Thanner J, Malchau H, Herberts P. Highly cross-linked polyethylene in cemented THA: randomized study of 61 hips. Clin Orthop Relat Res 2003;417:126–38.

[12] McKellop H, Shen FW, Lu B, Campbell P, Salovey R. Development of an extremely wear-resistant ultra high molecular weight polyethylene for total hip replacements. J Orthop Res 1999;17(2):157–67.

Questions? Contact FDA/CDRH/OCE/DID at CDRH-FOISTATUS@fda.hhs.gov or 301-796-8118

Records processed under FOIA Request #2014-8015; Released by CDRH on 12-8-2015

[13] Muratoglu OK, Wannomae K, Christensen S, Rubash HE, Harris WH. Ex vivo wear of conventional and cross-linked polyethylene acetabular liners. Clin Orthop Relat Res 2005;438:158–64.
[14] Shen FW, McKellop H. Surface-gradient cross-linked polyethylene acetabular cups: oxidation resistance and wear against smooth and rough femoral balls. Clin Orthop Relat Res 2005;430:80–8.
[15] Akagi M, Asano T, Clarke IC, Niiyama N, Kyomoto M, Nakamura T, et al. Wear and toughness of crosslinked polyethylene for total knee replacements: a study using a simulator and small-punch testing. J Orthop Res 2006;24(10):2021–7.
[16] Asano T, Akagi M, Clarke IC, Masuda S, Ishii T, Nakamura T. Dose effects of cross-linking polyethylene for total knee arthroplasty on wear performance and mechanical properties. J Biomed Mater Res B Appl Biomater 2007;83(2):615–22.
[17] Endo M, Tipper JL, Barton DC, Stone MH, Ingham E, Fisher J. Comparison of wear, wear debris and functional biological activity of moderately crosslinked and non-crosslinked polyethylenes in hip prostheses. Proc Inst Mech Eng [H] 2002;216(2):111–22.
[18] Scott M, Morrison M, Mishra SR, Jani S. Particle analysis for the determination of UHMWPE wear. J Biomed Mater Res B Appl Biomater 2005;73(2):325–37.
[19] Ries MD, Pruitt L. Effect of cross-linking on the microstructure and mechanical properties of ultra-high molecular weight polyethylene. Clin Orthop Relat Res 2005;440:149–56.
[20] Oral E, Wannomae KK, Hawkins N, Harris WH, Muratoglu OK. Alpha-tocopherol-doped irradiated UHMWPE for high fatigue resistance and low wear. Biomaterials 2004;25(24):5515–22.
[21] McEwen HM, Fisher J, Goldsmith AA, Auger DD, Hardaker C, Stone MH. Wear of fixed bearing and rotating platform mobile bearing knees subjected to high levels of internal and external tibial rotation. J Mater Sci Mater Med 2001;12(10–12):1049–52.
[22] McEwen HM, Barnett PI, Bell CJ, Farrar R, Auger DD, Stone MH, et al. The influence of design, materials and kinematics on the *in vitro* wear of total knee replacements. J Biomech 2005;38(2):357–65.
[23] Cheng CK, Huang CH, Liau JJ, Huang CH. The influence of surgical malalignment on the contact pressures of fixed and mobile bearing knee prostheses—a biomechanical study. Clin Biomech (Bristol, Avon) 2003;18(3):231–6.
[24] Ho FY, Ma HM, Liau JJ, Yeh CR, Huang CH. Mobile-bearing knees reduce rotational asymmetric wear. Clin Orthop Relat Res 2007;462: 143–9.
[25] Tamura J et al. Micro-wear patterns on UHMWPE tibial inserts in total knee joint simulation. J Biomed Mater Res 2002;61(2):218–25.
[26] International Standard ISO/FDIS 14243. Implants for surgery—wear of total knee-joint-prostheses—Part 1: Loading and displacement parameters for wear-testing machines with load control and corresponding enviromental conditions for tests, 2002.
[27] International Standard ISO/FDIS 14243. Implants for surgery—wear of total knee-joint-prostheses—Part 2: Methods of measurement, 2000.
[28] Niedzwiecki S, Klapperich C, Short J, Jani S, Ries M, Pruitt L. Comparison of three joint simulator wear debris isolation techniques: acid digestion, base digestion, and enzyme cleavage. J Biomed Mater Res 2001;56(2):245–9.
[29] International Standard ISO/FDIS 17853. Wear of implant particles—Polymer and metal wear particles—Isolation, characterization and quantification, 2002.
[30] Sieving A, Wu B, Mayton L, Nasser S, Wooley PH. Morphological characteristics of total joint arthroplasty-derived ultra-high molecular weight polyethylene (UHMWPE) wear debris that provoke inflammation in a murine model of inflammation. J Biomed Mater Res A 2003;64(3):457–64.
[31] Barnett PI, McEwen HM, Auger DD, Stone MH, Ingham E, Fisher J. Investigation of wear of knee prostheses in a new displacement/force-controlled simulator. Proc Inst Mech Eng [H] 2002;216(1): 51–61.
[32] Howling GI, Barnett PI, Tipper JL, Stone MH, Fisher J, Ingham E. Quantitative characterization of polyethylene debris isolated from periprosthetic tissue in early failure knee implants and early and late failure Charnley hip implants. J Biomed Mater Res 2001;58(4):415–20.
[33] Muratoglu OK, Bragdon CR, Jasty M, O'Connor DO, Von Knoch RS, Harris WH. Knee-simulator testing of conventional and cross-linked polyethylene tibial inserts. J Arthroplasty 2004;19(7):887–97.
[34] Affatato S, Leardini W, Rocchi M, Toni A, Viceconti M. Investigation on wear of knee prostheses under fixed kinematic conditions. Artif Organs 2008;32(1):13–8.
[35] Schmalzried TP, Campbell P, Schmitt AK, Brown IC, Amstutz HC. Shapes and dimensional characteristics of polyethylene wear particles generated in vivo by total knee replacements compared to total hip replacements. J Biomed Mater Res 1997;38(3):203–10.
[36] Wright TM, Rimnac CM, Stulberg SD, Mintz L, Tsao AK, Klein RW, et al. Wear of polyethylene in total joint replacements. Observations from retrieved PCA knee implants. Clin Orthop Relat Res 1992;276:126–34.
[37] Benz EB, Federman M, Godleski JJ, Bierbaum BE, Thornhill TS, Spector M. Transmission electron microscopy of intracellular particles of polyethylene from joint replacement prostheses: size distribution and cellular response. Biomaterials 2001;22(21):2835–42.
[38] Jasty M, Bragdon CR, Lee KR, Hanson AE, Goetz DD. Wear of polyethylene cups in THR: Analysis of 159 cups retrieved at revision surgery or autopsy. Trans Orthop Res Soc 1993;18:291.
[39] Minoda Y et al. Wear particle analysis of highly crosslinked polyethylene isolated from a failed total hip arthroplasty. J Biomed Mater Res B Appl Biomater 2008;86B(2):501–5.
[40] Laurent MP, Johnson TS, Crowninshield RD, Blanchard CR, Bhambri SK, Yao JQ. Characterization of a highly cross-linked ultrahigh molecular-weight polyethylene in clinical use in total hip arthroplasty. J Arthroplasty 2008;23(5):751–61.
[41] Essner A, Herrera L, Yau SS, Wang A, Dumbleton JH, Manley MT. Sequentially crosslinked and annealed UHMWPE CR knee wear. Trans Orthop Res Soc 2005:312.
[42] Scott M, Widding K, Jani S. Do current wear particle isolation procedures underestimate the number of particles generated by prosthetic bearing components? Wear 2001;251:1213–7.
[43] Minoda Y, Kobayashi A, Iwaki H, Miyaguchi M, Kadoya Y, Ohashi H, et al. Characteristics of polyethylene wear particles isolated from synovial fluid after mobile-bearing and posterior-stabilized total knee arthroplasties. J Biomed Mater Res B Appl Biomater 2004;71(1):1–6.
[44] Matthews JB, Besong AA, Green TR, Stone MH, Wroblewski BM, Fisher J, et al. Evaluation of the response of primary human peripheral blood mononuclear phagocytes to challenge with *in vitro* generated clinically relevant UHMWPE particles of known size and dose. J Biomed Mater Res 2000;52(2):296–307.
[45] Matthews JB, Green TR, Stone MH, Wroblewski BM, Fisher J, Ingham E. Comparison of the response of primary murine peritoneal macrophages and the U937 human histiocytic cell line to challenge with *in vitro* generated clinically relevant UHMWPE particles. Biomed Mater Eng 2000;10(3–4):229–40.
[46] Ingham E, Fisher J. Biological reactions to wear debris in total joint replacement. Proc Inst Mech Eng [H] 2000;214(1):21–37.
[47] Yang SY, Ren W, Park Y, Sieving A, Hsu S, Nasser S, et al. Diverse cellular and apoptotic responses to variant shapes of UHMWPE particles in a murine model of inflammation. Biomaterials 2002;23(17): 3535–43.
[48] Revell PA. Tissue reactions to joint prostheses and the products of wear and corrosion. Curr Top Pathol 1982;71:73–101.
[49] Szivek JA, Anderson PL, Benjamin JB. Average and peak contact stress distribution evaluation of total knee arthroplasties. J Arthroplasty 1996;11(8):952–63.
[50] Green TR, Fisher J, Matthews JB, Stone MH, Ingham E. Effect of size and dose on bone resorption activity of macrophages by *in vitro* clinically relevant ultra high molecular weight polyethylene particles. J Biomed Mater Res 2000;53(5):490–7.
[51] Revell PA, Al-Saffar N, Kobayashi A. Biological reaction to debris in relation to joint prostheses. Proc Inst Mech Eng [H] 1997;211(2): 187–97.

Questions? Contact FDA/CDRH/OCE/DID at CDRH-FOISTATUS@fda.hhs.gov or 301-796-8118

Records processed under FOIA Request #2014-8015; Released by CDRH on 12-8-2015

[52] Scott M, Widding K, Ries M, Shanbhag A. Wear particle analyses of conventional and crosslinked UHMWPE tested in an anatomic hip simulator. Trans Orthop Res Soc 2001:p0001.

[53] Hodrick JT, Severson EP, McAlister DS, Dahl B, Hofmann AA. Highly crosslinked polyethylene is safe for use in total knee arthroplasty. Clin Orthop Relat Res 2008;466:2806–12.

Questions? Contact FDA/CDRH/OCE/DID at CDRH-FOISTATUS@fda.hhs.gov or 301-796-8118

Records processed under FOIA Request #2014-8015; Released by CDRH on 12-8-2015

Reduction of total knee replacement wear with vitamin E blended highly cross-linked ultra-high molecular weight polyethylene

C Vaidya[1], **E Alvarez**[1], **J Vinciguerra**[2], **D A Bruce**[1], and **J D DesJardins**[1*]
[1]Clemson University, Clemson, South Carolina, USA
[2]DJO Surgical, Austin, Texas, USA

The manuscript was received on 16 November 2009 and was accepted after revision for publication on 28 May 2010.

DOI: 10.1243/09544119JEIM774

Abstract: Ultra-high molecular weight polyethylene (UHMWPE) is a common bearing component in total knee replacement (TKR) implants, and its susceptibility to wear continues to be the long-term limiting factor in the life of these implants. This study hypothesized that in TKR systems, a highly cross-linked (HXL) UHMWPE blended with vitamin E will result in reduced wear as compared to a direct compression-moulded (DCM) UHMWPE. A wear simulation study was conducted using an asymmetric lateral pivoting '3D Knee' design to compare the two inserts. The highly cross-linked UHMWPE was aged prior to the testing and force-controlled wear testing was carried out for 5 million cycles using a load-controlled ISO-14243 standard at a frequency of 1 Hz on both groups. Gravimetric measurements of DCM UHMWPE (4.4 ± 3.0 mg/million cycles) and HXL UHMWPE with vitamin E (1.9 ± 1.9 mg/ million cycles) showed significant statistical differences ($p < 0.01$) between the wear rates. Wear modes and surface roughness for both groups revealed no significant dissimilarities.

Keywords: wear, TKR, highly cross-linked UHMWPE with vitamin E, force-controlled simulator, GUR 1020

1 INTRODUCTION

The most common limiting factor in the performance of total knee replacement (TKR) joints has been the wear of ultra-high molecular weight polyethylene (UHMWPE) used as a bearing component. The efforts to reduce the wear of this polymer led to first-generation cross-linked UHMWPEs, which were irradiated with gamma radiation to form C–C bonds between polymer chains [**1**]. The cross-linking of UHMWPE reduced plastic deformation, resulting in less wear than in a conventional UHMWPE. Radiation cross-linking, however, generated residue free radicals that caused oxidative degeneration of the polyethylene, which has been shown to increase highly cross-linked (HXL) UHMWPE wear rates if allowed to oxidize. To overcome this, post-irradiation thermal treatment was proposed, which eliminated the residue free radicals, thereby stabilizing the cross-linked UHMWPE oxidatively. One such study compared wear rates of aged and unaged conventional UHMWPE with HXL UHMWPE [**2**]. The wear rate of thermally treated and aged HXL UHMWPE was found to be significantly lower than either the aged or unaged conventional UHMWPE [**3**]. Thermal treatment, however, has been found to decrease the fatigue strength of the cross-linked UHMWPE [**4**]. Second generation cross-linked UHMWPEs were then introduced in which the residue free radicals were stabilized by the addition of vitamin E, which is a natural antioxidant. The vitamin E doping is expected to inhibit oxidation, while maintaining the mechanical properties of the polyethylene in the long term, thereby reducing wear [**5–7**]. For example, pin-on-disc wear testing and hip simulator testing has shown that vitamin E stabilized irradiated UHMWPE exhibits lower wear rates as compared to conventional UHMWPE materials [**2, 8**]. Wannomae *et al.* [**9**] compared wear rates of aged UHMWPE doped with vitamin E and

*Corresponding author: Department of Bioengineering, Clemson University, 401 Rhodes Building, Clemson, SC 29634, USA.
email: jdesjar@clemson.edu*

Questions? Contact FDA/CDRH/OCE/DID at CDRH-FOISTATUS@fda.hhs.gov or 301-796-8118

Records processed under FOIA Request #2014-8015; Released by CDRH on 12-8-2015

conventional UHMWPE using a unidirectional reciprocating motion simulator that emulates knee motion and found that there was a significant difference in their wear rates. Specifically, no pitting or delamination was found in the vitamin E stabilized UHMWPE inserts in their study. In a separate study by Teramura *et al.* [**10**], a knee simulator was used to compare the wear performance of conventional UHMWPE with an unaged vitamin E added conventional UHMWPE. Their results showed lower wear volume in the vitamin E stabilized UHMWPE than in the conventional UHMWPE; however, the vitamin E was present in a conventional UHMWPE and not in a highly cross-linked UHMWPE.

Over the last few years, many accelerated ageing methods have been developed and standardized to simulate *in vivo* and shelf ageing of the polyethylene. Ageing is also a good indication of how oxidation of polyethylene can affect its wear behaviour. Wannomae *et al.* [**9**] conducted a knee simulator wear testing study and found that ageing of a conventional UHMWPE showed increased levels of oxidation and delamination after a 5 million cycles wear test, whereas aged HXL UHWMPE did not show any delamination after 5 million cycles. Highly cross-linked vitamin E blended UHMPE inserts in the present study were thus subjected to artificial ageing to increase the levels of oxidation, whereas the conventional UHMWPE inserts were left unaged as the effects of ageing on a conventional UHMWPE insert are significant and lead to failure of the inserts [**11**]. In the present study, the process is a blend wherein the vitamin E is blended into the UHMWPE powder prior to consolidation. It is then compressed into sheets, cross linked, and then machined into the final part.

The objective of the present study was to find if there is a better alternative to the conventional UHMWPE that is currently in use, which would possess lower wear rates than that of a HXL polyethylene under oxidatively challenged conditions. The authors hypothesized that vitamin E blended HXL UHMWPE inserts will exhibit a lower wear rate as compared to standard direct compression moulded (DCM) UHMWPE inserts under physiologic loading during TKR simulation.

2 MATERIALS AND METHODS

Eight 3D Knee (DJO Surgical, Texas) TKR systems were prepared for wear testing in this study. Eight CoCrMo femoral components (size 6, left) were paired with four HXL–VitE UHMWPE and four DCM UHMWPE tibial inserts (GUR1020, size 6, left, 11 mm). Prior to the test, all tibial inserts were visually inspected for damage and wear. They were cleaned according to ASTM F1715 cleaning protocol and baseline weights were measured ($\pm$ 0.1 mg, Sartorious Corporation, New York). The HXL–VitE UHMWPE inserts were subjected to accelerated ageing according to ASTM F2003 protocol by exposing the tibial inserts to an oxygen environment at 5 atm, 70 °C for 14 days. Following ageing, the inserts were visually inspected for damage, weighed again using the same scale, and monitored until off-gassing was complete and the specimen weights reached the pre-ageing values.

Non-contact surface profilometry was performed on the femoral components and tibial inserts at points where contact during loading was likely to occur (four points per condyle, $n = 8$; refer to Fig. 1) at 25× magnification using a Wyko NT2000 profilometer (Wyko Corp, Tucson, Arizona). Measurements of arithmetic average roughness R_a, root mean square roughness R_q, and maximum peak-to-valley height R_t were recorded.

Alignment of tibial components relative to the femoral components was conducted as per the literature [**12**]. Simulator buffer springs were set to 20 N/mm anterior/posterior (A/P) translational resistance and 0.28 N m/deg internal/external (I/E) rotational resistance with no laxity gap for the course of the test [**13**]. Both sets of implants were aligned identically to ensure that the test conditions remained the same. The axial compressive forces, A/P load, and I/E torques were provided pneumatically and according to the load-corrected ISO standard at a frequency of 1 Hz.

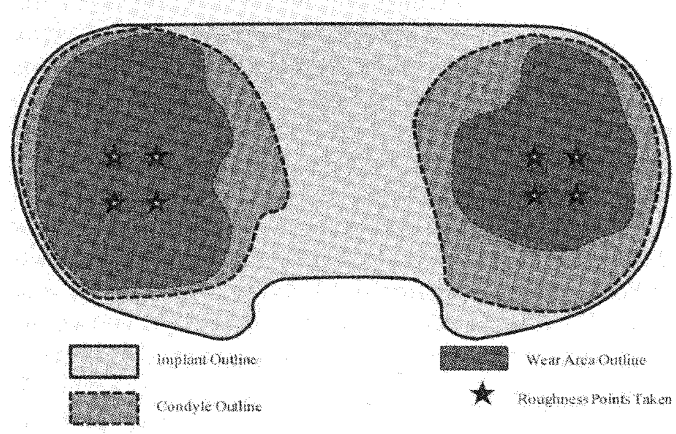

Fig. 1 A schematic diagram showing the locations of the surface roughness measurements on the polyethylene tibial insert and the femoral component

Questions? Contact FDA/CDRH/OCE/DID at CDRH-FOISTATUS@fda.hhs.gov or 301-796-8118

Records processed under FOIA Request #2014-8015; Released by CDRH on 12-8-2015

The unaged DCM and aged HXL–VitE UHMWPE specimens were tested serially on the same Instron-Stanmore KC four-station force-controlled wear-testing simulator for 5 million cycles each using a load-corrected ISO-14243-1 standard at a frequency of 1 Hz. Four additional inserts from each group were used as loaded ($n = 2$) (static load of 165 lb [74.8 KG]) and unloaded soaked controls ($n = 2$) to correct for weight changes caused due to immersion in lubricant fluid. A 25 per cent concentration of defined bovine calf serum (HyClone, Logan, Utah) with 0.2 per cent sodium azide (NaN3, Fisher Scientific: S227-100) was diluted with ultra-pure deionized water and used as lubricant for this test. The lubricant was replaced every 0.5 million cycles. The temperature of the testing environment was kept at $37 \pm 2\,^{\circ}$C to mimic physiological conditions.

Kinematic and kinetic data samples were recorded at 50 Hz for 15 s every 24 h (~ 84 000 cycles) to ensure that the simulator performance remained within ISO standards. The kinetic and kinematic performance of the TKR systems was also assessed, which included A/P displacement, A/P implant shear reaction force, I/E tibial rotation, I/E implant shear reaction torque, A/P soft tissue loading, and I/E soft tissue loading torque.

After every 0.5 million cycles the UHMWPE inserts were cleaned according to the ASTM F-1715 cleaning protocol and visually inspected for any signs of delamination and wear. Following cleaning and visual inspection, each of the tibial inserts was weighed for measures of gravimetric loss.

Non-contact surface profilometry was performed on the experimental tibial inserts and the femoral components on the same points as had been conducted at the outset of the test (four points/condyle ($n = 8$) using a WYKO NT 2000 profilometer (Wyko Corporation, Tucson, Arizona)) to compare surface roughness parameters at every 1 million cycles.

All of the tibial inserts and femoral components were photographed after 5 million cycles. One tibial insert each from DCM and aged HXL–VitE UHMWPE groups was analysed using a variable pressure (30 Pa) scanning electron microscope (SEM) at 55× and 1000×. Statistical differences between UHMWPE groups for measures of wear rate, surface roughness, and simulator/implant kinematics/kinetics were assessed using Student's t-test at $p < 0.05$.

3 RESULTS

The simulator was able to maintain the ISO standard walking cycle within operating tolerances reported in the literature [**11**, **14**]. The average full-scale profiles over the gait cycle for flexion, axial load, A/P load, and I/E torque for both of the groups did not exceed 3.6, 2.3, 6.7, and 4.9 per cent, respectively. Figure 2 shows the average inputs for both the groups for 15 cycles at the beginning of the test. The A/P displacement and I/E rotation values for both the groups were in agreement and both groups confirmed the lateral pivot nature of the 3D Knee design (Fig. 3).

ASTM F2003 was shown to increase the weights of the aged HXL–VitE UHMWPE significantly by (4.9 ± 0.21 mg, $p > 0.05$), which required 13 days to stabilize before the start of testing. All soaked control specimens steadily gained weight (0.3 ± 1.2 mg per million cycles) during testing, with no noticeable differences between static loaded and unloaded soak control specimens. The weights of the tibial inserts were corrected for fluid adsorption by subtracting the averaged weights of the unloaded soaked controls.

At the end of 5 million cycles of wear testing the unaged DCM UHMWPE showed 4.4 ($\pm$ 3.0) mg average weight loss per million cycles, whereas aged HXL–VitE UHMWPE incurred an average wear rate of 1.9 ($\pm$ 1.9) mg per million cycles (Fig. 4). The wear rates were statistically different ($p < 0.01$). Figure 4 shows the weight changes of the two groups over 5 million cycles.

Owing to the initial machined surfaces of the aged HXL–VitE UHMWPE surfaces, roughness values at 0 million were statistically higher than the DCM surfaces (Table 1). The aged HXL–VitE UHMWPE and DCM UHMWPE showed statistically significant changes in surface roughness between 0 (679.9 ± 119.5 and 106.3 ± 22.4, respectively) and 5 million cycles (105.2 ± 24.3 and 82.5 ± 31.7, respectively) (84.5 per cent and 22.4 per cent reduction, respectively, Table 1, $p < 0.05$), whereas the femoral surfaces of both groups did not show significant changes in roughness over testing cycles. Scanning electron microscopy at 55× and 1000× confirmed polishing and burnishing to be the primary modes of wear in both the UHMWPE groups.

4 DISCUSSION

The loading conditions for both DCM and aged HXL–VitE UHMWPE showed nearly identical trends within ISO tolerance during the course of the 5 million cycle wear test. Studies have shown that the femoral surface roughness greatly contributes to the wear of polyethylene [**9**]. In this study, the femoral surfaces of both the groups did not show statistically significant changes at the end of the wear test. There-

Questions? Contact FDA/CDRH/OCE/DID at CDRH-FOISTATUS@fda.hhs.gov or 301-796-8118

Records processed under FOIA Request #2014-8015; Released by CDRH on 12-8-2015

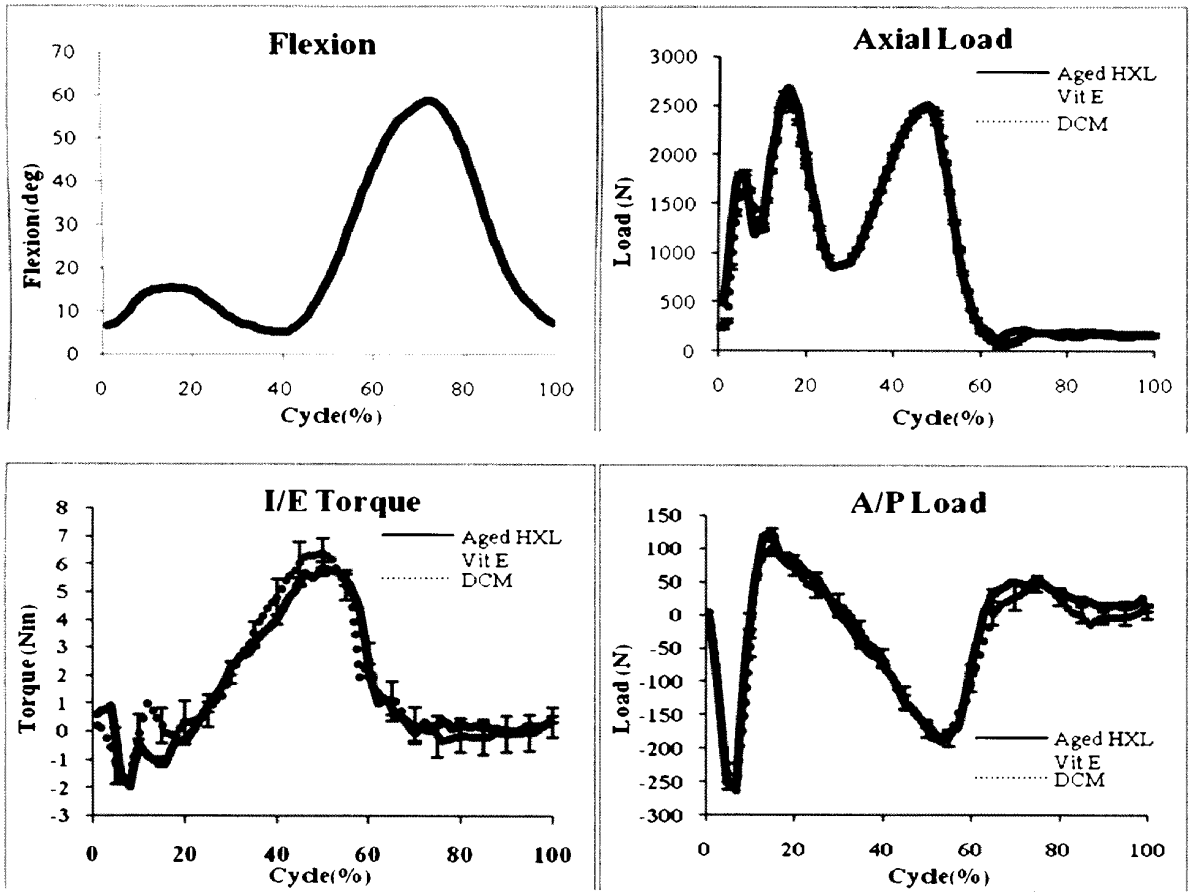

Fig. 2 Simulator inputs for Aged HXL-VitE and DCM groups at the start of the test

fore, the surface roughness of the femurs seems not to have contributed to the results obtained in this study.

The use of HXL–VitE UHMWPE in the 3D Knee design, even under aged conditions, was shown to reduce UHMWPE wear rates by 57 per cent as compared to unaged DCM UHMWPE. The results obtained in this study are similar to those of Teramura *et al.* [**10**] who reported a 45 per cent reduction in UHMWPE wear volume of vitamin E added UHMWPE TKR compared with that of conventional UHMWPE inserts. Significant differences in methodology include Teramura et al's use of ISO displacement-controlled simulation on a TKR system with a Ti–6Al–4V femoral component and flat tibial UHMWPE components made from GUR1050, which were not sterilized, highly cross-linked, or aged before testing. Titanium alloys, although extremely biocompatible and corrosion resistant, are known to have poor wear resistance and low shear strength. Furthermore, the resulting wear debris and metal ions arising from the gradual degradation of these metal alloys lead to implant failure [**15–17**]. This could be one of the reasons why this study saw better wear rate results than the study performed by Teramura *et al.* Specific methodology and materials contributions to the increased reduction in wear between the two tests are of interest for future studies.

Accelerated ageing has been described as a 'severe oxidative challenge' [**18**]. The accelerated ageing performed on the aged HXL–VitE UHMWPE for 14 days is designed to cause higher levels of surface degradation than seen in implants shelf aged for a duration of 5 years [**19**]. The HXL–VitE UHMWPE inserts were therefore subjected to a substantially greater degree of oxidative stress, prior to testing, as compared to DCM UHMWPE. The combination of high cross-linking and vitamin E blending worked well in this study to reduce the wear rate of the UHMWPE inserts significantly. Studies have shown delamination in tibial inserts that have undergone accelerated ageing and knee simulator wear testing; however, no such delamination was observed in the aged HXL–VitE UHMWPE inserts in this study. DCM UHMWPE was not subjected to accelerated ageing in this study, as it is already known that it shows delamination and wear when subjected to oxidation

Questions? Contact FDA/CDRH/OCE/DID at CDRH-FOISTATUS@fda.hhs.gov or 301-796-8118

Records processed under FOIA Request #2014-8015; Released by CDRH on 12-8-2015

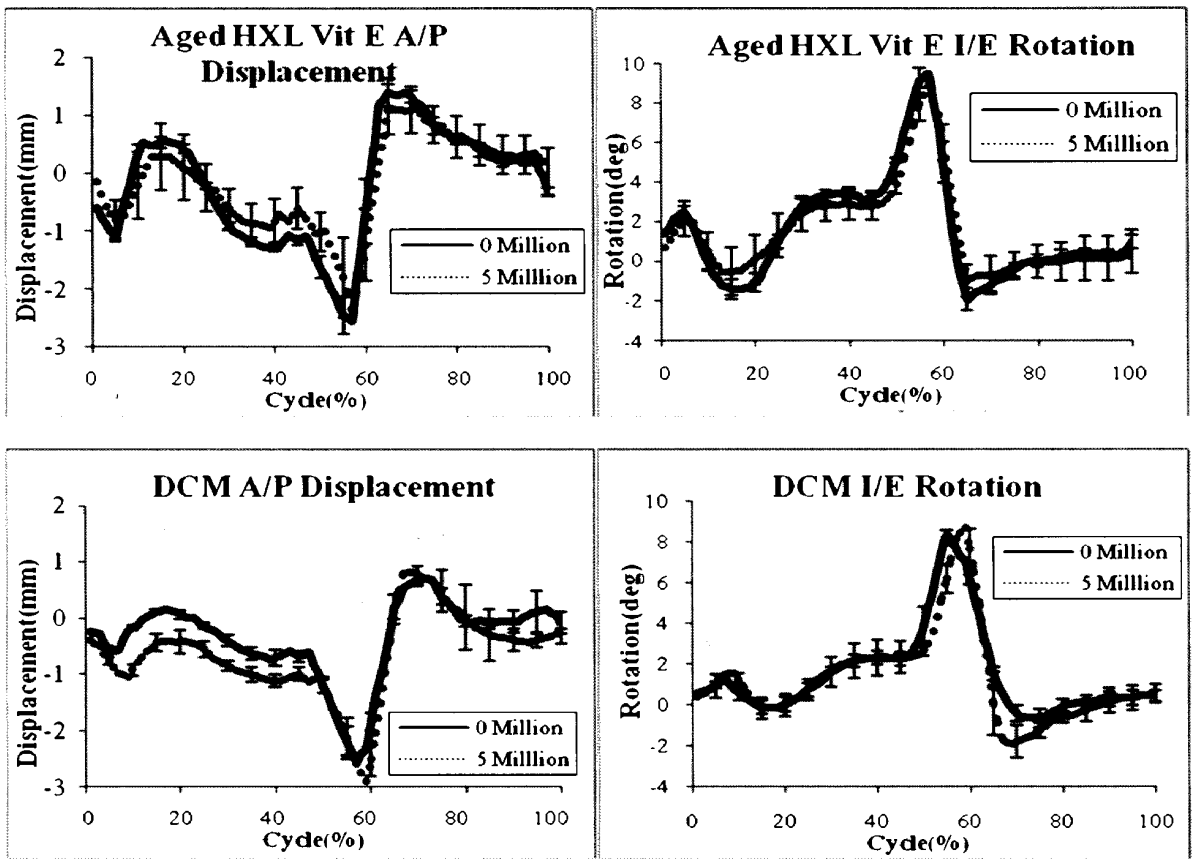

Fig. 3 A/P displacement and I/E rotation of the two groups at 0 and 5 million cycles

[**11, 20, 21**]. The relative contribution of the vitamin E blend versus the HXL processing of the UHMWPE on the resulting wear rate is unknown, and would lend itself to a future study to determine this relationship.

A slight increase in weight post ageing in the aged HXL–VitE UHMWPE was observed (4.9 ± 0.21 mg, $p > 0.05$). An increase in weight post ageing could affect the results of studies where low wear rates are observed. It therefore becomes crucial to monitor ageing to check for an increase in weight of the polyethylene. In this study, total weight loss measured 9.56 mg, with soaked control inserts accounting for 1.58 mg of the weight change. Undetected increases in weight during ageing could therefore influence resulting measures by as much as almost 50 per cent. Other studies have shown that UHMWPE inserts gain weight post sterilization with pressurized gas and can require approximately 14 days to stabilize [**22**]. This is in conjunction with the present authors' results, as in both cases UHMWPE was exposed to pressurized gas. This underlines the importance of allowing enough time for off-gassing post ageing.

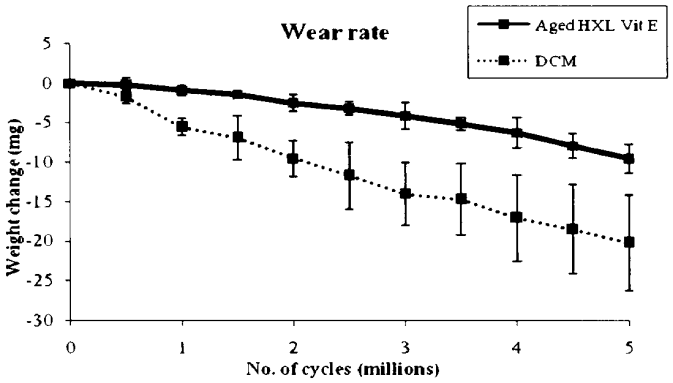

Fig. 4 Soak corrected weight change of Aged HXL-VitE and DCM groups over the 5 million cycles test

Moulded inserts show better wear performance as compared to machined inserts, as machined inserts are known to have a wear-in period owing to their relatively rougher surfaces [**13**]. In this study, although the aged HXL–VitE UHMWPE inserts were machined and the initial surface roughness values for aged HXL–VitE UHMWPE were found to be higher than DCM UHMWPE, they did not see any wear-in period. The wear data after the first 1 million cycles did not show a higher wear rate, which could occur

Questions? Contact FDA/CDRH/OCE/DID at CDRH-FOISTATUS@fda.hhs.gov or 301-796-8118

Records processed under FOIA Request #2014-8015; Released by CDRH on 12-8-2015

Table 1 Surface roughness parameters for the UHMWPE tibial surfaces

Surface	No. of cycles (million)	R_a (nm)	R_q (nm)
Aged HXL–VitE	0	679.9 ± 119.5*#	843.6 ± 136.6*#
Aged HXL–VitE	5	105.2 ± 24.3	134.2 ± 35.3
DCM	0	106.3 ± 22.4*	138.4 ± 27.9*
DCM	5	82.5 ± 31.7	110.4 ± 42.1

Note: * denotes a significant difference from the same surface at 5 million cycles; # denotes a significant difference from the DCM surface at the same time point ($p < 0.05$).

because of the machining marks wearing off. The surfaces of both DCM UHMWPE and aged HXL–VitE UHMWPE showed only polishing by the end of the test. No pitting or delamination was observed in the aged HXL–VitE UHMWPE inserts, which is in agreement with the results obtained by Wannomae *et al.* [**9**].

A vitamin E penetration assessment can be made using Fourier transform infrared spectroscopy (FTIR) (ASTM F2102-06 e1) to check whether full diffusion throughout the entire thickness of the HXL UHMWPE had taken place. Limiting the diffusion to the first few millimetres of UHMWPE has been shown to shift the oxidation below the subsurface where vitamin E levels are low [**8**, **23**]. This, coupled with oxidation assessment, will further our knowledge of whether a significant difference is observed post accelerated ageing and after completion of the wear test with regard to oxidation which, in turn, will help deduce specific contributions of aged HXL–VitE UHMWPE to observed reductions in wear.

5 CONCLUSIONS

This study hypothesized that in TKR systems, a HXL UHMWPE blened with vitamin E would result in reduced wear when compared to a DCM UHMWPE. Force-controlled ISO-14243-1 wear simulation was conducted using an asymmetric lateral pivoting 3D Knee design to test this typothesis. The HXL UHMWPE was ASTM-F2003 aged prior to the testing and wear testing was carried out for 5 million cycles at 1 Hz on both groups. Gravimetric measurements showed that use of aged HXL–VitE UHMWPE in the 3D Knee design (even under aged conditions) was shown to reduce UHMWPE wear rates by 57 per cent as compared to unaged DCM UHMWPE. Wear modes and surface roughness for both groups revealed no significant dissimilarities. The combination of high cross-linking and vitamin E blending worked well in this study to reduce the wear rate of the UHMWPE inserts significantly. This work supports the small volume of literature to date that indicates the addition of vitamin E to UHMWPE reduces the wear rates of these materials in TKR designs. Further work is necessary to deduce specific contributions of these two material variables to the observed reduction in wear.

ACKNOWLEDGEMENT

These studies were funded by DJO Surgical.

© Authors 2011

REFERENCES

1 **Tipper, J. L., Galvin, A. L., Williams, S., McEwen, H. M. J., Stone, M. H., Ingham, E.,** and **Fisher, J.** Isolation and characterization of UHMWPE wear particles down to ten nanometers in size from *in vitro* hip and knee joint simulators. *J. Biomed. Mater. Res., Part A*, 2006, **78A**(3), 473–480.

2 **Oral, E., Christensen, S. D., Malhi, A. S., Wannomae, K. K.,** and **Muratoglu, O. K.** Wear resistance and mechanical properties of highly cross-linked, ultrahigh-molecular weight polyethylene doped with vitamin E. *J. Arthroplasty*, 2006, **21**(4), 580–591.

3 **Muratoglu, O. K., Bragdon, C. R., O'Connor, D. O., Jasty, M.,** and **Harris, W. H.** A novel method of cross-linking ultra-high-molecular-weight polyethylene to improve wear, reduce oxidation, and retain mechanical properties: Recipient of the 1999 Hap Paul Award. *J. Arthroplasty*, 2001, **16**(2), 149–160.

4 **Oral, E., Malhi, A. S.,** and **Muratoglu, O. K.** Mechanisms of decrease in fatigue crack propagation resistance in irradiated and melted UHMWPE. *Biomater.*, 2006, **27**(6), 917–925.

5 **Costa, L., Brach, E. M., Bracco, P.,** and **Gallinaro, P.**. *In vivo* wear could be reduced by vitamin E stabilised UHMWPE. *J. Bone Joint Surg. Br.*, 2006, **88-B**(Suppl. I), 46.

6 **Oral, E.** and **Muratoglu, O. K.** Radiation cross-linking in ultra-high molecular weight polyethylene for orthopaedic applications. *Nucl. Instrum. Meth. Physics Res. Sec. B: Beam Interactions with Materials and Atoms*, 2007, **265**(1), 18–22.

7 **Oral, E., Rowell, S. L.,** and **Muratoglu, O. K.** The effect of alpha-tocopherol on the oxidation and free radical decay in irradiated UHMWPE. *Biomater.*, 2006, **27**(32), 5580–5587.

Questions? Contact FDA/CDRH/OCE/DID at CDRH-FOISTATUS@fda.hhs.gov or 301-796-8118

Records processed under FOIA Request #2014-8015; Released by CDRH on 12-8-2015

8 **Oral, E., Wannomae, K. K., Hawkins, N., Harris, W. H.,** and **Muratoglu, O. K.** Alpha-tocopherol-doped irradiated UHMWPE for high fatigue resistance and low wear. *Biomater.*, 2004, **25**(24), 5515–5522.

9 **Wannomae, K. K., Christensen, S. D., Micheli, B. R., Rowell, S. L., Schroeder, D. W.,** and **Muratoglu, O. K.** Delamination and adhesive wear behavior of (alpha)-tocopherol-stabilized irradiated ultrahigh-molecular-weight polyethylene. *J. Arthroplasty*, 2010, **25**(4), 635–643.

10 **Teramura, S., Sakoda, H., Terao, T., Endo, M. M., Fujiwara, K.,** and **Tomita, N.** Reduction of wear volume from ultrahigh molecular weight polyethylene knee components by the addition of vitamin E. *J. Orthop. Res.*, 2008, **26**(4), 460–464.

11 **DesJardins, J. D., Walker, P. S., Haider, H.,** and **Perry, J.** The use of a force-controlled dynamic knee simulator to quantify the mechanical performance of total knee replacement designs during functional activity. *J. Biomechanics*, 2000, **33**(10), 1231–1242.

12 **Affatato, S., Bersaglia, G., Rocchi, M., Taddei, P., Fagnano, C.,** and **Toni, A.** Wear behaviour of cross-linked polyethylene assessed in vitro under severe conditions. *Biomater.*, 2005, **26**(16), 3259–3267.

13 ISO/Cd 14243-1: *Implants for surgery: Wear of total knee joint prostheses, Part 1. Loading and displacement parameters for wear testing machines with load control and corresponding environmental conditions for test*, 1999 (International Organization for Standarization, London).

14 **DesJardins, J. D., Banks, S. A., Benson, L. C., Pace, T.,** and **LaBerge, M.** A direct comparison of patient and force-controlled simulator total knee replacement kinematics. *J. Biomechanics*, 2007, **40**(15), 3458–3466.

15 **American Society for Testing and Materials.** *Chemical and electrochemical aspects of biocompatibility of titanium and its alloys. Medical applications of titanium and its alloys: the material and biological issues*, 1996, ASTM Stp 1272, pp. 163–177 (American Society for Testing and Materials, Philadelphia, PA).

16 **Dearnley, P.** A review of metallic, ceramic and surface-treated metals used for bearing surfaces in human joint replacements. *Proc. IMechE, Part H: J. Engineering in Medicine*, 1999, **213**(2), 107–135. DOI: 10.1243/0954411991534843.

17 **Long, M.** and **Rack, H. J.** Titanium alloys in total joint replacement – a materials science perspective. *Biomater.*, 1998, **19**(18), 1621–1639.

18 **Greer, K., Schmidt, M.,** and **Hamilton, J.** The hip simulator wear of gamma-vacuum, gamma-air, and ethylene oxide sterilized UHMWPE following a severe oxidative challenge. *Trans. 44th Orthop. Res. Soc.*, 1998, **23**, 52.

19 **Lu, S., Buchanan, F. J.,** and **Orr, J. F.** Analysis of variables influencing the accelerated ageing behaviour of ultra-high molecular weight polyethylene (UHMWPE). *Polym. Testing*, 2002, **21**(6), 623–631.

20 **Hastings, R. S., Huston, D. E., Reber, E. W.,** and **Di Maio, W. G.** Knee wear testing of a radiation crosslinked and remelted UHMWPE. *Trans. Soc. Biomater.*, 1999, **XXII**, 328.

21 **Walker, P. S., Blunn, G. W., Perry, J. P., Bell, C. J., Sathasivam, S., Andriacchi, T. P., Paul, J. P., Haider, H.,** and **Campbell, P. A.** Methodology for long-term wear testing of total knee replacements. *Clin. Orthop. Related Res.*, 2000, **372**, 290–301.

22 **DesJardins, J. D., Hemmer, J., Matthews, M., Drews, M.,** and **LaBerge, M.** Wear and mechanical testing of supercritical carbon dioxide sterilized UHMWPE. In Proceedings of the 53rd Annual Meeting of the Orthopaedic Research Society, San Diego, California, 2007, p. 1785.

23 **Wright, T. M., Rimnac, C. M., Stulberg, S. D., Mintz, L., Tsao, A. K., Klein, R. W.,** and **McCrae, C.** Wear of polyethylene in total joint replacements: observations from retrieved PCA knee implants. *Clin. Orthop. Related Res.*, 1992, **276**, 126–134.

Questions? Contact FDA/CDRH/OCE/DID at CDRH-FOISTATUS@fda.hhs.gov or 301-796-8118

Records processed under FOIA Request #2014-8015; Released by CDRH on 12-8-2015

Polyethylene Wear Debris Produced in a Knee Simulator Model: Effect of Crosslinking and Counterface Material

Paul A. Williams,[1] Cindy M. Brown,[1] Riichro Tsukamoto,[2] Ian C. Clarke[1]

[1] Peterson Research Center, Loma Linda University, Loma Linda, California 92354

[2] Tsukamoto Orthopaedic Clinic, Tokyo, Japan

Received 30 January 2009; revised 28 May 2009; accepted 12 June 2009
Published online 2 October 2009 in Wiley InterScience (www.interscience.wiley.com). DOI: 10.1002/jbm.b.31491

Abstract: Polyethylene (PE) debris has been well studied in clinical retrievals and laboratory wear simulations of total hip replacements. However, little is known about PE debris from total knee replacements. In this study, we investigated the effects of crosslinking PE bearings and alternate counterface material. Mildly (35 kGy) and highly (70 kGy) crosslinked PE were studied in combination with CoCr and zirconia femoral counterfaces. Wear debris was isolated and its morphology characterized. Except for changes in PE debris size with the zirconia bearings, there were no morphological changes greater than 10%. The average submicron volume fraction decreased from about 65% to 45% with both increased crosslinking and changing counterface material from CoCr to zirconia. The averaged number of generated particles decreased by ~fourfold with increased crosslinking and threefold with changing counterface material from CoCr to zirconia. This showed that the degree of PE crosslinking and the choice of counterface material were important factors in the PE wear debris production in total knee simulator replacements. © 2009 Wiley Periodicals, Inc. J Biomed Mater Res Part B: Appl Biomater 92B: 78–85, 2010

Keywords: polyethylene; crosslinking; debris; knee; ceramic

INTRODUCTION

One of the principle goals in material science studies of total joint replacements is the reduction of wear, thereby reducing the risk of the bone disease termed osteolysis.[1–4] One such technology involves crosslinking of polyethylene (PE) bearings while taking steps to reduce the risk of oxidation.[5–8] Improved wear resistance of crosslinked PE has been well-demonstrated in both hip and knee bearings.[5,9–11] Gamma radiation (25–33 kGy) was originally introduced in 1977 for sterilization of PE hip cups. Now both laboratory and clinical data support the fact that PE wear could be reduced by 50–90% depending on the amount of crosslinking.[3] Similarly, crosslinked tibial inserts in total knee replacements (TKR) demonstrated 50% wear reduction in simulator studies with 70 kGy gamma-irradiated, highly crosslinked PE (HXPE).[9,11–15] The comparable reduction in hip simulator studies would be ~60%.[3]

The relationship between wear, the debris particles, and osteolysis is a complex issue.[16–21] The volumetric wear, number of particles, and volume fraction of submicron particles are important factors in the bioreactivity of the wear debris.[16,18,22] The submicron PE debris appears to be responsible for the bioreactive response involved in implant loosening (bone loss termed osteolysis).[16,17,19,22] Investigations of crosslinked PE hip bearings indicated that the wear debris decreased in size with increased crosslinking.[23–25] The largest decrease in particle diameter was ~50% when changing from noncrosslinked to 35 or 50 kGy crosslinked PE.[23,25,26] Crosslinking PE with more than 50 kGy of gamma irradiation appeared to decrease particle diameter by an additional 20% at most. However, it has been indicated that this size reduction could lead to higher bioreactivity.[16,18,19,27,28] It has also been suggested that this size decrease may offset any reduction in wear such that the osteolytic potential may be the same or higher.[19,20,22,24,29] Although the wear may be very low or nondetectable with some highly crosslinked bearings, large numbers of particles can still be generated.[26,30] Therefore, both the wear rate and the debris size are critical in determining the osteolytic potential.

PE wear in total knees has been reported as lower than in total hips.[22] The effect of crosslinking PE has been shown to be less in knees than that found in hips.[10,12,22] This difference in PE wear between knees and hips has been attributed to the differences in wear mechanisms.[10,22] The wear of PE

Correspondence to: P. A. Williams (e-mail: pwilliams@llu.edu)
Contract grant sponsor: Japan Medical Materials (JMM Inc., Osaka, Japan), Dr. Nakamura (Orthopaedic Surgery, Kyoto University, Japan), Western Center for Orthopaedics Research (Riverside, CA).

© 2009 Wiley Periodicals, Inc.

Questions? Contact FDA/CDRH/OCE/DID at CDRH-FOISTATUS@fda.hhs.gov or 301-796-8118

Records processed under FOIA Request #2014-8015; Released by CDRH on 12-8-2015

TABLE I. Summary of Noncrosslinked Polyethylene Wear Debris Isolated from Synovial Fluid of Patients with Medial-Pivot Knees[43]

Tibial Insert	Femoral Condyle	ECD (microns)	Numbers of Particles
Eto gas	CoCr	0.66 ± 0.06	$(57.0 \pm 28.2) \times 10^6$
	Alumina	0.78 ± 0.04	$(7.10 \pm 2.86) \times 10^6$

in knees is influenced by the kinematics, crosslinking, and conformity of the tibial insert.[9,10,31–34] The particulates produced in the knee joint also appear to be different from that of hips, tending to be slightly larger and more flakelike.[35–37] For moderately crosslinked (40 kGy) PE, the debris has been reported as mostly rounded submicron with a very small number of larger flake like particles.[38] PE bearings irradiated at 50 kGy yielded a submicron volumetric fraction of ~50% in a knee simulator with CoCr femoral condyles.[22] Highly crosslinked PE (>50 kGy) debris in the knee has not been extensively studied.

The role of ceramic bearings in reducing PE wear in hip joints has been somewhat controversial but there appeared to be clinical benefits.[39–41] Both alumina and zirconia ceramic knee components have been used in Asia for some time, but have not received FDA approval for use in the United States.[42–44] In the laboratory, knee simulator studies have indicated that ceramic counterfaces were much more effective at reducing PE wear than CoCr bearings.[11,45] Use of alumina bearings with noncrosslinked PE inserts generated fewer and more rounded particles compared to CoCr counterfaces.[43] The computed number of particles generated with the alumina/PE combination was eight times lower than the CoCr/PE combination (Table I). Although the particulates averaged 18% larger with alumina/PE, this difference was not statistically significant (Table I: $p = 0.12$).[43]

Figure 1. Image of total knee replacement specimens used in study. On the left in the picture is a CoCr femoral component, top center is a 70 kGy PE tibial insert, bottom center is a 35 kGy PE tibial insert, and right is a zirconia femoral component. [Color figure can be viewed in the online issue, which is available at www.interscience.wiley.com.]

A recent knee study showed that both increased crosslinking (35–70 kGy) and use of zirconia femoral condyles (Figure 1) reduced wear more than 60%.[11] It was also noted that the Y-TZP zirconia condyles did not exhibit phase transformation or other surface changes over five million cycle duration test.[46] However, very little is known about how PE debris production will be affected by use of crosslinked PE and ceramic material combinations in knee joints. Therefore, the objective of this study was to determine how increased PE crosslinking from 35 to 70 kGy and changing the counterface material from CoCr to zirconia would influence the particulate morphology in a knee wear model. The first hypothesis was that neither increased crosslinking (35; 70 kGy) nor counterface material (CoCr; zirconia) would significantly change debris morphology by more than 20%. The second hypothesis was that the submicron volume fractions would be ~50% or higher, implying that such a reduction in wear also represented a reduction in the particulate numbers, thereby lowering the osteolytic potential.[3,22,43]

MATERIALS AND METHODS

Lubricant samples were obtained from a prior knee simulator wear study.[11] The four implant groups (Table II) included CoCr (M) and zirconia ceramic (Zr) femoral components combined with 35 kGy (CXPE) and 70 kGy (HXPE) tibial inserts (Figure 1). A knee simulator (Shore Western Manufacturing, Monrovia, CA) was used with 20° flexion, 6 mm of anterior–posterior translation, and ±5° internal–external rotation. A Paul load profile with 2.6-kN peak load at 1.8 cycles/second were used and the lubricant was 50% alpha calf serum (20 mg of protein/mL) with EDTA added.[11] The lubricant samples selected at 2 and 4 Mc durations represented the stable, steady-state wear phase of the six million cycle (6 Mc) wear study.

Debris processing used a base (NaOH) for the protein digestion, a separation technique, and subsequent washing cycles for purification (Figure 2).[23,47,48] Debris samples were collected on 0.1-μm pore filters and mounted on SEM stubs. The specimens were imaged by SEM (Philips, XL30, FEG) and the micrographs processed for debris morphology (Image J software, NIH). Approximately 300–860 particles were analyzed per group (Tables III and IV). The equivalent circular diameter (ECD), aspect ratio (AR), and circular shape factor (CSF) were calculated.

Descriptive statistics were calculated and groups were compared using both parametric (one-way ANOVA with

TABLE II. Description of Knee Materials for Groups Studied

Group	Designation	Femoral Condyle	Tibial Insert
1	M-CXPE	CoCr	35 kGy XLPE
2	M-HXPE	CoCr	70 kGy XLPE
3	Zr-CXPE	Zirconia	35 kGy XLPE
4	Zr-HXPE	Zirconia	70 kgy XLPE

Questions? Contact FDA/CDRH/OCE/DID at CDRH-FOISTATUS@fda.hhs.gov or 301-796-8118

Records processed under FOIA Request #2014-8015; Released by CDRH on 12-8-2015

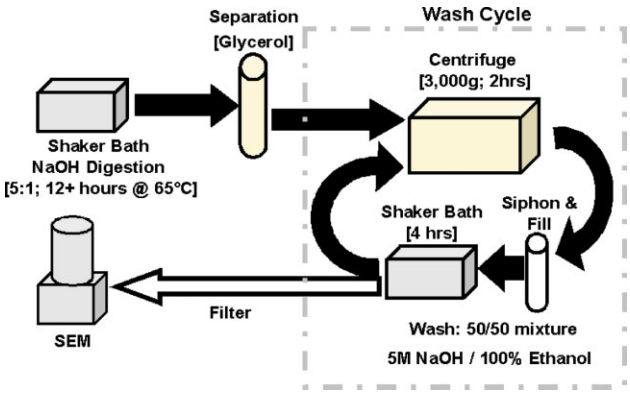

Figure 2. Schematic of the debris sample processing method used in isolating and separating the debris particulate from the serum lubricant. [Color figure can be viewed in the online issue, which is available at www.interscience.wiley.com.]

Tukey test for multiple comparisons) and nonparametric (Mann–Whitney) tests. To test for differences between 2 and 4 Mc, nonparametric statistics were used, but for differences between the four groups parametric multiple comparisons were required. To further characterize the debris morphology, box plots were performed on the ECD, AR, and CSF. It has been suggested that the size (ECD) distribution can be represented by a log-normal function.[49] Therefore, both number and volume fractions were generated and compared to log-normal distributions. The volumetric fractions were calculated as they directly related to wear rates (mm^3/Mc) and bioreactivity of the debris.[3,18,22] The number of particles generated was estimated from the volumetric wear rates and size distributions.[11,50] Number fractions were fitted to log-normal distributions and the Kolmogorov–Smirnov test was used to evaluate the goodness-of-fit.

RESULTS

With CoCr femoral condyles, debris morphology (size; shape) at 2 and 4 Mc showed little or no differences (<10%) between CXPE and HXPE inserts (Tables III and IV; Figures 3–5). With zirconia femoral condyles, the debris shape (AR; CSF) at 2 and 4 Mc also showed little difference (<10%) between CXPE and HXPE inserts (Figures 4 and 5). Compared to M-CXPE at 2 Mc, the Zr-CXPE reduced the median ECD by 15% whereas the Zr-HXPE inserts showed a 34% increase (Table III). This change meant that the debris size was ~50% larger at 2 Mc for Zr-HXPE compared to Zr-CXPE (Table III).

At 4 Mc duration, the only notable changes were that both Zr-CXPE and Zr-HXPE revealed a 13% reduction in ECD compared to M-CXPE controls (Table IV). This showed that there was no measurable difference (>10%) in debris size at 4 Mc for CXPE and HXPE with zirconia. Comparing the debris morphology between 2 and 4 Mc duration, the only notable changes were a 39% decrease in median ECD for Zr-HXPE compared to only 13% decrease for M-HXPE (Tables III and IV). For the CXPE, there was minimal decrease from 2 to 4 Mc with either CoCr or zirconia (Figure 3).

Because the largest particle was ~5 μm in size (ECD), the data consisted of submicron (<1 μm) and micron (1–5 μm) sized particles (Tables III and IV). Although the

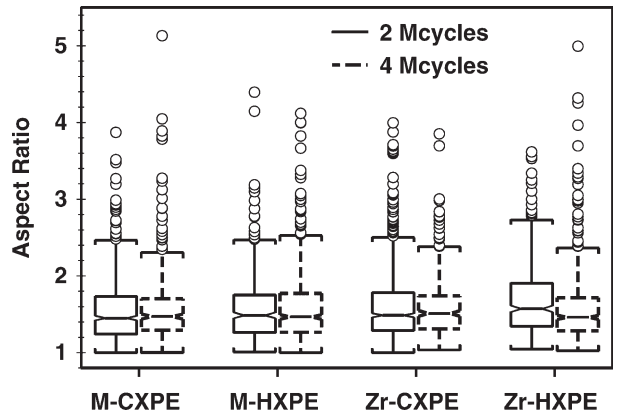

Figure 4. Box plot of aspect ratio for the four groups at 2 and 4 Mc.

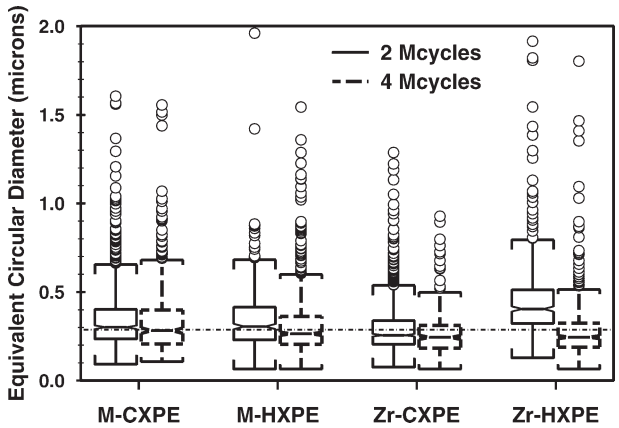

Figure 3. Box plot of ECD for the four groups at 2 and 4 Mc.

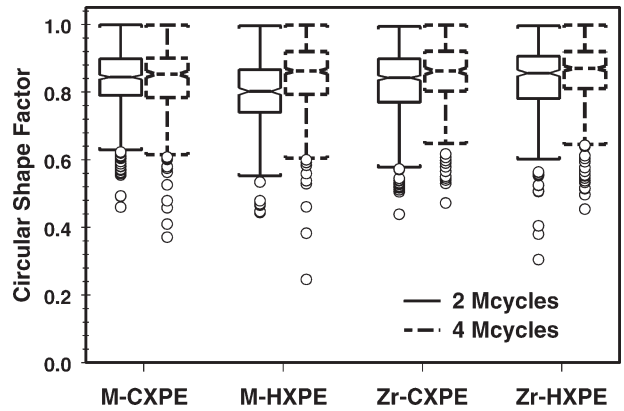

Figure 5. Box plot of the CSF for the four groups at 2 and 4 Mc.

Questions? Contact FDA/CDRH/OCE/DID at CDRH-FOISTATUS@fda.hhs.gov or 301-796-8118

Records processed under FOIA Request #2014-8015; Released by CDRH on 12-8-2015

TABLE III. Descriptive Statistics for the Debris for the Four Groups at 2Mc, with Number of Particles Measured (*N*), Mean ± 1 std, (Median), and [Minimum – Maximum]

	M-CXPE	M-HXPE	Zr-CXPE	Zr-HXPE
N	669	393	861	437
ECD (μ)	0.356 ± 0.202 (0.301) [0.092 – 1.605]	0.343 ± 0.181 (0.305) [0.065 – 1.961]	0.304 ± 0.240 (0.256) [0.075 – 3.862]	0.473 ± 0.349 (0.404) [0.128 – 5.204]
Aspect Ratio	1.55 ± 0.45 (1.45) [1.00 – 6.00]	1.57 ± 0.43 (1.49) [1.01 – 4.40]	1.60 ± 0.45 (1.49) [1.00 – 4.00]	1.69 ± 0.51 (1.57) [1.04 – 6.13]
CSF	0.834 ± 0.089 (0.844) [0.460 – 0.999]	0.796 ± 0.102 (0.802) [0.444 – 0.996]	0.826 ± 0.098 (0.842) [0.439 – 0.994]	0.835 ± 0.103 (0.856) [0.305 – 0.996]

micron-sized particles have been shown to be bioreactive, the submicron particles are considered the most bioreactive.[16,18,22,24,27] Therefore, the submicron particles were the main focus. Submicron number fractions demonstrated no specific sensitivity with respect to groups (Table V). However, submicron volume fractions showed differences between both groups and durations. With M-HXPE, the submicron volume fraction decreased from 2 to 4 Mc. The Zr-CXPE showed the opposite trend by increasing dramatically from 2 to 4 Mc (Table V). The Zr-HXPE demonstrated the lowest average submicron volume fraction of 45% compared to ~60% with the other groups (Table V).

Except for the Zr-CXPE with its particle generation showing a 3.3-fold increase from (2–4 Mc), the particulate numbers for the other groups were consistent at 2 and 4 Mc (Table VI). In general, changing from CoCr to zirconia yielded about a threefold decrease in the number of generated particles whereas increased PE crosslinking resulted in approximately a fourfold decrease (Table VI).

The number fractions for particle size (ECD) approximated a log-normal distribution (Figure 6). Statistical analysis showed that such data was significantly different ($p < 0.01$) from the log-normal distribution. ECD means estimated from the log-normal distribution (Table VII) were generally 13% lower than calculated from the debris data (Tables III and IV). The log-normal distribution also poorly represented the volume fractions from 1 to 2 μm (Figure 7). The volume fraction of the log-normal distribution approached zero similar to the number distribution (Figure 6). However, the data sets indicated that large particles (>1 μm) represented a higher volume fraction than predicted by the log-normal distribution (Figure 7).

DISCUSSION

The specific knee used in the previous study (Figure 1) used a bi-surface design with a spherical cam that engages at 80° of flexion, however, because the flexion was 20° this cam had no influence on the wear.[11,46] Although the PE wear rates were less than those for a total hip under similar conditions, this is common due to the differences in kinematics and wear mechanisms between total hips and total knees.[9,10,12,22,31] The wear rates from the previous knee simulator study were consistent with those from other knee simulator studies with similar designs under similar conditions.[11,46]

There were no differences greater than 10% with shape (AR and CSF) between any groups or between durations. However, at 2 Mc, the median ECD for Zr-HXPE was 34% higher than for M-CXPE, whereas Zr-CXPE was 15% lower. This 34% increase in size was counter to our first hypothesis. Previously, it was observed that the wear rate for highly crosslinked PE (HXPE) with a zirconia femoral condyle was nondetectable.[11] Although such a low-wearing, Zr-HXPE bearing may still be in an earlier stage at 2 Mc, it is unknown why this result was present. At 4 Mc, the size of the Zr-CXPE and Zr-HXPE was 13% less compared to the M-CXPE. Increased crosslinking had little effect with the CoCr femoral condyle. This was comparable to the 20% or less decrease in size reported by others.[23,25,26] Therefore, this result was consistent with our first hypothesis. Because the PE in this study was either moderately (35 kGy) or highly (70 kGy) crosslinked, the debris were mainly round submicron with a few larger flake like particles as previously described by others.[38]

TABLE IV. Descriptive Statistics for the Debris for the Four Groups at 4Mc, with Number of Particles Measured (*N*), Mean ± 1 std, (Median), and [Minimum – Maximum]

	M-CXPE	M-HXPE	Zr-CXPE	Zr-HXPE
N	368	733	337	581
ECD (μ)	0.348 ± 0.224 (0.282) [0.107 – 1.556]	0.315 ± 0.200 (0.264) [0.066 – 2.434]	0.265 ± 0.126 (0.244) [0.066 – 0.928]	0.284 ± 0.182 (0.245) [0.066 – 2.086]
Aspect Ratio	1.59 ± 0.50 (1.47) [1.00 – 5.13]	1.60 ± 0.53 (1.47) [1.00 – 7.79]	1.60 ± 0.42 (1.51) [1.03 – 3.85]	1.58 ± 0.48 (1.46) [1.02 – 5.00]
CSF	0.837 ± 0.097 (0.853) [0.371 – 0.998]	0.847 ± 0.093 (0.862) [0.246 – 0.998]	0.851 ± 0.094 (0.862) [0.472 – 0.998]	0.855 ± 0.093 (0.870) [0.454 – 0.998]

Questions? Contact FDA/CDRH/OCE/DID at CDRH-FOISTATUS@fda.hhs.gov or 301-796-8118

Records processed under FOIA Request #2014-8015; Released by CDRH on 12-8-2015

TABLE V. The Number and Volume Fractions of the Sub-Micron (<1 Micron) Particles for the Four Groups

	Number Fraction (%)		Volume Fraction (%)			
Groups	2 Mc	4 Mc	2 Mc	4 Mc	Difference	Average
M-CXPE	98.2	98.1	66.8	64.1	−2.7	65.5
M-HXPE	99.5	98.1	72.8	52.4	−20.4	62.6
Zr-CXPE	99.1	100	24.5	100	75.5	62.3
Zr-HXPE	96.6	98.8	43.0	47.2	4.2	45.1

The average submicron volumetric fractions for M-CXPE and M-HXPE were comparable to the 50% reported by others.[22] However, in this study, there was a difference in submicron volume fraction for both M-HXPE and Zr-CXPE from 2 to 4 Mc (Table V). There is little information in the literature to provide an explanation, but it could be hypothesized that these differences in submicron volume fractions were due to surface interactions with test duration. The average of submicron volume fractions at 2 and 4 Mc for both M-HXPE and Zr-CXPE gave ~60% ratio, comparable to M-CXPE (Table V). However, the Zr-HXPE had an average submicron volume fraction of 45% (Table V). Therefore, very little, if any, reduction would occur for the volume of bioreactive particles for H-HXPE or Zr-CXPE unless there was a reduction in wear. However, Zr-HXPE would have a decreased volume of bioreactive submicron particles in addition to any reduced wear. Previously, it has been shown that both the M-HXPE and Zr-CXPE had produced similar wear reductions compared to M-CXPE.[11] However, this was not necessarily reflected in the average submicron volume fractions in that they were comparable to M-CXPE. Therefore, the wear reduction probably related to a uniform decrease across the range of debris sizes.

Even given the minimal decrease in submicron volumetric fraction for M-HXPE and Zr-CXPE, due to their large wear decrease, there was at least a threefold decrease in particles generated compared to M-CXPE (Table VI).[11] The particulate numbers in this study were much higher than those measured *in vivo*.[43] However, in such studies, there were important differences in that the PE bearings were noncrosslinked, and the wear debris was extracted only from the patients' synovial fluid.[43] *In vitro* debris studies have shown that the size decrease affected by crosslinking greatly increased the number of particles per unit wear (Table VIII).[22,25,26] However, the number of PE particles produced in hip simulators studies was even higher than in the present knee study (Table VIII). Crosslinking PE with 100 kGy dose yielded a fivefold decrease in particle numbers compared to noncrosslinked PE in a hip simulator (Table VIII).[30] Scott and coworkers showed a 5.2-fold decrease in numbers of PE particles from 50 to 100 kGy (Table VIII). In this study, increasing the crosslinking from 35 to 70 KGy resulted in a fourfold decrease in PE particle numbers (Table VI). With increased crosslinking or the changing of counterface material, there was a reduction in the number of total particles generated, which could result in less biological activity produced by the debris.

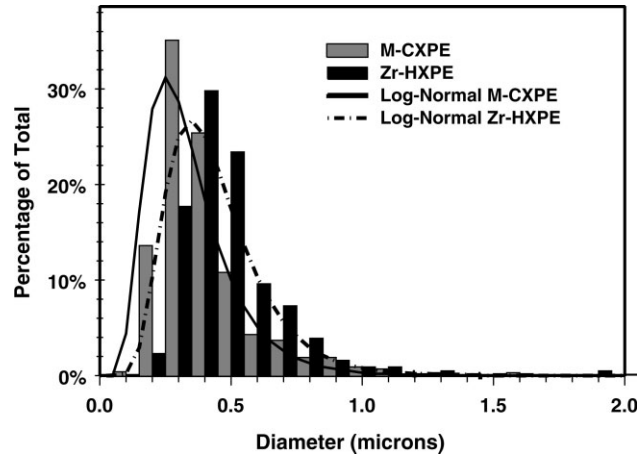

Figure 6. Number fraction histograms of the ECD data for M-CXPE and Zr-HXPE at 2Mc with log-normal distributions shown.

The distributions and log-normal fits revealed that any assumption of normal or log-normal behavior is not strongly supported. The previous study[49] suggesting that log-normal distributions fit the number fractions had four weaknesses:

1. No graphs of both data and log-normal fit.
2. No descriptive statistics from the data were provided.
3. Distributions of the volume fractions were not shown.
4. There were no debris particle <1 μm in diameter.

TABLE VI. Estimated number of particles generated per one million cycles for each group at 2 and 4 Mc

	Number of Particles (10^9/Mc)			
Groups	2Mc	4Mc	Average	Ratio
M-CXPE	203	207	205	
M-HXPE	51	49	50	4.10
Zr-CXPE	32	106	69	2.97
Zr-HXPE	N/A	N/A	N/A	N/A

Also shown are the average values and the ratios of M-CXPE to M-HXPE and Zr-CXPE.

TABLE VII. Results of Fitting Log-Normal Distributions for the Number Fraction of the Particle Size (ECD) Data for Each Group at 2 and 4 Mc

	Two Million Cycles		Four Million Cycles	
Groups	μ	σ	μ	σ
M-CXPE	−1.177	0.462	−1.237	0.546
M-HXPE	−1.184	0.446	−1.308	0.472
Zr-CXPE	−1.340	0.415	−1.426	0.405
Zr-HXPE	−0.901	0.398	−1.398	0.421

Shown are μ, the mean of ln(x), and σ, the standard deviation.

Questions? Contact FDA/CDRH/OCE/DID at CDRH-FOISTATUS@fda.hhs.gov or 301-796-8118

Records processed under FOIA Request #2014-8015; Released by CDRH on 12-8-2015

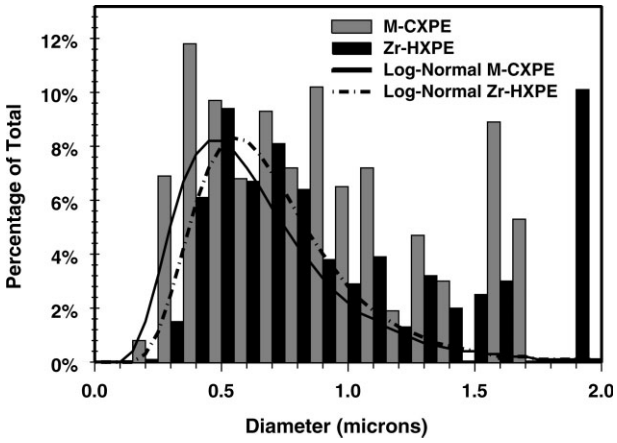

Figure 7. Volume fraction histograms of the ECD data for M-CXPE and Zr-HXPE at 2 Mc with the curves for log-normal distributions fitted to the data.

With PE debris in both total hips and knees submicron particles usually represent 80–95% of the number of particles.[22,25,36,51] The debris distributions of Ge and others[49] were inconsistent with those obtained by Elfick and coworkers[52] under similar conditions. In this study, the log-normal distribution appeared to represent the number fractions, but this was obviously not the case for the volume fraction (Figures 6 and 7). Elfick and coworkers demonstrated measurable affects in the volume fraction distributions, while showing very small, if any effects with the number fractions.[52] In addition, the volume fractions did not seem to correspond to a single distribution.[52,53] Previously, we have shown that the size distribution of PE debris from total hip simulators can be represented as a mixture model of at least two distributions.[53] The size distributions from this study behaved in a manner more consistent with those from Elfick et al. and our previous work.[52,53] Therefore, this study would suggest that care should be taken in the statistical analysis and interpretation of wear debris particle size. A better understanding of the debris size distribution could be of benefit.

In the previous knee study, wear was nondetectable for the Zr-HXPE combination.[11] PE weight changes of $\sim\geq$0.15 mg for can be confidently detected in such studies. This in combination with other factors such as fluid absorption[54] would permit discrimination of wear rates greater than 0.5 mm^3/Mc. If it were assumed that the effect of crosslinking and counterface material were cumulative, then from the previous study a 22-fold decrease would be possible for Zr-HXPE as compared to M-CXPE, that is, an estimated wear rate of circa 0.2 mm^3/Mc. Thus, the results from this knee study yielded a 12-fold decrease relating to 17×10^9 particles generated per million cycles. To provide a framework for this large number of particles, it can generally be assumed that an elderly patient can walk 10^6 cycles per year.[55] Thus, such knee joint wear is capable of releasing 17,000 PE particulates with every step the patient takes. This is much lower than the estimated 500,000 PE particles per step in the human hip joint,[55] but is still a sizeable quantity. Therefore, increased crosslinking and counterface material are important factors in the wear and numbers of generated particles. Combining these two effects provided additional improvement in wear performance.

CONCLUSIONS

In this study we found that

1. Except for the Zr-HXPE, overall there was no significant difference in particle size and shape with changes in crosslinking or counterface material.
2. Increasing the PE crosslinking created a fourfold decrease in the number of particles generated per million cycles.
3. Changing from the counterface of CoCr to one of zirconia created a threefold decrease in the number of particles generated per million cycles.
4. The averaged submicron volumetric fractions were comparable between the M-CXPE, M-HXPE, and Zr-CXPE, but the reduced wear decreased the number of particles for both the M-HXPE and Zr-CXPE.
5. The Zr-HXPE showed the largest difference in particle size and submicron volume fraction.

The authors thank the Peterson Family Foundation of Loma Linda University and the Department of Orthopaedic Surgery,

TABLE VIII. Comparison of the Number of Generated Particles from Two Simulator Studies

Bearing Combination (Femoral/PE)	Number of Particles (10^{12}/Mc)			Ratio (Normal to Control)		
	Good et al., 2003	Scott et al., 2005	Present Study	Good et al., 2003	Scott et al., 2005	Present Study
CoCr/PE	8.0 ± 1.2	6.6 ± 0.9		1.00	1.00	
OxZr/PE	5.6 ± 0.6			1.43		
CoCr/CXPE		12.0 ± 1.9	0.205		0.55	1.00
Zr/CXPE			0.069			2.97
CoCr/HXPE	2.2 ± 0.5	2.3 ± 0.2	0.050	3.64	2.87	4.10
Zr;OxZr/HXPE	1.6 ± 0.8		N/A	5.00		N/A

The ratios were normalized by the control group, which was CoCr with noncrosslinked PE for the studies of Good et al.[30] and Scott et al.[26] and for the present study CoCr with UHMWPE irradiated with 3.5 Mrad.

Questions? Contact FDA/CDRH/OCE/DID at CDRH-FOISTATUS@fda.hhs.gov or 301-796-8118

Records processed under FOIA Request #2014-8015; Released by CDRH on 12-8-2015

Loma Linda University School of Medicine for their support. Finally, grateful thanks are due to Krassimir Bozhilov, Central Facility for Advanced Microscopy and Microanalysis, University of California, Riverside for assistance with SEM.

REFERENCES

1. Clarke I, Donaldson T, Jobe C. Chapter 1: Total joint replacement: Effects of materials and designs on osteolysis. In: Garino J, Beredjiklian P, editors. Adult Reconstruction and Arthroplasty: Core Knowledge in Orthopaedics. Mosby, New York: Elsevier; 2007. pp 1–40.
2. Schmalzreid TP, Clarke IC, McKellop H. Bearing surfaces. In: Callaghan JJ, Rosenberg A, Rubash H, editors. The Adult Hip. Philadelphia: Lippincott-Raven; 1998. pp 247–265.
3. Williams PA, Yamamoto K, Masaoka T, Oonishi H, Clarke IC. Highly crosslinked polyethylenes in hip replacements: Improved wear performance or paradox? Tribol Trans 2007; 50:277–290.
4. Fisher J, Dowson D. Tribology of total artificial joints. Proc Inst Mech Eng [H] 1991;205:73–79.
5. McKellop H, Shen FW, Lu B, Campbell P, Salovey R. Development of an extremely wear-resistant ultra high molecular weight polyethylene for total hip replacements. J Orthop Res 1999;17:157–167.
6. Oonishi H, Clarke IC, Yamamoto K, Masaoka T, Fujisawa A, Masuda S. Assessment of wear in extensively irradiated UHMWPE cups in simulator studies. J Biomed Mater Res 2004;68A:52–60.
7. Muratoglu OK. The comparison of the wear behavior of four different types of crosslinked acetabular components. J Orthop Res 2001;19:1210.
8. Muratoglu OK, Bragdon CR, O'Connor DO, Jasty M, Harris WH. A novel method of cross-linking ultra-high-molecular-weight polyethylene to improve wear, reduce oxidation, and retain mechanical properties. Recipient of the 1999 HAP Paul Award. J Arthroplasty 2001;16:149–160.
9. Akagi M, Asano T, Clarke IC, Niiyama N, Kyomoto M, Nakamura T, Hamanishi C. Wear and toughness of cross-linked polyethylene for total knee replacements: A study using a simulator and small-punch testing. J Orthop Res 2006;24:2021–2027.
10. Wang A, Essner A, Polineni VK, Stark C, Dumbleton JH. Lubrication and wear of ultra-high molecular weight polyethylene in total joint replacements. Tribol Int 1998;31:17–33.
11. Tsukamoto R, Chen S, Asano T, Ogino M, Shoji H, Nakamura T, Clarke IC. Improved wear performance with cross-linked UHMWPE and zirconia implants in knee simulation. Acta Orthop 2006;77:505–511.
12. Asano T, Akagi M, Clarke IC, Masuda S, Ishii T, Nakamura T. Dose effects of cross-linking polyethylene for total knee arthroplasty on wear performance and mechanical properties. J Biomed Mater Res B Appl Biomater 2007;83:615–622.
13. Tsukamoto R, Williams PA, Shoji H, Hirakawa K, Yamamoto K, Tsukamoto M, Clarke IC. Wear of sequentially enhanced 9-Mrad polyethylene in 10 million cycle knee simulation study. J Biomed Mater Res B Appl Biomater 2008;86:119–124.
14. Hodrick JT, Severson EP, McAlister DS, Dahl B, Hofmann AA. Highly crosslinked polyethylene is safe for use in total knee arthroplasty. Clin Orthop Relat Res 2008;466:2806–2812.
15. Muratoglu OK, Bragdon CR, Jasty M, O'Connor DO, Von Knoch RS, Harris WH. Knee-simulator testing of conventional and cross-linked polyethylene tibial inserts. J Arthroplasty 2004;19:887–897.
16. Ingham E, Fisher J. Biological reactions to wear debris in total joint replacement. Proc Inst Mech Eng [H] 2000;214:21–37.
17. Ingham E, Fisher J. The role of macrophages in osteolysis of total joint replacement. Biomaterials 2005;26:1271–1286.
18. Fisher J, Bell J, Barbour PS, Tipper JL, Matthews JB, Besong AA, Stone MH, Ingham E. A novel method for the prediction of functional biological activity of polyethylene wear debris. Proc Inst Mech Eng [H] 2001;215:127–132.
19. Ingram JH, Stone M, Fisher J, Ingham E. The influence of molecular weight, crosslinking and counterface roughness on TNF-α production by macrophages in response to ultra high molecular weight polyethylene particles. Biomaterials 2004; 25:3511–3522.
20. Ingram J, Matthews JB, Tipper J, Stone M, Fisher J, Ingham E. Comparison of the biological activity of grade GUR 1120 and GUR 415HP UHMWPE wear debris. Biomed Mater Eng 2002;12:177–188.
21. Sundfeldt M, Carlsson LV, Johansson CB, Thomsen P, Gretzer C. Aseptic loosening, not only a question of wear: A review of different theories. Acta Orthop 2006;77:177–197.
22. Fisher J, McEwen HM, Tipper JL, Galvin AL, Ingram J, Kamali A, Stone MH, Ingham E. Wear, debris, and biologic activity of cross-linked polyethylene in the knee: Benefits and potential concerns. Clin Orthop 2004:114–119.
23. Yamamoto K, Clarke IC, Masaoka T, Oonishi H, Williams PA, Good VD, Imakiire A. Microwear phenomena of ultra-high molecular weight polyethylene cups and debris morphology related to gamma radiation dose in simulator study. J Biomed Mater Res 2001;56:65–73.
24. Endo M, Tipper JL, Barton DC, Stone MH, Ingham E, Fisher J. Comparison of wear, wear debris and functional biological activity of moderately crosslinked and non-crosslinked polyethylenes in hip prostheses. Proc Inst Mech Eng [H] 2002; 216:111–122.
25. Williams P, Yamamoto K, Oonishi H, Clarke I. Highly cross-linked polyethylenes in hip replacements: Improved wear performance or paradox? Tribol Trans 2007;50:277–290.
26. Scott M, Morrison M, Mishra SR, Jani S. Particle analysis for the determination of UHMWPE wear. J Biomed Mater Res B Appl Biomater 2005;73:325–337.
27. Green TR, Fisher J, Stone M, Wroblewski BM, Ingham E. Polyethylene particles of a 'critical size' are necessary for the induction of cytokines by macrophages in vitro. Biomaterials 1998;19:2297–2302.
28. Green TR, Fisher J, Matthews JB, Stone MH, Ingham E. Effect of size and dose on bone resorption activity of macrophages by in vitro clinically relevant ultra high molecular weight polyethylene particles. J Biomed Mater Res 2000;53:490–497.
29. Bowsher JG, Williams PA, Clarke IC, Green DD, Donaldson TK. "Severe" wear challenge to 36 mm mechanically enhanced highly crosslinked polyethylene hip liners. J Biomed Mater Res B Appl Biomater 2008;86:253–263.
30. Good V, Ries M, Barrack RL, Widding K, Hunter G, Heuer D. Reduced wear with oxidized zirconium femoral heads. J Bone Joint Surg Am 2003;85A (Suppl 4):105–110.
31. Kawanabe K, Clarke IC, Tamura J, Akagi M, Good VD, Williams PA, Yamamoto K. Effects of A-P translation and rotation on the wear of UHMWPE in a total knee joint simulator. J Biomed Mater Res 2001;54:400–406.
32. Kuster MS, Stachowiak GW. Factors affecting polyethylene wear in total knee arthroplasty. Orthopedics 2002;25 (2 Suppl):s235–s242.
33. Blunn GW, Joshi AB, Minns RJ, Lidgren L, Lilley P, Ryd L, Engelbrecht E, Walker PS. Wear in retrieved condylar knee arthroplasties. A comparison of wear in different designs of 280 retrieved condylar knee prostheses. J Arthroplasty 1997; 12:281–290.

Questions? Contact FDA/CDRH/OCE/DID at CDRH-FOISTATUS@fda.hhs.gov or 301-796-8118

Records processed under FOIA Request #2014-8015; Released by CDRH on 12-8-2015

34. Trent PS, Walker PS. Wear and conformity in total knee replacement. Wear 1976;36:175–187.
35. Kobayashi A, Bonfield W, Kadoya Y, Yamac T, Freeman MA, Scott G, Revell PA. The size and shape of particulate polyethylene wear debris in total joint replacements. Proc Inst Mech Eng [H] 1997;211:11–15.
36. Schmalzried TP, Campbell P, Schmitt AK, Brown IC, Amstutz HC. Shapes and dimensional characteristics of polyethylene wear particles generated in vivo by total knee replacements compared to total hip replacements. J Biomed Mater Res 1997;38:203–210.
37. Schmalzried TP, Jasty M, Rosenberg A, Harris WH. Polyethylene wear debris and tissue reactions in knee as compared to hip replacement prostheses. J Appl Biomater 1994;5:185–190.
38. Tipper JL, Galvin AL, Williams S, McEwen HM, Stone MH, Ingham E, Fisher J. Isolation and characterization of UHMWPE wear particles down to ten nanometers in size from in vitro hip and knee joint simulators. J Biomed Mater Res A 2006;78:473–480.
39. Heisel C, Silva M, Schmalzried TP. Bearing surface options for total hip replacement in young patients. Instr Course Lect 2004;53:49–65.
40. Urban JA, Garvin KL, Boese CK, Bryson L, Pedersen DR, Callaghan JJ, Miller RK. Ceramic-on-polyethylene bearing surfaces in total hip arthroplasty. Seventeen to twenty-one-year results. J Bone Joint Surg Am 2001;83A:1688–1694.
41. Haraguchi K, Sugano N, Nishii T, Sakai T, Yoshikawa H, Ohzono K. Influence of polyethylene and femoral head surface quality on wear: A retrieval study. Int Orthop 2001;25: 29–34.
42. Oonishi H, Kim SC, Clarke IC, Asano T, Bal BS, Kyomoto M, Masuda S. Retrieved ceramic total knee prosthesis in clinical use for 23 years. Bioceramics 15. Zurich-Uetikon: Trans Tech; 2003. pp 797–799.
43. Minoda Y, Kobayashi A, Iwaki H, Miyaguchi M, Kadoya Y, Ohashi H, Takaoka K. Polyethylene wear particle generation in vivo in an alumina medial pivot total knee prosthesis. Biomaterials 2005;26:6034–6040.
44. Oonishi H, Ueno M, Kim SC, Iwamoto M, Kyomoto M. Ceramic versus cobalt-chrome femoral components; Wear of polyethylene insert in total knee prosthesis. J Arthroplasty 2008;24:374–382.
45. Oonishi H, Clarke IC, Good V, Amino H, Ueno M, Masuda S, Oomamiuda K, Ishimaru H, Yamamoto M, Tsuji E. Needs of bioceramics to longevity of total joint arthroplasty. Bioceramics 15. Zurich-Uetikon: Trans Tech; 2003. pp 735–754.
46. Tsukamoto R, Williams PA, Clarke IC, Pezzotti G, Shoji H, Akagi M, Yamamoto K. Y-TZP zirconia run against highly crosslinked UHMWPE tibial inserts: Knee simulator wear and phase-transformation studies. J Biomed Mater Res B Appl Biomater 2008;86:145–153.
47. Campbell P, Ma S, Schmalzried T, Amstutz HC. Tissue digestion for wear debris particle isolation. J Biomed Mater Res 1994;28:523–526.
48. Campbell P, Ma S, Yeom B, McKellop H, Schmalzried TP, Amstutz HC. Isolation of predominantly submicron-sized UHMWPE wear particles from periprosthetic tissues. J Biomed Mater Res 1995;29:127–131.
49. Ge SR, Wang SB, Gitis N, Vinogradov M, Xiao J. Wear behavior and wear debris distribution of UHMWPE against Si3N4 ball in bi-directional sliding. Wear 2008264:571–578.
50. Williams P, Clarke I. A unified approach for evaluation of UHMWPE performance in a hip simulator using wear volume and debris size distribution: Effect of fabrication method. Proceedings of the 53rd Annual Meeting of the Orthopaedic Research Socciety, San Diego, California, February 11–14, 2007.
51. Endo MM, Barbour PS, Barton DC, Fisher J, Tipper JL, Ingham E, Stone MH. Comparative wear and wear debris under three different counterface conditions of crosslinked and non-crosslinked ultra high molecular weight polyethylene. Biomed Mater Eng 2001;11:23–35.
52. Elfick APD, Smith SL, Green SM, Unsworth A. The quantitative assessment of UHMWPE wear debris produced in hip simulator testing: The influence of head material and roughness, motion and loading. Wear 2001;249:517–527.
53. Williams PA, Clarke IC. Understanding polyethylene wear mechanisms by modeling of debris size distributions. Wear 17th Int Conf Wear Mater 2009;267:646–652.
54. Affatato S, Vandelli C, Bordini B, Toni A. Fluid absorption study in ultra-high molecular weight polyethylene (UHMWPE) sterilized and unsterilized acetabular cups. Proc Inst Mech Eng [H] 2001;215:107–111.
55. McKellop HA, Campbell P, Park SH, Schmalzried TP, Grigoris P, Amstutz HC, Sarmiento A. The origin of submicron polyethylene wear debris in total hip arthroplasty. Clin Orthop 1995:3–20.

Questions? Contact FDA/CDRH/OCE/DID at CDRH-FOISTATUS@fda.hhs.gov or 301-796-8118

Records processed under FOIA Request #2014-8015; Released by CDRH on 12-8-2015

Section 19
Performance Testing – Animal

This section does not apply to the current submission.

Questions? Contact FDA/CDRH/OCE/DID at CDRH-FOISTATUS@fda.hhs.gov or 301-796-8118

Records processed under FOIA Request #2014-8015; Released by CDRH on 12-8-2015

Section 20
Performance Testing – Clinical

This section does not apply to the current submission.

Questions? Contact FDA/CDRH/OCE/DID at CDRH-FOISTATUS@fda.hhs.gov or 301-796-8118

Records processed under FOIA Request #2014-8015; Released by CDRH on 12-8-2015

Barlow, Lenny *

From: Barlow, Lenny *
Sent: Thursday, October 17, 2013 3:55 PM
To: 'thaueter@orthodevelopment.com'
Cc: DCCLetters
Subject: k131337 Correspondence
Attachments: k131337.pdf

Questions? Contact FDA/CDRH/OCE/DID at CDRH-FOISTATUS@fda.hhs.gov or 301-796-8118

Records processed under FOIA Request #2014-8015; Released by CDRH on 12-8-2015

COVER SHEET MEMORANDUM

Food and Drug Administration
Office of Device Evaluation &
Office of In Vitro Diagnostics and
Radiological Health

From: Reviewer Name Michael C. Owens

Subject: 510(k) Number K131337

To: The Record

Please list CTS decision code: SE - Substantially Equivalent

☐ Refused to Accept (Note: this is considered the first review cycle. See screening checklist.)

☐ Hold (Additional Information or Telephone Hold)

☒ Final Decision (SE, SE with Limitations, NSE (select code below), Withdrawn, etc.)

Please complete the following for a final clearance decision (i.e, SE, SE with Limitations, etc.)	YES	NO
Indications for Use Page *(Attach IFU)*	X	
510(k) Summary or 510(k) Statement *(Attach Summary or Statement)*	X	
Truthful and Accurate Statement *(Must be present for a Final Decision)*	X	
Is the device Class III?		X
Does firm reference standards? (If yes, please attach Form 3654.)	X	
Is this a combination product?		X
Is this a reprocessed single use device? (See Guidance for Industry and FDA Staff - MDUFMA - Validation Data in 510(k)s for Reprocessed Single-Use Medical Devices.)		X
Is this device intended for pediatric use only?		X
Is this a prescription device? (If both prescription & OTC, check both boxes.)	X	
Is clinical data necessary to support the review of this 510(k)?		X
For United States based clinical studies only, did the application include a completed Form FDA 3674, Certification with Requirements of ClinicalTrials.gov Data Bank? (If study was conducted in the United States and Form FDA 3674 was not included or was incomplete, then applicant must be contacted to obtain completed form.)		X
Does this device include an Animal Tissue Source?		X
All Pediatric Patients age <= 21		X
Neonate/Newborn (Birth to 28 days)		X
Infant (29 days to < 2 years)		X
Child (2 years to <12 years)		X
Adolescent (12 years to <18 years)		X
Transitional Adolescent A (18 years to <21 years); Special considerations are being given to this group, different from adults age >= 21 (different device design or tesating, different protocol procedures, etc.)		X
Transitional Adolescent B (18 years to <21 years); No special considerations compared to adults >= 21 years)		X

Questions? Contact FDA/CDRH/OCE/DID at CDRH-FOISTATUS@fda.hhs.gov or 301-796-8118

Nanotechnology		X
Is this device subject to the Tracking Regulation? (Medical Device Tracking Guidance)		X

Regulation Number:	21 CFR 888.3560
Class:	II
Product Code:	JWH
Additional Product Codes:	OIY

Digital Signature Concurrence Table
(Not all signatures may be required)

Branch Chief Sign-Off	Casey Hanley -S 2013.10.11 11:50:46 -04'00'
Division Sign-Off	Erin I. Keith 2013.10.11 14:09:04 -04'00'

Records processed under FOIA Request #2014-8015; Released by CDRH on 12-8-2015

K131337-S001

12187 So. Business Park Drive
Draper, Utah 84020
801-553-9991/fax 553-9993

orthodevelopment.com

ORTHO DEVELOPMENT

FDA CDRH DMC
MAY 29 2013
Received

24 May 2013

To: Michael Owens

U.S. Food and Drug Administration
Center for Devices and Radiological Heath
Document Control Center - WO66-G609
10903 New Hampshire Avenue
Silver Spring, MD 20993-0002

RE: RTA Response to K131337

Dear Michael,

This letter is to provide response to the observations made in the Refuse To Accept (RTA) Checklist for K131337. The observations are listed below, with the response from Ortho Development. Per request from the agency, an electronic copy is also provided, which is the same as the paper copy.

RTA Issue:

23 b) A description of method to validate the sterilization parameters (e.g., half-cycle method and full citation of FDA-recognized standard, including date) is provided for each proposed sterilization method.

The sponsor has not describe the method used for validation (e.g., Bioburden or Overkill).

Ortho Development Response:

Section 14 of the submission has been updated to include the method used for the validation. A copy is attached.

Questions? Contact FDA/CDRH/OCE/DID at CDRH-FOISTATUS@fda.hhs.gov or 301-796-8118

20

Records processed under FOIA Request #2014-8015; Released by CDRH on 12-8-2015

RTA Issue:

24 b) A description of method to validate the sterilization parameters (e.g., half-cycle method and full citation of FDA-recognized standard, including date) is provided for each proposed sterilization method.

The sponsor did not provide a description of the method to validate the sterilization parameters.

Ortho Development Response:

Section 14 of the submission has been updated to include the method used for the validation. A copy is attached.

Please let me know if there is further information you may need to assist you in the review of this submission.

Kind Regards,

Tom Haueter

Regulatory Affairs Manager

Ortho Development

Questions? Contact FDA/CDRH/OCE/DID at CDRH-FOISTATUS@fda.hhs.gov or 301-796-8118

Records processed under FOIA Request #2014-8015; Released by CDRH on 12-8-2015

001_RTA Checklist Response Letter

Questions? Contact FDA/CDRH/OCE/DID at CDRH-FOISTATUS@fda.hhs.gov or 301-796-8118

Records processed under FOIA Request #2014-8015; Released by CDRH on 12-8-2015

24 May 2013

To: Michael Owens

U.S. Food and Drug Administration
Center for Devices and Radiological Heath
Document Control Center - WO66-G609
10903 New Hampshire Avenue
Silver Spring, MD 20993-0002

RE: RTA Response to K131337

Dear Michael,

This letter is to provide response to the observations made in the Refuse To Accept (RTA) Checklist for K131337. The observations are listed below, with the response from Ortho Development. Per request from the agency, an electronic copy is also provided, which is the same as the paper copy.

RTA Issue:

23 b) A description of method to validate the sterilization parameters (e.g., half-cycle method and full citation of FDA-recognized standard, including date) is provided for each proposed sterilization method.

The sponsor has not describe the method used for validation (e.g., Bioburden or Overkill).

Ortho Development Response:

Section 14 of the submission has been updated to include the method used for the validation. A copy is attached.

Questions? Contact FDA/CDRH/OCE/DID at CDRH-FOISTATUS@fda.hhs.gov or 301-796-8118

Records processed under FOIA Request #2014-8015; Released by CDRH on 12-8-2015

RTA Issue:

24 b) A description of method to validate the sterilization parameters (e.g., half-cycle method and full citation of FDA-recognized standard, including date) is provided for each proposed sterilization method.

The sponsor did not provide a description of the method to validate the sterilization parameters.

Ortho Development Response:

Section 14 of the submission has been updated to include the method used for the validation. A copy is attached.

Please let me know if there is further information you may need to assist you in the review of this submission.

Kind Regards,

Tom Haueter

Regulatory Affairs Manager

Ortho Development

Questions? Contact FDA/CDRH/OCE/DID at CDRH-FOISTATUS@fda.hhs.gov or 301-796-8118

Records processed under FOIA Request #2014-8015; Released by CDRH on 12-8-2015

002_Sterilization and Shelf Life

Questions? Contact FDA/CDRH/OCE/DID at CDRH-FOISTATUS@fda.hhs.gov or 301-796-8118

Records processed under FOIA Request #2014-8015; Released by CDRH on 12-8-2015

Sterilization and Shelf Life

14.1 Sterilization:

14.1.1 Implant Sterility:

The implants are sterilized by ethylene oxide in accordance with ISO 11135-1. Each lot is processed in a validated cycle to achieve a sterility assurance level (SAL) of 10^{-6}. ISO 11135-1:2007 half cycle method was used for validation.

Residual exposure limits for ethylene oxide and ethylene chlorohydrin comply with ISO 10993-7.

(b)(4) [redacted]

The sterilization validation method is conducted per ISO 11135-1. Sterilization is performed by (b)(4) [redacted] The responsibility of both parties is defined in a signed contract, consistent with FDA guidance on contract sterilization.

Ortho Development does not certify the sterile packaged device as pyrogen-free.

Refer to Section 14.2 for a description of the packaging used to maintain sterility. Refer to Section 13 for a copy of the labels identifying the product as STERILE.

14.1.2 Instrument Sterility:

Questions? Contact FDA/CDRH/OCE/DID at CDRH-FOISTATUS@fda.hhs.gov or 301-796-8118

Surgical instruments will be supplied non-sterile and are intended for sterilization or re-sterilization by the user.

14.1.3 Instrument Kit Sterility:

Surgical instrument kits will be supplied as non-sterile and are intended for sterilization or re-sterilization by the user. The validated steam sterilization cycles given below must be followed in order to ensure sterility. Cycles were validated using ISO 17665-1:2006 overkill.

(b)(4)

[redacted]

Instrument kits pertaining to Balanced Knee® System High Flex Vitamin E have been either revalidated or justified with a steam sterilization cycle, sterility assurance level (SAL) of 10^{-6}. Refer to the re-sterilization instructions in the IFU in Section 13.

14.1.4 Instrument Cleaning:

The IFU contains a statement that "all instruments shall be cleaned prior to sterilization" and provides cleaning instructions for reusable ODEV instruments. All the instruments pertaining to Balanced Knee® System High Flex Vitamin E are similar in material and similar or less complex than other instruments which have been validated for cleaning by Ortho Development and do not present new worst case instruments.

14.2 Implant Packaging:

14.2.1 The packaging configuration used for High Flex Vit E patella is identical to the packaging configuration used for BKS Revision tibial augments (K031201). The packaging configuration used for High Flex Vit E PS tibial inserts is identical to that used for the largest BKS High Flex femoral component (K123457).

(b)(4)

[redacted]

(b)(4)

[redacted]

14.3 Packaging Shelf Life:

(b)(4)

[redacted]

Records processed under FOIA Request #2014-8015; Released by CDRH on 12-8-2015

K131337/S2

12187 So. Business Park Drive
Draper, Utah 84020
801-553-9991/fax 553-9993

orthodevelopment.com

ORTHO DEVELOPMENT®

6 September 2013

U.S. Food and Drug Administration
Center for Devices and Radiological Health
Document Mail Center – WO66-G609
10903 New Hampshire Avenue
Silver Spring, MD 20993-0002

FDA CDRH DMC
SEP 09 2013
Received

ATTN:
Michael Owens
Biomedical Engineer
CDRH/ODE/DOD/JFOB
MichaelC.Owens@fda.hhs.gov

RE: K131337/S002 Additional Information Request Response

Dear Mr. Owens,

This letter is to detail the responses from Ortho Development to the letter dated 7/25/2013 received via e-mail. This letter will provide the responses and will refer the location of the documentation to support the responses. The Replacement eCopy is an exact duplicate of the paper copy.

ISSUE 1:

According to the device description, the subject component will come with yellow Radel trials. We acknowledge that the same trial material is used in your predicate devices. However, no biocompatibility information was provided on this material with the identified colorant in either submission. Therefore, please provide the following information on the yellow color additive used in the trial component:

- Chemical name and the Chemical Abstract Services (CAS) number of each key colorant in the formulation.
- Estimated absolute amount of colorant (in weight) per device.
- Size range of colorant.
- Purity level of colorant.
- Release capability of colorant.
- Material Safety Data Sheet (MSDS) for each colorant.
- Identification of other US marketed medical devices by device name, manufacturer, submission #, where the colorants have been previously used, if known.
- Biocompatibility testing of the device containing the colorant.

Questions? Contact FDA/CDRH/OCE/DID at CDRH-FOISTATUS@fda.hhs.gov or 301-796-8118

37

- Toxicity assessment of the colorant or a rational for why additional toxicity testing for the device containing the colorant is unnecessary.

Ortho Development Response:

(b)(4)

[redacted]

ISSUE 2:

(b)(4)

[redacted]

Ortho Development Response:

Pursuant to our phone conversation of August 8, 2013, the response to these questions is located in the attached "Response for Item 2."

ISSUE 3:

In your submission, you note that the re-usable instruments are provided in a storage tray/kit. Please provide a description of the tray/kit. Please clarify if this is a sterilization tray, if the sterilization tray is currently part of the submission, and if this tray is specific to your system. Please also confirm whether the tray was included in your validation testing. Please note that general sterilization trays are class II devices regulated under 21 CFR 880.6850 under the product code KCT. General sterilization trays are currently reviewed by the infection control branch in DAGID. As stated in our guidance titled "Bundling Multiple Devices or Multiple Indications in a Single Submission", which issued on June 22, 2007, devices with different indications for use in multiple medical specialties, which would require reviews by

Questions? Contact FDA/CDRH/OCE/DID at CDRH-FOISTATUS@fda.hhs.gov or 301-796-8118

Records processed under FOIA Request #2014-8015; Released by CDRH on 12-8-2015

different divisions, should have separate submissions. Therefore, if it is a general sterilization tray, please verify whether the tray mentioned has been previously cleared, and if so, please provide the 510(k) number. Alternatively, you may use a different commercially available tray and revalidate your device/instrument sterilization with the cleared tray. In this case, JFDB1 does not need to review the validation data (only the validation method and sterility assurance level achieved need to be supplied). Should you not wish to include the tray as accessories to your device for sterilizing the instruments in the tray, you may request the withdrawal of the trays by providing the appropriate withdrawal statement. In this case, you would need to validate your instrument/device sterilization without the use of a sterilization tray.

Ortho Development Response:

Pursuant to our discussion of August 8, 2013, the reusable instruments for this submission are unique to the Balanced Knee System and have been validated for the times indicated in the IFU.

ISSUE 4:

You provided draft instructions for use with your proposed labeling. The indications for use outlined the instructions do not include the method of fixation. Please provide a revised package insert that includes the method of fixation. In addition, please make sure that the instructions for use match the Indications for Use Statement. Finally, you have included additional intended use language in the package insert that should be separated from the indications for use statement. Therefore, please provide a revised package insert with this language separated from the indications for use.

Ortho Development Response:

The attached IFU has been modified to include the method of fixation in the 'INDICATIONS FOR USE' section. In addition, the additional language has been separated from the Indications for Use Statement. Section 4 has also been updated with the same language as used in the 'INDICATIONS FOR USE'.

ISSUE 5:

You provided a 510(K) Summary with your submission. However, the summary does not identify all of the correct product codes. Please provide a revised 510(K) Summary that identifies the OIY product code indicating your device contains a component manufactured from polyethylene containing an additive.

Ortho Development Response:

The attached 510(k) Summary has been modified to include the OIY product code.

Questions? Contact FDA/CDRH/OCE/DID at CDRH-FOISTATUS@fda.hhs.gov or 301-796-8118

Records processed under FOIA Request #2014-8015; Released by CDRH on 12-8-2015

Please do not hesitate to inform me if there are further requests or if more information is needed for this submission.

Kind Regards,

Tom Haueter
Regulatory Affairs Manager
Ortho Development
thaueter@odev.com

Questions? Contact FDA/CDRH/OCE/DID at CDRH-FOISTATUS@fda.hhs.gov or 301-796-8118

Records processed under FOIA Request #2014-8015; Released by CDRH on 12-8-2015

FDA CDRH DMC
SEP 03 2013
Received

K131337/S2

12187 So. Business Park Drive
Draper, Utah 84020
801-553-9991/fax 553-9993

orthodevelopment.com

ORTHO DEVELOPMENT

30 August 2013

U.S. Food and Drug Administration
Center for Devices and Radiological Health
Document Mail Center – WO66-G609
10903 New Hampshire Avenue
Silver Spring, MD 20993-0002

ATTN:
Michael Owens
Biomedical Engineer
CDRH/ODE/DOD/JFOB
MichaelC.Owens@fda.hhs.gov

RE: K131337- Response to requests for Additional Information

Dear Mr. Owens,

This letter is to detail the responses from Ortho Development to the letter dated 7/25/2013 received via e-mail. This letter will provide the responses and will refer the location of the documentation to support the responses.

ISSUE 1:

1. According to the device description, the subject component will come with yellow Radel trials. We acknowledge that the same trial material is used in your predicate devices. However, no biocompatibility information was provided on this material with the identified colorant in either submission. Therefore, please provide the following information on the yellow color additive used in the trial component:

   - Chemical name and the Chemical Abstract Services (CAS) number of each key colorant in the formulation.
   - Estimated absolute amount of colorant (in weight) per device.
   - Size range of colorant.
   - Purity level of colorant.
   - Release capability of colorant.
   - Material Safety Data Sheet (MSDS) for each colorant.
   - Identification of other US marketed medical devices by device name, manufacturer, submission #, where the colorants have been previously used, if known.
   - Biocompatibility testing of the device containing the colorant.

Questions? Contact FDA/CDRH/OCE/DID at CDRH-FOISTATUS@fda.hhs.gov or 301-796-8118

53

- **Toxicity assessment of the colorant or a rational for why additional toxicity testing for the device containing the colorant is unnecessary.**

Ortho Development Response:

(b)(4)

[redacted]

ISSUE 2:

(b)(4)

[redacted]

Ortho Development Response:

Pursuant to our phone conversation of August 8, 2013, the response to these questions is located in the attached "Response for Item 2."

ISSUE 3:

3. **In your submission, you note that the re-usable instruments are provided in a storage tray/kit. Please provide a description of the tray/kit. Please clarify if this is a sterilization tray, if the sterilization tray is currently part of the submission, and if this tray is specific to your system. Please also confirm whether the tray was included in your validation testing. Please note that general sterilization trays are class II devices regulated under 21 CFR 880.6850 under the product code KCT. General sterilization trays are currently reviewed by the infection control branch in DAGID. As stated in our guidance titled "Bundling Multiple Devices or Multiple Indications in a Single Submission", which issued on June 22, 2007, devices with different indications for use in multiple**

Questions? Contact FDA/CDRH/OCE/DID at CDRH-FOISTATUS@fda.hhs.gov or 301-796-8118

Records processed under FOIA Request #2014-8015; Released by CDRH on 12-8-2015

medical specialties, which would require reviews by different divisions, should have separate submissions. Therefore, if it is a general sterilization tray, please verify whether the tray mentioned has been previously cleared, and if so, please provide the 510(k) number. Alternatively, you may use a different commercially available tray and revalidate your device/instrument sterilization with the cleared tray. In this case, JFDB1 does not need to review the validation data (only the validation method and sterility assurance level achieved need to be supplied). Should you not wish to include the tray as accessories to your device for sterilizing the instruments in the tray, you may request the withdrawal of the trays by providing the appropriate withdrawal statement. In this case, you would need to validate your instrument/device sterilization without the use of a sterilization tray.

Ortho Development Response:

Pursuant to our discussion of August 8, 2013, the reusable instruments for this submission are unique to the Balanced Knee System and have been validated for the times indicated in the IFU.

ISSUE 4:

4. You provided draft instructions for use with your proposed labeling. The indications for use outlined the instructions do not include the method of fixation. Please provide a revised package insert that includes the method of fixation. In addition, please make sure that the instructions for use match the Indications for Use Statement. Finally, you have included additional intended use language in the package insert that should be separated from the indications for use statement. Therefore, please provide a revised package insert with this language separated from the indications for use.

Ortho Development Response:

The attached IFU has been modified to include the method of fixation in the 'INDICATIONS FOR USE' section. In addition, the additional language has been separated from the Indications for Use Statement. Section 4 has also been updated with the same language as used in the 'INDICATIONS FOR USE'.

ISSUE 5:

5. You provided a 510(K) Summary with your submission. However, the summary does not identify all of the correct product codes. Please provide a revised 510(K) Summary that identifies the OIY product code indicating your device contains a component manufactured from polyethylene containing an additive.

Ortho Development Response:

The attached 510(k) Summary has been modified to include the OIY product code.

Questions? Contact FDA/CDRH/OCE/DID at CDRH-FOISTATUS@fda.hhs.gov or 301-796-8118

Records processed under FOIA Request #2014-8015; Released by CDRH on 12-8-2015

Please do not hesitate to inform me if there are further requests or if more information is needed for this submission.

Kind Regards,

Tom Haueter
Regulatory Affairs Manager
Ortho Development
thaueter@odev.com

Questions? Contact FDA/CDRH/OCE/DID at CDRH-FOISTATUS@fda.hhs.gov or 301-796-8118

Records processed under FOIA Request #2014-8015; Released by CDRH on 12-8-2015

12187 So. Business Park Drive
Draper, Utah 84020
801-553-9991/fax 553-9993

orthodevelopment.com

6 September 2013

U.S. Food and Drug Administration
Center for Devices and Radiological Health
Document Mail Center – WO66-G609
10903 New Hampshire Avenue
Silver Spring, MD 20993-0002

ATTN:
Michael Owens
Biomedical Engineer
CDRH/ODE/DOD/JFOB
MichaelC.Owens@fda.hhs.gov

RE: K131337/S002 Additional Information Request Response

Dear Mr. Owens,

This letter is to detail the responses from Ortho Development to the letter dated 7/25/2013 received via e-mail. This letter will provide the responses and will refer the location of the documentation to support the responses. The Replacement eCopy is an exact duplicate of the paper copy.

ISSUE 1:

According to the device description, the subject component will come with yellow Radel trials. We acknowledge that the same trial material is used in your predicate devices. However, no biocompatibility information was provided on this material with the identified colorant in either submission. Therefore, please provide the following information on the yellow color additive used in the trial component:

- Chemical name and the Chemical Abstract Services (CAS) number of each key colorant in the formulation.
- Estimated absolute amount of colorant (in weight) per device.
- Size range of colorant.
- Purity level of colorant.
- Release capability of colorant.
- Material Safety Data Sheet (MSDS) for each colorant.
- Identification of other US marketed medical devices by device name, manufacturer, submission #, where the colorants have been previously used, if known.
- Biocompatibility testing of the device containing the colorant.

Questions? Contact FDA/CDRH/OCE/DID at CDRH-FOISTATUS@fda.hhs.gov or 301-796-8118

- Toxicity assessment of the colorant or a rational for why additional toxicity testing for the device containing the colorant is unnecessary.

Ortho Development Response:

(b)(4)

[redacted]

ISSUE 2:

(b)(4)

[redacted]

Ortho Development Response:

Pursuant to our phone conversation of August 8, 2013, the response to these questions is located in the attached "Response for Item 2."

ISSUE 3:

In your submission, you note that the re-usable instruments are provided in a storage tray/kit. Please provide a description of the tray/kit. Please clarify if this is a sterilization tray, if the sterilization tray is currently part of the submission, and if this tray is specific to your system. Please also confirm whether the tray was included in your validation testing. Please note that general sterilization trays are class II devices regulated under 21 CFR 880.6850 under the product code KCT. General sterilization trays are currently reviewed by the infection control branch in DAGID. As stated in our guidance titled "Bundling Multiple Devices or Multiple Indications in a Single Submission", which issued on June 22, 2007, devices with different indications for use in multiple medical specialties, which would require reviews by

different divisions, should have separate submissions. Therefore, if it is a general sterilization tray, please verify whether the tray mentioned has been previously cleared, and if so, please provide the 510(k) number. Alternatively, you may use a different commercially available tray and revalidate your device/instrument sterilization with the cleared tray. In this case, JFDB1 does not need to review the validation data (only the validation method and sterility assurance level achieved need to be supplied). Should you not wish to include the tray as accessories to your device for sterilizing the instruments in the tray, you may request the withdrawal of the trays by providing the appropriate withdrawal statement. In this case, you would need to validate your instrument/device sterilization without the use of a sterilization tray.

Ortho Development Response:

Pursuant to our discussion of August 8, 2013, the reusable instruments for this submission are unique to the Balanced Knee System and have been validated for the times indicated in the IFU.

ISSUE 4:

You provided draft instructions for use with your proposed labeling. The indications for use outlined the instructions do not include the method of fixation. Please provide a revised package insert that includes the method of fixation. In addition, please make sure that the instructions for use match the Indications for Use Statement. Finally, you have included additional intended use language in the package insert that should be separated from the indications for use statement. Therefore, please provide a revised package insert with this language separated from the indications for use.

Ortho Development Response:

The attached IFU has been modified to include the method of fixation in the 'INDICATIONS FOR USE' section. In addition, the additional language has been separated from the Indications for Use Statement. Section 4 has also been updated with the same language as used in the 'INDICATIONS FOR USE'.

ISSUE 5:

You provided a 510(K) Summary with your submission. However, the summary does not identify all of the correct product codes. Please provide a revised 510(K) Summary that identifies the OIY product code indicating your device contains a component manufactured from polyethylene containing an additive.

Ortho Development Response:

The attached 510(k) Summary has been modified to include the OIY product code.

Records processed under FOIA Request #2014-8015; Released by CDRH on 12-8-2015

Please do not hesitate to inform me if there are further requests or if more information is needed for this submission.

Kind Regards,

Tom Haueter
Regulatory Affairs Manager
Ortho Development
thaueter@odev.com

Questions? Contact FDA/CDRH/OCE/DID at CDRH-FOISTATUS@fda.hhs.gov or 301-796-8118

Records processed under FOIA Request #2014-8015; Released by CDRH on 12-8-2015

Device Description

1. Overview

The Balanced Knee® System High Flex Vitamin E (High Flex Vit E) PS tibial insert and patella are machined from extensively crosslinked, compression molded, Vitamin E UHMWPE. Both components are single use only. The High Flex Vit E PS insert must be used in conjunction with the High Flex PS femoral component (K123457). Used together, these components are designed to accommodate increased range of motion up to 150° of flexion. The High Flex Vit E patella may be used in conjunction with the Balanced Knee® System (BKS) femoral components (K994370), the BKS modular femoral components (K060569), or the High Flex PS femoral components (K123457). Both the High Flex Vit E PS insert and patella may be used in conjunction with the BKS standard and modular tibial trays, tibial augments, and stems to complete the semi-constrained modular knee prosthesis. The tibial trays, tibial augments, and stems were approved under K994370 and K031201. The High Flex Vit E PS system is designed for cemented use only. A basic configuration of the High Flex Vit E PS system is shown below. Part numbers for all implants are found in Appendix A and drawings of representative sizes of each component are found in Appendix B of this section.

(b)(4)

[redacted]

Questions? Contact FDA/CDRH/OCE/DID at CDRH-FOISTATUS@fda.hhs.gov or 301-796-8118

Records processed under FOIA Request #2014-8015; Released by CDRH on 12-8-2015

2. Intended Use

The Balanced Knee® System High Flex Vitamin E PS tibial insert and patella are intended for use in cemented total knee arthroplasty procedures with the following indications:

1. Loss of knee joint configuration and joint function.
2. Osteoarthritis of the knee joint.
3. Rheumatoid arthritis of the knee joint.
4. Post-traumatic arthritis of the knee joint.
5. Valgus, varus, or flexion deformities of the knee joint.
6. Revision procedures where other treatments or devices have failed.

3. Design Requirement

(b)(4) [redacted]

4. High Flex Vit E PS Tibial Insert

High Flex Vit E PS inserts are manufactured from Compression Molded Vitamin E Ultra High Molecular Weight Polyethylene (b)(4) [redacted]
(b)(4)

The High Flex Vit E PS inserts are available in identical sizes to the High Flex PS inserts (K123457). The seven insert sizes match each respective size of tibial tray. The insert is symmetric, not left/right specific. It is supplied in thicknesses of 7, 8, 9, 10, 11, 12, 13, 14, 16, 17, 18, and 20mm. Minimum polyethylene thickness, at the thinnest measurement point, is 7mm for every size of tibial insert. The anterior/posterior and medial/lateral dimensions are outlined for each size in the following table.

Questions? Contact FDA/CDRH/OCE/DID at CDRH-FOISTATUS@fda.hhs.gov or 301-796-8118

(b)(4) [redacted]

5. High Flex Vit E Patella

High Flex Vit E patellae are manufactured from Compression Molded Vitamin E Ultra High Molecular Weight Polyethylene (b)(4) [redacted]

(b)(4) [redacted]

The patella is available in five sizes. (b)(4) [redacted] The patella will work on either right or left knees; it is not side-specific. It is supplied in diameters of 29, 32, 35, 38 and 41 mm. (b)(4) [redacted]

(b)(4)

[redacted]

6. Size Compatibility

The High Flex Vit E PS inserts and High Flex PS femoral components (K123457) can be sized together according to the table below. The insert is matched to the tibial tray size, one-to-one.

(b)(4) [redacted]

7. System Compatibility

(b)(4) [redacted]

(b)(4) [redacted]

510(k) Number
K123457
K994370
K031201

(b)(4) [redacted]

(b)(4) [redacted]

510(k) Number
K994370
K123457
K060569

8. Surgical Instruments

All instruments are standard for the placement of total knee implants and do not represent new or novel technologies. Instrumentation is provided with the High Flex Vit E PS insert and patella for trialing the implants and preparing the patella. A summary of new instruments included in the system is provided in the table below. All other necessary instruments used with this system have been cleared in K994370, K031201, K060569, and K123457.

(b)(4) [redacted]

(b)(4)

[redacted]

Records processed under FOIA Request #2014-8015; Released by CDRH on 12-8-2015

(b)(4)

[redacted]

Questions? Contact FDA/CDRH/OCE/DID at CDRH-FOISTATUS@fda.hhs.gov or 301-796-8118

Records processed under FOIA Request #2014-8015; Released by CDRH on 12-8-2015

Appendix B, Representative Component Drawings

Questions? Contact FDA/CDRH/OCE/DID at CDRH-FOISTATUS@fda.hhs.gov or 301-796-8118

Records processed under FOIA Request #2014-8015; Released by CDRH on 12-8-2015

SOLVAY

August 13, 2013

Patricia Parish
Ortho Development Corporation
12187 S Business Park Dr.
Draper, Utah 84020
patriciap@orthodevelopment.com

Device Master File No. MAF-2122 for Radel®

Dear Customer:

Information on Solvay Specialty Polymers USA, L.L.C. Radel® Polyphenylsulfone has been submitted in our Device Master File No. MAF-2122. We hereby authorize the FDA Bureau of Devices to refer to information contained in Device Master File MAF-2122 in support of the Balanced Knee System High Flex Vitamin E PS Tibial Insert and Patella submitted by Ortho Development Corporation of Draper, Utah, whenever Solvay Specialty Polymers is proposed as a supplier. The specific Radel products are listed below:

(b)(4) [redacted]

Toxicology information can be found on pages 28-30 in the MAF.

As of the date of this letter, four Amendments have been submitted for this MAF.

The compositional information is confidential, as referred to in Section 1905, of Title 18, of the United States code Annotated and is exempt from disclosure under Section 552(b)(4), of Title 5, of the United States Code Annotated and Part 20, Subpart D of Title 21, Code of Federal Regulations.

Please direct any questions concerning the above products to me by telephone at 770-772-8584 or by e-mail at john.bankston@solvay.com.

Sincerely,

John Bankston

John Bankston
Regulatory Affairs & Product Stewardship Manager, Aromatic Polymers

Questions? Contact FDA/CDRH/OCE/DID at CDRH-FOISTATUS@fda.hhs.gov or 301-796-8118

(b)(4) Testing

(b)(4) Testing

(b)(4) Testing

(b)(4) Testing

(b)(4) Testing

(b)(4) Testing

(b)(4) Testing

(b)(4) Testing

(b)(4) Testing

(b)(4) Testing

(b)(4) Testing

(b)(4) Testing

(b)(4) Testing

(b)(4) Testing

(b)(4) Testing

(b)(4) Testing

(b)(4) Testing

(b)(4) Testing

(b)(4) Testing

(b)(4) Testing

(b)(4) Testing

(b)(4) Testing

(b)(4) Testing

(b)(4) Testing

(b)(4) Testing

(b)(4) Testing

(b)(4) Testing

(b)(4) Testing

Records processed under FOIA Request #2014-8015; Released by CDRH on 12-8-2015

Instructions for Use

Balanced Knee® System

Manufacturer
Ortho Development® Corporation
12187 South Business Park Drive
Draper, UT 84020
Phone 801-553-9991
Fax 801-553-9993
www.orthodevelopment.com

For cemented use only

DESCRIPTION

Balanced Knee® System, Balanced Knee® System High Flex, and Balanced Knee® System Revision are a multi-compartmental total knee replacement providing a system of components for posterior cruciate ligament retaining and substituting procedures. Balanced Knee® System, Balanced Knee® System High Flex, and Balanced Knee® System Revision are indicated for cemented use only. Choice of specific femoral and tibial components depends on whether the posterior cruciate ligament is retained or excised, and the extent and nature of anterior/posterior (A/P) and medial/lateral (M/L) stabilization.

Cobalt Chromium Alloy Femoral Component

The femoral components are cobalt chromium (Co-Cr-Mo, ASTM F-75).

Component	*510(k) Number*
BKS Cruciate Retaining (CR)	K994370
BKS Posterior Stabilized (PS)	K994370
High Flex Posterior Stabilized (High Flex PS)	K123457
Modular Femoral	K060569

Femoral components with porous coating are porous coated with cobalt chromium (Co-Cr-Mo, ASTM F-75).

The semi-constrained posterior stabilizing femoral components are designed to provide anterior/posterior (A/P) stability, but rely on collateral ligament balancing techniques for medial/lateral (M/L) stability.

The High Flex PS (HFPS) components are semi-constrained posterior stabilizing components designed to accommodate a higher level of flexion up to 150°, while providing anterior/posterior stability, but rely on collateral ligament balancing techniques for medial/lateral (M/L) stability.

The cruciate retaining femoral components are designed for use with a functional posterior cruciate ligament. These components also rely on collateral ligament balancing techniques for medial/lateral (M/L) stability.

The modular femoral components are posterior stabilized with the option of intramedullary stem extensions and are designed to provide additional anterior/posterior (A/P) and medial/lateral (M/L) stability if needed or desired.

Titanium Tibial Tray

The titanium tibial tray (Ti-6Al-4V ELI, ASTM F-136) is available either with or without porous coating of commercially pure titanium (CP Ti, ASTM F-1580).

Questions? Contact FDA/CDRH/OCE/DID at CDRH-FOISTATUS@fda.hhs.gov or 301-796-8118

Records processed under FOIA Request #2014-8015; Released by CDRH on 12-8-2015

Component	*510(k) Number*
BKS Non-Porous Tray	K994370
BKS Porous Tray	K994370
BKS Porous Pegged Tray	K020383
Modular Tray	K031201
Offset Tray	K103837

The porous coated tibial trays are available in two options. The first option is supplied with removable polyethylene screw hole plugs (UHMWPE, ASTM F-648) for optional screw fixation using cancellous bone screws. The second porous coated option is offered with titanium pegs (Ti-6Al-4V ELI, ASTM F-136) instead of screw holes.

The modular tibial trays (Ti-6Al-4V ELI, ASTM F-136) are supplied with a titanium keel cap (Ti-6Al-4V ELI, ASTM F-136) which is removable in cases where a stem extension is needed.

The offset tibial trays (Ti-6Al-4V ELI, ASTM F-136) are used with an offset adapter, offset screw, and stem extension to accommodate various tibial anatomies.

Polyethylene Tibial Insert
The polyethylene tibial inserts are available in six variations:

Component	*510(k) Number*
BKS Cruciate Retaining (CR)	K994370
BKS Posterior Stabilized (PS)	K994370
BKS Ultra Congruent (UC)	K090705
High Flex Posterior Stabilized (HFPS)	K123457
High Flex Crosslinked Vitamin E Posterior Stabilized (HFVPS)	K131337
Semi-Constrained Posterior Stabilized (SCPS)	K060569

The PS, HFPS, CR, UC, and High Flex PS variations are made of polyethylene (UHMWPE, ASTM F-648) and are to be used with the matching femoral component variation (i.e., PS femoral for PS insert, HFPS femoral for HFPS insert, CR femoral for CR or UC insert).

The High Flex Vitamin E PS is made of crosslinked Vitamin E polyethylene (Vitamin E UHMWPE, ASTM F-648) and is to be used with the matching femoral component variation (i.e. High Flex PS femoral with High Flex Vitamin E PS insert).

The SCPS variation is made of polyethylene (UHMWPE, ASTM F-648) and includes a titanium (Ti-6Al-4V ELI, ASTM F-136) reinforcement pin for added stability. The SCPS tibial insert is to be used with the matching femoral component (i.e., modular) when additional medial/lateral (M/L) stability is required. The SCPS tibial insert must also be used with the matching modular tibial tray or offset tibial tray.

Patella
The patellae are available in two variations:

Component	*510(k) Number*
Compression Molded Polyethylene Patella	K994370
Crosslinked Vitamin E Polyethylene Patella	K131377

Questions? Contact FDA/CDRH/OCE/DID at CDRH-FOISTATUS@fda.hhs.gov or 301-796-8118

The compression molded polyethylene patella (UHMWPE, ASTM F-648) is a resurfacing patellar prosthesis. 510(k) Number: K994370.

The Crosslinked Vitamin E Polyethylene Patella (Vitamin E UHMWPE, ASTM F-648) is a resurfacing patellar prosthesis. 510(k) Number: K131337.

Titanium Femoral Augments
The titanium femoral augments (Ti-6Al-4V ELI, ASTM F-136) are provided with a locking screw (Ti-6Al-4V ELI, ASTM F-136) and a locking ring (Ti-6Al-4V ELI, ASTM F-136). Femoral augments may only be used with the Balanced Knee® System Revision modular femoral components. 510(k) Number: K060569.

Femoral augments are provided for optional use in order to augment either the distal and/or posterior femur with bony deficiencies. Femoral augments are provided in assorted stepped configurations to facilitate surgeon selection for addressing typical bony defects.

Titanium Tibial Augments
The titanium tibial augments (Ti-6Al-4V ELI, ASTM F-136) are provided with a locking screw (Ti-6Al-4V ELI, ASTM F-136) and a locking ring (Ti-6Al-4V ELI, ASTM F-136). Tibial augments may only be used with the Balanced Knee® System Revision modular or offset tibial tray components. 510(k) Number: K031201.

Tibial augments are provided for optional use in order to augment a tibial plateau with bony deficiencies. Tibial augments are provided in assorted hemispherical stepped and angled configurations to facilitate surgeon selection for addressing typical bony defects.

Titanium Cemented and Fluted Stem Extensions
The titanium cemented and fluted stem extensions (Ti-6Al-4V ELI, ASTM F-136) are provided for optional use with Balanced Knee® System Revision femoral components and tibial trays to provide increased stability. The stem extensions attach into the modular femoral junction box, the modular tibial tray, or the offset adapter as needed. 510(k) Number: K031201.

Cobalt Chromium Alloy Junction Box
The junction box is manufactured from forged cobalt chromium (Co-Cr-Mo, ASTM F-799) and is used with the modular femoral component when a stem extension is needed. The junction box is available in 5° and 7° options. 510(k) Number: K060569.

Titanium Offset Adapter
The titanium offset adapters (Ti-6Al-4V ELI, ASTM F-136) are provided with one screw (Ti-6Al-4V ELI, ASTM F-136). Offset adapters must be used with Balanced Knee® System Revision offset tibial tray and stem extension components. One screw is required for sufficient fixation of the offset adapter. 510(k) Number: K103837.

Titanium Offset Screw
The titanium offset screws (Ti-6Al-4V ELI, ASTM F-136) are provided for optional use beyond the single screw that is required with the offset adapter. Offset screws may only be used with Balanced Knee® System Revision offset tibial tray and offset adapter components. 510(k) Number: K103837.

Records processed under FOIA Request #2014-8015; Released by CDRH on 12-8-2015

INDICATIONS FOR USE

Balanced Knee® System, Balanced Knee® System High Flex, and Balanced Knee® System Revision are intended for use in cemented total knee arthroplasty procedures.

Total knee arthroplasty is indicated for the following conditions:

1. Loss of knee joint configuration and joint function.
2. Osteoarthritis of the knee joint.
3. Rheumatoid arthritis of the knee joint.
4. Post-traumatic arthritis of the knee joint.
5. Valgus, varus, or flexion deformities of the knee joint.
6. Revision procedures where other treatments or devices have failed.

INTENDED USE

Balanced Knee® System, Balanced Knee® System High Flex, and Balanced Knee® System Revision are intended for total knee arthroplasty procedures.

Balanced Knee® System is intended in the salvage of previously failed surgical attempts where femoral bone loss does not require the use of augments or stem extensions and where collateral ligaments may be relied upon for medial/lateral (M/L) stability.

Balanced Knee® System High Flex is intended in the salvage of previously failed surgical attempts where femoral bone loss does not require the use of augments or stem extensions, where collateral ligaments may be relied upon for medial/lateral stability, where post-operative flexion up to 150° may be desirable, and the patient meets all indications/contraindications requirements.

Balanced Knee® System Revision is intended in the salvage of previously failed surgical attempts where femoral bone loss may require the use of augments or stem extensions.

Balanced Knee® System Revision SCPS Tibial Insert is intended for use with Balanced Knee® System Revision modular femoral and modular or offset tibial components where collateral ligaments may not be relied upon for medial/lateral (M/L) stability.

Balanced Knee® System Revision Offset Tibia is intended for use in the salvage of previously failed surgical attempts where bone loss may require the use of augments or stem extensions or in difficult primary surgical cases where a long extension stem is necessary.

CONTRAINDICATIONS

1. Any patient not experiencing a compromised quality of life by loss of joint function and/or joint configuration, or pain from arthritis disease.
2. Any patient whose knee cannot be returned to normal function and normal stability through reconstructive procedures, including ligamentous balancing.
3. Active infection in or near the knee joint, fever and/or local inflammation signs, and elevation of sedimentation rate unexplained by other diseases should not be treated unless preoperative infection is ruled out.
4. Distant foci of infection, such as genitourinary, pulmonary, skin (chronic lesions or ulcerations), and other sites, that may result in hematogenous spread to the implant site.
5. Rapid joint destruction or bone absorption apparent on roentgenograms.6. Neuromuscular disorders in which the potentially adverse effects on prosthesis function are not outweighed by the benefits gained by the patient from usage of the prosthesis.
7. Mental disorders that would compromise essential patient post-operative care.

Questions? Contact FDA/CDRH/OCE/DID at DIHF@fda.hhs.gov or 301-796-8118

Records processed under FOIA Request #2014-8015; Released by CDRH on 12-8-2015

8. A painless, stable arthrodesis in a functional position.
9. Allergic reactions to implant materials and/or tissue reactions to the products of corrosion or wear.
10. Skeletal immaturity.

INFORMATION FOR USE

To ensure proper placement and fit, only Balanced Knee® System, Balanced Knee® System High Flex, and Balanced Knee® System Revision instruments and trials manufactured by Ortho Development® Corporation should be used to implant the Balanced Knee® System, Balanced Knee® System High Flex, and Balanced Knee® System Revision components.

Components, trials, and instruments from other knee systems must not be used with components, trials, and instruments from Balanced Knee® System, Balanced Knee® System High Flex, and Balanced Knee® System Revision and vice versa, unless specifically labeled for such use. Different engineering specifications and dimensional incompatibilities among the various systems may cause premature wear or loosening of the implant.

Components of Balanced Knee® System, Balanced Knee® System High Flex, and Balanced Knee® System Revision are not compatible with components of any other knee system.

Optimal fixation and implant stability are achieved by maximizing bone coverage. Components are provided in a variety of sizes. The largest available components should be chosen that cover, but do not overhang, the femur, tibia, or patella.

Several thicknesses and styles of polyethylene tibial inserts are supplied separately from the tibial tray, but in corresponding sizes to the tibial tray. The surgeon should choose an insert of appropriate thickness and style to restore the original joint line and to achieve proper ligament tension.

PRECAUTIONS

Preoperative:

The surgeon should thoroughly understand all aspects of the surgical procedure and limitations of the device. The surgeon should instruct patients as to the limits of the prosthesis and the impact of excessive loading through patient weight or activity. Patients should also be taught to govern and/or restrict their activities accordingly.

Strict adherence to the indications, contraindications, precautions, and warnings for this product is essential to potentially maximize the success of the procedure and the service life of the implant.

Intraoperative:

If the implant site has been improperly prepared or excessive force is used to seat the implant, fracture of the proximal tibia or femoral condyles may occur.

Polyethylene tibial inserts can be removed after they have been snapped into place. Once removed, however, they must be discarded, as the removal process deforms the plastic and reduces attachment strength. Use trials to determine proper tibial insert sizing.

Questions? Contact FDA/CDRH/OCE/DID at CDRH-FOISTATUS@fda.hhs.gov or 301-796-8118

Records processed under FOIA Request #2014-8015; Released by CDRH on 12-8-2015

An implant should never be reused. Any implant, once used, should be discarded. Though it appears undamaged, it may have small defects and internal stress patterns that may eventually lead to failure. Likewise, care must be taken in handling new implants to avoid damage that could compromise the mechanical integrity of the device and cause early failure or loosening, such as marring, nicks, or notches caused by contact with metal or abrasive objects.

The SCPS polyethylene insert can only be used with the modular tibial tray or offset tibial tray. It is not compatible with the primary porous coated, non-coated or pegged tibial trays. The modular femoral component with augments and stem may be used with the primary tibial trays only if a standard tibial insert is used.

If loose fragments of bone cement become detached, they can act as an abrasive on the contact surfaces of the implant, greatly accelerating the wear rate of the prosthesis. Care should be taken to remove all excess cement from around the implant and its surfaces.

WARNINGS

Components of Balanced Knee® System, Balanced Knee® System High Flex, and Balanced Knee® System Revision are not compatible with the components of any other knee system. Different specifications and dimensional compatibilities among the various systems may cause premature wear or loosening of the implant.

1. Use only Balanced Knee® System, Balanced Knee® System High Flex, and Balanced Knee® System Revision femoral components with Balanced Knee® System, Balanced Knee® System High Flex, and Balanced Knee® System Revision tibial inserts and tibial trays.
2. Use only Balanced Knee® System High Flex femoral components with Balanced Knee® System High Flex tibial inserts.
3. Use only Balanced Knee® System patella prostheses with Balanced Knee® System, Balanced Knee® System High Flex, and Balanced Knee® System Revision femoral components.
4. If optional screw fixation is desired with the porous-coated tibial tray, use only Ortho Development® Corporation cancellous bone screws.
5. Components that are labeled as PS should be used only with other PS components. HFPS components should be used only with other HFPS components. Likewise, CR components should be used only with CR or UC components. In addition, components that are marked SCPS should be used only with other SCPS components. If no specification is made, the part can be used with all three systems.
6. The correct selection of the implant is extremely important. The potential for success in total joint replacement is increased by the selection of the proper size, shape, and design of the implant. Balanced Knee® System, Balanced Knee® System High Flex, and the Balanced Knee® System Revision have interchangeable part sizes as described by the following chart, where the number in the shaded box refers to the tibial insert size:

		Femoral Component Size						
		1	2	3	4	5	6	7
Tibial Tray Size	1	1	1					
	2	2	2	2				
	3		3	3	3			
	4			4	4	4		
	5				5	5	5	
	6					6	6	6
	7						7	7

Questions? Contact FDA/CDRH/OCE/DID at CDRH-FOISTATUS@fda.hhs.gov or 301-796-8118

7. The compatibility of the implants vary by what implant is being used. Correct implant choice is crucial in a successful joint replacement. Below is a compatibility chart which refers to the proper implants to be used:

		TIBIAL INSERT AND TRAY								
		BKS Tray				*Modular and Offset Tray*				
		CR	*UC*	*HFPS HFVPS*	*PS*	*CR*	*UC*	*HFPS HFVPS*	*PS*	*SCPS*
FEMORAL	*BKS CR*	●	●			●	●			
	High Flex PS			●				●		
	BKS PS				●				●	
	Modular Femoral				●				●	●

● = compatible

ADVERSE EFFECTS

Short-term complication rates may be similar to those occurring with any femoral joint replacement such as:

1. Changes in position and loosening of the implant.
2. Dislocation of implant.
3. Infection.
4. Reduced range of motion.
5. Heterotopic bone formation.
6. Incomplete pain relief.

MAGNETIC RESONANCE (MR)

Balanced Knee® System, Balanced Knee® System High Flex, and Balanced Knee® System Revision have not been evaluated for safety and compatibility in the MR environment. Balanced Knee® System, Balanced Knee® System High Flex, and Balanced Knee® System Revision have not been tested for heating or migration in the MR environment.

PACKAGING AND STERILITY

All implants are sterilized to Sterility Assurance Level 10^{-6}. All implants, except for the Vitamin E polyethylene components, are sterilized by a minimum of 25 kGy gamma irradiation. All Vitamin E polyethylene components are ethylene oxide sterilized.

All gamma irradiated polyethylene tibial inserts and polyethylene patellae are sterilized in an oxygen-free/nitrogen-rich environment.

Sterile product packaging should be inspected for flaws before and after opening. In the presence of a flaw, assume the product is non-sterile and do not implant it into a patient.

INSTRUMENT STERILITY

All Instruments should be thoroughly cleaned prior to sterilization. Please refer to Ortho Development Reusable Instrument Care Manual for instrument cleaning and sterilization details.

Unless otherwise indicated on the case labeling, the following Steam Sterilization Cycles must be followed in order to ensure sterility:

Records processed under FOIA Request #2014-8015; Released by CDRH on 12-8-2015

	Temperature	Cycle Time (Minutes)	Dry Time (Minutes)
Prevacuum	270 °F (132°C)	4	60
Gravity	270 °F (132°C)	30	90

Kit Number	Description	Prevac (Minutes)	Prevac Dry (Minutes)	Gravity (Minutes)	Gravity Dry (Minutes)
261-9301	BKS Femoral 1	6	45	30	90
261-9304(A)	BKS Tibial 1	5	5	50	50

PRODUCT HANDLING

Always store implants unopened in their respective protective packages. Prior to use, inspect the packaging for damage, which may compromise sterility. When removing the implant from its packaging, observe relevant aseptic techniques. Protect the prosthesis from contact with objects that may damage the surface finish. Inspect each implant prior to use for visual damage.

PRODUCT COMPLAINTS

Any complaint or dissatisfaction with product quality, performance, labeling, and/or safety should be reported to Ortho Development® Corporation. If any of the implants or instruments “malfunction” (i.e., do not meet any of their performance specifications or do not perform as intended), and/or are suspected to have caused or contributed to the death or serious injury of the patient, Ortho Development® Corporation should be notified immediately by phone, fax, or written correspondence.

When filing a complaint, please provide the product description, product number, lot number, complainant’s name and address, and the nature of the complaint.

CAUTION

Federal Law (USA) restricts this device to sale, distribution, and use by or on the order of a physician.

351-1-10627 04/2013

Questions? Contact FDA/CDRH/OCE/DID at CDRH-FOISTATUS@fda.hhs.gov or 301-796-8118

Records processed under FOIA Request #2014-8015; Released by CDRH on 12-8-2015

Indications for Use Form
Ortho Development
Balanced Knee® System High Flex Vitamin E
PS Tibial Insert and Patella 510(k)

510(k) Number (if known): _____

Device Name: Balanced Knee® System High Flex Vitamin E PS Tibial Insert and Patella

Indications for Use:

Balanced Knee® System, Balanced Knee® System High Flex, and Balanced Knee® System Revision are intended for use in cemented total knee arthroplasty procedures.

Total knee arthroplasty is indicated for the following conditions:

1. Loss of knee joint configuration and joint function.
2. Osteoarthritis of the knee joint.
3. Rheumatoid arthritis of the knee joint.
4. Post-traumatic arthritis of the knee joint.
5. Valgus, varus, or flexion deformities of the knee joint.
6. Revision procedures where other treatments or devices have failed.

Prescription Use ____X___ (Part 21 CFR 801 Subpart D)	AND/OR	Over-The-Counter Use _____ (21 CFR 801 Subpart C)

(PLEASE DO NOT WRITE BELOW THIS LINE-CONTINUE ON ANOTHER PAGE IF NEEDED)

Concurrence of CDRH, Office of Device Evaluation (ODE)

Questions? Contact FDA/CDRH/OCE/DID at CDRH-FOISTATUS@fda.hhs.gov or 301-796-8118

Records processed under FOIA Request #2014-8015; Released by CDRH on 12-8-2015

510(k) Summary

NAME OF SPONSOR:	Ortho Development Corporation 12187 South Business Park Drive Draper, Utah 84020
510(k) CONTACT:	Tom Haueter Regulatory Affairs Manager Telephone: (801) 553-9991 Facsimile: (801) 553-9993 Email: thaueter@orthodevelopment.com
DATE PREPARED:	April 24, 2013
PROPRIETARY NAME:	Balanced Knee® System High Flex Vitamin E PS Tibial Insert and Patella
COMMON NAME:	Total Knee Replacement Prosthesis
CLASSIFICATION:	21 CFR 888.3560, Knee joint, patellofemorotibial, polymer/metal/polymer semi-constrained cemented prosthesis, Class II device
DEVICE PRODUCT CODE:	JWH, OIY
PREDICATE DEVICES:	Balanced Knee® System (K994370), *Ortho Development Corp.* Balanced Knee® System High Flex PS (K123457), *Ortho Development Corp.* Highly Cross-Linked Vitamin E UHMWPE Tibial Insert (K091956), *DJO Surgical/Encore Medical*

Questions? Contact FDA/CDRH/OCE/DID at CDRH-FOISTATUS@fda.hhs.gov or 301-796-8118

Records processed under FOIA Request #2014-8015; Released by CDRH on 12-8-2015

Device Description

The Balanced Knee® System High Flex Vitamin E (High Flex Vit E) PS tibial insert and patella are machined from extensively crosslinked, compression molded, Vitamin E UHMWPE. Both components are single use only. The High Flex Vit E PS tibial insert must be used in conjunction with the High Flex PS femoral component (K123457). Used together, these components are designed to accommodate increased range of motion up to 150° of flexion. The High Flex Vit E patella may be used in conjunction with the Balanced Knee® System (BKS) femoral components (K994370), the BKS modular femoral components (K060569), or the High Flex PS femoral components (K123457). Both the High Flex Vit E PS tibial insert and patella may be used in conjunction with the BKS standard and modular tibial trays, tibial augments, and stems to complete the semi-constrained modular knee prosthesis. The tibial trays, tibial augments, and stems were approved under K994370 and K031201.

Intended Use

The Balanced Knee® System High Flex Vitamin E PS tibial insert and patella are intended for use in cemented total knee arthroplasty procedures with the following indications:

1. Loss of knee joint configuration and joint function.
2. Osteoarthritis of the knee joint.
3. Rheumatoid arthritis of the knee joint.
4. Post-traumatic arthritis of the knee joint.
5. Valgus, varus, or flexion deformities of the knee joint.
6. Revision procedures where other treatments or devices have failed.

Technological Characteristics

Feature	Equivalent Device
Indications for Use and Design	Ortho Development: Balanced Knee® System (K994370) Ortho Development: Balanced Knee® System High Flex PS (K123457)
Material: Extensively Crosslinked Vitamin E Polyethylene UHMWPE (α-tocopherol)	DJO Surgical/Encore Medical: Vit E UHMWPE Tibial Insert (K091956)

There is only one difference between the High Flex Vit E PS insert when compared to the BKS High Flex PS insert: the implementation of a different material, crosslinked Vitamin E UHMWPE. Likewise, the High Flex Vit E patella is identical to the BKS patella except for the crosslinked Vitamin E UHMWPE material. The indications for use for the High Flex Vit E PS tibial insert and patella are identical to the indications for use for the BKS High Flex. The crosslinked Vitamin E UHMWPE for the High Flex Vit E PS insert and patella undergoes substantially equivalent fabrication and final processing as its predicate, DJO/Encore's Vitamin E UHMWPE tibial insert.

Questions? Contact FDA/CDRH/OCE/DID at CDRH-FOISTATUS@fda.hhs.gov or 301-796-8118

Records processed under FOIA Request #2014-8015; Released by CDRH on 12-8-2015

Performance Data

The following non-clinical testing was performed to determined substantial equivalence to the predicate devices:

Property	Result
Range of Motion	Up to 150° flexion; Identical to predicate device, BKS High Flex
Femorotibial Constraint	Identical to predicate device, BKS High Flex
Femorotibial Contact Area	Identical to predicate device, BKS High Flex
Patellofemoral Constraint	Identical to predicate device, BKS High Flex
Patellofemoral Contact Area	Identical to predicate device, BKS High Flex
PS Spine Fatigue	Sufficient strength to survive in-vivo loading
Insert Assembly/ Disassembly	Sufficient strength to survive in-vivo loading
Crosslinking Characterization of High Flex Vit E	Substantially equivalent or better than BKS
Vitamin E Characterization of High Flex Vit E	Substantially equivalent or better than BKS
High Flex Knee Wear	56% decrease in wear over BKS

Basis for Substantial Equivalence

Ortho Development believes that the High Flex Vit E PS tibial insert and patella are substantially equivalent to the previously cleared predicate devices based on similarities in intended use, design, materials, manufacturing methods, packaging, and mechanical performance.

Questions? Contact FDA/CDRH/OCE/DID at CDRH-FOISTATUS@fda.hhs.gov or 301-796-8118